

# **Independent Review of the Chromium Interim Measures Remediation System in Mortandad Canyon Los Alamos, New Mexico**

---

Vedat Batu, PhD, P.E.  
Fred Day-Lewis, PhD  
Inci Demirkanli, PhD  
J.F. Devlin, PhD  
Scott Ellinger, M.S. P.G.  
J. Alexandra Hakala, PhD  
Brian B. Looney, PhD  
Charles J. Newell, PhD, P.E., BCEE  
Sorab Panday, PhD  
Mark J. Rigali, PhD  
Daniel B. Stephens, PhD  
Matthew Tonkin, PhD  
Ines Triay, PhD  
Haruko Wainwright, PhD  
David Wilson, MS, P.E.

**December 2024**

This page intentionally left blank.

## Executive Summary

In 2004, sampling of a monitoring well revealed chromium at concentrations exceeding the 50 parts per billion (ppb) State of New Mexico water quality standard in groundwater beneath a portion of Mortandad Canyon in Los Alamos, New Mexico. The subsequent investigation and cleanup efforts have been regulated since 2016 under a Resource Conservation and Recovery Act (RCRA) Corrective Action Order from the New Mexico Environment Department (NMED) Hazardous Waste Bureau. The U.S. Department of Energy (DOE) Office of Environmental Management Los Alamos Field Office (DOE-EM-LA) is responsible for oversight of the prime contractors implementing the investigation and cleanup, including interim measures (IM) that have been taken to mitigate plume migration until a final remedy is implemented.

The current IM is a groundwater pump-and-treat (P&T) hydraulic control measure together with chromium mass recovery, currently consisting of five extraction wells located in the center of the plume and five injection wells located on the south and east margins of the plume. Contaminated water recovered from the five extraction wells is treated before reinjection. The injection aims to create a hydraulic barrier such that the plume will not cross the Pueblo de San Ildefonso lands boundary to the south. A discharge permit for treated water injection was issued by the NMED Ground Water Quality Bureau (GWQB). The IM system began partial operations in 2017, and ramped up to full capacity in 2018.

In March 2023 during IM operations, unanticipated increases in chromium concentrations in two monitoring wells, as well as the discovery of contamination deeper than expected, caused NMED to issue an order to stop injection until DOE-EM-LA could ensure that chromium was not migrating beyond hydraulic control at concentrations above the 50 ppb standard. From September 2023 to March 2024, an exchange of correspondence took place between NMED and DOE-EM-LA to discuss restarting the IM, without resolution. DOE-EM-LA and NMED then agreed to convene an independent panel of 15 experts (the Independent Review Team [IRT]) to assess the issues in dispute and recommend possible solutions. The parties developed specific questions for the IRT to address and grouped them into five topics: (1) the performance of the IM in achieving hydraulic control of the chromium plume, (2) the modeling of the chromium plume, (3) the corrective actions proposed by NMED, (4) regulatory matters, and (5) well design issues. Each of these topics is summarized in the following paragraphs. The IRT was provided two days of briefings and a site tour in March 2024. This report represents the combined efforts of the IRT in answering the questions posed.

The first topic was chromium plume control by IM operation. The horizontal and vertical extents of chromium have been the subjects of several years of investigation, and although understanding is growing, at this time the plume is not sufficiently characterized to design a final remedy. It is also difficult to fully address the success of hydraulic containment when the plume boundaries are not yet confidently defined in some areas, and when there is some potential as inferred by the IRT that operation of the IM may increase downward migration potential in some areas. Nevertheless, during IM operations, the chromium plume appeared to shift northward (i.e., toward the extraction wells and away from the Pueblo de San Ildefonso lands boundary) and, over much of the plume, chromium concentrations declined during IM operations due—at

least in part—to the successful recovery of substantial chromium mass. Therefore, though the ability of the IM system to capture all the chromium during operations and prevent further migration on the east side is not clear, it *is* clear that chromium concentrations increased significantly in some wells following IM shutdown, including in the easternmost monitoring well where chromium was detected (R-70). The rate of chromium plume expansion with the IM turned off could be on the order of hundreds of feet per year in some places. Therefore, increasing areas and regions of the aquifer appear to be impacted following the cessation of the IM pumping, bringing a sense of urgency to renewing the IM abatement procedures. For this reason, *the single most important recommendation of the IRT is to restart the IM*—using a portion of the original system—while other studies and field investigations move forward.

The second topic was computer modeling of the chromium plume. DOE-EM-LA contractors used a sophisticated computer code referred to as FEHM (Finite Element Heat and Mass) to develop a groundwater model to simulate chromium behavior during and after IM operations. Although the IRT raised concerns regarding the complexity of the analyses that have been undertaken and the use of the FEHM code in preference to more common codes, the IRT has no concerns regarding the technical reliability of the FEHM code itself. Nonetheless, the FEHM code was not originally developed for groundwater simulation and is not widely used by groundwater professionals—including regulators and their consultants—which limits the ability of third parties to review or execute analyses. The IRT therefore recommends that the model be converted to another simulation code—preferably one of the MODFLOW family of codes—which would be equally or better suited to the technical tasks at hand, but also more widely accepted and more transparent to third parties. In addition, the IRT concluded that the chromium plume conceptual site model (CSM) should be revisited and that the numerical model should show improved correspondence with the CSM, including layering and aquifer parameters, with particular emphasis on horizontal and vertical hydraulic conductivities. Data for some aquifer tests were reanalyzed by members of the IRT, and details for these and other analyses are presented in report appendices. Although the IRT expressed concerns with the groundwater model, the IRT believes that the model is, at this time, the best tool for comparative analysis of IM system operational schemes to improve plume capture until an updated, preferably MODFLOW-based, model is implemented.

The third topic is NMED’s recommendation for a path forward, as described in Appendix A to their September 6, 2023 letter to DOE-EM-LA. Overall, the IRT finds the NMED proposal reasonable. NMED stated it would accept restarting the IM if certain wells were used for injection while an alternative means of treated water disposal was evaluated. The IRT urges DOE-EM-LA to consider the IRT’s concerns related to the computer modeling of the plume going forward. The IRT also urges NMED to be flexible in approving alternate well locations and flow rates that optimize capture without losing containment. The IRT suggests using at least two injection wells and two extraction wells, but also points out that significant modifications and expansion of the existing IM may be needed, especially on the east side of the plume. The IRT fully supports the drilling of the proposed new site characterization ‘data gap’ monitoring wells while the partial IM is restarted and evaluating options for returning cleaned treated water to the environment to support future groundwater cleanup.

The fourth topic pertains to regulatory matters. In addressing the questions within this topic, the IRT finds that the cleanup process generally follows standard practice. However, data gaps and uncertainties need to be addressed before committing to an alternative or final remedy. These data gaps include (1) improved understanding and representation of the horizontal and vertical extents of chromium contamination and, for any final remedy in particular, (2) improved characterization of the vadose zone sources. The IRT believes that an adaptive management strategy is well suited to guide remediation throughout the project.

The fifth topic is monitoring well design. This issue arose because OSE indicated that it would not approve any permit to drill a monitoring well that was constructed in the same manner as most of the existing IM monitor wells—that is, with dual well screens and bentonite clay seals in the well casing annulus. The IRT finds that the regional aquifer monitoring wells in the IM area function as intended, with no convincing evidence of cross-contamination within the regional aquifer due to drilling or comingling of water between well screens where bentonite has been used in well construction. The IRT recommends that new monitoring wells be constructed so that the casing annulus in the vadose zone is sealed with cement. Coated bentonite granules are recommended to seal the annulus in the regional aquifer. The use of dual-screen monitoring wells, constructed with appropriate supplemental documentation, procedures, and controls, to ensure that any risks of leakage or cross-contamination are mitigated and minimized, would also be beneficial to future plume characterization. The IRT recommends improved communication and coordination between DOE-EM-LA, NMED, and OSE in planning for and constructing additional monitoring wells.

# Contents

1.	Introduction .....	1
1.1	Review Panel Charge Questions .....	1
1.2	Summary of Findings and Recommendations .....	1
1.3	Committee Participants .....	3
1.4	Acknowledgements .....	9
1.5	Report Structure .....	10
2.	Site Overview .....	10
2.1	Background .....	10
2.1.1	Chromium Plume Discovery and Origin .....	10
2.1.2	Nature and Extent of the Chromium Contamination.....	10
2.1.3	Chromium Plume Control Interim Measure .....	11
2.1.4	State of New Mexico Regulatory Oversight and Concerns with the Interim Measure .....	11
2.1.5	Independent Technical Review 2024 .....	12
2.2	Conceptual Site Model of the LNAL Chromium Plume Site in Mortandad Canyon, New Mexico .....	13
2.2.1	The Chromium Remediation Area .....	13
2.2.2	Geology .....	14
2.2.3	Chromium Distribution .....	14
2.2.4	Groundwater Hydrology .....	16
2.2.5	Geomicrobiology .....	22
2.2.6	Transport of Chromium .....	22
3.	Committee Responses to Charge Questions.....	27
3.1	Topic 1: Chromium Plume Control Interim Measure Hydraulic Control.....	28
3.1.1	Do groundwater data and modeling results demonstrate that operation of the IM, as originally approved and in full operation, hydraulically control the plume?.....	29
3.1.2	Is there assurance that existing injection locations appear to be outside the current 50 µg/L, or ppb, plume boundary? .....	35
3.1.3	To what extent are the increasing chromium concentration trends in R-45 S2 and R-61 S1 the result of an adverse impact of current injection locations? .....	35
3.1.4	Will the current IM be protective of the environment until a remedial alternative is selected and implemented? .....	37
3.1.5	What are the recommendations for maintaining hydraulic control? .....	39
3.2	Topic 2: Chromium Plume Modeling .....	40
3.2.1	Overview of Modeling History and Needs .....	41
3.2.2	Question 1: Is the software currently used to model the chromium plume at LANL (Finite Element Heat and Mass [FEHM]) appropriate? .....	43
3.2.3	Question 2: Are modeling assumptions, inputs, and results reasonable and defensible? .....	45
3.2.4	Question 3: Are there technical issues or data gaps that significantly impair the project's or the regulator's ability to use the model results when making operational or regulatory decisions? .....	50
3.2.5	Question 4: To what extent can the modeling be relied upon (e.g., predictions) without the data gaps being fully closed? .....	52

3.2.6	Question 5: What limitations should be considered when using the model before the known data gaps are filled? .....	53
3.2.7	Question 6: What aspects of the existing model are sufficiently mature to predict future plume behavior, and what recommendation(s) does the team have to improve the model's ability to predict future plume behavior (e.g., aquifer test versus slug test)? .....	54
3.2.8	Summary .....	54
3.2.9	Recommended Actions .....	56
3.3	Topic 3: NMED Ground Water Quality Bureau Acceptable Corrective Actions and Conditions in September 6, 2023 Letter Appendix A Proposal .....	58
3.3.1	Overview of Interim Measure Operation and Dispute .....	58
3.3.2	Are the proposed Appendix A conditions appropriate as part of the IM or more suited for remedy selection? .....	61
3.3.3	Has a technical basis been established that demonstrates the existing extraction wells alone would control plume migration if the IM were modified for use of an alternative injection location that did not provide hydraulic control? .....	63
3.3.4	What are the team's recommendations for considering alternative injection locations? .....	64
3.3.5	Summary of Recommended Actions .....	66
3.4	Topic 4: Regulatory Matters .....	68
3.4.1	Is the current chromium plume characterization consistent with industry practices and EPA guidance for the maturity and understanding necessary to propose and begin evaluating potential remedial alternatives (i.e., conducting a corrective measures evaluation and preparing a corrective measures evaluation report)? .....	68
3.4.2	Has the project defined the needed data and uncertainties for designing a remedy (e.g., corrective measures implementation plan [CMIP])? .....	69
3.4.3	Which data gaps need to be closed, if any, before completing the comparison of the potential remedial alternatives? .....	69
3.4.4	Is use of an adaptive management strategy as a component of a final remedy appropriate? If so, how is regulatory oversight preserved during the CMIP phase as design evolves due to emerging information? .....	70
3.4.5	How is regulatory oversight preserved during the CMIP phase as design evolves due to emerging information? .....	71
3.4.6	Under what circumstances is it more favorable to apply an adaptive management strategy to IM versus the remedy itself? .....	74
3.4.7	Recommended Actions .....	75
3.5	Topic 5: Well Design .....	75
3.5.1	Do the monitoring wells constructed with bentonite in the chromium plume region demonstrate a seal between the screened intervals in the dual-screened monitoring wells that is adequate to ensure the prevention of comingling or interaquifer exchanges between the separate hydrogeologic units in the plume area? .....	76
3.5.2	Are there alternatives to bentonite that can be used to seal chromium monitoring wells at the LANL site that will not negatively impact or alter groundwater chemistry (e.g. cement in lieu of bentonite)? .....	78
3.5.3	Recommended Actions .....	79
4.	References .....	79

## Figures

- Figure 2-1. Photographic depiction of the position of the chromium plume in relation to the Power Plant source area, and the two canyons (Sandia and Mortandad) affected by the releases.
- Figure 2-2. Estimated extents of chromium plume showing monitoring wells, extraction wells (CrEX-1 through CrEx-5), and injection wells (CrIN-1 through CrIN-5).
- Figure 2-3. Locations of Sandia and Mortandad Canyons in relation to other nearby canyons.
- Figure 2-4. Aerial image of the region around Mortandad Canyon, and a section of the topographic changes from Los Alamos to the Rio Grande River.
- Figure 2-5. A simplified cross section of the regional geology.
- Figure 2-6. Map of study site and surrounding area. Locations of selected monitoring wells (R-x), extraction wells (CrEX-x), injection wells (CrIN-x) and water supply wells (PM-x) are shown.
- Figure 2-7. (A) Locations of selected monitors with chromium concentrations above background ( $> \sim 10$  ppb), above the New Mexico standard for chromium ( $> 50$  ppb). (B) Locations of 'windows' that explain observed chromium concentration distributions in Neptune modeling.
- Figure 2-8. (A) Manual contouring of plan-view chromium concentrations in the plume area in 2015-2016, before the initiation of the IM. (B) Computer generated contours of the data in (A) based on inverse distance weighting interpolation with a power of 4 and an x-axis weighting to permit contours to reflect the flow direction. (C) Manual contours of chromium concentrations for maximum concentrations at selected locations in 2023. (D) Computer generated contours of the data in (C) based on inverse distance weighting interpolation as described in (B).
- Figure 2-9. Change in plan-view chromium concentrations between 2015 (pre-IM) and 2023 (post-IM), based on the data in Figure 2-8.
- Figure 2-10. The extent of chromium contamination along the southern border of the site is uncertain.
- Figure 2-11. Example of water table decline trend since the year 2000.
- Figure 2-12. Comparison of plan-view water levels in the shallow aquifer in Mortandad Canyon between 1984 and 2023.
- Figure 2-13. Pumping history at the CrEX wells in the plume area.
- Figure 2-14. (A) Regional potentiometric surface through Mortandad Canyon and surroundings indicating eastward horizontal flow. (B) Effect of PM well and IM well pumping on vertical hydraulic gradients at R-45. (C) Density plots of hydraulic gradients are several wells in the plume area with influences similar to those at R-45 caused by PM-4 and IM well pumping.
- Figure 2-15. (A) Profile of estimated horizontal hydraulic conductivity values from grain size analysis through the Puye Formation and below. (B) Range of reported horizontal hydraulic conductivity values for the study area
- Figure 2-16. Borehole log of PM-3, showing reduced porosity and conductivity in the mineralogically distinct zones associated with the basalt.
- Figure 2-17. Map showing locations of wells and monitoring wells used in the estimation of effective porosity at the chromium plume site



- Figure 2-18. Background water chemistry in the regional aquifer beneath the Pajarito Plateau.
- Figure 2-19. (A) Major ion chemistry in the vicinity of the chromium plume in Mortandad Canyon (R 42) compared to vadose zone water in Sandia Canyon (LADP and LAOI). (B) Stiff diagrams showing similarities in the geochemistry of the vadose zone waters in Sandia Canyon and those in the plume area in Mortandad Canyon.
- Figure 2-20. CSM summary figures presented by (A) Katzman et al. (2018), (B) DOE-EM-LA (2023), and (C) Broxton (2024a).
- Figure 2-21. Speciation of dilute chromium in natural waters for the system Cr-O-H (1).
- Figure 2-22. (A) Subsurface formations underlying Mortandad Canyon, at borehole CrCH-3. (B) Classification of sediments from selected formation. (C) Units and abbreviations commonly used.
- Figure 3-1. Time-series concentrations of chromium (green), nitrate (brown), and sulfate (red) at perimeter monitoring wells in the plume area.
- Figure 3-2. Relative screen elevations and their interpreted geologic settings along two transects shown in the upper right inset.
- Figure 3-3. Plan-view hydraulic head contours for time (A) before IM pumping and injection and (B) after pumping.
- Figure 3-4. Approximate range of capture zone in plan view inferred from the time-series chromium data in Figure 3-1, up to early 2024.
- Figure 3-5. Comparison of plan-view chromium distributions in the regional aquifer while IM pumping and injection were inactive (A, B, May 2020) and while they were active (C, D, spring 2022) and immediately following the inactivation of the IM system in spring 2023 (Figures (E), (F)).
- Figure 3-6. Three-point problem flow direction vectors while the IM is off.
- Figure 3-7. Comparison of effective capture zones, in plan view
- Figure 3-8. (A) Transmissivity field, in plan view, used in all simulations (units are  $\text{ft}^2/\text{s}$ ). (B) Particle tracks, in plan view, and head contours for the base case in which no IM well were active.
- Figure 3-9. Approximate limits to capture (A), in plan view, with the IM in full operation and (B) with only the CrEX-4/CrEX-5 and CrIN-4/CrIN-5 wells operating.
- Figure 3-10. Plan-view locations of the injection wells in relation to the 50  $\mu\text{g}/\text{L}$  chromium contours as of spring 2023.
- Figure 3-11. Section through the plume area showing the vertical relationships between the injection wells, R-45 S2 and the R-70 S1 and S2 locations.
- Figure 3-12. Hydraulic head responses at R-61 S1 (shallow screen).
- Figure 3-13. Chromium concentration history at R-45 S2.
- Figure 3-14. Hydraulic head responses at R-45 S1 (shallow screen) and R-45 S2 (deep screen).
- Figure 3-15. Transects considered for visualization of vertical head distributions in the regional aquifer.
- Figure 3-16. Hydraulic head distributions along the north and south transects.
- Figure 3-17. Hypothetical capture of a groundwater plume by a groundwater extraction well.

- Figure 3-18. Approximate location and depths of chromium plume and water supply well PM-3 showing how PM-3 draws water from over a ~1,600-foot interval.
- Figure 3-19A. Schematic hydrogeologic conceptual site model (CSM) for site modeling purposes: Full section.
- Figure 3-19B. Schematic hydrogeologic conceptual site model (CSM) for site modeling purposes: Saturated section.
- Figure 3-20. Approximate illustration of the extents of dissolved chromium.
- Figure 3-21a. Example maps of aquifer parameters corresponding to elevation of 5,830 feet msl.
- Figure 3-21b. Example maps of aquifer parameters corresponding to elevation of 5,800 feet msl.
- Figure 3-21c. Example maps of aquifer parameters corresponding to elevation of 5,700 feet msl.
- Figure 3-22. Example property distributions for aquifer parameters and their ratios: (a) horizontal conductivity, (b) ratio of horizontal conductivities ( $p_{nx}/p_{ny}$ ) and (c) ratio of horizontal to vertical conductivities ( $PNX/PNZ$ ).
- Figure 3-23. Regional modeling reported by Frenzel (1995).
- Figure 3-24. Interim measure injection and extraction wells generally in operation 2020 to October 2022.
- Figure 3-25. Interim measure injection and extraction wells generally in operation 2020 to October 2022 showing chromium concentration trends during this period at R-61 S1 and R-45 S2.
- Figure 3-26. Interim measure injection and extraction wells generally in operation November 2022 to March 2023 (4s/5s Scenario). C
- Figure 3-27. NMED's proposed interim measure restart configuration (Letter #3).
- Figure 3-28. DOE-EM-LA's proposed interim measure restart configuration (Letter #4).
- Figure 3-29. Conceptual depiction of an alternative cleaned water return system using either a newly drilled deep well or repurposing existing water supply well PM-3.

## Tables

- |     |  |
|-----|--|
| 2-1 | Paraphrased Topics of Questions Posed to the Panel                             |
| 2-2 | Sources of the Water Table Maps in Figure 2-11                                 |
| 3-1 | Extraction Rate Statistics for the IM between June 28, 2016 and March 31, 2023 |
| 3-2 | Comparison of Modeling Platforms   |
| 3-3 | Key Characteristics of Potential Annular Sealants for LANL Wells               |

## Appendices

- A Summary of Simplified Modeling Calculations (*Demirkanli/Looney/Tonkin/Newell/Stephens*)
- B Batu (2024j) - Horizontal ( $K_h$ ) and Vertical Hydraulic Conductivity ( $K_v$ ) Values Determined from the Aquifer Tests of the CrIN, CrEX, PM-2, PM-4, PM-3 (with R-35a and R-35b), and R-13 Wells at the LANL Site
- C Batu (2024b) - Comparison of the Horizontal Hydraulic Conductivity ( $K_h$ ) Values at the CrEX and CrIN Well Locations, and PM-2 and PM-4 Aquifer Tests Well Locations with the  $K_h$  Values of Neptune, Los Alamos, New Mexico
- D Batu (2024c) - Comparison of the Horizontal Hydraulic Conductivity ( $K_h$ ) Values of the CrEX and CrIN Wells, the  $K_h$  Values Neptune, and the Average  $K_{h-x}$  and  $K_{h-y}$  Values in the CrEX and CrIN Areas of Compendium Technical Reports (Attachment 9, Figure 2.2-3), Los Alamos, New Mexico
- E Batu (2024a) - Hydraulic Conductivity Data Evaluation of the Neptune's Model for the LANL Site, Los Alamos, New Mexico.
- F Batu (2024g) - Evaluation of the Measured  $Cr^{6+}$  Concentrations and Flow Rates of PM-2, PM-3, PM-4, and PM-5 Water Supply Wells Between 2006 and 2024 Along with Their Well Diagrams, Los Alamos, New Mexico
- G Batu (2024f) - Evaluation of the Measured Temporal Chromium ( $Cr^{6+}$ ) Concentrations in the Unconfined Aquifer with Respect to the Transport in the Vadose Zone, Los Alamos, New Mexico
- H Batu (2024i) - Evaluation of the Flow Parameters and Chromium ( $Cr^{6+}$ ) Concentration Data to Estimate the Plume Extensions in the Longitudinal and Transverse Vertical Directions, Los Alamos, New Mexico
- I Batu (2024h) - Determination of the Zone of Influence of the PM-4 Water Supply Well and Evaluation of the Effects of All Water Supply Wells to the Chromium ( $Cr^{6+}$ ) Plume Area, Los Alamos, New Mexico
- J Batu (2024e) - Plots of Chromium ( $Cr^{6+}$ ) Concentrations vs. Date Between 2004 and 2024 and Their Interpretations, Los Alamos, New Mexico
- K Vertical Gradients and Their Impact on Cr Concentrations (*Wainwright, Newell, Stephens*)
- L Devlin (2024) - Derivation of Equation 1
- M Mass Flux Evaluation (*Newell*)
- N Batu (2024d) - The Conceptual Model for the Water-Bearing Formations Beneath the LANL Site and Determination Methods of the Breakthrough Curves at the Bottom of the Vadose Zone and Degradation Rates of Chromium ( $Cr^{6+}$ ), Los Alamos, New Mexico

- O      Compilation of Materials Regarding Well Construction and NMOSE Concerns and Correspondence (*Stephens/Looney/other*)
- P      Evaluation of Borehole Leakage (*Tonkin*)

## Acronyms

1D	one-dimensional
2D	two-dimensional
3D	three-dimensional
µg/g	micrograms per gram
µg/L	micrograms per liter
AEM	analytic element method
ANPRM	Advance Notice of Proposed Rulemaking
ASM	adaptive site management
bgs	below ground surface
CAP	corrective action plan
CERCLA	Comprehensive Environmental Response, Compensation, and Liability Act
CMIP	corrective measures implementation plan
Cr(VI)	hexavalent chromium
CSM	conceptual site model
DO	dissolved oxygen
DOE	Department of Energy
EM-LA	Environmental Management Los Alamos Field Office
EPA	U.S. Environmental Protection Agency
EWM	embedded wellbore model
F&T	fate and transport
FEHM	Finite Element Heat and Mass
ft/d	feet per day
ft/yr	feet per year
gpm	gallons per minute
GWF	groundwater flow
GWQB	Ground Water Quality Bureau [NMED]
HWB	Hazardous Waste Bureau [NMED]
HSU	hydrostratigraphic unit
IDW	inverse distance weighting
IMWP	Interim Measures and Characterization Work Plan
IM	[chromium plume control] interim measure
IRT	independent review team
ITRC	Interstate Technology and Regulatory Council
K <sub>h</sub>	horizontal hydraulic conductivity
K <sub>v</sub>	vertical hydraulic conductivity

LANL	Los Alamos National Laboratory
m/d	meters per day
mg/L	milligrams per liter
msl	above mean sea level
NMED	New Mexico Environment Department
NMR	nuclear magnetic resonance
NOD	notice of disapproval
OLEM	[EPA] Office of Land and Emergency Management
OSE	[New Mexico] Office of the State Engineer
P&T	pump and treat
PNNL	Pacific Northwest National Laboratory
ppb	parts per billion
ppm	parts per million
RCRA	Resource Conservation and Recovery Act
RDX	royal demolition explosive
SOP	standard operating procedure
STOMP	Subsurface Transport over Multiple Phases
TDS	total dissolved solids
USGS	U.S. Geological Survey

# 1. Introduction

In December 2023, the U.S. Department of Energy (DOE) Office of Environmental Management Los Alamos Field Office (DOE-EM-LA), together with the State of New Mexico Environment Department (NMED), prepared a letter requesting that an independent technical review be conducted of actions taken by EM-LA to characterize, model, and contain the hexavalent chromium [Cr(VI)] plume at Los Alamos National Laboratory (LANL) (the LANL Chromium Plume Site [the site]) and the efficacy of chromium plume control interim measures (IM) taken to prevent plume migration offsite (LANL, 2015). The expressed purpose of the review is to assess IM control of the plume, plume modeling, additional proposed corrective actions cited in an NMED letter to DOE-EM-LA dated September 6, 2023, project readiness to propose a remedy, and monitoring well design within the chromium plume. Assembly of the independent review team (IRT), led by Dr. Ines Triay, took place through the winter and the IRT first convened for a series of meetings starting in early March 2024. An on-site kickoff meeting was held in the third week of March 2024, during which the IRT members were provided a number of presentations and escorted on a tour of the area encompassing the chromium investigation area, including visiting monitoring, extraction, and injection wells, as well as the treatment components of the IM. This report, prepared throughout summer 2024, presents collaborative and overwhelmingly consensus responses to the five specific questions with which the assembled IRT was charged.

## 1.1 Review Panel Charge Questions

The IRT was tasked with responding to questions that lie within the following five overarching topic areas (the detailed questions are reiterated in Section 3):

- Chromium plume control IM hydraulic control
- Chromium plume modeling
- NMED Ground Water Quality Bureau (GWQB) acceptable corrective actions and conditions in September 6, 2023 letter (enclosure) Appendix A Proposal
- Regulatory matters
- Well design

## 1.2 Summary of Findings and Recommendations

It is a consensus finding of the IRT that the IM, at a limited and/or altered capacity, should be restarted as soon as possible. There is clear benefit to the near- and long-term cleanup objectives of containing and recovering chromium located upgradient of the extraction wells rather than allowing it to continue migrating without intercession. The IRT recognizes that aspects of the historical configuration and operation of the IM extraction and injection wells likely resulted in incomplete hydraulic containment of the chromium plume. Consequently, to continue contaminant mass recovery and maintain some degree of hydraulic containment of at least the (apparent) core of the plume, the IM needs to be operated in a revised configuration while further analyses improve the remedy. The IRT believes that, in a collaborative effort between

DOE-EM-LA, NMED, and other parties, a suitable near-term operating configuration can be determined through data-driven analyses supported by groundwater modeling of the chromium plume and capture zone analysis. This report also presents the results of empirical data analyses and model-based calculations that the IRT completed to demonstrate that the IM can be confidently restarted in one of several alternative configurations to achieve these limited near-term containment and recovery goals.

In support of, and in addition to, this primary recommendation, the IRT also reached the following responses to the five charge questions:

- Greater effort is needed to obtain consensus on the characterization, modeling, and remediation of the chromium contamination. This process may benefit from the establishment of small focused technical, regulatory, or managerial working groups to tackle challenging issues, such as those assigned to the IRT, so that the issues do not result in further delays.
- To transition from a limited start-up of the IM to expanded operations, alternative configurations should be considered that may include alternative treated water disposal options. However, because the identification, evaluation, and implementation of any alternatives would be time-consuming, seeking such alternatives at this time should not further delay a limited restart of the IM in the near-term.
- Certain aspects of the conceptual site model (CSM) should be reevaluated to ascertain the degree to which any uncertainty associated with them impacts site characterization approaches, fate and transport understanding, and remedial decisions. In particular, the following should be reassessed before undertaking further three-dimensional (3D) groundwater modeling:
  - ◇ Role of stratigraphy and property contrasts between major hydrostratigraphic units (HSUs) on model design, lateral and vertical hydraulic containment, and contaminant fate and transport.
  - ◇ Evaluation of the site-wide measured and estimated horizontal hydraulic conductivity ( $K_h$ ) and vertical hydraulic conductivity ( $K_v$ ) values. This evaluation will require understanding to a depth substantially greater than the depth of the plume, including the depths of the PM-series wells.
  - ◇ Causes of relatively small (flat) horizontal hydraulic gradient and significance of the notable downward vertical gradients in the IM area.
  - ◇ Role of the nearby water supply wells in vertical gradients and lateral and vertical plume migration and spread.
  - ◇ Further investigation of potential vadose zone sources of Cr(VI) contributing to the groundwater plume and their impacts through alternative conceptualization of location of fluxes and their time-dependent contributions. To date this has included vadose zone modeling to estimate breakthrough curves at the base of the vadose zone. Further modeling of this type will be necessary for long-term decision making at the site.



- Transition to a groundwater flow and transport simulator (e.g., MODFLOW-6) that has a wider user community with well-established application areas, similar to this site and its remedy design/implementation needs, is recommended, along with establishing a small collaborative modeling working group including members from EM-LA, NMED, and other stakeholders and technical experts. This recommendation is expected to facilitate refocusing of the modeling efforts to specific site needs.
- Chromium investigation and remediation efforts would benefit from more rapid and cost-effective drilling and well installation procedures to maximize the data that can be obtained with available time and funding. To facilitate this, the IRT recommends the following:
  - ◊ Using coated bentonite granules below the water table (ending just above the capillary fringe), and then using cement throughout the entire vadose zone. Uncoated bentonite granules would be an appropriate alternative to cement for the vadose zone due to their ability to swell in the presence of perched water.
  - ◊ It would be enormously beneficial if the New Mexico Office of the State Engineer (OSE) would permit dual-screen monitoring wells to be constructed with appropriate supplemental documentation, procedures, and controls, to ensure that risks of leakage or cross-contamination are mitigated and minimized.
- Implement an adaptive site management (ASM) strategy to take the site forward. Although the ASM term is not in wide use under the Resource Conservation and Recovery Act (RCRA), the RCRA program incorporated ASM elements and implementation of a RCRA-compatible process (perhaps based in part on the RCRA First process) that would streamline some decision making, including timely implementation of the recommendations presented in this IRT report. Many of the recommendations developed by the IRT would benefit from close collaboration between DOE-EM-LA, NMED, and other stakeholders.

Technical discussions supporting these recommendations and discussion of additional opportunities for improvement are included in the specific subsections addressing the five charge questions.

### 1.3 Committee Participants

The assembly and management of the IRT were directed by **Dr. Ines Triay**, the Interim Dean of the College of Engineering of Computing and the Executive Director for the Applied Research Center (ARC) at Florida International University (FIU). Dr. Triay has been at FIU for 12 years as ARC's Director, and most recently served as the Associate Dean for Research Innovation and Technology, where she has worked closely with the Knight Foundation to maximize the impact of resources on the growth of computing and information science at FIU. Dr. Triay is a foremost expert on environmental management and has worked tirelessly in this area as a researcher, a visionary leader, and a manager at LANL, DOE, and FIU. At DOE, she managed the largest, most complex nuclear environmental cleanup program in the world as Assistant Secretary for Environmental Management, a Presidential appointment, confirmed by the U.S. Senate, with a budget of \$6 billion per annum, and a workforce of 34,000 at 114 sites across the U.S. Dr. Triay has been widely recognized for her many accomplishments in science and engineering

including the Los Alamos Distinguished Performance Award, Presidential Rank Award, the DOE Secretary Exceptional Service Award, the National Award for Nuclear Science, and the Dixie Lee Ray Award from the American Society of Mechanical Engineers.

The following persons were retained to serve as active members of the IRT:

**Vedat Batu, PhD, P.E.** is a Surface and Subsurface Hydrologist and Argonne Associate at the Argonne National Laboratory. He has more than 30 years of environmental and civil engineering consulting experience. He also has more than 15 years of academic experience in the areas of fluid mechanics, hydraulic engineering, groundwater hydrology, and applied mathematics at several universities. Dr. Batu received his PhD in Hydraulic Engineering from the Civil Engineering Faculty of Istanbul Technical University in 1974. He prepared his associate professorship thesis at the University of Wisconsin-Madison in 1976-1977 by working mainly with soil physicists. He also served as the head of the Civil Engineering Department at Karadeniz (Blacksea) Technical University. His consulting experience includes aquifer testing, groundwater resources usage and protection, groundwater contamination assessment and remediation, and stormwater management, design of hydraulic structures, and surface water quality evaluation. He is the author of more than a dozen one-dimensional (1D), two-dimensional (2D), and 3D analytical solute transport models and computer programs. He is familiar with many groundwater flow and contaminant transport computer programs, as well as computer programs in surface hydraulics and hydrology areas. Dr. Batu is the author of a number of papers published in some internationally recognized journals such as *Groundwater*, *Journal of Hydrology*, *Water Resources Research*, *Soil Science Society of America Journal*, and several of the American Society of Civil Engineers (ASCE) journals. He is the author of the following books: (1) Batu, V., 1998, *Aquifer Hydraulics: A Comprehensive Guide to Hydrogeologic Data Analysis*, John Wiley & Sons New York, (2) Batu, V., 2006, *Applied Flow and Solute Transport Modeling in Aquifers: Fundamental Principles and Analytical and Numerical Models*, CRC Press, Boca Raton, Florida, and (3) Batu, V., 2024, *Fluid Mechanics and Hydraulics: Illustrative Worked Examples of Surface and Subsurface Flows*, CRC Press., Boca Raton, Florida. These books are being used as textbooks at various universities, as well by practitioners around the world.

**Fred Day-Lewis, PhD** is a Laboratory Fellow and Chief Geophysicist at Pacific Northwest National Laboratory (PNNL). He holds a joint faculty appointment at Colorado School of Mines. Prior to starting at PNNL, Dr. Day-Lewis worked for the U.S. Geological Survey (USGS) for 18 years as a Research Hydrologist. He has worked on a variety of applied-research projects related to subsurface characterization and monitoring, groundwater remediation, groundwater/surface-water exchange, geophysical inverse problems, thermal methods, and hydrologic parameter estimation. Dr. Day-Lewis currently serves as an associate editor for the journal *Groundwater*. He previously served as an associate editor for *Water Resources Research*, *Geosphere*, and *Hydrogeology Journal*. Dr. Day-Lewis is a past president of the American Geophysical Union Near Surface Geophysics Section. He was elected Fellow of the Geological Society of America (GSA) in 2015 for pioneering contributions to hydrogeophysics. He is a 2023 recipient of the Harold Mooney Award from the Society of Exploration Geophysicists for contributions to the near surface geophysics community and is the 2024

recipient of the Public Service Award from GSA. He received a PhD in Hydrogeology from Stanford University and B.A. and B.S. from the University of New Hampshire.

**Inci Demirkanli, PhD** is a senior hydrogeologist and technical advisor at PNNL with experience in analytical and numerical modeling of subsurface flow and transport with application in remediation research and radionuclide mobility in vadose zone, and subsurface energy and storage systems, such as geologic sequestration of carbon dioxide (CO<sub>2</sub>), enhanced oil recovery, and hydraulic fracturing. In her current capacity, Dr. Demirkanli provides technical support to DOE's Richland Office on integrated cleanup efforts, as well as programmatic and regulatory strategy development at the Hanford Site. She has managed and participated in large projects providing technical and programmatic support to DOE's Hanford Site for performance-based pump-and-treat (P&T) remedy optimization approaches, characterization and monitoring of contaminants in groundwater and vadose zone, in situ source remedy development, treatability studies, and implementation, as well as implementation of adaptive approaches for cleanup.

**J.F. Devlin, PhD** is a professor at the University of Kansas. He received his PhD in Earth Sciences from the University of Waterloo. Dr. Devlin is the Co-Director of the University Consortium for Field-Focused Research at the University of Guelph and is the Editor-in-Chief of GWMR. He was the Farvolden Lecturer in 2022. He serves on the Board of Trustees for the Tumbling Creek Cave Foundation. He has authored or co-authored three books: *Groundwater Velocity*, *Practical Groundwater Tracing with Fluorescent Dyes*, and *Sequenced Reactive Barriers for Groundwater Remediation*, and has held two patents: "Procedure for delivering a substance into an aquifer" (Pat. No. 5,456,550) and Groundwater velocity probe (Pat. no. 6,393,925 B1). His research currently focusses on aquifer characterization, in situ treatment of groundwater contaminated with nutrients from agricultural fields, instrument development, and the use of direct groundwater velocity measurements in groundwater studies, groundwater-surface water interaction studies, and to aid in modeling.

**Scott Ellinger, M.S. P.G.** is the Regional Groundwater Center Coordinator for the U.S. Environmental Protection Agency (EPA) Region 6 office in Dallas, Texas. He has 34 years of experience as a geologist at EPA and nine years as an adjunct geology professor and lecturer. His main areas of expertise include geological and hydrogeological site investigations, groundwater contaminant fate and transport modeling, designing groundwater recovery systems, hydrogeologic concerns from mining and mineral processing, hazardous and non-hazardous RCRA facilities, and underground injection control. Mr. Ellinger has extensive experience working on groundwater problems in New Mexico, Texas, Oklahoma, Arkansas, and Louisiana. Mr. Ellinger received his B.S. in geology from Texas Tech University and his M.S. from West Texas State University.

**J. Alexandra Hakala, PhD** is a Senior Physical Research Scientist and Senior Fellow at the Geological & Environmental Systems Research & Innovation Center (RIC) of the DOE's National Energy Technology Laboratory (NETL). Dr. Hakala is a geochemist and leader of multidisciplinary geoscience and engineering research teams executing research and development (R&D) focused on ensuring prudent development of natural resources for energy

extraction, water management, and climate change mitigation. She has 15 years of experience in applied geoscience and engineering research at NETL (2008-present), earned her PhD in Earth Sciences (Geochemistry focus) from Ohio State University (2008), where she was an EPA Science to Achieve Results Graduate Fellow, and earned her B.A. *Cum Laude* in Geosciences with a Certificate (minor) in Environmental Studies from Princeton University (2003). She actively engages in strategic planning and initiative development across the NETL and Fossil Energy Carbon Management Headquarters, and with external industrial, academic, and federal laboratory stakeholders on multidisciplinary and multi-organizational geologic and environmental R&D. Dr. Hakala is NETL's representative on the Network of National Laboratories for Environmental Management and Stewardship (through DOE-Environmental Management and DOE-Legacy Management) and is active in geothermal R&D through DOE-Energy Efficiency and Renewable Energy's Geothermal Technologies Office. She is the author of 60+ technical publications focused on multiple energy geoscience topics, including geologic CO<sub>2</sub> storage, unconventional oil and gas development, geothermal resources, produced water management, and environmental geochemistry, and has mentored 30+ students, including postdoctoral students. Dr. Hakala is a recipient of the Presidential Early Career Award for Scientists and Engineers (2017) and is an Oppenheimer Science and Energy Leadership Program Fellow (2023).

**Brian B. Looney, PhD** is a senior fellow environmental engineer at the DOE Savannah River National Laboratory (SRNL). Dr. Looney received his PhD in Environmental Engineering from the University of Minnesota in 1984. He is an environmental engineer at SRNL and an adjunct professor in the Environmental Engineering and Earth Science Department at Clemson University. Over the past 40 years, he has developed and deployed a wide range of environmental characterization and cleanup technologies for organic contaminants, metals, and radionuclides. His work focuses on matching characterization and cleanup technologies to the specific conditions and needs at each site and developing technical approaches for that matching process. He has focused on developing natural and enhanced attenuation remedies and developing strategies for remediating complex sites using combined or sequenced remedies and phased objectives. Specific past work has included development of environmental horizontal drilling, improved remediation methods (e.g., enhanced attenuation, sparging, bioremediation, and thermal methods), and improved characterization (e.g., tracer testing, soil gas methods and geophysics). Dr. Looney has 12 patents for environmental remediation or characterization methods. He received the 2006 National Groundwater Association Technology Award, 2005 American Chemical Society Industrial Innovation Award, 1996 and 2000 Federal Laboratory Award of Excellence in Technology Transfer, 2004 Worlds Best Technology Award, and 2000 Energy 100 Award.

**Charles J. Newell, PhD, P.E., BCEE** is Vice President of GSI Environmental Inc. (formerly Groundwater Services, Inc.). He is a member of the American Academy of Environmental Engineers, a National Groundwater Association (NGWA) Certified Ground Water Professional, and an Adjunct Professor at Rice University. He has co-authored five EPA publications, 12 environmental decision support software systems, numerous technical articles, and two books. With over 35 years of experience, his professional expertise includes groundwater flow modeling, groundwater contaminant transport modeling, natural attenuation, light nonaqueous-

phase liquid (LNAPL)/dense nonaqueous-phase liquid (DNAPL) issues, bioremediation, software/model development, optimizing long-term monitoring programs, per- and polyfluoroalkyl substances (PFAS) fate and transport, and PFAS remediation. He has also served as a technical facilitator for groups trying to reach consensus regarding complex environmental issues. He has taught graduate level groundwater courses at both the University of Houston and Rice University. Dr. Newell has been selected to serve on several expert panels to review site cleanups both nationally and internationally. He has served as a Principal or Co-Principal Investigator for numerous Department of Defense SERDP/ESTCP projects since 2003 and has extensive experience working with research teams comprised of mixed academic, industrial, and consulting members.

**Sorab Panday, PhD** is a Principal Engineer at GSI Environmental with 35 years of experience in directing, managing, developing, troubleshooting, and reviewing flow and transport models for subsurface contamination/remediation evaluations, groundwater/surface water interactions, and water resource management. He has worked on hydrologic and hydrogeologic modeling projects spanning a wide range of schedules and budgets. These projects involve multiple spatial and temporal scales, complex geological settings, diverse stakeholder concerns, extreme climatic conditions, unique water/contaminant management issues, and challenging numerical conditions. Dr. Panday has provided leadership, mentorship, training, and guidance on projects for clients and staff, executed and managed modeling projects for various industries and government agencies, managed regulator and stakeholder modeling committees, provided expert witness services, participated in expert panels, conducted workshops and webinars on water resource and subsurface contaminant transport modeling, and maintained effective communication with regulators and clients. Dr. Panday is also a part-time Research Professor at the University of Nebraska, Lincoln. He publishes regularly in leading industry journals and provides review and editorial support to industry publications and conferences. He was elected to the National Academy of Engineering in 2017 for the development of computer code for solving complex groundwater problems.

**Mark J. Rigali, PhD** earned a PhD in Geology/Geochemistry at the University of Arizona in 1997. His dissertation research focused on the roles of organic matter in the Oklo natural nuclear reactors. In 1998 he joined Advanced Ceramics Research, managing a team of engineers and scientists focused on developing novel composites for machine tool applications. This effort led to 10 issued patents, an R&D 100 Award (2002) and license agreements with Kyocera Industrial Ceramics and Smith International. He was hired by Sandia National Laboratories in 2003 and has served in several roles including manager of the Repository Performance Department (2003-2007), manager of the Geochemistry Department (2007-2014) and Principal Member of Technical Staff (2014-present). As a technical staff member, his research is focused on (1) development of novel water treatment technologies for the selective removal of heavy metals and radionuclides from groundwater and surface water (three issued patents), (2) development of phosphate-based cements/grouts for radioactive waste disposal applications (one provisional patent filed), and (3) development of novel catalysts to facilitate the advanced oxidation and destruction of PFAS. He has served as a team lead for Remediation Technologies on the DOE Legacy Management National Laboratories Network since 2018. He is also an NNLEMS team member and has co-authored independent site reviews at Los

Alamos, Shiprock, and Tuba City. In addition, he is a team member and co-author of the NNLEMS Roadmap for Accelerated Clean-up of Tank Waste at the Hanford Site. Over his career he has authored more than 40 publications and reports and has received two R&D 100 awards and a DOE Federal Laboratories Consortium Award for Excellence in Technology Transfer.

**Daniel B. Stephens, PhD** is the founder of Daniel B. Stephens & Associates, Inc. (DBS&A) in Albuquerque, New Mexico. He is currently retired from DBS&A and has on-call status there. For the past three years he served as the acting director of the Hantush-Deju National Hydrologic Innovation Center at New Mexico Tech. Dr. Stephens received his bachelor's degree in geological science from Pennsylvania State University, his master's degree in hydrology from Stanford University, and his doctorate in hydrology from the University of Arizona. He was on the faculty of the hydrology program at New Mexico Tech for 10 years and served as a department chair. In 2019, he was elected to the National Academy of Engineering. Dr. Stephens has published over 40 articles in peer-reviewed professional journals and has given over 100 presentations and articles in symposium proceedings. In 1996, he published *Vadose Zone Hydrology*. Dr. Stephens also specializes in water supply development, application of numerical models, and aquifer monitoring and contamination problems. His research has focused on developing methods to characterize the hydrologic properties of soil, as well as field investigations of natural soil-water movement and recharge in semiarid climates. Dr. Stephens has served on numerous technical review panels at DOE facilities, including Yucca Mountain, Yucca Flat, LANL, Hanford, and Fernald. He is currently on a review panel for SRNL regarding a cumulative impact assessment on the Central Plateau at Hanford. He was a reviewer of the Lawrence Berkeley Laboratory Earth Science Division. Dr. Stephens served as chairman on a 60-scientist team to develop a strategy to research vadose zone hydrology at DOE facilities nationwide, producing the Vadose Zone Roadmap. He was also a chair of the DOE Office of Technology, Innovation and Development, Advance Simulation Capability for Environmental Management (ASCEM).

**Matthew Tonkin, PhD** is the current President of S.S. Papadopoulos & Associates, Inc. (SSP&A). He has nearly 30 years of experience as a consulting hydrogeologist and environmental modeler. He provides subject matter expertise and manages or advises on many projects, specializing in data synthesis and modeling to support groundwater, surface water, soil and soil vapor studies, and leads projects for public, private, and legal clients. This includes planning data acquisition, collaborating with other experts, developing and applying models, and presenting to stakeholders. He received his PhD on the topic of model calibration and uncertainty analysis, and he has provided professional instruction and published on these and related topics, including time-series and spatial data analysis. Dr. Tonkin was a leading subject matter expert (SME) on numerous Comprehensive Environmental Response, Compensation, and Liability Act (CERCLA) actions at the DOE Hanford Site and has served in teaching or advisory positions with the Interstate Technology and Regulatory Council (ITRC), Integrated Groundwater Modeling Center (IGWMC) at Princeton, EPA, and other organizations.

**Haruko Wainwright, PhD** joined the Department of Nuclear Science and Engineering of the Massachusetts Institute of Technology (MIT) as an assistant professor in January 2022. She

received her BEng in Engineering Physics from Kyoto University, Japan in 2003, M.S. in nuclear engineering in 2006, M.A. in statistics in 2010, and PhD in nuclear engineering in 2010 from University of California, Berkeley (UC-Berkeley). Before joining MIT, Dr. Wainwright was a Staff Scientist in the Earth and Environmental Sciences Area at Lawrence Berkeley National Laboratory and an adjunct professor in Nuclear Engineering at UC-Berkeley. Her research focuses on environmental modeling and monitoring technologies, with a particular emphasis on nuclear waste and nuclear-related contamination. Dr. Wainwright has been developing Bayesian methods for multi-type multiscale data integration and model-data integration. She leads and co-leads multiple interdisciplinary projects, including DOE's Advanced Long-Term Environmental Monitoring Systems (ALTEMIS) project.

**David Wilson, MS, P.E.** has been with Longenecker & Associates (L&A) for over three years as a Senior Strategist. Prior to joining L&A, Mr. Wilson had a 37-year career with the South Carolina Department of Health and Environmental Control (DHEC). This included 20 years of implementing and providing direction for the state's hazardous waste programs. During this time, he was integrally involved in regulation of the DOE Savannah River Site (SRS), beginning with establishment of waste regulation oversight and cleanup. He was the state's lead regulatory/technical representative in development of the SRS Federal Facility Agreement and led the way for establishment of partnering with Department of Defense sites and the SRS Core Team. Mr. Wilson also directed the state's water and wastewater programs for 10 years. Mr. Wilson finished his career with DHEC as the Acting Agency Director, which included leading a 3,200-employee state agency with a budget of over \$600 million. He received a B.S. in Civil Engineering and M.S. in Civil Engineering from the University of South Carolina.

## 1.4 Acknowledgements

The activities of the IRT were supported and facilitated by the following, among other persons:

- Ming Zhu, DOE-EM Senior Advisor for Laboratory Policy, Network of National Laboratories for Environmental Management and Stewardship
- Ms. Cheryl Rodriguez, DOE-EM-LA, primary DOE-EM-LA point of contact
- John Rhoderick, Rick Shean, Caitlin Martinez, and Jason Herman, primary NMED points-of-contact throughout this review
- Susan Wacaster, DOE-EM-LA, Federal Cleanup Director
- Tom McCrory, DOE-EM-LA, Geologist
- David Broxton, Mei Ding, Catherine Goetz, Jeff Langman, Patrick Longmire, and David Schafer at N3B
- Lauren Foster, Neptune, Inc.
- David Schafer, Schafer & Associates, Inc.

## 1.5 Report Structure

The remainder of this report is organized in the following manner. Section 2 presents a site overview followed by a more detailed description of the CSM for the area encompassing the chromium plume. Section 3 provides a series of subsections that detail the committee responses to the five charge questions, including findings, conclusions, and recommendations. Section 4 provides cited references. Extensive appendices are included that present additional material supporting discussion provided in the main report.

## 2. Site Overview

### 2.1 Background

In this section, we provide a summary of information presented to or obtained by the IRT that we considered relevant background for addressing the ‘charge questions’ put to the IRT.

#### 2.1.1 Chromium Plume Discovery and Origin

As detailed in a summary provided by Katzman et al. (2018), chromium contamination was discovered beneath the site in 2004 during sampling and analysis of groundwater from a newly constructed characterization well that was drilled as part of a multi-year site-wide hydrogeologic characterization project. Routine sampling started in May 2005 at R-28, during which time chromium concentrations ranged from 360 to 389 micrograms per liter ( $\mu\text{g/L}$ ). The discovery triggered a regulatory driven investigation to identify the source(s) of the chromium, present as Cr(VI). Archival research undertaken after the discovery of contamination identified the source as LANL’s Power Plant, where potassium dichromate was used as a corrosion inhibitor in cooling towers from 1956 to 1972 (**Figure 2-1**). The combination of interviews with former LANL employees who worked at the Power Plant and purchase records for potassium dichromate provided the basis for an estimate that approximately 72,000 kilograms of chromium was released into an existing effluent stream during routine “blowdown” conducted at the Power Plant.

#### 2.1.2 Nature and Extent of the Chromium Contamination

As a result of the regulatory driven investigation, DOE-EM-LA began a significant effort to identify the source of infiltration and the nature and extent of the chromium contamination in all media from the ground-surface source to the deep aquifer. From 2006 through 2015, the investigations focused on the initial source area at the Power Plant to the deepest groundwater zone at approximately 1,000 feet below ground surface (bgs). A total of 20 monitoring wells (many with two screens to provide samples at two separate depths within the aquifer) were drilled over about 7 years to characterize the plume and monitor its behavior. Prior to installation of these wells, there was little local-scale understanding of groundwater flow. The new wells provided detailed information on plume thickness, flow direction, and pressure gradients at depth within the aquifer.



### **2.1.3 Chromium Plume Control Interim Measure**

By 2013, Cr(VI) trends in key monitoring wells (R-50 and R-45) at the downgradient plume edge to the east and along LANL's southern boundary with the neighboring Pueblo de San Ildefonso began to show increasing Cr(VI) concentrations with time. Studies were conducted to evaluate potential technologies for complete remediation of the chromium plume. Concurrently, an IM strategy was developed to control migration along the downgradient edge of the plume to the east and south. Implemented in 2018 and 2019, the IM involved the completion and use of four (and later five) extraction wells, chromium removal by P&T, treatment by ion exchange, and reinjection of the treated water into five injection wells (**Figure 2-2**) (McCrorry, 2024).

The primary objective of the IM is to provide hydraulic plume control along the leading edge of the plume. The downgradient injection wells were intended to create a hydraulic barrier to constrain downgradient plume movement (primarily east and south). When operating, the extraction wells recovered contaminated groundwater for chromium removal followed by reinjection of treated water into the injection wells near the plume boundary to the south and east to sustain the hydraulic barrier. Operation of the IM focused on sustained southern area operations until March 2023. Extraction wells recovered groundwater near the heart of the plume, which was then treated at the surface for chromium removal. The treated water was reinjected in wells near the southern plume boundary. An additional well (CrIN-6) was designed as an injection well but was converted to an extraction well (CrEX-5) after first samples revealed higher than anticipated chromium concentrations (270 µg/L). Sustained eastern area operations ran from November 2019 through October 2022 except for the fifth extraction well, which came on-line in 2022 and operated through March 2023.

Over a 3-year period ending in November 2022, more than 400 million gallons of water was treated, with the concomitant removal of approximately 680 pounds of chromium. Most importantly, the southern margin of the main plume was pushed back to the north away from the border of Pueblo de San Ildefonso. Because, before the IM operations started, chromium concentrations above the New Mexico standard were found in all three southern CrIN wells at roughly 50 to 90 µg/L, documents and data we reviewed suggest that some of the chromium there may have been pushed to the south and southeast.

### **2.1.4 State of New Mexico Regulatory Oversight and Concerns with the Interim Measure**

Regulatory oversight is provided by the NMED Hazardous Waste Bureau (HWB), which regulates the IM operation and characterization activities. The NMED GWQB regulates the use of the Underground Injection Control (UIC) wells within the IM P&T system. Three workplans were submitted to NMED in response to its consent orders. The first workplan (April 2013) focused primarily on extraction/mass recovery. It was followed by a second workplan (May 2015) (LANL, 2015) that included plume migration control. A third workplan followed in April 2018 that included a key assumption that the Cr(VI) plume was present in the top 50 feet of the aquifer. This workplan also included provisions for metrics and reporting, as well as a 3-year performance timeline including monitoring with semiannual and annual reports.

The drilling of downgradient monitoring well R-70 in 2019 revealed that the chromium contamination was deeper—approximately 100 feet—than the initial assumption of 50 feet or less when NMED approved the IM operations. In response, NMED issued numerous technical comments and asserted that the overarching assumption for the original work plans was not valid, requiring a new workplan. In response, the site delivered a revised workplan entitled *Chromium Interim Measures and Characterization Work Plan* (IMWP) to HWB in September 2022 (LANL, 2022). NMED reviewed the IMWP and delivered comments in a Notice of Disapproval (NOD), which included the following:

- A requirement that the document revision include alternative location(s) for injection outside the plume contamination boundary
- Agreement with the chromium extraction activities, but requiring that DOE-EM-LA must find an alternative location for injection of treated water to continue IM operations
- A goal to determine a final remedy after completing the data gap activities in the IMWP

The fourth quarterly report from the site in 2020 showed a chromium concentration in monitoring well R-45, Screen 2 of 55 parts per billion (ppb), exceeding the water quality standard. NMED responded by informing DOE-EM-LA that the IM permit required DOE-EM-LA to submit a corrective action plan to NMED if groundwater monitoring in the vicinity of the discharge indicates a significant increase in concentration of an analyte or toxic pollutant. The corrective action plan shall include a description of the actions to control the source and a completion schedule. NMED then issued DOE-EM-LA a Notice of Non-Compliance for this exceedance at R-45 in April 2022.

DOE-EM-LA responded to the Notice of Non-Compliance with a letter in May 2022, stating that there had been no demonstration of a significant increase in concentration, and that there was no demonstration that such increase is attributable to a discharge. NMED then issued a Notice of Violation in June 2022, requiring submission of a corrective action plan. In response, DOE-EM-LA complied and submitted an Action Plan in September 2022. GWQB issued a Corrective Plan Response and Further Action Required letter in December 2022, stating that the proposed actions were acceptable but had deficiencies. NMED then required additional corrective actions, with the cessation of all injection activities by April 2023.

Since the cessation of injection activities in 2023, NMED and DOE-EM-LA have continued to negotiate a solution that would enable resumption of the IM and extraction/ injection operations. Additional details of these negotiations can be found in Herman and Martinez (2024), presented to the IRT on March 21, 2024. In December 2023, NMED and DOE-EM-LA agreed to participate in an Independent Technical Review to provide insight on the impasse.

### **2.1.5 Independent Technical Review 2024**

An independent technical review is being conducted of actions taken by DOE-EM-LA to characterize and model the Cr(VI) plume at the LANL site and the efficacy of IM taken to prevent plume migration offsite. In early 2024, an IRT was selected and formed under the leadership of Professor Ines Triay.

## 2.2 Conceptual Site Model of the LNAL Chromium Plume Site in Mortandad Canyon, New Mexico

A CSM is described by EPA (U.S. EPA, 2011, pg.1) as follows:

*“The Conceptual Site Model (CSM) is an iterative, ‘living representation’ of a site that summarizes and helps project teams visualize and understand available information.”*

In a regulatory framework, a CSM may provide basic information on the sources of the contamination, migration pathways to the accessible environment and potential receptors that might be at risk (e.g., TechLaw and EPA Region 4, 2024). For the purposes of this document, the CSM is tailored to inform the IRT responses to the five charge questions (paraphrased in **Table 2-1**) with the aim of establishing common agreement on the physical and chemical systems that exist in the chromium affected portion of the aquifer in Mortandad Canyon.

As expressed by EPA (U.S. EPA, 2011), the CSM is a living document. As new information is received, the CSM can and should be revised to incorporate the new information, ensuring that future decision making is based on the most accurate understanding of the site that is available.

The CSM presented here describes the current (as of 2024) understanding of the site, geology, contaminant distribution, groundwater hydrology (including aquifer properties, hydrogeochemistry, and microbiology), and chromium transport.

### 2.2.1 The Chromium Remediation Area

The site lies in Mortandad Canyon, 2 to 3 miles southeast of the Power Plant (**Figure 2-1**), south of Los Alamos, New Mexico. The primary focus of this work is on dissolved chromium that has entered the regional aquifer in Mortandad Canyon at concentrations exceeding the New Mexico standard for chromium in groundwater (50 µg/L). The affected area and nearby surroundings host several municipal water supply wells, one of which (PM-3) is potentially in the path of the eastwardly migrating plume.

Mortandad Canyon is one of several canyons (**Figure 2-3**) eroded into volcanic deposits of the east side of the Jemez Mountains that range in thickness from 1,000 feet on the western side of the plateau to about 260 feet eastward above the Rio Grande (Broxton and Eller, 1995). The canyon extends 8 to 9 miles in length, and has an elevation drop of about 1,900 feet (Neptune, 2024) (**Figure 2-4**). Mortandad Canyon heads on the Pajarito Plateau and runoff passes through the canyons but rarely reaches the Rio Grande as surface flow due to limited flow durations and infiltration in canyons. According to N3B (2024, pg. 77):

*“The Mortandad watershed may be influenced by two significant tributaries: Ten Site Canyon and Cañada del Buey. Snowmelt runoff and stormwater runoff from seasonal snow and rainstorms flow for a limited distance in the upper canyon and occasionally reach as far as the sediment traps [a location in Mortandad Canyon just west of the plume area at Lat 35.86083333 and Long -106.26833333].”*

The Mortandad watershed covers approximately 10 square miles. The 10-year average annual volume recorded at a surface water flow gauge located at an elevation of 6,654 feet above mean sea level (feet msl) is 1.1 acre-feet (N3B, 2024, pg. 84). Industrial wastewater discharge has also occurred in Mortandad Canyon upgradient of the chromium remediation area in Technical Area 50.

### **2.2.2 Geology**

This summary focuses primarily on the geologic units that underlie the Los Alamos site on the Pajarito Plateau. Additional details on the regional geology can be found in Kelley (1978) and Broxton and Vaniman (2005). A simplified cross section of the regional geology was provided by Broxton (2024a), and is provided as **Figure 2-5**.

Rock units of the Pajarito Plateau beneath the site are described below in ascending order (oldest to youngest). Precambrian basement rocks are likely composed of granite, granitic gneiss, schist, and greenstone. These are overlain by Paleozoic (Mississippian to Permian) and Mesozoic marine and terrestrial sedimentary rocks. No wells have been drilled on or near the Los Alamos site that penetrate either the Precambrian or Paleozoic/Mesozoic basement rocks. However, the depth to, and thickness of, these basement rocks beneath the site are largely inferred, and are likely based on the regional geology of the Española Basin (Kelley, 1978; Broxton and Vaniman, 2005). Smith et al. (2004) and Cather (2004) believe that the upper Paleozoic and Mesozoic rocks were then eroded from the Española basin area during the Laramide Pajarito uplift. Miocene-aged sediments appear to rest directly and unconformably on the Precambrian and Paleozoic/Mesozoic basement rocks beneath the site. These Miocene sediments are part of the Santa Fe Group, a thick package consisting of fluvial deposits, volcanoclastic sediments, and basalts.

The geology of the immediate chromium plume site area comprises several geologic units that are briefly summarized here. The deepest geologic unit monitored in the IM area is the Chamita Formation of the Santa Fe Group. This unit is composed of sands and gravels, and is likely fluvial in origin. It is overlain by a Miocene tuffaceous unit. The overlying Puye Formation has a lower pumiceous subunit but is composed predominantly of fanglomerate deposits that interfinger with basalts of the Cerro del Rio Volcanic Series Basalts. These are overlain by the younger deposits of the Bandelier Tuff, which is composed predominantly of rhyolitic ignimbrites.

### **2.2.3 Chromium Distribution**

Available evidence indicates that practically all chromium contamination in groundwater in the IM area is in the hexavalent form. However, Cr(VI) has also been detectable in background samples collected from the aquifer at concentrations between 5 µg/L and 10 µg/L (see historical chromium records for wells in Mortandad Canyon in Neptune, 2023). By comparison, the New Mexico standard for chromium in groundwater is 50 µg/L (McCroory, 2024, slides 5 and 11; Langman, 2024, slide 16). The locations where chromium occurs in the groundwater regularly above the level of concern include CrEX-1, CrEX-2, CrEX-3, CrEX-4, CrEX-5, R-28, R-42, R-43 S1, R-44 S1, R-45 S2, R-50 S1, R-61 S1, R-62, and R-70 S2. This list is not exhaustive,

but allows readers to readily locate the zones of concerning chromium concentrations. Locations with concentrations repeatedly (not necessarily continuously) above background but below the level of concern include R-11, R-15, R-43 S2, R-44 S2, R-45 S1, R-45 S2, and R-70 S1 (see **Figures 2-6 and 2-7A** for locations). In addition, there are perched-intermediate monitoring wells, such as MCOI-6 and SCI-2, that also contain elevated concentrations of chromium (above 50 µg/L) for extended periods of time. These could serve as sources of chromium contamination to the groundwater in the regional aquifer. However, the extent of these detections is limited to the western and northern boundaries of the observed chromium plume in the groundwater, leaving significant uncertainty associated with locations of continuing fluxes of chromium into the regional aquifer and the time frames of the contributions to the groundwater plume.

Prior to activation of the IM system, the chromium plume was found to extend from about R-62 (chromium concentration of about 100 ppb), on the west side of the study site, to about R-45 (chromium concentration of about 40 ppb) on the east side of site, referred to here as the 'plume area' (**Figures 2-8A and 2-8B**). A manual rendering of the 50 ppb contour interpreted the leading edge of the plume to be near R-45. Computer-generated contours (using inverse distance weighting to interpolate and a x-axis scaling method to simulate the effects of anisotropy; see Section 3.1.3 for details) of the same data present a similar plume geometry, but do not close the leading edge of the plume. These versions of the plume reflect uncertainty in the plume boundaries (depending on the assumptions and judgements made in the contouring process) and represent the range of likely plume occurrence in 2015. It is noted that the maps represent the plume as it was known prior to the start of IM operations. There is uncertainty regarding the delineation of the northeast boundaries of the plume on the basis of high chromium concentrations detected in post-2015 wells (e.g., at R-70 S2).

The same exercise was undertaken for the plume using data from 2023—after the IM had been in operation, albeit discontinuously. Both the manual contours and the computer-generated contours show some plume recession in the southern portion of the site, but ambiguous improvements elsewhere. The central area of the plume appears to improve in the vicinity of CrEX-3. The west side of the plume center experienced an increase in chromium concentration at CrPZ-5 in 2023. This increase appears to be related to chromium capture from a more westerly location, possibly a vadose zone source, by the extraction wells.

Changes in chromium concentrations between the two dates can be visualized by subtracting values at common sampled locations and contouring the differences (**Figure 2-9**). Once again, there is consistency in the trends observed from manual and computer-generated contour plots. Improvements to the water quality are suggested to be occurring on the northern and southern sides of the study site and in the vicinity of CrEX-2 as a result of IM operations. On the other hand, the southwestern portion of the plume area is seen to have experienced moderate increases in chromium concentrations, as have the central and west central portions of the plume.

There is also uncertainty in the extent of chromium south of CrIN-3, CrIN-4, and CrIN-5 prior to IM startup. The extent of the chromium plume on the south side of the LANL site is important for

assessing any transgression of the border with San Ildefonso Pueblo. As of 2024, no data have been collected to show that such a transgression has occurred. However, tracer tests in the form of point dilution tests, cross-borehole tests, and push-pull tracer tests were used by N3B to qualitatively infer aquifer zones influenced by the IM well operations (**Figure 2-10A**). The zones from CrIN-3, CrIN-4, and CrIN-5 all approach or cross the border, raising the possibility that a small amount of chromium, present in and around the wells before injection, might have been pushed to the border and possibly crossed it. This possibility is also raised in a plume map prepared by the IRT (**Figure 2-10B**). Using maximum values of chromium in monitoring wells and IM wells from the time range 2014 to 2024, log-transformed concentration data were interpolated over the site by kriging and then contoured. The resulting graphic represents a likely upper limit of the plume footprint at the site. The plume map illustrates that there is at least some possibility that chromium at concentrations above 50 ppb extends, or extended in the past, south of the property boundary.

While the possibility that chromium reached the southern property boundary cannot be discounted, there are no direct measurements to confirm this possibility; the available evidence is only speculative and suggests that the amounts involved are/were small. Moreover, hydraulic information related to the IM operation, together with the ambient flow directions in the regional aquifer discussed in detail elsewhere in this report, are expected to cause northward flow across the southern boundary of the site, making any occurrence of chromium south of the border temporary. This area of the plume should be investigated further to better define the southern extent of chromium contamination.

#### **2.2.4 Groundwater Hydrology**

There are two types of water-bearing units relevant to the chromium plume investigation: the perched groundwater and the upper regional aquifer. Perched groundwater has been encountered during drilling in numerous locations above the regional aquifer. Infiltrating water from the canyon bottoms percolates downward in a partially saturated state until it encounters a low-permeability zone, a perching horizon, where saturated conditions develop. In the chromium study area, the perching zones are the Cerros del Rio basalts. Water in the perched zones may flow downward through fractures or discontinuities in the basalts or laterally along the slope of the basalts until the perching zone pinches out, at which point, the water continues to percolate downward through the underlying permeable sediments of the Puye Formation to recharge the upper regional aquifer. The net effect of the perched zones and underlying south-dipping sediments is to divert groundwater infiltrated from Sandia Canyon to the south, toward Mortandad Canyon.

The water table represents the top of the regional aquifer, roughly 800 to 1,000 feet bgs. The upper regional aquifer comprises primarily sediments of the Puye Formation, including a pumice-rich subunit of the Puye, and the underlying Miocene pumiceous sands and sediments of the Chamita Formation of the Santa Fe Group. The Puye is a fanglomerate with an origin in the uplands to the west. This Puye fanglomerate is primarily composed of a heterogeneous mix of various coarse-textured materials that are, individually, laterally discontinuous over great distances. The Santa Fe Group is primarily a thick sequence of ancestral Rio Grande fluvial deposits, composed mainly of sands and gravels. Thus, heterogeneous but permeable

sediments occur within all formations of the regional aquifer. Owing to large-scale stratification features in these sediments, the regional aquifer appears to be anisotropic, with lower permeability orthogonal to the bedding planes and higher permeability parallel to bedding planes. The upper regional aquifer where the chromium contamination is found is unconfined and extends to a depth of over 5,000 feet bgs.

In addition to recharge through the vadose zone, the regional aquifer is recharged along the Jemez Mountains front. The slope of the water table, and therefore the direction of groundwater flow, is primarily to the east, toward the Rio Grande, where the groundwater discharges as springs. The water table cuts across the Puye Formation, the Miocene pumiceous unit, and the Miocene sediments. Possibly because of the local recharge from the perched zones, along with the influence of pumping from deep high-capacity wells surrounding the IM site, there are also significant downward components to the hydraulic head in places, indicated by the water level difference between the dual well screens.

Miocene basalt flows have been encountered within the Santa Fe Group, approximately 500 feet below the water table in the chromium investigation area. The basalts dip to the southwest. Consequently, the basalts rise to the water table east of the plume area, in the primary direction of groundwater flow. The basalts appear to have relatively low permeability and may serve as an aquitard that separates the upper and lower regional aquifer.

#### **2.2.4.1 Recent Water Table History**

The position of the water table within the regional aquifer has changed over time. Pumping of the CrEX wells and injection at the CrIN wells, as well as natural variations in the water table in response to weather and climate changes, would naturally cause deviations from a baseline steady-state (pre-pumping) flow system. Foster (2024c) reported that the water table has been steadily declining in area since the turn of the millennium (**Figure 2-11**). Although the regional water table has declined at a rate of roughly 0.5 to 1.0 foot per year (ft/yr), the hydraulic head gradient has not changed appreciably in the IM area. A comparison of water table maps in 1984 and 2014 indicates that groundwater flow through the canyon could have changed somewhat at various times, based on horizontal gradient variations (**Figure 2-12**). However, the gradient does not follow a consistent trend, and appears to stay within a reasonable range given the approximate nature of the estimates in **Figure 2-12**. It is further noted that some of the differences arise from uncertainty associated with the comparatively sparse data pre-2014. Also, the choice of locations over which the gradient is measured introduces variability because it is not uniform over the site. **Figure 2-13** shows the times when these water level maps were prepared in the context of IM pumping.

The water levels shown in the **Figure 2-12** maps between 2020 and 2023 were comparatively stable during those years, even comparing periods of extraction well pumping and non-pumping (**Figure 2-13**). Hydraulic gradients across the site (from R-67 to R-36) remained roughly on the order of 0.005 (see **Figures 2-12C, 2-12E, and 2-12F**), disregarding gradients at pumping or injecting wells. However, these gradients were not uniform across the site. West of R-1, they were on the order of 0.01, while those in the plume area were about 0.0007 (from gradients calculated in the IRT flow model described in Section 3.1.1.4). Gradients steepened again east

of R-35. As expected, gradients in the immediate vicinity of the pumping or injecting wells were enhanced. Spatial changes in the horizontal hydraulic head gradient across the IM area may be related to the hydrogeologic character of the aquifer or possibly to effects of deep production well pumping.

Despite the variations mentioned above, the general spatial consistency in the hydraulic gradients at the site, as well as the rapid establishment of a new post-pumping steady state, can justify the use of simplified models with the steady-state assumption for prefatory and explorative work, as well as playing a role in confirming the reasonableness of output from complex models. Thus, models assuming a steady-state base case may be useful for simulating groundwater within the past 3 to 5 years, with or without pumping of the CrEX wells. Simplified modeling is discussed briefly in Sections 3.1, 3.2, and 3.3, and in more detail in **Appendix A**.

#### **2.2.4.2 Aquifer Properties at the IM Site**

As discussed above, flow in the shallowest portions of the regional aquifer beneath Mortandad Canyon is generally to the east (McCrary, 2024; DOE-EM-LA, 2023, pg. C2-C3; Neptune, 2023, pg. 62, 64; Purtyman, 1995, pg. 29; Frenzel, 1995, pg. 11) (**Figure 2-14A**). More local flow immediately beneath the plume area is much less well defined and can range from strongly southeast to northeast. In addition, there appears to be a vertical component to the hydraulic gradient in the downward direction, possibly related to pumping of the large regional water supply wells PM-1 to PM-5, recharge from the vadose zone, or some other natural cause (**Figures 2-14B and 2-14C**). Although in places the magnitude of the vertical gradient is greater than the horizontal hydraulic gradient, the effect of the downward component on the driving force is likely tempered by vertical anisotropy in the aquifer, which is estimated to be on the order of 0.020 ( $K_v/K_h$ ) based on the analysis of pumping test data (Batu, 2024j [**Appendix B**]). Grain size analyses reported by Broxton et al. (2021) also suggested vertical anisotropy in the sediments, although their preliminary  $K_v/K_h$  ratio estimates were less pronounced, on the order of 0.3.

##### **2.2.4.2.1 Hydraulic Conductivity**

The hydraulic conductivity of the Puye Formation is variable due to the heterogeneous nature of the sediments. Grain size analyses suggested variations in  $K_h$  on the order of a factor of 25 within the formation (**Figure 2-15A**). Foster (2024b) evaluated the hydraulic conductivity data for their model input, and found that  $K_{h(xy)}$  ranged from 0.2 to 686 feet per day (ft/d), with the highest values in the vicinity of R-35b and the lowest values near R-35a and R-62 (see **Figure 2-15B**). Batu (2024j [**Appendix B**], see Table 1 in Attachment 2) reevaluated aquifer testing in the CrEX and CrIN wells and found the horizontal hydraulic conductivity to range from 12.5 to 172 ft/d, with the highest values at CrEX-2 and CrEX-5. Likewise, Batu (2024j [**Appendix B**], see Table 1 in Attachment 1) reevaluated aquifer testing in the CrIN-series of wells and found the horizontal hydraulic conductivity to range from 26 to 72 ft/d, which is less variable compared to the CrEX wells. A comparison of the IRT reevaluations of hydraulic conductivity with the original estimates reported by Neptune (2023) reveals an overall higher mean in the IRT estimates (See **Appendix C** [Batu, 2024b] and **Appendix D** [Batu, 2024c]). Location-specific comparisons for 9 wells, including CrEX-1 through CrEX-4 and CrIN-1 through CrIN-5, were unable to verify the



estimates reported by Neptune (2023), with some values varying by an order of magnitude or more. Other analysis of aquifer tests is provided in **Appendix E** (Batu, 2024a)

These apparent differences in hydraulic conductivity estimates may have important implications for modeling scenarios involving hydraulic containment and migration of chromium, and should be investigated further to reconcile differences. The values obtained by Batu [**Appendix B**] were derived using well-established methods. With regard to assumptions that underly those methods, Hantush (1964) states that *“Despite the shortcomings of these assumptions, observations have shown that the Dupuit-Forchheimer well discharge formula predicts the well discharge with a very high degree of accuracy.”* The methods assume, for example, that (1) well losses are negligible, (2) there is no resistance to vertical flow in the aquifer (for the Dupuit solution), (3) an effective radius of influence within the aquifer applies and can be confidently determined, and (4) pumping is constant and conditions have achieved steady state (i.e., drawdown has stabilized). These assumptions are not perfectly met by the non-ideal data and conditions commonly encountered in the field and that were evaluated here. The consequences of non-idealities are difficult to determine. For example, the effect of assuming negligible well losses is—all other things being equal—to yield underestimates of transmissivity and hydraulic conductivity, which may explain some of the apparent systematic difference between estimates obtained by Batu [**Appendix B**] and Neptune (2023) and others.

Based on geology and the spatial distribution of hydraulic conductivity values, the IRT has seen no evidence of a confining layer or aquitard within the upper portion of the regional aquifer. Therefore, groundwater in the upper part of regional aquifer, where the chromium contamination occurs, appears to be unconfined. However, the deeper Miocene basalts that are roughly 300 to 500 feet beneath the chromium plume may exhibit aquitard properties (**Figure 2-16**). Broxton (2024b, slide 18) wrote:

*“The massive cores of the Miocene basalt flows form dense low permeability zones that can act as confining or semiconfining beds ... Pumping effects from PM-2, PM-4, and PM-5 occur above the Miocene basalts and propagate laterally along bedding towards the Chromium monitoring wells ... Pumping effects from PM-1, PM-3, O-1, and O-2 occur below the Miocene basalts. Chromium monitoring wells are isolated from these pumping effects, both by basalts acting as confining or semi-confining beds and by the lateral propagation of pressure responses to deeper levels of the aquifer southwestward along bedding.”*

While the Miocene basalts may have aquitard properties, Harp and Vesselinov (2013) reported evidence that PM-3 and PM-4, and to a much lesser degree PM-2, did cause mild drawdown responses in the chromium plume area wells. PM-5, located upgradient of the plume area, imparted no clear hydraulic response from the monitoring wells. Of these wells, PM-3 is the only one screened mostly beneath the basalt layer. It remains unclear whether the responses to PM-3 pumping are due to breaches in the basalt layer or the effects of the relatively small portion of the PM-3 screen and filter pack above the basalt layer. The well diagrams of the PM-series wells are shown in the figures in **Appendix F** (Batu, 2024g), along with the formations of the unconfined aquifer.

Overall, the Miocene-age sediments beneath the Puye Formation (e.g., Chamita Formation of the Santa Fe Group) appear to be sedimentologically similar to those within the Puye Formation down to an elevation of about 5,740 feet msl (note that due to the dipping beds, this elevation is variable across the site). The hydrogeologic properties of sediments down to an elevation of about 4,000 feet msl may be inferred from the reanalysis of PM-2 pumping test analyses reported by Batu (2024j, Attachment 3 in p. 107 [Appendix B], 2024b [Appendix C], and 2024g [Appendix F]). PM-2 has a screen length of 1,276 feet and extends from a maximum elevation of 5,711 feet msl to a minimum elevation of 4,435 feet msl, with a pump intake elevation of 5,735 feet msl (LANL, 2008, pg. 223). Batu reported a  $K_h$  of between 0.8 and 19.9 ft/d, depending on the observation well used for the analysis. These results suggest that the permeability of the deeper sediments are on average slightly less than those in the Puye Formation and upper Miocene sediments, though the significance of these apparent differences are difficult to gauge with high confidence. Foster (2024a, pg. 6) wrote:

*“While it was originally intended to develop unique distributions for different sedimentary units such as Tpf [including Tpf(p)], Tjfp, and Tcar, exploratory data analysis suggested that the distributions would not differ with statistical significance between the units and plausible ranges for K values would be so similar as to be within the range of uncertainty.”*

#### 2.2.4.2.2 Porosity

Total porosity can be defined as the fraction of porous medium volume that is not occupied by solids; in aquifers, it is the water-filled fraction. This quantity can be estimated using geophysical methods such as neutron probe logging or nuclear magnetic resonance (NMR), conducting grain size analysis, or conducting gravimetric analysis of core samples. At the Mortandad Canyon site, total porosity has been estimated to be in the range of 0.25 to 0.3 (Broxton et al., 2021; Reimus et al., 2021). For the purposes of estimating seepage velocities and solute transport rates, a more relevant quantity is the effective porosity, which is the portion of total porosity with connected pore space that permits fluid flow to occur. Effective porosity was estimated at the chromium plume site from cross borehole tracer tests performed with the tracers 1,5-naphthalene disulfonate (injected into CrIN-4) and 1,3,6-naphthalene trisulfonate (injected into CrIN-3) while CrEX-1 was pumped. Along with the sulfonate tracers, the aquifer parameters sulfate ( $\text{SO}_4^{2-}$ ), nitrate ( $\text{NO}_3^-$ ), chloride ( $\text{Cl}^-$ ), and Cr(VI) were tracked at R-50 S1, R-44 S1, and R-45 S1 (**Figure 2-17**).

Reimus et al. (2021) used the tracer breakthrough curves to estimate mean arrival times at CrEX-1 and the monitoring wells. Then, assuming radial flow around the pumping and injecting wells and ambient groundwater velocities of 0.25 meters per day (m/d) at R-50s1 (obtained from the borehole dilution tracer test conducted in R-50 S1) and 0.2 m/d at R-44 S1 and R-45 S1 (assumed), they used effective porosity as a fitting parameter to match a semi-analytical model to the observed chloride arrival times. The effective porosities were estimated to be 0.12 at CrEX-1, 0.14 at R-50 S1, 0.09 at R-44 S1, and 0.115 at R-45 S1, which suggests that 36% to 56% of the total porosity is associated with the majority of flow in the aquifer. On the basis of grain size analyses, Broxton et al. (2021) estimated this range of flowing porosity to be 55% to 62%, which is comparable but may be inflated due to the small sample sizes considered and other biases introduced by sieving samples (Devlin, 2015).

### 2.2.4.3 Hydrogeochemistry

The background water chemistry of the groundwater in the upper regional aquifer beneath the Pajarito Plateau is strikingly uniform across canyons in the area around the chromium plume. This is consistent with the notion that the upper regional aquifer behaves as a single hydrochemical unit and, by extension, a single hydrostratigraphic unit, in which the groundwater has equilibrated with the aquifer matrix material. Significant variations in the background major ion chemistry are generally restricted to areas near the discharge zone above the Rio Grande (**Figure 2-18**). However, the plume-affected groundwater is chemically distinct from the background water in several chemical components, including, among the major ions, sodium and calcium content (**Figure 2-19A**). Similarly, the vadose zone waters of Sandia Canyon are distinguishable from regional aquifer water at Mortandad Canyon and vadose zone water in Los Alamos Canyon on the basis of relatively higher total dissolved solids (TDS), sulfate, and calcium concentrations (**Figure 2-19B**). This fingerprint provides some evidence that the Sandia Canyon water is reaching the regional aquifer in Mortandad Canyon, in agreement with the hypothesis that dissolved chromium travels down Sandia Canyon and then laterally in the vadose zone southward to Mortandad Canyon.

### 2.2.4.4 Redox

The field work defining the plume boundaries indicated that the chromium plume was restricted to within 100 feet of the water table, mainly in the Puye Formation but also in the Miocene pumiceous unit in some locations to the east. The groundwater in the upper 100 feet of the regional aquifer is aerobic (generally >6 milligrams per liter [mg/L] dissolved oxygen [DO]) and permits chromium to persist in its mobile hexavalent form once it enters the saturated portion of the Puye Formation (Langman, 2024). Isotopic evidence suggests that chromium arriving at the top of the regional aquifer has followed a path from the source area that led to minimal chemical reduction (Heikoop et al., 2014). Once in the regional aquifer, transport of the chromium is largely in these upper 100 feet.

The upper portion of the regional aquifer, including the saturated zone of the Puye Formation, is aerobic and low in organic carbon. Bench-scale experiments have found no measurable chromium leaching difference between plume-affected sediments and background sediments in samples from the Puye, where the plume currently resides. In contrast, the underlying Miocene pumiceous sediments were found to contain a magnetic mineral fraction of up to 11% by weight with up to 0.2 micrograms per gram ( $\mu\text{g/g}$ ) leachable chromium (Ding et al., 2018). These minerals have the potential of providing some chromium attenuative capacity to the Miocene pumiceous sediments, particularly over large spatial scales. In addition, the Miocene sediments are underlain by a Miocene-age basalt layer that could contain reduced elements, including iron. This layer could also act as an aquitard, as discussed in Section 2.2.4 (**Figure 2-16**).

As the chromium plume travels eastward, the Miocene basalt layer, which is dipping (approximately  $3^\circ$ ) to the southwest (Broxton, 2024b), effectively causes the upper regional aquifer to thin, reducing the aquifer transmissivity and therefore increasing the hydraulic head gradient. The Miocene basalt also could act to partially dam the eastward flowing groundwater, perhaps contributing to the steepened water table east of the plume area. The impeding effect

of the Miocene basalt is illustrated near R-70 S1/S2, where a slight upward ambient hydraulic head gradient occurs, possibly caused by the top of the basalt layers that rise to the east. The basalt could also redirect water southward (see for example **Figure 2-14A**), though evidence of the basalt being the primary driver of such a diversion is weak. If the basalt layer is sufficiently leaky, water may pass through it with some potential for reactions between the oxidized chromium species and reduced elements in the basalt. In the horizontal direction, this process would take place some distance downgradient of the chromium plume area, beyond the scope of this work. As the chromium plume is restricted to zones hundreds of feet above the basalt, chromium reduction through contact with basalt minerals via vertical transport is currently unlikely.

### 2.2.5 Geomicrobiology

Microbial populations can be a dominant factor in establishing the geochemical environment in aquifers, both widespread and locally. There has been no direct microbial characterization of the vadose zone or aquifer at the site. However, indirect evidence of microbial activity capable of participating in chromium reduction was demonstrated in an in-situ injection of molasses (biostimulation) on September 9, 2017 (McCrary, 2024). In that demonstration, a local reducing environment was created in which Cr(VI) was reduced to Cr(III). Thus, microbial communities either directly or indirectly capable of attenuating chromium under reducing conditions are present.

Evidence for the reduction of chromium by aerobic bacteria has been reported in the literature (Palmer and Puls, 1994; Dey and Paul, 2013), though the mechanisms are poorly understood. Therefore, the role of microbial activity cannot be fully discounted despite the appearance that a geochemical environment generally stable for Cr(VI) exists at the site.

### 2.2.6 Transport of Chromium

#### 2.2.6.1 Sources

The first detection of chromium in Mortandad Canyon at concentrations above background (approximately 5 to 10 ppb) was at R-28 in 2004 (400 ppb). The date of the first arrival of chromium from Sandia Canyon at the water table in Mortandad Canyon is not known, but the presence of chromium in the aquifer in 2004 means that the travel time from source to aquifer was less than 50 years. In 2009, chromium was detected at R-42, upgradient of R-28, at a concentration on the order of 830 to 1,000 ppb.

Based on our review of the data, the IRT finds there are at least three source areas, and probably a fourth, where chromium reaches the water table. The first and main source is near a 'hotspot' (i.e., the area of highest chromium concentration) at R-42 (**Figure 2-7**). The perched zone contamination at SCI-2 is likely on the vadose zone flow path that contributed to the main plume near R-42 and R-28. R-43 may be on the fringe of this first source area. SCI-2, a perched-intermediate well, also depicted high concentrations of chromium in the vicinity of R-43, albeit in a slowly decreasing trend, from about 600 µg/L in 2009 to about 180 µg/L in 2024. Meanwhile, increased concentrations are observed in the groundwater nearby (R-43). These

increasing and decreasing trends indicated a response to the IM operation, as well as a potential source in this area.

The pathway of chromium from the source to the aquifer, projected to the surface, was depicted by McCrory (2024) (**Figure 2-1**). A notable portion of the chromium mass originally spilled is thought to have been attenuated by sorption and reduction in the organic sediments of the Sandia wetland (Heikoop et al., 2014). **Figures 2-1 and 2-6** suggest that transport occurs on the surface for much of the distance down Sandia Canyon until infiltration is achieved. McCrory (2024, slide 9) wrote:

*“Water containing chromium travelled down Sandia Canyon until reaching an infiltration window, then migrating laterally and vertically until reaching Mortandad Canyon.”*

The lateral migration is thought to be, at least partially, in response to the southerly dip of the Cerros del Rio basalts in the unsaturated zone (Heikoop et al., 2014).

Previous CSMs were revisited and updated by Katzman et al. (2018) (**Figure 2-20**). They summarized the earlier findings that the chromium apparently entered the regional aquifer at a depth of approximately 1,000 feet (elevation of about 5,850 feet msl) in Mortandad Canyon, eventually spreading throughout a zone approximately bounded by the red dashed line in **Figure 2-6**.

The pathway of chromium from the Power Plant to the regional aquifer was also depicted in cross section by Katzman et al. (2018) and Neptune (2023) (**Figures 2-20A and 2-20B**). An extended depiction of the area geology in section was presented by Broxton (2024a) (**Figure 2-20C**).

The second source is shown as a second zone of high chromium concentrations near CrPZ-5 (**Figure 2-8**). Because of its low perchlorate concentration, among other factors, as reported by N3B in the factual review, the origin of this source also appears to be from Sandia Canyon via the perched aquifer.

Regarding the third source, in 2012, chromium was detected at a concentration of 89.7 parts per million (ppm) in R-50 in 2012 (for reference, R-50 is east of R-61 and south of R-28 and R-42), raising the possibility of chromium migration toward San Ildefonso Pueblo land. Because the hydraulic gradient in the aquifer underlying Mortandad Canyon is predominantly to the east, the appearance of chromium as far south as R-50 could be evidence that the chromium migrated to R-50 from a source just west of that location. Groundwater transport from the R-42/R-28 locations does not seem likely based on currently known hydraulic gradients, which do not support southerly flow. The origin of this source may be discharge from the perched aquifer beneath Mortandad Canyon just west of the IM area. There are evidential lines of support for this supposition as explained below.

Perchlorate and tritium, along with chromium, are characteristics of a Mortandad Canyon source. In fact, their absence in the water originating from Sandia Canyon makes them a fingerprint of Mortandad Canyon source water, as alluded to in the discussion of the second

source area. The head of the Mortandad Canyon source area includes the area in the vicinity of R-61 and likely also extends toward to the northwest, somewhere near R-15. As elevated perchlorate, and sometimes tritium, occurs mostly in the southern part of the chromium plume, notably near R-50, R-61 and CrPZ-1 (Vesselinov et al., 2013), it is reasonable to infer that the source of the chromium is in the upper Mortandad Canyon area. Furthermore, the fact that chromium concentrations in R-61 increased at a time when the horizontal hydraulic gradient near R-61 was to the north-northeast, during IM operations, also supports a west to southwest source. Moreover, there was a continued increase in chromium concentrations at R-61 after IM shutdown, when the hydraulic gradient should have resumed a predominantly eastward direction. This again is consistent with a west-lying source area.

The fourth source is in the northwestern section of the plume, near R-62. About  $\frac{3}{4}$  mile to the west-northwest and upgradient of R-62 (**Figure 2-6**), chromium was found in CrCH-6 in July 2015. Chromium concentration in R-62, which is located downgradient of CrCH-6, increased before and during the IM operations. It is probable that the chromium here migrated southward in the vadose zone to R-62 and perhaps to CrCH-6, from discharges of chromium in Sandia Canyon, similar to the pathway to R-42. However, overall, the data from CrCH-6 are less certain than other data sources of Cr concentrations due to possible contamination from drilling fluid and some samples being collected unfiltered (factual review by N3B). Nevertheless, there are increasing concentrations of chromium in the regional aquifer near R-62, and the pathways to it through the vadose zone require delineation.

To explain the chromium concentration distributions shown in **Figures 2-8 and 2-9**, the occurrence of vadose zone ‘windows’ has been proposed by LANL for use in their model to designate areas of chromium input to the top of the regional aquifer (**Figure 2-7B**). Such sources must extend at least as far west as R-62, as alluded to above, to explain the rising chromium concentrations there since before 2011; they have approached 300  $\mu\text{g/L}$  since 2019. R-15 may also be affected by a western source, though chromium has not appeared there at concentrations greater than 20  $\mu\text{g/L}$ —below the New Mexico guideline, but above the regional background. In the IRT analysis, three of the four hydraulic windows are locations where Sandia Canyon power plant discharge enters the regional aquifer, and the other location is discharge from upper Mortandad Canyon.

In general, the four sources described above are reasonably consistent with the ‘hydraulic windows’ proposed by LANL (**Figure 2-7B**). However, the locations of these windows are based primarily on groundwater monitoring data, and their individual spatial extents are unknown. None of the contamination in the vadose zone has so far been explored in sufficient detail to evaluate the areas of impact or the mass discharge (chromium concentration times water flow rate) into the regional aquifer from the ‘windows.’ In the absence of more detailed information, the ‘windows’ are arbitrarily assigned ovoid shapes in the 3D numerical model (Finite Element Heat and Mass [FEHM]) to identify the most active locations (**Figure 2-7B**). One possible scenario involving such ‘windows,’ deduced from calibrating the numerical model of the site, illustrates the locations that multiple sources in the plume area might occupy to explain the observed concentrations (**Figure 2-7B**). This scenario is one of several that have been reported by Neptune (Foster, 2024b) and is shown here for illustrative purposes only.

### 2.2.6.2 Retardation

Chromium at the site occurs as both Cr(III) and Cr(VI). However, the majority of the mobile species is Cr(VI), which represents the largest health risk and occurs as an anion in solution ( $\text{CrO}_4^{2-}$ ) (**Figure 2-21**). Facilitated transport of Cr(III) species as colloids or attached to colloids cannot be ruled out, but this mechanism of transport is not required to explain the chromium mobility at the site. The anionic form of Cr(VI) is subject to neither cation exchange nor hydrophobic sorption, although interactions with clay mineral edges, which can be positively charged, may play a small role in retarding chromium in specific locations where clay content is high. Therefore, in general, retardation of the species is expected to be minimal in the Puye Formation and Miocene pumiceous unit, where the plume is currently found. This expectation is supported by the results of leaching experiments performed by Ding et al. (2018), who found:

*“Our results ... indicate that all samples taken from known contaminated horizons in comparison to non-contaminated ones within the Puye formation showed no statistical difference in the amount of Cr leached indicative of its insignificant Cr(VI) attenuation capacity.”*

However, analytical modeling (Batu, 2024i [**Appendix H**] and 2024f [**Appendix G**]) indicates that chromium degradation could possibly account for a loss of up to 10 to 15% of the chromium concentration.

### 2.2.6.3 Average Estimated Advective Velocity

In the absence of retardation and degradation, Cr(VI) will behave conservatively and, in an advection dominated system like the Mortandad Canyon site, will be transported at a rate similar to the average groundwater seepage velocity. Therefore, any data that provide insights into the groundwater velocity in the aquifer should be considered of high value. The first data of this kind that deserve consideration are those from a Darcy’s Law based estimate of seepage velocity. In this case, we assume that the hydraulic conductivity ranges from 12 to 150 ft/d, that the hydraulic gradient in the plume area is about 0.001, and that the effective porosity is approximately 0.15. With these parameters, the travel time of chromium in groundwater under ambient, non-pumping conditions in the central IM area likely ranges from roughly 12 to 365 ft/yr (e.g., showing high end of this range):

$$v = \frac{Ki}{\theta} = 150 \frac{ft}{day} \times \frac{0.001}{0.15} \times 365 \frac{days}{year} = 365 \frac{ft}{year}$$

The faster velocity appears to be in the more permeable northern part of the plume (e.g., near CrEX-5) (Section 2.2.4.2). If the effective porosity is closer to 0.10, as indicated from tracer tests (Section 2.2.4.2), the calculated range in average transport velocity rises to between 18 and 547 ft/yr. These estimates are helpful, but must be considered with caution; the distance of transport along a flow path over a specified period of time depends not only on the estimated values of hydraulic properties (either averaged or point-specific), but also on the continuity of the strata exhibiting these properties (e.g., N3B, 2021, Fig 2.4-1). Continuity issues are not accounted for in the above calculations.

A second data source for seepage velocity data at the site is direct, independent testing that does not depend on Darcy’s Law calculations. Borehole dilution tests were implemented at

10 locations in the chromium plume area and showed a geometric mean groundwater velocity of 229 ft/yr (Figure 2 of Reimus et al., 2021). On page 14, Reimus et al. (2021) state that “the cross-hole test provided a natural flow velocity estimate of ~1 m/d over a distance of ~125 m between CrPZ-2a and CrEX-3.” That is nearly 1,200 ft/yr.

As a check on the reasonableness of the velocity calculated from the borehole dilution tests, we divided the plume length, roughly 5,000 to 6,000 feet, by 229 ft/yr, and found that the average travel time to cover that distance was on the order of 20 to 25 years. This time range corresponds to the plume first appearing in the regional aquifer sometime near the turn of this century, which seems realistic. This calculation is only approximate, but is nonetheless noteworthy because it establishes an estimated date of plume origin in the Mortandad Canyon aquifer that is generally consistent with observation.

Additional predictions of chromium migration post-IM shutdown are given in **Appendix A**. These calculations are especially relevant to the containment east of R-70.

#### **2.2.6.4 Dispersion**

Hydrodynamic dispersion combines the processes of effective diffusion in an aquifer and spreading due to mechanical processes related to variability in seepage velocity at different scales. Dispersion has long been known to be scale dependent and related to the degree of heterogeneity in a porous medium (Skibitzke and Robinson, 1963). Early work on modeling dispersion, both deterministic and stochastic, tended to overestimate (macro) dispersion, especially where it was used to infer mixing and its effects on reactive transport (Kitanidis, 2017; Zech et al., 2023). Controlled field experiments in sandy aquifers with low to moderate heterogeneity have generally found that dispersion is a weak process, particularly in directions transverse to flow (Mackay et al., 1986; LeBlanc et al., 1991). Hadley and Newell (2014) proposed that the advection-dispersion approach to transport modeling be deemphasized in favor of an advection-diffusion approach originally introduced by Gillham et al. (1984). This view has yet to be generally accepted (Kitanidis, 2017; Cirpka et al., 2015). Cherry (2023, pg. 146), who wrote critically about the advection-dispersion equation (ADE), nonetheless noted that:

*“However, as I try to set the record straight concerning the problems of the ADE, I wish to be clear that I do not advocate its abandonment. The ADE models can be useful and even necessary given lack of practical alternatives, if used with judgment and care.”*

For the purposes of this conceptual site model, the ‘*judgment and care*’ standard mentioned by Cherry (2023, pg. 147) sets the default for the modeling of transport with dispersion in the predominantly sandy deposits beneath Mortandad Canyon:

*“I now recognize that, at the time, there were extreme differences between high-resolution field plumes and model plumes and that the field evidence overwhelmingly supported weak transverse dispersion in sandy aquifers of weak to moderate heterogeneity.”*

Accordingly, the transverse horizontal dimensions of the plume in Mortandad Canyon are probably defined foremost by the locations of vadose zone ‘windows’ in the plume area.



Longitudinal dispersion affects first arrival times at downgradient receptors but may be of secondary importance, as purely advective arrival times are likely to be only a few weeks, maybe months, later; they do not meaningfully change the risk scenario.

#### **2.2.6.5 Sinks**

The issue of chromium mobility and transformation was discussed in Sections 2.2.4.4, 2.2.5, and 2.2.6.2. Briefly, the chromium in the regional aquifer is present primarily as Cr(VI), which is unlikely to be removed from solution by either sorption or reduction, due to the lack of reductants in the sediments of the regional aquifer and the aerobic character of the groundwater.

Chromium could be temporarily removed from the fastest pathways in the aquifer by transport into the less permeable lenses of material that contribute to the heterogeneity of the aquifer. If the low-permeability features contain sufficient clay, the transport may be limited by matrix diffusion and storage. Storage times in cases like this can be decades or longer, effectively behaving as sinks for notable fractions of contaminants and establishing long-term sources of contamination, via back-diffusion, at considerably lower concentrations than the original sources—though these weak long-term sources may still present risk. If the strata and lenses in the aquifer are not clay-rich, the transport into the low-permeability features may occur by slow advection. In that case, the storage times, and breakthrough tailing, would also be extended in time but to a much lower degree than matrix diffusion and back-diffusion would cause.

Grain size analyses performed on sediments from the Puye and below indicate that the Puye has regions that are high in silt (**Figure 2-22A and 2-22B**) and low in ‘mud,’ which is understood to refer to clay-sized particles. Silt permeability is typically low, but still subject to conducting advective flow. Therefore, storage of chromium in these fine-grained lenses or layers should be expected, but may not be diffusion limited.

Pumping wells of the Pajarito well field, in addition to the CrEX wells, also need to be considered as potential sinks of chromium, including PM-3. Vesselinov (2004), along with calculations by Batu (2024j [**Appendix B**], 2024b [**Appendix C**], and 2024h [**Appendix I**]), show that the PM-series production wells have an influence on water levels in the IM area. These appendices note that these wells need to be considered in plume transport and containment.

### **3. Committee Responses to Charge Questions**

This section presents the IRT’s responses to the five main charge topics, and any subparts thereof, together with recommendations. For each topic in this section, the questions are given, as presented to the IRT, followed by a summary response by the IRT to each. Each response is then supported by more detailed discussions.

### 3.1 Topic 1: Chromium Plume Control Interim Measure Hydraulic Control

The following questions are addressed in this section:

1. Do groundwater data and modeling results demonstrate that operation of the IM, as originally approved and in full operation, hydraulically control the plume?

*Response:* The water level and chemical data are not sufficient to conclude that the IM operation has hydraulically contained the plume. However, a simple 2D model developed by the IRT indicates that most if not all of the plume may have been within the capture zone at full IM operations. In contrast, 3D modeling with FEHM clearly shows that the plume was not hydraulically controlled. As discussed in the following section, at this time FEHM remains the most capable tool for predicting capture for any IM well field configuration.

2. Is there assurance that existing injection locations are outside the current 50 µ/L, or ppb, plume boundary?

*Response:* Yes. The Intellus database indicates that, as of August 2024, the five CrIN wells do not have chromium concentrations exceeding 3 µg/L. Three CrIN wells lie south of the main chromium plume 50 µg/L contour. All CrIN wells should be resampled prior to restarting any IM operation.

3. To what extent are the increasing chromium concentration trends in R-45 S2 and R-61 S1 the result of an adverse impact of current injection locations?

*Response:* More likely than not, R-45 S2 has been adversely impacted by IM injection operations. Chromium concentrations at R-61 S1 appear to have been influenced by changes in IM-induced hydraulic gradient; however, the increase mostly reveals a source west to southwest of R-61. In contrast to R-45 S2, IM operations appear to have captured contamination at R-61.

4. Will the current IM be protective of the environment until a remedial alternative is selected and implemented?

*Response:* No. The current IM system at full operations will not contain all chromium migration.

5. If not, what are the recommendations for maintaining hydraulic control?

*Response:* As discussed in Sections 3.2 and 3.3, there are alternative approaches to operating the IM. Because the plume has yet to be sufficiently characterized from field data, the extent of chromium contamination that needs to be controlled is not known. The existing IM system will likely need to be modified, reconfigured, and possibly expanded with at least one additional extraction well in the vicinity of R-70.

### 3.1.1 Do groundwater data and modeling results demonstrate that operation of the IM, as originally approved and in full operation, hydraulically control the plume?

Four approaches have been reviewed regarding hydraulic control of the chromium plume: chromium time-series data, water level elevation data, 3D modeling using FEHM, and simplified 2D modeling.

#### 3.1.1.1 Chromium Time-Series Data to Demonstrate Plume Containment

The IRT was provided an extensive database and numerous technical reports relevant to plume containment. Graphs of chromium concentrations at monitoring wells in the chromium remediation area are shown in **Figure 3-1** and **Appendix J**.

The IRT is assuming in the question that “operation of the IM as it was originally approved and in full operation” means full operation with five extraction wells and five injection wells. This response is therefore focused on the IM operation with extraction wells CrEX-1 through CrEX-5 and CrIN-1 through CrIN-5. However, for completeness, some attention is also given to the partial IM operation, in which CrEX-4/CrEX-5 and CrIN-4/CrIN-5 are the only wells operating. All chromium concentration data are plotted and evaluated in **Appendix J**. In general, evidence for loss of containment would be an increase in chromium concentrations over time along the margins of the plume that was known prior to the start of IM operations.

An examination of the time-series chromium concentrations on the perimeter of the plume area reveals locations on the northwest (R-43, R-62) portion of the study site that may be affected by the IM. This source zone may be associated with the increasing trend in chromium concentrations that began shortly before initiation of the IM system, indicating that IM operations were not responsible for all—or possibly any—of the rising chromium concentrations in this area. This trend reversed early in 2021 (see **Figure 3-1** for concentrations and **Figure 3-2** for relative screen elevations). Notably, the discontinuation of IM pumping did not result in an immediate rise in chromium concentrations, as expected if IM pumping was drawing clean water from upgradient of R-62 into this portion of the aquifer. This raises the possibility that the chromium concentrations in these locations are governed to a greater extent by the sources than by IM pumping and injection. Note that according to the conceptual model, the regional aquifer behaves as an unconfined aquifer. The sources of chromium delivery to the aquifer are located in the vadose zone and are not expected to depend on pumping in the aquifer. Therefore, trends in chromium concentrations at these wells are explained best as the increasing capture of an unmonitored northwestern chromium plume segment and/or chromium delivery rates from the vadose zone rather than effects from IM pumping and injection.

Near the southwest and south sides of the plume, respectively, locations R-61 and R-50 were most notably affected by elevated chromium concentrations. In both cases, it was the shallowest screened portions of the wells that experienced increases in chromium concentrations (**Figure 3-1**). R-50 S2 never showed an impact from chromium, and R-61 S2 was compromised by drilling fluids and has not been deemed suitable for producing a representative sample. In the shallow screens, the rate of chromium concentration rise appeared to increase after the onset of IM pumping and injection in the southern area. This

timing suggests a causal link between the rising chromium concentrations at R-61 S1 and IM operations. However, it is noted that this trend persisted after pumping ceased at this location. An analysis by N3B (2023) suggested that R-61 S1 could be receiving chromium from a continuing nearby source (the southwestern source zone), as discussed further in **Appendix K**. Possible contributions could have arisen from vertical downward flow induced by IM operations, a shift from an upward gradient in the ambient condition, or other causes, such as inflow from Mortandad Canyon.

On the other hand, R-50 S1 displayed a strong decline in chromium concentrations about 2 years after IM pumping and injection were initiated in the southern portion of the site. The chromium concentration increased again once pumping ceased. These data at R-50 S1 are consistent with R-61 S1 up to the time of IM pumping. During that time, these monitoring locations likely responded primarily to increasing capture and/or source variations from the vadose zone (leaving possible vertical flow aside for the moment). Once IM pumping began, chromium concentrations at R-50 S1 appeared to depend on redirected flow imposed by IM pumping and injection, and began declining, while chromium concentrations at R-61 S1 continued on the rising trend already being shown.

On the south and southeast side of the plume area, the shallowest screen at the R-44 location responded in a fashion similar to R-50 S1, although the chromium concentrations at this location have never exceeded 50 µg/L (**Figure 3-1**). IM operations decreased the chromium concentrations to background. Cessation of pumping did not cause a rebound of chromium as of early 2024. This result suggests that R-44 S1 is outside the chromium plume, and the upgradient injection wells may be generating sufficient hydraulic barrier for preventing chromium migration into this area. However, the appearance of sulfate in the water after IM system activation indicates that the declines in chromium concentrations are at least partially due to injection water displacing and mixing with plume water at that location.

We note that other wells on the south side also contained chromium concentrations in excess of 50 µg/L prior to IM start up: CrIN-3, CrIN-4 and CrIN-5 (**Appendix J**). There is uncertainty regarding where this chromium has migrated as a result of treated water injection. But at this time, there is no evidence from field data or model results that chromium concentrations greater than 50 µg/L occur south of these three CrIN wells.

The eastern portion of the plume affected by rising chromium concentrations included monitoring wells R-45 and R-70. Locations R-35, R36, and R-13 are outside the plume boundary on the east, and never exhibited chromium concentrations above baseline. In the cases of R-35 and R-36, the locations are considerably east of the plume and may be unaffected because the plume has yet to reach them. R-13 may be too far downgradient to have been impacted or chromium travel times may be too slow for the well to have been impacted. However, R-13 may become impacted in the future because it is in the path of contaminated water from the west-northwest (**Figures 3-3A and 3-3B**). **Figure 3-2** illustrates the differences in monitoring well screen elevations, which should also be considered in evaluating potential future impacts of plume migration.

Wells R-45 and R-70, at both screen levels, exhibited chromium concentrations above background prior to (R-45) or shortly after (R-70) IM pumping and injection was initiated. During IM pumping and injection, chromium concentrations at both R-70 screen depths showed signs of declining slowly, and R-45 S1 experienced a rapid decline. During this time, R-45 S2, the deeper R-45 screen, experienced increasing chromium concentrations. With the cessation in IM pumping and injection in 2023, all these trends seemed to reverse, with the exception of R-45 S1, which has remained low in chromium but may be experiencing the onset of chromium concentration increases as of January 2024. Taken at face value, these trends suggest that IM pumping and injection drew chromium back from both depths of R-70 and the shallower depth of R-45. However, these same trends could have resulted from other causes. In the case of R-45 S1, the rapid decline in chromium concentration with the onset of full IM activation could have resulted from displacement and mixing of chromium contaminated groundwater by treated water that was injected at either CrIN-1 or CrIN-2, or both. The appearance of sulfate at R-45 S1 at this time supports this hypothesis, as sulfate is associated with source water that passed through treatment (e.g., see R-43 S1). On the other hand, it must be noted that chromium began decreasing in concentration at R-45 S1 very soon after activation of the southern IM, before the CrIN-1 and CrIN-2 injection wells were activated. There was little or no corresponding increase in sulfate during this time. This might be interpreted as evidence that R-45 S1 was inside the hydraulic capture zone of the southern IM, as well as being affected by injected water (**Figure 3-4**).

The continual rise in chromium concentrations at R-45 S2 prior to the partial IM operation phase may also be due to water injected at wells CrIN-1 and CrIN-2 (**Appendix K**). In this case, the injections may have caused enhanced downward migration of chromium in the vicinity of R-45. Reduction in IM operations, when only CrIN-4 and CrIN-5 and CrEX-4 and CrEX-5 operated, was followed by an abrupt decline in chromium concentration at R-45 S2, apparently in agreement with the hypothesis of enhanced downward flow and transport. However, the decline in chromium concentrations at the lower R-45 screen was not sustained and, as of January 2024, chromium concentrations resumed an increasing trend partway to the maximum value of December 2022, where they appear to have stabilized, as the main plume moved eastward uncontained by the IM. An understanding of the flow and chromium transport past R-45 S2 is confounded by the superposition of possible enhanced downward component to the hydraulic head gradient due to IM injections, and pre-existing downward flow, due to the natural flow system or pumping influences of the PM-series wells.

At R-70 S1 and S2, the decreasing chromium concentrations, particularly prior to the switch to partial IM operation, could have been the result of IM capture, but could also have occurred if the capture zone limits fell west of R-70, preventing most of the chromium plume from reaching R-70 after the IM was activated. In other words, the declining chromium concentrations would have been the result of the capture zone of the IM system essentially shielding R-70 from receiving most, but not all, of the chromium that had previously been migrating there. In this scenario, chromium that has recently arrived at R-70 or might reach R-70 in the future would likely continue to migrate to the east.

To further assess the effect of IM operations on the chromium plume, the chromium concentration contours were examined for three dates: (1) May 2020, when pumping was off, (2) spring (March through June) 2022, when the IM system was active, and (3) spring (March through June) 2023, immediately following deactivation of the IM system (**Figure 3-5**).

Contours were based on interpolated concentrations using inverse distance weighting (IDW). The IDW parameters were selected to produce a visualization of the chromium plume that closely resembled the 50 µg/L plume shape reported in prior work (**Figure 3-5F**). In addition, lower concentration contours were considered. It was found that contours less than 35 µg/L plotted as bullseyes and did not aid with plume visualization. Regardless of the outside plume contour chosen, the extent of the area with elevated chromium concentrations was diminished by spring 2023, consistent with the conclusions regarding plume capture discussed above.

The observations above provide tentative evidence that IM operations effectively constrained spreading of the chromium plume in the shallowest monitored regions of the plume area. The effects of pumping and injection are apparently evident as far east as R-70 (**Figure 3-4**).

However, post-IM shutdown at R-70 S2, over about a 5-month period since September 2023, chromium concentration has increased from about 150 to 250 µg/L, near the concentration detected when the well was first sampled in 2019. The chromium concentration has remained fairly constant at this value. Whatever mechanism is responsible for this increase, it is clear that chromium has migrated and continues to migrate east of R-70. Based on these observations, and in the interests of minimizing plume advancement going forward, an immediate restart of the IM in some fashion is justified and desirable. Also, additional characterization is warranted to properly define the eastern location of plume capture and evaluate the need for additional wells in the eastern portion of the site to contain the chromium migration.

### **3.1.1.2 Water Level Elevation Data to Demonstrate Plume Containment**

Ideally, a capture zone is defined by patterns in hydraulic head—for example, a demonstration of gradient reversal at the leading edge of the plume. However, the exact position of the capture zone is difficult to ascertain because the potentiometric surface in the plume area is very flat, making identification of the flow patterns challenging. This is shown graphically by the highly variable flow directions indicated by three-point problems conducted between wells in the plume area (**Figure 3-6**).

A water level dataset from June 15, 2021 was used by Neptune as input to three-point problems that generated ‘guide-points’ to increase the density of locations with hydraulic head estimates. From these data, hand-sketched equipotential lines were plotted and used to infer an ‘equipotential-based capture zone’ map (Neptune, 2023) (blue line in **Figure 3-7**). An IRT member developed a hand-drawn flow net from the Neptune contour maps from March 21, 2024. In both cases, the hand-drawn capture zones found that R-45 and R-70 were outside the zone of capture. However, the low hydraulic gradients and sparse data at this site introduce uncertainty in flow direction calculations from hydraulic head data. Thus, greater emphasis falls to models to estimate capture zone boundaries.

### 3.1.1.3 3D Modeling to Predict Chromium Plume Capture

Neptune calculated several capture zone realizations based on 3D particle tracking simulations with FEHM (Neptune, 2023) and once again found that R-45 and R-70 lay outside the zone of capture (green line in **Figure 3-7**). However, in these cases, the capture zone boundary was represented by a line demarking the 50% particle capture boundary. Thus, some capture beyond the indicated boundary is implied and the effective capture zone size at the study site remains in some doubt.

### 3.1.1.4 Simplified 2D Modeling

The IRT undertook two simple modeling exercises to evaluate and corroborate the estimated extent of capture in the plume area (**Appendix A**) as previously determined using the FEHM model and to make some comparative evaluations of the potential pattern of capture under alternative extraction and injection configurations.

First, a heterogeneous, 2D flow model was prepared to assess the capture of chromium during full IM operations (all injection and extraction wells active) and partial IM operations. The simple model was constructed in Microsoft Excel™ using non-proprietary methods. The base flow system model was prepared by adjusting boundary head values and the internal hydraulic conductivity distribution until the head contours observed in May 2020 (the IM was inactive at this time) were closely matched (**Figures 3-8A and 3-8B**). An aquifer depth of 1,000 feet was assumed for the purposes of mapping the transmissivity field, and reasonably represents the capacity of the aquifer to conduct flow when the IM was active and when it was not. The calculated particle tracks in the base case simulation indicate a chromium plume projected to migrate east-northeast in the plume area (**Figure 3-8B**).

The behavior of the IM system was then examined with two additional simulations: (1) with the IM system in full operation with all CrEX and CrIN wells active at the average values presented in **Table 3-1** and (2) with the IM system in partial operation with only CrEX-4 and CrEX-5 pumping and CrIN-4 and CrIN-5 injecting treated water. Particle tracks were calculated for each of these two simulations. These were used to delineate effective capture zones bounded by divergent particle paths (red lines in **Figure 3-9**). In these simulations, both R-61 and R-45 fell inside the capture zone, suggesting that both options have potential to prevent the chromium plume from spreading eastward from R-70 (**Figure 3-9**). Groundwater at R-70 was captured during full IM operation, but appears to be less likely to be captured under partial IM operation. In both cases, the 2D capture zones were more extensive than those found by Neptune (2023) (**Figures 3-7 and 3-9**).

A comparison of the two IRT simulations (**Figure 3-9**) shows that deactivation of CrEX-1, CrEX-2, and CrEX-3 and CrIN-1, CrIN-2, and CrIN-3 resulted in the southern extent of the capture zone moving very slightly northward, with CrEX-5 picking up some of the captured groundwater previously collected by CrEX-4. Given the uncertainty and simplifications associated with these calculations, a conservative restart of the IM system should consider adding a third extraction well to the CrEX-4/CrEX-5 pair. Perhaps converting CrIN-1 to an extraction well, along with other monitoring wells such as R-70, could provide meaningful

additional capture near the leading edge of the plume. The addition of one or more injection wells should be considered to take on the additional pumped discharges.

Following this numerical modeling exercise, additional calculations were performed using 2D analytical (Theis) superposition methods as described in **Appendix A**. The calculations were completed using a non-proprietary Fortran code developed over 20 years ago for purposes similar to that for which it was used here, and has previously been used numerous times at the U.S. DOE Hanford Site for screening-level analyses of P&T systems. The primary purpose of these calculations was *not* to obtain very accurate estimates of the extent of capture, but rather to obtain approximate extents that could then be used to demonstrate the utility of simple calculations for comparative purposes—for example, in this case, the effect of using alternate injection locations on the anticipated general geometry of capture. The use of 2D methods tends to overestimate the lateral extent of hydraulic containment unless the effects of partial penetration are specifically accounted for using methods such as described by Bair and Lahm (1996). Such adjustments for partial penetration were not implemented in this quick demonstration. Nonetheless, these analytical calculations led to similar conclusions regarding the approximate extents of hydraulic containment when representing similar well configurations as described above, suggesting that while both methods neglect the vertical component of flow, they provide similar conclusions in terms of lateral capture extents and—more importantly—patterns of hydraulic containment that may result from various alternate configurations of injection and extraction wells.

The issue of vertical plume containment has also been modeled in 3D by Neptune (2023). They calculated that vertical containment of contamination occurred to over 360 feet below the water table. For comparison, the deepest screen interval showing chromium concentration above 50 µ/L is at R-45 S2 at about 125 feet below the water table. Although the vertical extent of the chromium plume has not been characterized completely, the modeling strongly suggests that the deep contamination should be captured by the IM where groundwater flows upward to the extraction wells. In contrast to the modeling results, the field data are insufficient to provide evidence that vertical contamination is contained by the IM. This issue requires further evaluation in both data collection and modeling.

### **3.1.1.5 Summary**

Interpretations of data and modeling results remain inconclusive regarding the exact boundaries of capture, especially at the eastern end of the plume. On one hand, water level elevation data and 3D modeling indicate that at full IM conditions, the chromium plume was not contained on the east side. On the other hand, chemical time-series could be interpreted to mean that the plume either was or was not contained. Simplified 2D modeling by the IRT indicates that the capture zone was larger than indicated by the hand-drawn interpretations of the water level elevation data and the 3D modeling.

It is important to note that the size of the capture zone is inversely proportional to the hydraulic conductivity of the aquifer. Although it is not the case everywhere (e.g., **Figure 2-14**), there is some indication that the hydraulic conductivity was underestimated in the central IM area at most of the CrIN and CrEX wells (Tables 1 and 2 in **Appendix D**). If so, all other things being



equal, in this area the actual capture zone would be smaller than the one predicted by the current 3D model if the original data from these wells were used as model input.

### **3.1.2 Is there assurance that existing injection locations appear to be outside the current 50 µg/L, or ppb, plume boundary?**

Yes. The Intellus NM database indicates that as of August 2024, chromium concentrations at all five of the CrIN wells remain near the chromium detection limit of 3 µg/L. The IRT recommends that these CrIN wells be sampled prior to initiation of the IM in a full or partial configuration.

However, overlaying these CrIN locations on the plume footprint as of spring 2023, it is seen that CrIN-1 and possibly CrIN-2 may eventually lie within the 50 µg/L contour area of the plume and at risk of driving concerning levels of chromium outward in an easterly direction (**Figure 3-10**). These wells are in the vicinity of R-45 S1 and S2 and may therefore play a role in the rising chromium concentrations at those monitoring locations. In contrast, the increasing chromium concentrations observed at R-61 do not initially appear to be caused by southerly plume spreading due to groundwater injections. CrIN-3, CrIN-4, and CrIN-5 are all south of the 50 µg/L boundary of the main chromium plume.

### **3.1.3 To what extent are the increasing chromium concentration trends in R-45 S2 and R-61 S1 the result of an adverse impact of current injection locations?**

Following activation of the IM system, two monitoring wells—R-61 S1 and R-45 S2—showed notable increases in chromium concentrations that raised concerns over the effectiveness of the IM pumping and injection. As discussed above, the locations of the CrIN-5 and CrIN-4 wells are inconsistent with a southerly spread of the chromium plume toward R-61 due to injections. However, in combination with pumping at CrEX-2, chromium transported from a location southwest of R-61 could have been redirected to that well in response to the pumping and injection (**Figures 3-10 and 3-11**). This scenario might represent a desirable outcome, as it results in chromium plume capture at CrEX-2 from a western source.

A second alternative to explain rising chromium concentrations in R-61 S1 notes that the gradient in the vicinity of R-61 S1 is upward when the IM system is inactive and, on average, downward when the southern IM or full IM is active (**Figure 3-12 and Appendix K**). This raises the possibility that increases in chromium concentrations at R-61 could be due to higher chromium concentrations moving from the shallow aquifer (less than 50 feet) near the water table downward to the R-61 S1 screen zone during IM operation (**Figure 3-11**).

As noted above, a transitory and weak vertical downward hydraulic head gradient at R-61 developed while the IM system was active (**Figure 3-12A**). During this time, chromium concentrations began rising steadily in R-61 S1 (**Figure 3-12B**), a trend that continued into 2024, even after the IM was deactivated. Although the vertical component of the hydraulic head gradient reverted to upward after the shutdown, it was less pronounced than the ambient condition before IM pumping, which may be a response to increased pumping at PM-4 after PM-3 pumping was discontinued. The weak transitory downward component to the gradient that formed during IM operation frequently reversed for short durations until the IM system was

deactivated, when it began returning to the ambient condition (increased upward gradient). These observations, and the relative positions of the various well screens involved (CrEX-2, R-61 S1, S2), are consistent with a model involving horizontal transport of Cr to R-61 S1 from the southwestern source zone.

As with R-61 S1, the coincidence in timing of changes in chromium concentrations at R-45 with changes to the IM operations suggests a causal link (see **Figures 3-1 and 3-13**). Between January 2018 and fall 2019, when only the southern area IM wells were in operation, chromium concentrations at R-45 S1 appeared to stabilize after a period of increase dating back to 2009 (**Figure 3-1**). The chromium concentrations then began a period of decline that continued after activation of the full IM system. This decline only began to reverse after the 2023 deactivation of the IM system, probably due to resumption of the uncontained, ambient eastward plume migration.

The onset of sustained pumping and injection at CrEX-2, CrEX-4, CrIN-4, and CrIN-5 in early 2018 also coincided with an increase in chromium concentrations at R-45 S2 (**Figure 3-13**). The rate of increasing chromium concentrations was slightly enhanced with activation of the eastern area wells, in particular CrEX-5, CrIN-2, and CrIN-1, in late 2019. In mid-2021 the concentration of chromium in R-45 S2 rose above 50 µg/L. In response, in late 2022, the IM system was changed to operate with only two extraction wells, CrEX-4 and CrEX-5, and two injection wells, CrIN-4 and CrIN-5. This change was immediately followed by a decline in chromium concentrations at R-45 S2 that lasted until the entire IM system was deactivated in early 2023, when concentrations began to rebound.

Unlike the trends at R-61 S1, those at R-45 S2 can be plausibly explained in terms of increasing vertical downward head gradients arising from injection wells. As noted previously, CrIN-1 and CrIN-2 are located close to the leading edge of the chromium plume, as defined by the 50 µg/L contour (**Figures 3-10 and 3-11**). Operation of these wells therefore had the potential to drive chromium mass horizontally outward to the east and vertically downward. The head differences between R-45 S1 and R-45 S2 produced a near-zero vertical hydraulic gradient before IM activation that altered to a more downward gradient while the IM system was in operation (**Figure 3-14 and Appendix K**).

The water level data collected across the site were relatively sparse, and information on vertical hydraulic gradients is based mainly on heads measured in single boreholes containing monitoring wells with two screened intervals. To gain a preliminary view of vertical gradients in full cross section, two transects were examined: a north transect and a south transect (**Figure 3-15**).

Contours were based on IDW interpolations of head data collected in May 2020, before the full IM system was activated, and in March 2022, while the IM system was fully active. The IDW interpolations were conducted on a scale-adjusted x-axis and then transformed back to the original scale for plotting. Conceptually, the scale adjustment accounts for vertical anisotropy ( $\xi = \frac{K_v}{K_h}$ ). In principle, the ratio of fluxes in the vertical and horizontal directions can be corrected for anisotropy by scaling the horizontal (x) axis (Equation 1 [see **Appendix L**]).

$$\frac{q_v}{q_h} = -\frac{K_v \frac{\Delta H_v}{\Delta y}}{-K_h \frac{\Delta H_h}{\Delta x}} = \frac{\xi K_h \frac{\Delta H_v}{\Delta y}}{K_h \frac{\Delta H_h}{\Delta x}} = \frac{\xi x_1 - \xi x_2}{\Delta y} \frac{\Delta H_v}{\Delta H_h} = \xi \frac{i_v}{i_h} \quad (1)$$

Conducting the IDW interpolations on the scale-transformed data serves to weight the horizontal component of the interpolation in proportion to the scale factor, leading to contours that capture the effects of anisotropy. This manipulation is convenient and provides a visual aid for assessing head distributions in an anisotropic aquifer. It is a useful approximation suitable for preliminary calculations and for use in cases where data are sparse. More in-depth analyses require rigorous, geostatistically based schemes to represent anisotropy. However, the finding of higher chromium concentration in the lower well screen of R-70—about 100 feet below the water table—than in the upper screen provides some evidence for a plume that has moved primarily horizontally, but also vertically downward. The limited vertical transport distance compared to the horizontal transport distance (e.g., Herman and Martinez, 2024, p. 11) is attributable to anisotropy in the aquifer.

A comparison of the head distributions from the IDW interpolations along the north and south transects, with IM off and IM pumping on, reveals notable gradients generally leading to some downward flow component (**Figure 3-16**). The gradient is greatest on the west side of the site, apparently leading to an interesting side effect: the interpolated heads indicate the possibility that a tendency for upward flow exists from an elevation of about 5,700 feet msl upward in the vicinity of R-28 on the north transect and R-61 on the south transect. This effect is only weakly supported by measured data, particularly on the north transect, where data from deep screens on the west side of the site are absent. Nevertheless, the upward gradients in the ambient condition, based on field data from R-61 on the south transect, agree with these findings (**Appendix K**). It is further noted that the onset of IM pumping is coincident with the expansion of the zones of downward flow on both transects. These changes in vertical flow could have led to the escape of chromium in the vicinity of R-45 from the capture zone of the IM system.

### 3.1.4 Will the current IM be protective of the environment until a remedial alternative is selected and implemented?

The eastern extent of chromium contamination has not been sufficiently delineated. Groundwater generally flows to the east, and the easternmost extent of contamination lies somewhere east of R-70. The rate of chromium migration in groundwater in places could be as much as a couple hundred ft/yr or higher (Section 2.2.6.3). Chromium concentration has increased abruptly in the past year at R-70 from about 150 to 250 µg/L. Unless modeling or field data present a convincing argument otherwise, it appears unlikely that the full IM or a partial IM would capture contamination that has migrated beyond R-70. Thus, the current IM is not likely to protect groundwater from further degradation east of R-70. Although IM operations would capture and cut off further migration from the main plume flowing eastward toward R-70, the uncontained chromium mass already east of R-70 would be expected to continue to migrate eastward to points of discharge unless it is captured by an additional extraction well.

In the event that the IM is restarted and some chromium escapes capture, it is worth considering the risk that would result. A risk-based approach to remedial design is almost always used in groundwater cleanup projects, where the goal is to remove risks to potential

receptors rather than removing every last molecule of groundwater contamination, which is commonly a practical impossibility. A mass discharge analysis, where the plume size, groundwater flowrate, and plume concentrations are integrated, is a useful way for groundwater experts to gauge the general risk posed by a particular groundwater plume (**Appendix M**).

A mass discharge analysis was performed for the chromium plume site and indicated that (using the most likely site data) about 15 kilograms per year (33 pounds a year) of chromium is transported eastward in groundwater under natural groundwater flow conditions. Due to uncertainties in performing groundwater calculations, the chromium mass discharge could range from 3 to 75 kilograms per year. When a partial restart of the IM system was considered, this estimated mass discharge range dropped to between 0 and 5 kilograms per year (note: 1 kilogram equals about 2.2 pounds).

The IRT wanted to know the theoretical impact of the chromium plume on local users of groundwater. To answer this question, a *hypothetical worst-case scenario*—one that is highly unlikely for multiple reasons—was evaluated. In this scenario, the chromium plume reached the nearest downgradient water supply well, PM-3. The calculations assumed that 100% of the highest-concentration part of the chromium plume impacted water supply well PM-3 sometime in the future (**Figure 3-17**). This approach, commonly used when conducting mass discharge analysis, considers the amount of water and the location of the screened interval for the pumping well (**Figure 3-18**).

The analysis then assumed that there was a partial IM restart (the “4s/5s” Scenario where only CrEX-4/CrEX-5 and CrIN-4/CrIN-5 are operated) and that only the portion of the plume that was not controlled by the IM impacted water quality at the water supply well (To compare these mass discharge scenarios to the State of New Mexico drinking water standard of 50 µg/L, add about 5 µg/L to account for background chromium concentrations.).

The mass discharge analysis provided the following information about the general risk associated with the chromium plume (**Appendix M**):

- For an almost impossible, worst-case scenario where neither the IM nor a final corrective measure is ever enacted, the chromium concentration in the water supply well could increase between 4 and 85 µg/L with an estimated mid-range value of 17 µg/L. In other words, exceedance of the chromium drinking water standard is hypothetically possible but very unlikely.
- For another almost impossible, near worst-case scenario in which a partial restart of the IM occurs but never evolves into the final corrective measure, the chromium concentration in the water supply well could increase to between 1 and 28 µg/L with a mid-range value of 6 µg/L. In other words, exceedance of the chromium drinking water standard is again extremely unlikely to occur.

Overall these results provide the IRT some confidence that an extremely adverse outcome will not occur upon an immediate restart of the IM (or some version of the IM), even if some questions about the aquifer and plume are not fully resolved at restart time.

### 3.1.5 What are the recommendations for maintaining hydraulic control?

The IRT has the following recommendations for maintaining hydraulic control:

1. The IM system should be restarted in view of the results of the field data analysis, 3D modeling, and preliminary 2D simulations.
  - ◇ Accelerate in-depth modeling in 3D to reassess (1) the potential extent of migration beyond R-70 post-IM, (2) new capture zone boundaries for various configurations of a partial IM system, and (3) whether the CrIN wells are associated with downward and lateral flow at R-45.
  - ◇ While the model is being updated, potentially considering revised hydraulic conductivity values presented in **Appendices B, C, D, and E**, an initial IM restart limited to the operation of CrEX-4 and CrEX-5, together with CrIN-4 and CrIN-5, should be implemented.
  - ◇ After this initial restart, a conservative approach to extending the partial IM should consider adding a third extraction well, possibly CrEX-2, to maintain a southern capture boundary that is established south of R-61 and R-50. Also, conversion of CrIN-1 from an injection well to an extraction well should be considered to enhance capture at the plume leading edge. The nature of this extended IM depends on how much of the current injection well capacity is usable, if an alternative cleaned water return system is available, and other factors (see Section 3.3 for more detail on the partial IM restart).
  - ◇ Based on the expedited 3D (updated FEHM) modeling results to predict the downgradient extent of chromium or new field data (e.g., R-73 redrill and R-79 new data gap filling monitoring wells), it should be anticipated that the IM system may need to be expanded to the east with an additional CrEX well, perhaps at or near R-70.
2. Rising chromium concentration at R-45 may be occurring due to vertical migration issues needing further investigation.
  - ◇ Issues related to the occurrence of chromium at deep screens remain poorly understood and require further investigation. Opportunities to obtain data from as many depths as possible from new and existing boreholes are needed to improve our knowledge of the deeper plume.
  - ◇ The lower boundary of the chromium plume should be better defined to assess the possibility of a deep transport pathway.
  - ◇ Any restart of the IM should avoid activation of CrIN-1 (as an injection well), which presents the highest risk of exacerbating downward migration of chromium near R-45. CrIN-2 should only be reactivated with caution, as it is relatively close to R-45.
  - ◇ 3D modeling of the ambient flow system, including various combinations of injection rates (at various combinations of locations), should be conducted to assess the possibility of a downward migration pathway at some locations near the leading edge of the plume and advance the understanding of capture zone boundaries.

3. Rising chromium concentrations at R-61 are more likely to arise from a nearby source to the southwest than plume spreading due to IM operations. In fact, the analysis presented here suggests that the IM is capturing the chromium passing R-61 and should therefore continue operating.
4. Other recommendations are offered regarding control of the chromium plume.
  - ◇ During IM operations, trends in declining chromium concentrations at R-70, and possibly R-45 S1, are explainable without the wells being inside the IM capture zone. Additional effort is needed to gather field data that better define groundwater flow directions, and hence capture zone boundaries—particularly at the plume front.
  - ◇ An upward gradient component at R-70 has been documented under current conditions (i.e., with PM-3 not pumped). If PM-3 is reactivated as a water supply well, the vertical flow directions at R-70 and other leading-edge monitoring wells should be carefully monitored.
  - ◇ Beneficial plume capture and control near R-61 are expected to follow an initial IM restart that is limited to the operation of CrEX-4 and CrEX-5, together with CrIN-4 and CrIN-5.

### 3.2 Topic 2: Chromium Plume Modeling

The IRT was charged with responding to the following questions regarding the modeling being conducted at the site. Most IRT members provided input and opinions in response to the charge question posed regarding modeling. The list of questions is accompanied by abbreviated responses to each question. More detailed narrative follows, providing explanation and basis for the conclusions reached by the IRT.

- Is the software currently used to model the chromium plume at LANL (Finite Element Heat and Mass [FEHM]) appropriate?

*Response:* No. The FEHM code appears to be technically capable. However, there are other codes that are in much more widespread use, such as the MODFLOW family of codes, and more than amply meet the simulation needs. The IRT recommends that the model be converted to the MODFLOW family of codes.

- Are modeling assumptions, inputs, and results reasonable and defensible?

*Response:* The response depends on the specific task for which the model is deployed. It is clear how the current model design and parameterization were obtained (the latter through calibration procedures). However, the resulting parameterization does not adequately reflect site data and analyses, and the model does not reflect the effects of pumping at nearby public supply wells, as well as some other aspects of the CSM. Consequently, some improvements are needed.

- Are there technical issues or data gaps that significantly impair the project's or the regulator's ability to use the model results when making operational or regulatory decisions?

*Response:* Yes. The IRT identified some technical concerns regarding the groundwater model that warrant improvement, including the representation of aquifer parameters, responses to supply pumping, and data gaps regarding the vertical and lateral extents of contamination.

- To what extent can the modeling be relied upon (e.g., predictions) without the data gaps being fully closed?

*Response:* The foregoing concerns require mitigation. However, until that time, the current groundwater model is the best tool for comparative analysis of alternate configurations of injection and extraction for operation of the IM, such as conducting groundwater flow and particle tracking simulations. The IRT did conduct some calculations to demonstrate the potential utility of simpler modeling methods and tools as a companion to the existing 3D groundwater model.

- What limitations should be considered when using the model before the known data gaps are filled?

*Response:* Simulations conducted to date using FEHM are accompanied by uncertainty and limitations, primarily resulting from questionable/uncertain representation of aquifer parameters, incomplete knowledge of contaminant extents, and uncertainty regarding the degree and amount of vertical contaminant migration, among other factors identified in this report.

- What aspects of the existing model are sufficiently mature to predict future plume behavior, and what recommendation(s) does the team have to improve the model's ability to predict future plume behavior (e.g., aquifer test versus slug test)?

*Response:* As noted above, despite some concerns raised by the IRT, the current groundwater model is the best tool for comparative analysis of alternate configurations of injection and extraction for operation of the IM, such as conducting groundwater flow and particle tracking simulations. However, efforts should be undertaken to mitigate concerns raised by the IRT, improve understanding, and update the model including reanalysis of (1) existing aquifer tests (such as presented in appendices to this report) and (2) the hydrostratigraphic CSM, together with new analyses of (a) sedimentary textures, structure, and methods of representation and (b) use of recirculated water quality as de-facto tracers, which are recommended to improve understanding and representation of the subsurface.

### **3.2.1 Overview of Modeling History and Needs**

The IRT was tasked to evaluate containment of the dissolved chromium plume, and whether the modeling conducted toward that effort is appropriate and reasonable. The IM remedy is in place to contain further migration of the plume while a permanent solution is developed, and modeling has been used to guide design and operation of the IM. Groundwater flow (GWF) and contaminant fate and transport (F&T) modeling is often used to support water resource management issues, including analysis of contaminant sources and migration, simulation of alternate interim and final groundwater remedies, evaluation of remedy performance, and

optimization of remedy design and operations. Throughout the stages of site assessment, investigation, remediation, and closure, modeling assists with furthering conceptual understanding, interpreting data, testing hypothesis, evaluating uncertainties (or bracketing results), and predicting future conditions under plausible alternative future decisions so that robust decisions can be made.

GWF and F&T models can be constructed using analytical solutions, the analytic element method (AEM), and numerical simulators for which calculations are made using a discretized “grid.” Many analytical, AEM, and numerical GWF and F&T codes are available that provide widely varying capabilities (e.g., **Table 3-2**). Model applications can also range from simple retrospective (reconstructive) and forward (deterministic) calculations, through inverse modeling (calibration) and beyond into predictive analysis accompanied by parameter or scenario uncertainty. The appropriateness of each modeling method, simulation code, and model application varies at different stages in the lifecycle of large complex projects like the LANL chromium investigation area. In light of this variability, the most suitable modeling methods, simulation codes, and calculations to be used at a particular site can be determined over time by assessing the project status and the current and anticipated modeling needs, recognizing that these often evolve as the knowledge base and needs of the site evolve.

Given the complexity of conditions encountered at the chromium investigation and remediation area, GWF and F&T modeling presents many challenges. The development and application of models has evolved over about 20 years and, at this point in time, the primary modeling objective is to evaluate containment of the dissolved chromium plume by the IM. This objective primarily requires simulation of saturated groundwater flow attended by particle tracking to represent dissolved-phase contaminant transport (refer to **Figure 3-19b**). At a later date, work toward this objective may benefit from simulation of vadose zone flow and migration (refer to **Figure 3-19a**), given that the plume within the regional aquifer is located nearly 1,000 feet beneath the ground surface and that the sources of contamination to groundwater traversed this thick vadose zone (**Figure 3-20**). To achieve this objective of evaluating and improving plume containment, the primary tasks appear to be the following:

- *Hydraulic*: Estimation of aquifer parameters, estimation of the extent of capture developed by various configurations of extraction and injection wells, and estimation of the influence of nearby supply wells on heads and horizontal and vertical gradients within the investigation area.
- *Chemical*: Estimation of the recent 3D extent of chromium dissolved within groundwater, and its approximate conservative (non-reactive) directions and rates of migration so that extraction and injection wells can be appropriately placed and operated.

There is also some value to estimating the locations of chromium sources to groundwater, as well as the associated rates and directions of chromium migration from those sources, to better understand what conditions caused the current estimated plume configuration. This may improve predictions of where the plume is likely to migrate further. However, for purposes of an



interim remedy, this level of understanding is less critical and the lack of knowledge of sources may be mitigated through more extensive delineation of the plume in groundwater.

### **3.2.2 Question 1: Is the software currently used to model the chromium plume at LANL (Finite Element Heat and Mass [FEHM]) appropriate?**

Most GWF and F&T modeling of the chromium plume has been undertaken using the FEHM simulation code (LANL, 2024). FEHM is a 3D finite element code that solves for the flow of a water phase, an air phase, and other nonaqueous-phase liquids with partitioning of constituents among the phases and associated transport of the constituents, along with transport of heat and the overall impacts of solutes and heat, to flow of the fluids. As noted by N3B (2023), FEHM *“can account for complexities associated with partially penetrating wells, aquifer heterogeneity, and complex boundary conditions and has been benchmarked against MODFLOW.”*

The chromium plume model developed in FEHM is a 3D transient GWF and F&T model that represents aquifer properties using a spatially varying parameterization obtained via calibration of both the flow and transport components of the model using the pilot point technique (Doherty, 2003). The model has been used to conduct uncertainty analyses using Monte Carlo techniques that generated 100,000 realizations. During this review, the panel was provided a comprehensive presentation of the development and application of the FEHM chromium plume model and received responses to submitted questions regarding the model development and parameterization, among other topics. Overall, while the majority of the IRT has expressed no fundamental concerns regarding the technical capabilities or simulation accuracy of the FEHM code, it is the consensus opinion of the IRT that selection of and rigid adherence to the FEHM code has contributed to communication and transparency challenges with regulators and the public at large, which have hampered constructive conversation and decision making.

The FEHM code, while capable, was developed primarily to simulate multi-phase and heat-moderated processes, and is both unnecessarily complex and opaque for examining the primary near-term modeling requirements—groundwater flow (only the water phase) and the migration and containment of a single dissolved solute. Furthermore, the FEHM code is rarely used for groundwater analysis and P&T remedy simulations outside of LANL, and does not appear to bring any critical simulation capabilities for the chromium plume modeling effort that are not offered by more widely used simulation codes—in particular, the MODFLOW family of codes (**Table 3-2**). The following are the most recent public-domain and open-source releases of the flow, transport, and integrated versions of the MODFLOW family of codes (other freeware versions of these codes are available from third parties that offer extended capabilities beyond those available with these USGS distributed releases):

- MODFLOW 6: USGS Modular Hydrologic Model – Current Version 6.5.0, Released May 2024 (USGS, 2024)
- MODFLOW-2005: USGS Three-Dimensional Finite-Difference Ground-Water Model – Current Version 1.12.00, Released March 2019 (USGS, 2019a)

- MODFLOW-USG: An Unstructured Grid Version of MODFLOW for Simulating Groundwater Flow and Tightly Coupled Processes Using a Control Volume Finite-Difference Formulation - Current Version 1.5, Released October 2017 (USGS, 2017)
- MT3D-USGS: Groundwater Solute Transport Simulator for MODFLOW – Current Version 1.0.1, Released June 2019 (USGS, 2019b)

As a particular example of simulation capabilities relevant to the chromium investigation and remediation, it is not clear how FEHM is being used to simulate the presence, operation, and impact to horizontal and vertical flows and migration of long-screened “multi-aquifer” wells. Documentation of the FEHM capabilities (e.g., Zyvoloski, 2007) indicates that the code includes an embedded wellbore model (EWM), described as a high-resolution wellbore model for use in carbon sequestration, soil vapor extraction, and petroleum industry applications. This is described by Zyvoloski (2007) as follows:

*“Yield(ing) a complete high-resolution, numerical radial model that is, like the GDPM model, independent of the physics package. The wellbore model simply replaces existing control volumes with the wellbore package.”*

However, it is unclear to the IRT without further investigation whether this package is being used to simulate wells at the chromium investigation site and, if it is, how these numerical capabilities align with the needs for simulating containment and mass recovery at LANL.

In contrast, the MODFLOW family of codes is universally used and was specifically designed to simulate groundwater flow and migration of dissolved solutes—a critical requirement for the current chromium plume modeling exercises—and provides accessible core functionality for such assessments, including explicit simulation of features such as drains, rivers, flow to a wellbore, and flow to wells that tap multiple hydrogeologic units. As one example, the MODFLOW family of codes includes a number of specialized capabilities for simulation of long-screened pumping and monitoring (zero net flow) wells (Neville and Tonkin, 2004; Neville and Zhang, 2010; Ma et al., 2011 and 2012), which would be ideally suited to simulation of both the remedy injection and extraction wells (Cr-In and Cr-Ex) and the nearby supply wells (i.e., PM-series wells). Similar capabilities are available with the PNNL simulator Subsurface Transport over Multiple Phases (STOMP) (PNNL, 2024), but it is not clear if these capabilities are available or in use with FEHM at the LANL chromium site, and STOMP may lack other capabilities desirable for the chromium investigation area analyses.

In addition to the foregoing technical concerns, a brief internet-based review of local news sources indicates that concerns have been raised regarding the technical veracity and transparency of the FEHM code (e.g., CCNS, 2023; Arends, 2023).

While the foundations of any technical concerns raised in such articles regarding the FEHM code have not been demonstrated to our knowledge, these examples further illustrate that trust in the modeling conducted at the chromium investigation site is hampered, rather than supported, through the use of FEHM.

In conclusion, the response to Question 1 is “no.” The FEHM code appears to be technically capable. However, there are other codes that are in much more widespread use, such as the MODFLOW family of codes, and more than amply meet the simulation needs. The IRT recommends that the model be converted to the MODFLOW family of codes. The IRT recognizes that NMED may not possess substantial internal subject matter expertise in hands-on modeling with either FEHM or MODFLOW, such that the selection of code might not appear to be consequential with respect to NMED’s capabilities and engagement. However, there is a much larger community of MODFLOW users that could bring valuable modeling expertise to NMED, facilitating a more collaborative project atmosphere, especially considering that NMED has specifically requested that MODFLOW be used. It is also understood by the IRT that NMED has on previous occasions contracted with specialized companies to obtain technical modeling services. It is the opinion of the IRT that a transition to modeling with the MODFLOW platform would not add undue effort or complexity to the modeling efforts; rather, it would fairly quickly simplify and streamline the modeling process, while at the same time providing for greater transparency and independent review.

### **3.2.3 Question 2: Are modeling assumptions, inputs, and results reasonable and defensible?**

In very general terms, it can be appreciated that the current assumptions and inputs to the existing FEHM model were developed based upon many years of model development, application, calibration, and uncertainty analysis. The monitoring network is (as is typical) not sufficient to provide the horizontal and vertical spatial data to identify all potentially significant heterogeneities and produce a unique calibration. Given the spatial limitations in well and borehole data, the DOE-EM-LA and regulator teams have done a commendable job in opportunistically collecting and using data, including detailed chemistry and multi-well tracer data, during investigations and IM P&T operation. The modeling approach uses state-of-the-art calibration techniques to infer aquifer properties from available data; however, because the data available are—as is often the case—insufficient to identify these properties uniquely, uncertainty analysis has been conducted.

However, despite these commendable efforts, the IRT is concerned that the structure and parameterization of the method rests on a CSM and some particular assumptions that are no longer the “best” assumptions. Also, the parameterization has strayed from the most plausible representation of conditions, and would now benefit from revisions and updates—possibly using alternate methods of representing aquifer heterogeneity. These concerns are detailed in the following subsections.

#### **3.2.3.1 Hydraulic Conductivity**

Several IRT members raised concerns that the parameterization of aquifer properties (i.e., hydraulic conductivity, anisotropy, and storage) in the model does not appear consistent with general expectations given the depositional character of the relevant geological formations. For example, investigations indicate that the subsurface around the investigation area exhibits geologic formations that, though similar in many characteristics, demonstrate moderately different central-tendency values for hydraulic conductivity. These formations are in hydraulic

connection and do not exhibit differences over orders of magnitude. Therefore, they do not serve to separate the subsurface into different aquifers; they simply represent differing bulk properties within the unconfined aquifer. The IRT understands that, perhaps as a result of these differences being apparently moderate, the calibration represented these materials as a single “unit” exhibiting a single central-tendency about which substantial variation is inferred using pilot points. However, doing so may have inhibited the ability of the calibration to identify meaningful differences in properties associated with different strata, which may be informative regarding the potential for vertical migration of contamination and the relative lateral and vertical extents of hydraulic containment developed by the IM. An alternate parameterization and regularization approach that enables the mean values to differ between these units without penalty may have elucidated such systematic contrasts.

In addition—or possibly, as a consequence—the ranges of parameter values obtained using the pilot point technique appear implausible. To determine this, the IRT examined the parameters assigned to the FEHM model nodes/cells. The values had been allowed to range widely, suggesting that there were insufficient regularization constraints applied to ensure plausibility of the inferred parameters. The IRT identified conceptually unlikely and incongruous parameter combinations. For example, calibrated values for the horizontal and vertical hydraulic conductivity span several orders of magnitude, resulting in (1) values for vertical anisotropy that also span orders of magnitude, including values that are much greater than 1 and also much smaller than 1 (e.g., **Figures 3-21 and 3-22**), and (2) values for horizontal anisotropy that in places are orthogonal to those that would typically be expected based on the deposition environment for the sedimentary units. This appears to occur because the single aquifer anchor/pilot point calibration process is agnostic to the process-based subsurface structure, and improvements may be possible based on sequence stratigraphy principles and the expected facies-based structure of these deposits. For example, as detailed in Section 2.2, the Puye Formation is a fanglomerate, and fanglomerates typically comprise “*heterogeneous fragments of all sizes, initially deposited in an alluvial fan and later cemented into a firmer rock...*” Deposition of alluvial fans produces channel features (“lineaments”) that would constitute preferential pathways in the groundwater system. Such pathways are one hypothesis that would provide a basis for connectivity (or lack of thereof) in the aquifer beneath LANL. The existing model attempts to represent this through statistical correlations and anisotropy; however, this does not reproduce geometries, spacing, and shapes expected in an alluvial fan.

There are numerous literature studies and published model applications in which expected depositional features are incorporated into the model setup and calibration. One possible CSM that could be explored for the chromium plume might be to build in expected fanglomerate geometries with constraints based on tracer results. Such a “facies-informed” modeling approach, along with other parameterization alternatives, could be initially explored outside of the main model to assess if the alternative would be useful and defensible, would provide improved fidelity to the real system, and would provide more robust support to DOE-EM-LA, NMED, and others. Closer fidelity of the numerical model to recognizable facies may also improve communication of, and confidence in, the model.

The IRT also expressed concern that in addition to exhibiting a large and unsubstantiated degree of variability of hydraulic parameters—that does not conceptually align with the expected patterns given the sedimentary deposits—the central tendency of the estimated parameter fields does not correspond well with estimates obtained independently from the analysis of both planned and opportunistic aquifer testing data (See Section 2.2.4.2). In brief, though the hydraulic conductivity of the Puye Formation should be variable due to its heterogeneous nature, it is important that the bulk properties represented in the groundwater model reflect bulk values obtained independently. Members of the IRT reevaluated aquifer test data from the CrEX and CrIN series of wells and found the horizontal hydraulic conductivity range from 12.5 ft/d to 172 ft/d, with the highest values at CrEX-2 and CrEX-5; data for the CrIN wells were less variable in  $K_h$  (26 ft/d to 75 ft/d). Comparing these values for hydraulic conductivity with the estimates obtained by Neptune reveals an overall higher mean in the IRT estimates. Details of these analyses are addressed further in several analyses presented in their complete form under **Appendices B, C, D, and E**).

Systematic misestimation of aquifer hydraulic conductivity could have substantial implications. It is well known that for a single extraction well pumping from an (ideally, confined) aquifer exhibiting a uniform (planar) hydraulic gradient, the width of the capture zone is given by the relationship  $W = Q/KBi$ , where  $W$  is the width,  $Q$  is the pumping rate,  $i$  is the hydraulic gradient,  $B$  is the aquifer thickness, and  $K$  is the aquifer hydraulic conductivity. From this admittedly simplified relationship, it is seen that systematic underestimation of the aquifer conductivity would tend to lead to (1) underestimates of the migration rate of chromium and (2) overestimates of the width of hydraulic containment developed by pumping at extraction wells. This could potentially result in underdesign and undersizing of the IM and final groundwater P&T remedies. Given that these apparent differences in estimated aquifer properties could have important implications for modeled scenarios involving migration and containment of chromium, the IRT recommends that the sources of the values provided by Neptune and included in the groundwater model be further investigated and reconciled before proceeding with further modeling.

### **3.2.3.2 Representation of PM Wells**

The IRT expressed concern that the potential influence of the nearby public supply wells on groundwater conditions and the lateral and, perhaps most importantly, vertical migration of chromium is not considered in the current FEHM model. The location and inferred potential influence of the nearby public supply (PM-series) wells on groundwater in the unconfined aquifer at the chromium investigation area is discussed in Section 2.2.4. In brief, although the PM-series wells have very long screened intervals and the majority of the screen is below the Miocene basalts, Harp and Vesselinov (2011) reported evidence that PM-3 and PM-4, and to a much lesser degree PM-2, cause drawdown responses in the chromium plume area wells. Furthermore, Broxton (2024b, slide 18) wrote:

*“... Pumping effects from PM-2, PM-4, and PM-5 occur above the Miocene basalts and propagate laterally along bedding towards the Chromium monitoring wells.”*

In addition, there appears to be a vertical hydraulic gradient component that leads to downward flow, possibly related to pumping of the regional supply wells—likely in addition to other causal factors (recharge, etc.).

None of the foregoing potential impacts of the PM-series wells are, to the knowledge of the IRT, currently included in the FEHM modeling.

### **3.2.3.3 Model Scale**

The IRT expressed some concern that the fairly local scale of the FEHM model may overdetermine some of the simulation results.

GWF and F&T modeling at these fairly local scales has so far required models with relatively small domains that do not include important hydrogeological features, such as the Miocene basalt layer at depth, which rises to elevations comparable to the plume elevation about 1.5 miles east of the present plume location. In addition, the PM supply wells are not included in plume-scale models although these wells pump at significant rates that may influence water levels in the plume area. Lastly, water levels in the canyon have been steadily declining for the past decade, partly in response to the PM pumping (Foster, 2024c). In contrast, regional models of the Pajarito Plateau have been performed (e.g., Frenzel, 1995), which reflect the general features of flow in the Mortandad Canyon area (**Figure 3-23**). However, they lack detail in the plume area and would not be suitable for purposes of the chromium investigation and remediation. For example, the boundaries might be extended to include significant regional water production wells and LANL facility operations (currently including supercomputers and other activities that require large amounts of groundwater), and the Los Alamos community shares the groundwater production well infrastructure. The production wells that provide the needed quantities of water (circa 1.6 billion gallons per year) are generally screened below the shallow groundwater zone (where the chromium plume resides) and to substantial depths. Although PM-3 is currently not being pumped (due to concerns about drawing in contamination from upgradient), the overall operation of the production wells and discharge of some water into surface water features that redistribute water downcanyon may contribute to flattening of the water table locally. The existing FEHM model does not appear to adequately predict this flattening gradient and revisions to the geology (described elsewhere in this report), and the model boundaries may facilitate improved correspondence. It is noted, however, that if the eastern boundary were to be extended too far (e.g., past the Rio Grande), this would encroach on the Buckman wells, which would likely add complexity and other concerns without adding value to the local simulations. Therefore, a compromise scale of simulation is needed; that compromise might be met by extending the groundwater model boundaries or using alternate model discretization techniques, or by using a combination of these approaches.

### **3.2.3.4 Uncertainty Analysis**

Another concern raised by the IRT regarding the modeling efforts is that although substantial computational effort was expended on parameter uncertainty (potential variability) analysis, too much emphasis has been placed on the use of Monte Carlo techniques for parameter analysis, and sufficient emphasis has not been placed on other important and higher-level aspects of

uncertainty. Recognizing that parameter uncertainty (variability) must be evaluated, communicated, and discussed with NMED and other stakeholders and that this is an important aspect of the modeling work, the utility and cost-benefit of conducting computationally intensive Monte Carlo calculations generating 100,000 realizations is—for most applications at the chromium investigation area—questionable. In particular, the uncertainty analysis emphasized varying the parameters of the numerical model, while setting aside the potentially larger implications of uncertainties arising from using the “lumped” geologic conceptualization and regularization scheme versus alternate conceptualizations that represent either textural and facies relationships and/or mean-adjusted values for different geologic formations. The IRT concluded that alternate conceptualizations and representation of the formations and deposits within them should be evaluated before conducting further numerical Monte Carlo type analyses. When calibration and uncertainty analyses are conducted, additional constraints (“rules”) may be needed to ensure that the parameter estimates so obtained are realistic and technically defensible (i.e., that they are consistent with the CSM). The use of supplemental rules or guardrails should improve future statistics-based calibrations so that the combination of parameters better aligns with conceptual expectations—for example, so that the ratio  $K_h/K_v$  lies between 1 and 200 with a typical value in the 50 range for these types of materials.

Lastly, it appears that while uncertainty analyses conducted using the model incorporated a range of porosity values, typical simulations used a uniform porosity value while varying hydraulic conductivity and storage values that represented inferred confined storage conditions for the different formations. The use of a uniform porosity value throughout the model and in all geologic units contrasts strongly with the variability in other aquifer parameters, particularly the very wide range of horizontal and vertical conductivities inferred through calibration, as well as the resulting anisotropy values. These and other similar conflicts in the relationship between different aquifer parameters and the underlying stratigraphic CSM could be alleviated through use of sequence-stratigraphy and/or texture-based techniques for developing parameter fields (structures/patterns) and inferring parameter values through both the calibration (inverse) and uncertainty analysis procedures. For example, the program Texture2Par (Scantlebury et al, 2022), developed for the California Department of Water Resources (DWR), was designed specifically to assist in the use of sediment texture data to derive and estimate aquifer parameters in groundwater models (non-proprietary, available at S.S. Papadopulos & Associates, Inc. website under [Aquifer Parameter Tool \(Texture2Par\) Development](#)). Although developed primarily for models constructed using MODFLOW and the DWR Integrated Water Flow Model (IWFM), Texture2Par could be easily adapted for use with FEHM, and already incorporates the pilot point technique used by Neptune (2023) in their model calibration, but combined with texture information.

### **3.2.3.5 Conclusion**

The response to Question 2 is “no.” The response depends on the specific task for which the model is deployed. It is clear how the current model design and parameterization were obtained (the latter through calibration procedures). However, the resulting parameterization does not adequately reflect site data and analyses, and the model does not reflect the effects of pumping at nearby public supply wells, as well as some other aspects of the CSM. The model

parameterization and uncertainty analysis appear to “blur” the representation of the major formations as identified in the geological CSM. Consequently, some improvements are needed. Some of these issues may be alleviated through the use of sequence-stratigraphy and/or texture-based techniques for model parameterization.

### **3.2.4 Question 3: Are there technical issues or data gaps that significantly impair the project’s or the regulator’s ability to use the model results when making operational or regulatory decisions?**

It is important to recognize that there are always data gaps in groundwater investigations, no matter how much data are collected and analyses undertaken; nonetheless, decisions have to be made. It is common in modeling projects that many assumptions can be reasonably challenged—in broad strokes—including representation of the hydrogeologic system, unit thicknesses, and hydraulic properties. The impact to decision making of assumptions and data gaps can often be bridged by communicating the degree and likely impact of data gaps, determining whether the gaps can be mitigated through further data collection or accommodated via uncertainty analysis, and evaluating the relative worth to required decisions of alternate data collection or analysis activities. Such an adaptive management strategy can in turn be facilitated by developing a model framework that is easy to understand, flexible, and robust. This framework is important for quick turnarounds and conducting conceptual uncertainty analyses to fill in the “what-ifs” that are unknown so that the reliability of the results is assessed. The data gaps that the IRT identified at the chromium investigation area are fairly typical, and result in uncertainty in predicted flow directions and magnitude, contaminant transport, and the efficacy of the IM. Some of these gaps in knowledge and/or representation in the FEHM model are detailed in previous sections of this report. These include the need to better address the potential impact from operation of the PM-series wells and representation of aquifer properties, particularly hydraulic conductivity. Additional data gaps identified by the IRT are listed in the following subsections, with limited accompanying discussion:

#### **3.2.4.1 *Horizontal and Vertical Hydraulic Gradients***

The existing FEHM model does not appear to adequately predict the changing slope of the horizontal hydraulic gradient moving from west (upgradient) to east (downgradient), where a noteworthy “flattening” is evidenced in the area of the chromium plume. Specifically, an important aspect of the hydrogeology in the plume area is the notable decline in eastward hydraulic gradient that begins immediately west of the plume. The gradient increases again east of the plume, where it alters direction to the southeast. The existing regional models do not fully explain this variation in horizontal hydraulic gradients. The local models go some way to duplicating this change in gradient by adjusting model boundaries—mimicking the effects—rather than incorporating the actual causes which, based on the IRT review, may include but are not limited to operation of the PM-series wells and relevant geologic features. It is likely that revisions to the geology (described elsewhere in this report) and to the model boundaries may facilitate improved correspondence with this change in horizontal hydraulic gradient and, relatedly, groundwater flow and chromium migration rates.



With regard to vertical gradients, analyses undertaken by the IRT (detailed in **Appendix K**) suggest that vertical gradients respond strongly to operation of the CrEX and Cr-In wells, but may also respond to other system stresses. The IRT is concerned that the current model does not include sufficient representation of the vertical structure (i.e., layering and stratification) to confidently test for these various potential causes. Consequently, it cannot be determined with confidence whether operation of the IM CrEX and CrIN wells develops sufficient capture in the vertical direction to prevent further migration and contain the contamination within the existing footprint.

#### **3.2.4.2 Chromium Sources and Transport**

The IRT identified three particular concerns regarding the sources, transport, and fate of chromium. Although these concerns are most pertinent to longer-term simulations and final groundwater remedy design considerations—including the estimated time to cleanup under a final remedy—these concerns are raised here so they can be considered as the current modeling moves forward.

First, there is insufficient information regarding the location and rates of chromium mass flux to groundwater—encompassing the geographical location, lateral extents, historical loading rates, and potential future loading rates. This is recognized by the DOE-EM-LA modeling team, which has undertaken a large number of history-matching simulations as one effort to reproduce sampled concentrations of chromium in groundwater while representing the loading of chromium from the vadose zone via multiple “drip zones.” The drip zones are typically represented as ellipses, with the centroid and the lengths and orientation of the major and minor axes apparently determined via calibration/sensitivity analyses.

Second, the transport of chromium is currently represented in the FEHM model as the movement of a conservative, non-reactive solute. While this may be appropriate for an interim remedy, for final remedy design, both attenuation and possible reduction processes should be considered in the event that a combined P&T and monitored natural attenuation (MNA) “hybrid” remedy is considered. For example, at the present time, transport modeling neglects the possible contribution to chromium migration and attenuation of reduced and metals-bearing minerals within the Miocene sediments and basalt formations. This is reasonable, and typically conservative (i.e., predicts the most rapid and extensive migration). However, when non-reactive transport is assumed in coupled GWF and F&T model calibration—as has been done in this case—it can lead to bias in estimated values for the flow model parameters, which can have implications for capture zone determination and other aspects of remedy design.

Third, as noted elsewhere in this report, the specific types of sedimentary facies encountered in the chromium investigation area would be anticipated to exhibit preferential patterns of longitudinally oriented connectivity resulting from deposition of coarse-grained materials in channels. This facies-driven anisotropy would exert a strong influence on chromium migration patterns and rates. Site characterization data may never clearly elucidate these patterns. They may need to be assumed based on geological principals and depositional understanding (sequence stratigraphy and textural analysis) and incorporated into the model on that basis.

### **3.2.4.3 FEHM Code Formulation**

A technical concern regarding FEHM was raised by the IRT that was resolved late in the period of review of the FEHM modeling and underlying simulation code. Concerns were raised regarding the formulations presented in the FEHM documentation—specifically regarding Equations 76 and 77 of the FEHM model documentation (Zyvoloski et al., 1999, pp. 40-41). In the FEHM documentation, the velocity term is defined as the Darcy velocity (Zyvoloski et al., 1999, p. 16); however, it is understood that this should not be a Darcy velocity, but rather the groundwater velocity, which is the Darcy velocity divided by the effective porosity. This issue was resolved through correspondence between the IRT and technical representatives of DOE-EM-LA and determined to arise from typographical errors in the documentation, which the IRT was informed will be resolved. Late in the IRT review process, in part due to these concerns that were raised by some members of the IRT, the IRT was provided and reviewed documentation describing several “benchmark” calculations comparing the FEHM code outputs to other analytical and numerical simulators, which provided assurance that the FEHM code properly implements the underlying equations. If DOE-EM-LA is agreeable to and undertakes the transition to a more commonly used, preferably MODFLOW-based, simulation platform as recommended by the IRT, that transition process is the ideal opportunity to prepare a benchmark comparison of FEHM with MODFLOW for the particular conditions encountered at the chromium investigation area, providing confidence in both past and future modeling efforts.

### **3.2.4.4 Conclusion**

The response to Question 3 is “yes.” The IRT identified some technical concerns regarding the groundwater model that warrant improvement, including the representation of aquifer parameters, responses to supply pumping, and data gaps regarding the vertical and lateral extents of contamination.

### **3.2.5 Question 4: To what extent can the modeling be relied upon (e.g., predictions) without the data gaps being fully closed?**

DOE-EM-LA and its contractors conducted a large number of hydraulic and chemical simulations using the existing groundwater model. The FEHM model was developed using available field data and interpreted geology, and was calibrated against observed water levels and conceptual migration pathways. The model was also calibrated to observed chromium concentrations and was further used to estimate impacts of the extraction and injection system currently in place. The model has been documented in a series of reports and presentations and, based on the IRT review, the model has performed fairly well in reproducing measured groundwater levels, inferred groundwater flow gradients, and overall patterns of area-wide chromium plume migration through part of 2022.

The IRT has not been provided with plume maps to show post-IM predicted spatial extent of chromium. The FEHM modeling does not appear to have provided insight with regard to certain important aspects of the chromium migration:

- Modeling did not appear to provide insights into the migration behavior noted near CrIN-06 (which was later converted to CrEX-5) and new monitoring well R-70 on the eastern side of

the plume, where chromium appears to have migrated deeper into the aquifer than anticipated.

- Modeling did not appear to provide sufficient insight into the chromium migration and extents to prevent the installation of injection wells in areas exhibiting chromium concentrations above applicable standards.

These findings suggest that while the overall area-wide flow simulations produced with the FEHM model are plausible, the resulting transport simulations have not proven as reliable and instructive as hoped for by the DOE-EM-LA team. The possible causes of these shortcomings are many and are detailed throughout this report, and recommendations are provided at the end of this section in an effort to reconcile them. However, in general terms, the IRT is of the opinion that the flow component of the FEHM model (attended by particle tracking) continues to be useful for comparative assessments of alternate remedies, but neither the flow nor transport components of the FEHM model should be relied upon quantitatively until improvements are made along the lines of those recommended in this report. Furthermore, if the FEHM model continues to be used, the IRT recommends that conclusions drawn on the basis of flow and particle tracking simulations should be corroborated using simpler calculation methods and tools to provide assurance to NMED and others that the results are both plausible and reliable. To demonstrate this, the IRT prepared a series of calculations to demonstrate the utility of simpler modeling methods and tools for the purpose of comparative remedy analyses. The results of these simple analyses are presented in **Appendix A** and discussed in various sections of this report where restart of the IM in alternative configurations is addressed.

The response to Question 4 is that the concerns raised in response to Questions 1, 2, and 3 require mitigation. Until that time, the FEHM model is the best tool for comparative analysis of alternate configurations of injection and extraction for operation of the IM (i.e., flow and particle tracking simulations only).

### **3.2.6 Question 5: What limitations should be considered when using the model before the known data gaps are filled?**

The responses to Questions 2, 3, and 4 provide the technical basis for responding to Question 5.

The response to Question 5 is that simulations conducted using FEHM are currently accompanied by uncertainty and limitations in several areas, primarily resulting from questionable representation of aquifer parameters, partial knowledge of contaminant extents, and uncertainty regarding the degree and amount of vertical contaminant migration, among other factors. For this reason, while the FEHM model is currently the most capable tool available for comparative analysis of alternate configurations of injection and extraction for operation of the IM (i.e., flow and particle tracking simulations only), its use should be accompanied by simpler calculation methods and tools to provide assurance to NMED and others that the results are both plausible and reliable. The IRT completed demonstration calculations for this purpose.

### **3.2.7 Question 6: What aspects of the existing model are sufficiently mature to predict future plume behavior, and what recommendation(s) does the team have to improve the model's ability to predict future plume behavior (e.g., aquifer test versus slug test)?**

The responses to Questions 2, 3, and 4 provide much of the technical basis for responding to Question 6. Although the IRT has not seen results of FEHM predictions beyond mid-2022, the IRT concluded that, given the absence of other tools at the present time, the existing model could be used to evaluate alternative configurations of the IM for capturing contamination, including whether to convert some wells from injection to extraction (i.e., flow and particle tracking calculations). The current model could also be used to test the impact of a quick restart of the IM in regions where it is inferred to be currently reliable and where the consequences of recognized limitations and data gaps are small. However, such simulations should be accompanied by simpler calculations (such as those demonstrated in this report) to provide confidence in the results so that consensus might be obtained with NMED and other parties such that the IM can be restarted, contaminant mass removed, and growth of the plume mitigated. The detailed simulation of system operations should only be implemented after a more consensus-derived model is developed and various uncertainties identified throughout this report are further evaluated.

For far-field modeling, long-term predictions, and (reactive) transport simulations, the existing model requires further development and testing. This is because, among other factors, (1) the causes of hydraulic gradient patterns are not well understood, (2) the source term boundary conditions from the vadose zone are highly uncertain such that the input locations and rates, and therefore migration rates and arrival times and projected source mass flux, are poorly constrained, and (3) there is significant uncertainty in contaminant mass distribution and aquifer heterogeneity, and representation of the latter in the model is questionable.

The response to Question 6 is that, until the foregoing concerns are resolved, the FEHM model is the best tool for comparative analysis of alternate configurations of injection and extraction for operation of the IM (i.e., flow and particle tracking simulations only). Reanalysis of (1) existing aquifer tests (such as presented in appendices to this report) and (2) the hydrostratigraphic CSM, together with new analyses of (a) sedimentary textures and structure, and (b) recirculated water quality as de-facto tracers, among other activities, are recommended to improve understanding and representation of subsurface conditions. A complete list of recommendations for improving the modeling at the chromium investigation area is provided at the end of this report section.

### **3.2.8 Summary**

The panel concludes that this is an opportune time to take a step back in the development and application of models at the site and conduct a "lessons learned" activity to determine a best-value determination for current and projected future modeling needs. Modeling will be required throughout the remedy lifecycle, and a decision must be made as to which modeling methods and codes bring the most value to the project needs. It was partly due to concerns raised regarding modeling (together with other unanticipated developments in the field) that the IM was

shut down until the IRT convened to develop recommendations. Considering the diverging opinions of DOE-EM-LA and NMED and the resulting temporary impasse regarding IM operation, the IRT considered it critical that consensus be built on the use of modeling during IM operation and transition to a final remedy, as modeling could play a critical role in such processes.

The current FEHM model—supported by decades of groundwater levels, concentrations, and other data—was implemented using state-of-the-art tools for model calibration and estimation of uncertainty considering contaminant concentrations and groundwater levels. The model has been refined and updated in response to new data, including several years of IM operation. However, significant issues were identified that need to be addressed to implement a modeling framework and process that is sufficiently robust to support the longer-term remedy selection and formal remedy documentation. All models are simplifications of the natural system, and will therefore not capture/represent all potentially important features and processes. This model is no exception, but the simplifications are potentially significant in this heterogeneous system when the current model is applied to specific scenarios/objectives, and the IRT has developed a series of recommendations to take modeling forward. The recommendations attempt to harmonize the model with the CSM and available data so that it reflects regional heads and hydraulic gradients without prescribing them by (1) extending boundaries beyond the LANL/community production wells horizontally and vertically to the bottom of the Miocene sediments having around 5,000-foot aquifer thickness, (2) minimizing the occurrences of unrealistic parameter combinations, (3) simplifying the model while discretizing key geologic layers (e.g., basalt) and including structural geometry such as the layers dipping to the west, (4) validating modeled aquifer parameters and considering the potential of facies structure and texture when assigning those parameters, and (5) performing modeling using codes that support independent verification.

To begin, the IRT recommends that a new base-case model be developed in a more accessible simulation code and platform using a structure and parameterization that is more consistent with the CSM and independent information regarding aquifer parameters. Furthermore, considering that the current numerical model cannot explain certain aspects of recent plume behavior, the IRT suggests revisiting features of the CSM and considering different plausible variations of those features that may also simulate site conditions and fit available data. To accomplish this, the IRT suggests undertaking some analyses using a multi-model approach whereby alternate conceptualizations are tested and used to assess uncertainties, with the most behavioral of those carried forward into one or more “best” models. These efforts should be undertaken in collaboration with NMED and OSE. From this baseline, further model development should be undertaken to the extent possible while engaging regulators in a transparent process possibly facilitated by workshops at key project milestones or decision points. A recent example of such an exercise is provided at Kirtland Air Force Base, where NMED participated and was instrumental in past modeling activities for the ethylene dibromide plume. The IRT recommends strongly that elements of the IM be reactivated. Considering site observations and understanding gained from IM system startup to shutdown and beyond, the IM should be reactivated without waiting for these modeling suggestions to be implemented in full.

### 3.2.9 Recommended Actions

The following are recommended actions to mitigate concerns raised by regulatory representatives, to which the IRT is largely sympathetic. All recommended actions should be coordinated with NMED to the extent practical:

1. Lessons learned from previous groundwater modeling efforts should be documented concisely to provide a basis for improvements.
2. A concise “groundwater modeling needs assessment” should be conducted to identify required core or priority simulation capabilities, as well as additional capabilities that may be desirable or necessary for future analyses.
  - ◇ Recognizing that vadose zone modeling may be required, this needs assessment should identify likely capabilities required for that purpose.
  - ◇ The needs assessment should identify whether fully coupled variably saturated simulation capabilities are necessary, or whether future vadose simulations could be “linked” to a saturated (groundwater) simulator providing computation efficiencies. Note: *It is the majority opinion of the IRT that the latter is sufficient and appropriate for the conditions encountered at the LANL Cr(VI) investigation area.*
3. Future groundwater modeling should be undertaken using the MODFLOW code platform.
  - ◇ The specific variant of the MODFLOW platform to be used should be determined at the conclusion of the lessons learned (Recommendation 1) and modeling needs assessment (Recommendation 2) in collaboration with NMED among others. Note: *It is the majority opinion of the IRT that either MODFLOW-6 or another public-domain/freeware version of MODFLOW and MT3D are likely to be suitable for all presently envisioned simulation requirements.*
  - ◇ If necessary, in the interim, a companion to the existing FEHM model could be developed using the MODFLOW code platform to facilitate review by the regulatory agencies and their consultants, so that updates can be made to the underlying CSM, discretization, boundary conditions, and simulation packages (among other aspects of the model), concluding with a consensus 3D model built from the MODFLOW platform.
4. During this transition, evaluate the model geographic and vertical extents and the potential benefits of hybrid-scale (dual-model or flexible local area grid refinement) modeling approaches that provide for sub-regional modeling capabilities to ensure consistency with water budgets and boundaries, as well as refined local-scale flow and transport capabilities.
5. The “base” initial model obtained at the conclusion of the transition to the MODFLOW platform should employ simpler parameterization founded on the lessons learned and modeling needs assessment. Typical forward simulations should be undertaken using this more parsimonious parameterization that is, on average, consistent with bulk properties. Model selection criteria, L-curve analysis, other trade-off analysis, or other methods may be used to identify this “base” model parameterization for most applications. Greater parameter and scenario flexibility is encouraged during analysis of parameter uncertainty or remedy

performance or, for example, when evaluating the likely robustness of potential remedy improvements (i.e., optimization).

6. During model calibration and uncertainty analyses, parameterization and regularization schemes should be more firmly anchored to the underlying hydrogeological CSM. For example (1) mean property values should be allowed to differ between different contrasting formations, with any regularization (similarity) constraints only applying within formations and not across them and (2) regularization strategies (and post-audits/reviews) should emphasize the plausibility of estimated parameter fields (e.g., presence of “inverted” anisotropies).
7. Also, during the model development and calibration, depositional process and facies-informed methods of model parameterization should be explored in both forward and inverse modeling phases. Although such parameterization methods can be challenging to calibrate, their use tends to result in more plausible representation of the geologic system and consequently greater understanding by relevant parties and more acceptable simulation results.
8. Use alternative conceptual models (ACMs)—facilitated by the simpler “base-case” model parameterization and accessible simulation code—to investigate the potential impact of important conceptual questions such as (1) the potential impact of vertical gradients, partial penetration, and PM-series well pumping, on hydraulic containment, (2) the potential sensitivity of the interim remedy efficacy to the presumed properties of the basalt, and (3) the potential for substantial inflows to the area from adjacent canyons.
9. Provide workshops or establish technical working groups for the regulators, other stakeholders, and any contracted SMEs regarding the use of modeling at the site, enabling them to engage more directly. Subsequently, develop communication channels to keep stakeholders apprised of model developments.

The following recommendations pertain primarily to longer-term applications of the F&T component of the groundwater model, particularly as progress is made toward transitioning to a final remedy when efforts will be needed to estimate the time required to achieve remedial action objectives:

1. Consider alternative source mass flux prediction strategies such as transfer function methods to better match past and projected chromium input from the vadose zone. Improvements and lessons learned from these methods may help inform decisions related to future vadose zone source flushing or control activities (e.g., by contrasting the potential value of vadose flushing, surface infiltration relocation/reduction, chromium stabilization, or various alternative sequenced/combined actions).
2. Refine estimates and projections of source mass flux from the vadose zone, and the locations and sizes of the entry locations, based on characterization information and the methods described above.
3. Evaluate appropriate methods for simulating the reactive transport of chromium in groundwater using methods that can reproduce probable transport characteristics discussed

in this report, including bulk mass transport, fast pathways, and attenuation via ion exchange/surface complexation and other processes specific to chromium. These simulation capabilities will be required to design, scale, and provide time-to-cleanup projections for a final remedy.

### **3.3 Topic 3: NMED Ground Water Quality Bureau Acceptable Corrective Actions and Conditions in September 6, 2023 Letter Appendix A Proposal**

The following charge questions are addressed in this section:

1. Are the proposed Appendix A conditions appropriate as part of the IM or more suited for remedy selection?

*Response:* NMED's proposed conditions do not appear to be unreasonable to include in the restart of partial IM operations. However, maximum flexibility regarding the requirement of an alternative cleaned water return system should be provided to expedite plume characterization and timely capture.

2. Has a technical basis been established that demonstrates the existing extraction wells alone would control plume migration if the IM were modified for use of an alternative injection location that did not provide hydraulic control?

*Response:* The demonstration of hydraulic control might be achieved with existing extraction wells, especially if greater pumping capacity and treated water disposal rates could be applied. However, additional extraction capability may be needed to control chromium migration on the east side, depending on the extent of the plume.

3. What are the team's recommendations for considering alternative injection locations?

*Response:* Alternative locations considered by the IRT included PM-3, a new deep disposal well, discharge to Sandia Canyon, vadose zone wells, and a new spreading basin.

#### **3.3.1 Overview of Interim Measure Operation and Dispute**

The DOE-EM-LA IM was constructed in stages:

- *2017-2018:* Southern area wells CrEX-1, CrEX-3, and CrEX-4 and CrIN-3, CrIN-4, and CrIN-5 were installed.
- *2019-2020:* Wells CrEX-5, CrIN-1, and CrIN-2 were installed, mainly focused on the eastern edge of the plume, and CrEX-2 was installed on the central portion of the plume. Injection well CrIN-6 in the original configuration was converted to extraction well CrEX-5 immediately following installation when a chromium concentration of 270 µg/L was measured in the well. Extraction from this well started in late 2019.

**Figure 3-24** shows this general configuration of the IM as it was operated from about January 2020 to October 2022. Note that operation was not continuous; there were stoppages due to the



Covid pandemic in spring/summer 2020 and some temporary stoppages at other times. During this period, increasing chromium concentrations were observed in two monitoring wells: R-61 and R-45 S2. This was an unexpected outcome of the operation of the IM (**Figure 3-25**). The cumulative extraction flowrate from the five extraction wells was about 280 gallons per minute (gpm), with the same total amount of about 280 gpm injected into the five injection wells. Most of the wells were pumped at about 40 to 70 gpm when they were in operation, except for CrEX-3 and CrIN-3, which typically operated at about half the flowrate of the other wells.

Due to increasing chromium concentrations in R-45 S2, NMED issued a Notice of Non-Compliance in April 2022. In response, DOE-EM-LA submitted an Action Plan in September 2022. In December 2022, NMED required cessation of all injection by April 2023 until DOE-EM-LA “could definitely prove that further migration is not occurring.” In February 2023, NMED also identified that increasing chromium concentrations in R-61 were of concern.

In October 2022, DOE-EM-LA changed the operation of the IM so that only four wells were left in operation: CrEX-4, CrEX-5, CrIN-4, and CrIN-5 (**Figure 3-26**) (referred to by the IRT as the “4s/5s Scenario”). During the next five months, each of the four wells was operated at about 70 gpm (140 gpm total extraction, 140 gpm total injection). During this time, the chromium concentrations continued to increase at R-61 but decreased sharply at R-45 S2 (**Figure 3-26**). Despite some fluctuations in the water elevation data, the “4s/5s Scenario” also reduced the downward vertical gradients in the aquifer at R-45 (see **Appendix K**) during the period in which the chromium concentrations were decreasing in R-45 S2. On March 31, 2023, the IM was completely shut down, and has not yet been restarted as of August 2024.

### **3.3.1.1 Overview of Four Letters in Late 2023-Early 2024 Between NMED and DOE-EM-LA**

Between September 2023 and March 2024, NMED and DOE-EM-LA exchanged four letters regarding shutdown of the IM.

**Letter #1:** NMED’s September 6, 2023 letter to DOE-EM-LA (Letter #1) stated that NMED would accept restart of injection in a revised Corrective Action Plan (CAP) that would include the following terms (see Appendix A of Letter #1) (**Figure 3-27**):

1. Recommence injection for 1 year while DOE-EM-LA develops, installs, and operates an alternative treated water disposal area (referred to by the IRT as an “alternative cleaned water return system”) 1,200 feet or more outside the plume boundary.
2. Recommence injection into CrIN-3 and CrIN-4 for one year and during this time install and sample monitoring well SIMR-3. If the new well does not contain chromium at concentrations above background, start injection into CrIN-5 in addition to CrIN-3 and CrIN-4. However, if SIMR-3 is impacted, stop all injections.
3. Do not inject into CrIN-1 and CrIN-2 until R-80 (located to the south east of R-45) is installed, sampled, and evaluated. If data show that operation of CrIN-1 and CrIN-2 would continue to impact R-45 S2, do not use CrIN-1 or CrIN-2.

**Letter #2:** DOE-EM-LA replied on December 5, 2023 (Letter #2), saying that “EM-LA do not agree” with NMED’s shutdown and restart requirements, and requesting that operation of the IM be resumed with injection in CrIN-2, CrIN-3, CrIN-4, and CrIN-5.

**Letter #3:** On February 6, 2024, NMED issued Letter #3, which proposed “another compromise for partial operation” with a 2-year time frame where only two injection wells, CrIN-3 and CrIN-4, were to be used to support pumping from two or more extraction wells. NMED relaxed the required capacity of the alternative cleaned water return system from Letter #1’s “full amount of water to be extracted” to Letter #3’s “amount of water extracted from a minimum of two extraction wells.” From a flowrate perspective, Letter #3 effectively reduced the alternative cleaned water return system’s required flow capacity from about 280 gpm to about 112 gpm.

**Letter #4:** DOE-EM-LA replied on April 10, 2024, saying that DOE-EM-LA “does not agree with the conditions” specified by NMED in Letter #3, and requesting permission to resume partial operation of the IM with operation of these injection wells (**Figure 3-28**):

- “CrIN-3 to provide additional injection volume.”
- “Injection wells CrIN-4 and CrIN-5 to prevent migration of the plume . . . onto Pueblo de San Ildefonso.”
- “Based on the response of R-45 Screen 2 to operation of CrEX-5, consideration could be given to restarting CrIN-2.”

In addition, DOE-EM-LA stated that NMED did not provide DOE-EM-LA with any supporting analysis on why an alternative cleaned water return system is necessary, and that the technical specifications were arbitrary and without scientific basis.

### **3.3.1.2 Key Issues**

The main issue for NMED appears to be how the injection wells are operated rather than how the extraction wells are operated. Their initial concern was that the injection into the existing injection system (the CrIN wells) is “spreading the chromium plume” (Letter #1) near monitoring well R-45, and they stipulated that injection should be limited to CrIN-3 and CrIN-4 (**Figure 3-27**) with the possibility of operating CrIN-5 if new monitoring confirmed that the chromium extent was not expanding in the southern area of the plume. In Letter #3, DOE-EM-LA recommended a revised, smaller-scale compromise injection program using only CrIN-3 and CrIN-4.

In Letter #4, DOE-EM-LA states that they want to operate a different configuration: inject into CrIN-3, CrIN-4, and CrIN-5 and, based on the response of R-45 S2 to extraction from CrEX-5, potentially restart injection at CrIN-2.

While not directly mentioned in the four letters, NMED also expressed concern about rising chromium concentrations at monitoring well R-61, stating in February 2023 that additional investigation or modification to the IM may be required if chromium trends exceed regulatory standards.

### **3.3.1.3 Areas of Agreement Between the Parties**

- Injection wells for the IM restart: Both parties generally agree:
  - ◊ No injection at CrIN-1 at the eastern edge of the chromium plume
  - ◊ Yes injection in CrIN-3 and CrIN-4

### **3.3.1.4 Areas of Disagreement Between the Parties**

- Alternative cleaned water return system: NMED wants DOE-EM-LA to have an alternative cleaned water return system that could handle the flow from at least two extraction wells (about 112 gpm). DOE-EM-LA disagrees and stated that it is not needed for the IM.
- Injection wells for the IM restart:
  - ◊ NMED puts a condition on potentially restarting injection at CrIN-5: Monitoring well SIMR-3 is drilled and sampled, and does not show elevated chromium concentrations.
  - ◊ DOE-EM-LA suggests a condition on potentially restarting CrIN-2 based on data from the R-45 monitoring wells after CrEX-5 starts extracting groundwater.
  - ◊ DOE-EM-LA suggests restarting CrIN-5 immediately.

### **3.3.2 Are the proposed Appendix A conditions appropriate as part of the IM or more suited for remedy selection?**

Overall, it is clear to the IRT that:

- Despite potential issues with the current IM and some unresolved questions, the objectives of controlling the plume and removing chromium from the aquifer will be served with a carefully focused partial restart of the IM with associated benefits that outweigh any negative impacts.
- The data show that the full IM has increased the downward vertical hydraulic gradient and has contributed to the loss of containment at R-45.
- There is a strong likelihood that chromium has migrated east of the IM capture zone boundary in the vicinity of R-70.
- The IM was capturing chromium in the vicinity of monitoring well R-61, thereby increasing the chromium concentrations in this well. However, this chromium near R-61 will be removed from groundwater by the IM; therefore, from an environmental perspective, this chromium will be controlled.
- As long as CrEX-1 through CrEX-5 continue operation, injection into CrIN-5 appears to be beneficial in directing chromium in groundwater near R-61 northward toward two of the closest extraction wells, CrEX-1 and CrEX-2. However, additional modeling is recommended to better understand the behavior of the chromium plume southwest of R-61.
- In Letters #1, #2, #3, and #4, the dispute between the two parties appears to be over which injection wells to operate rather than which extraction wells to use.

### 3.3.2.1 Key Issues Regarding Existing IM Wells Activation

There are two key elements to the proposed conditions for a compromise, as stated in NMED's revised Appendix A in Letter #2 (February 6, 2022):

- *Issue 1:* NMED wants DOE-EM-LA to have an alternative cleaned water return system that could handle the flow from at least two extraction wells (about 112 gpm in total), with any other extraction well flow handled by the existing, NMED-approved injection wells. DOE-EM-LA disagrees and states that this system is not needed for the IM.
- *Issue 2:* NMED specifies that injection of treated clean groundwater should be into CrIN-3, CrIN-4, and maybe CrIN-5.

*Alternative Location:* The IRT believes that the complexity of the hydrogeology, chromium transport, and hydraulics of the IM at the site means that more injection capacity would greatly simplify control of the chromium plume and make an ASM approach easier to implement for both the IM restart and final corrective measure. The IRT believes that having an "alternative cleaned water return system" would greatly benefit the IM and provide benefits when the final corrective measure is designed. Finally, the IRT recommends an immediate partial restart of the IM while DOE-EM-LA locates, designs, and constructs this new alternative cleaned water return system on a schedule that is acceptable to both parties but at the earliest practical date. In addition, the IRT recommends that DOE-EM-LA and NMED engage more closely in a cooperative process to locate, design, construct, and operate the alternative cleaned water return system.

*Restart Injection Wells:* While the IRT recommends that Appendix A conditions be implemented, a different injection scheme has been developed by the team relative to the NMED and DOE-EM-LA approaches. We recommend an immediate, initially partial restart of the IM as it was operating from late October 2022 to late March 2023 (the 4s/5s Scenario) using these wells:

- Injection: CrIN-4, CrIN-5 (injecting at ~65 to 70 gpm per well)
- Extraction: CrEX-4, CrEX-5 (pumping at ~65 to 70 gpm well)

This system removed chromium and resulted in marked improvement in chromium concentrations in R-45 S2. Capture zone modeling of the 4s/5s Scenario by the IRT (Section 3.1 and **Appendix A**) and best available technical information currently suggest capture of groundwater at R-61 but uncertain capture at R-45 and R-70. It is noted that these IRT models do not consider vertical gradients, which contributes to uncertainty in the boundaries of the capture zone. Overall, this partial restart should be conducted concurrently with DOE-EM-LA's work to locate, design, and build the new alternative cleaned water return system as described above.

The IRT believes that significant adverse effects from operating injection well CrIN-5 are unlikely. Chromium concentrations at CrIN-5 before injection commenced in December 2016 ranged from about 15 to 95 µg/L, somewhat lower than CrIN-4 prestart concentrations. This is

notable because CrIN-4 is a well that NMED considers acceptable for continued injection (see **Figure 3-27** for NMED's recommended restart injection wells).

On the issue of increasing chromium concentrations at monitoring well R-61 S1 during the 4s/5s Scenario, the available data (measured heads and modeling) show that the groundwater in this area of the chromium plume is being captured, so these increasing concentrations are being managed. Once SIMR-3 is installed, the chromium concentration data can guide the parties on future decisions regarding continued injection at CrIN-5. For that reason, we encourage the parties to drill monitoring well SIMR-3 as soon as possible, following the IRT recommendations on well construction matters provided in Section 3.5. Subsequently, the restart of additional injection wells is also encouraged by the IRT if both parties agree. Because both parties have included CrIN-3 as an acceptable injection location, consideration should be given to restarting CrIN-3 as a next step to expand the IM restart capacity.

### **3.3.2.2 Key Issues Regarding New Wells**

As with development of the alternative cleaned water return system, the IRT recommends that DOE-EM-LA and NMED engage more closely in a cooperative process to develop a mutually acceptable set of drilling practices for future site monitoring wells.

Plans should be made to ensure that the chromium near and downgradient of monitoring wells R-45 and R-70 be quickly characterized and controlled. DOE-EM-LA's modeling and analysis (N3B, 2023) shows that at full IM, R-45 and R-70 are outside the capture zone. The IRT also supports drilling and sampling the site's "planned data gap wells" (R-73 redrill, R-76, R-77, R-79, R-80, and SIMR-3) over the next 2 years. For the area near R-45, the following potential modifications to the IM restart should be investigated and, if the parties agree, implemented:

- Increasing the relative CrEX-5 pumping rate and lowering Cr-Ex-4 pumping to maintain consistent total pumping for the IM.
- Increasing the total pumping in both of these existing extraction wells once new cleaned water return capacity is available.
- Potentially converting CrIN-1 to an extraction well.
- If other measures do not capture chromium in groundwater east of monitoring well R-70, a high priority would be to install additional extraction capacity in this area.

### **3.3.3 Has a technical basis been established that demonstrates the existing extraction wells alone would control plume migration if the IM were modified for use of an alternative injection location that did not provide hydraulic control?**

This question asks whether there would be containment (i.e., hydraulic control) of the plume if the IM were restarted without any injection wells and only the extraction wells operating.

Demonstrating plume capture/containment from water level elevations is relatively difficult at this site due to the relatively flat groundwater hydraulic gradient and the location of the existing

monitoring wells. However, a combination of field measurements and groundwater modeling can be effective.

The IRT currently believes that the chromium plume may have already migrated beyond the reach of the existing extraction wells under their average IM pumping rates in the areas of monitoring wells R-45 and R-70. The capture zone analysis presented in Section 3.1 and **Appendix A** shows a range of results about the degree of potential capture under the 4s/5s Scenario for these areas, showing some uncertainty. Therefore, after the extent of migration has been assessed with new monitoring wells, the restarted 4s/5s Scenario IM may need to be expanded or operated in a different way to capture the chromium excursions to the east and potentially to the south.

However, containment of the chromium plume east of CrEX-5 and R-70 might be achieved with extraction wells only (see Question 3.2) under all three of these conditions:

1. No IM injection wells are used to inject water' only extraction wells are operated.
2. A high volume alternative cleaned water return system with a capacity of 300+ gpm is available along with added treatment capacity.
3. Increasing extraction flowrates in existing extraction wells and/or converting some of the injection wells to extraction wells.

For example, if converted to extraction wells, CrIN-1(EX), CrIN-2(EX), and perhaps CrIN-3(EX), along with the existing CrEX-5 extraction well, would form a line of four extraction wells that might achieve hydraulic control east of the plume, and there is a high likelihood that pumping from CrEX-1 and CrEX-2 would continue to control the plume along the southern boundary if sufficient water treatment and water return capacity are available to achieve the necessary flowrates for hydraulic control.

### **3.3.4 What are the team's recommendations for considering alternative injection locations?**

The IRT is using the term "alternative cleaned water return system" to describe this recommended addition to the IM for additional capacity. The IRT evaluated six potential locations/design for this system, listed here from most to least promising. These are not the only possible locations/designs for the alternative cleaned water return system, but are six alternatives that appeared to the IRT to be the most promising for implementation. The IRT recognizes that DOE-EM-LA and NMED must collaborate closely to locate, design, and develop the alternative cleaned water return system design. One approach is to form a working group of DOE-EM-LA, NMED, and any needed additional parties based on the proposed alternative, to meet this goal.

1. *Repurpose water supply well PM-3*: Los Alamos County water supply well PM-3 is not currently being used for water supply. While there may be non-technical reasons for rejecting this option, from a technical perspective the IRT feels that adding PM-3 to the collective of injecting wells could serve as a safe, easily implemented modification to the IM.

This option is viewed as an environmentally sustainable alternative cleaned water return system that would significantly improve both the reliability of the IM and potentially the final corrective measure (**Figure 3-29**). Key considerations of this repurposing include the following:

- ◇ This well demonstrated extraction rates of up to 1,400 gpm from the 1,576-foot-long well screen; almost any injection flowrate up to this rate is likely possible.
  - ◇ Connecting the existing IM to PM-3 would require a water supply line only a few thousand feet in length. Horizontal drilling might be useful for constructing this water supply line.
  - ◇ The IRT believes that overall injection into PM-3 would likely have either very limited effect, or even a potentially beneficial hydraulic effect by reducing any vertical gradients that may be present that drive downward flow in the area of the chromium plume. However, if needed, hydraulic effects of the PM-3 injection on the upper portion of the aquifer, containing the chromium plume, could be considerably diminished by using an inflatable packer to isolate the portion of the well screen above the Miocene basalt from the portion below; the basalt is thought to behave as an aquitard in the subsurface. This measure would still leave over 1,200 feet of well screen below the basalt to receive treated injected water. Additional declines of hydraulic effects experienced in the plume area could be realized by sealing of the gravel pack of PM-3 (which currently extends the entire depth of the well) in the zone of the Miocene basalt by a specialty well contractor.
  - ◇ The treated water would be released back into the aquifer, so water rights issues could be averted and the environmental sustainability metrics of this project would be positive. While the treated water from the LANL treatment system is currently injected into shallow groundwater with no obvious issues, the parties would need to confirm that the treated water can also be injected into the deeper aquifer without adverse impacts.
  - ◇ Significant cost and time savings could accrue to the project, as no new well would need to be drilled. Overall, this option is also the most environmentally sustainable option, as there would be no water loss and modest construction requirements. However, to implement this approach, the owners of the well, Los Alamos County, the State of New Mexico, and other stakeholders may need to give their permission. If this approach has not already been evaluated and rejected, a joint request by the two parties might increase the chance for quick acceptance by other stakeholders. Potential arrangements include DOE-EM-LA acquiring or leasing PM-3 for recharging the aquifer with cleaned water for just a few years or potentially for the lifetime of the final corrective measure.
2. *Construct a deep injection well:* For example, this well could be 1,000 to 2,000 feet deep, potentially screened below the Miocene basalt (**Figure 3-29**). The IRT suggests that this well could be located inside the 1,200-foot radius of NMED's proposed exclusion zone, as it is unlikely to significantly affect capture, and might even have a positive effect by diminishing any downward flow in the area. Note that a very small change in hydraulic gradient from injection is likely to not be a problem due to the vertical anisotropy of the

aquifer. While NMED's requirement that any injection well "not hydrologically affect the plume" is a laudable goal, this goal is more practical and attainable if it is understood to mean "not adversely affect the plume" by not causing the plume to grow.

3. *North of the chromium plume:* This alternative would involve piping treated water back in a northern direction, into the east end of Sandia Canyon, perhaps via a pipeline through a gap in the finger mesa (e.g., near R-36 and east of the chromium plume). Here, treated water discharged to the alluvium would flow as surface water and infiltrate (if permitting and water rights issues are resolvable).
4. *Land application:* This alternative would expand the capacity of the current DOE-EM-LA land application system from ~28 gpm to ~112 gpm. While there are some operational, permitting, and financial constraints, the IRT feels that, with the appropriate level of engineering, this could be a legitimate option for handling some fraction of the treated groundwater.
5. *Vadose zone injection wells:* This alternative involves using vadose zone injection wells in the source areas to dispose of the treated groundwater and to flush contaminants out of the vadose zone and into the regional aquifer, where they would be intercepted and retreated. However, the IRT feels that any form of injection of treated water upgradient of a groundwater extraction system at this time is very operationally complex and has the potential for incomplete capture or indeterminate redirection of chromium in the vadose zone. Nonetheless, this could be part of the solution to remediating the impacted vadose zone in the future.
6. *Spreading basin:* Managing treated water at a rate of 112 gpm would require an infiltration area of about 5 acres, assuming the infiltration rate is 0.1 ft/d. During winter, the basin could be kept from freezing using solar heat and/or aeration bubblers. An automated system would need to be designed to stop infiltration and halt the IM in the event of a chromium breakthrough or water overflow. Water would need to be piped out of the exclusion zone requested by NMED, outside an area 1,200 feet from the chromium plume edge, to a 5-acre plot free of soil or groundwater contamination. A site free of basalts in the vadose zone would be favorable.

Note that in their February 6, 2024 letter (Letter #3), NMED indicated that an alternative cleaned water return system that had the capacity to manage treated water from two extraction wells would be sufficient to meet their expectations for such a system. This would have a total system capacity of about 112 gpm. The IRT feels that even a small system of this size would be a significant step forward, but also encourages all parties to determine if a higher-capacity system (e.g., 300 gpm or more) could be installed at relatively little extra cost (likely the case for the deep well systems in Options 1 and 2 above) to provide potential capacity for the final corrective measure (if needed).

### **3.3.5 Summary of Recommended Actions**

1. *Alternative location for treated water:* While acknowledging drawbacks, overall, the IRT has concluded that having an alternative cleaned water return system would greatly benefit the IM and the final corrective measure. The IRT concluded that the complexity of the



hydrogeology, chromium transport, and hydraulics of the IM at the site means that more capacity for returning clean, treated water to the environment is needed. This would greatly simplify the control of the chromium plume and make an ASM approach easier to implement for both the IM restart and final corrective measure. Therefore, the IRT recommends an immediate partial restart of the IM while DOE-EM-LA locates, designs, and constructs this new alternative cleaned water return system that could supplement or eventually replace the entire existing injection well system.

The IRT reviewed six different configurations for this system, with the following two most promising options:

- ◇ Repurposing currently unused Los Alamos County well PM-3 for injection of treated water (**Figure 3-29**). While complicated from a jurisdictional and regulatory perspective, an approach where DOE-EM-LA buys or leases this well is technically feasible, would likely save many months or potentially years for solving the chromium plume problem, and greatly reduces the cost of the alternative cleaned water return system.
  - ◇ Drilling a new deep injection well similar to the design of a local water supply well.
2. *Immediate partial restart of IM:* While the IRT appreciates the thinking behind the NMED and DOE-EM-LA restart proposals, it recommends a different configuration for an immediate, initially partial restart of the IM using the pumping/injection approach used in late October 2022 to late March 2023 (the 4s/5s Scenario) using these wells:
- ◇ Injection: CrIN-4, CrIN-5 (starting injection at ~65 to 75 gpm per well)
  - ◇ Extraction: CrEX-4, CrEX-5 (starting pumping at ~65 to 70 gpm well)

The IRT has concluded that it is unlikely for there to be significant adverse effects from operating injection well CrIN-5 at this time, and it should be put back in operation immediately. Once monitoring well SIMR-3 is installed, the chromium concentration data can guide the parties on the issue of continued injection in CrIN-5. For that reason, we encourage the parties to drill monitoring well SIMR-3 as soon as possible, following the IRT's advice on well construction matters provided in Section 3.5.

3. *Control of downgradient eastern portion of chromium plume:* Finally, plans should be made to ensure that the chromium plume near and downgradient of monitoring well R-70 is quickly controlled. Potential future IM modifications that should be investigated to achieve full capture include:
- ◇ Increasing the CrEX-5 pumping rate by lowering CrEX-4 pumping rate.
  - ◇ Bringing CrIN-3 on line for more injection capacity and therefore more extraction capacity in CrEX-5.
  - ◇ Converting CrIN-1 and potentially other current injection wells to extraction wells.
  - ◇ If needed, adding extraction capacity in the vicinity of monitoring well R-70.
  - ◇ When available, converting to a mostly extraction or extraction-only system (limited or no shallow reinjection) using the capacity of the alternative cleaned water return system.

### 3.4 Topic 4: Regulatory Matters

The following questions on regulatory matters are addressed in this section:

1. Is the current chromium plume characterization consistent with industry practices and EPA guidance for the maturity and understanding necessary to propose and begin evaluating potential remedial alternatives (i.e., conducting a corrective measures evaluation and preparing a corrective measures evaluation report)?

*Response:* The techniques DOE-EM-LA has used are standard practices, but have not resulted in adequate information.

2. Has the project defined the needed data and uncertainties for designing a remedy (e.g., corrective measures implementation plan [CMIP])?

*Response:* No. The project has not defined the data gaps and uncertainties adequately for designing a remedy.

3. Which data gaps need to be closed, if any, before completing the comparison of the potential remedial alternatives?

*Response:* Various categories of data gaps need to be closed before comparing potential remedial alternatives.

4. Is use of an adaptive management strategy as a component of a final remedy appropriate?

*Response:* Yes. Adaptive management is an appropriate strategy.

5. If so, how is regulatory oversight preserved during the CMIP phase as design evolves due to emerging information?

*Response:* Tailored oversight and results-based corrective action can be used to preserve regulatory oversight.

6. Under what circumstances is it more favorable to apply an adaptive management strategy to interim measures vice the remedy itself?

*Response:* Adaptive management is considered an overarching process that is best suited to guide remediation throughout a project rather than being implemented during a single phase of remediation.

#### **3.4.1 Is the current chromium plume characterization consistent with industry practices and EPA guidance for the maturity and understanding necessary to propose and begin evaluating potential remedial alternatives (i.e., conducting a corrective measures evaluation and preparing a corrective measures evaluation report)?**

The site investigation techniques DOE-EM-LA has used to characterize the presence of the chromium plume, including characterization of the hydrogeological setting and associated physical and chemical characteristics, are consistent with industry practices and EPA guidance.

However, due to the complex nature of the site, they have not provided sufficient information to propose and evaluate potential remedial alternatives.

In considering consistency with industry practices, characterization of the chromium plume is not comparable to groundwater plume characterization typical of the RCRA corrective action process. Most groundwater plumes are found in the shallow subsurface in much simpler geology than the chromium plume, underlie thin vadose zones, and do not lie below perched aquifers. Factors unique to the chromium plume, including its depth, size, presence and movement through the vadose zone, perched aquifers, and complicated geology and hydrogeology, make the selection of remedial alternatives for the chromium plume more difficult than for typical plumes. The site investigation techniques are consistent with industry practices and EPA guidance, and have provided extensive amounts of data, but have not resolved site uncertainties to the extent necessary to advance the project from IM to a corrective measures evaluation and corrective measures evaluation report.

### **3.4.2 Has the project defined the needed data and uncertainties for designing a remedy (e.g., corrective measures implementation plan [CMIP])?**

The chromium plume is in a complex hydrogeologic setting, and data gaps and uncertainties have been identified, but have not been sufficiently resolved to design a final remedy.

An evaluation of technical and non-technical factors for both the chromium plume and the royal demolition explosive (RDX) plume identified the setting for both plumes as complex sites (DOE, 2022). The typical expected sequence for the RCRA corrective action process (i.e., RCRA facility assessment, RCRA facility investigation, corrective measures study, and corrective measures implementation) is not the best approach for the chromium plume due to the complex site conditions and because flexible site investigation approaches (i.e., adaptive management) are better suited to address the remaining data gaps needed for remedy selection.

To protect human health and the environment and keep chromium from reaching water supply wells and off-site locations, the IRT believes it is possible to restart the chromium plume IM (or certain extraction and injection wells) without needing to close all remaining data gaps. The remaining data gaps can be addressed through adaptive management while IM is taking place.

### **3.4.3 Which data gaps need to be closed, if any, before completing the comparison of the potential remedial alternatives?**

Discussions of specific data gaps that need to be closed before completing a comparison of potential remedial alternatives are more appropriately found in technically oriented sections of the IRT report, and thus are not included here. They fall within the general categories of plume delineation, aquifer properties, influences of county production wells, effects of basalt strata, precise groundwater flow directions, entry points for chromium to the regional aquifer, modeling uncertainties, influences of the interim measure wells, and others. Factors contributing to the prevailing data gaps relate to restrictions on where and how many monitoring wells can be installed due to the terrain, cost, and the presence of cultural features that limit the density of groundwater monitoring data over the plume footprint. The continuing presence of chromium mass in the vadose zone is another important factor as evaluated by the IRT (**Appendices G**

**and N).** Although a fundamental aspect of RCRA corrective action is source removal, and the original source of chromium at the Power Plant was removed, the remaining chromium in the vadose zone continues to provide chromium mass to the regional aquifer. The pathways that chromium follows as it migrates through the vadose zone are not well understood, and the locations where chromium enters the regional aquifer (hydraulic windows) are only approximated.

#### **3.4.4 Is use of an adaptive management strategy as a component of a final remedy appropriate? If so, how is regulatory oversight preserved during the CMIP phase as design evolves due to emerging information?**

The use of an adaptive management strategy (also referred to as adaptive management or adaptive site management [ASM]) as a component of a final remedy for the chromium plume is appropriate and is supported by EPA's directives and guidance. On May 1, 1996, EPA published an Advance Notice of Proposed Rulemaking (ANPRM) for Corrective Action from Releases at Solid Waste Management Units at Hazardous Waste Management Facilities (61 FR 19432) (U.S. EPA, 1996). One of the purposes of the ANPRM was to emphasize flexibility inherent to implementing the RCRA corrective action program and to describe improvements to the program underway or under consideration at that time. Section III of the ANPRM (U.S. EPA, 1996), p. 19440) discusses corrective action program implementation and emphasizes that corrective action is intended to support flexible approaches to site remediation. It further emphasizes that facility owners/operators should take advantage of flexibility to improve the corrective action process and expedite cleanups. The notice points out that interim actions (measures) should be compatible with or a component of a final remedy. The final remedy as well as IM can be a component of adaptive management. The following excerpt from U.S. EPA (1996) attests to RCRA flexibility and selecting a final remedy:

*“On July 27, 1990 (55 FR 30798), EPA proposed detailed regulations to govern the RCRA corrective action program. The 1990 proposal was designed to be the analogue to the CERCLA program's National Oil and Hazardous Substances Pollution Contingency Plan (NCP). As such, it addressed both technical (e.g., cleanup levels, remedy selection, points of compliance) and procedural (e.g., definitions, permitting, reporting) elements of the corrective action program. In the 1990 proposal, EPA emphasized the need for site-specific flexibility in cleanup programs. The Agency stated, “Because of the wide variety of sites likely to be subject to corrective action, EPA believes that a flexible approach, based on site-specific analyses is necessary. No two cleanups will follow exactly the same course, and therefore, the program has to allow significant latitude to the decision maker in structuring the process, selecting the remedy, and setting cleanup standards appropriate to the specifics of the situation.”*

The ANPRM discusses consistencies between RCRA corrective action and cleanup under CERCLA, or Superfund. EPA is committed to consistency of results between the RCRA corrective action and Superfund remedial programs (U.S. EPA, 1996). On June 23, 2022, the EPA Office of Land and Emergency Management (OLEM) issued Directive 9200.3-123 (Considerations for Adaptive Management at Superfund Sites) following the establishment of an adaptive management workgroup and implementation of adaptive management pilot efforts

(U.S. EPA, 2022). This directive provides a working definition of adaptive management as the following:

*“Adaptive management is a formal and systematic site or project management approach centered on rigorous site planning and a firm understanding of site conditions and uncertainties. This technique, rooted in the sound use of science and technology, encourages continuous re-evaluation and management prioritization of site activities to account for new information and changing site conditions. A structured and continuous planning, implementation and assessment process allows EPA, states, other federal agencies (OFAs), or responsible parties (PRPs) to target management and resource decisions with the goal of incrementally reducing site uncertainties while supporting continued site progress.”*

The OLEM directive differentiates how adaptive management can be applied at either the project level or site level for the Superfund remedial program. At the site level, adaptive management is focused on achieving broad site objectives, making it generally better suited for complex sites; whereas, at the project level, adaptive management can target specific project uncertainties in the remedial investigation or remedial design process. The directive further states that adaptive management may be applicable to projects where remedial progress may appear stalled in the long-term operation and maintenance.

In addition to the ANPRM and the OLEM directive, on March 24, 2000, EPA published Federal Register Notice 65 FR 15905, which requested feedback on the RCRA cleanup reforms and related guidance documents (U.S. EPA, 2000). The RCRA cleanup reforms were intended to achieve faster, more efficient cleanups at RCRA sites that have actual or potential contamination. These reforms were designed to, in part, foster maximum use of program flexibility and practical approaches through training, outreach, and new uses of enforcement tools.

In 2017, the ITRC published comprehensive guidance on the application of ASM at complex sites (ITRC, 2017). The guidance provides four steps of adaptive management in Section 4.1: (1) identify complexity attributes within the conceptual site model and assess whether ASM is warranted (the reader is referred to the IRT’s work on the conceptual model found in responses to Questions 1 and 2 of the December 19, 2023 NMED EM-LA letter), (2) refine the conceptual site model, (3) set or revisit site objectives, and (4) develop interim objectives and adaptive remedial strategy. The guidance further points out that these steps are “particularly relevant at sites that are selecting an interim or final remedy or revisiting the existing remedial strategy because insufficient progress has been made towards meeting site remediation objectives.” The guidance addresses the use of ASM for technical and regulatory considerations for both CERCLA and RCRA and provides an excellent procedural framework for implementing adaptive management at the chromium plume.

### **3.4.5 How is regulatory oversight preserved during the CMIP phase as design evolves due to emerging information?**

Preserving regulatory oversight during the CMIP phase as the design evolves during ASM can be accomplished by implementing tailored oversight and results-based corrective action. EPA

presents guidance on the use of both tailored oversight and results-based corrective action including the planning, benefits, roles of regulatory agencies, and use of performance standards (U.S. EPA, 2003). EPA's 2003 guidance states that tailored oversight involves regulators and facilities, where appropriate, developing a plan that allows for the appropriate level of oversight for a particular facility rather than a pre-determined "one-size-fits-all" process. Results-based corrective action emphasizes outcomes or results and establishes process requirements needed for the characteristics of the specific corrective action needs. Regarding performance standards, the 1996 ANPRM (U.S. EPA, 1996) states that EPA favors performance-based approaches provided that the remedial goals are clear, the oversight during remedy implementation is appropriate to the complexity of the facility-specific circumstances of the corrective action needs, and there is substantial public involvement.

Based on EPA's 2003 guidance, results-based approaches for the chromium plume site can involve setting goals and providing procedural flexibility in how those goals are met, inviting innovative technical approaches and focused data collections, and having DOE-EM-LA undertake cleanup with an appropriate level of oversight based on NMED's assessment of the actions. However, under risk-based corrective action and tailored oversight, DOE-EM-LA would still be held fully accountable for the results they agree to achieve. A tailored oversight plan should be based on facility-specific conditions and capabilities, and tailored oversight is considered a significant tool in the overall diversified strategy of results-based project management. EPA points out that tailored oversight does not result in less protective cleanups and does not change the overall expected results of the corrective action program. Additionally, tailored oversight does not result in reduced data quality, and a facility is still responsible for providing sufficient quality data to verify that agreed upon results are met. Tailored oversight is appropriate for both IM and final remedies.

EPA recommends five core results-based approaches that facilities and regulators consider at any corrective action site to promote results-based corrective action, in addition to four supplemental approaches not discussed in this report. The five core approaches are (1) tailored oversight, (2) holistic approach, (3) procedural flexibility, (4) performance standards, and (5) targeted data collection. The following paragraphs are quoted from the guidance, and the footnotes are included below for reference.

***Tailored oversight*** - Oversight, in general, is the responsibility of the lead regulator<sup>4</sup> to ensure the facility implements corrective action. Tailored oversight is an oversight plan developed based on facility-specific conditions such as site complexity, compliance history, and financial and technical capability of the facility. In addition to discussing and using results-based approaches with facilities, we recommend regulators evaluate the facility-specific conditions and

---

<sup>4</sup> A "lead regulator" is typically the first-line staff person for the government authority that is responsible for ensuring that a facility implements corrective action as necessary to meet facility-specific corrective action goals. The lead regulator, could depending on the circumstances, either be a federal employee working in an EPA regional office or an employee of a particular State or Territory (EPA, 2001)

*develop a plan with an appropriate level of oversight that will enhance timely, efficient, and protective cleanups. Tailored oversight may result in the elimination of administrative or technical steps, usually for facilities who have agreed to, and have demonstrated that they are capable of, meeting the environmental objectives and specific requirements established for their facility. In some instances, an analysis of facility capabilities may result in greater oversight to ensure environmental results are achieved in a timely manner.*

**Holistic Approach** - *The 1996 ANPRM states, “In general, EPA believes that a holistic approach to corrective action, could increase cleanup efficiency and reduce transaction costs.” (61 FR 19432, May 1, 1996, 19456). The term “holistic” in this context means taking a “big picture” look so facility representatives and regulators can prioritize their resources based on risk<sup>5</sup> to human health and the environment. For example, in a situation where there are many on-site sources of contamination contributing to an off-site plume of contaminated groundwater, a holistic approach could first focus on identifying and controlling, in the near-term, current risks to humans from the site as a whole. Subsequent to controlling these risks, the facility could then conduct additional focused investigations to help evaluate additional cleanup activities needed to achieve other short- and long-term cleanup objectives associated with individual sources. EPA believes that viewing corrective action sites holistically is particularly appropriate to help meet Environmental Indicator goals. Ultimately, the facility would still be responsible for meeting final remedy corrective action goals.*

**Procedural flexibility** - *Regulators and facilities place their primary focus on environmental results and ensure that each corrective action-related activity at a given facility directly supports cleanup goals at that site. Corrective action is generally structured around seven elements common to most cleanups: initial facility assessment, site characterization, short-term (interim) actions, remedy evaluation and selection, remedy implementation, remedy completion and public participation. EPA emphasizes that no individual results-based approach that implements these cleanup elements is likely to be appropriate for all corrective action facilities. EPA continues to encourage regulators and facilities to focus on the desired result of cleanup rather than a predetermined (or “generic”) step-by-step cleanup process that does not reflect site-specific circumstances. We recommend these seven elements be viewed as evaluations generally necessary to make good cleanup decisions. By focusing on results, regulators are encouraged to use the most effective approaches for facility management and oversight.*

**Performance Standards** - *The regulator, working (as appropriate) with the facility, develops general performance standards to prescribe the scientific, technical, and administrative requirements the facility must fulfill in order to implement and ultimately complete corrective action. Under this approach, it is anticipated that the facility, not the regulator, is responsible for determining the methods by which the performance standards are attained, e.g., designing a*

---

<sup>5</sup> “Risk-based decision making is especially important in the corrective action program, where it should be used to ensure that corrective action activities are fully protective given reasonable exposure assumptions and consistent with the degree of threat to human health and the environment at a given facility.” (EPA, 1996; page 19441)

*remedy that will meet the required performance standard. That is, the regulator establishes clear, reasonable, and protective performance standards, while the facility (with an appropriate level of regulatory oversight) determines how those standards are met.*

**Targeted (or Focused) Data Collection** - *As described in the 1996 ANPRM, there are a variety of results-based approaches that regulators and facilities might use to focus data gathering efforts to identify and implement appropriate responses at a corrective action facility. For example, EPA encourages facilities and regulators to develop and use a conceptual site model<sup>6</sup> (CSM) to identify and prioritize data needs based on a particular corrective action goal. Additionally, facilities might dramatically improve the effectiveness and efficiency of data collection by taking advantage of numerous innovative site characterization techniques<sup>7</sup>. Also, EPA recommends using data quality objectives<sup>8</sup> (DQOs) to identify the amount, type, and quality of data needed to support corrective action decisions (EPA, 1994; page 19445).*

The IRT suggests that to implement tailored oversight and results-based corrective action, DOE-EM-LA and NMED consider identifying the specific phases needed and develop an agreement that includes performance standards, timing, and how the needed flexibility will be managed. This type of agreement could preserve regulatory oversight during the CMIP phase.

#### **3.4.6 Under what circumstances is it more favorable to apply an adaptive management strategy to IM versus the remedy itself?**

EPA and ITRC characterize adaptive management as a project management tool intended to assist decision making about site remediation as information becomes available during remediation activities. Adaptive management is described as a comprehensive process that is especially useful for managing the remediation of complex sites because it allows flexibility to adapt to new information and changing conditions regardless of the phase of remediation. The National Research Council (NRC, 2003 and 2005) refers to adaptive management as “an innovative approach to resource management in which policies are implemented with the express recognition that the response is uncertain, but with the intent that the response will be monitored, interpreted, and used to adjust programs in an iterative manner, leading to ongoing improvements.” Each of these descriptions considers adaptive management as an overarching process that is best suited to guide remediation throughout a project rather than being implemented during a single phase of remediation.

Section 4 of the 2017 ITRC guidance (Adaptive Site Management) presents a detailed description of how to implement adaptive site management in terms of both RCRA and CERCLA. The guidance reports that the first steps in the ASM process are to identify

---

<sup>6</sup> A Conceptual Site Model is a three-dimensional representation of what is known or suspected about the sources, releases, and release mechanisms, contaminant fate and transport, exposure pathways and potential receptors, and risk.

<sup>7</sup> To access detailed information, guidance and other resources pertaining to innovative site characterization tools and approaches, see <http://www.clu-in.org/char1.cfm>.



complexities within the conceptual model and determine if ASM is warranted. As previously mentioned, these steps are followed by (1) refining the conceptual site model, (2) setting or revisiting the objectives, and (3) developing interim objectives and an adaptive remedial strategy. The IRT recognizes the complex history of the chromium plume investigation and that an appropriate amount of planning would be needed to implement ASM so that it is inclusive of existing investigations and ongoing remedial activities. Further, Section 7 of the 2017 ITRC guidance discusses the importance of obtaining stakeholder perspectives and expectations during the ASM process.

### 3.4.7 Recommended Actions

The recommendations regarding this topic are as follows:

- Implement an ASM strategy.
- Consider using tools such as EPA's RCRA First approach and EPA's 2015 Region 6 corrective action strategy. Also use ITRC's guidance on adaptive management. These tools will facilitate and streamline important decisions and provide a RCRA-safe procedure for using ASM concepts. The concepts of ASM laid out by ITRC directly address many concerns raised by the IRT (e.g., CSM).
- Data gaps need to be closed and a procedure needs to be developed for doing this quickly and effectively. To do so would benefit enormously from the ability to install more sample intervals (well screens) more rapidly, and also take advantage of other technologies (e.g., downhole geophysics). This can only be done if conducted collaboratively with NMED, and a working group may be needed to accomplish this, perhaps through an ASM approach as noted above.

## 3.5 Topic 5: Well Design

The following questions are addressed in this section:

1. Do the monitoring wells constructed with bentonite in the chromium plume region demonstrate a seal between the screened intervals in the dual-screened monitoring wells that is adequate to ensure the prevention of comingling or interaquifer exchanges between the separate hydrogeologic units in the plume area?

*Response:* Yes.

2. Are there alternatives to bentonite that can be used to seal chromium monitoring wells at the site that will not negatively impact or alter groundwater chemistry (e.g., cement in lieu of bentonite)?

*Response:* Yes. However, granular bentonite should be used above and below the sand filter pack that surrounds the monitor well screen.

**3.5.1 Do the monitoring wells constructed with bentonite in the chromium plume region demonstrate a seal between the screened intervals in the dual-screened monitoring wells that is adequate to ensure the prevention of comingling or interaquifer exchanges between the separate hydrogeologic units in the plume area?**

The IRT received a briefing on the construction of the monitoring wells from Catherine Goetz. Our impression was that considerable care was taken to ensure the proper placement of bentonite in the annular space of the monitoring wells. Using R-50 as an example, the borehole diameter is 12.75 inches, and the stainless steel casing and screen have an outer diameter of about 5.5 inches, with centralizers 2 feet above and below the screens. This leaves about 3.6 inches of annular space between the casing and the formation to place the bentonite. The annular interval for the bentonite seal is about 38 feet. Thus, our sense is that this is a reasonable design to ensure a proper seal. The screens are below the water table; therefore, the bentonite will remain hydrated. In the regional aquifer, the vertical hydraulic gradients are on the order of 0.001 to 0.01, so there is low potential for significant mass transfer via a bentonite defect.

In the vadose zone the perched water should also keep the bentonite hydrated to ideally prevent downward migration of contaminants via the annulus. However, hydraulic head gradients in the vadose zone are on the order of 1.0. The impact of a defect in the bentonite seal on the potential significance of chromium mass transfer from perched zones into the regional aquifer via the well annulus has not been evaluated.

Based on the technical literature, consensus standards, and guidelines from the OSE, both bentonite and cement sealants can be effectively used as annular sealants, both in the groundwater zone and the vadose zone. However, the various annular seal materials exhibit nuanced differences in their relative performance. The IRT has attempted to summarize some of these key characteristics in **Table 3-3**. A few of the key differences are highlighted in the following narrative paragraphs.

In **Table 3-3**, the annular sealants are organized into columns and include cements (i.e., standard grouts and cements as highlighted by OSE), bentonite amended grouts and cements, bentonite slurries, uncoated bentonite chips, uncoated bentonite granules, and coated bentonite granules. A key difference in the bentonite materials (chips and granules) relates to their shape and properties. Chips are irregularly shaped. They do not flow smoothly/easily through the tremie pipe, do not pack as densely in the annulus, and have a higher potential to bridge and leave voids in the emplaced seal. Granules are compact regular shapes that overcome these negatives. Coated granules have a layer that slowly dissolves in water, providing additional working time below the water table to help ensure for high quality emplacement and an effective seal (but this layer would inhibit the sealing in a low moisture vadose setting). Based on data in the technical literature, bentonite slurries and bentonite amended cements underperformed relative to some of the other sealants in the vadose zone due to shrinking following hydrated emplacement and from shrinking and swelling in response to varying moisture conditions. Thus, the bentonite chips, bentonite slurries, and bentonite-amended cements were included primarily for completeness, as these materials may not be optimal for the thick LANL site vadose zone

scenario. Some of the other summary scoring factors relate to logistics (the need to premix cements and clean equipment), the ability to easily and accurately tag the layer as a quality assurance check, the timing of emplacement below the water table (i.e., the urgency for continuing to the next layer after emplacement), and potential geochemical impacts. In general, the optimal annular sealing materials for use below the water table was coated bentonite granules (cement and bentonite-amended cement were also rated as good). No materials were rated as good for the vadose zone; however, cement and uncoated bentonite granules were rated as acceptable overall.

The IRT posed a list of questions to OSE regarding their concerns on monitoring well construction and the IRT response (**Appendix O**). OSE also presented its evidence that bentonite seals leak in a “Well Construction Memorandum” dated May 21, 2024 and the IRT response is also provided in **Appendix O**.

Regarding the well construction memorandum, the emphasis of the OSE analysis is on wells that are screened into or have tapped through the perched zone, not on the dual-screen monitoring wells in the regional aquifer. OSE’s review of literature found that in chromium-contaminated areas, the integrity of bentonite may be compromised by the chromium (Ajitha et al., 2018). However, the study they refer to actually concluded that there was only a marginal effect of the chromium on clay permeability. Moreover, that study used calcium bentonite, which does not swell as much as the sodium bentonite used in the site wells. The effect of Cr(VI) on bentonite was one example of a general emphasis in the interactions between OSE and the DOE-EM-LA team regarding the possibility chemical impacts of the annular sealant (i.e., alteration of collected samples, or impacts of the plume of Cr(VI) on the sealant properties). The IRT believes that both bentonite and cement sealants will have negligible geochemical impacts and interactions when installed according to DOE-EM-LA standard designs. In the nominal configuration, sealants are isolated from the screen zone by a buffer interval of sand pack. In this scenario, neither bentonite nor cement sealants would impact the geochemistry of a groundwater sample. Importantly, incursion of sealant into the screen zone is more likely with cement compared to bentonite, and such incursion has the potential to significantly alter the pH, geochemistry, and validity of groundwater samples. Thus, the potential for adverse geochemical impacts under non-ideal conditions is higher for cement.

We have seen no evidence that the bentonite seals in the regional aquifer have failed to do their job in the chromium plume remediation area. In reviewing the data from many of the monitoring wells, it is apparent that the behavior in the dual-screen monitoring wells in the regional aquifer is consistent with a good bentonite seal. If the seal had failed, one would see similar water levels and similar chemistry in the two sampling intervals. Instead, each interval seems to have different water levels and different chemistry. The behavior of water levels and chemistry over time in the regional aquifer is also different. There is also a finite time lag between some of the responses, which is consistent with a sound bentonite seal that prevents “short-circuiting” in the casing annulus. Interpretations of the data lead us to conclude that the dual-screen monitoring wells are quite useful in providing a vertical perspective on the directions of groundwater flow and the extent of contamination. Dual-screen wells are a very cost-effective way to obtain data essential to redesign of the IM in a timely manner.

Although there are also publications in the scientific literature indicating that bentonite is a suitable sealant in the vadose zone (e.g., Dunnivant et al., 1997) and in aquifers that are consistent with observations of the IRT in the chromium area regional aquifer, OSE's position appears to be intractable.

### **3.5.2 Are there alternatives to bentonite that can be used to seal chromium monitoring wells at the LANL site that will not negatively impact or alter groundwater chemistry (e.g. cement in lieu of bentonite)?**

Yes, there are alternatives to seal wells using bentonite alone. As noted above, it is possible to add bentonite to cement grout to minimize the tendency for cement to shrink away from the borehole wall in the presence of water. However, bentonite-amended cements and bentonite slurries deploy the clay in its swollen/expanded state, and these materials have a high potential for long-term shrinkage or cracking in dry vadose zone conditions. As noted above, under nominal conditions, neither cement/grout nor bentonite would be expected to impact groundwater samples and water chemistry, and neither material would be expected to be adversely impacted by plume chemistry. If there were any specific concerns, such as the findings of Dr. Patrick Longmire that some cements contain chromium, these could be tested before the material is used in drilling. Notably, cement on its own potentially may alter the pH of water in cases where incursion into the screen zone occurs; however, this was not discussed as a concern by OSE (e.g., Blackmer, 1988).

Bentonite on its own has been widely used in the environmental industry, including in dual-screened wells (e.g., Korte and Kearl, 1991). The swelling properties of a type of bentonite clay called sodium montmorillonite are especially good for forming strong seals.

The petroleum industry also uses bentonite for sealing annular spaces, as shown in the approved production well diagram presented by OSE to N3B/DOE-EM-LA (Angel, 2024, slide 27/43) where, for example, 50 feet of bentonite was placed between the underlying sand pack and overlying neat cement, evidently to help prevent communication across the contact between the Artesian Group Sandstone from the San Andres Limestone.

The IRT recognizes OSE's concerns with dual-screen wells. In this type of construction, there may be a potential for vertical movement of contamination unless appropriate engineering and procedural protections are in place to mitigate the risks. In the case of the LANL Cr(VI) plume, the most important challenges faced by DOE-EM-LA and the regulators are data gaps and uncertainties. Given the depth of the plume, the required time frames, challenges and costs for installing monitoring wells, and the need to maximize the value of each drilling campaign, the IRT believes that there is a compelling need to use dual-screen wells. Further, the DOE-EM-LA team documented that their mitigation strategy is effective and robust, using the highest-quality packer systems (e.g., Baski) with automated monitoring and real-time alarms so that any loss of isolation is reported to the local control room for immediate response. Calculations prepared by the IRT (**Appendix P**) to assess upper-bound values for the likely rates of leakage via borehole flow should a packer fail suggest that these rates are, under most conditions encountered at the site, small and could be recovered if necessary, and that the risk posed by such release does not outweigh the value of the dual-screen well completions to obtain data from a single boring.

Based on this strategy, the IRT recommends that OSE consider allowing the use of dual-screen wells with appropriate documentation and controls (i.e., using reviewed and approved standard operating procedures [SOPs], maintaining spare parts for contingencies, and providing clear time frames for restoring isolation if needed).

### 3.5.3 Recommended Actions

The IRT developed the following two specific recommendations:

- To support more quickly moving the remedial process ahead, the IRT believes it would be prudent and expedient for DOE-EM-LA to implement key aspects of the OSE requests. Specifically the IRT recommends use of coated bentonite granules below the water table (ending just above the capillary fringe), and then using cement (not bentonite amended) throughout the entire vadose zone. In the past, DOE-EM-LA has used uncoated bentonite chips in the vadose zone and then completed the upper (e.g., 50 to 100 feet) using cement. Uncoated bentonite granules would be an appropriate alternative to cement for the vadose zone due to its ability to swell in the presence of perched water.
- In the regional aquifer, it would be beneficial to the urgent need for site characterization for OSE to allow dual-screen monitoring wells to be constructed with supplemental documentation and controls to assure that risks are mitigated and minimized. The IRT recommends that coated bentonite granules be placed above and below the filter sand pack intervals to isolate the sample intervals.

## 4. References

- Angel, C. 2024. *Artesian well plan of operations & contamination present form*. New Mexico Office of the State Engineer presentation to Los Alamos National Laboratory. March 18, 2024.
- Arends, J. 2023. To eradicate the plume, use the same models. *Santa Fe New Mexican*. September 2, 2023. Available at <[https://www.santafenewmexican.com/opinion/my\\_view/to-eradicate-the-plume-use-the-same-models/article\\_b93f3b86-4849-11ee-b322-63fe35d4d7db.html](https://www.santafenewmexican.com/opinion/my_view/to-eradicate-the-plume-use-the-same-models/article_b93f3b86-4849-11ee-b322-63fe35d4d7db.html)>.
- Batu, V. 2024a. *Hydraulic conductivity data evaluation of the Neptune model for the LANL Site, Los Alamos, New Mexico*. Report to the IRT. April 3, 2024.
- Batu, V. 2024b. *Comparison of the horizontal hydraulic conductivity ( $K_h$ ) values at the CrEX and CrIN well locations, and PM-2 and PM-4 aquifer tests well locations with the  $K_h$  values of Neptune, Los Alamos, New Mexico*. Report to the IRT. August 12, 2024.
- Batu, V. 2024c. *Comparison of the horizontal hydraulic conductivity ( $K_h$ ) values of the CrEX and CrIN Wells, the  $K_h$  values Neptune, and the average  $K_{h-x}$  and  $K_{h-y}$  values in the CrEX and CrIN areas of compendium technical reports (Attachment 9, Figure 2.2-3), Los Alamos, New Mexico*. Report to the IRT. August 12, 2024.

- Batu, V. 2024d. *The conceptual model for the water-bearing formations beneath the LANL Site and determination methods of the breakthrough curves at the bottom of the vadose zone and degradation rates of chromium ( $\text{Cr}^{6+}$ )*, Los Alamos, New Mexico. Report to the IRT. August 16, 2024.
- Batu, V. 2024e. *Plots of chromium ( $\text{Cr}^{6+}$ ) concentrations vs. date between 2004 and 2024 and their interpretations*, Los Alamos, New Mexico. Report to the IRT. August 17, 2024.
- Batu, V. 2024f. *Evaluation of the measured temporal chromium ( $\text{Cr}^{6+}$ ) concentrations in the unconfined aquifer with respect to the transport in the vadose zone*, Los Alamos, New Mexico. Report to the IRT. August 18, 2024.
- Batu, V. 2024g. *Evaluation of the measured  $\text{Cr}^{6+}$  concentrations and flow rates of PM-2, PM-3, PM-4, and PM-5 water supply wells between 2006 and 2024 along with their well diagrams*, Los Alamos, New Mexico. Report to the IRT. August 19, 2024.
- Batu, V. 2024h. *Determination of the zone of influence of the PM-4 water supply well and evaluation of the effects of all water supply wells to the chromium ( $\text{Cr}^{6+}$ ) plume area*, Los Alamos, New Mexico. Report to the IRT. August 23, 2024.
- Batu, V. 2024i. *Evaluation of the flow parameters and chromium ( $\text{Cr}^{6+}$ ) concentration data to estimate the plume extensions in the longitudinal and transverse vertical directions*, Los Alamos, New Mexico. Report to the IRT. August 23, 2024.
- Batu, V. 2024j. *Horizontal ( $K_h$ ) and vertical hydraulic conductivity ( $K_v$ ) values determined from the aquifer tests of the CrIN, CrEX, PM-2, PM-4, PM-3 (with R-35a and R-35b), and R-13 wells at the LANL Site*. Report to the IRT. August 25, 2024.
- Blackmer, G.C. 1988. *Review of monitoring wells exhibiting elevated pH in F and H Area*. Prepared for the U.S. Department of Energy under Contract DE-AC09-76SR00001. E. I. du Pont de Nemours & Co. Savannah River Plant. July 1988.
- Broxton, D. 2024a. *Geology of the chromium investigation area*. Presentation to the IRT. March 21, 2024. Santa Fe, New Mexico.
- Broxton, D. 2024b. *Miocene basalts as potential confining beds*. Presentation to the IRT. March 21, 2024. Santa Fe, New Mexico.
- Broxton D.E. and P.G. Eller. 1995. *Earth science investigations for environmental restoration - Los Alamos National Laboratory Technical Area 21*. Los Alamos National Laboratory, Los Alamos, New Mexico.
- Broxton, D.E. and D.T. Vaniman. 2005. Geologic framework of a groundwater system on the margin of a rift basin, Pajarito Plateau, north-central New Mexico. *Vadose Zone Journal* 4(3): 522-550.

- Broxton, D., G. WoldeGabriel, D. Katzman, and R. Harris. 2021. *Using high-resolution stratigraphic characterization to inform remediation strategies for a chromium plume at Los Alamos National Laboratory*. 21116.WM2021 Conference, March 8–12, 2021. Phoenix, Arizona.
- Cather, S.M. 2004. Laramide orogeny in central and northern New Mexico and southern Colorado. p. 203-248 in Mack, G.H. and K.A. Giles, *The Geology of New Mexico, A Geologic History*, New Mexico Geological Society.
- Cherry, J.A. 2023. In My Experience: the lessons from dispersion—don't believe everything you read. *Groundwater Monitoring & Remediation* 43(3): 145–147.
- Cirpka, O.A., G. Chiogna, M. Rolle, and A. Bellin. 2015. Transverse mixing in three-dimensional nonstationary anisotropic heterogeneous porous media. *Water Resources Research* 51: 241–260. doi:10.1002/2014WR015331.
- Concerned Citizens for Nuclear Safety (CCNS). 2023. LANL's toxic hexavalent chromium plume must remain a priority. <<https://nuclearactive.org/lanls-toxic-hexavalent-chromium-plume-must-remain-a-priority/>>. August 31, 2023.
- Devlin, J.F. 2015. HydrogeoSieveXL: An Excel-based tool to estimate hydraulic conductivity from grain-size analysis. *Hydrogeology Journal* 23: 837-844.
- Dey, S. and A.K. Paul. 2013. Hexavalent chromium reduction by aerobic heterotrophic bacteria indigenous to chromite mine overburden. *Brazilian Journal of Microbiology* 44(1): 307-315.
- Ding, M., D. Musa, R. Harris, M. Rearick, G. Perkins, P. Reimus, Paul, G. WoldeGabriel, E. Kluk, D. Ware, J. Heikoop, Jeff, and D. Katzman. 2018. *Characterizing natural attenuation of Cr(VI) in a chromium plume at Los Alamos National Laboratory*.
- DOE-EM-LA. 2023. *Draft chromium interim measure and final remedy environmental assessment, Los Alamos, New Mexico*. U.S. Department of Energy Environmental Management Los Alamos Field Office. EMID-703015, DOE/EA-2216. November 2023.
- Doherty, J. 2003. Ground water model calibration using pilot points and regularization. *Ground Water* 41(2): 170-177.
- Foster, L. 2024a. Kxy and Kz Notes - draft for IRT.
- Foster, L. 2024b. *Numerical modeling of the Cr plume*. Presentation to the IRT. March 21, 2024. Santa Fe, New Mexico.
- Foster, L. 2024c. *Hydrology of the Pajarito Plateau and regional aquifer*. Presentation to the IRT. March 21, 2024. Santa Fe, New Mexico.
- Frenzel, P.F. 1995. *Geohydrology and simulation of groundwater flow near Los Alamos, north-central New Mexico*. U.S. Geological Survey Water-Resources Investigations Report 95-4091.

- Geological Survey of Japan. 2005. *Atlas of Eh-pH diagrams, Intercomparison of thermodynamic databases*. Open File Report No.419.
- Gillham, R.W., E.A. Sudicky, J.A. Cherry, and E.O. Frind. 1984. An advection–diffusion concept for solute transport in heterogeneous unconsolidated geological deposits. *Water Resources Research* 20(3): 369–378. DOI:10.1029/WR020i003p00369.
- Hadley, P.W. and C. Newell. 2014. The new potential for understanding groundwater contaminant transport. *Groundwater* 52(2): 174–186.
- Hantush, M.S. 1964. Hydraulics of wells. p. 281-442 in Chow, V.T. (Ed.), *Advances in hydroscience*. Academic Press.
- Harp, D.R. and V.V. Vesselinov. 2011. Identification of pumping influences in long-term water level fluctuations. *Ground Water Journal* 49(3): 403-414.
- Harp, D.R. and V.V. Vesselinov. 2013. Contaminant remediation decision analysis using information. *Stochastic Environmental Research and Risk Assessment* 27: 159–168.
- Herman, J. and C. Martinez. 2024. *Los Alamos National Laboratory chromium plume cleanup*, New Mexico Environment Department. Power Point Presentation. March 21, 2024.
- Heikoop, J.M., T.M. Johnson, K.H. Birdsell, P. Longmire, D.D. Hickmott, E.P. Jacobs, D.E. Broxton, D. Katzman, V.V. Vesselinov, M. Ding, D.T. Vaniman, S.L. Reneau, T.J. Goering, J. Glessner, and A. Basu. 2014. Isotopic evidence for reduction of anthropogenic hexavalent chromium in Los Alamos National Laboratory groundwater. *Chemical Geology* 373. doi: 0.1016/j.chemgeo.2014.02.022.
- Interstate Technology and Regulatory Council (ITRC). 2017. *Remediation management of complex sites*. RMCS-1.
- Katzman, D., V. Vesselinov, P. Reimus, D. Broxton, J. Heikoop, G. WoldeGabriel, M. Everett, K. Birdsell, and C. Rodriguez. 2018. *Chromium plume at LANL: From conceptual site model to development of complex remediation strategies*. WM2018 Conference, March 18–22, 2018. Phoenix, Arizona.
- Kelley, V.C. 1978. *Geology of the Española Basin, New Mexico*. New Mexico Bureau of Mines and Mineral Resources Geologic Map GM-48. Scale 1:250,000.
- Kitanidis, P.K. 2017. Teaching and communicating dispersion in hydrogeology, with emphasis on the applicability of the Fickian model. *Advances in Water Resources* 106: 11–23.
- Korte, N.E. and P.M. Kearl. 1991. The utility of multiple-completion monitoring wells for describing a solvent plume. *Ground Water Monitoring Review* 11(2): 153.
- Langman, J. 2024. *Chromium chemistry and regional aquifer contamination*. Presentation to the IRT. March 21, 2024.



- Los Alamos National Laboratory (LANL). 2008. *Groundwater level status report for 2008, Los Alamos National Laboratory*. LA-14397-PR Progress Report.
- LANL. 2015. *Interim measures work plan for chromium plume control*. LA-UR-15-23126.
- LANL. 2016. *Geochemical analysis of potential impacts of injecting treated water into injection wells in Mortandad Canyon*. EPC-D0-16-118, LA-UR-16-22806, 7 pp.
- LANL. 2018. Stratigraphic and sedimentological studies and their hydrogeological features in the chromium investigation area, Los Alamos National Laboratory. Attachment 3, p. 210-223, in *Compendium of Technical Reports Conducted Under the Work Plan for Chromium Plume Center Characterization*. LA-UR-18-21450. March 2018, EP2018-0026.
- LANL. 2022. *Chromium interim measures and characterization work plan*. September 2022.
- LANL. 2024. FEHM: Finite Element Heat and Mass Transfer Code. <<https://fehm.lanl.gov/>>. Accessed September 2024.
- LeBlanc, D.R., S.P. Garabedian, K.M. Hess, L.W. Gelhar, R.D. Quadri, K.G. Stollenwerk, and W.W. Wood. 1991. Large scale natural gradient tracer test in sand and gravel, Cape Cod, Massachusetts, Experimental design and observed tracer movement. *Water Resources Research* 27(5): 895-910.
- Longmire, P.A., S. Kung, J.M. Boak, A.I. Adams, F. Caporuscio, and R.N. Gray. 1996. Aqueous geochemistry of upper Los Alamos Canyon, New Mexico. p. 473-480 in *New Mexico Geological Society Guidebook, 47th Field Conference, Jemez Mountains Region*.
- Ma, R., C. Zheng, M. Tonkin, and J. Zachara. 2011. Importance of considering intraborehole flow in solute transport modeling under highly dynamic flow conditions. *Journal of Contaminant Hydrology* 123(1-2): 11-19.
- Ma, R., C. Zheng, J. Zachara, and M. Tonkin. 2012. Utility of bromide and heat tracers for aquifer characterization affected by highly transient flow conditions. *Water Resources Research* 48(8). Doi: 10.1029/2011WR011281.
- Mackay, D.M., D.L. Freyberg, and P.V. Roberts. 1986. A natural gradient experiment on solute transport in a sand aquifer, Approach and overview of plume movement. *Water Resources Research* 22(13): 2017-2029.
- McCrary, T. 2024. *Background of hexavalent chromium plume in the regional aquifer*. Presentation to the IRT. March 21, 2024. Santa Fe, New Mexico.
- N3B. 2023. *Initial five-year evaluation of the interim measures for chromium plume control with an assessment of potential modifications to operations*. Prepared for the U.S. Department of Energy Office of Environmental Management (DOE-EM) Los Alamos (LA). February 2023. EM2023-0067.

- National Research Council (NRC). 2003. *Environmental cleanup at Navy facilities: Adaptive site management*. National Academies Press, Washington, D.C.
- NRC. 2005. *Contaminants in the subsurface, Source zone assessment and remediation*. National Academies Press, Washington, D.C.
- Neptune. 2023. *Annual progress report on chromium plume control interim measure performance, April 2022 through March 2023*. EM2023-0392. June 2023.
- Neptune. 2024. *Surface water data at Los Alamos National Laboratory, Water year 2023*. EM2024-0164.
- Neville, C. and M. Tonkin, 2004. Modeling multi-aquifer wells with MODFLOW. *Ground Water* 42(6): 910-919.
- Neville, C. and J. Zhang. 2010. Benchmark analysis of solute transport with multi-aquifer wells. *Ground Water* 48(6): 884–891.
- New Mexico Environment Department (NMED). 2024. List of contaminants for new water sources, Drinking Water Bureau. <[https://cloud.env.nm.gov/resources/\\_translator.php/HKA~sl~mnAhFiTd2yWeBAialqR+PaKNAPF7Hpqc9NTXnM~sl~E8lyNw~sl~+y8O~sl~fFFw5pbQGTA+whRjHjfONDAq8YHBeJQzHxTvnUrpfEni8U8SH~sl~JE02HtikMgvhg==.pdf](https://cloud.env.nm.gov/resources/_translator.php/HKA~sl~mnAhFiTd2yWeBAialqR+PaKNAPF7Hpqc9NTXnM~sl~E8lyNw~sl~+y8O~sl~fFFw5pbQGTA+whRjHjfONDAq8YHBeJQzHxTvnUrpfEni8U8SH~sl~JE02HtikMgvhg==.pdf)>. Accessed July 22, 2024.
- Pacific Northwest National Laboratory (PNNL). 2024. STOMP User Guide: Subsurface Transport Over Multiple Phases. <<https://stomp-userguide.pnnl.gov/>>. Accessed September 2024.
- Palmer, C.D. and R.W. Puls. 1994. *Natural attenuation of hexavalent chromium in groundwater and soils*. EPA154015-941505.
- Purtymun, W.D. 1984. *Hydrologic characteristics of the main aquifer in the Los Alamos area: Development of ground water supplies*. LANL report LA-9967-MS.
- Purtymun, W.D. 1995. *Geologic and hydrologic records of observation wells, test holes, test wells, supply wells, springs, and surface water stations in the Los Alamos Area*. LA-12883-MS, UC-903 and UC-940.
- Reimus, P., D. Katzman, M. Ding, and B. Willis. 2021. *Using tracers and opportunistic geochemical signatures to inform modeling of Cr(VI) migration at LANL*. WM2021 Conference, March 7–11, 2021, Phoenix, Arizona.
- Scantlebury, L., V. Bedekar, M. Karanovic, M.J. Tonkin, and T.J. Durbin. 2022. *Texture2Par USER'S GUIDE: A parameterization utility for IWFm and MODFLOW*. Version 1.0.0.
- Skibitzke, H.E. and G.M. Robinson. 1963. *Dispersion in ground water flowing through heterogeneous materials*. U.S. Geological Survey Professional Paper 386-B.

- Smith, G.A., M.N. Gaud, and J.M. Timmons. 2004. *Geologic map of the Truchas quadrangle, Rio Arriba, Santa Fe, and Taos Counties, New Mexico*. New Mexico Bureau of Geology and Mineral Resources OF-GM-84. Scale: 1:24,000.
- Stephens, D. 2024. *Conceptual site model for chromium*. Unpublished letter.
- Stephens, D., H. Wainwright, and C.W. Newell. 2024. *Vertical gradients and their impact on Cr concentrations*. Report to the IRT..
- TechLaw and EPA Region 4. 2024. Conceptual Site Model (CSM). <<https://archive.epa.gov/epawaste/hazard/web/pdf/csm.pdf>>. Accessed August 17, 2024.
- U.S. Department of Energy (DOE). 2022. Network of National Laboratories for Environmental Management and Stewardship, Independent Review of Groundwater Remediation Strategy for Hexavalent Chromium and RDX Groundwater Plumes and Los Alamos National Laboratory. NNLEMS-2022-00003.
- U.S. DOE. 2023. *Annual progress report on chromium plume control interim measure performance, April 2022 through March 2023*. EMLA-23-BF25 I-2-I.
- U.S. DOE Environmental Management Los Alamos Field Office. 2023. *Draft chromium interim measure and final remedy environmental assessment, Los Alamos, New Mexico*. DOE/EA-2216, EMID-703015. November 2023.
- U.S. Environmental Protection Agency (EPA). 1990. Corrective Action for Solid Waste Management Units (SWMUs) at Hazardous Waste Management Facilities, 55 Fed. Reg. 30793. July 27, 1990.
- U.S. EPA. 1996. Corrective Action for Releases from Solid Waste Management Units at Hazardous Waste Management Facilities, 61 Fed. Reg., 19432. May 1, 1996.
- U.S. EPA. 2000. Announcement of Schedule for Resource Conservation and Recovery Act (RCRA) Corrective Action Guidance Documents and Request for Feedback on RCRA Cleanup Reforms, 65 Fed. Reg. 15905. March 24, 2000.
- U.S. EPA. 2003. *Results based corrective action and tailored oversight guidance for facilities subject to corrective action under Subtitle C of the Resource Conservation and Recovery Act*. EPA 530-R-03-012.
- U.S. EPA. 2011. *Environmental cleanup best management practices: Effective use of the project life cycle conceptual site model*. EPA 542-F-11-011.
- U.S. EPA. 2022. Office of Land and Emergency Management Directive 9200.3-123. June 23, 2022.
- U.S. Geological Survey (USGS). 2017. *MODFLOW-USG: An Unstructured Grid Version of MODFLOW for Simulating Groundwater Flow and Tightly Coupled Processes Using a Control Volume Finite-Difference Formulation*. <<https://www.usgs.gov/software/modflow->

usg-unstructured-grid-version-modflow-simulating-groundwater-flow-and-tightly>.  
October 27, 2017.

USGS. 2019a. *MODFLOW-2005: USGS Three-Dimensional Finite-Difference Ground-Water Model*. Release information. <<https://www.usgs.gov/software/modflow-2005-usgs-three-dimensional-finite-difference-ground-water-model>> March 4, 2019.

USGS. 2019b. *MT3D-USGS: Groundwater Solute Transport Simulator for MODFLOW*. <<https://www.usgs.gov/software/mt3d-usgs-groundwater-solute-transport-simulator-modflow>>. Released June 28, 2019.

USGS. 2024. *MODFLOW 6: USGS Modular Hydrologic Model*. Release information <<https://www.usgs.gov/software/modflow-6-usgs-modular-hydrologic-model>>. May 23, 2024.

Vesselinov, V.V. 2004. *An alternative conceptual model of groundwater flow and transport in saturated zone beneath the Pajarito Plateau*. Los Alamos National Laboratory. LA-UR-05-6741.

Vesselinov, V.V., D. Katzman, D. Broxton, K. Birdsell, S. Reneau, D. Vaniman, P. Longmire, J. Fabryka-Martin, J. Heikoop, M. Ding, D. Hickmott, E. Jacobs, T. Goering, D. Harp, and M. Phoolendra. 2013. *Data and model-driven decision support for environmental management of a chromium plume at Los Alamos National Laboratory*. 13264, WM2013 Conference. February 24–28, 2013. Phoenix, Arizona.

Wainright, H., and D. Stephens. 2024. *Does IM have adverse impacts?* Presentation to the IRT. July 2024.

Zech, A., S. Attinger, A. Bellin, V. Cvetkovic, G. Dagan, P. Dietrich, A. Fiori, and G. Teutsch. 2023. Evidence based estimation of macrodispersivity for groundwater transport applications. *Groundwater* 61(3): 346–362. <https://doi.org/10.1111/gwat.13252>.

Zyvoloski, G. 2007. *FEHM: A control volume finite element code for simulating subsurface multi-phase multi-fluid heat and mass transfer*. LAUR-07-3359. May 18, 2007.

Zyvoloski, G.A., B.A. Robinson, and Z.V. Dash. 1999. *FEHM application*. SC-194. MOL.19990810.0029.

## Figures



**Figure 2-1.** Photographic depiction of the position of the chromium plume in relation to the Power Plant source area, and the two canyons (Sandia and Mortandad) affected by the releases (taken from McCrory, 2024).

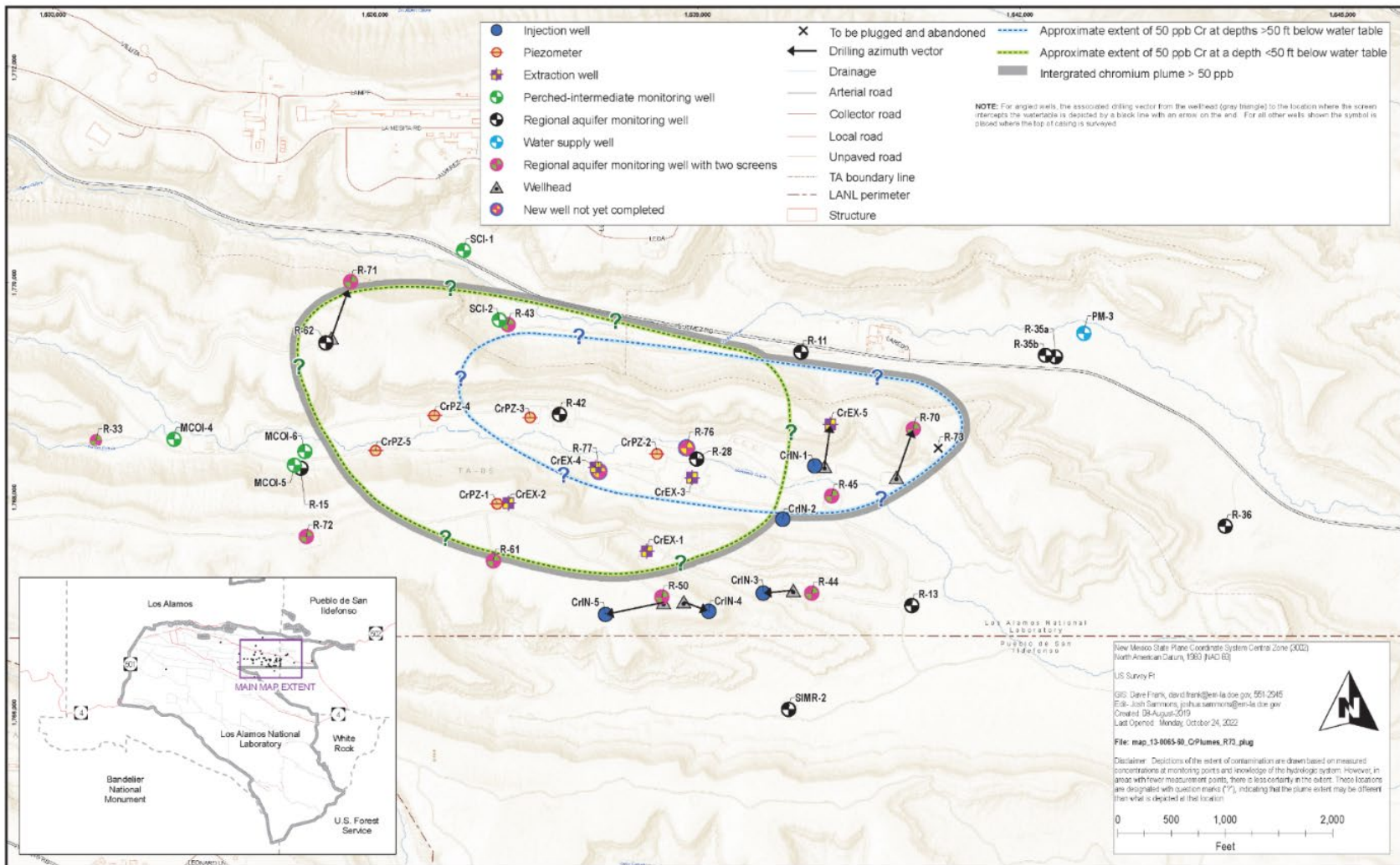


Figure 2-2. Estimated extents of chromium plume showing monitoring wells, extraction wells (CrEX-1 thru CrEX-5) and injection wells (CrIN-1 thru CrIN-5) and extent of chromium in groundwater as estimated by LANL (2019).

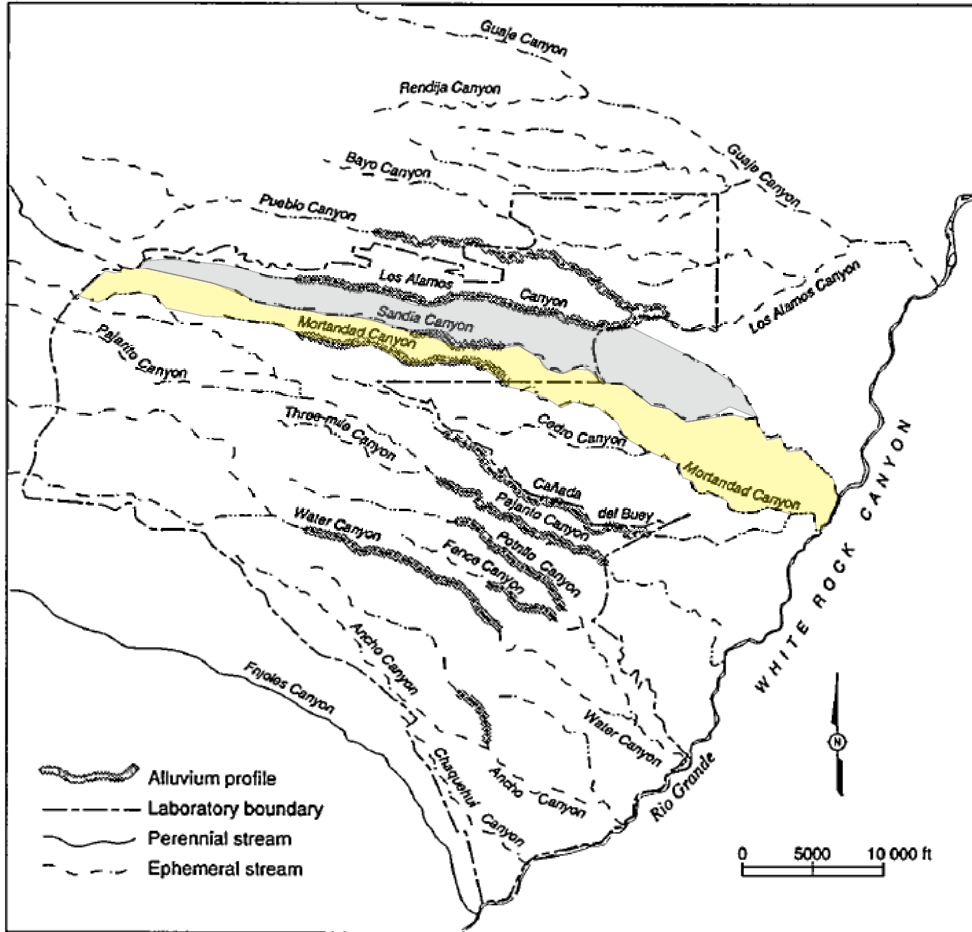
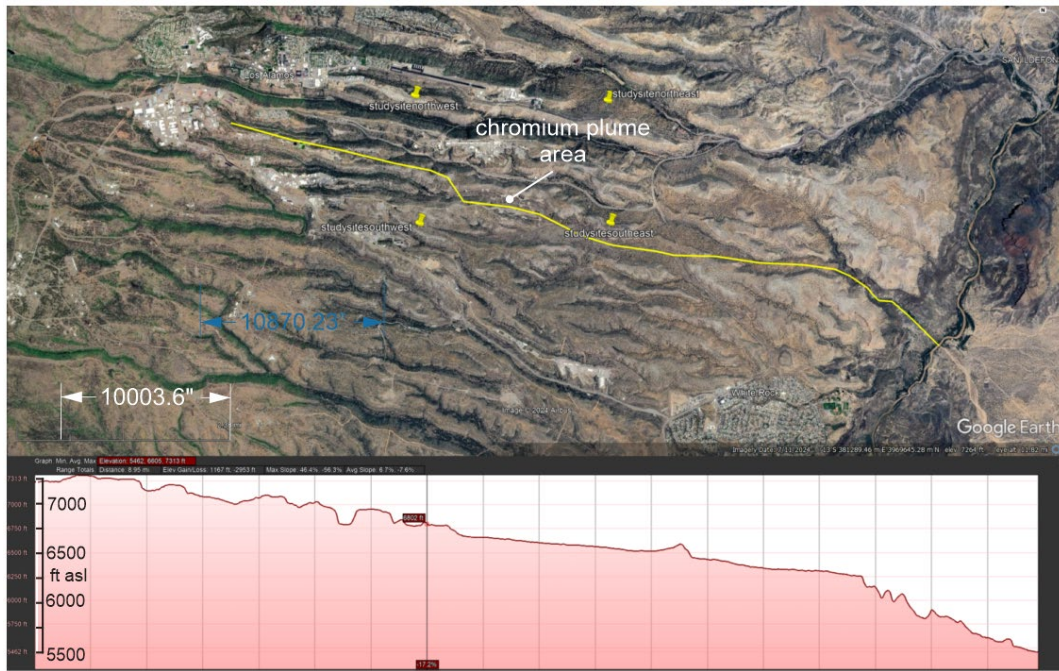


Figure 2-3. Locations of Sandia and Mortandad Canyons in relation to other nearby canyons (from Purtyman, 1995, Figure I-P).





**Figure 2-4.** Aerial image of the region around Mortandad Canyon, and a section of the topographic changes from Los Alamos to the Rio Grande River. The chromium plume area lies on a topographically flat portion of the canyon.

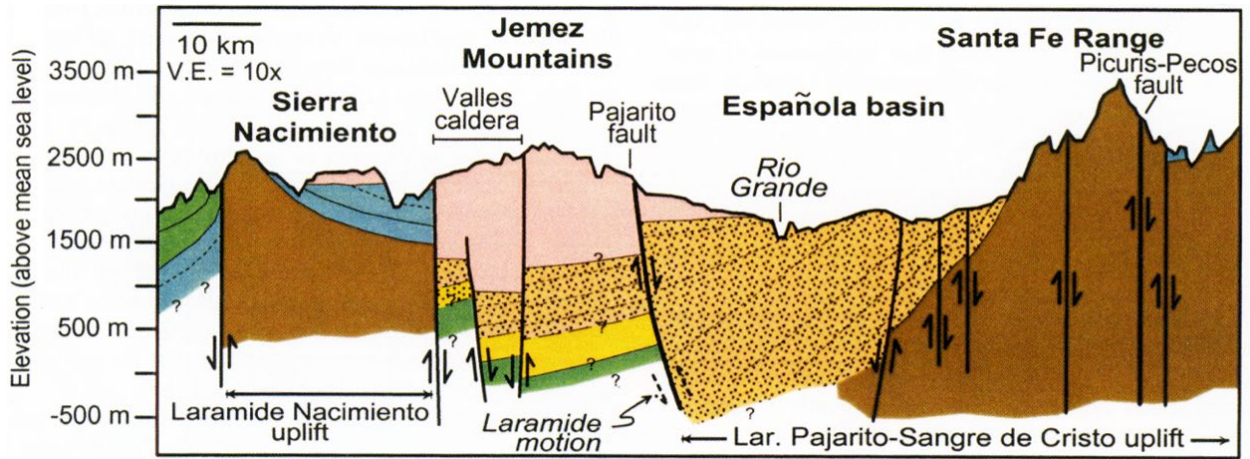
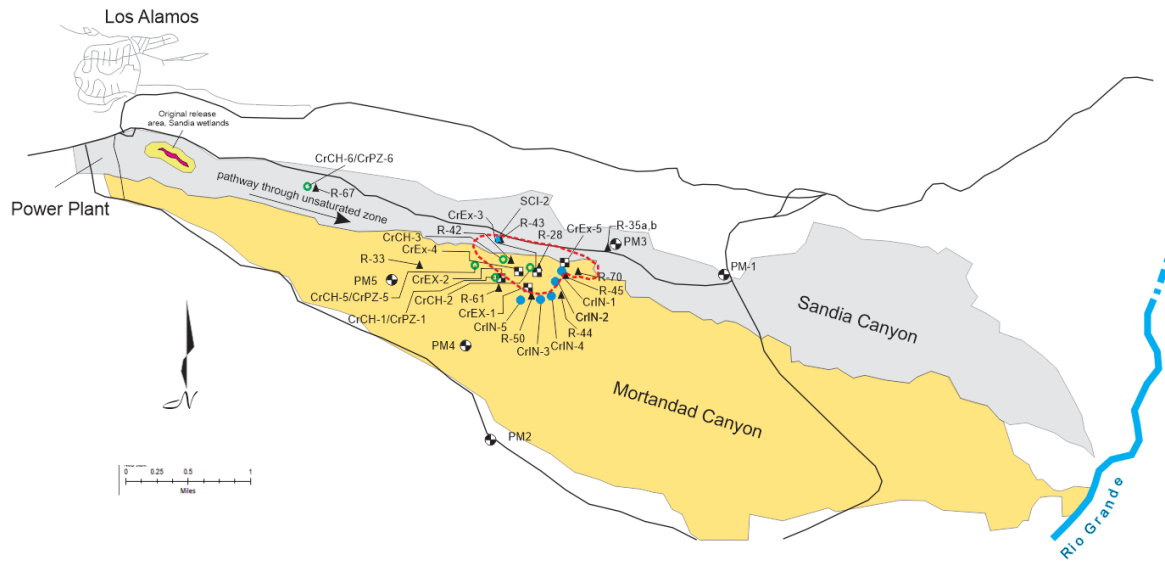
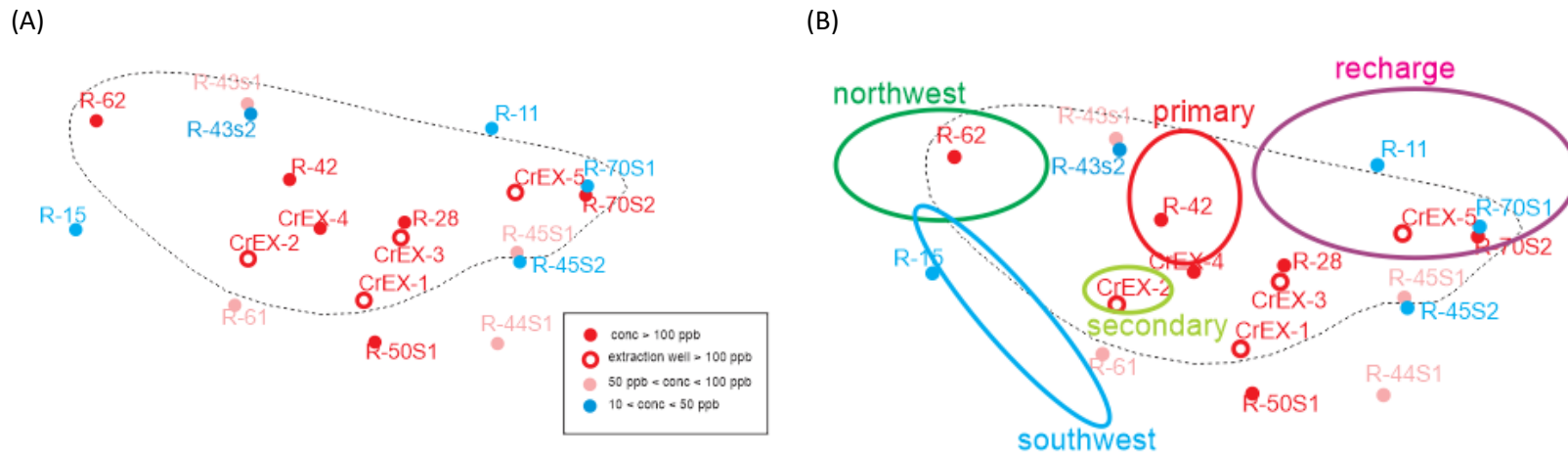


Figure 2-5. A simplified cross section of the regional geology (provided by Broxton, 2024)

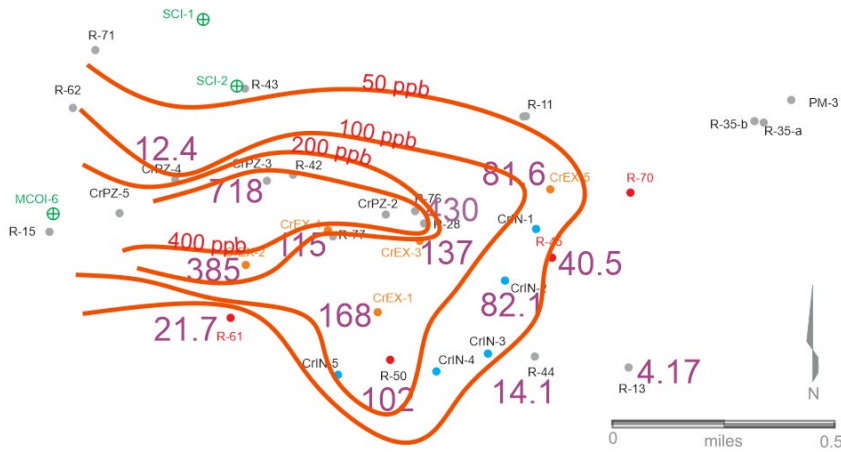


**Figure 2-6. Map of study site and surrounding area, modified from map\_20-0010-12d\_revised\_well\_location\_plate\_2024\_cheryl\_version and DOE-EM-LA, 2023. Locations of selected monitoring wells (R-x), extraction wells (CrEX-x), injection wells (CrIN-x) and water supply wells (PM-x) are shown. Colors show locations of Sandia and Mortandad Canyons (see also Figure 2-2).**

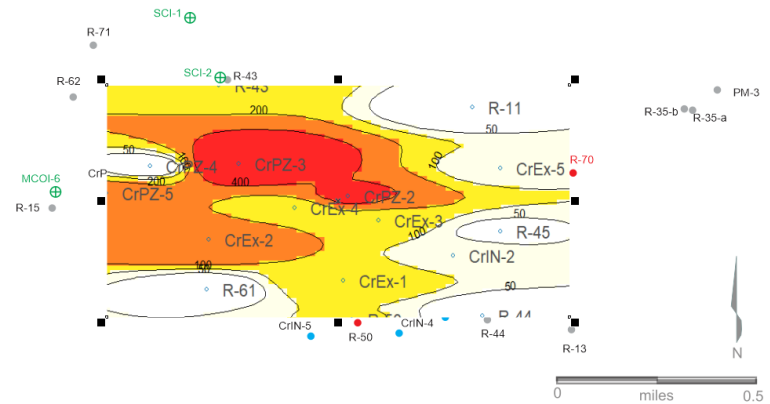


**Figure 2-7.** (A) Locations of selected monitors with chromium concentrations above background (>~10 ppb), above the New Mexico standard for chromium (>50 ppb) (from map\_MCP\_126\_chromium\_monitoring\_Q2\_2024.tiff; Department of Energy, 2023). (B) Locations of 'windows' that explain observed chromium concentration distributions in Neptune modeling. These locations are non-unique and represent one realization (Foster, 2024b, slide 42).

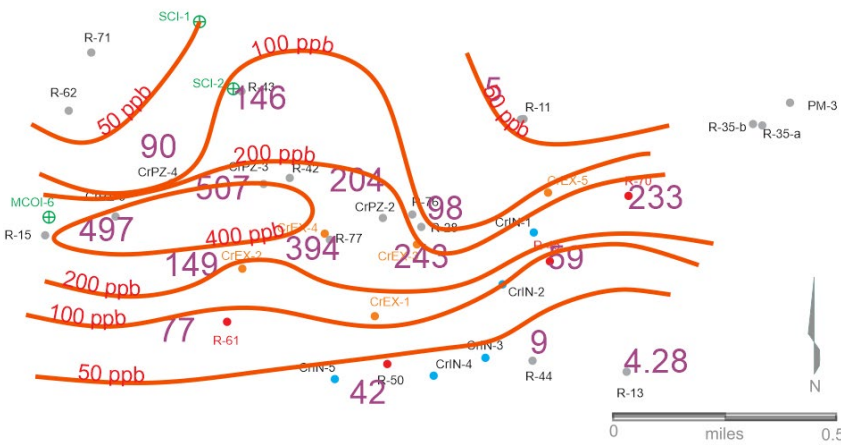
(A)



(B)



(C)



(D)

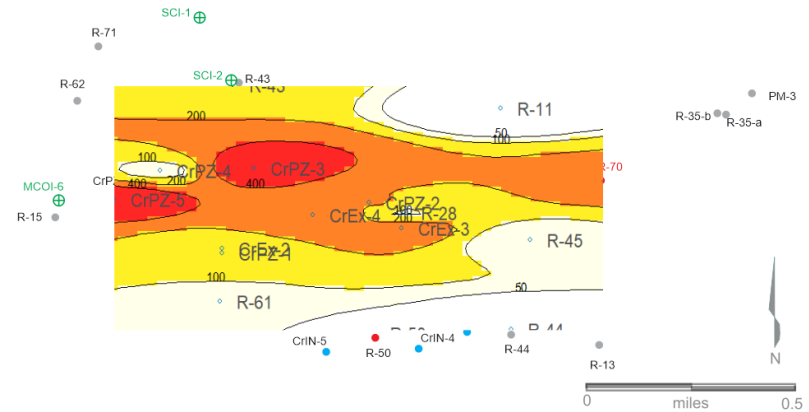
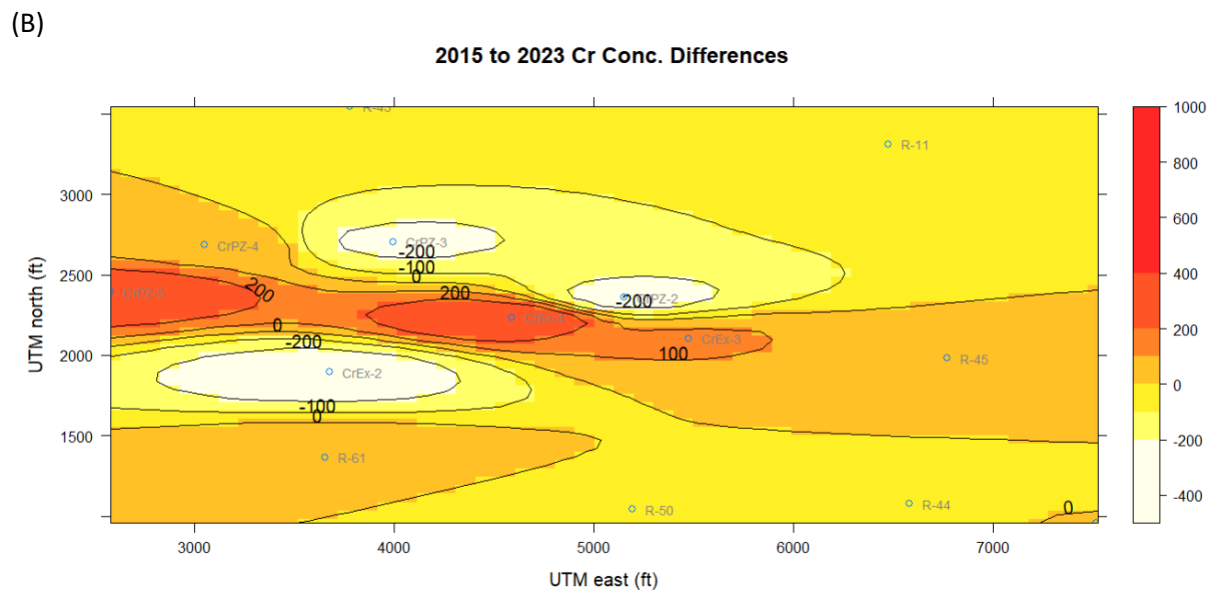
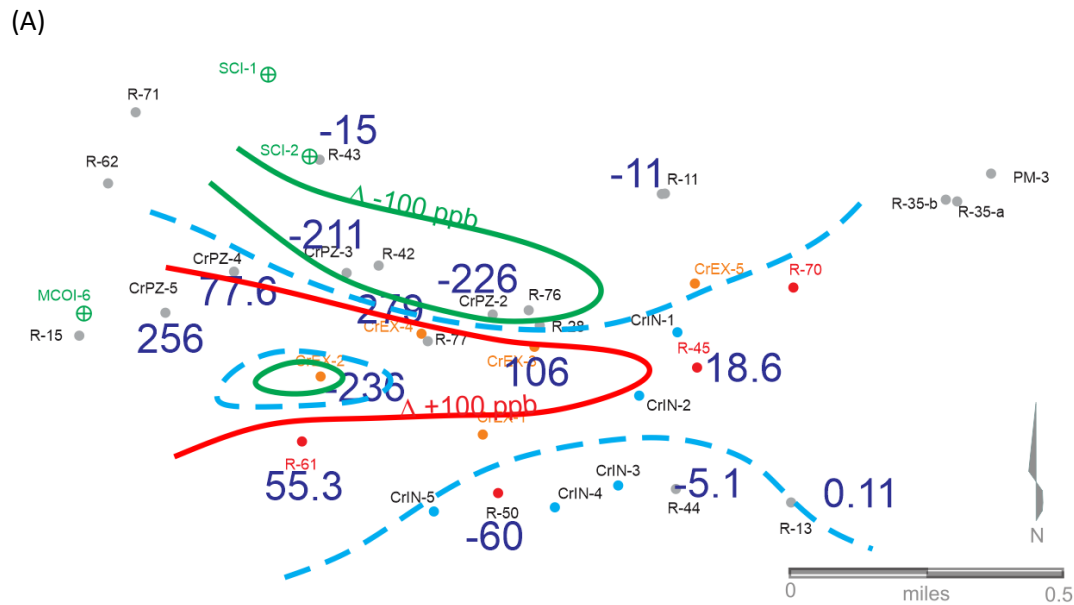


Figure 2-8.

(A) Manual contouring of plan-view chromium concentrations in the plume area in 2015-2016, before the initiation of the IM. Values shown represent maximum values at either S1 or S2 screens. (B) Computer generated contours of the data in (A) based on inverse distance weighting interpolation with a power of 4 and an x-axis weighting to permit contours to reflect the flow direction (see Section 3.1.2.2 for details). (C) Manual contours of chromium concentrations for maximum concentrations at selected locations in 2023. (D) Computer generated contours of the data in (C) based on inverse distance weighting interpolation as described in (B).



**Figure 2-9.** Change in plan-view chromium concentrations between 2015 (pre-IM) and 2023 (post-IM), based on the data in Figure 2-8. (A) Manual contouring of differences suggests chromium mass increases in the central area of the plume and diminishing chromium to the north and south. The dashed blue lines represent the zero-change contour, green lines bound zones of chromium concentration declines equal to or greater than 100 ppb, and red lines bound zones of chromium concentration increases equal to or greater and 100 ppb. Purple values are chromium concentrations in parts per billion. (B) Computer contours, calculated as described in Figure 2-8, of the chromium concentration differences in (A) show similar trends. The greatest increases in concentration between the two dates correspond to locations of extractions wells, suggesting some level of success in the capture and removal of chromium mass from the aquifer.

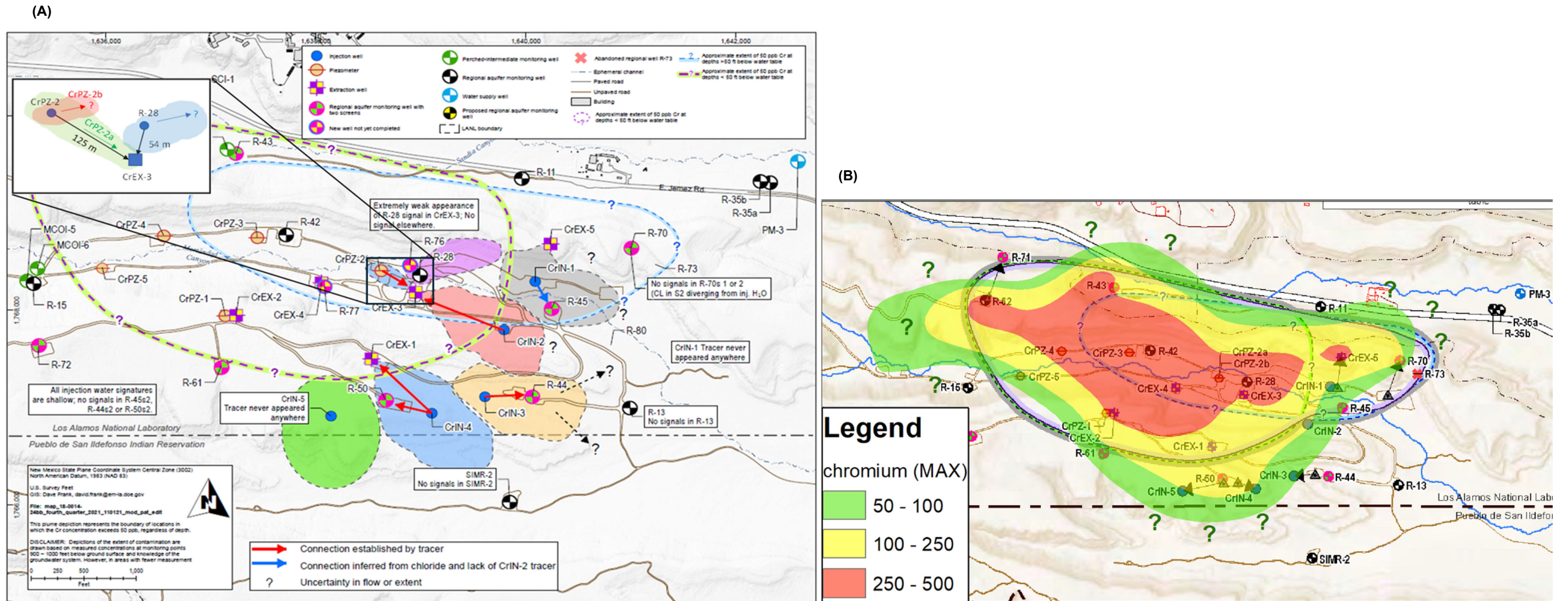
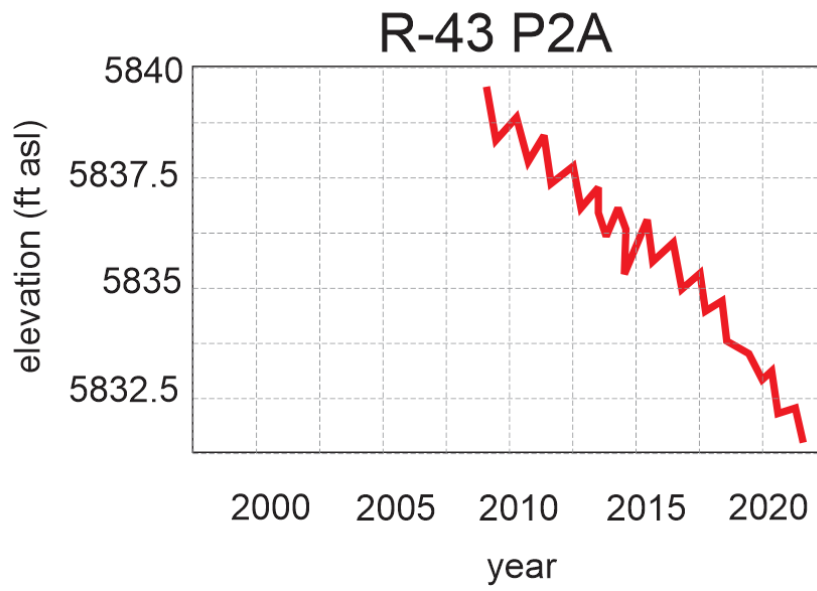
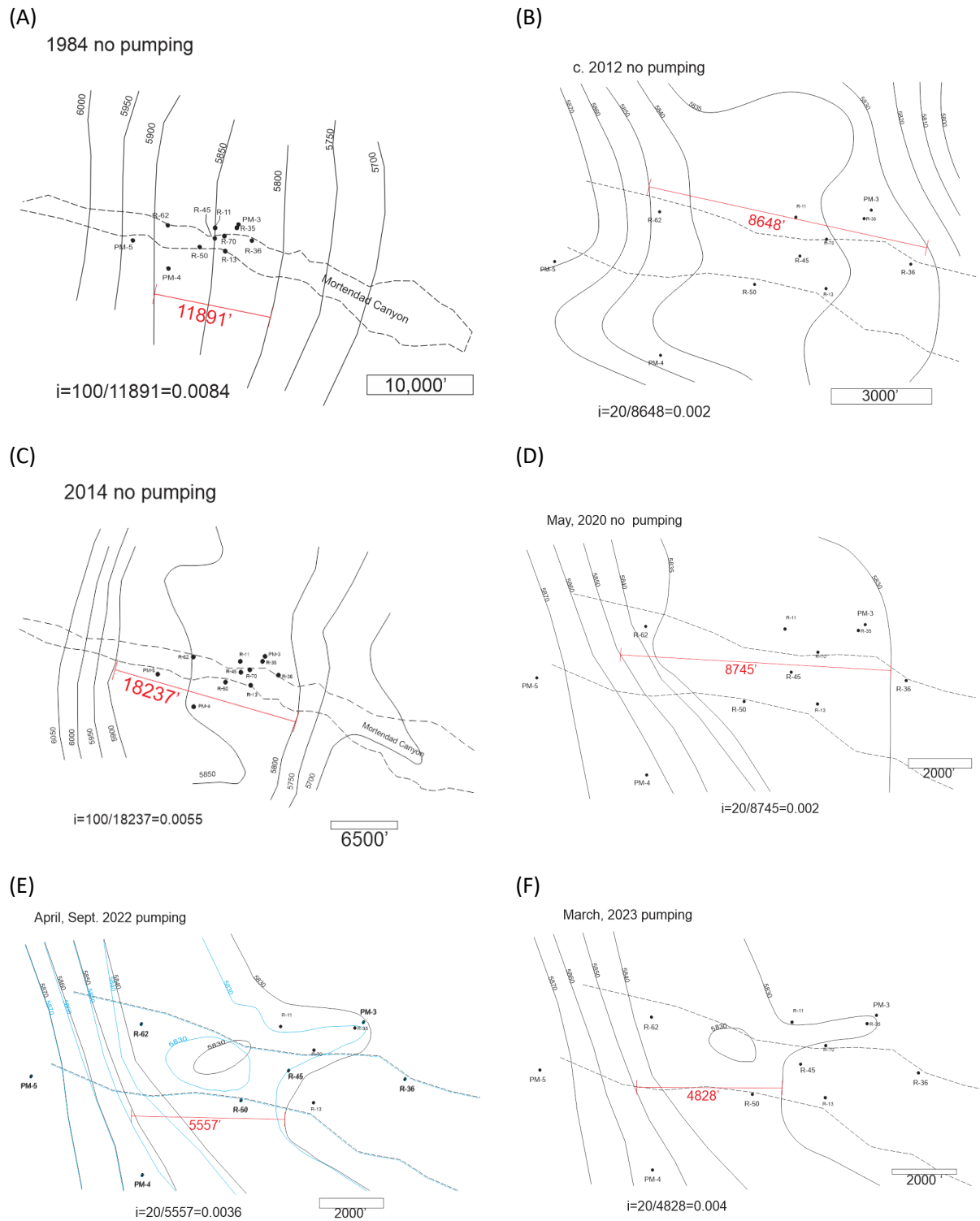


Figure 2-10. The extent of chromium contamination along the southern border of the site is uncertain. The available data are suggestive of a small portion of the chromium plume reaching or possibly crossing the San Ildefonso Pueblo border. (A) Areas of influence of wells inferred on the basis of tracer testing cross the boundary raising the possibility of a small amount of plume water moving in that direction with the onset of injection well pumping. Image reproduced from N3B (2023, Figure 5.4-7, pg. 76). (B) Composite plume consisting of maximum values detected at the wells shown up to 2023. The data were interpolated by kriging the log-concentration values and then contoured. The resulting graphic shows a small portion of the plume south of the border with the San Ildefonso Pueblo.



**Figure 2-11.** Example of water table decline trend since the year 2000. At R-43 in the plume area the decline has been on the order of 8 feet (Foster, 2024c).





**Figure 2-12. Comparison of plan-view water levels in the shallow aquifer in Mortandad Canyon between 1984 and 2023. The approximate hydraulic gradient between PM-5 and R-50 was used as a metric to compare flow conditions across the decades and in the presence/absence of pumping at the CrEX wells. Sources of the data are given in Table 2-2.**

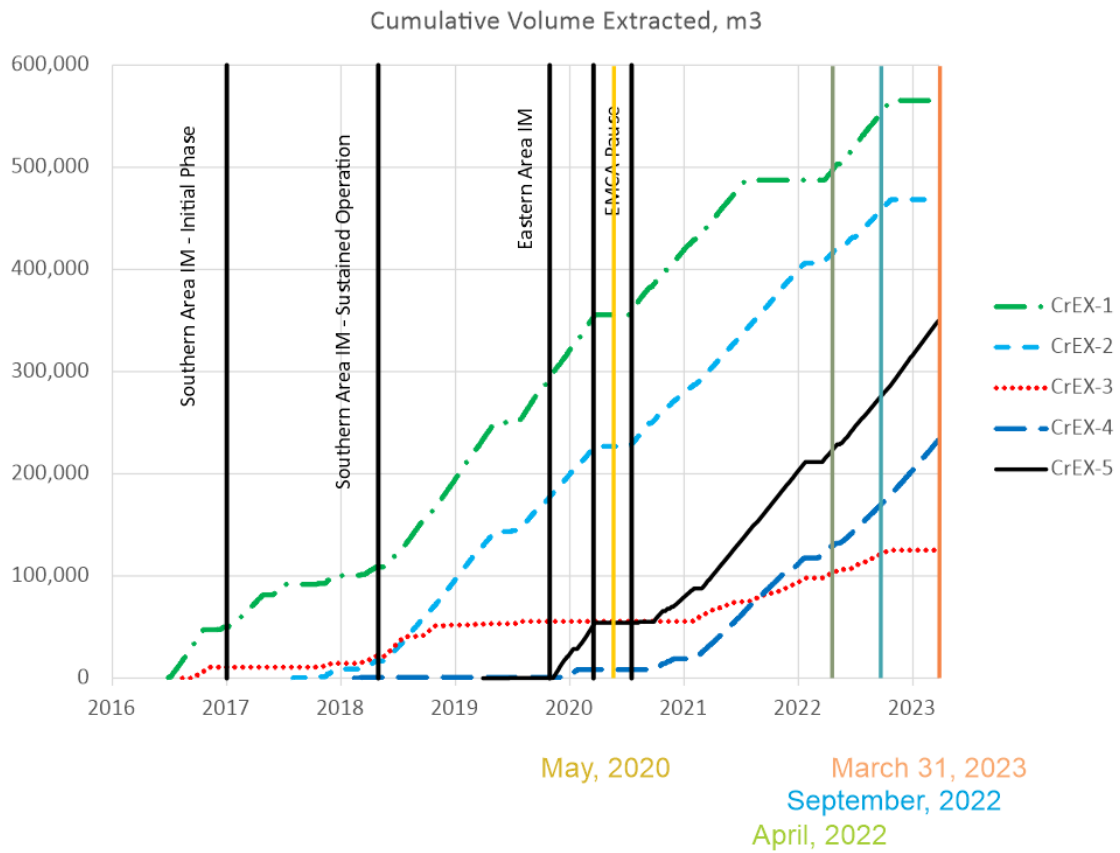


**Figure 2-13. Pumping history at the CrEX wells in the plume area. Times of the water levels shown in are indicated as colored vertical lines. Note that maps before 2016 predated pumping from the CrEX wells. The May 2020 data were also collected during a time when the CrEX wells were not pumping.**

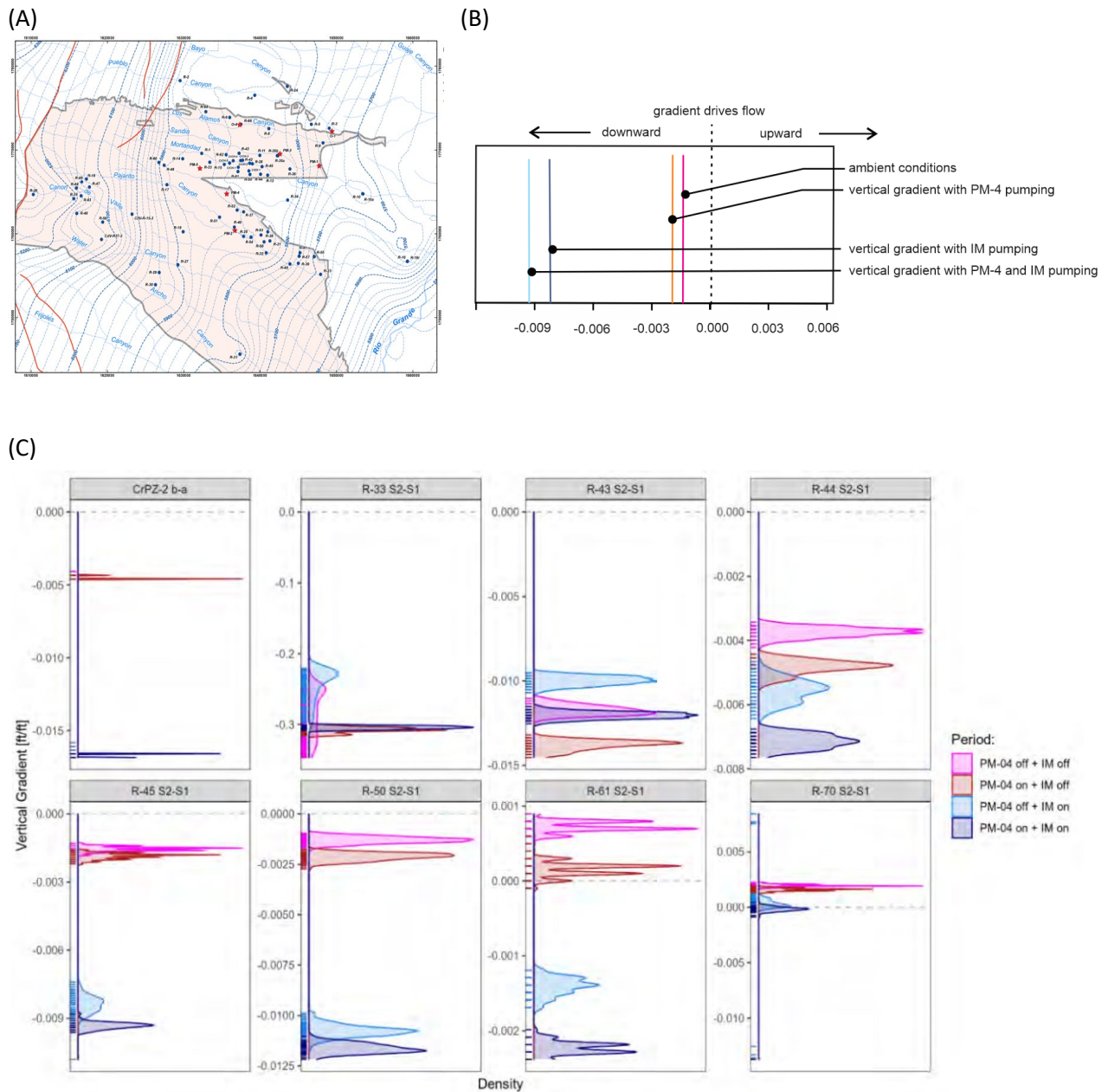


**Figure 2-14.** (A) Regional potentiometric surface through Mortandad Canyon and surroundings indicating eastward horizontal flow. Flow exhibits local deviations to the north and to the south (taken from McCrory, 2024). (B) Effect of PM well and IM well pumping on vertical hydraulic gradients at R-45. Flow has a consistent downward driving force, with the greatest effects caused by IM well pumping. (C) Density plots of hydraulic gradients are several wells in the plume area with influences similar to those at R-45 caused by PM-4 and IM well pumping. Note the plots in C are rotated 90° to show the highest potentials for downward flow lower on the y-axis (reproduced from Neptune (2023 enclosure, pg. 41). The density plots show that the vertical gradients for downward flow are routinely present beyond the range of measurement noise, with the exceptions of R-33 and to a lesser degree R-43.

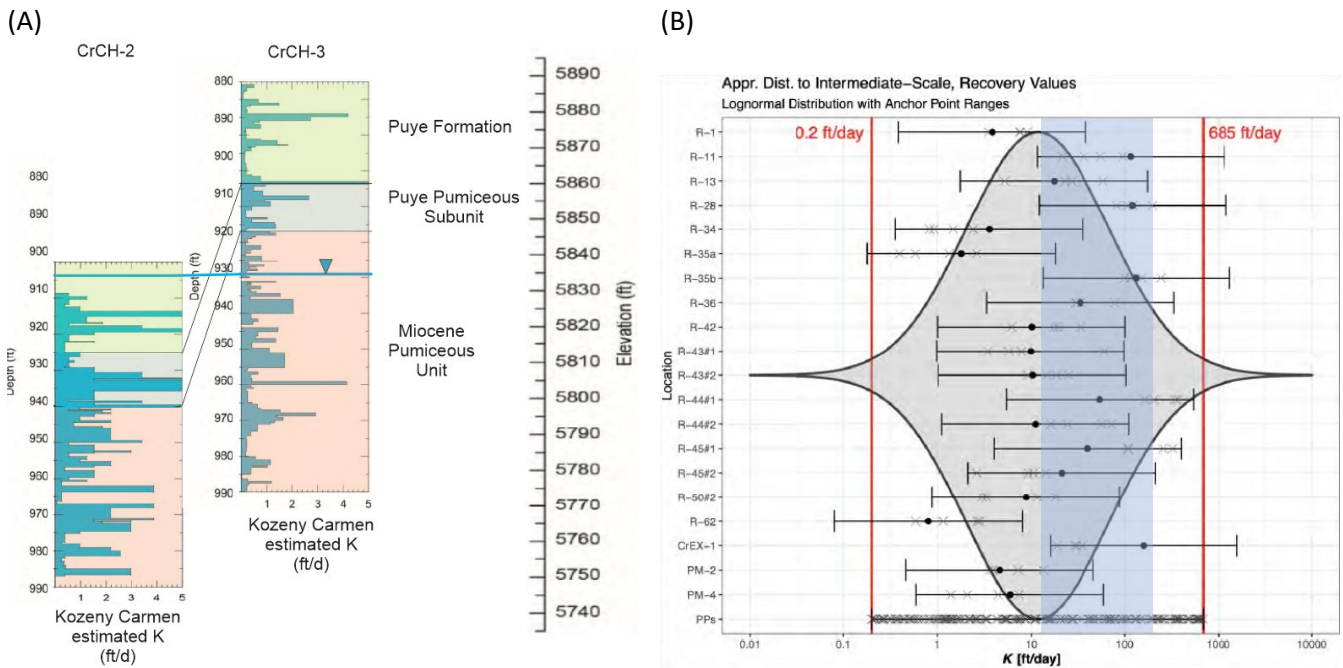


**Figure 2-15. (A) Profile of estimated horizontal hydraulic conductivity values from grain size analysis through the Puye Formation and below. The range at CrCH-3 is shown and is between about 0.2 ft/d to 5 ft/d, a factor of 25 difference. Depending on the horizontal continuity of these variations, they could be responsible for much of the observed vertical anisotropy (modified from LANL, 2018, Attachment 3, pg. 210-231). (B) Range of reported horizontal hydraulic conductivity values for the study area (from Neptune, 2023; Foster, 2024b, Figure 10). Blue highlighted zone is the range determined from Batu (2024d) based on the analysis of pumping records from the CrEX wells (12 ft/d to 172 ft/d).**

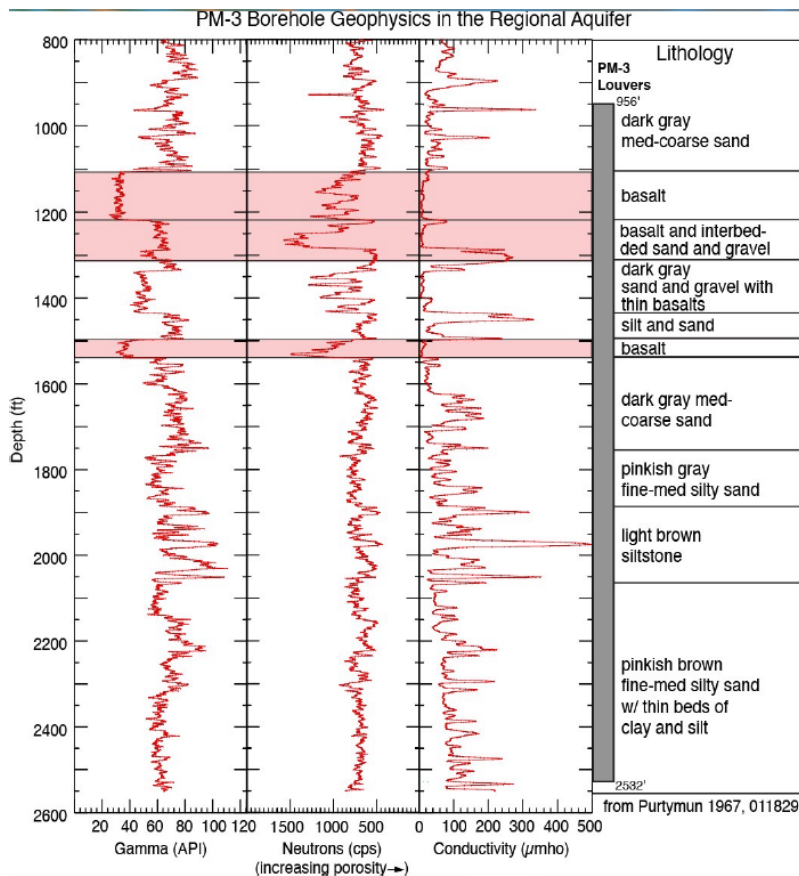


**Figure 2-16. Borehole log of PM-3, showing reduced porosity and conductivity in the mineralogically distinct zones associated with the basalt. These data are consistent with the basalt serving as an aquitard in the system (from Broxton, 2024b, slide 13).**

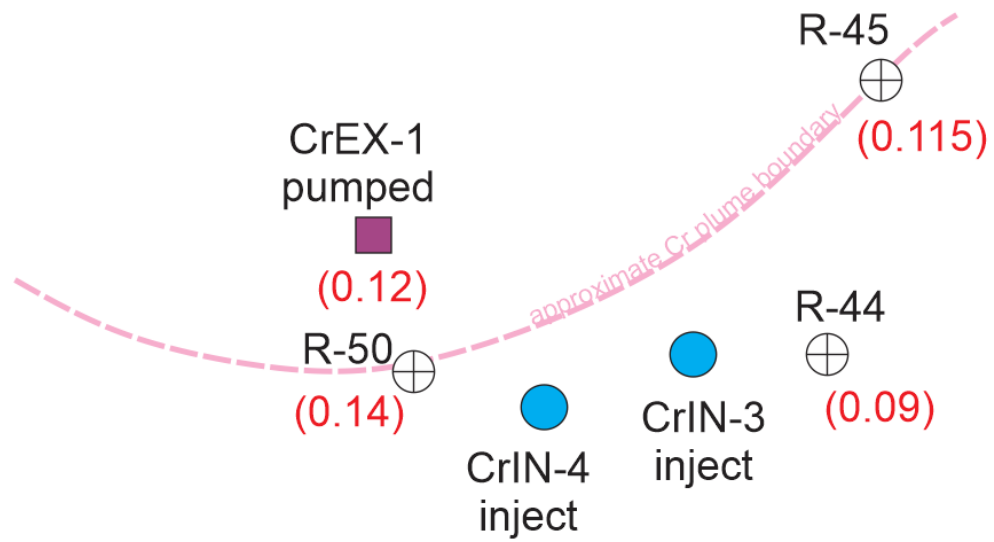
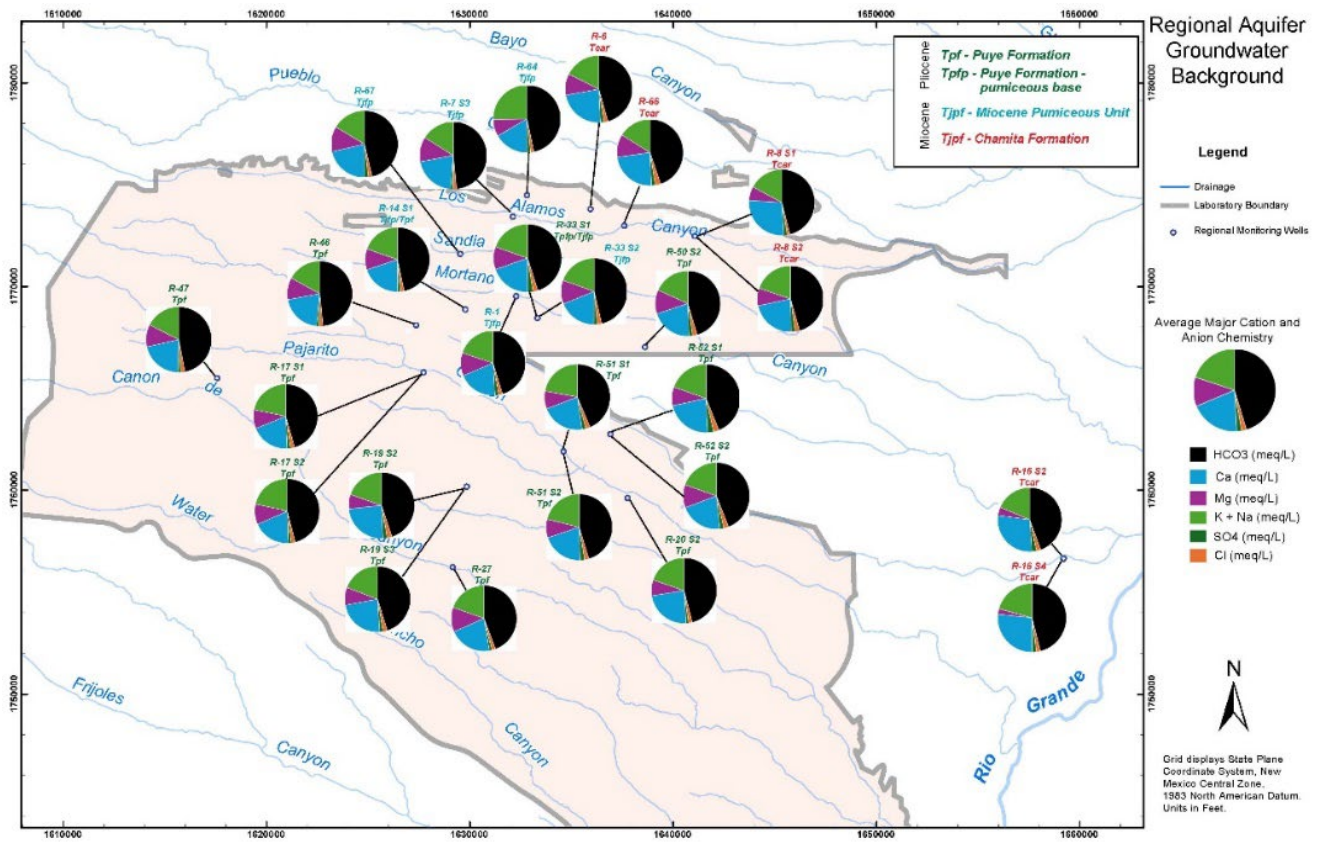
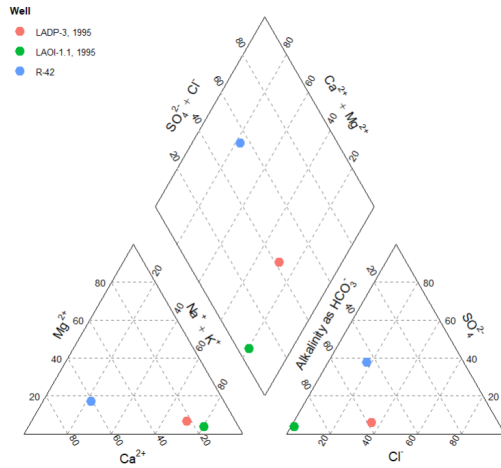


Figure 2-17. Map showing locations of wells and monitoring wells used in the estimation of effective porosity at the chromium plume site (values shown in red) (modified from Reimus et al., 2021).



**Figure 2-18. Background water chemistry in the regional aquifer beneath the Pajarito Plateau. The uniformity of the fingerprint through most of the region suggests a single hydrogeologic unit in near equilibrium with the groundwater (Figure provided by Pat Longmire and Dave Broxton, 2024).**

(A)



(B)

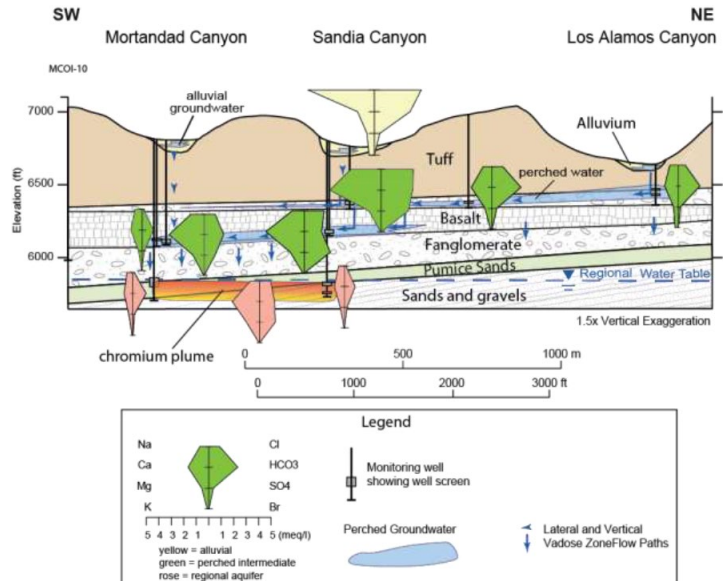


**Figure 2-19. (A) Major ion chemistry in the vicinity of the chromium plume in Mortandad Canyon (R-42) compared to vadose zone water in Sandia Canyon (LADP and LAOI). The background water chemistry is a calcium/bicarbonate/sulfate water in the Mortandad Canyon aquifer compared to a sodium/bicarbonate/chloride chemistry in the Sandia vadose zone. The two waters are distinct from one another (sources Longmire et al., 1996; LANL, 2016). (B) Stiff diagrams showing similarities in the geochemistry of the vadose zone waters in Sandia Canyon and those in the plume area in Mortandad Canyon (Katzman et al., 2018).**



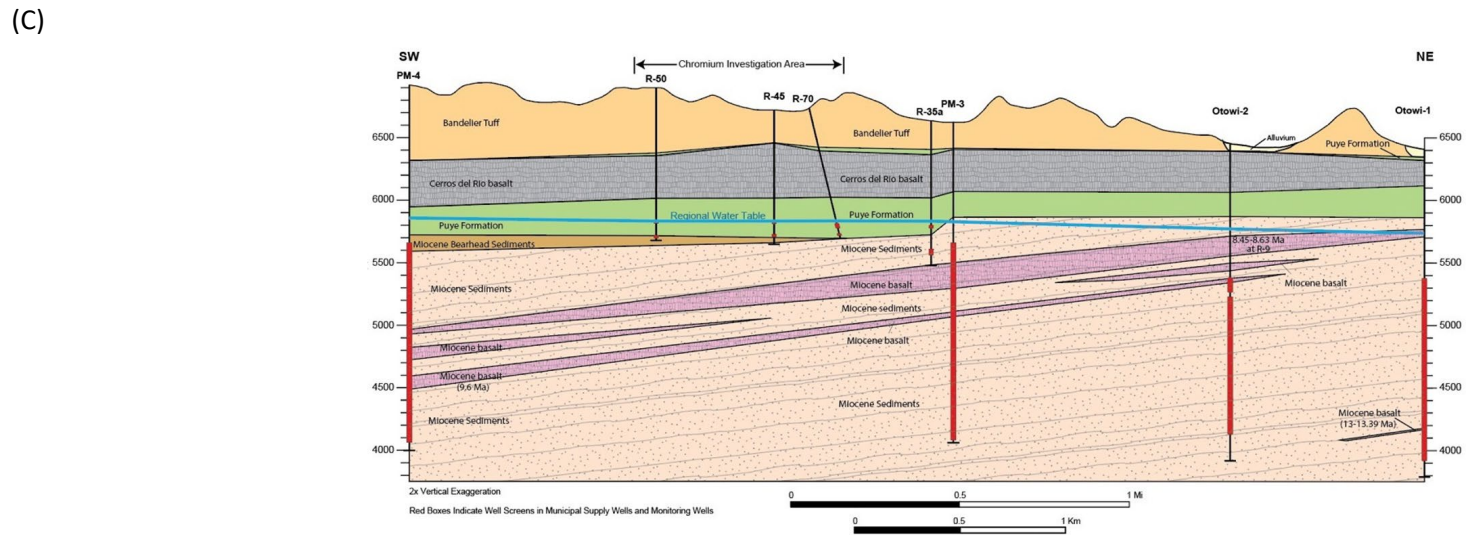
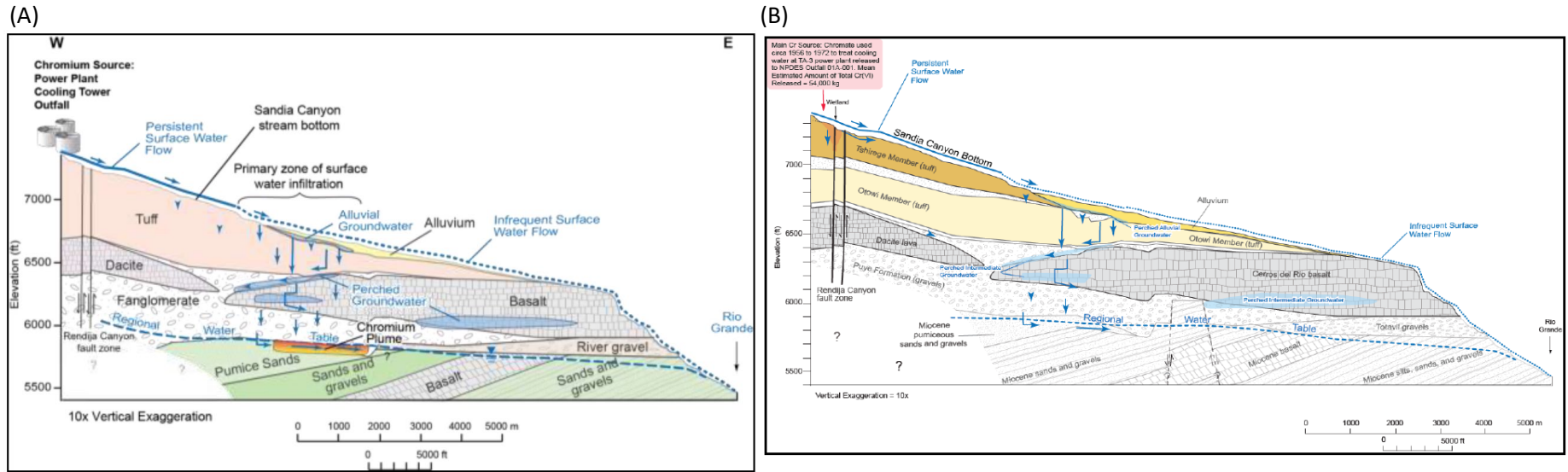


Figure 2-20. CSM summary figures presented by (A) Katzman et al. (2018), (B) DOE-EM-LA (2023), and (C) Broxton (2024a).

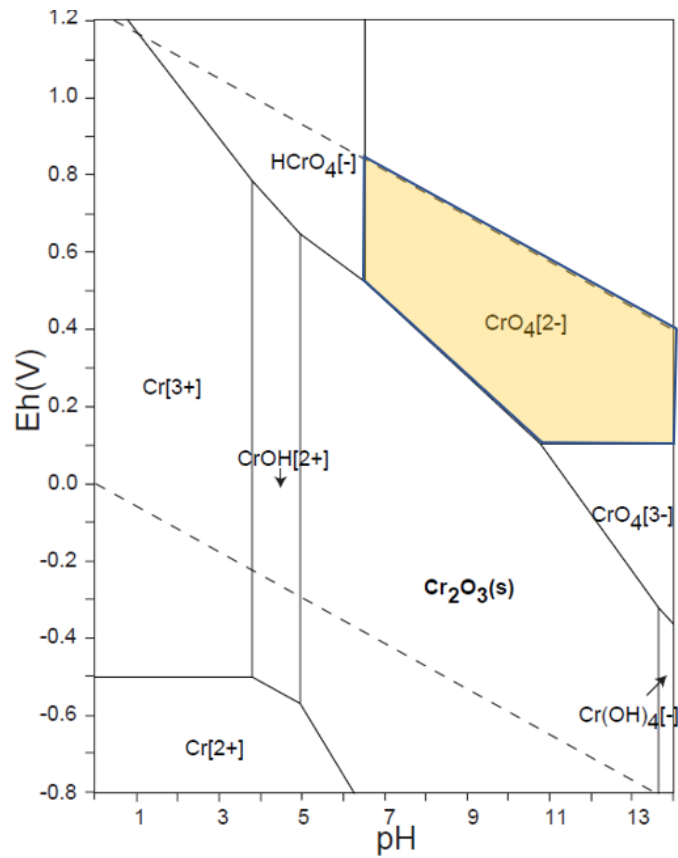


Figure 2-21. Speciation of dilute chromium in natural waters for the system Cr-O-H (1).  $\Sigma\text{Cr} = 10^{-10}$ , 298.15K,  $10^5$  Pa (Geological Survey of Japan, 2005). The highlighted region of the Eh-pH diagram coincides with aerobic conditions and is the region of stability for the species of hexavalent chromium that may be dominating transport at the site.

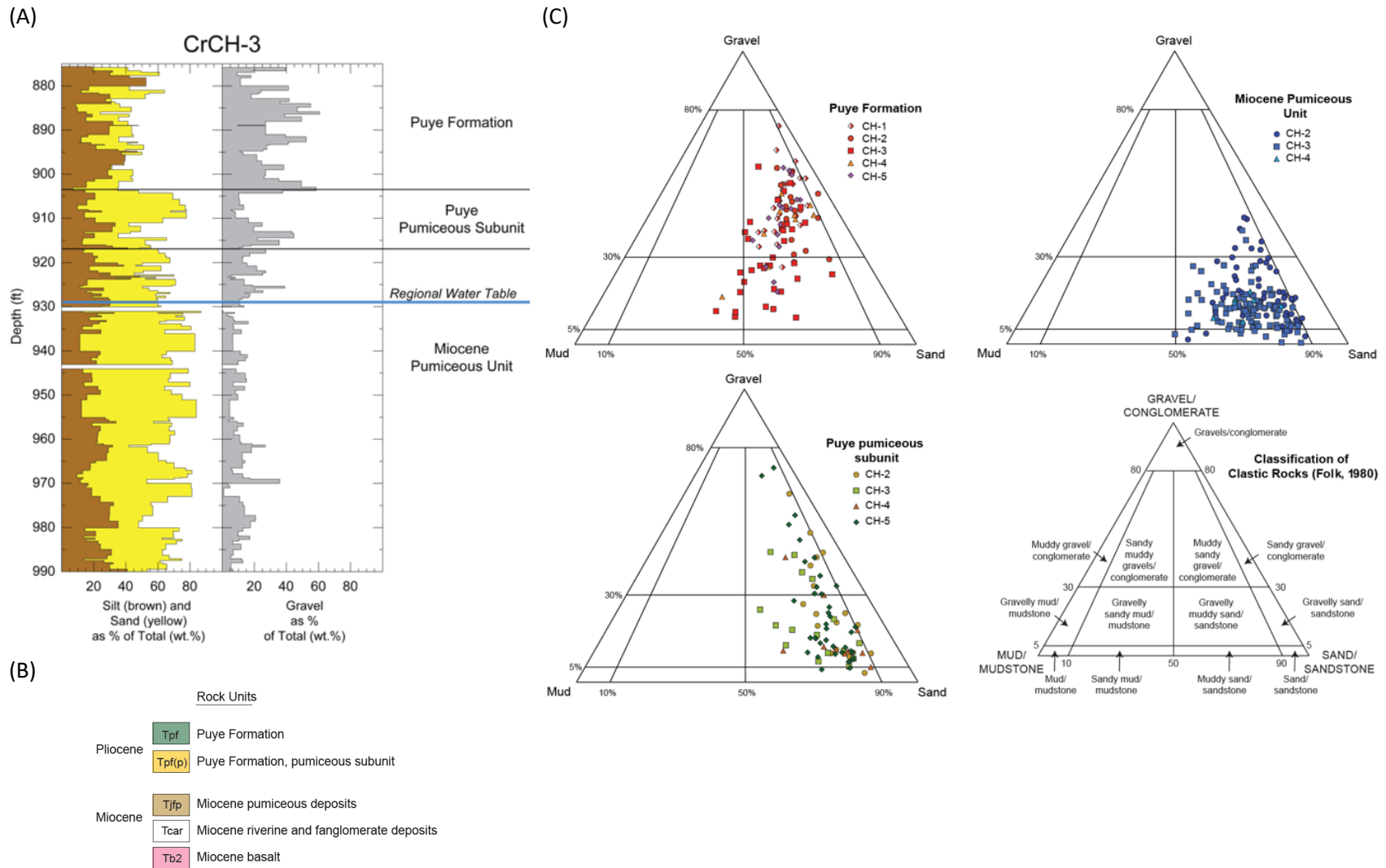


Figure 2-22. (A) Subsurface formations underlying Mortandad Canyon, at borehole CrCH-3 from Broxton (2014) and LANL, 2018, Attachment 3, pg. 210-231. (B) Classification of sediments from selected formation (taken from Broxton et al., 2021). (C) Units and abbreviations commonly used (Broxton, 2024a).

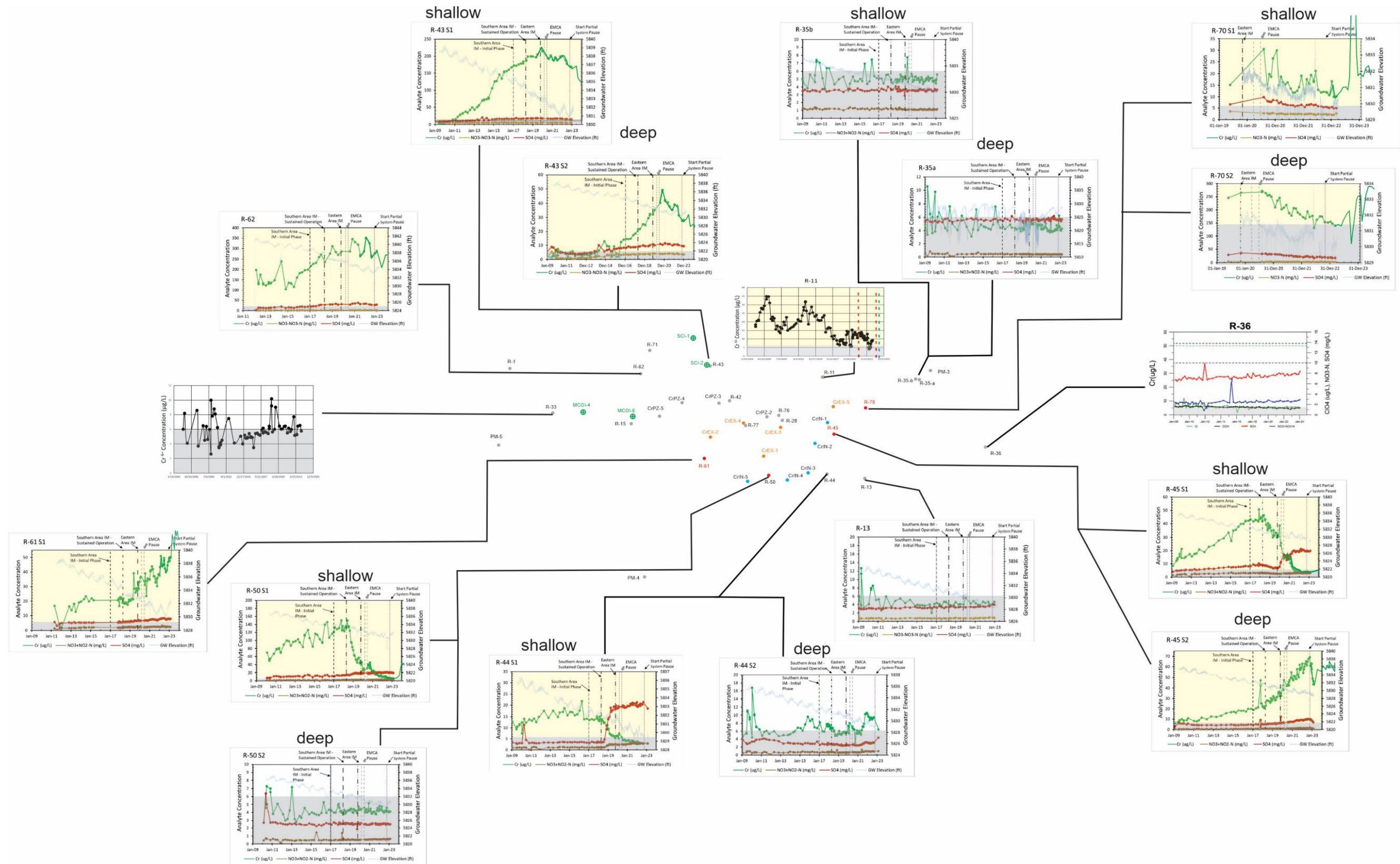
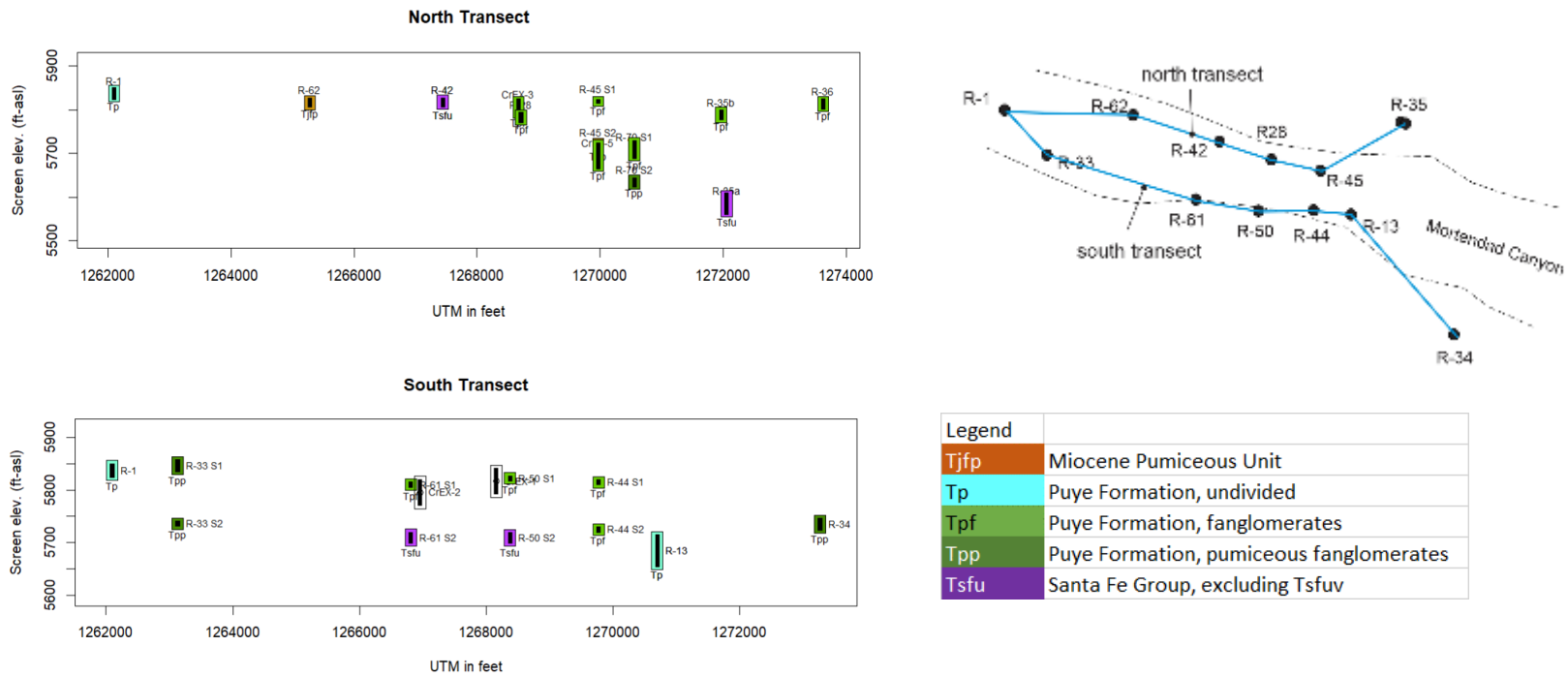


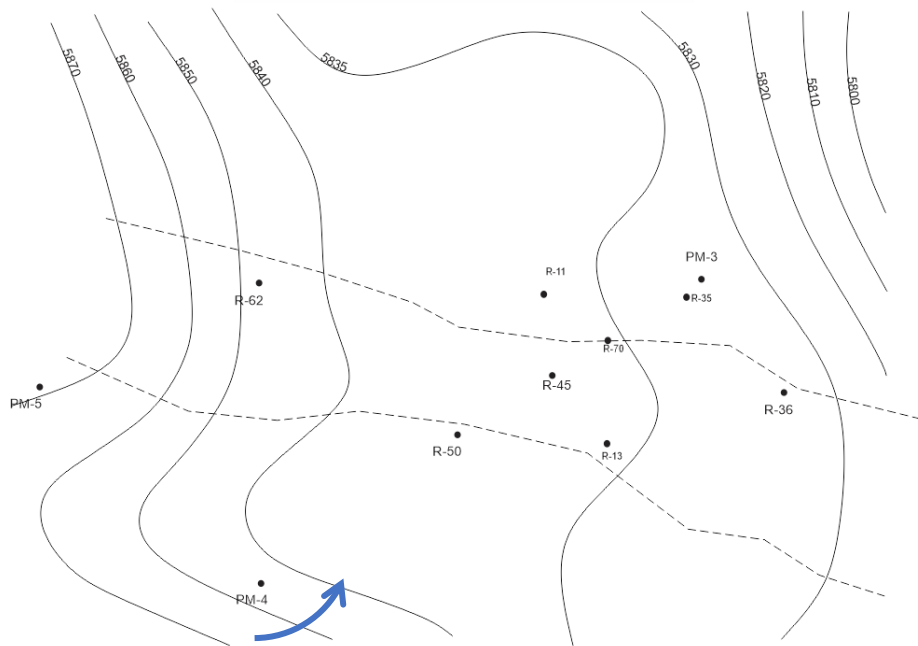
Figure 3-1. Time-series concentrations of chromium (green), nitrate (brown), and sulfate (red) at perimeter monitoring wells in the plume area. The figures were taken from Neptune (2023) with selected locations appended to March 2024 from file Time-Series Quarterly Plots\_FYQ1\_020724.pptx. Plots highlighted in yellow are those with persistent chromium concentrations above background (~6 µg/L).



**Figure 3-2.** Relative screen elevations and their interpreted geologic settings along two transects shown in the upper right inset. For simplicity, the angled nature of some screens is not shown. See Figure 3-11 for a depiction of the angles on wells.

(A)

c. 2012 - no pumping



B)

April, Sept. 2022- pumping

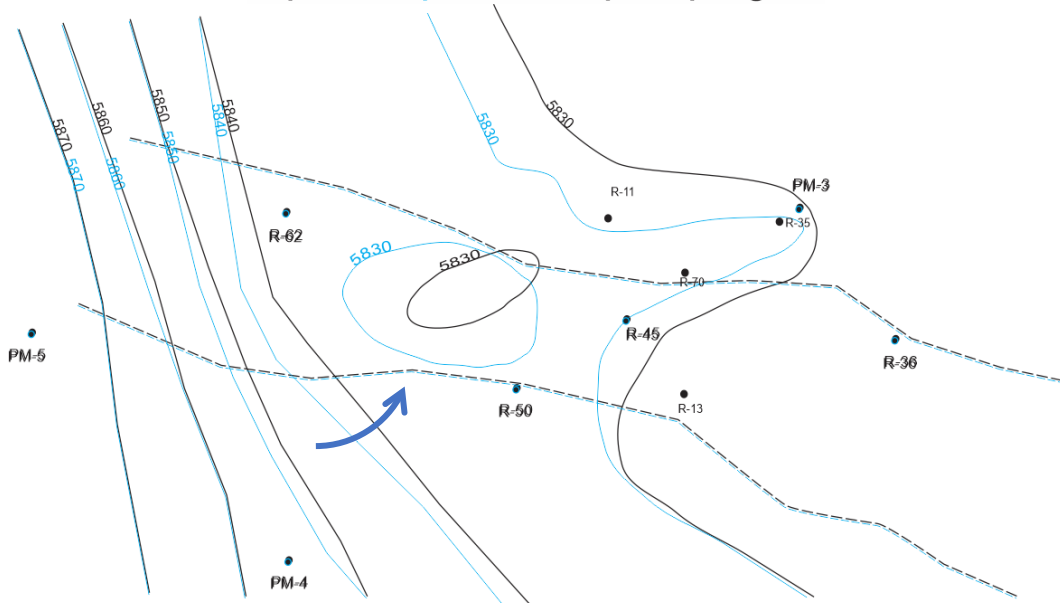


**Figure 3-3.** Plan-view hydraulic head contours for time (A) before IM pumping and injection and (B) after pumping. In both cases, the gradient between R-50 and R-45, along the southeastern portion of the plume, is northeast. This suggests that the IM pumping wells are capturing uncontaminated groundwater from south of the site, and redirecting plume water northward in this area (see blue arrows). This condition may prevail with and without IM pumping and injection, though it seems more assured with IM pumping and injection (maps from (A) Vesselinov et al., 2013; (B) Neptune (2023), Figures 3.3.3 and 3.3.5).

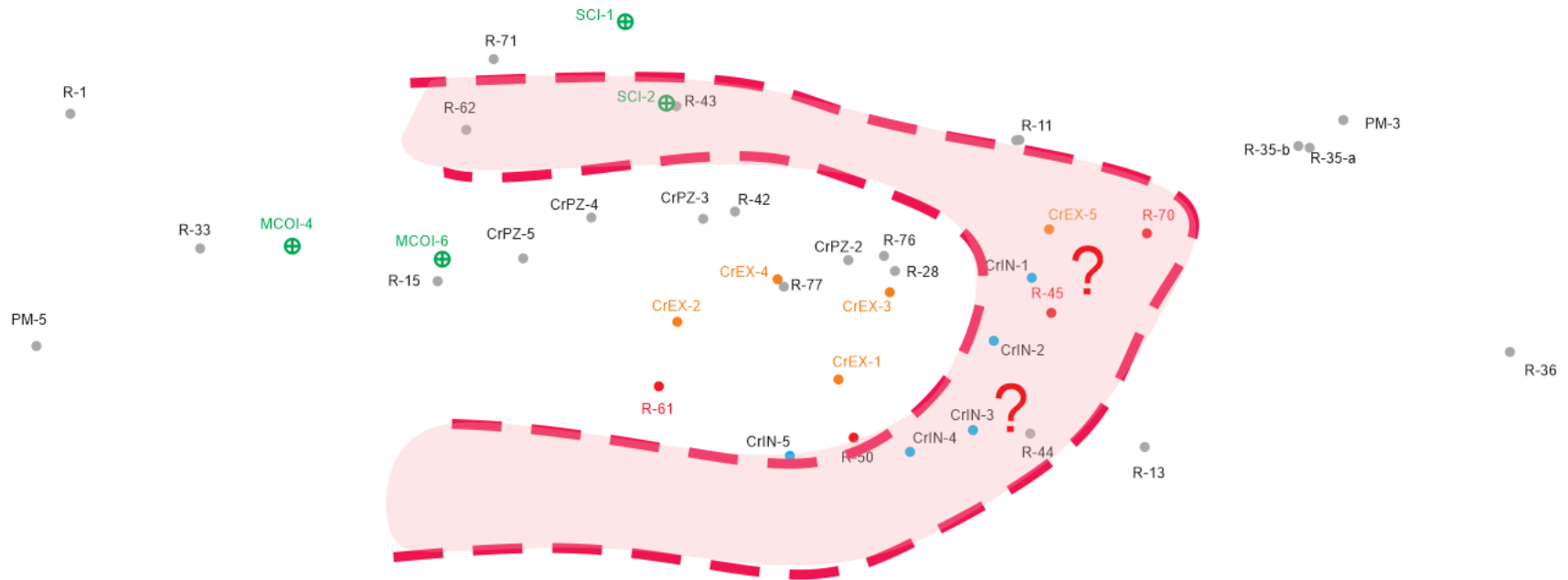


**Figure 3-4.** Approximate range of capture zone in plan view inferred from the time-series chromium data in Figure 3-1, up to early 2024. The exact location of the eastern edge of the capture zone is ambiguously defined on the basis of where chromium concentration trends at the monitoring wells appeared to be affected by IM.

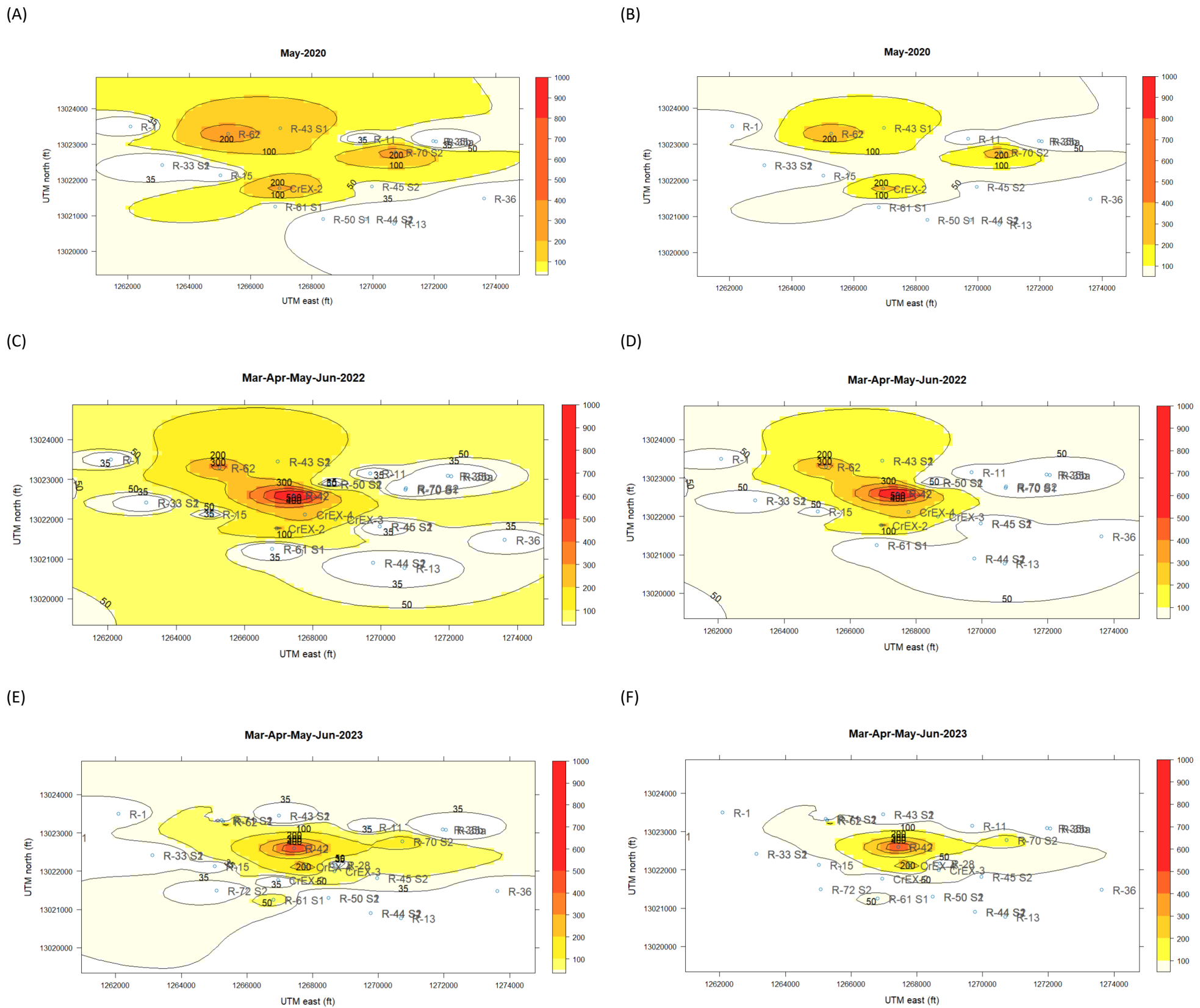


**Figure 3-5. Comparison of plan-view chromium distributions in the regional aquifer while IM pumping and injection were inactive (A, B, May 2020) and while they were active (C, D, spring 2022) and immediately following the inactivation of the IM system in spring 2023 (Figures (E), (F)). Figures (A), (C), and (D) show plume boundaries for maximum values at each location the 35 µg/L contour and Figures (B), (D) and (F) show the 50 µg/L plume boundaries for maximum values at each location. Lower concentration contours plot as bullseyes and do not facilitate the perception of a plume boundary. All plots were made using inverse distance weighting (IDW factor = 2) and an x-axis compression of 0.25 to provide visual elongation of the plume reflective of current understanding of the plume shape (inset in F) (taken from Neptune, 2023, Figure1.0-1). Note: the total contoured area is larger than the region shown, extending from R-26 on the west to R-10 on the east, and R-19 to the south and R-2 to the north. Note also that prior to 2019, chromium concentration was above 50 µg/L at R-50, which is not represented in the above plots based on more recent data.**



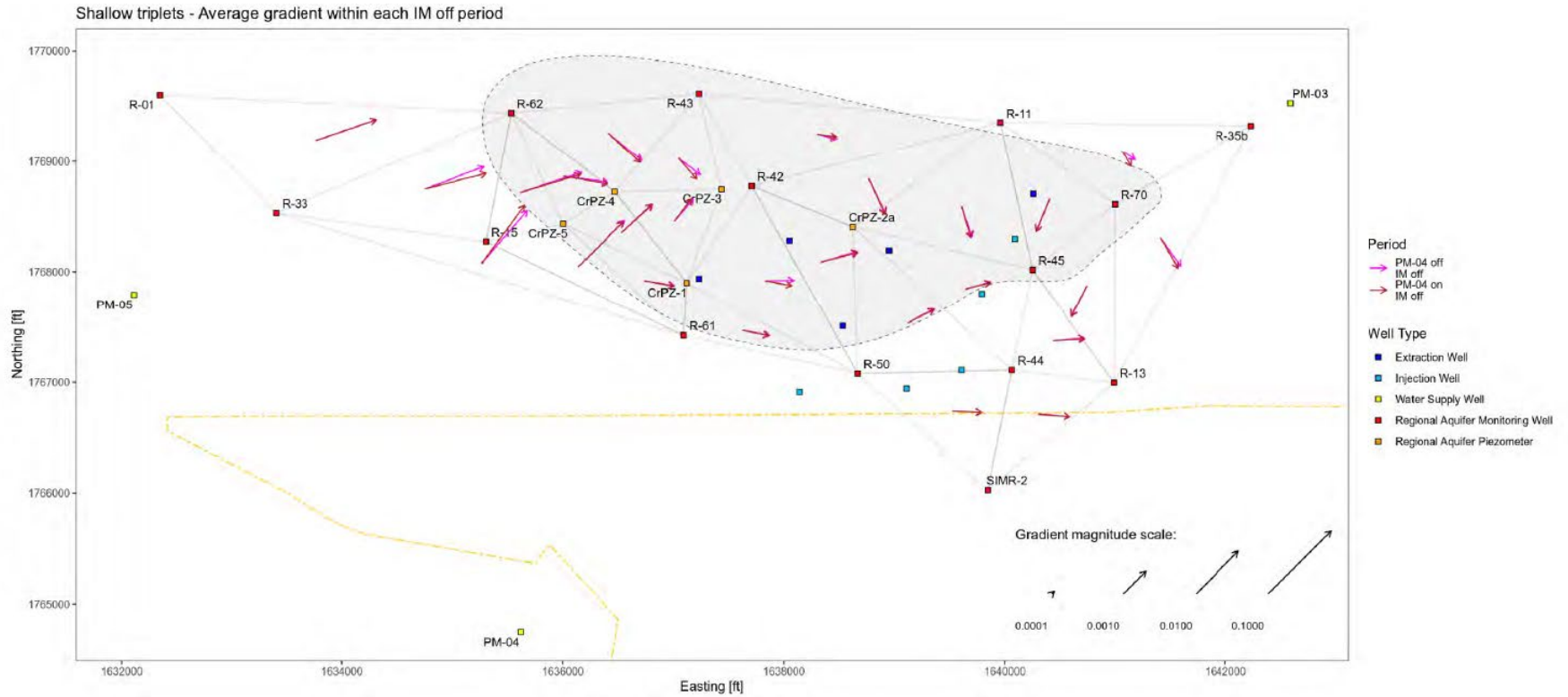


**Figure 3-6. Three-point problem flow direction vectors while the IM is off. Red vectors show directions when PM-4 (regional pumping well) is on, and brown arrows show flow directions when PM-4 is off. Arrow lengths are scaled to gradient magnitude (figure taken from Neptune, 2023).**

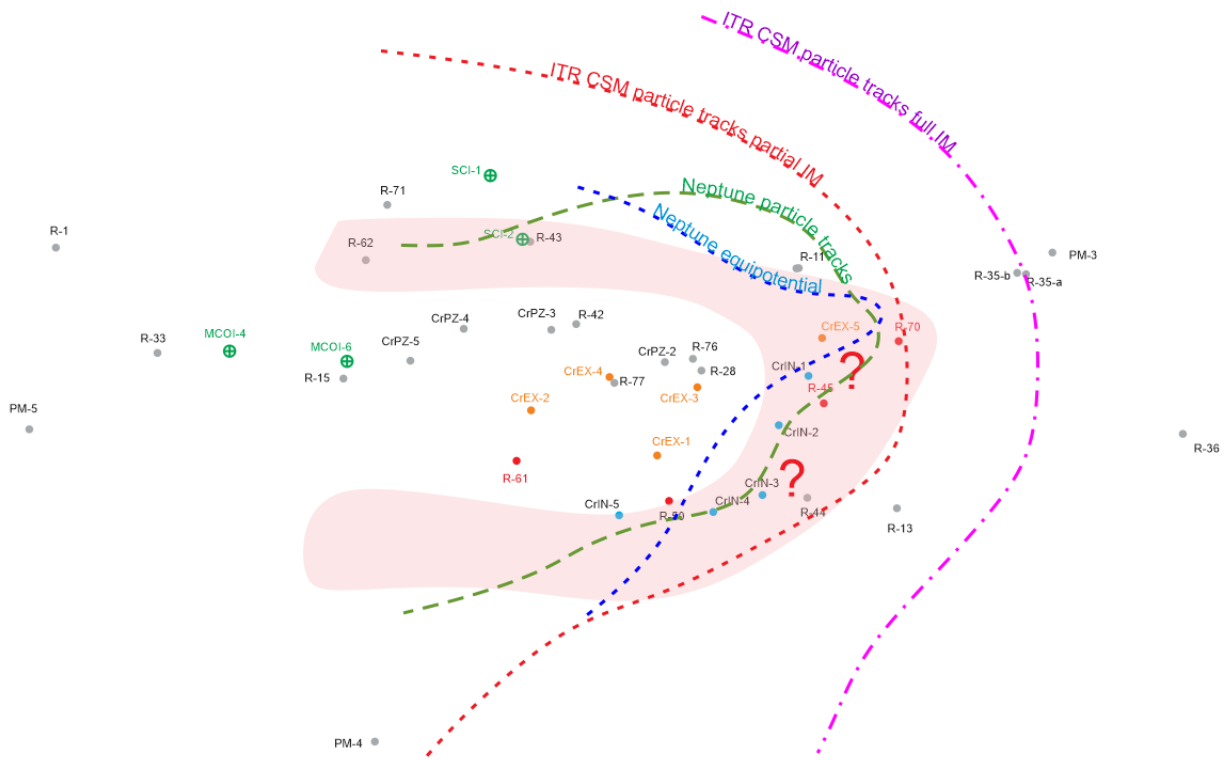
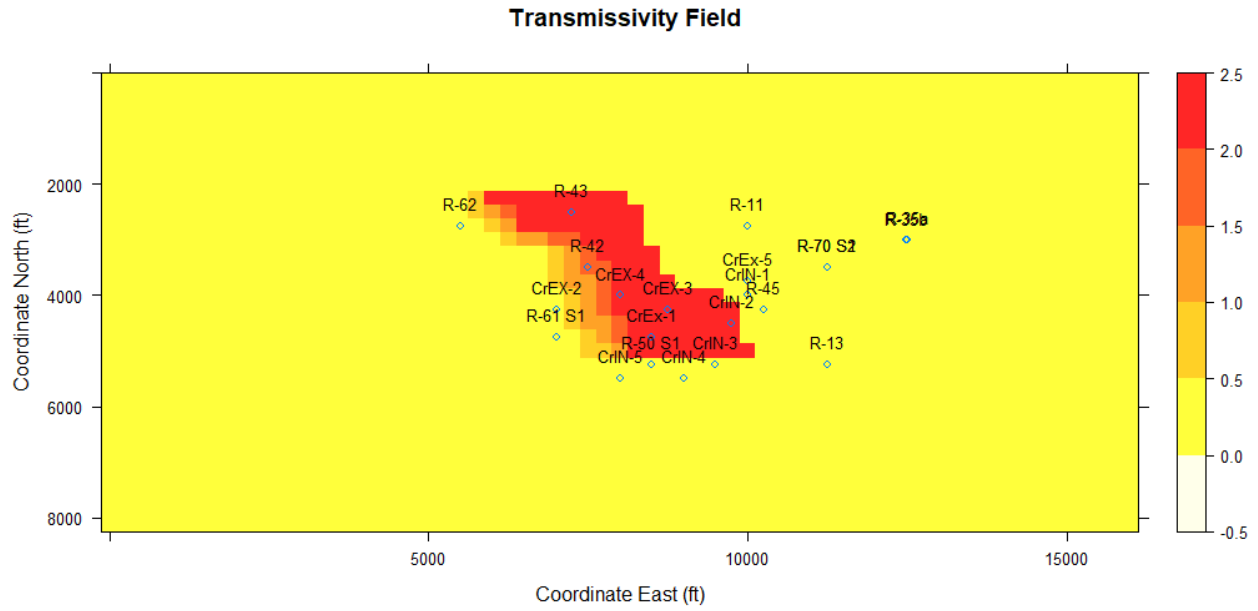


**Figure 3-7.** Comparison of effective capture zones, in plan view, inferred in Figure 3-4 (red shaded area) and from two-dimensional models simulating full IM operation (purple line) and partial IM operation with two extraction and two injection wells (red line). Also shown are capture zone limits reported by Neptune (2023) from particle tracking calculations (green line shows capture zone for 50% of particles) and equipotential modeling (blue line, based on hand-drawn contours inferred from three-point problems of hydraulic head). The location of the capture zone boundary with respect to R-70 is in question for all but the two-dimensional, full IM model simulation. The capture zone in that case is only roughly estimated, and should not be regarded as highly accurate. Nonetheless, it suggests a meaningful expansion of the capture zone between partial and full IM operation.

(A)



(B)

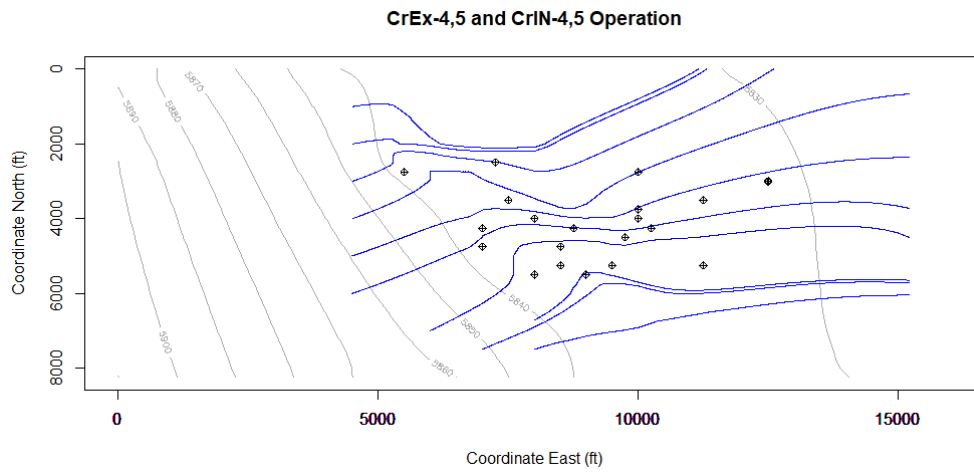
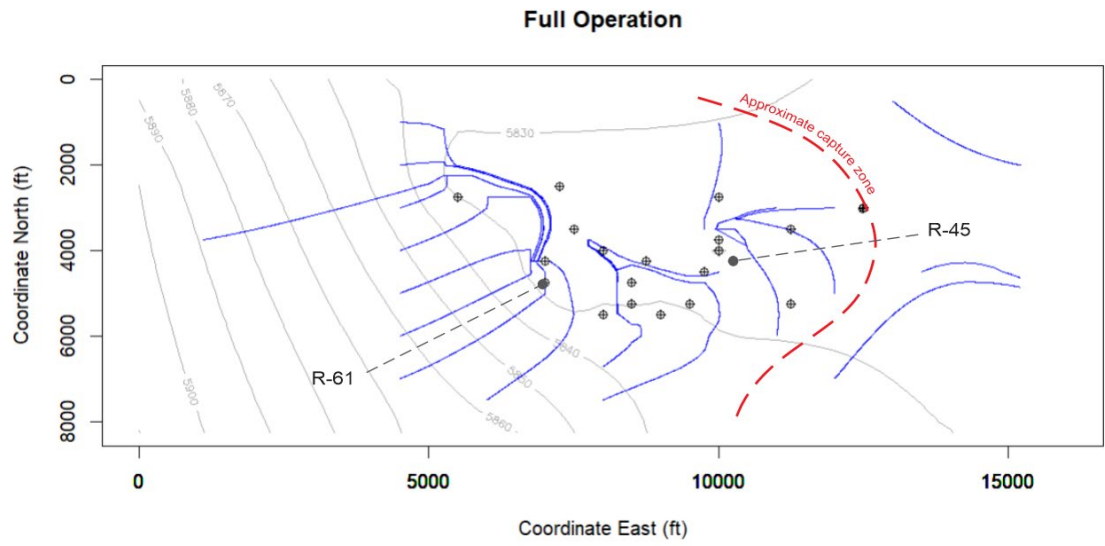


**Figure 3-8. (A) Transmissivity field, in plan view, used in all simulations (units are  $\text{ft}^2/\text{s}$ ). (B) Particle tracks, in plan view, and head contours for the base case in which no IM well were active.**

(A)



(B)

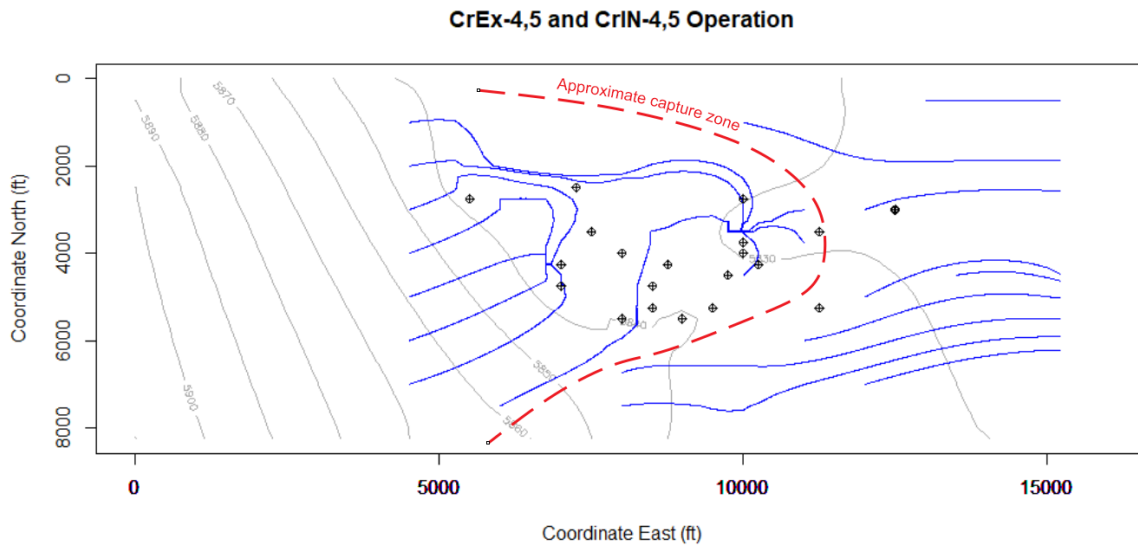
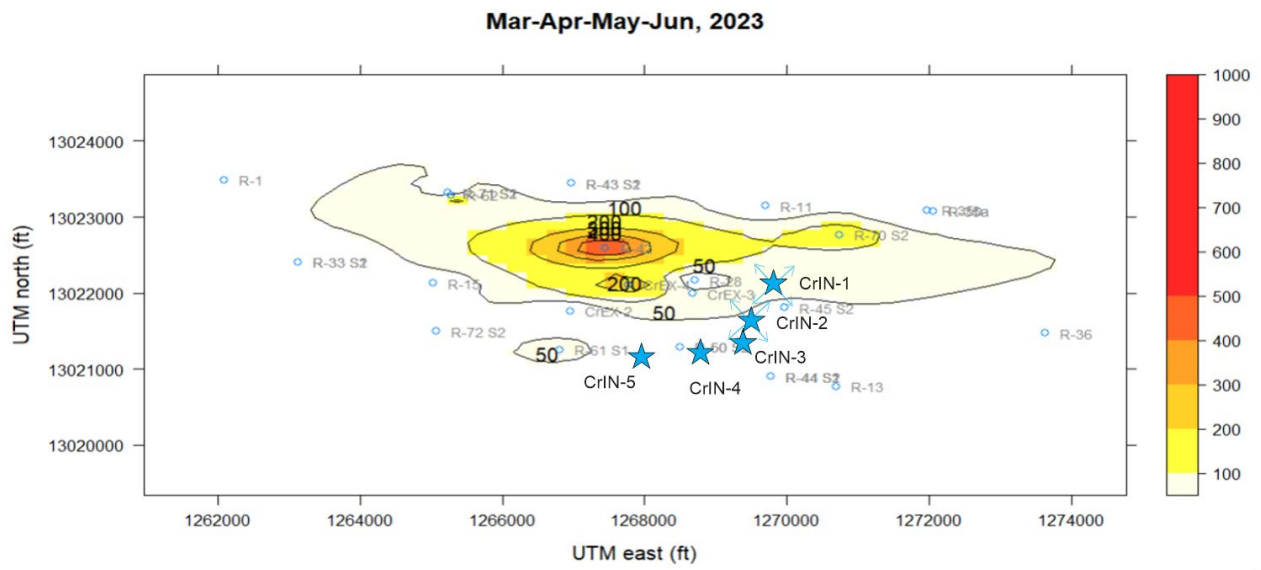


Figure 3-9. Approximate limits to capture (A), in plan view, with the IM in full operation and (B) with only the CrEX-4/CrEX-5 and CrIN-4/CrIN-5 wells operating.



**Figure 3-10.** Plan-view locations of the injection wells in relation to the 50 µg/L chromium contours as of spring 2023. Note radial arrows on CrIN-1 and CrIN-2 illustrating how these wells might have influence over chromium concentrations at R-45.

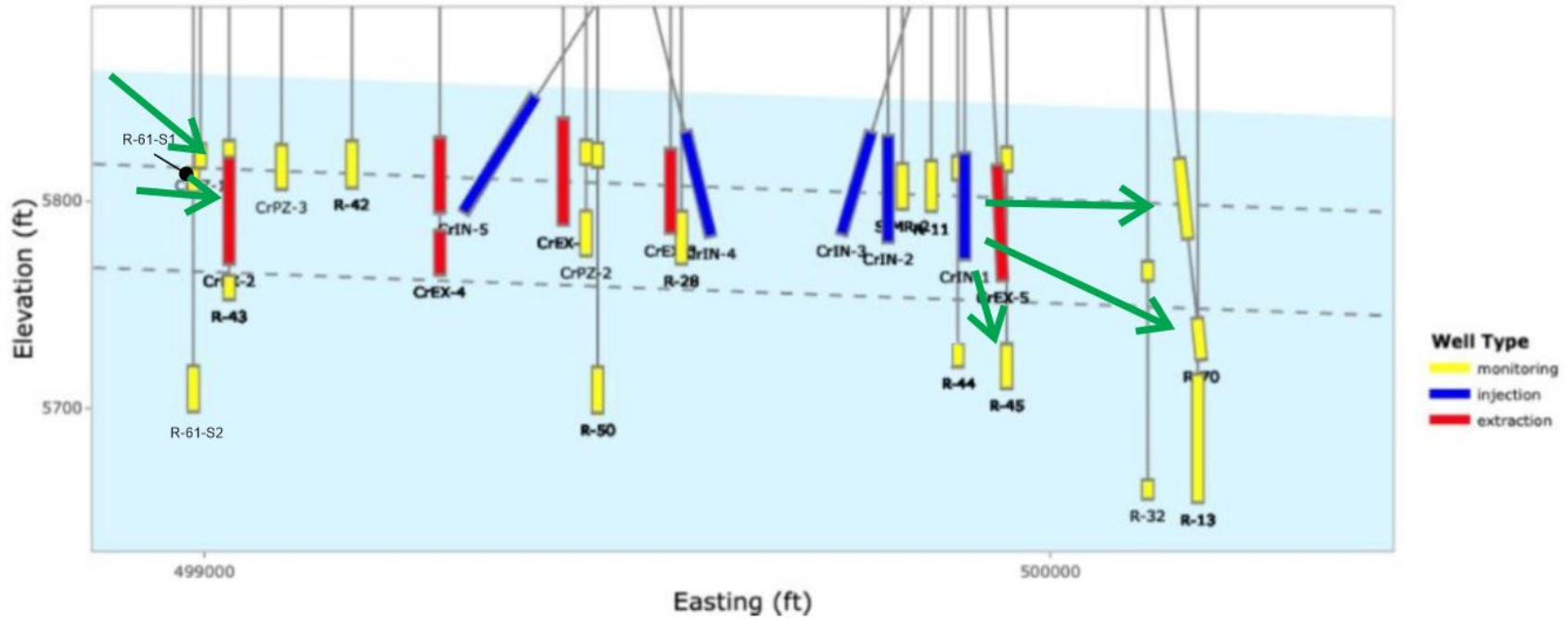
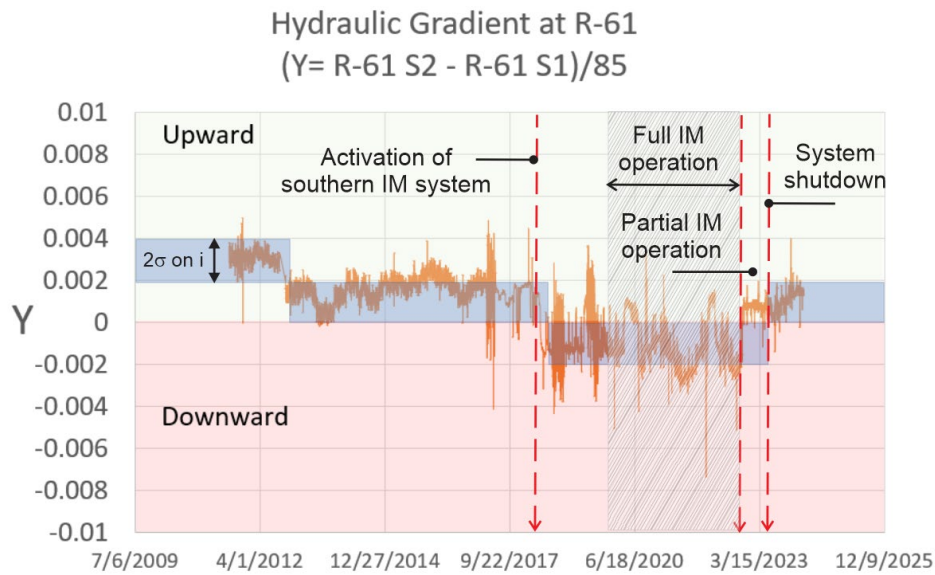
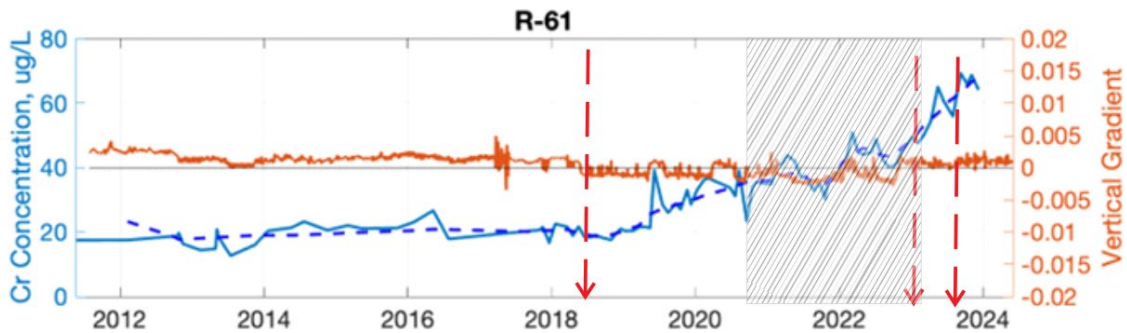


Figure 3-11. Section through the plume area showing the vertical relationships between the injection wells, R-45 S2 and the R-70 S1 and S2 locations. Green arrows show pathlines between CrIN-1 and the outer-lying well locations at R-45 and R-70. See Appendix K.

(A)



(B)



**Figure 3-12.** Hydraulic head responses at R-61 S1 (shallow screen) (after Appendix K). Note: this graph has omitted some outlying data points. The blue shaded areas in (A) represent 2 standard deviations on the estimated gradients. There appears to be a statistically meaningful change from upward to downward mean gradients that coincides with the activation of the IM system. The majority of the change appears to be associated with the southern IM system. (B) Overlay of the response of hydraulic gradient and chromium concentration history at R-61 S1 (Appendix K).

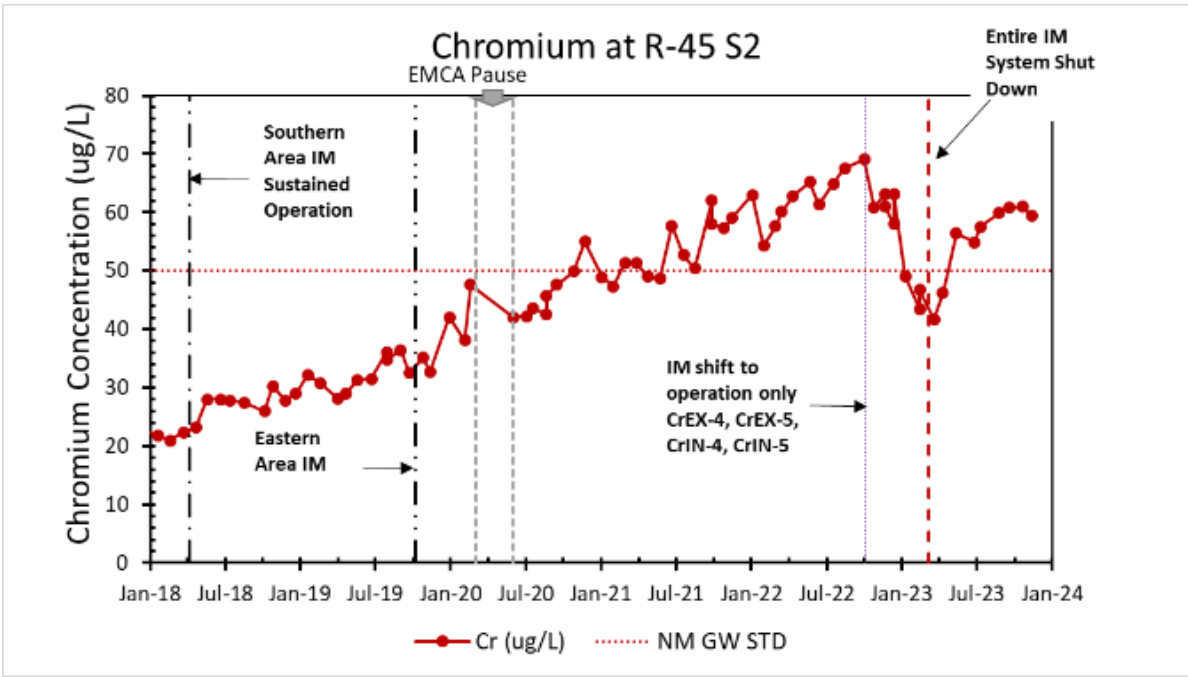
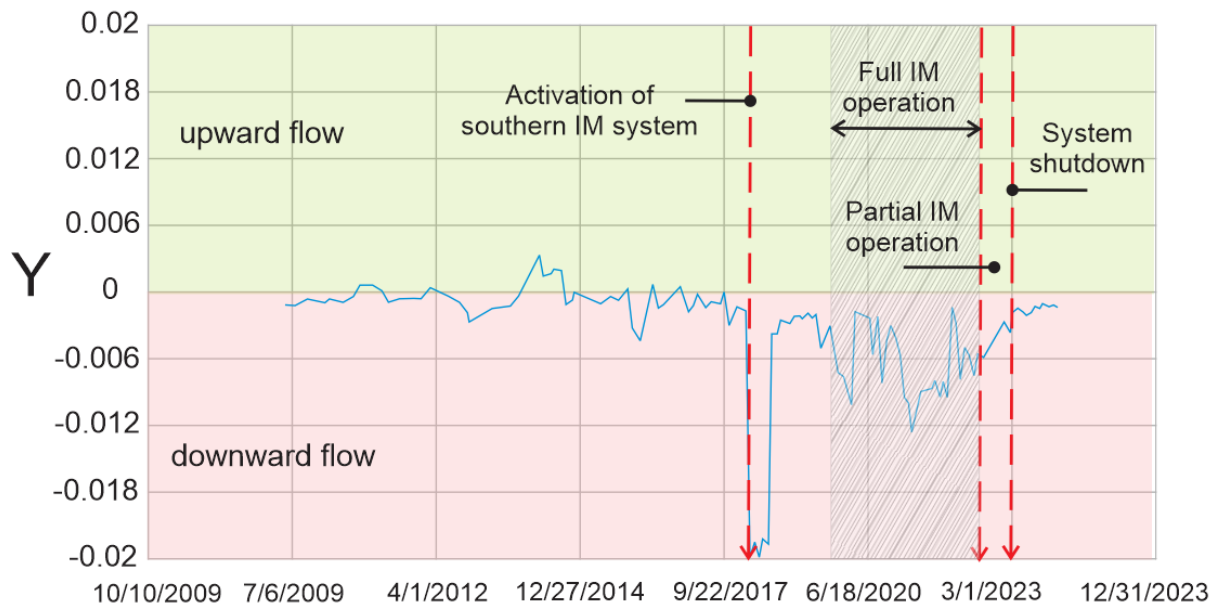


Figure 3-13. Chromium concentration history at R-45 S2 (Appendix K).



Hydraulic gradient response over time at R-45  
( $Y = R-45 S2 - R-45 S1$ )/85



**Figure 3-14.** Hydraulic head responses at R-45 S1 (shallow screen) and R-45 S2 (deep screen). Note: this graph has omitted some outlying data points identified to the IRT by Haruko. In particular, the head data collected during the partial IM operation were considered untrustworthy, and are not shown in this figure.

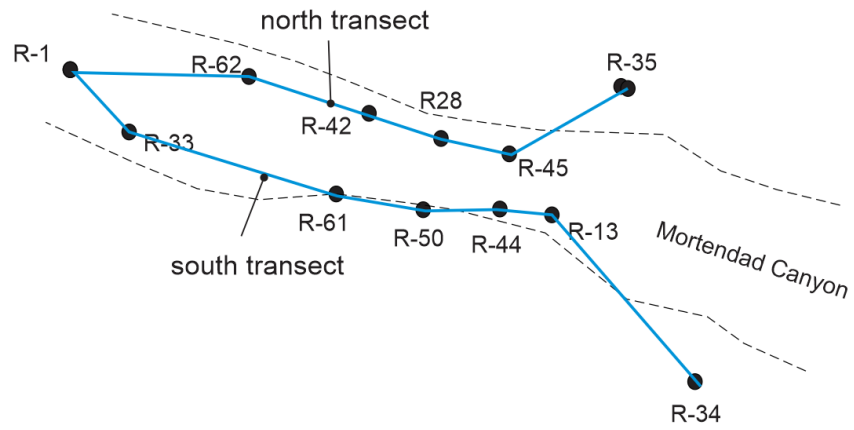
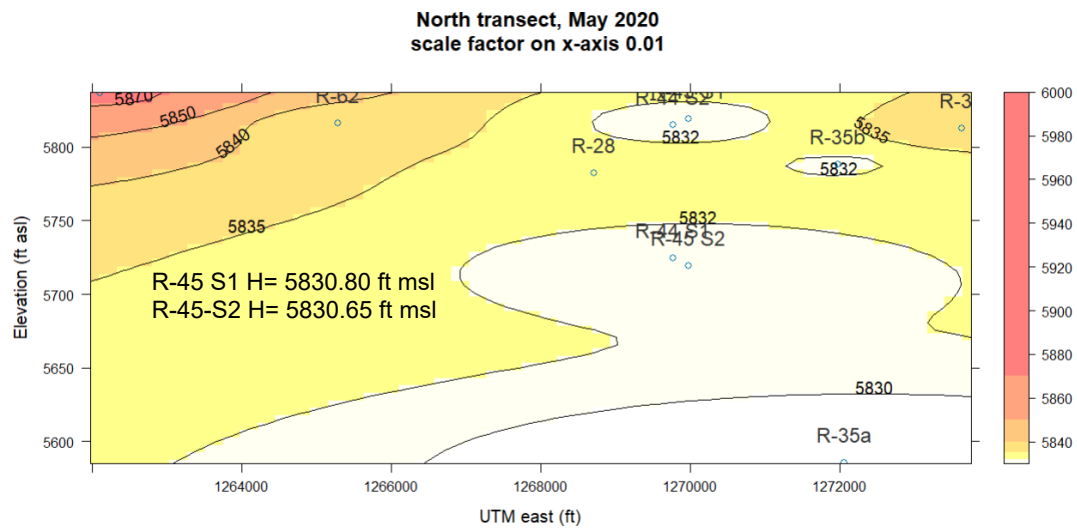
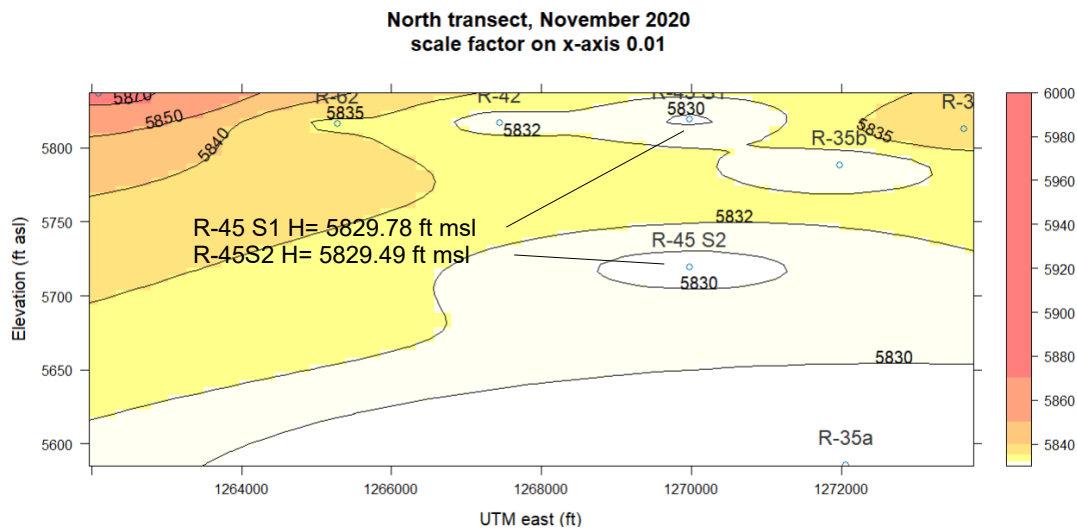


**Figure 3-15.** Transects considered for visualization of vertical head distributions in the regional aquifer.

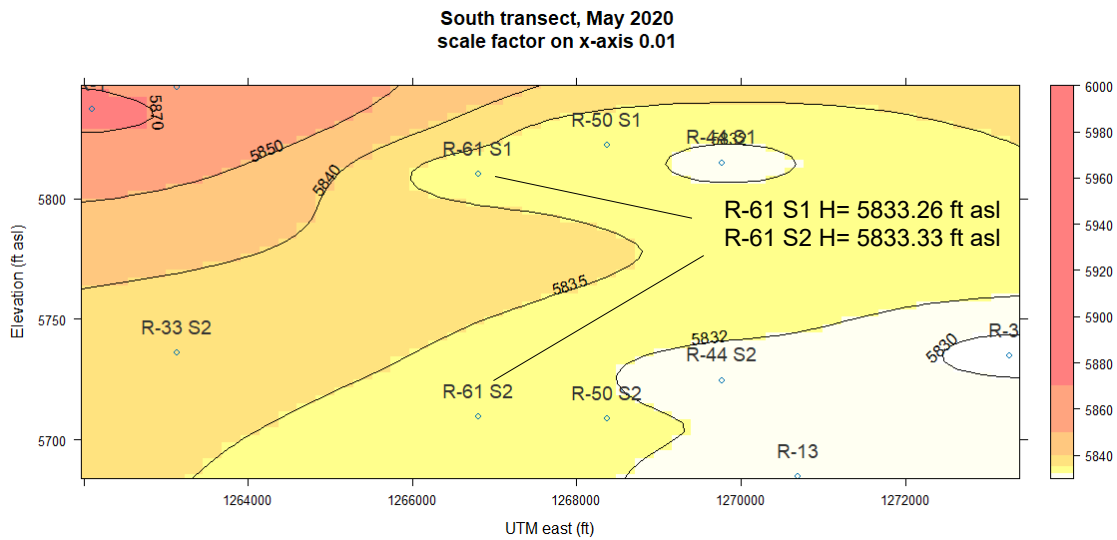
(A)



B)



(C)



(D)

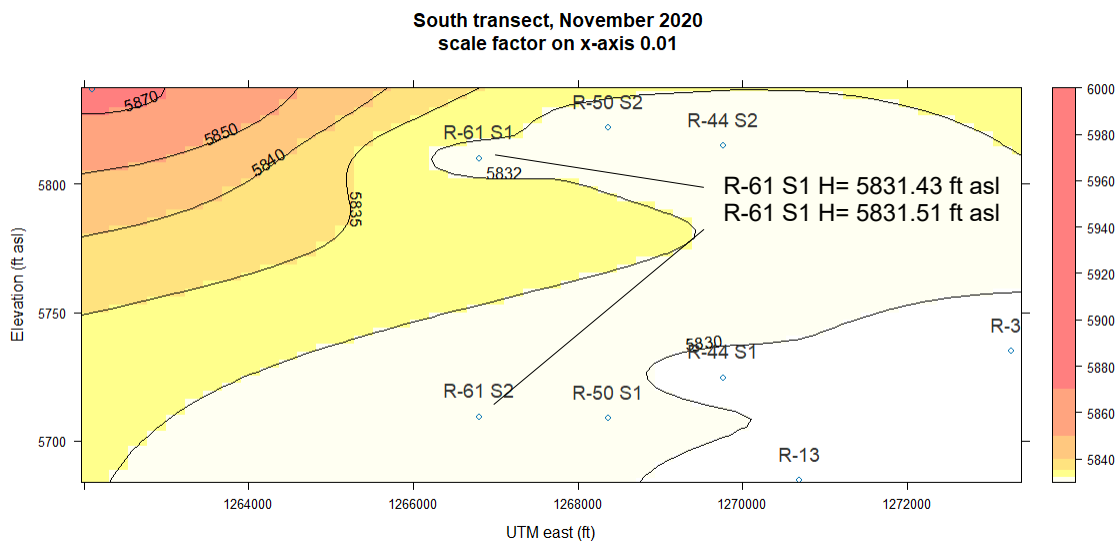


**Figure 3-16. Hydraulic head distributions along the north and south transects. (A) North transect, May 2020, while IM pumping was inactive. (B) North transect, November 2020, while IM pumping was active. (C) South transect, May 2020, while IM pumping was inactive. (D) South transect, November 2020, while IM pumping was active. On both dates selected, hydraulic gradients were consistent with downward flow at R-45 and upward flow at R-61. In the latter case, flow was on average downward while the IM system was active. The upward flow in (D) appears to be associated with a transient variation.**

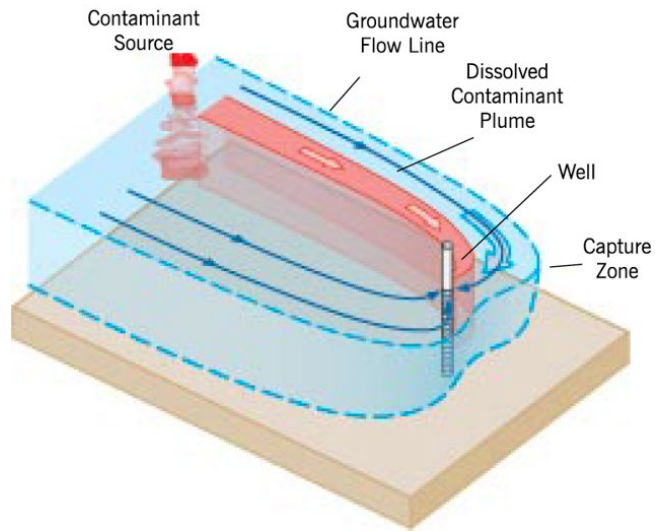


**Figure 3-17. Hypothetical capture of a groundwater plume by a groundwater extraction well (ITRC, 2010).**

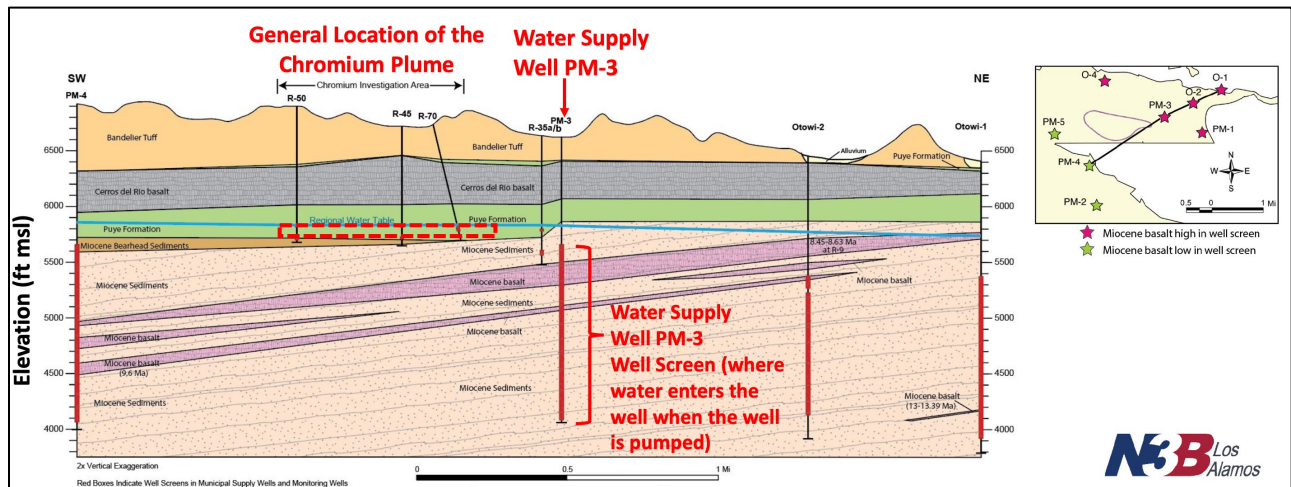


**Figure 3-18.** Approximate location and depths of chromium plume and water supply well PM-3 showing how PM-3 draws water from over a ~1,600-foot interval. This compares to the chromium plume, which has an approximate thickness of less than 100 feet. Original figure from “Miocene Basalts” presentation by D. Broxton (2024) with annotations by C. Newell. Location of chromium plume is conceptual and not to scale.

(A)

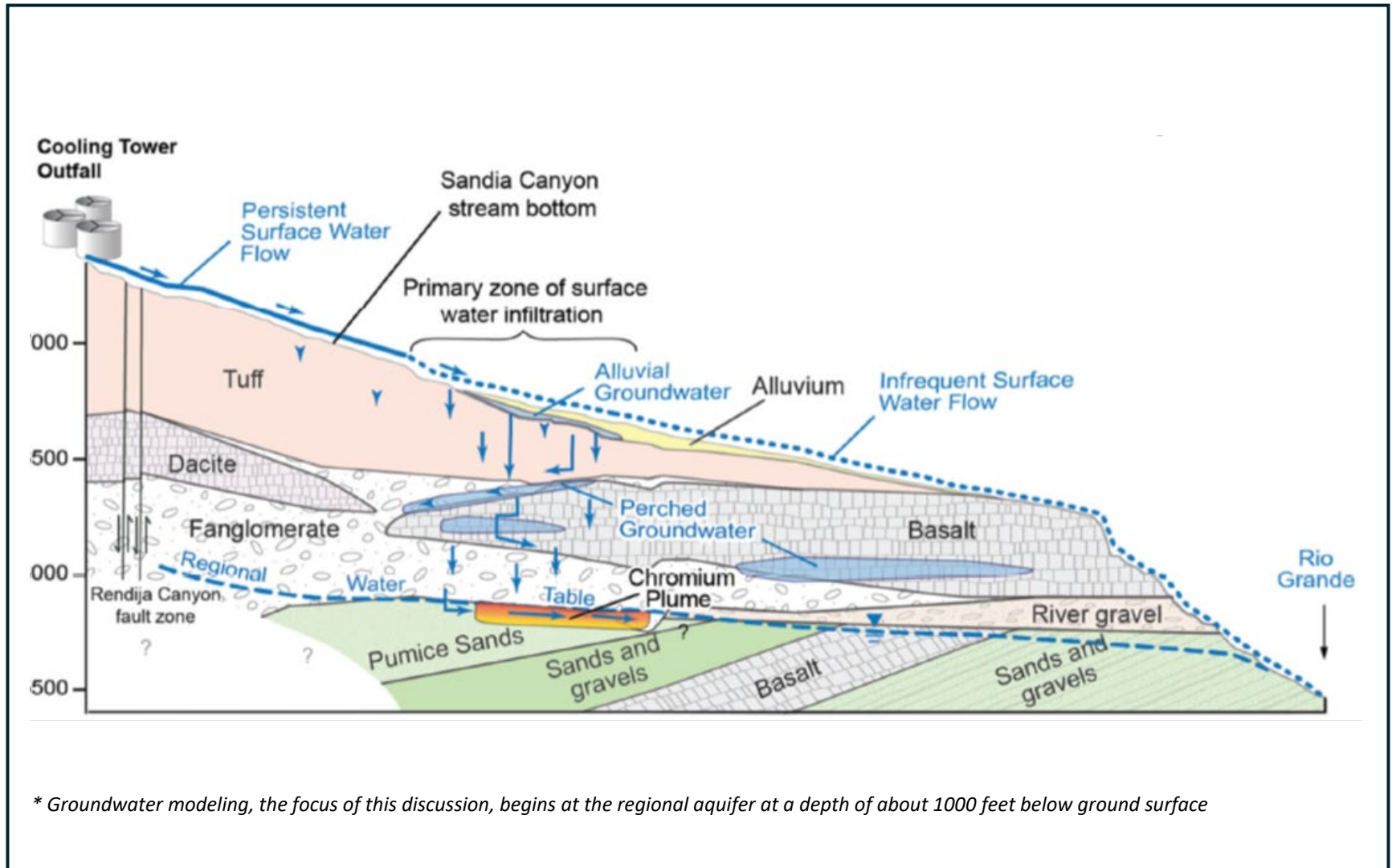


Figure 3-19A. Schematic hydrogeologic conceptual site model (CSM) for site modeling purposes: Full section.

(B)

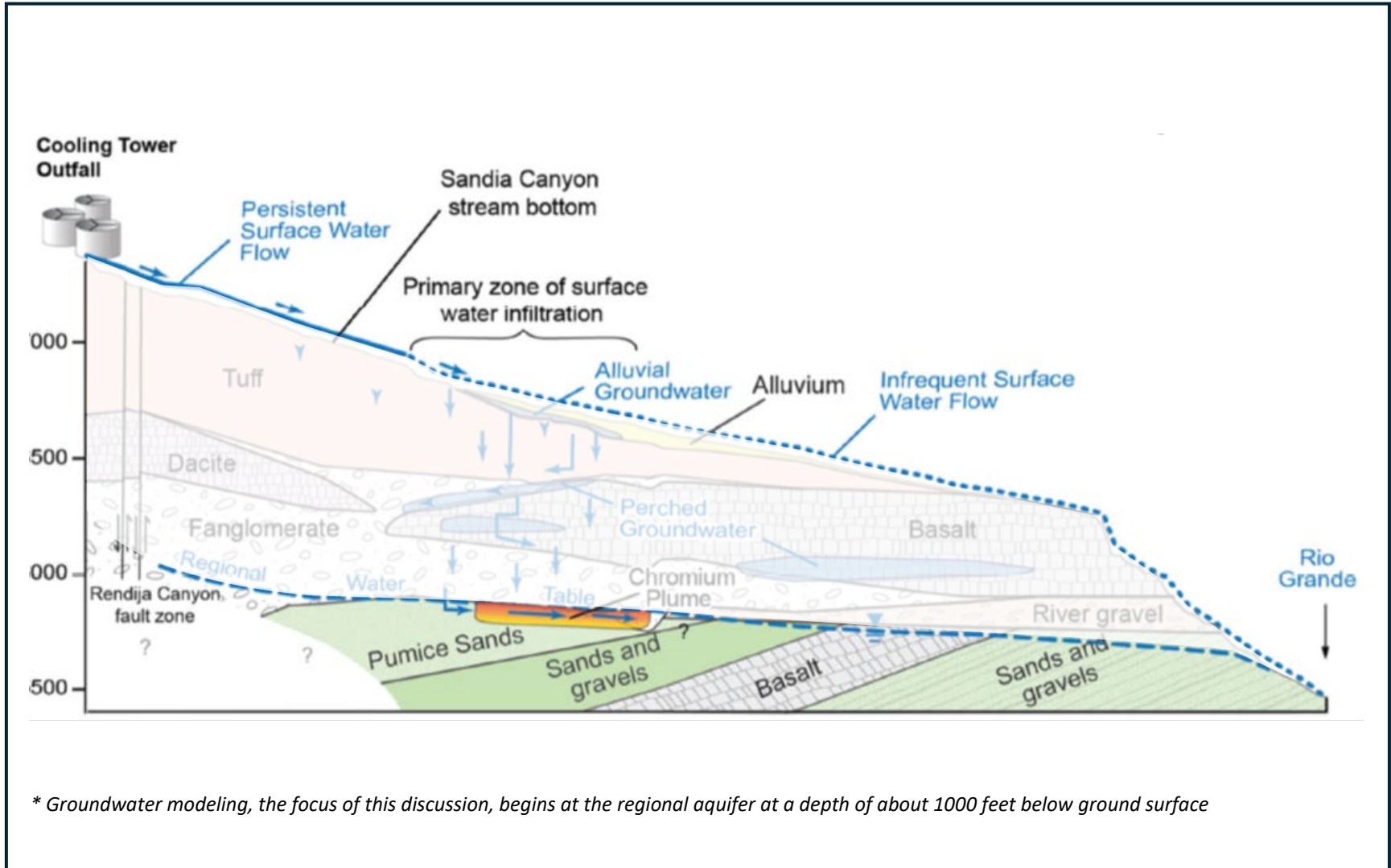


Figure 3-19B. Schematic hydrogeologic conceptual site model (CSM) for site modeling purposes: Saturated section.



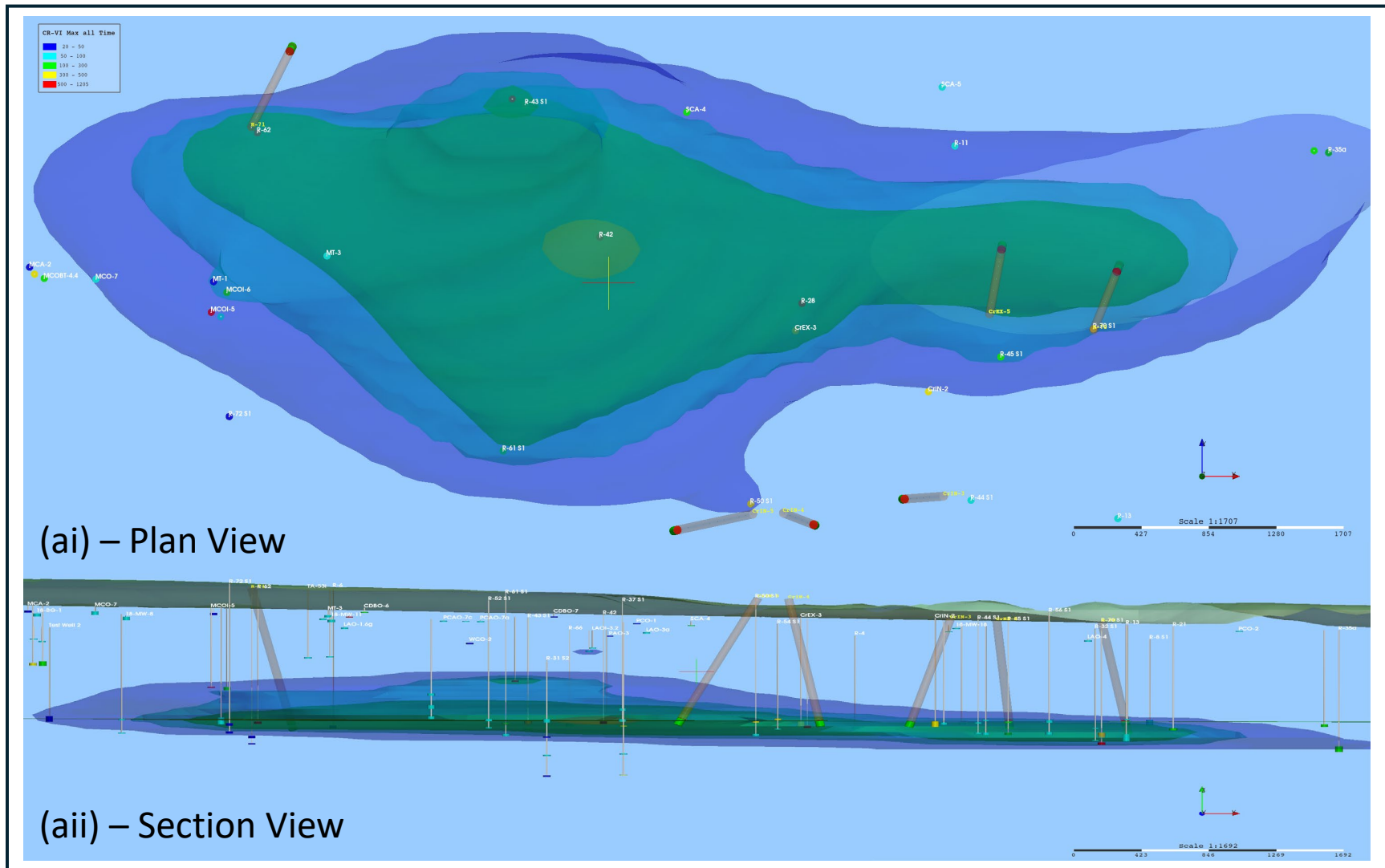
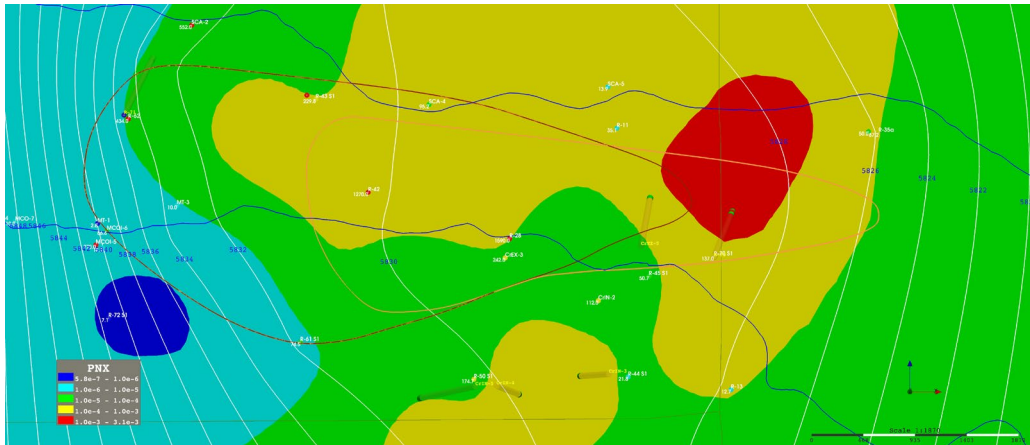
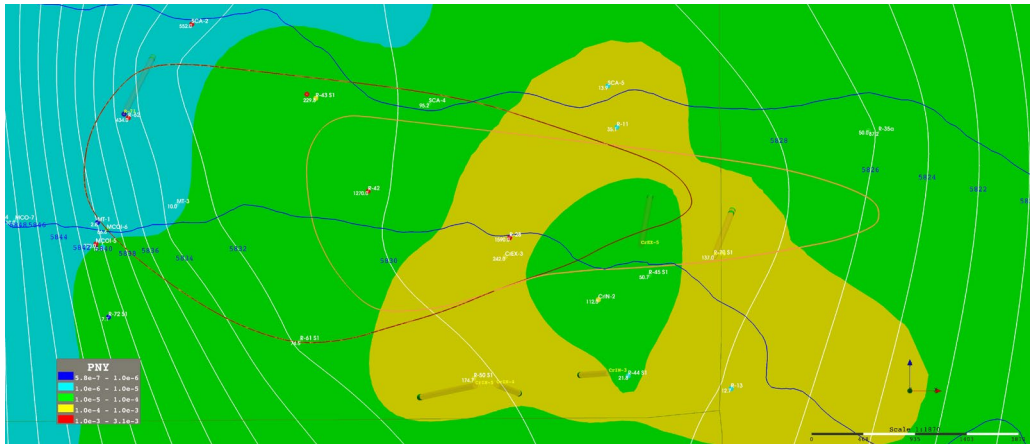


Figure 3-20. Approximate illustration of the extents of dissolved chromium depicted (ai) IN PLAN VIEW and (aii) in section view, prepared using uniform-score (quantile) kriging, with the objective of depicting the approximate lateral extents, thick vadose zone, and angled borings.

(ai) – Horizontal Conductivity in the Easting Direction (PNX)



(aii) – Horizontal Conductivity in the Northing Direction (PNY)



(aiii) – Vertical Conductivity (PNZ)

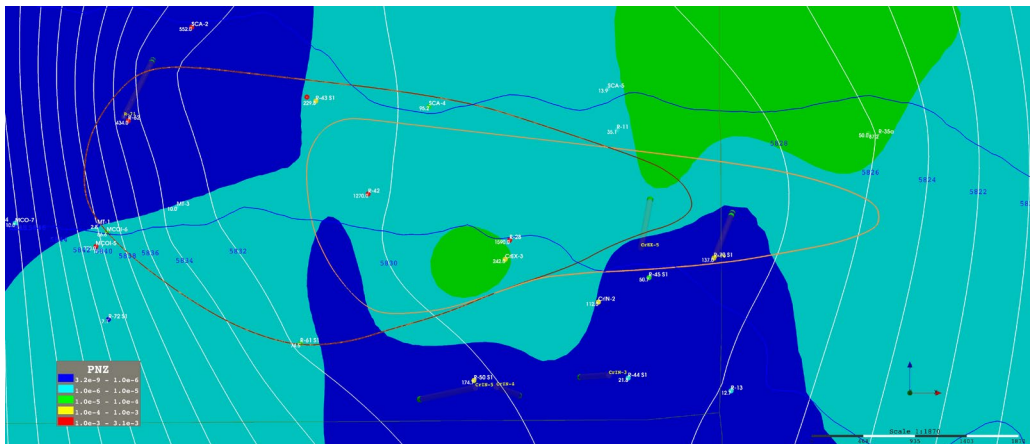
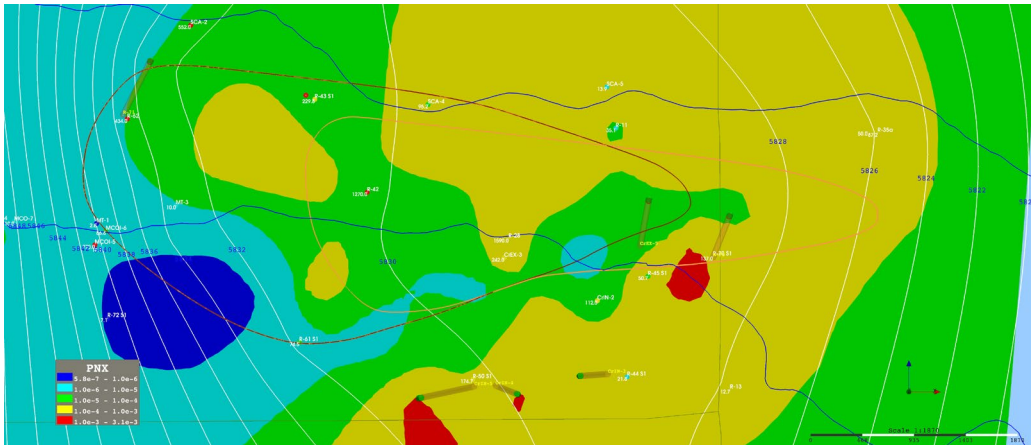
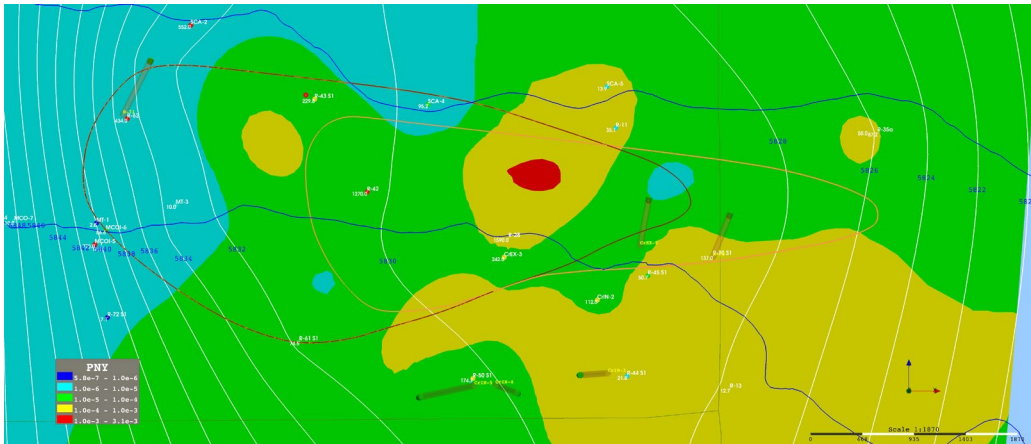


Figure 3-21a. Example maps of aquifer parameters corresponding to elevation of 5,830 feet msl.

(bi) – Horizontal Conductivity in the Easting Direction (PNX)



(bii) – Horizontal Conductivity in the Northing Direction (PNY)



(biii) – Vertical Conductivity (PNZ)

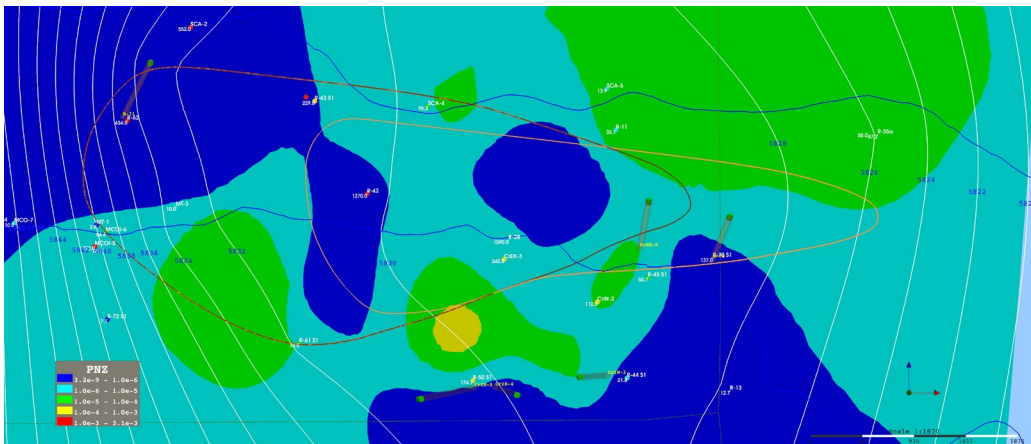
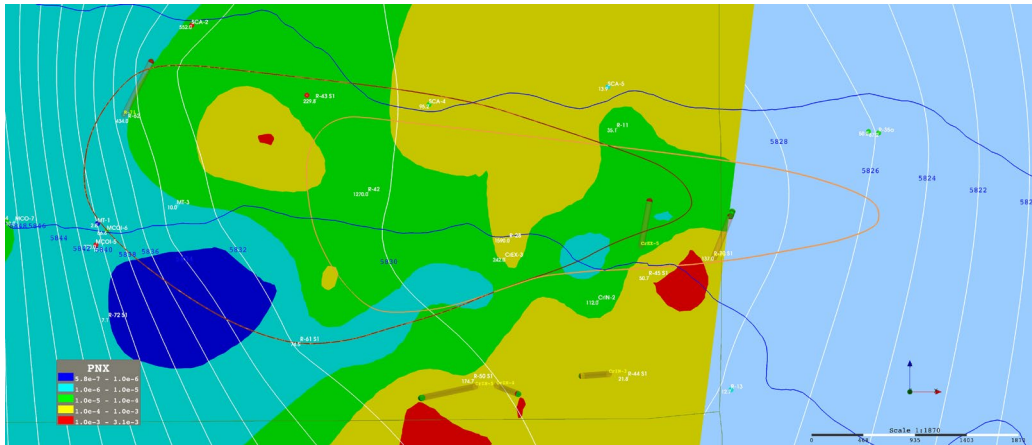
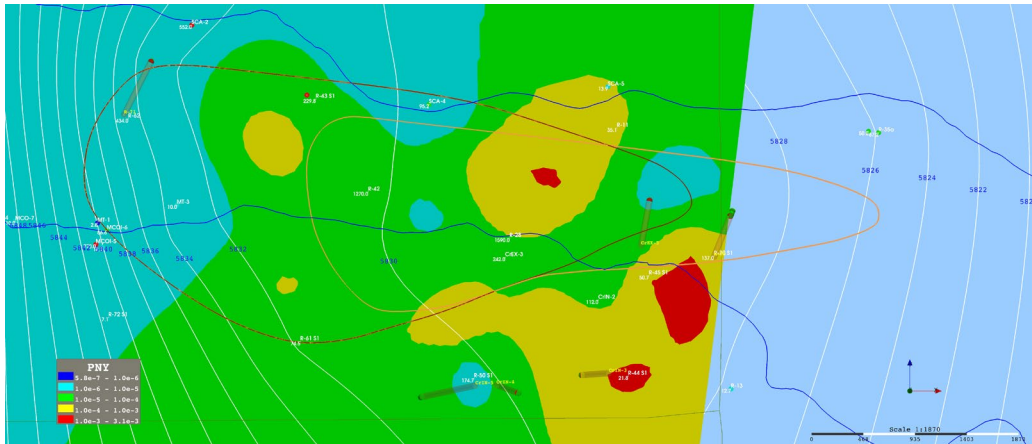


Figure 3-21b. Example maps of aquifer parameters corresponding to elevation of 5,800 feet msl.

(ci) – Horizontal Conductivity in the Easting Direction (PNX)



(cii) – Horizontal Conductivity in the Northing Direction (PNY)



(ciii) – Vertical Conductivity (PNZ)

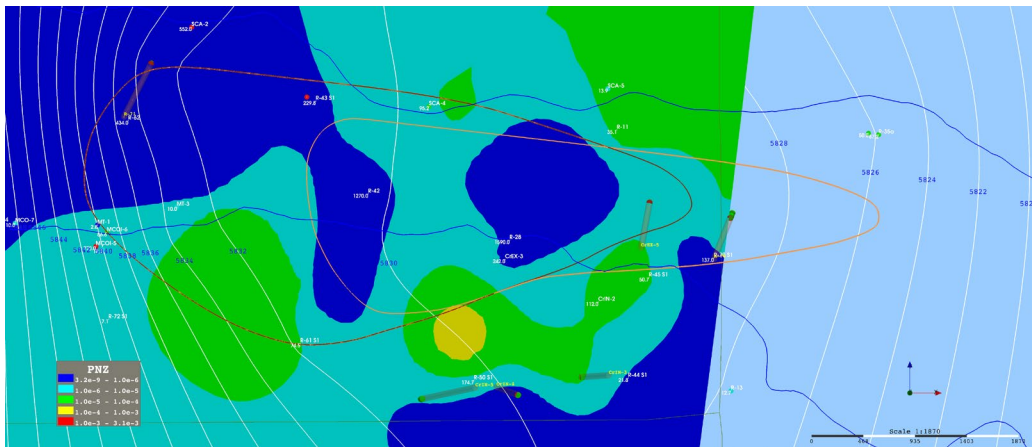
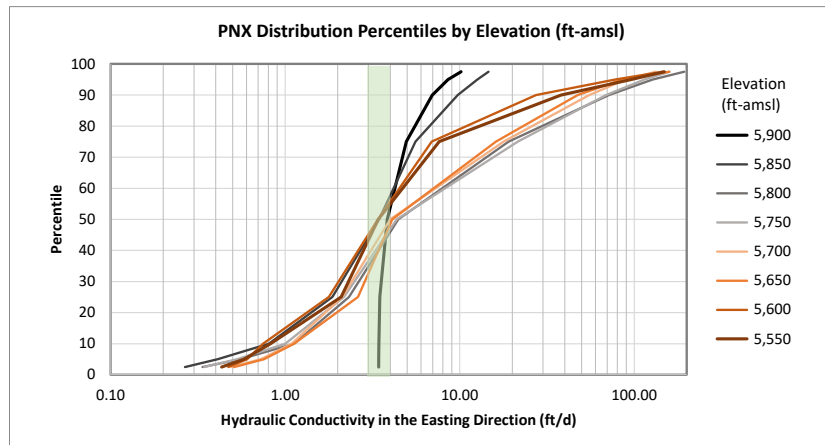
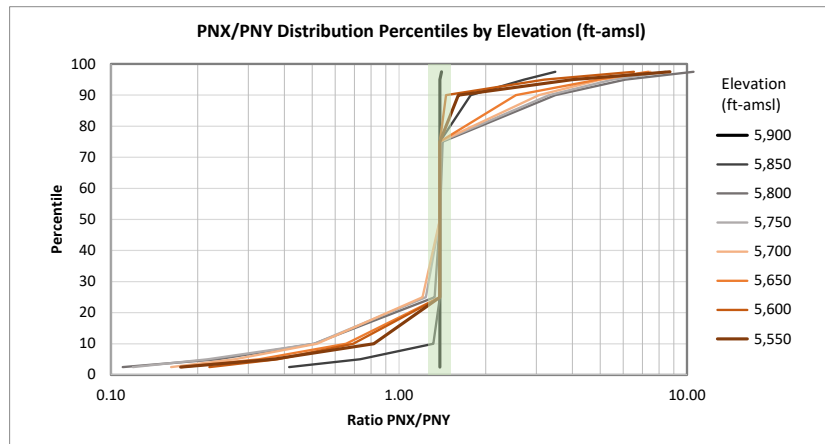


Figure 3-21c. Example maps of aquifer parameters corresponding to elevation of 5,700 feet msl.

(a) Horizontal Conductivity in the Easting Direction (PNX)



(b) Ratio of Horizontal Conductivities (PNX/PNY)



(c) Ratio of Horizontal to Vertical Conductivities (PNX/PNZ)

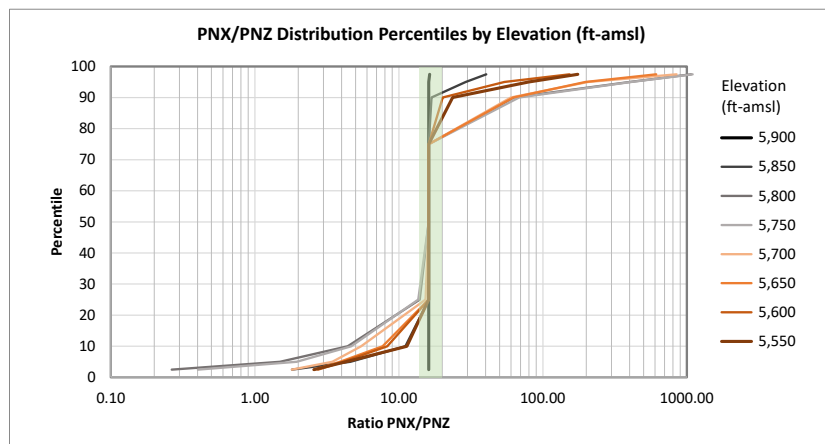
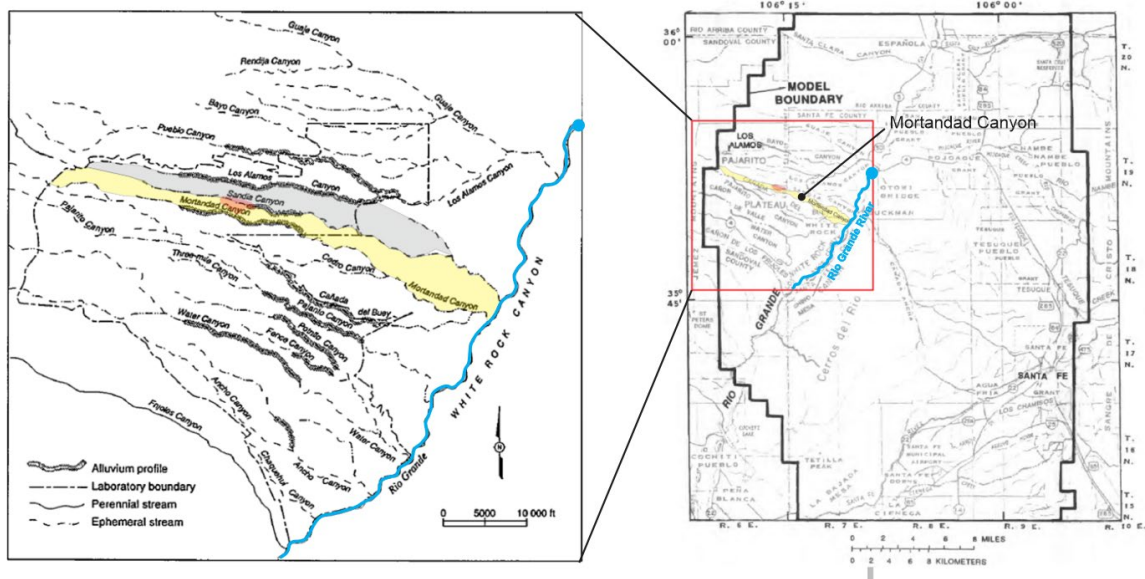


Figure 3-22. Example property distributions for aquifer parameters and their ratios: (a) horizontal conductivity, (b) ratio of horizontal conductivities (pnx/pny) and (c) ratio of horizontal to vertical conductivities (PNX/PNZ).

(A)



(B)

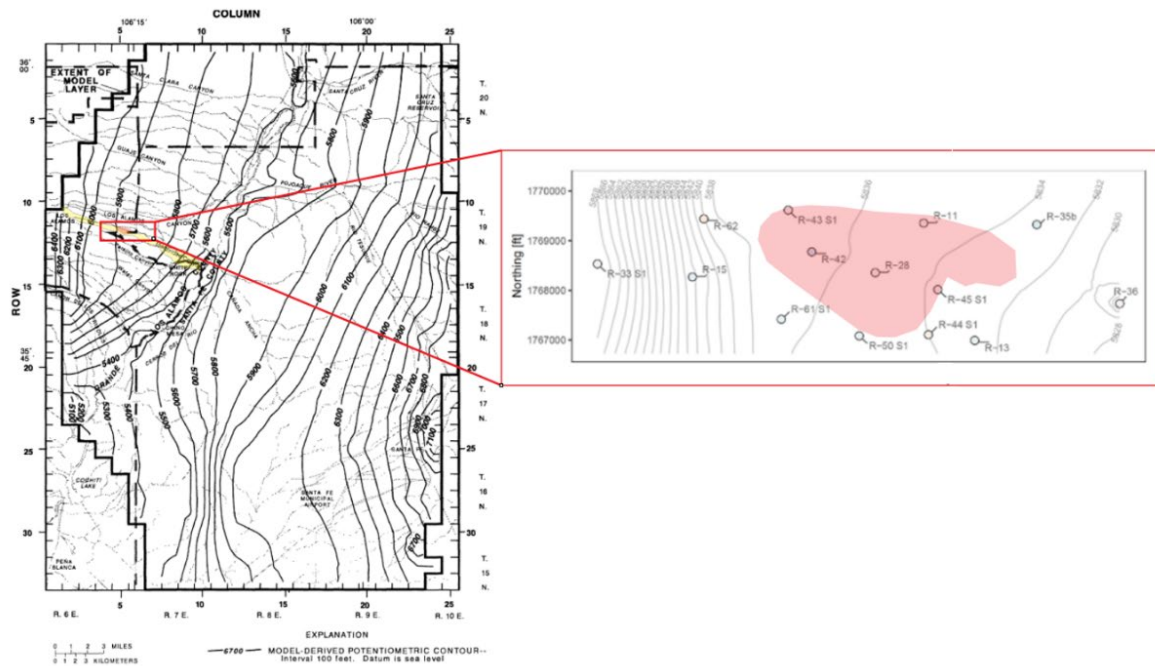


Figure 3-23. Regional modeling reported by Frenzel (1995). (A) Maps showing the relationships between the plume area in Mortandad Canyon, in red, and the regional model area. (B) Potentiometric surface of the top layer of the regional model, 200 feet thick. Also shown is one example of a deterministic plot of the Neptune modeled local-scale equipotentials, with approximate plume outline for reference (Foster, 2024b).

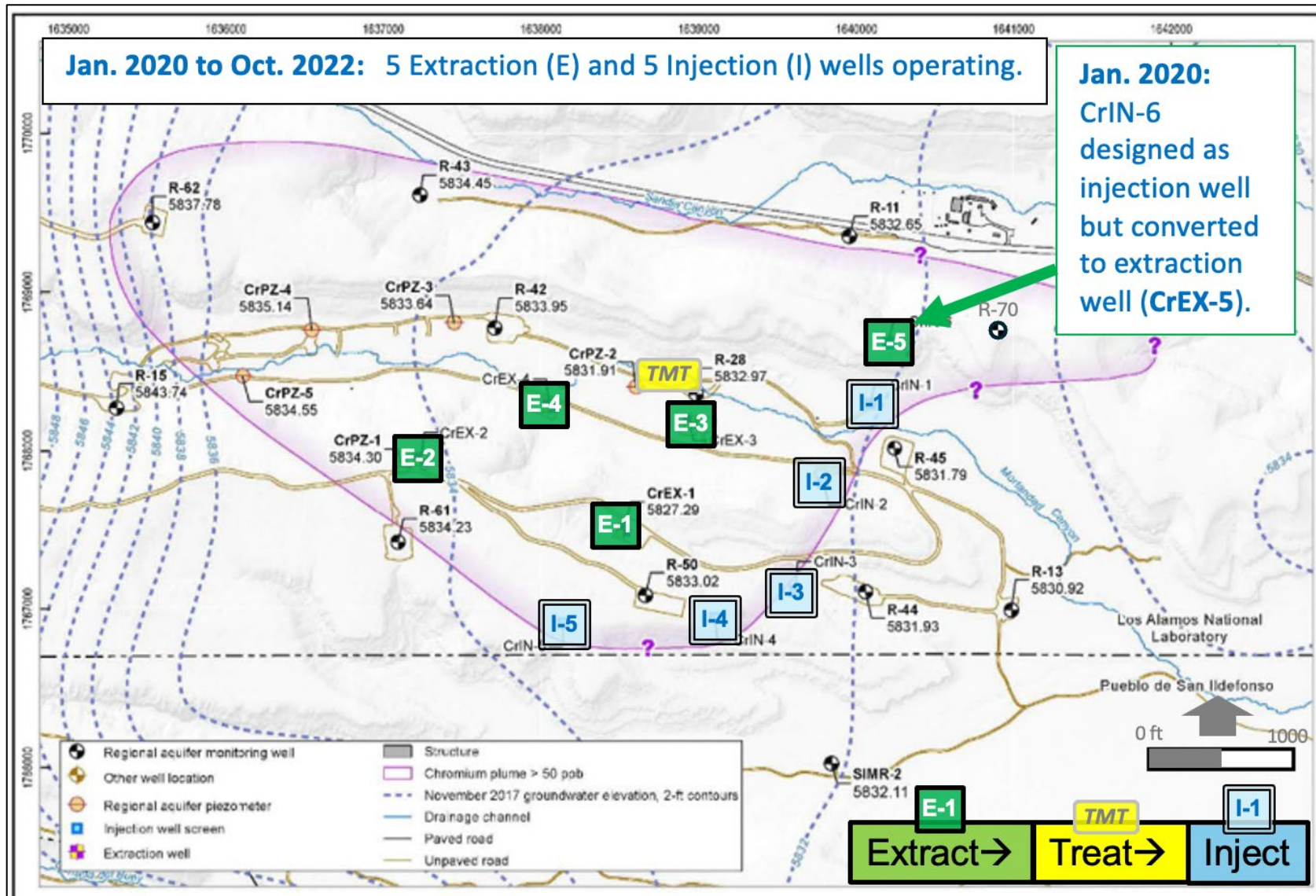


Figure 3-24. Interim measure injection and extraction wells generally in operation 2020 to October 2022. Scale is approximate.

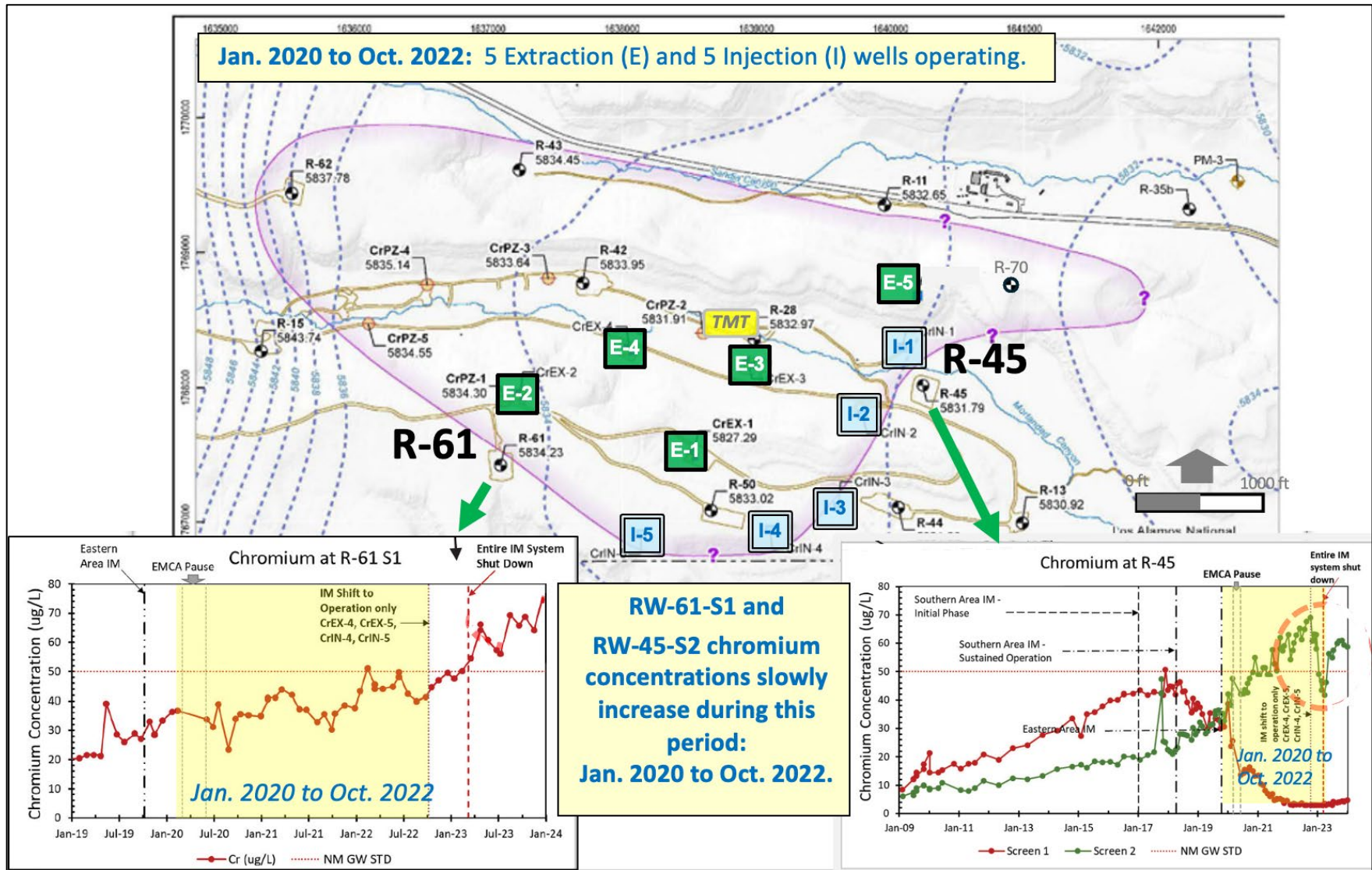


Figure 3-25. Interim measure injection and extraction wells generally in operation 2020 to October 2022 showing chromium concentration trends during this period (yellow highlight) at R-61 S1 and R-45 S2.



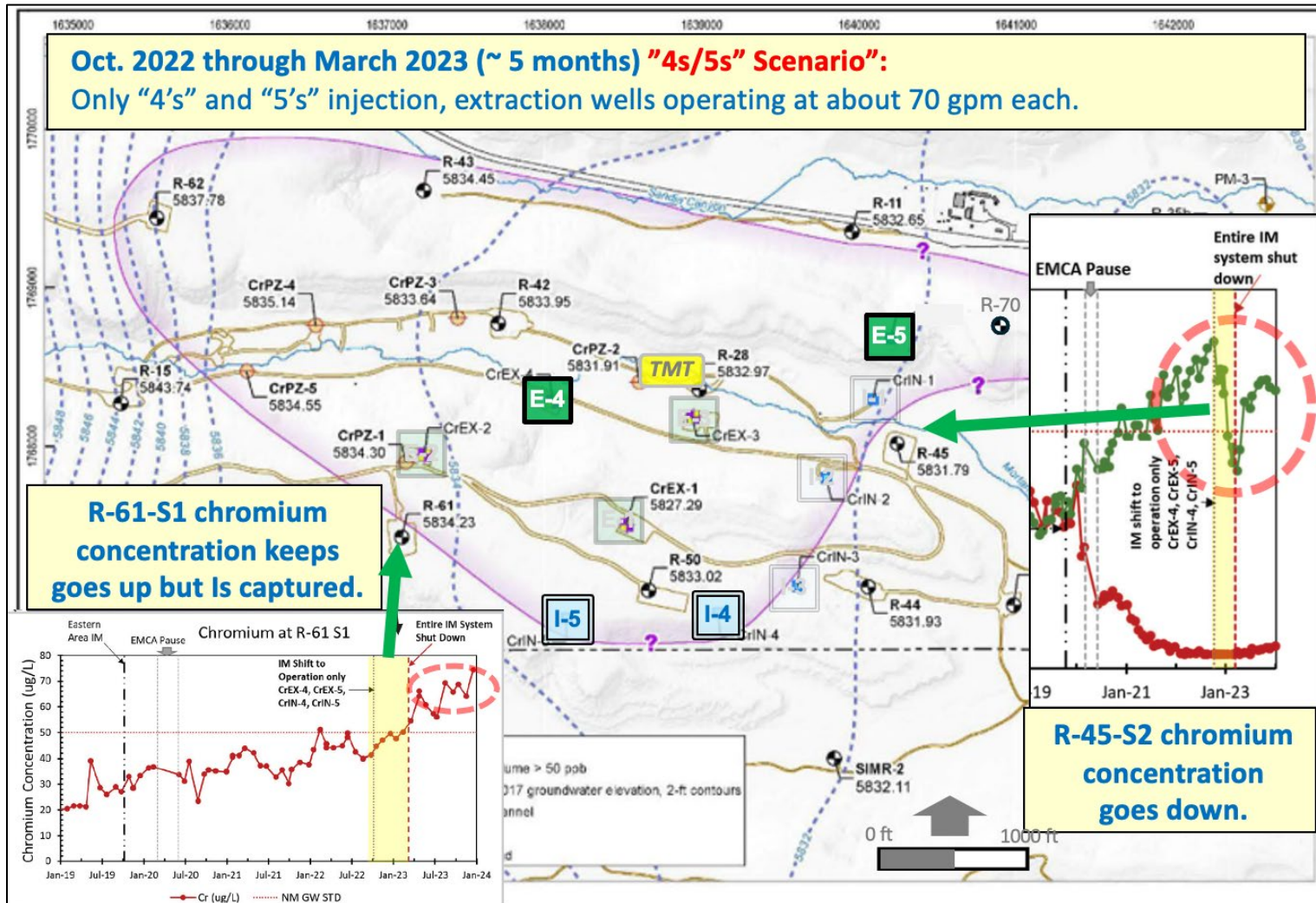


Figure 3-26. Interim measure injection and extraction wells generally in operation November 2022 to March 2023 (4s/5s Scenario). Chromium concentrations increased in R-61 S1, but groundwater in this area was being captured by the partial IM operation. The chromium concentrations in R-45-S2 decreased dramatically after nearby injection wells were shut off. (The plume outline used in this figure is from the previous time period and should be considered to only a general representation of the plume at the time in the figure).

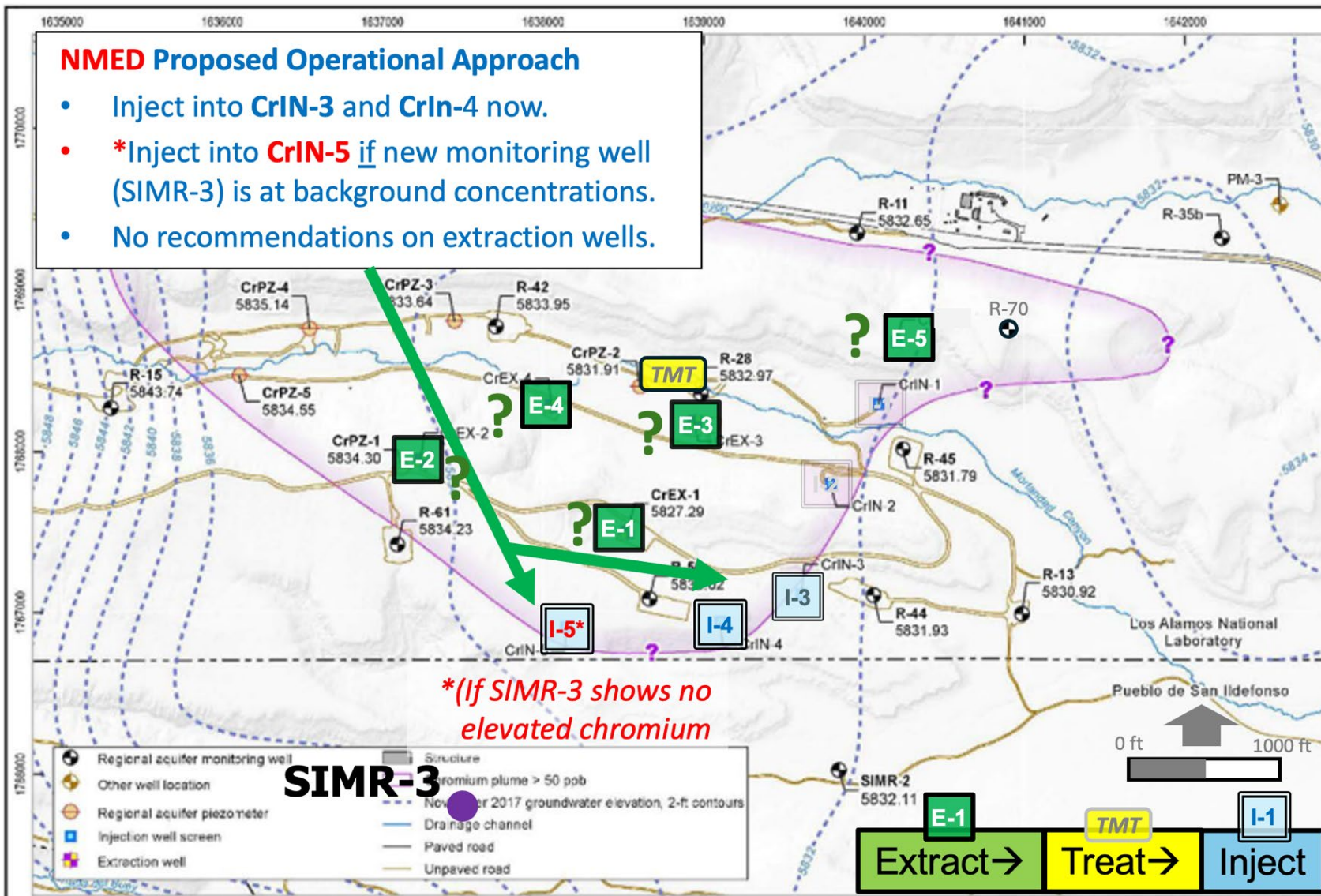


Figure 3-27. NMED's proposed interim measure restart configuration (Letter #3).

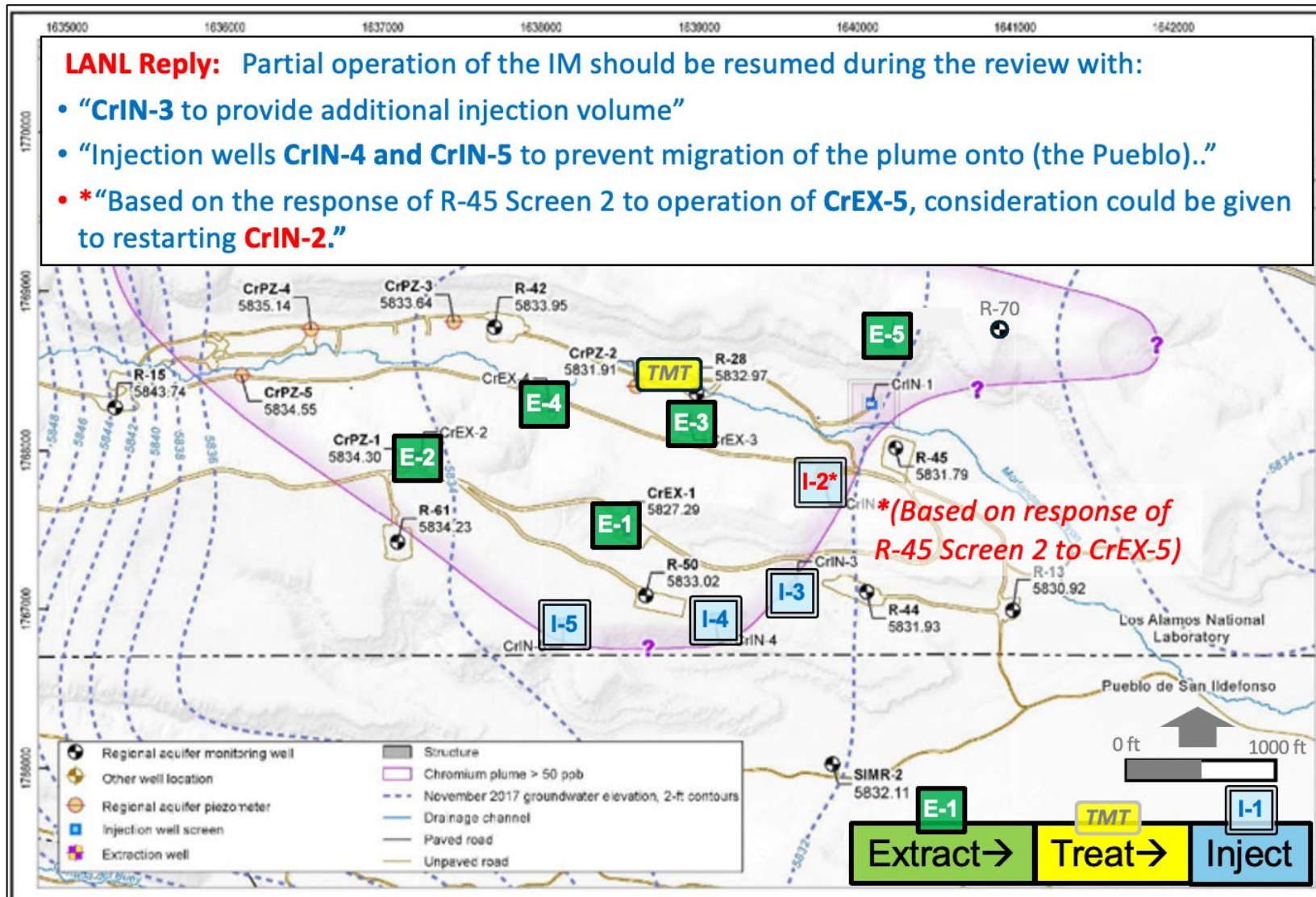


Figure 3-28. DOE-EM-LA's proposed interim measure restart configuration (Letter #4).

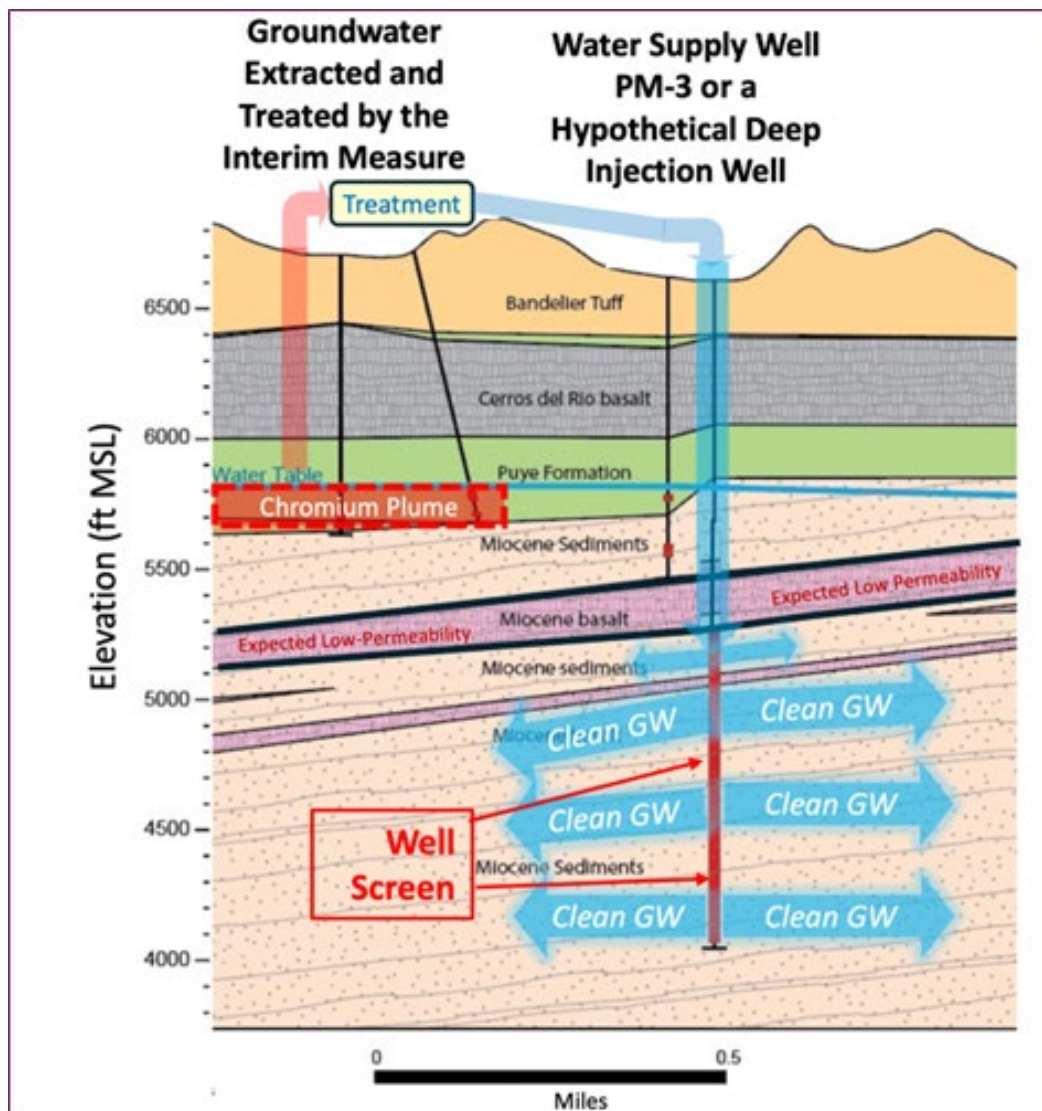


Figure 3-29. Conceptual depiction of an alternative cleaned water return system using either a newly drilled deep well or repurposing existing water supply well PM-3. Original figure: Broxton et al., 2021. Note PM-3 has a gravel pack around the well from 0 to 2,552 feet (the well depth).

## Tables

**Table 2-1. Paraphrased Topics of Questions Posed to the Panel**

1	2	3	4	5
Does evidence (field and modeling) support that the IM is protective or is it responsible for increasing chromium in R-45 and R-61?	Is FEHM software suitable for this project, and is the model with its assumptions suffering from data gaps or accessibility by all concerned parties?	Are the current placement and numbers of wells in the IM sufficient to contain chromium and inform remedy selection or are more wells or different pumping schemes needed?	Is the IM, or its modified form, going to be successful with adaptive management practices and will the current characterization meet EPA requirements for remedy selection?	What are the options available for sealing wells beyond bentonite or cement, and what will the effects of these alternatives be on water chemistry?

**Table 2-2. Sources of the Water Table Maps in Figure 2-11**

Panel	Source
A	Purtymun, 1984
B	Vesselinov et al., 2013
C	Foster, 2024a, presentation slide 9
D	Neptune. 2023, pg. 60. May 2020
E	Neptune. 2023, pg. 62, 64. April, September, 2022
F	Neptune. 2023, pg. 66. March, 2023

**Table 3-1. Extraction Rate Statistics for the IM between June 28, 2016 and March 31, 2023**

	Extraction					Injection				
	CrEx-1	CrEx-2	CrEx-3	CrEx-4	CrEx-5	CrIn-1	CrIn-2	CrIn-3	CrIn-4	CrIn-5
Min (gpm)	8	7	7	8	8	8	8	8	8	8
Max (gpm)	241	76	62	71	102	86	129	236	79	102
Average (gpm)	71	62	32	55	68	56	57	38	56	55

Note: The average values were used in all simulations for which a CrEx pumping rate was > 0 gallons per minute (gpm). Minimum values are the lowest pumping rates greater than 7 gpm, chosen to filter out pumping and injection rates not representative of normal IM operations (e.g., zero pumping rates while the IM was inactive).

**Table 3-2. Comparison of Modeling Platforms**

Code / Code Family	Most recent release (VERSION, YEAR)	Dimensions	Fluid Flow							Material Transport							Heat Transport			Deformation			Discretization		Parallel Computing	Preprocessor	Manual			Operating System(s)		Status			Comments	Ref.																
			Surface Flow	Richards eqn (VS)	Water	Air	Water Vapor	NAPL	Density Flow	Compressibility	Viscosity	Advection	Dispersion/Diffusion	Adsorption	Dissolution	Precipitation	Volatilization	Ion Exchange	Chemical Reaction	Decay	Discrete fracture flow/transport	Dual domain/dual-porosity	Advection	Conduction			Eradiation	Heat Exchange	Phase-Transfer	Elastic	Inelastic	Coupled Flow	Spatial	Temporal			Theoretical	Operating	V&V	UNIX	Windows/DOS	Proprietary (\$)	Freeware	Open-source	License needed?							
Modflow/MT3D	Modflow USG "Flow"	V1.5, 2019	3D	X	X	X																						unstructured	FI		?	X	X		X	X		X	X													
	Modflow USG "Transport"	V1.10.0, 2022	3D	X	X	X				X	X	X									X	X						unstructured	varying, user-def.	?		X	X		X	X		X	X													
	Modflow USG with PHREEQ		3D		X																																															
Modflow/MT3D	Modflow 6	V6.3.0, 2022	3D	X		X				X																		variable	FI		?	X	X		X	X		X	X		X	X										
	Modflow 2000	?, 2000	3D	X		X																		X	X	X		IFDM	FI		X	X	X		X	X		X	X		X	X										
National Labs	MT3D-USGS	V1.0.1, 2019	3D			X				X	X	X							X	X								IFDM	FI		X	X	X	X	X	X		X	X		X	X										
	STOMP	?	3D		X	X	X	X	X**	X	X	X	X	X	X	X	X	X			X	X						IFDM	FI		X	X	X	X	X	X		X	X		X	X				X	Capabilities require customized builds/compilation					
	Parflow+Crunch	V?, 2015	3D	X	X	X				X	X	?	?	?	?	?	?											?	?		X	?	X		X	X		X	X		X	X										
	Tough 2	V2, 1999	3D		X	X	X	X	X	X	X	X	X	X	X	X	X	X	X	X	X	X	X					IFDM	FI		X	X		?	X		?	X		X	X		X	X								
	Tough 3	V1, 2018	3D		X	X	X	X	X	X	X	X	X	X	X	X	X	X	X	X	X	X	X					IFDM	FI		X	X	X		?	?		X	X		X	X										
	FEHM	V3.4, 2019	3D		X	X	X	X	X	X	X	X	X	X	X	X	X	X	X	X	X	X	X					IFDM	FI		X	X	X	X	X	X		X	X		X	X		?								
	JOINT LAB CODE (Name?)		3D																																																	
	Propri.	Feflow	V7.5, 2022	3D		?	X				X	X	?	?	?	?	?	?	X	X	?								?															X	X	X						
Modflow-Surfact*		V4, 2018	3D	?	X	X			X	X	?	?	?				X	X	X									varying	varying			X	X		?	?	X				X											
Eclipse		V?, 2014	3D		X				?	?	?	?	?				X	X	X									?	?		?	?		?	?	X				X												
UTCHEM		V9, 2000	3D			X	X	?	X**	?	X	X	X	X	X	X	X	X	X	X	X	X						varying	varying			X		?	X	X																
Other	MAGNAS	V3, 1993	3D			X			X																																											

**Legend / Explanation**

Modflow-2000 or Modflow-6 can obtain their transport capabilities via MT3D-USGS

Modflow-USG "Transport" includes both flow and transport capabilities

X: the code has the marked capability

?: sources unclear regarding this capability

IFDM: integral finite difference method

FI: fully implicit

\* Part of Modflow code family, but proprietary

\*\*NAPL representation includes residualization/entrapment

Note the following 2009 source document used for reference

[Microsoft PowerPoint - 101222 FunctionalCompaisionChart.pptx \(getc.co.jp\)](#)

**References:**

- 1 <https://www.usgs.gov/software/modflow-usg-unstructured-grid-version-modflow-simulating-groundwater-flow-and-tightly>
- 2 <https://www.gsienv.com/product/modflow-usg/>
- 3
- 4 <https://www.usgs.gov/software/modflow-6-usgs-modular-hydrologic-model>
- 5 [ofr00-92.pdf \(usgs.gov\)](#)
- 6 [MT3D-USGS: Groundwater Solute Transport Simulator for MODFLOW | U.S. Geological Survey](#)
- 7 <https://www.pnnl.gov/projects/stomp>
- 8 [ParCrunchFlow: an efficient, parallel reactive transport simulation tool for physically and chemically heterogeneous saturated subsurface environments | SpringerLink](#)
- 9 [Microsoft PowerPoint - 101222 FunctionalCompaisionChart.pptx \(getc.co.jp\)](#)
- 10 [Scientists Unveil New Version of TOUGH3 Users Guide v2.pdf - Google Drive](#)
- 11 [| LANL | EES | FEHM | LA-CC-2012-083](#)
- 12
- 13 <https://www.mikepoweredbydhi.com/products/feflow>
- 14 <https://www.hgl.com/softwareproducts-new/modflow-surfact/>
- 15 [Product Library \(slb.com\)](#)
- 16 <https://cee.engr.utexas.edu/re:http://gmstuto http://gm:https://link.springer.com/article/10.1007/s13201-013-0090-5>
- 17 <https://agupubs.onlinelibrary.wiley.com/doi/full/10.1029/2004GL020541>



**Table 3-3. Key Characteristics of Potential Annular Sealants for LANL Wells**

	Cement	Cement with Bentonite	Bentonite Slurry	Uncoated Bentonite Chips	Uncoated Bentonite Granules	Coated Bentonite Granules
performance in groundwater aone	☀	☀	☉	☉	○	☀
performance in vadose zone	○	☉	☉	☉	○	☉
geochemical impacts (nominal)	☀	☀	☀	☀	☀	☀
deployment logistics						
field logistics	☀	☀	○	○	☀	☀
tremie logistics	☀	☀	☀	○	☀	☀
tagging logistics	○	○	○	☀	☀	☀
timing logistics (groundwater zone)	○	○	○	☉	☉	○
Resilience (e.g. self healing) in perched vadose interval	☉	○	○	○	○	○
potential for adverse collateral impacts						
Geochemical impacts (incursion into screen zone)	☉	☉	○	○	○	○
leaking/cracking risks (groundwater zone)	☀	☀	☀	○	○	☀
leaking/cracking risks (vadose zone)	○	☉	☉	○	○	○
key -->	☀	= good				
	○	= acceptable				
	☉	= poor				

## **Appendix A**

### **Summary of Simplified Modeling Calculations (*Demirkanli/Looney/Tonkin/Newell/Stephens*)**

## **Appendix A: Summary of Simplified Modeling Calculations**

In recognition that there is disagreement between DOE-EM-LA, NMED, and other stakeholders regarding the operation of the IM and whether the hydraulic containment of the plume is achieved during full and/or partial operations of the system, and further, that there has been communicated a lack of confidence in the existing FEHM groundwater model, calculations were performed to illustrate potential capture zones of the IM system and the effect of alternate configurations and rates of Cr-EX and Cr-IN wells that might be implemented as part of a limited restart of the IM to continue recovering mass and containing a substantial portion of the chromium plume (preventing further plume expansion from these areas) while longer-term solutions are found. The calculations fall into two broad categories:

- Simple numerical calculations
- Calculations performed using analytical superposition

The following sections present these calculations. Assumptions and limitations are summarized; however, limited discussion of the results, conclusions, or recommendations are provided herein. The main narrative sections of the report to which this appendix is attached provide the contextualized interpretation of these calculations.

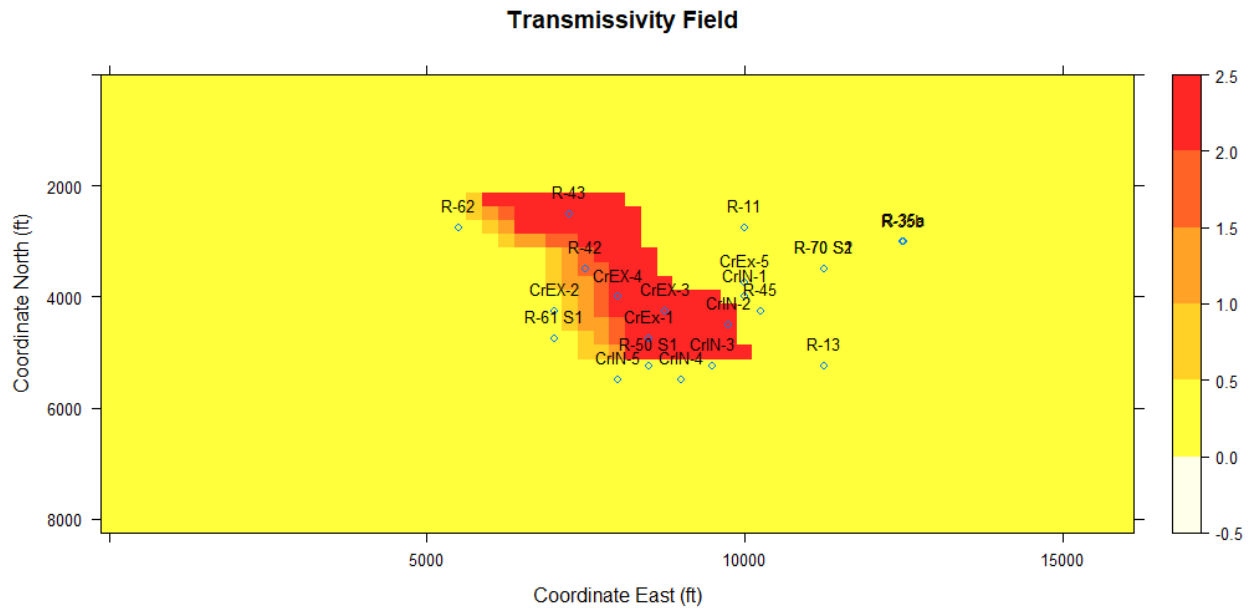
### **1. Numerical Capture Zone Analysis to Evaluate Plume Containment for Full or Partial IM Operations**

Capture zone evaluations are ideally conducted based on observations of patterns in hydraulic head. However, due to low hydraulic gradients and sparse data for the LANL chromium plume site, the capture zones estimated based only on hydraulic head data (particularly in the southeastern portion of the plume area where R-45 and R-70 are located), present a high level of uncertainty. Therefore, the IRT undertook a simple exercise to re-evaluate the capture zones in the plume area.

A simple heterogeneous, 2-dimensional flow model was prepared to assess the capture of Cr during full IM operations (all injection and extraction wells active) and partial IM operations (CrEx-2, CrEx-5, CrIN-4, CrIN-5 active). The base flow system model was prepared by adjusting boundary head values and the internal hydraulic conductivity distribution until the head contours observed in May, 2020 (the IM was inactive at this time) were closely matched (Figure 1A, B). An aquifer depth of 1000 feet was assumed for the purposes of mapping the transmissivity field and reasonably represent the capacity of the aquifer to conduct flow when the IM was active and when it was not. This exercise was done with the purpose of guiding thinking about the site and assisting with data interpretation. The results are not intended to replace more detailed modeling aimed at quantitatively assessing parameter sensitivity, guiding remedial design, or assessing flow and capture in the vertical direction. The calculated particle tracks in the base case simulation indicate a Cr plume projected to migrate east-northeast in the plume area (Figure 1B).

The behavior of the IM system was then examined with two additional simulations: (1) With the IM system in full operation with all CrEx and CrIN wells active at the average values presented in Table 1. Note that the complete record of pumping and injection rates during the times the IM was active or partially active is quite complex and beyond the scope of this evaluation to reproduce in detail in simulations. (2) With the IM system in partial operation with only CrEx-4 and CrEx-5 pumping groundwater and CrIN-4 and CrIN-5 reinjecting the pumped (and treated) water. The second simulation is useful because it establishes a simulated capture zone in the absence of CrIN-1 and CrIN-2, which could have added to hydraulic gradients driving downward flow and Cr transport near R-45.

A)



B)

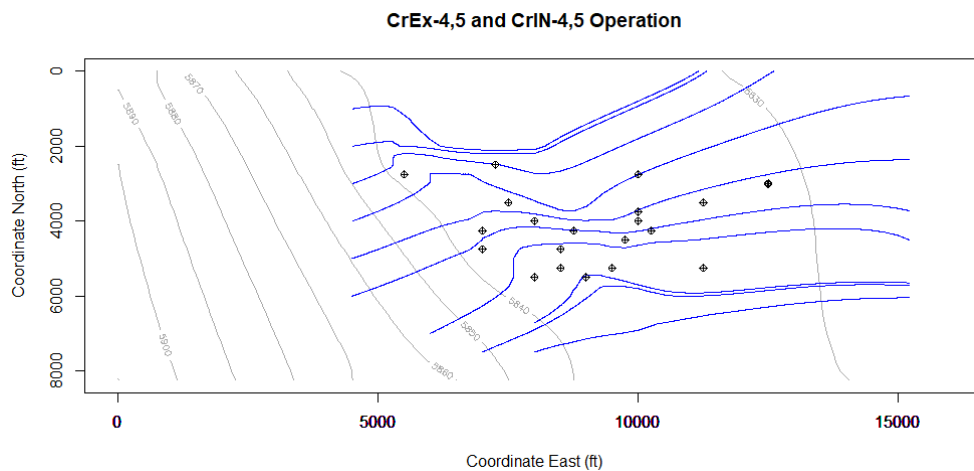


Figure 1. (A) Transmissivity field used in all simulations (units are  $\text{ft}^2/\text{s}$ ) (B) Particle tracks and head contours for the base case in which no IM well were active.

Table1. Summary of extraction rate statistics for the IM between June 28, 2016 and March 31, 2023. The average values were used in all simulations for which a CrEx pumping rate was > 0 gallons/min. Minimum values are the lowest pumping rates greater than 7 gal/min, chosen to filter out pumping and injection rates not representative of normal IM operations (e.g., zero pumping rates while the IM was inactive).

	extraction					injection				
values in gal/min	CrEX-1	CrEX-2	CrEX-3	CrEX-4	CrEX-5	CrIN-1	CrIN-2	CrIN-3	CrIN-4	CrIN-5
min	8	7	7	8	8	8	8	8	8	8
max	241	76	62	71	102	86	129	236	79	102
average	71	62	32	55	68	56	57	38	56	55

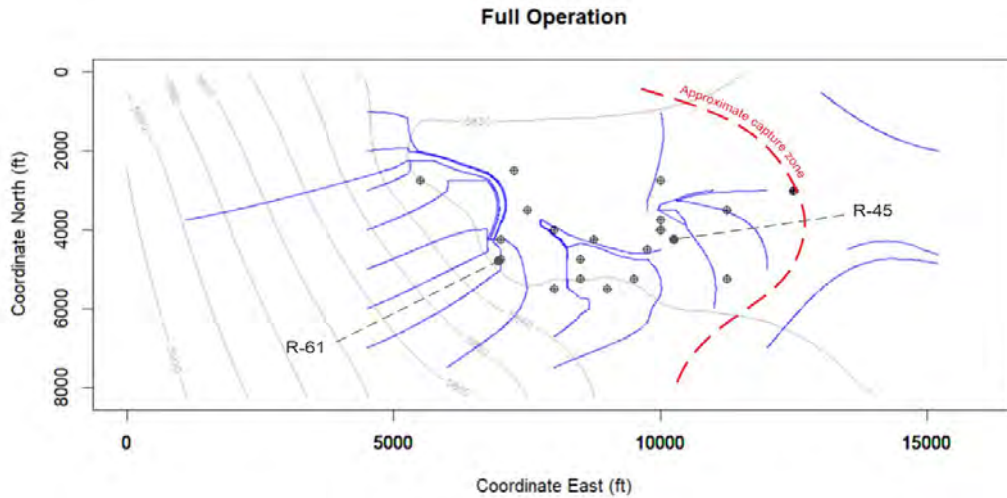
Particle tracks were calculated for each of the two simulations above. These were used to delineate effective capture zones bounded by divergent particle paths (red lines in Figure 2). In these simulations, both R-61 and R-45, fell inside the capture zone, suggesting both options have potential to prevent the Cr plume from spreading eastward from R-70 (Figure 2). Groundwater at R-70 was captured during full IM operation but less likely to be captured under partial IM operation. In both cases, the capture zones were more extensive than those found by Neptune (2023d) (Figure 2). The differences are probably due to a combination of the conservative nature of the Neptune boundaries, and accuracy limitations in the simple IRT model.

In both IRT simulations, R-35 appears to lie east of the estimated capture zones (Figure 2A, B). Therefore, the IM is unlikely to contain portions of the plume that have passed R-70 and are approaching R-35, according to these preliminary calculations. Also, the northern extent of the capture zone in the IRT models are likely exaggerated due to the proximity of the northern model boundary. Taking these limitations, and those discussed previously, into account, these estimated capture zones compare to those predicted by Neptune (2023d) reasonably well. Regardless, the necessity to better understand the position of the capture zone boundaries requires additional careful evaluation with higher level modeling and additional field data.

A comparison of the two IRT simulations (Figure 2) shows that the deactivation of CrEx-1,2,3 and CrIN-1,2,3 resulted in the southern extent of the capture zone moving very slightly northward with CrEx-5 picking up some of the captured groundwater previously collected by CrEx-4. Given the unavoidable uncertainty in these simplified calculations, a conservative restart of the IM system should consider adding a third extraction well to the CrEx-4,5 pair. Perhaps changing CrIN-1 to an extraction well could provide meaningful additional capture near the leading edge of the plume. The addition of one or more injection wells should be considered to take on the additional pumped discharges. A possible future injection well is PM-3. If the portion of the well screen above the Miocene basalt can be isolated from the deeper screen,

injections to this location should exert little or no effect on the shallow portions of the Puye Formation where the Cr contamination resides. This use of PM-3 would not have to disqualify it from future use as a water supply well as long as the treated, injected water maintained the required standards. Additional work is needed to evaluate this possibility, including field testing the basalt hydraulic properties and modeling the response of groundwater to PM-3 pumping and injections across the basalt layer(s).

A)



B)

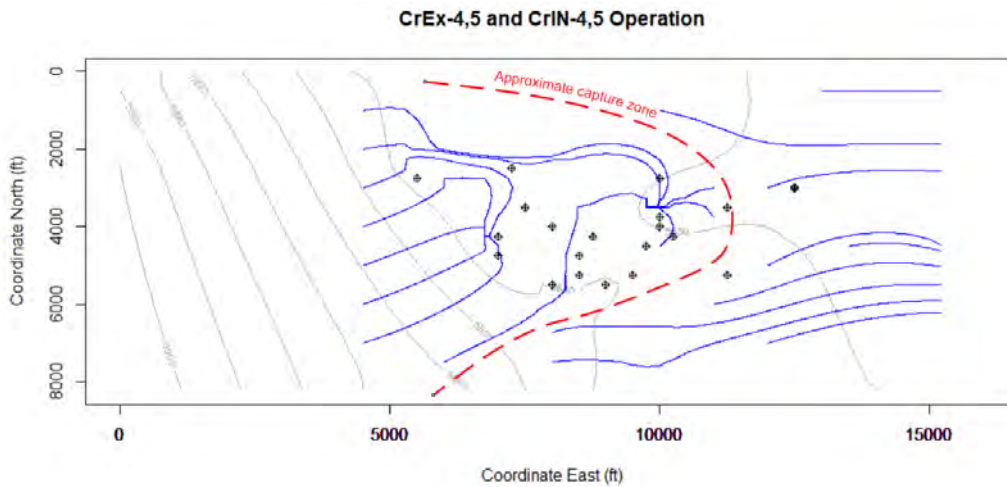


Figure 2. Approximate limits to capture (A) with the IM in full operation and (B) with only the CrEx-5,5 and CrIN-4,5 wells operating.

The simulation results presented above provide tentative insights based on horizontal flow and a single, simplified realization of the aquifer heterogeneity. The issue of vertical plume capture has also been modeled by Neptune (2023d). They calculated that vertical containment of contamination occurred to over 360 ft below the water table. For comparison, the deepest screen interval showing chromium in excess of 50 u/L is at R-45 S2 at about 125 feet below the water table. Although the vertical extent of the chromium plume has not been characterized completely, the modeling strongly suggests that the deep contamination should be captured by the IM where groundwater flows upward to the extraction wells. However, during operation of the IM, downward vertical gradients increased, even at Cr PZ-2 which is between CrEx-3 and CrEx-4. Stratification and the associated anisotropy may limit the amount of vertical flow, and hence transport of contaminants. Nevertheless, in contrast to the modeling results, the field data provide no evidence that vertical contamination is contained by the IM. This issue requires further evaluation both in data collection and modeling.

## 2. Capture Zone Calculations Performed using Analytical Superposition

Two methods that share many commonalities, assumptions, and limitations were used to evaluate groundwater levels, the effects of extraction and injection at the Cr-EX and Cr-IN wells, and to make simple estimates of the lateral extents and patterns of hydraulic containment developed by some hypothetical alternate well configurations. The methods used are:

1. Universal Kriging (UK) with analytic element trends to represent extraction and injection.
2. Superposition with Theis (TS)

### 2.1 UK Method and Results

UK is at its heart a generalized least squares (GLS) regression technique that can be used, once the kriging system of equations has been solved, to predict values at intermediate unsampled locations such as on a grid. Under many conditions, UK with a linear trend and point sink/sources can be used to map water level data in areas with a broad regional trend impacted by extraction and injection. This is described by Tonkin and Larson (2002), Tonkin et al (2009) and Tonkin et al, (2015) and is not detailed further here. The form of the trend equation is presented below:

$$h(x,y) = a + bx + cy + d \sum_{i=1}^m Q \log_{10}(r_i) + e(x,y)$$

Where:

- h(x,y) is the head at any location (x,y)
- A is the global mean (unbiased) term
- B is the regression coefficient in the eastern direction
- C is the regression coefficient in the northern direction
- E(x,y) represents the regression residuals

And:

$$d \sum_1^m Q \log_{10}(r_i)$$

is the summed effect of extraction and injection occurring at  $m$  locations, at rates  $Q$ , each at separation distances of  $r$  from the estimation location, and  $d$  is the regression coefficient for the summed pumping effects. It can be shown (Tonkin and Larson, 2002) that the term  $d$  approximates the value of  $1/(2\pi T)$  from which an estimate of the transmissivity,  $T$ , can be obtained. Often pumping stresses are collected in a single trend term however terms can be grouped – e.g.: separate terms may be specified for two wells believed to be screened within aquifer units that exhibit different transmissivities.

The UK method was used to obtain estimates of the hydraulic gradient in the chromium investigation area to be used as constraints in the capture calculations completed using the TS method. The following values were obtained via a series of water level mapping exercises:

- Hydraulic gradient: ranging 0.001 to 0.003 ft/ft at 079 degrees (i.e., slightly north of east).
- Transmissivity: ranging 600 to 1400 ft<sup>2</sup>/d. Note that this value may be biased low as a consequence of the change in hydraulic gradient moving eastward across the area of interest.

## 2.2 TS Method and Results

Similarly to the UK method, a linear trend can be combined with the superposition of extraction and injection effects (i.e. point sink/sources) represented by the Theis equation, to “model” water level data in areas with a broad regional trend impacted by extraction and injection. The form of this simple model equation, which can be calibrated to measured water level data to obtain the required regression coefficients, is presented below:

$$h = a + bx + cy + d \sum_{i=1}^n Q_i W(u_i)$$

Where:

$h(x,y)$  is the head at any location  $(x,y)$

$A$  is the global mean (unbiased) term

$B$  is the regression coefficient in the eastern direction

$C$  is the regression coefficient in the northern direction

And where  $W(u_i)$  is the Theis well function (exponential integral) with argument:

$$u_i = \frac{r_i^2 S}{4Tt}$$



The values for the gradient terms can be estimated through calibration, or specified by the user. In this application presented here, these values were based on those obtained using the UK method as described above.

The TS method was then used in a screening-level analysis to compare and contrast several alternative strategies for combinations of extraction and injection. The alternatives are bulleted below and the rates are further tabulated (Table 1). Each scenario was simulated assuming two transmissivities: 600 and 1400 ft<sup>2</sup>/d. The estimated extents of hydraulic containment are illustrated in a series of simple figures.

- Scenario 1a – Original configuration (T-600)
- Scenario 1b – Original configuration (T-1400)
- Scenario 2a – Cr-EX as for original configuration, but no injection (T-600)
- Scenario 2b – Cr-EX as for original configuration, but no injection (T-1400)
- Scenario 3a – Cr-EX as for original configuration, all injection to east (T-600)
- Scenario 3b – Cr-EX as for original configuration, all injection to east (T-1400)
- Scenario 4a – Cr-EX as for original configuration, all injection to west (T-600)
- Scenario 4b – Cr-EX as for original configuration, all injection to west (T-1400)
- Scenario 5a – Cr-EX as for original configuration, injection to east and west (T-600)
- Scenario 5b – Cr-EX as for original configuration, injection to east and west (T-1400)
- Scenario 6a – Cr-EX as for original configuration, envelop of injection (T-600)
- Scenario 6b – Cr-EX as for original configuration, envelop of injection (T-1400)
- Scenario 7a – Reduced configuration 1 (T-600)
- Scenario 7b – Reduced configuration 1 (T-1400)
- Scenario 8a – Reduced configuration 2 (T-600)
- Scenario 8b – Reduced configuration 2 (T-1400)

Table 1. Scenario pumping rates

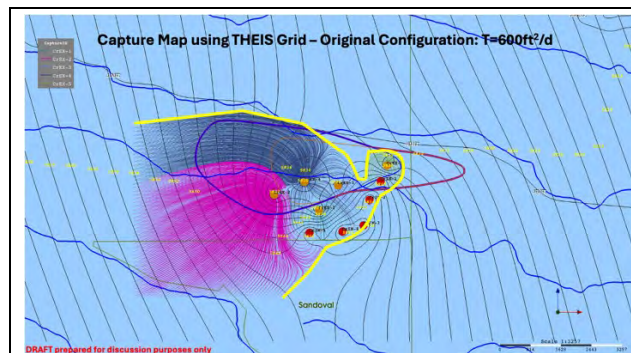
Well	X	Y	Rate (ft3/d)	Rate (gpm)	Well	X	Y	Rate (ft3/d)	Rate (gpm)
<b>Scenario 1: Original Configuration</b>					<b>Scenario 5: Injection Combined on East and West Side</b>				
CrEX-1	1638440.0	1767520.7	-14437.5	-75.0	CrEX-1	1638440.0	1767520.7	-14437.5	-75.0
CrEX-2	1637238.8	1767934.3	-12512.5	-65.0	CrEX-2	1637238.8	1767934.3	-12512.5	-65.0
CrEX-3	1638949.3	1768184.2	-5775.0	-30.0	CrEX-3	1638949.3	1768184.2	-5775.0	-30.0
CrEX-4	1638052.6	1768280.8	-9625.0	-50.0	CrEX-4	1638052.6	1768280.8	-9625.0	-50.0
CrEX-5	1640257.8	1768714.8	-12512.5	-65.0	CrEX-5	1640257.8	1768714.8	-12512.5	-65.0
CrIN-1	1640089.6	1768293.7	11550.0	60.0	CrIN-1	1634810.0	1767640.0	11550.0	60.0
CrIN-2	1639791.8	1767797.5	11550.0	60.0	CrIN-2	1642800.0	1768080.0	11550.0	60.0
CrIN-3	1639633.8	1767117.6	8662.5	45.0	CrIN-3	1642800.0	1768520.0	8662.5	45.0
CrIN-4	1639069.1	1766953.8	11550.0	60.0	CrIN-4	1642800.0	1768960.0	11550.0	60.0
CrIN-5	1638188.1	1766918.7	11550.0	60.0	CrIN-5	1634810.0	1769400.0	11550.0	60.0
<b>Scenario 2: No Injection</b>					<b>Scenario 6: Injection Enveloped Plume</b>				
CrEX-1	1638440.0	1767520.7	-14437.5	-75.0	CrEX-1	1638440.0	1767520.7	-14437.5	-75.0
CrEX-2	1637238.8	1767934.3	-12512.5	-65.0	CrEX-2	1637238.8	1767934.3	-12512.5	-65.0
CrEX-3	1638949.3	1768184.2	-5775.0	-30.0	CrEX-3	1638949.3	1768184.2	-5775.0	-30.0
CrEX-4	1638052.6	1768280.8	-9625.0	-50.0	CrEX-4	1638052.6	1768280.8	-9625.0	-50.0
CrEX-5	1640257.8	1768714.8	-12512.5	-65.0	CrEX-5	1640257.8	1768714.8	-12512.5	-65.0
CrIN-1	1640089.6	1768293.7	0.0	0.0	CrIN-1	1636274.0	1766840.0	11550.0	60.0
CrIN-2	1639791.8	1767797.5	0.0	0.0	CrIN-2	1639832.0	1766060.0	11550.0	60.0

CrIN-3	1639633. 8	1767117. 6	0.0	0.0
CrIN-4	1639069. 1	1766953. 8	0.0	0.0
CrIN-5	1638188. 1	1766918. 7	0.0	0.0
<b>Scenario 3: All Injection on East Side</b>				
CrEX-1	1638440. 0	1767520. 7	-14437.5	-75.0
CrEX-2	1637238. 8	1767934. 3	-12512.5	-65.0
CrEX-3	1638949. 3	1768184. 2	-5775.0	-30.0
CrEX-4	1638052. 6	1768280. 8	-9625.0	-50.0
CrEX-5	1640257. 8	1768714. 8	-12512.5	-65.0
CrIN-1	1642800. 0	1767640. 0	11550.0	60.0
CrIN-2	1642800. 0	1768080. 0	11550.0	60.0
CrIN-3	1642800. 0	1768520. 0	8662.5	45.0
CrIN-4	1642800. 0	1768960. 0	11550.0	60.0
CrIN-5	1642800. 0	1769400. 0	11550.0	60.0
<b>Scenario 4: All Injection on West Side</b>				
CrEX-1	1638440. 0	1767520. 7	-14437.5	-75.0
CrEX-2	1637238. 8	1767934. 3	-12512.5	-65.0
CrEX-3	1638949. 3	1768184. 2	-5775.0	-30.0
CrEX-4	1638052. 6	1768280. 8	-9625.0	-50.0
CrEX-5	1640257. 8	1768714. 8	-12512.5	-65.0
CrIN-1	1634810. 0	1767640. 0	11550.0	60.0

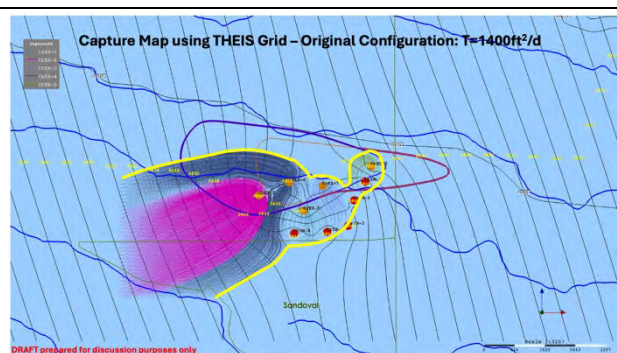
CrIN-3	1642800. 0	1768520. 0	8662.5	45.0
CrIN-4	1638560. 0	1770170. 0	11550.0	60.0
CrIN-5	1634810. 0	1769400. 0	11550.0	60.0
<b>Scenario 7: Reduced Configuration 1</b>				
CrEX-1	1638440. 0	1767520. 7	0.0	0.0
CrEX-2	1637238. 8	1767934. 3	0.0	0.0
CrEX-3	1638949. 3	1768184. 2	0.0	0.0
CrEX-4	1638052. 6	1768280. 8	-9625.0	-50.0
CrEX-5	1640257. 8	1768714. 8	-12512.5	-65.0
CrIN-1	1640089. 6	1768293. 7	0.0	0.0
CrIN-2	1639791. 8	1767797. 5	0.0	0.0
CrIN-3	1639633. 8	1767117. 6	0.0	0.0
CrIN-4	1639069. 1	1766953. 8	11550.0	60.0
CrIN-5	1638188. 1	1766918. 7	11550.0	60.0
<b>Scenario 8: Reduced Configuration 2</b>				
CrEX-1	1638440. 0	1767520. 7	0.0	0.0
CrEX-2	1637238. 8	1767934. 3	0.0	0.0
CrEX-3	1638949. 3	1768184. 2	0.0	0.0
CrEX-4	1638052. 6	1768280. 8	-12512.5	-65.0
CrEX-5	1640257. 8	1768714. 8	-14437.5	-75.0
CrIN-1	1640089. 6	1768293. 7	0.0	0.0

CrIN-2	1634810. 0	1768080. 0	11550.0	60.0
CrIN-3	1634810. 0	1768520. 0	8662.5	45.0
CrIN-4	1634810. 0	1768960. 0	11550.0	60.0
CrIN-5	1634810. 0	1769400. 0	11550.0	60.0

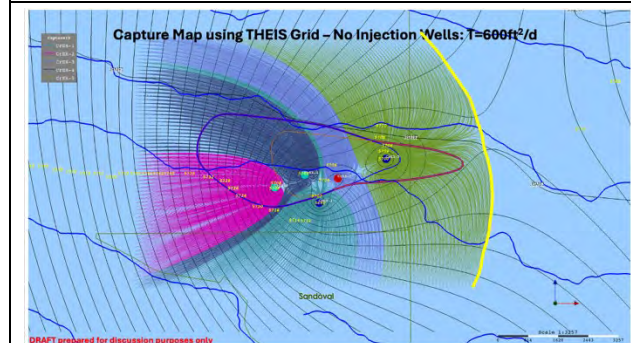
CrIN-2	1639791. 8	1767797. 5	0.0	0.0
CrIN-3	1639633. 8	1767117. 6	0.0	0.0
CrIN-4	1639069. 1	1766953. 8	13475.0	70.0
CrIN-5	1638188. 1	1766918. 7	13475.0	70.0



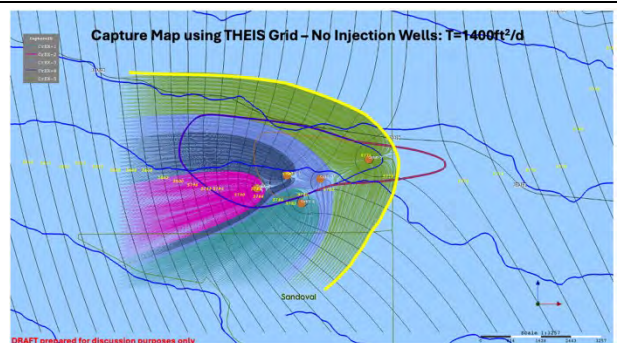
1a



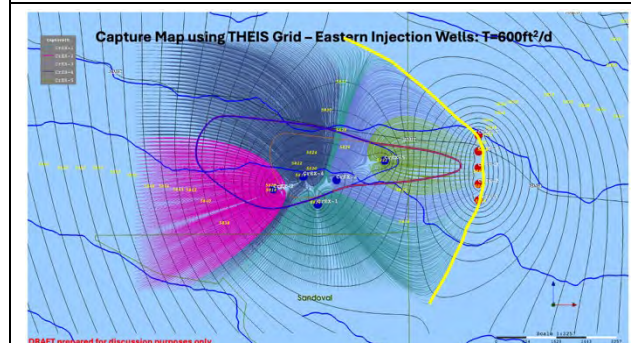
1b



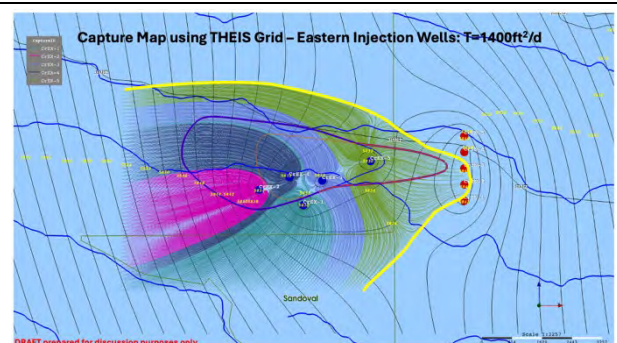
2a



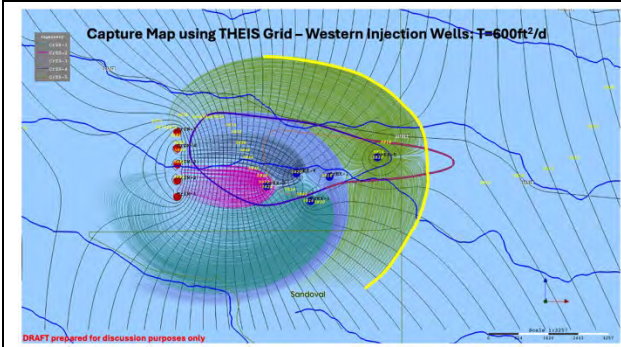
2b



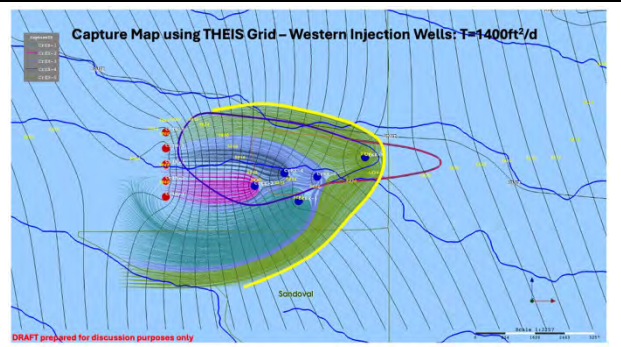
3a



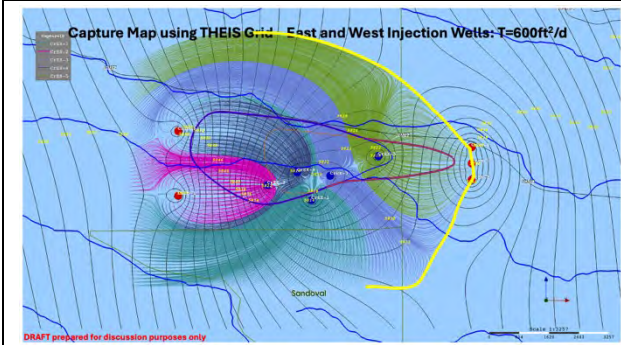
3b



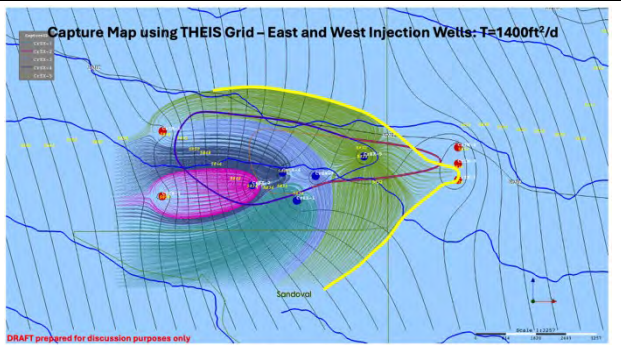
4a



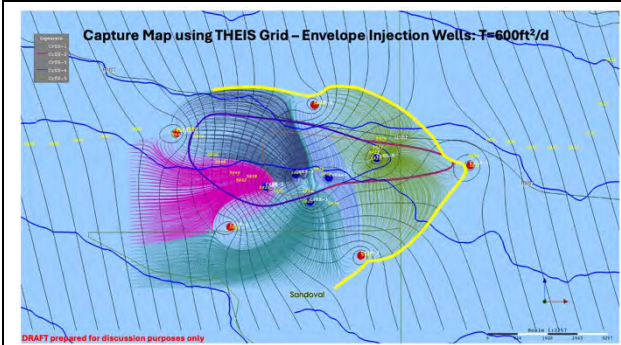
4b



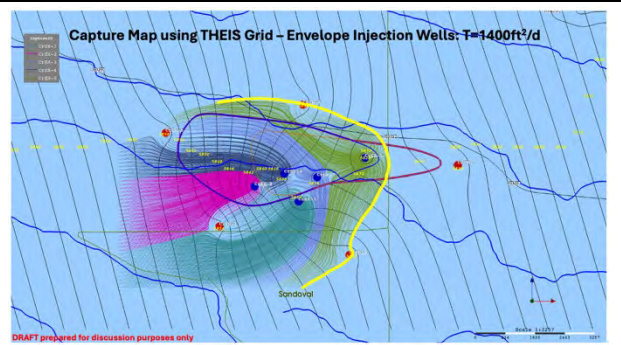
5a



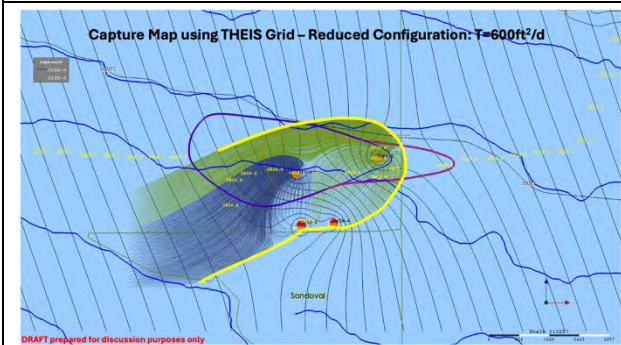
5b



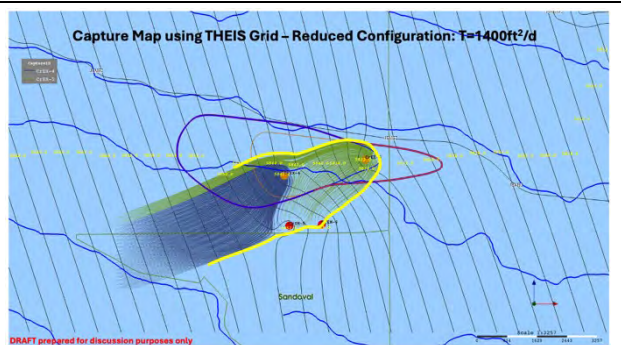
6a



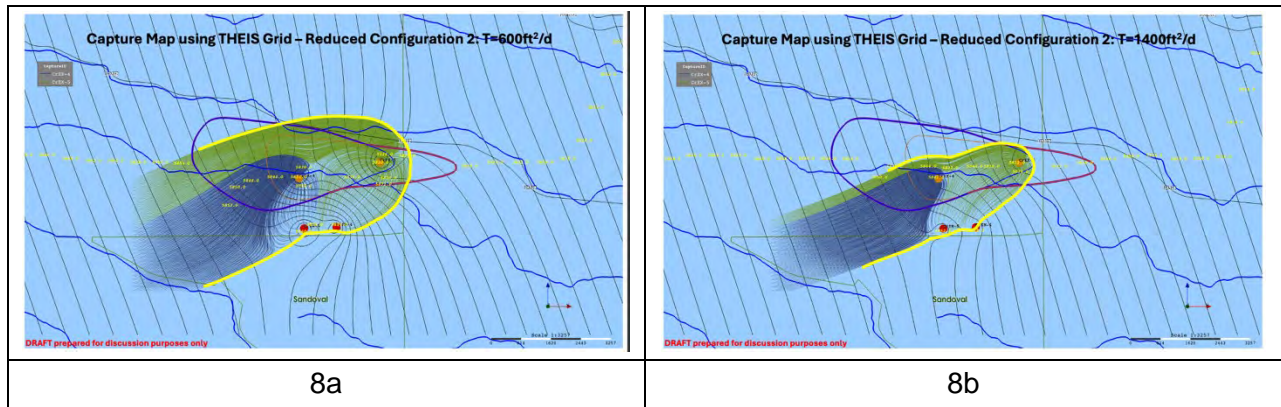
6b



7a



7b



The extent of hydraulic containment under varying operational scenarios for the IM system: 1a – Original configuration (T-600); 1b – Original configuration (T-1400); 2a – Cr-EX as for original configuration, but no injection (T-600); 2b – Cr-EX as for original configuration, but no injection (T-1400); 3a – Cr-EX as for original configuration, all injection to east (T-600); 3b – Cr-EX as for original configuration, all injection to east (T-1400); 4a – Cr-EX as for original configuration, all injection to west (T-600); 4b – Cr-EX as for original configuration, all injection to west (T-1400); 5a – Cr-EX as for original configuration, injection to east and west (T-600); 5b – Cr-EX as for original configuration, injection to east and west (T-1400); 6a – Cr-EX as for original configuration, envelop of injection (T-600); 6b – Cr-EX as for original configuration, envelop of injection (T-1400); 7a – Reduced configuration 1 (T-600); 7b – Reduced configuration 1 (T-1400); 8a – Reduced configuration 2 (T-600); and 8b – Reduced configuration 2 (T-1400).

### 3. Assumptions and Limitations

The calculations presented in this appendix are not considered design-basis calculations, and should not be interpreted as such. These calculations were completed to help visualize the different extents and patterns of capture using different well configurations; provide points of discussion when considering a restart of the IM system (particularly with regards to full or partial operational conditions). While utilizing different methods, collectively, the results from these simpler approaches indicate a consistent overall behavior of the capture zones in response to varying operational conditions, and demonstrate that some decisions at the site may not require such sophisticated numerical modeling as has been the focus in the past.

The main assumptions underlying use of both the method described above are listed below, together with an indication as to whether the assumption is met in this specific application. Several of these assumptions are violated to some extent, whereas others are not applicable or are not consequential to the purpose of the calculations here:

- The piezometric surface was horizontal prior to pumping. **N/A**
- The well is pumped at a constant rate. **N/A**
- The aquifer is homogeneous, isotropic, and confined. **No**

- Water removed from storage is discharged instantaneously with decline in head. **No**
- Flow is two dimensional (there is no vertical component of flow). **No**
- The well is fully penetrating and well storage is negligible. **No**
- The aquifer is (appears) infinite and of uniform thickness. **No**

## References

- Tonkin, M.J., J. Kennel, W. Huber, and J. Lambie, 2015. Multi-Event Universal Kriging (MEUK), *Advances in Water Resources*, v. 87, pp. 92–105, January.  
doi:10.1016/j.advwatres.2015.11.001.
- Tonkin, M., S. Dadi, and R. Shannon, 2009. Collection and Mapping of Water Levels to Assist in the Evaluation of Groundwater Pump-and-Treat Remedy Performance. SGW-42305 (Rev. 0). Prepared for the US Department of Energy, Richland, WA, September 2009.
- Tonkin, M., and S. Larson, 2002. Kriging Water Levels with a Regional-Linear and Point-Logarithmic Drift. *Ground Water*, v. 40, no. 2, pp. 185-193.

## **Appendix B**

**Batu (2024j) - Horizontal ( $K_h$ ) and Vertical Hydraulic  
Conductivity ( $K_v$ ) Values Determined from the  
Aquifer Tests of the CrIN, CrEX, PM-2, PM-4, PM-3  
(with R 35a and R-35b), and R-13 Wells at the LANL Site**



# Horizontal ( $K_h$ ) and Vertical Hydraulic Conductivity ( $K_v$ ) Values Determined from the Aquifer Tests of the CrIN, CrEX, PM-2, PM-4, PM-3 (with R-35a and R-35b), and R-13 Wells at the LANL Site

---

Vedat Batu, Ph.D., P.E.  
Argonne Associate  
Argonne National Laboratory  
Lemont, Illinois

**August 25, 2024**

This page intentionally left blank.

## Executive Summary

In this report, the aquifer test data for CrIN, CrEX, PM-2, PM-3, and PM-4 are analyzed and the results are as follows.

### IN Wells Aquifer Tests

The drawdown data as well as the methods used for them are given in Attachment 1 of this report.

The resulted horizontal hydraulic conductivity ( $K_h$ ) values for the 5 CrIN wells are as follows:

$$\text{CrIN} - 1: K_h = 26 \text{ ft/d} = 9.17 \times 10^{-3} \text{ cm/s}$$

$$\text{CrIN} - 2: K_h = 37 \text{ ft/d} = 1.31 \times 10^{-2} \text{ cm/s}$$

$$\text{CrIN} - 3: K_h = 38 \text{ ft/d} = 1.34 \times 10^{-2} \text{ cm/s}$$

$$\text{CrIN} - 4: K_h = 60 \text{ ft/d} = 2.11 \times 10^{-2} \text{ cm/s}$$

$$\text{CrIN} - 5: K_h = 72 \text{ ft/d} = 2.54 \times 10^{-2} \text{ cm/s}$$

Their arithmetic average is  $47 \text{ ft/d}$  ( $1.66 \times 10^{-2} \text{ cm/s}$ ). These values correspond to silty sand, clean sand and gravel (e.g., Freeze and Cherry, 1979, p. 29, Table 2.3). These wells are approximately along a line which is perpendicular to the main flow direction which is towards the southeast direction. It can be noticed that the aquifer is more permeable around CrIN-4 and CrIN-5 injection wells ( $60 \text{ ft/d}$  and  $72 \text{ ft/d}$ ). Also, these values indicate that the  $K_h$  values at CrIN-1, CrIN-2, and CrIN-3 ( $26 \text{ ft/d}$ ,  $37 \text{ ft/d}$ , and  $38 \text{ ft/d}$ ) are about 50% of the previous two values.

### EX Wells Aquifer Tests

The drawdown data as well as the methods used for them are given in Attachment 2 of this report.

The resulted horizontal hydraulic conductivity ( $K_h$ ) values for the five CrEX extraction wells are as follows:

$$\text{CrEX} - 1: K_h = 12.5 \text{ ft/d} = 4.41 \times 10^{-3} \text{ cm/s}$$

$$\text{CrEX} - 2: K_h = 51.0 \text{ ft/d} = 1.80 \times 10^{-2} \text{ cm/s}$$

$$\text{CrEX} - 3: K_h = 21.5 \text{ ft/d} = 7.58 \times 10^{-3} \text{ cm/s}$$

$$\text{CrEX} - 4: K_h = 12.5 \text{ ft/d} = 4.41 \times 10^{-3} \text{ cm/s}$$

CrEX – 5:  $K_h = 172.0 \text{ ft/d} = 6.07 \times 10^{-2} \text{ cm/s}$

Their arithmetic average is  $53.9 \text{ ft/d}$  ( $1.90 \times 10^{-2} \text{ cm/s}$ ). These values correspond to silty sand, clean sand, and gravel (e.g., Freeze and Cherry, 1979, p. 29, Table 2.3). It can be noticed that the aquifer is more permeable around CrEX-2( $51.0 \text{ ft/d}$ ) and CrEX-5 ( $172.0 \text{ ft/d}$ ) extraction wells.

## PM-2 Aquifer Test

The drawdown data as well as the methods used for them are given in Attachment 3 of this report.

The drawdown data for PM-4 (0.83 ft/d), PM-5 (3.34 ft/d), R-20 Screen 3 (2.84 ft/d), and PM-2 (1.20 ft/d) recovery are generally good. The values in the parentheses are the  $K_h$  values. And their average  $K_h$  value is  $2.05 \text{ ft/d}$  ( $7.23 \times 10^{-4} \text{ cm/s}$ ). The anisotropy ratio ( $K_v/K_h$ ) for PM-4, PM-5, and R-20 Screen 3 are 0.035, 0.010, 0.016, respectively. And their average is 0.020. Therefore,  $K_v = 0.041 \text{ ft/d} = 1.45 \times 10^{-5} \text{ cm/s}$

The storage coefficient ( $S$ ) for PM-4, PM-5, and R-20 Screen 3 are  $6.73 \times 10^{-4}$ ,  $1.31 \times 10^{-3}$ ,  $6.54 \times 10^{-3}$  respectively. And their average is  $2.84 \times 10^{-3}$ . According to the literature, storage coefficients generally vary between 0.00005 and 0.005 (e.g., Freeze and Cherry, 1979, p. 60). And the value 0.00284 is in this range.

The specific yield ( $S_y$ ) values in Table 2 of Attachment 3 are not reliable. Potential reasons may be (a) the screen intervals are significantly below the water table and (b) the pump test period was not long enough.

The  $K_h$  value determined from the steady-state drawdown value of PM-2 is  $K_h = 2.60 \text{ ft/d} = 9.17 \times 10^{-4} \text{ cm/s}$  for which the calculation details are given in Appendix A of Attachment 3. This value compares favorably with the  $K_h = 1.20 \text{ ft/d} = 4.23 \times 10^{-4} \text{ cm/s}$  determined from the PM-2 recovery analysis. The  $K_h = 2.60 \text{ ft/d}$  steady-state drawdown value is even closer to the average  $K_h = 2.05 \text{ ft/d}$  determined from the transient drawdown data analysis.

## PM-4 Aquifer Test

The drawdown data as well as the methods used for them are given in Attachment 4 of this report.

The values of  $K_h$  vary between  $0.3 \text{ ft/d}$  and  $1.5 \text{ ft/d}$ . The average of the rest of seven values (1.2, 0.8, 0.3, 1.1, 1.0, 1.5, and  $0.7 \text{ ft/d}$ ) is  $K_{h-avg} = 0.9 \text{ ft/d}$ . The  $K_h$  value determined from the steady-state drawdown value of PM-4 is  $K_h = 2.3 \text{ ft/d}$ .

The average of the six  $a = K_v/K_h$  values (0.016, 0.225, 0.012, 0.022, 0.040, and 0.016) is  $a_{avg} = K_{v-avg}/K_{h-avg} = 0.055$ . Therefore,  $K_{v-avg} = aK_h = 0.05 \text{ ft/d}$ .

The storage coefficient ( $S$ ) values range from  $2.91E - 04$  to  $7.17E - 04$ . According to the literature, storage coefficients generally vary between 0.00005 and 0.005 (e.g., Freeze and Cherry, 1979, p. 60).

The specific yield ( $S_y$ ) values in Table 2 are not reliable. Potential reasons may be (a) the screen intervals are significantly below the water table; (b) the pump test period was not long enough; and (c) the observation wells are significantly far away from the pumped well (4,463 *ft* to 5,508 *ft*).

### **PM-3, R-35a, and R-35b Aquifer Tests**

The drawdown data as well as the methods used for them are given in Attachment 5 of this report.

Horizontal hydraulic conductivity ( $K_h$ ) and vertical hydraulic conductivity ( $K_v$ ) at R-35a are determined using transient drawdown data. Also with the use of steady state drawdowns at R-35a and R-35b the  $K_h$  values are determined.

The results for the transient drawdown data analyses are given in Table 2 which shows that there is a total of two set of values determined from the Neuman (1974, 1975) method. From the values in Table 2, the conclusions drawn are as follows:

1. Based on the Neuman method, the values corresponding to drawdown and recovery for horizontal hydraulic conductivity ( $K_h$ ) are 5.56 *ft/d* and 6.19 *ft/d*, respectively, and their average is 5.875 *ft/d*.
2. The corresponding values of storage coefficient ( $S$ ) to drawdown and recovery are 0.001002 and 0.001032 respectively. According to the literature, storage coefficients generally vary between 0.00005 and 0.005 (e.g., Freeze and Cherry, 1979, p. 60).
3. The anisotropy  $a = K_v/K_h$  values corresponding to drawdown and recovery are 0.1437 and 0.0704, respectively. And their average is 0.12205 which close to 0.10 and this value generally is being used in practice whenever  $a = K_v/K_h$  is not available.
4. The specific yield ( $S_y$ ) values in Table 2 are not realistic. Potential reasons may be (a) the screen interval of R-35a is significantly below the water table and (b) the aquifer test period was not long enough.

From the steady state drawdown at R-35a, the  $K_h$  value was determined as  $K_h = 2.2 \text{ ft/d} = 0.000007761 \text{ m/s} = 7.76 \times 10^{-4} \text{ cm/s}$ .

From the steady state drawdown at R-35b, the  $K_h$  value was determined as  $K_h = 73.0 \text{ ft/d} = 0.000257528 \text{ m/s} = 2.58 \times 10^{-2} \text{ cm/s}$ .

The  $K_h$  values based on steady state drawdowns at R-35a and R-35b are compared with the  $K_h$  values of Neptune in Table 4. Some key points are as follows:

1. At R-35a, the  $K_h$  values of the steady state drawdown and  $K_{h-Neptune}$  values are  $2.2 \text{ ft/d}$  and  $3.1 \text{ ft/d}$ , respectively, and the  $K_{h-Neptune}/K_h$  is 1.409. Neptune described the formation name as “Tcar” whereas in Koch and Schmeer (2009, p. 54) it is described as “Tsfu”.
2. At R-35b, the  $K_h$  values of the steady state drawdown and  $K_{h-Neptune}$  values are  $73.0 \text{ ft/d}$  and  $133.0 \text{ ft/d}$ , respectively, and the  $K_{h-Neptune}/K_h$  is 1.822. Both Neptune and in Koch and Schmeer (2009, p. 55) describe the formation name as “Tpf”.

### **R-13 Aquifer Test Results**

The drawdown data as well as the methods used for them are given in Attachment 6 of this report.

Using the method described in Section 4.0, calculation details for the horizontal hydraulic conductivity ( $K_h$ ) are given in Appendix A. The value is

$$K_h = 25 \text{ ft/d} = 0.000088194 \text{ m/s} = 8.82 \times 10^{-3} \text{ cm/s}$$

# Contents

Executive Summary .....	ES-1
1. Purpose.....	1
1.1 Purpose of Attachment 1 .....	1
1.2 Purpose of Attachment 2.....	1
1.3 Purpose of Attachment 3.....	1
1.4 Purpose of Attachment 4.....	1
1.5 Purpose of Attachment 5.....	1
1.6 Purpose of Attachment 6.....	1
2. Results .....	2
2.1 Results of CrIN-1, CrIN-2, CrIN-3, CrIN-4, and CrIN-5 Injection Wells Data Analyses.....	2
2.2 Results of CrEX-1, CrEX-2, CrEX-3, CrEX-4, and CrEX-5 Extraction Wells Data Analyses.....	2
2.3 Results of the PM-2 Aquifer Test Data Analyses .....	3
2.3.1 Transient Drawdown Data at the Observation Wells and PM-2 Recovery Analyses Results.....	3
2.3.2 Horizontal Hydraulic Conductivity ( $K_h$ ) Value Determined from the Steady-State Drawdown Value at the PM-2 Pumped Well.....	3
2.4 Results of the PM-4 Aquifer Test Data Analyses .....	3
2.4.1 Transient Drawdown Data at the Observation Wells and PM-4 Recovery Analyses Results.....	3
2.4.2 Horizontal Hydraulic Conductivity ( $K_h$ ) Value Determined from the Steady-State Drawdown Value at the PM-4 Pumped Well.....	4
2.5 Results of the PM-3 Aquifer Test Data Analyses .....	4
2.5.1 Results of the Transient Drawdown Data Analyses .....	4
2.5.2 Results of the Steady State Drawdown Data Analysis.....	5
2.6 Result of the R-13 Aquifer Test Data Analysis.....	5

## Attachments

- Attachment 1 Determination of the Horizontal Hydraulic Conductivity ( $K_h$ ) Values from the Steady-State Drawdowns of the CrIN-1, CrIN-2, CrIN-3, CrIN-4, and CrIN-5 Injection Wells Los Alamos, New Mexico
- Attachment 2 Determination of the Horizontal Hydraulic Conductivity ( $K_h$ ) Values from the Steady-State Drawdown Values of the CrEX-1, CrEX-2, CrEX-3, CrEX-4, and CrEX-5 Extraction Wells, Los Alamos, New Mexico
- Attachment 3 Analyses of Aquifer Test Data for PM-2 to Determine Horizontal ( $K_h$ ) and Vertical Hydraulic Conductivities ( $K_v$ ), Los Alamos, New Mexico
- Attachment 4 Analyses of Aquifer Test Data for PM-4 to Determine Horizontal ( $K_h$ ) and Vertical Hydraulic Conductivities ( $K_v$ ), Los Alamos, New Mexico
- Attachment 5 Analyses of Aquifer Test Data for PM-3 to Determine Horizontal ( $K_h$ ) and Vertical Hydraulic Conductivities ( $K_v$ ) at R-35a and Use of Steady State Drawdowns at R-35a and R-35b to Determine  $K_h$  Values and Comparison with the Neptune  $K_h$  Values, Los Alamos, New Mexico

Attachment 6 Determination of the Horizontal Hydraulic Conductivity ( $K_h$ ) Value from the Steady-State Drawdown Value of the R-13 Extraction Well, Los Alamos, New Mexico



# 1. Purpose

This report has six attachments and their purposes are described below.

## 1.1 Purpose of Attachment 1

The purpose of Attachment 1 is to determine horizontal hydraulic conductivity ( $K_h$ ) values using the measured steady-state drawdowns at CrIN-1, CrIN-2, CrIN-3, CrIN-4, and CrIN-5 injection wells. The method is based on the *Dupuit-Forchheimer well discharge formula* along with the *Sichardt empirical zone of influence radius* to determine the values of  $K_h$  around each CrIN injection well using the data in the report of Los Alamos National Laboratory (2017).

## 1.2 Purpose of Attachment 2

The purpose of Attachment 2 is to determine horizontal hydraulic conductivity ( $K_h$ ) values using the measured steady-state drawdown at CrEX-1, CrEX-2, CrEX-3, CrEX-3, and CrEX-5 extraction wells. The method is based on the *Dupuit-Forchheimer well discharge formula* for unconfined aquifers and *Thiem's discharge formula* for confined aquifers along with the *Sichardt empirical zone of influence radius* to determine the values of  $K_h$  around each CrEX extraction well using the data in the report of Los Alamos National Laboratory (2015, 20016, 2017a, 2017b, and 2018).

## 1.3 Purpose of Attachment 3

The purpose of Attachment 3 is to analyze the aquifer test data of PM-2 using multiple observation wells. The test was performed in 2003 and described in a 2005 report entitled "*Analyses of the PM-2 Aquifer Test Using Multiple Observation Wells, LA-14225-MS*" authored by Stephen G. McLin.

## 1.4 Purpose of Attachment 4

The purpose of Attachment 4 is to analyze the aquifer test data of PM-4 using multiple observation wells. The test was performed in February and March 2005 and described in a 2006 report entitled "*Analyses of the PM-4 Aquifer Test Using Multiple Observation Wells, LA-14252-MS*" authored by Stephen G. McLin.

## 1.5 Purpose of Attachment 5

The purpose of Attachment 5 is to analyze the aquifer test data of PM-3 to determine horizontal hydraulic conductivity ( $K_h$ ) and vertical hydraulic conductivity ( $K_v$ ) at R-35a and with the use of steady state drawdowns at R-35a and R-35b to determine  $K_h$  values.

## 1.6 Purpose of Attachment 6

The purpose of Attachment 6 is to determine horizontal hydraulic conductivity ( $K_h$ ) value using the measured steady-state drawdown value at R-13 extraction well. The method is based on

*Thiem's discharge formula* for confined aquifers along with the *Sichardt empirical zone of influence radius* to determine the values of  $K_h$  around R-13 extraction well using the data in the report of Los Alamos National Laboratory (Stone and McLin, 2003).

## 2. Results

### 2.1 Results of CrIN-1, CrIN-2, CrIN-3, CrIN-4, and CrIN-5 Injection Wells Data Analyses

The drawdown data as well as the methods used for them are given in Attachment 1. The resulted horizontal hydraulic conductivity ( $K_h$ ) values for the 5 CrIN wells are as follows:

$$\text{CrIN} - 1: K_h = 26 \text{ ft/d} = 9.17 \times 10^{-3} \text{ cm/s}$$

$$\text{CrIN} - 2: K_h = 37 \text{ ft/d} = 1.31 \times 10^{-2} \text{ cm/s}$$

$$\text{CrIN} - 3: K_h = 38 \text{ ft/d} = 1.34 \times 10^{-2} \text{ cm/s}$$

$$\text{CrIN} - 4: K_h = 60 \text{ ft/d} = 2.11 \times 10^{-2} \text{ cm/s}$$

$$\text{CrIN} - 5: K_h = 72 \text{ ft/d} = 2.54 \times 10^{-2} \text{ cm/s}$$

Their arithmetic average is  $47 \text{ ft/d}$  ( $1.66 \times 10^{-2} \text{ cm/s}$ ). These values correspond to silty sand, clean sand and gravel (e.g., Freeze and Cherry, 1979, p. 29, Table 2.3). These wells are approximately along a line which is perpendicular to the main flow direction which is towards the southeast direction. It can be noticed that the aquifer is more permeable around CrIN-4 and CrIN-5 injection wells ( $60 \text{ ft/d}$  and  $72 \text{ ft/d}$ ). Also, these values indicate that the  $K_h$  values at CrIN-1, CrIN-2, and CrIN-3 ( $26 \text{ ft/d}$ ,  $37 \text{ ft/d}$ , and  $38 \text{ ft/d}$ ) are about 50% of the previous two values.

### 2.2 Results of CrEX-1, CrEX-2, CrEX-3, CrEX-4, and CrEX-5 Extraction Wells Data Analyses

The drawdown data as well as the methods used for them are given in Attachment 2. The resulted horizontal hydraulic conductivity ( $K_h$ ) values for the five CrEX extraction wells are as follows:

$$\text{CrEX} - 1: K_h = 12.5 \text{ ft/d} = 4.41 \times 10^{-3} \text{ cm/s}$$

$$\text{CrEX} - 2: K_h = 51.0 \text{ ft/d} = 1.80 \times 10^{-2} \text{ cm/s}$$

$$\text{CrEX} - 3: K_h = 21.5 \text{ ft/d} = 7.58 \times 10^{-3} \text{ cm/s}$$

$$\text{CrEX} - 4: K_h = 12.5 \text{ ft/d} = 4.41 \times 10^{-3} \text{ cm/s}$$

$$\text{CrEX} - 5: K_h = 172.0 \text{ ft/d} = 6.07 \times 10^{-2} \text{ cm/s}$$

Their arithmetic average is  $53.9 \text{ ft/d}$  ( $1.90 \times 10^{-2} \text{ cm/s}$ ). These values correspond to silty sand, clean sand, and gravel (e.g., Freeze and Cherry, 1979, p. 29, Table 2.3). It can be noticed that the aquifer is more permeable around CrEX-2 ( $51.0 \text{ ft/d}$ ) and CrEX-5 ( $172.0 \text{ ft/d}$ ) extraction wells.

## **2.3 Results of the PM-2 Aquifer Test Data Analyses**

### **2.3.1 Transient Drawdown Data at the Observation Wells and PM-2 Recovery Analyses Results**

The drawdown data as well as the methods used for them are given in Attachment 3. The drawdown data for PM-4 ( $0.83 \text{ ft/d}$ ), PM-5 ( $3.34 \text{ ft/d}$ ), R-20 Screen 3 ( $2.84 \text{ ft/d}$ ), and PM-2 ( $1.20 \text{ ft/d}$ ) recovery are generally good. The values in the parentheses are the  $K_h$  values. And their average  $K_h$  value is  $2.05 \text{ ft/d}$  ( $7.23 \times 10^{-4} \text{ cm/s}$ ). The anisotropy ratio ( $K_v/K_h$ ) for PM-4, PM-5, and R-20 Screen 3 are 0.035, 0.010, 0.016, respectively. And their average is 0.020. Therefore,  $K_v = 0.041 \text{ ft/d} = 1.45 \times 10^{-5} \text{ cm/s}$ .

The storage coefficient ( $S$ ) for PM-4, PM-5, and R-20 Screen 3 are  $6.73 \times 10^{-4}$ ,  $1.31 \times 10^{-3}$ ,  $6.54 \times 10^{-3}$  respectively. And their average is  $2.84 \times 10^{-3}$ . According to the literature, storage coefficients generally vary between 0.00005 and 0.005 (e.g., Freeze and Cherry, 1979, p. 60). And the value 0.00284 is in this range.

The specific yield ( $S_y$ ) values in Table 2 are not reliable. Potential reasons may be (a) the screen intervals are significantly below the water table; (b) the aquifer is relatively less permeable; and the pump test period was not long enough.

### **2.3.2 Horizontal Hydraulic Conductivity ( $K_h$ ) Value Determined from the Steady-State Drawdown Value at the PM-2 Pumped Well**

The  $K_h$  value determined from the steady-state drawdown value of PM-2 is  $K_h = 2.60 \text{ ft/d} = 9.17 \times 10^{-4} \text{ cm/s}$  for which the calculation details are given in Appendix A of Attachment 3. This value compares favorably with the  $K_h = 1.20 \text{ ft/d} = 4.23 \times 10^{-4} \text{ cm/s}$  in Table 2 of Attachment 3 determined from the PM-2 recovery analysis. The  $K_h = 2.60 \text{ ft/d}$  steady-state drawdown value is even closer to the average  $K_h = 2.05 \text{ ft/d}$  determined from the transient drawdown data analysis.

## **2.4 Results of the PM-4 Aquifer Test Data Analyses**

### **2.4.1 Transient Drawdown Data at the Observation Wells and PM-4 Recovery Analyses Results**

The results for the transient drawdown data analyses are given in Table 2 which shows that there is a total of seven set of values determined from the Neuman (1974, 1975) method. The last line shows the  $K_h$  value determined from the steady-state drawdown value at the pumped well PM-4 using the Thiem (1906) well discharge formula under confined aquifer conditions. From the values in Table 2 Attachment 4, the conclusions drawn are given as follows:

1. Based on the Neuman method, the values of  $K_h$  vary between  $0.3 \text{ ft/d}$  and  $1.5 \text{ ft/d}$ . The average of the rest of seven values ( $1.2, 0.8, 0.3, 1.1, 1.0, 1.5,$  and  $0.7 \text{ ft/d}$ ) is  $K_{h-avg} = 0.9 \text{ ft/d}$ .
2. The last line of Table 2 includes  $K_h = 2.3 \text{ ft/d}$  value determined from the steady-state drawdown at the pumped well PM-4 using Thiem (1906) well discharge formula under confined aquifer conditions (see Section 6.2 Attachment 4 for its determination method).
3. The average of the six  $a = K_v/K_h$  values ( $0.016, 0.225, 0.012, 0.022, 0.040,$  and  $0.016$ ) is  $a_{avg} = K_{v-avg}/K_{h-avg} = 0.055$ . Therefore,  $K_{v-avg} = aK_h = 0.05 \text{ ft/d}$ .
4. The storage coefficient ( $S$ ) values range from  $2.91E - 04$  to  $7.17E - 04$ . According to the literature, storage coefficients generally vary between  $0.00005$  and  $0.005$  (e.g., Freeze and Cherry, 1979, p. 60).
5. The specific yield ( $S_y$ ) values in Table 2 are not reliable. Potential reasons may be (a) the screen intervals are significantly below the water table; (b) the aquifer is relatively less permeable; (c) the pump test period was not long enough; and (c) the observation wells are significantly far away from the pumped well ( $4,463 \text{ ft}$  to  $5,508 \text{ ft}$ ).

#### **2.4.2 Horizontal Hydraulic Conductivity ( $K_h$ ) Value Determined from the Steady-State Drawdown Value at the PM-4 Pumped Well**

The  $K_h$  value determined from the steady-state drawdown value of PM-4 is  $K_h = 2.3 \text{ ft/d}$  for which the calculation details are given in Appendix A of Attachment 4.

### **2.5 Results of the PM-3 Aquifer Test Data Analyses**

#### **2.5.1 Results of the Transient Drawdown Data Analyses**

The results for the transient drawdown data analyses are given in Table 2 which shows that there is a total of two set of values determined from the Neuman (1974, 1975) method. From the values in Table 2, the conclusions drawn are as follows:

1. Based on the Neuman method, the values corresponding to drawdown and recovery for horizontal hydraulic conductivity ( $K_h$ ) are  $5.56 \text{ ft/d}$  and  $6.19 \text{ ft/d}$ , respectively, and their average is  $5.875 \text{ ft/d}$ .
2. The corresponding values of storage coefficient ( $S$ ) to drawdown and recovery are  $0.001002$  and  $0.001032$  respectively. According to the literature, storage coefficients generally vary between  $0.00005$  and  $0.005$  (e.g., Freeze and Cherry, 1979, p. 60).
3. The anisotropy  $a = K_v/K_h$  values corresponding to drawdown and recovery are  $0.1437$  and  $0.0704$ , respectively. And their average is  $0.12205$  which is close to  $0.10$  and this value generally is being used in practice whenever  $a = K_v/K_h$  is not available.
4. The specific yield ( $S_y$ ) values in Table 2 are not realistic. Potential reasons may be (a) the screen interval of R-35a is significantly below the water table and (b) the aquifer test period was not long enough.

### **2.5.2 Results of the Steady State Drawdown Data Analysis**

For steady state drawdown data analysis at R-35a gave the following result for the horizontal hydraulic conductivity ( $K_h$ ):

$$K_h = 2.2 \text{ ft/d} = 0.000007761 \text{ m/s} = 7.76 \times 10^{-4} \text{ cm/s}.$$

For steady state drawdown data analysis at R-35b gave the following result for the horizontal hydraulic conductivity ( $K_h$ ):

$$K_h = 73.0 \text{ ft/d} = 0.000257528 \text{ m/s} = 2.58 \times 10^{-3} \text{ cm/s}.$$

### **2.6 Result of the R-13 Aquifer Test Data Analysis**

For steady state drawdown data analysis at R-13 gave the following result for the horizontal hydraulic conductivity ( $K_h$ ):

$$K_h = 25 \text{ ft/d} = 0.000088194 \text{ m/s} = 8.82 \times 10^{-3} \text{ cm/s}$$

## **ATTACHMENT 1**

**Determination of the Horizontal Hydraulic Conductivity ( $K_h$ ) Values from the Steady-State Drawdowns of the CrIN-1, CrIN-2, CrIN-3, CrIN-4, and CrIN-5 Injection Wells**

---

This page intentionally left blank.

## Executive Summary

In Attachment 1, horizontal hydraulic conductivity ( $K_h$ ) values are determined using the measured steady-state drawdowns at CrIN-1, CrIN-2, CrIN-3, CrIN-4, and CrIN-5 injection wells. The method is based on the Dupuit-Forchheimer well discharge formula along with the Sichardt empirical zone of influence radius equation to determine the values of  $K_h$  around each CrIN injection well using the data in the report of Los Alamos National Laboratory. The measured drawdown as well as other data for CrIN-1, CrIN-2, CrIN-3, CrIN-4, and CrIN-5 injection wells are taken from the report of Los Alamos National Laboratory entitled “*Well Completion Report for Chromium Plume Control Interim Measure and Plume-Center Characterization Injection Wells CrIN-1, CrIN-2, CrIN-3, CrIN-4, and CrIN-5, LA-UR-22162, EP2017-0006, 2017*”. From this report, some key information are as follows:

1. The wells were completed as single-screen wells within the uppermost portion of the regional aquifer. The screened intervals are all within Puye Formation sediments.
2. CrIN-1, CrIN-2, CrIN-3, and CrIN-4 injection wells were designed with nominal 50-ft screened intervals to hydraulically manipulate chromium-contaminated groundwater near the top of the regional aquifer within the Puye Formation.
3. CrIN-1 and CrIN-2 were designed as vertical wells.
4. CrIN-3 and CrIN-4 were designed with 17-degree and 11-degree angles from vertical, respectively.
5. CrIN-5 was designed with a 60-ft screen to yield an effective vertical submergence of 54 ft because of its 25-degree angle.
6. All CrIN wells were constructed of 8.0-in.-I.D./8.63-in.-O.D.

The resulted horizontal hydraulic conductivity ( $K_h$ ) values for the 5 CrIN wells are as follows:

$$\text{CrIN} - 1: K_h = 26 \text{ ft/d} = 9.17 \times 10^{-3} \text{ cm/s}$$

$$\text{CrIN} - 2: K_h = 37 \text{ ft/d} = 1.31 \times 10^{-2} \text{ cm/s}$$

$$\text{CrIN} - 3: K_h = 38 \text{ ft/d} = 1.34 \times 10^{-2} \text{ cm/s}$$

$$\text{CrIN} - 4: K_h = 60 \text{ ft/d} = 2.11 \times 10^{-2} \text{ cm/s}$$

$$\text{CrIN} - 5: K_h = 72 \text{ ft/d} = 2.54 \times 10^{-2} \text{ cm/s}$$

Their arithmetic average is 47 ft/d ( $1.66 \times 10^{-2}$  cm/s). These values correspond to silty sand, clean sand and gravel (e.g., Freeze and Cherry, 1979, p. 29, Table 2.3). These wells are approximately along a line which is perpendicular to the main flow direction which is towards the southeast direction. It can be noticed that the aquifer is more permeable around CrIN-4 and CrIN-5 injection wells (60 ft/d and 72 ft/d). Also, these values indicate that the  $K_h$  values at



CrIN-1, CrIN-2, and CrIN-3 (26 *ft/d*, 37 *ft/d*, and 38 *ft/d*) are about 50% of the previous two values.

In Figure 6, based on the Dupuit assumptions, the approximate form of the cone is also shown. In reality, the intersection of the cone of depression with the well edge ( $h_s$ ) is higher than  $h_w$  and the Dupuit-Forchheimer well discharge formula is based on the Dupuit assumptions, namely  $h_s = h_w$ . For  $(h_s - h_w)$ , an approximate expression is given by Boulton (1951), which is given by Eq. (A-11) in Appendix A. The  $(h_s - h_w)/h_w$  ratio is determined for each well and they are 0.13 (CrIN-1), 0.06 (CrIN-2), 0.06 (CrIN-3), 0.03 (CRIN-4), and 0.03 (CrIN-5). Therefore, assuming  $h_s = h_w$  does not generate significant errors in determining the  $K_h$  values.

# Attachment 1 Contents

1.	Purpose.....	1
2.	CrIN Injection Wells and Steady-State Drawdown Data .....	1
2.1	Data for the CrIN Injection Wells .....	1
2.2	CrIN-1 Injection Well Data.....	2
2.3	CrIN-2 Injection Well Data.....	2
2.4	CrIN-3 Injection Well Data.....	3
2.5	CrIN-4 Injection Well Data.....	4
2.6	CrIN-5 Injection Well Data.....	5
3.	Method for Determining Horizontal Hydraulic Conductivity With Steady State Drawdown at the Extraction Well .....	6
4.	Results for the Horizontal Hydraulic Conductivity Values .....	6

## Figures

- Figure 1 Measured drawdowns at CrIN-1 injection well.
- Figure 2 Measured drawdowns at CrIN-2 injection well.
- Figure 3 Measured drawdowns at CrIN-3 injection well.
- Figure 4 Measured drawdowns at CrIN-4 injection well.
- Figure 5 Measured drawdowns at CrIN-5 injection well.
- Figure 6 Well in an unconfined aquifer.

## Tables

- Table 1. Determined horizontal hydraulic conductivity ( $K_h$ ) values using the drawdown data at the CrIN injection wells.

## Appendices

- Appendix A Dupuit-Forchheimer Well Discharge Formula and Determination Method of Horizontal Hydraulic Conductivity
- Appendix B Determination Of Horizontal Hydraulic Conductivity Using Dupuit-Forchheimer Well Discharge Formula for the CrIN-1, CrIN-2, CrIN-3, CrIN-4, and CrIN-5 Steady State Drawdown Values

## 1. Purpose

The purpose of this report is to determine horizontal hydraulic conductivity ( $K_h$ ) values using the measured steady-state drawdowns at CrIN-1, CrIN-2, CrIN-3, CrIN-4, and CrIN-5 injection wells. The method is based on the *Dupuit-Forchheimer well discharge formula* along with the *Sichardt empirical zone of influence radius* to determine the values of  $K_h$  around each CrIN injection well using the data in the report of Los Alamos National Laboratory (2017).

## 2. CrIN Injection Wells and Steady-State Drawdown Data

### 2.1 Data for the CrIN Injection Wells

In the analyses, the measured drawdown data at CrIN-1, CrIN-2, CrIN-3, CrIN-4, and CrIN-5 injection wells included in the report of Los Alamos National Laboratory entitled "*Well Completion Report for Chromium Plume Control Interim Measure and Plume-Center Characterization Injection Wells CrIN-1, CrIN-2, CrIN-3, CrIN-4, and CrIN-5, LA-UR-22162, EP2017-0006, 2017, pp. 37-58*" are used to determine horizontal hydraulic conductivity ( $K_h$ ) values. The report (p. 7) states that following development, the wells underwent aquifer testing consisting of step drawdown tests and 24-h constant rate tests. Constant rate pumping was followed by a 24-h recovery period. Table 8.2-1 (pp. 37-58) of the report presents a summary of testing dates and pumping rates. From the report, some key data and information are given below:

The wells were completed as single-screen wells within the uppermost portion of the regional aquifer. The screened intervals are all within Puye Formation sediments (Executive Summary, p. v).

From this report, some key information are as follows:

1. The wells were completed as single-screen wells within the uppermost portion of the regional aquifer. The screened intervals are all within Puye Formation sediments.
2. CrIN-1, CrIN-2, CrIN-3, and CrIN-4 injection wells were designed with nominal 50-ft screened intervals to hydraulically manipulate chromium-contaminated groundwater near the top of the regional aquifer within the Puye Formation.
3. CrIN-1 and CrIN-2 were designed as vertical wells.
4. CrIN-3 and CrIN-4 were designed with 17-degree and 11-degree angles from vertical, respectively.
5. CrIN-5 was designed with a 60-ft screen to yield an effective vertical submergence of 54 ft because of its 25-degree angle.
6. All CrIN wells were constructed of 8.0-in.-I.D./8.63-in.-O.D.

## 2.2 CrIN-1 Injection Well Data

The CrIN-1 injection well water levels (LANL, 2017, p. 5):

*Depth to water in the completed well on June 21, 2016 = 879.0 ft*

*Depth to water in the completed well on July 17, 2016 = 871.4 ft*

The CrIN-1 injection well data are (LANL, 2017, p. 18, Figure 7.2-1):

*Depth of top of screen interval = 883.9 ft*

*Depth of bottom of screen interval = 933.9 ft*

From these data,

$$\text{Screen interval} = L = 933.9 \text{ ft} - 883.9 \text{ ft} = 50 \text{ ft} = 15.24 \text{ m}$$

From Figure 1, the steady-state average drawdown is

$$s_{w-CrIN-1} = 12.0 \text{ ft} = 3.6576 \text{ m}$$

Then,

$$H_{0-CrIN-1} = 933.9 \text{ ft} - 879.0 \text{ ft} = 54.9 \text{ ft} = 16.73 \text{ m}$$

$$h_{w-CrIN-1} = H_{0-CrIN-1} - s_{w-CrIN-1} = 54.9 \text{ ft} - 12.0 \text{ ft} = 42.9 \text{ ft} = 13.08 \text{ m}$$

With

$$1 \text{ gpm} = 0.0000630902 \frac{\text{m}^3}{\text{s}}$$

the extraction rate of CrIN-1 is

$$Q_{CrIN-1} = 70 \text{ gpm} = 70 \frac{\text{gallon}}{\text{day}} = (70 \text{ gpm}) \left( \frac{0.0000630902 \frac{\text{m}^3}{\text{s}}}{\text{gpm}} \right) = 0.004416 \frac{\text{m}^3}{\text{s}}$$

## 2.3 CrIN-2 Injection Well Data

The CrIN-2 injection well water levels (LANL, 2017, p. 5):

*Depth to water in the completed well on May 10, 2016 = 899.0 ft*

*Depth to water in the completed well on May 27, 2016 = 899.1 ft*

The CrIN-2 injection well data are (LANL, 2017, p. 19, Figure 7.2-2):

*Depth of top of screen interval = 902.5 ft*

*Depth of bottom of screen interval = 952.5 ft*

From these data,

*Screen interval = L = 952.5 ft – 902.5 ft = 50 ft = 15.24 m*

From Figure 2, the steady-state average drawdown is

*s<sub>w-CrIN-2</sub> = 6.4 ft = 1.95072 m*

Then,

*H<sub>0-CrIN-2</sub> = 952.5 ft – 899.1 ft = 59.4 ft = 16.28 m*

*h<sub>w-CrIN-2</sub> = H<sub>0-CrIN-2</sub> – s<sub>w-CrIN-2</sub> = 53.4 ft – 6.4 ft = 47.0 ft = 14.33 m*

With

*1 gpm = 0.0000630902  $\frac{m^3}{s}$*

the extraction rate of CrIN-2 is

$$Q_{CrIN-2} = 58 \text{ gpm} = 58 \frac{\text{gallon}}{\text{day}} = (58 \text{ gpm}) \left( \frac{0.0000630902 \frac{m^3}{s}}{\text{gpm}} \right) = 0.00365922 \frac{m^3}{s}$$

## **2.4 CrIN-3 Injection Well Data**

The CrIN-3 injection well water levels (LANL, 2017, p. 5):

*Water level (linear) below the top of drill casing on August 17, 2016 before installation = 924.0 ft*

*Depth to water (linear) below the top of drill casing on September 7, 20016 = 928.8 ft*

The CrIN-3 injection well data are (LANL, 2017, p. 20, Figure 7.2-3):

*Well angle from vertical = 17°*

*Depth of top of screen interval (linear) below top of drill casing = 930.4 ft*

*Depth of bottom of screen interval (linear) below top of drill casing = 980.4 ft*

From these data,

$$\text{Vertical screen interval} = L = (980.4 \text{ ft} - 930.4 \text{ ft}) \cos (17^\circ) = 47.82 \text{ ft} = 14.57 \text{ m}$$

From Figure 3, the steady-state average drawdown is

$$s_{w-CrIN-3} = 6.5 \text{ ft} = 1.9812 \text{ m}$$

Then,

$$H_{0-CrIN-3} = (980.4 \text{ ft} - 928.8 \text{ ft}) \cos (17^\circ) = 48.92 \text{ ft} = 14.91 \text{ m}$$

$$h_{w-CrIN-3} = H_{0-CrIN-3} - s_{w-CrIN-3} = 49.35 \text{ ft} - 6.5 \text{ ft} = 42.85 \text{ ft} = 13.06 \text{ m}$$

With

$$1 \text{ gpm} = 0.0000630902 \frac{\text{m}^3}{\text{s}}$$

the extraction rate of CrIN-3 is

$$Q_{CrIN-3} = 58 \text{ gpm} = 58 \frac{\text{gallon}}{\text{day}} = (58 \text{ gpm}) \left( \frac{0.0000630902 \frac{\text{m}^3}{\text{s}}}{\text{gpm}} \right) = 0.00365922 \frac{\text{m}^3}{\text{s}}$$

## 2.5 CrIN-4 Injection Well Data

The CrIN-4 injection well water levels (LANL, 2017, p. 5):

*Water level (linear) below the top of drill casing on May 11, 2016 before installation = 1,078.1 ft*

*Depth to water (linear) below the top of drill casing on June 15, 2016 = 1,059.1 ft*

The CrIN-4 injection well data are (LANL, 2017, p. 21, Figure 7.2-4):

*Well angle from vertical = 11°*

*Depth of top of screen interval (linear) below top of drill casing = 1,083.0 ft*

*Depth of bottom of screen interval (linear) below top of drill casing = 1,133.0 ft*

From these data,

$$\text{Vertical screen interval} = L = (1,133.0 \text{ ft} - 1,083.0 \text{ ft}) \cos (11^\circ) = 49.08 \text{ ft} = 14.96 \text{ m}$$

From Figure 4, the steady-state average drawdown is

$$s_{w-CrIN-4} = 3.9 \text{ ft} = 1.18872 \text{ m}$$

Then,

$$H_{0-CrIN-4} = (1,133.0 \text{ ft} - 1,078.1 \text{ ft}) \cos(11^\circ) = 53.89 \text{ ft} = 16.43 \text{ m}$$

$$h_{w-CrIN-4} = H_{0-CrIN-4} - s_{w-CrIN-4} = 53.89 \text{ ft} - 3.9 \text{ ft} = 49.99 \text{ ft} = 15.24 \text{ m}$$

With

$$1 \text{ gpm} = 0.0000630902 \frac{\text{m}^3}{\text{s}}$$

the extraction rate of CrIN-4 is

$$Q_{CrIN-4} = 62 \text{ gpm} = 62 \frac{\text{gallon}}{\text{day}} = (62 \text{ gpm}) \left( \frac{0.0000630902 \frac{\text{m}^3}{\text{s}}}{\text{gpm}} \right) = 0.00391158 \frac{\text{m}^3}{\text{s}}$$

## 2.6 CrIN-5 Injection Well Data

The CrIN-5 injection well water levels (LANL, 2017, p. 5):

*Water level (linear) below the top of drill casing on July 1, 2016 before installation = 1,156.8 ft*

*Depth to water (linear) below the top of drill casing on July 30, 2016 = 1,159.1 ft*

The CrIN-5 injection well data are (LANL, 2017, p. 22, Figure 7.2-5):

*Well angle from vertical = 25°*

*Depth of top of screen interval (linear) below top of drill casing = 1,162.0 ft*

*Depth of bottom of screen interval (linear) below top of drill casing = 1,222.0 ft*

From these data,

$$\text{Vertical screen interval} = L = (1,222 \text{ ft} - 1,162 \text{ ft}) \cos(25^\circ) = 54.38 \text{ ft} = 16.58 \text{ m}$$

From Figure 5, the steady-state average drawdown is

$$s_{w-CrIN-5} = 2.75 \text{ ft} = 0.8382 \text{ m}$$

Then,

$$H_{0-CrIN-5} = (1,222.0 \text{ ft} - 1,156.8 \text{ ft}) \cos(25^\circ) = 59.09 \text{ ft} = 18.01 \text{ m}$$

$$h_{w-CrIN-5} = H_{0-CrIN-5} - s_{w-CrIN-5} = 59.09 \text{ ft} - 2.75 \text{ ft} = 56.34 \text{ ft} = 17.17 \text{ m}$$

With

$$1 \text{ gpm} = 0.0000630902 \frac{\text{m}^3}{\text{s}}$$

the extraction rate of CrIN-5 is

$$Q_{\text{CrIN-5}} = 62 \text{ gpm} = 62 \frac{\text{gallon}}{\text{day}} = (62 \text{ gpm}) \left( \frac{0.0000630902 \frac{\text{m}^3}{\text{s}}}{\text{gpm}} \right) = 0.00391158 \frac{\text{m}^3}{\text{s}}$$

### 3. Method for Determining Horizontal Hydraulic Conductivity With Steady State Drawdown at the Extraction Well

In order to determine the value of horizontal hydraulic conductivity ( $K_h$ ) with steady-state drawdown at a well, the *Dupuit-Forchheimer well discharge formula* along with empirical zone of influence radius can be used. The geometry of the Dupuit-Forchheimer solution for an unconfined aquifer under steady-state flow conditions is given in Figure 6, which shows the radial flow to a well fully penetrating a homogeneous and isotropic unconfined aquifer. The initial aquifer thickness is  $H_0$  and the aquifer has infinite extent. Its horizontal hydraulic conductivity is  $K_h$ . The constant extraction rate of the well is  $Q_w$ . Details of the method are given in Appendix A.

### 4. Results for the Horizontal Hydraulic Conductivity Values

Using the method described in Section 3, the resulted horizontal hydraulic conductivity ( $K_h$ ) values for the 5 CrIN wells are as follows:

$$\text{CrIN} - 1: K_h = 26 \text{ ft/d} = 9.17 \times 10^{-3} \text{ cm/s}$$

$$\text{CrIN} - 2: K_h = 37 \text{ ft/d} = 1.31 \times 10^{-2} \text{ cm/s}$$

$$\text{CrIN} - 3: K_h = 38 \text{ ft/d} = 1.34 \times 10^{-2} \text{ cm/s}$$

$$\text{CrIN} - 4: K_h = 60 \text{ ft/d} = 2.11 \times 10^{-2} \text{ cm/s}$$

$$\text{CrIN} - 5: K_h = 72 \text{ ft/d} = 2.54 \times 10^{-2} \text{ cm/s}$$

Their arithmetic average is  $47 \text{ ft/d}$  ( $1.66 \times 10^{-2} \text{ cm/s}$ ). These values correspond to silty sand, clean sand and gravel (e.g., Freeze and Cherry, 1979, p. 29, Table 2.3). These wells are approximately along a line which is perpendicular to the main flow direction which is towards the southeast direction. It can be noticed that the aquifer is more permeable around CrIN-4 and CrIN-5 injection wells ( $60 \text{ ft/d}$  and  $72 \text{ ft/d}$ ). Also, these values indicate that the  $K_h$  values at CrIN-1, CrIN-2, and CrIN-3 ( $26 \text{ ft/d}$ ,  $37 \text{ ft/d}$ , and  $38 \text{ ft/d}$ ) are about 50% of the previous two values.



In Figure 6, based on the Dupuit assumptions, the approximate form of the cone is also shown. In reality, the intersection of the cone of depression with the well edge ( $h_s$ ) is higher than  $h_w$  and the Dupuit-Forchheimer well discharge formula is based on the Dupuit assumptions, namely  $h_s = h_w$ . For  $(h_s - h_w)$ , an approximate expression is given by Boulton (1951), which is given by Eq. (A-11) in Appendix A. The  $(h_s - h_w)/h_w$  ratio is determined for each well and they are 0.13 (CrIN-1), 0.06 (CrIN-2), 0.06 (CrIN-3), 0.03 (CrIN-4), and 0.03 (CrIN-5). Therefore, assuming  $h_s = h_w$  does not generate significant errors in determining the  $K_h$  values.

## References

- Batu, V., *Fluid Mechanics and Hydraulics: Illustrative Worked Examples of Surface and Subsurface Flows*, Taylor & Francis CRC Press, Boca Raton, Florida, 1240 pp., 2024.
- Bear, J., *Hydraulics of Groundwater*, McGraw-Hill Book Company, New York, 569 pp., 1979.
- Boulton, N.S., "The Flow Pattern Near a Gravity Well in a Uniform Water Bearing Unit, *Journal of the Institutions of Civil Engineers* (London), Vol. 36, pp. 534-550, 1951.
- Chertousov, M.D., *Hydraulics* (in Russian), Gosenergouzdat, 630 pp., Moscow, Russia, 1962.
- De Filippi, F.M., S. Iacurto, F. Ferranti, and G. Sappa, "Hydraulic Conductivity Estimation Using Low-Flow Purging Data Elaboration in Contaminated Sites," *Water*, Vol. 12, pp. 898-914, 2020.
- Dupuit, J., *Études Théoriques et Pratiques sur le Mouvement des Eaux*, Second edition, Paris, France, 304 pp., 1863.
- Forchheimer, P., "Über die Ergiebigkeit von Brunnen-Anlagen und Sickerschlitzten Zeitschrift," *Der Architekten-und Ingenieur-Verein*, Vol. 32, p. 539, Hannover, Germany, 1886.
- Freeze, R.A., And J.A. Cherry, *Groundwater*, Prentice-Hall, Inc., Englewood Cliffs, New Jersey, 604, pp., 1979.
- Los Alamos National Laboratory, "Well Completion Report for Chromium Plume Control Interim Measure and Plume-Center Characterization Injection Wells CrIN-1, CrIN-2, CrIN-3, CrIN-4, and CrIN-5," LA-UR-22162, EP2017-0006, 2017.

## Figures

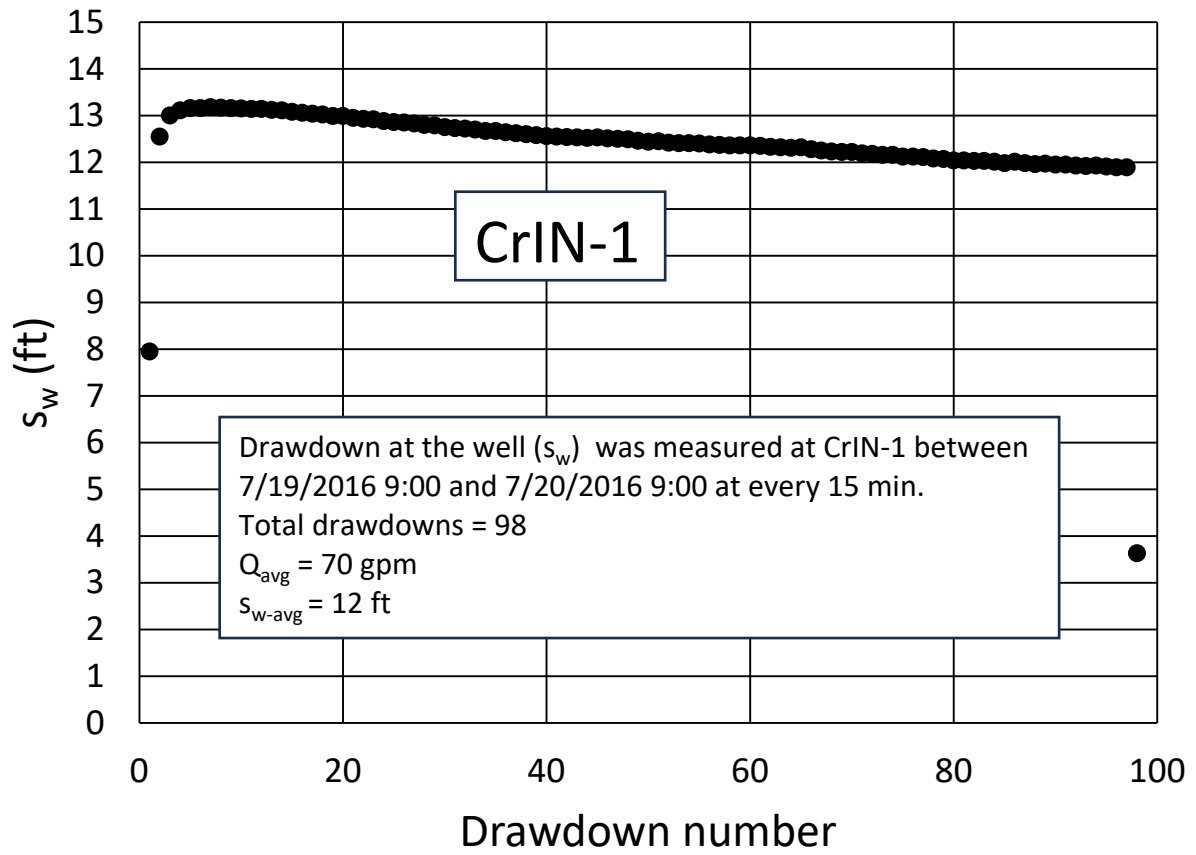


Figure 1. Measured drawdowns at CrIN-1 injection well.

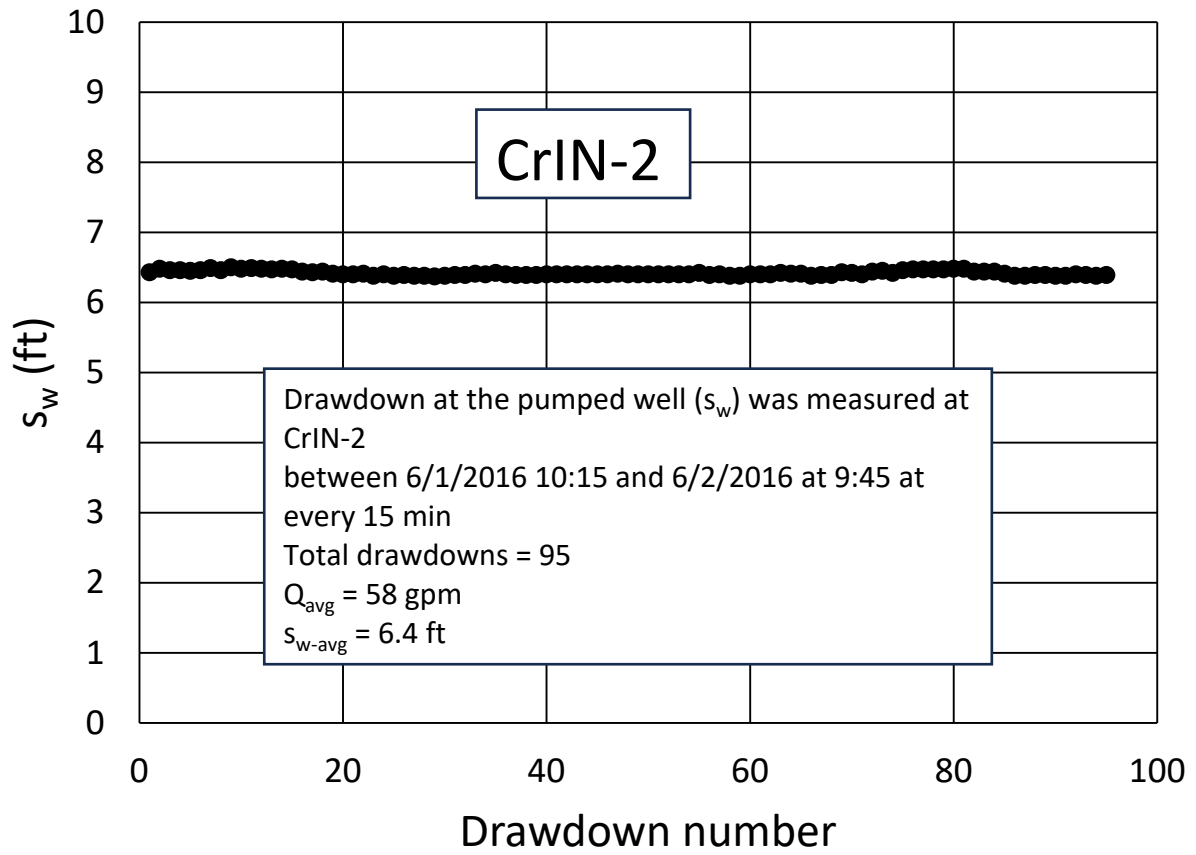


Figure 2. Measured drawdowns at CrIN-2 injection well.

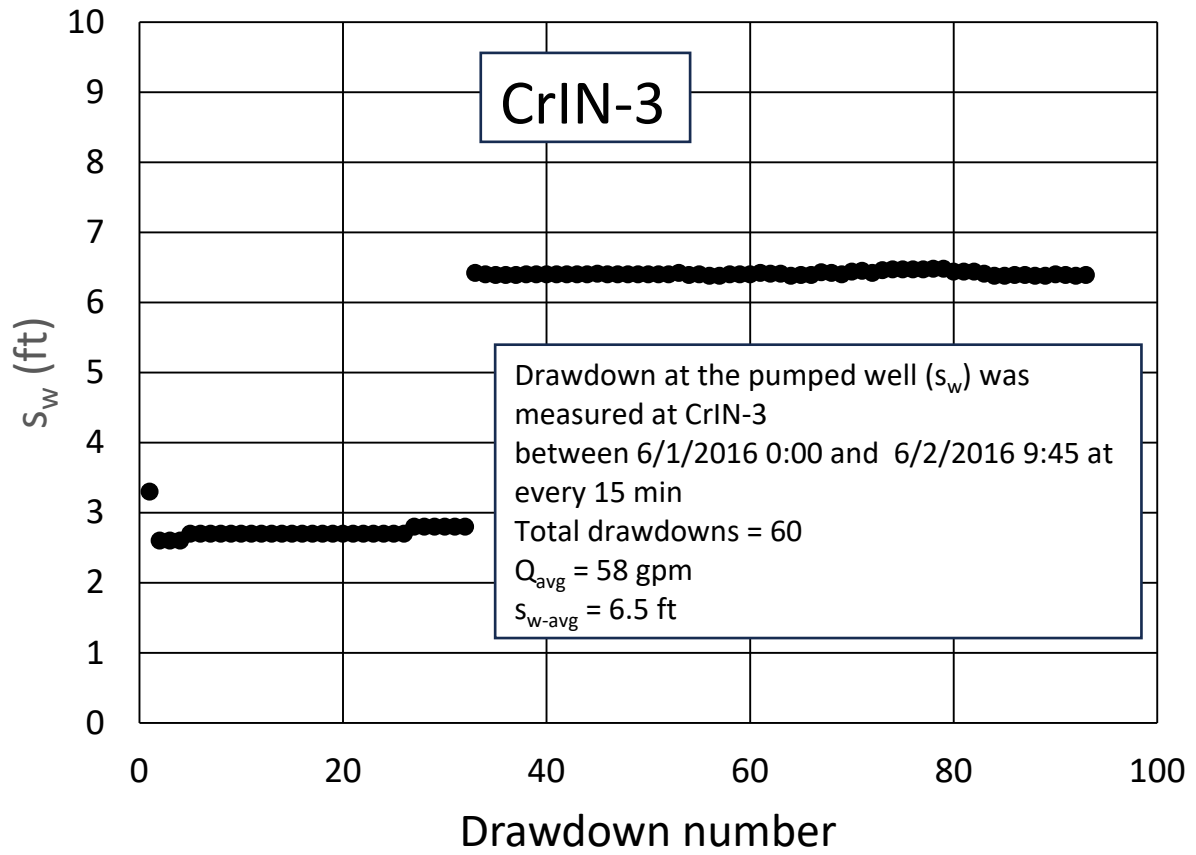


Figure 3. Measured drawdowns at CrIN-3 injection well.

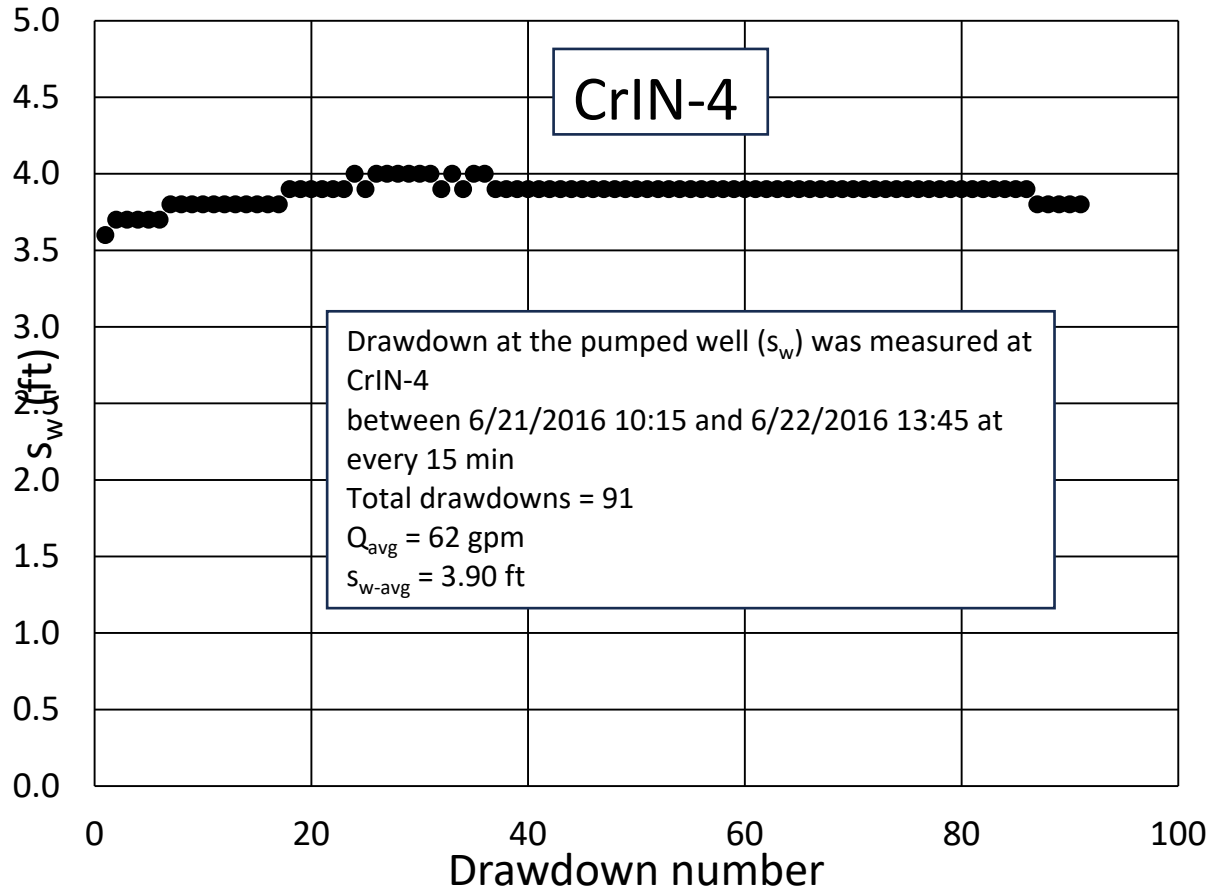


Figure 4. Measured drawdowns at CrIN-4 injection well.

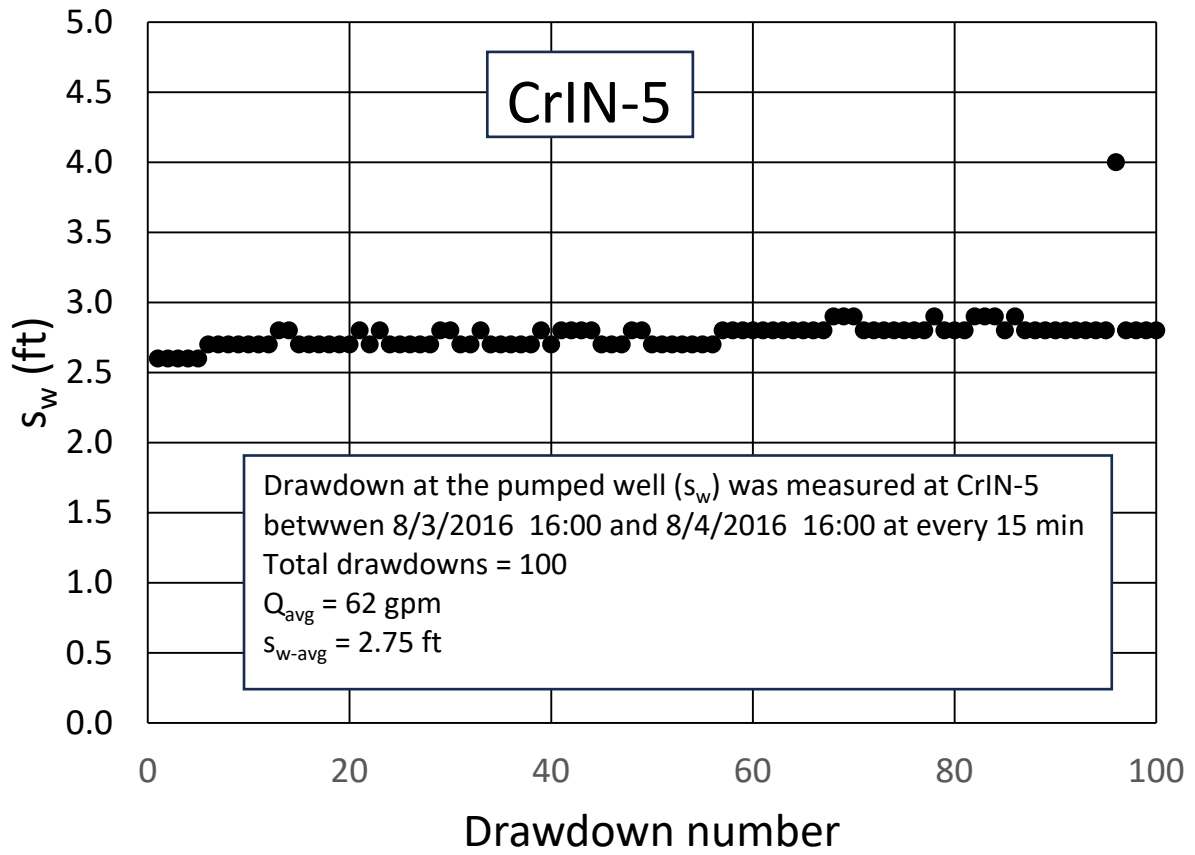


Figure 5. Measured drawdowns at CrIN-5 injection well.

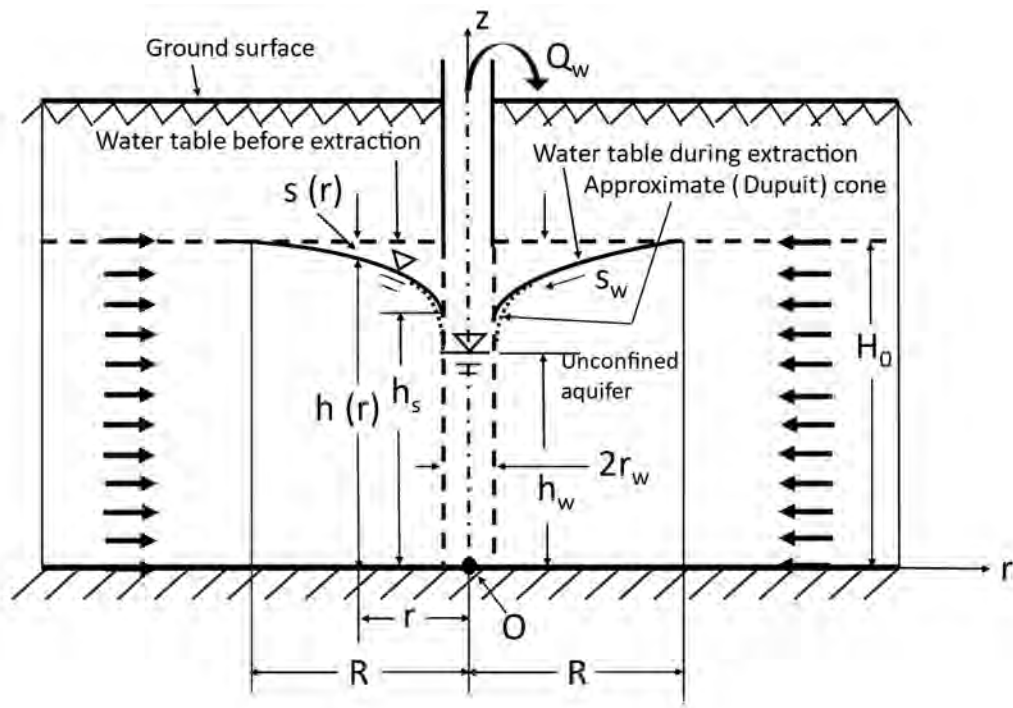


Figure 6. Well in an unconfined aquifer.



## Tables

Table 1. Determined horizontal hydraulic conductivity ( $K_h$ ) values using the drawdown data at the CrIN injection wells.

Well ID	$K_h$	
	ft/d	cm/s
CrIN-1	26	$9.17 \times 10^{-3}$
CrIN-2	37	$1.31 \times 10^{-2}$
CrIN-3	38	$1.34 \times 10^{-2}$
CrIN-4	60	$2.11 \times 10^{-2}$
CrIN-5	72	$2.54 \times 10^{-2}$
<b>Average</b>	<b>47</b>	<b><math>1.64 \times 10^{-2}</math></b>

## **Appendices**

## APPENDIX A: DUPUIT-FORCHHEIMER WELL DISCHARGE FORMULA AND DETERMINATION METHOD OF HORIZONTAL HYDRAULIC CONDUCTIVITY

### A.1 DUPUI-FORCHHEIMER SOLUTION FOR UNCONFINED AQUIFERS

#### A.1.1 Problem Definition

The Dupuit-Forchheimer solution for a well in an unconfined aquifer was derived by Dupuit (1863) and Forchheimer (1886) without being ware of each other. And that it is why it is called *Dupuit-Forchheimer well discharge formula* in aquifer hydraulics.

The geometry of the Dupuit-Forchheimer well discharge formula for an unconfined aquifer under steady state flow conditions is given in Figure 6, which shows that the radial flow to a well fully penetrates a homogeneous and isotropic unconfined aquifer. The initial aquifer thickness is  $H_0$  and the aquifer is assumed to have infinite extent. Its horizontal hydraulic conductivity is  $K_h$ . The constant extraction rate of the well is  $Q_w$ . Under extraction conditions, a cone of depression is formed and the drawdown at  $r$  distance is

$$s(r) = H_0 - h(r) \quad (\text{A-1})$$

$h(r)$  is the aquifer thickness at distance  $r$ . In Figure 6,  $R$  is the radius of influence beyond which the drawdown is zero. The drawdown at the well is  $s_w$  and the water elevation at the well is  $h_w$  which is based on the Dupuit assumptions (Dupuit, 1864). In Figure 6, based on the Dupuit assumptions, the approximate form of the cone is also shown. In reality, the intersection of the cone of depression with the well edge ( $h_s$ ) is higher than  $h_w$  and an expression for  $(h_s - h_w)$  will be given in Section A.2.

#### A.1.2 Drawdown Solution at the Well

The solution for drawdown at the well was determined by Dupuit (1863) and Forchheimer (1896) and is given as [e.g., Bear 1979, p. 310, Eq. (8-23); Batu, 2024, p. 1095, Eq. (29-258)]

$$H_0^2 - h_w^2 = \frac{Q_w}{\pi K_h} \quad (\text{A-2})$$

which is exactly the same as included in some books [e.g., Bear, 1979, p. 310, Eq. (8-23); Batu, 2024, p. 1095, Eq. (29-258)] with the exception of notation.

From Figure 6, the drawdown at the well is

$$s_w = H_0 - h_w \quad (\text{A-3})$$

Eq. (A-1) can also be written as

$$(H_0 - h_w)(H_0 + h_w) = \frac{Q_w}{\pi K_h} \ln \left( \frac{R}{r_w} \right) \quad (\text{A-4})$$

And with Eq. (A-3) and solving it for  $s_w$ , the drawdown at the well can be determined as

$$s_w = \frac{Q_w}{\pi K_h (H_0 + h_w)} \ln \left( \frac{R}{r_w} \right) \quad (\text{A-5})$$

### A.1.3 Radius of Influence

The radius of influence  $R$  is the distance from the well where drawdown is zero. Since the 1880s, many attempts have been made to relate it to well, aquifer, and flow parameters in both steady and unsteady flow conditions in confined and unconfined aquifers. Some semi-empirical formulas are given in Bear (1979, p. 306). Of these formulas, the one developed by Sichardt is given in Bear [1979, p. 306, Eq. (8-11) as presented in Chertousov (1962)] is widely being used [e.g., De Filippi et al., 2020; Batu, 2024, p. 1088, Eq. (29-249)]:

$$R = 3000 s_w K_h^{\frac{1}{2}} \quad (\text{A-6})$$

in which  $R$  and  $s_w$  are in meters (m), and  $K_h$  in meters per second (m/s).

### A.1.4 Estimation Method of the Horizontal Hydraulic Conductivity

The estimation method is described in Batu (2024, pp. 1097-1099). Substitution of Eq. (A-6) into Eq. (A-5) and solving for  $K_h$ ,

$$K_h = \frac{Q_w}{\pi s_w (H_0 + h_w)} \ln \left( \frac{3000 s_w K_h^{\frac{1}{2}}}{r_w} \right) \quad (\text{A-7})$$

And after some manipulations,

$$K_h = m \left[ \ln(3000) + \frac{1}{2} \ln(K_h) + \ln \left( \frac{s_w}{r_w} \right) \right] \quad (\text{A-8})$$

in which

$$m = \frac{Q_w}{\pi s_w (H_0 + h_w)} \quad (\text{A-9})$$

Eq. (A-8) can also be written as

$$K_h - m \frac{1}{2} \ln(K_h) = m \left[ \ln(3000) + \ln \left( \frac{s_w}{r_w} \right) \right] \quad (\text{A-10})$$

In Eq. (A-10), with the known values of  $Q_w$ ,  $s_w$ ,  $H_0$ ,  $h_w$ , and  $r_w$ , the value of  $K_h$  can be determined with the trial-and-error method. Since the units for Eq. (A-6) for  $R$  are in the metric system, calculations will be made using metric units. Further details for the method can be found in a recent book Batu (2024, pp. 1090-1099).

## A.2 AN APPROXIMATE EXPRESSION FOR $(h_s - h_w)$

Boulton (1951) suggests the relationship

$$h_s - h_w \approx (H_0 - h_w) - 3.75 \frac{Q_w}{2\pi K_h H_0} \quad (\text{A-11})$$

where 3.75 is replaced by 3.5 if  $r_w/H_0$  is of the order 0.25. Eq. (A-11) is also included in Bear [1979, p. 310, Eq. (8-21)].

**APPENDIX B: DETERMINATION OF HORIZONTAL HYDRAULIC CONDUCTIVITY USING DUPUIT-FORCHHEIMER WELL DISCHARGE FORMULA FOR THE CrIN-1, CrIN-2, CrIN-3, CrIN-4, AND CrIN-5 STEADY STATE DRAWDOWN VALUES**

In this appendix, calculation details of the horizontal hydraulic conductivity determination are presented.

**B.1 DETERMINATION OF HORIZONTAL HYDRAULIC CONDUCTIVITY FROM CrIN-1 DATA**

**B.1.1 Input Data Summary**

From Section 2.2 , the input data for CrIN-1 are as follows:

$$s_{w-CrIN-1} = 12.0 \text{ ft} = 3.6576 \text{ m}$$

$$H_{0-CrIN-1} = 933.9 \text{ ft} - 879.0 \text{ ft} = 54.9 \text{ ft} = 16.73 \text{ m}$$

$$h_{w-CrIN-1} = H_{0-CrIN-1} - s_{w-CrIN-1} = 54.9 \text{ ft} - 12.0 \text{ ft} = 42.9 \text{ ft} = 13.08 \text{ m}$$

The radius of the well is

$$r_w = 4 \text{ in} = 0.1016 \text{ m}$$

With

$$1 \text{ gpm} = 0.0000630902 \frac{\text{m}^3}{\text{s}}$$

the extraction rate of CrIN-1 is

$$Q_{CrIN-1} = 70 \text{ gpm} = 70 \frac{\text{gallon}}{\text{day}} = (70 \text{ gpm}) \left( \frac{0.0000630902 \frac{\text{m}^3}{\text{s}}}{\text{gpm}} \right) = 0.004416 \frac{\text{m}^3}{\text{s}}$$

**B.1.2 Horizontal Hydraulic Conductivity Determination**

The horizontal hydraulic conductivity ( $K_h$ ) will be determined with the trial-and-error method.

From Eq. (A-9),

$$m_{CrIN-1} = \frac{Q_{CrIN-1}}{\pi s_{w-CrIN-1} (H_{0-CrIN-1} + h_{w-CrIN-1})} = \frac{0.004416 \frac{\text{m}^3}{\text{s}}}{\pi (3.6576 \text{ m}) (16.73 \text{ m} + 13.08 \text{ m})} = 0.000012892 \frac{\text{m}}{\text{s}}$$

From Eq. (A-10),

$$K_h - m_{CrIN-1} \frac{1}{2} \ln(K_h) = m_{CrIN-1} [\ln(3,000) + \ln\left(\frac{s_{w-CrIN-1}}{r_w}\right)]$$

$$\text{Trial 1: } K_h = 20 \frac{ft}{d} = 0.000070566 \frac{m}{s}$$

$$0.000070566 - (0.000012892) \frac{1}{2} \ln(0.000070566)$$

$$= (0.000012892) [8.006368 + \ln\left(\frac{3.6576 \text{ m}}{0.1016 \text{ m}}\right)]$$

$$0.000132184 \neq 0.000149417$$

$$\text{Trial 2: } K_h = 30 \frac{ft}{d} = 0.000105833 \frac{m}{s}$$

$$0.000105833 - (0.000012892) \frac{1}{2} \ln(0.000105833)$$

$$= 0.000149417$$

$$0.000164837 \neq 0.000149417$$

$$\text{Trial 3: } K_h = 27 \frac{ft}{d} = 0.000098778 \frac{m}{s}$$

$$0.00009525 - (0.000012892) \frac{1}{2} \ln(0.00009525)$$

$$= 0.000149417$$

$$0.000154934 \neq 0.000149417$$

$$\text{Trial 4: } K_h = 26 \frac{ft}{d} = 0.000091722 \frac{m}{s}$$

$$0.000091722 - (0.000012892) \frac{1}{2} \ln(0.000091722)$$

$$= 0.000149417$$

$$0.000151649 \neq 0.000149417$$

Therefore,

$$K_h = 26 \frac{ft}{d} = 0.000091722 \frac{m}{s} = 0.0091722 \frac{cm}{s} = 9.17 \times 10^{-3} \frac{cm}{s}$$

### **B.1.3 Determination of $h_s - h_w$**

From Section 2.2, the input data for CrIN-1 are as follows:

$$H_{0-CrIN-1} = 933.9 \text{ ft} - 879.0 \text{ ft} = 54.9 \text{ ft} = 16.73 \text{ m}$$

$$h_{w-CrIN-1} = H_{0-CrIN-1} - s_{w-CrIN-1} = 54.9 \text{ ft} - 12.0 \text{ ft} = 42.9 \text{ ft} = 13.08 \text{ m}$$



$$Q_{CrIN-1} = 70 \text{ gpm} = 70 \frac{\text{gallon}}{\text{day}} = (70 \text{ gpm}) \left( \frac{0.0000630902 \frac{\text{m}^3}{\text{s}}}{\text{gpm}} \right) = 0.004416 \frac{\text{m}^3}{\text{s}}$$

$$\frac{r_w}{H_0} = \frac{0.1016 \text{ m}}{16.73 \text{ m}} = 0.0061 < 0.25$$

With these values, Eq. (A-11) gives

$$h_s - h_w \approx (H_0 - h_w) - 3.75 \frac{Q_w}{2\pi K_h H_0}$$

$$h_s - h_w \approx (16.73 \text{ m} - 13.08 \text{ m}) - 3.75 \frac{0.004416 \frac{\text{m}^3}{\text{s}}}{2\pi(0.000091722 \frac{\text{m}}{\text{s}})(16.73 \text{ m})} = 1.93 \text{ m}$$

$$h_s = h_w + 1.93 \text{ m} = 13.08 \text{ m} + 1.93 \text{ m} = 15.01 \text{ m}$$

$$\frac{h_s - h_w}{h_s} = \frac{1.93 \text{ m}}{15.01 \text{ m}} = 0.13$$

## B.2 DETERMINATION OF HORIZONTAL HYDRAULIC CONDUCTIVITY FROM CrIN-2 DATA

### B.2.1 Input Data Summary

From Section 2.3, the input data for CrIN-2 are as follows:

$$s_{w-CrIN-2} = 6.4 \text{ ft} = 1.95072 \text{ m}$$

$$H_{0-CrIN-2} = 952.5 \text{ ft} - 899.1 \text{ ft} = 53.4 \text{ ft} = 16.28 \text{ m}$$

$$h_{w-CrIN-2} = H_{0-CrIN-2} - s_{w-CrIN-2} = 53.4 \text{ ft} - 6.4 \text{ ft} = 47.0 \text{ ft} = 14.33 \text{ m}$$

The radius of the well is

$$r_w = 4 \text{ in} = 0.1016 \text{ m}$$

With

$$1 \text{ gpm} = 0.0000630902 \frac{\text{m}^3}{\text{s}}$$

the extraction rate of CrIN-2 is

$$Q_{CrIN-2} = 58 \text{ gpm} = 58 \frac{\text{gallon}}{\text{day}} = (58 \text{ gpm}) \left( \frac{0.0000630902 \frac{\text{m}^3}{\text{s}}}{\text{gpm}} \right) = 0.00365922 \frac{\text{m}^3}{\text{s}}$$

## B.2.2 Horizontal Hydraulic Conductivity Determination

The horizontal hydraulic conductivity ( $K_h$ ) will be determined with the trial-and-error method.

From Eq. (A-9),

$$m_{CrIN-2} = \frac{Q_{CrIN-2}}{\pi s_{w-CrIN-2}(H_0 - CrIN-2 + h_{w-CrIN-2})} = \frac{0.00365922 \frac{m^3}{s}}{\pi(1.95072 m)(16.28 m + 14.33 m)} = 0.000019507 \frac{m}{s}$$

From Eq. (A-10),

$$K_h - m_{CrIN-2} \frac{1}{2} \ln(K_h) = m_{CrIN-2} [\ln(3,000) + \ln\left(\frac{s_{w-CrIN-2}}{r_w}\right)]$$

$$\text{Trial 1: } K_h = 20 \frac{ft}{d} = 0.000070556 \frac{m}{s}$$

$$0.000070556 - (0.000019507) \frac{1}{2} \ln(0.000070556)$$

$$= (0.000019507) [\ln(3,000) + \ln\left(\frac{1.95072 m}{0.1016 m}\right)]$$

$$0.000163791 \neq 0.000213822$$

$$\text{Trial 2: } K_h = 30 \frac{ft}{d} = 0.000105833 \frac{m}{s}$$

$$0.000105833 - (0.000019507) \frac{1}{2} \ln(0.000105833)$$

$$= 0.000213822$$

$$0.000195113 \neq 0.000213822$$

$$\text{Trial 3: } K_h = 34 \frac{ft}{d} = 0.000119994 \frac{m}{s}$$

$$0.000119994 - (0.000019507) \frac{1}{2} \ln(0.000119994)$$

$$= 0.000213822$$

$$0.000208049 \neq 0.000213822$$

$$\text{Trial 5: } K_h = 38 \frac{ft}{d} = 0.000134056 \frac{m}{s}$$

$$0.000134056 - (0.000019507) \frac{1}{2} \ln(0.000134056)$$

$$= 0.000213822$$

$$0.00022103 \neq 0.000213822$$

$$\text{Trial 6: } K_h = 37 \frac{ft}{d} = 0.000130528 \frac{m}{s}$$

$$0.000130528 - (0.000019507) \frac{1}{2} \ln(0.000130528)$$

$$= 0.000213822$$

$$0.000217763 \cong 0.000213822$$

Therefore,

$$K_h = 37 \frac{ft}{d} = 0.000130528 \frac{m}{s} = 0.0130528 \frac{cm}{s} = 1.31 \times 10^{-2} \frac{cm}{s}$$

### **B.2.3 Determination of $h_s - h_w$**

From Section 2.4, the input data for CrIN-2 are as follows:

$$H_{0-CrIN-2} = 952.5 ft - 899.1 ft = 59.4 ft = 16.28 m$$

$$h_{w-CrIN-2} = H_{0-CrIN-2} - s_{w-CrIN-2} = 53.4 ft - 6.4 ft = 47.0 ft = 14.33 m$$

$$Q_{CrIN-2} = 58 gpm = 58 \frac{gallon}{day} = (58 gpm) \left( \frac{0.0000630902 \frac{m^3}{s}}{gpm} \right) = 0.00365922 \frac{m^3}{s}$$

$$\frac{r_w}{H_0} = \frac{0.1016 m}{16.28 m} = 0.0062 < 0.25$$

With these values, Eq. (A-11) gives

$$h_s - h_w \approx (H_0 - h_w) - 3.75 \frac{Q_w}{2\pi K_h H_0}$$

$$h_s - h_w \approx (16.28 m - 14.33 m) - 3.75 \frac{0.00365922 \frac{m^3}{s}}{2\pi(0.000130528 \frac{m}{s})(16.28 m)} = 0.92 m$$

$$h_s = h_w + 0.92 m = 14.33 m + 0.92 m = 15.25 m$$

$$\frac{h_s - h_w}{h_s} = \frac{0.92 m}{15.25 m} = 0.06$$

## **B.3 DETERMINATION OF HORIZONTAL HYDRAULIC CONDUCTIVITY FROM CrIN-3 DATA**

### **B.3.1 Input Data Summary**

From Section 2.4 , the input data for CrIN-3 are as follows:

$$s_{w-CrIN-3} = 6.5 \text{ ft} = 1.9812 \text{ m}$$

$$H_{0-CrIN-3} = (980.4 \text{ ft} - 928.8 \text{ ft}) \cos (17^\circ) = 49.35 \text{ ft} = 15.04 \text{ m}$$

$$h_{w-CrIN-3} = H_{0-CrIN-3} - s_{w-CrIN-3} = 49.35 \text{ ft} - 6.5 \text{ ft} = 42.85 \text{ ft} = 13.06 \text{ m}$$

The radius of the well is

$$r_w = 4 \text{ in} = 0.1016 \text{ m}$$

With

$$1 \text{ gpm} = 0.0000630902 \frac{\text{m}^3}{\text{s}}$$

the extraction rate of CrIN-3 is

$$Q_{CrIN-3} = 58 \text{ gpm} = 58 \frac{\text{gallon}}{\text{day}} = (58 \text{ gpm}) \left( \frac{0.0000630902 \frac{\text{m}^3}{\text{s}}}{\text{gpm}} \right) = 0.00365922 \frac{\text{m}^3}{\text{s}}$$

### **B.3.2 Horizontal Hydraulic Conductivity Determination**

The horizontal hydraulic conductivity ( $K_h$ ) will be determined with the trial-and-error method.

From Eq. (A-9),

$$m_{CrIN-3} = \frac{Q_{CrIN-3}}{\pi s_{w-CrIN-3} (H_{0-CrIN-3} + h_{w-CrIN-3})} = \frac{0.00365922 \frac{\text{m}^3}{\text{s}}}{\pi (1.9812 \text{ m}) (15.04 \text{ m} + 13.06 \text{ m})} = 0.000020922 \frac{\text{m}}{\text{s}}$$

From Eq. (A-10),

$$K_h - m_{CrIN-3} \frac{1}{2} \ln(K_h) = m_{CrIN-3} [\ln(3,000) + \ln\left(\frac{s_{w-CrIN-3}}{r_w}\right)]$$

$$\text{Trial 1: } K_h = 20 \frac{\text{ft}}{\text{d}} = 0.000070556 \frac{\text{m}}{\text{s}}$$

$$0.000070556 - (0.000020922) \frac{1}{2} \ln(0.000070556)$$

$$= (0.000020922) [\ln(3,000) + \ln\left(\frac{1.9812 \text{ m}}{0.1016 \text{ m}}\right)]$$

$$0.000170554 \neq 0.000229656$$

$$\text{Trial 2: } K_h = 30 \frac{\text{ft}}{\text{d}} = 0.000105833 \frac{\text{m}}{\text{s}}$$

$$0.000105833 - (0.000020922) \frac{1}{2} \ln(0.000105833)$$

$$= 0.000229656$$

$$0.000201589 \neq 0.000229656$$

$$\text{Trial 3: } K_h = 34 \frac{ft}{d} = 0.000119994 \frac{m}{s}$$

$$0.000119994 - (0.000020922) \frac{1}{2} \ln(0.000119994)$$

$$= 0.000229656$$

$$0.000214437 \neq 0.000229656$$

$$\text{Trial 5: } K_h = 38 \frac{ft}{d} = 0.000134056 \frac{m}{s}$$

$$0.000134056 - (0.000020922) \frac{1}{2} \ln(0.000134056)$$

$$= 0.000229656$$

$$0.000227339 \cong 0.000229656$$

Therefore,

$$K_h = 38 \frac{ft}{d} = 0.000134056 \frac{m}{s} = 0.0134056 \frac{cm}{s} = 1.34 \times 10^{-2} \frac{cm}{s}$$

### B.3.3 Determination of $h_s - h_w$

From Section 2.4, the input data for CrIN-3 are as follows:

$$H_{0-CrIN-3} = (980.4 ft - 928.8 ft) \cos(17^\circ) = 49.35 ft = 15.04 m$$

$$h_{w-CrIN-3} = H_{0-CrIN-3} - s_{w-CrIN-3} = 49.35 ft - 6.5 ft = 42.85 ft = 13.06 m$$

$$Q_{CrIN-3} = 58 gpm = 58 \frac{gallon}{day} = (58 gpm) \left( \frac{0.0000630902 \frac{m^3}{s}}{gpm} \right) = 0.00365922 \frac{m^3}{s}$$

$$\frac{r_w}{H_0} = \frac{0.1016 m}{14.91 m} = 0.0068 < 0.25$$

With these values, Eq. (A-11) gives

$$h_s - h_w \approx (H_0 - h_w) - 3.75 \frac{Q_w}{2\pi K_h H_0}$$

$$h_s - h_w \approx (15.04 m - 13.06 m) - 3.75 \frac{0.00365922 \frac{m^3}{s}}{2\pi(0.000134056 \frac{m}{s})(15.04 m)} = 0.90 m$$

$$h_s = h_w + 0.90 \text{ m} = 13.06 \text{ m} + 0.90 \text{ m} = 13.96 \text{ m}$$

$$\frac{h_s - h_w}{h_s} = \frac{0.90 \text{ m}}{13.96 \text{ m}} = 0.06$$

## B.4 DETERMINATION OF HORIZONTAL HYDRAULIC CONDUCTIVITY FROM CrIN-4 DATA

### B.4.1 Input Data Summary

From Section 2.5, the input data for CrIN-4 are as follows:

$$s_{w-CrIN-4} = 3.9 \text{ ft} = 1.18872 \text{ m}$$

$$H_{0-CrIN-4} = (1,133.0 \text{ ft} - 1,078.1 \text{ ft}) \cos(11^\circ) = 53.89 \text{ ft} = 16.43 \text{ m}$$

$$h_{w-CrIN-4} = H_{0-CrIN-4} - s_{w-CrIN-4} = 53.89 \text{ ft} - 3.9 \text{ ft} = 49.99 \text{ ft} = 15.24 \text{ m}$$

With

$$1 \text{ gpm} = 0.0000630902 \frac{\text{m}^3}{\text{s}}$$

the extraction rate of CrIN-4 is

$$Q_{CrIN-4} = 62 \text{ gpm} = 62 \frac{\text{gallon}}{\text{day}} = (62 \text{ gpm}) \left( \frac{0.0000630902 \frac{\text{m}^3}{\text{s}}}{\text{gpm}} \right) = 0.00391158 \frac{\text{m}^3}{\text{s}}$$

### B.4.2 Horizontal Hydraulic Conductivity Determination

The horizontal hydraulic conductivity ( $K_h$ ) will be determined with the trial-and-error method.

From Eq. (A-9),

$$m_{CrIN-4} = \frac{Q_{CrIN-4}}{\pi s_{w-CrIN-4} (H_{0-CrIN-4} + h_{w-CrIN-4})} = \frac{0.00391158 \frac{\text{m}^3}{\text{s}}}{\pi (1.18872 \text{ m}) (16.43 \text{ m} + 15.24 \text{ m})} = 0.000033073 \frac{\text{m}}{\text{s}}$$

From Eq. (A-10),

$$K_h - m_{CrIN-4} \frac{1}{2} \ln(K_h) = m_{CrIN-4} [\ln(3,000) + \ln\left(\frac{s_{w-CrIN-4}}{r_w}\right)]$$

$$\text{Trial 1: } K_h = 38 \frac{\text{ft}}{\text{d}} = 0.000134056 \frac{\text{m}}{\text{s}}$$

$$0.000134056 - (0.000033073) \frac{1}{2} \ln(0.000134056)$$

$$= (0.000033073) [\ln(3,000) + \ln\left(\frac{1.18872 \text{ m}}{0.1016 \text{ m}}\right)]$$

$$0.000281516 \neq 0.000346141$$

$$\text{Trial 2: } K_h = 44 \frac{ft}{d} = 0.000155222 \frac{m}{s}$$

$$0.000155222 - (0.000033073) \frac{1}{2} \ln(0.000155222)$$

$$= 0.000346141$$

$$0.000300258 \neq 0.000346141$$

$$\text{Trial 4: } K_h = 52 \frac{ft}{d} = 0.000183444 \frac{m}{s}$$

$$0.000183444 - (0.000033073) \frac{1}{2} \ln(0.000183444)$$

$$= 0.000346141$$

$$0.000325717 \neq 0.000346141$$

$$\text{Trial 5: } K_h = 60 \frac{ft}{d} = 0.000211667 \frac{m}{s}$$

$$0.000211667 - (0.000033073) \frac{1}{2} \ln(0.000211667)$$

$$= 0.000346141$$

$$0.000351574 \cong 0.000346141$$

Therefore,

$$K_h = 60 \frac{ft}{d} = 0.000211667 \frac{m}{s} = 0.0211667 \frac{cm}{s} = 2.11 \times 10^{-2} \frac{cm}{s}$$

### **B.4.3 Determination of $h_s - h_w$**

From Section 2.5, the input data for CrIN-4 are as follows:

$$H_{0-CrIN-4} = (1,133.0 \text{ ft} - 1,078.1 \text{ ft}) \cos(11^\circ) = 53.89 \text{ ft} = 16.43 \text{ m}$$

$$h_{w-CrIN-4} = H_{0-CrIN-4} - s_{w-CrIN-4} = 53.89 \text{ ft} - 3.9 \text{ ft} = 49.99 \text{ ft} = 15.24 \text{ m}$$

$$Q_{CrIN-4} = 62 \text{ gpm} = 62 \frac{\text{gallon}}{\text{day}} = (62 \text{ gpm}) \left( \frac{0.0000630902 \frac{\text{m}^3}{\text{s}}}{\text{gpm}} \right) = 0.00391158 \frac{\text{m}^3}{\text{s}}$$

$$\frac{r_w}{H_0} = \frac{0.1016 \text{ m}}{16.43 \text{ m}} = 0.0062 < 0.25$$

With these values, Eq. (A-11) gives

$$h_s - h_w \approx (H_0 - h_w) - 3.75 \frac{Q_w}{2\pi K_h H_0}$$

$$h_s - h_w \approx (16.43 \text{ m} - 15.24 \text{ m}) - 3.75 \frac{0.00391158 \frac{\text{m}^3}{\text{s}}}{2\pi(0.000211667 \frac{\text{m}}{\text{s}})(16.43 \text{ m})} = 0.52 \text{ m}$$

$$h_s = h_w + 0.52 \text{ m} = 15.24 \text{ m} + 0.90 \text{ m} = 15.76 \text{ m}$$

$$\frac{h_s - h_w}{h_s} = \frac{0.52 \text{ m}}{15.76 \text{ m}} = 0.03$$

## B.5 DETERMINATION OF HORIZONTAL HYDRAULIC CONDUCTIVITY FROM CrIN-5 DATA

### B.5.1 Input Data Summary

From Section 2.6, the input data for CrIN-5 are as follows:

$$s_{w-CrIN-5} = 2.75 \text{ ft} = 0.8382 \text{ m}$$

$$H_{0-CrIN-5} = (1,222.0 \text{ ft} - 1,156.8 \text{ ft}) \cos(25^\circ) = 59.09 \text{ ft} = 18.01 \text{ m}$$

$$h_{w-CrIN-5} = H_{0-CrIN-5} - s_{w-CrIN-5} = 59.09 \text{ ft} - 2.75 \text{ ft} = 54.34 \text{ ft} = 17.17 \text{ m}$$

The radius of the well is

$$r_w = 4 \text{ in} = 0.1016 \text{ m}$$

With

$$1 \text{ gpm} = 0.0000630902 \frac{\text{m}^3}{\text{s}}$$

the extraction rate of CrIN-5 is

$$Q_{CrIN-5} = 62 \text{ gpm} = 62 \frac{\text{gallon}}{\text{day}} = (62 \text{ gpm}) \left( \frac{0.0000630902 \frac{\text{m}^3}{\text{s}}}{\text{gpm}} \right) = 0.00391158 \frac{\text{m}^3}{\text{s}}$$

### B.5.2 Horizontal Hydraulic Conductivity Determination

The horizontal hydraulic conductivity ( $K_h$ ) will be determined with the trial-and-error method.

From Eq. (A-9),



$$m_{CrIN-5} = \frac{Q_{CrIN-5}}{\pi s_{w-CrIN-5}(H_{0-CrIN-5} + h_{w-CrIN-5})} = \frac{0.00391158 \frac{m^3}{s}}{\pi(0.8382 m)(18.01 m + 17.17 m)} = 0.000042224 \frac{m}{s}$$

From Eq. (A-10),

$$K_h - m_{CrIN-5} \frac{1}{2} \ln(K_h) = m_{CrIN-5} [\ln(3,000) + \ln\left(\frac{s_{w-CrIN-5}}{r_w}\right)]$$

$$\text{Trial 1: } K_h = 65 \frac{ft}{d} = 0.000229306 \frac{m}{s}$$

$$0.000229306 - (0.000042224) \frac{1}{2} \ln(0.000229306)$$

$$= (0.000042224) [\ln(3,000) + \ln\left(\frac{0.8382 m}{0.1016 m}\right)]$$

$$0.000406234 \neq 0.000427163$$

$$\text{Trial 2: } K_h = 80 \frac{ft}{d} = 0.000282222 \frac{m}{s}$$

$$0.000282222 - (0.000042224) \frac{1}{2} \ln(0.000282222)$$

$$= 0.000427163$$

$$0.000454766 \neq 0.000427163$$

$$\text{Trial 3: } K_h = 72 \frac{ft}{d} = 0.000254 \frac{m}{s}$$

$$0.000254 - (0.000042224) \frac{1}{2} \ln(0.000254)$$

$$= 0.000420496$$

$$0.000428769 \cong 0.000427163$$

Therefore,

$$K_h = 72 \frac{ft}{d} = 0.000254 \frac{m}{s} = 0.0254 \frac{cm}{s} = 2.54 \times 10^{-2} \frac{cm}{s}$$

### **B.5.3 Determination of $h_s - h_w$**

From Section 2.6, the input data for CrIN-5 are as follows:

$$H_{0-CrIN-5} = (1,222.0 ft - 1,156.8 ft) \cos(25^\circ) = 59.09 ft = 18.01 m$$

$$h_{w-CrIN-5} = H_{0-CrIN-5} - s_{w-CrIN-5} = 59.09 ft - 2.75 ft = 54.34 ft = 17.17 m$$

$$Q_{CrIN-5} = 62 \text{ gpm} = 62 \frac{\text{gallon}}{\text{day}} = (62 \text{ gpm}) \left( \frac{0.0000630902 \frac{\text{m}^3}{\text{s}}}{\text{gpm}} \right) = 0.00391158 \frac{\text{m}^3}{\text{s}}$$

$$\frac{r_w}{H_0} = \frac{0.1016 \text{ m}}{18.01 \text{ m}} = 0.0056 < 0.25$$

With these values, Eq. (A-11) gives

$$h_s - h_w \approx (H_0 - h_w) - 3.75 \frac{Q_w}{2\pi K_h H_0}$$

$$h_s - h_w \approx (18.01 \text{ m} - 17.17 \text{ m}) - 3.75 \frac{0.00391158 \frac{\text{m}^3}{\text{s}}}{2\pi(0.000254 \frac{\text{m}}{\text{s}})(18.01 \text{ m})} = 0.51 \text{ m}$$

$$h_s = h_w + 0.51 \text{ m} = 17.17 \text{ m} + 0.51 \text{ m} = 17.68 \text{ m}$$

$$\frac{h_s - h_w}{h_s} = \frac{0.51 \text{ m}}{17.68 \text{ m}} = 0.03$$

## **ATTACHMENT 2**

**Determination of the Horizontal  
Hydraulic Conductivity ( $K_h$ ) Values  
from the Steady-State Drawdown  
Values of the CrEX-1, CrEX-2, CrEX-3,  
CrEX-4, and CrEX-5 Extraction Wells**

---

This page intentionally left blank.

## Executive Summary

In Attachment 2, horizontal hydraulic conductivity ( $K_h$ ) values are determined using the measured steady-state drawdowns at CrEX-1, CrEX-2, CrEX-3, CrEX-4, and CrEX-5 extraction wells. The chromium injection well CrIN-6 was completed in 2017 as part of IM. In 2019, owing to high measured concentration, CrIN-6 was converted to the chromium extraction well CrEX-5 (Susan Wacaster, email to Vedat Batu, 6/28/2024). The method is based on the Dupuit-Forchheimer and Thiem well discharge formulas along with the Sichardt empirical zone of influence radius equation to determine the values of  $K_h$  around each CrEX extraction. The measured drawdown as well as other data for CrEX-1, CrEX-2, CrEX-3, CrEX-4, and CrEX-5 extraction wells are taken from the reports given below:

Los Alamos National Laboratory (LANL), "Completion Report for Groundwater Extraction Well CrEX-1," LA-UR-15-20165, EP2015-0005, Los Alamos, New Mexico, January, 2015.

Los Alamos National Laboratory (LANL), "Completion Report for Groundwater Extraction Well CrEX-3," LA-UR-16-26486, EP2016-0077, Los Alamos, New Mexico, September, 2016.

Los Alamos National Laboratory (LANL), "Completion Report for Groundwater Extraction Well CrEX-2," LA-UR-17-27466, EP2017-0104, Los Alamos, New Mexico, September, 2017a.

Los Alamos National Laboratory (LANL), "Completion Report for Groundwater Extraction Well CrIN-6," LA-UR-17-28238, EP2017-0115, Los Alamos, New Mexico, September, 2017b.

Los Alamos National Laboratory (LANL), "Completion Report for Groundwater Extraction Well CrEX-4," LA-UR-18-23083, EP2018-0037, Los Alamos, New Mexico, April, 2018.

From these report, some key information are as follows:

1. The well CrEX-1 was completed as having two screens within the uppermost portion of the regional aquifer. The screened intervals are all within Puye Formation sediments.
2. The well CrEX-2 was completed as having one screen within the uppermost portion of the regional aquifer. The screen interval is within Puye Formation sediments.
3. The well CrEX-3 was completed as having one screen within the uppermost portion of the regional aquifer. The screen interval is within Puye Formation sediments.
4. The well CrEX-4 was completed as having two screens within the uppermost portion of the regional aquifer. The screened intervals are all within Puye Formation sediments.
5. CrEX-5 was designed as having one inclined screen interval with 25-degree angle within the uppermost portion of the regional aquifer. The screen interval is within Puye Formation sediments.
6. All CrEX wells were constructed of 8.0-in.-I.D./8.63-in.-O.D.

The resulted horizontal hydraulic conductivity ( $K_h$ ) values for the 5 CrEX wells are as follows:

$$\text{CrEX} - 1: K_h = 12.5 \text{ ft/d} = 4.41 \times 10^{-3} \text{ cm/s}$$

$$\text{CrEX} - 2: K_h = 51.0 \text{ ft/d} = 1.80 \times 10^{-2} \text{ cm/s}$$

$$\text{CrEX} - 3: K_h = 21.5 \text{ ft/d} = 7.58 \times 10^{-2} \text{ cm/s}$$

$$\text{CrEX} - 4: K_h = 12.5 \text{ ft/d} = 4.41 \times 10^{-3} \text{ cm/s}$$

$$\text{CrEX} - 5: K_h = 172.0 \text{ ft/d} = 6.07 \times 10^{-2} \text{ cm/s}$$

Their arithmetic average is  $53.9 \text{ ft/d}$  ( $1.90 \times 10^{-2} \text{ cm/s}$ ). These values correspond to silty sand, clean sand and gravel (e.g., Freeze and Cherry, 1979, p. 29, Table 2.3). It can be noticed that the aquifer is more permeable around CrEX-2 ( $51.0 \text{ ft/d}$ ) and CrEX-5 ( $172.0 \text{ ft/d}$ ) extraction wells.

## Attachment 2 Contents

1.	Purpose.....	1
2.	CrEX Extraction Wells and Steady-State Drawdown Data .....	1
2.1	Geometrical Data for the CrEX Extraction Wells.....	1
2.2	CrEX-1 Extraction Well Data .....	2
2.3	CrEX-2 Extraction Well Data .....	3
2.4	CrEX-3 Extraction Well Data .....	4
2.5	CrEX-4 Extraction Well Data .....	5
2.6	CrEX-5 Extraction Well Data .....	6
3.	Method for Determining Horizontal Hydraulic Conductivity With Steady State Drawdown at the Extraction Well .....	7
4.	Results for the Horizontal Hydraulic Conductivity Values .....	7

## Figures

- Figure 1. Measured drawdowns at CrEX-1 extraction well.
- Figure 2. Measured extraction rates at CrEX-1 extraction well.
- Figure 3. Measured drawdowns at CrEX-3 extraction well.
- Figure 4. Measured extraction rates at CrEX-2 extraction well.
- Figure 5. Measured drawdowns at CrEX-3 extraction well.
- Figure 6. Measured extraction rates at CrEX-3 extraction well.
- Figure 7. Measured drawdowns at CrEX-4 extraction well.
- Figure 8. Measured flow rates at CrEX-4 extraction well.
- Figure 9. Measured drawdowns at CrEX-5 extraction well.
- Figure 10. Measured flow rates at CrEX-5 extraction well.
- Figure 11. Well in an unconfined aquifer.
- Figure 12. Well in a confined aquifer.

## Tables

- Table 1. Determined horizontal hydraulic conductivity ( $K_h$ ) values using the drawdown data at the CrEX injection wells.

## Appendices

- Appendix A Dupuit-Forchheimer Well Discharge Formula and Determination Method of Horizontal Hydraulic Conductivity
- Appendix B Determination of Horizontal Hydraulic Conductivity Using Thiem Well Discharge Formula for Steady State Drawdown Value at the Well

Appendix C Determination of Horizontal Hydraulic Conductivity Values Using the CrEX-1, CrEX-2, CrEX-3, CrEX-4, and CrEX-5 Wells Steady State Drawdown Values



## 1. Purpose

The purpose of Attachment 2 is to determine horizontal hydraulic conductivity ( $K_h$ ) values using the measured steady-state drawdown values at CrEX-1, CrEX-2, CrEX-3, CrEX-3, and CrEX-5 extraction wells. The method is based on the *Dupuit-Forchheimer well discharge formula* for unconfined aquifers and *Thiem's discharge formula* for confined aquifers along with the *Sichardt empirical zone of influence radius* to determine the values of  $K_h$  around each CrEX extraction well using the data in the report of Los Alamos National Laboratory (2015, 20016, 2017a, 217b, and 2018).

## 2. CrEX Extraction Wells and Steady-State Drawdown Data

### 2.1 Geometrical Data for the CrEX Extraction Wells

In the analyses, the measured drawdown data at CrEX-1, CrEX-2, CrEX-3, CrEX-4, and CrEX-5 extraction wells included as five separate reports of Los Alamos National Laboratory are used to determine horizontal hydraulic conductivity ( $K_h$ ) values. From these reports, some key data and information are given below:

The wells are completed within the uppermost portion of the regional aquifer. The screened intervals are all within Puye Formation sediments.

From these reports, some key information are as follows:

1. The CrEX-1 extraction well contains an upper screen 50 ft in length and lower screen 20 ft in length, separated by 30 ft blank pipe (LANL, 2015, p. v).
2. The CrEX-2 extraction is completed as a single-screen well within the regional aquifer. The screened interval is between 1,129.9 ft and 1,179.9 ft below ground surface (bgs) within Puye Formation sediments having 50 ft screen interval. The static depth to water after well installation was measured at 1,113.7 ft bgs (LANL, 2017a, p. v).
3. The CrEX-3 extraction well is completed as a single-screen well within the aquifer. The screened interval is set between 909.6 ft 948.8 ft bgs within the Puye Formation Sediments having 39.2 ft screen interval. The static depth to water after well installation was measured at 898.5 ft bgs (LANL, 2016, p. v).
4. The CrEX-4 extraction well is completed as a dual-screen well within the regional aquifer. The screen intervals are set between 929.9 ft and 964.9 ft (upper) ft bgs and 974.9 ft and 994.9 ft (lower) within Puye Formation sediments having 35 ft and 20 ft screen intervals with 10 ft apart. The static depth to water after well installation was measured at 920.0 ft bgs (LANL, 2018, p. v).
5. The chromium injection well CrIN-6 was completed in 2017 as part of IM. In 2019, owing to high measured concentration, CrIN-6 was converted to the chromium extraction well CrEX-5 (Susan Wacaster, email to Vedat Batu, 6/28/2024). The CrEX-5 extraction well was designed as having one inclined screen interval with 25-degree angle within the uppermost

portion of the regional aquifer. The screen interval is within Puye Formation sediments. The screened interval was set between 980 ft bgs and 1,040 ft bgs within the Puye Formation sediments having 60 ft screen interval (LANL, 217b, p. 6).

6. All CrEX extraction wells were constructed of 8.0-in.-I.D./8.63-in.-O.D.

## 2.2 CrEX-1 Extraction Well Data

The CrEX-1 extraction well data (LANL, 2015, p. 18, Figure 7.2-1):

*Depth to water in the completed well measured on September 24, 2014 = 997.2 ft*

*Depth of top of screen interval 1 = 990.0 ft*

*Depth of bottom of screen interval 1 = 1,040.0 ft*

From these values,

*Screen interval 1 =  $L_1 = 1,040 \text{ ft} - 990.0 \text{ ft} = 50 \text{ ft} = 15.24 \text{ m}$*

*Depth of top of screen interval 2 = 1,070.0 ft*

*Depth of bottom of screen interval 2 = 1,090.0 ft*

From these values,

*Screen interval 2 =  $L_2 = 1,090 \text{ ft} - 1,070.0 \text{ ft} = 20 \text{ ft} = 6.096 \text{ m}$*

*Total screen interval =  $L_1 + L_2 = 50 \text{ ft} + 20 \text{ ft} = 70 \text{ ft} = 21.336 \text{ m}$*

From Figure 1, the steady-state average drawdown is

*$s_{w-CrEX-1} = 20.0 \text{ ft} = 6.096 \text{ m}$*

Then,

*$H_{0-CrEX-1} = \text{Depth of bottom of screen interval 2} - \text{Depth to water level}$*

*$= 1,090 \text{ ft} - 997.2 \text{ ft} = 92.8 \text{ ft} = 28.28544 \text{ m}$*

*$h_{w-CrEX-1} = H_{0-CrEX-1} - s_{w-CrEX-1} = 92.8 \text{ ft} - 20.0 \text{ ft} = 72.8 \text{ ft} = 22.18944 \text{ m}$*

*Depth of bottom of screen interval 2 – Depth of top of screen interval 1*

*$= 1,090 \text{ ft} - 990 \text{ ft} = 100 \text{ ft} = 30.48 \text{ m} > h_{w-CrEX-1} = 72.8 \text{ ft} = 22.18944 \text{ m}$*

Therefore, the water level in the well interferes with the screen intervals and the Dupuit-Forchheimer well discharge formula will be used.

With

$$1 \text{ gpm} = 0.0000630902 \frac{\text{m}^3}{\text{s}}$$

the extraction rate of CrEX-1 is (Figure 2)

$$Q_{CrEX-1} = 95 \text{ gpm} = 95 \frac{\text{gallon}}{\text{day}} = (95 \text{ gpm}) \left( \frac{0.0000630902 \frac{\text{m}^3}{\text{s}}}{\text{gpm}} \right) = 0.00599355 \frac{\text{m}^3}{\text{s}}$$

### 2.3 CrEX-2 Extraction Well Data

The CrEX-2 extraction well data (LANL, 2017a, p. 16, Figure 8.3-1a):

*Depth to water in the completed well measured on May 6, 2017 = 1,113.7 ft*

*Depth of top of screen interval = 1,129.9 ft*

*Depth of bottom of screen interval = 1,179.9 ft*

From these values,

$$\text{Screen interval} = L = 1,179.9 \text{ ft} - 1,129.9 \text{ ft} = 50 \text{ ft} = 15.24 \text{ m}$$

From Figure 3, the steady-state average drawdown is

$$s_{w-CrEX-2} = 11.2 \text{ ft} = 3.41376 \text{ m}$$

Then,

$$H_{0-CrEX-2} = \text{Depth of bottom of screen interval} - \text{Depth to water level}$$

$$= 1,179.9 \text{ ft} - 1,113.7 \text{ ft} = 66.2 \text{ ft} = 20.17776 \text{ m}$$

$$h_{w-CrEX-2} = H_{0-CrEX-2} - s_{w-CrEX-2} = 66.2 \text{ ft} - 11.2 \text{ ft} = 55.0 \text{ ft} = 16.764 \text{ m}$$

$$h_{w-CrEX-2} = 55.0 \text{ ft} = 16.764 \text{ m} > \text{Screen interval} = L = 50 \text{ ft} = 15.24 \text{ m}$$

Therefore, the water level in the well does not interfere with the screen interval and the Thiem equation will be used.

With

$$1 \text{ gpm} = 0.0000630902 \frac{\text{m}^3}{\text{s}}$$

the extraction rate of CrEX-2 is (Figure 4)

$$Q_{CrEX-2} = 65 \text{ gpm} = 65 \frac{\text{gallon}}{\text{day}} = (65 \text{ gpm}) \left( \frac{0.0000630902 \frac{\text{m}^3}{\text{s}}}{\text{gpm}} \right) = 0.00410085 \frac{\text{m}^3}{\text{s}}$$

## 2.4 CrEX-3 Extraction Well Data

The CrEX-3 extraction well data (LANL, 2016, p. 13, Figure 7.2-1):

*Depth to water in the completed well measured on April 19, 2016 = 898.5 ft*

*Depth of top of screen interval = 909.6 ft*

*Depth of bottom of screen interval = 948.8 ft*

From these values,

*Screen interval = L = 948.8 ft – 909.6 ft = 39.2 ft = 11.94816 m*

From Figure 5, the steady-state average drawdown is

*s<sub>w-CrEX-3</sub> = 11.2 ft = 3.41376 m*

Then,

*H<sub>0-CrEX-3</sub> = Depth of bottom of screen interval – Depth to water level*

$$= 948.8 \text{ ft} - 898.5 \text{ ft} = 50.3 \text{ ft} = 15.33144 \text{ m}$$

*h<sub>w-CrEX-3</sub> = H<sub>0-CrEX-3</sub> – s<sub>w-CrEX-3</sub> = 50.3 ft – 11.2 ft = 39.1 ft = 11.91768 m*

*h<sub>w-CrEX-3</sub> = 39.1 ft = 11.91768 ft < Screen interval = L = 39.2 ft = 11.94816 m*

Therefore, the water level in the well will interfere with the screen interval and the Dupuit-Forchheimer well discharge formula will be used.

With

$$1 \text{ gpm} = 0.0000630902 \frac{\text{m}^3}{\text{s}}$$

the extraction rate of CrEX-3 is (Figure 6)

$$Q_{CrEX-2} = 53 \text{ gpm} = 53 \frac{\text{gallon}}{\text{day}} = (53 \text{ gpm}) \left( \frac{0.0000630902 \frac{\text{m}^3}{\text{s}}}{\text{gpm}} \right) = 0.00334377 \frac{\text{m}^3}{\text{s}}$$

## 2.5 CrEX-4 Extraction Well Data

The CrEX-4 extraction well data (LANL, 2018, p. 15, Figure 7.2-1):

*Depth to water in the completed well measured on November 14, 2017 = 920.02 ft*

*Depth of top of screen interval 1 = 929.9 ft*

*Depth of bottom of screen interval 1 = 964.9 ft*

From these values,

*Screen interval 1 =  $L_1 = 964.9 \text{ ft} - 929.9 \text{ ft} = 35 \text{ ft} = 10.668 \text{ m}$*

*Depth of top of screen interval 2 = 974.9 ft*

*Depth of bottom of screen interval 2 = 994.9 ft*

From these values,

*Screen interval 2 =  $L_2 = 994.9 \text{ ft} - 974.9 \text{ ft} = 20 \text{ ft} = 6.096 \text{ m}$*

*Total screen interval =  $L_1 + L_2 = 35 \text{ ft} + 20 \text{ ft} = 55 \text{ ft} = 16.764 \text{ m}$*

From Figure 7, the steady-state average drawdown is

$s_{w-CrEX-4} = 20.1 \text{ ft} = 6.12648 \text{ m}$

Then,

$H_{0-CrEX-4} = \text{Depth of bottom of screen interval 2} - \text{Depth to water level}$   
 $= 994.9 \text{ ft} - 920.02 \text{ ft} = 74.88 \text{ ft} = 22.8234 \text{ m}$

$h_{w-CrEX-4} = H_{0-CrEX-4} - s_{w-CrEX-4} = 74.88 \text{ ft} - 20.1 \text{ ft} = 54.78 \text{ ft} = 16.6969 \text{ m}$

*Depth of bottom of screen interval 2 – Depth of top of screen interval 1*

$= 994.9 \text{ ft} - 929.9 \text{ ft} = 65 \text{ ft} = 19.812 \text{ m} > h_{w-CrEX-4} = 54.78 \text{ ft} = 16.6969 \text{ m}$

Therefore, the water level in the well interferes with the screen intervals and the Dupuit-Forchheimer well discharge formula will be used.

With

$1 \text{ gpm} = 0.0000630902 \frac{\text{m}^3}{\text{s}}$

the extraction rate of CrEX-4 is (Figure 8)

$$Q_{CrEX-4} = 76 \text{ gpm} = 76 \frac{\text{gallon}}{\text{day}} = (76 \text{ gpm}) \left( \frac{0.0000630902 \frac{\text{m}^3}{\text{s}}}{\text{gpm}} \right) = 0.00479484 \frac{\text{m}^3}{\text{s}}$$

## 2.6 CrEX-5 Extraction Well Data

The chromium injection well CrIN-6 was completed in 2017 as part of IM. In 2019, owing to high measured concentration, CrIN-6 was converted to the chromium extraction well CrEX-5 (Susan Wacaster, email to Vedat Batu, 6/28/2024).

The CrIN-6 extraction well data (LANL, 2017b, p. 16, Figure 7.2-1):

The CrIN-6 injection well water levels (LANL, 2017b, p. 16, Figure 7.2-1):

*Depth to water (linear) following installation on July 13, 2017 = 966.5 ft*

The CrIN-6 injection well data are (LANL, 2017b, p. 16, Figure 7.2-1):

*Well angle from vertical = 25°*

*Depth of top of screen interval (linear) below top of drill casing = 980.0 ft*

*Depth of bottom of screen interval (linear) below top of drill casing = 1,040.0 ft*

From these data,

$$\text{Vertical screen interval} = L = (1,040.0 \text{ ft} - 980.0 \text{ ft}) \cos (25^\circ) = 54.38 \text{ ft} = 16.58 \text{ m}$$

From Figure 9, the steady-state average drawdown is

$$s_{w-CrEX-5} = 4.0 \text{ ft} = 1.2192 \text{ m}$$

Then,

$$H_{0-CrEX-5} = (1,040.0 \text{ ft} - 966.5 \text{ ft}) \cos (25^\circ) = 66.61 \text{ ft} = 20.30 \text{ m}$$

$$h_{w-CrEX-5} = H_{0-CrEX-5} - s_{w-CrEX-5} = 66.61 \text{ ft} - 4.0 \text{ ft} = 62.61 \text{ ft} = 19.08 \text{ m}$$

$$\text{Vertical screen interval} = L = 54.38 \text{ ft} = 16.58 \text{ m} < h_{w-CrEX-5} = 66.61 \text{ ft} = 19.08 \text{ m}$$

Therefore, the water level in the well does not interfere with the screen interval and the Thiem well discharge formula will be used.

The radius of the well is

$$r_w = 4 \text{ in} = 0.1016 \text{ m}$$

With

$$1 \text{ gpm} = 0.0000630902 \frac{\text{m}^3}{\text{s}}$$

From Figure 10, the extraction rate of CrEX-5 is

$$Q_{CrEX-5} = 90 \text{ gpm} = 90 \frac{\text{gallon}}{\text{day}} = (90 \text{ gpm}) \left( \frac{0.0000630902 \frac{\text{m}^3}{\text{s}}}{\text{gpm}} \right) = 0.0056781 \frac{\text{m}^3}{\text{s}}$$

### 3. Method for Determining Horizontal Hydraulic Conductivity With Steady State Drawdown at the Extraction Well

In order to determine the value of horizontal hydraulic conductivity ( $K_h$ ) with the steady-state drawdown value at a well, the *Dupuit-Forchheimer well discharge formula* under unconfined aquifer conditions or the *Thiem well discharge formula* under confined aquifer conditions along with empirical zone of influence radius can be used.

The geometry of the Dupuit-Forchheimer well discharge formula in an unconfined aquifer under steady-state flow conditions is given in Figure 11. The initial aquifer thickness is  $H_0$  and the aquifer has infinite extent. Its horizontal hydraulic conductivity is  $K_h$ . The constant extraction rate of the well is  $Q_w$ . Details of the method are given in Appendix A.

The geometry of the Thiem solution for a confined aquifer under steady-state flow conditions is given in Figure 12. The initial aquifer thickness is  $H$  and the aquifer has infinite extent. Its horizontal hydraulic conductivity is  $K_h$ . The constant extraction rate of the well is  $Q_w$ . Details of the method are given in Appendix B.

### 4. Results for the Horizontal Hydraulic Conductivity Values

Using the method described in Section 3, the resulted horizontal hydraulic conductivity ( $K_h$ ) values for the five CrEX extraction wells are as follows:

$$CrEX - 1: K_h = 12.5 \text{ ft/d} = 4.41 \times 10^{-3} \text{ cm/s}$$

$$CrEX - 2: K_h = 51.0 \text{ ft/d} = 1.80 \times 10^{-2} \text{ cm/s}$$

$$CrEX - 3: K_h = 21.5 \text{ ft/d} = 7.58 \times 10^{-2} \text{ cm/s}$$

$$CrEX - 4: K_h = 12.5 \text{ ft/d} = 4.41 \times 10^{-3} \text{ cm/s}$$

$$CrEX - 5: K_h = 172.0 \text{ ft/d} = 6.07 \times 10^{-2} \text{ cm/s}$$

Their arithmetic average is  $53.9 \text{ ft/d}$  ( $1.90 \times 10^{-2} \text{ cm/s}$ ). These values correspond to silty sand, clean sand, and gravel (e.g., Freeze and Cherry, 1979, p. 29, Table 2.3). It can be noticed that

the aquifer is more permeable around CrEX-2(51.0 *ft/d*) and CrEX-5 (172.0 *ft/d*) extraction wells.

In Figure 11, based on the Dupuit assumptions, the approximate form of the cone is also shown. In reality, the intersection of the cone of depression with the well edge ( $h_s$ ) is higher than  $h_w$  and the Dupuit-Forchheimer well discharge formula is based on the Dupuit assumptions, namely  $h_s = h_w$ . For  $(h_s - h_w)$ , an approximate expression is given by Boulton (1951), which is given by Eq. (A-11) in Appendix A. The  $(h_s - h_w)/h_w$  ratio is only determined for CrEX-1 [ $(h_s - h_w)/h_w = 0.13$ ], CrEX-3 [ $(h_s - h_w)/h_w = 0.12$ ], and CrEX-4 [ $(h_s - h_w)/h_w = 0.16$ ] for which the requirements are given in Section 2.2, Section 2.4, and Section 2.6, respectively. Calculation details are given in Appendix C. Therefore, assuming  $h_s = h_w$  does not generate significant errors in determining the  $K_h$  values.

For CrEX-2 and CrEX-5 extraction wells Thiem well discharge formula is used because the screen intervals are below the water levels in the wells. Details are given Section 2.3 and Section 2.6 for CrEX-2 and CrEX-5, respectively, as well as in Appendix C.

## References

- Batu, V., *Fluid Mechanics and Hydraulics: Illustrative Worked Examples of Surface and Subsurface Flows*, Taylor & Francis CRC Press, Boca Raton, Florida, 1240 pp., 2024.
- Bear, J., *Hydraulics of Groundwater*, McGraw-Hill Book Company, New York, 569 pp., 1979.
- Boulton, N.S., "The Flow Pattern Near a Gravity Well in a Uniform Water Bearing Unit, *Journal of the Institutions of Civil Engineers* (London), Vol. 36, pp. 534-550, 1951.
- Chertousov, M.D., *Hydraulics* (in Russian), Gosenergouzdat, 630 pp., Moscow, Russia, 1962.
- De Filippi, F.M., S. Iacurto, F. Ferranti, and G. Sappa, "Hydraulic Conductivity Estimation Using Low-Flow Purging Data Elaboration in Contaminated Sites," *Water*, Vol. 12, pp. 898-914, 2020.
- Dupuit, J., *Études Théoriques et Pratiques sur le Mouvement des Eaux*, Second edition, Paris, France, 304 pp., 1863.
- Forchheimer, P., "Über die Ergiebigkeit von Brunnen-Anlagen und Sickerschlitzzen Zeitschrift," *Der Architekten-und Ingenieur-Verein*, Vol. 32, p. 539, Hannover, Germany, 1886.
- Freeze, R.A., And J.A. Cherry, *Groundwater*, Prentice-Hall, Inc., Englewood Cliffs, New Jersey, 604, pp., 1979.
- Los Alamos National Laboratory (LANL), "Completion Report for Groundwater Extraction Well CrEX-1," LA-UR-15-20165, EP2015-0005, Los Alamos, New Mexico, January, 2015.
- Los Alamos National Laboratory (LANL), "Completion Report for Groundwater Extraction Well CrEX-3," LA-UR-16-26486, EP2016-0077, Los Alamos, New Mexico, September, 2016.



Los Alamos National Laboratory (LANL), "Completion Report for Groundwater Extraction Well CrEX-2," LA-UR-17-27466, EP2017-0104, Los Alamos, New Mexico, September, 2017a.

Los Alamos National Laboratory (LANL), "Completion Report for Groundwater Extraction Well CrIN-6," LA-UR-17-28238, EP2017-0115, Los Alamos, New Mexico, September, 2017b.

Los Alamos National Laboratory (LANL), "Completion Report for Groundwater Extraction Well CrEX-4," LA-UR-18-23083, EP2018-0037, Los Alamos, New Mexico, April, 2018.

Thiem, G., *Hydrologische Methoden* (in German), J.M. Gebhardt, Leipzig, Germany, 56 pp., 1906.

## Figures

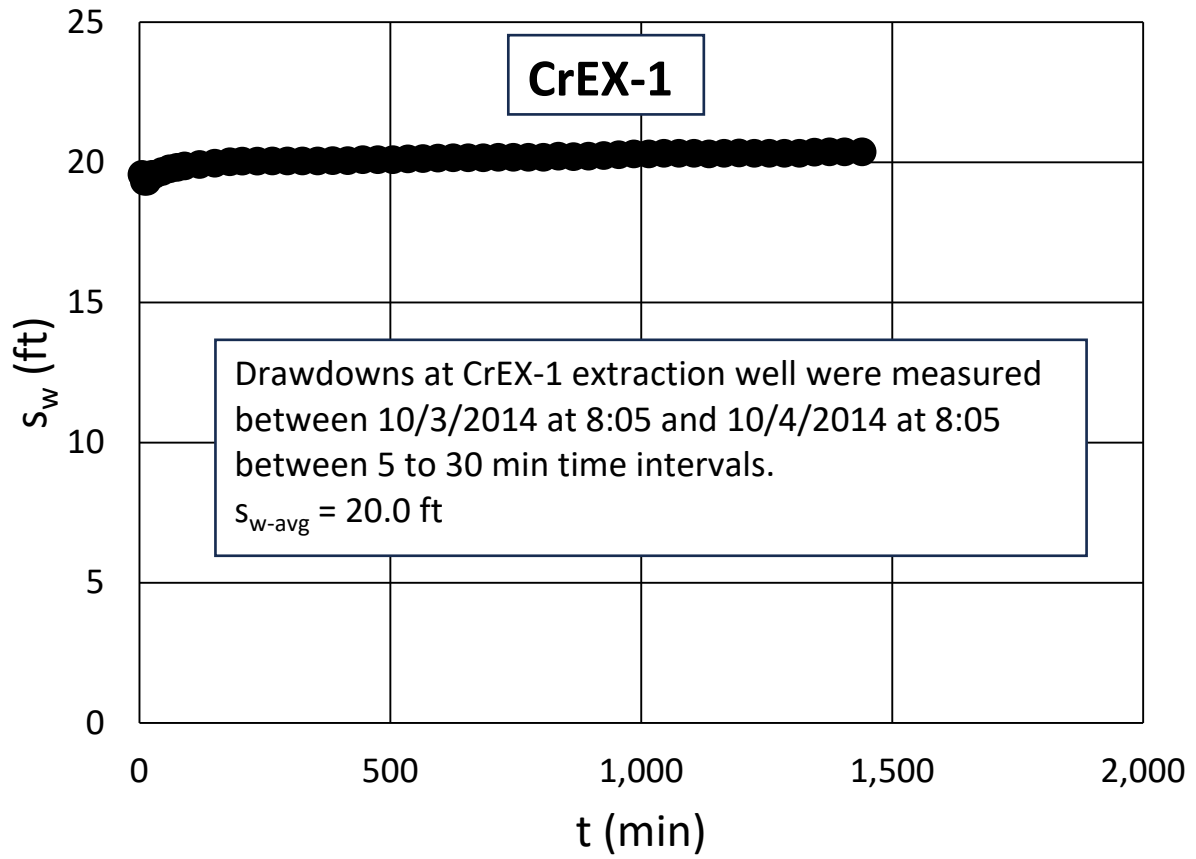


Figure 1. Measured drawdowns at CrEX-1 extraction well.

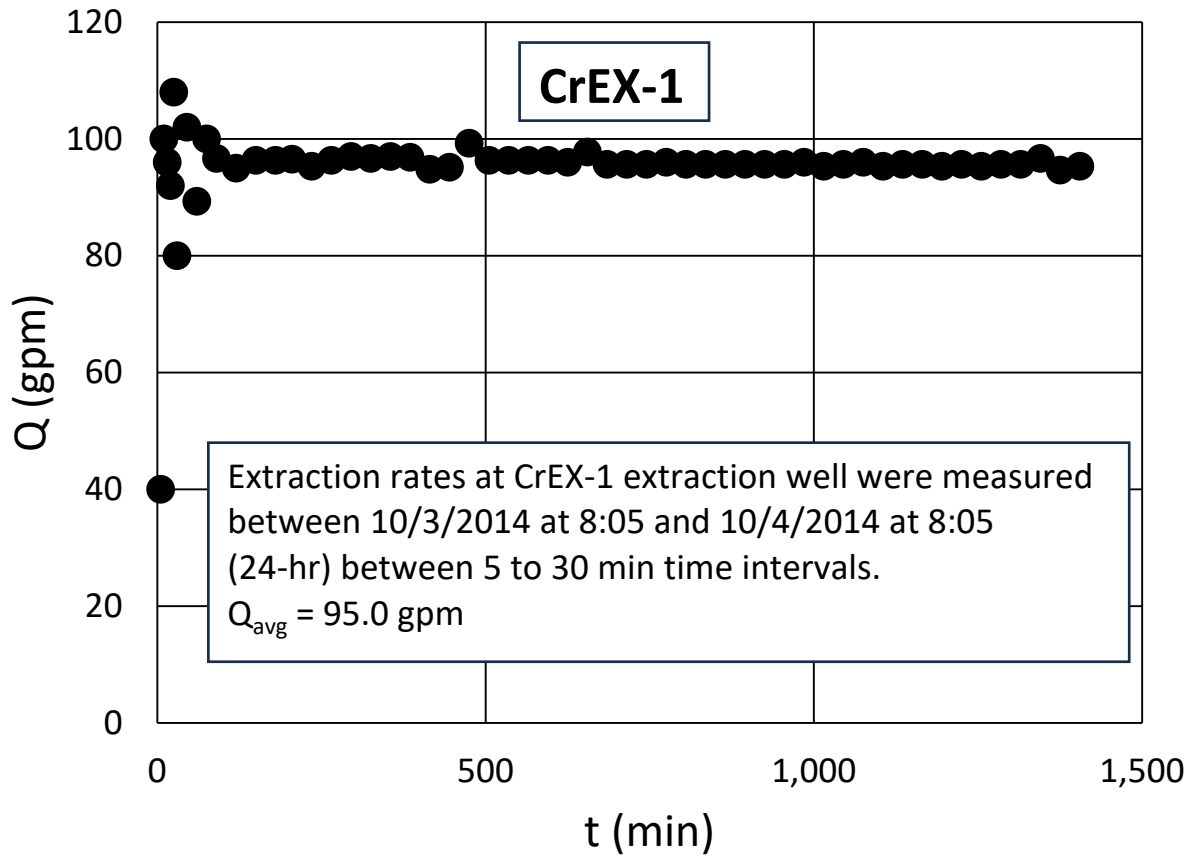


Figure 2. Measured extraction rates at CrEX-1 extraction well.

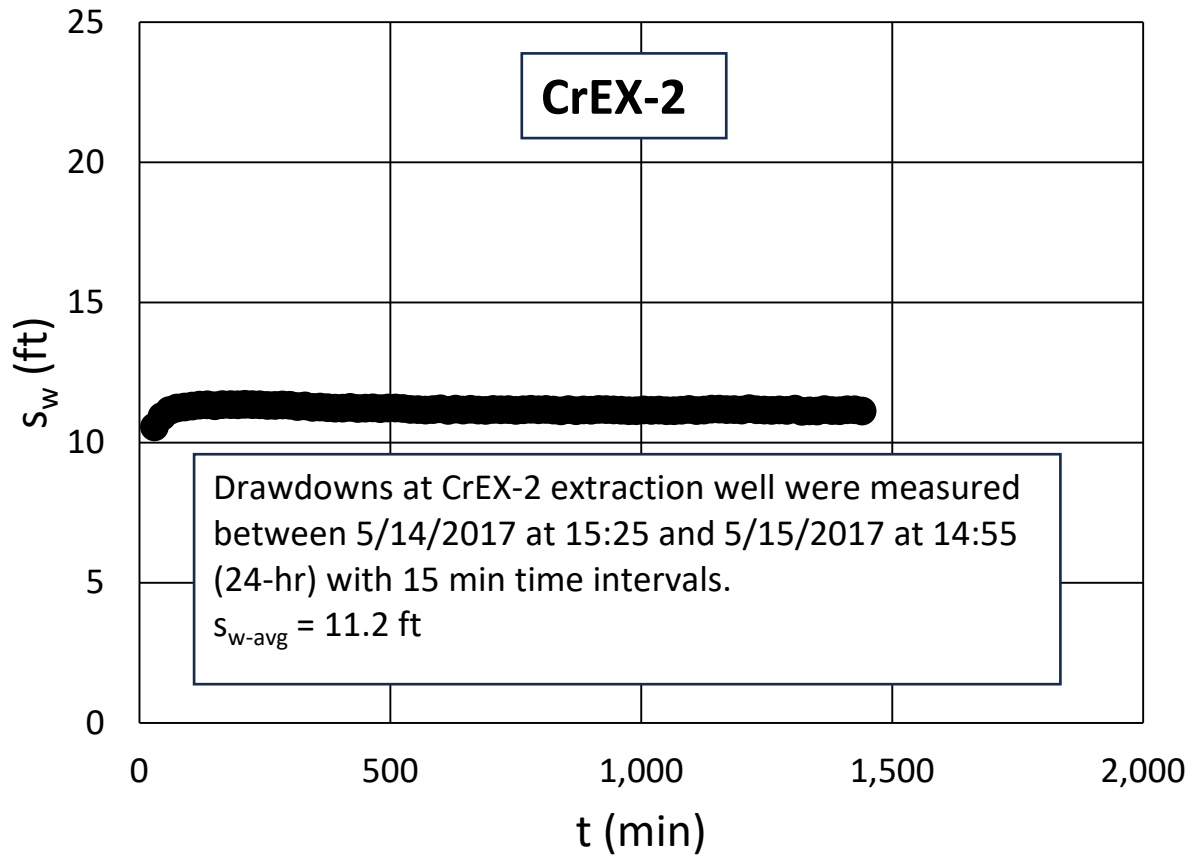


Figure 3. Measured drawdowns at CrEX-3 extraction well.

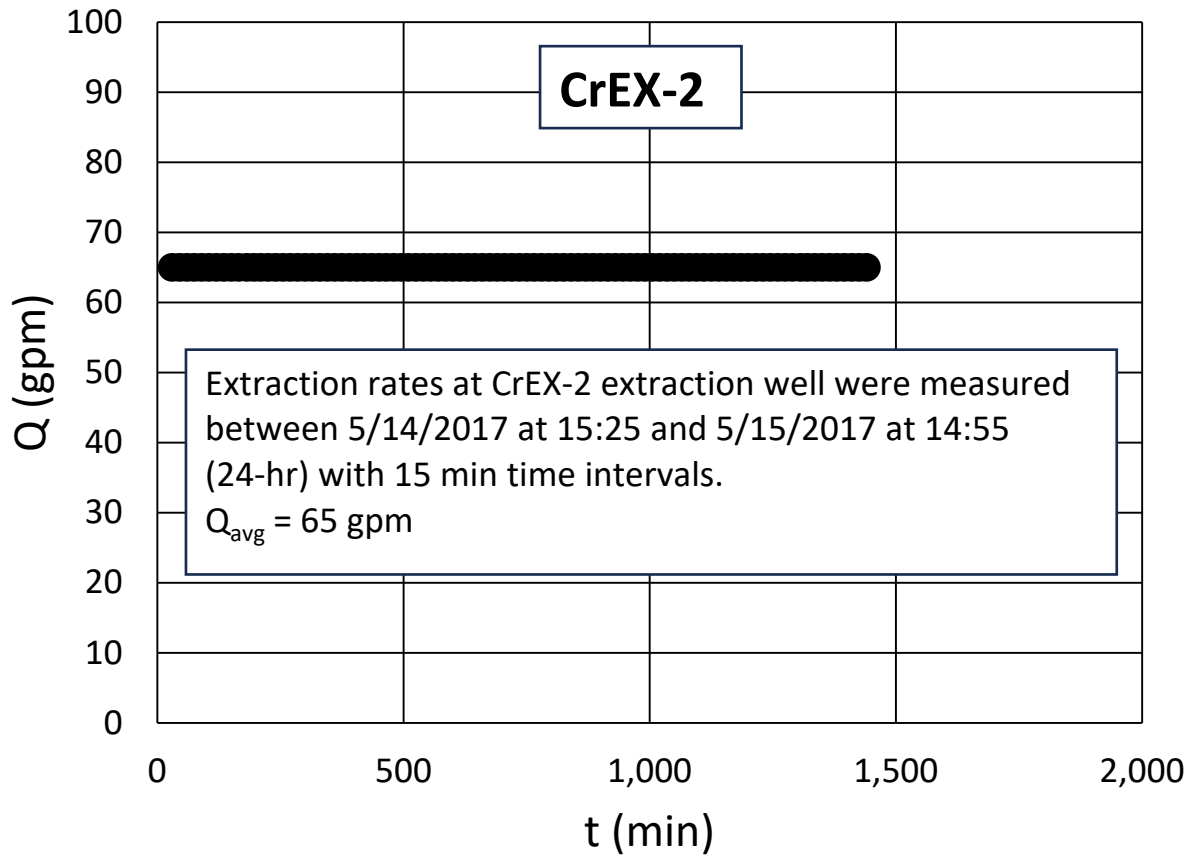


Figure 4. Measured extraction rates at CrEX-2 extraction well.

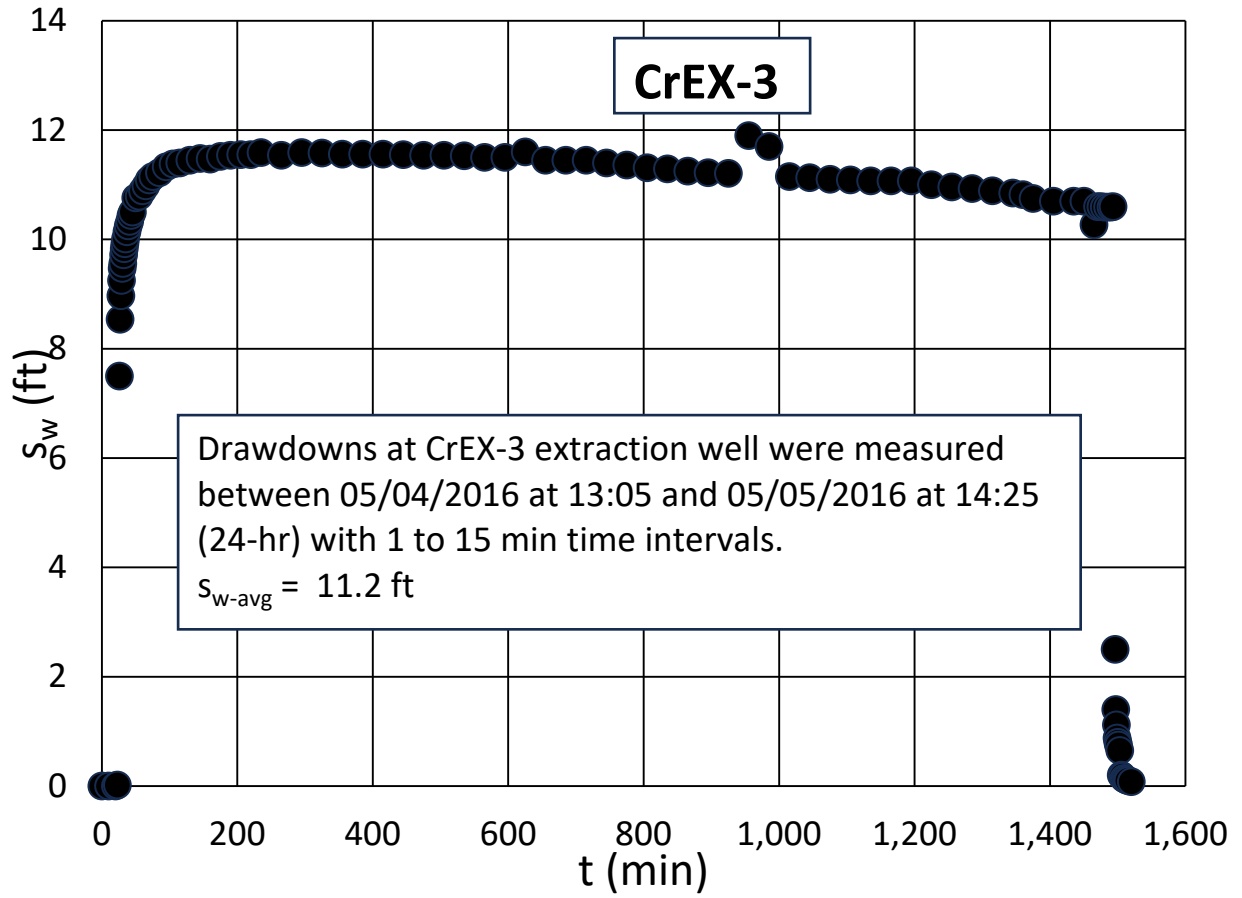


Figure 5. Measured drawdowns at CrEX-3 extraction well.

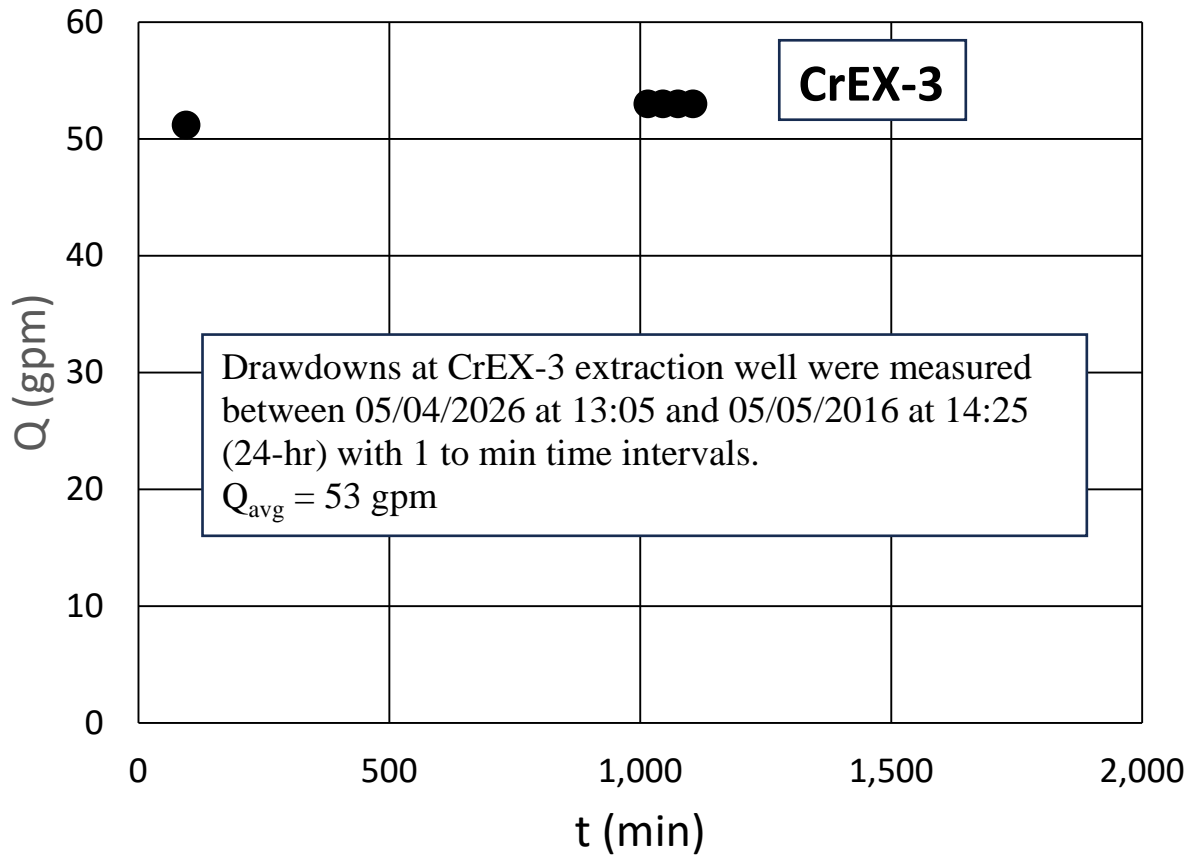


Figure 6. Measured extraction rates at CrEX-3 extraction well.



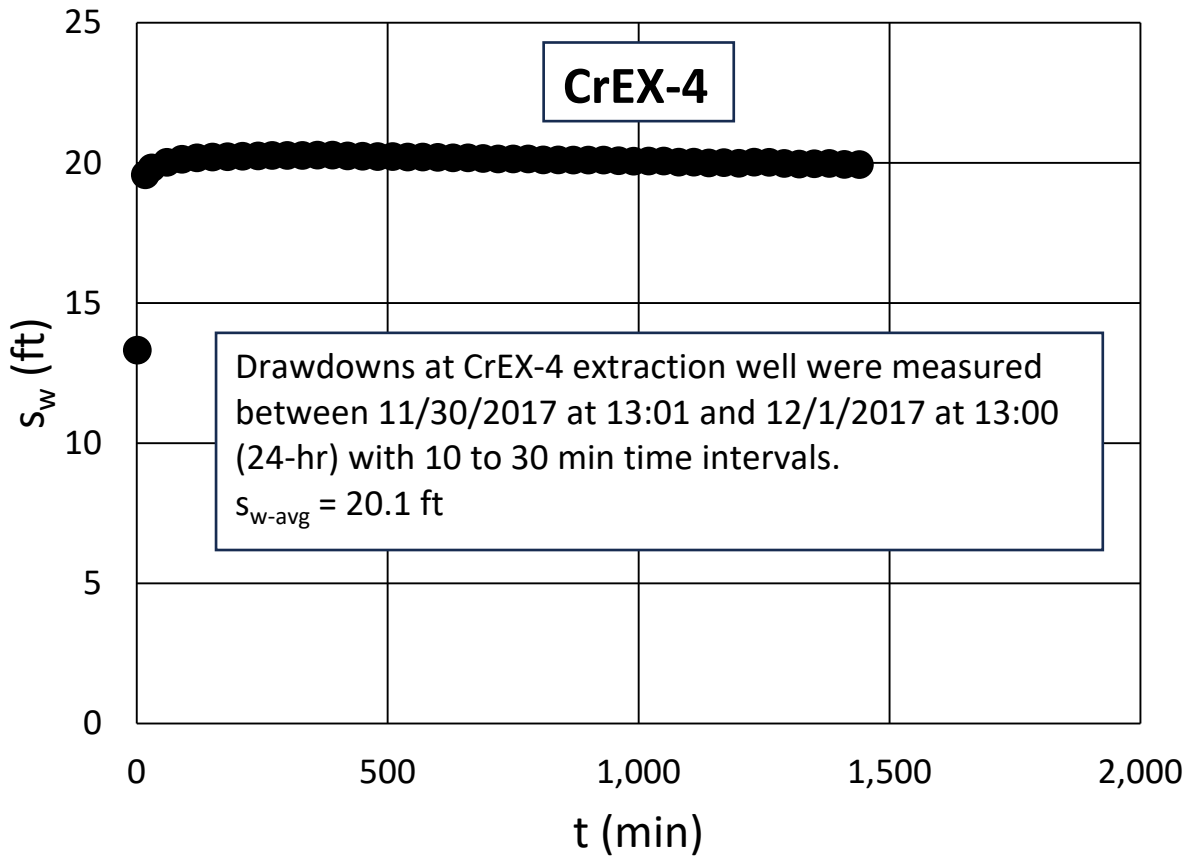


Figure 7. Measured drawdowns at CrEX-4 extraction well.

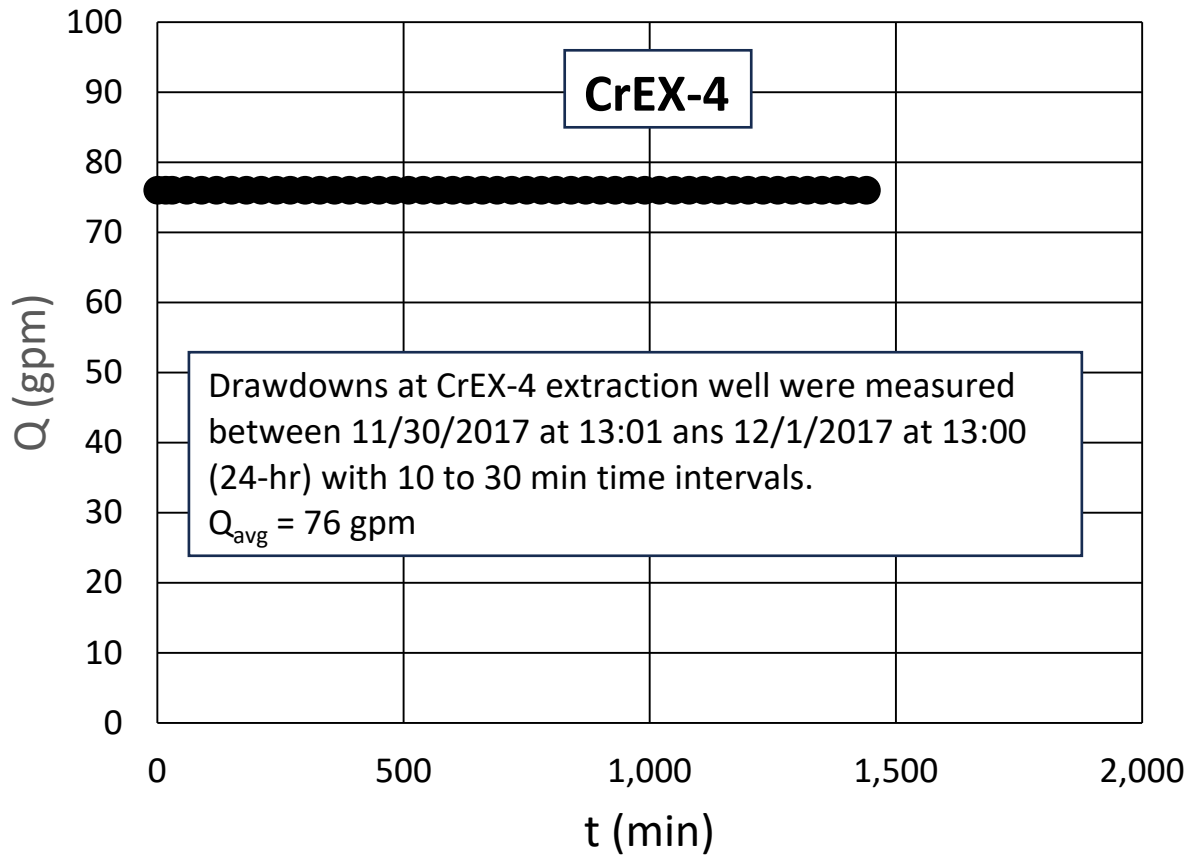


Figure 8. Measured flow rates at CrEX-4 extraction well.

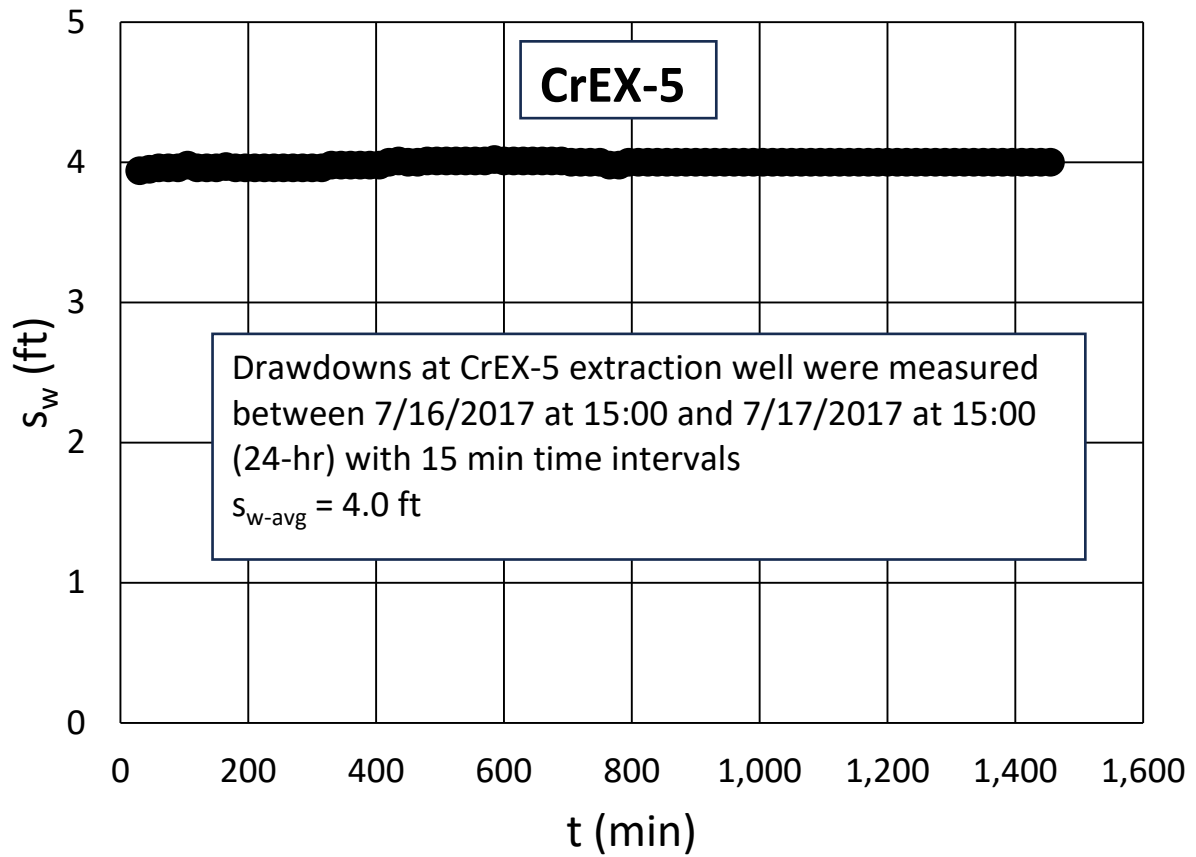


Figure 9. Measured drawdowns at CrEX-5 extraction well.

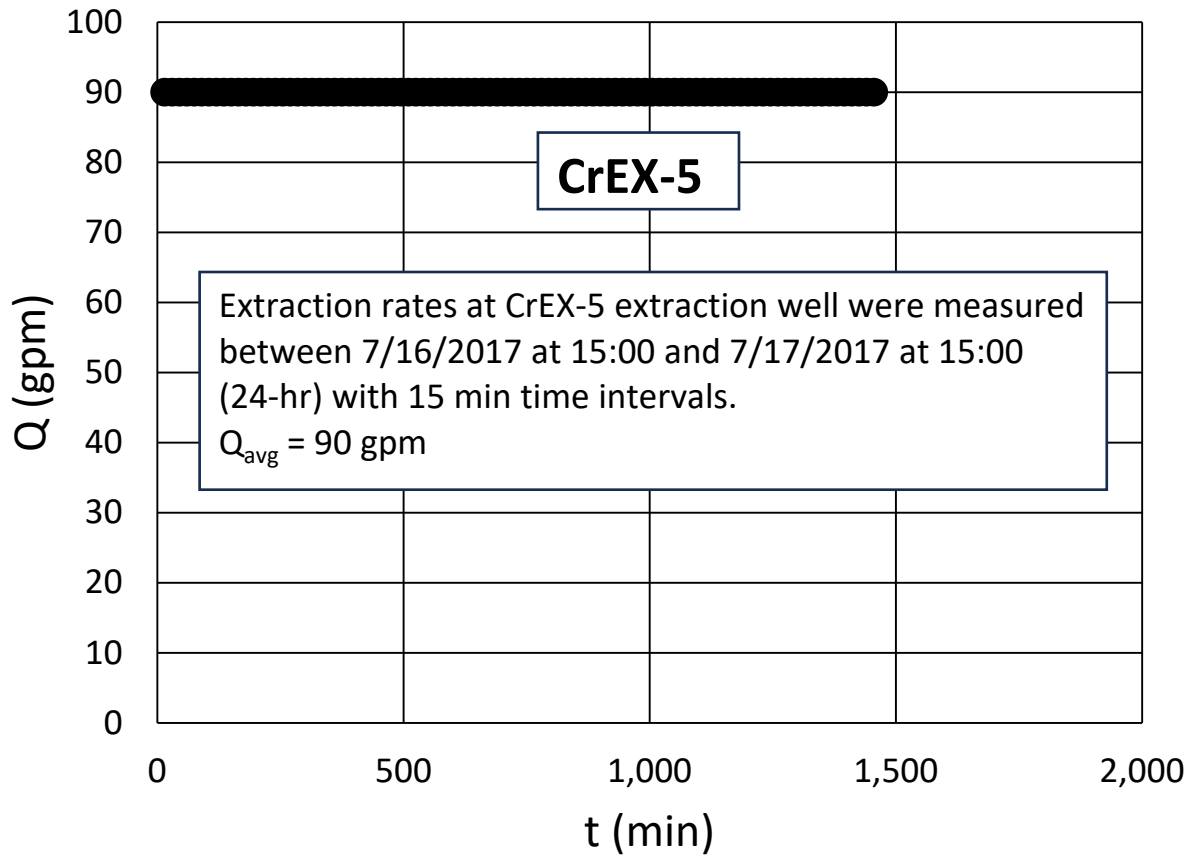


Figure 10. Measured flow rates at CrEX-5 extraction well.

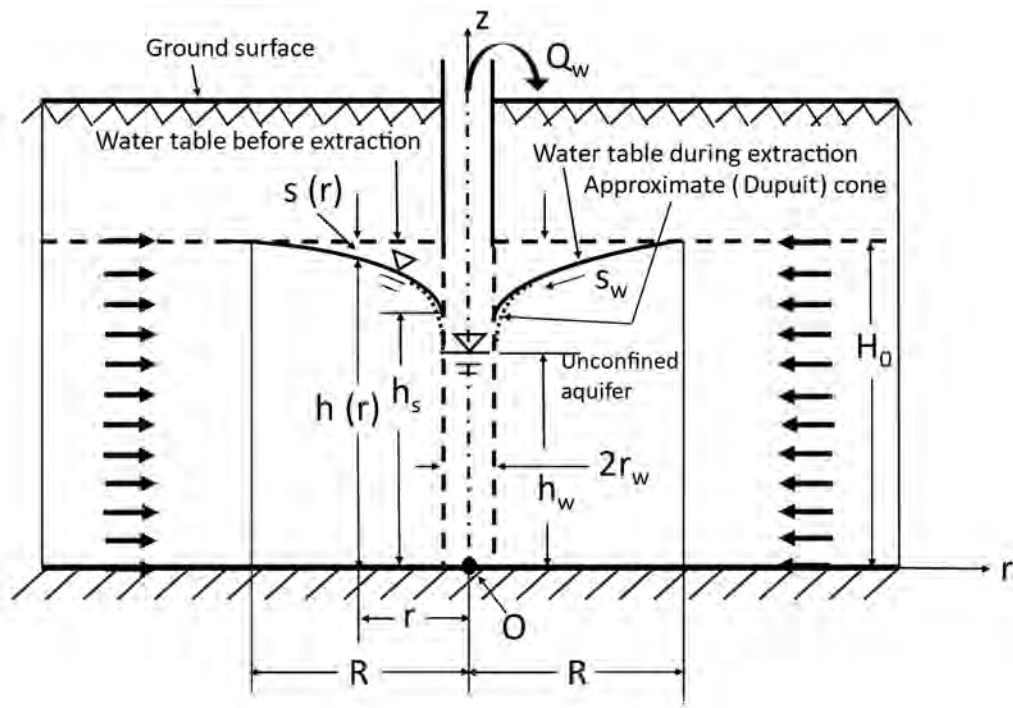


Figure 11. Well in an unconfined aquifer.

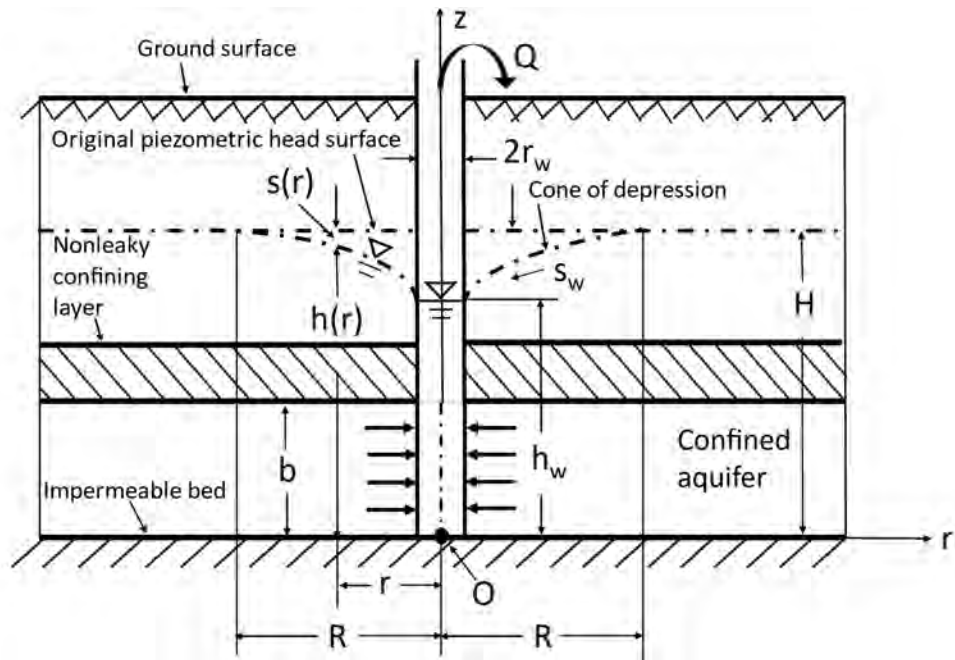


Figure 12. Well in a confined aquifer.

## Tables

Table 1. Determined horizontal hydraulic conductivity ( $K_h$ ) values using the drawdown data at the CrEX extraction wells.

Well ID	$K_h$	
	ft/d	cm/s
CrEX-1	12.5	$4.41 \times 10^{-3}$
CrEX-2	51.0	$1.80 \times 10^{-2}$
CrEX-3	21.5	$7.58 \times 10^{-3}$
CrEX-4	12.5	$4.41 \times 10^{-3}$
CrEX-5	172.0	$6.07 \times 10^{-2}$
<b>Average</b>	<b>53.9</b>	<b><math>1.90 \times 10^{-2}</math></b>



## **Appendices**

## APPENDIX A: DUPUIT-FORCHHEIMER WELL DISCHARGE FORMULA AND DETERMINATION METHOD OF HORIZONTAL HYDRAULIC CONDUCTIVITY

### A.1 DUPUI-FORCHHEIMER SOLUTION FOR UNCONFINED AQUIFERS

#### A.1.1 Problem Definition

The Dupuit-Forchheimer solution for a well in an unconfined aquifer was derived by Dupuit (1863) and Forchheimer (1886) without being ware of each other. And that it is why it is called *Dupuit-Forchheimer well discharge formula* in aquifer hydraulics.

The geometry of the Dupuit-Forchheimer well discharge formula for an unconfined aquifer under steady-state flow conditions is given in Figure 11, which shows that the radial flow to a well fully penetrates a homogeneous and isotropic unconfined aquifer. The initial aquifer thickness is  $H_0$  and the aquifer is assumed to have infinite extent. Its horizontal hydraulic conductivity is  $K_h$ . The constant extraction rate of the well is  $Q_w$ . Under water extraction conditions, a cone of depression is formed and the drawdown at  $r$  distance is

$$s(r) = H_0 - h(r) \quad (\text{A-1})$$

$h(r)$  is the aquifer thickness at distance  $r$ . In Figure 11,  $R$  is the radius of influence beyond which the drawdown is zero. The drawdown at the well is  $s_w$  and the water elevation at the well is  $h_w$  which is based on the Dupuit assumptions (Dupuit, 1864). In Figure 11, based on the Dupuit assumptions, the approximate form of the cone is also shown. In reality, the intersection of the cone of depression with the well edge ( $h_s$ ) is higher than  $h_w$  and an expression for  $(h_s - h_w)$  will be given in Section A.2.

#### A.1.2 Drawdown Solution at the Well

The solution for drawdown at the well was determined by Dupuit (1863) and Forchheimer (1896) and is given as [e.g., Bear 1979, p. 310, Eq. (8-23); Batu, 2024, p. 1095, Eq. (29-258)]

$$H_0^2 - h_w^2 = \frac{Q_w}{\pi K_h} \quad (\text{A-2})$$

which is exactly the same as included in some books [e.g., Bear, 1979, p. 310, Eq. (8-23); Batu, 2024, p. 1095, Eq. (29-258)] with the exception of notation.

From Figure 11, the drawdown at the well is

$$s_w = H_0 - h_w \quad (\text{A-3})$$

Eq. (A-1) can also be written as

$$(H_0 - h_w)(H_0 + h_w) = \frac{Q_w}{\pi K_h} \ln \left( \frac{R}{r_w} \right) \quad (\text{A-4})$$

And with Eq. (A-3) and solving it for  $s_w$ , the drawdown at the well can be determined as

$$s_w = \frac{Q_w}{\pi K_h (H_0 + h_w)} \ln \left( \frac{R}{r_w} \right) \quad (\text{A-5})$$

### A.1.3 Radius of Influence

The radius of influence  $R$  is the distance from the well where drawdown is zero. Since the 1880s, many attempts have been made to relate it to well, aquifer, and flow parameters in both steady and unsteady flow conditions in confined and unconfined aquifers. Some semi-empirical formulas are given in Bear (1979, p. 306). Of these formulas, the one developed by Sichardt is given in Bear [1979, p. 306, Eq. (8-11) as presented in Chertousov (1962)] is widely being used [e.g., De Filippi et al., 2020; Batu, 2024, p. 1088, Eq. (29-249)]:

$$R = 3000 s_w K_h^{\frac{1}{2}} \quad (\text{A-6})$$

in which  $R$  and  $s_w$  are in meters (m), and  $K_h$  in meters per second (m/s).

### A.1.4 Estimation Method of the Horizontal Hydraulic Conductivity

The estimation method is described in Batu (2024, pp. 1097-1099). Substitution of Eq. (A-6) into Eq. (A-5) and solving for  $K_h$ ,

$$K_h = \frac{Q_w}{\pi s_w (H_0 + h_w)} \ln \left( \frac{3000 s_w K_h^{\frac{1}{2}}}{r_w} \right) \quad (\text{A-7})$$

And after some manipulations,

$$K_h = m \left[ \ln(3000) + \frac{1}{2} \ln(K_h) + \ln \left( \frac{s_w}{r_w} \right) \right] \quad (\text{A-8})$$

in which

$$m = \frac{Q_w}{\pi s_w (H_0 + h_w)} \quad (\text{A-9})$$

Eq. (A-8) can also be written as

$$K_h - m \frac{1}{2} \ln(K_h) = m \left[ \ln(3000) + \ln \left( \frac{s_w}{r_w} \right) \right] \quad (\text{A-10})$$

In Eq. (A-10), with the known values of  $Q_w$ ,  $s_w$ ,  $H_0$ ,  $h_w$ , and  $r_w$ , the value of  $K_h$  can be determined with the trial-and-error method. Since the units for Eq. (A-6) for  $R$  are in the metric system, calculations will be made using metric units. Further details for the method can be found in a recent book Batu (2024, pp. 1090-1099).

## A.2 AN APPROXIMATE EXPRESSION FOR $(h_s - h_w)$

Boulton (1951) suggests the relationship

$$h_s - h_w \approx (H_0 - h_w) - 3.75 \frac{Q_w}{2\pi K_h H_0} \quad (\text{A-11})$$

where 3.75 is replaced by 3.5 if  $r_w/H_0$  is of the order 0.25. Eq. (A-11) is also included in Bear [1979, p. 310, Eq. (8-21)].

## APPENDIX B: DETERMINATION OF HORIZONTAL HYDRAULIC CONDUCTIVITY USING THIEM WELL DISCHARGE FORMULA FOR STEADY STATE DRAWDOWN VALUE AT THE WELL

### B.1 FULLY-PENETRATING WELL SOLUTION IN A NONLEAKY CONFINED AQUIFER: THIEM EQUATION

Thiem (1906) was the first to derive the hydraulic head and drawdown solution for a well in a fully penetrating well in a confined aquifer under steady-state conditions and is given by [e.g., Bear, 1979, p. 306, Eq. (8-6); Batu, 2024, p. 187, Eq. (29-246)]

$$h(R) - h(r) = H - h(r) = \frac{Q}{2\pi T} \ln\left(\frac{R}{r}\right) \quad (\text{B-1})$$

The geometry of the Thiem solution is shown in Figure 12.

### B.2 RADIUS OF INFLUENCE

The radius of influence  $R$  is the distance from the well where drawdown is zero. Since the 1880s, many attempts have been made to relate it to well, aquifer, and flow parameters in both steady and unsteady flow conditions in confined and unconfined aquifers. Some semi-empirical formulas are given in Bear (1979, p. 306). Of these formulas, the one developed by Sichardt is given in Bear [1979, p. 306, Eq. (8-11) as presented in Chertousov (1962)] is widely being used [e.g., De Filippi et al., 2020; Batu, 2024, p. 1088, Eq. (29-249)]:

$$R = 3000 s_w K_h^{\frac{1}{2}} \quad (\text{B-2})$$

in which  $R$  and  $s_w$  are in meters (m), and  $K_h$  in meters per second (m/s).

### B.3 ESTIMATION OF THE HORIZONTAL HYDRAULIC CONDUCTIVITY

The method is described in Batu (2024, pp. 1088-1090). Using the measured steady state drawdown  $s_w$  at the well, with Eqs. (B-1), the horizontal hydraulic conductivity  $K_h$  of the aquifer can be estimated. With  $T = K_h b$ , substitution of Eq. (B-2) into Eq. (B-1) and solving for  $K_h$ ,

$$K_h = \frac{Q}{2\pi s_w b} \ln\left(\frac{3000 s_w K_h^{\frac{1}{2}}}{r_w}\right) \quad (\text{B-3})$$

And after some manipulations,

$$K_h = m \left[ \ln(3000) + \frac{1}{2} \ln(K_h) + \ln\left(\frac{s_w}{r_w}\right) \right] \quad (\text{B-4})$$

in which

$$m = \frac{Q}{2\pi s_w b} \quad (\text{B-5})$$

Eq. (B-4) can also be written as

$$K_h - m \frac{1}{2} \ln(K_h) = m [\ln(3,000) + \ln\left(\frac{s_w}{r_w}\right)] \quad (\text{B-6})$$

In Eq. (B-6), with the known values of  $Q$ ,  $s_w$ ,  $b$ , and  $r_w$ , the value of  $K_h$  can be determined with the trial-and-error method. Since the units for Eq. (B-3) for  $R$  are in the metric unit system, calculations must be made using metric units.

## APPENDIX C: DETERMINATION OF HORIZONTAL HYDRAULIC CONDUCTIVITY VALUES USING THE CrEX-1, CrEX-2, CrEX-3, CrEX-4, AND CrEX-5 WELLS STEADY STATE DRAWDOWN VALUES

In this appendix, calculation details of the horizontal hydraulic conductivity determination are presented.

### C.1 DETERMINATION OF HORIZONTAL HYDRAULIC CONDUCTIVITY FROM CrEX-1 DATA

#### C.1.1 Input Data Summary

From Section 2.2 , the input data for CrEX-1 are as follows:

$$s_{w-CrEX-1} = 20.0 \text{ ft} = 6.096 \text{ m}$$

$$\begin{aligned} H_{0-CrEX-1} &= \text{Depth of bottom of screen interval 2} - \text{Depth to water level} \\ &= 1,090 \text{ ft} - 997.2 \text{ ft} = 92.8 \text{ ft} = 28.28544 \text{ m} \end{aligned}$$

$$h_{w-CrEX-1} = H_{0-CrEX-1} - s_{w-CrEX-1} = 92.8 \text{ ft} - 20.0 \text{ ft} = 72.8 \text{ ft} = 22.18944 \text{ m}$$

$$\begin{aligned} &\text{Depth of bottom of screen interval 2} - \text{Depth of top of screen interval 1} \\ &= 1,090 \text{ ft} - 990 \text{ ft} = 100 \text{ ft} = 30.48 \text{ m} > h_{w-CrEX-1} = 72.8 \text{ ft} = 22.18944 \text{ m} \end{aligned}$$

Therefore, the water level in the well interferes with the screen intervals and the Dupuit-Forchheimer well discharge formula must be used.

The radius of the well is

$$r_w = 4 \text{ in} = 0.1016 \text{ m}$$

With

$$1 \text{ gpm} = 0.0000630902 \frac{\text{m}^3}{\text{s}}$$

the extraction rate of CrEX-1 is

$$Q_{CrEX-1} = 95 \text{ gpm} = 95 \frac{\text{gallon}}{\text{day}} = (95 \text{ gpm}) \left( \frac{0.0000630902 \frac{\text{m}^3}{\text{s}}}{\text{gpm}} \right) = 0.00599355 \frac{\text{m}^3}{\text{s}}$$

#### C.1.2 Horizontal Hydraulic Conductivity Determination

The horizontal hydraulic conductivity ( $K_h$ ) will be determined with the trial-and-error method.

From Eq. (A-9),

$$m_{CrEX-1} = \frac{Q_{CrEX-1}}{\pi s_{w-CrEX-1}(H_0 - CrEX-1 + h_{w-CrEX-1})} = \frac{0.00599355 \frac{m^3}{s}}{\pi(6.096 m)(28.28544 m + 22.18944 m)}$$

$$= 0.0000062 \frac{m}{s}$$

From Eq. (A-10),

$$K_h - m_{CrEX-1} \frac{1}{2} \ln(K_h) = m_{CrEX-1} [\ln(3,000) + \ln\left(\frac{s_w - CrEX-1}{r_w}\right)]$$

**Trial 1:**  $K_h = 20 \frac{ft}{d} = 0.000070556 \frac{m}{s}$

$$0.000070556 - (0.0000062) \frac{1}{2} \ln(0.000070556)$$

$$= (0.0000062) [8.006368 + \ln\left(\frac{6.096 m}{0.1016 m}\right)]$$

$$0.000100189 \neq 0.000075024$$

**Trial 2:**  $K_h = 10 \frac{ft}{d} = 0.000035278 \frac{m}{s}$

$$0.000035278 - (0.0000062) \frac{1}{2} \ln(0.000035278)$$

$$= 0.000075024$$

$$0.00006706 \neq 0.000075024$$

**Trial 3:**  $K_h = 15 \frac{ft}{d} = 0.000052917 \frac{m}{s}$

$$0.000052917 - (0.0000062) \frac{1}{2} \ln(0.000052917)$$

$$= 0.000075024$$

$$0.000083442 \neq 0.000075024$$

**Trial 4:**  $K_h = 12 \frac{ft}{d} = 0.000042233 \frac{m}{s}$

$$0.000042233 - (0.0000062) \frac{1}{2} \ln(0.000042233)$$



$$= 0.000075024$$

$$0.00007345 \neq 0.000075024$$

$$\text{Trial 5: } K_h = 13 \frac{ft}{d} = 0.000045861 \frac{m}{s}$$

$$0.000045861 - (0.0000062)^{\frac{1}{2}} \ln(0.000045861)$$

$$= 0.000075024$$

$$0.00007683 \cong 0.000075024$$

$$\text{Trial 6: } K_h = 12.8 \frac{ft}{d} = 0.000045156 \frac{m}{s}$$

$$0.000045156 - (0.0000062)^{\frac{1}{2}} \ln(0.000045156)$$

$$= 0.000075024$$

$$0.000076173 \neq 0.000075024$$

$$\text{Trial 7: } K_h = 12.5 \frac{ft}{d} = 0.000044097 \frac{m}{s}$$

$$0.000044097 - (0.0000062)^{\frac{1}{2}} \ln(0.000044097)$$

$$= 0.000075024$$

$$0.000075187 \cong 0.000075024$$

Therefore,

$$K_h = 12.5 \frac{ft}{d} = 0.000044097 \frac{m}{s} = 0.0044097 \frac{cm}{s} = 4.41 \times 10^{-3} \frac{cm}{s}$$

### C.1.3 Determination of $h_s - h_w$

From Section 2.2, the input data for CrEX-1 are as follows:

$$H_{0-CrEX-1} = \text{Depth of bottom of screen interval 2} - \text{Depth to water level}$$

$$= 1,090 \text{ ft} - 997.2 \text{ ft} = 92.8 \text{ ft} = 28.28544 \text{ m}$$

$$h_{w-CrEX-1} = H_{0-CrEX-1} - s_{w-CrEX-1} = 92.8 \text{ ft} - 20.0 \text{ ft} = 72.8 \text{ ft} = 22.18944 \text{ m}$$

$$Q_{CrEX-1} = 95 \text{ gpm} = 95 \frac{\text{gallon}}{\text{day}} = (95 \text{ gpm}) \left( \frac{0.0000630902 \frac{\text{m}^3}{\text{s}}}{\text{gpm}} \right) = 0.00599355 \frac{\text{m}^3}{\text{s}}$$

$$\frac{r_w}{H_0} = \frac{0.1016 \text{ m}}{28.28544 \text{ m}} = 0.0036 < 0.25$$

With these values, Eq. (A-11) gives

$$h_s - h_w \approx (H_0 - h_w) - 3.75 \frac{Q_w}{2\pi K_h H_0}$$

$$h_s - h_w \approx (28.28544 \text{ m} - 22.18944 \text{ m}) - 3.75 \frac{0.00599355 \frac{\text{m}^3}{\text{s}}}{2\pi(0.000044097 \frac{\text{m}}{\text{s}})(28.28544 \text{ m})} = 3.22 \text{ m}$$

$$h_s = h_w + 3.22 \text{ m} = 22.18944 \text{ m} + 3.22 \text{ m} = 25.41 \text{ m}$$

$$\frac{h_s - h_w}{h_s} = \frac{3.22 \text{ m}}{25.41 \text{ m}} = 0.13$$

## C.2 DETERMINATION OF HORIZONTAL HYDRAULIC CONDUCTIVITY FROM CrEX-2 DATA

### C.2.1 Input Data Summary

From Section 2.3 , the input data for CrEX-2 are as follows:

$$s_{w-CrEX-2} = 11.2 \text{ ft} = 3.41376 \text{ m}$$

$$H_{0-CrEX-2} = \text{Depth of bottom of screen interval} - \text{Depth to water level}$$

$$= 1,179.9 \text{ ft} - 1,113.7 \text{ ft} = 66.2 \text{ ft} = 20.17776 \text{ m}$$

$$h_{w-CrEX-2} = H_{0-CrEX-2} - s_{w-CrEX-2} = 66.2 \text{ ft} - 11.2 \text{ ft} = 55.0 \text{ ft} = 16.764 \text{ m}$$

$$\text{Screen interval} = L = 1,179.9 \text{ ft} - 1,129.9 \text{ ft} = 50 \text{ ft} = 15.24 \text{ m}$$

$$h_{w-CrEX-2} = 55.0 \text{ ft} = 16.764 \text{ ft} > \text{Screen interval} = L = 50 \text{ ft} = 15.24 \text{ m}$$

Therefore, the water level in the well does not interfere with the screen interval and the Thiem equation must be used.

The radius of the well is

$$r_w = 4 \text{ in} = 0.1016 \text{ m}$$

With

$$1 \text{ gpm} = 0.0000630902 \frac{\text{m}^3}{\text{s}}$$

the extraction rate of CrEX-2 is (Figure 4)

$$Q_{CrEX-2} = 65 \text{ gpm} = 65 \frac{\text{gallon}}{\text{day}} = (65 \text{ gpm}) \left( \frac{0.0000630902 \frac{\text{m}^3}{\text{s}}}{\text{gpm}} \right) = 0.00410085 \frac{\text{m}^3}{\text{s}}$$

### **C.2.2 Horizontal Hydraulic Conductivity Determination**

The horizontal hydraulic conductivity ( $K_h$ ) will be determined with the trial-and-error method.

From Eq. (B-5),

$$m_{CrEX-2} = \frac{Q_{CrEX-2}}{2\pi s_w - CrEX-2 L} = \frac{0.00410085 \frac{\text{m}^3}{\text{s}}}{\pi(3.41376 \text{ m})(15.24 \text{ m})} = 0.00002509 \frac{\text{m}}{\text{s}}$$

From Eq. (B-6),

$$K_h - m_{CrEX-2} \frac{1}{2} \ln(K_h) = m_{CrEX-2} [\ln(3,000) + \ln\left(\frac{s_w - CrEX-2}{r_w}\right)]$$

$$\text{Trial 1: } K_h = 20 \frac{\text{ft}}{\text{d}} = 0.000070556 \frac{\text{m}}{\text{s}}$$

$$0.000070556 - (0.00002509) \frac{1}{2} \ln(0.000070556)$$

$$= (0.00002509) [8.006367568 + \ln\left(\frac{3.41376 \text{ m}}{0.1016 \text{ m}}\right)]$$

$$0.000190475 \neq 0.000289059$$

$$\text{Trial 2: } K_h = 30 \frac{\text{ft}}{\text{d}} = 0.000105833 \frac{\text{m}}{\text{s}}$$

$$0.000105833 - (0.00002509) \frac{1}{2} \ln(0.000105833)$$

$$= 0.000289059$$

$$0.000220665 \neq 0.000289059$$

$$\text{Trial 3: } K_h = 35 \frac{\text{ft}}{\text{d}} = 0.000123472 \frac{\text{m}}{\text{s}}$$

$$0.000123472 - (0.00002509) \frac{1}{2} \ln(0.000123472)$$

$$= 0.000289059$$

$$0.000236371 \neq 0.000289059$$

$$\text{Trial 4: } K_h = 52 \frac{ft}{d} = 0.000183444 \frac{m}{s}$$

$$0.000183444 - (0.00002509) \frac{1}{2} \ln(0.000183444)$$

$$= 0.000289059$$

$$0.000291376 \neq 0.000289059$$

$$\text{Trial 5: } K_h = 51 \frac{ft}{d} = 0.000179917 \frac{m}{s}$$

$$0.000179917 - (0.00002509) \frac{1}{2} \ln(0.000179917)$$

$$= 0.000289059$$

$$0.000288093 \cong 0.000289059$$

Therefore,

$$K_h = 51 \frac{ft}{d} = 0.000179917 \frac{m}{s} = 0.0179917 \frac{cm}{s} = 1.80 \times 10^{-2} \frac{cm}{s}$$

### C.3 DETERMINATION OF HORIZONTAL HYDRAULIC CONDUCTIVITY FROM CrEX-3 DATA

#### C.3.1 Input Data Summary

From Section 2.4, the input data for CrEX-3 are as follows:

$$s_{w-CrEX-3} = 11.2 ft = 3.41376 m$$

Then,

$$H_{0-CrEX-3} = \text{Depth of bottom of screen interval} - \text{Depth to water level}$$

$$= 948.8 ft - 898.5 ft = 50.3 ft = 15.33144 m$$

$$h_{w-CrEX-3} = H_{0-CrEX-3} - s_{w-CrEX-3} = 50.3 ft - 11.2 ft = 39.1 ft = 11.91768 m$$

$$h_{w-CrEX-3} = 39.1 \text{ ft} = 11.91768 \text{ ft} < \text{Screen interval} = L = 39.2 \text{ ft} = 11.94816 \text{ m}$$

Therefore, the water level in the well will interfere with the screen interval and the Dupuit-Forchheimer well discharge formula must be used.

The radius of the well is

$$r_w = 4 \text{ in} = 0.1016 \text{ m}$$

With

$$1 \text{ gpm} = 0.0000630902 \frac{\text{m}^3}{\text{s}}$$

the extraction rate of CrEX-3 is (Figure 6)

$$Q_{CrEX-3} = 53 \text{ gpm} = 53 \frac{\text{gallon}}{\text{day}} = (53 \text{ gpm}) \left( \frac{0.0000630902 \frac{\text{m}^3}{\text{s}}}{\text{gpm}} \right) = 0.00334377 \frac{\text{m}^3}{\text{s}}$$

### C.3.2 Horizontal Hydraulic Conductivity Determination

The horizontal hydraulic conductivity ( $K_h$ ) will be determined with the trial-and-error method.

From Eq. (A-9),

$$m_{CrEX-3} = \frac{Q_{CrEX-3}}{\pi s_{w-CrEX-3} (H_{0-CrEX-3} + h_{w-CrEX-3})} = \frac{0.00334377 \frac{\text{m}^3}{\text{s}}}{\pi (3.41376 \text{ m}) (15.33144 \text{ m} + 11.91768 \text{ m})}$$

$$= 0.000011442$$

From Eq. (A-10),

$$K_h - m_{CrEX-3} \frac{1}{2} \ln(K_h) = m_{CrEX-3} [\ln(3,000) + \ln\left(\frac{s_{w-CrEX-3}}{r_w}\right)]$$

$$\text{Trial 1: } K_h = 20 \frac{\text{ft}}{\text{d}} = 0.000070556 \frac{\text{m}}{\text{s}}$$

$$0.000070556 - (0.000011442) \frac{1}{2} \ln(0.000070556)$$

$$= (0.000011442) [8.006367568 + \ln\left(\frac{3.41376 \text{ m}}{0.1016 \text{ m}}\right)]$$

$$0.000125244 \neq 0.000131822$$

**Trial 2:**  $K_h = 25 \frac{ft}{d} = 0.000088195 \frac{m}{s}$

$$0.000088195 - (0.000011442) \frac{1}{2} \ln(0.000088195)$$

$$0.000141606 \neq 0.000131822$$

**Trial 3:**  $K_h = 23 \frac{ft}{d} = 0.000081139 \frac{m}{s}$

$$0.000081139 - (0.000011442) \frac{1}{2} \ln(0.000081139)$$

$$0.000135027 \neq 0.000131822$$

**Trial 4:**  $K_h = 21.5 \frac{ft}{d} = 0.000075847 \frac{m}{s}$

$$0.000075847 - (0.000011442) \frac{1}{2} \ln(0.000075847)$$

$$0.000130121 \cong 0.000131822$$

Therefore,

$$K_h = 21.5 \frac{ft}{d} = 0.000075847 \frac{m}{s} = 0.0075847 \frac{cm}{s} = 7.58 \times 10^{-3} \frac{cm}{s}$$

### C.3.3 Determination of $h_s - h_w$

From Section 2.4, the input data for CrEX-3 are as follows:

$$H_{0-CrEX-3} = \text{Depth of bottom of screen interval} - \text{Depth to water level}$$

$$= 948.8 \text{ ft} - 898.5 \text{ ft} = 50.3 \text{ ft} = 15.33144 \text{ m}$$

$$h_{w-CrEX-3} = H_{0-CrEX-3} - s_{w-CrEX-3} = 50.3 \text{ ft} - 11.2 \text{ ft} = 39.1 \text{ ft} = 11.91768 \text{ m}$$

$$Q_{CrEX-3} = 53 \text{ gpm} = 53 \frac{\text{gallon}}{\text{day}} = (53 \text{ gpm}) \left( \frac{0.0000630902 \frac{m^3}{s}}{\text{gpm}} \right) = 0.00334377 \frac{m^3}{s}$$

$$\frac{r_w}{H_0} = \frac{0.1016 \text{ m}}{15.33144 \text{ m}} = 0.0066 < 0.25$$

With these values, Eq. (A-11) gives

$$h_s - h_w \approx (H_0 - h_w) - 3.75 \frac{Q_w}{2\pi K_h H_0}$$

$$h_s - h_w \approx (15.33144 \text{ m} - 11.91768 \text{ m}) - 3.75 \frac{0.00334377 \frac{\text{m}^3}{\text{s}}}{2\pi(0.000075847 \frac{\text{m}}{\text{s}})(15.33144 \text{ m})} = 1.698 \text{ m}$$

$$h_s = h_w + 1.698 \text{ m} = 11.91768 \text{ m} + 1.698 \text{ m} = 13.62 \text{ m}$$

$$\frac{h_s - h_w}{h_s} = \frac{1.698 \text{ m}}{13.62 \text{ m}} = 0.12$$

## C.4 DETERMINATION OF HORIZONTAL HYDRAULIC CONDUCTIVITY FROM CrEX-4 DATA

### C.4.1 Input Data Summary

From Section 2.5, the input data for CrEX-4 are as follows:

$$s_{w-CrEX-4} = 20.1 \text{ ft} = 6.12648 \text{ m}$$

$$\begin{aligned} H_{0-CrEX-4} &= \text{Depth of bottom of screen interval 2} - \text{Depth to water level} \\ &= 994.9 \text{ ft} - 920.02 \text{ ft} = 74.88 \text{ ft} = 22.8234 \text{ m} \end{aligned}$$

$$h_{w-CrEX-4} = H_{0-CrEX-4} - s_{w-CrEX-4} = 74.88 \text{ ft} - 20.1 \text{ ft} = 54.78 \text{ ft} = 16.6969 \text{ m}$$

$$\text{Depth of bottom of screen interval 2} - \text{Depth of top of screen interval 1}$$

$$= 994.9 \text{ ft} - 929.9 \text{ ft} = 65 \text{ ft} = 19.812 \text{ m} > h_{w-CrEX-4} = 54.78 \text{ ft} = 16.6969 \text{ m}$$

Therefore, the water level in the well interferes with the screen intervals and the Dupuit-Forchheimer well discharge formula must be used.

With

$$1 \text{ gpm} = 0.0000630902 \frac{\text{m}^3}{\text{s}}$$

the extraction rate of CrEX-4 is (Figure 8)

$$Q_{CrEX-4} = 76 \text{ gpm} = 76 \frac{\text{gallon}}{\text{day}} = (76 \text{ gpm}) \left( \frac{0.0000630902 \frac{\text{m}^3}{\text{s}}}{\text{gpm}} \right) = 0.00479484 \frac{\text{m}^3}{\text{s}}$$

### C.4.2 Horizontal Hydraulic Conductivity Determination

The horizontal hydraulic conductivity ( $K_h$ ) will be determined with the trial-and-error method.

From Eq. (A-9),

$$m_{CrEX-4} = \frac{Q_{CrEX-4}}{\pi s_{w-CrEX-4}(H_0 - CrEX-4 + h_{w-CrEX-4})} = \frac{0.00479484 \frac{m^3}{s}}{\pi(6.12648 m)(22.8234 m + 16.6969 m)}$$

$$= 0.000006304 \frac{m}{s}$$

From Eq. (A-10),

$$K_h - m_{CrEX-4} \frac{1}{2} \ln(K_h) = m_{CrEX-4} [\ln(3,000) + \ln\left(\frac{s_{w-CrEX-4}}{r_w}\right)]$$

**Trial 1:**  $K_h = 20 \frac{ft}{d} = 0.000070556 \frac{m}{s}$

$$0.000070556 - (0.000006304) \frac{1}{2} \ln(0.000070556)$$

$$= (0.000006304) [8.006367568 + \ln\left(\frac{6.12648 m}{0.1016 m}\right)]$$

$$0.000100686 \neq 0.000076314$$

**Trial 2:**  $K_h = 10 \frac{ft}{d} = 0.000035278 \frac{m}{s}$

$$0.000035278 - (0.000006304) \frac{1}{2} \ln(0.000035278)$$

$$= 0.000076314$$

$$0.000067593 \neq 0.000076314$$

**Trial 3:**  $K_h = 12 \frac{ft}{d} = 0.000042333 \frac{m}{s}$

$$0.000042333 - (0.000006304) \frac{1}{2} \ln(0.000042333)$$

$$= 0.000076314$$

$$0.000074073 \neq 0.000076314$$

**Trial 4:**  $K_h = 13 \frac{ft}{d} = 0.000045861 \frac{m}{s}$

$$0.000045861 - (0.000006304) \frac{1}{2} \ln(0.000045861)$$

$$= 0.000076314$$



$$0.000077349 \neq 0.000076314$$

$$\text{Trial 5: } K_h = 12.6 \frac{ft}{d} = 0.00004445 \frac{m}{s}$$

$$0.00004445 - (0.000006304) \frac{1}{2} \ln(0.00004445) \\ = 0.000076314$$

$$0.000077037 \neq 0.000076314$$

$$\text{Trial 6: } K_h = 12.5 \frac{ft}{d} = 0.000044097 \frac{m}{s}$$

$$0.000044097 - (0.000006304) \frac{1}{2} \ln(0.000044097) \\ = 0.000076314$$

$$0.000075709 \cong 0.000076314$$

Therefore,

$$K_h = 12.5 \frac{ft}{d} = 0.000044097 \frac{m}{s} = 0.0044097 \frac{cm}{s} = 4.41 \times 10^{-3} \frac{cm}{s}$$

### C.4.3 Determination of $h_s - h_w$

From Section 2.5, the input data for CrEX-4 are as follows:

$$H_{0-CrEX-4} = \text{Depth of bottom of screen interval 2} - \text{Depth to water level} \\ = 994.9 \text{ ft} - 920.02 \text{ ft} = 74.88 \text{ ft} = 22.8234 \text{ m}$$

$$h_{w-CrEX-4} = H_{0-CrEX-4} - s_{w-CrEX-4} = 74.88 \text{ ft} - 20.1 \text{ ft} = 54.78 \text{ ft} = 16.6969 \text{ m}$$

$$Q_{CrEX-4} = 76 \text{ gpm} = 76 \frac{\text{gallon}}{\text{day}} = (76 \text{ gpm}) \left( \frac{0.0000630902 \frac{m^3}{s}}{\text{gpm}} \right) = 0.00479484 \frac{m^3}{s}$$

$$\frac{r_w}{H_0} = \frac{0.1016 \text{ m}}{22.8234 \text{ m}} = 0.0045 < 0.25$$

With these values, Eq. (A-11) gives

$$h_s - h_w \approx (H_0 - h_w) - 3.75 \frac{Q_w}{2\pi K_h H_0}$$

$$h_s - h_w \approx (22.8234 \text{ m} - 16.6969 \text{ m}) - 3.75 \frac{0.00479484 \frac{\text{m}^3}{\text{s}}}{2\pi(0.000044097 \frac{\text{m}}{\text{s}})(22.8234 \text{ m})} = 3.28 \text{ m}$$

$$h_s = h_w + 3.28 \text{ m} = 16.6969 \text{ m} + 3.28 \text{ m} = 19.98 \text{ m}$$

$$\frac{h_s - h_w}{h_s} = \frac{3.28 \text{ m}}{19.98 \text{ m}} = 0.16$$

## C.5 DETERMINATION OF HORIZONTAL HYDRAULIC CONDUCTIVITY FROM CrEX-5 DATA

### C.5.1 Input Data Summary

From Section 2.6, the input data for CrEX-5 are as follows:

$$s_{w-CrEX-5} = 4.0 \text{ ft} = 1.2192 \text{ m}$$

Then,

$$H_{0-CrEX-5} = (1,040.0 \text{ ft} - 966.5 \text{ ft}) \cos(25^\circ) = 66.61 \text{ ft} = 20.30 \text{ m}$$

$$h_{w-CrEX-5} = H_{0-CrEX-5} - s_{w-CrEX-5} = 66.61 \text{ ft} - 4.0 \text{ ft} = 62.61 \text{ ft} = 19.08 \text{ m}$$

$$\text{Vertical screen interval} = L = 54.38 \text{ ft} = 16.58 \text{ m} < h_{w-CrEX-5} = 66.61 \text{ ft} = 19.08 \text{ m}$$

Therefore, the water level in the well does not interfere with the screen interval and the Thiem well discharge formula must be used.

The radius of the well is

$$r_w = 4 \text{ in} = 0.1016 \text{ m}$$

With

$$1 \text{ gpm} = 0.0000630902 \frac{\text{m}^3}{\text{s}}$$

From Figure 10, the extraction rate of CrEX-5 is

$$Q_{CrEX-5} = 90 \text{ gpm} = 90 \frac{\text{gallon}}{\text{day}} = (90 \text{ gpm}) \left( \frac{0.0000630902 \frac{\text{m}^3}{\text{s}}}{\text{gpm}} \right) = 0.0056781 \frac{\text{m}^3}{\text{s}}$$

### C.5.2 Horizontal Hydraulic Conductivity Determination

The horizontal hydraulic conductivity ( $K_h$ ) will be determined with the trial-and-error method.

From Eq. (B-5),

$$m_{CrEX-5} = \frac{Q_{CrEX-5}}{2\pi s_{w-CrEX-5}L} = \frac{0.0056781 \frac{m^3}{s}}{\pi(1.2192 m)(16.58 m)} = 0.000089412 \frac{m}{s}$$

From Eq. (B-6),

$$K_h - m_{CrEX-5} \frac{1}{2} \ln(K_h) = m_{CrEX-5} [\ln(3,000) + \ln\left(\frac{s_{w-CrEX-5}}{r_w}\right)]$$

$$\text{Trial 1: } K_h = 45 \frac{ft}{d} = 0.00015875 \frac{m}{s}$$

$$0.00015875 - (0.000089412) \frac{1}{2} \ln(0.00015875)$$

$$= (0.000089412) [8.006367568 + \ln\left(\frac{1.2192 m}{0.1016 m}\right)]$$

$$0.000549846 \neq 0.000938046$$

$$\text{Trial 2: } K_h = 60 \frac{ft}{d} = 0.000211667 \frac{m}{s}$$

$$0.000211667 - (0.000089412) \frac{1}{2} \ln(0.000211667)$$

$$0.000589902 \neq 0.000938046$$

$$\text{Trial 3: } K_h = 80 \frac{ft}{d} = 0.000282222 \frac{m}{s}$$

$$0.000282222 - (0.000089412) \frac{1}{2} \ln(0.000282222)$$

$$0.000647596 \neq 0.000938046$$

$$\text{Trial 4: } K_h = 120 \frac{ft}{d} = 0.000423333 \frac{m}{s}$$

$$0.000423333 - (0.000089412) \frac{1}{2} \ln(0.000423333)$$

$$0.00077058 \neq 0.000938046$$

$$\text{Trial 5: } K_h = 140 \frac{ft}{d} = 0.000493889 \frac{m}{s}$$

$$0.000493889 - (0.000089412) \frac{1}{2} \ln(0.000493889)$$

$$0.000834245 \neq 0.000938046$$

$$\text{Trial 6: } K_h = 155 \frac{ft}{d} = 0.000546806 \frac{m}{s}$$

$$0.000546806 - (0.000089412) \frac{1}{2} \ln(0.000546806)$$

$$0.000882611 \neq 0.000938046$$

$$\text{Trial 7: } K_h = 158 \frac{ft}{d} = 0.000557389 \frac{m}{s}$$

$$0.000557389 - (0.000089412) \frac{1}{2} \ln(0.000557389)$$

$$0.000892337 \neq 0.000938046$$

$$\text{Trial 8: } K_h = 162 \frac{ft}{d} = 0.0005715 \frac{m}{s}$$

$$0.0005715 - (0.000089412) \frac{1}{2} \ln(0.0005715)$$

$$0.000905331 \neq 0.000938046$$

$$\text{Trial 9: } K_h = 168 \frac{ft}{d} = 0.000592667 \frac{m}{s}$$

$$0.000592667 - (0.000089412) \frac{1}{2} \ln(0.000592667)$$

$$0.000924872 \neq 0.000938046$$

$$\text{Trial 10: } K_h = 172 \frac{ft}{d} = 0.000606778 \frac{m}{s}$$

$$0.000606778 - (0.000089412) \frac{1}{2} \ln(0.000606778)$$

$$0.000937931 \neq 0.000938046$$

Therefore,

$$K_h = 172 \frac{ft}{d} = 0.000606778 \frac{m}{s} = 0.0606778 \frac{cm}{s} = 6.07 \times 10^{-2} \frac{cm}{s}$$

## **ATTACHMENT 3**

**Analyses of Aquifer Test Data for  
PM-2 to Determine Horizontal ( $K_h$ ) and  
Vertical Hydraulic Conductivities ( $K_v$ )**

---

This page intentionally left blank.

## Executive Summary

The purpose of Attachment 3 is to reanalyze the aquifer test data of PM-2 using multiple observation wells and determine especially the values of horizontal hydraulic conductivity ( $K_h$ ) and vertical hydraulic conductivity ( $K_v$ ). The used data are associated with a report entitled “*Analyses of the PM-2 Aquifer Test Using Multiple Observation Wells, LA-14225-MS*” published in 2005 authored by Stephen G. McLin.

The results for the transient drawdown data analyses are given in Table 2. The drawdown data for PM-4 (0.83 ft/d), PM-5 (3.34 ft/d), R-20 Screen 3 (2.84 ft/d), and PM-2 (1.20 ft/d; recovery period) are generally good. And their average  $K_h$  value is 2.05 ft/d ( $7.23 \times 10^{-4}$  cm/s). The anisotropy ratio ( $K_v/K_h$ ) for PM-4, PM-5, and R-20 Screen 3 are 0.035, 0.010, 0.016, respectively. And their average is 0.020. Therefore,  $K_v = 0.041$  ft/d =  $1.45 \times 10^{-5}$  cm/s.

The storage coefficient ( $S$ ) for PM-4, PM-5, and R-20 Screen 3 are  $6.73 \times 10^{-4}$ ,  $1.31 \times 10^{-3}$ ,  $6.54 \times 10^{-3}$ , respectively. And their average is  $2.84 \times 10^{-3}$ . According to the literature, storage coefficients generally vary between 0.00005 and 0.005 (e.g., Freeze and Cherry, 1979, p. 60). And the value 0.00284 is in this range.

The specific yield ( $S_y$ ) values in Table 2 are not reliable. Potential reasons may be (a) the screen intervals are significantly below the water table and (b) the pump test period was not long enough.

The  $K_h$  value determined from the steady-state drawdown value from PM-2 is  $K_h = 2.60$  ft/d =  $9.17 \times 10^{-4}$  cm/s for which the calculation details are given in Appendix A. This value compares favorably with the average value (2.05 ft/d) in Section 6.1.

## Attachment 3 Contents

1.	Purpose.....	1
2.	Aquifer Test Procedure .....	1
3.	Wells Geometry and Initial Water Levels .....	1
4.	Measured Well Drawdowns and Their Interpretations .....	1
4.1	Measured Steady-State Drawdown at the PM-2 Pumped Well.....	1
4.2	Measured Transient Drawdowns at the Observation Wells .....	2
5.	Drawdowns Data Analysis Methods.....	2
5.1	Pumped Well Steady-State Drawdown Data Analysis Method .....	2
5.2	Observation Wells Transient Drawdown Data Analysis Methods .....	3
6.	Results and Discussion.....	3
6.1	Transient Drawdown Data at the Observation Wells and PM-2 Recovery Analyses Results.....	3
6.2	Horizontal Hydraulic Conductivity (Kh) Value Determined from the Steady-State Drawdown Value at the PM-2 Pumped Well .....	4

## Figures

- Figure 1. PM-2 pumped well drawdown versus time.
- Figure 2. PM-4 pumped well drawdown versus time.
- Figure 3. PM-5 pumped well drawdown versus time.
- Figure 4. R-20 Screen 1, Screen 2, and Screen 3 observation well drawdowns vs time.
- Figure 5. R-32 Screen 1, Screen 2, and Screen 3 observation well drawdowns vs time.
- Figure 6. Well in a confined aquifer.

## Tables

- Table 1. Wells geometry and initial water levels.
- Table 2. PM-2 aquifer test data analysis results.

## Appendices

- Appendix A Determination of Horizontal Hydraulic Conductivity Using Thiem Well Discharge Formula for PM-2 Steady State Drawdown Value
- Appendix B AQTESOLV Output for PM-4 Drawdown Analysis
- Appendix C AQTESOLV Output for PM-5 Drawdown Analysis
- Appendix D AQTESOLV Output for R-20 Screen 1 Drawdown Analysis
- Appendix E AQTESOLV Output for R-20 Screen 2 Drawdown Analysis
- Appendix F AQTESOLV Output for R-20 Screen 3 Drawdown Analysis



Appendix G	AQTESOLV Output for R-32 Screen 1 Drawdown Analysis
Appendix H	AQTESOLV Output for R-32 Screen 2 Drawdown Analysis
Appendix I	AQTESOLV Output for R-32 Screen 3 Drawdown Analysis
Appendix J	AQTESOLV Output for PM-2 Recovery Analysis

## 1. Purpose

The purpose of Attachment 3 is to analyze the aquifer test data of PM-2 using multiple observation wells. The test was performed in 2003 and described in a 2005 report entitled “*Analyses of the PM-2 Aquifer Test Using Multiple Observation Wells, LA-14225-MS*” authored by Stephen G. McLin.

## 2. Aquifer Test Procedure

The aquifer test procedure is described as follows (McLin, 2005, pp. 15-16):

*“A traditional aquifer test procedure was followed at well PM-2. This procedure consisted of turning off all surrounding water supply wells and allowing hydrostatic conditions in the aquifer to become reestablished before the start of actual test pumping. This initial nonpumping, or recovery period (i.e., November 5, 2002, to February 3, 2003), was intentionally set at approximately three times the length of the planned pumping interval to ensure near-complete recovery. Then well PM-2 was turned on for 25 days (i.e., February 3–28, 2003), and drawdown was recorded in surrounding wells. Finally, PM-2 was turned off, and this pumping period was followed by a second recovery period that was about as long as the pumping period (i.e., February 28 to March 26, 2003). Data from the second recovery period were used to verify drawdown behavior recorded during the pumping phase of the aquifer test and to verify a return to hydrostatic conditions after pumping stopped. Nearly 45 million gallons of water were produced during the 25-day aquifer test at PM-2. These waters were directed into the Los Alamos County water distribution system for normal consumptive use, an arrangement facilitated by Los Alamos County personnel with the Department of Public Utilities. This procedure represents nearly ideal conditions for a conventional aquifer test. Typically, pumping test waters are discharged directly into the environment because distribution systems are usually unavailable.”*

## 3. Wells Geometry and Initial Water Levels

The wells geometry and initial water levels are given in Table 1. PM-2 was the pumped well with 1,249 gpm extraction rate. The municipal wells PM-4 and PM-5 were used as observation wells. Also R-20 and R-32 (with three screen intervals each) were used as observation wells.

## 4. Measured Well Drawdowns and Their Interpretations

### 4.1 Measured Steady-State Drawdown at the PM-2 Pumped Well

The measured drawdown variation at the PM-2 pumped well is shown in Figure 1 which shows that the drawdown at the well is  $s_w = 85 \text{ ft}$ . As shown in Table 1, the initial head at PM-2 was 869 ft bgs (Below the ground surface). The top elevation of the screen interval is 1,004 ft bgs. Therefore, the distance between the water level and the top elevation of the screen interval is 135 ft. This means that the screen interval does not interfere with the water level under extraction condition because  $s_w = 85 \text{ ft} < 135 \text{ ft}$ . As shown in Figure 1, after 25 d extraction of

water was stopped and after approximately 17.5 d of elapsed time, the water level reached to the original level before extraction.

## 4.2 Measured Transient Drawdowns at the Observation Wells

The measured drawdown variation at the PM-4 observation well is shown in Figure 2. As shown in Table 1, the top elevation of the screen interval is 184.7 ft. Figure 2 indicates that during the 25-d extraction rate period, delayed yield has not occurred due to the potential reasons that (a) the screen interval is not close to the water table and (b) the aquifer is relatively less permeable around PM-4 well.

The measured drawdown variation at the PM-5 observation well is shown in Figure 3. As shown in Table 1, the top elevation of the screen interval is 198.7 ft. Figure 3 indicates that after around 12-d from the beginning of extraction, delayed yield effects started to occur. However, since the extraction rate period was not long enough, the whole delayed drawdown curve had not been developed (e.g., Boulton, 1951, 1954a, 1954b, 1963; Neuman, 1972, 1974, 1975). Under delayed yield effects, the drawdown curve for an observation well has *S*-shape (e.g., Batu, 1998, p. 461, Figure 9-2).

The measured drawdown variations at the R-20 S1, R-20 S2, and R-20 S3 observation wells are shown in Figure 4. As shown in Table 1, the distances between the water levels and the top elevation of the three screen intervals are 79.3 ft, 317.6 ft, and 479.1 ft, respectively. Figure 4 indicates that during the 25-d extraction rate period, delayed yield has not occurred due to the potential reasons that (a) the screen interval is not close to the water table and (b) the aquifer is relatively less permeable around R-20 observation well.

The measured drawdown variations at the R-32 S1, R-32 S2, and R-32 S3 observation wells are shown in Figure 5. As shown in Table 1, the distances between the water levels and the top elevation of the three screen intervals are 88.8 ft, 146.2 ft, and 185.2 ft, respectively. Figure 5 indicates that during the 25-d extraction rate period, delayed yield has not occurred due to the potential reasons that (a) the screen interval is not close to the water table and (b) the aquifer is relatively less permeable around R-32 observation well.

## 5. Drawdowns Data Analysis Methods

### 5.1 Pumped Well Steady-State Drawdown Data Analysis Method

As mentioned in Section 4.1, the measured drawdown variation at the PM-2 pumped well is shown in Figure 1 which shows that the drawdown at the well is  $s_w = 85 \text{ ft}$ . As shown in Table 1, the distance between the water level and the top elevation of the screen interval is 135 ft. This means that the screen interval does not interfere with the with the water level under extraction condition because  $s_w = 85 \text{ ft} < 135 \text{ ft}$ . With the steady-state drawdown at a pumped well, only the horizontal hydraulic conductivity ( $K_h$ ) can be determined. And the *Thiem well discharge formula* (Thiem, 1906) as given by Eq. (A-1) is the appropriate equation for the determination of the value of  $K_h$ . Further details about the method as well as calculation details

for the determination of  $K_h$  are given in Appendix A. The geometry of the Thiem formula is shown in Figure 6.

## 5.2 Observation Wells Transient Drawdown Data Analysis Methods

The drawdown data at the 4 observation wells and recovery data at the PM-2 pumped well have been analyzed with the Neuman type-curve method (Neuman, 1974, 1975) with the Version 4.5 of the AQTESOLV software (HydroSOLVE, Inc., 2023).

The AQTESOLV output for the PM-4 drawdown data is given in Appendix B.

The AQTESOLV output for the PM-5 drawdown data is given in Appendix C.

The AQTESOLV outputs for the R-20 Screen 1, R-20 Screen 2, and R-20 Screen 3 drawdown data are given in Appendix D, Appendix E, and Appendix F, respectively.

The AQTESOLV outputs for the R-32 Screen 1, R-32 Screen 2, and R-32 Screen 3 drawdown data are given in Appendix G, Appendix H, and Appendix I, respectively.

The AQTESOLV output for the PM-2 recovery data is given in Appendix J.

## 6. Results and Discussion

### 6.1 Transient Drawdown Data at the Observation Wells and PM-2 Recovery Analyses Results

The results for the transient drawdown data analyses results are given in Table 2. The drawdown data for PM-4 (0.83 ft/d), PM-5 (3.34 ft/d), R-20 Screen 3 (2.84 ft/d), and PM-2 (1.20 ft/d) recovery are generally good. The values in the parentheses are the  $K_h$  values. And their average  $K_h$  value is 2.05 ft/d ( $7.23 \times 10^{-4}$  cm/s). The anisotropy ratio ( $K_v/K_h$ ) for PM-4, PM-5, and R-20 Screen 3 are 0.035, 0.010, 0.016, respectively. And their average is 0.020. Therefore,  $K_v = 0.041$  ft/d =  $1.45 \times 10^{-5}$  cm/s.

The storage coefficient ( $S$ ) for PM-4, PM-5, and R-20 Screen 3 are  $6.73 \times 10^{-4}$ ,  $1.31 \times 10^{-3}$ ,  $6.54 \times 10^{-3}$  respectively. And their average is  $2.84 \times 10^{-3}$ . According to the literature, storage coefficients generally vary between 0.00005 and 0.005 (e.g., Freeze and Cherry, 1979, p. 60). And the value 0.00284 is in this range.

The specific yield ( $S_y$ ) values in Table 2 are not reliable. Potential reasons may be (a) the screen intervals are significantly below the water table; (b) the aquifer is relatively less permeable; and the pump test period was not long enough.

## 6.2 Horizontal Hydraulic Conductivity ( $K_h$ ) Value Determined from the Steady-State Drawdown Value at the PM-2 Pumped Well

The  $K_h$  value determined from the steady-state drawdown value of PM-2 is  $K_h = 2.60 \text{ ft/d} = 9.17 \times 10^{-4} \text{ cm/s}$  for which the calculation details are given in Appendix A. This value compares favorably with the  $K_h = 1.20 \text{ ft/d} = 4.23 \times 10^{-4} \text{ cm/s}$  in Table 2 determined from the PM-2 recovery analysis. The  $K_h = 2.60 \text{ ft/d}$  steady-state drawdown value is even closer to the average  $K_h = 2.05 \text{ ft/d}$  given in Section 6.1.

## References

- Batu, V., *Aquifer Hydraulics: A Comprehensive Guide to Hydrogeologic Data Analysis*, John Wiley & Sons, Inc., New York, 727 pp., 1998.
- Batu, V., *Fluid Mechanics and Hydraulics: Illustrative Worked Examples of Surface and Subsurface Flows*, Taylor & Francis CRC Press, 1,240 pp., Boca Raton, Florida, 2024.
- Bear, J., *Hydraulics of Groundwater*, McGraw-Hill Inc., 569 pp., New York, 1979.
- Boulton, N.S., "The Flow Pattern Near a Gravity Well in a Uniform Water Bearing Medium," *Journal of the Institution of Civil Engineers*, London, Great Britain, Vol. 36, pp. 534-550, December, 1951.
- Boulton, N.S., "The Drawdown of the Water-Table Under Non-Steady Conditions Near a Pumped Well in an Unconfined Formation," *Journal of the Institution of Civil Engineers*, London, Great Britain, Part III, pp. 564-579, December, 1954a.
- Boulton, N.S., "Unsteady Radial Flow to a Pumped Well Allowing Delayed Yield from Storage," *International Association of Scientific Hydrology*, London, Great Britain, Vol. II, pp. 472-477, 1954b.
- Boulton, N.S., "Unsteady Radial Flow to a Pumped Well Allowing Delayed Yield from Storage," *International Association of Scientific Hydrology*, London, Great Britain, Vol. 26 pp. 469-482, December, 1963.
- Chertousov, M.D., *Hydraulics* (in Russian), Gosenergouzdat, 630 pp., Moscow, Russia, 1962.
- HydroSOLVE, Inc., AQTESOLV: Advanced Aquifer Test Analysis Software, v4.5., Reston, Virginia, 2023.
- Freeze, R.A., And J.A. Cherry, *Groundwater*, Prentice-Hall, Inc., Englewood Cliffs, New Jersey, 604, pp., 1979.
- McLin, S.G., "Analysis of the PM-2 Aquifer Test Using Multiple Observation Wells, LA-14225-MS, Los Alamos National Laboratory," Los Alamos, New Mexico, July, 2005.

Neuman, S.P., 'Effect of Partial Penetration on Flow in Unconfined Aquifers Considering Delayed Gravity Response,' *Water Resources Research*, Vol. 10, No.2, pp. 303-312, April, 1974.

Neuman, S.P., "Analysis of Pumping Test Data From Anisotropic Unconfined Aquifers Considering Delayed Gravity Response," *Water Resources Research*, Vol. 11, No. 2, pp. 329-342, April, 1975.

Neuman, S.P., "Theory of Flow in Unconfined Aquifers Considering Delayed Response of the Water Table," *Water Resources Research*, Vol. 8, No. 4, pp. 1031-1045, August, 1972.

Thiem, G., *Hydrologische Methoden* (in German), J.M. Gebhardt, Leipzig, Germany, 56 pp., 1906.

## Figures

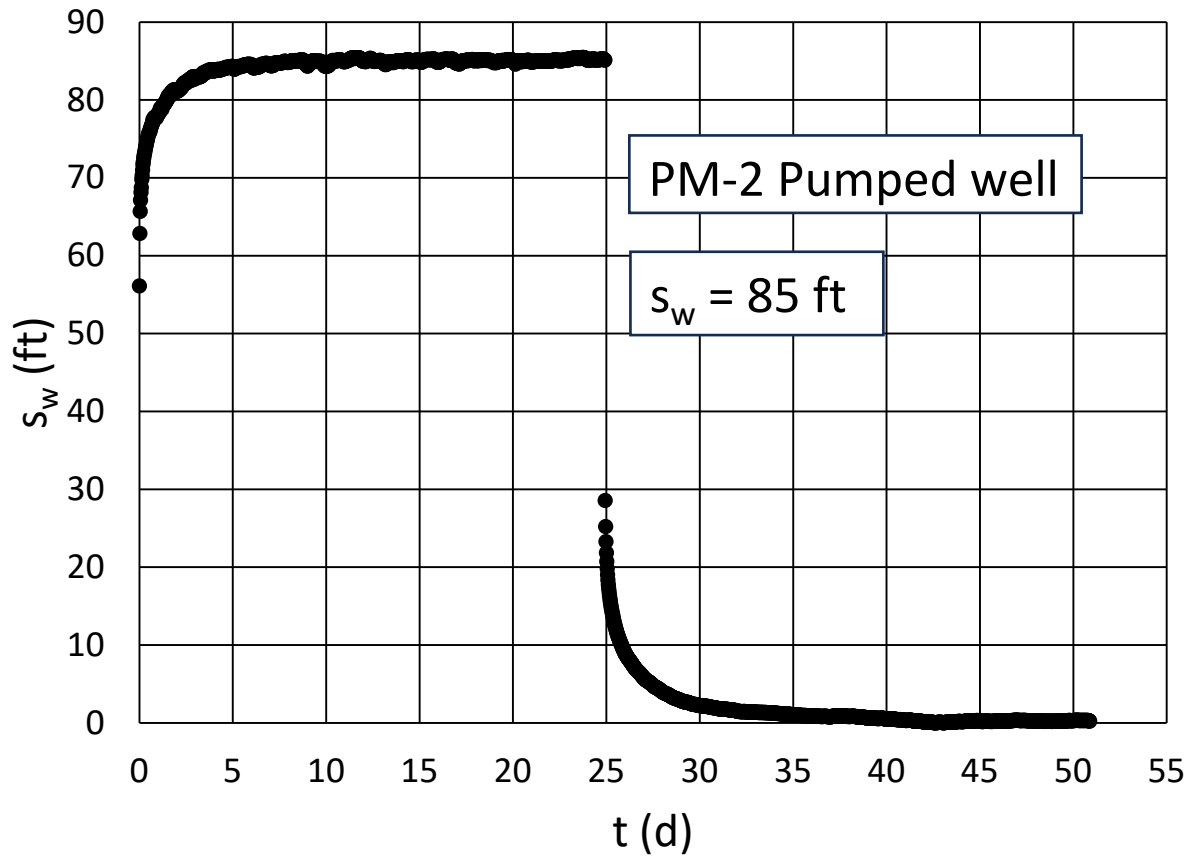


Figure 1. PM-2 pumped well drawdown versus time.



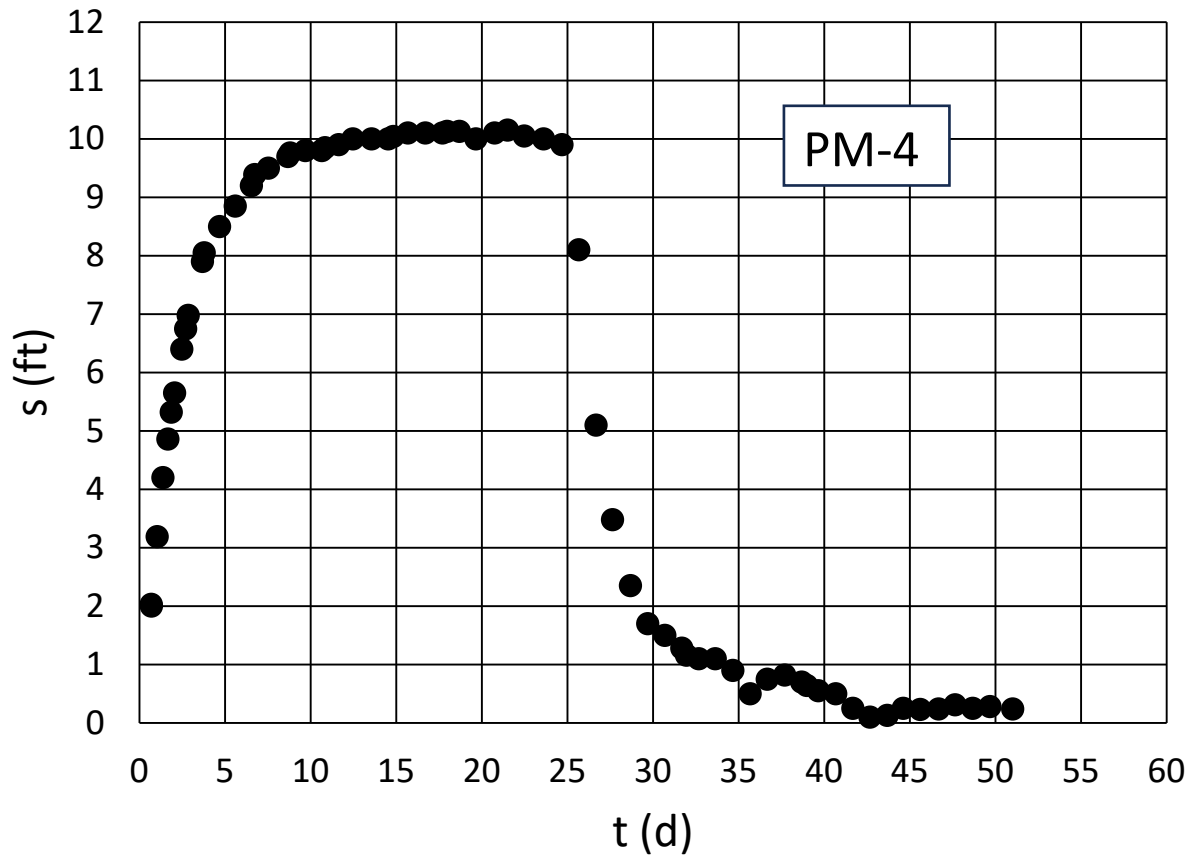


Figure 2. PM-4 observation well drawdown versus time.

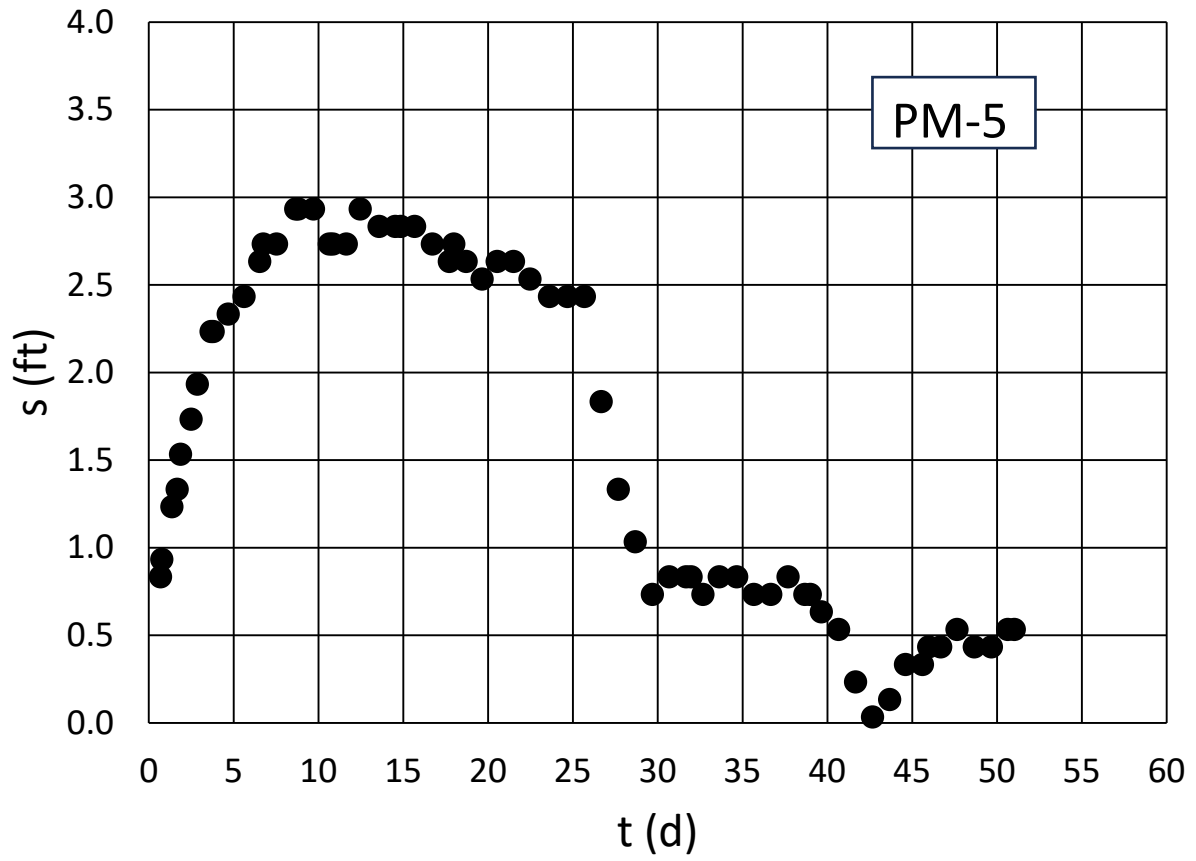


Figure 3. PM-5 observation well drawdown versus time.

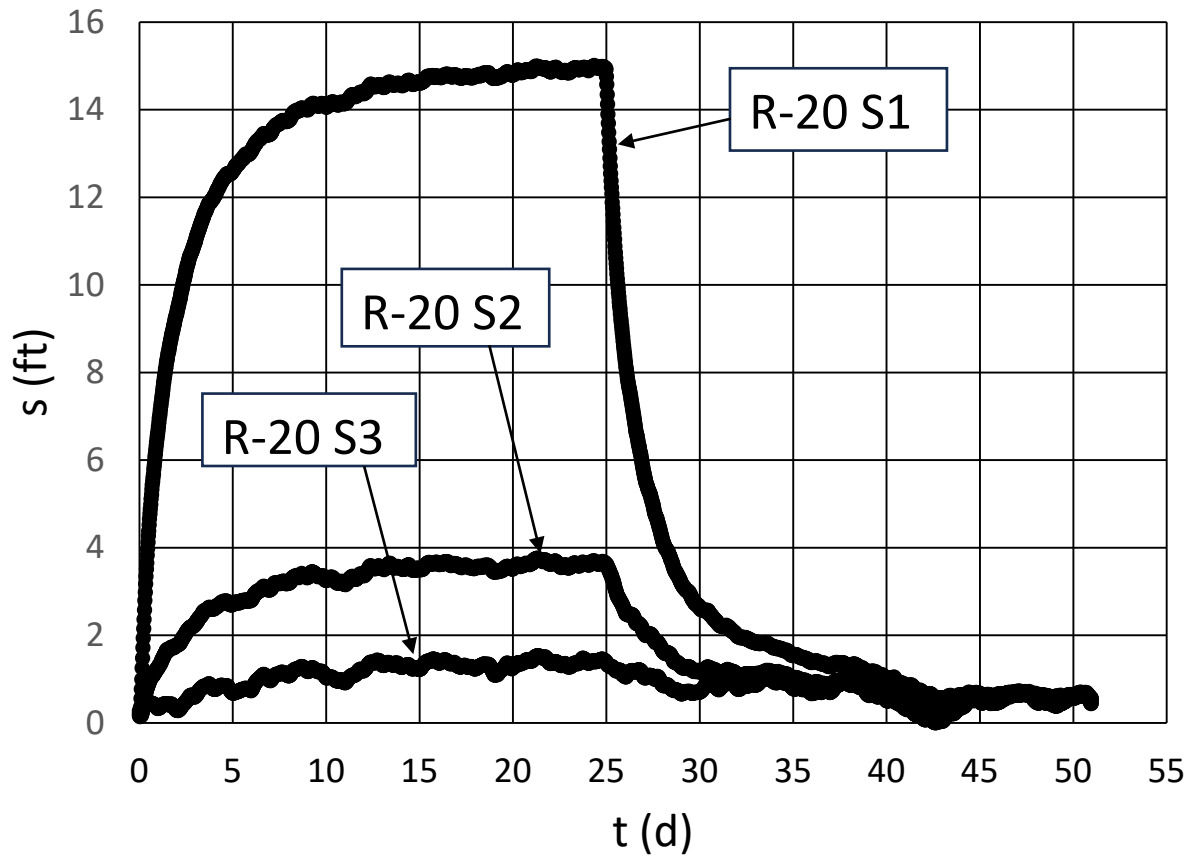


Figure 4. R-20 Screen 1, Screen 2, and Screen 3 observation well drawdowns versus time.

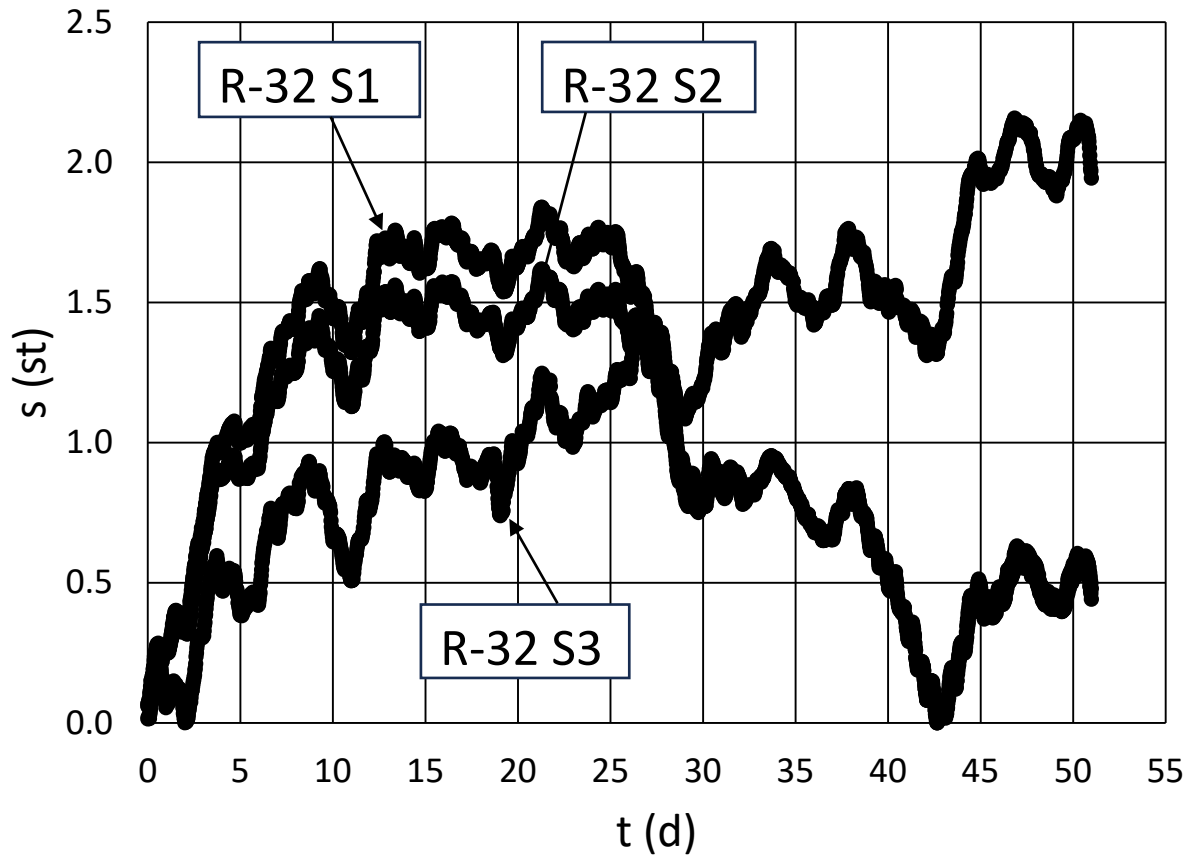


Figure 5. R-32 Screen 1, Screen 2, and Screen 3 observation well drawdowns versus time.

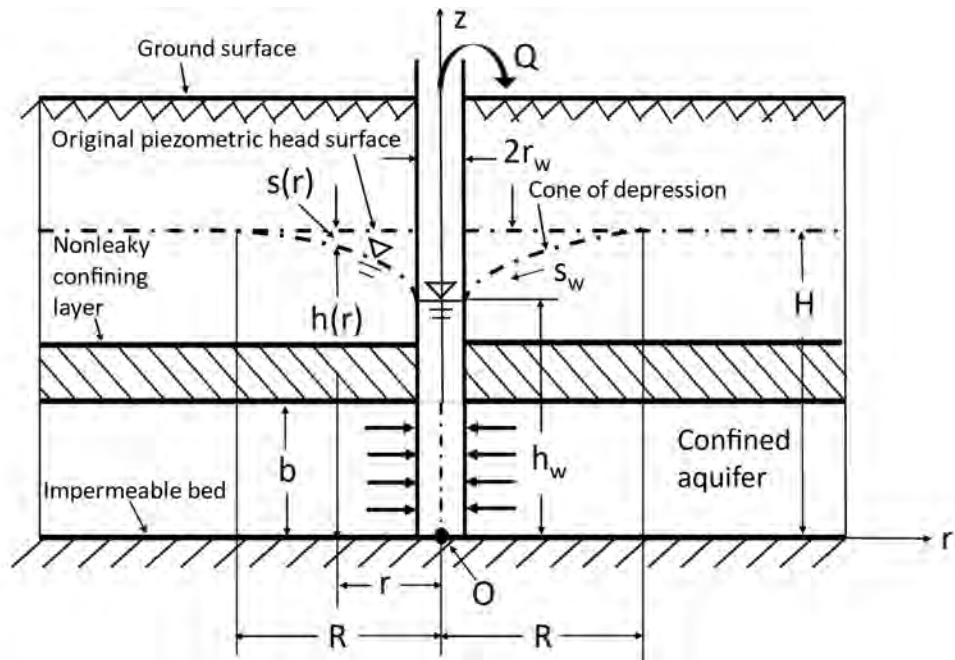


Figure 6. Well in a confined aquifer.

## Tables

Table 1. Wells geometry and initial water levels.

Well	Distance r (ft)	Water Level (ft bgs)	Top of screen (ft bgs)	Bottom of screen (ft bgs)	Screen Length L (ft)	Depth to screen from water table d (ft)	Inside radius of well casing $r_c$ (ft)	Radius of well $r_w$ (ft)
PM-2	-	869	1004	2280	1276	135	0.5833	1.0000
PM-4	4478	1075.3	1260	2854	1594	184.7	0.6667	1.0833
PM-5	8808	1241.3	1440	3072	1632	198.7	0.6667	1.0833
R20-1	1225	825.3	904.6	912.2	7.6	79.3	0.1875	0.2083
R20-2	1225	829.5	1147.1	1154.7	7.6	317.6	0.1875	0.2083
R20-3	1225	849.7	1328.8	1336.5	7.7	479.1	0.1875	0.2083
R32-1	4779	778.7	867.5	875.2	7.7	88.8	0.1875	0.2083
R32-2	4779	785.6	931.8	934.9	3.1	146.2	0.1875	0.2083
R32-3	4779	787.7	972.9	980.6	7.7	185.2	0.1875	0.2083

bgs: Below the ground surface

Source: Table 1 and Figures 5-9 of McLin (2005).

Table 2. PM-2 aquifer test data analysis results.

<b>Well</b>	<b>r (ft)</b>	<b>T (ft<sup>2</sup>/d)</b>	<b>S</b>	<b>S<sub>y</sub></b>	<b>β</b>	<b>b (ft)</b>	<b>K<sub>h</sub> (ft/d)</b>	<b>K<sub>v</sub>/K<sub>h</sub></b>
PM-4	4478	4139.5	6.73E-04	0.5 <sup>a</sup>	0.02846	5000	0.83	0.035
PM-5	8808	16710	1.31E-03	0.5 <sup>a</sup>	0.03086	5000	3.34	0.010
R-20 Screen 1	1225	13930	2.86E-03	0.20750	0.03000	5000	2.79	0.500
R-20 Screen 2	1225	47590	2.68E-02	0.5 <sup>a</sup>	0.00100	5000	9.52	0.017
R-20 Screen 3	1225	14220	6.54E-03	0.5 <sup>a</sup>	0.00094	5000	2.84	0.016
R32 Screen 1	4779	16410	3.06E-04	0.01603	0.06000	5000	3.28	0.066
R32 Screen 2	4779	99550	1.33E-03	0.00093	0.03000	5000	19.91	0.033
R32 Screen 3	4779	80890	2.51E-03	0.00079	0.03000	5000	16.18	0.033
PM-2 recovery	-	5996.4	3.87E-03	0.5 <sup>a</sup>	0.00024	5000	1.20	

<sup>a</sup>Upper bound value for S<sub>y</sub> during matching was 0.5 (AQTESOLV default).



## **Appendices**

## APPENDIX A: DETERMINATION OF HORIZONTAL HYDRAULIC CONDUCTIVITY USING THIEM WELL DISCHARGE FORMULA FOR PM-2 STEADY STATE DRAWDOWN VALUE

### A.1 Fully Penetrating Well Solution in a Nonleaky Confined Aquifer: Thiem Equation

Thiem (1906) was the first to derive the hydraulic head and drawdown solution for a well in a fully penetrating well in a confined aquifer under steady state conditions and is given by [e.g., Bear, 1979, p. 306, Eq. (8-6); Batu, 2024, p. 187, Eq. (29-246)]

$$h(R) - h(r) = H - h(r) = \frac{Q}{2\pi T} \ln\left(\frac{R}{r}\right) \quad (\text{A-1})$$

The geometry of the Thiem solution is shown in Figure 6.

### A.2 Radius of Influence

The radius of influence  $R$  is the distance from the well where drawdown is zero. Since the 1880s, many attempts have been made to relate it to well, aquifer, and flow parameters in both steady and unsteady flow conditions in confined and unconfined aquifers. Some semi-empirical formulas are given in Bear (1979, p. 306). Of these formulas, the one developed by Sichardt is given in Bear [1979, p. 306, Eq. (8-11) as presented in Chertousov (1962)] is widely being used [e.g., De Filippi et al., 2020; Batu, 2024, p. 1088, Eq. (29-249)]:

$$R = 3000 s_w K_h^{\frac{1}{2}} \quad (\text{A-2})$$

in which  $R$  and  $s_w$  are in meters (m), and  $K_h$  in meters per second (m/s).

### A.3 Estimation of the Horizontal Hydraulic Conductivity with the PM-2 Drawdown

The method is described in Batu (2024, pp. 1088-1090). Using the measured steady state drawdown  $s_w$  at the well, with Eqs. (A-1), the horizontal hydraulic conductivity  $K_h$  of the aquifer can be estimated. With  $T = K_h b$ , substitution of Eq. (A-2) into Eq. (29-242) and solving for  $K_h$ ,

$$K_h = \frac{Q}{2\pi s_w b} \ln\left(\frac{3000 s_w K_h^{\frac{1}{2}}}{r_w}\right) \quad (\text{A-3})$$

And after some manipulations,

$$K_h = m \left[ \ln(3000) + \frac{1}{2} \ln(K_h) + \ln\left(\frac{s_w}{r_w}\right) \right] \quad (\text{A-4})$$

in which

$$m = \frac{Q}{2\pi s_w b} \quad (\text{A-5})$$

Eq. (A-4) can also be written as

$$K_h - m \frac{1}{2} \ln(K_h) = m [\ln(3,000) + \ln\left(\frac{s_w}{r_w}\right)] \quad (\text{A-6})$$

In Eq. (A-6), with the known values of  $Q$ ,  $s_w$ ,  $b$ , and  $r_w$ , the value of  $K_h$  can be determined with the trial-and-error method. Since the units for Eq. (A-3) for  $R$  are in the metric unit system, calculations must be made using metric units.

The relevant PM-2 data are as follows:

$$b = 2,280 \text{ ft} - 1,004 \text{ ft} = 1,276 \text{ ft} = 388.92 \text{ m} \quad (\text{McLin, 2005, p.11, Figure 7})$$

$$s_w = 85.0 \text{ ft} = 25.908 \text{ m} \quad (\text{From Figure 1})$$

$$2r_c = 2r_w = 14 \text{ in} = 1.1667 \text{ ft} = 0.3556 \text{ m} \quad (\text{McLin, 2005, p.11, Figure 7})$$

$$r_w = 0.5833 \text{ ft} = 0.1778 \text{ m}$$

$$Q = 1249 \text{ gpm} \quad (\text{p. 16}) \quad (\text{McLin, 2005, p.16})$$

$$1 \text{ gpm} = 0.0000630902 \frac{\text{m}^3}{\text{s}}$$

$$Q = 1,249.0 \text{ gpm} = 1,249.0 \frac{\text{gallon}}{\text{day}} = (1,249.0 \text{ gpm}) \left( \frac{0.0000630902 \frac{\text{m}^3}{\text{s}}}{\text{gpm}} \right) = 0.07879941 \frac{\text{m}^3}{\text{s}}$$

From Eq. (A-5),

$$m = \frac{Q}{2\pi s_w b} = \frac{(0.07879941 \frac{\text{m}^3}{\text{s}})}{2\pi(25.908 \text{ m})(388.92 \text{ m})} = 0.000001245 \text{ s}^{-1}$$

$$\text{Trial 1: } K_h = 50 \text{ ft/d} = 0.000176389 \text{ m/s}$$

From Eq. (A-6),

$$K_h - m \frac{1}{2} \ln(K_h) = m [\ln(3,000) + \ln\left(\frac{s_w}{r_w}\right)]$$

$$0.000176389 - (0.000001245) \frac{1}{2} \ln(0.000176389)$$

$$= (0.000001245) [\ln(3,000) + \ln\left(\frac{25.908}{0.1778}\right)]$$

$$0.000181769 \neq 0.00001617$$

$$\text{Trial 2: } K_h = 30 \text{ ft/d} = 0.000105833 \text{ m/s}$$

From Eq. (A-6),

$$K_h - m \frac{1}{2} \ln(K_h) = m[\ln(3,000) + \ln\left(\frac{s_w}{r_w}\right)]$$

$$0.000105833 - (0.000001245) \frac{1}{2} \ln(0.000105833)$$

$$0.000111531 \neq 0.00001617$$

**Trial 3:  $K_h = 15 \text{ ft/d} = 0.000052917 \text{ m/s}$**

From Eq. (A-6),

$$K_h - m \frac{1}{2} \ln(K_h) = m[\ln(3,000) + \ln\left(\frac{s_w}{r_w}\right)]$$

$$0.000052917 - (0.000001245) \frac{1}{2} \ln(0.000052917)$$

$$0.000059047 \neq 0.00001617$$

**Trial 4:  $K_h = 5 \text{ ft/d} = 0.000017639 \text{ m/s}$**

From Eq. (A-6),

$$K_h - m \frac{1}{2} \ln(K_h) = m[\ln(3,000) + \ln\left(\frac{s_w}{r_w}\right)]$$

$$0.000017639 - (0.000001245) \frac{1}{2} \ln(0.000017639)$$

$$0.000024183 \neq 0.00001617$$

**Trial 5:  $K_h = 4 \text{ ft/d} = 0.000014111 \text{ m/s}$**

From Eq. (A-6),

$$K_h - m \frac{1}{2} \ln(K_h) = m[\ln(3,000) + \ln\left(\frac{s_w}{r_w}\right)]$$

$$0.000014111 - (0.000001245) \frac{1}{2} \ln(0.000014111)$$

$$0.000021063 \neq 0.00001617$$

**Trial 6:  $K_h = 2 \text{ ft/d} = 0.000007056 \text{ m/s}$**

From Eq. (A-6),

$$K_h - m \frac{1}{2} \ln(K_h) = m[\ln(3,000) + \ln\left(\frac{s_w}{r_w}\right)]$$

$$0.000007056 - (0.000001245) \frac{1}{2} \ln(0.000007056)$$

$$0.00001444 \neq 0.00001617$$

$$\text{Trial 7: } K_h = 3 \text{ ft/d} = 0.000010583 \text{ m/s}$$

From Eq. (A-6),

$$K_h - m \frac{1}{2} \ln(K_h) = m [\ln(3,000) + \ln\left(\frac{s_w}{r_w}\right)]$$

$$0.000010583 - (0.000001245) \frac{1}{2} \ln(0.000010583)$$

$$0.000017715 \cong 0.00001617$$

$$\text{Trial 8: } K_h = 2.8 \text{ ft/d} = 0.000009878 \text{ m/s}$$

From Eq. (A-6),

$$K_h - m \frac{1}{2} \ln(K_h) = m [\ln(3,000) + \ln\left(\frac{s_w}{r_w}\right)]$$

$$0.000009878 - (0.000001245) \frac{1}{2} \ln(0.000009878)$$

$$0.000017052 \cong 0.00001617$$

$$\text{Trial 9: } K_h = 2.6 \text{ ft/d} = 0.000009172 \text{ m/s}$$

From Eq. (29-253),

$$K_h - m \frac{1}{2} \ln(K_h) = m [\ln(3,000) + \ln\left(\frac{s_w}{r_w}\right)]$$

$$0.000009172 - (0.000001245) \frac{1}{2} \ln(0.000009172)$$

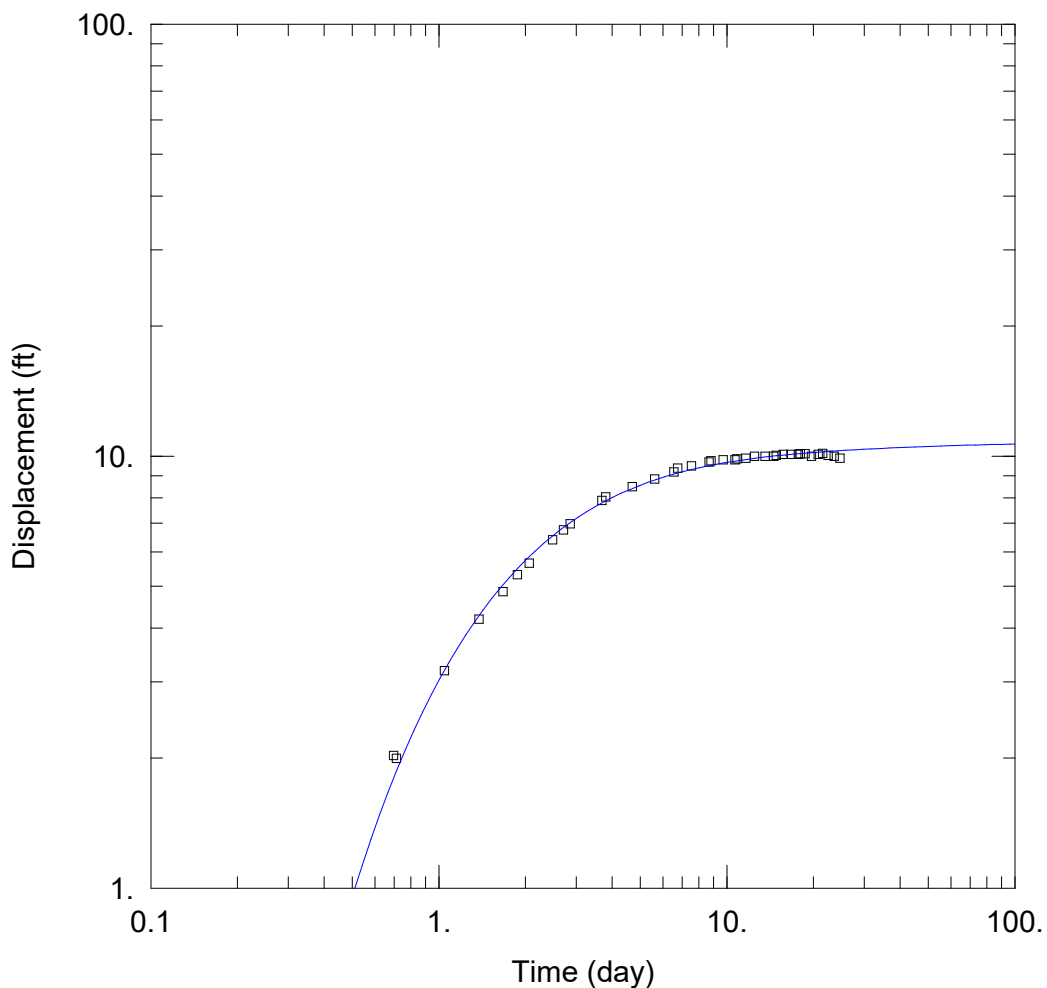
$$0.000016393 \cong 0.00001617$$

Therefore,

$$K_h = 2.6 \text{ ft/d} = 0.000009172 \text{ m/s} = 0.0009172 \text{ cm/s} = 9.17 \times 10^{-4} \text{ cm/s}$$

**APPENDIX B**

**AQTESOLV OUTPUT FOR PM-4 DRAWDOWN ANALYSIS**



WELL TEST ANALYSIS

Data Set: D:\hugo \Downloads\LANL NM PROJECT\AQTESOLV files\PM-4 data.aqt  
 Date: 06/07/24 Time: 13:33:22

PROJECT INFORMATION

Test Well: PM-2

AQUIFER DATA

Saturated Thickness: 5000. ft

WELL DATA

Pumping Wells			Observation Wells		
Well Name	X (ft)	Y (ft)	Well Name	X (ft)	Y (ft)
PM-2	0	0	□ PM-4	4478	0

SOLUTION

Aquifer Model: Unconfined

Solution Method: Neuman

T = 4139.5 ft<sup>2</sup>/day

S = 0.0006728

Sy = 0.5

β = 0.02846

Data Set: D:\hugo\_\Downloads\LANL NM PROJECT\AQTESOLV files\PM-4 data.aqt

Date: 06/07/24

Time: 13:33:38

---

PROJECT INFORMATION

Test Well: PM-2

---

AQUIFER DATA

Saturated Thickness: 5000. ft

Anisotropy Ratio (Kz/Kr): 0.03548

---

PUMPING WELL DATA

No. of pumping wells: 1

Pumping Well No. 1: PM-2

X Location: 0. ft

Y Location: 0. ft

Casing Radius: 0.5833 ft

Well Radius: 1. ft

Partially Penetrating Well

Depth to Top of Screen: 135. ft

Depth to Bottom of Screen: 1411. ft

No. of pumping periods: 1

Pumping Period Data

<u>Time (day)</u>	<u>Rate (gal/min)</u>
0.	1249.

---

OBSERVATION WELL DATA

No. of observation wells: 1

Observation Well No. 1: PM-4

X Location: 4478. ft

Y Location: 0. ft

Radial distance from PM-2: 4478. ft

Partially Penetrating Well

Depth to Top of Screen: 184.7 ft

Depth to Bottom of Screen: 1778.7 ft

No. of Observations: 38

Observation Data

<u>Time (day)</u>	<u>Displacement (ft)</u>	<u>Time (day)</u>	<u>Displacement (ft)</u>
-------------------	--------------------------	-------------------	--------------------------

---



0.697	2.028	9.7	9.798
0.713	1.997	10.66	9.798
1.045	3.188	10.85	9.848
1.379	4.197	11.65	9.898
1.669	4.858	12.48	9.997
1.872	5.318	13.57	9.997
2.06	5.648	14.54	9.997
2.485	6.398	14.84	10.04
2.71	6.747	15.69	10.1
2.861	6.977	16.7	10.1
3.686	7.898	17.71	10.1
3.797	8.048	17.98	10.13
4.693	8.497	18.7	10.13
5.61	8.848	19.66	9.997
6.548	9.197	20.76	10.1
6.75	9.388	21.51	10.15
7.544	9.497	22.48	10.05
8.676	9.697	23.61	9.997
8.809	9.757	24.69	9.898

SOLUTION

Pumping Test  
 Aquifer Model: Unconfined  
 Solution Method: Neuman

VISUAL ESTIMATION RESULTS

Estimated Parameters

Parameter	Estimate	
T	4141.2	ft <sup>2</sup> /day
S	0.000673	
Sy	0.25	
β	0.02847	

K = T/b = 0.8282 ft/day (0.0002922 cm/sec)  
 Ss = S/b = 1.346E-7 1/ft

AUTOMATIC ESTIMATION RESULTS

Estimated Parameters

Parameter	Estimate	Std. Error	Approx. C.I.	t-Ratio	
T	4139.5	870.9	+/- 1769.6	4.753	ft <sup>2</sup> /day
S	0.0006728	7.127E-5	+/- 0.0001448	9.44	
Sy	0.5	6.289	+/- 12.78	0.0795	
β	0.02846	0.009227	+/- 0.01875	3.084	

C.I. is approximate 95% confidence interval for parameter  
 t-ratio = estimate/std. error  
 No estimation window

K = T/b = 0.8279 ft/day (0.0002921 cm/sec)

Ss = S/b = 1.346E-7 1/ft

Parameter Correlations

	<u>T</u>	<u>S</u>	<u>Sy</u>	<u>β</u>
T	1.00	0.99	0.56	-1.00
S	0.99	1.00	0.63	-0.99
Sy	0.56	0.63	1.00	-0.59
β	-1.00	-0.99	-0.59	1.00

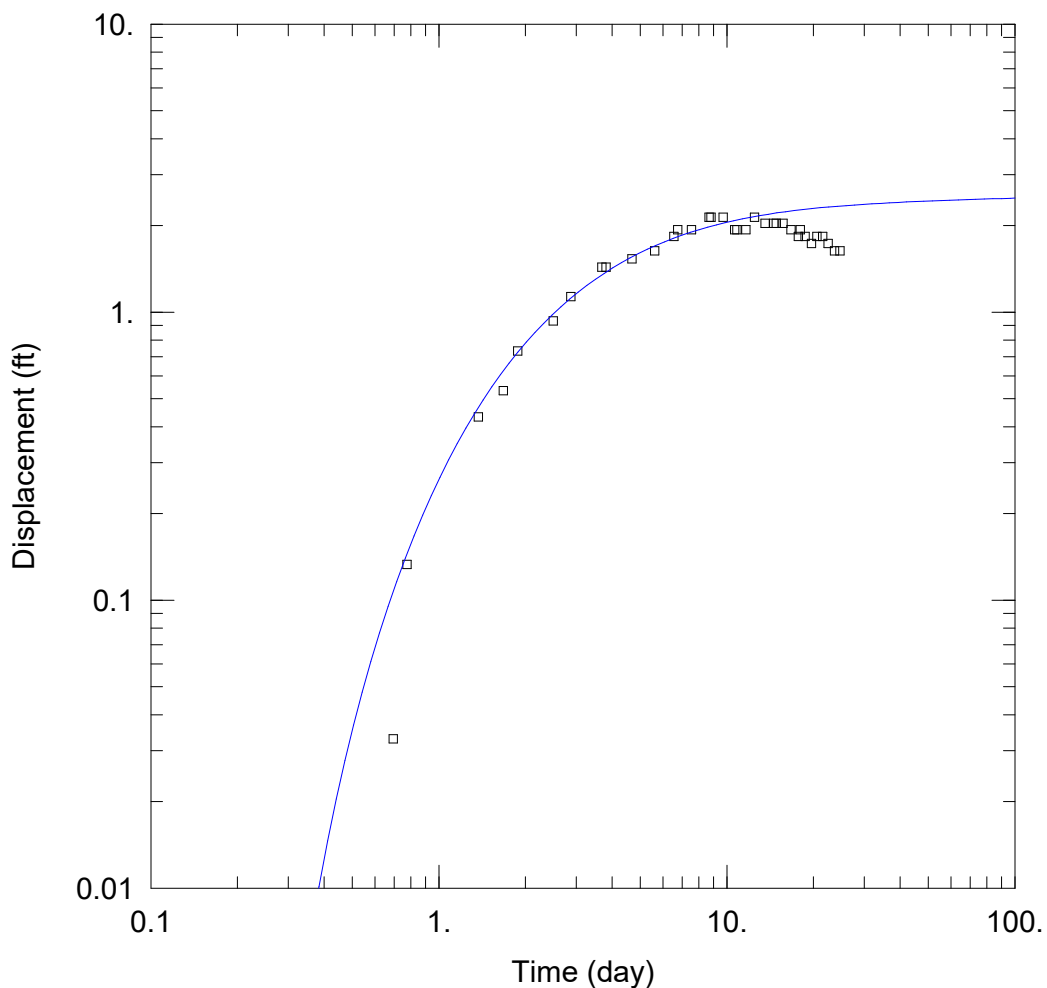
Residual Statistics

for weighted residuals

Sum of Squares... 0.8484 ft<sup>2</sup>  
Variance ..... 0.02495 ft<sup>2</sup>  
Std. Deviation ..... 0.158 ft  
Mean ..... 0.001709 ft  
No. of Residuals .. 38  
No. of Estimates .. 4

**APPENDIX C**

**AQTESOLV OUTPUT FOR PM-5 DRAWDOWN ANALYSIS**



WELL TEST ANALYSIS

Data Set: D:\hugo \Downloads\LANL NM PROJECT\AQTESOLV files\PM-5 data.aqt  
 Date: 06/07/24 Time: 13:40:13

PROJECT INFORMATION

Test Well: PM-2

AQUIFER DATA

Saturated Thickness: 5000. ft

WELL DATA

Pumping Wells			Observation Wells		
Well Name	X (ft)	Y (ft)	Well Name	X (ft)	Y (ft)
PM-2	0	0	□ PM-5	8808	0

SOLUTION

Aquifer Model: Unconfined

Solution Method: Neuman

T = 1.671E+4 ft<sup>2</sup>/day

S = 0.001314

Sy = 0.5

β = 0.03086

Data Set: D:\hugo\_\Downloads\LANL NM PROJECT\AQTESOLV files\PM-5 data.aqt  
Date: 06/07/24  
Time: 13:40:25

---

PROJECT INFORMATION

Test Well: PM-2

---

AQUIFER DATA

Saturated Thickness: 5000. ft  
Anisotropy Ratio (Kz/Kr): 0.009944

---

PUMPING WELL DATA

No. of pumping wells: 1

Pumping Well No. 1: PM-2

X Location: 0. ft  
Y Location: 0. ft

Casing Radius: 0.5833 ft  
Well Radius: 1. ft

Partially Penetrating Well  
Depth to Top of Screen: 135. ft  
Depth to Bottom of Screen: 1411. ft

No. of pumping periods: 1

<u>Pumping Period Data</u>	
<u>Time (day)</u>	<u>Rate (gal/min)</u>
0.	1249.

---

OBSERVATION WELL DATA

No. of observation wells: 1

Observation Well No. 1: PM-5

X Location: 8808. ft  
Y Location: 0. ft

Radial distance from PM-2: 8808. ft

Partially Penetrating Well  
Depth to Top of Screen: 198.7 ft  
Depth to Bottom of Screen: 1830.7 ft

No. of Observations: 35

<u>Observation Data</u>			
<u>Time (day)</u>	<u>Displacement (ft)</u>	<u>Time (day)</u>	<u>Displacement (ft)</u>

---

0.695	0.033	10.85	1.933
0.776	0.133	11.64	1.933
1.37	0.433	12.47	2.133
1.675	0.533	13.58	2.033
1.878	0.733	14.53	2.033
2.499	0.933	14.85	2.033
2.871	1.133	15.68	2.033
3.683	1.433	16.72	1.933
3.803	1.433	17.72	1.833
4.684	1.533	17.98	1.933
5.621	1.633	18.71	1.833
6.542	1.833	19.65	1.733
6.757	1.933	20.54	1.833
7.535	1.933	21.5	1.833
8.669	2.133	22.48	1.733
8.816	2.133	23.63	1.633
9.71	2.133	24.68	1.633
10.65	1.933		

---

SOLUTION

Pumping Test  
 Aquifer Model: Unconfined  
 Solution Method: Neuman

---

VISUAL ESTIMATION RESULTS

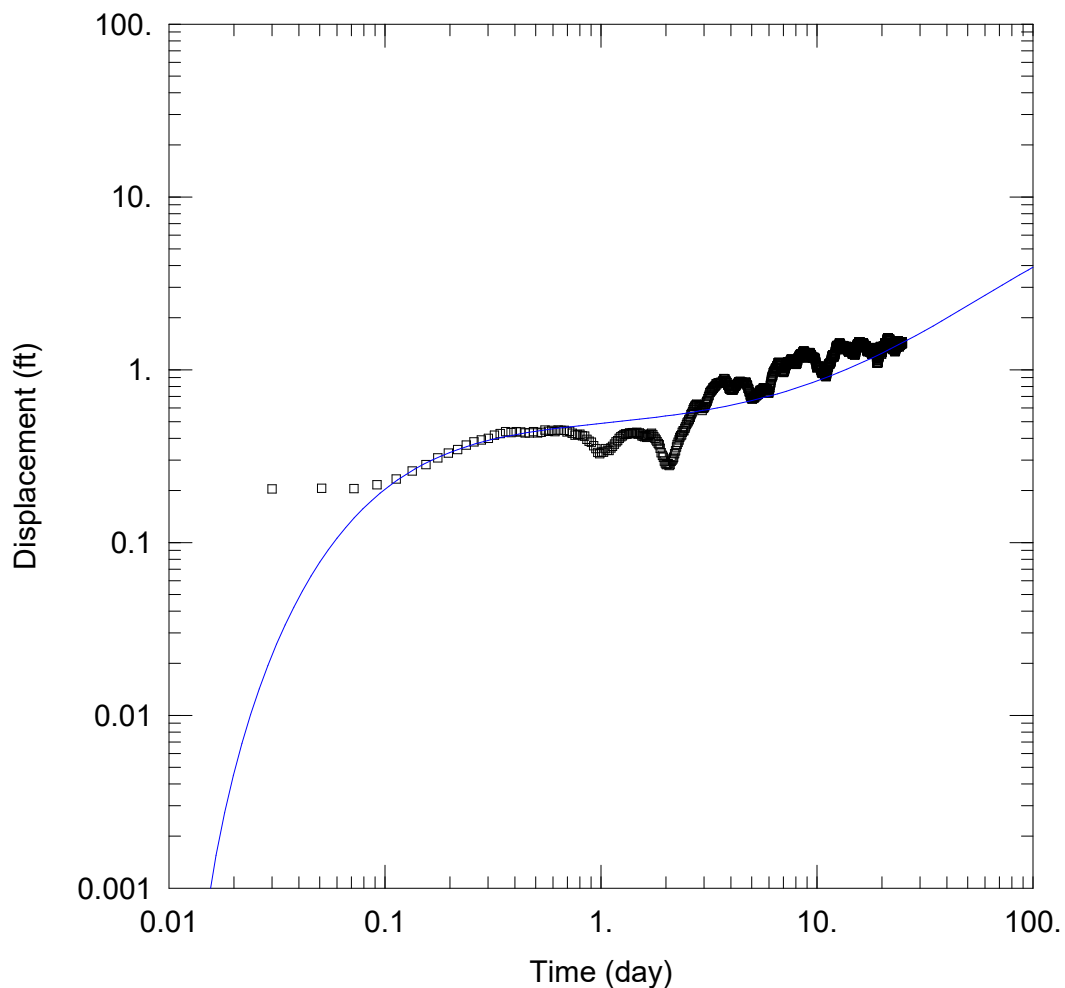
Estimated Parameters

<u>Parameter</u>	<u>Estimate</u>	
T	1.654E+4	ft <sup>2</sup> /day
S	0.001253	
Sy	0.5	
β	0.03	

$K = T/b = 3.309 \text{ ft/day (0.001167 cm/sec)}$   
 $Ss = S/b = 2.507E-7 \text{ 1/ft}$

**APPENDIX D**

**AQTESOLV OUTPUT FOR R-20 SCREEN 1 DRAWDOWN ANALYSIS**



WELL TEST ANALYSIS

Data Set: D:\hugo \Downloads\LANL NM PROJECT\AQTESOLV files\R20 S1 data.aqt  
 Date: 06/07/24 Time: 13:49:46

PROJECT INFORMATION

Test Well: PM-2

AQUIFER DATA

Saturated Thickness: 5000. ft

WELL DATA

Pumping Wells			Observation Wells		
Well Name	X (ft)	Y (ft)	Well Name	X (ft)	Y (ft)
PM-2	0	0	□ R20 S1	1225	0

SOLUTION

Aquifer Model: Unconfined

Solution Method: Neuman

T = 1.393E+4 ft<sup>2</sup>/day

S = 0.002862

Sy = 0.2075

β = 0.03



Data Set: D:\hugo\_\Downloads\LANL NM PROJECT\AQTESOLV files\R20 S1 data.aqt

Date: 06/07/24

Time: 13:49:58

---

PROJECT INFORMATION

Test Well: PM-2

---

AQUIFER DATA

Saturated Thickness: 5000. ft

Anisotropy Ratio (Kz/Kr): 0.4998

---

PUMPING WELL DATA

No. of pumping wells: 1

Pumping Well No. 1: PM-2

X Location: 0. ft

Y Location: 0. ft

Casing Radius: 0.5833 ft

Well Radius: 1. ft

Partially Penetrating Well

Depth to Top of Screen: 135. ft

Depth to Bottom of Screen: 1411. ft

No. of pumping periods: 1

Pumping Period Data

<u>Time (day)</u>	<u>Rate (gal/min)</u>
0.	1249.

---

OBSERVATION WELL DATA

No. of observation wells: 1

Observation Well No. 1: R20 S1

X Location: 1225. ft

Y Location: 0. ft

Radial distance from PM-2: 1225. ft

Partially Penetrating Well

Depth to Top of Screen: 79.3 ft

Depth to Bottom of Screen: 86.9 ft

No. of Observations: 1197

Observation Data

<u>Time (day)</u>	<u>Displacement (ft)</u>	<u>Time (day)</u>	<u>Displacement (ft)</u>
-------------------	--------------------------	-------------------	--------------------------

---

0.009	0.207	12.49	1.378
0.03	0.204	12.51	1.37
0.051	0.206	12.53	1.372
0.072	0.205	12.55	1.366
0.092	0.216	12.57	1.372
0.113	0.233	12.59	1.368
0.134	0.259	12.61	1.374
0.155	0.283	12.63	1.384
0.176	0.309	12.65	1.39
0.197	0.329	12.68	1.397
0.217	0.345	12.7	1.405
0.238	0.366	12.72	1.428
0.259	0.383	12.74	1.421
0.28	0.392	12.76	1.422
0.301	0.4	12.78	1.419
0.322	0.419	12.8	1.421
0.342	0.427	12.82	1.41
0.363	0.438	12.84	1.418
0.384	0.432	12.86	1.406
0.405	0.439	12.88	1.391
0.426	0.436	12.9	1.38
0.447	0.43	12.93	1.372
0.467	0.43	12.95	1.344
0.488	0.438	12.97	1.335
0.509	0.43	12.99	1.33
0.53	0.435	13.01	1.316
0.551	0.447	13.03	1.314
0.572	0.441	13.05	1.308
0.592	0.446	13.07	1.319
0.613	0.439	13.09	1.31
0.634	0.448	13.11	1.31
0.655	0.445	13.13	1.319
0.676	0.446	13.15	1.326
0.697	0.436	13.18	1.339
0.717	0.44	13.2	1.347
0.738	0.429	13.22	1.337
0.759	0.419	13.24	1.341
0.78	0.421	13.26	1.349
0.801	0.423	13.28	1.364
0.822	0.415	13.3	1.379
0.842	0.413	13.32	1.365
0.863	0.395	13.34	1.36
0.884	0.386	13.36	1.369
0.905	0.38	13.38	1.37
0.926	0.363	13.4	1.35
0.947	0.349	13.43	1.354
0.967	0.332	13.45	1.358
0.988	0.327	13.47	1.346
1.009	0.334	13.49	1.337
1.03	0.333	13.51	1.327
1.051	0.349	13.53	1.331
1.072	0.342	13.55	1.326
1.092	0.341	13.57	1.319
1.113	0.352	13.59	1.313

---

<u>Time (day)</u>	<u>Displacement (ft)</u>	<u>Time (day)</u>	<u>Displacement (ft)</u>
1.134	0.36	13.61	1.327
1.155	0.371	13.63	1.33
1.176	0.382	13.65	1.329
1.197	0.389	13.68	1.347
1.217	0.401	13.7	1.36
1.238	0.409	13.72	1.364
1.259	0.415	13.74	1.357
1.28	0.421	13.76	1.36
1.301	0.426	13.78	1.357
1.322	0.424	13.8	1.352
1.342	0.427	13.82	1.362
1.363	0.431	13.84	1.349
1.384	0.429	13.86	1.338
1.405	0.433	13.88	1.329
1.426	0.427	13.9	1.326
1.447	0.431	13.93	1.309
1.467	0.434	13.95	1.296
1.488	0.424	13.97	1.291
1.509	0.431	13.99	1.285
1.53	0.425	14.01	1.272
1.551	0.414	14.03	1.266
1.572	0.412	14.05	1.266
1.592	0.41	14.07	1.272
1.613	0.416	14.09	1.283
1.634	0.406	14.11	1.281
1.655	0.416	14.13	1.283
1.676	0.421	14.15	1.278
1.697	0.424	14.18	1.293
1.717	0.429	14.2	1.295
1.738	0.42	14.22	1.298
1.759	0.41	14.24	1.304
1.78	0.4	14.26	1.311
1.801	0.393	14.28	1.305
1.822	0.384	14.3	1.312
1.842	0.375	14.32	1.321
1.863	0.368	14.34	1.311
1.884	0.351	14.36	1.321
1.905	0.331	14.38	1.327
1.926	0.319	14.4	1.327
1.947	0.311	14.43	1.321
1.967	0.296	14.45	1.311
1.988	0.289	14.47	1.3
2.009	0.282	14.49	1.294
2.03	0.285	14.51	1.281
2.051	0.286	14.53	1.267
2.072	0.279	14.55	1.256
2.092	0.283	14.57	1.25
2.113	0.295	14.59	1.236
2.134	0.3	14.61	1.241
2.155	0.305	14.63	1.23
2.176	0.312	14.65	1.228
2.197	0.326	14.68	1.24
2.217	0.339	14.7	1.241

<u>Time (day)</u>	<u>Displacement (ft)</u>	<u>Time (day)</u>	<u>Displacement (ft)</u>
2.238	0.357	14.72	1.247
2.259	0.369	14.74	1.248
2.28	0.38	14.76	1.252
2.301	0.393	14.78	1.249
2.322	0.405	14.8	1.248
2.342	0.414	14.82	1.248
2.363	0.42	14.84	1.247
2.384	0.435	14.86	1.251
2.405	0.444	14.88	1.244
2.426	0.443	14.9	1.237
2.447	0.458	14.93	1.233
2.467	0.468	14.95	1.22
2.488	0.482	14.97	1.217
2.509	0.492	14.99	1.219
2.53	0.501	15.01	1.224
2.551	0.511	15.03	1.225
2.572	0.518	15.05	1.229
2.592	0.532	15.07	1.236
2.613	0.549	15.09	1.252
2.634	0.558	15.11	1.263
2.655	0.572	15.13	1.278
2.676	0.588	15.15	1.292
2.697	0.602	15.18	1.3
2.717	0.613	15.2	1.308
2.738	0.621	15.22	1.332
2.759	0.624	15.24	1.33
2.78	0.631	15.26	1.351
2.801	0.625	15.28	1.359
2.822	0.627	15.3	1.376
2.842	0.627	15.32	1.379
2.863	0.619	15.34	1.377
2.884	0.61	15.36	1.378
2.905	0.608	15.38	1.398
2.926	0.605	15.4	1.401
2.947	0.581	15.43	1.406
2.967	0.596	15.45	1.409
2.988	0.599	15.47	1.406
3.009	0.603	15.49	1.399
3.03	0.61	15.51	1.401
3.051	0.63	15.53	1.398
3.072	0.642	15.55	1.406
3.092	0.653	15.57	1.403
3.113	0.661	15.59	1.414
3.134	0.68	15.61	1.412
3.155	0.696	15.63	1.421
3.176	0.712	15.65	1.431
3.197	0.737	15.68	1.445
3.217	0.742	15.7	1.45
3.238	0.753	15.72	1.446
3.259	0.759	15.74	1.45
3.28	0.77	15.76	1.452
3.301	0.786	15.78	1.452
3.322	0.779	15.8	1.444

<u>Time (day)</u>	<u>Displacement (ft)</u>	<u>Time (day)</u>	<u>Displacement (ft)</u>
3.342	0.794	15.82	1.442
3.363	0.799	15.84	1.437
3.384	0.805	15.86	1.442
3.405	0.812	15.88	1.432
3.426	0.832	15.9	1.438
3.447	0.831	15.93	1.423
3.467	0.83	15.95	1.399
3.488	0.838	15.97	1.393
3.509	0.837	15.99	1.384
3.53	0.839	16.01	1.384
3.551	0.843	16.03	1.368
3.572	0.844	16.05	1.366
3.592	0.843	16.07	1.361
3.613	0.843	16.09	1.368
3.634	0.842	16.11	1.379
3.655	0.852	16.13	1.378
3.676	0.864	16.16	1.385
3.697	0.871	16.18	1.394
3.717	0.888	16.2	1.403
3.738	0.887	16.22	1.409
3.759	0.882	16.24	1.412
3.78	0.864	16.26	1.426
3.801	0.858	16.28	1.424
3.822	0.846	16.3	1.422
3.842	0.84	16.32	1.433
3.863	0.818	16.34	1.432
3.884	0.813	16.36	1.431
3.905	0.804	16.38	1.435
3.926	0.784	16.41	1.429
3.947	0.774	16.43	1.425
3.967	0.777	16.45	1.417
3.988	0.767	16.47	1.407
4.009	0.77	16.49	1.412
4.03	0.763	16.51	1.398
4.051	0.766	16.53	1.387
4.072	0.763	16.55	1.378
4.092	0.763	16.57	1.376
4.113	0.772	16.59	1.362
4.134	0.78	16.61	1.356
4.155	0.793	16.63	1.354
4.176	0.804	16.66	1.347
4.197	0.803	16.68	1.354
4.217	0.805	16.7	1.354
4.238	0.817	16.72	1.35
4.259	0.821	16.74	1.361
4.28	0.829	16.76	1.362
4.301	0.836	16.78	1.359
4.322	0.834	16.8	1.364
4.342	0.847	16.82	1.372
4.363	0.851	16.84	1.37
4.384	0.848	16.86	1.377
4.405	0.856	16.88	1.366
4.426	0.857	16.91	1.363

---

<u>Time (day)</u>	<u>Displacement (ft)</u>	<u>Time (day)</u>	<u>Displacement (ft)</u>
4.447	0.844	16.93	1.35
4.467	0.845	16.95	1.334
4.488	0.849	16.97	1.332
4.509	0.844	16.99	1.325
4.53	0.842	17.01	1.319
4.551	0.836	17.03	1.305
4.572	0.839	17.05	1.301
4.592	0.834	17.07	1.293
4.613	0.843	17.09	1.287
4.634	0.838	17.11	1.284
4.655	0.842	17.13	1.28
4.676	0.847	17.16	1.288
4.697	0.845	17.18	1.277
4.717	0.838	17.2	1.273
4.738	0.82	17.22	1.276
4.759	0.813	17.24	1.275
4.78	0.805	17.26	1.289
4.801	0.783	17.28	1.299
4.822	0.776	17.3	1.302
4.842	0.766	17.32	1.304
4.863	0.747	17.34	1.301
4.884	0.74	17.36	1.299
4.905	0.717	17.38	1.305
4.926	0.706	17.41	1.31
4.947	0.702	17.43	1.311
4.967	0.689	17.45	1.307
4.988	0.679	17.47	1.301
5.009	0.68	17.49	1.29
5.03	0.677	17.51	1.29
5.051	0.68	17.53	1.281
5.072	0.688	17.55	1.276
5.092	0.685	17.57	1.274
5.113	0.686	17.59	1.266
5.134	0.694	17.61	1.271
5.155	0.7	17.63	1.275
5.176	0.695	17.66	1.278
5.197	0.712	17.68	1.275
5.217	0.711	17.7	1.283
5.238	0.712	17.72	1.283
5.259	0.706	17.74	1.282
5.28	0.718	17.76	1.273
5.301	0.717	17.78	1.275
5.322	0.72	17.8	1.272
5.342	0.723	17.82	1.262
5.363	0.724	17.84	1.268
5.384	0.734	17.86	1.262
5.405	0.731	17.88	1.248
5.426	0.747	17.91	1.244
5.447	0.751	17.93	1.234
5.467	0.759	17.95	1.233
5.488	0.757	17.97	1.224
5.509	0.76	17.99	1.236
5.53	0.766	18.01	1.243

---

<u>Time (day)</u>	<u>Displacement (ft)</u>	<u>Time (day)</u>	<u>Displacement (ft)</u>
5.551	0.756	18.03	1.24
5.572	0.761	18.05	1.241
5.592	0.769	18.07	1.248
5.613	0.769	18.09	1.249
5.634	0.769	18.11	1.262
5.655	0.784	18.13	1.265
5.676	0.785	18.16	1.271
5.697	0.779	18.18	1.291
5.717	0.786	18.2	1.289
5.738	0.773	18.22	1.296
5.759	0.766	18.24	1.297
5.78	0.765	18.26	1.302
5.801	0.765	18.28	1.305
5.822	0.77	18.3	1.31
5.842	0.78	18.32	1.317
5.863	0.776	18.34	1.315
5.884	0.769	18.36	1.328
5.905	0.761	18.38	1.322
5.926	0.745	18.41	1.323
5.947	0.743	18.43	1.332
5.967	0.738	18.45	1.346
5.988	0.732	18.47	1.342
6.009	0.744	18.49	1.33
6.03	0.758	18.51	1.332
6.051	0.776	18.53	1.328
6.072	0.788	18.55	1.325
6.092	0.812	18.57	1.318
6.113	0.831	18.59	1.333
6.134	0.847	18.61	1.329
6.155	0.871	18.63	1.332
6.176	0.894	18.66	1.336
6.197	0.903	18.68	1.331
6.217	0.918	18.7	1.335
6.238	0.921	18.72	1.327
6.259	0.933	18.74	1.321
6.28	0.959	18.76	1.303
6.301	0.961	18.78	1.3
6.322	0.975	18.8	1.279
6.342	0.98	18.82	1.268
6.363	0.982	18.84	1.247
6.384	0.989	18.86	1.227
6.405	1.005	18.88	1.199
6.426	1.012	18.91	1.178
6.447	1.021	18.93	1.166
6.467	1.028	18.95	1.145
6.488	1.022	18.97	1.132
6.509	1.038	18.99	1.107
6.53	1.054	19.01	1.09
6.551	1.056	19.03	1.092
6.572	1.06	19.05	1.094
6.592	1.075	19.07	1.093
6.613	1.094	19.09	1.097
6.634	1.096	19.11	1.093

---

<u>Time (day)</u>	<u>Displacement (ft)</u>	<u>Time (day)</u>	<u>Displacement (ft)</u>
6.655	1.102	19.13	1.102
6.676	1.105	19.16	1.104
6.697	1.09	19.18	1.098
6.717	1.085	19.2	1.109
6.738	1.078	19.22	1.127
6.759	1.077	19.24	1.153
6.78	1.063	19.26	1.157
6.801	1.053	19.28	1.161
6.822	1.053	19.3	1.172
6.842	1.049	19.32	1.184
6.863	1.033	19.34	1.185
6.884	1.029	19.36	1.197
6.905	1.013	19.38	1.202
6.926	0.988	19.41	1.203
6.947	0.977	19.43	1.215
6.967	0.971	19.45	1.227
6.988	0.97	19.47	1.231
7.009	0.964	19.49	1.246
7.03	0.963	19.51	1.25
7.051	0.982	19.53	1.257
7.072	0.979	19.55	1.267
7.092	0.999	19.57	1.283
7.113	1.014	19.59	1.295
7.134	1.016	19.61	1.307
7.155	1.033	19.63	1.323
7.176	1.046	19.66	1.332
7.197	1.059	19.68	1.36
7.217	1.065	19.7	1.361
7.238	1.08	19.72	1.355
7.259	1.083	19.74	1.343
7.28	1.097	19.76	1.349
7.301	1.095	19.78	1.351
7.322	1.106	19.8	1.344
7.342	1.108	19.82	1.337
7.363	1.106	19.84	1.333
7.384	1.108	19.86	1.291
7.405	1.11	19.88	1.309
7.426	1.11	19.91	1.238
7.447	1.111	19.93	1.274
7.467	1.115	19.95	1.231
7.488	1.112	19.97	1.259
7.509	1.114	19.99	1.255
7.53	1.118	20.01	1.26
7.551	1.125	20.03	1.262
7.572	1.14	20.05	1.277
7.592	1.149	20.07	1.284
7.613	1.15	20.09	1.286
7.634	1.152	20.11	1.3
7.655	1.146	20.13	1.303
7.676	1.151	20.16	1.323
7.697	1.149	20.18	1.33
7.717	1.145	20.2	1.348
7.738	1.136	20.22	1.36



---

<u>Time (day)</u>	<u>Displacement (ft)</u>	<u>Time (day)</u>	<u>Displacement (ft)</u>
7.759	1.137	20.24	1.359
7.78	1.125	20.26	1.362
7.801	1.124	20.28	1.364
7.822	1.116	20.3	1.369
7.842	1.112	20.32	1.365
7.863	1.101	20.34	1.363
7.884	1.093	20.36	1.349
7.905	1.091	20.38	1.334
7.926	1.085	20.41	1.351
7.947	1.085	20.43	1.356
7.967	1.076	20.45	1.359
7.988	1.076	20.47	1.358
8.009	1.072	20.49	1.366
8.03	1.078	20.51	1.368
8.051	1.08	20.53	1.366
8.072	1.087	20.55	1.368
8.092	1.094	20.57	1.372
8.113	1.113	20.59	1.382
8.134	1.118	20.61	1.389
8.155	1.141	20.63	1.398
8.176	1.158	20.66	1.4
8.197	1.171	20.68	1.415
8.217	1.175	20.7	1.429
8.238	1.188	20.72	1.429
8.259	1.194	20.74	1.432
8.28	1.193	20.76	1.436
8.301	1.21	20.78	1.433
8.322	1.213	20.8	1.435
8.342	1.204	20.82	1.436
8.363	1.218	20.84	1.423
8.384	1.229	20.86	1.417
8.405	1.224	20.88	1.418
8.426	1.232	20.91	1.417
8.447	1.229	20.93	1.409
8.467	1.229	20.95	1.411
8.488	1.236	20.97	1.404
8.509	1.237	20.99	1.413
8.53	1.24	21.01	1.41
8.551	1.238	21.03	1.422
8.572	1.237	21.05	1.418
8.592	1.253	21.07	1.434
8.613	1.254	21.09	1.448
8.634	1.267	21.11	1.463
8.655	1.272	21.13	1.47
8.676	1.282	21.16	1.484
8.697	1.284	21.18	1.497
8.717	1.28	21.2	1.501
8.738	1.278	21.22	1.514
8.759	1.268	21.24	1.515
8.78	1.27	21.26	1.522
8.801	1.255	21.28	1.523
8.822	1.244	21.3	1.527
8.842	1.236	21.32	1.525

---

<u>Time (day)</u>	<u>Displacement (ft)</u>	<u>Time (day)</u>	<u>Displacement (ft)</u>
8.863	1.227	21.34	1.526
8.884	1.234	21.36	1.531
8.905	1.223	21.38	1.523
8.926	1.214	21.41	1.512
8.947	1.201	21.43	1.52
8.967	1.188	21.45	1.516
8.988	1.177	21.47	1.514
9.009	1.177	21.49	1.504
9.03	1.175	21.51	1.503
9.051	1.169	21.53	1.497
9.072	1.178	21.55	1.489
9.092	1.187	21.57	1.48
9.113	1.187	21.59	1.481
9.134	1.212	21.61	1.483
9.155	1.224	21.63	1.485
9.176	1.239	21.66	1.488
9.197	1.243	21.68	1.486
9.217	1.247	21.7	1.495
9.238	1.254	21.72	1.503
9.259	1.254	21.74	1.504
9.28	1.257	21.76	1.484
9.301	1.252	21.78	1.472
9.322	1.241	21.8	1.47
9.342	1.231	21.82	1.465
9.363	1.214	21.84	1.441
9.384	1.212	21.86	1.431
9.405	1.217	21.88	1.411
9.426	1.214	21.91	1.401
9.447	1.208	21.93	1.392
9.467	1.192	21.95	1.371
9.488	1.189	21.97	1.368
9.509	1.185	21.99	1.365
9.53	1.172	22.01	1.351
9.551	1.171	22.03	1.356
9.572	1.165	22.05	1.359
9.592	1.166	22.07	1.356
9.613	1.181	22.09	1.356
9.634	1.169	22.11	1.362
9.655	1.163	22.13	1.364
9.676	1.169	22.16	1.366
9.697	1.175	22.18	1.378
9.717	1.17	22.2	1.375
9.738	1.176	22.22	1.388
9.759	1.174	22.24	1.396
9.78	1.167	22.26	1.394
9.801	1.16	22.28	1.396
9.822	1.158	22.3	1.395
9.842	1.147	22.32	1.392
9.863	1.13	22.34	1.382
9.884	1.117	22.36	1.377
9.905	1.097	22.38	1.37
9.926	1.078	22.41	1.362
9.947	1.065	22.43	1.362

---

<u>Time (day)</u>	<u>Displacement (ft)</u>	<u>Time (day)</u>	<u>Displacement (ft)</u>
9.967	1.057	22.45	1.366
9.988	1.042	22.47	1.358
10.01	1.032	22.49	1.345
10.03	1.022	22.51	1.33
10.05	1.037	22.53	1.323
10.07	1.033	22.55	1.314
10.09	1.03	22.57	1.31
10.11	1.035	22.59	1.305
10.13	1.036	22.61	1.312
10.15	1.043	22.63	1.318
10.18	1.049	22.66	1.312
10.2	1.041	22.68	1.314
10.22	1.045	22.7	1.315
10.24	1.045	22.72	1.33
10.26	1.047	22.74	1.339
10.28	1.036	22.76	1.34
10.3	1.04	22.78	1.346
10.32	1.036	22.8	1.351
10.34	1.039	22.82	1.34
10.36	1.026	22.84	1.336
10.38	1.022	22.86	1.331
10.4	1.01	22.88	1.312
10.43	1.002	22.91	1.307
10.45	0.999	22.93	1.289
10.47	0.995	22.95	1.279
10.49	0.986	22.97	1.273
10.51	0.965	22.99	1.285
10.53	0.965	23.01	1.281
10.55	0.966	23.03	1.274
10.57	0.962	23.05	1.288
10.59	0.955	23.07	1.288
10.61	0.953	23.09	1.281
10.63	0.953	23.11	1.288
10.65	0.951	23.13	1.299
10.68	0.961	23.16	1.314
10.7	0.959	23.18	1.321
10.72	0.956	23.2	1.326
10.74	0.966	23.22	1.337
10.76	0.978	23.24	1.341
10.78	0.977	23.26	1.353
10.8	0.973	23.28	1.354
10.82	0.981	23.3	1.359
10.84	0.973	23.32	1.362
10.86	0.957	23.34	1.36
10.88	0.952	23.36	1.359
10.9	0.941	23.38	1.352
10.93	0.931	23.41	1.35
10.95	0.922	23.43	1.349
10.97	0.922	23.45	1.357
10.99	0.926	23.47	1.353
11.01	0.913	23.49	1.349
11.03	0.914	23.51	1.357
11.05	0.921	23.53	1.362

---

<u>Time (day)</u>	<u>Displacement (ft)</u>	<u>Time (day)</u>	<u>Displacement (ft)</u>
11.07	0.933	23.55	1.368
11.09	0.938	23.57	1.371
11.11	0.951	23.59	1.39
11.13	0.961	23.61	1.399
11.15	0.975	23.63	1.414
11.18	0.994	23.66	1.423
11.2	1.001	23.68	1.437
11.22	1.006	23.7	1.448
11.24	1.029	23.72	1.458
11.26	1.032	23.74	1.474
11.28	1.041	23.76	1.468
11.3	1.057	23.78	1.468
11.32	1.05	23.8	1.454
11.34	1.068	23.82	1.457
11.36	1.074	23.84	1.447
11.38	1.082	23.86	1.439
11.4	1.079	23.88	1.43
11.43	1.083	23.91	1.423
11.45	1.092	23.93	1.415
11.47	1.086	23.95	1.395
11.49	1.086	23.97	1.38
11.51	1.082	23.99	1.374
11.53	1.085	24.01	1.375
11.55	1.091	24.03	1.362
11.57	1.104	24.05	1.365
11.59	1.107	24.07	1.357
11.61	1.11	24.09	1.37
11.63	1.118	24.11	1.372
11.65	1.135	24.13	1.379
11.68	1.147	24.16	1.387
11.7	1.158	24.18	1.391
11.72	1.167	24.2	1.393
11.74	1.189	24.22	1.404
11.76	1.201	24.24	1.406
11.78	1.205	24.26	1.399
11.8	1.208	24.28	1.4
11.82	1.221	24.3	1.411
11.84	1.22	24.32	1.404
11.86	1.214	24.34	1.405
11.88	1.216	24.36	1.411
11.9	1.21	24.38	1.407
11.93	1.199	24.41	1.394
11.95	1.188	24.43	1.393
11.97	1.185	24.45	1.402
11.99	1.193	24.47	1.405
12.01	1.186	24.49	1.406
12.03	1.196	24.51	1.406
12.05	1.204	24.53	1.404
12.07	1.21	24.55	1.411
12.09	1.222	24.57	1.411
12.11	1.226	24.59	1.415
12.13	1.239	24.61	1.426
12.15	1.258	24.63	1.431

<u>Time (day)</u>	<u>Displacement (ft)</u>	<u>Time (day)</u>	<u>Displacement (ft)</u>
12.18	1.27	24.66	1.435
12.2	1.284	24.68	1.438
12.22	1.297	24.7	1.436
12.24	1.316	24.72	1.448
12.26	1.332	24.74	1.449
12.28	1.338	24.76	1.448
12.3	1.356	24.78	1.453
12.32	1.365	24.8	1.448
12.34	1.372	24.82	1.449
12.36	1.378	24.84	1.438
12.38	1.382	24.86	1.441
12.4	1.379	24.88	1.424
12.43	1.381	24.91	1.417
12.45	1.377	24.93	1.418
12.47	1.379		

---

### SOLUTION

Pumping Test  
Aquifer Model: Unconfined  
Solution Method: Neuman

---

### VISUAL ESTIMATION RESULTS

#### Estimated Parameters

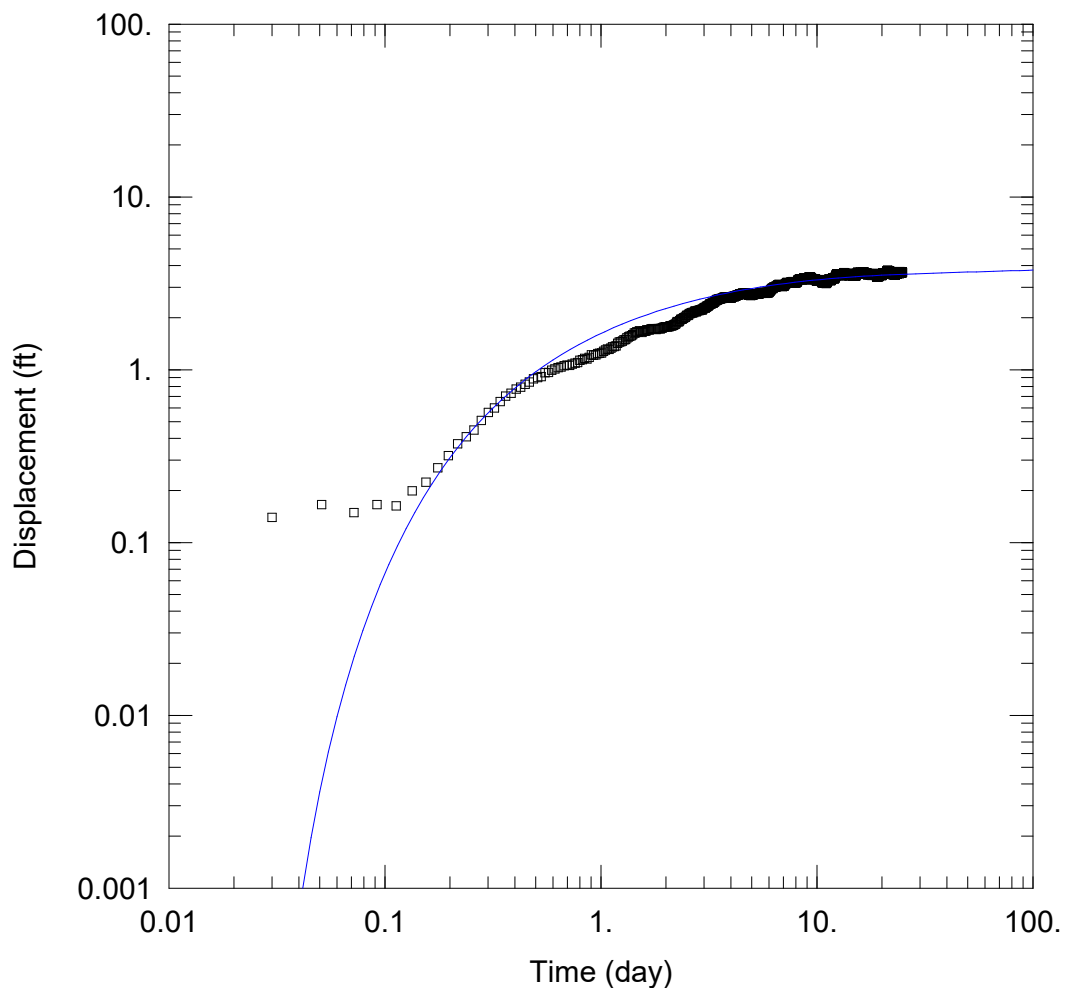
<u>Parameter</u>	<u>Estimate</u>	
T	1.393E+4	ft <sup>2</sup> /day
S	0.002862	
Sy	0.2075	
$\beta$	0.03	

$K = T/b = 2.787 \text{ ft/day (0.0009832 cm/sec)}$

$S_s = S/b = 5.724E-7 \text{ 1/ft}$

**APPENDIX E**

**AQTESOLV OUTPUT FOR R-20 SCREEN 2 DRAWDOWN ANALYSIS**



WELL TEST ANALYSIS

Data Set: D:\hugo \Downloads\LANL NM PROJECT\AQTESOLV files\R20 S2 data.aqt  
 Date: 06/07/24 Time: 14:00:56

PROJECT INFORMATION

Test Well: PM-2

AQUIFER DATA

Saturated Thickness: 5000. ft

WELL DATA

Pumping Wells			Observation Wells		
Well Name	X (ft)	Y (ft)	Well Name	X (ft)	Y (ft)
PM-2	0	0	□ R20 S2	1225	0

SOLUTION

Aquifer Model: Unconfined

Solution Method: Neuman

T = 4.759E+4 ft<sup>2</sup>/day

S = 0.02677

Sy = 0.5

β = 0.001

Data Set: D:\hugo\_\Downloads\LANL NM PROJECT\AQTESOLV files\R20 S2 data.aqt  
Date: 06/07/24  
Time: 14:01:07

---

PROJECT INFORMATION

Test Well: PM-2

---

AQUIFER DATA

Saturated Thickness: 5000. ft  
Anisotropy Ratio (Kz/Kr): 0.01666

---

PUMPING WELL DATA

No. of pumping wells: 1

Pumping Well No. 1: PM-2

X Location: 0. ft  
Y Location: 0. ft

Casing Radius: 0.5833 ft  
Well Radius: 1. ft

Partially Penetrating Well  
Depth to Top of Screen: 135. ft  
Depth to Bottom of Screen: 1411. ft

No. of pumping periods: 1

<u>Pumping Period Data</u>	
<u>Time (day)</u>	<u>Rate (gal/min)</u>
0.	1249.

---

OBSERVATION WELL DATA

No. of observation wells: 1

Observation Well No. 1: R20 S2

X Location: 1225. ft  
Y Location: 0. ft

Radial distance from PM-2: 1225. ft

Partially Penetrating Well  
Depth to Top of Screen: 317.6 ft  
Depth to Bottom of Screen: 325.2 ft

No. of Observations: 1197

<u>Observation Data</u>			
<u>Time (day)</u>	<u>Displacement (ft)</u>	<u>Time (day)</u>	<u>Displacement (ft)</u>

---



0.009	0.157	12.49	3.569
0.03	0.14	12.51	3.562
0.051	0.166	12.53	3.535
0.072	0.149	12.55	3.529
0.092	0.166	12.57	3.53
0.113	0.163	12.59	3.515
0.134	0.199	12.61	3.527
0.155	0.223	12.63	3.537
0.176	0.271	12.65	3.518
0.197	0.318	12.68	3.537
0.217	0.372	12.7	3.527
0.238	0.409	12.72	3.567
0.259	0.447	12.74	3.571
0.28	0.508	12.76	3.573
0.301	0.567	12.78	3.562
0.322	0.601	12.8	3.574
0.342	0.654	12.82	3.57
0.363	0.704	12.84	3.582
0.384	0.732	12.86	3.57
0.405	0.772	12.88	3.565
0.426	0.792	12.9	3.554
0.447	0.822	12.93	3.557
0.467	0.85	12.95	3.535
0.488	0.886	12.97	3.544
0.509	0.902	12.99	3.521
0.53	0.911	13.01	3.514
0.551	0.959	13.03	3.524
0.572	0.965	13.05	3.524
0.592	0.993	13.07	3.511
0.613	1.009	13.09	3.515
0.634	1.029	13.11	3.498
0.655	1.037	13.13	3.517
0.676	1.054	13.15	3.542
0.697	1.063	13.18	3.531
0.717	1.06	13.2	3.543
0.738	1.077	13.22	3.553
0.759	1.09	13.24	3.568
0.78	1.103	13.26	3.588
0.801	1.132	13.28	3.587
0.822	1.143	13.3	3.6
0.842	1.163	13.32	3.6
0.863	1.155	13.34	3.628
0.884	1.18	13.36	3.63
0.905	1.22	13.38	3.642
0.926	1.212	13.4	3.629
0.947	1.221	13.43	3.633
0.967	1.239	13.45	3.637
0.988	1.245	13.47	3.615
1.009	1.251	13.49	3.606
1.03	1.28	13.51	3.595
1.051	1.301	13.53	3.583
1.072	1.318	13.55	3.568
1.092	1.313	13.57	3.549
1.113	1.335	13.59	3.545

---

<u>Time (day)</u>	<u>Displacement (ft)</u>	<u>Time (day)</u>	<u>Displacement (ft)</u>
1.134	1.355	13.61	3.539
1.155	1.365	13.63	3.544
1.176	1.376	13.65	3.532
1.197	1.423	13.68	3.539
1.217	1.447	13.7	3.544
1.238	1.453	13.72	3.548
1.259	1.464	13.74	3.542
1.28	1.493	13.76	3.548
1.301	1.497	13.78	3.545
1.322	1.531	13.8	3.552
1.342	1.549	13.82	3.571
1.363	1.564	13.84	3.559
1.384	1.574	13.86	3.559
1.405	1.594	13.88	3.543
1.426	1.628	13.9	3.557
1.447	1.637	13.93	3.547
1.467	1.658	13.95	3.543
1.488	1.653	13.97	3.532
1.509	1.677	13.99	3.526
1.53	1.671	14.01	3.52
1.551	1.643	14.03	3.521
1.572	1.675	14.05	3.51
1.592	1.674	14.07	3.517
1.613	1.673	14.09	3.51
1.634	1.7	14.11	3.502
1.655	1.697	14.13	3.51
1.676	1.701	14.15	3.506
1.697	1.716	14.18	3.52
1.717	1.72	14.2	3.532
1.738	1.729	14.22	3.505
1.759	1.718	14.24	3.522
1.78	1.719	14.26	3.57
1.801	1.705	14.28	3.546
1.822	1.731	14.3	3.581
1.842	1.727	14.32	3.577
1.863	1.729	14.34	3.574
1.884	1.723	14.36	3.594
1.905	1.737	14.38	3.6
1.926	1.748	14.4	3.6
1.947	1.763	14.43	3.612
1.967	1.758	14.45	3.584
1.988	1.776	14.47	3.591
2.009	1.773	14.49	3.574
2.03	1.77	14.51	3.561
2.051	1.778	14.53	3.54
2.072	1.777	14.55	3.529
2.092	1.799	14.57	3.529
2.113	1.792	14.59	3.512
2.134	1.798	14.61	3.51
2.155	1.804	14.63	3.483
2.176	1.81	14.65	3.487
2.197	1.831	14.68	3.481
2.217	1.837	14.7	3.482

<u>Time (day)</u>	<u>Displacement (ft)</u>	<u>Time (day)</u>	<u>Displacement (ft)</u>
2.238	1.871	14.72	3.488
2.259	1.901	14.74	3.483
2.28	1.895	14.76	3.503
2.301	1.902	14.78	3.493
2.322	1.924	14.8	3.48
2.342	1.957	14.82	3.504
2.363	1.957	14.84	3.508
2.384	1.964	14.86	3.509
2.405	1.985	14.88	3.521
2.426	2.001	14.9	3.532
2.447	2.004	14.93	3.527
2.467	2.019	14.95	3.497
2.488	2.051	14.97	3.488
2.509	2.066	14.99	3.514
2.53	2.063	15.01	3.514
2.551	2.078	15.03	3.515
2.572	2.109	15.05	3.502
2.592	2.113	15.07	3.498
2.613	2.124	15.09	3.497
2.634	2.139	15.11	3.497
2.655	2.135	15.13	3.512
2.676	2.152	15.15	3.509
2.697	2.143	15.18	3.511
2.717	2.177	15.2	3.508
2.738	2.185	15.22	3.541
2.759	2.157	15.24	3.546
2.78	2.181	15.26	3.561
2.801	2.193	15.28	3.563
2.822	2.205	15.3	3.579
2.842	2.198	15.32	3.593
2.863	2.201	15.34	3.585
2.884	2.22	15.36	3.609
2.905	2.212	15.38	3.626
2.926	2.236	15.4	3.635
2.947	2.219	15.43	3.634
2.967	2.239	15.45	3.644
2.988	2.259	15.47	3.658
3.009	2.268	15.49	3.652
3.03	2.293	15.51	3.66
3.051	2.272	15.53	3.639
3.072	2.325	15.55	3.64
3.092	2.301	15.57	3.616
3.113	2.345	15.59	3.645
3.134	2.329	15.61	3.633
3.155	2.352	15.63	3.624
3.176	2.374	15.65	3.634
3.197	2.397	15.68	3.625
3.217	2.397	15.7	3.636
3.238	2.402	15.72	3.632
3.259	2.426	15.74	3.635
3.28	2.43	15.76	3.631
3.301	2.427	15.78	3.635
3.322	2.445	15.8	3.633

---

<u>Time (day)</u>	<u>Displacement (ft)</u>	<u>Time (day)</u>	<u>Displacement (ft)</u>
3.342	2.463	15.82	3.642
3.363	2.469	15.84	3.643
3.384	2.509	15.86	3.652
3.405	2.509	15.88	3.66
3.426	2.533	15.9	3.669
3.447	2.549	15.93	3.654
3.467	2.532	15.95	3.642
3.488	2.556	15.97	3.642
3.509	2.555	15.99	3.633
3.53	2.569	16.01	3.643
3.551	2.566	16.03	3.617
3.572	2.567	16.05	3.633
3.592	2.584	16.07	3.611
3.613	2.583	16.09	3.623
3.634	2.578	16.11	3.617
3.655	2.593	16.13	3.617
3.676	2.605	16.16	3.619
3.697	2.618	16.18	3.628
3.717	2.629	16.2	3.637
3.738	2.628	16.22	3.626
3.759	2.638	16.24	3.629
3.78	2.615	16.26	3.629
3.801	2.626	16.28	3.628
3.822	2.613	16.3	3.649
3.842	2.6	16.32	3.664
3.863	2.59	16.34	3.663
3.884	2.612	16.36	3.68
3.905	2.601	16.38	3.677
3.926	2.599	16.41	3.664
3.947	2.599	16.43	3.664
3.967	2.612	16.45	3.68
3.988	2.603	16.47	3.67
4.009	2.599	16.49	3.668
4.03	2.633	16.51	3.679
4.051	2.629	16.53	3.65
4.072	2.639	16.55	3.653
4.092	2.656	16.57	3.656
4.113	2.648	16.59	3.632
4.134	2.64	16.61	3.626
4.155	2.671	16.63	3.606
4.176	2.664	16.66	3.624
4.197	2.686	16.68	3.589
4.217	2.665	16.7	3.596
4.238	2.687	16.72	3.599
4.259	2.697	16.74	3.603
4.28	2.705	16.76	3.598
4.301	2.699	16.78	3.601
4.322	2.704	16.8	3.616
4.342	2.716	16.82	3.635
4.363	2.715	16.84	3.633
4.384	2.752	16.86	3.626
4.405	2.735	16.88	3.627
4.426	2.742	16.91	3.635

---

<u>Time (day)</u>	<u>Displacement (ft)</u>	<u>Time (day)</u>	<u>Displacement (ft)</u>
4.447	2.758	16.93	3.621
4.467	2.753	16.95	3.623
4.488	2.749	16.97	3.613
4.509	2.745	16.99	3.63
4.53	2.778	17.01	3.607
4.551	2.772	17.03	3.617
4.572	2.768	17.05	3.612
4.592	2.753	17.07	3.605
4.613	2.772	17.09	3.594
4.634	2.757	17.11	3.596
4.655	2.777	17.13	3.563
4.676	2.776	17.16	3.565
4.697	2.774	17.18	3.561
4.717	2.766	17.2	3.557
4.738	2.743	17.22	3.549
4.759	2.746	17.24	3.559
4.78	2.737	17.26	3.539
4.801	2.722	17.28	3.56
4.822	2.708	17.3	3.568
4.842	2.703	17.32	3.564
4.863	2.702	17.34	3.578
4.884	2.698	17.36	3.576
4.905	2.693	17.38	3.582
4.926	2.705	17.41	3.58
4.947	2.687	17.43	3.581
4.967	2.71	17.45	3.589
4.988	2.717	17.47	3.606
5.009	2.712	17.49	3.577
5.03	2.715	17.51	3.588
5.051	2.712	17.53	3.579
5.072	2.719	17.55	3.592
5.092	2.716	17.57	3.572
5.113	2.724	17.59	3.57
5.134	2.731	17.61	3.559
5.155	2.755	17.63	3.562
5.176	2.757	17.66	3.542
5.197	2.742	17.68	3.552
5.217	2.748	17.7	3.56
5.238	2.749	17.72	3.56
5.259	2.733	17.74	3.542
5.28	2.755	17.76	3.532
5.301	2.738	17.78	3.539
5.322	2.758	17.8	3.536
5.342	2.743	17.82	3.532
5.363	2.738	17.84	3.531
5.384	2.765	17.86	3.536
5.405	2.746	17.88	3.522
5.426	2.772	17.91	3.523
5.447	2.759	17.93	3.518
5.467	2.783	17.95	3.528
5.488	2.787	17.97	3.536
5.509	2.785	17.99	3.549
5.53	2.767	18.01	3.53

---

<u>Time (day)</u>	<u>Displacement (ft)</u>	<u>Time (day)</u>	<u>Displacement (ft)</u>
5.551	2.792	18.03	3.552
5.572	2.778	18.05	3.553
5.592	2.786	18.07	3.55
5.613	2.785	18.09	3.569
5.634	2.803	18.11	3.557
5.655	2.788	18.13	3.549
5.676	2.796	18.16	3.563
5.697	2.796	18.18	3.575
5.717	2.79	18.2	3.57
5.738	2.8	18.22	3.559
5.759	2.794	18.24	3.543
5.78	2.792	18.26	3.565
5.801	2.769	18.28	3.551
5.822	2.797	18.3	3.555
5.842	2.783	18.32	3.556
5.863	2.796	18.34	3.555
5.884	2.8	18.36	3.561
5.905	2.797	18.38	3.555
5.926	2.78	18.41	3.567
5.947	2.79	18.43	3.558
5.967	2.802	18.45	3.589
5.988	2.795	18.47	3.596
6.009	2.8	18.49	3.59
6.03	2.838	18.51	3.585
6.051	2.833	18.53	3.581
6.072	2.844	18.55	3.595
6.092	2.875	18.57	3.588
6.113	2.883	18.59	3.597
6.134	2.9	18.61	3.576
6.155	2.925	18.63	3.603
6.176	2.947	18.66	3.583
6.197	2.944	18.68	3.591
6.217	2.959	18.7	3.589
6.238	2.963	18.72	3.569
6.259	2.951	18.74	3.574
6.28	2.976	18.76	3.538
6.301	3.002	18.78	3.54
6.322	2.992	18.8	3.543
6.342	2.992	18.82	3.542
6.363	2.993	18.84	3.509
6.384	3.	18.86	3.511
6.405	3.011	18.88	3.494
6.426	3.012	18.91	3.484
6.447	3.031	18.93	3.458
6.467	3.033	18.95	3.465
6.488	3.021	18.97	3.457
6.509	3.025	18.99	3.439
6.53	3.047	19.01	3.445
6.551	3.066	19.03	3.44
6.572	3.072	19.05	3.449
6.592	3.085	19.07	3.448
6.613	3.08	19.09	3.458
6.634	3.101	19.11	3.455

---

<u>Time (day)</u>	<u>Displacement (ft)</u>	<u>Time (day)</u>	<u>Displacement (ft)</u>
6.655	3.117	19.13	3.458
6.676	3.095	19.16	3.45
6.697	3.11	19.18	3.451
6.717	3.093	19.2	3.468
6.738	3.099	19.22	3.451
6.759	3.091	19.24	3.472
6.78	3.071	19.26	3.477
6.801	3.074	19.28	3.463
6.822	3.084	19.3	3.474
6.842	3.074	19.32	3.468
6.863	3.058	19.34	3.47
6.884	3.058	19.36	3.482
6.905	3.058	19.38	3.469
6.926	3.027	19.41	3.47
6.947	3.045	19.43	3.482
6.967	3.045	19.45	3.494
6.988	3.031	19.47	3.498
7.009	3.048	19.49	3.489
7.03	3.054	19.51	3.51
7.051	3.053	19.53	3.517
7.072	3.057	19.55	3.51
7.092	3.094	19.57	3.525
7.113	3.119	19.59	3.544
7.134	3.111	19.61	3.55
7.155	3.122	19.63	3.55
7.176	3.141	19.66	3.565
7.197	3.153	19.68	3.568
7.217	3.16	19.7	3.57
7.238	3.192	19.72	3.569
7.259	3.179	19.74	3.565
7.28	3.186	19.76	3.564
7.301	3.197	19.78	3.559
7.322	3.195	19.8	3.552
7.342	3.185	19.82	3.562
7.363	3.183	19.84	3.551
7.384	3.185	19.86	3.537
7.405	3.188	19.88	3.538
7.426	3.187	19.91	3.522
7.447	3.189	19.93	3.514
7.467	3.187	19.95	3.516
7.488	3.183	19.97	3.514
7.509	3.174	19.99	3.509
7.53	3.195	20.01	3.538
7.551	3.185	20.03	3.558
7.572	3.193	20.05	3.548
7.592	3.219	20.07	3.555
7.613	3.22	20.09	3.576
7.634	3.198	20.11	3.571
7.655	3.216	20.13	3.581
7.676	3.214	20.16	3.601
7.697	3.212	20.18	3.614
7.717	3.236	20.2	3.616
7.738	3.21	20.22	3.61

<u>Time (day)</u>	<u>Displacement (ft)</u>	<u>Time (day)</u>	<u>Displacement (ft)</u>
7.759	3.21	20.24	3.616
7.78	3.206	20.26	3.619
7.801	3.21	20.28	3.598
7.822	3.207	20.3	3.613
7.842	3.19	20.32	3.597
7.863	3.18	20.34	3.603
7.884	3.171	20.36	3.595
7.905	3.187	20.38	3.587
7.926	3.204	20.41	3.567
7.947	3.192	20.43	3.589
7.967	3.189	20.45	3.592
7.988	3.193	20.47	3.598
8.009	3.184	20.49	3.576
8.03	3.195	20.51	3.595
8.051	3.197	20.53	3.598
8.072	3.22	20.55	3.601
8.092	3.212	20.57	3.605
8.113	3.229	20.59	3.597
8.134	3.245	20.61	3.598
8.155	3.274	20.63	3.613
8.176	3.291	20.66	3.609
8.197	3.311	20.68	3.63
8.217	3.296	20.7	3.644
8.238	3.322	20.72	3.626
8.259	3.315	20.74	3.624
8.28	3.338	20.76	3.628
8.301	3.338	20.78	3.631
8.322	3.334	20.8	3.632
8.342	3.332	20.82	3.621
8.363	3.345	20.84	3.632
8.384	3.362	20.86	3.626
8.405	3.341	20.88	3.626
8.426	3.348	20.91	3.612
8.447	3.345	20.93	3.62
8.467	3.328	20.95	3.633
8.488	3.335	20.97	3.634
8.509	3.336	20.99	3.635
8.53	3.332	21.01	3.639
8.551	3.313	21.03	3.644
8.572	3.33	21.05	3.648
8.592	3.339	21.07	3.681
8.613	3.352	21.09	3.705
8.634	3.359	21.11	3.668
8.655	3.364	21.13	3.717
8.676	3.373	21.16	3.706
8.697	3.411	21.18	3.736
8.717	3.366	21.2	3.73
8.738	3.387	21.22	3.743
8.759	3.37	21.24	3.745
8.78	3.358	21.26	3.734
8.801	3.345	21.28	3.753
8.822	3.357	21.3	3.757
8.842	3.342	21.32	3.754



---

<u>Time (day)</u>	<u>Displacement (ft)</u>	<u>Time (day)</u>	<u>Displacement (ft)</u>
8.863	3.357	21.34	3.738
8.884	3.357	21.36	3.743
8.905	3.347	21.38	3.746
8.926	3.338	21.41	3.724
8.947	3.329	21.43	3.714
8.967	3.321	21.45	3.722
8.988	3.312	21.47	3.708
9.009	3.323	21.49	3.709
9.03	3.336	21.51	3.708
9.051	3.33	21.53	3.702
9.072	3.333	21.55	3.694
9.092	3.36	21.57	3.697
9.113	3.367	21.59	3.697
9.134	3.377	21.61	3.681
9.155	3.396	21.63	3.683
9.176	3.411	21.66	3.714
9.197	3.433	21.68	3.702
9.217	3.419	21.7	3.71
9.238	3.448	21.72	3.718
9.259	3.437	21.74	3.719
9.28	3.433	21.76	3.7
9.301	3.439	21.78	3.699
9.322	3.435	21.8	3.701
9.342	3.419	21.82	3.684
9.363	3.418	21.84	3.677
9.384	3.416	21.86	3.668
9.405	3.4	21.88	3.664
9.426	3.402	21.91	3.655
9.447	3.391	21.93	3.633
9.467	3.375	21.95	3.628
9.488	3.365	21.97	3.642
9.509	3.367	21.99	3.628
9.53	3.355	22.01	3.626
9.551	3.336	22.03	3.619
9.572	3.341	22.05	3.644
9.592	3.342	22.07	3.624
9.613	3.357	22.09	3.641
9.634	3.345	22.11	3.658
9.655	3.339	22.13	3.65
9.676	3.338	22.16	3.662
9.697	3.356	22.18	3.675
9.717	3.339	22.2	3.671
9.738	3.356	22.22	3.668
9.759	3.347	22.24	3.692
9.78	3.334	22.26	3.69
9.801	3.35	22.28	3.693
9.822	3.348	22.3	3.674
9.842	3.355	22.32	3.672
9.863	3.331	22.34	3.667
9.884	3.335	22.36	3.662
9.905	3.309	22.38	3.645
9.926	3.29	22.41	3.637
9.947	3.264	22.43	3.625

---

<u>Time (day)</u>	<u>Displacement (ft)</u>	<u>Time (day)</u>	<u>Displacement (ft)</u>
9.967	3.256	22.45	3.617
9.988	3.254	22.47	3.585
10.01	3.272	22.49	3.602
10.03	3.261	22.51	3.57
10.05	3.259	22.53	3.574
10.07	3.255	22.55	3.565
10.09	3.262	22.57	3.544
10.11	3.285	22.59	3.563
10.13	3.293	22.61	3.58
10.15	3.275	22.63	3.552
10.18	3.309	22.66	3.563
10.2	3.29	22.68	3.552
10.22	3.298	22.7	3.583
10.24	3.316	22.72	3.575
10.26	3.328	22.74	3.583
10.28	3.318	22.76	3.601
10.3	3.298	22.78	3.573
10.32	3.312	22.8	3.605
10.34	3.32	22.82	3.602
10.36	3.307	22.84	3.591
10.38	3.297	22.86	3.586
10.4	3.291	22.88	3.567
10.43	3.268	22.91	3.572
10.45	3.27	22.93	3.554
10.47	3.265	22.95	3.532
10.49	3.239	22.97	3.549
10.51	3.233	22.99	3.533
10.53	3.208	23.01	3.536
10.55	3.219	23.03	3.557
10.57	3.21	23.05	3.547
10.59	3.185	23.07	3.553
10.61	3.207	23.09	3.557
10.63	3.206	23.11	3.581
10.65	3.187	23.13	3.575
10.68	3.185	23.16	3.59
10.7	3.188	23.18	3.596
10.72	3.203	23.2	3.601
10.74	3.207	23.22	3.613
10.76	3.2	23.24	3.634
10.78	3.21	23.26	3.639
10.8	3.212	23.28	3.64
10.82	3.231	23.3	3.652
10.84	3.223	23.32	3.648
10.86	3.201	23.34	3.628
10.88	3.196	23.36	3.627
10.9	3.184	23.38	3.621
10.93	3.192	23.41	3.633
10.95	3.166	23.43	3.596
10.97	3.183	23.45	3.605
10.99	3.162	23.47	3.594
11.01	3.163	23.49	3.586
11.03	3.164	23.51	3.587
11.05	3.154	23.53	3.592

---

<u>Time (day)</u>	<u>Displacement (ft)</u>	<u>Time (day)</u>	<u>Displacement (ft)</u>
11.07	3.176	23.55	3.581
11.09	3.182	23.57	3.58
11.11	3.194	23.59	3.603
11.13	3.204	23.61	3.601
11.15	3.202	23.63	3.616
11.18	3.231	23.66	3.608
11.2	3.238	23.68	3.633
11.22	3.278	23.7	3.643
11.24	3.277	23.72	3.654
11.26	3.278	23.74	3.669
11.28	3.298	23.76	3.656
11.3	3.302	23.78	3.656
11.32	3.314	23.8	3.654
11.34	3.325	23.82	3.655
11.36	3.332	23.84	3.64
11.38	3.329	23.86	3.638
11.4	3.344	23.88	3.646
11.43	3.338	23.91	3.649
11.45	3.329	23.93	3.619
11.47	3.33	23.95	3.616
11.49	3.306	23.97	3.618
11.51	3.298	23.99	3.618
11.53	3.283	24.01	3.612
11.55	3.306	24.03	3.606
11.57	3.295	24.05	3.619
11.59	3.276	24.07	3.601
11.61	3.274	24.09	3.607
11.63	3.288	24.11	3.627
11.65	3.292	24.13	3.651
11.68	3.309	24.16	3.629
11.7	3.321	24.18	3.638
11.72	3.347	24.2	3.653
11.74	3.363	24.22	3.674
11.76	3.35	24.24	3.664
11.78	3.366	24.26	3.692
11.8	3.374	24.28	3.687
11.82	3.398	24.3	3.68
11.84	3.391	24.32	3.691
11.86	3.374	24.34	3.686
11.88	3.387	24.36	3.698
11.9	3.398	24.38	3.67
11.93	3.381	24.41	3.663
11.95	3.393	24.43	3.653
11.97	3.373	24.45	3.662
11.99	3.374	24.47	3.652
12.01	3.356	24.49	3.648
12.03	3.366	24.51	3.638
12.05	3.381	24.53	3.625
12.07	3.362	24.55	3.625
12.09	3.392	24.57	3.637
12.11	3.396	24.59	3.634
12.13	3.403	24.61	3.621
12.15	3.428	24.63	3.628

<u>Time (day)</u>	<u>Displacement (ft)</u>	<u>Time (day)</u>	<u>Displacement (ft)</u>
12.18	3.434	24.66	3.637
12.2	3.454	24.68	3.658
12.22	3.461	24.7	3.65
12.24	3.496	24.72	3.655
12.26	3.498	24.74	3.656
12.28	3.523	24.76	3.661
12.3	3.54	24.78	3.676
12.32	3.567	24.8	3.683
12.34	3.556	24.82	3.66
12.36	3.58	24.84	3.656
12.38	3.584	24.86	3.669
12.4	3.57	24.88	3.652
12.43	3.566	24.91	3.651
12.45	3.562	24.93	3.663
12.47	3.557		

---

### SOLUTION

Pumping Test  
Aquifer Model: Unconfined  
Solution Method: Neuman

---

### VISUAL ESTIMATION RESULTS

#### Estimated Parameters

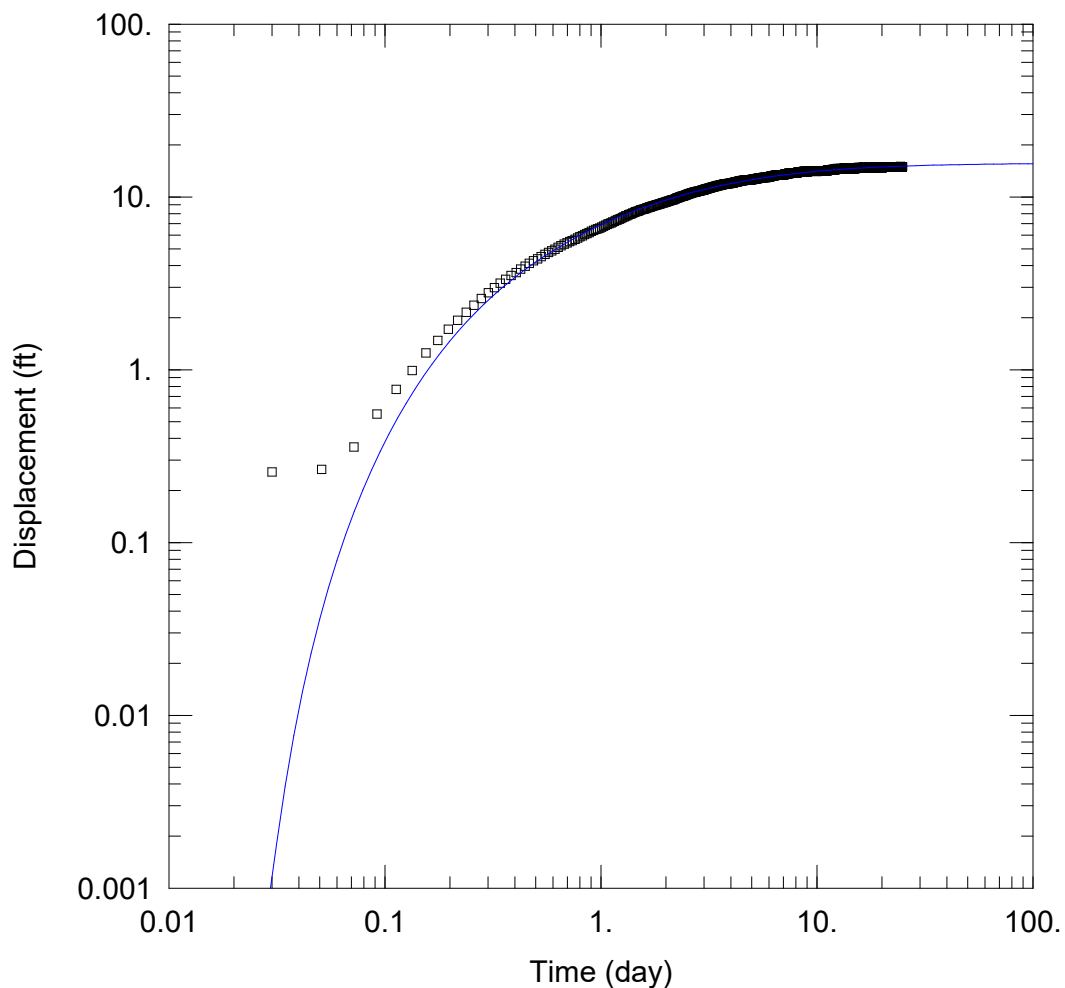
<u>Parameter</u>	<u>Estimate</u>	
T	4.759E+4	ft <sup>2</sup> /day
S	0.02677	
Sy	0.5	
β	0.001	

$K = T/b = 9.517 \text{ ft/day (0.003357 cm/sec)}$

$S_s = S/b = 5.354E-6 \text{ 1/ft}$

**APPENDIX F**

**AQTESOLV OUTPUT FOR R-20 SCREEN 3 DRAWDOWN ANALYSIS**



WELL TEST ANALYSIS

Data Set: D:\hugo \Downloads\LANL NM PROJECT\AQTESOLV files\R20 S3 data.aqt  
 Date: 06/07/24 Time: 14:30:31

PROJECT INFORMATION

Test Well: PM-2

AQUIFER DATA

Saturated Thickness: 5000. ft

WELL DATA

Pumping Wells			Observation Wells		
Well Name	X (ft)	Y (ft)	Well Name	X (ft)	Y (ft)
PM-2	0	0	□ R20 S3	1225	0

SOLUTION

Aquifer Model: Unconfined

Solution Method: Neuman

T = 1.422E+4 ft<sup>2</sup>/day

S = 0.006537

Sy = 0.5

β = 0.0009417

Data Set: D:\hugo\_\Downloads\LANL NM PROJECT\AQTESOLV files\R20 S3 data.aqt

Date: 06/07/24

Time: 14:31:01

---

PROJECT INFORMATION

Test Well: PM-2

---

AQUIFER DATA

Saturated Thickness: 5000. ft

Anisotropy Ratio (Kz/Kr): 0.01569

---

PUMPING WELL DATA

No. of pumping wells: 1

Pumping Well No. 1: PM-2

X Location: 0. ft

Y Location: 0. ft

Casing Radius: 0.5833 ft

Well Radius: 1. ft

Partially Penetrating Well

Depth to Top of Screen: 135. ft

Depth to Bottom of Screen: 1411. ft

No. of pumping periods: 1

Pumping Period Data

<u>Time (day)</u>	<u>Rate (gal/min)</u>
0.	1249.

---

OBSERVATION WELL DATA

No. of observation wells: 1

Observation Well No. 1: R20 S3

X Location: 1225. ft

Y Location: 0. ft

Radial distance from PM-2: 1225. ft

Partially Penetrating Well

Depth to Top of Screen: 479.1 ft

Depth to Bottom of Screen: 486.8 ft

No. of Observations: 1197

Observation Data

<u>Time (day)</u>	<u>Displacement (ft)</u>	<u>Time (day)</u>	<u>Displacement (ft)</u>
-------------------	--------------------------	-------------------	--------------------------

---

0.009	0.272	12.49	14.55
0.03	0.256	12.51	14.56
0.051	0.265	12.53	14.55
0.072	0.357	12.55	14.52
0.092	0.553	12.57	14.53
0.113	0.769	12.59	14.53
0.134	0.991	12.61	14.52
0.155	1.251	12.63	14.53
0.176	1.477	12.65	14.53
0.197	1.714	12.68	14.54
0.217	1.935	12.7	14.53
0.238	2.15	12.72	14.53
0.259	2.361	12.74	14.55
0.28	2.577	12.76	14.56
0.301	2.791	12.78	14.56
0.322	2.98	12.8	14.55
0.342	3.172	12.82	14.57
0.363	3.342	12.84	14.56
0.384	3.508	12.86	14.56
0.405	3.652	12.88	14.56
0.426	3.827	12.9	14.57
0.447	3.972	12.93	14.53
0.467	4.121	12.95	14.55
0.488	4.266	12.97	14.54
0.509	4.381	12.99	14.53
0.53	4.521	13.01	14.53
0.551	4.655	13.03	14.52
0.572	4.772	13.05	14.52
0.592	4.879	13.07	14.5
0.613	4.988	13.09	14.51
0.634	5.111	13.11	14.51
0.655	5.211	13.13	14.51
0.676	5.327	13.15	14.52
0.697	5.428	13.18	14.54
0.717	5.511	13.2	14.54
0.738	5.597	13.22	14.55
0.759	5.673	13.24	14.56
0.78	5.79	13.26	14.57
0.801	5.876	13.28	14.58
0.822	5.968	13.3	14.6
0.842	6.068	13.32	14.6
0.863	6.142	13.34	14.63
0.884	6.229	13.36	14.61
0.905	6.32	13.38	14.62
0.926	6.4	13.4	14.63
0.947	6.483	13.43	14.61
0.967	6.552	13.45	14.62
0.988	6.61	13.47	14.61
1.009	6.686	13.49	14.6
1.03	6.766	13.51	14.59
1.051	6.857	13.53	14.59
1.072	6.948	13.55	14.59
1.092	7.006	13.57	14.58
1.113	7.075	13.59	14.58



<u>Time (day)</u>	<u>Displacement (ft)</u>	<u>Time (day)</u>	<u>Displacement (ft)</u>
1.134	7.152	13.61	14.55
1.155	7.232	13.63	14.57
1.176	7.299	13.65	14.55
1.197	7.376	13.68	14.58
1.217	7.445	13.7	14.59
1.238	7.509	13.72	14.58
1.259	7.583	13.74	14.59
1.28	7.658	13.76	14.58
1.301	7.749	13.78	14.58
1.322	7.799	13.8	14.59
1.342	7.881	13.82	14.6
1.363	7.925	13.84	14.57
1.384	7.998	13.86	14.58
1.405	8.076	13.88	14.6
1.426	8.115	13.9	14.57
1.447	8.193	13.93	14.6
1.467	8.248	13.95	14.57
1.488	8.284	13.97	14.58
1.509	8.337	13.99	14.57
1.53	8.406	14.01	14.55
1.551	8.447	14.03	14.57
1.572	8.479	14.05	14.56
1.592	8.524	14.07	14.56
1.613	8.575	14.09	14.54
1.634	8.636	14.11	14.56
1.655	8.673	14.13	14.58
1.676	8.736	14.15	14.56
1.697	8.756	14.18	14.57
1.717	8.823	14.2	14.58
1.738	8.86	14.22	14.58
1.759	8.891	14.24	14.59
1.78	8.931	14.26	14.6
1.801	8.964	14.28	14.61
1.822	9.012	14.3	14.61
1.842	9.065	14.32	14.63
1.863	9.085	14.34	14.64
1.884	9.126	14.36	14.66
1.905	9.173	14.38	14.65
1.926	9.224	14.4	14.67
1.947	9.25	14.43	14.66
1.967	9.293	14.45	14.67
1.988	9.315	14.47	14.66
2.009	9.347	14.49	14.64
2.03	9.396	14.51	14.64
2.051	9.439	14.53	14.62
2.072	9.477	14.55	14.6
2.092	9.511	14.57	14.61
2.113	9.551	14.59	14.61
2.134	9.598	14.61	14.59
2.155	9.638	14.63	14.57
2.176	9.662	14.65	14.59
2.197	9.705	14.68	14.58
2.217	9.762	14.7	14.6

---

<u>Time (day)</u>	<u>Displacement (ft)</u>	<u>Time (day)</u>	<u>Displacement (ft)</u>
2.238	9.808	14.72	14.59
2.259	9.85	14.74	14.59
2.28	9.884	14.76	14.59
2.301	9.926	14.78	14.59
2.322	9.971	14.8	14.6
2.342	10.02	14.82	14.61
2.363	10.05	14.84	14.6
2.384	10.09	14.86	14.62
2.405	10.12	14.88	14.63
2.426	10.15	14.9	14.62
2.447	10.2	14.93	14.63
2.467	10.23	14.95	14.63
2.488	10.3	14.97	14.61
2.509	10.33	14.99	14.62
2.53	10.37	15.01	14.62
2.551	10.4	15.03	14.62
2.572	10.44	15.05	14.6
2.592	10.47	15.07	14.62
2.613	10.49	15.09	14.62
2.634	10.54	15.11	14.62
2.655	10.57	15.13	14.63
2.676	10.61	15.15	14.63
2.697	10.64	15.18	14.64
2.717	10.67	15.2	14.65
2.738	10.68	15.22	14.66
2.759	10.71	15.24	14.65
2.78	10.72	15.26	14.69
2.801	10.75	15.28	14.67
2.822	10.77	15.3	14.7
2.842	10.79	15.32	14.69
2.863	10.81	15.34	14.71
2.884	10.85	15.36	14.71
2.905	10.86	15.38	14.73
2.926	10.9	15.4	14.75
2.947	10.92	15.43	14.76
2.967	10.96	15.45	14.74
2.988	10.98	15.47	14.76
3.009	10.98	15.49	14.76
3.03	11.04	15.51	14.76
3.051	11.08	15.53	14.76
3.072	11.11	15.55	14.74
3.092	11.14	15.57	14.76
3.113	11.15	15.59	14.77
3.134	11.19	15.61	14.75
3.155	11.21	15.63	14.76
3.176	11.24	15.65	14.75
3.197	11.26	15.68	14.75
3.217	11.28	15.7	14.78
3.238	11.33	15.72	14.76
3.259	11.34	15.74	14.75
3.28	11.38	15.76	14.75
3.301	11.4	15.78	14.75
3.322	11.42	15.8	14.73

<u>Time (day)</u>	<u>Displacement (ft)</u>	<u>Time (day)</u>	<u>Displacement (ft)</u>
3.342	11.44	15.82	14.74
3.363	11.48	15.84	14.76
3.384	11.48	15.86	14.78
3.405	11.52	15.88	14.76
3.426	11.54	15.9	14.75
3.447	11.56	15.93	14.76
3.467	11.61	15.95	14.75
3.488	11.62	15.97	14.77
3.509	11.65	15.99	14.76
3.53	11.65	16.01	14.75
3.551	11.68	16.03	14.74
3.572	11.68	16.05	14.74
3.592	11.72	16.07	14.74
3.613	11.73	16.09	14.75
3.634	11.76	16.11	14.73
3.655	11.8	16.13	14.73
3.676	11.81	16.16	14.74
3.697	11.84	16.18	14.73
3.717	11.85	16.2	14.74
3.738	11.87	16.22	14.75
3.759	11.87	16.24	14.75
3.78	11.87	16.26	14.75
3.801	11.88	16.28	14.79
3.822	11.89	16.3	14.77
3.842	11.9	16.32	14.77
3.863	11.93	16.34	14.79
3.884	11.93	16.36	14.79
3.905	11.94	16.38	14.8
3.926	11.96	16.41	14.79
3.947	11.96	16.43	14.81
3.967	11.97	16.45	14.8
3.988	11.99	16.47	14.79
4.009	12.03	16.49	14.8
4.03	12.03	16.51	14.78
4.051	12.04	16.53	14.81
4.072	12.06	16.55	14.79
4.092	12.06	16.57	14.8
4.113	12.09	16.59	14.77
4.134	12.12	16.61	14.76
4.155	12.15	16.63	14.78
4.176	12.16	16.66	14.78
4.197	12.18	16.68	14.76
4.217	12.2	16.7	14.75
4.238	12.2	16.72	14.77
4.259	12.22	16.74	14.74
4.28	12.25	16.76	14.74
4.301	12.27	16.78	14.78
4.322	12.27	16.8	14.77
4.342	12.32	16.82	14.78
4.363	12.32	16.84	14.79
4.384	12.33	16.86	14.78
4.405	12.35	16.88	14.79
4.426	12.36	16.91	14.8

---

<u>Time (day)</u>	<u>Displacement (ft)</u>	<u>Time (day)</u>	<u>Displacement (ft)</u>
4.447	12.39	16.93	14.78
4.467	12.39	16.95	14.79
4.488	12.41	16.97	14.78
4.509	12.43	16.99	14.77
4.53	12.43	17.01	14.78
4.551	12.46	17.03	14.77
4.572	12.45	17.05	14.77
4.592	12.47	17.07	14.74
4.613	12.46	17.09	14.74
4.634	12.49	17.11	14.74
4.655	12.5	17.13	14.74
4.676	12.53	17.16	14.72
4.697	12.53	17.18	14.73
4.717	12.53	17.2	14.73
4.738	12.54	17.22	14.72
4.759	12.52	17.24	14.72
4.78	12.53	17.26	14.74
4.801	12.53	17.28	14.72
4.822	12.53	17.3	14.73
4.842	12.53	17.32	14.74
4.863	12.53	17.34	14.73
4.884	12.54	17.36	14.75
4.905	12.54	17.38	14.76
4.926	12.55	17.41	14.75
4.947	12.56	17.43	14.77
4.967	12.58	17.45	14.75
4.988	12.6	17.47	14.76
5.009	12.6	17.49	14.77
5.03	12.61	17.51	14.74
5.051	12.63	17.53	14.75
5.072	12.64	17.55	14.75
5.092	12.65	17.57	14.75
5.113	12.69	17.59	14.75
5.134	12.68	17.61	14.73
5.155	12.72	17.63	14.77
5.176	12.72	17.66	14.74
5.197	12.74	17.68	14.74
5.217	12.74	17.7	14.75
5.238	12.73	17.72	14.73
5.259	12.75	17.74	14.73
5.28	12.77	17.76	14.72
5.301	12.76	17.78	14.74
5.322	12.79	17.8	14.73
5.342	12.77	17.82	14.74
5.363	12.81	17.84	14.74
5.384	12.81	17.86	14.73
5.405	12.82	17.88	14.75
5.426	12.82	17.91	14.74
5.447	12.85	17.93	14.74
5.467	12.85	17.95	14.75
5.488	12.85	17.97	14.76
5.509	12.87	17.99	14.77
5.53	12.89	18.01	14.77

---

<u>Time (day)</u>	<u>Displacement (ft)</u>	<u>Time (day)</u>	<u>Displacement (ft)</u>
5.551	12.88	18.03	14.78
5.572	12.88	18.05	14.76
5.592	12.9	18.07	14.78
5.613	12.94	18.09	14.78
5.634	12.92	18.11	14.78
5.655	12.95	18.13	14.78
5.676	12.95	18.16	14.79
5.697	12.98	18.18	14.8
5.717	12.97	18.2	14.78
5.738	12.97	18.22	14.77
5.759	12.96	18.24	14.79
5.78	12.96	18.26	14.77
5.801	12.98	18.28	14.8
5.822	12.98	18.3	14.79
5.842	12.97	18.32	14.79
5.863	13.	18.34	14.79
5.884	12.98	18.36	14.8
5.905	12.99	18.38	14.79
5.926	13.01	18.41	14.82
5.947	13.03	18.43	14.81
5.967	13.03	18.45	14.84
5.988	13.04	18.47	14.83
6.009	13.06	18.49	14.83
6.03	13.07	18.51	14.83
6.051	13.09	18.53	14.82
6.072	13.1	18.55	14.82
6.092	13.14	18.57	14.81
6.113	13.15	18.59	14.82
6.134	13.16	18.61	14.82
6.155	13.17	18.63	14.83
6.176	13.19	18.66	14.83
6.197	13.22	18.68	14.82
6.217	13.24	18.7	14.84
6.238	13.22	18.72	14.82
6.259	13.23	18.74	14.8
6.28	13.27	18.76	14.8
6.301	13.27	18.78	14.79
6.322	13.29	18.8	14.77
6.342	13.29	18.82	14.77
6.363	13.29	18.84	14.76
6.384	13.3	18.86	14.75
6.405	13.32	18.88	14.74
6.426	13.32	18.91	14.73
6.447	13.33	18.93	14.74
6.467	13.33	18.95	14.71
6.488	13.35	18.97	14.71
6.509	13.34	18.99	14.72
6.53	13.38	19.01	14.72
6.551	13.38	19.03	14.72
6.572	13.39	19.05	14.73
6.592	13.4	19.07	14.72
6.613	13.41	19.09	14.73
6.634	13.42	19.11	14.72

<u>Time (day)</u>	<u>Displacement (ft)</u>	<u>Time (day)</u>	<u>Displacement (ft)</u>
6.655	13.45	19.13	14.73
6.676	13.45	19.16	14.74
6.697	13.44	19.18	14.72
6.717	13.45	19.2	14.75
6.738	13.45	19.22	14.73
6.759	13.42	19.24	14.75
6.78	13.44	19.26	14.74
6.801	13.42	19.28	14.74
6.822	13.43	19.3	14.74
6.842	13.43	19.32	14.75
6.863	13.43	19.34	14.77
6.884	13.43	19.36	14.75
6.905	13.42	19.38	14.77
6.926	13.43	19.41	14.75
6.947	13.43	19.43	14.78
6.967	13.43	19.45	14.78
6.988	13.43	19.47	14.78
7.009	13.45	19.49	14.79
7.03	13.45	19.51	14.79
7.051	13.46	19.53	14.8
7.072	13.48	19.55	14.81
7.092	13.49	19.57	14.8
7.113	13.5	19.59	14.83
7.134	13.54	19.61	14.83
7.155	13.56	19.63	14.84
7.176	13.57	19.66	14.84
7.197	13.59	19.68	14.86
7.217	13.59	19.7	14.85
7.238	13.61	19.72	14.86
7.259	13.62	19.74	14.85
7.28	13.62	19.76	14.85
7.301	13.63	19.78	14.84
7.322	13.65	19.8	14.83
7.342	13.65	19.82	14.83
7.363	13.65	19.84	14.83
7.384	13.65	19.86	14.8
7.405	13.65	19.88	14.82
7.426	13.67	19.91	14.81
7.447	13.67	19.93	14.8
7.467	13.68	19.95	14.8
7.488	13.69	19.97	14.79
7.509	13.68	19.99	14.79
7.53	13.7	20.01	14.8
7.551	13.7	20.03	14.8
7.572	13.71	20.05	14.81
7.592	13.72	20.07	14.8
7.613	13.72	20.09	14.83
7.634	13.74	20.11	14.84
7.655	13.73	20.13	14.85
7.676	13.75	20.16	14.87
7.697	13.75	20.18	14.86
7.717	13.74	20.2	14.86
7.738	13.75	20.22	14.89

---

<u>Time (day)</u>	<u>Displacement (ft)</u>	<u>Time (day)</u>	<u>Displacement (ft)</u>
7.759	13.75	20.24	14.86
7.78	13.74	20.26	14.9
7.801	13.73	20.28	14.9
7.822	13.74	20.3	14.88
7.842	13.73	20.32	14.88
7.863	13.73	20.34	14.89
7.884	13.73	20.36	14.88
7.905	13.73	20.38	14.87
7.926	13.74	20.41	14.86
7.947	13.73	20.43	14.87
7.967	13.74	20.45	14.84
7.988	13.75	20.47	14.86
8.009	13.75	20.49	14.86
8.03	13.77	20.51	14.85
8.051	13.77	20.53	14.86
8.072	13.77	20.55	14.87
8.092	13.8	20.57	14.88
8.113	13.82	20.59	14.86
8.134	13.83	20.61	14.86
8.155	13.84	20.63	14.88
8.176	13.88	20.66	14.88
8.197	13.9	20.68	14.88
8.217	13.91	20.7	14.91
8.238	13.91	20.72	14.89
8.259	13.93	20.74	14.91
8.28	13.95	20.76	14.9
8.301	13.94	20.78	14.88
8.322	13.94	20.8	14.88
8.342	13.96	20.82	14.89
8.363	13.96	20.84	14.88
8.384	13.97	20.86	14.9
8.405	13.95	20.88	14.87
8.426	13.97	20.91	14.88
8.447	13.99	20.93	14.87
8.467	13.97	20.95	14.88
8.488	13.96	20.97	14.88
8.509	13.98	20.99	14.88
8.53	13.98	21.01	14.87
8.551	13.98	21.03	14.89
8.572	13.98	21.05	14.9
8.592	13.98	21.07	14.91
8.613	14.	21.09	14.94
8.634	14.	21.11	14.95
8.655	14.03	21.13	14.95
8.676	14.03	21.16	14.94
8.697	14.04	21.18	14.96
8.717	14.03	21.2	14.98
8.738	14.03	21.22	14.97
8.759	14.01	21.24	14.99
8.78	14.02	21.26	14.98
8.801	14.01	21.28	14.98
8.822	14.02	21.3	14.97
8.842	14.02	21.32	14.98

---

<u>Time (day)</u>	<u>Displacement (ft)</u>	<u>Time (day)</u>	<u>Displacement (ft)</u>
8.863	14.	21.34	14.99
8.884	14.02	21.36	14.97
8.905	14.01	21.38	14.96
8.926	14.	21.41	14.96
8.947	14.01	21.43	14.96
8.967	14.	21.45	14.96
8.988	14.01	21.47	14.96
9.009	14.01	21.49	14.94
9.03	13.99	21.51	14.96
9.051	14.01	21.53	14.95
9.072	14.03	21.55	14.94
9.092	14.04	21.57	14.93
9.113	14.04	21.59	14.95
9.134	14.06	21.61	14.93
9.155	14.09	21.63	14.93
9.176	14.1	21.66	14.93
9.197	14.09	21.68	14.93
9.217	14.11	21.7	14.94
9.238	14.11	21.72	14.95
9.259	14.13	21.74	14.96
9.28	14.13	21.76	14.95
9.301	14.14	21.78	14.91
9.322	14.13	21.8	14.93
9.342	14.14	21.82	14.94
9.363	14.11	21.84	14.91
9.384	14.11	21.86	14.9
9.405	14.11	21.88	14.9
9.426	14.12	21.91	14.89
9.447	14.1	21.93	14.89
9.467	14.1	21.95	14.88
9.488	14.09	21.97	14.87
9.509	14.1	21.99	14.87
9.53	14.1	22.01	14.86
9.551	14.1	22.03	14.86
9.572	14.07	22.05	14.87
9.592	14.09	22.07	14.89
9.613	14.1	22.09	14.89
9.634	14.09	22.11	14.89
9.655	14.09	22.13	14.9
9.676	14.11	22.16	14.91
9.697	14.11	22.18	14.92
9.717	14.1	22.2	14.95
9.738	14.14	22.22	14.94
9.759	14.13	22.24	14.96
9.78	14.14	22.26	14.94
9.801	14.13	22.28	14.96
9.822	14.13	22.3	14.94
9.842	14.14	22.32	14.97
9.863	14.11	22.34	14.94
9.884	14.1	22.36	14.93
9.905	14.09	22.38	14.91
9.926	14.09	22.41	14.9
9.947	14.09	22.43	14.92



---

<u>Time (day)</u>	<u>Displacement (ft)</u>	<u>Time (day)</u>	<u>Displacement (ft)</u>
9.967	14.08	22.45	14.9
9.988	14.07	22.47	14.89
10.01	14.05	22.49	14.89
10.03	14.06	22.51	14.87
10.05	14.07	22.53	14.88
10.07	14.09	22.55	14.87
10.09	14.08	22.57	14.88
10.11	14.08	22.59	14.87
10.13	14.11	22.61	14.85
10.15	14.11	22.63	14.86
10.18	14.11	22.66	14.87
10.2	14.12	22.68	14.86
10.22	14.13	22.7	14.87
10.24	14.15	22.72	14.88
10.26	14.16	22.74	14.88
10.28	14.16	22.76	14.89
10.3	14.17	22.78	14.9
10.32	14.15	22.8	14.89
10.34	14.15	22.82	14.89
10.36	14.18	22.84	14.88
10.38	14.16	22.86	14.89
10.4	14.15	22.88	14.85
10.43	14.16	22.91	14.88
10.45	14.15	22.93	14.84
10.47	14.15	22.95	14.84
10.49	14.14	22.97	14.85
10.51	14.12	22.99	14.85
10.53	14.13	23.01	14.86
10.55	14.12	23.03	14.84
10.57	14.12	23.05	14.86
10.59	14.11	23.07	14.88
10.61	14.13	23.09	14.86
10.63	14.11	23.11	14.89
10.65	14.11	23.13	14.87
10.68	14.11	23.16	14.91
10.7	14.14	23.18	14.92
10.72	14.13	23.2	14.9
10.74	14.14	23.22	14.92
10.76	14.14	23.24	14.92
10.78	14.16	23.26	14.92
10.8	14.17	23.28	14.94
10.82	14.15	23.3	14.95
10.84	14.16	23.32	14.95
10.86	14.15	23.34	14.93
10.88	14.15	23.36	14.95
10.9	14.14	23.38	14.95
10.93	14.15	23.41	14.94
10.95	14.14	23.43	14.95
10.97	14.14	23.45	14.93
10.99	14.14	23.47	14.92
11.01	14.13	23.49	14.92
11.03	14.14	23.51	14.93
11.05	14.15	23.53	14.91

<u>Time (day)</u>	<u>Displacement (ft)</u>	<u>Time (day)</u>	<u>Displacement (ft)</u>
11.07	14.16	23.55	14.91
11.09	14.16	23.57	14.92
11.11	14.17	23.59	14.93
11.13	14.2	23.61	14.92
11.15	14.21	23.63	14.94
11.18	14.22	23.66	14.93
11.2	14.23	23.68	14.94
11.22	14.24	23.7	14.95
11.24	14.25	23.72	14.94
11.26	14.27	23.74	14.96
11.28	14.27	23.76	14.94
11.3	14.3	23.78	14.96
11.32	14.28	23.8	14.97
11.34	14.31	23.82	14.96
11.36	14.31	23.84	14.95
11.38	14.34	23.86	14.96
11.4	14.34	23.88	14.95
11.43	14.33	23.91	14.94
11.45	14.34	23.93	14.95
11.47	14.32	23.95	14.93
11.49	14.31	23.97	14.93
11.51	14.31	23.99	14.9
11.53	14.31	24.01	14.92
11.55	14.32	24.03	14.91
11.57	14.3	24.05	14.89
11.59	14.3	24.07	14.9
11.61	14.31	24.09	14.91
11.63	14.32	24.11	14.93
11.65	14.33	24.13	14.94
11.68	14.32	24.16	14.94
11.7	14.33	24.18	14.96
11.72	14.34	24.2	14.95
11.74	14.36	24.22	14.97
11.76	14.36	24.24	14.97
11.78	14.37	24.26	14.98
11.8	14.39	24.28	14.96
11.82	14.39	24.3	14.98
11.84	14.39	24.32	14.99
11.86	14.39	24.34	14.98
11.88	14.4	24.36	15.01
11.9	14.37	24.38	14.96
11.93	14.4	24.41	14.97
11.95	14.4	24.43	14.96
11.97	14.38	24.45	14.97
11.99	14.37	24.47	14.97
12.01	14.39	24.49	14.96
12.03	14.36	24.51	14.97
12.05	14.37	24.53	14.95
12.07	14.37	24.55	14.97
12.09	14.39	24.57	14.94
12.11	14.39	24.59	14.96
12.13	14.4	24.61	14.96
12.15	14.4	24.63	14.96

<u>Time (day)</u>	<u>Displacement (ft)</u>	<u>Time (day)</u>	<u>Displacement (ft)</u>
12.18	14.42	24.66	14.96
12.2	14.45	24.68	14.96
12.22	14.46	24.7	14.98
12.24	14.49	24.72	14.97
12.26	14.49	24.74	14.98
12.28	14.52	24.76	14.98
12.3	14.52	24.78	14.98
12.32	14.54	24.8	14.98
12.34	14.55	24.82	14.97
12.36	14.56	24.84	14.98
12.38	14.58	24.86	14.98
12.4	14.58	24.88	14.95
12.43	14.56	24.91	14.96
12.45	14.55	24.93	14.95
12.47	14.54		

---

### SOLUTION

Pumping Test  
Aquifer Model: Unconfined  
Solution Method: Neuman

---

### VISUAL ESTIMATION RESULTS

#### Estimated Parameters

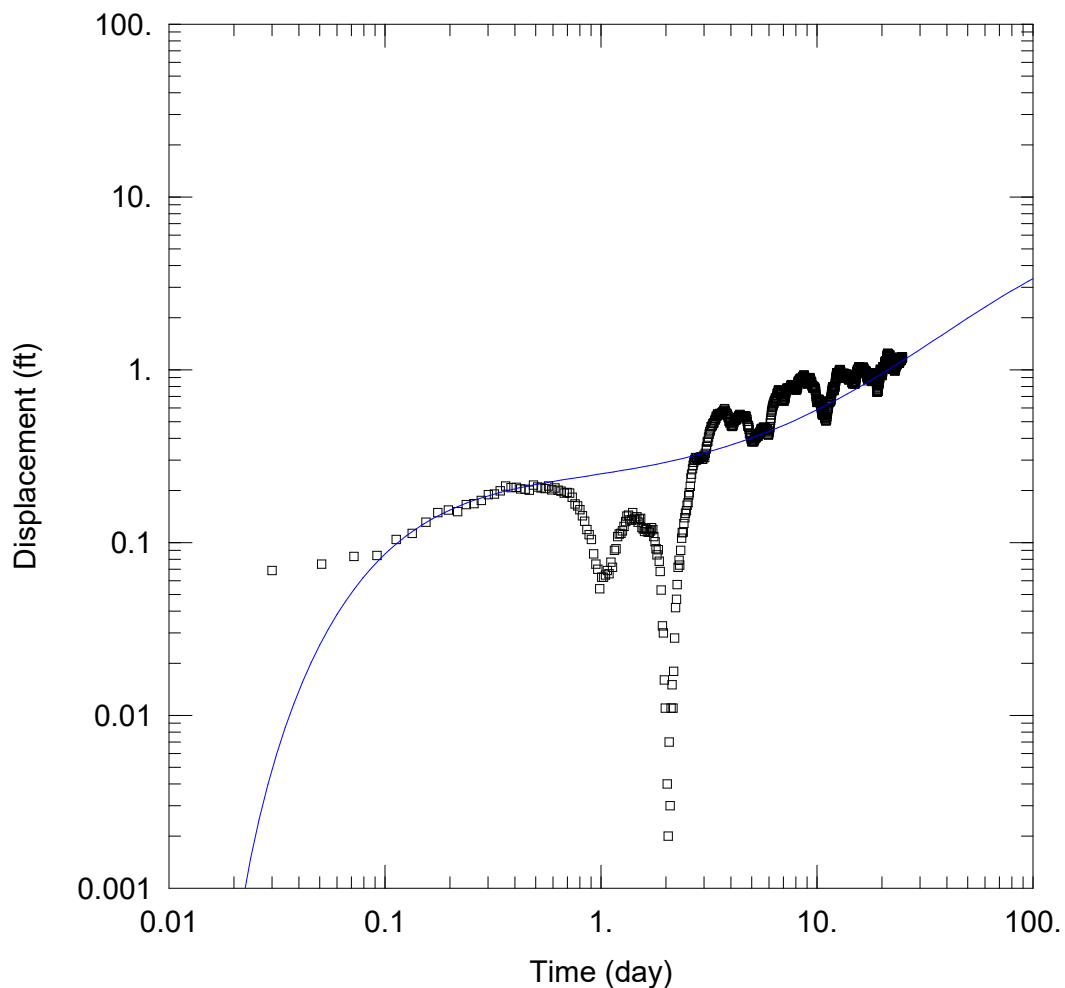
<u>Parameter</u>	<u>Estimate</u>	
T	1.428E+4	ft <sup>2</sup> /day
S	0.005615	
Sy	0.5	
β	0.001	

$K = T/b = 2.857 \text{ ft/day (0.001008 cm/sec)}$

$S_s = S/b = 1.123\text{E-}6 \text{ 1/ft}$

**APPENDIX G**

**AQTESOLV OUTPUT FOR R-32 SCREEN 1 DRAWDOWN ANALYSIS**



WELL TEST ANALYSIS

Data Set: D:\hugo \Downloads\LANL NM PROJECT\AQTESOLV files\R32 S1 data.aqt  
 Date: 06/07/24 Time: 14:48:05

PROJECT INFORMATION

Test Well: PM-2

AQUIFER DATA

Saturated Thickness: 5000. ft

WELL DATA

Pumping Wells			Observation Wells		
Well Name	X (ft)	Y (ft)	Well Name	X (ft)	Y (ft)
PM-2	0	0	□ R32 S1	4779	0

SOLUTION

Aquifer Model: Unconfined

Solution Method: Neuman

T = 1.641E+4 ft<sup>2</sup>/day

S = 0.0003064

Sy = 0.01603

β = 0.06

Data Set: D:\hugo\_\Downloads\LANL NM PROJECT\AQTESOLV files\R32 S1 data.aqt

Date: 06/07/24

Time: 14:48:52

---

PROJECT INFORMATION

Test Well: PM-2

---

AQUIFER DATA

Saturated Thickness: 5000. ft

Anisotropy Ratio (Kz/Kr): 0.06568

---

PUMPING WELL DATA

No. of pumping wells: 1

Pumping Well No. 1: PM-2

X Location: 0. ft

Y Location: 0. ft

Casing Radius: 0.5833 ft

Well Radius: 1. ft

Partially Penetrating Well

Depth to Top of Screen: 135. ft

Depth to Bottom of Screen: 1411. ft

No. of pumping periods: 1

Pumping Period Data

<u>Time (day)</u>	<u>Rate (gal/min)</u>
0.	1249.

---

OBSERVATION WELL DATA

No. of observation wells: 1

Observation Well No. 1: R32 S1

X Location: 4779. ft

Y Location: 0. ft

Radial distance from PM-2: 4779. ft

Partially Penetrating Well

Depth to Top of Screen: 88.8 ft

Depth to Bottom of Screen: 96.5 ft

No. of Observations: 1197

<u>Observation Data</u>			
<u>Time (day)</u>	<u>Displacement (ft)</u>	<u>Time (day)</u>	<u>Displacement (ft)</u>

---

0.009	0.068	12.49	0.955
0.03	0.069	12.51	0.95
0.051	0.075	12.53	0.951
0.072	0.083	12.55	0.946
0.092	0.084	12.57	0.946
0.113	0.104	12.59	0.948
0.134	0.113	12.61	0.947
0.155	0.131	12.63	0.952
0.176	0.149	12.65	0.967
0.197	0.154	12.68	0.957
0.217	0.151	12.7	0.966
0.238	0.166	12.72	0.994
0.259	0.168	12.74	0.988
0.28	0.175	12.76	1.001
0.301	0.189	12.78	0.995
0.322	0.191	12.8	1.002
0.342	0.199	12.82	0.996
0.363	0.212	12.84	0.995
0.384	0.208	12.86	0.99
0.405	0.209	12.88	0.974
0.426	0.204	12.9	0.964
0.447	0.203	12.93	0.949
0.467	0.201	12.95	0.929
0.488	0.215	12.97	0.924
0.509	0.21	12.99	0.916
0.53	0.207	13.01	0.916
0.551	0.205	13.03	0.908
0.572	0.212	13.05	0.895
0.592	0.202	13.07	0.894
0.613	0.207	13.09	0.898
0.634	0.201	13.11	0.897
0.655	0.198	13.13	0.903
0.676	0.193	13.15	0.906
0.697	0.195	13.18	0.912
0.717	0.193	13.2	0.924
0.738	0.183	13.22	0.927
0.759	0.167	13.24	0.935
0.78	0.163	13.26	0.93
0.801	0.155	13.28	0.94
0.822	0.143	13.3	0.943
0.842	0.133	13.32	0.955
0.863	0.119	13.34	0.941
0.884	0.111	13.36	0.946
0.905	0.104	13.38	0.934
0.926	0.086	13.4	0.936
0.947	0.075	13.43	0.947
0.967	0.07	13.45	0.935
0.988	0.054	13.47	0.933
1.009	0.063	13.49	0.926
1.03	0.063	13.51	0.911
1.051	0.065	13.53	0.909
1.072	0.069	13.55	0.905
1.092	0.066	13.57	0.905
1.113	0.077	13.59	0.898

---

<u>Time (day)</u>	<u>Displacement (ft)</u>	<u>Time (day)</u>	<u>Displacement (ft)</u>
1.134	0.072	13.61	0.907
1.155	0.09	13.63	0.91
1.176	0.092	13.65	0.911
1.197	0.108	13.68	0.927
1.217	0.112	13.7	0.939
1.238	0.113	13.72	0.938
1.259	0.117	13.74	0.946
1.28	0.124	13.76	0.937
1.301	0.132	13.78	0.94
1.322	0.142	13.8	0.937
1.342	0.144	13.82	0.938
1.363	0.135	13.84	0.936
1.384	0.135	13.86	0.933
1.405	0.149	13.88	0.93
1.426	0.138	13.9	0.917
1.447	0.135	13.93	0.921
1.467	0.141	13.95	0.902
1.488	0.131	13.97	0.901
1.509	0.137	13.99	0.888
1.53	0.138	14.01	0.883
1.551	0.122	14.03	0.876
1.572	0.12	14.05	0.881
1.592	0.116	14.07	0.881
1.613	0.12	14.09	0.878
1.634	0.119	14.11	0.878
1.655	0.115	14.13	0.876
1.676	0.115	14.15	0.877
1.697	0.117	14.18	0.888
1.717	0.122	14.2	0.893
1.738	0.119	14.22	0.89
1.759	0.108	14.24	0.89
1.78	0.101	14.26	0.901
1.801	0.092	14.28	0.9
1.822	0.085	14.3	0.903
1.842	0.091	14.32	0.907
1.863	0.078	14.34	0.907
1.884	0.068	14.36	0.913
1.905	0.053	14.38	0.912
1.926	0.033	14.4	0.926
1.947	0.03	14.43	0.916
1.967	0.016	14.45	0.919
1.988	0.011	14.47	0.901
2.009	0.	14.49	0.89
2.03	0.004	14.51	0.884
2.051	0.002	14.53	0.874
2.072	0.007	14.55	0.849
2.092	0.003	14.57	0.846
2.113	0.011	14.59	0.842
2.134	0.015	14.61	0.837
2.155	0.011	14.63	0.835
2.176	0.018	14.65	0.829
2.197	0.028	14.68	0.837
2.217	0.042	14.7	0.828



<u>Time (day)</u>	<u>Displacement (ft)</u>	<u>Time (day)</u>	<u>Displacement (ft)</u>
2.238	0.047	14.72	0.845
2.259	0.057	14.74	0.847
2.28	0.072	14.76	0.853
2.301	0.079	14.78	0.847
2.322	0.074	14.8	0.845
2.342	0.09	14.82	0.845
2.363	0.106	14.84	0.846
2.384	0.114	14.86	0.841
2.405	0.115	14.88	0.84
2.426	0.129	14.9	0.841
2.447	0.139	14.93	0.834
2.467	0.148	14.95	0.827
2.488	0.153	14.97	0.826
2.509	0.164	14.99	0.831
2.53	0.17	15.01	0.849
2.551	0.187	15.03	0.832
2.572	0.194	15.05	0.842
2.592	0.211	15.07	0.84
2.613	0.236	15.09	0.857
2.634	0.249	15.11	0.86
2.655	0.267	15.13	0.88
2.676	0.28	15.15	0.889
2.697	0.291	15.18	0.897
2.717	0.301	15.2	0.909
2.738	0.31	15.22	0.91
2.759	0.298	15.24	0.924
2.78	0.308	15.26	0.936
2.801	0.302	15.28	0.945
2.822	0.308	15.3	0.958
2.842	0.31	15.32	0.968
2.863	0.305	15.34	0.97
2.884	0.311	15.36	0.976
2.905	0.312	15.38	0.978
2.926	0.311	15.4	0.992
2.947	0.304	15.43	0.989
2.967	0.304	15.45	1.004
2.988	0.313	15.47	1.005
3.009	0.319	15.49	1.003
3.03	0.31	15.51	1.
3.051	0.328	15.53	0.998
3.072	0.348	15.55	0.998
3.092	0.358	15.57	0.996
3.113	0.381	15.59	1.008
3.134	0.386	15.61	1.014
3.155	0.407	15.63	1.015
3.176	0.424	15.65	1.015
3.197	0.439	15.68	1.033
3.217	0.448	15.7	1.035
3.238	0.467	15.72	1.04
3.259	0.47	15.74	1.037
3.28	0.478	15.76	1.025
3.301	0.487	15.78	1.031
3.322	0.49	15.8	1.034

<u>Time (day)</u>	<u>Displacement (ft)</u>	<u>Time (day)</u>	<u>Displacement (ft)</u>
3.342	0.494	15.82	1.029
3.363	0.508	15.84	1.025
3.384	0.513	15.86	1.033
3.405	0.524	15.88	1.02
3.426	0.537	15.9	1.022
3.447	0.537	15.93	1.018
3.467	0.554	15.95	1.006
3.488	0.547	15.97	0.997
3.509	0.552	15.99	0.99
3.53	0.55	16.01	0.99
3.551	0.559	16.03	0.979
3.572	0.553	16.05	0.97
3.592	0.554	16.07	0.969
3.613	0.554	16.09	0.972
3.634	0.564	16.11	0.979
3.655	0.565	16.13	0.973
3.676	0.572	16.16	0.988
3.697	0.576	16.18	0.991
3.717	0.583	16.2	0.997
3.738	0.596	16.22	1.01
3.759	0.583	16.24	1.008
3.78	0.573	16.26	1.008
3.801	0.56	16.28	1.011
3.822	0.559	16.3	1.022
3.842	0.552	16.32	1.022
3.863	0.543	16.34	1.033
3.884	0.533	16.36	1.032
3.905	0.522	16.38	1.025
3.926	0.505	16.41	1.031
3.947	0.5	16.43	1.024
3.967	0.491	16.45	1.015
3.988	0.494	16.47	1.013
4.009	0.477	16.49	1.011
4.03	0.471	16.51	1.006
4.051	0.475	16.53	0.999
4.072	0.47	16.55	0.984
4.092	0.478	16.57	0.982
4.113	0.485	16.59	0.97
4.134	0.497	16.61	0.975
4.155	0.51	16.63	0.966
4.176	0.512	16.66	0.959
4.197	0.513	16.68	0.966
4.217	0.511	16.7	0.962
4.238	0.519	16.72	0.958
4.259	0.515	16.74	0.964
4.28	0.528	16.76	0.974
4.301	0.528	16.78	0.969
4.322	0.528	16.8	0.976
4.342	0.539	16.82	0.98
4.363	0.538	16.84	0.989
4.384	0.546	16.86	0.974
4.405	0.551	16.88	0.972
4.426	0.544	16.91	0.967

---

<u>Time (day)</u>	<u>Displacement (ft)</u>	<u>Time (day)</u>	<u>Displacement (ft)</u>
4.447	0.542	16.93	0.963
4.467	0.539	16.95	0.951
4.488	0.538	16.97	0.95
4.509	0.541	16.99	0.935
4.53	0.538	17.01	0.945
4.551	0.529	17.03	0.936
4.572	0.529	17.05	0.925
4.592	0.531	17.07	0.915
4.613	0.535	17.09	0.906
4.634	0.538	17.11	0.903
4.655	0.543	17.13	0.899
4.676	0.54	17.16	0.9
4.697	0.535	17.18	0.893
4.717	0.528	17.2	0.884
4.738	0.518	17.22	0.882
4.759	0.503	17.24	0.865
4.78	0.481	17.26	0.884
4.801	0.471	17.28	0.898
4.822	0.475	17.3	0.901
4.842	0.463	17.32	0.898
4.863	0.452	17.34	0.902
4.884	0.428	17.36	0.894
4.905	0.426	17.38	0.904
4.926	0.415	17.41	0.909
4.947	0.408	17.43	0.904
4.967	0.397	17.45	0.91
4.988	0.388	17.47	0.915
5.009	0.383	17.49	0.902
5.03	0.386	17.51	0.891
5.051	0.384	17.53	0.888
5.072	0.386	17.55	0.883
5.092	0.382	17.57	0.883
5.113	0.388	17.59	0.884
5.134	0.392	17.61	0.887
5.155	0.402	17.63	0.881
5.176	0.405	17.66	0.884
5.197	0.399	17.68	0.889
5.217	0.409	17.7	0.888
5.238	0.405	17.72	0.898
5.259	0.407	17.74	0.903
5.28	0.413	17.76	0.894
5.301	0.416	17.78	0.89
5.322	0.419	17.8	0.891
5.342	0.412	17.82	0.878
5.363	0.423	17.84	0.881
5.384	0.425	17.86	0.877
5.405	0.425	17.88	0.871
5.426	0.43	17.91	0.864
5.447	0.433	17.93	0.861
5.467	0.436	17.95	0.86
5.488	0.444	17.97	0.856
5.509	0.452	17.99	0.857
5.53	0.455	18.01	0.868

<u>Time (day)</u>	<u>Displacement (ft)</u>	<u>Time (day)</u>	<u>Displacement (ft)</u>
5.551	0.458	18.03	0.873
5.572	0.45	18.05	0.871
5.592	0.448	18.07	0.882
5.613	0.454	18.09	0.882
5.634	0.457	18.11	0.885
5.655	0.46	18.13	0.896
5.676	0.466	18.16	0.898
5.697	0.463	18.18	0.907
5.717	0.463	18.2	0.911
5.738	0.463	18.22	0.922
5.759	0.452	18.24	0.918
5.78	0.447	18.26	0.925
5.801	0.442	18.28	0.92
5.822	0.45	18.3	0.931
5.842	0.452	18.32	0.928
5.863	0.455	18.34	0.939
5.884	0.447	18.36	0.941
5.905	0.451	18.38	0.945
5.926	0.426	18.41	0.944
5.947	0.424	18.43	0.945
5.967	0.419	18.45	0.957
5.988	0.422	18.47	0.957
6.009	0.432	18.49	0.952
6.03	0.442	18.51	0.95
6.051	0.457	18.53	0.941
6.072	0.465	18.55	0.941
6.092	0.492	18.57	0.946
6.113	0.508	18.59	0.947
6.134	0.525	18.61	0.946
6.155	0.546	18.63	0.945
6.176	0.569	18.66	0.948
6.197	0.577	18.68	0.956
6.217	0.593	18.7	0.959
6.238	0.606	18.72	0.957
6.259	0.617	18.74	0.944
6.28	0.623	18.76	0.923
6.301	0.636	18.78	0.915
6.322	0.637	18.8	0.912
6.342	0.648	18.82	0.892
6.363	0.66	18.84	0.883
6.384	0.658	18.86	0.876
6.405	0.669	18.88	0.843
6.426	0.685	18.91	0.826
6.447	0.683	18.93	0.8
6.467	0.676	18.95	0.782
6.488	0.683	18.97	0.767
6.509	0.698	18.99	0.763
6.53	0.708	19.01	0.745
6.551	0.727	19.03	0.741
6.572	0.73	19.05	0.739
6.592	0.735	19.07	0.747
6.613	0.741	19.09	0.746
6.634	0.755	19.11	0.755

---

<u>Time (day)</u>	<u>Displacement (ft)</u>	<u>Time (day)</u>	<u>Displacement (ft)</u>
6.655	0.765	19.13	0.751
6.676	0.754	19.16	0.749
6.697	0.748	19.18	0.761
6.717	0.748	19.2	0.756
6.738	0.747	19.22	0.787
6.759	0.735	19.24	0.811
6.78	0.722	19.26	0.814
6.801	0.721	19.28	0.816
6.822	0.733	19.3	0.814
6.842	0.726	19.32	0.826
6.863	0.721	19.34	0.83
6.884	0.701	19.36	0.835
6.905	0.695	19.38	0.838
6.926	0.677	19.41	0.846
6.947	0.67	19.43	0.853
6.967	0.668	19.45	0.875
6.988	0.665	19.47	0.869
7.009	0.662	19.49	0.886
7.03	0.658	19.51	0.89
7.051	0.66	19.53	0.894
7.072	0.672	19.55	0.91
7.092	0.678	19.57	0.93
7.113	0.685	19.59	0.947
7.134	0.696	19.61	0.944
7.155	0.708	19.63	0.965
7.176	0.725	19.66	0.984
7.197	0.736	19.68	0.998
7.217	0.752	19.7	1.006
7.238	0.763	19.72	1.004
7.259	0.773	19.74	0.993
7.28	0.78	19.76	0.989
7.301	0.782	19.78	0.994
7.322	0.779	19.8	0.986
7.342	0.779	19.82	0.989
7.363	0.77	19.84	0.982
7.384	0.773	19.86	0.976
7.405	0.783	19.88	0.971
7.426	0.778	19.91	0.964
7.447	0.777	19.93	0.949
7.467	0.784	19.95	0.938
7.488	0.786	19.97	0.939
7.509	0.78	19.99	0.924
7.53	0.785	20.01	0.929
7.551	0.794	20.03	0.937
7.572	0.802	20.05	0.941
7.592	0.811	20.07	0.951
7.613	0.815	20.09	0.956
7.634	0.816	20.11	0.959
7.655	0.815	20.13	0.969
7.676	0.819	20.16	0.983
7.697	0.814	20.18	0.995
7.717	0.805	20.2	1.011
7.738	0.798	20.22	1.022

---

<u>Time (day)</u>	<u>Displacement (ft)</u>	<u>Time (day)</u>	<u>Displacement (ft)</u>
7.759	0.795	20.24	1.038
7.78	0.795	20.26	1.04
7.801	0.786	20.28	1.031
7.822	0.79	20.3	1.026
7.842	0.782	20.32	1.024
7.863	0.776	20.34	1.03
7.884	0.772	20.36	1.021
7.905	0.772	20.38	1.024
7.926	0.779	20.41	1.025
7.947	0.765	20.43	1.019
7.967	0.769	20.45	1.021
7.988	0.765	20.47	1.026
8.009	0.768	20.49	1.026
8.03	0.767	20.51	1.027
8.051	0.764	20.53	1.024
8.072	0.774	20.55	1.035
8.092	0.78	20.57	1.04
8.113	0.798	20.59	1.045
8.134	0.789	20.61	1.053
8.155	0.815	20.63	1.067
8.176	0.839	20.66	1.074
8.197	0.855	20.68	1.085
8.217	0.847	20.7	1.099
8.238	0.855	20.72	1.105
8.259	0.859	20.74	1.109
8.28	0.865	20.76	1.121
8.301	0.878	20.78	1.119
8.322	0.878	20.8	1.125
8.342	0.873	20.82	1.122
8.363	0.883	20.84	1.115
8.384	0.886	20.86	1.12
8.405	0.888	20.88	1.121
8.426	0.892	20.91	1.123
8.447	0.887	20.93	1.107
8.467	0.878	20.95	1.104
8.488	0.878	20.97	1.109
8.509	0.887	20.99	1.111
8.53	0.89	21.01	1.115
8.551	0.892	21.03	1.126
8.572	0.882	21.05	1.139
8.592	0.903	21.07	1.144
8.613	0.903	21.09	1.152
8.634	0.912	21.11	1.166
8.655	0.915	21.13	1.186
8.676	0.921	21.16	1.19
8.697	0.928	21.18	1.202
8.717	0.932	21.2	1.211
8.738	0.929	21.22	1.23
8.759	0.91	21.24	1.226
8.78	0.905	21.26	1.233
8.801	0.9	21.28	1.239
8.822	0.902	21.3	1.247
8.842	0.9	21.32	1.236

---

<u>Time (day)</u>	<u>Displacement (ft)</u>	<u>Time (day)</u>	<u>Displacement (ft)</u>
8.863	0.886	21.34	1.236
8.884	0.891	21.36	1.24
8.905	0.886	21.38	1.224
8.926	0.875	21.41	1.22
8.947	0.865	21.43	1.228
8.967	0.855	21.45	1.23
8.988	0.848	21.47	1.217
9.009	0.842	21.49	1.207
9.03	0.827	21.51	1.203
9.051	0.833	21.53	1.195
9.072	0.828	21.55	1.201
9.092	0.837	21.57	1.19
9.113	0.835	21.59	1.193
9.134	0.845	21.61	1.185
9.155	0.866	21.63	1.186
9.176	0.879	21.66	1.184
9.197	0.871	21.68	1.199
9.217	0.892	21.7	1.204
9.238	0.894	21.72	1.215
9.259	0.891	21.74	1.222
9.28	0.899	21.76	1.2
9.301	0.888	21.78	1.163
9.322	0.884	21.8	1.156
9.342	0.869	21.82	1.153
9.363	0.853	21.84	1.142
9.384	0.85	21.86	1.13
9.405	0.857	21.88	1.117
9.426	0.849	21.91	1.107
9.447	0.848	21.93	1.09
9.467	0.841	21.95	1.078
9.488	0.819	21.97	1.073
9.509	0.811	21.99	1.069
9.53	0.807	22.01	1.073
9.551	0.795	22.03	1.069
9.572	0.784	22.05	1.067
9.592	0.788	22.07	1.052
9.613	0.8	22.09	1.069
9.634	0.803	22.11	1.064
9.655	0.789	22.13	1.065
9.676	0.781	22.16	1.079
9.697	0.789	22.18	1.082
9.717	0.794	22.2	1.087
9.738	0.793	22.22	1.105
9.759	0.784	22.24	1.106
9.78	0.783	22.26	1.107
9.801	0.778	22.28	1.102
9.822	0.775	22.3	1.104
9.842	0.773	22.32	1.103
9.863	0.757	22.34	1.089
9.884	0.75	22.36	1.084
9.905	0.721	22.38	1.074
9.926	0.699	22.41	1.07
9.947	0.684	22.43	1.055

---

<u>Time (day)</u>	<u>Displacement (ft)</u>	<u>Time (day)</u>	<u>Displacement (ft)</u>
9.967	0.674	22.45	1.059
9.988	0.662	22.47	1.057
10.01	0.649	22.49	1.045
10.03	0.645	22.51	1.032
10.05	0.66	22.53	1.016
10.07	0.653	22.55	1.006
10.09	0.653	22.57	1.004
10.11	0.651	22.59	1.01
10.13	0.667	22.61	1.01
10.15	0.665	22.63	1.008
10.18	0.674	22.66	1.012
10.2	0.674	22.68	1.014
10.22	0.667	22.7	1.019
10.24	0.67	22.72	1.03
10.26	0.671	22.74	1.04
10.28	0.659	22.76	1.035
10.3	0.663	22.78	1.05
10.32	0.658	22.8	1.045
10.34	0.659	22.82	1.057
10.36	0.651	22.84	1.049
10.38	0.641	22.86	1.04
10.4	0.634	22.88	1.024
10.43	0.625	22.91	1.017
10.45	0.619	22.93	0.998
10.47	0.613	22.95	0.988
10.49	0.6	22.97	0.983
10.51	0.59	22.99	0.988
10.53	0.586	23.01	1.009
10.55	0.572	23.03	0.993
10.57	0.562	23.05	1.002
10.59	0.554	23.07	1.014
10.61	0.555	23.09	0.998
10.63	0.546	23.11	1.001
10.65	0.549	23.13	1.017
10.68	0.554	23.16	1.036
10.7	0.554	23.18	1.043
10.72	0.545	23.2	1.051
10.74	0.551	23.22	1.06
10.76	0.57	23.24	1.061
10.78	0.567	23.26	1.065
10.8	0.566	23.28	1.073
10.82	0.559	23.3	1.079
10.84	0.558	23.32	1.084
10.86	0.554	23.34	1.077
10.88	0.543	23.36	1.08
10.9	0.534	23.38	1.081
10.93	0.521	23.41	1.078
10.95	0.519	23.43	1.079
10.97	0.51	23.45	1.082
10.99	0.507	23.47	1.076
11.01	0.507	23.49	1.071
11.03	0.508	23.51	1.069
11.05	0.508	23.53	1.077



---

<u>Time (day)</u>	<u>Displacement (ft)</u>	<u>Time (day)</u>	<u>Displacement (ft)</u>
11.07	0.509	23.55	1.083
11.09	0.514	23.57	1.089
11.11	0.532	23.59	1.089
11.13	0.535	23.61	1.101
11.15	0.551	23.63	1.118
11.18	0.568	23.66	1.13
11.2	0.575	23.68	1.134
11.22	0.583	23.7	1.149
11.24	0.595	23.72	1.161
11.26	0.598	23.74	1.171
11.28	0.603	23.76	1.174
11.3	0.617	23.78	1.181
11.32	0.628	23.8	1.17
11.34	0.636	23.82	1.163
11.36	0.646	23.84	1.172
11.38	0.647	23.86	1.155
11.4	0.653	23.88	1.147
11.43	0.655	23.91	1.144
11.45	0.657	23.93	1.138
11.47	0.655	23.95	1.128
11.49	0.654	23.97	1.114
11.51	0.653	23.99	1.104
11.53	0.66	24.01	1.111
11.55	0.653	24.03	1.096
11.57	0.658	24.05	1.091
11.59	0.665	24.07	1.097
11.61	0.676	24.09	1.105
11.63	0.677	24.11	1.105
11.65	0.695	24.13	1.107
11.68	0.697	24.16	1.123
11.7	0.718	24.18	1.118
11.72	0.734	24.2	1.131
11.74	0.749	24.22	1.128
11.76	0.756	24.24	1.137
11.78	0.766	24.26	1.138
11.8	0.783	24.28	1.138
11.82	0.791	24.3	1.151
11.84	0.789	24.32	1.151
11.86	0.794	24.34	1.145
11.88	0.795	24.36	1.145
11.9	0.789	24.38	1.152
11.93	0.78	24.41	1.133
11.95	0.766	24.43	1.133
11.97	0.764	24.45	1.144
11.99	0.757	24.47	1.139
12.01	0.769	24.49	1.131
12.03	0.77	24.51	1.139
12.05	0.778	24.53	1.152
12.07	0.788	24.55	1.141
12.09	0.789	24.57	1.145
12.11	0.795	24.59	1.148
12.13	0.81	24.61	1.139
12.15	0.816	24.63	1.15

<u>Time (day)</u>	<u>Displacement (ft)</u>	<u>Time (day)</u>	<u>Displacement (ft)</u>
12.18	0.836	24.66	1.161
12.2	0.857	24.68	1.168
12.22	0.861	24.7	1.184
12.24	0.876	24.72	1.182
12.26	0.892	24.74	1.179
12.28	0.902	24.76	1.179
12.3	0.914	24.78	1.186
12.32	0.929	24.8	1.187
12.34	0.943	24.82	1.179
12.36	0.946	24.84	1.182
12.38	0.959	24.86	1.186
12.4	0.957	24.88	1.179
12.43	0.956	24.91	1.168
12.45	0.957	24.93	1.17
12.47	0.952		

---

SOLUTION

Pumping Test  
 Aquifer Model: Unconfined  
 Solution Method: Neuman

---

VISUAL ESTIMATION RESULTS

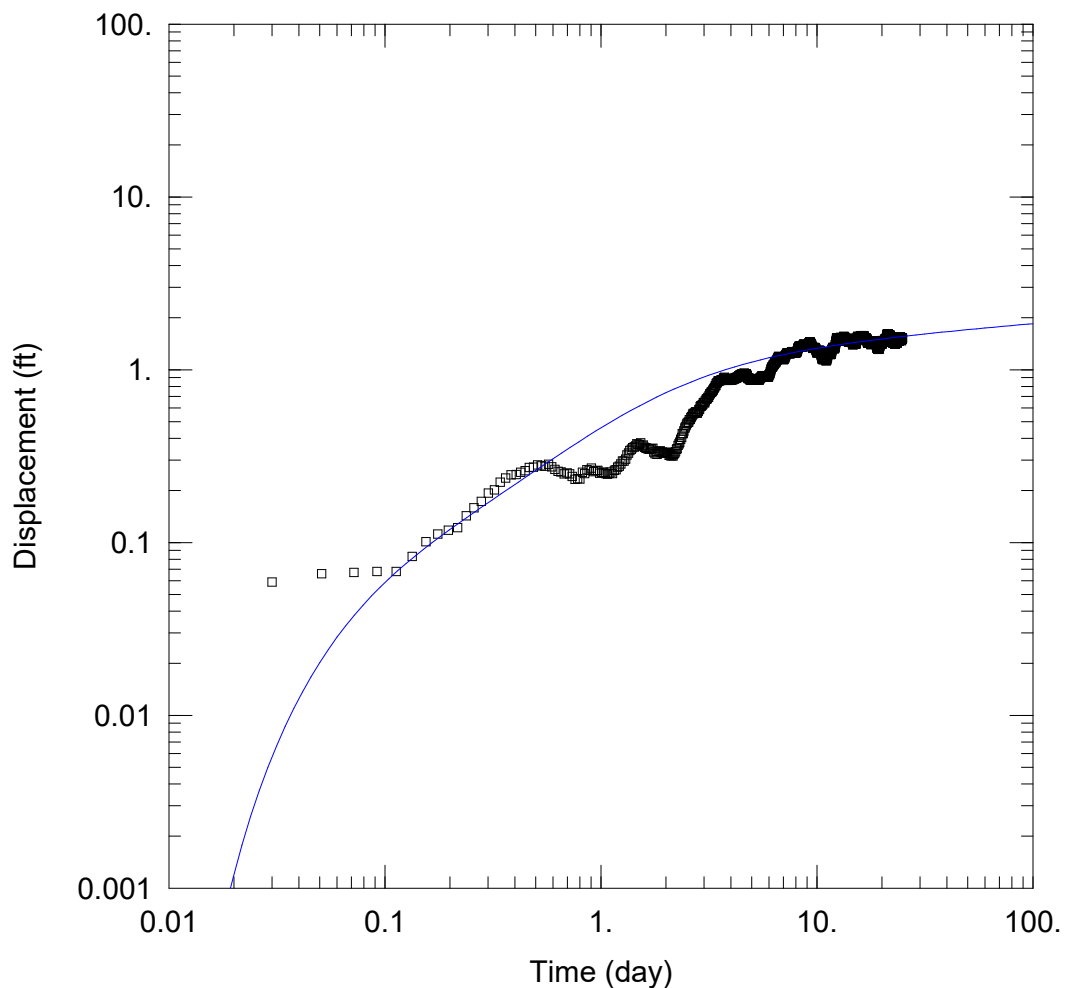
Estimated Parameters

<u>Parameter</u>	<u>Estimate</u>	
T	1.641E+4	ft <sup>2</sup> /day
S	0.0003064	
Sy	0.01603	
β	0.06	

K = T/b = 3.282 ft/day (0.001158 cm/sec)  
 Ss = S/b = 6.129E-8 1/ft

**APPENDIX H**

**AQTESOLV OUTPUT FOR R-32 SCREEN 2 DRAWDOWN ANALYSIS**



WELL TEST ANALYSIS

Data Set: D:\hugo \Downloads\LANL NM PROJECT\AQTESOLV files\R32 S2 data.aqt  
 Date: 06/07/24 Time: 15:00:34

PROJECT INFORMATION

Test Well: PM-2

AQUIFER DATA

Saturated Thickness: 5000. ft

WELL DATA

Pumping Wells			Observation Wells		
Well Name	X (ft)	Y (ft)	Well Name	X (ft)	Y (ft)
PM-2	0	0	□ R32 S2	4779	0

SOLUTION

Aquifer Model: Unconfined

Solution Method: Neuman

T = 9.955E+4 ft<sup>2</sup>/day

S = 0.00133

Sy = 0.0009298

β = 0.03

Data Set: D:\hugo\_\Downloads\LANL NM PROJECT\AQTESOLV files\R32 S2 data.aqt

Date: 06/07/24

Time: 15:00:46

---

PROJECT INFORMATION

Test Well: PM-2

---

AQUIFER DATA

Saturated Thickness: 5000. ft

Anisotropy Ratio (Kz/Kr): 0.03284

---

PUMPING WELL DATA

No. of pumping wells: 1

Pumping Well No. 1: PM-2

X Location: 0. ft

Y Location: 0. ft

Casing Radius: 0.5833 ft

Well Radius: 1. ft

Partially Penetrating Well

Depth to Top of Screen: 135. ft

Depth to Bottom of Screen: 1411. ft

No. of pumping periods: 1

Pumping Period Data

<u>Time (day)</u>	<u>Rate (gal/min)</u>
0.	1249.

---

OBSERVATION WELL DATA

No. of observation wells: 1

Observation Well No. 1: R32 S2

X Location: 4779. ft

Y Location: 0. ft

Radial distance from PM-2: 4779. ft

Partially Penetrating Well

Depth to Top of Screen: 146.2 ft

Depth to Bottom of Screen: 149.3 ft

No. of Observations: 1197

<u>Observation Data</u>			
<u>Time (day)</u>	<u>Displacement (ft)</u>	<u>Time (day)</u>	<u>Displacement (ft)</u>

---

0.009	0.059	12.49	1.503
0.03	0.059	12.51	1.504
0.051	0.066	12.53	1.498
0.072	0.067	12.55	1.481
0.092	0.068	12.57	1.48
0.113	0.068	12.59	1.482
0.134	0.083	12.61	1.475
0.155	0.101	12.63	1.473
0.176	0.112	12.65	1.481
0.197	0.118	12.68	1.485
0.217	0.122	12.7	1.487
0.238	0.143	12.72	1.495
0.259	0.159	12.74	1.509
0.28	0.173	12.76	1.516
0.301	0.193	12.78	1.53
0.322	0.202	12.8	1.536
0.342	0.223	12.82	1.531
0.363	0.236	12.84	1.536
0.384	0.246	12.86	1.538
0.405	0.247	12.88	1.535
0.426	0.255	12.9	1.532
0.447	0.261	12.93	1.524
0.467	0.272	12.95	1.511
0.488	0.273	12.97	1.499
0.509	0.281	12.99	1.497
0.53	0.278	13.01	1.49
0.551	0.276	13.03	1.483
0.572	0.284	13.05	1.469
0.592	0.274	13.07	1.469
0.613	0.265	13.09	1.472
0.634	0.258	13.11	1.465
0.655	0.256	13.13	1.464
0.676	0.25	13.15	1.467
0.697	0.253	13.18	1.48
0.717	0.25	13.2	1.492
0.738	0.241	13.22	1.495
0.759	0.232	13.24	1.516
0.78	0.234	13.26	1.518
0.801	0.233	13.28	1.528
0.822	0.255	13.3	1.538
0.842	0.251	13.32	1.549
0.863	0.264	13.34	1.549
0.884	0.262	13.36	1.561
0.905	0.269	13.38	1.549
0.926	0.257	13.4	1.551
0.947	0.26	13.43	1.555
0.967	0.262	13.45	1.543
0.988	0.252	13.47	1.534
1.009	0.255	13.49	1.527
1.03	0.255	13.51	1.519
1.051	0.251	13.53	1.504
1.072	0.248	13.55	1.493
1.092	0.251	13.57	1.48
1.113	0.256	13.59	1.473

---

<u>Time (day)</u>	<u>Displacement (ft)</u>	<u>Time (day)</u>	<u>Displacement (ft)</u>
1.134	0.251	13.61	1.462
1.155	0.262	13.63	1.464
1.176	0.264	13.65	1.459
1.197	0.273	13.68	1.462
1.217	0.277	13.7	1.473
1.238	0.285	13.72	1.479
1.259	0.296	13.74	1.481
1.28	0.296	13.76	1.485
1.301	0.304	13.78	1.481
1.322	0.321	13.8	1.485
1.342	0.329	13.82	1.492
1.363	0.341	13.84	1.498
1.384	0.347	13.86	1.501
1.405	0.354	13.88	1.505
1.426	0.357	13.9	1.505
1.447	0.361	13.93	1.495
1.467	0.373	13.95	1.491
1.488	0.37	13.97	1.482
1.509	0.369	13.99	1.469
1.53	0.377	14.01	1.471
1.551	0.361	14.03	1.458
1.572	0.366	14.05	1.456
1.592	0.355	14.07	1.449
1.613	0.352	14.09	1.446
1.634	0.351	14.11	1.446
1.655	0.348	14.13	1.443
1.676	0.347	14.15	1.439
1.697	0.349	14.18	1.443
1.717	0.348	14.2	1.448
1.738	0.351	14.22	1.444
1.759	0.333	14.24	1.458
1.78	0.326	14.26	1.462
1.801	0.338	14.28	1.475
1.822	0.324	14.3	1.484
1.842	0.337	14.32	1.495
1.863	0.337	14.34	1.496
1.884	0.34	14.36	1.515
1.905	0.332	14.38	1.514
1.926	0.333	14.4	1.521
1.947	0.33	14.43	1.51
1.967	0.329	14.45	1.514
1.988	0.33	14.47	1.503
2.009	0.333	14.49	1.498
2.03	0.33	14.51	1.485
2.051	0.329	14.53	1.475
2.072	0.32	14.55	1.457
2.092	0.322	14.57	1.447
2.113	0.317	14.59	1.437
2.134	0.321	14.61	1.419
2.155	0.317	14.63	1.416
2.176	0.324	14.65	1.397
2.197	0.328	14.68	1.398
2.217	0.335	14.7	1.396

<u>Time (day)</u>	<u>Displacement (ft)</u>	<u>Time (day)</u>	<u>Displacement (ft)</u>
2.238	0.346	14.72	1.4
2.259	0.35	14.74	1.402
2.28	0.365	14.76	1.407
2.301	0.372	14.78	1.408
2.322	0.381	14.8	1.406
2.342	0.396	14.82	1.413
2.363	0.405	14.84	1.42
2.384	0.427	14.86	1.429
2.405	0.428	14.88	1.428
2.426	0.442	14.9	1.43
2.447	0.459	14.93	1.429
2.467	0.467	14.95	1.422
2.488	0.479	14.97	1.427
2.509	0.49	14.99	1.425
2.53	0.496	15.01	1.424
2.551	0.499	15.03	1.413
2.572	0.513	15.05	1.416
2.592	0.516	15.07	1.408
2.613	0.528	15.09	1.412
2.634	0.535	15.11	1.408
2.655	0.546	15.13	1.414
2.676	0.559	15.15	1.41
2.697	0.557	15.18	1.418
2.717	0.56	15.2	1.423
2.738	0.569	15.22	1.431
2.759	0.57	15.24	1.432
2.78	0.56	15.26	1.45
2.801	0.561	15.28	1.473
2.822	0.574	15.3	1.486
2.842	0.589	15.32	1.489
2.863	0.591	15.34	1.504
2.884	0.611	15.36	1.511
2.905	0.618	15.38	1.526
2.926	0.617	15.4	1.54
2.947	0.623	15.43	1.544
2.967	0.63	15.45	1.552
2.988	0.646	15.47	1.559
3.009	0.645	15.49	1.551
3.03	0.643	15.51	1.541
3.051	0.661	15.53	1.539
3.072	0.674	15.55	1.54
3.092	0.678	15.57	1.537
3.113	0.681	15.59	1.536
3.134	0.692	15.61	1.535
3.155	0.693	15.63	1.536
3.176	0.71	15.65	1.536
3.197	0.725	15.68	1.528
3.217	0.727	15.7	1.536
3.238	0.74	15.72	1.534
3.259	0.743	15.74	1.531
3.28	0.751	15.76	1.526
3.301	0.76	15.78	1.525
3.322	0.769	15.8	1.541



---

<u>Time (day)</u>	<u>Displacement (ft)</u>	<u>Time (day)</u>	<u>Displacement (ft)</u>
3.342	0.78	15.82	1.543
3.363	0.788	15.84	1.546
3.384	0.806	15.86	1.554
3.405	0.81	15.88	1.561
3.426	0.83	15.9	1.563
3.447	0.837	15.93	1.572
3.467	0.846	15.95	1.568
3.488	0.86	15.97	1.558
3.509	0.859	15.99	1.558
3.53	0.863	16.01	1.552
3.551	0.865	16.03	1.554
3.572	0.866	16.05	1.545
3.592	0.867	16.07	1.537
3.613	0.873	16.09	1.527
3.634	0.876	16.11	1.527
3.655	0.871	16.13	1.521
3.676	0.878	16.16	1.522
3.697	0.888	16.18	1.519
3.717	0.896	16.2	1.518
3.738	0.903	16.22	1.525
3.759	0.895	16.24	1.522
3.78	0.879	16.26	1.522
3.801	0.873	16.28	1.532
3.822	0.871	16.3	1.537
3.842	0.878	16.32	1.55
3.863	0.869	16.34	1.554
3.884	0.872	16.36	1.56
3.905	0.868	16.38	1.572
3.926	0.871	16.41	1.572
3.947	0.873	16.43	1.572
3.967	0.871	16.45	1.57
3.988	0.874	16.47	1.567
4.009	0.87	16.49	1.572
4.03	0.878	16.51	1.56
4.051	0.875	16.53	1.56
4.072	0.877	16.55	1.552
4.092	0.878	16.57	1.537
4.113	0.878	16.59	1.532
4.134	0.883	16.61	1.523
4.155	0.89	16.63	1.514
4.176	0.899	16.66	1.507
4.197	0.893	16.68	1.501
4.217	0.891	16.7	1.503
4.238	0.892	16.72	1.493
4.259	0.901	16.74	1.498
4.28	0.908	16.76	1.495
4.301	0.901	16.78	1.497
4.322	0.908	16.8	1.504
4.342	0.919	16.82	1.508
4.363	0.924	16.84	1.517
4.384	0.926	16.86	1.509
4.405	0.931	16.88	1.519
4.426	0.931	16.91	1.522

---

<u>Time (day)</u>	<u>Displacement (ft)</u>	<u>Time (day)</u>	<u>Displacement (ft)</u>
4.447	0.929	16.93	1.525
4.467	0.94	16.95	1.519
4.488	0.945	16.97	1.511
4.509	0.948	16.99	1.51
4.53	0.945	17.01	1.506
4.551	0.943	17.03	1.504
4.572	0.943	17.05	1.499
4.592	0.951	17.07	1.483
4.613	0.955	17.09	1.475
4.634	0.945	17.11	1.464
4.655	0.95	17.13	1.454
4.676	0.94	17.16	1.448
4.697	0.949	17.18	1.441
4.717	0.948	17.2	1.432
4.738	0.932	17.22	1.43
4.759	0.924	17.24	1.42
4.78	0.901	17.26	1.432
4.801	0.891	17.28	1.432
4.822	0.895	17.3	1.442
4.842	0.897	17.32	1.432
4.863	0.886	17.34	1.436
4.884	0.881	17.36	1.449
4.905	0.873	17.38	1.458
4.926	0.869	17.41	1.464
4.947	0.875	17.43	1.459
4.967	0.871	17.45	1.465
4.988	0.875	17.47	1.463
5.009	0.877	17.49	1.464
5.03	0.873	17.51	1.459
5.051	0.878	17.53	1.456
5.072	0.873	17.55	1.444
5.092	0.882	17.57	1.444
5.113	0.876	17.59	1.439
5.134	0.88	17.61	1.435
5.155	0.89	17.63	1.429
5.176	0.885	17.66	1.425
5.197	0.887	17.68	1.424
5.217	0.883	17.7	1.423
5.238	0.879	17.72	1.419
5.259	0.881	17.74	1.411
5.28	0.873	17.76	1.408
5.301	0.883	17.78	1.404
5.322	0.88	17.8	1.398
5.342	0.879	17.82	1.399
5.363	0.877	17.84	1.402
5.384	0.872	17.86	1.411
5.405	0.872	17.88	1.405
5.426	0.884	17.91	1.412
5.447	0.88	17.93	1.422
5.467	0.896	17.95	1.414
5.488	0.897	17.97	1.417
5.509	0.905	17.99	1.425
5.53	0.909	18.01	1.436

---

<u>Time (day)</u>	<u>Displacement (ft)</u>	<u>Time (day)</u>	<u>Displacement (ft)</u>
5.551	0.919	18.03	1.435
5.572	0.911	18.05	1.426
5.592	0.915	18.07	1.43
5.613	0.915	18.09	1.43
5.634	0.918	18.11	1.427
5.655	0.92	18.13	1.424
5.676	0.926	18.16	1.426
5.697	0.924	18.18	1.435
5.717	0.917	18.2	1.432
5.738	0.917	18.22	1.43
5.759	0.906	18.24	1.426
5.78	0.907	18.26	1.426
5.801	0.909	18.28	1.421
5.822	0.903	18.3	1.426
5.842	0.912	18.32	1.429
5.863	0.923	18.34	1.427
5.884	0.915	18.36	1.435
5.905	0.912	18.38	1.439
5.926	0.913	18.41	1.445
5.947	0.911	18.43	1.446
5.967	0.906	18.45	1.451
5.988	0.916	18.47	1.458
6.009	0.933	18.49	1.459
6.03	0.936	18.51	1.457
6.051	0.944	18.53	1.462
6.072	0.952	18.55	1.462
6.092	0.973	18.57	1.46
6.113	0.982	18.59	1.461
6.134	0.999	18.61	1.46
6.155	1.014	18.63	1.46
6.176	1.03	18.66	1.463
6.197	1.031	18.68	1.464
6.217	1.04	18.7	1.453
6.238	1.039	18.72	1.445
6.259	1.051	18.74	1.439
6.28	1.064	18.76	1.424
6.301	1.063	18.78	1.416
6.322	1.071	18.8	1.413
6.342	1.075	18.82	1.399
6.363	1.093	18.84	1.397
6.384	1.092	18.86	1.397
6.405	1.096	18.88	1.384
6.426	1.111	18.91	1.374
6.447	1.103	18.93	1.369
6.467	1.116	18.95	1.363
6.488	1.123	18.97	1.355
6.509	1.132	18.99	1.351
6.53	1.135	19.01	1.34
6.551	1.147	19.03	1.336
6.572	1.15	19.05	1.334
6.592	1.162	19.07	1.335
6.613	1.168	19.09	1.334
6.634	1.182	19.11	1.329

---

<u>Time (day)</u>	<u>Displacement (ft)</u>	<u>Time (day)</u>	<u>Displacement (ft)</u>
6.655	1.192	19.13	1.325
6.676	1.195	19.16	1.324
6.697	1.189	19.18	1.316
6.717	1.188	19.2	1.31
6.738	1.18	19.22	1.314
6.759	1.162	19.24	1.325
6.78	1.156	19.26	1.322
6.801	1.162	19.28	1.324
6.822	1.167	19.3	1.315
6.842	1.166	19.32	1.32
6.863	1.154	19.34	1.318
6.884	1.155	19.36	1.323
6.905	1.155	19.38	1.319
6.926	1.151	19.41	1.327
6.947	1.151	19.43	1.334
6.967	1.148	19.45	1.342
6.988	1.146	19.47	1.343
7.009	1.15	19.49	1.353
7.03	1.146	19.51	1.357
7.051	1.154	19.53	1.361
7.072	1.16	19.55	1.371
7.092	1.165	19.57	1.384
7.113	1.179	19.59	1.401
7.134	1.197	19.61	1.398
7.155	1.202	19.63	1.419
7.176	1.206	19.66	1.425
7.197	1.223	19.68	1.431
7.217	1.226	19.7	1.44
7.238	1.244	19.72	1.432
7.259	1.241	19.74	1.421
7.28	1.241	19.76	1.416
7.301	1.25	19.78	1.415
7.322	1.246	19.8	1.42
7.342	1.24	19.82	1.417
7.363	1.244	19.84	1.416
7.384	1.24	19.86	1.417
7.405	1.244	19.88	1.419
7.426	1.239	19.91	1.412
7.447	1.238	19.93	1.41
7.467	1.245	19.95	1.412
7.488	1.233	19.97	1.407
7.509	1.241	19.99	1.412
7.53	1.246	20.01	1.416
7.551	1.248	20.03	1.418
7.572	1.249	20.05	1.435
7.592	1.258	20.07	1.439
7.613	1.262	20.09	1.437
7.634	1.263	20.11	1.44
7.655	1.269	20.13	1.443
7.676	1.273	20.16	1.464
7.697	1.275	20.18	1.462
7.717	1.272	20.2	1.472
7.738	1.265	20.22	1.47

---

<u>Time (day)</u>	<u>Displacement (ft)</u>	<u>Time (day)</u>	<u>Displacement (ft)</u>
7.759	1.255	20.24	1.479
7.78	1.248	20.26	1.474
7.801	1.253	20.28	1.472
7.822	1.25	20.3	1.467
7.842	1.249	20.32	1.465
7.863	1.25	20.34	1.464
7.884	1.246	20.36	1.455
7.905	1.253	20.38	1.451
7.926	1.247	20.41	1.452
7.947	1.252	20.43	1.446
7.967	1.25	20.45	1.448
7.988	1.252	20.47	1.453
8.009	1.262	20.49	1.446
8.03	1.261	20.51	1.447
8.051	1.258	20.53	1.451
8.072	1.268	20.55	1.449
8.092	1.274	20.57	1.461
8.113	1.285	20.59	1.465
8.134	1.29	20.61	1.467
8.155	1.315	20.63	1.481
8.176	1.327	20.66	1.474
8.197	1.342	20.68	1.486
8.217	1.341	20.7	1.5
8.238	1.349	20.72	1.499
8.259	1.36	20.74	1.503
8.28	1.366	20.76	1.508
8.301	1.365	20.78	1.513
8.322	1.366	20.8	1.512
8.342	1.361	20.82	1.509
8.363	1.357	20.84	1.509
8.384	1.367	20.86	1.514
8.405	1.369	20.88	1.508
8.426	1.366	20.91	1.51
8.447	1.361	20.93	1.507
8.467	1.359	20.95	1.505
8.488	1.359	20.97	1.51
8.509	1.354	20.99	1.518
8.53	1.357	21.01	1.529
8.551	1.352	21.03	1.526
8.572	1.363	21.05	1.539
8.592	1.363	21.07	1.551
8.613	1.37	21.09	1.559
8.634	1.379	21.11	1.567
8.655	1.389	21.13	1.58
8.676	1.395	21.16	1.59
8.697	1.402	21.18	1.602
8.717	1.405	21.2	1.612
8.738	1.409	21.22	1.604
8.759	1.39	21.24	1.606
8.78	1.399	21.26	1.613
8.801	1.387	21.28	1.619
8.822	1.389	21.3	1.614
8.842	1.388	21.32	1.617

---

<u>Time (day)</u>	<u>Displacement (ft)</u>	<u>Time (day)</u>	<u>Displacement (ft)</u>
8.863	1.387	21.34	1.616
8.884	1.391	21.36	1.607
8.905	1.393	21.38	1.605
8.926	1.382	21.41	1.601
8.947	1.372	21.43	1.601
8.967	1.369	21.45	1.591
8.988	1.369	21.47	1.584
9.009	1.369	21.49	1.581
9.03	1.362	21.51	1.577
9.051	1.367	21.53	1.575
9.072	1.369	21.55	1.574
9.092	1.378	21.57	1.57
9.113	1.383	21.59	1.573
9.134	1.4	21.61	1.572
9.155	1.414	21.63	1.573
9.176	1.42	21.66	1.578
9.197	1.419	21.68	1.579
9.217	1.433	21.7	1.578
9.238	1.435	21.72	1.589
9.259	1.452	21.74	1.589
9.28	1.447	21.76	1.587
9.301	1.443	21.78	1.57
9.322	1.446	21.8	1.57
9.342	1.43	21.82	1.574
9.363	1.421	21.84	1.556
9.384	1.418	21.86	1.557
9.405	1.405	21.88	1.544
9.426	1.404	21.91	1.534
9.447	1.389	21.93	1.518
9.467	1.389	21.95	1.519
9.488	1.373	21.97	1.507
9.509	1.358	21.99	1.509
9.53	1.355	22.01	1.514
9.551	1.343	22.03	1.516
9.572	1.339	22.05	1.515
9.592	1.329	22.07	1.506
9.613	1.341	22.09	1.516
9.634	1.337	22.11	1.518
9.655	1.337	22.13	1.52
9.676	1.335	22.16	1.526
9.697	1.343	22.18	1.53
9.717	1.341	22.2	1.528
9.738	1.347	22.22	1.546
9.759	1.338	22.24	1.546
9.78	1.338	22.26	1.541
9.801	1.339	22.28	1.543
9.822	1.343	22.3	1.538
9.842	1.341	22.32	1.53
9.863	1.331	22.34	1.523
9.884	1.325	22.36	1.518
9.905	1.309	22.38	1.508
9.926	1.294	22.41	1.497
9.947	1.285	22.43	1.489

---

<u>Time (day)</u>	<u>Displacement (ft)</u>	<u>Time (day)</u>	<u>Displacement (ft)</u>
9.967	1.276	22.45	1.48
9.988	1.27	22.47	1.471
10.01	1.257	22.49	1.459
10.03	1.253	22.51	1.453
10.05	1.261	22.53	1.437
10.07	1.255	22.55	1.426
10.09	1.254	22.57	1.431
10.11	1.253	22.59	1.424
10.13	1.268	22.61	1.424
10.15	1.266	22.63	1.428
10.18	1.283	22.66	1.419
10.2	1.289	22.68	1.421
10.22	1.289	22.7	1.433
10.24	1.298	22.72	1.437
10.26	1.286	22.74	1.447
10.28	1.287	22.76	1.449
10.3	1.291	22.78	1.457
10.32	1.293	22.8	1.453
10.34	1.287	22.82	1.457
10.36	1.279	22.84	1.443
10.38	1.27	22.86	1.447
10.4	1.263	22.88	1.437
10.43	1.247	22.91	1.431
10.45	1.233	22.93	1.419
10.47	1.227	22.95	1.408
10.49	1.214	22.97	1.404
10.51	1.198	22.99	1.402
10.53	1.187	23.01	1.409
10.55	1.173	23.03	1.407
10.57	1.164	23.05	1.416
10.59	1.156	23.07	1.415
10.61	1.15	23.09	1.406
10.63	1.154	23.11	1.415
10.65	1.143	23.13	1.431
10.68	1.155	23.16	1.437
10.7	1.155	23.18	1.45
10.72	1.146	23.2	1.458
10.74	1.166	23.22	1.474
10.76	1.165	23.24	1.468
10.78	1.168	23.26	1.479
10.8	1.174	23.28	1.474
10.82	1.174	23.3	1.479
10.84	1.179	23.32	1.478
10.86	1.175	23.34	1.484
10.88	1.171	23.36	1.474
10.9	1.155	23.38	1.469
10.93	1.156	23.41	1.472
10.95	1.141	23.43	1.459
10.97	1.138	23.45	1.456
10.99	1.135	23.47	1.456
11.01	1.128	23.49	1.445
11.03	1.129	23.51	1.443
11.05	1.129	23.53	1.43

---

<u>Time (day)</u>	<u>Displacement (ft)</u>	<u>Time (day)</u>	<u>Displacement (ft)</u>
11.07	1.131	23.55	1.429
11.09	1.136	23.57	1.442
11.11	1.14	23.59	1.45
11.13	1.156	23.61	1.448
11.15	1.166	23.63	1.458
11.18	1.177	23.66	1.463
11.2	1.183	23.68	1.475
11.22	1.204	23.7	1.483
11.24	1.223	23.72	1.501
11.26	1.227	23.74	1.504
11.28	1.231	23.76	1.514
11.3	1.246	23.78	1.522
11.32	1.257	23.8	1.517
11.34	1.265	23.82	1.51
11.36	1.274	23.84	1.512
11.38	1.268	23.86	1.515
11.4	1.275	23.88	1.508
11.43	1.269	23.91	1.498
11.45	1.265	23.93	1.492
11.47	1.257	23.95	1.488
11.49	1.249	23.97	1.481
11.51	1.241	23.99	1.485
11.53	1.241	24.01	1.478
11.55	1.228	24.03	1.47
11.57	1.227	24.05	1.471
11.59	1.233	24.07	1.464
11.61	1.223	24.09	1.472
11.63	1.232	24.11	1.472
11.65	1.243	24.13	1.481
11.68	1.245	24.16	1.49
11.7	1.259	24.18	1.499
11.72	1.275	24.2	1.505
11.74	1.297	24.22	1.515
11.76	1.304	24.24	1.524
11.78	1.321	24.26	1.531
11.8	1.324	24.28	1.539
11.82	1.332	24.3	1.538
11.84	1.343	24.32	1.544
11.86	1.341	24.34	1.539
11.88	1.343	24.36	1.546
11.9	1.343	24.38	1.533
11.93	1.335	24.41	1.521
11.95	1.334	24.43	1.514
11.97	1.332	24.45	1.517
11.99	1.325	24.47	1.506
12.01	1.33	24.49	1.504
12.03	1.324	24.51	1.493
12.05	1.333	24.53	1.499
12.07	1.336	24.55	1.482
12.09	1.336	24.57	1.485
12.11	1.342	24.59	1.481
12.13	1.351	24.61	1.472
12.15	1.364	24.63	1.484



Time (day)	Displacement (ft)	Time (day)	Displacement (ft)
12.18	1.39	24.66	1.487
12.2	1.404	24.68	1.494
12.22	1.416	24.7	1.497
12.24	1.438	24.72	1.502
12.26	1.453	24.74	1.499
12.28	1.463	24.76	1.506
12.3	1.475	24.78	1.513
12.32	1.504	24.8	1.52
12.34	1.524	24.82	1.526
12.36	1.521	24.84	1.529
12.38	1.527	24.86	1.519
12.4	1.531	24.88	1.526
12.43	1.53	24.91	1.515
12.45	1.518	24.93	1.51
12.47	1.513		

SOLUTION

Pumping Test  
 Aquifer Model: Unconfined  
 Solution Method: Neuman

VISUAL ESTIMATION RESULTS

Estimated Parameters

Parameter	Estimate	
T	9.955E+4	ft <sup>2</sup> /day
S	0.00133	
Sy	0.0009298	
β	0.03	

K = T/b = 19.91 ft/day (0.007024 cm/sec)  
 Ss = S/b = 2.66E-7 1/ft

AUTOMATIC ESTIMATION RESULTS

Estimated Parameters

Parameter	Estimate	Std. Error	Approx. C.I.	t-Ratio	
T	8.521E+4	2.38E+4	+/- 4.67E+4	3.58	ft <sup>2</sup> /day
S	0.005636	0.002853	+/- 0.005597	1.976	
Sy	0.0009298	0.0007065	+/- 0.001386	1.316	
β	0.02722	0.0313	+/- 0.06141	0.8697	

C.I. is approximate 95% confidence interval for parameter  
 t-ratio = estimate/std. error  
 Estimation window: 0.1 to 25 day

K = T/b = 17.04 ft/day (0.006012 cm/sec)  
 Ss = S/b = 1.127E-6 1/ft

Parameter Correlations

	T	S	Sy	β
T	1.00	0.94	-0.96	-1.00
S	0.94	1.00	-1.00	-0.95
Sy	-0.96	-1.00	1.00	0.97
β	-1.00	-0.95	0.97	1.00

Residual Statistics

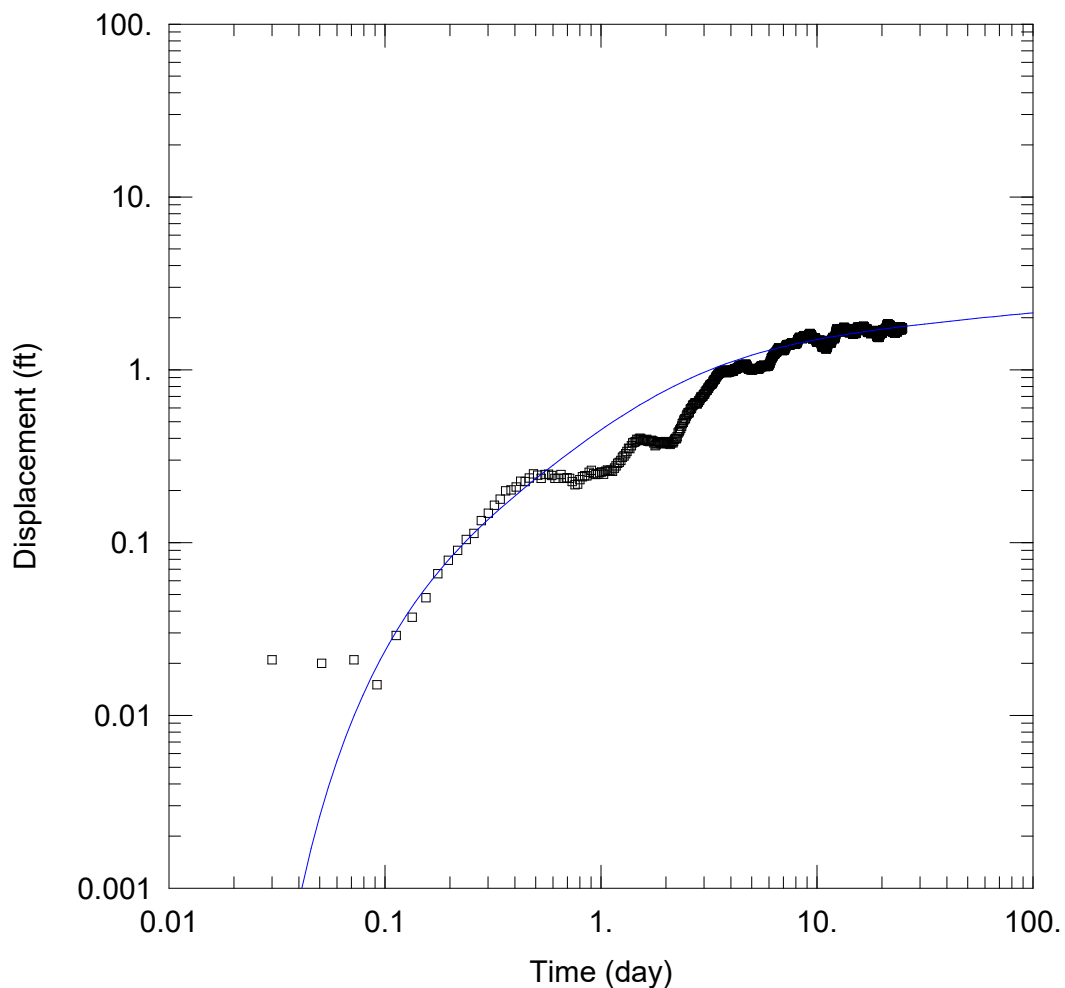
for weighted residuals

Sum of Squares... 11.25 ft<sup>2</sup>  
 Variance ..... 0.009466 ft<sup>2</sup>  
 Std. Deviation ..... 0.09729 ft  
 Mean ..... 0.001092 ft  
 No. of Residuals .. 1192  
 No. of Estimates .. 4

Estimation window from 0.1 to 25 day.

**APPENDIX I**

**AQTESOLV OUTPUT FOR R-32 SCREEN 3 DRAWDOWN ANALYSIS**



WELL TEST ANALYSIS

Data Set: D:\hugo \Downloads\LANL NM PROJECT\AQTESOLV files\R32 S3 data.aqt  
 Date: 06/07/24 Time: 15:14:12

PROJECT INFORMATION

Test Well: PM-2

AQUIFER DATA

Saturated Thickness: 5000. ft

WELL DATA

Pumping Wells			Observation Wells		
Well Name	X (ft)	Y (ft)	Well Name	X (ft)	Y (ft)
PM-2	0	0	□ R32 S3	4779	0

SOLUTION

Aquifer Model: Unconfined

Solution Method: Neuman

T = 8.089E+4 ft<sup>2</sup>/day

S = 0.002508

Sy = 0.00079

β = 0.03

Data Set: D:\hugo\_\Downloads\LANL NM PROJECT\AQTESOLV files\R32 S3 data.aqt

Date: 06/07/24

Time: 15:14:31

---

PROJECT INFORMATION

Test Well: PM-2

---

AQUIFER DATA

Saturated Thickness: 5000. ft

Anisotropy Ratio (Kz/Kr): 0.03284

---

PUMPING WELL DATA

No. of pumping wells: 1

Pumping Well No. 1: PM-2

X Location: 0. ft

Y Location: 0. ft

Casing Radius: 0.5833 ft

Well Radius: 1. ft

Partially Penetrating Well

Depth to Top of Screen: 135. ft

Depth to Bottom of Screen: 1411. ft

No. of pumping periods: 1

Pumping Period Data

<u>Time (day)</u>	<u>Rate (gal/min)</u>
0.	1249.

---

OBSERVATION WELL DATA

No. of observation wells: 1

Observation Well No. 1: R32 S3

X Location: 4779. ft

Y Location: 0. ft

Radial distance from PM-2: 4779. ft

Partially Penetrating Well

Depth to Top of Screen: 185.2 ft

Depth to Bottom of Screen: 192.9 ft

No. of Observations: 1197

Observation Data

<u>Time (day)</u>	<u>Displacement (ft)</u>	<u>Time (day)</u>	<u>Displacement (ft)</u>
-------------------	--------------------------	-------------------	--------------------------

---

0.009	0.014	12.49	1.702
0.03	0.021	12.51	1.703
0.051	0.02	12.53	1.69
0.072	0.021	12.55	1.679
0.092	0.015	12.57	1.678
0.113	0.029	12.59	1.66
0.134	0.037	12.61	1.672
0.155	0.048	12.63	1.671
0.176	0.066	12.65	1.672
0.197	0.079	12.68	1.676
0.217	0.09	12.7	1.678
0.238	0.104	12.72	1.693
0.259	0.113	12.74	1.693
0.28	0.134	12.76	1.707
0.301	0.148	12.78	1.708
0.322	0.164	12.8	1.715
0.342	0.178	12.82	1.723
0.363	0.199	12.84	1.729
0.384	0.202	12.86	1.724
0.405	0.21	12.88	1.721
0.426	0.226	12.9	1.718
0.447	0.225	12.93	1.71
0.467	0.236	12.95	1.704
0.488	0.25	12.97	1.699
0.509	0.245	12.99	1.691
0.53	0.235	13.01	1.684
0.551	0.247	13.03	1.676
0.572	0.248	13.05	1.669
0.592	0.244	13.07	1.655
0.613	0.235	13.09	1.665
0.634	0.235	13.11	1.664
0.655	0.247	13.13	1.664
0.676	0.235	13.15	1.661
0.697	0.237	13.18	1.672
0.717	0.235	13.2	1.679
0.738	0.225	13.22	1.695
0.759	0.216	13.24	1.71
0.78	0.218	13.26	1.719
0.801	0.231	13.28	1.715
0.822	0.24	13.3	1.719
0.842	0.243	13.32	1.743
0.863	0.243	13.34	1.744
0.884	0.255	13.36	1.756
0.905	0.262	13.38	1.757
0.926	0.251	13.4	1.746
0.947	0.247	13.43	1.75
0.967	0.249	13.45	1.745
0.988	0.254	13.47	1.736
1.009	0.256	13.49	1.729
1.03	0.249	13.51	1.72
1.051	0.258	13.53	1.705
1.072	0.263	13.55	1.694
1.092	0.259	13.57	1.687
1.113	0.263	13.59	1.68

---

<u>Time (day)</u>	<u>Displacement (ft)</u>	<u>Time (day)</u>	<u>Displacement (ft)</u>
1.134	0.258	13.61	1.676
1.155	0.27	13.63	1.664
1.176	0.278	13.65	1.673
1.197	0.287	13.68	1.675
1.217	0.291	13.7	1.68
1.238	0.299	13.72	1.679
1.259	0.311	13.74	1.68
1.28	0.317	13.76	1.678
1.301	0.326	13.78	1.681
1.322	0.336	13.8	1.692
1.342	0.351	13.82	1.699
1.363	0.349	13.84	1.698
1.384	0.363	13.86	1.695
1.405	0.377	13.88	1.699
1.426	0.38	13.9	1.7
1.447	0.384	13.93	1.697
1.467	0.396	13.95	1.692
1.488	0.393	13.97	1.691
1.509	0.4	13.99	1.684
1.53	0.401	14.01	1.68
1.551	0.392	14.03	1.666
1.572	0.389	14.05	1.664
1.592	0.392	14.07	1.657
1.613	0.39	14.09	1.647
1.634	0.395	14.11	1.647
1.655	0.385	14.13	1.651
1.676	0.384	14.15	1.639
1.697	0.387	14.18	1.644
1.717	0.391	14.2	1.649
1.738	0.388	14.22	1.638
1.759	0.378	14.24	1.653
1.78	0.364	14.26	1.657
1.801	0.368	14.28	1.676
1.822	0.375	14.3	1.686
1.842	0.382	14.32	1.691
1.863	0.382	14.34	1.697
1.884	0.379	14.36	1.71
1.905	0.372	14.38	1.716
1.926	0.379	14.4	1.73
1.947	0.383	14.43	1.72
1.967	0.376	14.45	1.717
1.988	0.384	14.47	1.706
2.009	0.374	14.49	1.701
2.03	0.377	14.51	1.688
2.051	0.376	14.53	1.671
2.072	0.374	14.55	1.66
2.092	0.37	14.57	1.656
2.113	0.378	14.59	1.639
2.134	0.382	14.61	1.627
2.155	0.378	14.63	1.625
2.176	0.385	14.65	1.612
2.197	0.395	14.68	1.613
2.217	0.401	14.7	1.604

---

<u>Time (day)</u>	<u>Displacement (ft)</u>	<u>Time (day)</u>	<u>Displacement (ft)</u>
2.238	0.399	14.72	1.608
2.259	0.41	14.74	1.617
2.28	0.431	14.76	1.622
2.301	0.439	14.78	1.623
2.322	0.447	14.8	1.621
2.342	0.457	14.82	1.621
2.363	0.472	14.84	1.629
2.384	0.487	14.86	1.638
2.405	0.495	14.88	1.638
2.426	0.51	14.9	1.632
2.447	0.52	14.93	1.638
2.467	0.521	14.95	1.625
2.488	0.541	14.97	1.63
2.509	0.552	14.99	1.628
2.53	0.564	15.01	1.633
2.551	0.56	15.03	1.622
2.572	0.568	15.05	1.625
2.592	0.591	15.07	1.624
2.613	0.596	15.09	1.62
2.634	0.602	15.11	1.623
2.655	0.62	15.13	1.622
2.676	0.626	15.15	1.624
2.697	0.63	15.18	1.626
2.717	0.64	15.2	1.631
2.738	0.643	15.22	1.638
2.759	0.644	15.24	1.653
2.78	0.634	15.26	1.657
2.801	0.635	15.28	1.674
2.822	0.648	15.3	1.687
2.842	0.664	15.32	1.697
2.863	0.666	15.34	1.706
2.884	0.679	15.36	1.719
2.905	0.694	15.38	1.727
2.926	0.693	15.4	1.742
2.947	0.699	15.43	1.753
2.967	0.699	15.45	1.754
2.988	0.716	15.47	1.761
3.009	0.721	15.49	1.76
3.03	0.726	15.51	1.763
3.051	0.743	15.53	1.761
3.072	0.757	15.55	1.755
3.092	0.761	15.57	1.752
3.113	0.764	15.59	1.744
3.134	0.782	15.61	1.743
3.155	0.782	15.63	1.744
3.176	0.799	15.65	1.737
3.197	0.814	15.68	1.742
3.217	0.816	15.7	1.743
3.238	0.822	15.72	1.748
3.259	0.832	15.74	1.745
3.28	0.832	15.76	1.74
3.301	0.849	15.78	1.739
3.322	0.858	15.8	1.742



---

<u>Time (day)</u>	<u>Displacement (ft)</u>	<u>Time (day)</u>	<u>Displacement (ft)</u>
3.342	0.869	15.82	1.744
3.363	0.877	15.84	1.754
3.384	0.882	15.86	1.762
3.405	0.9	15.88	1.769
3.426	0.912	15.9	1.765
3.447	0.92	15.93	1.767
3.467	0.93	15.95	1.763
3.488	0.944	15.97	1.767
3.509	0.942	15.99	1.761
3.53	0.954	16.01	1.761
3.551	0.962	16.03	1.757
3.572	0.963	16.05	1.761
3.592	0.965	16.07	1.74
3.613	0.964	16.09	1.736
3.634	0.974	16.11	1.736
3.655	0.975	16.13	1.73
3.676	0.983	16.16	1.731
3.697	0.979	16.18	1.735
3.717	0.986	16.2	1.733
3.738	0.993	16.22	1.733
3.759	1.	16.24	1.744
3.78	0.977	16.26	1.744
3.801	0.97	16.28	1.741
3.822	0.962	16.3	1.752
3.842	0.977	16.32	1.759
3.863	0.967	16.34	1.77
3.884	0.964	16.36	1.769
3.905	0.981	16.38	1.775
3.926	0.97	16.41	1.781
3.947	0.973	16.43	1.782
3.967	0.978	16.45	1.78
3.988	0.981	16.47	1.777
4.009	0.984	16.49	1.776
4.03	0.978	16.51	1.777
4.051	0.982	16.53	1.77
4.072	0.992	16.55	1.756
4.092	0.979	16.57	1.754
4.113	0.985	16.59	1.748
4.134	1.004	16.61	1.74
4.155	1.011	16.63	1.724
4.176	1.012	16.66	1.717
4.197	1.013	16.68	1.717
4.217	1.012	16.7	1.712
4.238	1.012	16.72	1.709
4.259	1.015	16.74	1.707
4.28	1.029	16.76	1.704
4.301	1.021	16.78	1.706
4.322	1.029	16.8	1.707
4.342	1.039	16.82	1.717
4.363	1.045	16.84	1.727
4.384	1.047	16.86	1.725
4.405	1.051	16.88	1.73
4.426	1.052	16.91	1.725

---

<u>Time (day)</u>	<u>Displacement (ft)</u>	<u>Time (day)</u>	<u>Displacement (ft)</u>
4.447	1.057	16.93	1.728
4.467	1.054	16.95	1.723
4.488	1.059	16.97	1.729
4.509	1.056	16.99	1.721
4.53	1.067	17.01	1.717
4.551	1.058	17.03	1.722
4.572	1.065	17.05	1.703
4.592	1.059	17.07	1.694
4.613	1.071	17.09	1.685
4.634	1.066	17.11	1.688
4.655	1.072	17.13	1.672
4.676	1.076	17.16	1.659
4.697	1.071	17.18	1.658
4.717	1.07	17.2	1.65
4.738	1.054	17.22	1.653
4.759	1.039	17.24	1.644
4.78	1.03	17.26	1.649
4.801	1.02	17.28	1.656
4.822	1.011	17.3	1.645
4.842	1.006	17.32	1.656
4.863	1.008	17.34	1.653
4.884	1.005	17.36	1.659
4.905	1.01	17.38	1.669
4.926	1.006	17.41	1.661
4.947	0.999	17.43	1.676
4.967	1.009	17.45	1.669
4.988	0.999	17.47	1.681
5.009	1.002	17.49	1.681
5.03	0.998	17.51	1.67
5.051	1.002	17.53	1.674
5.072	1.004	17.55	1.662
5.092	1.007	17.57	1.662
5.113	1.014	17.59	1.656
5.134	1.011	17.61	1.659
5.155	1.014	17.63	1.647
5.176	1.017	17.66	1.649
5.197	1.011	17.68	1.648
5.217	1.008	17.7	1.64
5.238	1.017	17.72	1.643
5.259	1.012	17.74	1.635
5.28	1.011	17.76	1.618
5.301	1.014	17.78	1.621
5.322	1.01	17.8	1.629
5.342	1.01	17.82	1.622
5.363	1.014	17.84	1.626
5.384	1.009	17.86	1.622
5.405	1.016	17.88	1.623
5.426	1.028	17.91	1.63
5.447	1.025	17.93	1.64
5.467	1.034	17.95	1.639
5.488	1.042	17.97	1.636
5.509	1.043	17.99	1.643
5.53	1.053	18.01	1.655

---

<u>Time (day)</u>	<u>Displacement (ft)</u>	<u>Time (day)</u>	<u>Displacement (ft)</u>
5.551	1.05	18.03	1.653
5.572	1.042	18.05	1.651
5.592	1.046	18.07	1.648
5.613	1.052	18.09	1.648
5.634	1.049	18.11	1.644
5.655	1.051	18.13	1.648
5.676	1.064	18.16	1.65
5.697	1.055	18.18	1.645
5.717	1.061	18.2	1.649
5.738	1.054	18.22	1.64
5.759	1.044	18.24	1.65
5.78	1.045	18.26	1.649
5.801	1.04	18.28	1.637
5.822	1.048	18.3	1.649
5.842	1.05	18.32	1.653
5.863	1.054	18.34	1.65
5.884	1.052	18.36	1.652
5.905	1.056	18.38	1.656
5.926	1.052	18.41	1.661
5.947	1.057	18.43	1.663
5.967	1.052	18.45	1.675
5.988	1.062	18.47	1.675
6.009	1.072	18.49	1.677
6.03	1.069	18.51	1.668
6.051	1.083	18.53	1.68
6.072	1.091	18.55	1.686
6.092	1.112	18.57	1.678
6.113	1.128	18.59	1.679
6.134	1.131	18.61	1.684
6.155	1.159	18.63	1.67
6.176	1.167	18.66	1.674
6.197	1.169	18.68	1.668
6.217	1.178	18.7	1.671
6.238	1.191	18.72	1.669
6.259	1.196	18.74	1.656
6.28	1.208	18.76	1.648
6.301	1.221	18.78	1.627
6.322	1.222	18.8	1.623
6.342	1.233	18.82	1.624
6.363	1.231	18.84	1.628
6.384	1.236	18.86	1.608
6.405	1.247	18.88	1.596
6.426	1.256	18.91	1.6
6.447	1.254	18.93	1.581
6.467	1.261	18.95	1.576
6.488	1.275	18.97	1.576
6.509	1.269	18.99	1.572
6.53	1.28	19.01	1.561
6.551	1.292	19.03	1.557
6.572	1.301	19.05	1.555
6.592	1.306	19.07	1.563
6.613	1.306	19.09	1.555
6.634	1.326	19.11	1.55

---

<u>Time (day)</u>	<u>Displacement (ft)</u>	<u>Time (day)</u>	<u>Displacement (ft)</u>
6.655	1.336	19.13	1.553
6.676	1.333	19.16	1.544
6.697	1.334	19.18	1.543
6.717	1.333	19.2	1.537
6.738	1.318	19.22	1.547
6.759	1.314	19.24	1.544
6.78	1.307	19.26	1.554
6.801	1.307	19.28	1.542
6.822	1.305	19.3	1.547
6.842	1.305	19.32	1.539
6.863	1.313	19.34	1.542
6.884	1.301	19.36	1.547
6.905	1.301	19.38	1.55
6.926	1.297	19.41	1.558
6.947	1.29	19.43	1.558
6.967	1.295	19.45	1.566
6.988	1.299	19.47	1.567
7.009	1.296	19.49	1.577
7.03	1.293	19.51	1.582
7.051	1.301	19.53	1.586
7.072	1.307	19.55	1.595
7.092	1.312	19.57	1.602
7.113	1.326	19.59	1.611
7.134	1.337	19.61	1.615
7.155	1.349	19.63	1.63
7.176	1.353	19.66	1.642
7.197	1.37	19.68	1.648
7.217	1.38	19.7	1.664
7.238	1.384	19.72	1.655
7.259	1.394	19.74	1.644
7.28	1.395	19.76	1.64
7.301	1.397	19.78	1.638
7.322	1.392	19.8	1.644
7.342	1.393	19.82	1.641
7.363	1.398	19.84	1.633
7.384	1.394	19.86	1.641
7.405	1.398	19.88	1.629
7.426	1.399	19.91	1.636
7.447	1.398	19.93	1.622
7.467	1.398	19.95	1.624
7.488	1.393	19.97	1.626
7.509	1.394	19.99	1.631
7.53	1.399	20.01	1.636
7.551	1.408	20.03	1.637
7.572	1.409	20.05	1.641
7.592	1.417	20.07	1.651
7.613	1.421	20.09	1.663
7.634	1.423	20.11	1.66
7.655	1.422	20.13	1.662
7.676	1.434	20.16	1.683
7.697	1.429	20.18	1.681
7.717	1.432	20.2	1.684
7.738	1.419	20.22	1.695

---

<u>Time (day)</u>	<u>Displacement (ft)</u>	<u>Time (day)</u>	<u>Displacement (ft)</u>
7.759	1.416	20.24	1.691
7.78	1.415	20.26	1.699
7.801	1.407	20.28	1.69
7.822	1.404	20.3	1.692
7.842	1.416	20.32	1.689
7.863	1.404	20.34	1.682
7.884	1.407	20.36	1.674
7.905	1.414	20.38	1.682
7.926	1.414	20.41	1.677
7.947	1.413	20.43	1.671
7.967	1.405	20.45	1.68
7.988	1.413	20.47	1.671
8.009	1.417	20.49	1.671
8.03	1.422	20.51	1.672
8.051	1.42	20.53	1.662
8.072	1.429	20.55	1.673
8.092	1.436	20.57	1.679
8.113	1.447	20.59	1.683
8.134	1.452	20.61	1.691
8.155	1.47	20.63	1.698
8.176	1.488	20.66	1.699
8.197	1.497	20.68	1.703
8.217	1.503	20.7	1.71
8.238	1.511	20.72	1.71
8.259	1.515	20.74	1.714
8.28	1.521	20.76	1.719
8.301	1.527	20.78	1.724
8.322	1.541	20.8	1.729
8.342	1.529	20.82	1.72
8.363	1.525	20.84	1.733
8.384	1.535	20.86	1.738
8.405	1.53	20.88	1.733
8.426	1.534	20.91	1.734
8.447	1.522	20.93	1.726
8.467	1.519	20.95	1.723
8.488	1.52	20.97	1.735
8.509	1.529	20.99	1.736
8.53	1.525	21.01	1.741
8.551	1.527	21.03	1.738
8.572	1.51	21.05	1.758
8.592	1.53	21.07	1.763
8.613	1.545	21.09	1.771
8.634	1.553	21.11	1.779
8.655	1.557	21.13	1.792
8.676	1.556	21.16	1.802
8.697	1.576	21.18	1.807
8.717	1.573	21.2	1.817
8.738	1.577	21.22	1.829
8.759	1.551	21.24	1.824
8.78	1.561	21.26	1.838
8.801	1.549	21.28	1.838
8.822	1.558	21.3	1.839
8.842	1.556	21.32	1.835

---

<u>Time (day)</u>	<u>Displacement (ft)</u>	<u>Time (day)</u>	<u>Displacement (ft)</u>
8.863	1.549	21.34	1.827
8.884	1.56	21.36	1.832
8.905	1.555	21.38	1.829
8.926	1.551	21.41	1.819
8.947	1.548	21.43	1.826
8.967	1.545	21.45	1.815
8.988	1.545	21.47	1.809
9.009	1.539	21.49	1.799
9.03	1.531	21.51	1.795
9.051	1.537	21.53	1.8
9.072	1.538	21.55	1.799
9.092	1.541	21.57	1.782
9.113	1.56	21.59	1.785
9.134	1.563	21.61	1.784
9.155	1.577	21.63	1.792
9.176	1.59	21.66	1.797
9.197	1.582	21.68	1.798
9.217	1.603	21.7	1.803
9.238	1.605	21.72	1.807
9.259	1.616	21.74	1.815
9.28	1.618	21.76	1.806
9.301	1.62	21.78	1.789
9.322	1.616	21.8	1.782
9.342	1.601	21.82	1.786
9.363	1.592	21.84	1.775
9.384	1.588	21.86	1.77
9.405	1.589	21.88	1.764
9.426	1.581	21.91	1.747
9.447	1.573	21.93	1.744
9.467	1.559	21.95	1.739
9.488	1.543	21.97	1.734
9.509	1.542	21.99	1.73
9.53	1.538	22.01	1.734
9.551	1.52	22.03	1.73
9.572	1.516	22.05	1.728
9.592	1.505	22.07	1.733
9.613	1.518	22.09	1.736
9.634	1.521	22.11	1.739
9.655	1.52	22.13	1.74
9.676	1.519	22.16	1.747
9.697	1.52	22.18	1.75
9.717	1.518	22.2	1.748
9.738	1.524	22.22	1.76
9.759	1.522	22.24	1.76
9.78	1.528	22.26	1.761
9.801	1.523	22.28	1.764
9.822	1.52	22.3	1.765
9.842	1.526	22.32	1.757
9.863	1.509	22.34	1.737
9.884	1.503	22.36	1.731
9.905	1.488	22.38	1.728
9.926	1.479	22.41	1.724
9.947	1.457	22.43	1.716

---

<u>Time (day)</u>	<u>Displacement (ft)</u>	<u>Time (day)</u>	<u>Displacement (ft)</u>
9.967	1.468	22.45	1.713
9.988	1.462	22.47	1.698
10.01	1.442	22.49	1.678
10.03	1.445	22.51	1.68
10.05	1.447	22.53	1.67
10.07	1.447	22.55	1.653
10.09	1.44	22.57	1.658
10.11	1.445	22.59	1.65
10.13	1.461	22.61	1.644
10.15	1.458	22.63	1.648
10.18	1.469	22.66	1.646
10.2	1.469	22.68	1.648
10.22	1.468	22.7	1.653
10.24	1.471	22.72	1.664
10.26	1.48	22.74	1.674
10.28	1.473	22.76	1.669
10.3	1.485	22.78	1.67
10.32	1.48	22.8	1.679
10.34	1.481	22.82	1.677
10.36	1.473	22.84	1.67
10.38	1.463	22.86	1.661
10.4	1.449	22.88	1.658
10.43	1.44	22.91	1.644
10.45	1.44	22.93	1.645
10.47	1.42	22.95	1.636
10.49	1.414	22.97	1.631
10.51	1.391	22.99	1.629
10.53	1.38	23.01	1.63
10.55	1.366	23.03	1.627
10.57	1.37	23.05	1.636
10.59	1.354	23.07	1.642
10.61	1.349	23.09	1.633
10.63	1.354	23.11	1.635
10.65	1.349	23.13	1.652
10.68	1.354	23.16	1.664
10.7	1.354	23.18	1.671
10.72	1.345	23.2	1.679
10.74	1.358	23.22	1.694
10.76	1.37	23.24	1.696
10.78	1.367	23.26	1.7
10.8	1.36	23.28	1.701
10.82	1.367	23.3	1.707
10.84	1.372	23.32	1.712
10.86	1.368	23.34	1.712
10.88	1.372	23.36	1.708
10.9	1.348	23.38	1.696
10.93	1.343	23.41	1.692
10.95	1.341	23.43	1.686
10.97	1.338	23.45	1.683
10.99	1.335	23.47	1.676
11.01	1.321	23.49	1.671
11.03	1.322	23.51	1.676
11.05	1.322	23.53	1.656

<u>Time (day)</u>	<u>Displacement (ft)</u>	<u>Time (day)</u>	<u>Displacement (ft)</u>
11.07	1.324	23.55	1.662
11.09	1.328	23.57	1.661
11.11	1.339	23.59	1.669
11.13	1.349	23.61	1.666
11.15	1.352	23.63	1.683
11.18	1.369	23.66	1.682
11.2	1.376	23.68	1.693
11.22	1.397	23.7	1.708
11.24	1.41	23.72	1.72
11.26	1.42	23.74	1.722
11.28	1.424	23.76	1.726
11.3	1.439	23.78	1.734
11.32	1.45	23.8	1.736
11.34	1.458	23.82	1.743
11.36	1.454	23.84	1.731
11.38	1.475	23.86	1.735
11.4	1.461	23.88	1.727
11.43	1.462	23.91	1.731
11.45	1.465	23.93	1.719
11.47	1.463	23.95	1.708
11.49	1.455	23.97	1.708
11.51	1.44	23.99	1.698
11.53	1.433	24.01	1.699
11.55	1.433	24.03	1.69
11.57	1.432	24.05	1.691
11.59	1.43	24.07	1.698
11.61	1.428	24.09	1.699
11.63	1.436	24.11	1.699
11.65	1.441	24.13	1.708
11.68	1.449	24.16	1.71
11.7	1.456	24.18	1.719
11.72	1.473	24.2	1.726
11.74	1.488	24.22	1.737
11.76	1.495	24.24	1.752
11.78	1.505	24.26	1.753
11.8	1.509	24.28	1.754
11.82	1.523	24.3	1.76
11.84	1.535	24.32	1.766
11.86	1.533	24.34	1.76
11.88	1.534	24.36	1.767
11.9	1.528	24.38	1.761
11.93	1.533	24.41	1.749
11.95	1.526	24.43	1.742
11.97	1.517	24.45	1.738
11.99	1.524	24.47	1.734
12.01	1.522	24.49	1.731
12.03	1.509	24.51	1.727
12.05	1.525	24.53	1.719
12.07	1.527	24.55	1.708
12.09	1.521	24.57	1.711
12.11	1.534	24.59	1.708
12.13	1.55	24.61	1.705
12.15	1.556	24.63	1.71



<u>Time (day)</u>	<u>Displacement (ft)</u>	<u>Time (day)</u>	<u>Displacement (ft)</u>
12.18	1.575	24.66	1.714
12.2	1.589	24.68	1.721
12.22	1.607	24.7	1.724
12.24	1.609	24.72	1.728
12.26	1.639	24.74	1.732
12.28	1.655	24.76	1.732
12.3	1.674	24.78	1.74
12.32	1.682	24.8	1.74
12.34	1.703	24.82	1.74
12.36	1.706	24.84	1.749
12.38	1.719	24.86	1.746
12.4	1.717	24.88	1.739
12.43	1.709	24.91	1.736
12.45	1.717	24.93	1.73
12.47	1.712		

---

### SOLUTION

Pumping Test  
Aquifer Model: Unconfined  
Solution Method: Neuman

---

### VISUAL ESTIMATION RESULTS

#### Estimated Parameters

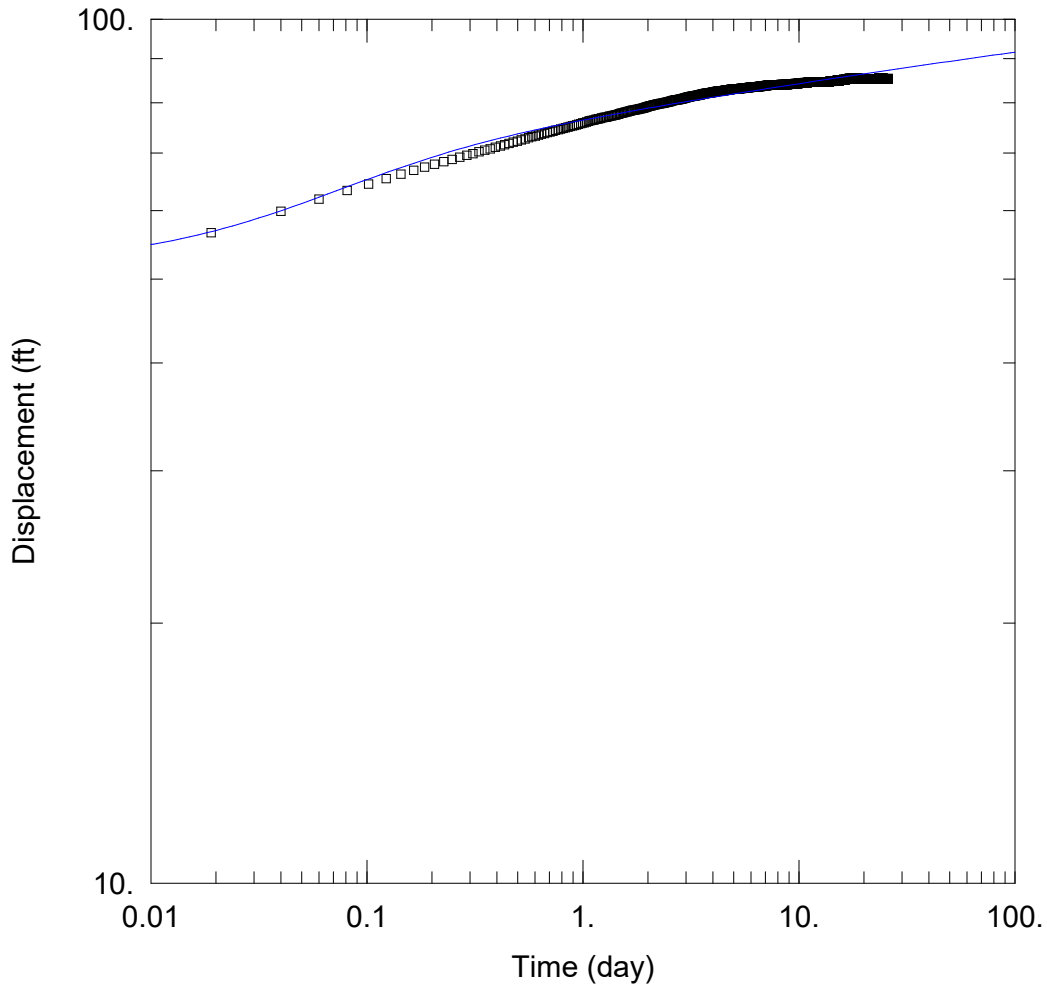
<u>Parameter</u>	<u>Estimate</u>	
T	8.089E+4	ft <sup>2</sup> /day
S	0.002508	
Sy	0.00079	
$\beta$	0.03	

$K = T/b = 16.18 \text{ ft/day (0.005707 cm/sec)}$

$S_s = S/b = 5.016E-7 \text{ 1/ft}$

**APPENDIX J**

**AQTESOLV OUTPUT FOR PM-2 RECOVERY ANALYSIS**



WELL TEST ANALYSIS

Data Set: D:\hugo \Downloads\LANL NM PROJECT\AQTESOLV files\PM-2 recovery data.aqt  
 Date: 06/07/24 Time: 16:46:22

PROJECT INFORMATION

Test Well: PM-2

AQUIFER DATA

Saturated Thickness: 5000. ft

WELL DATA

Pumping Wells			Observation Wells		
Well Name	X (ft)	Y (ft)	Well Name	X (ft)	Y (ft)
PM-2	0	0	□ PM-2 recovery	1	0

SOLUTION

Aquifer Model: Unconfined

Solution Method: Neuman

T = 5996.4 ft<sup>2</sup>/day

S = 0.003874

Sy = 0.5

β = 0.0002363

Data Set: D:\hugo\_\Downloads\LANL NM PROJECT\AQTESOLV files\PM-2 recovery data.aqt  
Date: 06/07/24  
Time: 16:46:34

---

PROJECT INFORMATION

Test Well: PM-2

---

AQUIFER DATA

Saturated Thickness: 5000. ft  
Anisotropy Ratio (Kz/Kr): 5907.9

---

PUMPING WELL DATA

No. of pumping wells: 1

Pumping Well No. 1: PM-2

X Location: 0. ft  
Y Location: 0. ft

Casing Radius: 0.5833 ft  
Well Radius: 1. ft

Partially Penetrating Well  
Depth to Top of Screen: 135. ft  
Depth to Bottom of Screen: 1411. ft

No. of pumping periods: 1

<u>Pumping Period Data</u>	
<u>Time (day)</u>	<u>Rate (gal/min)</u>
0.	1249.

---

OBSERVATION WELL DATA

No. of observation wells: 1

Observation Well No. 1: PM-2 recovery

X Location: 1. ft  
Y Location: 0. ft

Radial distance from PM-2: 1. ft

Partially Penetrating Well  
Depth to Top of Screen: 135. ft  
Depth to Bottom of Screen: 1411. ft

No. of Observations: 1246

<u>Observation Data</u>			
<u>Time (day)</u>	<u>Displacement (ft)</u>	<u>Time (day)</u>	<u>Displacement (ft)</u>

---

0.019	56.62	13.	84.57
0.04	59.95	13.02	84.57
0.06	61.89	13.04	84.57
0.081	63.32	13.06	84.57
0.102	64.44	13.08	84.57
0.123	65.36	13.1	84.57
0.144	66.15	13.12	84.57
0.165	66.83	13.14	84.57
0.185	67.42	13.16	84.56
0.206	67.94	13.19	84.56
0.227	68.39	13.21	84.54
0.248	68.81	13.23	84.54
0.269	69.2	13.25	84.54
0.29	69.56	13.27	84.53
0.31	69.89	13.29	84.54
0.331	70.21	13.31	84.54
0.352	70.49	13.33	84.54
0.373	70.78	13.35	84.55
0.394	71.06	13.37	84.56
0.415	71.31	13.39	84.57
0.435	71.56	13.41	84.58
0.456	71.8	13.44	84.59
0.477	72.03	13.46	84.59
0.498	72.25	13.48	84.62
0.519	72.48	13.5	84.62
0.54	72.68	13.52	84.63
0.56	72.88	13.54	84.62
0.581	73.08	13.56	84.64
0.602	73.24	13.58	84.65
0.623	73.43	13.6	84.65
0.644	73.59	13.62	84.65
0.665	73.75	13.64	84.64
0.685	73.9	13.66	84.65
0.706	74.05	13.69	84.65
0.727	74.19	13.71	84.65
0.748	74.34	13.73	84.65
0.769	74.45	13.75	84.65
0.79	74.59	13.77	84.65
0.81	74.71	13.79	84.65
0.831	74.85	13.81	84.65
0.852	74.98	13.83	84.65
0.873	75.1	13.85	84.67
0.894	75.21	13.87	84.67
0.915	75.33	13.89	84.68
0.935	75.46	13.91	84.71
0.956	75.59	13.94	84.71
0.977	75.69	13.96	84.73
0.998	75.82	13.98	84.74
1.019	75.92	14.	84.76
1.04	76.04	14.02	84.77
1.06	76.14	14.04	84.77
1.081	76.25	14.06	84.8
1.102	76.34	14.08	84.8
1.123	76.42	14.1	84.8

---

<u>Time (day)</u>	<u>Displacement (ft)</u>	<u>Time (day)</u>	<u>Displacement (ft)</u>
1.144	76.51	14.12	84.8
1.165	76.58	14.14	84.79
1.185	76.68	14.16	84.77
1.206	76.76	14.19	84.77
1.227	76.84	14.21	84.78
1.248	76.9	14.23	84.78
1.269	76.97	14.25	84.76
1.29	77.03	14.27	84.76
1.31	77.1	14.29	84.75
1.331	77.19	14.31	84.75
1.352	77.25	14.33	84.75
1.373	77.32	14.35	84.75
1.394	77.39	14.37	84.73
1.415	77.46	14.39	84.75
1.435	77.54	14.41	84.76
1.456	77.61	14.44	84.77
1.477	77.69	14.46	84.78
1.498	77.77	14.48	84.78
1.519	77.84	14.5	84.79
1.54	77.91	14.52	84.81
1.56	77.98	14.54	84.84
1.581	78.06	14.56	84.84
1.602	78.11	14.58	84.85
1.623	78.2	14.6	84.85
1.644	78.26	14.62	84.85
1.665	78.33	14.64	84.84
1.685	78.37	14.66	84.85
1.706	78.43	14.69	84.86
1.727	78.47	14.71	84.84
1.748	78.53	14.73	84.83
1.769	78.58	14.75	84.83
1.79	78.62	14.77	84.83
1.81	78.68	14.79	84.83
1.831	78.72	14.81	84.83
1.852	78.78	14.83	84.83
1.873	78.82	14.85	84.81
1.894	78.88	14.87	84.83
1.915	78.94	14.89	84.83
1.935	79.01	14.91	84.84
1.956	79.07	14.94	84.86
1.977	79.13	14.96	84.86
1.998	79.18	14.98	84.89
2.019	79.25	15.	84.92
2.04	79.31	15.02	84.93
2.06	79.37	15.04	84.93
2.081	79.43	15.06	84.95
2.102	79.47	15.08	84.95
2.123	79.55	15.1	84.95
2.144	79.59	15.12	84.95
2.165	79.63	15.14	84.93
2.185	79.67	15.16	84.92
2.206	79.7	15.19	84.92
2.227	79.75	15.21	84.92

---

<u>Time (day)</u>	<u>Displacement (ft)</u>	<u>Time (day)</u>	<u>Displacement (ft)</u>
2.248	79.78	15.23	84.91
2.269	79.81	15.25	84.91
2.29	79.85	15.27	84.91
2.31	79.88	15.29	84.89
2.331	79.91	15.31	84.89
2.352	79.94	15.33	84.89
2.373	79.98	15.35	84.89
2.394	80.01	15.37	84.89
2.415	80.05	15.39	84.89
2.435	80.09	15.41	84.91
2.456	80.12	15.44	84.91
2.477	80.17	15.46	84.91
2.498	80.21	15.48	84.94
2.519	80.25	15.5	84.95
2.54	80.3	15.52	84.97
2.56	80.37	15.54	84.98
2.581	80.41	15.56	85.
2.602	80.46	15.58	84.98
2.623	80.5	15.6	84.98
2.644	80.55	15.62	85.
2.665	80.59	15.64	85.01
2.685	80.6	15.66	85.01
2.706	80.63	15.69	85.02
2.727	80.65	15.71	85.02
2.748	80.67	15.73	85.02
2.769	80.69	15.75	85.02
2.79	80.72	15.77	85.02
2.81	80.76	15.79	85.
2.831	80.78	15.81	85.02
2.852	80.82	15.83	85.02
2.873	80.85	15.85	85.02
2.894	80.88	15.87	85.02
2.915	80.92	15.89	85.02
2.935	80.95	15.91	85.05
2.956	81.	15.94	85.05
2.977	81.05	15.96	85.05
2.998	81.08	15.98	85.08
3.019	81.13	16.	85.08
3.04	81.15	16.02	85.09
3.06	81.2	16.04	85.09
3.081	81.24	16.06	85.11
3.102	81.27	16.08	85.11
3.123	81.3	16.1	85.12
3.144	81.34	16.12	85.12
3.165	81.36	16.14	85.14
3.185	81.39	16.16	85.12
3.206	81.4	16.18	85.12
3.227	81.43	16.21	85.11
3.248	81.46	16.23	85.11
3.269	81.47	16.25	85.11
3.29	81.49	16.27	85.1
3.31	81.52	16.29	85.1
3.331	81.52	16.31	85.1

---

<u>Time (day)</u>	<u>Displacement (ft)</u>	<u>Time (day)</u>	<u>Displacement (ft)</u>
3.352	81.56	16.33	85.1
3.373	81.58	16.35	85.1
3.394	81.61	16.37	85.1
3.415	81.63	16.39	85.1
3.435	81.65	16.41	85.11
3.456	81.69	16.43	85.13
3.477	81.71	16.46	85.14
3.498	81.75	16.48	85.16
3.519	81.78	16.5	85.17
3.54	81.82	16.52	85.19
3.56	81.85	16.54	85.2
3.581	81.88	16.56	85.23
3.602	81.91	16.58	85.23
3.623	81.94	16.6	85.23
3.644	81.97	16.62	85.25
3.665	81.98	16.64	85.25
3.685	82.01	16.66	85.23
3.706	82.04	16.68	85.22
3.727	82.06	16.71	85.23
3.748	82.07	16.73	85.22
3.769	82.09	16.75	85.22
3.79	82.1	16.77	85.22
3.81	82.11	16.79	85.22
3.831	82.14	16.81	85.21
3.852	82.16	16.83	85.21
3.873	82.17	16.85	85.21
3.894	82.19	16.87	85.21
3.915	82.2	16.89	85.24
3.935	82.23	16.91	85.24
3.956	82.25	16.93	85.24
3.977	82.26	16.96	85.27
3.998	82.29	16.98	85.27
4.019	82.32	17.	85.3
4.04	82.33	17.02	85.31
4.06	82.35	17.04	85.33
4.081	82.39	17.06	85.34
4.102	82.41	17.08	85.34
4.123	82.44	17.1	85.35
4.144	82.45	17.12	85.36
4.165	82.47	17.14	85.36
4.185	82.5	17.16	85.34
4.206	82.5	17.18	85.34
4.227	82.53	17.21	85.34
4.248	82.53	17.23	85.34
4.269	82.54	17.25	85.33
4.29	82.55	17.27	85.31
4.31	82.55	17.29	85.31
4.331	82.57	17.31	85.3
4.352	82.57	17.33	85.3
4.373	82.58	17.35	85.3
4.394	82.6	17.37	85.3
4.415	82.61	17.39	85.32
4.435	82.61	17.41	85.32



---

<u>Time (day)</u>	<u>Displacement (ft)</u>	<u>Time (day)</u>	<u>Displacement (ft)</u>
4.456	82.63	17.43	85.32
4.477	82.64	17.46	85.33
4.498	82.66	17.48	85.35
4.519	82.67	17.5	85.36
4.54	82.7	17.52	85.38
4.56	82.72	17.54	85.39
4.581	82.75	17.56	85.41
4.602	82.76	17.58	85.42
4.623	82.79	17.6	85.42
4.644	82.81	17.62	85.44
4.665	82.82	17.64	85.45
4.685	82.85	17.66	85.45
4.706	82.85	17.68	85.44
4.727	82.86	17.71	85.45
4.748	82.86	17.73	85.45
4.769	82.88	17.75	85.45
4.79	82.88	17.77	85.44
4.81	82.88	17.79	85.41
4.831	82.89	17.81	85.42
4.852	82.89	17.83	85.41
4.873	82.91	17.85	85.41
4.894	82.91	17.87	85.41
4.915	82.94	17.89	85.4
4.935	82.94	17.91	85.4
4.956	82.95	17.93	85.4
4.977	82.97	17.96	85.4
4.998	82.98	17.98	85.41
5.019	83.	18.	85.41
5.04	83.	18.02	85.41
5.06	83.01	18.04	85.43
5.081	83.03	18.06	85.43
5.102	83.04	18.08	85.43
5.123	83.06	18.1	85.43
5.144	83.06	18.12	85.44
5.165	83.07	18.14	85.44
5.185	83.07	18.16	85.44
5.206	83.09	18.18	85.44
5.227	83.09	18.21	85.43
5.248	83.09	18.23	85.42
5.269	83.1	18.25	85.42
5.29	83.1	18.27	85.4
5.31	83.1	18.29	85.39
5.331	83.1	18.31	85.39
5.352	83.1	18.33	85.36
5.373	83.12	18.35	85.35
5.394	83.12	18.37	85.35
5.415	83.13	18.39	85.35
5.435	83.13	18.41	85.35
5.456	83.12	18.43	85.33
5.477	83.14	18.46	85.33
5.498	83.15	18.48	85.33
5.519	83.16	18.5	85.33
5.54	83.18	18.52	85.35

---

<u>Time (day)</u>	<u>Displacement (ft)</u>	<u>Time (day)</u>	<u>Displacement (ft)</u>
5.56	83.19	18.54	85.36
5.581	83.21	18.56	85.38
5.602	83.21	18.58	85.38
5.623	83.22	18.6	85.38
5.644	83.24	18.62	85.39
5.665	83.25	18.64	85.39
5.685	83.27	18.66	85.41
5.706	83.27	18.68	85.41
5.727	83.27	18.71	85.4
5.748	83.28	18.73	85.4
5.769	83.3	18.75	85.38
5.79	83.31	18.77	85.37
5.81	83.31	18.79	85.35
5.831	83.31	18.81	85.34
5.852	83.31	18.83	85.34
5.873	83.33	18.85	85.33
5.894	83.33	18.87	85.31
5.915	83.34	18.89	85.31
5.935	83.34	18.91	85.3
5.956	83.36	18.93	85.3
5.977	83.39	18.96	85.3
5.998	83.4	18.98	85.3
6.019	83.42	19.	85.3
6.04	83.43	19.02	85.3
6.06	83.43	19.04	85.32
6.081	83.45	19.06	85.32
6.102	83.46	19.08	85.32
6.123	83.46	19.1	85.32
6.144	83.48	19.12	85.32
6.165	83.48	19.14	85.32
6.185	83.49	19.16	85.32
6.206	83.49	19.18	85.32
6.227	83.51	19.21	85.32
6.248	83.51	19.23	85.3
6.269	83.51	19.25	85.3
6.29	83.51	19.27	85.29
6.31	83.51	19.29	85.29
6.331	83.51	19.31	85.26
6.352	83.51	19.33	85.26
6.373	83.51	19.35	85.25
6.394	83.51	19.37	85.25
6.415	83.52	19.39	85.23
6.435	83.51	19.41	85.23
6.456	83.52	19.43	85.23
6.477	83.53	19.46	85.24
6.498	83.53	19.48	85.22
6.519	83.54	19.5	85.24
6.54	83.54	19.52	85.24
6.56	83.56	19.54	85.24
6.581	83.57	19.56	85.25
6.602	83.57	19.58	85.25
6.623	83.58	19.6	85.25
6.644	83.58	19.62	85.27

---

<u>Time (day)</u>	<u>Displacement (ft)</u>	<u>Time (day)</u>	<u>Displacement (ft)</u>
6.665	83.6	19.64	85.27
6.685	83.61	19.66	85.27
6.706	83.63	19.68	85.27
6.727	83.63	19.71	85.27
6.748	83.63	19.73	85.25
6.769	83.63	19.75	85.25
6.79	83.63	19.77	85.26
6.81	83.63	19.79	85.24
6.831	83.63	19.81	85.23
6.852	83.63	19.83	85.23
6.873	83.63	19.85	85.21
6.894	83.65	19.87	85.21
6.915	83.66	19.89	85.22
6.935	83.68	19.91	85.2
6.956	83.69	19.93	85.2
6.977	83.69	19.96	85.22
6.998	83.72	19.98	85.22
7.019	83.73	20.	85.22
7.04	83.75	20.02	85.23
7.06	83.75	20.04	85.25
7.081	83.77	20.06	85.25
7.102	83.81	20.08	85.26
7.123	83.79	20.1	85.28
7.144	83.81	20.12	85.29
7.165	83.81	20.14	85.29
7.185	83.82	20.16	85.29
7.206	83.83	20.18	85.32
7.227	83.84	20.21	85.33
7.248	83.84	20.23	85.33
7.269	83.84	20.25	85.32
7.29	83.84	20.27	85.31
7.31	83.86	20.29	85.31
7.331	83.86	20.31	85.31
7.352	83.86	20.33	85.29
7.373	83.86	20.35	85.31
7.394	83.84	20.37	85.3
7.415	83.86	20.39	85.3
7.435	83.84	20.41	85.3
7.456	83.84	20.43	85.3
7.477	83.84	20.46	85.3
7.498	83.84	20.48	85.3
7.519	83.86	20.5	85.3
7.54	83.86	20.52	85.3
7.56	83.87	20.54	85.3
7.581	83.89	20.56	85.31
7.602	83.89	20.58	85.33
7.623	83.9	20.6	85.33
7.644	83.9	20.62	85.33
7.665	83.9	20.64	85.33
7.685	83.9	20.66	85.33
7.706	83.9	20.68	85.33
7.727	83.92	20.71	85.33
7.748	83.91	20.73	85.33

<u>Time (day)</u>	<u>Displacement (ft)</u>	<u>Time (day)</u>	<u>Displacement (ft)</u>
7.769	83.92	20.75	85.33
7.79	83.91	20.77	85.33
7.81	83.91	20.79	85.33
7.831	83.91	20.81	85.32
7.852	83.91	20.83	85.3
7.873	83.91	20.85	85.3
7.894	83.91	20.87	85.29
7.915	83.89	20.89	85.29
7.935	83.89	20.91	85.29
7.956	83.92	20.93	85.28
7.977	83.92	20.96	85.28
7.998	83.92	20.98	85.28
8.019	83.94	21.	85.28
8.04	83.94	21.02	85.29
8.06	83.94	21.04	85.28
8.081	83.94	21.06	85.28
8.102	83.94	21.08	85.29
8.123	83.94	21.1	85.29
8.144	83.94	21.12	85.29
8.165	83.94	21.14	85.29
8.185	83.96	21.16	85.31
8.206	83.97	21.18	85.31
8.227	83.97	21.21	85.31
8.248	83.97	21.23	85.31
8.269	83.97	21.25	85.31
8.29	83.96	21.27	85.31
8.31	83.97	21.29	85.3
8.331	83.97	21.31	85.3
8.352	83.97	21.33	85.3
8.373	83.97	21.35	85.3
8.394	83.97	21.37	85.3
8.415	83.97	21.39	85.28
8.435	83.97	21.41	85.28
8.456	83.97	21.43	85.27
8.477	83.97	21.46	85.27
8.498	83.97	21.48	85.25
8.519	83.98	21.5	85.26
8.54	83.99	21.52	85.26
8.56	83.99	21.54	85.27
8.581	83.98	21.56	85.26
8.602	83.98	21.58	85.26
8.623	83.98	21.6	85.26
8.644	83.99	21.62	85.26
8.665	83.99	21.64	85.26
8.685	83.99	21.66	85.26
8.706	84.01	21.68	85.26
8.727	84.01	21.71	85.26
8.748	84.01	21.73	85.26
8.769	84.01	21.75	85.25
8.79	84.01	21.77	85.25
8.81	84.	21.79	85.25
8.831	84.	21.81	85.23
8.852	84.02	21.83	85.22

---

<u>Time (day)</u>	<u>Displacement (ft)</u>	<u>Time (day)</u>	<u>Displacement (ft)</u>
8.873	84.03	21.85	85.22
8.894	84.03	21.87	85.22
8.915	84.03	21.89	85.22
8.935	84.04	21.91	85.22
8.956	84.04	21.93	85.21
8.977	84.06	21.96	85.21
8.998	84.06	21.98	85.21
9.019	84.06	22.	85.21
9.04	84.07	22.02	85.21
9.06	84.07	22.04	85.21
9.081	84.08	22.06	85.21
9.102	84.08	22.08	85.21
9.123	84.1	22.1	85.21
9.144	84.09	22.12	85.21
9.165	84.09	22.14	85.21
9.185	84.1	22.16	85.24
9.206	84.1	22.18	85.24
9.227	84.09	22.21	85.24
9.248	84.1	22.23	85.24
9.269	84.1	22.25	85.25
9.29	84.12	22.27	85.24
9.31	84.13	22.29	85.25
9.331	84.13	22.31	85.24
9.352	84.13	22.33	85.24
9.373	84.13	22.35	85.24
9.394	84.13	22.37	85.24
9.415	84.14	22.39	85.24
9.435	84.14	22.41	85.24
9.456	84.15	22.43	85.24
9.477	84.15	22.46	85.24
9.498	84.16	22.48	85.24
9.519	84.16	22.5	85.24
9.54	84.18	22.52	85.24
9.56	84.19	22.54	85.24
9.581	84.18	22.56	85.26
9.602	84.19	22.58	85.26
9.623	84.19	22.6	85.26
9.644	84.21	22.62	85.26
9.665	84.21	22.64	85.26
9.685	84.21	22.66	85.28
9.706	84.21	22.68	85.26
9.727	84.21	22.71	85.28
9.748	84.23	22.73	85.26
9.769	84.21	22.75	85.28
9.79	84.21	22.77	85.28
9.81	84.21	22.79	85.26
9.831	84.21	22.81	85.26
9.852	84.23	22.83	85.28
9.873	84.23	22.85	85.28
9.894	84.24	22.87	85.28
9.915	84.24	22.89	85.28
9.935	84.24	22.91	85.28
9.956	84.26	22.93	85.28

---

<u>Time (day)</u>	<u>Displacement (ft)</u>	<u>Time (day)</u>	<u>Displacement (ft)</u>
9.977	84.26	22.96	85.28
10.	84.29	22.98	85.28
10.02	84.29	23.	85.28
10.04	84.29	23.02	85.32
10.06	84.29	23.04	85.31
10.08	84.29	23.06	85.31
10.1	84.29	23.08	85.31
10.12	84.29	23.1	85.31
10.14	84.31	23.12	85.31
10.16	84.29	23.14	85.33
10.19	84.31	23.16	85.31
10.21	84.31	23.18	85.31
10.23	84.31	23.21	85.33
10.25	84.32	23.23	85.33
10.27	84.31	23.25	85.33
10.29	84.31	23.27	85.33
10.31	84.32	23.29	85.33
10.33	84.32	23.31	85.33
10.35	84.34	23.33	85.33
10.37	84.34	23.35	85.34
10.39	84.35	23.37	85.34
10.41	84.35	23.39	85.34
10.44	84.37	23.41	85.36
10.46	84.37	23.43	85.36
10.48	84.37	23.46	85.36
10.5	84.38	23.48	85.36
10.52	84.4	23.5	85.36
10.54	84.4	23.52	85.36
10.56	84.4	23.54	85.38
10.58	84.4	23.56	85.38
10.6	84.4	23.58	85.36
10.62	84.4	23.6	85.36
10.64	84.4	23.62	85.36
10.66	84.4	23.64	85.36
10.69	84.4	23.66	85.36
10.71	84.4	23.68	85.36
10.73	84.4	23.71	85.35
10.75	84.4	23.73	85.36
10.77	84.4	23.75	85.35
10.79	84.42	23.77	85.35
10.81	84.43	23.79	85.35
10.83	84.42	23.81	85.35
10.85	84.43	23.83	85.35
10.87	84.43	23.85	85.35
10.89	84.43	23.87	85.35
10.91	84.45	23.89	85.37
10.94	84.46	23.91	85.38
10.96	84.46	23.93	85.38
10.98	84.46	23.96	85.38
11.	84.48	23.98	85.37
11.02	84.48	24.	85.37
11.04	84.49	24.02	85.37
11.06	84.49	24.04	85.37

<u>Time (day)</u>	<u>Displacement (ft)</u>	<u>Time (day)</u>	<u>Displacement (ft)</u>
11.08	84.48	24.06	85.37
11.1	84.48	24.08	85.37
11.12	84.48	24.1	85.37
11.14	84.48	24.12	85.37
11.16	84.48	24.14	85.39
11.19	84.47	24.16	85.37
11.21	84.47	24.18	85.37
11.23	84.47	24.21	85.37
11.25	84.47	24.23	85.37
11.27	84.47	24.25	85.36
11.29	84.48	24.27	85.34
11.31	84.48	24.29	85.34
11.33	84.48	24.31	85.35
11.35	84.5	24.33	85.36
11.37	84.5	24.35	85.36
11.39	84.51	24.37	85.36
11.41	84.5	24.39	85.38
11.44	84.5	24.41	85.38
11.46	84.51	24.43	85.38
11.48	84.51	24.46	85.38
11.5	84.53	24.48	85.36
11.52	84.53	24.5	85.36
11.54	84.54	24.52	85.36
11.56	84.54	24.54	85.36
11.58	84.54	24.56	85.36
11.6	84.54	24.58	85.36
11.62	84.55	24.6	85.37
11.64	84.55	24.62	85.37
11.66	84.55	24.64	85.35
11.69	84.55	24.66	85.35
11.71	84.53	24.68	85.35
11.73	84.53	24.71	85.32
11.75	84.53	24.73	85.32
11.77	84.53	24.75	85.31
11.79	84.53	24.77	85.3
11.81	84.53	24.79	85.3
11.83	84.53	24.81	85.3
11.85	84.55	24.83	85.28
11.87	84.55	24.85	85.28
11.89	84.55	24.87	85.28
11.91	84.56	24.89	85.28
11.94	84.55	24.91	85.31
11.96	84.56	24.93	85.3
11.98	84.58	24.96	85.3
12.	84.59	24.98	85.3
12.02	84.58	25.	85.3
12.04	84.58	25.02	85.3
12.06	84.59	25.04	85.3
12.08	84.58	25.06	85.3
12.1	84.58	25.08	85.29
12.12	84.57	25.1	85.29
12.14	84.55	25.12	85.29
12.16	84.55	25.14	85.29

<u>Time (day)</u>	<u>Displacement (ft)</u>	<u>Time (day)</u>	<u>Displacement (ft)</u>
12.19	84.54	25.16	85.27
12.21	84.53	25.18	85.27
12.23	84.51	25.21	85.26
12.25	84.51	25.23	85.26
12.27	84.51	25.25	85.26
12.29	84.51	25.27	85.26
12.31	84.51	25.29	85.26
12.33	84.51	25.31	85.26
12.35	84.51	25.33	85.26
12.37	84.51	25.35	85.28
12.39	84.51	25.37	85.29
12.41	84.53	25.39	85.28
12.44	84.52	25.41	85.28
12.46	84.52	25.43	85.28
12.48	84.53	25.46	85.29
12.5	84.53	25.48	85.28
12.52	84.53	25.5	85.29
12.54	84.55	25.52	85.29
12.56	84.55	25.54	85.29
12.58	84.53	25.56	85.3
12.6	84.55	25.58	85.3
12.62	84.53	25.6	85.3
12.64	84.53	25.62	85.3
12.66	84.52	25.64	85.3
12.69	84.52	25.66	85.3
12.71	84.52	25.68	85.3
12.73	84.51	25.71	85.28
12.75	84.51	25.73	85.3
12.77	84.51	25.75	85.3
12.79	84.51	25.77	85.28
12.81	84.51	25.79	85.28
12.83	84.51	25.81	85.3
12.85	84.51	25.83	85.3
12.87	84.51	25.85	85.3
12.89	84.51	25.87	85.3
12.91	84.52	25.89	85.31
12.94	84.52	25.91	85.33
12.96	84.52	25.93	85.36
12.98	84.54	25.96	85.37

SOLUTION

Pumping Test  
 Aquifer Model: Unconfined  
 Solution Method: Neuman

VISUAL ESTIMATION RESULTS

Estimated Parameters

<u>Parameter</u>	<u>Estimate</u>	
T	5176.4	ft <sup>2</sup> /day
S	0.01046	



Sy	0.4156
β	0.001

$K = T/b = 1.035 \text{ ft/day (0.0003652 cm/sec)}$

$Ss = S/b = 2.093E-6 \text{ 1/ft}$

## **ATTACHMENT 4**

**Analyses of Aquifer Test Data for  
PM-4 to Determine Horizontal ( $K_h$ ) and  
Vertical Hydraulic Conductivities ( $K_v$ )**

---

This page intentionally left blank.

## Executive Summary

The purpose of Attachment 4 is to reanalyze the aquifer test data of PM-4 using multiple observation wells and determine especially the values of horizontal hydraulic conductivity ( $K_h$ ) and vertical hydraulic conductivity ( $K_v$ ). The used data are associated with a report entitled “*Analyses of the PM-2 Aquifer Test Using Multiple Observation Wells, LA-14252-MS*” published in January 2006 authored by Stephen G. McLin.

The results for the transient drawdown data analysis are given in Table 2 which shows that there is a total of seven set of values determined from the Neuman (1974, 1975) method. The last line shows the  $K_h$  value determined from the steady-state drawdown value at the pumped well PM-4 using the Thiem (1906) well discharge formula under confined aquifer conditions. From the values in Table 2, the conclusions drawn are given as follows:

1. Based on the Neuman method, the values of  $K_h$  vary between 0.3 *ft/d* and 1.5 *ft/d*. The average of the rest of seven values (1.2, 0.8, 0.3, 1.1, 1.0, 1.5, and 0.7 *ft/d*) is  $K_{h-avg} = 0.9$  *ft/d*.
2. The last line of Table 2 includes  $K_h = 2.3$  *ft/d* value determined from the steady-state drawdown at the pumped well PM-4 using Thiem (1906) well discharge formula under confined aquifer conditions (see Section 6.2 for its determination method).
3. The average of the six  $a = K_v/K_h$  values (0.016, 0.225, 0.012, 0.022, 0.040, and 0.016) is  $a_{avg} = K_{v-avg}/K_{h-avg} = 0.055$ . Therefore,  $K_{v-avg} = aK_h = 0.05$  *ft/d*.
4. The storage coefficient ( $S$ ) values range from  $2.91E - 04$  to  $7.17E - 04$ . According to the literature, storage coefficients generally vary between 0.00005 and 0.005 (e.g., Freeze and Cherry, 1979, p. 60).
5. The specific yield ( $S_y$ ) values in Table 2 are not reliable. Potential reasons may be (a) the screen intervals are significantly below the water table; (c) the pump test period was not long enough; and (c) the observation wells are significantly far away from the pumped well (4,463 *ft* to 5,508 *ft*).

Comparisons are of the  $K_h$  and  $K_{h-Neptune}$  are shown in Table 3. As can be seen from Table 3,  $K_{h-Neptune}/K_h$  ratio varies between 3.447 and 9.744. These values mean that  $K_{h-Neptune}$  values are higher approximately between one-half order and one order of magnitudes than the  $K_h$  values of the drawdown analysis.

## Attachment 4 Contents

1.	Purpose.....	1
2.	Aquifer Test Procedure .....	1
3.	Wells Geometry and Initial Water Levels .....	1
4.	Measured Well Drawdowns and Their Interpretations .....	1
4.1	Measured Steady-State Drawdown at the PM-4 Pumped Well.....	1
4.2	Measured Transient Drawdowns at the Observation Wells .....	2
5.	Drawdowns Data Analysis Methods.....	2
5.1	Pumped Well Steady-State Drawdown Data Analysis Method .....	2
5.2	Observation Wells Transient Drawdown Data Analysis Methods .....	3
6.	Results and Discussion.....	3
6.1	Transient Drawdown Data at the Observation Wells and PM-2 Recovery Analyses Results.....	3
6.2	Horizontal Hydraulic Conductivity (Kh) Value Determined from the Steady-State Drawdown Value at the PM-4 Pumped Well .....	4

## Figures

- Figure 1. PM-4 pumped well drawdown versus time.
- Figure 2. PM-2 observation well drawdown versus time.
- Figure 3. PM-5 observation well drawdown versus time.
- Figure 4. R-20 S1 observation well drawdowns versus time.
- Figure 5. R-20 S2 observation well drawdowns versus time.
- Figure 6. R-20 S3 observation well drawdowns versus time.
- Figure 7. R-32 S1 observation well drawdowns versus time.
- Figure 8. R-32 S2 observation well drawdowns versus time.
- Figure 9. R-32 S3 observation well drawdowns versus time.
- Figure 10. R-19 S4 observation well drawdowns versus time.
- Figure 11. R-19 S5 observation well drawdowns versus time.
- Figure 12. R-19 S6 observation well drawdowns versus time.
- Figure 13. R-19 S7 observation well drawdowns versus time.
- Figure 14. R-14 S1 observation well drawdowns versus time.
- Figure 15. R-14 S2 observation well drawdowns versus time.
- Figure 16. R-13 observation well drawdowns versus time.
- Figure 17. Well in a confined aquifer.

## Tables

Table 1. Wells geometry and initial water levels.

Table 2. PM-2 aquifer test data analysis results.

## Appendices

- Appendix A Determination of Horizontal Hydraulic Conductivity Using Thiem Well Discharge Formula for PM-2 Steady State Drawdown Value
- Appendix B AQTESOLV Output for PM-2 Drawdown Analysis
- Appendix C AQTESOLV Output for PM-5 Drawdown Analysis
- Appendix D AQTESOLV Output for R-20 S3 Drawdown Analysis
- Appendix E AQTESOLV Output for PM-4 Recovery Analysis
- Appendix F AQTESOLV Output for PM-2 Recovery Analysis
- Appendix G AQTESOLV Output for PM-5 Recovery Analysis
- Appendix H AQTESOLV Output for R-20 S3 Recovery Analysis

## 1. Purpose

The purpose of Attachment 4 is to analyze the aquifer test data of PM-4 using multiple observation wells. The test was performed in February and March 2005 and described in a 2006 report entitled “*Analyses of the PM-4 Aquifer Test Using Multiple Observation Wells, LA-14252-MS*” authored by Stephen G. McLin.

## 2. Aquifer Test Procedure

The purpose and scope of the aquifer test is described as follows (McLin, 2006, pp. 2):

*“A long-term aquifer test was conducted at municipal water supply well PM-4 during February and March of 2005. This test consisted of a 21-day pumping interval followed by a 21-day recovery period. Both drawdown and recovery data were collected at PM-4 and numerous observation wells. The purpose of this aquifer test was the experimental determination of regional aquifer parameters that characterize the saturated porous media below Pajarito Plateau. This test consisted of pumping PM-4 at a constant discharge rate and observing water level changes in both the pumping and surrounding observation wells.”*

McLin (2006, pp. 6-7) states that for the PM-4 aquifer test, usable drawdown data were recorded in wells PM-4, PM-2, PM-5, R-20, and R-32. In addition, small drawdown values were also recorded in wells R-15, R-13, R-14, R-19, and TW-8.

## 3. Wells Geometry and Initial Water Levels

The wells geometry and initial water levels are given in Table 1. PM-4 was the pumped well with 1,494 gpm extraction rate. The municipal wells PM-2 and PM-5 were used as observation wells. Also R-20 (with three screen intervals each), R-32 (with three screen intervals each), R-19 (with four screen intervals of each), R-14 (with two screen intervals of each), R-13, and R-15 were used as observation wells.

## 4. Measured Well Drawdowns and Their Interpretations

### 4.1 Measured Steady-State Drawdown at the PM-4 Pumped Well

The measured drawdown variation at the PM-4 pumped well is shown in Figure 1, which shows that the equilibrium drawdown at the well is  $s_w = 70 \text{ ft}$ . As shown in Table 1, the initial head at PM-4 was 1,082.4 ft bgs (below the ground surface). The top elevation of the screen interval is 1,260 ft bgs. Therefore, the distance between the water level and the top elevation of the screen interval is 177.6 ft. This means that the screen interval does not interfere with the with the water level under extraction condition because  $s_w = 70 \text{ ft} < 177.6 \text{ ft}$ . As shown in Figure 1, after 21 d extraction of water was stopped and after approximately 40 d of elapsed time, the water level reached to the original level before extraction.

## 4.2 Measured Transient Drawdowns at the Observation Wells

The measured drawdown variation at the PM-2 observation well is shown in Figure 2. As shown in Table 1, the upper end of the screen interval of PM-2 is 130.4 ft bgs. Figure 2 indicates that during the 21-d extraction rate period, delayed yield has not occurred due to the potential reasons that (a) the screen interval is not close to the water table; (b) the aquifer is relatively less permeable around PM-4 well; and (c) PM-2 has significantly large distance (4,463 ft) from the pumped well PM-4.

The measured drawdown variation at the PM-5 observation well is shown in Figure 3. As shown in Table 1, the upper end of the screen interval of PM-5 is 195.3 ft bgs. Figure 3 indicates that during the 21-d extraction rate period, delayed yield has not occurred due to the potential reasons that (a) the screen interval is not close to the water table; (b) the aquifer is relatively less permeable around PM-4 well; and (c) PM-5 has significantly large distance (4,651 ft) from the pumped well PM-4.

Figure 4 and Figure 5 show the drawdown variation at R-20 S1 and R-20 S2, respectively, and they exhibit noise effects. Figure 6 shows the drawdown variation at R-20 S3 and does not exhibit noise effects. Likewise, Figure 6 indicates that during the 21-d extraction rate period, delayed yield has not occurred due to the potential reasons that (a) the screen interval is not close to the water table; (b) the aquifer is relatively less permeable around R-20 well; and (c) R-20 has significantly large distance (5,508 ft) from the pumped well PM-4.

Figures 7 through 16 show that the rest of drawdown versus time curves for R-32 S1, R-32 S2, R-32 S3, R-19 S4, R-19 S5, R-19 S6, R-19 S7, R14 S1, R-14 S2, and R-13, and all have noise effects.

## 5. Drawdowns Data Analysis Methods

### 5.1 Pumped Well Steady-State Drawdown Data Analysis Method

As mentioned in Section 4.1, the measured drawdown variation at the PM-4 pumped well is shown in Figure 1, which shows that the equilibrium drawdown at the well is  $s_w = 70 \text{ ft}$ . As shown in Table 1, the initial head at PM-4 was 1,082.4 ft bgs (below the ground surface). The top elevation of the screen interval is 1,260 ft bgs. Therefore, the distance between the water level and the top elevation of the screen interval is 177.6 ft. This means that the screen interval does not interfere with the with the water level under extraction condition because  $s_w = 70 \text{ ft} < 177.6 \text{ ft}$ . As shown in Figure 1, after 21 d extraction of water was stopped and after approximately 40 d of elapsed time, the water level reached to the original level before extraction.

With the steady-state drawdown at a pumped well, only the horizontal hydraulic conductivity ( $K_h$ ) can be determined. And the *Thiem well discharge formula* (Thiem, 1906) as given by Eq. (A-1) is the appropriate equation for the determination of the value of  $K_h$ . Further details about



the method as well as calculation details for the determination of  $K_h$  are given in Appendix A. The geometry of the Thiem formula is shown in Figure 17.

## 5.2 Observation Wells Transient Drawdown Data Analysis Methods

The drawdown and recovery data at the 6 observation wells and recovery data at the PM-4 pumped well have been analyzed with the Neuman type-curve method (Neuman, 1974, 1975) with Version 4.5 of the AQTESOLV software (HydroSOLVE, Inc., 2023).

The AQTESOLV output for the PM-2 drawdown data is given in Appendix B.

The AQTESOLV output for the PM-5 drawdown data is given in Appendix C.

The AQTESOLV outputs for the R-20 S3 is given Appendix D.

The AQTESOLV output for PM-4 recovery is given in Appendix E.

The AQTESOLV output for the PM-2 recovery is given in Appendix F.

The AQTESOLV output for the PM-5 recovery is given in Appendix G.

The AQTESOLV output for the R-20 S3 recovery is given in Appendix H.

## 6. Results and Discussion

### 6.1 Transient Drawdown Data at the Observation Wells and PM-2 Recovery Analyses Results

The results for the transient drawdown data analyses are given in Table 2 which shows that there is a total of seven set of values determined from the Neuman (1974, 1975) method. The last line shows the  $K_h$  value determined from the steady-state drawdown value at the pumped well PM-4 using the Thiem (1906) well discharge formula under confined aquifer conditions. From the values in Table 2, the conclusions drawn are given as follows:

1. Based on the Neuman method, the values of  $K_h$  vary between  $0.3 \text{ ft/d}$  and  $1.5 \text{ ft/d}$ . The average of the rest of seven values (1.2, 0.8, 0.3, 1.1, 1.0, 1.5, and  $0.7 \text{ ft/d}$ ) is  $K_{h-avg} = 0.9 \text{ ft/d}$ .
2. The last line of Table 2 includes  $K_h = 2.3 \text{ ft/d}$  value determined from the steady-state drawdown at the pumped well PM-4 using Thiem (1906) well discharge formula under confined aquifer conditions (see Section 6.2 for its determination method).
3. The average of the six  $a = K_v/K_h$  values (0.016, 0.225, 0.012, 0.022, 0.040, and 0.016) is  $a_{avg} = K_{v-avg}/K_{h-avg} = 0.055$ . Therefore,  $K_{v-avg} = aK_h = 0.05 \text{ ft/d}$ .
4. The storage coefficient ( $S$ ) values range from  $2.91E - 04$  to  $7.17E - 04$ . According to the literature, storage coefficients generally vary between 0.00005 and 0.005 (e.g., Freeze and Cherry, 1979, p. 60).

5. The specific yield ( $S_y$ ) values in Table 2 are not reliable. Potential reasons may be (a) the screen intervals are significantly below the water table; (b) the pump test period was not long enough; and (c) the observation wells are significantly far away from the pumped well (4,463 ft to 5,508 ft).

## 6.2 Horizontal Hydraulic Conductivity ( $K_h$ ) Value Determined from the Steady-State Drawdown Value at the PM-4 Pumped Well

The  $K_h$  value determined from the steady-state drawdown value of PM-4 is  $K_h = 2.3 \text{ ft/d}$  for which the calculation details are given in Appendix A.

## References

- Batu, V., *Aquifer Hydraulics: A Comprehensive Guide to Hydrogeologic Data Analysis*, John Wiley & Sons, Inc., New York, 727 pp., 1998.
- Batu, V., *Fluid Mechanics and Hydraulics: Illustrative Worked Examples of Surface and Subsurface Flows*, Taylor & Francis CRC Press, 1,240 pp., Boca Raton, Florida, 2024.
- Bear, J., *Hydraulics of Groundwater*, McGraw-Hill Inc., 569 pp., New York, 1979.
- Chertousov, M.D., *Hydraulics* (in Russian), Gosenergouzdat, 630 pp., Moscow, Russia, 1962.
- HydroSOLVE, Inc., AQTESOLV: Advanced Aquifer Test Analysis Software, v4.5., Reston, Virginia, 2023.
- Doherty, J., "Ground Water Model Calibration Using Pilot Points and Regularization," *Ground Water*, Vol. 41, No. 2, pp. 170-177, March-April, 2003.
- Freeze, R.A., And J.A. Cherry, *Groundwater*, Prentice-Hall, Inc., Englewood Cliffs, New Jersey, 604, pp., 1979.
- McLin, S.G., "Analysis of the PM-4 Aquifer Test Using Multiple Observation Wells, LA-14252-MS, Los Alamos National Laboratory," Los Alamos, New Mexico, January, 2006.
- Neptune and Company, Inc., Excel file: K and S LANL – For ITR – 5 – 6 – 24, May 6, 2024.
- Neuman, S.P., "Effect of Partial Penetration on Flow in Unconfined Aquifers Considering Delayed Gravity Response," *Water Resources Research*, Vol. 10, No.2, pp. 303-312, April, 1974.
- Neuman, S.P., "Analysis of Pumping Test Data From Anisotropic Unconfined Aquifers Considering Delayed Gravity Response," *Water Resources Research*, Vol. 11, No. 2, pp. 329-342, April, 1975.
- Thiem, G., *Hydrologische Methoden* (in German), J.M. Gebhardt, Leipzig, Germany, 56 pp., 1906.

## Figures

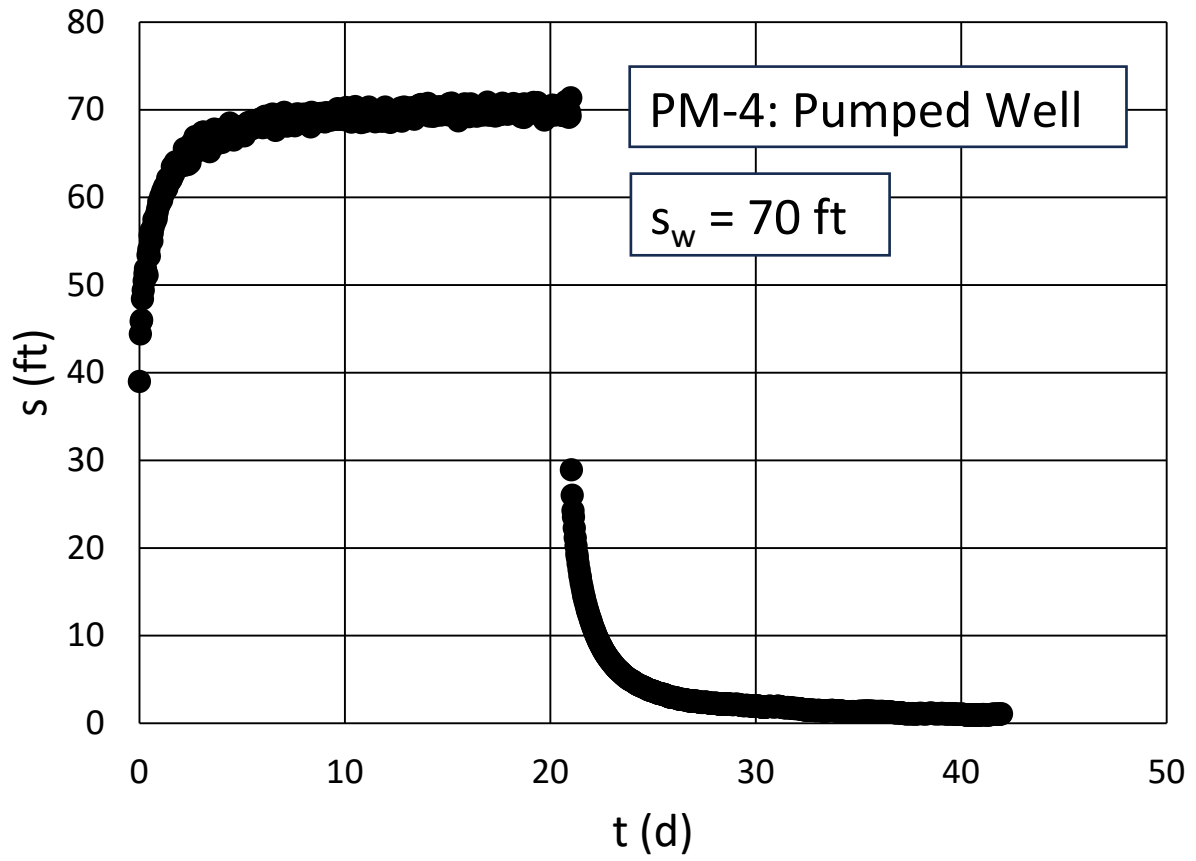


Figure 1. PM-4 pumped well drawdown versus time.

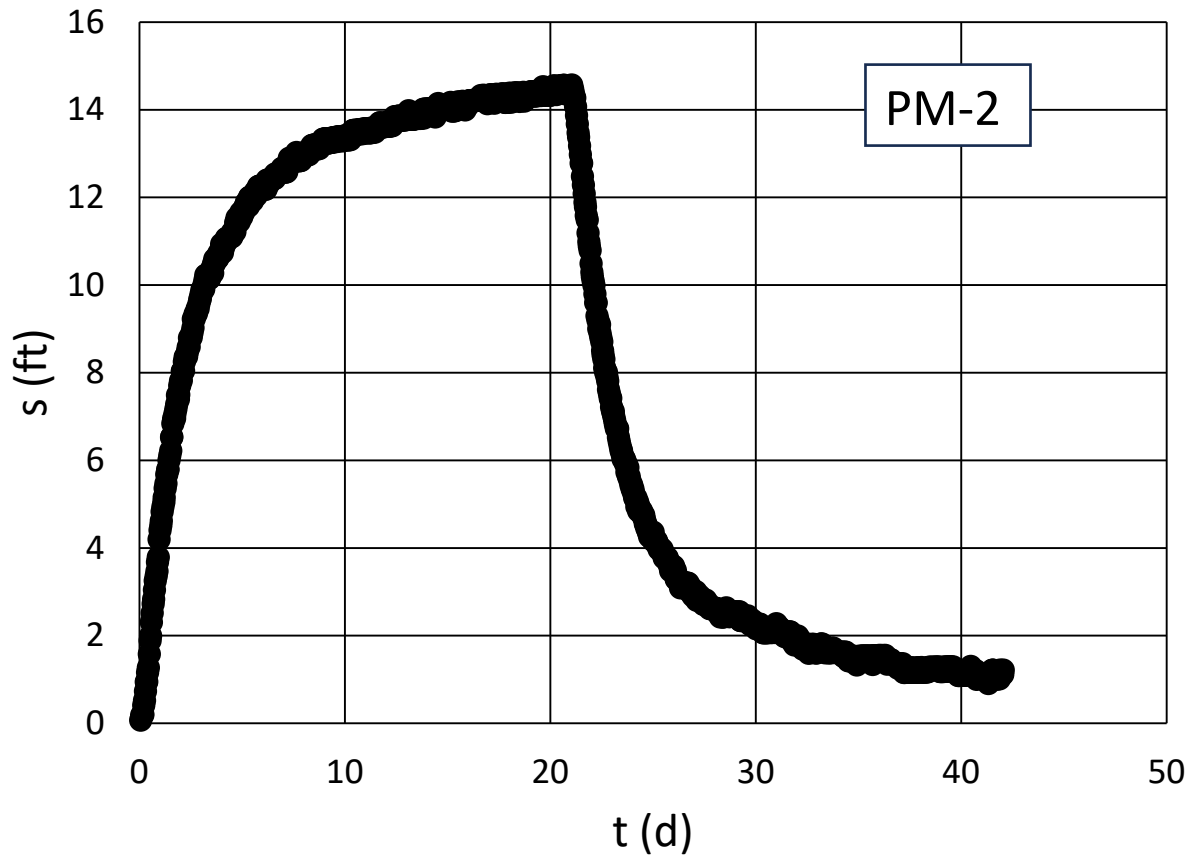


Figure 2. PM-2 observation well drawdown versus time.

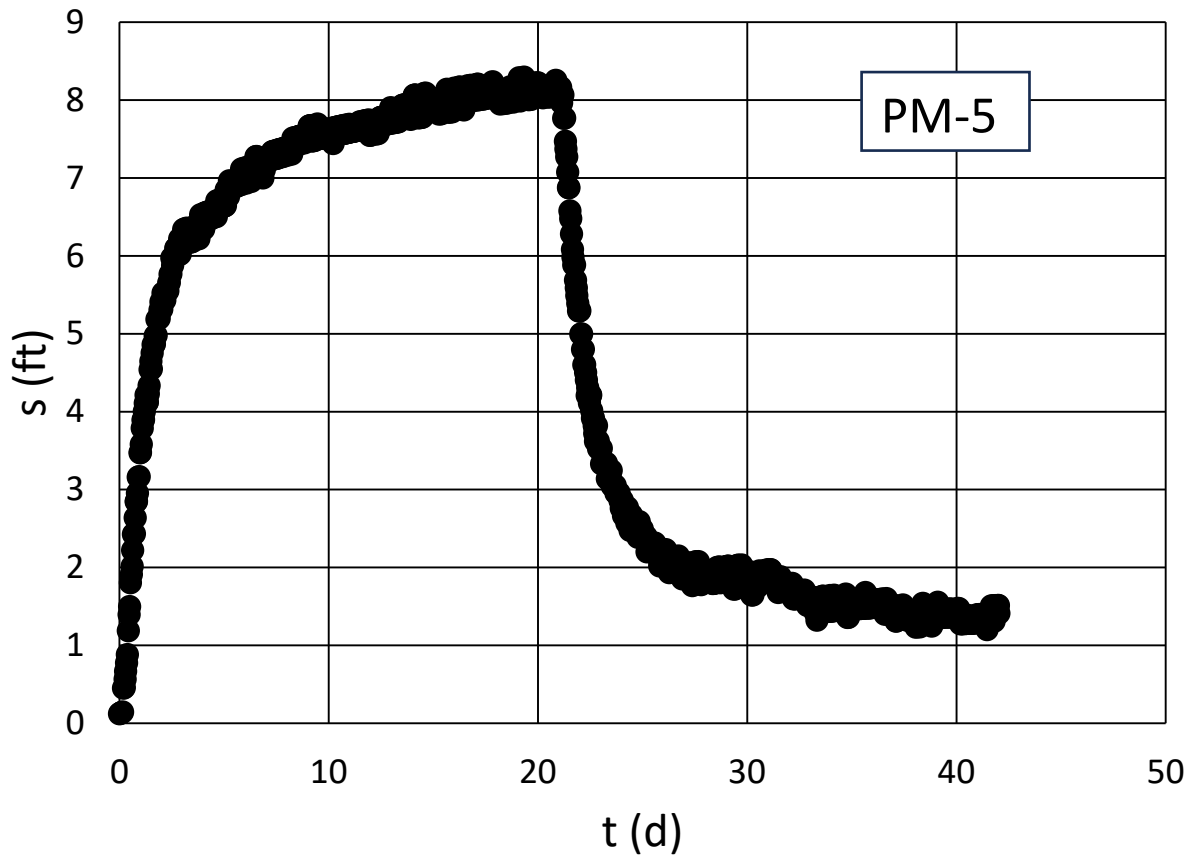


Figure 3. PM-5 observation well drawdown versus time.

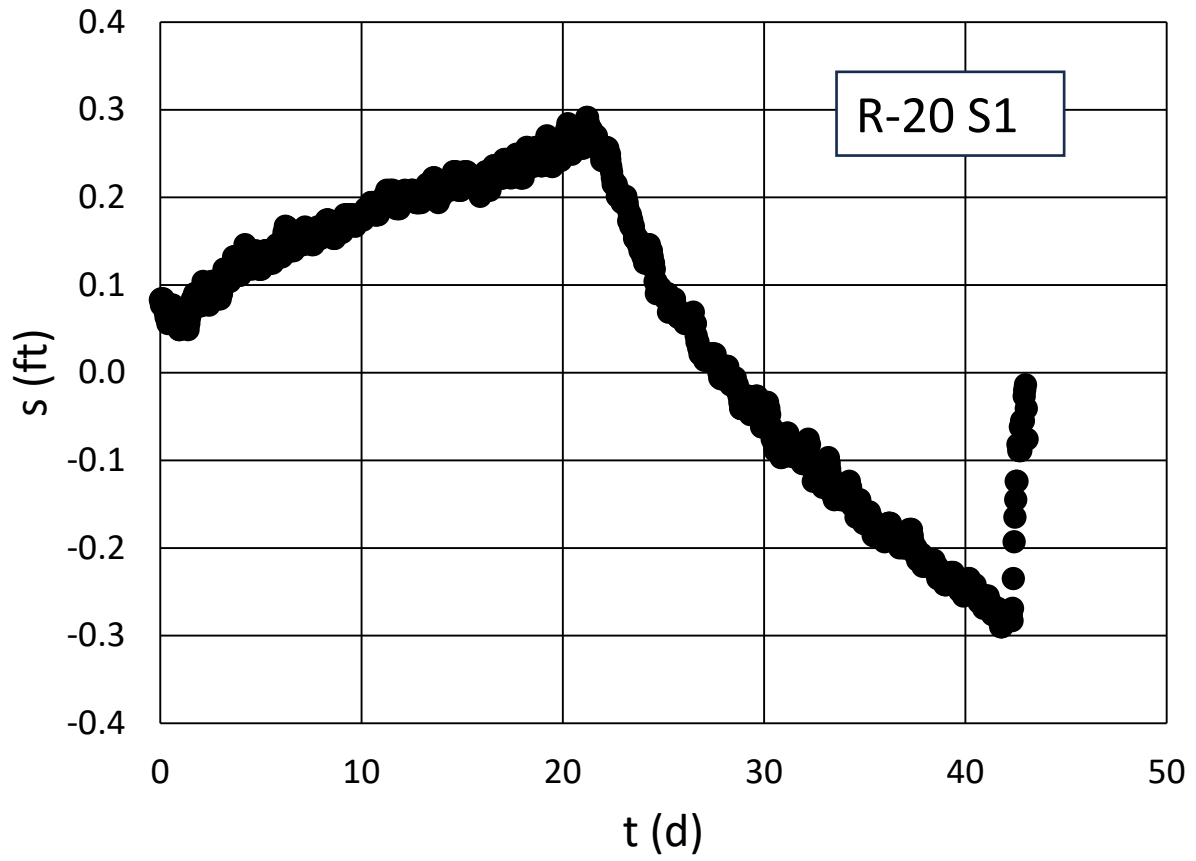


Figure 4. R-20 S1 observation well drawdowns versus time.

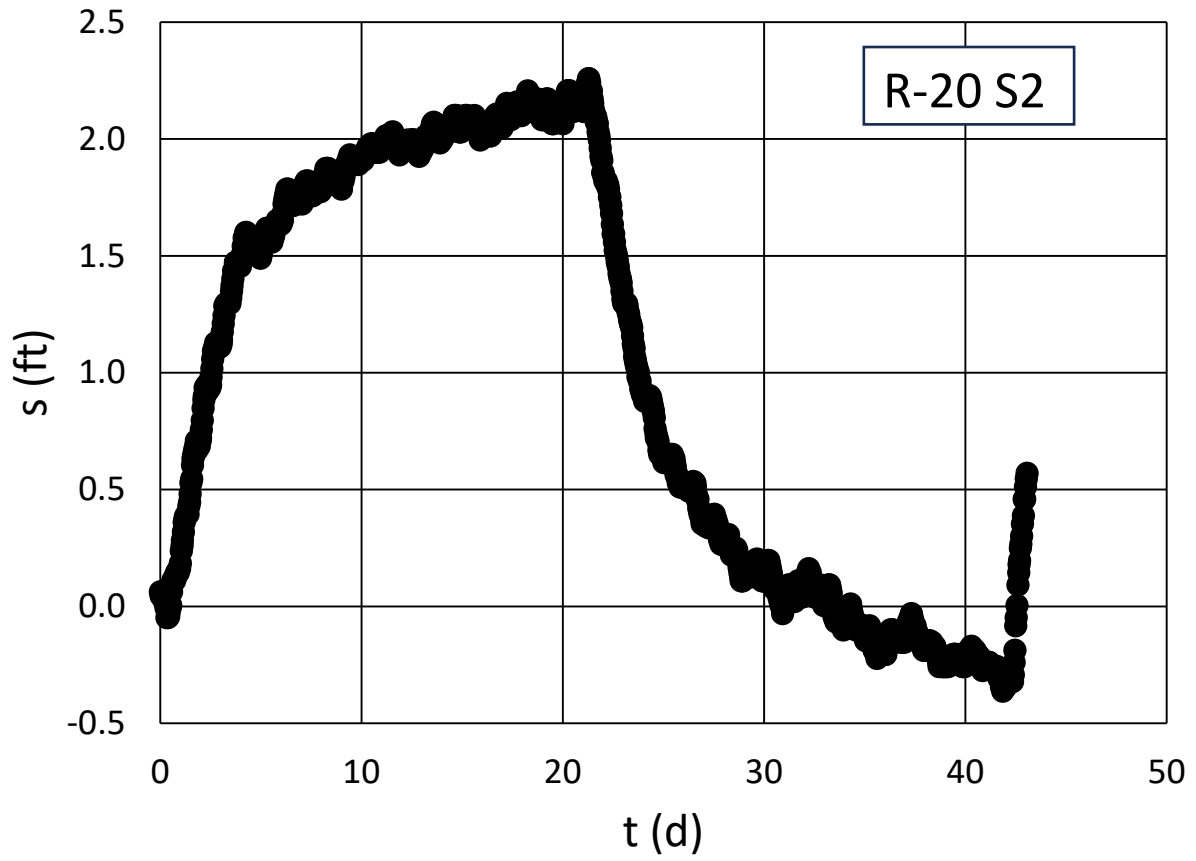


Figure 5. R-20 S2 observation well drawdowns versus time.



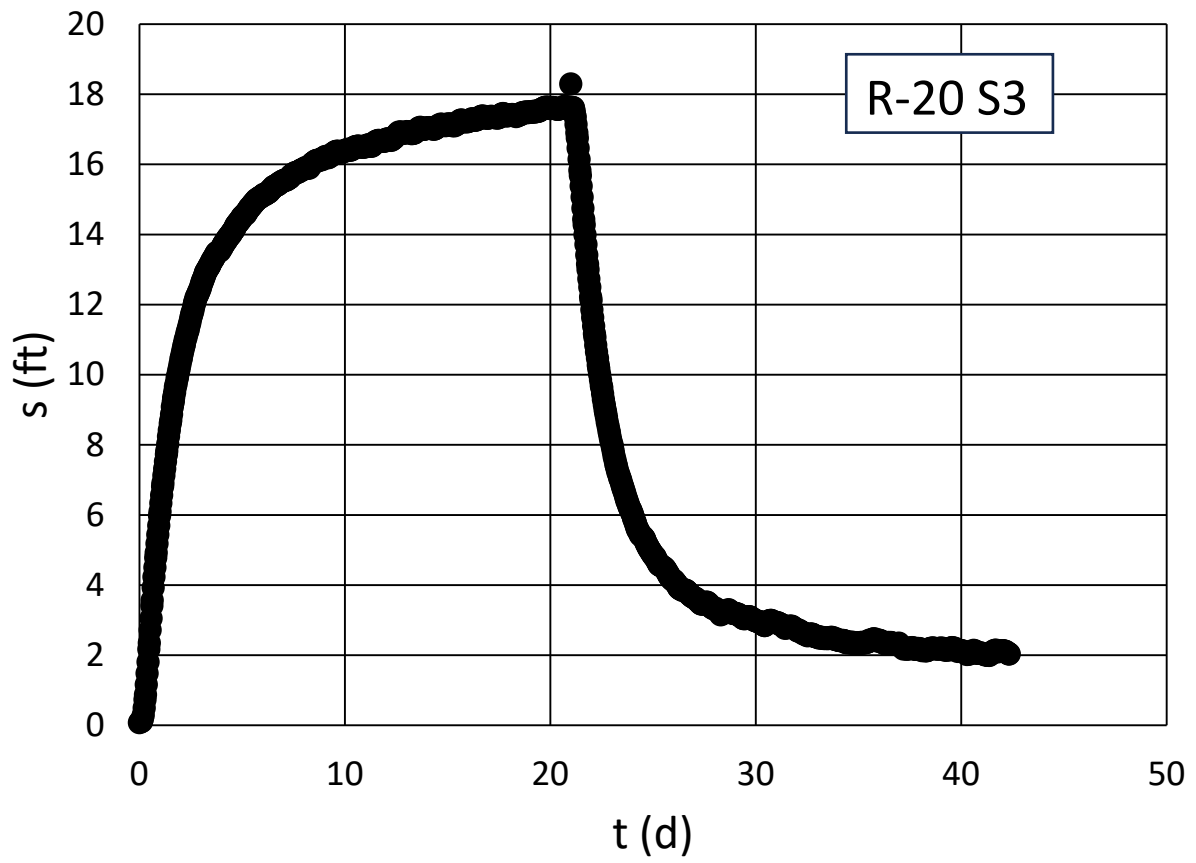


Figure 6. R-20 S3 observation well drawdowns versus time.

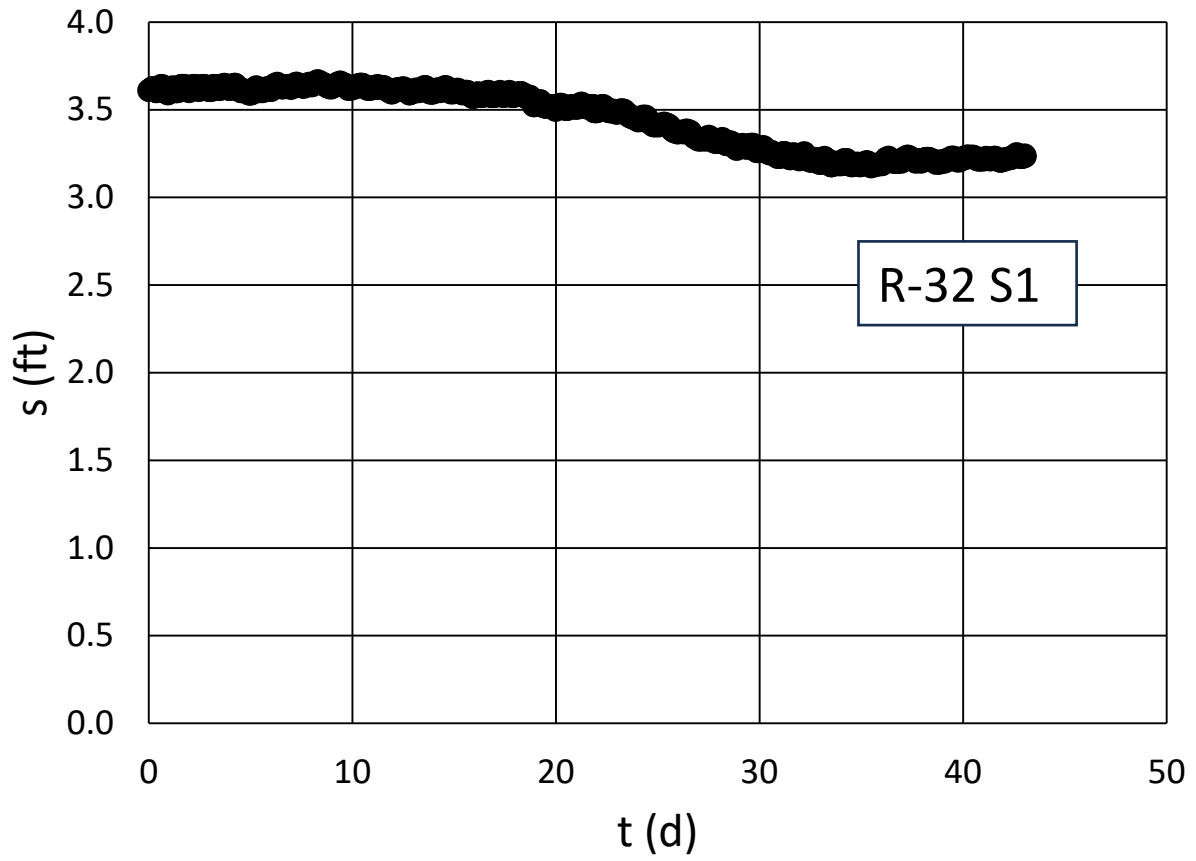


Figure 7. R-32 S1 observation well drawdowns versus time.

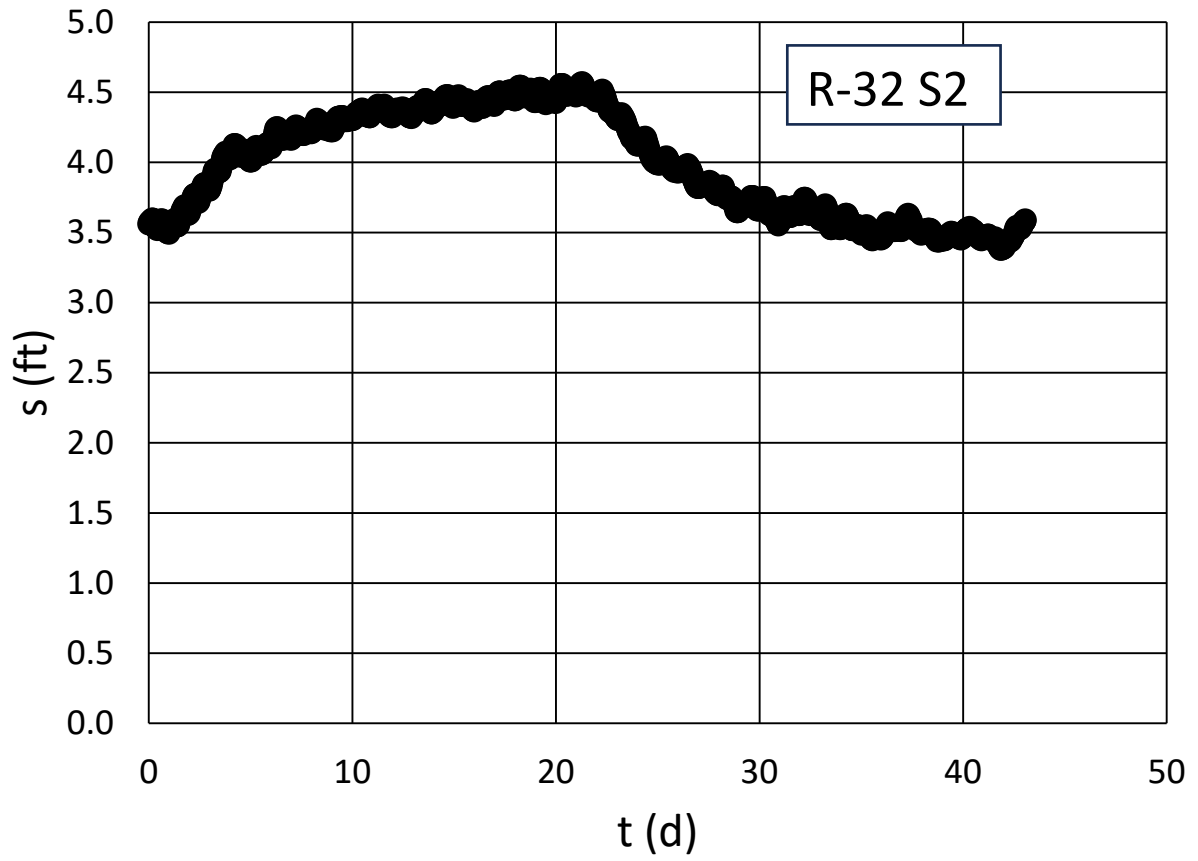


Figure 8. R-32 S2 observation well drawdowns versus time.

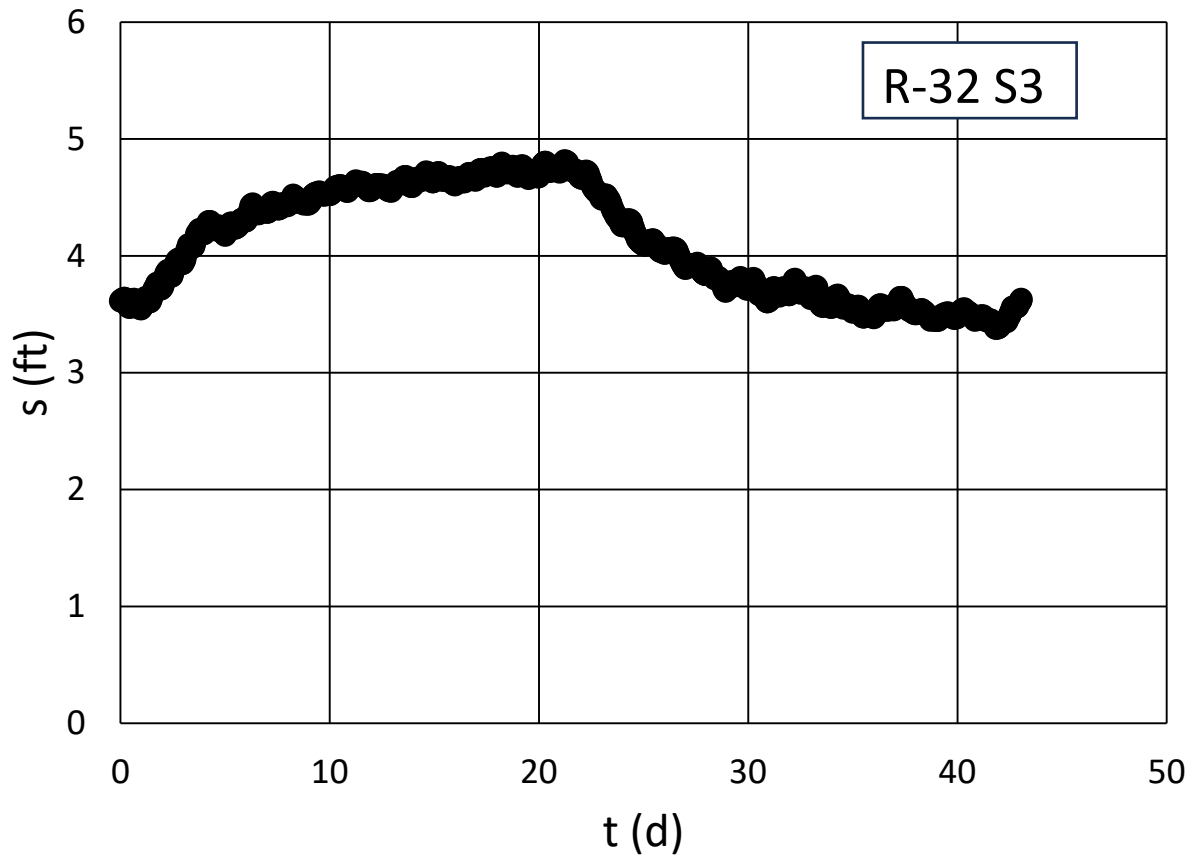


Figure 9. R-32 S3 observation well drawdowns versus time.

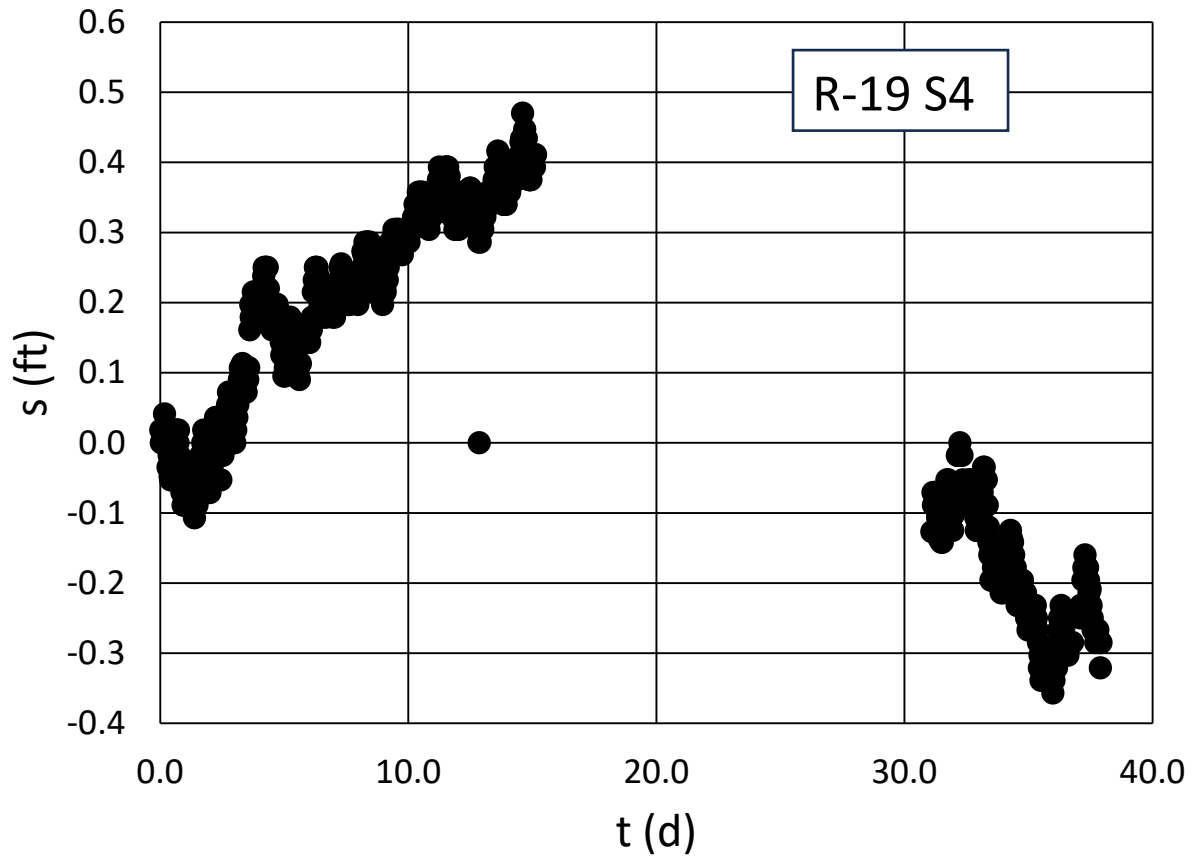


Figure 10. R-19 S4 observation well drawdowns versus time.

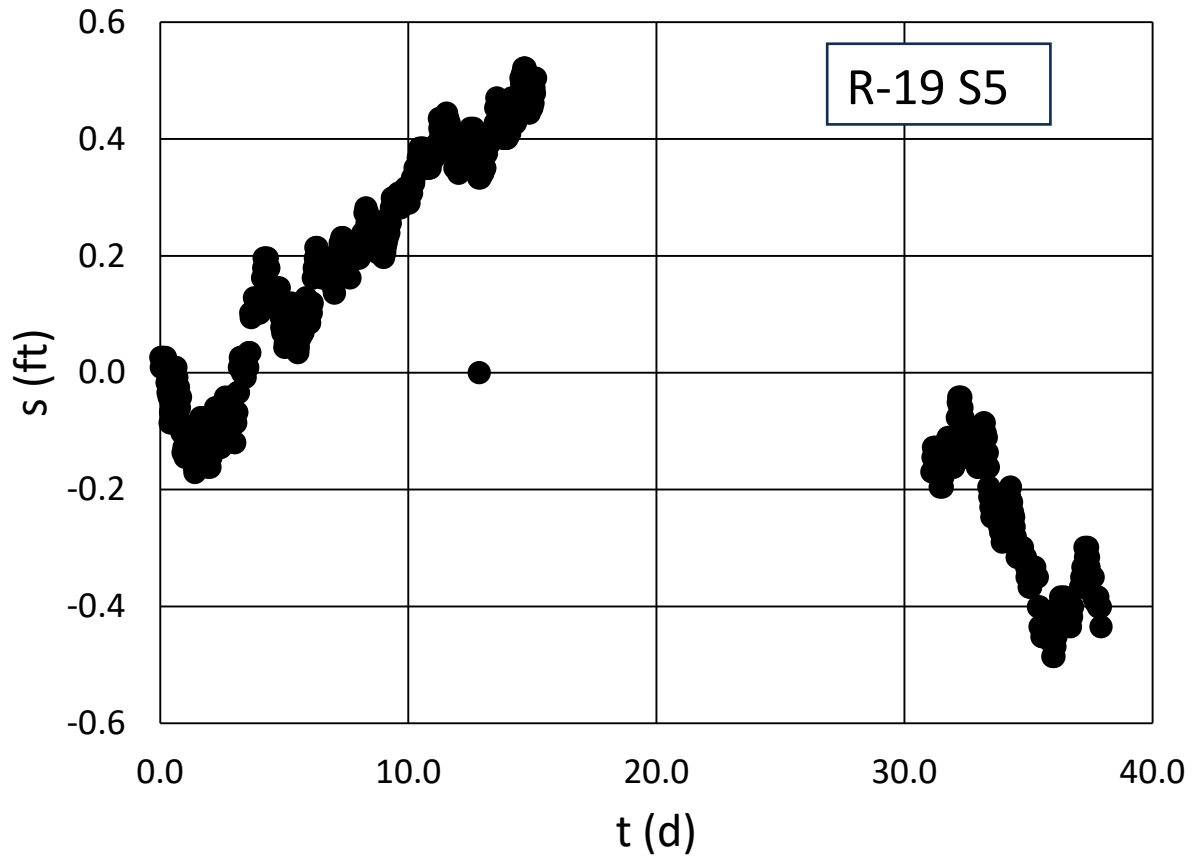


Figure 11. R-19 S5 observation well drawdowns versus time.

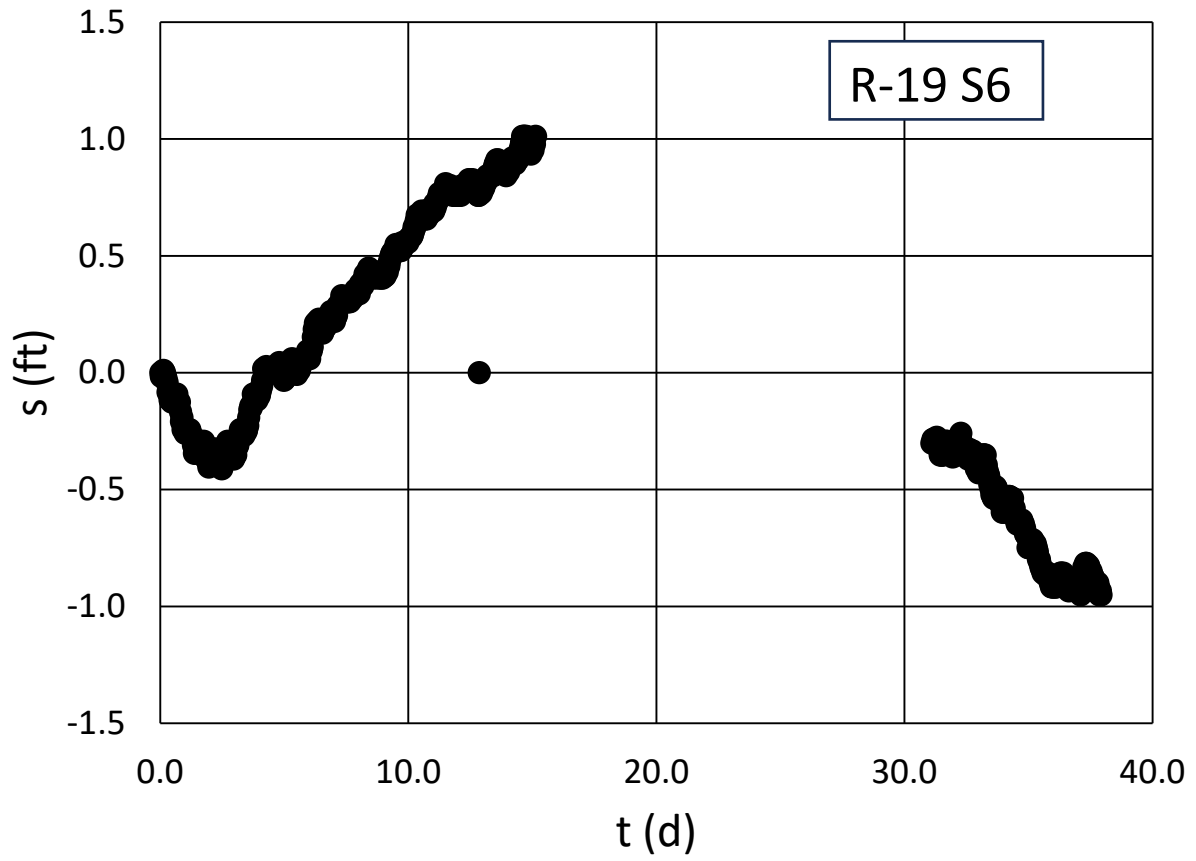


Figure 12. R-19 S6 observation well drawdowns versus time.

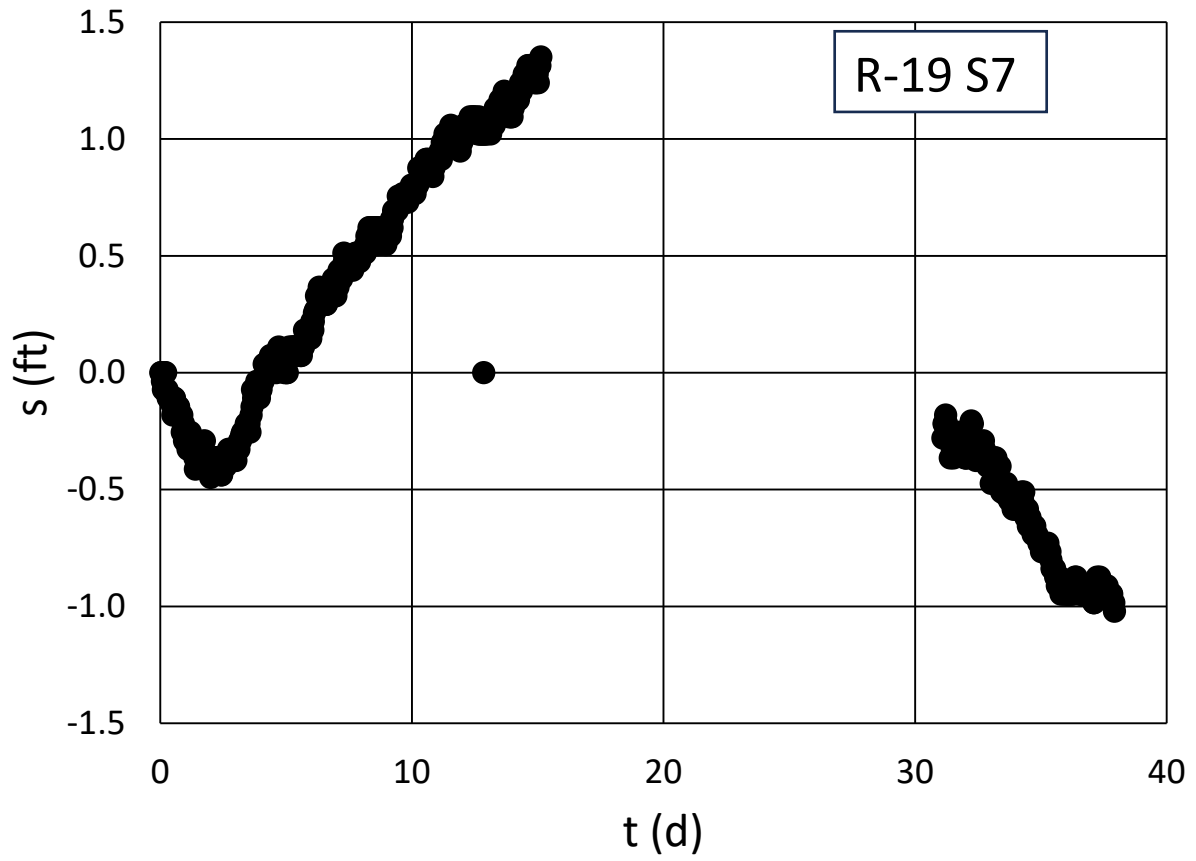


Figure 13. R-19 S7 observation well drawdowns versus time.



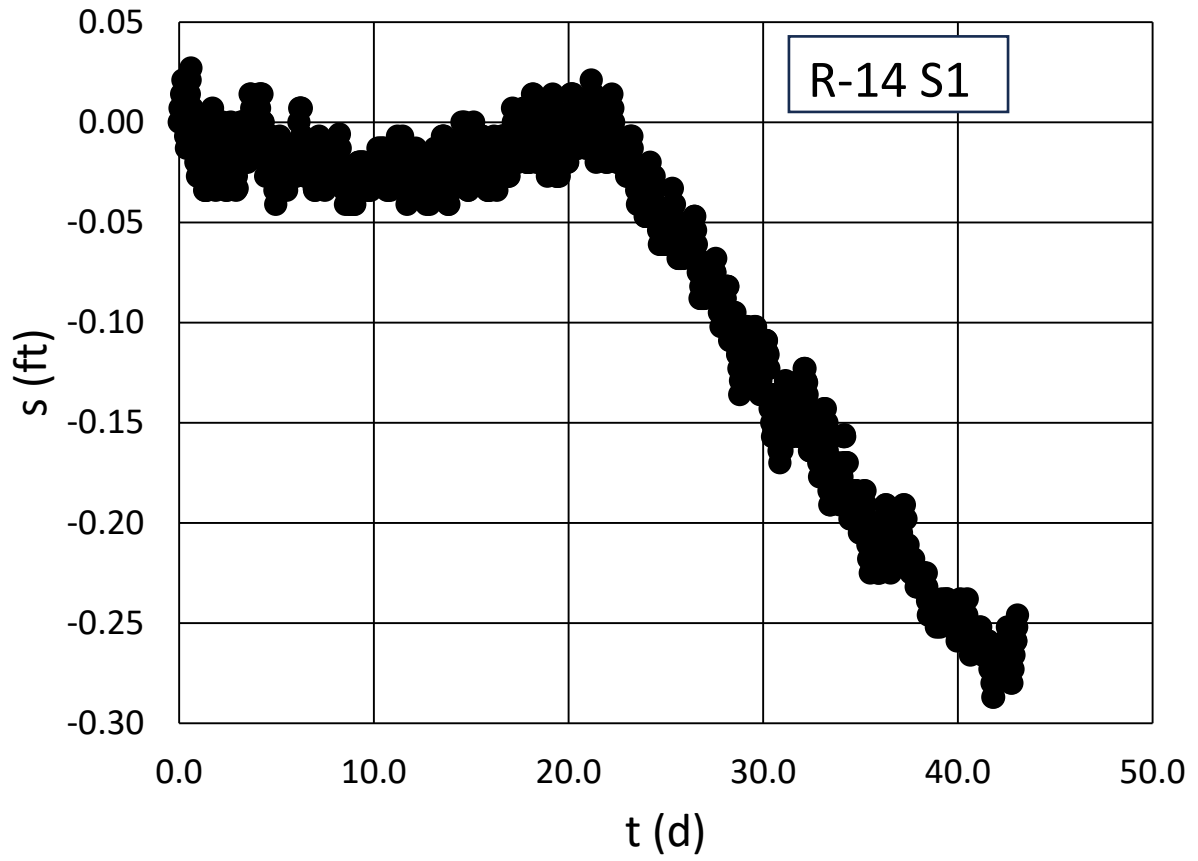


Figure 14. R-14 S1 observation well drawdowns versus time.

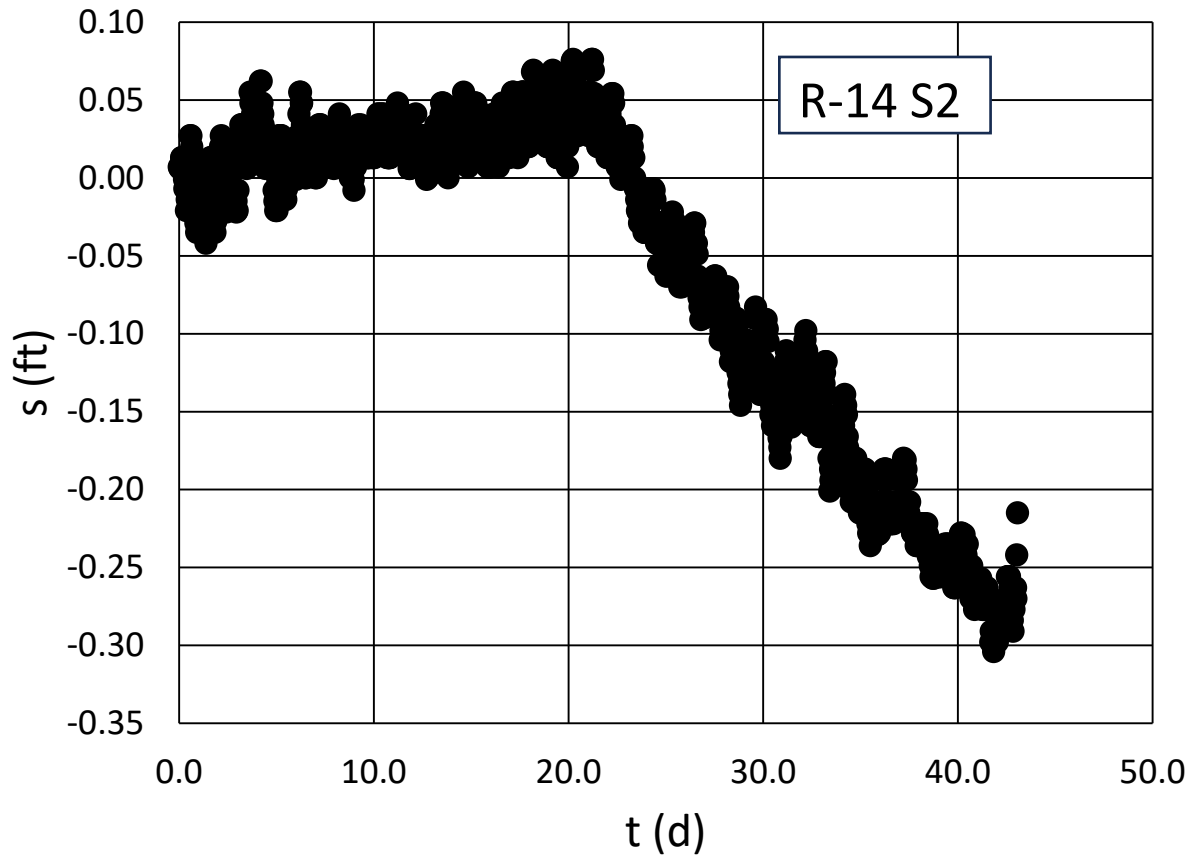


Figure 15. R-14 S2 observation well drawdowns versus time.

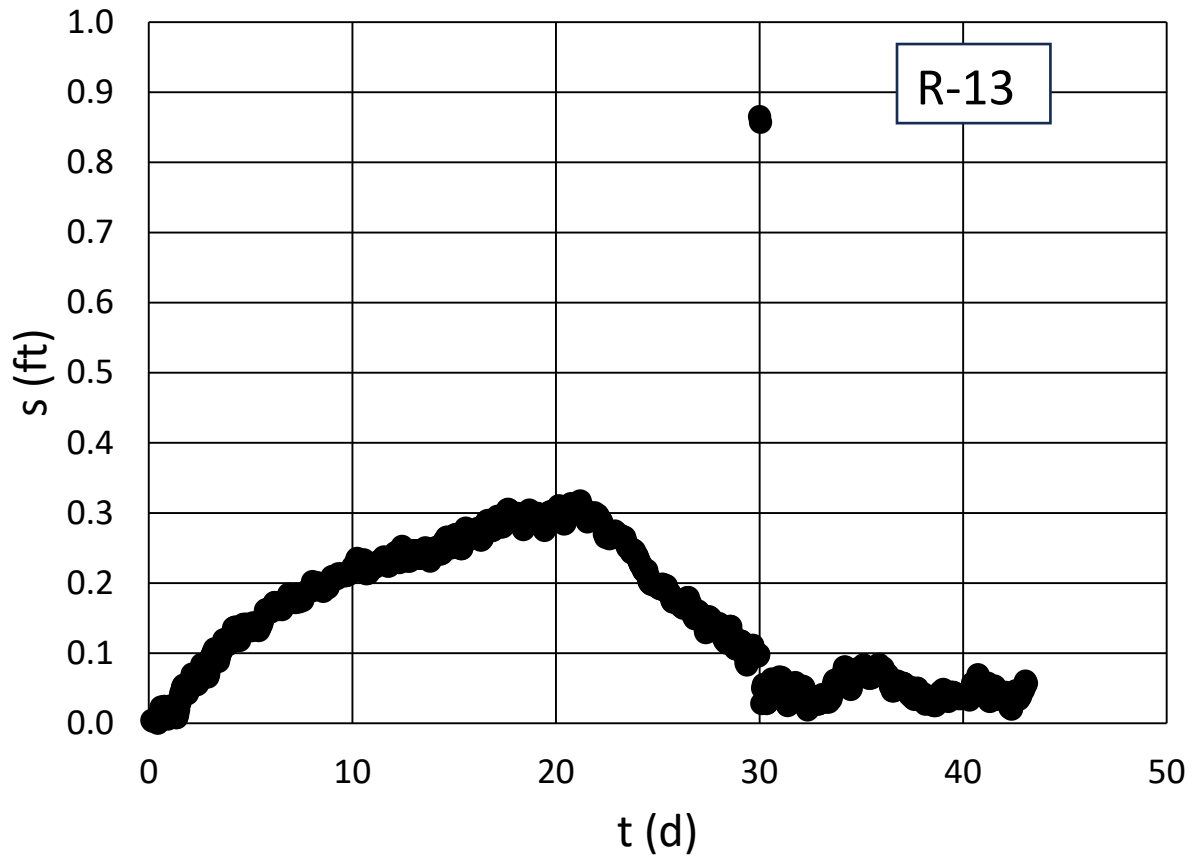


Figure 16. R-13 observation well drawdowns versus time.

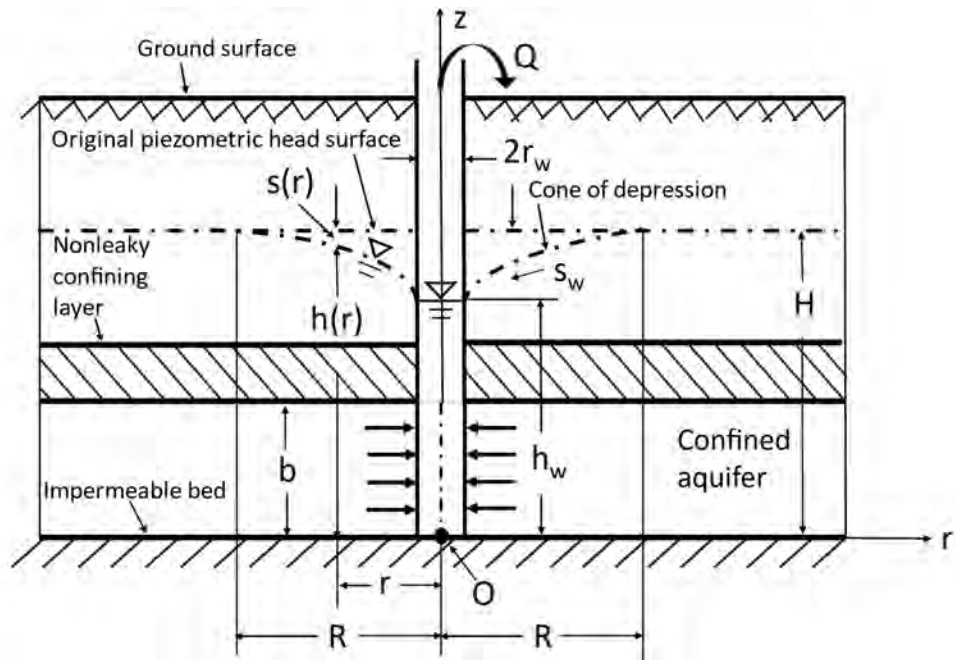


Figure 17. Well in a confined aquifer.

## Tables

Table 1. Wells geometry and initial water levels.

Well	Distance, r (ft)	Hydrostatic Water Level (ft bgs)	Top of screen (ft bgs)	Bottom of screen (ft bgs)	Screen Length, L (ft)	Depth to screen from water table, d (ft)	Inside radius of well casing, $r_c$ (ft)	Radius of well, $r_w$ (ft)
PM-4	0	1082.4	1260	2854	1594	177.6	0.6667	1.0833
PM-2	4463	873.6	1004	2280	1276	130.4	0.5833	1.0000
PM-5	4651	1244.7	1440	3072	1632	195.3	0.6667	1.0833
R20-1	5508	827.9	904.6	912.2	7.6	76.7	0.1875	0.2083
R20-2	5508	832.2	1147.1	1154.7	7.6	314.9	0.1875	0.2083
R20-3	5508	853.3	1328.8	1336.5	7.7	475.5	0.1875	0.2083
R32-1	8713	779.4	867.5	875.2	7.7	88.1	0.1875	0.2083
R32-2	8713	788.2	931.8	934.9	3.1	143.6	0.1875	0.2083
R32-3	8713	787.8	972.9	980.6	7.7	185.1	0.1875	0.2083
R19-4	7253	1178	1410.2	1417.4	7.2	232.2	0.1875	0.2188
R19-5	7253	1178	1582.6	1589.8	7.2	404.6	0.1875	0.2188
R19-6	7253	1178	1726.8	1733.9	7.1	548.8	0.1875	0.2188
R19-7	7253	1178	1832.4	1839.5	7.1	654.4	0.1875	0.2188
R14-1	7141	1182	1200.6	1233.1	32.5	18.6	0.1875	0.2083
R14-2	7141	1182	1286.5	1293.1	6.6	104.5	0.1875	0.2083
R13	5828	833	958.3	1018.7	60.4	125.3	0.1875	0.2083
R15	3549	964	958.6	1020.3	61.7	-5.4	0.2083	0.2292

Hydrostatic water levels from Table 1 or Figures A1, A8, A9 and A10 of the PM-4 Aquifer Test Report (McLin, 2006).

Distances (r) from Table A-1 of the McLin (2006) report.

Well geometry from Figures A1-A10 of the McLin (2006) report.

d = depth to top of well screen from water table.

Table 2. PM-4 aquifer test data analysis results.

<i>Well</i>	$r$ (ft)	$T$ (ft <sup>2</sup> /d)	$s$	$S_y$	$\beta = \left(\frac{K_v}{K_h}\right)\left(\frac{r}{b}\right)^2$	$K_h$ (ft/d)	$a = \frac{K_v}{K_h}$
PM-2 (a)	4463	5751.7	7.17E-04	0.015	0.01268	1.2	0.016
PM-5 (a)	4651	1568.9	2.35E-04	0.020	0.19460	0.3	0.225
R-20 S3 (a)	5508	3849.1	3.02E-04	0.004	0.01407	0.8	0.012
PM-4 recovery (a)	0	5653.2	(c)	(c)	0.00100	1.1	(c)
PM-2 recovery (a)	4463	5233.2	7.33E-04	0.010	0.01709	1.0	0.022
PM-5 recovery (a)	4651	7303.3	6.90E-04	0.009	0.03480	1.5	0.040
R-20 S3 recovery (a)	5508	3339.3	2.91E-04	0.007	0.01952	0.7	0.016
PM-4 (b)	0	11500	(d)	(d)	(d)	2.3	(d)

- (a) Neuman (1974, 1975) methods
- (b) Thiem (1906) method
- (c) Unrealistic value
- (d) Value cannot be determined

## **Appendices**



## APPENDIX A: DETERMINATION OF HORIZONTAL HYDRAULIC CONDUCTIVITY USING THIEM WELL DISCHARGE FORMULA FOR PM-2 STEADY STATE DRAWDOWN VALUE

### A.1 Fully Penetrating Well Solution in a Nonleaky Confined Aquifer: Thiem Equation

Thiem (1906) was the first to derive the hydraulic head and drawdown solution for a well in a fully penetrating well in a confined aquifer under steady state conditions and is given by [e.g., Bear, 1979, p. 306, Eq. (8-6); Batu, 2024, p. 187, Eq. (29-246)]

$$h(R) - h(r) = H - h(r) = \frac{Q}{2\pi T} \ln\left(\frac{R}{r}\right) \quad (\text{A-1})$$

The geometry of the Thiem solution is shown in Figure 17.

### A.2 Radius of Influence

The radius of influence  $R$  is the distance from the well where drawdown is zero. Since the 1880s, many attempts have been made to relate it to well, aquifer, and flow parameters in both steady and unsteady flow conditions in confined and unconfined aquifers. Some semi-empirical formulas are given in Bear (1979, p. 306). Of these formulas, the one developed by Sichardt is given in Bear [1979, p. 306, Eq. (8-11) as presented in Chertousov (1962)] is widely being used [e.g., De Filippi et al., 2020; Batu, 2024, p. 1088, Eq. (29-249)]:

$$R = 3000 s_w K_h^{\frac{1}{2}} \quad (\text{A-2})$$

in which  $R$  and  $s_w$  are in meters (m), and  $K_h$  in meters per second (m/s).

### A.3 Estimation of the Horizontal Hydraulic Conductivity with the PM-2 Drawdown

The method is described in Batu (2024, pp. 1088-1090). Using the measured steady state drawdown  $s_w$  at the well, with Eqs. (A-1), the horizontal hydraulic conductivity  $K_h$  of the aquifer can be estimated. With  $T = K_h b$ , substitution of Eq. (A-2) into Eq. (29-242) and solving for  $K_h$ ,

$$K_h = \frac{Q}{2\pi s_w b} \ln\left(\frac{3000 s_w K_h^{\frac{1}{2}}}{r_w}\right) \quad (\text{A-3})$$

And after some manipulations,

$$K_h = m \left[ \ln(3000) + \frac{1}{2} \ln(K_h) + \ln\left(\frac{s_w}{r_w}\right) \right] \quad (\text{A-4})$$

in which

$$m = \frac{Q}{2\pi s_w b} \quad (\text{A-5})$$

Eq. (A-4) can also be written as

$$K_h - m \frac{1}{2} \ln(K_h) = m [\ln(3,000) + \ln\left(\frac{s_w}{r_w}\right)] \quad (\text{A-6})$$

In Eq. (A-6), with the known values of  $Q$ ,  $s_w$ ,  $b$ , and  $r_w$ , the value of  $K_h$  can be determined with the trial-and-error method. Since the units for Eq. (A-3) for  $R$  are in the metric unit system, calculations must be made using metric units.

The relevant PM-2 data are as follows:

$$b = 1,594 \text{ ft} = 485.85 \text{ m} \text{ (From Table 1)}$$

$$s_w = 70 \text{ ft} = 21.336 \text{ m} \text{ (From Figure 2)}$$

$$2r_c = 2r_w = 16 \text{ in} = 1.3333 \text{ ft} = 0.4064 \text{ m} \text{ (McLin, 2006, p.65, Figure A-3)}$$

$$r_w = 0.6667 \text{ ft} = 0.2032 \text{ m}$$

$$Q = 1,494 \text{ gpm} \text{ (McLin, 2006, p.1)}$$

$$1 \text{ gpm} = 0.0000630902 \frac{\text{m}^3}{\text{s}}$$

$$Q = 1,494.0 \text{ gpm} = 1,494.0 \frac{\text{gallon}}{\text{day}} = (1,494.0 \text{ gpm}) \left( \frac{0.0000630902 \frac{\text{m}^3}{\text{s}}}{\text{gpm}} \right) = 0.09425646 \frac{\text{m}^3}{\text{s}}$$

From Eq. (A-5),

$$m = \frac{Q}{2\pi s_w b} = \frac{(0.07879941 \frac{\text{m}^3}{\text{s}})}{2\pi(25.908 \text{ m})(388.92 \text{ m})} = 0.000001245 \text{ s}^{-1}$$

$$\text{Trial 1: } K_h = 1 \text{ ft/d} = 0.000003528 \text{ m/s}$$

From Eq. (A-6),

$$K_h - m \frac{1}{2} \ln(K_h) = m [\ln(3,000) + \ln\left(\frac{s_w}{r_w}\right)]$$

$$0.000003528 - (0.000001447) \frac{1}{2} \ln(0.000003528)$$

$$= (0.000001447) [\ln(3,000) + \ln\left(\frac{6.401}{0.2032}\right)]$$

$$0.000012611 \neq 0.000016577$$

$$\text{Trial 2: } K_h = 1.5 \text{ ft/d} = 0.000005292 \text{ m/s}$$

From Eq. (A-6),

$$K_h - m \frac{1}{2} \ln(K_h) = m [\ln(3,000) + \ln\left(\frac{s_w}{r_w}\right)]$$

$$0.000005292 - (0.000001447) \frac{1}{2} \ln(0.000005292)$$

$$0.000014082 \neq 0.000016577$$

**Trial 3:  $K_h = 1.7 \text{ ft/d} = 0.000005997 \text{ m/s}$**

From Eq. (A-6),

$$K_h - m \frac{1}{2} \ln(K_h) = m [\ln(3,000) + \ln\left(\frac{s_w}{r_w}\right)]$$

$$0.000005997 - (0.000001447) \frac{1}{2} \ln(0.000005997)$$

$$0.000014697 \neq 0.000016577$$

**Trial 4:  $K_h = 2.0 \text{ ft/d} = 0.000007056 \text{ m/s}$**

From Eq. (A-6),

$$K_h - m \frac{1}{2} \ln(K_h) = m [\ln(3,000) + \ln\left(\frac{s_w}{r_w}\right)]$$

$$0.000007056 - (0.000001447) \frac{1}{2} \ln(0.000007056)$$

$$0.000015658 \neq 0.000016577$$

**Trial 5:  $K_h = 2.2 \text{ ft/d} = 0.000007761 \text{ m/s}$**

From Eq. (A-6),

$$K_h - m \frac{1}{2} \ln(K_h) = m [\ln(3,000) + \ln\left(\frac{s_w}{r_w}\right)]$$

$$0.000007761 - (0.000001447) \frac{1}{2} \ln(0.000007761)$$

$$0.000016274 \neq 0.000016577$$

**Trial 6:  $K_h = 2.3 \text{ ft/d} = 0.000008114 \text{ m/s}$**

From Eq. (A-6),

$$K_h - m \frac{1}{2} \ln(K_h) = m [\ln(3,000) + \ln\left(\frac{s_w}{r_w}\right)]$$

$$0.000008114 - (0.000001447) \frac{1}{2} \ln(0.000008114)$$

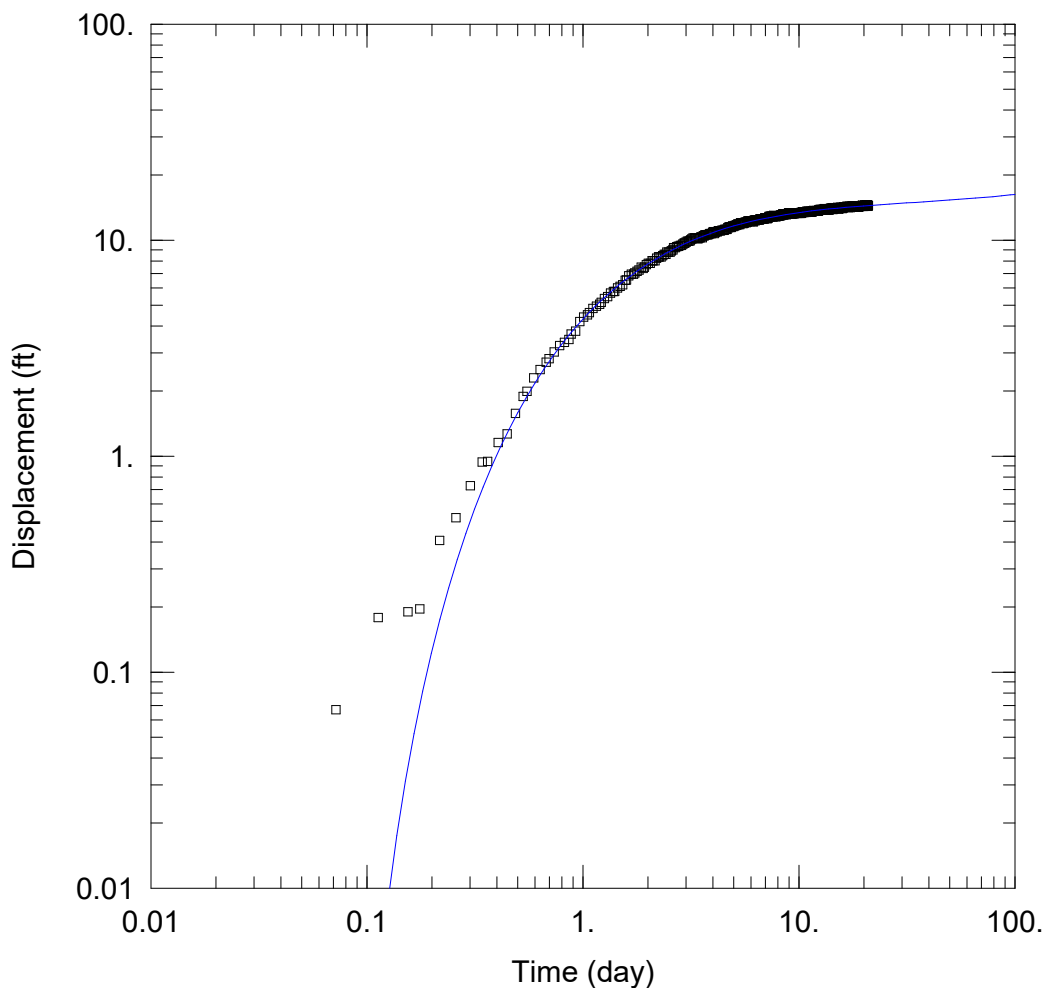
$$0.000016595 \cong 0.000016577$$

Therefore,

$$K_h = 2.3 \text{ ft/d}$$

**APPENDIX B**

**AQTESOLV OUTPUT FOR PM-2 DRAWDOWN ANALYSIS**



WELL TEST ANALYSIS

Data Set: D:\hugo \Downloads\LANL NM PROJECT\PM-4 Aquifer test\AQTESOLV files\PM-2 Data.aqt  
 Date: 07/18/24 Time: 15:25:24

PROJECT INFORMATION

Test Well: PM-4

AQUIFER DATA

Saturated Thickness: 5000. ft

WELL DATA

Pumping Wells			Observation Wells		
Well Name	X (ft)	Y (ft)	Well Name	X (ft)	Y (ft)
PM-4	0	0	□ PM-2	4463	0

SOLUTION

Aquifer Model: Unconfined

Solution Method: Neuman

T = 5751.7 ft<sup>2</sup>/day

S = 0.0007168

Sy = 0.01528

β = 0.01268

Data Set: D:\hugo\_\Downloads\LANL NM PROJECT\PM-4 Aquifer test\AQTESOLV files\PM-2 Data.aqt  
Date: 07/18/24  
Time: 15:25:39

---

PROJECT INFORMATION

Test Well: PM-4

---

AQUIFER DATA

Saturated Thickness: 5000. ft  
Anisotropy Ratio (Kz/Kr): 0.01591

---

PUMPING WELL DATA

No. of pumping wells: 1

Pumping Well No. 1: PM-4

X Location: 0. ft  
Y Location: 0. ft

Casing Radius: 0.6667 ft  
Well Radius: 1.083 ft

Partially Penetrating Well  
Depth to Top of Screen: 177.6 ft  
Depth to Bottom of Screen: 1771.6 ft

No. of pumping periods: 1

<u>Pumping Period Data</u>	
<u>Time (day)</u>	<u>Rate (gal/min)</u>
0.	1494.

---

OBSERVATION WELL DATA

No. of observation wells: 1

Observation Well No. 1: PM-2

X Location: 4463. ft  
Y Location: 0. ft

Radial distance from PM-4: 4463. ft

Partially Penetrating Well  
Depth to Top of Screen: 130.4 ft  
Depth to Bottom of Screen: 1406.4 ft

No. of Observations: 566

<u>Observation Data</u>			
<u>Time (day)</u>	<u>Displacement (ft)</u>	<u>Time (day)</u>	<u>Displacement (ft)</u>

---

0.072	0.067	10.57	13.43
0.113	0.179	10.61	13.44
0.155	0.19	10.65	13.54
0.176	0.196	10.7	13.54
0.217	0.407	10.72	13.54
0.259	0.518	10.76	13.55
0.301	0.729	10.8	13.45
0.342	0.94	10.84	13.55
0.363	0.946	10.86	13.55
0.405	1.156	10.9	13.55
0.447	1.267	10.95	13.46
0.488	1.578	10.99	13.56
0.53	1.888	11.03	13.56
0.551	1.993	11.05	13.56
0.592	2.304	11.09	13.56
0.634	2.514	11.13	13.57
0.676	2.724	11.18	13.47
0.697	2.829	11.22	13.47
0.738	3.039	11.24	13.57
0.78	3.249	11.28	13.48
0.822	3.359	11.32	13.58
0.863	3.469	11.36	13.48
0.884	3.674	11.38	13.58
0.926	3.784	11.43	13.58
0.967	4.193	11.47	13.49
1.009	4.403	11.51	13.59
1.051	4.512	11.55	13.59
1.072	4.617	11.57	13.59
1.113	4.826	11.61	13.59
1.155	4.936	11.65	13.6
1.197	5.045	11.7	13.7
1.217	5.149	11.74	13.7
1.259	5.359	11.76	13.6
1.301	5.468	11.8	13.61
1.342	5.677	11.84	13.61
1.384	5.785	11.88	13.61
1.405	5.79	11.9	13.61
1.447	5.999	11.95	13.61
1.488	6.107	11.99	13.62
1.53	6.216	12.03	13.62
1.572	6.524	12.07	13.72
1.592	6.529	12.09	13.62
1.634	6.837	12.13	13.62
1.676	6.946	12.18	13.63
1.717	6.954	12.22	13.63
1.738	7.058	12.26	13.63
1.78	7.166	12.28	13.73
1.822	7.274	12.32	13.63
1.863	7.483	12.36	13.73
1.905	7.391	12.4	13.74
1.926	7.495	12.43	13.84
1.967	7.703	12.47	13.74
2.009	7.81	12.51	13.84
2.051	7.818	12.55	13.85



<u>Time (day)</u>	<u>Displacement (ft)</u>	<u>Time (day)</u>	<u>Displacement (ft)</u>
2.092	8.026	12.59	13.85
2.113	8.03	12.61	13.85
2.155	8.038	12.65	13.85
2.197	8.245	12.7	13.75
2.238	8.353	12.74	13.75
2.259	8.357	12.78	13.76
2.301	8.364	12.8	13.86
2.342	8.472	12.84	13.86
2.384	8.579	12.88	13.86
2.426	8.586	12.93	13.76
2.447	8.79	12.95	13.77
2.488	8.797	12.99	13.87
2.53	8.805	13.03	13.87
2.572	8.912	13.07	13.87
2.613	9.019	13.11	13.97
2.634	9.222	13.13	13.87
2.676	9.229	13.18	13.88
2.717	9.336	13.22	13.78
2.759	9.343	13.26	13.78
2.78	9.347	13.3	13.78
2.822	9.454	13.32	13.78
2.863	9.46	13.36	13.79
2.905	9.567	13.4	13.89
2.947	9.674	13.45	13.79
2.967	9.677	13.47	13.89
3.009	9.784	13.51	13.89
3.051	9.891	13.55	13.89
3.092	9.897	13.59	13.9
3.134	9.904	13.63	13.8
3.155	10.01	13.65	13.8
3.197	10.11	13.7	13.8
3.238	10.22	13.74	13.9
3.28	10.23	13.78	13.9
3.301	10.23	13.82	14.01
3.342	10.24	13.84	13.81
3.384	10.14	13.88	14.01
3.426	10.15	13.93	14.01
3.467	10.25	13.97	13.91
3.488	10.26	13.99	13.91
3.53	10.36	14.03	14.02
3.572	10.27	14.07	14.02
3.613	10.48	14.11	14.02
3.655	10.48	14.15	13.92
3.676	10.59	14.18	13.92
3.717	10.59	14.22	14.03
3.759	10.6	14.26	14.03
3.801	10.6	14.3	14.03
3.822	10.61	14.34	13.93
3.863	10.71	14.36	14.03
3.905	10.72	14.4	13.83
3.947	10.72	14.45	14.04
3.988	10.83	14.49	14.04
4.009	10.93	14.51	13.94

---

<u>Time (day)</u>	<u>Displacement (ft)</u>	<u>Time (day)</u>	<u>Displacement (ft)</u>
4.051	10.74	14.55	14.14
4.092	10.84	14.59	14.04
4.134	10.95	14.63	14.04
4.176	10.95	14.68	14.05
4.197	10.96	14.7	14.05
4.238	11.06	14.74	14.05
4.28	11.07	14.78	14.05
4.322	11.07	14.82	14.05
4.342	11.08	14.86	14.05
4.384	11.08	14.88	14.05
4.426	11.09	14.93	14.06
4.467	11.09	14.97	14.06
4.509	11.1	15.01	14.06
4.53	11.2	15.03	14.06
4.572	11.21	15.07	14.06
4.613	11.21	15.11	14.06
4.655	11.22	15.15	14.16
4.697	11.42	15.2	14.07
4.717	11.42	15.22	13.97
4.759	11.53	15.26	13.97
4.801	11.43	15.3	14.07
4.842	11.54	15.34	13.97
4.863	11.44	15.38	13.98
4.905	11.55	15.4	14.07
4.947	11.65	15.45	14.08
4.988	11.56	15.49	14.08
5.03	11.66	15.53	14.18
5.051	11.66	15.55	14.08
5.092	11.67	15.59	14.08
5.134	11.77	15.63	14.09
5.176	11.78	15.68	14.09
5.217	11.88	15.72	14.09
5.238	11.79	15.74	14.19
5.28	11.89	15.78	14.09
5.322	11.79	15.82	14.09
5.363	12.	15.86	13.99
5.384	12.	15.9	14.1
5.426	12.01	15.93	14.1
5.467	12.01	15.97	14.1
5.509	11.91	16.01	14.1
5.551	12.02	16.05	14.2
5.572	12.02	16.07	14.2
5.613	12.03	16.11	14.2
5.655	12.13	16.16	14.21
5.697	12.04	16.2	14.21
5.738	12.14	16.24	14.21
5.759	12.14	16.26	14.21
5.801	12.25	16.3	14.21
5.842	12.25	16.34	14.21
5.884	12.26	16.38	14.21
5.905	12.26	16.43	14.22
5.947	12.16	16.45	14.22
5.988	12.27	16.49	14.22

<u>Time (day)</u>	<u>Displacement (ft)</u>	<u>Time (day)</u>	<u>Displacement (ft)</u>
6.03	12.27	16.53	14.22
6.072	12.28	16.57	14.22
6.092	12.28	16.59	14.22
6.134	12.18	16.63	14.32
6.176	12.19	16.68	14.23
6.217	12.39	16.72	14.23
6.259	12.39	16.76	14.33
6.28	12.3	16.78	14.23
6.322	12.4	16.82	14.23
6.363	12.4	16.86	14.23
6.405	12.41	16.91	14.23
6.426	12.41	16.95	14.13
6.467	12.41	16.97	14.23
6.509	12.42	17.01	14.24
6.551	12.42	17.05	14.24
6.592	12.43	17.09	14.34
6.613	12.53	17.11	14.34
6.655	12.53	17.16	14.24
6.697	12.54	17.2	14.24
6.738	12.54	17.24	14.24
6.78	12.54	17.26	14.25
6.801	12.55	17.28	14.15
6.842	12.55	17.32	14.25
6.884	12.55	17.36	14.25
6.926	12.56	17.38	14.35
6.947	12.66	17.43	14.25
6.988	12.66	17.47	14.25
7.03	12.67	17.51	14.25
7.072	12.67	17.55	14.26
7.113	12.57	17.57	14.26
7.134	12.58	17.61	14.26
7.176	12.58	17.66	14.36
7.217	12.68	17.7	14.36
7.259	12.79	17.74	14.26
7.301	12.89	17.76	14.26
7.322	12.79	17.8	14.16
7.363	12.8	17.84	14.17
7.405	12.9	17.88	14.17
7.447	12.9	17.91	14.17
7.467	12.91	17.95	14.17
7.509	12.81	17.99	14.37
7.551	12.91	18.03	14.27
7.592	12.82	18.07	14.37
7.634	12.92	18.09	14.17
7.655	13.02	18.13	14.18
7.697	12.93	18.18	14.28
7.738	12.93	18.22	14.28
7.78	12.83	18.26	14.38
7.822	12.84	18.28	14.28
7.842	12.94	18.32	14.38
7.884	12.84	18.36	14.28
7.926	12.95	18.41	14.29
7.967	12.95	18.43	14.39

<u>Time (day)</u>	<u>Displacement (ft)</u>	<u>Time (day)</u>	<u>Displacement (ft)</u>
7.988	12.95	18.47	14.29
8.03	12.95	18.51	14.19
8.072	12.96	18.55	14.29
8.113	12.96	18.59	14.29
8.155	12.96	18.61	14.29
8.176	12.97	18.66	14.29
8.217	13.07	18.7	14.39
8.259	12.97	18.74	14.2
8.301	13.07	18.78	14.3
8.342	13.08	18.8	14.3
8.363	13.08	18.84	14.3
8.405	13.18	18.88	14.3
8.447	13.19	18.93	14.3
8.488	13.19	18.95	14.3
8.509	13.09	18.99	14.3
8.551	13.19	19.03	14.4
8.592	13.2	19.07	14.41
8.634	13.1	19.11	14.41
8.655	13.2	19.13	14.41
8.676	13.2	19.18	14.31
8.717	13.21	19.22	14.31
8.759	13.11	19.26	14.41
8.78	13.21	19.3	14.31
8.822	13.21	19.32	14.41
8.863	13.22	19.36	14.32
8.905	13.22	19.41	14.42
8.947	13.32	19.45	14.42
8.967	13.32	19.47	14.42
9.009	13.33	19.51	14.42
9.051	13.33	19.55	14.32
9.092	13.33	19.59	14.42
9.134	13.34	19.63	14.42
9.155	13.24	19.66	14.52
9.197	13.24	19.7	14.43
9.238	13.24	19.74	14.33
9.28	13.25	19.78	14.43
9.301	13.25	19.82	14.43
9.342	13.25	19.84	14.43
9.384	13.36	19.88	14.33
9.426	13.26	19.93	14.43
9.467	13.36	19.95	14.43
9.488	13.36	19.97	14.33
9.53	13.27	19.99	14.33
9.572	13.37	20.01	14.33
9.613	13.37	20.03	14.44
9.655	13.27	20.07	14.34
9.676	13.38	20.11	14.44
9.717	13.38	20.16	14.44
9.759	13.38	20.18	14.54
9.801	13.38	20.22	14.54
9.822	13.39	20.26	14.44
9.863	13.29	20.3	14.34
9.905	13.39	20.34	14.44

Time (day)	Displacement (ft)	Time (day)	Displacement (ft)
9.947	13.29	20.36	14.44
9.988	13.4	20.41	14.45
10.01	13.4	20.45	14.45
10.05	13.4	20.49	14.55
10.09	13.4	20.51	14.45
10.13	13.31	20.55	14.45
10.18	13.41	20.59	14.55
10.2	13.31	20.63	14.55
10.24	13.41	20.68	14.55
10.28	13.32	20.7	14.55
10.32	13.42	20.74	14.46
10.34	13.42	20.78	14.36
10.38	13.52	20.82	14.46
10.43	13.52	20.86	14.36
10.47	13.53	20.88	14.46
10.51	13.43	20.93	14.36
10.53	13.53	20.97	14.46

SOLUTION

Pumping Test  
 Aquifer Model: Unconfined  
 Solution Method: Neuman

VISUAL ESTIMATION RESULTS

Estimated Parameters

Parameter	Estimate	
T	1301.5	ft <sup>2</sup> /day
S	0.0003659	
Sy	0.1	
β	0.1	

K = T/b = 0.2603 ft/day (9.183E-5 cm/sec)  
 Ss = S/b = 7.318E-8 1/ft

AUTOMATIC ESTIMATION RESULTS

Estimated Parameters

Parameter	Estimate	Std. Error	Approx. C.I.	t-Ratio	
T	5751.7	100.4	+/- 197.2	57.29	ft <sup>2</sup> /day
S	0.0007168	4.236E-6	+/- 8.319E-6	169.2	
Sy	0.01528	0.001667	+/- 0.003274	9.169	
β	0.01268	0.0004507	+/- 0.0008853	28.13	

C.I. is approximate 95% confidence interval for parameter  
 t-ratio = estimate/std. error  
 Estimation window: 0.2 to 21 day

K = T/b = 1.15 ft/day (0.0004058 cm/sec)  
 Ss = S/b = 1.434E-7 1/ft

Parameter Correlations

	<u>T</u>	<u>S</u>	<u>Sy</u>	<u>β</u>
T	1.00	0.92	0.62	-1.00
S	0.92	1.00	0.77	-0.94
Sy	0.62	0.77	1.00	-0.67
β	-1.00	-0.94	-0.67	1.00

Residual Statistics

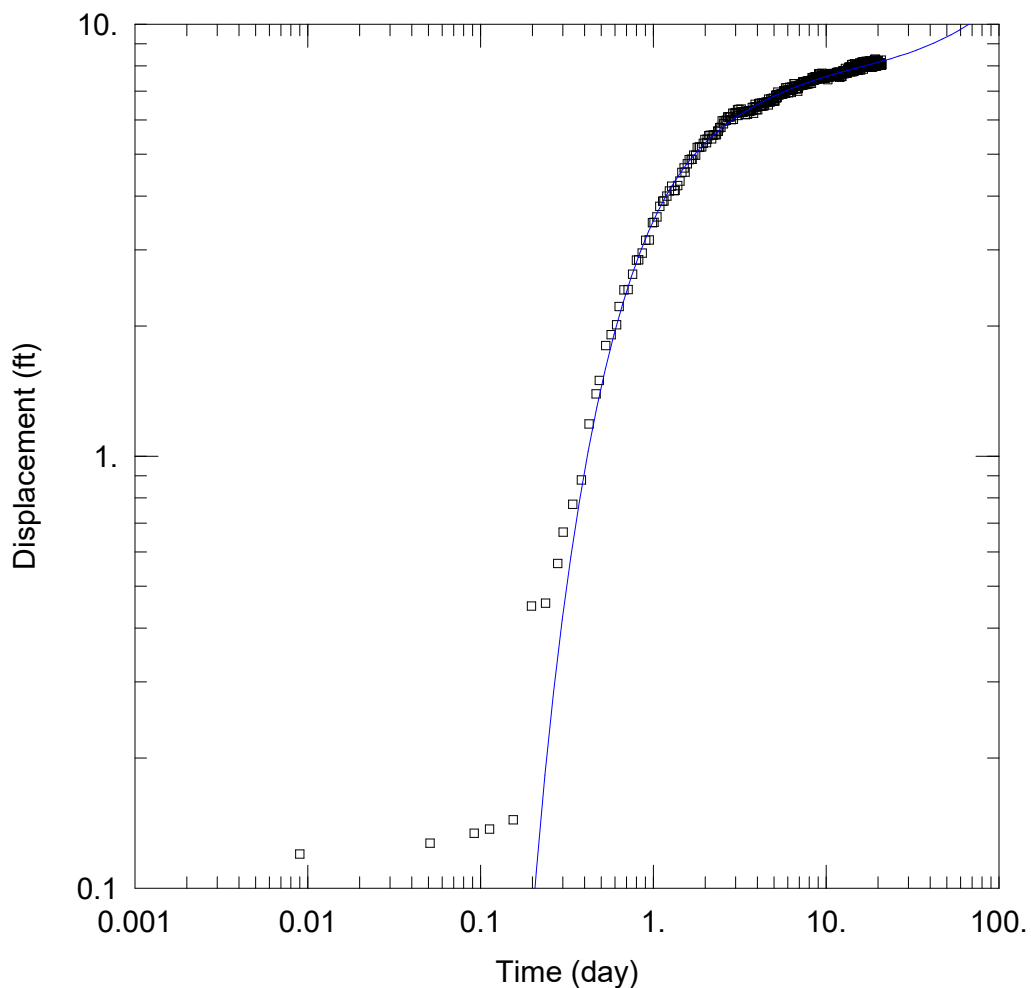
for weighted residuals

Sum of Squares... 3.336 ft<sup>2</sup>  
 Variance ..... 0.005979 ft<sup>2</sup>  
 Std. Deviation ..... 0.07732 ft  
 Mean ..... 0.001685 ft  
 No. of Residuals .. 562  
 No. of Estimates .. 4

Estimation window from 0.2 to 21 day.

**APPENDIX C**

**AQTESOLV OUTPUT FOR PM-5 DRAWDOWN ANALYSIS**



WELL TEST ANALYSIS

Data Set: D:\hugo \Downloads\LANL NM PROJECT\PM-4 Aquifer test\AQTESOLV files\PM-5 Data.aqt  
 Date: 07/18/24 Time: 16:10:05

PROJECT INFORMATION

Test Well: PM-4

AQUIFER DATA

Saturated Thickness: 5000. ft

WELL DATA

Pumping Wells			Observation Wells		
Well Name	X (ft)	Y (ft)	Well Name	X (ft)	Y (ft)
PM-4	0	0	□ PM-5	4651	0

SOLUTION

Aquifer Model: Unconfined

Solution Method: Neuman

T = 1568.9 ft<sup>2</sup>/day

S = 0.0002346

Sy = 0.02016

β = 0.1946



Data Set: D:\hugo\_\Downloads\LANL NM PROJECT\PM-4 Aquifer test\AQTESOLV files\PM-5 Data.aqt  
Date: 07/18/24  
Time: 16:10:16

---

PROJECT INFORMATION

Test Well: PM-4

---

AQUIFER DATA

Saturated Thickness: 5000. ft  
Anisotropy Ratio (Kz/Kr): 0.2249

---

PUMPING WELL DATA

No. of pumping wells: 1

Pumping Well No. 1: PM-4

X Location: 0. ft  
Y Location: 0. ft

Casing Radius: 0.6667 ft  
Well Radius: 1.083 ft

Partially Penetrating Well  
Depth to Top of Screen: 177.6 ft  
Depth to Bottom of Screen: 1771.6 ft

No. of pumping periods: 1

<u>Pumping Period Data</u>	
<u>Time (day)</u>	<u>Rate (gal/min)</u>
0.	1494.

---

OBSERVATION WELL DATA

No. of observation wells: 1

Observation Well No. 1: PM-5

X Location: 4651. ft  
Y Location: 0. ft

Radial distance from PM-4: 4651. ft

Partially Penetrating Well  
Depth to Top of Screen: 195.3 ft  
Depth to Bottom of Screen: 1827.3 ft

No. of Observations: 567

<u>Observation Data</u>			
<u>Time (day)</u>	<u>Displacement (ft)</u>	<u>Time (day)</u>	<u>Displacement (ft)</u>

---

0.009	0.12	10.55	7.66
0.051	0.127	10.59	7.562
0.092	0.134	10.63	7.565
0.113	0.137	10.65	7.666
0.155	0.144	10.7	7.669
0.197	0.45	10.74	7.571
0.238	0.457	10.78	7.574
0.28	0.564	10.8	7.575
0.301	0.667	10.84	7.678
0.342	0.774	10.88	7.58
0.384	0.88	10.93	7.583
0.426	1.187	10.97	7.585
0.467	1.393	10.99	7.687
0.488	1.496	11.03	7.589
0.53	1.803	11.07	7.592
0.572	1.909	11.11	7.594
0.613	2.015	11.15	7.597
0.634	2.219	11.18	7.598
0.676	2.425	11.22	7.601
0.717	2.431	11.26	7.603
0.759	2.637	11.3	7.605
0.801	2.843	11.32	7.607
0.822	2.847	11.36	7.609
0.863	2.953	11.4	7.612
0.905	3.159	11.45	7.614
0.947	3.165	11.49	7.717
0.988	3.471	11.51	7.618
1.009	3.474	11.55	7.72
1.051	3.58	11.59	7.623
1.092	3.786	11.63	7.625
1.134	3.892	11.68	7.628
1.155	3.895	11.7	7.729
1.197	4.001	11.74	7.731
1.238	4.106	11.78	7.634
1.28	4.212	11.82	7.636
1.322	4.118	11.84	7.737
1.342	4.121	11.88	7.64
1.384	4.227	11.93	7.742
1.426	4.332	11.97	7.544
1.467	4.538	12.01	7.547
1.509	4.644	12.03	7.648
1.53	4.547	12.07	7.65
1.572	4.752	12.11	7.653
1.613	4.858	12.15	7.655
1.655	4.863	12.2	7.657
1.676	4.866	12.22	7.659
1.717	4.972	12.26	7.561
1.759	4.977	12.3	7.663
1.801	5.182	12.34	7.666
1.842	5.188	12.36	7.567
1.863	5.191	12.4	7.669
1.905	5.196	12.45	7.771
1.947	5.301	12.49	7.774
1.988	5.407	12.53	7.776

---

<u>Time (day)</u>	<u>Displacement (ft)</u>	<u>Time (day)</u>	<u>Displacement (ft)</u>
2.03	5.312	12.55	7.777
2.051	5.415	12.59	7.779
2.092	5.52	12.63	7.782
2.134	5.525	12.68	7.784
2.176	5.43	12.72	7.686
2.197	5.533	12.74	7.687
2.238	5.538	12.78	7.79
2.28	5.543	12.82	7.792
2.322	5.549	12.86	7.694
2.363	5.654	12.88	7.795
2.384	5.656	12.93	7.698
2.426	5.761	12.97	7.9
2.467	5.766	13.01	7.802
2.509	5.971	13.05	7.804
2.551	5.876	13.07	7.705
2.572	5.979	13.11	7.708
2.613	5.984	13.15	7.71
2.655	5.989	13.2	7.712
2.697	6.094	13.24	7.814
2.717	6.096	13.26	7.815
2.759	6.101	13.3	7.718
2.801	6.106	13.34	7.72
2.842	6.011	13.38	7.822
2.884	6.216	13.4	7.823
2.905	6.018	13.45	7.825
2.947	6.223	13.49	7.828
2.988	6.228	13.53	7.93
3.03	6.232	13.57	7.932
3.072	6.337	13.59	7.933
3.092	6.14	13.63	7.835
3.134	6.344	13.68	7.937
3.176	6.249	13.72	7.939
3.217	6.354	13.76	7.842
3.238	6.256	13.78	7.943
3.28	6.261	13.82	7.945
3.322	6.265	13.86	7.947
3.363	6.27	13.9	7.849
3.405	6.174	13.93	7.75
3.426	6.177	13.97	7.852
3.467	6.281	14.01	7.954
3.509	6.186	14.05	7.857
3.551	6.29	14.09	8.059
3.592	6.295	14.11	8.06
3.613	6.297	14.15	8.062
3.655	6.302	14.2	7.964
3.697	6.306	14.24	7.966
3.738	6.41	14.28	7.768
3.759	6.313	14.3	7.869
3.801	6.217	14.34	7.871
3.842	6.421	14.38	7.773
3.884	6.526	14.43	7.875
3.926	6.43	14.45	7.776
3.947	6.332	14.49	7.779

<u>Time (day)</u>	<u>Displacement (ft)</u>	<u>Time (day)</u>	<u>Displacement (ft)</u>
3.988	6.437	14.53	7.881
4.03	6.341	14.57	8.083
4.072	6.545	14.61	7.885
4.113	6.549	14.63	8.086
4.134	6.552	14.68	7.888
4.176	6.456	14.72	7.99
4.217	6.46	14.76	7.992
4.259	6.564	14.8	7.894
4.28	6.466	14.82	7.995
4.322	6.471	14.86	7.997
4.363	6.575	14.9	7.899
4.405	6.479	14.95	7.901
4.447	6.583	14.97	7.902
4.467	6.585	15.01	7.904
4.509	6.589	15.05	7.906
4.551	6.593	15.09	8.008
4.592	6.597	15.13	7.91
4.634	6.501	15.15	8.011
4.655	6.704	15.2	8.013
4.697	6.608	15.24	8.015
4.738	6.612	15.28	7.817
4.78	6.616	15.32	7.919
4.801	6.718	15.34	7.92
4.842	6.622	15.38	7.822
4.884	6.726	15.43	7.924
4.926	6.63	15.47	7.926
4.967	6.733	15.49	8.027
4.988	6.635	15.53	7.929
5.03	6.639	15.57	7.931
5.072	6.643	15.61	8.033
5.113	6.847	15.65	8.135
5.155	6.751	15.68	8.036
5.176	6.853	15.72	7.938
5.217	6.757	15.76	7.84
5.259	6.961	15.8	7.942
5.301	6.865	15.84	8.044
5.322	6.866	15.86	7.945
5.363	6.87	15.9	7.846
5.405	6.874	15.95	7.948
5.447	6.878	15.99	7.95
5.488	6.882	16.01	8.151
5.509	6.884	16.05	7.953
5.551	6.887	16.09	7.955
5.592	6.891	16.13	7.957
5.634	6.895	16.18	8.059
5.676	6.998	16.2	8.06
5.697	7.	16.24	8.162
5.738	7.004	16.28	8.164
5.78	7.008	16.32	7.966
5.822	6.911	16.36	8.067
5.842	7.113	16.38	8.068
5.884	7.017	16.43	7.97
5.926	7.02	16.47	7.872

<u>Time (day)</u>	<u>Displacement (ft)</u>	<u>Time (day)</u>	<u>Displacement (ft)</u>
5.967	7.124	16.51	8.074
6.009	7.028	16.53	8.075
6.03	7.029	16.57	7.977
6.072	6.933	16.61	8.079
6.113	7.037	16.66	8.181
6.155	7.14	16.7	8.082
6.197	7.044	16.72	8.083
6.217	7.045	16.76	8.085
6.259	7.049	16.8	8.187
6.301	6.953	16.84	8.089
6.342	7.056	16.88	7.991
6.363	7.158	16.91	8.092
6.405	7.061	16.95	8.093
6.447	7.065	16.99	8.095
6.488	7.068	17.03	7.997
6.53	7.272	17.05	8.098
6.551	7.273	17.09	8.2
6.592	7.177	17.13	8.202
6.634	7.18	17.18	8.003
6.676	7.184	17.2	8.104
6.717	7.087	17.22	8.005
6.738	7.089	17.26	8.107
6.78	7.092	17.3	8.109
6.822	7.096	17.32	8.11
6.863	6.999	17.36	8.012
6.884	7.201	17.41	8.013
6.926	7.104	17.45	8.015
6.967	7.207	17.49	8.117
7.009	7.211	17.51	8.118
7.051	7.214	17.55	8.12
7.072	7.216	17.59	8.121
7.113	7.219	17.63	8.023
7.155	7.222	17.68	8.125
7.197	7.226	17.7	8.126
7.238	7.229	17.74	8.128
7.259	7.23	17.78	8.129
7.301	7.334	17.82	8.131
7.342	7.337	17.84	8.232
7.384	7.34	17.88	8.134
7.405	7.242	17.93	8.136
7.447	7.345	17.97	8.037
7.488	7.248	18.01	8.039
7.53	7.251	18.03	8.14
7.572	7.355	18.07	8.142
7.592	7.256	18.11	8.043
7.634	7.359	18.16	8.145
7.676	7.362	18.2	7.947
7.717	7.366	18.22	8.048
7.759	7.269	18.26	8.049
7.78	7.37	18.3	8.051
7.822	7.373	18.34	8.053
7.863	7.277	18.36	7.954
7.905	7.38	18.41	8.055

---

<u>Time (day)</u>	<u>Displacement (ft)</u>	<u>Time (day)</u>	<u>Displacement (ft)</u>
7.926	7.381	18.45	8.057
7.967	7.384	18.49	7.959
8.009	7.387	18.53	8.061
8.051	7.291	18.55	7.961
8.092	7.394	18.59	8.063
8.113	7.395	18.63	8.065
8.155	7.398	18.68	8.167
8.197	7.401	18.72	8.068
8.238	7.304	18.74	8.069
8.28	7.407	18.78	8.071
8.301	7.509	18.82	7.972
8.342	7.412	18.86	8.074
8.384	7.515	18.88	8.175
8.426	7.418	18.93	8.077
8.447	7.419	18.97	8.178
8.488	7.422	19.01	8.08
8.53	7.525	19.05	8.182
8.572	7.528	19.07	8.082
8.592	7.53	19.11	8.284
8.613	7.431	19.16	7.986
8.655	7.534	19.2	8.187
8.697	7.537	19.24	8.089
8.717	7.539	19.26	8.19
8.759	7.541	19.3	8.192
8.801	7.544	19.34	8.293
8.842	7.447	19.38	8.095
8.884	7.55	19.41	8.096
8.905	7.552	19.45	8.097
8.947	7.555	19.49	8.099
8.988	7.557	19.53	8.201
9.03	7.56	19.57	8.002
9.072	7.663	19.59	8.103
9.092	7.665	19.63	8.105
9.134	7.667	19.68	8.006
9.176	7.67	19.72	8.208
9.217	7.473	19.76	8.11
9.238	7.475	19.78	8.11
9.28	7.577	19.82	8.212
9.322	7.48	19.86	8.114
9.363	7.483	19.91	8.215
9.405	7.586	19.93	8.116
9.426	7.587	19.97	8.218
9.467	7.69	20.01	8.219
9.509	7.593	20.05	8.121
9.551	7.596	20.09	8.122
9.592	7.598	20.11	8.123
9.613	7.6	20.16	8.125
9.655	7.602	20.2	8.126
9.697	7.505	20.24	8.028
9.738	7.508	20.28	8.13
9.759	7.609	20.3	8.13
9.801	7.612	20.34	8.132
9.842	7.515	20.38	8.133

Time (day)	Displacement (ft)	Time (day)	Displacement (ft)
9.884	7.517	20.43	8.135
9.926	7.52	20.45	8.136
9.947	7.521	20.49	8.037
9.988	7.624	20.53	8.039
10.03	7.627	20.57	8.041
10.07	7.53	20.61	8.142
10.11	7.532	20.63	8.043
10.13	7.534	20.68	8.044
10.18	7.636	20.72	8.146
10.22	7.439	20.76	8.048
10.26	7.542	20.8	8.049
10.28	7.643	20.82	8.05
10.32	7.545	20.86	8.251
10.36	7.648	20.91	8.053
10.4	7.651	20.95	8.054
10.45	7.553	20.97	8.055
10.47	7.655	21.01	8.057
10.51	7.557		

SOLUTION

Pumping Test  
 Aquifer Model: Unconfined  
 Solution Method: Neuman

VISUAL ESTIMATION RESULTS

Estimated Parameters

Parameter	Estimate	
T	2761.8	ft <sup>2</sup> /day
S	0.0003665	
Sy	0.1	
β	0.1	

$K = T/b = 0.5524$  ft/day (0.0001949 cm/sec)  
 $S_s = S/b = 7.329E-8$  1/ft

AUTOMATIC ESTIMATION RESULTS

Estimated Parameters

Parameter	Estimate	Std. Error	Approx. C.I.	t-Ratio	
T	1568.9	115.	+/- 225.9	13.64	ft <sup>2</sup> /day
S	0.0002346	1.528E-5	+/- 3.0E-5	15.36	
Sy	0.02016	0.0006067	+/- 0.001192	33.23	
β	0.1946	0.0149	+/- 0.02927	13.06	

C.I. is approximate 95% confidence interval for parameter  
 t-ratio = estimate/std. error  
 Estimation window: 0.2 to 22 day

$K = T/b = 0.3138$  ft/day (0.0001107 cm/sec)

$S_s = S/b = 4.693E-8 \text{ 1/ft}$

Parameter Correlations

	<u>T</u>	<u>S</u>	<u>Sy</u>	<u>β</u>
T	1.00	1.00	0.14	-1.00
S	1.00	1.00	0.21	-1.00
Sy	0.14	0.21	1.00	-0.17
β	-1.00	-1.00	-0.17	1.00

Residual Statistics

for weighted residuals

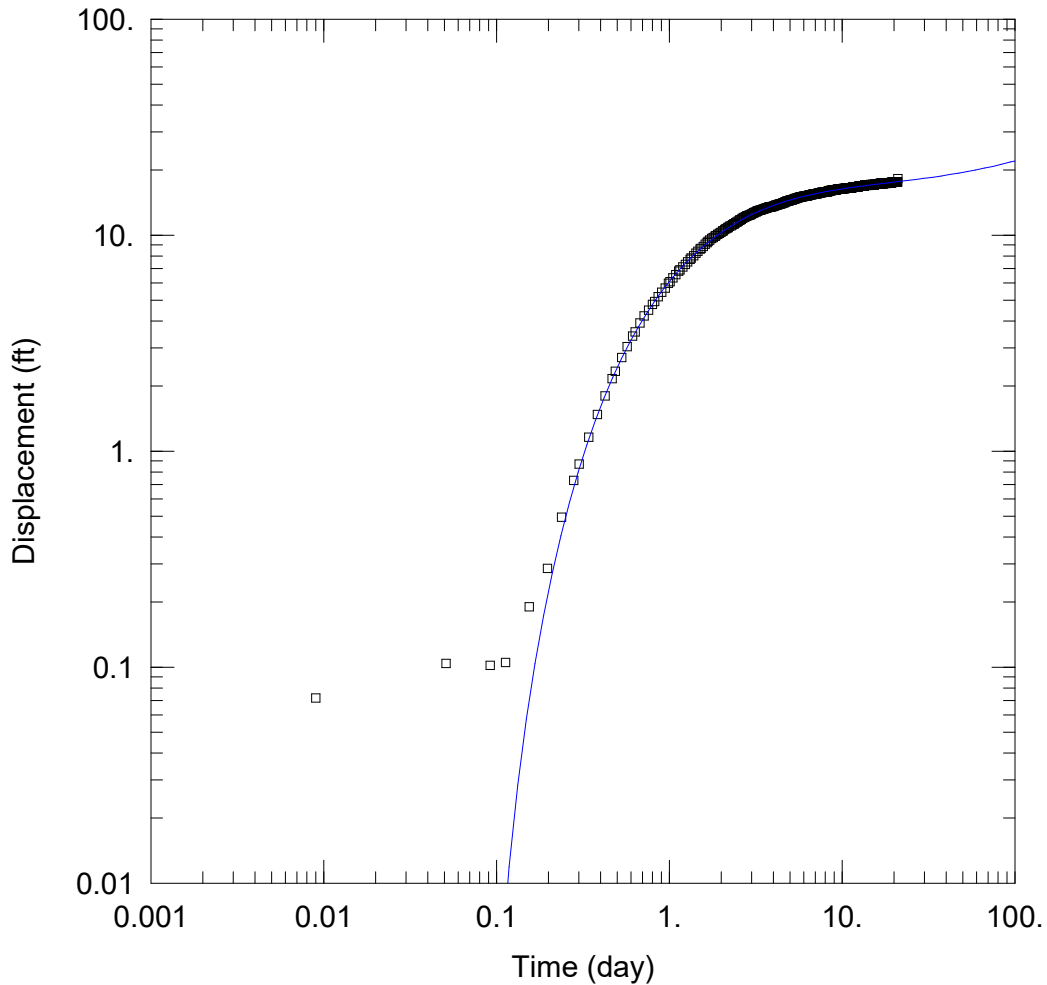
Sum of Squares... 4.533 ft<sup>2</sup>  
Variance ..... 0.008139 ft<sup>2</sup>  
Std. Deviation ..... 0.09022 ft  
Mean ..... 0.00167 ft  
No. of Residuals .. 561  
No. of Estimates .. 4

Estimation window from 0.2 to 22 day.



**APPENDIX D**

**AQTESOLV OUTPUT FOR R-20 S3 DRAWDOWN ANALYSIS**



WELL TEST ANALYSIS

Data Set: D:\...\R20-S3 Data.aqt  
 Date: 07/18/24

Time: 16:58:26

PROJECT INFORMATION

Test Well: PM-4

AQUIFER DATA

Saturated Thickness: 5000. ft

WELL DATA

Pumping Wells

Observation Wells

Well Name	X (ft)	Y (ft)
PM-4	0	0

Well Name	X (ft)	Y (ft)
□ R20-S3	5508	0

SOLUTION

Aquifer Model: Unconfined

Solution Method: Neuman

T = 3849.1 ft<sup>2</sup>/day

S = 0.0003019

Sy = 0.004026

β = 0.01407

Data Set: D:\hugo\_\Downloads\LANL NM PROJECT\PM-4 Aquifer test\AQTESOLV files\R20-S3 Data.aqt  
Date: 07/18/24  
Time: 16:59:02

---

PROJECT INFORMATION

Test Well: PM-4

---

AQUIFER DATA

Saturated Thickness: 5000. ft  
Anisotropy Ratio (Kz/Kr): 0.01159

---

PUMPING WELL DATA

No. of pumping wells: 1

Pumping Well No. 1: PM-4

X Location: 0. ft  
Y Location: 0. ft

Casing Radius: 0.6667 ft  
Well Radius: 1.083 ft

Partially Penetrating Well  
Depth to Top of Screen: 177.6 ft  
Depth to Bottom of Screen: 1771.6 ft

No. of pumping periods: 1

<u>Pumping Period Data</u>	
<u>Time (day)</u>	<u>Rate (gal/min)</u>
0.	1494.

---

OBSERVATION WELL DATA

No. of observation wells: 1

Observation Well No. 1: R20-S3

X Location: 5508. ft  
Y Location: 0. ft

Radial distance from PM-4: 5508. ft

Partially Penetrating Well  
Depth to Top of Screen: 475.5 ft  
Depth to Bottom of Screen: 483.2 ft

No. of Observations: 567

<u>Observation Data</u>			
<u>Time (day)</u>	<u>Displacement (ft)</u>	<u>Time (day)</u>	<u>Displacement (ft)</u>

---

0.009	0.072	10.55	16.49
0.051	0.104	10.59	16.51
0.092	0.102	10.63	16.52
0.113	0.105	10.65	16.51
0.155	0.19	10.7	16.5
0.197	0.286	10.74	16.51
0.238	0.494	10.78	16.5
0.28	0.731	10.8	16.49
0.301	0.872	10.84	16.49
0.342	1.16	10.88	16.49
0.384	1.476	10.93	16.49
0.426	1.802	10.97	16.52
0.467	2.165	10.99	16.49
0.488	2.345	11.03	16.52
0.53	2.715	11.07	16.53
0.572	3.048	11.11	16.53
0.613	3.407	11.15	16.55
0.634	3.561	11.18	16.56
0.676	3.923	11.22	16.52
0.717	4.231	11.26	16.51
0.759	4.501	11.3	16.53
0.801	4.778	11.32	16.52
0.822	4.919	11.36	16.54
0.863	5.18	11.4	16.57
0.905	5.435	11.45	16.6
0.947	5.694	11.49	16.64
0.988	5.975	11.51	16.64
1.009	6.093	11.55	16.66
1.051	6.332	11.59	16.66
1.092	6.563	11.63	16.68
1.134	6.809	11.68	16.67
1.155	6.902	11.7	16.67
1.197	7.121	11.74	16.67
1.238	7.316	11.78	16.66
1.28	7.521	11.82	16.66
1.322	7.725	11.84	16.66
1.342	7.823	11.88	16.66
1.384	8.015	11.93	16.66
1.426	8.237	11.97	16.67
1.467	8.413	12.01	16.7
1.509	8.608	12.03	16.71
1.53	8.691	12.07	16.7
1.572	8.864	12.11	16.73
1.613	9.08	12.15	16.72
1.655	9.228	12.2	16.71
1.676	9.344	12.22	16.7
1.717	9.486	12.26	16.68
1.759	9.647	12.3	16.7
1.801	9.742	12.34	16.72
1.842	9.89	12.36	16.73
1.863	9.946	12.4	16.75
1.905	10.07	12.45	16.77
1.947	10.18	12.49	16.82
1.988	10.3	12.53	16.83

---

<u>Time (day)</u>	<u>Displacement (ft)</u>	<u>Time (day)</u>	<u>Displacement (ft)</u>
2.03	10.43	12.55	16.86
2.051	10.49	12.59	16.85
2.092	10.6	12.63	16.91
2.134	10.72	12.68	16.91
2.176	10.81	12.72	16.91
2.197	10.87	12.74	16.91
2.238	10.98	12.78	16.89
2.28	11.07	12.82	16.9
2.322	11.18	12.86	16.88
2.363	11.25	12.88	16.89
2.384	11.3	12.93	16.9
2.426	11.41	12.97	16.9
2.467	11.49	13.01	16.93
2.509	11.61	13.05	16.92
2.551	11.71	13.07	16.92
2.572	11.76	13.11	16.91
2.613	11.84	13.15	16.92
2.655	11.95	13.2	16.91
2.697	12.05	13.24	16.88
2.717	12.09	13.26	16.87
2.759	12.18	13.3	16.88
2.801	12.24	13.34	16.88
2.842	12.28	13.38	16.89
2.884	12.34	13.4	16.9
2.905	12.38	13.45	16.92
2.947	12.43	13.49	16.94
2.988	12.5	13.53	16.99
3.03	12.59	13.57	17.
3.072	12.66	13.59	17.03
3.092	12.7	13.63	17.03
3.134	12.75	13.68	17.06
3.176	12.82	13.72	17.02
3.217	12.89	13.76	17.04
3.238	12.92	13.78	17.
3.28	12.97	13.82	16.99
3.322	13.01	13.86	17.01
3.363	13.05	13.9	17.01
3.405	13.1	13.93	17.01
3.426	13.1	13.97	17.01
3.467	13.16	14.01	17.04
3.509	13.22	14.05	17.02
3.551	13.26	14.09	17.04
3.592	13.29	14.11	17.05
3.613	13.31	14.15	17.04
3.655	13.36	14.2	17.04
3.697	13.4	14.24	17.03
3.738	13.44	14.28	17.
3.759	13.47	14.3	17.02
3.801	13.49	14.34	17.
3.842	13.5	14.38	17.01
3.884	13.52	14.43	17.02
3.926	13.52	14.45	17.05
3.947	13.55	14.49	17.05

---

<u>Time (day)</u>	<u>Displacement (ft)</u>	<u>Time (day)</u>	<u>Displacement (ft)</u>
3.988	13.59	14.53	17.09
4.03	13.62	14.57	17.11
4.072	13.68	14.61	17.11
4.113	13.72	14.63	17.1
4.134	13.74	14.68	17.14
4.176	13.78	14.72	17.13
4.217	13.8	14.76	17.13
4.259	13.86	14.8	17.12
4.28	13.87	14.82	17.11
4.322	13.9	14.86	17.13
4.363	13.94	14.9	17.1
4.405	13.96	14.95	17.11
4.447	14.	14.97	17.11
4.467	14.01	15.01	17.15
4.509	14.05	15.05	17.13
4.551	14.08	15.09	17.15
4.592	14.12	15.13	17.14
4.634	14.15	15.15	17.13
4.655	14.19	15.2	17.14
4.697	14.24	15.24	17.1
4.738	14.28	15.28	17.12
4.78	14.31	15.32	17.11
4.801	14.33	15.34	17.1
4.842	14.36	15.38	17.13
4.884	14.39	15.43	17.13
4.926	14.42	15.47	17.16
4.967	14.45	15.49	17.15
4.988	14.49	15.53	17.18
5.03	14.52	15.57	17.23
5.072	14.53	15.61	17.25
5.113	14.56	15.65	17.24
5.155	14.59	15.68	17.26
5.176	14.57	15.72	17.25
5.217	14.61	15.76	17.23
5.259	14.66	15.8	17.22
5.301	14.69	15.84	17.21
5.322	14.71	15.86	17.23
5.363	14.76	15.9	17.22
5.405	14.77	15.95	17.21
5.447	14.8	15.99	17.23
5.488	14.84	16.01	17.22
5.509	14.86	16.05	17.23
5.551	14.87	16.09	17.25
5.592	14.92	16.13	17.26
5.634	14.93	16.18	17.28
5.676	14.97	16.2	17.3
5.697	14.99	16.24	17.28
5.738	14.99	16.28	17.29
5.78	15.01	16.32	17.25
5.822	15.04	16.36	17.26
5.842	15.04	16.38	17.26
5.884	15.06	16.43	17.27
5.926	15.06	16.47	17.29

<u>Time (day)</u>	<u>Displacement (ft)</u>	<u>Time (day)</u>	<u>Displacement (ft)</u>
5.967	15.09	16.51	17.29
6.009	15.11	16.53	17.31
6.03	15.12	16.57	17.33
6.072	15.15	16.61	17.36
6.113	15.13	16.66	17.37
6.155	15.15	16.7	17.36
6.197	15.17	16.72	17.38
6.217	15.17	16.76	17.36
6.259	15.19	16.8	17.35
6.301	15.2	16.84	17.33
6.342	15.22	16.88	17.35
6.363	15.25	16.91	17.31
6.405	15.28	16.95	17.32
6.447	15.29	16.99	17.32
6.488	15.32	17.03	17.34
6.53	15.36	17.05	17.33
6.551	15.35	17.09	17.35
6.592	15.38	17.13	17.37
6.634	15.38	17.18	17.35
6.676	15.4	17.2	17.35
6.717	15.41	17.22	17.34
6.738	15.43	17.26	17.33
6.78	15.43	17.3	17.34
6.822	15.46	17.32	17.34
6.863	15.48	17.36	17.34
6.884	15.48	17.41	17.32
6.926	15.49	17.45	17.32
6.967	15.52	17.49	17.36
7.009	15.53	17.51	17.33
7.051	15.54	17.55	17.37
7.072	15.54	17.59	17.41
7.113	15.54	17.63	17.43
7.155	15.55	17.68	17.43
7.197	15.56	17.7	17.45
7.238	15.59	17.74	17.43
7.259	15.59	17.78	17.42
7.301	15.6	17.82	17.42
7.342	15.62	17.84	17.4
7.384	15.68	17.88	17.37
7.405	15.67	17.93	17.4
7.447	15.69	17.97	17.4
7.488	15.72	18.01	17.41
7.53	15.74	18.03	17.41
7.572	15.74	18.07	17.41
7.592	15.76	18.11	17.4
7.634	15.75	18.16	17.42
7.676	15.77	18.2	17.4
7.717	15.77	18.22	17.39
7.759	15.78	18.26	17.39
7.78	15.79	18.3	17.4
7.822	15.81	18.34	17.36
7.863	15.83	18.36	17.38
7.905	15.84	18.41	17.38

<u>Time (day)</u>	<u>Displacement (ft)</u>	<u>Time (day)</u>	<u>Displacement (ft)</u>
7.926	15.84	18.45	17.39
7.967	15.86	18.49	17.41
8.009	15.87	18.53	17.41
8.051	15.87	18.55	17.42
8.092	15.9	18.59	17.45
8.113	15.9	18.63	17.47
8.155	15.88	18.68	17.45
8.197	15.88	18.72	17.47
8.238	15.92	18.74	17.48
8.28	15.89	18.78	17.48
8.301	15.94	18.82	17.48
8.342	15.96	18.86	17.48
8.384	15.98	18.88	17.47
8.426	16.02	18.93	17.47
8.447	16.03	18.97	17.49
8.488	16.04	19.01	17.48
8.53	16.06	19.05	17.49
8.572	16.09	19.07	17.48
8.592	16.09	19.11	17.49
8.613	16.08	19.16	17.5
8.655	16.11	19.2	17.49
8.697	16.1	19.24	17.49
8.717	16.11	19.26	17.49
8.759	16.12	19.3	17.52
8.801	16.13	19.34	17.51
8.842	16.13	19.38	17.51
8.884	16.13	19.41	17.52
8.905	16.15	19.45	17.52
8.947	16.17	19.49	17.53
8.988	16.19	19.53	17.55
9.03	16.21	19.57	17.56
9.072	16.22	19.59	17.58
9.092	16.2	19.63	17.58
9.134	16.21	19.68	17.6
9.176	16.18	19.72	17.61
9.217	16.23	19.76	17.62
9.238	16.2	19.78	17.62
9.28	16.23	19.82	17.63
9.322	16.24	19.86	17.62
9.363	16.25	19.91	17.61
9.405	16.29	19.93	17.62
9.426	16.31	19.97	17.6
9.467	16.3	20.01	17.59
9.509	16.34	20.05	17.6
9.551	16.36	20.09	17.61
9.592	16.37	20.11	17.62
9.613	16.36	20.16	17.6
9.655	16.36	20.2	17.61
9.697	16.37	20.24	17.59
9.738	16.35	20.28	17.59
9.759	16.36	20.3	17.59
9.801	16.36	20.34	17.57
9.842	16.34	20.38	17.56



Time (day)	Displacement (ft)	Time (day)	Displacement (ft)
9.884	16.35	20.43	17.59
9.926	16.37	20.45	17.58
9.947	16.36	20.49	17.59
9.988	16.39	20.53	17.6
10.03	16.39	20.57	17.6
10.07	16.39	20.61	17.59
10.11	16.4	20.63	17.62
10.13	16.42	20.68	17.65
10.18	16.42	20.72	17.63
10.22	16.41	20.76	17.64
10.26	16.4	20.8	17.63
10.28	16.4	20.82	17.62
10.32	16.41	20.86	17.63
10.36	16.44	20.91	17.63
10.4	16.44	20.95	17.61
10.45	16.46	20.97	17.62
10.47	16.48	21.	18.29
10.51	16.5		

SOLUTION

Pumping Test  
 Aquifer Model: Unconfined  
 Solution Method: Neuman

VISUAL ESTIMATION RESULTS

Estimated Parameters

Parameter	Estimate	
T	779.5	ft <sup>2</sup> /day
S	0.0001205	
Sy	0.1	
β	0.1	

K = T/b = 0.1559 ft/day (5.5E-5 cm/sec)  
 Ss = S/b = 2.409E-8 1/ft

AUTOMATIC ESTIMATION RESULTS

Estimated Parameters

Parameter	Estimate	Std. Error	Approx. C.I.	t-Ratio	
T	3849.1	41.32	+/- 81.16	93.14	ft <sup>2</sup> /day
S	0.0003019	1.405E-6	+/- 2.759E-6	214.9	
Sy	0.004026	5.406E-5	+/- 0.0001062	74.47	
β	0.01407	0.0002633	+/- 0.0005171	53.43	

C.I. is approximate 95% confidence interval for parameter  
 t-ratio = estimate/std. error  
 Estimation window: 0.2 to 21 day

K = T/b = 0.7698 ft/day (0.0002716 cm/sec)

$S_s = S/b = 6.038E-8 \text{ 1/ft}$

Parameter Correlations

	<u>T</u>	<u>S</u>	<u>Sy</u>	<u>β</u>
T	1.00	0.96	0.02	-1.00
S	0.96	1.00	0.20	-0.97
Sy	0.02	0.20	1.00	-0.07
β	-1.00	-0.97	-0.07	1.00

Residual Statistics

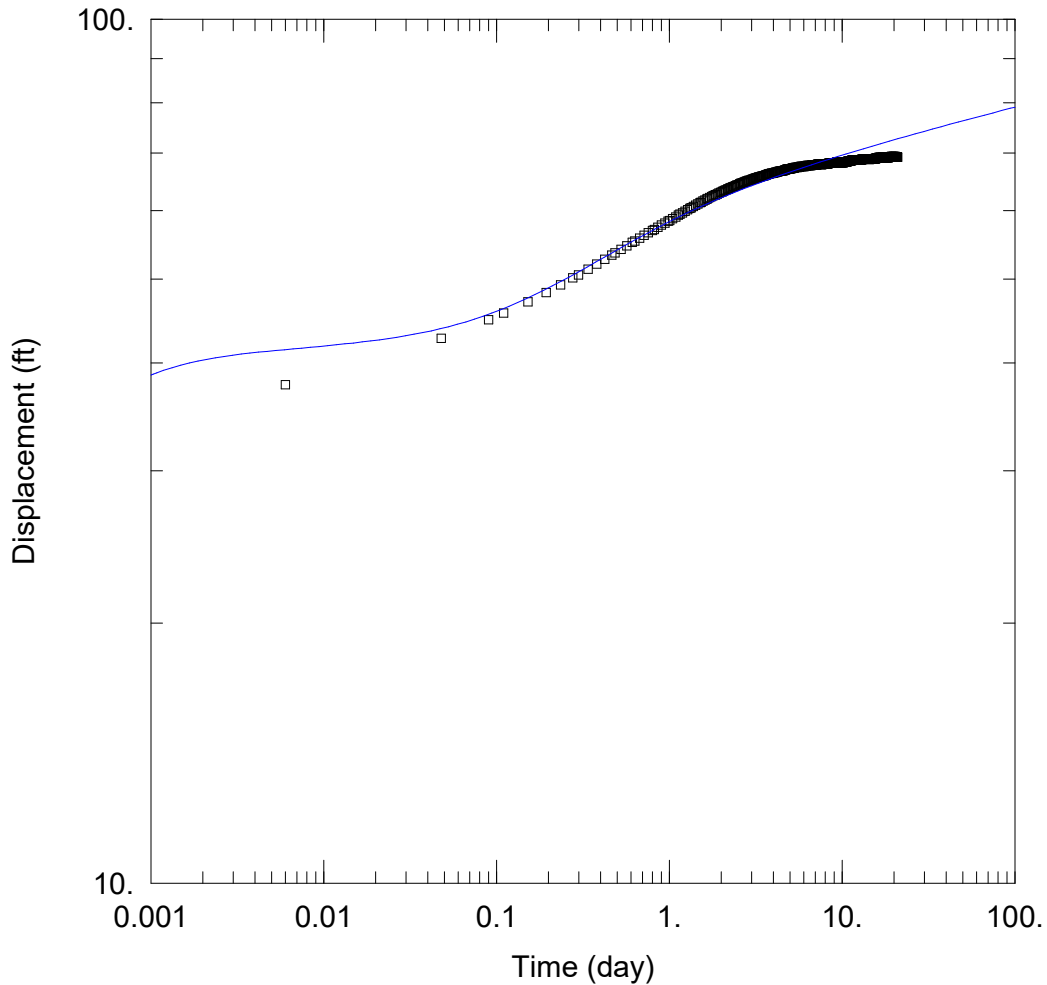
for weighted residuals

Sum of Squares... 1.333 ft<sup>2</sup>  
Variance ..... 0.002397 ft<sup>2</sup>  
Std. Deviation ..... 0.04896 ft  
Mean ..... 0.000155 ft  
No. of Residuals .. 560  
No. of Estimates .. 4

Estimation window from 0.2 to 21 day.

**APPENDIX E**

**AQTESOLV OUTPUT FOR PM-4 RECOVERY ANALYSIS**



WELL TEST ANALYSIS

Data Set: D:\...\PM-4o Data Recovery.aqt  
 Date: 07/18/24

Time: 17:35:37

PROJECT INFORMATION

Test Well: PM-4

AQUIFER DATA

Saturated Thickness: 5000. ft

WELL DATA

Pumping Wells

Observation Wells

Well Name	X (ft)	Y (ft)
PM-4	0	0

Well Name	X (ft)	Y (ft)
□ PM-4o recovery	1	0

SOLUTION

Aquifer Model: Unconfined

Solution Method: Neuman

T = 5653.2 ft<sup>2</sup>/day

S = 0.1326

Sy = 7.376

β = 0.001

Data Set: D:\hugo\_\Downloads\LANL NM PROJECT\PM-4 Aquifer test\AQTESOLV files\PM-4o Data Recovery.aqt  
Date: 07/18/24  
Time: 17:35:50

---

PROJECT INFORMATION

Test Well: PM-4

---

AQUIFER DATA

Saturated Thickness: 5000. ft  
Anisotropy Ratio (Kz/Kr): 2.13E+4

---

PUMPING WELL DATA

No. of pumping wells: 1

Pumping Well No. 1: PM-4

X Location: 0. ft  
Y Location: 0. ft

Casing Radius: 0.6667 ft  
Well Radius: 1.083 ft

Partially Penetrating Well  
Depth to Top of Screen: 177.6 ft  
Depth to Bottom of Screen: 1771.6 ft

No. of pumping periods: 1

<u>Pumping Period Data</u>	
<u>Time (day)</u>	<u>Rate (gal/min)</u>
0.	1494.

---

OBSERVATION WELL DATA

No. of observation wells: 1

Observation Well No. 1: PM-4o recovery

X Location: 1. ft  
Y Location: 0. ft

Radial distance from PM-4: 1. ft

Partially Penetrating Well  
Depth to Top of Screen: 177.6 ft  
Depth to Bottom of Screen: 1771.6 ft

No. of Observations: 566

<u>Observation Data</u>			
<u>Time (day)</u>	<u>Displacement (ft)</u>	<u>Time (day)</u>	<u>Displacement (ft)</u>

---

0.006	37.76	10.51	68.36
0.048	42.71	10.55	68.36
0.09	44.87	10.59	68.36
0.11	45.67	10.63	68.37
0.152	47.06	10.65	68.37
0.194	48.23	10.69	68.39
0.235	49.26	10.73	68.4
0.277	50.16	10.78	68.43
0.298	50.58	10.8	68.43
0.34	51.36	10.84	68.46
0.381	52.06	10.88	68.47
0.423	52.72	10.92	68.47
0.465	53.33	10.97	68.49
0.485	53.62	10.98	68.47
0.527	54.16	11.03	68.49
0.569	54.67	11.07	68.49
0.61	55.14	11.11	68.49
0.631	55.37	11.15	68.5
0.673	55.79	11.17	68.52
0.715	56.19	11.22	68.53
0.756	56.58	11.26	68.56
0.798	56.93	11.3	68.59
0.819	57.09	11.32	68.6
0.86	57.42	11.36	68.62
0.902	57.75	11.4	68.63
0.944	58.05	11.44	68.65
0.985	58.34	11.48	68.66
1.006	58.48	11.51	68.65
1.048	58.77	11.55	68.66
1.09	59.03	11.59	68.66
1.131	59.32	11.63	68.66
1.152	59.45	11.67	68.66
1.194	59.69	11.69	68.66
1.235	59.94	11.73	68.67
1.277	60.18	11.78	68.69
1.319	60.38	11.82	68.7
1.34	60.51	11.84	68.7
1.381	60.71	11.88	68.72
1.423	60.91	11.92	68.73
1.465	61.12	11.97	68.72
1.506	61.3	12.01	68.72
1.527	61.39	12.03	68.7
1.569	61.56	12.07	68.72
1.61	61.75	12.11	68.72
1.652	61.92	12.15	68.72
1.673	61.99	12.19	68.73
1.715	62.14	12.22	68.75
1.756	62.3	12.26	68.76
1.798	62.45	12.3	68.76
1.84	62.58	12.34	68.76
1.86	62.66	12.36	68.76
1.902	62.77	12.4	68.76
1.944	62.9	12.44	68.76
1.985	63.03	12.48	68.76

<u>Time (day)</u>	<u>Displacement (ft)</u>	<u>Time (day)</u>	<u>Displacement (ft)</u>
2.027	63.15	12.53	68.75
2.048	63.22	12.55	68.73
2.09	63.33	12.59	68.73
2.131	63.46	12.63	68.73
2.173	63.58	12.67	68.73
2.194	63.63	12.72	68.7
2.235	63.73	12.73	68.72
2.277	63.84	12.78	68.73
2.319	63.92	12.82	68.75
2.36	64.01	12.86	68.75
2.381	64.05	12.88	68.76
2.423	64.15	12.92	68.78
2.465	64.24	12.97	68.76
2.506	64.34	13.01	68.78
2.548	64.43	13.05	68.78
2.569	64.47	13.07	68.78
2.61	64.57	13.11	68.81
2.652	64.64	13.15	68.81
2.694	64.73	13.19	68.82
2.715	64.77	13.23	68.83
2.756	64.84	13.26	68.83
2.798	64.92	13.3	68.85
2.84	64.97	13.34	68.86
2.881	65.03	13.38	68.86
2.902	65.08	13.4	68.88
2.944	65.12	13.44	68.86
2.985	65.18	13.48	68.89
3.027	65.23	13.53	68.89
3.069	65.31	13.57	68.89
3.09	65.33	13.59	68.88
3.131	65.41	13.63	68.88
3.173	65.46	13.67	68.88
3.215	65.54	13.72	68.86
3.235	65.56	13.76	68.88
3.277	65.62	13.78	68.88
3.319	65.67	13.82	68.88
3.36	65.69	13.86	68.88
3.402	65.75	13.9	68.88
3.423	65.78	13.92	68.88
3.465	65.81	13.97	68.86
3.506	65.85	14.01	68.86
3.548	65.89	14.05	68.85
3.59	65.94	14.09	68.83
3.61	65.97	14.11	68.83
3.652	66.03	14.15	68.83
3.694	66.08	14.19	68.83
3.735	66.14	14.23	68.83
3.756	66.17	14.28	68.82
3.798	66.21	14.3	68.83
3.84	66.24	14.34	68.83
3.881	66.27	14.38	68.83
3.923	66.3	14.42	68.82
3.944	66.31	14.44	68.82

<u>Time (day)</u>	<u>Displacement (ft)</u>	<u>Time (day)</u>	<u>Displacement (ft)</u>
3.985	66.34	14.48	68.82
4.027	66.36	14.53	68.83
4.069	66.42	14.57	68.85
4.11	66.44	14.61	68.85
4.131	66.47	14.63	68.85
4.173	66.52	14.67	68.85
4.215	66.56	14.72	68.85
4.256	66.6	14.76	68.86
4.277	66.62	14.8	68.86
4.319	66.64	14.82	68.86
4.36	66.66	14.86	68.86
4.402	66.69	14.9	68.86
4.444	66.7	14.94	68.86
4.465	66.72	14.97	68.86
4.506	66.73	15.01	68.86
4.548	66.76	15.05	68.86
4.59	66.79	15.09	68.86
4.631	66.85	15.13	68.86
4.652	66.86	15.15	68.86
4.694	66.9	15.19	68.88
4.735	66.96	15.23	68.89
4.777	67.	15.28	68.91
4.798	67.02	15.32	68.91
4.84	67.05	15.34	68.91
4.881	67.08	15.38	68.92
4.923	67.08	15.42	68.92
4.965	67.09	15.47	68.94
4.985	67.09	15.48	68.95
5.027	67.11	15.53	68.94
5.069	67.12	15.57	68.94
5.11	67.15	15.61	68.95
5.152	67.19	15.65	68.98
5.173	67.22	15.67	68.98
5.215	67.25	15.72	68.99
5.256	67.28	15.76	69.01
5.298	67.31	15.8	69.02
5.319	67.31	15.84	69.02
5.36	67.32	15.86	69.01
5.402	67.34	15.9	69.01
5.444	67.35	15.94	69.01
5.485	67.35	15.98	69.04
5.506	67.36	16.01	69.02
5.548	67.36	16.05	69.04
5.59	67.39	16.09	69.05
5.631	67.41	16.13	69.08
5.673	67.44	16.17	69.09
5.694	67.45	16.19	69.11
5.735	67.49	16.23	69.11
5.777	67.52	16.28	69.14
5.819	67.54	16.32	69.14
5.84	67.54	16.36	69.14
5.881	67.54	16.38	69.14
5.923	67.54	16.42	69.12



---

<u>Time (day)</u>	<u>Displacement (ft)</u>	<u>Time (day)</u>	<u>Displacement (ft)</u>
5.965	67.52	16.47	69.12
6.006	67.52	16.51	69.14
6.027	67.52	16.53	69.14
6.069	67.54	16.57	69.15
6.11	67.55	16.61	69.14
6.152	67.58	16.65	69.15
6.194	67.61	16.69	69.15
6.215	67.62	16.72	69.15
6.256	67.67	16.76	69.17
6.298	67.68	16.8	69.17
6.34	67.7	16.84	69.15
6.36	67.7	16.88	69.14
6.402	67.7	16.9	69.14
6.444	67.7	16.94	69.12
6.485	67.68	16.98	69.12
6.527	67.68	17.03	69.12
6.548	67.67	17.05	69.12
6.59	67.68	17.09	69.12
6.631	67.7	17.13	69.14
6.673	67.72	17.17	69.14
6.715	67.74	17.19	69.14
6.735	67.77	17.22	69.15
6.777	67.8	17.26	69.15
6.819	67.8	17.3	69.14
6.86	67.81	17.32	69.14
6.881	67.83	17.36	69.14
6.923	67.83	17.4	69.12
6.965	67.81	17.44	69.14
7.006	67.8	17.48	69.11
7.048	67.8	17.51	69.09
7.069	67.8	17.55	69.11
7.11	67.81	17.59	69.12
7.152	67.86	17.63	69.12
7.194	67.88	17.67	69.14
7.235	67.93	17.69	69.15
7.256	67.93	17.73	69.14
7.298	67.91	17.78	69.17
7.34	67.94	17.82	69.15
7.381	67.94	17.84	69.15
7.402	67.94	17.88	69.15
7.444	67.93	17.92	69.14
7.485	67.91	17.97	69.14
7.527	67.88	18.01	69.14
7.569	67.88	18.03	69.12
7.59	67.88	18.07	69.14
7.631	67.88	18.11	69.14
7.673	67.88	18.15	69.15
7.715	67.91	18.19	69.15
7.756	67.94	18.22	69.17
7.777	67.94	18.26	69.17
7.819	67.96	18.3	69.17
7.86	67.97	18.34	69.17
7.902	67.97	18.36	69.18

---

<u>Time (day)</u>	<u>Displacement (ft)</u>	<u>Time (day)</u>	<u>Displacement (ft)</u>
7.923	67.97	18.4	69.17
7.965	67.96	18.44	69.17
8.006	67.94	18.48	69.17
8.048	67.94	18.53	69.17
8.09	67.94	18.55	69.17
8.11	67.94	18.59	69.15
8.152	67.96	18.63	69.19
8.194	68.	18.67	69.19
8.235	68.01	18.72	69.22
8.277	68.04	18.73	69.24
8.298	68.06	18.78	69.25
8.34	68.07	18.82	69.24
8.381	68.08	18.86	69.25
8.423	68.1	18.88	69.25
8.444	68.1	18.92	69.22
8.485	68.08	18.97	69.22
8.527	68.08	19.01	69.22
8.569	68.08	19.05	69.22
8.59	68.08	19.07	69.24
8.61	68.08	19.11	69.25
8.652	68.08	19.15	69.27
8.694	68.1	19.19	69.28
8.715	68.11	19.23	69.31
8.756	68.13	19.26	69.31
8.798	68.16	19.3	69.32
8.84	68.17	19.34	69.34
8.881	68.17	19.38	69.31
8.902	68.16	19.4	69.32
8.944	68.17	19.44	69.3
8.985	68.17	19.48	69.3
9.027	68.14	19.53	69.3
9.069	68.14	19.57	69.3
9.09	68.16	19.59	69.3
9.131	68.17	19.63	69.3
9.173	68.2	19.67	69.31
9.215	68.23	19.72	69.34
9.235	68.24	19.76	69.34
9.277	68.27	19.78	69.34
9.319	68.3	19.82	69.34
9.36	68.32	19.86	69.32
9.402	68.32	19.9	69.32
9.423	68.32	19.92	69.31
9.465	68.29	19.97	69.3
9.506	68.26	20.01	69.28
9.548	68.24	20.05	69.28
9.59	68.23	20.09	69.28
9.61	68.22	20.11	69.28
9.652	68.22	20.15	69.3
9.694	68.2	20.19	69.31
9.735	68.2	20.23	69.32
9.756	68.23	20.28	69.32
9.798	68.23	20.3	69.32
9.84	68.24	20.34	69.32

<u>Time (day)</u>	<u>Displacement (ft)</u>	<u>Time (day)</u>	<u>Displacement (ft)</u>
9.881	68.24	20.38	69.31
9.923	68.24	20.42	69.3
9.944	68.24	20.44	69.28
9.985	68.23	20.48	69.27
10.03	68.22	20.53	69.27
10.07	68.22	20.57	69.25
10.11	68.2	20.61	69.25
10.13	68.23	20.63	69.25
10.17	68.24	20.67	69.24
10.22	68.26	20.72	69.25
10.26	68.3	20.76	69.25
10.28	68.3	20.8	69.25
10.32	68.33	20.82	69.25
10.36	68.36	20.86	69.24
10.4	68.37	20.9	69.24
10.44	68.37	20.94	69.21
10.47	68.37	20.97	69.19

---

SOLUTION

Pumping Test  
 Aquifer Model: Unconfined  
 Solution Method: Neuman

---

VISUAL ESTIMATION RESULTS

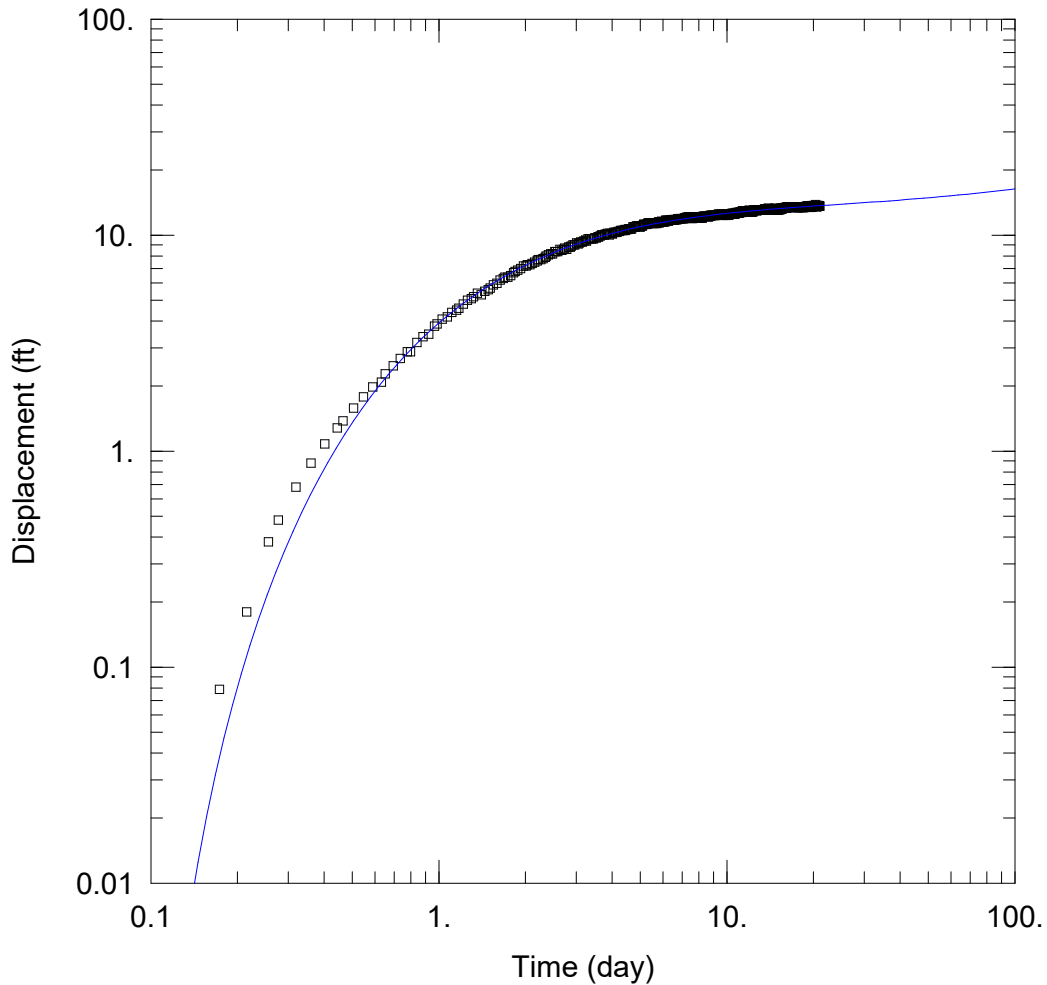
Estimated Parameters

<u>Parameter</u>	<u>Estimate</u>	
T	5653.2	ft <sup>2</sup> /day
S	0.1326	
Sy	7.376	
β	0.001	

K = T/b = 1.131 ft/day (0.0003989 cm/sec)  
 Ss = S/b = 2.651E-5 1/ft

**APPENDIX F**

**AQTESOLV OUTPUT FOR PM-2 RECOVERY ANALYSIS**



WELL TEST ANALYSIS

Data Set: D:\...\PM-2 Data Recovery.aqt  
 Date: 07/18/24

Time: 17:34:04

PROJECT INFORMATION

Test Well: PM-4

AQUIFER DATA

Saturated Thickness: 5000. ft

WELL DATA

Pumping Wells

Observation Wells

Well Name	X (ft)	Y (ft)
PM-4	0	0

Well Name	X (ft)	Y (ft)
□ PM-2 recovery	4463	0

SOLUTION

Aquifer Model: Unconfined

Solution Method: Neuman

T = 5233.2 ft<sup>2</sup>/day

S = 0.0007326

Sy = 0.01017

β = 0.01709

Data Set: D:\hugo\_\Downloads\LANL NM PROJECT\PM-4 Aquifer test\AQTESOLV files\PM-2 Data Recovery.aqt  
Date: 07/18/24  
Time: 17:34:16

---

PROJECT INFORMATION

Test Well: PM-4

---

AQUIFER DATA

Saturated Thickness: 5000. ft  
Anisotropy Ratio (Kz/Kr): 0.02145

---

PUMPING WELL DATA

No. of pumping wells: 1

Pumping Well No. 1: PM-4

X Location: 0. ft  
Y Location: 0. ft

Casing Radius: 0.6667 ft  
Well Radius: 1.083 ft

Partially Penetrating Well  
Depth to Top of Screen: 177.6 ft  
Depth to Bottom of Screen: 1771.6 ft

No. of pumping periods: 1

<u>Pumping Period Data</u>	
<u>Time (day)</u>	<u>Rate (gal/min)</u>
0.	1494.

---

OBSERVATION WELL DATA

No. of observation wells: 1

Observation Well No. 1: PM-2 recovery

X Location: 4463. ft  
Y Location: 0. ft

Radial distance from PM-4: 4463. ft

Partially Penetrating Well  
Depth to Top of Screen: 130.4 ft  
Depth to Bottom of Screen: 1406.4 ft

No. of Observations: 565

<u>Observation Data</u>			
<u>Time (day)</u>	<u>Displacement (ft)</u>	<u>Time (day)</u>	<u>Displacement (ft)</u>

---

0.173	0.079	10.67	12.52
0.215	0.18	10.72	12.62
0.256	0.38	10.76	12.72
0.277	0.48	10.8	12.72
0.319	0.681	10.82	12.62
0.36	0.881	10.86	12.72
0.402	1.081	10.9	12.72
0.444	1.282	10.94	12.72
0.465	1.382	10.97	12.72
0.506	1.582	11.01	12.72
0.548	1.783	11.05	12.62
0.59	1.983	11.09	12.72
0.631	2.083	11.13	12.82
0.652	2.283	11.15	12.82
0.694	2.484	11.19	12.72
0.735	2.684	11.23	12.82
0.777	2.884	11.28	12.82
0.798	2.885	11.32	12.92
0.84	3.185	11.34	12.92
0.881	3.385	11.38	12.92
0.923	3.485	11.42	12.92
0.965	3.786	11.47	12.82
0.985	3.886	11.48	12.92
1.027	4.086	11.53	12.82
1.069	4.187	11.57	12.92
1.11	4.387	11.61	12.82
1.152	4.487	11.65	12.92
1.173	4.587	11.67	12.92
1.215	4.788	11.72	12.92
1.256	4.988	11.76	12.92
1.298	5.088	11.8	12.82
1.319	5.188	11.84	12.82
1.36	5.389	11.86	12.92
1.402	5.289	11.9	12.92
1.444	5.489	11.94	13.02
1.485	5.589	11.98	13.02
1.506	5.69	12.01	12.92
1.548	5.89	12.05	12.92
1.59	5.99	12.09	12.92
1.631	6.19	12.13	12.82
1.673	6.291	12.17	12.93
1.694	6.391	12.19	12.82
1.735	6.391	12.23	12.82
1.777	6.491	12.28	12.93
1.819	6.692	12.32	12.82
1.84	6.792	12.36	13.03
1.881	6.892	12.38	13.03
1.923	6.992	12.42	12.93
1.965	7.193	12.47	13.03
2.006	7.193	12.51	13.03
2.027	7.293	12.53	13.03
2.069	7.293	12.57	13.03
2.11	7.394	12.61	13.03
2.152	7.494	12.65	13.03

<u>Time (day)</u>	<u>Displacement (ft)</u>	<u>Time (day)</u>	<u>Displacement (ft)</u>
2.194	7.594	12.69	13.03
2.215	7.694	12.72	12.93
2.256	7.694	12.76	13.03
2.298	7.795	12.8	13.03
2.34	7.895	12.84	13.13
2.36	7.995	12.88	13.03
2.402	8.095	12.9	13.03
2.444	8.195	12.94	13.03
2.485	8.196	12.98	13.03
2.527	8.396	13.03	13.03
2.548	8.396	13.05	13.03
2.59	8.396	13.09	13.03
2.631	8.597	13.13	13.03
2.673	8.497	13.17	13.13
2.715	8.597	13.22	13.03
2.735	8.697	13.23	13.03
2.777	8.597	13.28	13.13
2.819	8.798	13.32	13.13
2.86	8.798	13.36	13.03
2.881	8.898	13.4	13.13
2.923	8.998	13.42	13.13
2.965	8.998	13.47	13.13
3.006	9.199	13.51	13.23
3.048	9.099	13.55	13.13
3.069	9.199	13.57	13.23
3.11	9.299	13.61	13.13
3.152	9.299	13.65	13.23
3.194	9.4	13.69	13.13
3.235	9.5	13.73	13.13
3.256	9.4	13.76	13.13
3.298	9.6	13.8	13.13
3.34	9.6	13.84	13.23
3.381	9.601	13.88	13.23
3.402	9.601	13.92	13.33
3.444	9.601	13.94	13.23
3.485	9.701	13.98	13.23
3.527	9.701	14.03	13.13
3.569	9.801	14.07	13.23
3.59	9.802	14.09	13.23
3.631	9.902	14.13	13.23
3.673	10.	14.17	13.13
3.715	10.	14.22	13.13
3.756	10.	14.26	13.13
3.777	10.1	14.28	13.23
3.819	10.1	14.32	13.23
3.86	10.2	14.36	13.23
3.902	10.	14.4	13.13
3.923	10.2	14.44	13.23
3.965	10.2	14.47	13.13
4.006	10.1	14.51	13.23
4.048	10.3	14.55	13.23
4.09	10.3	14.59	13.23
4.11	10.3	14.61	13.23



<u>Time (day)</u>	<u>Displacement (ft)</u>	<u>Time (day)</u>	<u>Displacement (ft)</u>
4.152	10.3	14.65	13.13
4.194	10.4	14.69	13.33
4.235	10.4	14.73	13.13
4.277	10.51	14.78	13.23
4.298	10.51	14.8	13.13
4.34	10.51	14.84	13.23
4.381	10.51	14.88	13.23
4.423	10.61	14.92	13.23
4.444	10.51	14.97	13.13
4.485	10.61	14.98	13.13
4.527	10.61	15.03	13.13
4.569	10.71	15.07	13.13
4.61	10.71	15.11	13.13
4.631	10.71	15.13	13.13
4.673	10.71	15.17	13.23
4.715	10.91	15.22	13.13
4.756	10.91	15.26	13.23
4.798	10.91	15.3	13.13
4.819	10.91	15.32	13.23
4.86	11.01	15.36	13.23
4.902	11.01	15.4	13.33
4.944	11.01	15.44	13.23
4.965	10.91	15.48	13.23
5.006	10.91	15.51	13.23
5.048	11.01	15.55	13.23
5.09	11.01	15.59	13.23
5.131	11.21	15.63	13.33
5.152	11.21	15.65	13.33
5.194	11.21	15.69	13.33
5.235	11.21	15.73	13.33
5.277	11.21	15.78	13.33
5.319	11.31	15.82	13.33
5.34	11.41	15.84	13.33
5.381	11.31	15.88	13.33
5.423	11.31	15.92	13.43
5.465	11.41	15.97	13.33
5.485	11.41	16.01	13.33
5.527	11.31	16.03	13.33
5.569	11.31	16.07	13.43
5.61	11.31	16.11	13.43
5.652	11.31	16.15	13.33
5.673	11.31	16.17	13.43
5.715	11.31	16.22	13.53
5.756	11.41	16.26	13.53
5.798	11.51	16.3	13.43
5.84	11.41	16.34	13.53
5.86	11.51	16.36	13.53
5.902	11.51	16.4	13.53
5.944	11.61	16.44	13.43
5.985	11.51	16.48	13.43
6.006	11.51	16.53	13.43
6.048	11.51	16.55	13.53
6.09	11.51	16.59	13.53

<u>Time (day)</u>	<u>Displacement (ft)</u>	<u>Time (day)</u>	<u>Displacement (ft)</u>
6.131	11.71	16.63	13.43
6.173	11.61	16.67	13.53
6.194	11.71	16.69	13.53
6.235	11.71	16.73	13.53
6.277	11.61	16.78	13.53
6.319	11.71	16.82	13.53
6.36	11.71	16.86	13.43
6.381	11.71	16.88	13.53
6.423	11.71	16.92	13.53
6.465	11.81	16.97	13.43
6.506	11.81	17.01	13.53
6.527	11.81	17.05	13.53
6.569	11.71	17.07	13.43
6.61	11.81	17.11	13.53
6.652	11.81	17.15	13.53
6.694	11.81	17.19	13.53
6.715	11.81	17.22	13.53
6.756	11.91	17.26	13.53
6.798	11.91	17.3	13.53
6.84	11.91	17.34	13.53
6.881	11.91	17.36	13.53
6.902	11.91	17.38	13.53
6.944	11.91	17.42	13.43
6.985	11.91	17.47	13.53
7.027	11.91	17.48	13.43
7.048	11.91	17.53	13.43
7.09	11.91	17.57	13.43
7.131	12.02	17.61	13.43
7.173	12.02	17.65	13.43
7.215	12.02	17.67	13.43
7.235	12.02	17.72	13.43
7.277	12.12	17.76	13.43
7.319	12.02	17.8	13.43
7.36	12.12	17.84	13.53
7.402	12.12	17.86	13.43
7.423	12.12	17.9	13.43
7.465	12.12	17.94	13.53
7.506	12.02	17.98	13.43
7.548	12.02	18.01	13.53
7.569	11.92	18.05	13.53
7.61	12.02	18.09	13.53
7.652	12.02	18.13	13.53
7.694	12.12	18.17	13.43
7.735	12.12	18.19	13.53
7.756	12.12	18.23	13.43
7.798	12.02	18.28	13.43
7.84	12.02	18.32	13.53
7.881	12.02	18.36	13.43
7.923	12.02	18.38	13.43
7.944	12.02	18.42	13.43
7.985	12.02	18.47	13.43
8.027	12.12	18.51	13.43
8.069	12.02	18.53	13.43

<u>Time (day)</u>	<u>Displacement (ft)</u>	<u>Time (day)</u>	<u>Displacement (ft)</u>
8.09	12.12	18.57	13.53
8.131	12.12	18.61	13.43
8.173	12.02	18.65	13.53
8.215	12.02	18.69	13.53
8.256	12.22	18.72	13.53
8.277	12.22	18.76	13.53
8.319	12.22	18.8	13.53
8.36	12.22	18.84	13.53
8.402	12.22	18.88	13.53
8.444	12.22	18.9	13.63
8.465	12.22	18.94	13.53
8.506	12.22	18.98	13.53
8.548	12.22	19.03	13.63
8.59	12.22	19.05	13.53
8.61	12.12	19.09	13.63
8.652	12.22	19.13	13.53
8.694	12.22	19.17	13.53
8.735	12.32	19.22	13.63
8.756	12.22	19.23	13.63
8.777	12.32	19.28	13.63
8.819	12.32	19.32	13.63
8.86	12.32	19.36	13.63
8.881	12.32	19.4	13.63
8.923	12.32	19.42	13.53
8.965	12.32	19.47	13.43
9.006	12.32	19.51	13.63
9.048	12.32	19.55	13.53
9.069	12.32	19.57	13.53
9.11	12.32	19.61	13.53
9.152	12.32	19.65	13.53
9.194	12.42	19.69	13.53
9.235	12.42	19.73	13.63
9.256	12.42	19.76	13.73
9.298	12.42	19.8	13.63
9.34	12.52	19.84	13.53
9.381	12.42	19.88	13.63
9.402	12.52	19.92	13.63
9.444	12.42	19.94	13.63
9.485	12.42	19.98	13.63
9.527	12.52	20.03	13.73
9.569	12.42	20.05	13.63
9.59	12.52	20.07	13.63
9.631	12.42	20.09	13.63
9.673	12.32	20.11	13.63
9.715	12.42	20.13	13.63
9.756	12.42	20.17	13.63
9.777	12.42	20.22	13.63
9.819	12.42	20.26	13.73
9.86	12.42	20.28	13.63
9.902	12.42	20.32	13.83
9.923	12.42	20.36	13.63
9.965	12.52	20.4	13.63
10.01	12.32	20.44	13.63

<u>Time (day)</u>	<u>Displacement (ft)</u>	<u>Time (day)</u>	<u>Displacement (ft)</u>
10.05	12.52	20.47	13.63
10.09	12.42	20.51	13.53
10.11	12.42	20.55	13.53
10.15	12.42	20.59	13.63
10.19	12.42	20.61	13.63
10.23	12.52	20.65	13.63
10.28	12.52	20.69	13.63
10.3	12.52	20.73	13.73
10.34	12.52	20.78	13.73
10.38	12.52	20.8	13.63
10.42	12.52	20.84	13.63
10.44	12.62	20.88	13.63
10.48	12.52	20.92	13.63
10.53	12.52	20.97	13.63
10.57	12.62	20.98	13.63
10.61	12.52	21.03	13.63
10.63	12.52		

---

SOLUTION

Pumping Test  
 Aquifer Model: Unconfined  
 Solution Method: Neuman

---

VISUAL ESTIMATION RESULTS

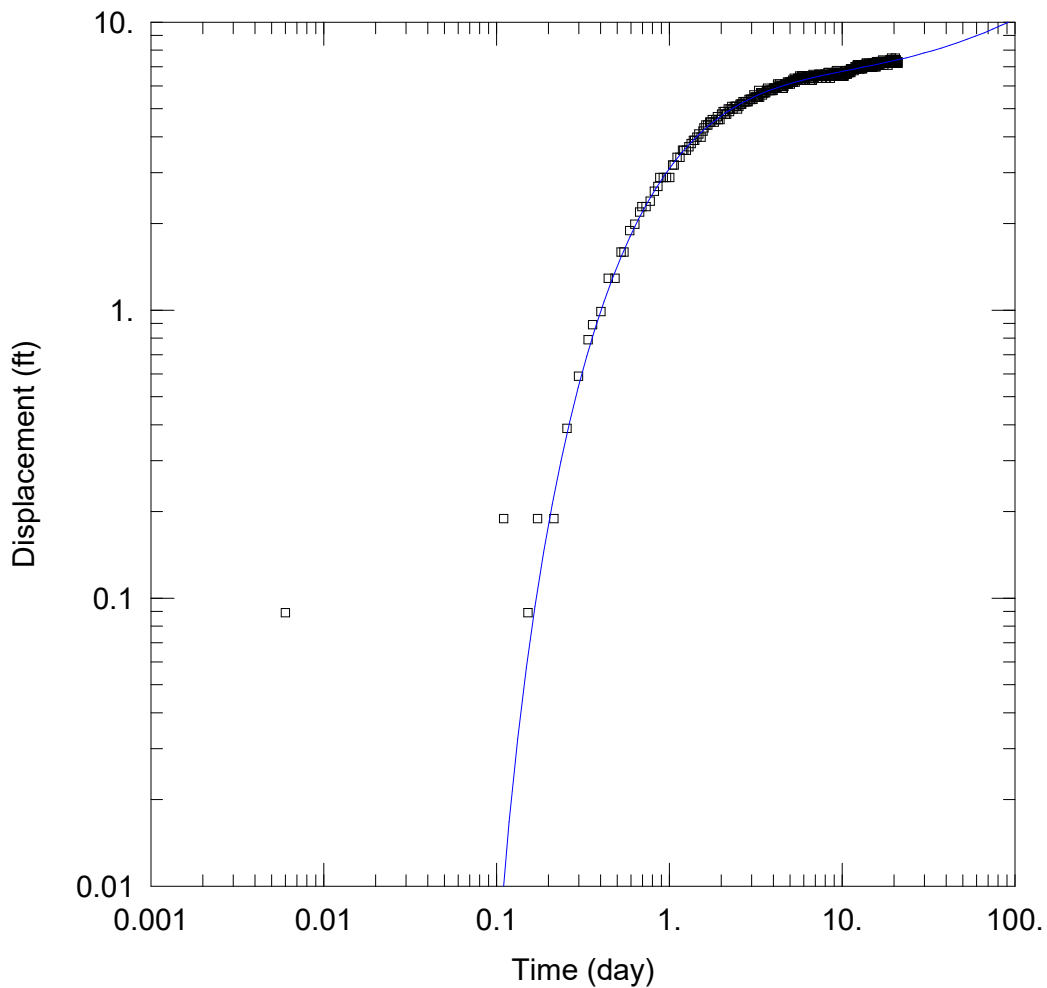
Estimated Parameters

<u>Parameter</u>	<u>Estimate</u>	
T	5233.2	ft <sup>2</sup> /day
S	0.0007326	
Sy	0.01017	
β	0.01709	

K = T/b = 1.047 ft/day (0.0003692 cm/sec)  
 Ss = S/b = 1.465E-7 1/ft

**APPENDIX G**

**AQTESOLV OUTPUT FOR PM-5 RECOVERY ANALYSIS**



WELL TEST ANALYSIS

Data Set: D:\...\PM-5 Data Recovery.aqt  
 Date: 07/18/24

Time: 17:42:06

PROJECT INFORMATION

Test Well: PM-4

AQUIFER DATA

Saturated Thickness: 5000. ft

WELL DATA

Pumping Wells

Observation Wells

Well Name	X (ft)	Y (ft)	Well Name	X (ft)	Y (ft)
PM-4	0	0	□ PM-5 recovery	4651	0

SOLUTION

Aquifer Model: Unconfined

Solution Method: Neuman

T = 7303.3 ft<sup>2</sup>/day

S = 0.0006898

Sy = 0.008996

β = 0.0348

Data Set: D:\hugo\_\Downloads\LANL NM PROJECT\PM-4 Aquifer test\AQTESOLV files\PM-5 Data Recovery.aqt  
Date: 07/18/24  
Time: 17:42:16

---

PROJECT INFORMATION

Test Well: PM-4

---

AQUIFER DATA

Saturated Thickness: 5000. ft  
Anisotropy Ratio (Kz/Kr): 0.04022

---

PUMPING WELL DATA

No. of pumping wells: 1

Pumping Well No. 1: PM-4

X Location: 0. ft  
Y Location: 0. ft

Casing Radius: 0.6667 ft  
Well Radius: 1.083 ft

Partially Penetrating Well  
Depth to Top of Screen: 177.6 ft  
Depth to Bottom of Screen: 1771.6 ft

No. of pumping periods: 1

<u>Pumping Period Data</u>	
<u>Time (day)</u>	<u>Rate (gal/min)</u>
0.	1494.

---

OBSERVATION WELL DATA

No. of observation wells: 1

Observation Well No. 1: PM-5 recovery

X Location: 4651. ft  
Y Location: 0. ft

Radial distance from PM-4: 4651. ft

Partially Penetrating Well  
Depth to Top of Screen: 195.3 ft  
Depth to Bottom of Screen: 1827.3 ft

No. of Observations: 566

<u>Observation Data</u>			
<u>Time (day)</u>	<u>Displacement (ft)</u>	<u>Time (day)</u>	<u>Displacement (ft)</u>

---

0.006	0.089	10.57	6.791
0.11	0.189	10.61	6.691
0.152	0.089	10.65	6.691
0.173	0.189	10.69	6.691
0.215	0.189	10.72	6.591
0.256	0.389	10.76	6.691
0.298	0.589	10.8	6.691
0.34	0.789	10.84	6.691
0.36	0.889	10.86	6.791
0.402	0.989	10.9	6.791
0.444	1.289	10.94	6.791
0.485	1.289	10.98	6.691
0.527	1.589	11.03	6.691
0.548	1.589	11.05	6.791
0.59	1.889	11.09	6.791
0.631	1.989	11.13	6.791
0.673	2.189	11.17	6.791
0.694	2.289	11.22	6.891
0.735	2.289	11.23	6.691
0.777	2.389	11.28	6.791
0.819	2.589	11.32	6.891
0.86	2.689	11.36	6.891
0.881	2.889	11.38	6.891
0.923	2.889	11.42	6.891
0.965	2.889	11.47	6.891
1.006	2.889	11.51	6.891
1.048	3.189	11.55	6.891
1.069	3.189	11.57	6.891
1.11	3.39	11.61	6.891
1.152	3.39	11.65	6.891
1.194	3.59	11.69	6.891
1.215	3.59	11.73	6.791
1.256	3.59	11.76	6.891
1.298	3.69	11.8	6.891
1.34	3.79	11.84	6.891
1.381	3.89	11.88	6.991
1.402	3.89	11.9	6.891
1.444	3.99	11.94	6.891
1.485	4.09	11.98	6.891
1.527	3.99	12.03	6.991
1.569	4.19	12.07	6.891
1.59	4.29	12.09	6.891
1.631	4.39	12.13	6.891
1.673	4.39	12.17	6.991
1.715	4.49	12.22	6.991
1.735	4.49	12.26	7.091
1.777	4.59	12.28	7.091
1.819	4.49	12.32	7.091
1.86	4.59	12.36	7.091
1.902	4.69	12.4	6.991
1.923	4.59	12.42	7.091
1.965	4.59	12.47	7.091
2.006	4.79	12.51	6.991
2.048	4.89	12.55	6.991



<u>Time (day)</u>	<u>Displacement (ft)</u>	<u>Time (day)</u>	<u>Displacement (ft)</u>
2.09	4.89	12.59	6.891
2.11	4.79	12.61	7.091
2.152	4.79	12.65	6.991
2.194	4.99	12.69	6.891
2.235	4.89	12.73	7.091
2.256	4.99	12.78	7.091
2.298	5.09	12.8	6.991
2.34	4.99	12.84	6.891
2.381	5.09	12.88	6.991
2.423	5.09	12.92	7.091
2.444	5.09	12.94	6.991
2.485	4.99	12.98	7.091
2.527	5.09	13.03	7.091
2.569	5.19	13.07	6.891
2.61	5.19	13.11	6.991
2.631	5.19	13.13	6.991
2.673	5.29	13.17	6.891
2.715	5.29	13.22	6.991
2.756	5.29	13.26	6.991
2.777	5.29	13.3	6.991
2.819	5.29	13.32	6.991
2.86	5.29	13.36	6.991
2.902	5.39	13.4	7.091
2.944	5.39	13.44	6.991
2.965	5.39	13.47	6.991
3.006	5.39	13.51	6.991
3.048	5.39	13.55	6.991
3.09	5.59	13.59	6.991
3.131	5.49	13.63	7.091
3.152	5.49	13.65	6.991
3.194	5.49	13.69	7.091
3.235	5.49	13.73	6.991
3.277	5.49	13.78	7.091
3.298	5.79	13.82	7.191
3.34	5.49	13.84	7.191
3.381	5.69	13.88	7.091
3.423	5.69	13.92	6.991
3.465	5.59	13.97	6.991
3.485	5.69	13.98	6.991
3.527	5.69	14.03	6.991
3.569	5.69	14.07	6.991
3.61	5.69	14.11	7.091
3.652	5.79	14.15	7.091
3.673	5.79	14.17	7.091
3.715	5.89	14.22	7.091
3.756	5.79	14.26	7.091
3.798	5.79	14.3	7.191
3.819	5.79	14.34	6.991
3.86	5.79	14.36	6.991
3.902	5.79	14.4	7.091
3.944	5.79	14.44	7.091
3.985	5.79	14.48	7.091
4.006	5.89	14.51	7.091

<u>Time (day)</u>	<u>Displacement (ft)</u>	<u>Time (day)</u>	<u>Displacement (ft)</u>
4.048	5.89	14.55	7.091
4.09	5.89	14.59	7.091
4.131	5.89	14.63	7.091
4.173	5.89	14.67	7.091
4.194	5.89	14.69	6.991
4.235	6.09	14.73	7.091
4.277	5.99	14.78	7.091
4.319	5.99	14.82	7.091
4.34	6.09	14.86	7.191
4.381	5.99	14.88	7.091
4.423	5.99	14.92	7.091
4.465	5.99	14.97	6.991
4.506	5.99	15.01	7.091
4.527	5.89	15.03	6.991
4.569	5.89	15.07	7.091
4.61	5.99	15.11	6.991
4.652	6.09	15.15	6.991
4.694	6.09	15.19	7.191
4.715	6.09	15.22	7.091
4.756	6.09	15.26	7.091
4.798	6.09	15.3	7.091
4.84	6.19	15.34	7.091
4.86	6.09	15.38	7.091
4.902	6.09	15.4	7.091
4.944	6.19	15.44	7.091
4.985	6.19	15.48	7.091
5.027	6.09	15.53	6.991
5.048	6.19	15.55	7.091
5.09	6.19	15.59	7.191
5.131	6.19	15.63	7.091
5.173	6.29	15.67	7.091
5.215	6.19	15.72	6.991
5.235	6.19	15.73	7.091
5.277	6.39	15.78	7.191
5.319	6.29	15.82	7.291
5.36	6.19	15.86	7.091
5.381	6.29	15.9	7.191
5.423	6.29	15.92	7.191
5.465	6.29	15.97	7.191
5.506	6.29	16.01	7.091
5.548	6.39	16.05	7.191
5.569	6.29	16.07	7.091
5.61	6.29	16.11	7.291
5.652	6.39	16.15	7.191
5.694	6.49	16.19	7.191
5.735	6.29	16.23	7.091
5.756	6.39	16.26	7.191
5.798	6.29	16.3	7.191
5.84	6.49	16.34	7.191
5.881	6.49	16.38	7.191
5.902	6.49	16.42	7.191
5.944	6.39	16.44	7.091
5.985	6.39	16.48	7.191

---

<u>Time (day)</u>	<u>Displacement (ft)</u>	<u>Time (day)</u>	<u>Displacement (ft)</u>
6.027	6.39	16.53	7.091
6.069	6.39	16.57	7.191
6.09	6.39	16.59	7.191
6.131	6.29	16.63	7.191
6.173	6.39	16.67	7.291
6.215	6.49	16.72	7.291
6.256	6.39	16.76	7.291
6.277	6.49	16.78	7.291
6.319	6.49	16.82	7.291
6.36	6.49	16.86	7.191
6.402	6.49	16.9	7.291
6.423	6.39	16.94	7.291
6.465	6.39	16.97	7.291
6.506	6.39	17.01	7.291
6.548	6.29	17.05	7.291
6.59	6.39	17.09	7.291
6.61	6.39	17.11	7.191
6.652	6.39	17.15	7.291
6.694	6.29	17.19	7.191
6.735	6.29	17.23	7.291
6.777	6.49	17.26	7.391
6.798	6.59	17.28	7.191
6.84	6.49	17.32	7.291
6.881	6.49	17.36	7.291
6.923	6.49	17.38	7.191
6.944	6.49	17.42	7.091
6.985	6.49	17.47	7.191
7.027	6.49	17.51	7.291
7.069	6.49	17.55	7.191
7.11	6.49	17.57	7.291
7.131	6.49	17.61	7.291
7.173	6.49	17.65	7.291
7.215	6.49	17.69	7.291
7.256	6.49	17.73	7.291
7.298	6.59	17.76	7.291
7.319	6.49	17.8	7.291
7.36	6.59	17.84	7.291
7.402	6.59	17.88	7.291
7.444	6.49	17.9	7.291
7.465	6.49	17.94	7.291
7.506	6.49	17.98	7.191
7.548	6.59	18.03	7.191
7.59	6.49	18.07	7.191
7.631	6.39	18.09	7.191
7.652	6.39	18.13	7.191
7.694	6.39	18.17	7.291
7.735	6.49	18.22	7.191
7.777	6.49	18.26	7.291
7.819	6.49	18.28	7.291
7.84	6.49	18.32	7.291
7.881	6.49	18.36	7.291
7.923	6.59	18.4	7.191
7.965	6.59	18.42	7.291

<u>Time (day)</u>	<u>Displacement (ft)</u>	<u>Time (day)</u>	<u>Displacement (ft)</u>
7.985	6.59	18.47	7.091
8.027	6.39	18.51	7.191
8.069	6.49	18.55	7.291
8.11	6.39	18.59	7.291
8.152	6.49	18.61	7.291
8.173	6.49	18.65	7.291
8.215	6.49	18.69	7.291
8.256	6.49	18.73	7.191
8.298	6.69	18.78	7.291
8.34	6.59	18.8	7.291
8.36	6.69	18.84	7.291
8.402	6.49	18.88	7.391
8.444	6.49	18.92	7.291
8.485	6.49	18.94	7.291
8.506	6.49	18.98	7.291
8.548	6.39	19.03	7.291
8.59	6.49	19.07	7.291
8.631	6.59	19.11	7.191
8.652	6.49	19.13	7.391
8.673	6.59	19.17	7.291
8.715	6.59	19.22	7.391
8.756	6.49	19.26	7.391
8.777	6.59	19.3	7.391
8.819	6.49	19.32	7.491
8.86	6.59	19.36	7.291
8.902	6.59	19.4	7.291
8.944	6.59	19.44	7.391
8.965	6.59	19.47	7.391
9.006	6.59	19.51	7.391
9.048	6.59	19.55	7.291
9.09	6.49	19.59	7.391
9.131	6.49	19.63	7.391
9.152	6.59	19.65	7.391
9.194	6.69	19.69	7.391
9.235	6.69	19.73	7.391
9.277	6.79	19.78	7.391
9.298	6.69	19.82	7.391
9.34	6.69	19.84	7.391
9.381	6.59	19.88	7.391
9.423	6.691	19.92	7.391
9.465	6.691	19.97	7.291
9.485	6.691	19.98	7.391
9.527	6.591	20.03	7.391
9.569	6.591	20.07	7.391
9.61	6.591	20.11	7.391
9.652	6.591	20.15	7.291
9.673	6.591	20.17	7.391
9.715	6.591	20.22	7.391
9.756	6.491	20.26	7.391
9.798	6.591	20.3	7.391
9.819	6.591	20.34	7.391
9.86	6.491	20.36	7.491
9.902	6.491	20.4	7.291

Time (day)	Displacement (ft)	Time (day)	Displacement (ft)
9.944	6.491	20.44	7.291
9.985	6.491	20.48	7.391
10.01	6.591	20.51	7.291
10.05	6.491	20.55	7.391
10.09	6.491	20.59	7.291
10.13	6.491	20.63	7.291
10.17	6.591	20.67	7.191
10.19	6.591	20.69	7.191
10.23	6.591	20.73	7.291
10.28	6.491	20.78	7.291
10.32	6.691	20.82	7.191
10.34	6.691	20.86	7.191
10.38	6.691	20.88	7.291
10.42	6.591	20.92	7.191
10.47	6.791	20.97	7.191
10.51	6.691	21.01	7.191
10.53	6.591	21.03	7.291

SOLUTION

Pumping Test  
 Aquifer Model: Unconfined  
 Solution Method: Neuman

VISUAL ESTIMATION RESULTS

Estimated Parameters

Parameter	Estimate	
T	1568.9	ft <sup>2</sup> /day
S	0.0002346	
Sy	0.02016	
β	0.1946	

K = T/b = 0.3138 ft/day (0.0001107 cm/sec)  
 Ss = S/b = 4.693E-8 1/ft

AUTOMATIC ESTIMATION RESULTS

Estimated Parameters

Parameter	Estimate	Std. Error	Approx. C.I.	t-Ratio	
T	7303.3	486.2	+/- 954.9	15.02	ft <sup>2</sup> /day
S	0.0006898	2.156E-5	+/- 4.234E-5	32.	
Sy	0.008996	0.000584	+/- 0.001147	15.4	
β	0.0348	0.003504	+/- 0.006882	9.931	

C.I. is approximate 95% confidence interval for parameter  
 t-ratio = estimate/std. error  
 Estimation window: 0.2 to 22 day

K = T/b = 1.461 ft/day (0.0005153 cm/sec)  
 Ss = S/b = 1.38E-7 1/ft

Parameter Correlations

	<u>T</u>	<u>S</u>	<u>Sy</u>	<u>β</u>
T	1.00	0.98	-0.91	-1.00
S	0.98	1.00	-0.85	-0.98
Sy	-0.91	-0.85	1.00	0.90
β	-1.00	-0.98	0.90	1.00

Residual Statistics

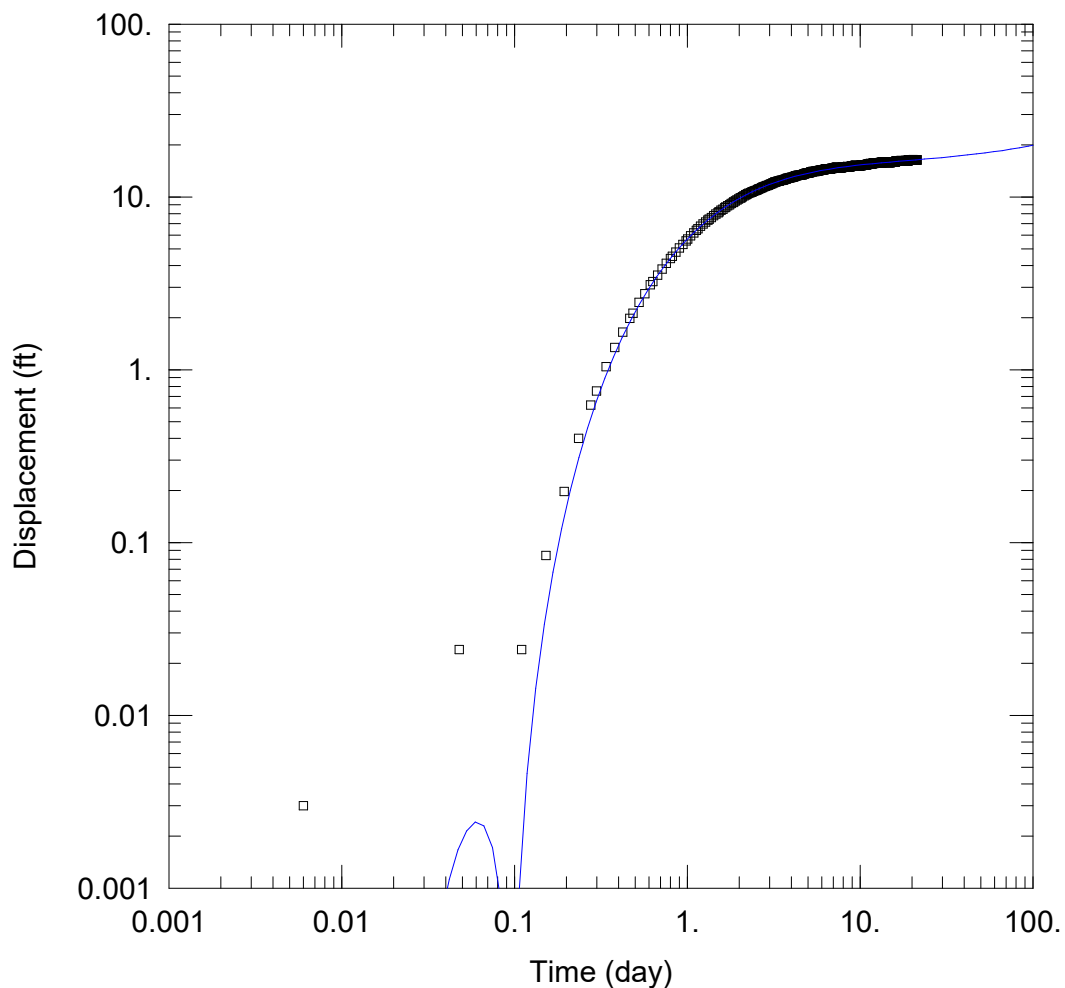
for weighted residuals

Sum of Squares... 4.452 ft<sup>2</sup>  
 Variance ..... 0.007978 ft<sup>2</sup>  
 Std. Deviation ..... 0.08932 ft  
 Mean ..... 0.0001997 ft  
 No. of Residuals .. 562  
 No. of Estimates .. 4

Estimation window from 0.2 to 22 day.

**APPENDIX H**

**AQTESOLV OUTPUT FOR R-20 S3 RECOVERY ANALYSIS**



WELL TEST ANALYSIS

Data Set: D:\...\R20-S3 Data Recovery.aqt

Date: 07/18/24

Time: 17:46:04

PROJECT INFORMATION

Test Well: PM-4

AQUIFER DATA

Saturated Thickness: 5000. ft

WELL DATA

Pumping Wells

Observation Wells

Well Name	X (ft)	Y (ft)
PM-4	0	0

Well Name	X (ft)	Y (ft)
□ R20-S3 recovery	5508	0

SOLUTION

Aquifer Model: Unconfined

Solution Method: Neuman

T = 3339.3 ft<sup>2</sup>/day

S = 0.0002912

Sy = 0.006684

β = 0.01952



Data Set: D:\hugo\_\Downloads\LANL NM PROJECT\PM-4 Aquifer test\AQTESOLV files\R20-S3 Data Recovery.aq  
Date: 07/18/24  
Time: 17:46:16

---

PROJECT INFORMATION

Test Well: PM-4

---

AQUIFER DATA

Saturated Thickness: 5000. ft  
Anisotropy Ratio (Kz/Kr): 0.01609

---

PUMPING WELL DATA

No. of pumping wells: 1

Pumping Well No. 1: PM-4

X Location: 0. ft  
Y Location: 0. ft

Casing Radius: 0.6667 ft  
Well Radius: 1.083 ft

Partially Penetrating Well  
Depth to Top of Screen: 177.6 ft  
Depth to Bottom of Screen: 1771.6 ft

No. of pumping periods: 1

<u>Pumping Period Data</u>	
<u>Time (day)</u>	<u>Rate (gal/min)</u>
0.	1494.

---

OBSERVATION WELL DATA

No. of observation wells: 1

Observation Well No. 1: R20-S3 recovery

X Location: 5508. ft  
Y Location: 0. ft

Radial distance from PM-4: 5508. ft

Partially Penetrating Well  
Depth to Top of Screen: 475.5 ft  
Depth to Bottom of Screen: 483.2 ft

No. of Observations: 576

<u>Observation Data</u>			
<u>Time (day)</u>	<u>Displacement (ft)</u>	<u>Time (day)</u>	<u>Displacement (ft)</u>

---

0.006	0.003	10.69	15.3
0.048	0.024	10.73	15.31
0.09	0.	10.78	15.32
0.11	0.024	10.8	15.33
0.152	0.084	10.84	15.34
0.194	0.197	10.88	15.36
0.235	0.401	10.92	15.38
0.277	0.625	10.97	15.41
0.298	0.752	10.98	15.4
0.34	1.043	11.03	15.42
0.381	1.347	11.07	15.44
0.423	1.651	11.11	15.43
0.465	1.98	11.15	15.45
0.485	2.125	11.17	15.46
0.527	2.452	11.22	15.46
0.569	2.758	11.26	15.49
0.61	3.101	11.3	15.49
0.631	3.238	11.32	15.54
0.673	3.532	11.36	15.54
0.715	3.828	11.4	15.56
0.756	4.128	11.44	15.58
0.798	4.408	11.48	15.59
0.819	4.531	11.51	15.57
0.86	4.799	11.55	15.58
0.902	5.07	11.59	15.56
0.944	5.32	11.63	15.57
0.985	5.568	11.67	15.56
1.006	5.712	11.69	15.56
1.048	5.952	11.73	15.56
1.09	6.196	11.78	15.59
1.131	6.418	11.82	15.6
1.152	6.535	11.84	15.61
1.194	6.756	11.88	15.63
1.235	6.96	11.92	15.64
1.277	7.149	11.97	15.65
1.319	7.351	12.01	15.68
1.34	7.439	12.03	15.66
1.381	7.603	12.07	15.65
1.423	7.777	12.11	15.67
1.465	7.952	12.15	15.66
1.506	8.09	12.19	15.68
1.527	8.196	12.22	15.68
1.569	8.369	12.26	15.68
1.61	8.499	12.3	15.7
1.652	8.655	12.34	15.71
1.673	8.738	12.36	15.7
1.715	8.887	12.4	15.7
1.756	9.027	12.44	15.7
1.798	9.144	12.48	15.69
1.84	9.292	12.53	15.72
1.86	9.342	12.55	15.7
1.902	9.47	12.59	15.68
1.944	9.592	12.63	15.7
1.985	9.72	12.67	15.7

<u>Time (day)</u>	<u>Displacement (ft)</u>	<u>Time (day)</u>	<u>Displacement (ft)</u>
2.027	9.832	12.72	15.69
2.048	9.909	12.73	15.68
2.09	10.04	12.78	15.72
2.131	10.15	12.82	15.71
2.173	10.27	12.86	15.73
2.194	10.31	12.88	15.74
2.235	10.42	12.92	15.75
2.277	10.5	12.97	15.78
2.319	10.58	13.01	15.78
2.36	10.66	13.05	15.78
2.381	10.72	13.07	15.77
2.423	10.78	13.11	15.79
2.465	10.86	13.15	15.78
2.506	10.94	13.19	15.8
2.548	11.03	13.23	15.79
2.569	11.04	13.26	15.79
2.61	11.13	13.3	15.82
2.652	11.21	13.34	15.83
2.694	11.31	13.38	15.85
2.715	11.34	13.4	15.83
2.756	11.43	13.44	15.86
2.798	11.5	13.48	15.85
2.84	11.55	13.53	15.86
2.881	11.62	13.57	15.84
2.902	11.65	13.59	15.87
2.944	11.7	13.63	15.87
2.985	11.77	13.67	15.87
3.027	11.84	13.72	15.85
3.069	11.91	13.76	15.86
3.09	11.96	13.78	15.88
3.131	12.02	13.82	15.88
3.173	12.11	13.86	15.9
3.215	12.17	13.9	15.9
3.235	12.2	13.92	15.89
3.277	12.26	13.97	15.9
3.319	12.3	14.01	15.9
3.36	12.35	14.05	15.9
3.402	12.36	14.09	15.87
3.423	12.41	14.11	15.89
3.465	12.44	14.15	15.87
3.506	12.46	14.19	15.88
3.548	12.5	14.23	15.91
3.59	12.52	14.28	15.88
3.61	12.55	14.3	15.87
3.652	12.61	14.34	15.88
3.694	12.66	14.38	15.87
3.735	12.71	14.42	15.86
3.756	12.75	14.44	15.87
3.798	12.81	14.48	15.86
3.84	12.84	14.53	15.83
3.881	12.9	14.57	15.81
3.923	12.91	14.61	15.83
3.944	12.95	14.63	15.83

<u>Time (day)</u>	<u>Displacement (ft)</u>	<u>Time (day)</u>	<u>Displacement (ft)</u>
3.985	12.97	14.67	15.82
4.027	12.99	14.72	15.8
4.069	13.02	14.76	15.81
4.11	13.06	14.8	15.81
4.131	13.1	14.82	15.83
4.173	13.13	14.86	15.84
4.215	13.21	14.9	15.85
4.256	13.23	14.94	15.84
4.277	13.26	14.97	15.83
4.319	13.28	15.01	15.84
4.36	13.31	15.05	15.84
4.402	13.34	15.09	15.88
4.444	13.35	15.13	15.88
4.465	13.35	15.15	15.88
4.506	13.37	15.19	15.89
4.548	13.4	15.23	15.93
4.59	13.42	15.28	15.92
4.631	13.45	15.32	15.93
4.652	13.48	15.34	15.95
4.694	13.52	15.38	15.94
4.735	13.54	15.42	15.91
4.777	13.61	15.47	15.91
4.798	13.63	15.48	15.92
4.84	13.68	15.53	15.94
4.881	13.7	15.57	15.92
4.923	13.73	15.61	15.91
4.965	13.76	15.65	15.93
4.985	13.75	15.67	15.96
5.027	13.77	15.72	15.95
5.069	13.82	15.76	15.96
5.11	13.83	15.8	15.98
5.152	13.87	15.84	15.95
5.173	13.89	15.86	15.98
5.215	13.95	15.9	15.97
5.256	13.99	15.94	15.96
5.298	14.	15.98	15.98
5.319	14.02	16.01	16.01
5.36	14.04	16.05	16.03
5.402	14.03	16.09	16.04
5.444	14.06	16.13	16.06
5.485	14.06	16.17	16.09
5.506	14.05	16.19	16.12
5.548	14.07	16.23	16.09
5.59	14.08	16.28	16.11
5.631	14.08	16.32	16.12
5.673	14.1	16.36	16.13
5.694	14.13	16.38	16.13
5.735	14.16	16.42	16.12
5.777	14.2	16.47	16.11
5.819	14.24	16.51	16.08
5.84	14.23	16.53	16.1
5.881	14.26	16.57	16.12
5.923	14.28	16.61	16.09

<u>Time (day)</u>	<u>Displacement (ft)</u>	<u>Time (day)</u>	<u>Displacement (ft)</u>
5.965	14.28	16.65	16.13
6.006	14.28	16.69	16.13
6.027	14.31	16.72	16.13
6.069	14.34	16.76	16.15
6.11	14.34	16.8	16.13
6.152	14.35	16.84	16.14
6.194	14.39	16.88	16.13
6.215	14.41	16.9	16.15
6.256	14.45	16.94	16.13
6.298	14.47	16.98	16.13
6.34	14.52	17.03	16.15
6.36	14.5	17.05	16.16
6.402	14.5	17.09	16.19
6.444	14.51	17.13	16.17
6.485	14.49	17.17	16.19
6.527	14.48	17.19	16.17
6.548	14.47	17.22	16.21
6.59	14.46	17.26	16.21
6.631	14.46	17.3	16.19
6.673	14.48	17.32	16.2
6.715	14.5	17.36	16.17
6.735	14.52	17.4	16.17
6.777	14.57	17.44	16.18
6.819	14.6	17.48	16.14
6.86	14.62	17.51	16.15
6.881	14.62	17.55	16.14
6.923	14.65	17.59	16.13
6.965	14.64	17.63	16.14
7.006	14.66	17.67	16.15
7.048	14.69	17.69	16.13
7.069	14.68	17.73	16.14
7.11	14.69	17.78	16.17
7.152	14.73	17.82	16.17
7.194	14.75	17.84	16.15
7.235	14.79	17.88	16.16
7.256	14.81	17.92	16.16
7.298	14.85	17.97	16.15
7.34	14.81	18.01	16.17
7.381	14.83	18.03	16.15
7.402	14.81	18.07	16.18
7.444	14.8	18.11	16.15
7.485	14.79	18.15	16.17
7.527	14.78	18.19	16.19
7.569	14.77	18.22	16.18
7.59	14.74	18.26	16.2
7.631	14.73	18.3	16.21
7.673	14.72	18.34	16.2
7.715	14.74	18.36	16.2
7.756	14.74	18.4	16.2
7.777	14.79	18.44	16.2
7.819	14.8	18.48	16.18
7.86	14.8	18.53	16.18
7.902	14.84	18.55	16.15

---

<u>Time (day)</u>	<u>Displacement (ft)</u>	<u>Time (day)</u>	<u>Displacement (ft)</u>
7.923	14.82	18.59	16.16
7.965	14.84	18.63	16.16
8.006	14.85	18.67	16.16
8.048	14.85	18.72	16.2
8.09	14.85	18.73	16.21
8.11	14.86	18.78	16.23
8.152	14.86	18.82	16.24
8.194	14.89	18.86	16.23
8.235	14.92	18.88	16.25
8.277	14.91	18.92	16.24
8.298	14.94	18.97	16.23
8.34	14.96	19.01	16.25
8.381	14.99	19.05	16.26
8.423	14.99	19.07	16.26
8.444	15.	19.11	16.26
8.485	14.97	19.15	16.27
8.527	14.98	19.19	16.3
8.569	14.96	19.23	16.32
8.59	14.97	19.26	16.34
8.61	14.96	19.3	16.35
8.652	14.96	19.34	16.32
8.694	14.98	19.38	16.36
8.715	14.96	19.4	16.35
8.756	14.98	19.44	16.33
8.798	14.99	19.48	16.3
8.84	15.03	19.53	16.28
8.881	15.05	19.57	16.3
8.902	15.04	19.59	16.29
8.944	15.05	19.63	16.28
8.985	15.07	19.67	16.31
9.027	15.09	19.72	16.29
9.069	15.1	19.76	16.33
9.09	15.1	19.78	16.35
9.131	15.09	19.82	16.35
9.173	15.12	19.86	16.35
9.215	15.12	19.9	16.34
9.235	15.13	19.92	16.34
9.277	15.17	19.97	16.34
9.319	15.2	20.01	16.36
9.36	15.22	20.05	16.36
9.402	15.21	20.09	16.35
9.423	15.23	20.11	16.37
9.465	15.22	20.15	16.35
9.506	15.2	20.19	16.38
9.548	15.18	20.23	16.41
9.59	15.14	20.28	16.4
9.61	15.14	20.3	16.4
9.652	15.12	20.34	16.42
9.694	15.11	20.38	16.39
9.735	15.08	20.42	16.38
9.756	15.1	20.44	16.35
9.798	15.13	20.48	16.34
9.84	15.14	20.53	16.31

Time (day)	Displacement (ft)	Time (day)	Displacement (ft)
9.881	15.15	20.57	16.3
9.923	15.17	20.61	16.32
9.944	15.16	20.63	16.27
9.985	15.17	20.67	16.28
10.03	15.19	20.72	16.27
10.07	15.18	20.76	16.3
10.11	15.19	20.8	16.31
10.13	15.18	20.82	16.33
10.17	15.21	20.86	16.31
10.22	15.22	20.9	16.31
10.26	15.21	20.94	16.3
10.28	15.25	20.97	16.3
10.32	15.25	21.01	16.29
10.36	15.3	21.05	16.3
10.4	15.33	21.09	16.31
10.44	15.32	21.13	16.32
10.47	15.34	21.15	16.32
10.51	15.33	21.19	16.34
10.55	15.3	21.23	16.38
10.59	15.32	21.28	16.38
10.63	15.31	21.32	16.4
10.65	15.29	21.34	16.39

SOLUTION

Pumping Test  
 Aquifer Model: Unconfined  
 Solution Method: Neuman

VISUAL ESTIMATION RESULTS

Estimated Parameters

Parameter	Estimate	
T	3849.1	ft <sup>2</sup> /day
S	0.0003019	
Sy	0.004026	
β	0.01407	

$K = T/b = 0.7698$  ft/day (0.0002716 cm/sec)  
 $Ss = S/b = 6.038E-8$  1/ft

AUTOMATIC ESTIMATION RESULTS

Estimated Parameters

Parameter	Estimate	Std. Error	Approx. C.I.	t-Ratio	
T	3339.3	52.84	+/- 103.8	63.2	ft <sup>2</sup> /day
S	0.0002912	2.235E-6	+/- 4.39E-6	130.3	
Sy	0.006684	0.0001379	+/- 0.0002709	48.46	
β	0.01952	0.0004833	+/- 0.0009492	40.39	

C.I. is approximate 95% confidence interval for parameter

t-ratio = estimate/std. error

Estimation window: 0.2 to 21 day

$K = T/b = 0.6679 \text{ ft/day (0.0002356 cm/sec)}$

$S_s = S/b = 5.824E-8 \text{ 1/ft}$

Parameter Correlations

	<u>T</u>	<u>S</u>	<u>Sy</u>	<u>β</u>
T	1.00	0.98	0.14	-1.00
S	0.98	1.00	0.27	-0.98
Sy	0.14	0.27	1.00	-0.18
β	-1.00	-0.98	-0.18	1.00

Residual Statistics

for weighted residuals

Sum of Squares... 1.943 ft<sup>2</sup>  
Variance ..... 0.003495 ft<sup>2</sup>  
Std. Deviation ..... 0.05912 ft  
Mean ..... 0.0008341 ft  
No. of Residuals .. 560  
No. of Estimates .. 4

Estimation window from 0.2 to 21 day.



## **ATTACHMENT 5**

**Analyses of Aquifer Test Data for PM-3 to Determine Horizontal ( $K_h$ ) and Vertical Hydraulic Conductivities ( $K_v$ ) at R-35a and Use of Steady State Drawdowns at R-35a and R-35b to Determine  $K_h$  Values and Comparison with the Neptune  $K_h$  Values, Los Alamos, New Mexico**

---

This page intentionally left blank.

## Executive Summary

In Attachment 5, horizontal hydraulic conductivity ( $K_h$ ) and vertical hydraulic conductivity ( $K_v$ ) at R-35a are determined using transient drawdown data. Also with the use of steady state drawdowns at R-35a and R-35b the  $K_h$  values are determined.

The results for the transient drawdown data analyses are given in Table 2, which shows that there is a total of two set of values determined from the Neuman (1974, 1975) method. From the values in Table 2, the conclusions drawn are as follows:

1. Based on the Neuman method, the values corresponding to drawdown and recovery for horizontal hydraulic conductivity ( $K_h$ ) are  $5.56 \text{ ft/d}$  and  $6.19 \text{ ft/d}$ , respectively, and their average is  $5.875 \text{ ft/d}$ .
2. The corresponding values of storage coefficient ( $S$ ) to drawdown and recovery are 0.001002 and 0.001032 respectively. According to the literature, storage coefficients generally vary between 0.00005 and 0.005 (e.g., Freeze and Cherry, 1979, p. 60).
3. The anisotropy  $a = K_v/K_h$  values corresponding to drawdown and recovery are 0.1437 and 0.0704, respectively. And their average is 0.12205 which close to 0.10 and this value generally is being used in practice whenever  $a = K_v/K_h$  is not available.
4. The specific yield ( $S_y$ ) values in Table 2 are not realistic. Potential reasons may be (a) the screen interval of R-35a is significantly below the water table and (b) the aquifer test period was not long enough.

From the steady state drawdown at R-35a, the  $K_h$  value was determined as  $K_h = 2.2 \text{ ft/d} = 0.000007761 \text{ m/s} = 7.76 \times 10^{-4} \text{ cm/s}$ .

From the steady state drawdown at R-35b, the  $K_h$  value was determined as  $K_h = 73.0 \text{ ft/d} = 0.000257528 \text{ m/s} = 2.58 \times 10^{-2} \text{ cm/s}$ .

The  $K_h$  values based on steady state drawdowns at R-35a and R-35b are compared with the  $K_h$  values of Neptune in Table 4. Some key points are as follows:

1. At R-35a, the  $K_h$  values of the steady state drawdown and  $K_{h-Neptune}$  values are  $2.2 \text{ ft/d}$  and  $3.1 \text{ ft/d}$ , respectively, and the  $K_{h-Neptune}/K_h$  is 1.409. Neptune described the formation name as "Tcar" whereas in Koch and Schmeer (2009, p. 54) it is described as "Tsfu".
2. At R-35b, the  $K_h$  values of the steady state drawdown and  $K_{h-Neptune}$  values are  $73.0 \text{ ft/d}$  and  $133.0 \text{ ft/d}$ , respectively, and the  $K_{h-Neptune}/K_h$  is 1.822. Both Neptune and in Koch and Schmeer (2009, p. 55) describe the formation name as "Tpf".

## Attachment 5 Contents

1.	Purpose and Data Sources .....	1
2.	Aquifer Test Procedure .....	1
3.	Wells Geometry and Initial Water Levels .....	1
4.	Measured Transient Well Drawdowns and Their Analysis.....	1
4.1	Measured Drawdown .....	1
4.2	Drawdown Data Analysis Method .....	2
4.3	Results and Discussion .....	2
5.	Measured Steady State Drawdowns and Their Analysis .....	2
5.1	Measured Steady State Drawdown Analysis at R-35a and Results.....	2
5.2	Measured Steady State Drawdown Analysis at R-35b and Results.....	3
6.	Comparisons of the Kh Values with the Kh Values of Neptune .....	4
6.1	Comparison the PM-3 Aquifer Test Kh Value and Neptune Kh Value at R-35a.....	4
6.2	Comparison of the Kh Values Based on Steady State Drawdowns at R-35a and R-35b with the Kh Values of Neptune .....	4

## Figures

- Figure 1. Drawdown versus time date at R-35a of the PM-3 aquifer test.
- Figure 2. Drawdown versus time date at R-35b of the PM-3 aquifer test.
- Figure 3. Drawdown versus time at R-35a under constant extraction constant extraction rate.
- Figure 4. Well in a confined aquifer.

## Tables

- Table 1. Wells geometry and initial water levels for the PM-3 aquifer test.
- Table 2. PM-3 aquifer test data analysis results for R-35a with the Neuman (1974, 1975) type-curve method.
- Table 3. Comparison with the  $K_h$  values of PM-3 aquifer test and Neptune at R-35a.
- Table 4. Comparison with the  $K_h$  values determined from steady state drawdowns at R-35a and R-35b determined from the Thiem (1906) method with the  $K_h$  values of Neptune.

## **Appendices**

- Appendix A Determination of Horizontal Hydraulic Conductivity Using Thiem Well Discharge Formula for R-35a Steady State Drawdown Value
- Appendix B Determination of Horizontal Hydraulic Conductivity Using Thiem Well Discharge Formula for R-35b Steady State Drawdown Value
- Appendix C AQTESOLV Output for R-35a Drawdown Analysis
- Appendix D AQTESOLV Output for R-35a Recovery Analysis

## 1. Purpose and Data Sources

The purpose of Attachment 5 is to analyze the aquifer test data of PM-3 to determine horizontal hydraulic conductivity ( $K_h$ ) and vertical hydraulic conductivity ( $K_v$ ) at R-35a and with the use of steady state drawdowns at R-35a and R-35b to determine  $K_h$  values.

The aquifer test is described in a report entitled “*Appendix E: R-35 and PM-3 Pumping Test Analysis*” sent by Susan Wacaster to Vedat Batu along with Excel files. The aforementioned report and Excel files were sent to Susan Wacaster by David Schafer in July 2024.

The wells geometry data are taken from LANL (2007) and Koch and Schmeer (2009) reports.

## 2. Aquifer Test Procedure

The aquifer test procedure is described in p. 1 of Appendix E mentioned in Section 1.0 as follows:

*“This report describes the hydraulic analysis of formation sediments at wells R-35a and R-35b located in Sandia Canyon adjacent to Los Alamos County supply well PM-3. The primary objective of the analysis was to determine the hydraulic properties of the zones screened by R-35a and R-35b, as well as the intervening aquitard between the two screen zones. Testing consisted primarily of constant-rate pumping tests conducted on R-35a and R-35b. During the tests, water levels were monitored in the two R-35 wells, several Los Alamos County supply wells, and several other R wells in the area. Monitored zones included PM-1, PM-3, PM-4, PM-5, R-5 screens 3 and 4, R-8 screens 1 and 2, R-9, R-11, R-13 and R-28.”*

## 3. Wells Geometry and Initial Water Levels

The wells geometry data and initial water levels are given in Table 1. PM-3 was the pumped well with 1,450 gpm extraction rate. The thickness of the unconfined aquifer is  $b = 5,000ft$ . Water levels were recorded at some wells mentioned in Section 2.0, but only the drawdowns data of R-35a are noise free.

## 4. Measured Transient Well Drawdowns and Their Analysis

### 4.1 Measured Drawdown

Only the drawdown data at R-35a shown in Figure 1 are in good condition without noise effects. The other ones have noise effects. The drawdown data at R-35b are shown in Figure 2, which has significant noise effects and not analyzed. The drawdown data at PM-3 extraction well itself are not available.

## 4.2 Drawdown Data Analysis Method

The drawdown and recovery data at the R-35a observation well have been analyzed with the Neuman type-curve method (Neuman, 1974, 1975) using Version 4.5 of the AQTESOLV software (HydroSOLVE, Inc., 2023).

The AQTESOLV output for the R-35a drawdown data is given in Appendix C.

The AQTESOLV output for R-35a recovery is given in Appendix D.

## 4.3 Results and Discussion

The results for the transient drawdown data analyses are given in Table 2 which shows that there is a total of two set of values determined from the Neuman (1974, 1975) method. From the values in Table 2, the conclusions drawn are as follows:

1. Based on the Neuman method, the values corresponding to drawdown and recovery for horizontal hydraulic conductivity ( $K_h$ ) are  $5.56 \text{ ft/d}$  and  $6.19 \text{ ft/d}$ , respectively, and their average is  $5.875 \text{ ft/d}$ .
2. The corresponding values of storage coefficient ( $S$ ) to drawdown and recovery are 0.001002 and 0.001032 respectively. According to the literature, storage coefficients generally vary between 0.00005 and 0.005 (e.g., Freeze and Cherry, 1979, p. 60).
3. The anisotropy  $a = K_v/K_h$  values corresponding to drawdown and recovery are 0.1437 and 0.0704, respectively. And their average is 0.12205 which is close to 0.10 and this value generally is being used in practice whenever  $a = K_v/K_h$  is not available.
4. The specific yield ( $S_y$ ) values in Table 2 are not realistic. Potential reasons may be (a) the screen interval of R-35a is significantly below the water table and (b) the aquifer test period was not long enough.

## 5. Measured Steady State Drawdowns and Their Analysis

### 5.1 Measured Steady State Drawdown Analysis at R-35a and Results

For steady state drawdown data analysis at R-35a are as follows:

$$b = 49.1 \text{ ft} = 14.9657 \text{ m} \text{ (From the reports mentioned in Section 1.0)}$$

$$s_w = 47.3 \text{ ft} = 14.417 \text{ m} \text{ (From Figure 3)}$$

$$2r_c = 2r_w = 4.375 \text{ in} = 0.3646 \text{ ft} = 0.1111 \text{ m} \text{ (LANL, 2007, p. 18, Figure 7.2-1)}$$

$$r_c = r_w = 0.1823 \text{ ft} = 0.0556 \text{ m}$$

$$Q = 21.4 \text{ gpm} \text{ (From the report mentioned in Section 1.0, p. 4)}$$

$$1 \text{ gpm} = 0.0000630902 \frac{\text{m}^3}{\text{s}}$$

$$Q = 21.4 \text{ gpm} = 21.4 \frac{\text{gallon}}{\text{day}} = (21.4 \text{ gpm}) \left( \frac{0.0000630902 \frac{\text{m}^3}{\text{s}}}{\text{gpm}} \right) = 0.00135013 \frac{\text{m}^3}{\text{s}}$$

The water level in the well before extraction is 791.0 *ft* below the ground surface (bgs). The upper end of the screen interval is 1,013.1 *ft* bgs. Therefore, the upper end of the screen interval is 222.1 *ft* below the water table and  $s_w = 47.3 \text{ ft} = 14.417 \text{ m} < 222.1 \text{ ft}$ . Therefore, Thiem (1906) equation will be used to determine the horizontal hydraulic conductivity ( $K_h$ ). Calculation details are given in Appendix A and calculated  $K_h$  value is  $K_h = 2.2 \text{ ft/d} = 0.000007761 \text{ m/s} = 7.76 \times 10^{-4} \text{ cm/s}$ .

## 5.2 Measured Steady State Drawdown Analysis at R-35b and Results

For steady state drawdown data analysis at R-35b are as follows:

$$b = 23.1 \text{ ft} = 7.04088 \text{ m} \text{ (From the reports mentioned in Section 1.0)}$$

$$s_w = 2.75 \text{ ft} = 0.8382 \text{ m} \text{ [From Appendix E (p. 46, Figure 49) mentioned in Section 1.0]}$$

$$2r_c = 2r_w = 4.375 \text{ in} = 0.3646 \text{ ft} = 0.1111 \text{ m} \text{ (LANL, 2007, p. 19, Figure 7.2-2)}$$

$$r_c = r_w = 0.1823 \text{ ft} = 0.0556 \text{ m}$$

$$Q = 22.6 \text{ gpm} \text{ [From Appendix E (p. 46, Figure 49) mentioned in Section 1.0]}$$

$$1 \text{ gpm} = 0.0000630902 \frac{\text{m}^3}{\text{s}}$$

$$Q = 22.6 \text{ gpm} = 22.6 \frac{\text{gallon}}{\text{day}} = (22.6 \text{ gpm}) \left( \frac{0.0000630902 \frac{\text{m}^3}{\text{s}}}{\text{gpm}} \right) = 0.00142588 \frac{\text{m}^3}{\text{s}}$$

The water level in the well before extraction is 787.1 *ft* below the ground surface (bgs). The upper end of the screen interval is 825.4 *ft* bgs. Therefore, the upper end of the screen interval is 38.3 *ft* below the water table and  $s_w = 2.75 \text{ ft} = 0.8382 \text{ m} < 38.3 \text{ ft}$ . Therefore, Thiem (1906) equation will be used to determine the horizontal hydraulic conductivity ( $K_h$ ). Calculation details are given in Appendix B and calculated  $K_h$  value is  $K_h = 73.0 \text{ ft/d} = 0.000257528 \text{ m/s} = 2.58 \times 10^{-3} \text{ cm/s}$ .



## 6. Comparisons of the $K_h$ Values with the $K_h$ Values of Neptune

### 6.1 Comparison the PM-3 Aquifer Test $K_h$ Value and Neptune $K_h$ Value at R-35a

The  $K_h$  values are compared with the  $K_h$  values of Neptune (Neptune and Company, 2024) determined using the pilot point method as described in Doherty (2003). The  $K_h$  values of Neptune have been provided in the following references:

Foster, L., Neptune and Company, Inc., Excel file: K and S LANL – For ITR – 5 – 6 – 24, sent by Lauren Foster of Neptune to Susan Wacaster of DOE, May 6, 2024a.

Foster, L., Neptune and Company, Inc., “Untitled Notes”, sent by Daniel Stephens, 22. pp., July 23, 2024b.

Figure 7 of Foster (2024b) was generated from the Excel file in Foster (2024a). Here are comparison results (Table 3) for the  $K_h$  values of the Neuman type-curve analysis and  $K_{h-Neptune}$  values:

1. Foster (2024a) includes 16 different  $K_{h-Neptune}$  values at R-35a between 1.8 *ft/d* and 9.2 *ft/d* and their average is 3.1 *ft/d* which is almost half of the Neuman type-curve value (5.88 *ft/d*) at R-35a.
2. Neptune described the formation name as “Tcar” whereas in Koch and Schmeer (2009, p. 54) it is described as “Tsfu”.

### 6.2 Comparison of the $K_h$ Values Based on Steady State Drawdowns at R-35a and R-35b with the $K_h$ Values of Neptune

The  $K_h$  values based on steady state drawdowns at R-35a and R-35b are compared with the  $K_h$  values of Neptune in Table 4. Some key points are as follows:

1. At R-35a, the  $K_h$  values of the steady state drawdown and  $K_{h-Neptune}$  values are 2.2 *ft/d* and 3.1 *ft/d*, respectively, and the  $K_{h-Neptune}/K_h$  is 1.409. Neptune described the formation name as “Tcar” whereas in Koch and Schmeer (2009, p. 54) it is described as “Tsfu”.

At R-35b, the  $K_h$  values of the steady state drawdown and  $K_{h-Neptune}$  values are 73.0 *ft/d* and 133.0 *ft/d*, respectively, and the  $K_{h-Neptune}/K_h$  is 1.822. Both Neptune and in Koch and Schmeer (2009, p. 55) describe the formation name as “Tpf”.

## References

Batu, V., *Fluid Mechanics and Hydraulics: Illustrative Worked Examples of Surface and Subsurface Flows*, Taylor & Francis CRC Press, 1,240 pp., Boca Raton, Florida, 2024.

- Bear, J., *Hydraulics of Groundwater*, McGraw-Hill Inc., 569 pp., New York, 1979.
- Chertousov, M.D., *Hydraulics* (in Russian), Gosenergouzdat, 630 pp., Moscow, Russia, 1962.
- De Filippi, F.M., S. Iacurto, F. Ferranti, and G. Sappa, "Hydraulic Conductivity Estimation Using Low-Flow Purging Data Elaboration in Contaminated Sites," *Water*, Vol. 12, pp. 898-914, 2020.
- HydroSOLVE, Inc., AQTESOLV: Advanced Aquifer Test Analysis Software, v4.5., , Reston, Virginia, 2023.
- Doherty, J., "Ground Water Model Calibration Using Pilot Points and Regularization," *Ground Water*, Vol. 41, No. 2, pp. 170-177, March-April, 2003.
- Foster, L., Neptune and Company, Inc., Excel file: K and S LANL – For ITR – 5 – 6 – 24, sent by Lauren Foster of Neptune to Susan Wacaster of DOE, May 6, 2024a.
- Foster, L., Neptune and Company, Inc., "Untitled Notes", sent by Daniel Stephens, 22. pp., July 23, 2024b.
- Freeze, R.A., And J.A. Cherry, *Groundwater*, Prentice-Hall, Inc., Englewood Cliffs, New Jersey, 604, pp., 1979.
- Koch, R.J., and S. Schmeer, *Groundwater Status Report for 2008: Los Alamos National Laboratory*, LA-14397-PR, Progress Report, 248 pp., March, 2009.
- LANL, *Completion Report for Regional Aquifer Wells R-35a and R-35b*, LA-UR-07-5324, EP20007-0462, September, 2007.
- Neuman, S.P., 'Effect of Partial Penetration on Flow in Unconfined Aquifers Considering Delayed Gravity Response,' *Water Resources Research*, Vol. 10, No.2, pp. 303-312, April, 1974.
- Neuman, S.P., "Analysis of Pumping Test Data From Anisotropic Unconfined Aquifers Considering Delayed Gravity Response," *Water Resources Research*, Vol. 11, No. 2, pp. 329-342, April, 1975.
- Thiem, G., *Hydrologische Methoden* (in German), J.M. Gebhardt, Leipzig, Germany, 56 pp., 1906.

## Figures

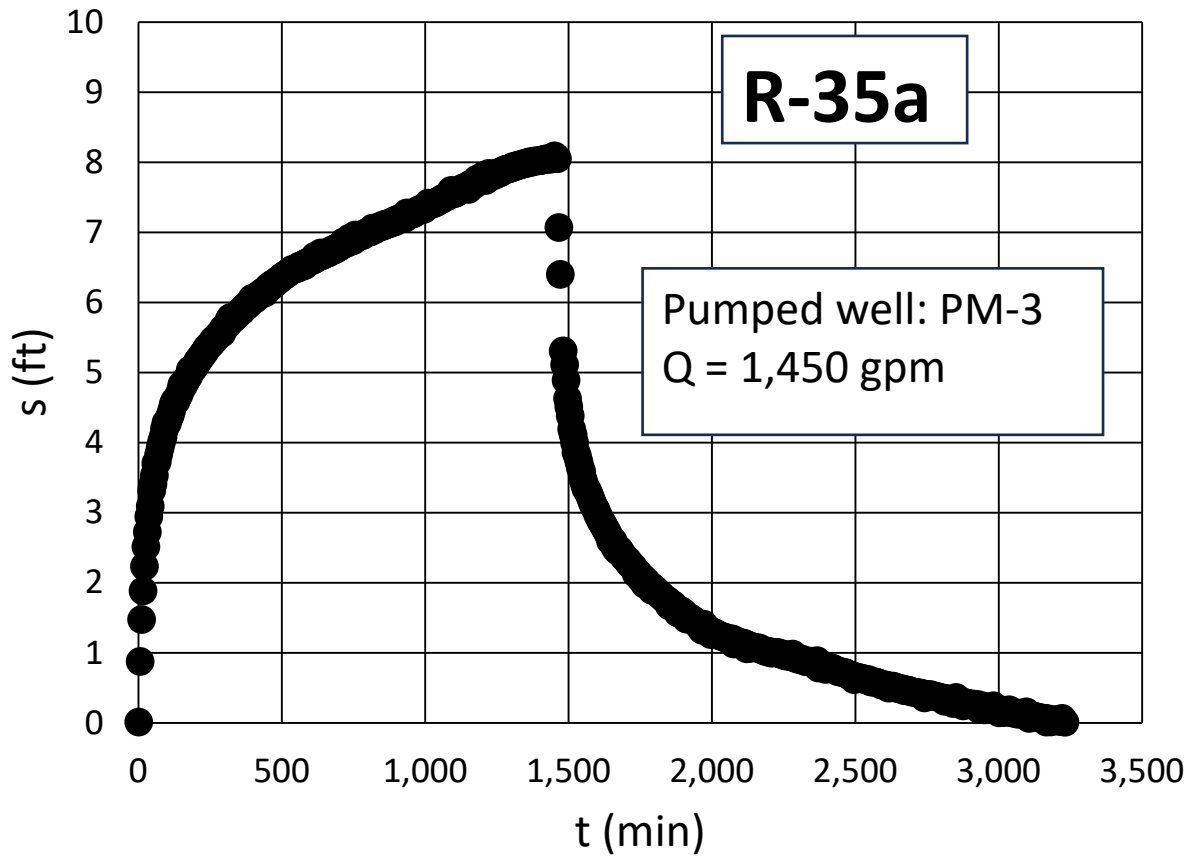


Figure 1. Drawdown versus time date at R-35a of the PM-3 aquifer test.

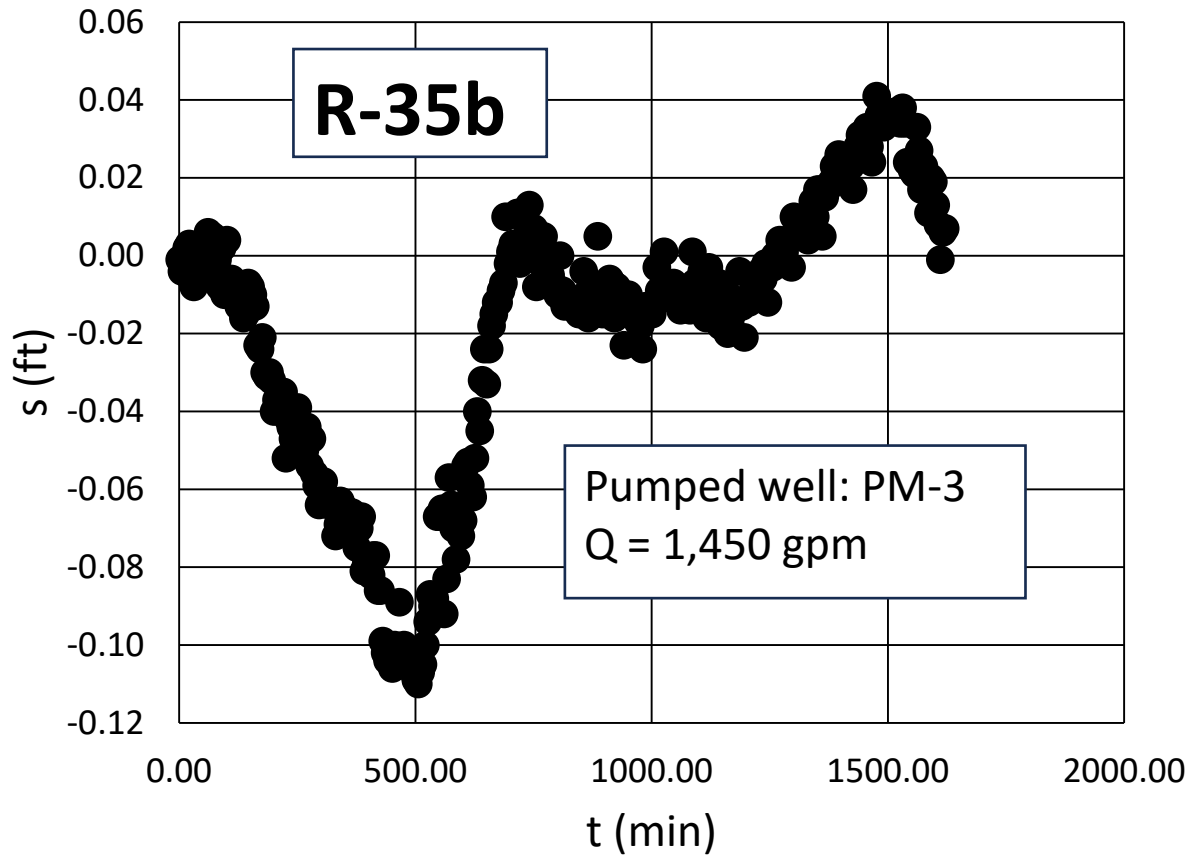


Figure 2. Drawdown versus time date at R-35b of the PM-3 aquifer test.

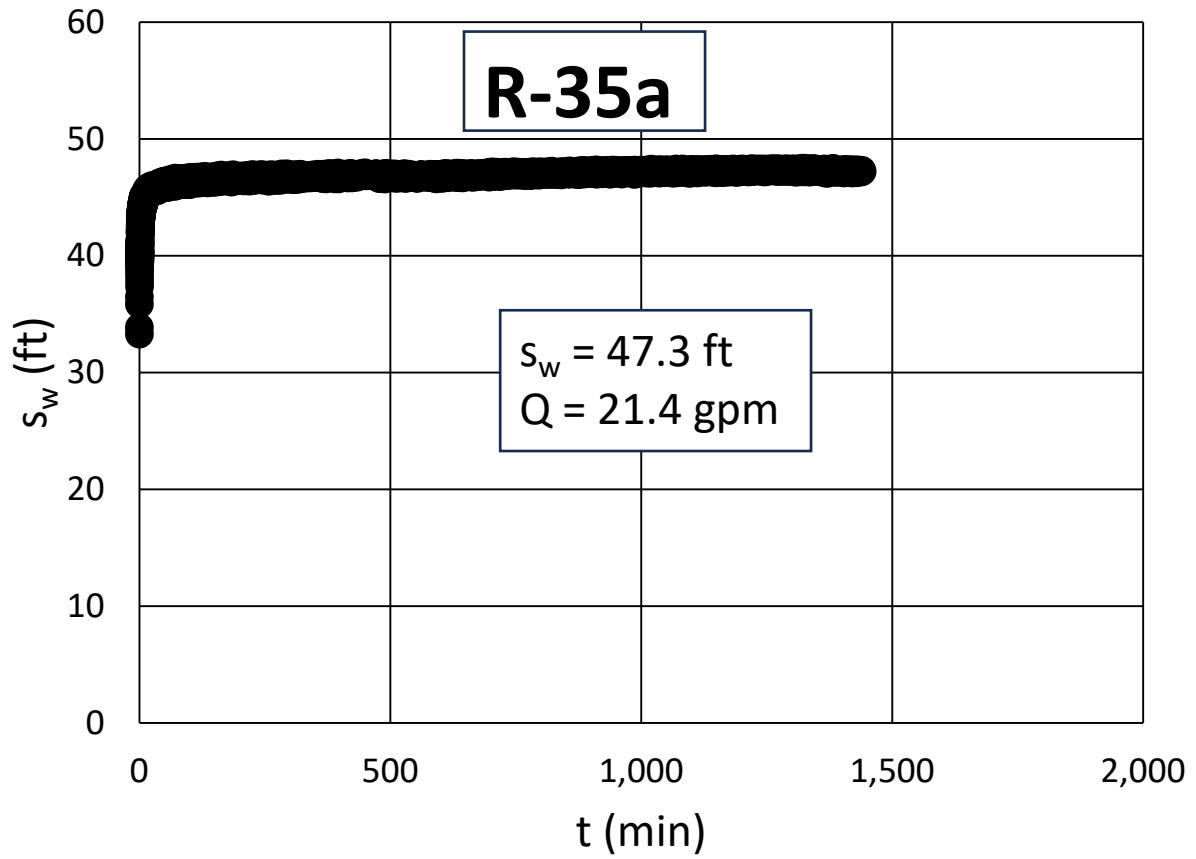


Figure 3. Drawdown versus time at R-35a under constant extraction constant extraction rate.

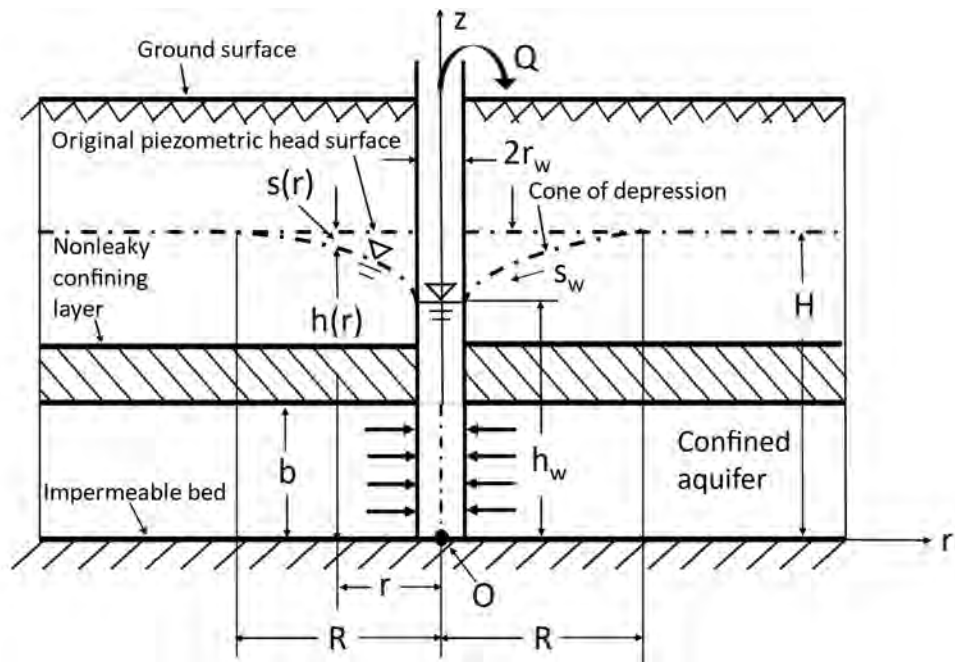


Figure 4. Well in a confined aquifer.

## Tables



Table 1. Wells geometry and initial water levels for the PM-3 aquifer test.

Well ID	Distance r (ft)	Initial Water Level (ft bgs)	Top of screen (ft bgs)	Bottom of screen (ft bgs)	Screen Length L (ft)	Depth to screen top from water table d (ft)	Inside radius of well casing, $r_c$ (ft)	Radius of well $r_w$ (ft)
PM-3	-	812.87	956	2532	1576	143.127	0.9792	1.00
R-35a	343	791.67	1013.1	1062.2	49.1	221.43	0.4896	0.51
R-35b	343	791.67	825.4	848.5	23.1	33.87	0.4896	0.51

Table 2. PM-3 aquifer test data analysis results for R-35a with the Neuman (1974, 1975) type-curve method.

<i>Well</i>	<i>r</i> (ft)	<i>T</i> (ft <sup>2</sup> /d)	<i>S</i>	<i>S<sub>y</sub></i>	$\beta = \left(\frac{K_v}{K_h}\right)\left(\frac{r}{b}\right)^2$	<i>K<sub>h</sub></i> (ft/d)	$a = \frac{K_v}{K_h}$
R-35a	343	2.780E+04	3.167E-03	1.002E-03	0.00068	5.56	0.1437
R-35a recovery	343	3.093E+04	2.644E-03	1.032E-03	0.00033	6.19	0.0704

Table 3. Comparison with the  $K_h$  values of PM-3 aquifer test and Neptune at R-35a.

<i>Well</i>	$K_h$ (ft/d)	$K_{h-Neptune}$ (ft/d)	<i>Number of Neptune values</i>	$K_{h-Neptune}/K_h$
R-35a	5.88 (a)	3.1 (b)	16	0.527

(a) Average of 5.56 and 6.19 ft/d values in Table 2.

(b) Neptune described the formation name as "Tcar" whereas in Koch and Schmeer (2009, p. 54) it is described as "Tsfu".

Table 4. Comparison with the  $K_h$  values determined from steady state drawdowns at R-35a and R-35b determined from the Thiem (1906) method with the  $K_h$  values of Neptune.

<i>Well</i>	$K_h$ (ft/d)	$K_{h-Neptune}$ (ft/d)	<i>Number of Neptune values</i>	$K_{h-Neptune}/K_h$
R-35a	2.2	3.1 (a)	16	1.409
R-35b	73.0	133.0 (b)	12	1.822

1. Neptune described the formation name as "Tcar" whereas in Koch and Schmeer (2009, p. 54) it is described as "Tsfu".
2. Both Neptune and in Koch and Schmeer (2009, p. 55) described the formation name as "Tpf".

## **Appendices**

## APPENDIX A: DETERMINATION OF HORIZONTAL HYDRAULIC CONDUCTIVITY USING THIEM WELL DISCHARGE FORMULA FOR R-35a STEADY STATE DRAWDOWN VALUE

### A.1 Fully Penetrating Well Solution in a Nonleaky Confined Aquifer: Thiem Equation

Thiem (1906) was the first to derive the hydraulic head and drawdown solution for a well in a fully penetrating well in a confined aquifer under steady state conditions and is given by [e.g., Bear, 1979, p. 306, Eq. (8-6); Batu, 2024, p. 187, Eq. (29-246)]

$$h(R) - h(r) = H - h(r) = \frac{Q}{2\pi T} \ln\left(\frac{R}{r}\right) \quad (\text{A-1})$$

The geometry of the Thiem solution is shown in Figure 4.

### A.2 Radius of Influence

The radius of influence  $R$  is the distance from the well where drawdown is zero. Since the 1880s, many attempts have been made to relate it to well, aquifer, and flow parameters in both steady and unsteady flow conditions in confined and unconfined aquifers. Some semi-empirical formulas are given in Bear (1979, p. 306). Of these formulas, the one developed by Sichardt is given in Bear [1979, p. 306, Eq. (8-11) as presented in Chertousov (1962)] is widely being used [e.g., De Filippi et al., 2020; Batu, 2024, p. 1088, Eq. (29-249)]:

$$R = 3000 s_w K_h^{\frac{1}{2}} \quad (\text{A-2})$$

in which  $R$  and  $s_w$  are in meters (m), and  $K_h$  in meters per second (m/s).

### A.3 Estimation of the Horizontal Hydraulic Conductivity with the R-35a Drawdown

The method is described in Batu (2024, pp. 1088-1090). Using the measured steady state drawdown  $s_w$  at the well, with Eqs. (A-1), the horizontal hydraulic conductivity  $K_h$  of the aquifer can be estimated. With  $T = K_h b$ , substitution of Eq. (A-2) into Eq. (29-242) and solving for  $K_h$ ,

$$K_h = \frac{Q}{2\pi s_w b} \ln\left(\frac{3000 s_w K_h^{\frac{1}{2}}}{r_w}\right) \quad (\text{A-3})$$

And after some manipulations,

$$K_h = m \left[ \ln(3000) + \frac{1}{2} \ln(K_h) + \ln\left(\frac{s_w}{r_w}\right) \right] \quad (\text{A-4})$$

in which

$$m = \frac{Q}{2\pi s_w b} \quad (\text{A-5})$$

Eq. (A-4) can also be written as

$$K_h - m \frac{1}{2} \ln(K_h) = m [\ln(3,000) + \ln\left(\frac{s_w}{r_w}\right)] \quad (\text{A-6})$$

In Eq. (A-6), with the known values of  $Q$ ,  $s_w$ ,  $b$ , and  $r_w$ , the value of  $K_h$  can be determined with the trial-and-error method. Since the units for Eq. (A-3) for  $R$  are in the metric unit system, calculations must be made using metric units.

The relevant R-35a data are as follows:

$$b = 49.1 \text{ ft} = 14.9657 \text{ m} \text{ (From the reports mentioned in Section 1.0)}$$

$$s_w = 47.3 \text{ ft} = 14.417 \text{ m} \text{ (From Figure 3)}$$

$$2r_c = 2r_w = 4.375 \text{ in} = 0.3646 \text{ ft} = 0.1111 \text{ m} \text{ (LANL, 2007, p. 18, Figure 7.2-1)}$$

$$r_c = r_w = 0.1823 \text{ ft} = 0.0556 \text{ m}$$

$$Q = 21.4 \text{ gpm} \text{ (From the report mentioned in Section 1.0, p. 4)}$$

$$1 \text{ gpm} = 0.0000630902 \frac{\text{m}^3}{\text{s}}$$

$$Q = 21.4 \text{ gpm} = 21.4 \frac{\text{gallon}}{\text{day}} = (21.4 \text{ gpm}) \left( \frac{0.0000630902 \frac{\text{m}^3}{\text{s}}}{\text{gpm}} \right) = 0.00135013 \frac{\text{m}^3}{\text{s}}$$

From Eq. (A-5),

$$m = \frac{Q}{2\pi s_w b} = \frac{(0.00135013 \frac{\text{m}^3}{\text{s}})}{2\pi(14.417 \text{ m})(14.9657 \text{ m})} = 0.000000996 \text{ s}^{-1}$$

$$\text{Trial 1: } K_h = 1 \text{ ft/d} = 0.000003528 \text{ m/s}$$

From Eq. (A-6),

$$K_h - m \frac{1}{2} \ln(K_h) = m [\ln(3,000) + \ln\left(\frac{s_w}{r_w}\right)]$$

$$0.000003528 - (0.000000996) \frac{1}{2} \ln(0.000003528)$$

$$= (0.000000996) [\ln(3,000) + \ln\left(\frac{14.417}{0.0556}\right)]$$

$$0.000000978 \neq 0.00001351$$

$$\text{Trial 2: } K_h = 3.0 \text{ ft/d} = 0.000010583 \text{ m/s}$$

From Eq. (A-6),

$$K_h - m \frac{1}{2} \ln(K_h) = m [\ln(3,000) + \ln\left(\frac{s_w}{r_w}\right)]$$

$$0.000010583 - (0.000000996) \frac{1}{2} \ln(0.000010583)$$

$$= 0.000016288 \neq 0.00001351$$

**Trial 3:  $K_h = 2.5 \text{ ft/d} = 0.000008819 \text{ m/s}$**

From Eq. (A-6),

$$K_h - m \frac{1}{2} \ln(K_h) = m [\ln(3,000) + \ln\left(\frac{s_w}{r_w}\right)]$$

$$0.000008819 - (0.000000996) \frac{1}{2} \ln(0.000008819)$$

$$= 0.000014615 \neq 0.00001351$$

**Trial 4:  $K_h = 2.0 \text{ ft/d} = 0.000007056 \text{ m/s}$**

From Eq. (A-6),

$$K_h - m \frac{1}{2} \ln(K_h) = m [\ln(3,000) + \ln\left(\frac{s_w}{r_w}\right)]$$

$$0.000007056 - (0.000000996) \frac{1}{2} \ln(0.000007056)$$

$$= 0.000012963 \neq 0.00001351$$

**Trial 5:  $K_h = 2.2 \text{ ft/d} = 0.000007761 \text{ m/s}$**

From Eq. (A-6),

$$K_h - m \frac{1}{2} \ln(K_h) = m [\ln(3,000) + \ln\left(\frac{s_w}{r_w}\right)]$$

$$0.000007761 - (0.000000996) \frac{1}{2} \ln(0.000007761)$$

$$= 0.000013621 \cong 0.00001351$$

Therefore,



$$K_h = 2.2 \text{ ft/d}$$

## APPENDIX B: DETERMINATION OF HORIZONTAL HYDRAULIC CONDUCTIVITY USING THIEM WELL DISCHARGE FORMULA FOR R-35b STEADY STATE DRAWDOWN VALUE

### B.1 Fully Penetrating Well Solution in a Nonleaky Confined Aquifer: Thiem Equation

Thiem (1906) was the first to derive the hydraulic head and drawdown solution for a well in a fully penetrating well in a confined aquifer under steady state conditions and is given by [e.g., Bear, 1979, p. 306, Eq. (8-6); Batu, 2024, p. 187, Eq. (29-246)]

$$h(R) - h(r) = H - h(r) = \frac{Q}{2\pi T} \ln\left(\frac{R}{r}\right) \quad (\text{B-1})$$

The geometry of the Thiem solution is shown in Figure 4.

### B.2 Radius of Influence

The radius of influence  $R$  is the distance from the well where drawdown is zero. Since the 1880s, many attempts have been made to relate it to well, aquifer, and flow parameters in both steady and unsteady flow conditions in confined and unconfined aquifers. Some semi-empirical formulas are given in Bear (1979, p. 306). Of these formulas, the one developed by Sichardt is given in Bear [1979, p. 306, Eq. (8-11) as presented in Chertousov (1962)] is widely being used [e.g., De Filippi et al., 2020; Batu, 2024, p. 1088, Eq. (29-249)]:

$$R = 3000 s_w K_h^{\frac{1}{2}} \quad (\text{B-2})$$

in which  $R$  and  $s_w$  are in meters (m), and  $K_h$  in meters per second (m/s).

### B.3 Estimation of the Horizontal Hydraulic Conductivity with the R-35b Drawdown

The method is described in Batu (2024, pp. 1088-1090). Using the measured steady state drawdown  $s_w$  at the well, with Eqs. (B-1), the horizontal hydraulic conductivity  $K_h$  of the aquifer can be estimated. With  $T = K_h b$ , substitution of Eq. (B-2) into Eq. (29-242) and solving for  $K_h$ ,

$$K_h = \frac{Q}{2\pi s_w b} \ln\left(\frac{3000 s_w K_h^{\frac{1}{2}}}{r_w}\right) \quad (\text{B-3})$$

And after some manipulations,

$$K_h = m \left[ \ln(3000) + \frac{1}{2} \ln(K_h) + \ln\left(\frac{s_w}{r_w}\right) \right] \quad (\text{B-4})$$

in which

$$m = \frac{Q}{2\pi s_w b} \quad (\text{B-5})$$

Eq. (B-4) can also be written as

$$K_h - m \frac{1}{2} \ln(K_h) = m [\ln(3,000) + \ln\left(\frac{s_w}{r_w}\right)] \quad (\text{B-6})$$

In Eq. (B-6), with the known values of  $Q$ ,  $s_w$ ,  $b$ , and  $r_w$ , the value of  $K_h$  can be determined with the trial-and-error method. Since the units for Eq. (B-3) for  $R$  are in the metric unit system, calculations must be made using metric units.

The relevant R-35b data are as follows:

$$b = 23.1 \text{ ft} = 7.04088 \text{ m} \text{ (From the reports mentioned in Section 1.0)}$$

$$s_w = 2.75 \text{ ft} = 0.8382 \text{ m} \text{ [From Appendix E (p. 46, Figure 49) mentioned in Section 1.0]}$$

$$2r_c = 2r_w = 4.375 \text{ in} = 0.3646 \text{ ft} = 0.1111 \text{ m} \text{ (LANL, 2007, p. 19, Figure 7.2-2)}$$

$$r_c = r_w = 0.1823 \text{ ft} = 0.0556 \text{ m}$$

$$Q = 22.6 \text{ gpm} \text{ [From Appendix E (p. 46, Figure 49) mentioned in Section 1.0]}$$

$$1 \text{ gpm} = 0.0000630902 \frac{\text{m}^3}{\text{s}}$$

$$Q = 22.6 \text{ gpm} = 22.6 \frac{\text{gallon}}{\text{day}} = (22.6 \text{ gpm}) \left( \frac{0.0000630902 \frac{\text{m}^3}{\text{s}}}{\text{gpm}} \right) = 0.00142588 \frac{\text{m}^3}{\text{s}}$$

From Eq. (B-5),

$$m = \frac{Q}{2\pi s_w b} = \frac{(0.00142588 \frac{\text{m}^3}{\text{s}})}{2\pi(0.8382 \text{ m})(7.04088 \text{ m})} = 0.000038453 \text{ s}^{-1}$$

$$\text{Trial 1: } K_h = 20 \text{ ft/d} = 0.000070556 \text{ m/s}$$

From Eq. (B-6),

$$K_h - m \frac{1}{2} \ln(K_h) = m [\ln(3,000) + \ln\left(\frac{s_w}{r_w}\right)]$$

$$0.000070556 - (0.000038453) \frac{1}{2} \ln(0.000070556)$$

$$= (0.000038453) [\ln(3,000) + \ln\left(\frac{0.8382}{0.0556}\right)]$$

$$0.000254344 \neq 0.000412195$$

$$\text{Trial 2: } K_h = 50 \text{ ft/d} = 0.000176389 \text{ m/s}$$

From Eq. (B-6),

$$K_h - m \frac{1}{2} \ln(K_h) = m [\ln(3,000) + \ln\left(\frac{s_w}{r_w}\right)]$$

$$0.000176389 - (0.000038453) \frac{1}{2} \ln(0.000176389)$$

$$= 0.00034256 \neq 0.000412195$$

**Trial 3:  $K_h = 60 \text{ ft/d} = 0.000211667 \text{ m/s}$**

From Eq. (B-6),

$$K_h - m \frac{1}{2} \ln(K_h) = m [\ln(3,000) + \ln\left(\frac{s_w}{r_w}\right)]$$

$$0.000211667 - (0.000038453) \frac{1}{2} \ln(0.000211667)$$

$$= 0.000374333 \neq 0.000412195$$

**Trial 4:  $K_h = 75 \text{ ft/d} = 0.000264583 \text{ m/s}$**

From Eq. (B-6),

$$K_h - m \frac{1}{2} \ln(K_h) = m [\ln(3,000) + \ln\left(\frac{s_w}{r_w}\right)]$$

$$0.000264583 - (0.000038453) \frac{1}{2} \ln(0.000264583)$$

$$= 0.0000422559 \cong 0.000412195$$

**Trial 5:  $K_h = 73 \text{ ft/d} = 0.000257528 \text{ m/s}$**

From Eq. (B-6),

$$K_h - m \frac{1}{2} \ln(K_h) = m [\ln(3,000) + \ln\left(\frac{s_w}{r_w}\right)]$$

$$0.000257528 - (0.000038453) \frac{1}{2} \ln(0.000257528)$$

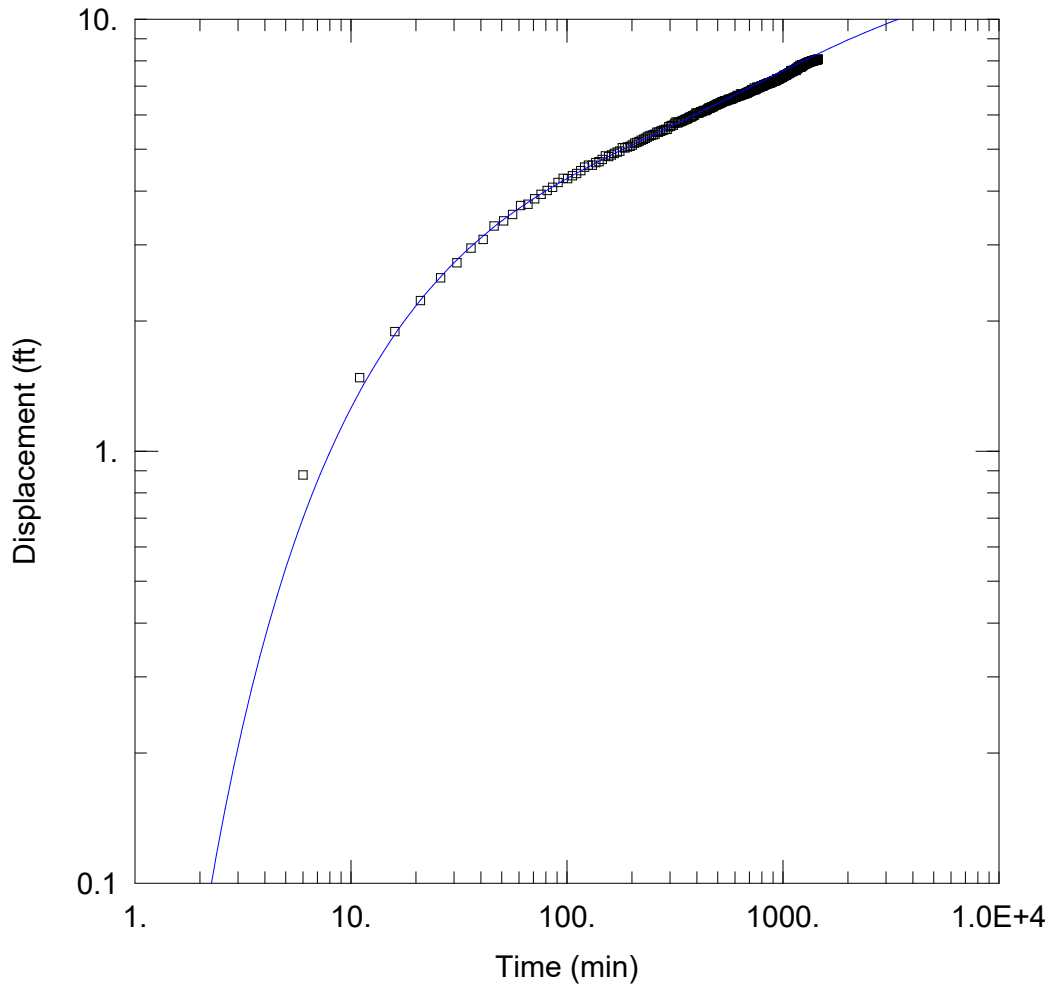
$$= 0.000416423 \cong 0.000412195$$

Therefore,

$$K_h = 73 \text{ ft/d}$$

**APPENDIX C**

**AQTESOLV OUTPUT FOR R-35a DRAWDOWN ANALYSIS**



WELL TEST ANALYSIS

Data Set: D:\hugo \Downloads\LANL NM PROJECT\R-35 Aquifer test\AQTESOLV files\R-35a Data.aqt  
 Date: 08/09/24 Time: 13:12:31

PROJECT INFORMATION

Test Well: PM-3

AQUIFER DATA

Saturated Thickness: 5000. ft

WELL DATA

Pumping Wells			Observation Wells		
Well Name	X (ft)	Y (ft)	Well Name	X (ft)	Y (ft)
PM-3	0	0	□ R-35a	343	0

SOLUTION

Aquifer Model: Unconfined

Solution Method: Neuman

T = 2.78E+4 ft<sup>2</sup>/day

S = 0.003167

Sy = 0.001002

β = 0.0006762

Data Set: D:\hugo\_\Downloads\LANL NM PROJECT\R-35 Aquifer test\AQTESOLV files\R-35a Data.aqt  
Date: 08/09/24  
Time: 13:12:47

---

PROJECT INFORMATION

Test Well: PM-3

---

AQUIFER DATA

Saturated Thickness: 5000. ft  
Anisotropy Ratio (Kz/Kr): 0.1437

---

PUMPING WELL DATA

No. of pumping wells: 1

Pumping Well No. 1: PM-3

X Location: 0. ft  
Y Location: 0. ft

Casing Radius: 0.9792 ft  
Well Radius: 1. ft

Partially Penetrating Well  
Depth to Top of Screen: 143.1 ft  
Depth to Bottom of Screen: 1719.1 ft

No. of pumping periods: 1

<u>Pumping Period Data</u>	
<u>Time (min)</u>	<u>Rate (gal/min)</u>
0.	1450.

---

OBSERVATION WELL DATA

No. of observation wells: 1

Observation Well No. 1: R-35a

X Location: 343. ft  
Y Location: 0. ft

Radial distance from PM-3: 343. ft

Partially Penetrating Well  
Depth to Top of Screen: 221.4 ft  
Depth to Bottom of Screen: 270.5 ft

No. of Observations: 292

<u>Observation Data</u>			
<u>Time (min)</u>	<u>Displacement (ft)</u>	<u>Time (min)</u>	<u>Displacement (ft)</u>

---



1.	0.01	731.	6.87
6.	0.88	736.	6.92
11.	1.48	741.	6.88
16.	1.89	746.	6.87
21.	2.23	751.	6.89
26.	2.52	756.	6.96
31.	2.73	761.	6.92
36.	2.95	766.	6.93
41.	3.09	771.	6.95
46.	3.32	776.	6.96
51.	3.41	781.	6.95
56.	3.53	786.	6.97
61.	3.7	791.	6.99
66.	3.73	796.	7.
71.	3.84	801.	7.
76.	3.93	806.	7.
81.	4.01	811.	7.01
86.	4.08	816.	7.06
91.	4.19	821.	7.04
96.	4.28	826.	7.04
101.	4.27	831.	7.06
106.	4.34	836.	7.07
111.	4.39	841.	7.08
116.	4.46	846.	7.08
121.	4.54	851.	7.1
126.	4.59	856.	7.09
131.	4.59	861.	7.12
136.	4.65	866.	7.11
141.	4.68	871.	7.12
146.	4.73	876.	7.13
151.	4.82	881.	7.13
156.	4.81	886.	7.15
161.	4.85	891.	7.16
166.	4.89	896.	7.15
171.	4.92	901.	7.18
176.	4.95	906.	7.18
181.	5.04	911.	7.2
186.	5.03	916.	7.19
191.	5.06	921.	7.21
196.	5.08	926.	7.2
201.	5.11	931.	7.21
206.	5.16	936.	7.28
211.	5.18	941.	7.24
216.	5.21	946.	7.25
221.	5.24	951.	7.26
226.	5.27	956.	7.26
231.	5.3	961.	7.27
236.	5.33	966.	7.29
241.	5.36	971.	7.31
246.	5.38	976.	7.31
251.	5.4	981.	7.33
256.	5.42	986.	7.32
261.	5.47	991.	7.34
266.	5.47	996.	7.33

<u>Time (min)</u>	<u>Displacement (ft)</u>	<u>Time (min)</u>	<u>Displacement (ft)</u>
271.	5.5	1001.	7.36
276.	5.52	1006.	7.38
281.	5.54	1011.	7.41
286.	5.56	1016.	7.39
291.	5.56	1021.	7.4
296.	5.63	1026.	7.41
301.	5.65	1031.	7.41
306.	5.67	1036.	7.43
311.	5.68	1041.	7.43
316.	5.74	1046.	7.45
321.	5.78	1051.	7.46
326.	5.75	1056.	7.47
331.	5.78	1061.	7.49
336.	5.79	1066.	7.49
341.	5.81	1071.	7.51
346.	5.83	1076.	7.51
351.	5.85	1081.	7.52
356.	5.87	1086.	7.57
361.	5.88	1091.	7.6
366.	5.91	1096.	7.56
371.	5.93	1101.	7.55
376.	5.94	1106.	7.56
381.	5.97	1111.	7.57
386.	5.98	1116.	7.59
391.	6.	1121.	7.61
396.	6.06	1126.	7.61
401.	6.06	1131.	7.63
406.	6.05	1136.	7.62
411.	6.07	1141.	7.63
416.	6.1	1146.	7.66
421.	6.1	1151.	7.61
426.	6.12	1156.	7.68
431.	6.15	1161.	7.69
436.	6.15	1166.	7.68
441.	6.14	1171.	7.68
446.	6.18	1176.	7.71
451.	6.21	1181.	7.76
456.	6.23	1186.	7.74
461.	6.22	1191.	7.74
466.	6.26	1196.	7.74
471.	6.26	1201.	7.81
476.	6.27	1206.	7.76
481.	6.3	1211.	7.74
486.	6.31	1216.	7.78
491.	6.33	1221.	7.84
496.	6.35	1226.	7.83
501.	6.37	1231.	7.79
506.	6.37	1236.	7.82
511.	6.39	1241.	7.84
516.	6.4	1246.	7.82
521.	6.42	1251.	7.85
526.	6.44	1256.	7.85
531.	6.45	1261.	7.85

---

<u>Time (min)</u>	<u>Displacement (ft)</u>	<u>Time (min)</u>	<u>Displacement (ft)</u>
536.	6.47	1266.	7.87
541.	6.47	1271.	7.88
546.	6.48	1276.	7.88
551.	6.48	1281.	7.9
556.	6.49	1286.	7.9
561.	6.52	1291.	7.91
566.	6.51	1296.	7.91
571.	6.52	1301.	7.92
576.	6.54	1306.	7.94
581.	6.53	1311.	7.93
586.	6.56	1316.	7.94
591.	6.57	1321.	7.95
596.	6.59	1326.	7.96
601.	6.59	1331.	7.96
606.	6.6	1336.	7.97
611.	6.61	1341.	7.98
616.	6.66	1346.	7.98
621.	6.63	1351.	7.98
626.	6.65	1356.	7.99
631.	6.65	1361.	8.01
636.	6.71	1366.	8.
641.	6.67	1371.	8.
646.	6.68	1376.	8.01
651.	6.69	1381.	8.02
656.	6.71	1386.	8.02
661.	6.7	1391.	8.02
666.	6.71	1396.	8.02
671.	6.73	1401.	8.02
676.	6.75	1406.	8.03
681.	6.75	1411.	8.03
686.	6.75	1416.	8.04
691.	6.78	1421.	8.05
696.	6.78	1426.	8.05
701.	6.79	1431.	8.04
706.	6.81	1436.	8.04
711.	6.82	1441.	8.05
716.	6.86	1446.	8.06
721.	6.84	1451.	8.09
726.	6.84	1456.	8.07

---

SOLUTION

Pumping Test  
 Aquifer Model: Unconfined  
 Solution Method: Neuman

---

VISUAL ESTIMATION RESULTS

Estimated Parameters

<u>Parameter</u>	<u>Estimate</u>	
T	2564.6	ft <sup>2</sup> /day
S	0.001036	

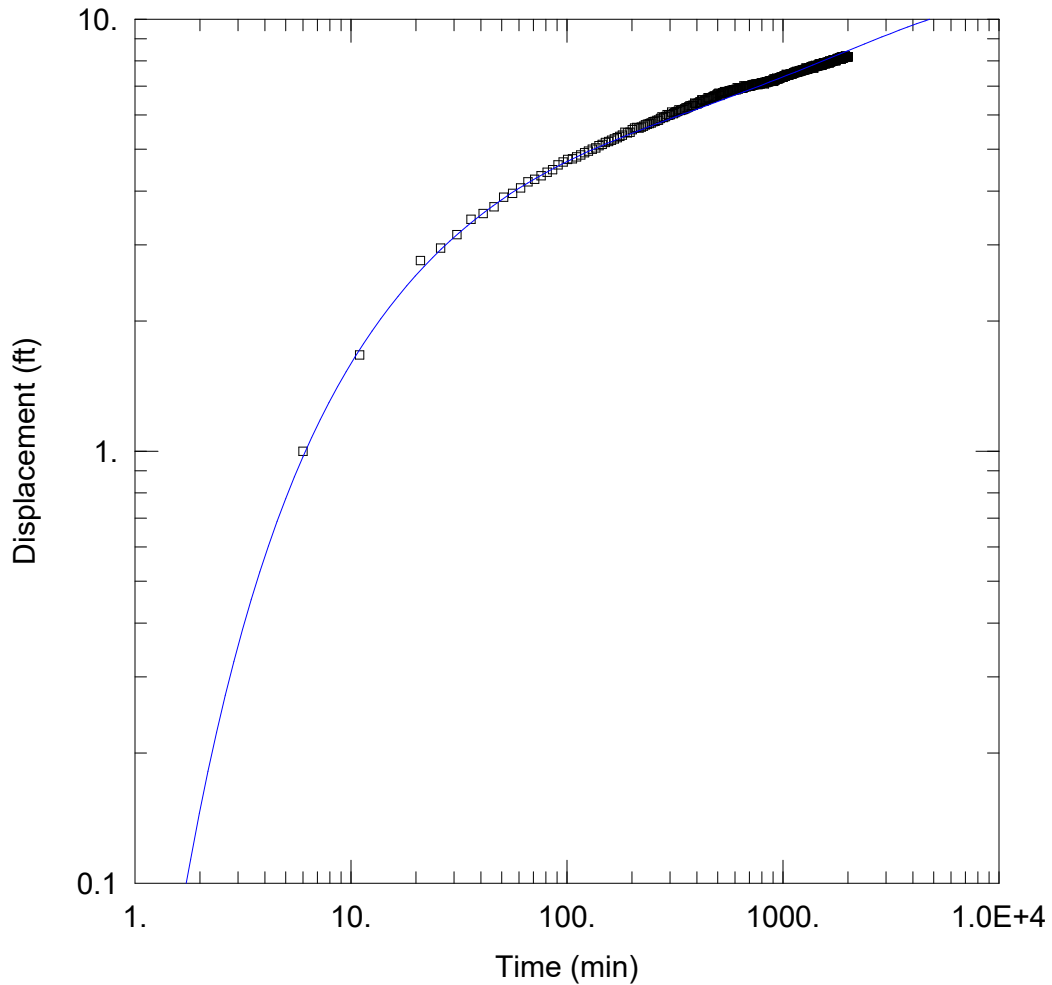
Sy	0.02
β	0.06

$K = T/b = 0.5129 \text{ ft/day (0.0001809 cm/sec)}$

$Ss = S/b = 2.072E-7 \text{ 1/ft}$

**APPENDIX D**

**AQTESOLV OUTPUT FOR R-35a RECOVERY ANALYSIS**



WELL TEST ANALYSIS

Data Set: D:\...\R-35a Data Recovery.aqt

Date: 08/09/24

Time: 14:40:57

PROJECT INFORMATION

Test Well: PM-3

AQUIFER DATA

Saturated Thickness: 5000. ft

WELL DATA

Pumping Wells

Observation Wells

Well Name	X (ft)	Y (ft)
PM-3	0	0

Well Name	X (ft)	Y (ft)
□ R-35a	343	0

SOLUTION

Aquifer Model: Unconfined

Solution Method: Neuman

T = 3.092E+4 ft<sup>2</sup>/day

S = 0.002644

Sy = 0.001032

β = 0.0003311

Data Set: D:\hugo\_\Downloads\LANL NM PROJECT\R-35 Aquifer test\AQTESOLV files\R-35a Data Recovery.aqt  
Date: 08/09/24  
Time: 14:41:10

---

PROJECT INFORMATION

Test Well: PM-3

---

AQUIFER DATA

Saturated Thickness: 5000. ft  
Anisotropy Ratio (Kz/Kr): 0.07036

---

PUMPING WELL DATA

No. of pumping wells: 1

Pumping Well No. 1: PM-3

X Location: 0. ft  
Y Location: 0. ft

Casing Radius: 0.9792 ft  
Well Radius: 1. ft

Partially Penetrating Well  
Depth to Top of Screen: 143.1 ft  
Depth to Bottom of Screen: 1719.1 ft

No. of pumping periods: 1

<u>Pumping Period Data</u>	
<u>Time (min)</u>	<u>Rate (gal/min)</u>
0.	1450.

---

OBSERVATION WELL DATA

No. of observation wells: 1

Observation Well No. 1: R-35a

X Location: 343. ft  
Y Location: 0. ft

Radial distance from PM-3: 343. ft

Partially Penetrating Well  
Depth to Top of Screen: 221.4 ft  
Depth to Bottom of Screen: 270.5 ft

No. of Observations: 403

<u>Observation Data</u>			
<u>Time (min)</u>	<u>Displacement (ft)</u>	<u>Time (min)</u>	<u>Displacement (ft)</u>

---

1.	0.02	1011.	7.37
6.	1.	1016.	7.39
11.	1.67	1021.	7.39
16.	-21.09	1026.	7.39
21.	2.76	1031.	7.39
26.	2.95	1036.	7.45
31.	3.17	1041.	7.41
36.	3.44	1046.	7.42
41.	3.55	1051.	7.42
46.	3.68	1056.	7.42
51.	3.87	1061.	7.43
56.	3.95	1066.	7.43
61.	4.07	1071.	7.44
66.	4.2	1076.	7.45
71.	4.26	1081.	7.45
76.	4.34	1086.	7.45
81.	4.42	1091.	7.47
86.	4.48	1096.	7.48
91.	4.6	1101.	7.48
96.	4.67	1106.	7.48
101.	4.73	1111.	7.48
106.	4.75	1116.	7.49
111.	4.8	1121.	7.5
116.	4.85	1126.	7.51
121.	4.91	1131.	7.53
126.	4.95	1136.	7.52
131.	5.	1141.	7.53
136.	5.03	1146.	7.53
141.	5.09	1151.	7.53
146.	5.13	1156.	7.57
151.	5.18	1161.	7.55
156.	5.21	1166.	7.55
161.	5.24	1171.	7.54
166.	5.28	1176.	7.56
171.	5.32	1181.	7.56
176.	5.35	1186.	7.57
181.	5.39	1191.	7.57
186.	5.47	1196.	7.57
191.	5.45	1201.	7.59
196.	5.47	1206.	7.59
201.	5.55	1211.	7.61
206.	5.59	1216.	7.59
211.	5.61	1221.	7.6
216.	5.59	1226.	7.6
221.	5.62	1231.	7.61
226.	5.65	1236.	7.63
231.	5.69	1241.	7.62
236.	5.71	1246.	7.63
241.	5.73	1251.	7.63
246.	5.75	1256.	7.63
251.	5.79	1261.	7.65
256.	5.8	1266.	7.64
261.	5.83	1271.	7.65
266.	5.84	1276.	7.65



<u>Time (min)</u>	<u>Displacement (ft)</u>	<u>Time (min)</u>	<u>Displacement (ft)</u>
271.	5.89	1281.	7.71
276.	5.94	1286.	7.66
281.	5.92	1291.	7.68
286.	5.95	1296.	7.66
291.	6.01	1301.	7.66
296.	5.99	1306.	7.68
301.	6.01	1311.	7.69
306.	6.09	1316.	7.69
311.	6.04	1321.	7.68
316.	6.07	1326.	7.7
321.	6.1	1331.	7.7
326.	6.11	1336.	7.71
331.	6.17	1341.	7.71
336.	6.14	1346.	7.72
341.	6.17	1351.	7.76
346.	6.18	1356.	7.72
351.	6.2	1361.	7.73
356.	6.23	1366.	7.74
361.	6.24	1371.	7.74
366.	6.26	1376.	7.73
371.	6.29	1381.	7.79
376.	6.3	1386.	7.74
381.	6.31	1391.	7.7
386.	6.32	1396.	7.76
391.	6.39	1401.	7.77
396.	6.37	1406.	7.77
401.	6.37	1411.	7.76
406.	6.39	1416.	7.82
411.	6.42	1421.	7.78
416.	6.44	1426.	7.78
421.	6.5	1431.	7.78
426.	6.5	1436.	7.79
431.	6.46	1441.	7.8
436.	6.49	1446.	7.81
441.	6.49	1451.	7.8
446.	6.52	1456.	7.81
451.	6.58	1461.	7.82
456.	6.56	1466.	7.8
461.	6.56	1471.	7.87
466.	6.57	1476.	7.87
471.	6.59	1481.	7.83
476.	6.61	1486.	7.82
481.	6.63	1491.	7.88
486.	6.63	1496.	7.84
491.	6.64	1501.	7.85
496.	6.68	1506.	7.85
501.	6.71	1511.	7.85
506.	6.74	1516.	7.87
511.	6.66	1521.	7.82
516.	6.72	1526.	7.87
521.	6.72	1531.	7.87
526.	6.75	1536.	7.87
531.	6.74	1541.	7.92

---

<u>Time (min)</u>	<u>Displacement (ft)</u>	<u>Time (min)</u>	<u>Displacement (ft)</u>
536.	6.8	1546.	7.91
541.	6.77	1551.	7.88
546.	6.77	1556.	7.92
551.	6.79	1561.	7.89
556.	6.79	1566.	7.89
561.	6.81	1571.	7.9
566.	6.82	1576.	7.88
571.	6.83	1581.	7.92
576.	6.83	1586.	7.9
581.	6.84	1591.	7.93
586.	6.84	1596.	7.92
591.	6.86	1601.	7.93
596.	6.87	1606.	7.94
601.	6.87	1611.	7.93
606.	6.88	1616.	7.94
611.	6.87	1621.	7.95
616.	6.94	1626.	7.94
621.	6.89	1631.	7.96
626.	6.92	1636.	7.91
631.	6.91	1641.	7.95
636.	6.92	1646.	8.
641.	6.93	1651.	7.97
646.	6.93	1656.	7.97
651.	6.93	1661.	7.97
656.	6.94	1666.	7.98
661.	7.01	1671.	7.98
666.	6.96	1676.	7.98
671.	7.	1681.	7.99
676.	6.97	1686.	8.
681.	6.98	1691.	7.99
686.	6.99	1696.	8.
691.	6.99	1701.	8.
696.	7.	1706.	8.05
701.	6.99	1711.	8.01
706.	7.	1716.	8.03
711.	7.01	1721.	8.05
716.	7.03	1726.	8.02
721.	7.03	1731.	8.04
726.	7.04	1736.	8.03
731.	7.05	1741.	8.02
736.	7.05	1746.	8.04
741.	7.05	1751.	8.04
746.	7.07	1756.	8.04
751.	7.07	1761.	8.
756.	7.07	1766.	8.04
761.	7.06	1771.	8.06
766.	7.07	1776.	8.07
771.	7.06	1781.	8.07
776.	7.08	1786.	8.08
781.	7.09	1791.	8.07
786.	7.08	1796.	8.08
791.	7.1	1801.	8.12
796.	7.11	1806.	8.09

<u>Time (min)</u>	<u>Displacement (ft)</u>	<u>Time (min)</u>	<u>Displacement (ft)</u>
801.	7.1	1811.	8.09
806.	7.11	1816.	8.09
811.	7.12	1821.	8.1
816.	7.12	1826.	8.11
821.	7.08	1831.	8.11
826.	7.14	1836.	8.14
831.	7.14	1841.	8.11
836.	7.13	1846.	8.11
841.	7.16	1851.	8.11
846.	7.16	1856.	8.13
851.	7.15	1861.	8.17
856.	7.17	1866.	8.07
861.	7.17	1871.	8.14
866.	7.19	1876.	8.13
871.	7.19	1881.	8.13
876.	7.19	1886.	8.19
881.	7.18	1891.	8.18
886.	7.2	1896.	8.13
891.	7.2	1901.	8.15
896.	7.21	1906.	8.13
901.	7.22	1911.	8.15
906.	7.18	1916.	8.15
911.	7.28	1921.	8.15
916.	7.23	1926.	8.16
921.	7.23	1931.	8.17
926.	7.26	1936.	8.17
931.	7.26	1941.	8.16
936.	7.3	1946.	8.22
941.	7.27	1951.	8.17
946.	7.28	1956.	8.18
951.	7.28	1961.	8.17
956.	7.29	1966.	8.18
961.	7.29	1971.	8.16
966.	7.31	1976.	8.18
971.	7.31	1981.	8.18
976.	7.32	1986.	8.17
981.	7.34	1991.	8.18
986.	7.34	1996.	8.18
991.	7.34	2001.	8.18
996.	7.35	2006.	8.18
1001.	7.34	2011.	8.18
1006.	7.35		

---

SOLUTION

Pumping Test  
 Aquifer Model: Unconfined  
 Solution Method: Neuman

---

VISUAL ESTIMATION RESULTS

Estimated Parameters

<u>Parameter</u>	<u>Estimate</u>	
T	3.092E+4	ft <sup>2</sup> /day
S	0.002644	
Sy	0.001032	
β	0.0003311	

$K = T/b = 6.185 \text{ ft/day (0.002182 cm/sec)}$

$S_s = S/b = 5.288\text{E-}7 \text{ 1/ft}$

## **ATTACHMENT 6**

**Determination of the Horizontal  
Hydraulic Conductivity ( $K_h$ ) Value  
from the Steady-State Drawdown  
Value of the R-13 Extraction Well,  
Los Alamos, New Mexico**

---

This page intentionally left blank.

## Executive Summary

In Attachment 6, horizontal hydraulic conductivity ( $K_h$ ) value is determined using the measured steady-state drawdown at R-13 extraction well.

Using the method described in Section 4.0, calculation details for the horizontal hydraulic conductivity ( $K_h$ ) are given in Appendix A. The determined value for the horizontal hydraulic conductivity ( $K_h$ ) is

$$K_h = 25 \text{ ft/d} = 0.000088194 \text{ m/s} = 8.82 \times 10^{-3} \text{ cm/s}$$

The  $K_h$  value is compared with the  $K_{h-Neptune}$  values of Neptune (Foster, 2024a, 2024b) determined using the pilot point method as described in Doherty (2003). The  $K_h$  values of Neptune have been provided in the following references:

Foster, L., Neptune and Company, Inc., Excel file: K and S LANL – For ITR – 5 – 6 – 24, sent by Lauren Foster of Neptune to Susan Wacaster of DOE, May 6, 2024a.

Foster, L., Neptune and Company, Inc., “Untitled Notes”, sent by Daniel Stephens, 22. pp., July 23, 2024b.

Figure 7 of Foster (2024b) was generated from the Excel file in Foster (2024a). Foster (2024a) includes 3 different  $K_{h-Neptune}$  values at R-13 which are 17.6 ft/d, 13.7 ft/d, and 8.0 – 39.7 ft/d. Neptune described the formation name as “Tpf”. Therefore, the minimum and maximum  $K_{h-Neptune}$  values are 8.0 ft/d and 39.7 ft/d, respectively. These values are compared in Table 1 which shows that  $K_{h-Neptune-min}/K_h$  ratios are 0.320 and 1.588, respectively.

## Attachment 6 Contents

1. Purpose and Data Sources .....	1
2. Relevant Data for R-13 Well .....	1
3. Method for Determining Horizontal Hydraulic Conductivity With Steady State Drawdown at the Extraction Well .....	1
4. Result for the Horizontal Hydraulic Conductivity Value .....	2
5. Comparisons of the Kh Value with the Kh Value of Neptune .....	2

## Figures

Figure 1. Drawdown vs. time at R-13 extraction well (Stone and McLin, 2003, p. B-3, Table B-2).

Figure 2. Well in a confined aquifer.

## Tables

Table 1. Comparison with the  $K_h$  value determined from steady state drawdown at R-13 determined from the Thiem (1906) method with the  $K_h$  values of Neptune (Foster, 2024a, 2024b).

## Appendices

Appendix A Determination of Horizontal Hydraulic Conductivity Using Thiem Well Discharge Formula for R-13 Steady State Drawdown Value



## 1. Purpose and Data Sources

The purpose of Attachment 6 is to determine horizontal hydraulic conductivity ( $K_h$ ) value using the measured steady-state drawdown value at R-13 extraction well. The method is based on *Thiem's discharge formula* for confined aquifers along with the *Sichardt empirical zone of influence radius* to determine the values of  $K_h$  around R-13 extraction well using the data in the report of Los Alamos National Laboratory (Stone and McLin, 2003).

## 2. Relevant Data for R-13 Well

From Stone and McLin (2003, p. 21, Figure 11) the screen interval is

$$b = L = 1018.7 \text{ ft} - 958.3 \text{ ft} = 60.4 \text{ ft} = 18.40992 \text{ m}$$

From Figure 1, steady state drawdown is:

$$s_w = 2.3 \text{ ft} = 0.70104 \text{ m}$$

From Stone and McLin (2003, p. 6):

$$2r_c = 2r_w = 4.5 \text{ in} = 0.375 \text{ ft} = 0.1143 \text{ m}$$

$$r_c = r_w = 0.1875 \text{ ft} = 0.05715 \text{ m}$$

From Stone and McLin (2003, p. 22, Table 9), the average extraction rate is

$$Q = 19 \text{ gpm}$$

$$1 \text{ gpm} = 0.0000630902 \frac{\text{m}^3}{\text{s}}$$

$$Q = 19 \text{ gpm} = 19 \frac{\text{gallon}}{\text{day}} = (19 \text{ gpm}) \left( \frac{0.0000630902 \frac{\text{m}^3}{\text{s}}}{\text{gpm}} \right) = 0.00119871 \frac{\text{m}^3}{\text{s}}$$

The water level in the well before extraction is 833.0 ft below the ground surface (bgs). The upper end of the screen interval is 958.3 ft bgs. Therefore, the upper end of the screen interval is 12.53 ft below the water table and  $s_w = 2.3 \text{ ft} = 0.70104 \text{ m} < 12.53 \text{ ft}$ . Therefore, Thiem (1906) equation will be used to determine the horizontal hydraulic conductivity ( $K_h$ ).

## 3. Method for Determining Horizontal Hydraulic Conductivity With Steady State Drawdown at the Extraction Well

In order to determine the value of horizontal hydraulic conductivity ( $K_h$ ) with the steady-state drawdown value at a well, the *Thiem well discharge formula* under confined aquifer conditions along with empirical zone of influence radius can be used.

The geometry of the Thiem solution for a confined aquifer under steady-state flow conditions is given in Figure 2. The aquifer thickness is  $b$  and the aquifer has infinite extent. Its horizontal hydraulic conductivity is  $K_h$ . The constant extraction rate of the well is  $Q_w$ . Details of the method are given in Appendix A.

#### 4. Result for the Horizontal Hydraulic Conductivity Value

Using the method described in Section 4.0, calculation details for the horizontal hydraulic conductivity ( $K_h$ ) are given in Appendix A. The value is

$$K_h = 25 \text{ ft/d} = 0.000088194 \text{ m/s} = 8.82 \times 10^{-3} \text{ cm/s}$$

#### 5. Comparisons of the $K_h$ Value with the $K_h$ Value of Neptune

The  $K_h$  value is compared with the  $K_h$  values of Neptune (Foster, 2024a, 2024b) determined using the pilot point method as described in Doherty (2003). The  $K_h$  values of Neptune have been provided in the following references:

Foster, L., Neptune and Company, Inc., Excel file: K and S LANL – For ITR – 5 – 6 – 24, sent by Lauren Foster of Neptune to Susan Wacaster of DOE, May 6, 2024a.

Foster, L., Neptune and Company, Inc., “Untitled Notes”, sent by Daniel Stephens, 22. pp., July 23, 2024b.

Figure 7 of Foster (2024b) was generated from the Excel file in Foster (2024a). Foster (2024a) includes 3 different  $K_{h-Neptune}$  values at R-13 which are  $17.6 \text{ ft/d}$ ,  $13.7 \text{ ft/d}$ , and  $8.0 - 39.7 \text{ ft/d}$ . Neptune described the formation name as “Tpf”. Therefore, the minimum and maximum  $K_{h-Neptune}$  values are  $8.0 \text{ ft/d}$  and  $39.7 \text{ ft/d}$ , respectively. These values are compared in Table 1 which shows that  $K_{h-Neptune-min}/K_h$  are 0.320 and 1.588, respectively.

#### References

- Batu, V., *Fluid Mechanics and Hydraulics: Illustrative Worked Examples of Surface and Subsurface Flows*, Taylor & Francis CRC Press, Boca Raton, Florida, 1240 pp., 2024.
- Bear, J., *Hydraulics of Groundwater*, McGraw-Hill Book Company, New York, 569 pp., 1979.
- Chertousov, M.D., *Hydraulics* (in Russian), Gosenergouzdat, 630 pp., Moscow, Russia, 1962.
- De Filippi, F.M., S. Iacurto, F. Ferranti, and G. Sappa, “Hydraulic Conductivity Estimation Using Low-Flow Purging Data Elaboration in Contaminated Sites,” *Water*, Vol. 12, pp. 898-914, 2020.
- Doherty, J., “Ground Water Model Calibration Using Pilot Points and Regularization,” *Ground Water*, Vol. 41, No. 2, pp. 170-177, March-April, 2003.

Foster, L., Neptune and Company, Inc., Excel file: K and S LANL – For ITR – 5 – 6 – 24, sent by Lauren Foster of Neptune to Susan Wacaster of DOE, May 6, 2024a.

Foster, L., Neptune and Company, Inc., “Untitled Notes”, sent by Daniel Stephens, 22. pp., July 23, 2024b.

Freeze, R.A., And J.A. Cherry, *Groundwater*, Prentice-Hall, Inc., Englewood Cliffs, New Jersey, 604, pp., 1979.

Stone, W.J., and S.G. McLin, “Hydrologic Tests at Characterization Wells R-9i, R-13, R-19, R-22, and R-31,” Los Alamos National Laboratory, LA-13987-MS, 46 pp., March, 2003

Thiem, G., *Hydrologische Methoden* (in German), J.M. Gebhardt, Leipzig, Germany, 56 pp., 1906., *Hydrologische Methoden* (in German), J.M. Gebhardt, Leipzig, Germany, 56 pp., 1906.

## Figures

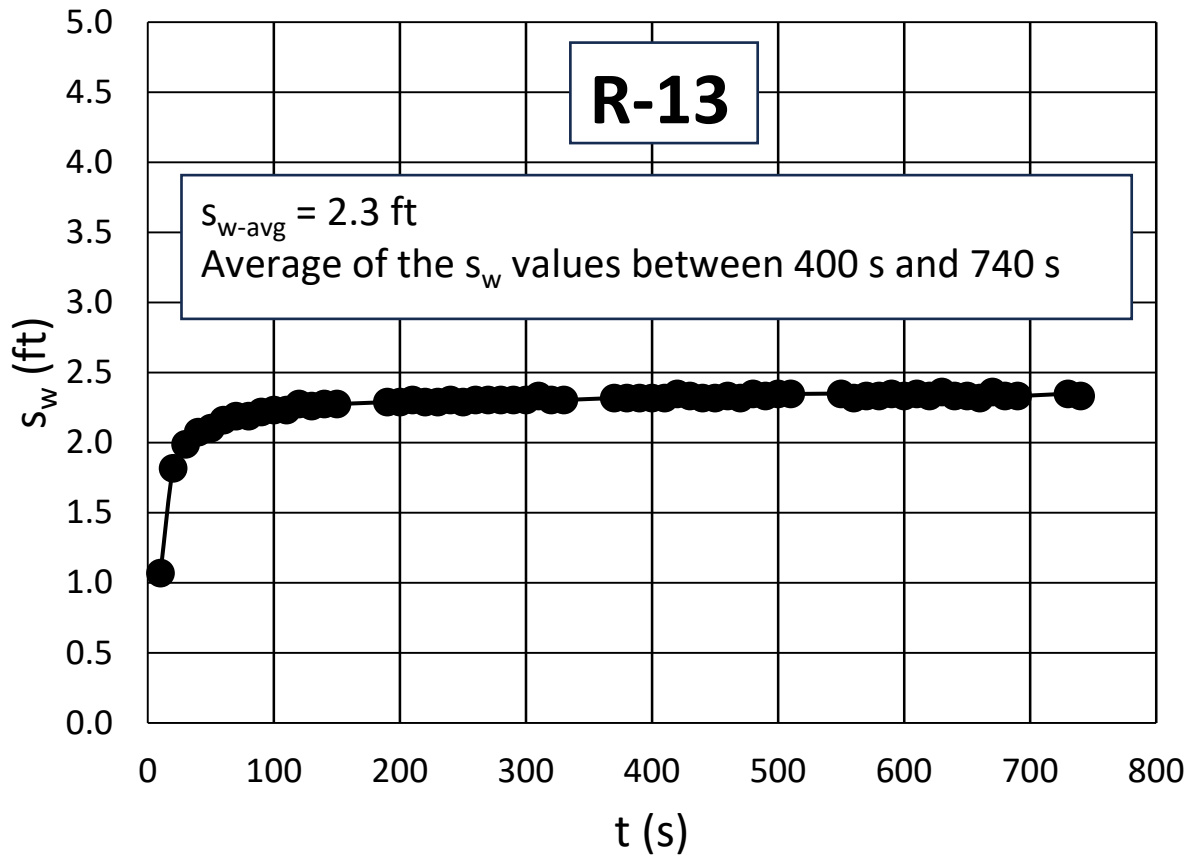


Figure 1. Drawdown vs. time at R-13 extraction well (Stone and McLin, 2003, p. B-3, Table B-2).

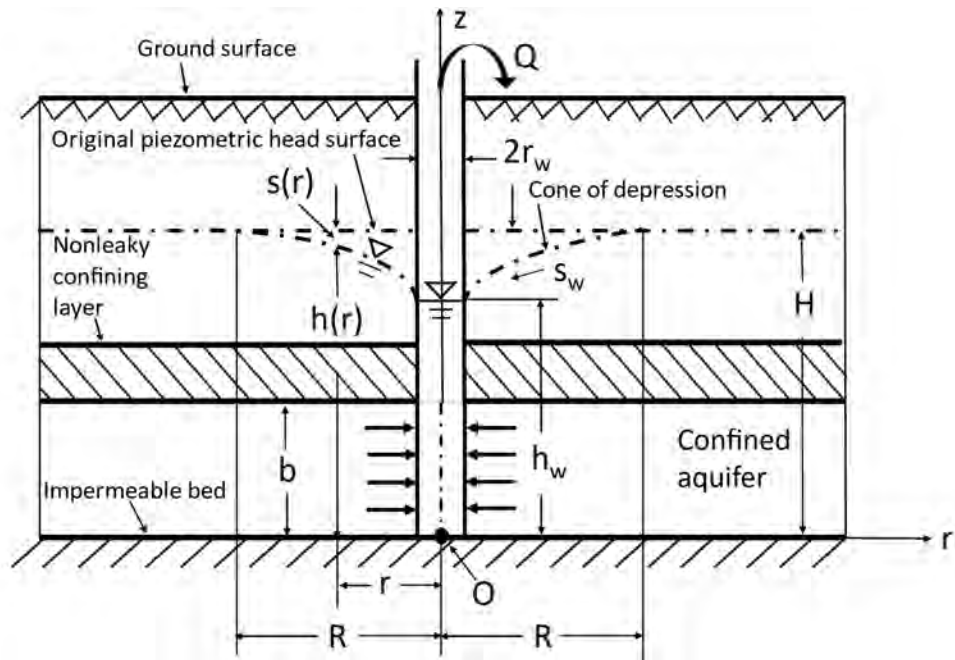


Figure 2. Well in a confined aquifer.

## Tables

Table 1. Comparison with the  $K_h$  value determined from steady state drawdown at R-13 determined from the Thiem (1906) method with the  $K_h$  values of Neptune (Foster, 2024a, 2024b).

<i>Well</i>	$K_h$ (ft/d)	$K_{h-Neptune}$ (ft/d)	<i>Number of Neptune values</i>	$K_{h-Neptune}/K_h$
R-13	25	8.0 (a)	1	0.320
R-13	25	39.7 (b)	1	1.588

- (1) Neptune's minimum  $K_h$  value.
- (2) Neptune's maximum  $K_h$  value.



## **Appendices**

## APPENDIX A: DETERMINATION OF HORIZONTAL HYDRAULIC CONDUCTIVITY USING THIEM WELL DISCHARGE FORMULA FOR R-13 STEADY STATE DRAWDOWN VALUE

### A.1 Fully Penetrating Well Solution in a Nonleaky Confined Aquifer: Thiem Equation

Thiem (1906) was the first to derive the hydraulic head and drawdown solution for a well in a fully penetrating well in a confined aquifer under steady state conditions and is given by [e.g., Bear, 1979, p. 306, Eq. (8-6); Batu, 2024, p. 187, Eq. (29-246)]

$$h(R) - h(r) = H - h(r) = \frac{Q}{2\pi T} \ln\left(\frac{R}{r}\right) \quad (\text{A-1})$$

The geometry of the Thiem solution is shown in Figure 2.

### A.2 Radius of Influence

The radius of influence  $R$  is the distance from the well where drawdown is zero. Since the 1880s, many attempts have been made to relate it to well, aquifer, and flow parameters in both steady and unsteady flow conditions in confined and unconfined aquifers. Some semi-empirical formulas are given in Bear (1979, p. 306). Of these formulas, the one developed by Sichardt is given in Bear [1979, p. 306, Eq. (8-11) as presented in Chertousov (1962)] is widely being used [e.g., De Filippi et al., 2020; Batu, 2024, p. 1088, Eq. (29-249)]:

$$R = 3000 s_w K_h^{\frac{1}{2}} \quad (\text{A-2})$$

in which  $R$  and  $s_w$  are in meters (m), and  $K_h$  in meters per second (m/s).

### A.3 Estimation of the Horizontal Hydraulic Conductivity with the R-13 Drawdown

The method is described in Batu (2024, pp. 1088-1090). Using the measured steady state drawdown  $s_w$  at the well, with Eqs. (A-1), the horizontal hydraulic conductivity  $K_h$  of the aquifer can be estimated. With  $T = K_h b$ , substitution of Eq. (A-2) into Eq. (29-242) and solving for  $K_h$ ,

$$K_h = \frac{Q}{2\pi s_w b} \ln\left(\frac{3000 s_w K_h^{\frac{1}{2}}}{r_w}\right) \quad (\text{A-3})$$

And after some manipulations,

$$K_h = m \left[ \ln(3000) + \frac{1}{2} \ln(K_h) + \ln\left(\frac{s_w}{r_w}\right) \right] \quad (\text{A-4})$$

in which

$$m = \frac{Q}{2\pi s_w b} \quad (\text{A-5})$$

Eq. (A-4) can also be written as

$$K_h - m \frac{1}{2} \ln(K_h) = m [\ln(3,000) + \ln\left(\frac{s_w}{r_w}\right)] \quad (\text{A-6})$$

In Eq. (A-6), with the known values of  $Q$ ,  $s_w$ ,  $b$ , and  $r_w$ , the value of  $K_h$  can be determined with the trial-and-error method. Since the units for Eq. (A-3) for  $R$  are in the metric unit system, calculations must be made using metric units.

From Section 2, the relevant R-13 data are as follows:

From Stone and McLin (2003, p. 21, Figure 11) the screen interval is

$$b = L = 1,018.7 \text{ ft} - 958.3 \text{ ft} = 60.4 \text{ ft} = 18.40992 \text{ m}$$

From Figure 1, steady state drawdown is:

$$s_w = 2.3 \text{ ft} = 0.70104 \text{ m}$$

From Stone and McLin (2003, p. 6):

$$2r_c = 2r_w = 4.5 \text{ in} = 0.375 \text{ ft} = 0.1143 \text{ m}$$

$$r_c = r_w = 0.1875 \text{ ft} = 0.05715 \text{ m}$$

From Stone and McLin (2003, p. 22, Table 9), the average extraction rate is

$$Q = 19 \text{ gpm}$$

$$1 \text{ gpm} = 0.0000630902 \frac{\text{m}^3}{\text{s}}$$

$$Q = 19 \text{ gpm} = 19 \frac{\text{gallon}}{\text{day}} = (19 \text{ gpm}) \left( \frac{0.0000630902 \frac{\text{m}^3}{\text{s}}}{\text{gpm}} \right) = 0.00119871 \frac{\text{m}^3}{\text{s}}$$

The water level in the well before extraction is 833.0 *ft* below the ground surface (bgs). The upper end of the screen interval is 958.3 *ft* bgs. Therefore, the upper end of the screen interval is 125.3 *ft* below the water table and  $s_w = 2.3 \text{ ft} = 0.70104 \text{ m} < 125.3 \text{ ft}$ . Therefore, Thiem (1906) equation will be used to determine the horizontal hydraulic conductivity ( $K_h$ ).

From Eq. (A-5),

$$m = \frac{Q}{2\pi s_w b} = \frac{(0.00119871 \frac{\text{m}^3}{\text{s}})}{2\pi(0.70104 \text{ m})(18.40992 \text{ m})} = 0.000014782 \text{ s}^{-1}$$

**Trial 1:  $K_h = 10 \text{ ft/d} = 0.000035278 \text{ m/s}$**

From Eq. (A-6),

$$K_h - m \frac{1}{2} \ln(K_h) = m [\ln(3,000) + \ln\left(\frac{s_w}{r_w}\right)]$$

$$0.000035278 - (0.000014782) \frac{1}{2} \ln(0.000035278)$$

$$= (0.000014782) [\ln(3,000) + \ln\left(\frac{0.70104}{0.05715}\right)]$$

$$0.000111052 \neq 0.000155407$$

**Trial 2:  $K_h = 15 \text{ ft/d} = 0.000052917 \text{ m/s}$**

From Eq. (A-6),

$$K_h - m \frac{1}{2} \ln(K_h) = m [\ln(3,000) + \ln\left(\frac{s_w}{r_w}\right)]$$

$$0.000052917 - (0.000014782) \frac{1}{2} \ln(0.000052917)$$

$$= 0.000125695 \neq 0.000155407$$

**Trial 3:  $K_h = 25 \text{ ft/d} = 0.000088194 \text{ m/s}$**

From Eq. (A-6),

$$K_h - m \frac{1}{2} \ln(K_h) = m [\ln(3,000) + \ln\left(\frac{s_w}{r_w}\right)]$$

$$0.00008819 - (0.000014782) \frac{1}{2} \ln(0.00008819)$$

$$= 0.0000157192 \cong 0.000155407$$

Therefore,

$$K_h = 25 \text{ ft/d}$$

## **Appendix C**

**Batu (2024b) - Comparison of the Horizontal Hydraulic Conductivity ( $K_h$ ) Values at the CrEX and CrIN Well Locations, and PM-2 and PM-4 Aquifer Tests Well Locations with the  $K_h$  Values of Neptune, Los Alamos, New Mexico**

# **Comparison of the Horizontal Hydraulic Conductivity ( $K_h$ ) Values at the CrEX and CrIN Well Locations, and PM-2 and PM-4 Aquifer Tests Well Locations with the $K_h$ Values of Neptune, Los Alamos, New Mexico**

---

Vedat Batu, Ph.D., P.E.  
Argonne Associate  
Argonne National Laboratory  
Lemont, Illinois

**August 12, 2024**

This page intentionally left blank.

## Executive Summary

The purpose of this report is to compare the horizontal hydraulic conductivity ( $K_h$ ) values determined from the steady-state drawdown values of the CrEX extraction wells and CrIN injection wells at the Los Alamos (New Mexico) site determined from the Dupuit-Forchheimer and Thiem ( $D - F & T$ ) well discharge formulas, and PM-2 and PM-4 aquifer tests well locations with the  $K_h$  values of Neptune (Foster, 2024a, 2024b) determined using the pilot point method as described in Doherty (2003). The conclusions reached are as follows:

1. There are more than one order of magnitude discrepancies between the  $K_h$  values at two EX well locations. The  $K_h$  value of Neptune at CrEX-1 (161.0  $ft/d$ ) is more than one order of magnitude higher than the  $K_h$  value (12.5  $ft/d$ ) determined from  $D - F & T$  well discharge formulas method. And the  $K_h$  value of Neptune at CrEX-2 (4.7  $ft/d$ ) is less than one order of magnitude of the  $K_h$  value (51.0  $ft/d$ ) determined from the  $D - F & T$  well discharge formulas method. The  $K_h$  values at the CrEX-3 and CrEX-4 locations of Neptune are 41% and 42% of the  $K_h$  values determined from the  $D - F & T$  well discharge formulas method, respectively.
2. For the five injection wells, the  $K_h$  values of Neptune have values between 41% and 200% of the  $K_h$  values determined from the  $D - F & T$  well discharge formulas method.
3. At the seven well locations of the PM-2 aquifer test, the  $K_{h-Neptune}/K_h$  ratio varies between 0.061 and 7.060. The 0.061 value means that the  $K_{h-Neptune}$  value is more than one and half orders of magnitude less than the  $K_h$  value of the PM-2 aquifer test value. Likewise, the 7.060 value means that the  $K_{h-Neptune}$  value is almost one order of magnitude higher than the PM-2 aquifer test value.
4. At the four well locations of the PM-4 aquifer test, the  $K_{h-Neptune}/K_h$  ratio varies between 3.447 and 9.744. At PM-5, the  $K_{h-Neptune}$  value is almost one order of magnitude higher than the  $K_h$  value of the PM-4 aquifer test. At R-20 S3, the  $K_{h-Neptune}$  value is more than one-half order of magnitude higher than the  $K_h$  value of the PM-4 aquifer test.



# Contents

Executive Summary .....	ES-1
1. Purpose.....	1
2. Neptune’s Horizontal Hydraulic Conductivity (Kh) Values at the Extraction Wells and Their Comparisons with the Ones Determined from the D-F & T Well Discharge Formulas .....	1
2.1 The Kh Values of Neptune .....	1
2.2 The Kh Values from the D-F & T Well Discharge Formulas Method.....	2
2.3 Comparative Evaluation of the Kh Values of Neptune and the Kh Values Determined from the D-F & T Well Discharge Formulas Method.....	3
3. Neptune’s Horizontal Hydraulic Conductivity (Kh) Values at the Injection Wells and Their Comparisons with the Ones Determined from the D-F & T Well Discharge Formulas Method .....	3
3.1 The Kh Values of Neptune .....	3
3.2 The Kh Values from the D-F & T Well Discharge Formulas Method.....	3
3.3 Comparative Evaluation of the Kh Values of Neptune and the Kh Values Determined from the D-F & T Well Discharge Formulas Method.....	3
4. Comparison of Horizontal Hydraulic Conductivity (Kh) Values of PM-2 Aquifer Test with the Kh Values of Neptune.....	4
4.1 The Kh Values of Neptune .....	4
4.2 The Kh Values from the PM-2 Aquifer Test.....	4
4.3 Comparative Evaluation of the Kh Values of Neptune and the Kh Values Determined from the PM-2 Aquifer Test.....	4
5. Comparison of Horizontal Hydraulic Conductivity (Kh) Values of PM-4 Aquifer Test with the Kh Values of Neptune.....	5
5.1 The Kh Values of Neptune .....	5
5.2 The Kh Values from the PM-4 Aquifer Test.....	5
5.3 Comparative Evaluation of the Kh Values of Neptune and the Kh Values Determined from the PM-2 Aquifer Test.....	5
6. The Kv/Kh Anisotropy Ratios.....	6
7. Conclusions .....	6
References.....	7

## Figures

- Figure 1. Comparison of the D-F & T and Neptune  $K_h$  values at the CrEX wells.
- Figure 2. Comparison of the D-F & T and Neptune  $K_h$  values at the CrIN wells.
- Figure 3. Comparison of the PM-2 Aquifer Test and Neptune  $K_h$  values at the seven well locations in Table 3 (The numbers in the horizontal axis represents the well numbers).
- Figure 4. Comparison of the PM-4 Aquifer Test and Neptune  $K_h$  values at the seven well locations in Table 4 (The numbers in the horizontal axis represents the well numbers).

## Tables

- Table 1. Determined horizontal hydraulic conductivity ( $K_h$ ) values using the drawdown data at the CrEX extraction wells and comparisons with Neptune's values.
- Table 2. Determined horizontal hydraulic conductivity ( $K_h$ ) values using the drawdown data at the CrIN injection wells and comparison with the Neptune's values.
- Table 3. Comparison of the  $K_h$  values of PM-2 aquifer test with the  $K_h$  values of Neptune.
- Table 4. Comparison of the  $K_h$  values of PM-4 aquifer test with the  $K_h$  values of Neptune.

# 1. Purpose

The purpose of this report is to compare the horizontal hydraulic conductivity ( $K_h$ ) values determined from the steady-state drawdown values of the CrEX extraction wells and CrIN injection wells at the Los Alamos (New Mexico) site determined from the Dupuit-Forchheimer and Thiem ( $D - F$  &  $T$ ) well discharge formulas, and PM-2 and PM-4 aquifer tests well locations with the  $K_h$  values of Neptune (Foster, 2024a, 2024b) determined using the pilot point method as described in Doherty (2003).

## 2. Neptune's Horizontal Hydraulic Conductivity ( $K_h$ ) Values at the Extraction Wells and Their Comparisons with the Ones Determined from the $D - F$ & $T$ Well Discharge Formulas

### 2.1 The $K_h$ Values of Neptune

The  $K_h$  values of Neptune have been provided in the references below:

Foster, L., Neptune and Company, Inc., Excel file: K and S LANL – For ITR – 5 – 6 – 24, sent by Lauren Foster of Neptune to Susan Wacaster of DOE, May 6, 2024a.

Foster, L., Neptune and Company, Inc., "Untitled Notes", sent by Daniel Stephens, 22 pp., July 23, 2024b.

The chromium injection well CrIN-6 was completed in 2017 as part of IM. In 2019, owing to high measured concentration, CrIN-6 was converted to the chromium extraction well CrEX-5 (Susan Wacaster, email to Vedat Batu, 6/28/2024) that is why Figure 7 of Neptune has just four EX wells.

In Foster (2024b, p. 1), the purpose of the document is described as

*"The purpose of document is to describe parameter distribution development for saturated hydraulic conductivity ( $K$ ) and  $K$  anisotropy ( $K_z/K_{xy}$ ) in the Cr project area at Los Alamos National Laboratory. These parameters are required for the Cr Regional Model (CRM) of Cr transport at the site. Their values are uncertain, and  $K$  is likely to be a sensitive parameter."*

Three-dimensional hydraulic conductivity tensor is [e.g., Bear, 1979, p. 72, Eq. (4-38)]

$$[K] = \begin{bmatrix} K_{xx} & K_{xy} & K_{xz} \\ K_{yx} & K_{yy} & K_{yz} \\ K_{zx} & K_{zy} & K_{zz} \end{bmatrix} \quad (1)$$

Its two-dimensional form is

$$[K] = \begin{bmatrix} K_{xx} & K_{xy} \\ K_{yx} & K_{yy} \end{bmatrix} \quad (2)$$

According to the quoted statements, the vertical anisotropy is defined by  $K_z/K_{xy}$  without mentioning  $K_{xx}$  and  $K_{yy}$ .

If  $K_{xx} = K_{yy} \neq K_{zz}$ , as in common in sedimentary horizontal deposits, the formation is said to be *transversely anisotropic* (e.g., Freeze and Cherry, 1979, p. 32).

Foster (2024b, p. 4), makes the following statement:

*“Along with a high degree of heterogeneity, the Puye Formation in the Cr area is also characterized by strong vertical anisotropy ( $K_z/K_{xy} < 1$ ), which is thought to explain observations of aquifer behavior in response to pumping.”*

Foster (2024b, p. 5), further makes the following statements:

*“Information is typically not given that would help identify whether the measurement represents  $K_{xx}$  or  $K_{yy}$  relative to any coordinate system, and therefore  $K$  values are assumed to be for any horizontal direction and are used for a single distribution for  $K_{xy}$ . Vertical anisotropy is difficult to estimate from pumping tests and was typically not within the scope of  $K$  estimations made for LANL well completion reports, e.g., (LANL 2002), but several of the pumping test analyses do provide rough anisotropy estimates, e.g., (LANL 2007, 2009). These provide the basis for the  $K_z$  distributions, as discussed below, along with literature reviews. If storativity estimates are also given in the same reference, they are also entered into the database.”*

The  $K_{xy} = K_{yx}$  in Eq. (2) can only be determined with methods described in some well-known literature (e.g., Papadopoulos, 1965; Neuman et al., 1984) with multiple wells. Foster (2004b) does not give information regarding measured  $K_{xy}$  values based on aquifer tests. In the quoted paragraph, the phrase *“Information is typically not given that would help identify whether the measurement represents  $K_{xx}$  or  $K_{yy}$  relative to any coordinate system, and therefore  $K$  values are assumed to be for any horizontal direction and are used for a single distribution for  $K_{xy}$ .”* needs additional explanation. Does it mean that the  $K_{xy}$  values are assumed to be the measured  $K$  (perhaps meant  $K_r$ ) values?

Based on the aforementioned points, comparisons will be made on the assumption that  $K_{xy} = K_{yx} \equiv K_r$ .

## **2.2 The $K_h$ Values from the $D - F$ & $T$ Well Discharge Formulas Method**

In Table 1, the  $K_h$  values based on the  $D - F$  &  $T$  formulas are taken from Batu (2024, August 10, p. 90, Table 1 of Attachment 2). The reason of having  $K_h$  value at CrEX-5 is given in Section 2.1 above.

### **2.3 Comparative Evaluation of the $K_h$ Values of Neptune and the $K_h$ Values Determined from the $D - F$ & $T$ Well Discharge Formulas Method**

By comparing the  $K_h$  values of Neptune and the  $K_h$  values determined from the  $D - F$  &  $T$  well discharge formulas in Table 1, the following observations can be made:

1. The  $K_h$  value of Neptune at CrEX-1 (161.0  $ft/d$ ) is more than one order of magnitude higher than the  $K_h$  value (12.5  $ft/d$ ) determined from  $D - F$  &  $T$  well discharge formulas method.
2. The  $K_h$  value of Neptune at CrEX-2 (4.7  $ft/d$ ) is less than one order of magnitude from the  $K_h$  value (51.0  $ft/d$ ) determined from the  $D - F$  &  $T$  well discharge formulas method.
3. The  $K_h$  value of Neptune at CrEX-3 (8.9  $ft/d$ ) is 41% of the  $K_h$  value (21.5  $ft/d$ ) of the  $D - F$  &  $T$  well discharge formulas method.
4. The  $K_h$  value of Neptune at CrEX-4 (5.2  $ft/d$ ) is 42% of the  $K_h$  value (12.5  $ft/d$ ) determined from the  $D - F$  &  $T$  well discharge formulas method.

Figure 1 presents the graphical comparisons of the  $K_h$  values determined from the  $D - F$  &  $T$  well discharge formulas method and Neptune at the CrEX extraction wells.

### **3. Neptune's Horizontal Hydraulic Conductivity ( $K_h$ ) Values at the Injection Wells and Their Comparisons with the Ones Determined from the $D - F$ & $T$ Well Discharge Formulas Method**

#### **3.1 The $K_h$ Values of Neptune**

The  $K_h$  values of Neptune have been provided in the references below:

Foster, L., Neptune and Company, Inc., Excel file: K and S LANL – For ITR – 5 – 6 – 24, sent by Lauren Foster of Neptune to Susan Wacaster of DOE, May 6, 2024a.

Foster, L., Neptune and Company, Inc., “Untitled Notes”, sent by Daniel Stephens, 22 pp., July 23, 2024b.

#### **3.2 The $K_h$ Values from the $D - F$ & $T$ Well Discharge Formulas Method**

In Table 2, the  $K_h$  values based on the  $D - F$  &  $T$  formulas method are taken from Batu (2024, August 10, Table 1 of Attachment 2, p. 43).

### **3.3 Comparative Evaluation of the $K_h$ Values of Neptune and the $K_h$ Values Determined from the $D - F$ & $T$ Well Discharge Formulas Method**

By comparing the  $K_h$  values of Neptune and the  $K_h$  values determined from the  $D - F$  &  $T$  well discharge formulas method in Table 2, the following observations can be made:

1. The  $K_h$  value of Neptune at CrIN-1 (13.0 *ft/d*) is 50% of the  $K_h$  value (26.0 *ft/d*) of  $D - F$  &  $T$  formulas method.
2. The  $K_h$  value of Neptune at CrIN-2 (19.6 *ft/d*) is 53% of the  $K_h$  value (37.0 *ft/d*) of  $D - F$  &  $T$  formulas method.
3. The  $K_h$  value of Neptune at CrIN-3 (76.3 *ft/d*) is twice of the  $K_h$  value (38.0 *ft/d*) of  $D - F$  &  $T$  formulas method.
4. The  $K_h$  value of Neptune at CrIN-4 (35.5 *ft/d*) is 59% of the  $K_h$  value (60.0 *ft/d*) of  $D - F$  &  $T$  formulas method.
5. The  $K_h$  value of Neptune at CrIN-5 (29.4 *ft/d*) is 41% of the  $K_h$  value (72.0 *ft/d*) of  $D - F$  &  $T$  formulas method.

Figure 2 presents the graphical comparisons of the  $K_h$  values determined from the  $D - F$  &  $T$  well discharge formulas method and Neptune at the CrIN injection wells.

#### **4. Comparison of Horizontal Hydraulic Conductivity ( $K_h$ ) Values of PM-2 Aquifer Test with the $K_h$ Values of Neptune**

##### **4.1 The $K_h$ Values of Neptune**

The  $K_h$  values of Neptune have been provided in the references below:

Foster, L., Neptune and Company, Inc., Excel file: K and S LANL – For ITR – 5 – 6 – 24, sent by Lauren Foster of Neptune to Susan Wacaster of DOE, May 6, 2024a.

Foster, L., Neptune and Company, Inc., “Untitled Notes”, sent by Daniel Stephens, 22 pp., July 23, 2024b.

##### **4.2 The $K_h$ Values from the PM-2 Aquifer Test**

In Table 3, the  $K_h$  values based on the PM-2 aquifer test are taken from Batu (2024, August 10, Table 2 of Attachment 3, p. 116).

##### **4.3 Comparative Evaluation of the $K_h$ Values of Neptune and the $K_h$ Values Determined from the PM-2 Aquifer Test**

By comparing the  $K_h$  values of Neptune and the  $K_h$  values determined from the PM-2 aquifer test in Table 3, the following observations can be made:

1. The  $K_h$  value of Neptune at PM-2 (1.2 *ft/d*) is 26% of the  $K_h$  value (4.55 *ft/d*) of the PM-2 aquifer test method.
2. The  $K_h$  value of Neptune at PM-4 (5.86 *ft/d*) is almost one order of magnitude higher than the  $K_h$  value (0.83 *ft/d*).

3. The  $K_h$  value of Neptune at PM-5 (8.77 *ft/d*) is almost three times higher than the  $K_h$  value (3.34 *ft/d*).
4. The  $K_h$  value of Neptune at R-20 S1 (0.17 *ft/d*) is more than one and half orders of magnitude lower than the  $K_h$  value (2.79 *ft/d*).
5. The  $K_h$  value of Neptune at R-20 S2 (1.6 *ft/d*) is more than one-half order of magnitude lower than the  $K_h$  value (9.52 *ft/d*).
6. The  $K_h$  value of Neptune at R-20 S3 (3.89 *ft/d*) is 1.4 times higher than the  $K_h$  value (2.84 *ft/d*).
7. The  $K_h$  value of Neptune at R-32 S3 (1.2 *ft/d*) is more than order of magnitude lower than the  $K_h$  value (16.18 *ft/d*).

Figure 3 presents the graphical comparisons of the aforementioned values.

## **5. Comparison of Horizontal Hydraulic Conductivity ( $K_h$ ) Values of PM-4 Aquifer Test with the $K_h$ Values of Neptune**

### **5.1 The $K_h$ Values of Neptune**

The  $K_h$  values of Neptune have been provided in the references below:

Foster, L., Neptune and Company, Inc., Excel file: K and S LANL – For ITR – 5 – 6 – 24, sent by Lauren Foster of Neptune to Susan Wacaster of DOE, May 6, 2024a.

Foster, L., Neptune and Company, Inc., “Untitled Notes”, sent by Daniel Stephens, 22 pp., July 23, 2024b.

### **5.2 The $K_h$ Values from the PM-4 Aquifer Test**

In Table 4, the  $K_h$  values based on the PM-4 aquifer test are taken from Batu (2024, August 10, Table 2 of Attachment 4, p. 151).

### **5.3 Comparative Evaluation of the $K_h$ Values of Neptune and the $K_h$ Values Determined from the PM-2 Aquifer Test**

By comparing the  $K_h$  values of Neptune and the  $K_h$  values determined from the PM-2 aquifer test in Table 4, the following observations can be made:

1. The  $K_h$  value of Neptune at PM-2 (4.55 *ft/d*) is more than four times higher than the  $K_h$  value (1.1 *ft/d*) of the PM-2 aquifer test method.
2. The  $K_h$  value of Neptune at PM-4 (5.86 *ft/d*) is more than three times higher than the  $K_h$  value (1.7 *ft/d*)

3. The  $K_h$  value of Neptune at PM-5 (8.77 *ft/d*) is almost one order of higher than the  $K_h$  value (0.9 *ft/d*).
4. The  $K_h$  value of Neptune at R-20 S3 (3.89 *ft/d*) is more than one-half order of magnitude higher than the  $K_h$  value (0.7 *ft/d*).

Figure 4 presents the graphical comparisons of the aforementioned values.

## 6. The $K_v/K_h$ Anisotropy Ratios

Foster (2024b, p. 15, Table 1) gives the  $K_v/K_h$  anisotropy ratios at a total of 14 well locations including CrEX-3, CrEX-4, CrIN-1, CrIN-2, CrIN-3, CrIN-4, and Cr-IN-5. However, comparisons cannot be made because the  $K_v/K_h$  anisotropy ratios cannot be determined with the  $D - F$  &  $T$  well discharge formulas method. The PM-2 and PM-4 aquifer tests provide the  $K_v/K_h$  anisotropy ratios, but Foster (2024b, p. 15, Table 1) does not provide  $K_v/K_h$  values for the wells of these tests.

## 7. Conclusions

Based on the foregoing analyses, the conclusions are as follows:

1. There are more than one order of magnitude discrepancies between the  $K_h$  values at two EX well locations. The  $K_h$  value of Neptune at CrEX-1 (161.0 *ft/d*) is more than one order of magnitude higher than the  $K_h$  value (12.5 *ft/d*) determined from  $D - F$  &  $T$  well discharge formulas method. And the  $K_h$  value of Neptune at CrEX-2 (4.7 *ft/d*) is less than one order of magnitude of the  $K_h$  value (51.0 *ft/d*) determined from the  $D - F$  &  $T$  well discharge formulas method. The  $K_h$  values at the CrEX-3 and CrEX-4 locations of Neptune are 41% and 42% of the  $K_h$  values determined from the  $D - F$  &  $T$  well discharge formulas method, respectively.
2. For the five injection wells, the  $K_h$  values of Neptune have values between 41% and 200% of the  $K_h$  values determined from the  $D - F$  &  $T$  well discharge formulas method.
3. At the seven well locations of the PM-2 aquifer test, the  $K_{h-Neptune}/K_h$  ratio varies between 0.061 and 7.060. The 0.061 value means that the  $K_{h-Neptune}$  value is more than one and half orders of magnitude less than the  $K_h$  value of the PM-2 aquifer test value. Likewise, the 7.060 value means that the  $K_{h-Neptune}$  value is almost one order of magnitude higher than the PM-2 aquifer test value.
4. At the four well locations of the PM-4 aquifer test, the  $K_{h-Neptune}/K_h$  ratio varies between 3.447 and 9.744. At PM-5, the  $K_{h-Neptune}$  value is almost one order of magnitude higher than the  $K_h$  value of the PM-4 aquifer test. At R-20 S3, the  $K_{h-Neptune}$  value is more than one-half order of magnitude higher than the  $K_h$  value of the PM-4 aquifer test.



## References

- Batu, V., "Horizontal ( $K_h$ ) and Vertical Hydraulic Conductivity ( $K_v$ ) Values Determined from the Aquifer Tests of CrIN, CrEX, PM-2, and PM-4 at the LANL Site," August 10, 2024.
- Bear, J., *Hydraulics of Groundwater*, McGraw-Hill Book Company, New York, 569 pp., New York, 1979.
- Doherty, J., "Ground Water Model Calibration Using Pilot Points and Regularization," *Ground Water*, Vol. 41, No. 2, pp. 170-177, March-April, 2003.
- Foster, L., Neptune and Company, Inc., Excel file: K and S LANL – For ITR – 5 – 6 – 24, sent by Lauren Foster of Neptune to Susan Wacaster of DOE, May 6, 2024a.
- Foster, L., Neptune and Company, Inc., "Untitled Notes", sent by Daniel Stephens, 22. pp., July 23, 2024b.
- Freeze, R.A., and J.A. Cherry, *Groundwater*, Prentice-Hall, Inc, Englewood Cliffs, New Jersey, 604, pp., 1979.
- Neuman, S.P., G.R. Walter, H.W. Bentley, J.J. Ward, and D.D. Gonzalez, "Determination of Horizontal Anisotropy with Three Wells," *Ground Water*, Vol. 22, No. 1, pp. 66-72, January-February, 1984.
- Papadopoulos, I.S., "Nonsteady Flow to a Well in an Infinite Anisotropic Aquifer," *Proceedings, of Dubrovnik Symposium on the Hydrology of Fractured Rocks*, International Association of Scientific Hydrology, Dubrovnik, Yugoslavia, pp. 21-31, 1965.

## Figures

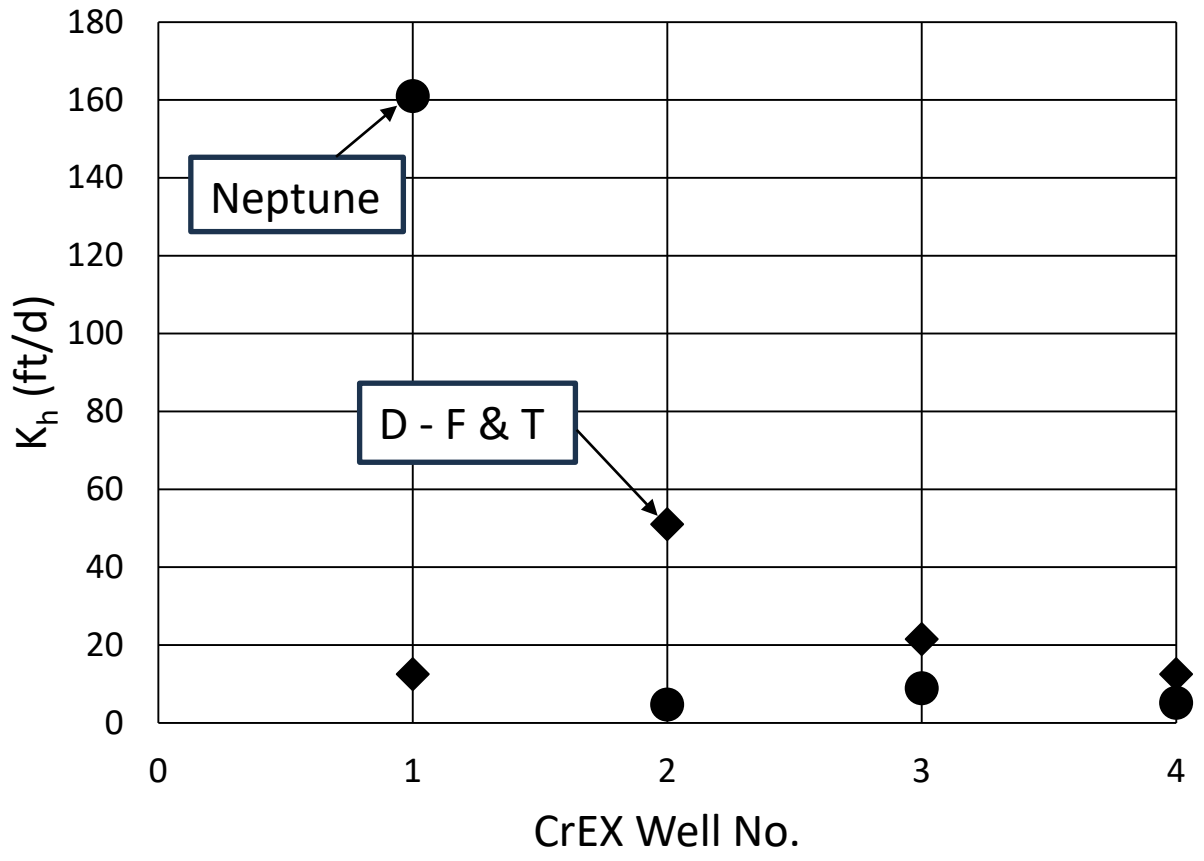


Figure 1. Comparison of the D-F & T and Neptune  $K_h$  values at CrEX wells.

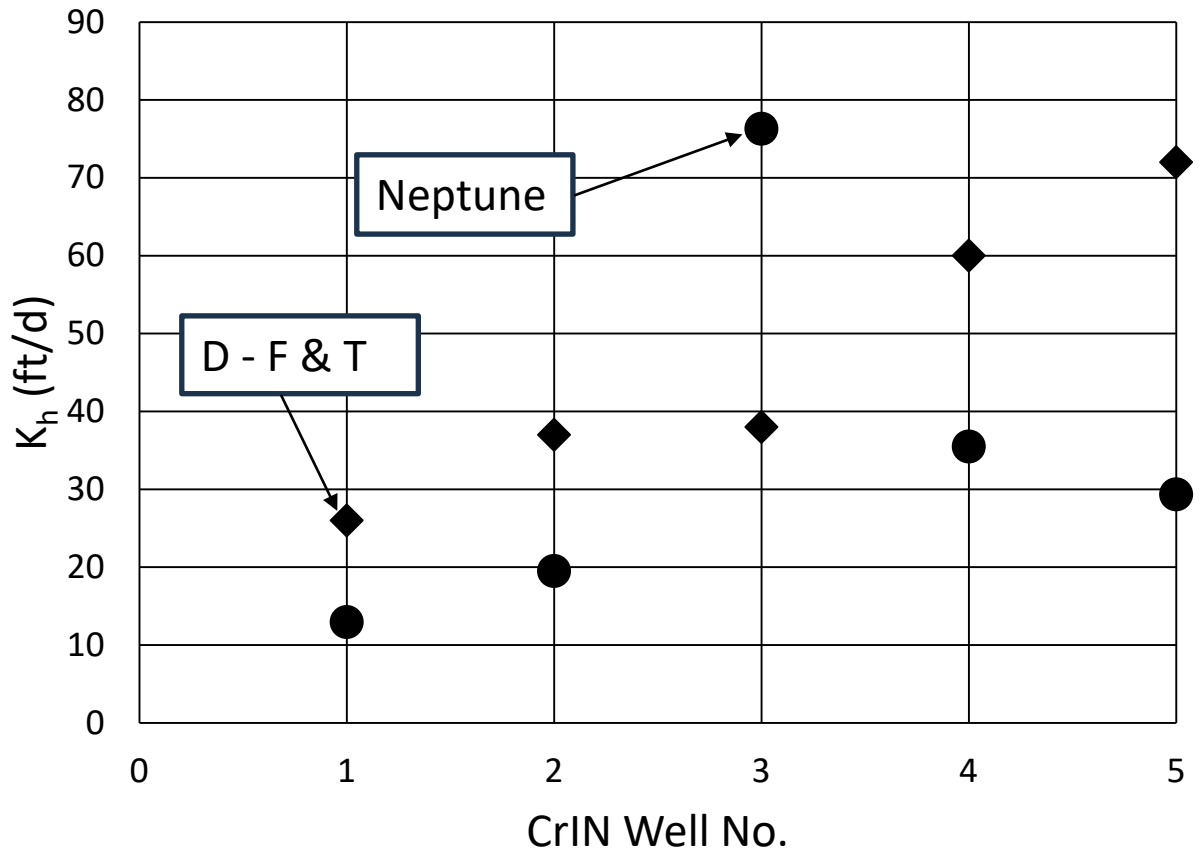


Figure 2. Comparison of the D-F & T and Neptune  $K_h$  values at CrIN wells.

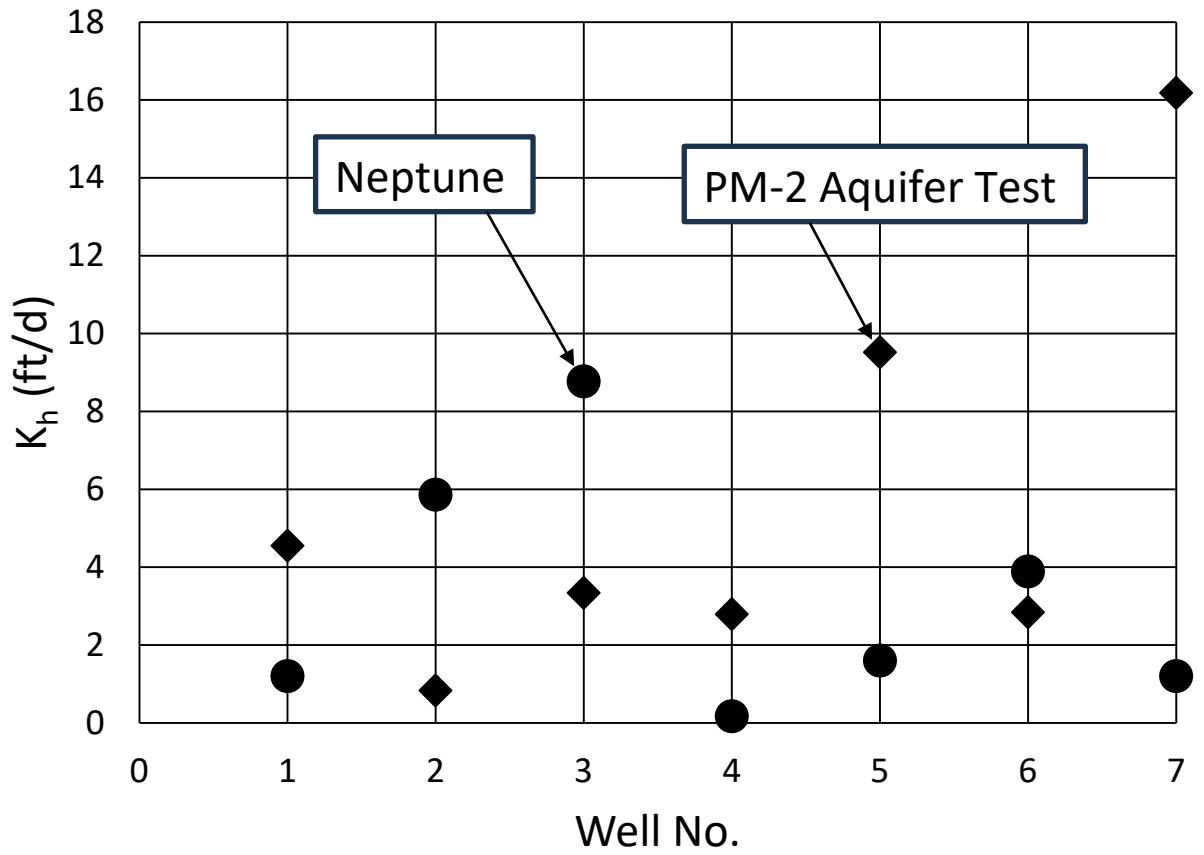


Figure 3. Comparison of the PM-2 Aquifer Test and Neptune  $K_h$  values at the seven well locations in Table 3 (The numbers in the horizontal axis represents the well numbers).

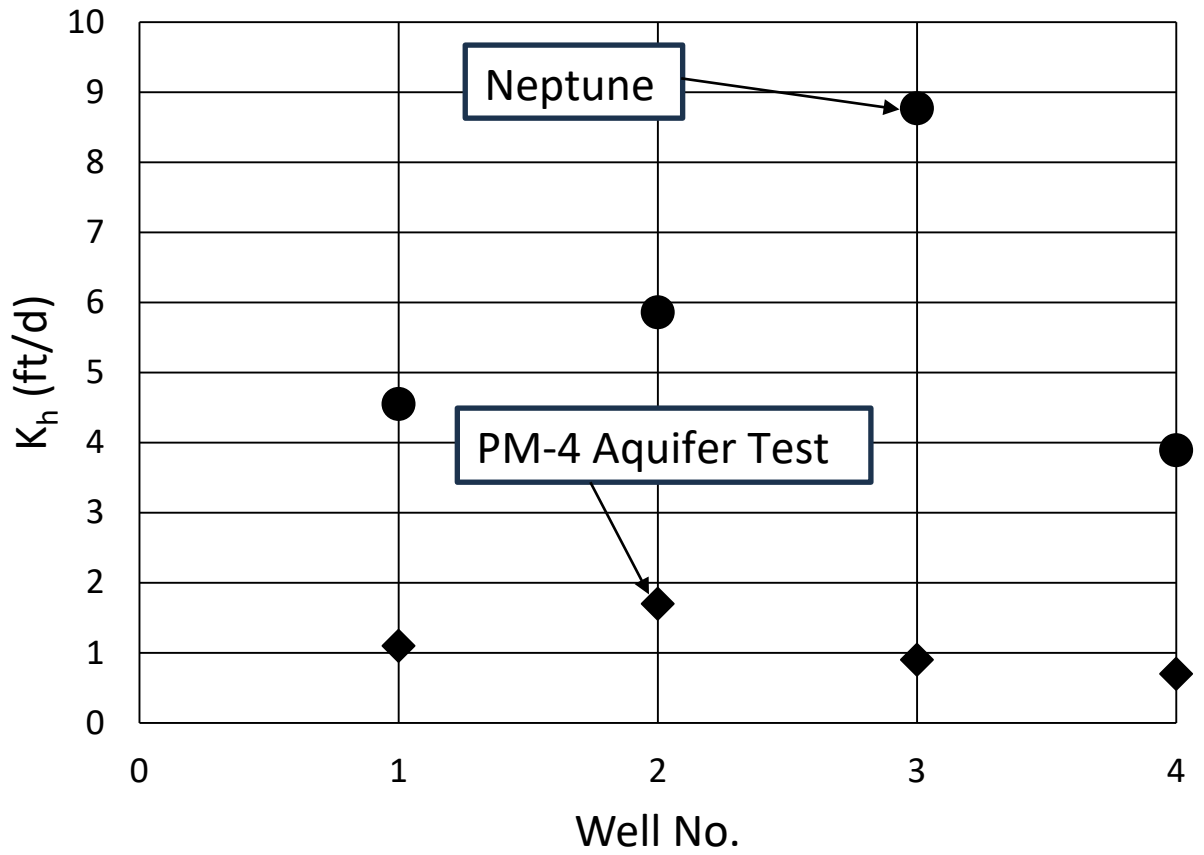


Figure 4. Comparison of the PM-4 Aquifer Test and Neptune  $K_h$  values at the seven well locations in Table 4 (The numbers in the horizontal axis represents the well numbers).

## Tables

Table 1. Horizontal hydraulic conductivity ( $K_h$ ) values using the drawdown data at the CrEX extraction wells and comparisons with Neptune’s values.

Well No.	Well	$K_h$ (ft/d) (a)	$K_{h-Neptune}$ (ft/d) (b)	Number of Neptune values	$K_{h-Neptune}/K_h$
1	CrEX-1	12.5	161.0	1	12.880
2	CrEX-2	51.0	4.7	1	0.092
3	CeEX-3	21.5	8.9	1	0.414
4	CrEX-4	12.5	5.2	2	0.416
5	CrEX-5	172.0	-	-	-

(a) Batu (2024, August 10, Table 1 of Attachment 2, p. 90).

(b) Foster, L., Neptune and Company, Inc., Excel file: K and S LANL – For ITR – 5 – 6 – 24, sent by Lauren Foster of Neptune to Susan Wacaster of DOE, May 6, 2024a.



Table 2. Horizontal hydraulic conductivity ( $K_h$ ) values using the drawdown data at the CrIN injection wells and comparison with the Neptune's values.

Well No.	Well	$K_h$ (ft/d) (a)	$K_{h-Neptune}$ (ft/d) (b)	Number of Neptune values	$K_{h-Neptune}/K_h$
1	CrIN-1	26.0	13.0	2	0.5
2	CrIN-2	37.0	19.6	2	0.530
3	CeIN-3	38.0	76.3	2	2.008
4	CrIN-4	60.0	35.5	2	0.592
5	CrEX-5	72.0	29.4	2	0.408

(a) Batu (2024, August 10, Table 1 of Attachment 2, p. 43).

(b) Foster, L., Neptune and Company, Inc., Excel file: K and S LANL – For ITR – 5 – 6 – 24, sent by Lauren Foster of Neptune to Susan Wacaster of DOE, May 6, 2024a.

Table 3. Comparison of the  $K_h$  values of PM-2 aquifer test with the  $K_h$  values of Neptune.

Well No.	Well	$K_h$ (ft/d) (a)	$K_{h-Neptune}$ (ft/d) (b)	Number of Neptune values	$K_{h-Neptune}/K_h$
1	PM-2	4.55	1.20	16	0.264
2	PM-4	0.83	5.86	16	7.060
3	PM-5	3.34	8.77	16	2.626
4	R-20 S1	2.79	0.17	1	0.061
5	R-20 S2	9.52	1.6	1	0.168
6	R-20 S3	2.84	3.89	12	1.370
7	R-32 S3	16.18	1.2	1	0.074

(a) Batu (2024, August 10, Table 2 of Attachment 3, p. 116).

(b) Foster, L., Neptune and Company, Inc., Excel file: K and S LANL – For ITR – 5 – 6 – 24, sent by Lauren Foster of Neptune to Susan Wacaster of DOE, May 6, 2024a.

Table 4. Comparison of the  $K_h$  values of PM-4 aquifer test with the  $K_h$  values of Neptune.

Well No.	Well	$K_h$ (ft/d) (a)	$K_{h-Neptune}$ (ft/d) (b)	Number of Neptune values	$K_{h-Neptune}$ / $K_h$
1	PM-2	1.1	4.55	16	4.136
2	PM-4	1.7	5.86	16	3.447
3	PM-5	0.9	8.77	16	9.744
4	R-20 S3	0.7	3.89	12	5.557

(a) Batu (2024, August 10, Table 2 of Attachment 4, p. 151).

(b) Foster, L., Neptune and Company, Inc., Excel file: K and S LANL – For ITR – 5 – 6 – 24, sent by Lauren Foster of Neptune to Susan Wacaster of DOE, May 6, 2024a.

## **Appendix D**

**Batu (2024c) - Comparison of the Horizontal Hydraulic Conductivity ( $K_h$ ) Values of the CrEX and CrIN Wells, the  $K_h$  Values of Neptune, and the Average  $K_{h-x}$  and  $K_{h-y}$  Values in the CrEX and CrIN Areas of Compendium Technical Reports (Attachment 9, Figure 2.2-3), Los Alamos, New Mexico**

# **Comparison of the Horizontal Hydraulic Conductivity ( $K_h$ ) Values of the CrEX and CrIN Wells, the $K_h$ Values Neptune, and the Average $K_{h-x}$ and $K_{h-y}$ Values in the CrEX and CrIN Areas of Compendium Technical Reports (Attachment 9, Figure 2.2-3), Los Alamos, New Mexico**

---

Vedat Batu, Ph.D., P.E.  
Argonne Associate  
Argonne National Laboratory  
Lemont, Illinois

**August 12, 2024**

This page intentionally left blank.

## Executive Summary

In this report, the horizontal hydraulic conductivity ( $K_h$ ) values determined from the steady-state drawdown values of the CrEX extraction wells and CrIN injection wells at the Los Alamos National Laboratory (New Mexico) site determined from the Dupuit-Forchheimer and Thiem ( $D - F & T$ ) well discharge formulas are compared with the average  $K_{h-x}$  and  $K_{h-y}$  values in the Compendium Technical Reports (Attachment 9, Figure 2.2-3) of Los Alamos National Laboratory (LANL, 2018a, 2018b). The Compendium Technical Reports values are also compared with the Neptune values.

The conclusions drawn are as follows:

1. The  $K_h$  values of LANL are approximately one to three orders of magnitude less than the  $K_h$  values determined from the  $D - F & T$  well discharge formulas method for the CrEX extraction wells and CrIN injection wells.

The  $K_h$  values of LANL are approximately one to three orders of magnitude less than the  $K_h$  values of Neptune for the CrEX extraction wells and CrIN injection wells.

## Contents

Executive Summary .....	ES-1
1. Purpose.....	1
2. Average Horizontal Hydraulic Conductivity ( $K_h$ ) Values in the Compendium Technical Reports of Los Alamos National Laboratory for the CrEX Extraction and CrIN Injection Wells Area.....	1
2.1 The Source Reports of LANL for the Horizontal Hydraulic Conductivity ( $K_h$ ) Values .....	1
2.1.1 Theoretical Background for the Hydraulic Conductivity Tensor .....	1
2.1.2 The Status of the $k_x$ and $k_y$ Values in the Compendium Technical Reports....	2
2.2 The $K_{h-x}$ and $K_{h-y}$ Values from the Compendium Technical Reports .....	2
3. Comparison of the LANL $K_h$ Values with the Ones Determined from the D-F & T Well Discharge Formulas Method.....	2
3.1 Comparison with the $K_h$ Values of the CrEX Wells.....	2
3.2 Comparison with the $K_h$ Values of the CrIN Wells.....	3
4. Comparison of the LANL $K_h$ Values with the Ones of Neptune .....	4
4.1 Comparison with the $K_h$ Values of the CrEX Wells.....	4
4.2 Comparison with the $K_h$ Values of the CrIN Wells.....	4
5. Conclusions .....	5
References.....	5

## Tables

- Table 1. Horizontal hydraulic conductivity ( $K_h$ ) values using the drawdown data at the CrEX extraction wells and comparisons with Neptune's values.
- Table 2. Horizontal hydraulic conductivity ( $K_h$ ) values using the drawdown data at the CrIN injection wells and comparison with the Neptune's values.



# 1. Purpose

The purpose of this report is to compare the horizontal hydraulic conductivity ( $K_h$ ) values determined from the steady-state drawdown values of the CrEX extraction wells and CrIN injection wells at the Los Alamos National Laboratory (New Mexico) site determined from the Dupuit-Forchheimer and Thiem ( $D - F$  &  $T$ ) well discharge formulas and with the average  $K_{h-x}$  and  $K_{h-y}$  values in the Compendium Technical Reports (CTR) (Attachment 9, Figure 2.2-3) of Los Alamos National Laboratory (LANL, 2018a, 2018b). The other purpose is to compare the CTR values with the Neptune values.

## 2. Average Horizontal Hydraulic Conductivity ( $K_h$ ) Values in the Compendium Technical Reports of Los Alamos National Laboratory for the CrEX Extraction and CrIN Injection Wells Area

### 2.1 The Source Reports of LANL for the Horizontal Hydraulic Conductivity ( $K_h$ ) Values

The main source report is entitled “Compendium of Technical Reports Conducted Under the Work Plan for Chromium Plume Center Characterization” and its reference is:

LANL, “Compendium of Technical Reports Conducted Under the Work Plan for Chromium Plume Center Characterization, LA-UR-18-21450, EP2018, EP2018-0026,” 641 pp., March, 2018a.

The  $K_h$  values are in the following report which is a part of the LANL (2018a) report:

LANL, “Groundwater Modeling Status Report, LA-UR-18-21450, EP2018, EP2018-0035,” March, pp. 577-641, 2018b.

which is Attachment 9 of the first report above.

The figures regarding the  $K_{h-x}$  and  $K_{h-y}$  values are given in Figure 2.2-3 in p. 612 entitled “Maps of model-predicted heterogeneity and anisotropy in the hydraulic conductivity along the top of the regional aquifer; hydraulic conductivity along  $x$ ,  $y$ , and  $z$  axes (north-south, east-west, and vertical axes, respectively) are shown in the  $a$ ,  $b$ , and  $c$  graphs above”.

#### 2.1.1 Theoretical Background for the Hydraulic Conductivity Tensor

Three-dimensional hydraulic conductivity tensor is [e.g., Bear, 1979, p. 72, Eq. (4-38)]

$$[K] = \begin{bmatrix} K_{xx} & K_{xy} & K_{xz} \\ K_{yx} & K_{yy} & K_{yz} \\ K_{zx} & K_{zy} & K_{zz} \end{bmatrix} \quad (1)$$

When the principal directions are used as the coordinate system, Eq. (1) becomes [e.g., Bear, 1979, p. 72, Eq. (4-40)]

$$[K] = \begin{bmatrix} K_{xx} & 0 & 0 \\ 0 & K_{yy} & 0 \\ 0 & 0 & K_{zz} \end{bmatrix} \quad (2)$$

in which

$$K_{xx} \equiv K_x \quad K_{yy} \equiv K_y \quad K_{zz} \equiv K_z \quad (3)$$

### 2.1.2 The Status of the $k_x$ and $k_y$ Values in the Compendium Technical Reports

Based on the expressions in Section 2.1.1, the  $k_x$  and  $k_y$  values in the Compendium Technical Reports (Attachment 9, Figure 2.2-3) of Los Alamos National Laboratory (LANL, 2018a, 2018b) are  $k_x \equiv K_x = K_{h-x}$  and  $k_y \equiv K_y = K_{h-y}$ .

It must be pointed out that in the aforementioned report, the  $K_{h-x}$  and  $K_{h-y}$  values are presented on the zonal bases with colors. Therefore, individual values at the CrEX and CrIN wells are not available. Under the framework of the aforementioned figure, the  $K_{h-x}$  and  $K_{h-y}$  values are presented in the following section.

## 2.2 The $K_{h-x}$ and $K_{h-y}$ Values from the Compendium Technical Reports

From Figure 2.2-3 (a) of the Compendium Technical Reports, the  $K_{h-x}$  values is

$$K_{h-x} = 10^{-5.6} \frac{m}{s} = 2.512 \times 10^{-6} \frac{m}{s} = 2.512 \times 10^{-4} \frac{cm}{s} = 0.712 \frac{ft}{d}$$

From Figure 2.2-3 (b), the  $K_{h-y}$  values is

$$K_{h-y} = 10^{-5.4} \frac{m}{s} = 3.981 \times 10^{-6} \frac{m}{s} = 3.981 \times 10^{-4} \frac{cm}{s} = 1.128 \frac{ft}{d}$$

## 3. Comparison of the LANL $K_h$ Values with the Ones Determined from the $D - F$ & $T$ Well Discharge Formulas Method

### 3.1 Comparison with the $K_h$ Values of the CrEX Wells

The  $K_h$  values determined from the  $D - F$  &  $T$  well discharge formulas method for the CrEX wells are given in Table 1 (Batu, 2024, August 10, p. 90, Table 1 of Attachment 2) in which  $K_h$  has values between  $K_{h-min} = 12.5 \text{ ft/d}$  and  $K_{h-max} = 172.0 \text{ ft/d}$ . Therefore, using the values in Section 2.2, one can write

$$\frac{K_{h-x}}{K_{h-min}} = \frac{0.712 \frac{ft}{d}}{12.5 \frac{ft}{d}} = 6.0 \times 10^{-2}$$

$$\frac{K_{h-x}}{K_{h-max}} = \frac{0.712 \frac{ft}{d}}{172.0 \frac{ft}{d}} = 4.1 \times 10^{-3}$$

$$\frac{K_{h-y}}{K_{h-min}} = \frac{1.128 \frac{ft}{d}}{12.5 \frac{ft}{d}} = 9.0 \times 10^{-2}$$

$$\frac{K_{h-y}}{K_{h-max}} = \frac{1.128 \frac{ft}{d}}{172.0 \frac{ft}{d}} = 6.6 \times 10^{-3}$$

The above results indicate that the  $K_h$  values of LANL are approximately one to three orders of magnitude less than the ones determined from the  $D - F$  &  $T$  well discharge formulas method for the CrEX wells.

### 3.2 Comparison with the $K_h$ Values of the CrIN Wells

The  $K_h$  values determined from the  $D - F$  &  $T$  well discharge formulas method for the CrIN wells are given in Table 2 (Batu, 2024, August 10, p. 43, Table 1 of Attachment 2) in which  $K_h$  has values between  $K_{h-min} = 26.0 \text{ ft/d}$  and  $K_{h-max} = 72.0 \text{ ft/d}$ . Therefore, using the values in Section 2.2, one can write

$$\frac{K_{h-x}}{K_{h-min}} = \frac{0.712 \frac{ft}{d}}{26.0 \frac{ft}{d}} = 2.7 \times 10^{-2}$$

$$\frac{K_{h-x}}{K_{h-max}} = \frac{0.712 \frac{ft}{d}}{72.0 \frac{ft}{d}} = 9.9 \times 10^{-3}$$

$$\frac{K_{h-y}}{K_{h-min}} = \frac{1.128 \frac{ft}{d}}{26.0 \frac{ft}{d}} = 4.3 \times 10^{-2}$$

$$\frac{K_{h-y}}{K_{h-max}} = \frac{1.128 \frac{ft}{d}}{72.0 \frac{ft}{d}} = 1.6 \times 10^{-2}$$

The above results indicate that the  $K_h$  values of LANL are approximately two orders of magnitude less than the ones determined from the  $D - F$  &  $T$  well discharge formulas method for the CrIN wells.

## 4. Comparison of the LANL $K_h$ Values with the Ones of Neptune

### 4.1 Comparison with the $K_h$ Values of the CrEX Wells

The  $K_h$  values of Neptune for the CrEX wells are given in Table 1 (Batu, 2024, August 10, p. 90, Table 1 of Attachment 2) in which  $K_h$  has values between  $K_{h-min} = 5.2 \text{ ft/d}$  and  $K_{h-max} = 161.0 \text{ ft/d}$ . Therefore, using the values in Section 2.2, one can write

$$\frac{K_{h-x}}{K_{h-min}} = \frac{0.712 \frac{ft}{d}}{5.2 \frac{ft}{d}} = 1.4 \times 10^{-1}$$

$$\frac{K_{h-x}}{K_{h-max}} = \frac{0.712 \frac{ft}{d}}{161.0 \frac{ft}{d}} = 4.4 \times 10^{-3}$$

$$\frac{K_{h-y}}{K_{h-min}} = \frac{1.128 \frac{ft}{d}}{5.2 \frac{ft}{d}} = 2.2 \times 10^{-1}$$

$$\frac{K_{h-y}}{K_{h-max}} = \frac{1.128 \frac{ft}{d}}{161.0 \frac{ft}{d}} = 7.0 \times 10^{-3}$$

The above results indicate that the  $K_h$  values of LANL are approximately one to three orders of magnitude less than the ones of Neptune for the CrEX wells.

### 4.2 Comparison with the $K_h$ Values of the CrIN Wells

The  $K_h$  values of Neptune for the CrIN wells are given in Table 2 (Batu, 2024, August 10, p. 43, Table 1 of Attachment 2) in which  $K_h$  has values between  $K_{h-min} = 13.0 \text{ ft/d}$  and  $K_{h-max} = 76.3 \text{ ft/d}$ . Therefore, using the values in Section 2.2, one can write

$$\frac{K_{h-x}}{K_{h-min}} = \frac{0.712 \frac{ft}{d}}{13.0 \frac{ft}{d}} = 5.5 \times 10^{-2}$$

$$\frac{K_{h-x}}{K_{h-max}} = \frac{0.712 \frac{ft}{d}}{76.3 \frac{ft}{d}} = 9.3 \times 10^{-3}$$

$$\frac{K_{h-y}}{K_{h-min}} = \frac{1.128 \frac{ft}{d}}{13.0 \frac{ft}{d}} = 8.7 \times 10^{-2}$$

$$\frac{K_{h-y}}{K_{h-max}} = \frac{1.128 \frac{ft}{d}}{76.3 \frac{ft}{d}} = 1.50 \times 10^{-2}$$

The above results indicate that the  $K_h$  values of LANL are approximately one to two orders of magnitude less than the  $K_h$  values of Neptune for CrIN wells.

## 5. Conclusions

Based on the foregoing analyses, the conclusions drawn are as follows:

1. The  $K_h$  values of LANL are approximately one to three orders of magnitude less than the  $K_h$  values determined from the  $D - F$  &  $T$  well discharge formulas method for the CrEX extraction wells and CrIN injection wells.
2. The  $K_h$  values of LANL are approximately one to three orders of magnitude less than the  $K_h$  values of Neptune for the CrEX extraction wells and CrIN injection wells.

## References

Batu, V., "Horizontal ( $K_h$ ) and Vertical Hydraulic Conductivity ( $K_v$ ) Values Determined from the Aquifer Tests of CrIN, CrEX, PM-2, and PM-4 at the LANL Site," August 10, 2024.

Bear, J., *Hydraulics of Groundwater*, McGraw-Hill Book Company, New York, 569 pp., New York, 1979.

Foster, L., Neptune and Company, Inc., Excel file: K and S LANL – For ITR – 5 – 6 – 24, sent by Lauren Foster of Neptune to Susan Wacaster of DOE, May 6, 2024a.

Foster, L., Neptune and Company, Inc., "Untitled Notes", sent by Daniel Stephens, 22. pp., July 23, 2024b.

LANL, "Compendium of Technical Reports Conducted Under the Work Plan for Chromium Plume Center Characterization, LA-UR-18-21450, EP2018, EP2018-0026," 641 pp., March, 2018a.

LANL, "Groundwater Modeling Status Report, LA-UR-18-21450, EP2018, EP2018-0035," March, 2018b.

## Tables

Table 1. Horizontal hydraulic conductivity ( $K_h$ ) values using the drawdown data at the CrEX extraction wells and comparisons with Neptune’s values.

Well No.	Well	$K_h$ (ft/d) (a)	$K_{h-Neptune}$ (ft/d) (b)	Number of Neptune values	$K_{h-Neptune}/K_h$
1	CrEX-1	12.5	161.0	1	12.880
2	CrEX-2	51.0	4.7	1	0.092
3	CeEX-3	21.5	8.9	1	0.414
4	CrEX-4	12.5	5.2	2	0.416
5	CrEX-5	172.0	-	-	-

(a) Batu (2024, August 10, Table 1 of Attachment 2, p. 90).

(b) Foster, L., Neptune and Company, Inc., Excel file: K and S LANL – For ITR – 5 – 6 – 24, sent by Lauren Foster of Neptune to Susan Wacaster of DOE, May 6, 2024a.

Table 2. Horizontal hydraulic conductivity ( $K_h$ ) values using the drawdown data at the CrIN injection wells and comparison with the Neptune's values.

Well No.	Well	$K_h$ (ft/d) (a)	$K_{h-Neptune}$ (ft/d) (b)	Number of Neptune values	$K_{h-Neptune}/K_h$
1	CrIN-1	26.0	13.0	2	0.5
2	CrIN-2	37.0	19.6	2	0.530
3	CeIN-3	38.0	76.3	2	2.008
4	CrIN-4	60.0	35.5	2	0.592
5	CrEX-5	72.0	29.4	2	0.408

(a) Batu (2024, August 10, Table 1 of Attachment 2, p. 43).

(a) Foster, L., Neptune and Company, Inc., Excel file: K and S LANL – For ITR – 5 – 6 – 24, sent by Lauren Foster of Neptune to Susan Wacaster of DOE, May 6, 2024a.



## **Appendix E**

**Batu (2024a) - Hydraulic Conductivity Data Evaluation of the Neptune Model for the LANL Site, Los Alamos, New Mexico**

# **Hydraulic Conductivity Data Evaluation of the Neptune Model for the LANL Site, Los Alamos, New Mexico**

---

Vedat Batu, Ph.D., P.E.  
Argonne Associate  
Argonne National Laboratory  
Lemont, Illinois

**April 3, 2024**

This page intentionally left blank.

## Executive Summary

In this report, first, the horizontal hydraulic conductivity ( $K_h$ ) values in Neptune (2023b) report are discussed along with the  $K_h$  values calculated from the transmissivity values in Figure 13 of the Neptune (2023b, p. 34) as well as the  $K_h$  values in McLin (2007, p. 488, Table1) reports. Comparing the calculated  $K_h$  values with the median value  $K_h = 12 \text{ ft/d}$  in Table 1 of Neptune report (2023b, p. 12), it has been found out that the Neptune's value is 4 to 6 times greater than the values determined from the pump test drawdown data analysis, almost one-half order of magnitude greater. No vertical hydraulic conductivity ( $K_v$ ) value is included in the Neptune's model report. Only an anisotropy ratio is included in Table 1 of Neptune's modeling report. Determination of vertical hydraulic conductivity ( $K_v$ ) for this type of site is crucial. In order to determine the vertical hydraulic conductivity ( $K_v$ ) and specific yield ( $S_y$ ) besides the horizontal hydraulic conductivity ( $K_h$ ) and storage coefficient (S) values, three-dimensional unconfined aquifer well hydraulics solutions need to be used. As a result, reanalysis of the aforementioned drawdown data analysis is proposed.

# Contents

Executive Summary .....	ES-1
1. Introduction .....	1
2. Horizontal Hydraulic Conductivity Values Based on Pump Tests Analysis and Comments on the Values of Neptune .....	1
2.1 Hydraulic Conductivity Values Used in the Neptune Model .....	1
2.2 Lengths of Screen Data of the PM-2 and PM-4 Wells.....	2
2.3 Calculated Horizontal Hydraulic Conductivity ( $K_h$ ) Values from Figure 13 of Neptune (2023a) Report Based on the Theis Type-Curve (1935) Solution .....	3
2.4 Horizontal Hydraulic Conductivity Values from the McLin (2007) Report.....	4
2.5 Proposed Reanalysis of the Drawdown Data of Some Wells.....	4
2.5.1 Methods of Analysis of the PM-2 and PM-4 Drawdown Data in Figure 13 of Neptune (2023a) .....	4
2.5.2 Drawdown Data in the McLin (2007) Paper .....	5
2.6 Comments on the Anisotropy Ratio ( $K_v/K_h$ ) .....	5
3. Conclusions .....	5
References.....	6

# 1. Introduction

In the past, pump tests were conducted in the aquifer beneath LANL, but the drawdown data were analyzed with two-dimensional well hydraulics solutions (Theis, 1935; Hantush and Jacob, 1955) with which only the horizontal hydraulic conductivity ( $K_h$ ) and storage coefficient ( $S$ ) can be determined. Besides these, with the Hantush and Jacob (1955) solution, the leakage factor can also be determined.

In this report, first, the horizontal hydraulic conductivity ( $K_h$ ) values of in Neptune (2023b) report are discussed along with the  $K_h$  values calculated from the transmissivity values in Figure 13 of the Neptune (2023b, p. 34) as well as the  $K_h$  values in McLin (2007, p. 488, Table1) reports.

Comparing the calculated  $K_h$  values with the median value  $K_h = 12 \text{ ft/d}$  in Table 1 of Neptune report (2023b, p. 12), it has been found out that the Neptune's value is 4 to 6 times greater than the values determined from the pump test drawdown data analysis, almost one-half order of magnitude greater. No vertical hydraulic conductivity ( $K_v$ ) values are included in the Neptune's report. Only an anisotropy ratio is included in Table 1 of Neptune's modeling report.

Determination of vertical hydraulic conductivity ( $K_v$ ) for this type of site is crucial. In order to determine the vertical hydraulic conductivity ( $K_v$ ) and specific yield ( $S_y$ ) besides the horizontal hydraulic conductivity ( $K_h$ ) and storage coefficient ( $S$ ) values, three-dimensional unconfined aquifer well hydraulics solutions need to be used. As a result, reanalysis of the aforementioned drawdown data analysis is proposed.

## 2. Horizontal Hydraulic Conductivity Values Based on Pump Tests Analysis and Comments on the Values of Neptune

### 2.1 Hydraulic Conductivity Values Used in the Neptune Model

In the Neptune (2023b) report, the only information available for the input data of the model is Table 1 (p. 12) and Figure 10 (p. 16). According to Table 1, the sources of information are well data and literature. But for these, fairly limited information was included in Neptune's reports. Based on the statements below (Neptune, 2023a), additional aquifer tests were also conducted ,but only the McLin (2007) report was found. The McLin (2005) and McLin (2006) reports. Neptune is also mentioned aquifer tests at R-13 and R-15. But these reports are not found, either.

Neptune (2023b, p. 12, Table 1; p. 16, Figure 10) includes the following values:

Median hydraulic conductivity =  $12 \text{ ft/d}$

The 1<sup>st</sup> percentile =  $0.2 \text{ ft/d}$

The 99<sup>th</sup> percentile =  $695 \text{ ft/d}$

Neptune does not give information whether these are related with the horizontal hydraulic conductivity ( $K_h$ ) or not. And Neptune states that in Table 1 that the sources of information are well data and literature, but they are not available in the reports.

It appears that search for site-related reports as well as pumping test data analyses were not done properly in order to determine values of horizontal hydraulic conductivity ( $K_h$ ) and vertical hydraulic conductivity ( $K_v$ ). In the Neptune (2023a, p. 34, Figure 13) report, type-curve matchings are presented for pump tests at PM-2 and PM-4 using Theis (1935) fully-penetrating confined aquifer solution and Hantush and Jacob (1955) fully-penetrating leaky aquifer solution. However, it is not clear as to why the Hantush and Jacob (1955) solution was used because Figure 1 does not include any confining layer.

Regarding aquifer tests, Neptune (2023a, pp. 33-34) states:

*“In both aquifer tests, the observed water-level displacement at the other supply well (PM-02 when PM-04 is in operation, and vice versa) diminishes after two to three weeks of sustained operation. The top two charts in Figure 13 show the aquifer test drawdown data fit to a confined aquifer Theis solution (blue curve), and the bottom two charts show the data fit to the Hantush and Jacob leaky aquifer solution. As described earlier, the confined aquifer Theis solution provides a good fit to early time data, but departs substantially from the observed data after only a few days. In contrast, the leaking aquifer solutions, which accounts for recharge from an overlying leaky layer, shows a much better overall fit to both early and late-time data. The range of estimated values of transmissivity (3,000 to 4,235 ft<sup>2</sup> /day) for the regional aquifer reflect the uncertainty in parameter estimates obtained from aquifer tests.*

*The PM-02 and PM-04 pump tests are examples of ways to estimate the maximum impact a well has in an aquifer. However, they are logistically difficult to plan (ideally all surrounding wells are turned off) and therefore these types of tests occur at most a few times in a well’s lifetime, and often only once following completion of the well. The PM-02 and PM-04 pump tests occurred in 2005 and 2006 (McLin 2005, 2006), respectively, when few monitoring wells existed in the Cr plume. Fortunately, when PM-02’s 25-day aquifer test was conducted, R-13 and R-15 along the Cr plume’s southern and western boundary, and PM-03 to the northeast of the Cr plume, were already installed. No water-level changes were observed at any of the three wells; they are thought to be too shallow and do not penetrate into the water-bearing units that yield water to PM-02 (R-13 and R-15) and/or the distance too great (PM-03, despite it being completed in similar water-bearing unit). Therefore, the impacts from pumping at PM-02 are ignored in this analysis.”*

## **2.2 Lengths of Screen Data of the PM-2 and PM-4 Wells**

In Neptune (2023a, p. 34, Figure 13),  $b = 850 \text{ ft}$ , but it is not specified whether it is the length of screen of the PM-2 and PM-4 wells. But the report of Purtymun and Stoker (1988, pp. 13-14, Tables 1 and 2) include much greater length of screen values for PM-2 and PM-4. For PM-2,  $b = 1,291 \text{ ft}$  and for PM-4,  $b = 1,594 \text{ ft}$ . The report of Koch et al. (1999, p. 5, Figure 2) includes

the construction information and stratigraphy of PM-4. The references of Neptune (2023a, 2023b) do not include the aforementioned reports.

### 2.3 Calculated Horizontal Hydraulic Conductivity ( $K_h$ ) Values from Figure 13 of Neptune (2023a) Report Based on the Theis Type-Curve (1935) Solution

The horizontal hydraulic conductivity ( $K_h$ ) values are calculated below using different length of screen values of the PM-2 and PM-4 wells given above. The values are as follows:

$K_h$  Value from the PM-2 Data for  $b = 850 \text{ ft}$  (Neptune, 2023a, p. 34, Figure 13):

$$K_h = \frac{T}{b} = \frac{3,999 \frac{ft^2}{d}}{850 \text{ ft}} = 4.71 \frac{ft}{d} = 1.66 \times 10^{-3} \frac{cm}{s}$$

$K_h$  Value from the PM-4 Data for  $b = 850 \text{ ft}$  (Neptune, 2023a, p. 34, Figure 13):

$$K_h = \frac{T}{b} = \frac{3,638 \frac{ft^2}{d}}{850 \text{ ft}} = 4.28 \frac{ft}{d} = 1.51 \times 10^{-3} \frac{cm}{s}$$

Their average is

$$K_{h-avg} = 4.49 \frac{ft}{d} = 1.37 \frac{m}{d} = 1.59 \times 10^{-3} \frac{cm}{s}$$

$K_h$  Value the from PM-2 Data for  $b = 1,291 \text{ ft}$  (Purtymun and Stoker, 988, pp. 13-14, Tables 1 and 2):

$$K_h = \frac{T}{b} = \frac{3,999 \frac{ft^2}{d}}{1,291 \text{ ft}} = 3.10 \frac{ft}{d} = 1.09 \times 10^{-3} \frac{cm}{s}$$

$K_h$  Value from PM-4 Data for  $b = 1,594 \text{ ft}$  (Purtymun and Stoker, 988, pp. 13-14, Tables 1 and 2):

$$K_h = \frac{T}{b} = \frac{3,638 \frac{ft^2}{d}}{1,594 \text{ ft}} = 2.28 \frac{ft}{d} = 8.05 \times 10^{-4} \frac{cm}{s}$$

Their average is

$$K_{h-avg} = 2.69 \frac{ft}{d} = 0.82 \frac{m}{d} = 0.95 \times 10^{-3} \frac{cm}{s}$$

Comparing these values with the median value  $K_h = 12 \text{ ft/d}$  of Table 1 of Neptune (2023b, p. 12) value (see Attachment D), it can be seen that this value is 4 to 6 times higher than the pump test  $K_h$  values given above. In other words, Neptune's value is almost one-half order of magnitude greater.



## 2.4 Horizontal Hydraulic Conductivity Values from the McLin (2007) Report

McLin (2007, p. 488, Table1) presents horizontal hydraulic conductivity ( $K_h$ ) values using the drawdown data at wells G-1A (7.5 ft/d), G-2a (7.9 ft/d), G-3a (6.2 ft/d), G-4a (7.1 ft/d), and G-5a (2.2 ft/d) based on Theis (1935) type-curve analysis. And their arithmetic average is 6.18 ft/d (1.884 m/d) which is around 50% of the median  $K_h = 12 \text{ ft/d}$  value of Neptune (2023b, p. 12, Table 1). Figure 2 in p. 486 of McLin (2007) paper includes the screen locations of these wells along with aquifer material zones. These wells are in the close proximity of the PM-2 and PM-4 wells.

The following references are in Neptune (2023a, p. 63) report:

McLin, S.G., 2005. *Analyses of the PM-2 Aquifer Test Using Multiple Observation Wells*, LA-14225-MS, Los Alamos National Laboratory, Los Alamos NM, July 2005.

McLin, S.G., 2006. *Analyses of the PM-4 Aquifer Test Using Multiple Observation Wells*, LA-14252-MS, Los Alamos National Laboratory, Los Alamos NM, January 2006.

The McLin (2005) is also a reference in McLin (2007) as well.

## 2.5 Proposed Reanalysis of the Drawdown Data of Some Wells

### 2.5.1 Methods of Analysis of the PM-2 and PM-4 Drawdown Data in Figure 13 of Neptune (2023a)

Inspection of the drawdown vs. time curves for PM-2 and PM-4 wells in Neptune (2023a, p. 34, Figure 13) reveal that after certain elapsed times, the drawdowns start to decrease which is the typical behavior of *delayed yield* of unconfined (water table) aquifer conditions (Boulton, 1954a, 1954b, 1963, 1970; Neuman, 1972,1974, 1975; Moench, 1993, 1995, 1996). The delayed yield phenomenon is well-explained in the related literature (e.g., Freeze and Cherry, 1979, pp. 324-327; Batu, 1998, 459-461). The drawdown data in the report of Neptune (2023a, p. 34, Figure 13) further reveals that the delayed yield effects were not fully developed because the pump tests periods were not long enough.

As can be seen from Figure 1, the water table and bottom elevations of the unconfined aquifer are 5,585 ft MSL and 3,500 ft MSL, respectively. Therefore, the aquifer thickness is  $b = 2,085 \text{ ft}$  and the length of screens of PM-2 and PM-4 wells are under partially-penetrating well conditions.

Based on the aforementioned points, it is recommended that the pump test data of PM-2 and PM-4 wells be reanalyzed using the unconfined aquifer well hydraulics solutions mentioned above. With type-curve analysis, besides the horizontal hydraulic conductivity ( $K_h$ ) and vertical hydraulic conductivity ( $K_v$ ), both the values of storage coefficient ( $S$ ) and specific yield ( $S_y$ ) can also be determined. There are softwares to analyze the drawdown data for unconfined under partially-penetrating well conditions.

## 2.5.2 Drawdown Data in the McLin (2007) Paper

Likewise, inspection of the drawdown vs. time curves in McLin (2007, Figures 4, 5, and 6), one can observe the *delayed yield* behavior, which is described in Section 2.5.1 with some relevant literature. Therefore, it is recommended that the pump test data curves shown in McLin (2007, Figures 4, 5, and 6) be reanalyzed using the unconfined aquifer well hydraulics solutions mentioned above in Section 2.5.1. With the type-curve analysis, besides the horizontal hydraulic conductivity ( $K_h$ ) and vertical hydraulic conductivity ( $K_v$ ), both the values of storage coefficient ( $S$ ) and specific yield ( $S_y$ ) can be determined. There are softwares to analyze the drawdown data for unconfined aquifers under partially-penetrating well conditions.

## 2.6 Comments on the Anisotropy Ratio ( $K_v/K_h$ )

In Neptune (2023b, p. 12, Table 1), an anisotropy ratio  $K_v/K_h = 0.27$  is included and called “Krige anisotropy ratio”. It is not clear as to how this value was determined.

The primary cause of anisotropy on a small scale is the orientation of clay minerals in sedimentary rocks and unconsolidated sediments. Core samples of clays and shales seldom show the anisotropy ratio ( $K_v/K_h$ ) greater than to 0.1, and usually less than 0.33 (e.g., Freeze and Cherry, 1979, p. 32). As can be seen from Section 3.1.2, the field-determined  $K_h$  value is around  $1.0 \times 10^{-3}$  cm/s, which is relatively a low value. In general, low-permeable aquifer materials tend to have lower anisotropy ratio ( $K_v/K_h$ ) value. Based on the aquifer materials shown in Figure 1 of Neptune (2023b, p. 28) and Figure 2 of McLin (2007, p. 486), the  $K_v/K_h = 0.27$  anisotropy ratio is high. And this value implies that the reanalysis of the pump test data for PM-2 and PM-4 is crucial. Also, additional pumping tests should be conducted.

As can be seen from Neptune (2023a, p. 34, Figure 13), the anisotropy ratio is  $K_h/K_v = 1$ , which is meaningless due to the fact that with the Theis (1935) and Hantush and Jacob (1955) solutions, the anisotropy ratio cannot be determined because these solutions are valid for two-dimensional radial flows towards the extraction wells.

## 3. Conclusions

The conclusions drawn from the analysis of the Neptune’s modeling report as well as pump tests conducted in the aquifer under LANL, are as follows:

1. Comparing the calculated  $K_h$  values with the median value  $K_h = 12 \text{ ft/d}$  in Table 1 of Neptune report (2023b, p. 12), it has been found out that the Neptune’s value is 4 to 6 times greater than the values determined from the pump test drawdown data analysis, almost one-half order of magnitude greater.
2. No vertical hydraulic conductivity ( $K_v$ ) values are included in Neptune’s model report. Only an anisotropy ratio is included in Table 1 of Neptune’s modeling report without providing any justification.
3. Determination of vertical hydraulic conductivity ( $K_v$ ) with aquifer tests for this type of site is crucial. In order to determine the vertical hydraulic conductivity ( $K_v$ ) and specific yield ( $S_y$ )

besides the horizontal hydraulic conductivity ( $K_h$ ) and storage coefficient (S) values, three-dimensional unconfined aquifer well hydraulics solutions need to be used. As a result, reanalysis of the aforementioned drawdown data analysis is proposed.

4. Also, additional pumping tests should be conducted.

## References

- Batu, V., *Aquifer Hydraulics: A Comprehensive Guide to Hydrogeologic Data Analysis*, John Wiley & Sons, Inc., 727 pp., New York, 1998.
- Boulton, N.S., "The Drawdown of the Water-Table Under Non-Steady Conditions Near a Pumped Well in an Unconfined Formation," *Proceedings of the Institution of Civil Engineers*, London, Great Britain, Part III, pp. 564-579, 1954a.
- Boulton, N.S., "Unsteady Radial Flow to a Pumped Well Allowing for Delayed Yield from Storage," *International Association of Scientific Hydrology*, Vol. II, pp. 472-477, 1954b.
- Boulton, N.S., "Analysis of Data from Non-equilibrium Pumping Tests Allowing for Delayed Yield from Storage," *Proceedings of the Institution of Civil Engineers*, London, Great Britain, Vol. 26, pp. 469-482, 1963.
- Boulton, N.S., "Analysis of Data from Pumping Tests in Unconfined Anisotropic Aquifers," *Journal of Hydrology*, Vol. 10, pp. 369-378, 1970.
- Freeze, R.A., and J.A. Cherry, *Groundwater*, Prentice-Hall, Inc., Englewood Cliffs, New Jersey, 604 pp., 1979.
- Hantush, M.S., and C.E. Jacob, "Non-Steady Radial Flow in an Infinite Leaky Aquifer," *Transactions*, American Geophysical Union, Vol. 36, No. 1, pp. 95-100, 1955.
- Koch, R.J., P. Longmire, D.B. Rogers, and K. Mullen, "Report of Testing and Sampling of Municipal Supply Well PM-4," Los Alamos National Laboratory, LA-13648, 40 pp., December, 1988.
- McLin, S.G., *Analyses of the PM-2 Aquifer Test Using Multiple Observation Wells*, LA-14225-MS, Los Alamos National Laboratory, Los Alamos NM, July 2005.
- McLin, S.G., *Analyses of the PM-4 Aquifer Test Using Multiple Observation Wells*, LA-14252-MS, Los Alamos National Laboratory, Los Alamos NM, January 20, 2006.
- McLin, S.G., "Hydrogeologic Characterization of Groundwater System Using Sequential Aquifer Tests and Flowmeter Logs," *New Mexico Geological Society Guidebook*, 58<sup>th</sup> Field Conference, Jemez Mountains II, pp. 485-491, 2007.
- Moench, A.F., "Computation of Type Curves for Flow to Partially Penetrating Wells in Water-Table Aquifers," *Ground Water*, Vol. 31, No. 6, pp. 966-971, 1993.

- Moench, A.F., "Combining the Neuman and Boulton Models for Flow to a Well in An unconfined Aquifer, *Ground Water*, Vol. 33, No. 3, pp. 378-384, 1995.
- Moench, A.F., "Flow to a Well in a Water-Table Aquifer: An Improved Laplace Transform Solution," *Ground Water*, Vol. 34, No. 4, pp. 593-596, 1996.
- Neptune and Company, Inc., "*Hydraulic Analysis of the Pajarito Plateau*", EMID-702780, prepared by Neptune and Company, Inc. for the U.S. Department of Energy Environmental Management Los Alamos Field Office, Neptune and Company Inc., Los Alamos NM, 64 pp., June 16, 2023a.
- Neptune and Company, Inc., "*Chromium Model: Calibrated with Uncertainty through 2022*", prepared by Neptune and Company, Inc. for the U.S. Department of Energy Environmental Management Los Alamos Field Office, Neptune and Company Inc., Los Alamos NM, 69 pp., June 16, 2023b.
- Neptune and Company, Inc., "*Chromium Interim Measure Capture Zone Analysis*", prepared by Neptune and Company, Inc. for the U.S. Department of Energy Environmental Management Los Alamos Field Office, Neptune and Company Inc., Los Alamos NM, 46 pp., June 16, 2023c.
- Neuman, S.P., "Theory of Flow in Unconfined Aquifers Considering Delayed Gravity Response of the Water Table," *Water Resources Research*, Vol. 8, No. 4, pp. 1031-1045, 1972.
- Neuman, S.P., "Effect of Partial Penetration on Flow in Unconfined Aquifers Considering Delayed Gravity Response," *Water Resources Research*, Vol. 10, No. 2, pp. 303-312, 1974.
- Neuman, S.P., "Analysis of Pumping Test Data from Anisotropic Unconfined Aquifers Considering Delayed Gravity Response," *Water Resources Research*, Vol. 11, No. 2, pp. 329-342, 1975.
- N3B Los Alamos, "Annual Progress Report on Chromium Plume Control Interim Measure Performance, April 2022 through March 2023," EM2023-0392, June, 2023.
- Theis, C.V., "The Relation between the Lowering of the Piezometric Surface and the Rate and Duration of Discharge of a Well Using Ground-Water Storage," *Transactions, American Geophysical Union*, Vol. 16, pp. 519-524, August, 1935.
- Purtymun, W.D., and A.K. Stoker, "Water Supply at Los Alamos: Current Status of Wells and Future Supply Wells," Los Alamos National Laboratory, LA-11332-MS, 16 pp., August, 1988.

## **Appendix F**

**Batu (2024g) - Evaluation of the Measured  
Cr<sup>6+</sup> Concentrations and Flow Rates of PM-2, PM-3, PM-4, and  
PM-5 Water Supply Wells Between 2006 and 2024 Along with  
Their Well Diagrams, Los Alamos, New Mexico**

# **Evaluation of the Measured $Cr^{6+}$ Concentrations and Flow Rates of PM-2, PM-3, PM-4, and PM-5 Water Supply Wells Between 2006 and 2024 Along with Their Well Diagrams, Los Alamos, New Mexico**

---

Vedat Batu, Ph.D., P.E.  
Argonne Associate  
Argonne National Laboratory  
Lemont, Illinois

**August 19, 2024**

This page intentionally left blank.

## Executive Summary

In this report, the measured chromium ( $Cr^{6+}$ ) concentrations and flow rates of the water supply wells (PM-2, PM-3, PM-4, and PM-5) between 2006 and 2024 along with their well diagrams are evaluated. In this evaluation, PM-1 is not included because its concentration and flow rate data are not available. The other point is that before 2006, chromium ( $Cr^{6+}$ ) concentration and flow rate data of the water supply wells PM-2, PM-3, PM-4, and PM-5 are not available. The plume is primarily located inside the polygon formed by PM-2, PM-3, PM-4, and PM-5 and their significantly high extraction rates potentially need to be taken into account in the remedial design activities. In order to achieve this task more efficiently, it is concluded that the temporal chromium ( $Cr^{6+}$ ) concentration variations of these wells as well as nearby monitoring wells need to be analyzed with their temporal flow rates.

In another report (Batu, 2024) entitled “Determination of the Zone of Influence of the PM-4 Water Supply Well and Evaluation of the Effects of All Water Supply Wells to the  $Cr^{6+}$  Plume Area, Los Alamos, New Mexico”, of these four PM wells, the zone of influence of the PM-4 water supply well with a partially-penetrating three-dimensional analytical well hydraulics solution for unconfined aquifers has been determined. Specifically, the drawdown variation at the location of R-28, which is located in the plume area, is determined. The PM-4 well is the second closest water supply well to the main plume (around R-28) after PM-3 water supply well. In Batu (2024) report the following conclusions were drawn:

1. After 30 d (1 month) of elapsed time the drawdown at R-28 is around 0.1 ft. After 300 d of elapsed time the drawdown at R-28 will be 0.88 ft. And after 1,000 d, the drawdown will be 3.19 ft. The key point is that with the significantly high extraction rates at PM-4 (1,400 *gpm*), the zone of influence of PM-4 will be noticeably at R-28 even after 1 month of elapsed time. And these results are consistent with the results in McLin (2005, pp. 6-7) report which are based on the actual drawdown measurements when water was extracted from PM-2.
2. The chromium ( $Cr^{6+}$ ) plume is inside of the polygon formed by PM-2, PM-3, PM-4, and PM-5 having recorded extraction rates up to 1,500 *gpm*. Based on the available reports, potentially these wells may extract water simultaneously from the aquifer under intermittent conditions. Therefore, in order to take under control of the plume, inward hydraulic gradients need to be generated with CrEx-1, CrEx-2, CrEx-3, and CrEx-4 with comparable water extraction rates. But the screen intervals of these wells are in the Puye Formation and close to the water table which is a drawback as compared with the long and deep screen intervals of the water supply wells.



# Contents

Executive Summary .....	ES-1
1. Purpose.....	1
2. Well Diagrams of the PM Wells and Their Distances to the Chromium Plume Center .....	1
2.1 Well Diagrams of the PM Wells.....	1
2.1.1 PM-1 Status in the Aquifer .....	1
2.1.2 PM-2 Status in the Aquifer .....	1
2.1.3 PM-3 Status in the Aquifer .....	1
2.1.4 PM-4 Status in the Aquifer .....	2
2.1.5 PM-5 Status in the Aquifer .....	2
2.2 Distances of the PM Wells to the Center of the Chromium (Cr <sup>6+</sup> ) Plume .....	2
2.2.1 Distance of PM-1 to R-42 .....	2
2.2.2 Distance of PM-2 to R-42 .....	2
2.2.3 Distance of PM-3 to R-42 .....	2
2.2.4 Distance of PM-4 to R-42 .....	2
2.2.5 Distance of PM-5 to R-42 .....	2
3. Measured Chromium (Cr <sup>6+</sup> ) Concentrations at the PM Wells and Their Average Flow Rates.....	2
3.1 Measured Chromium (Cr <sup>6+</sup> ) Concentrations at PM-1.....	2
3.2 Measured Chromium (Cr <sup>6+</sup> ) Concentrations at PM-2.....	2
3.3 Measured Chromium (Cr <sup>6+</sup> ) Concentrations at PM-3.....	3
3.4 Measured Chromium (Cr <sup>6+</sup> ) Concentrations at PM-4.....	3
3.5 Measured Chromium (Cr <sup>6+</sup> ) Concentrations at PM-5.....	3
4. Zone of Influence of the PM Wells .....	3
5. Conclusions .....	4
References.....	5

# Figures

- Figure 1. The conceptual model of the LANL site.
- Figure 2. PM well diagrams in the conceptual model of the LANL site.
- Figure 3. Measured Cr<sup>6+</sup> concentrations at PM-2 in 2006 and 2007.
- Figure 4. Measured flow rates at PM-2 between 02/19/2014 and 12/18/2023.
- Figure 5. Measured Cr<sup>6+</sup> concentrations at PM-3 in 2006 and 2007.
- Figure 6. Measured flow rates at PM-3 between 11/16/2010 and 03/25/2022.
- Figure 7. Measured Cr<sup>6+</sup> concentrations at R-35a between 8/30/2007 to 2/16/2024.
- Figure 8. Measured Cr<sup>6+</sup> concentrations at R-35b between 8/29/2007 to 2/9/2024.
- Figure 9. Measured Cr<sup>6+</sup> concentrations at PM-4 in 2006 and 2007.
- Figure 10. Measured flow rates at PM-4 between 09/09/2014 and 03/25/2024.

Figure 11. Measured  $Cr^{6+}$  concentrations at PM-5 in 2006 and 2007.

Figure 12. Measured flow rates at PM-5 between 11/16/2010 and 03/25/2024.

## **Appendices**

Appendix A PM Wells Geometry Data

## 1. Purpose

The purpose of this report is to evaluate the measured chromium ( $Cr^{6+}$ ) concentrations and flow rates of the water supply wells (PM-2, PM-3, PM-4, and PM-5) between 2006 and 2024 along with their well diagrams. The flow rates of the PM wells were provided by Susan Wacaster in an Excel file entitled “**PM2-5-Field Parameters EXPORT 06-20-2024**” on June 20, 2024.

In this evaluation, PM-1 is not included because its concentration and flow rate data are not available. The other point is that before 2006, chromium ( $Cr^{6+}$ ) concentrations and flow rates data of the water supply wells PM-2, PM-3, PM-4, and PM-5 are not available. The plume is primarily located inside the polygon formed by PM-2, PM-3, PM-4, and PM-5 and their significantly high extraction rates potentially need to be taken into account in the remedial design activities. In order to achieve this task more efficiently, the temporal chromium ( $Cr^{6+}$ ) concentration variations of these wells as well as nearby monitoring wells need to be analyzed with their temporal flow rates.

## 2. Well Diagrams of the PM Wells and Their Distances to the Chromium Plume Center

The conceptual model of the LANL site is shown in Figure 1. The dimensions of the formations in the conceptual model are all approximate and the dips range from southwest to southeast, depending on location. Figure 2 shows the PM well diagrams in the conceptual model of the LANL site. The well construction data of the PM wells are taken from the report of Los Alamos National Laboratory (LANL, 2009). The water table is assumed to be located approximately at 1,000 ft below the ground surface (bgs). The well diagrams of the PM wells are discussed below.

### 2.1 Well Diagrams of the PM Wells

#### 2.1.1 PM-1 Status in the Aquifer

As can be seen from Figure 2, the screen interval of PM-1 is 1,534 ft and it extends from 55 ft above the water table to almost to the lower boundary of the Miocene basalt. Namely, the screen interval of PM-2 cover the whole thicknesses of the Puye Formation and Miocene Sediments of Miocene basalt below the regional water table of the unconfined aquifer.

#### 2.1.2 PM-2 Status in the Aquifer

The screen interval of PM-2 is 1,276 ft (Figure 2) and is submerged 126 ft (as of 2012), with Miocene basalts in the lower part of the screen.

#### 2.1.3 PM-3 Status in the Aquifer

As can be seen from Figure 2, the screen interval of PM-3 is 1,576 ft and is submerged 167 ft (as of 2012) and the well screen extends 1,002 ft below the Miocene basalt. The top of the screen is in Miocene sediment (i.e., there is no Puye Formation in the well screen interval).

#### **2.1.4 PM-4 Status in the Aquifer**

The screen interval of PM-4 is 1,594 ft and is submerged 174 ft (as of 2013) and the well screen extends 424 ft below the Miocene basalt. There is no Puye Formation in the well screen interval.

#### **2.1.5 PM-5 Status in the Aquifer**

The status of PM-5 is similar to PM-4. The screen interval of PM-5 is 1,632 ft and is submerged 187 ft (as of 2012) and the well screen extends 332 ft below the Miocene basalt. There is no Puye Formation in the well screen interval.

### **2.2 Distances of the PM Wells to the Center of the Chromium ( $Cr^{6+}$ ) Plume**

By considering that the R-42 well, which has the maximum measured chromium ( $Cr^{6+}$ ) concentration ( $1,240 \mu g/L$ ), is the center of the chromium ( $Cr^{6+}$ ) plume, their distances are given below.

#### **2.2.1 Distance of PM-1 to R-42**

The distance between PM-1 and R-42 is approximately 10,000 ft.

#### **2.2.2 Distance of PM-2 to R-42**

The distance between PM-2 and R-42 is approximately 8,400 ft.

#### **2.2.3 Distance of PM-3 to R-42**

The distance between PM-2 and R-42 is approximately 5,000 ft. Most importantly, PM-3 is approximately 2,500 ft off from the main flow direction which is to the southwest direction.

#### **2.2.4 Distance of PM-4 to R-42**

The distance between PM-4 and R-42 is approximately 4,700 ft.

#### **2.2.5 Distance of PM-5 to R-42**

The distance between PM-5 and R-42 is approximately 5,800 ft. Most importantly, PM-5 is in the upgradient direction from R-42.

### **3. Measured Chromium ( $Cr^{6+}$ ) Concentrations at the PM Wells and Their Average Flow Rates**

#### **3.1 Measured Chromium ( $Cr^{6+}$ ) Concentrations at PM-1**

Neither the measured chromium ( $Cr^{6+}$ ) concentrations nor the flow rates at PM-1 are available.

#### **3.2 Measured Chromium ( $Cr^{6+}$ ) Concentrations at PM-2**

Measured chromium ( $Cr^{6+}$ ) Concentrations at PM-2 in 2006 and 2007 are shown in Figure 3, which shows that they are around  $4 \mu g/L$  which is far below than the threshold limit ( $50 \mu g/L$ ).

The flow rates at PM-2 between 02/19/2014 and 12/18/2023 are shown in Figure 4 with 1,142 *gpm* average flow rate.

### 3.3 Measured Chromium ( $Cr^{6+}$ ) Concentrations at PM-3

Measured chromium ( $Cr^{6+}$ ) Concentrations at PM-3 in 2006 and 2007 are shown in Figure 5, which shows that they are around 4  $\mu g/L$  which is far below than the threshold limit (50  $\mu g/L$ ). The flow rates at PM-3 between 11/16/2010 and 03/25/2022 are shown in Figure 6 with 1,404 *gpm* average flow rate.

The closest monitoring wells to PM-3 are R-35a and R-35b which are approximately 440 ft southwest of PM-3. The screen length of R-35a and R-35b are 49.1 ft and 23.1 ft, respectively, and they start nearby the water table. Figure 7 shows the measured chromium ( $Cr^{6+}$ ) concentrations at R-35a between 8/30/2007 and 2/16/2024 and their average is 4.9  $\mu g/L$ . Likewise, Figure 8 shows the measured chromium ( $Cr^{6+}$ ) concentrations at R-35b between 8/29/2007 and 2/9/2024 and their average is 6.1  $\mu g/L$ . These values are close to the average value at PM-3 in 2006 and 2007. Although, measured chromium ( $Cr^{6+}$ ) concentrations do not exist at PM-3 after 2007, one may deduce that its concentrations were perhaps around these values.

### 3.4 Measured Chromium ( $Cr^{6+}$ ) Concentrations at PM-4

Measured chromium ( $Cr^{6+}$ ) Concentrations at PM-4 in 2006 and 2007 are shown in Figure 9, which shows that they are around 5.5  $\mu g/L$  which is far below than the threshold limit (50  $\mu g/L$ ). The flow rates at PM-4 between 09/09/2014 and 03/25/2024 are shown in Figure 10 with 1,196 *gpm* average flow rate.

### 3.5 Measured Chromium ( $Cr^{6+}$ ) Concentrations at PM-5

Measured chromium ( $Cr^{6+}$ ) Concentrations at PM-5 in 2006 and 2007 are shown in Figure 11, which shows that they are around 5.5  $\mu g/L$  which is far below than the threshold limit (50  $\mu g/L$ ). The flow rates at PM-5 between 11/16/2010 and 03/25/2024 are shown in Figure 12 with 952 *gpm* average flow rate.

## 4. Zone of Influence of the PM Wells

As mentioned in Section 1.0, the chromium ( $Cr^{6+}$ ) plume is primarily located inside the polygon formed by PM-2, PM-3, PM-4, and PM-5 and their significantly high extraction rates potentially need to be taken into account in the remedial design activities. In another report (Batu, 2024) entitled “**Determination of the Zone of Influence of the PM-4 Water Supply Well and Evaluation of the Effects of All Water Supply Wells to the  $Cr^{6+}$  Plume Area, Los Alamos, New Mexico**”, of these four PM wells, the zone of influence of the PM-4 water supply well with a partially-penetrating three-dimensional analytical well hydraulics solution for unconfined aquifers has been determined. Specifically, the drawdown variation at the location of R-28, which is located in the plume area, is determined. PM-4 is the second closest water supply well to the

main plume (around R-28) after PM-3 water supply well. In the aforementioned Batu (2024) report, the following conclusions were drawn:

1. After 30 d (1 month) of elapsed time the drawdown at R-28 is around 0.1 ft. After 300 d of elapsed time the drawdown at R-28 will be 0.88 ft. And after 1,000 d, the drawdown will be 3.19 ft. The key point is that with the significantly high extraction rate at PM-4 (1,400 *gpm*), the zone of influence of PM-4 will be noticeably at R-28 even after 1 month of elapsed time. And these results are consistent with the points in McLin (2005, pp. 6-7) which are based on the actual drawdown measurements when water was extracted from PM-2.
2. The chromium ( $Cr^{6+}$ ) plume is inside of the polygon formed by PM-2, PM-3, PM-4, and PM-5 having recorded extraction rates up to 1,500 *gpm*. Based on the available reports, potentially these wells may extract water simultaneously from the aquifer under intermittent conditions. Therefore, in order to take under the control of the plume, inward gradients need to be generated with CrEx-1, CrEx-2, CrEx-3, and CrEx-4 extraction wells with comparable water extraction rates. But the screen intervals of these wells are in the Puye Formation and close to the water table which is a drawback as compared with the long and deep screen intervals of the water supply wells.

## 5. Conclusions

The measured chromium ( $Cr^{6+}$ ) concentrations and flow rates of the water supply wells (PM-2, PM-3, PM-4, and PM-5) between 2006 and 2024 along with their well diagrams are critically evaluated. In this evaluation, PM-1 is not included because its concentrations and flow rates data are not available. The other point is that before 2006, chromium ( $Cr^{6+}$ ) concentration and flow rate data of the water supply wells PM-2, PM-3, PM-4, and PM-5 are not available. The plume is primarily located inside the polygon formed by PM-2, PM-3, PM-4, and PM-5 and their significantly high extraction rates potentially need to be taken into account in the remedial design activities. In order to achieve this task more efficiently, the temporal chromium ( $Cr^{6+}$ ) concentration variations of these wells as well as nearby monitoring wells need to be analyzed with their temporal flow rates.

In another report (Batu, 2024) entitled “Determination of the Zone of Influence of the PM-4 Water Supply Well and Evaluation of the Effects of All Water Supply Wells to the  $Cr^{6+}$  Plume Area, Los Alamos, New Mexico”, of these four PM wells, the zone of influence of the PM-4 water supply well with a partially-penetrating three-dimensional analytical well hydraulics solution for unconfined aquifers has been determined. Specifically, the drawdown variation at the location of R-28, which is located in the plume area, is determined. PM-4 is the second closest water supply well to the main plume (Around R-28) after PM-3 water supply well. Some key conclusions have been drawn in Batu (2024) report and they are as follows:

1. After 30 d (1 month) of elapsed time the drawdown at R-28 is around 0.1 ft. After 300 d of elapsed time the drawdown at R-28 will be 0.88 ft. And after 1,000 d, the drawdown will be 3.19 ft. The key point is that with the significantly high extraction rate at PM-4 (1,400 *gpm*), the zone of influence of PM-4 will be noticeably at R-28 even after 1 month of elapsed time.

And these results are consistent with the points in McLin (2005, pp. 6-7) which are based on the actual drawdown measurements when water was extracted from PM-2.

2. The chromium ( $Cr^{6+}$ ) plume is inside of the polygon formed by PM-2, PM-3, PM-4, and PM-5 having recorded extraction rates up to 1,500 *gpm*. Based on the available reports, potentially these wells may extract water simultaneously from the aquifer under intermittent conditions. Therefore, in order to take under control of the plume, inward gradients need to be generated with CrEx-1, CrEx-2, CrEx-3, and CrEx-4 with comparable water extraction rates. But the screen intervals of these wells are in the Puye Formation and close to the water table which is a drawback as compared with the long and deep screen intervals of the water supply wells.

## References

Batu, V., "Determination of the Zone of Influence of the PM-4 Water Supply Well and Evaluation of the Effects of All Water Supply Wells to the  $Cr^{6+}$  Plume Area, Los Alamos, New Mexico," 14 pp., 2024.

LANL, "Groundwater Level Status Report for 2008, Los Alamos National Laboratory," LA-14397-PR, Progress Report, 247 pp., March, 2009.

McLin, S.G., "Analysis of the PM-2 Aquifer Test Using Multiple Observation Wells, LA-14225-MS, Los Alamos National Laboratory," Los Alamos, New Mexico, July, 2005.

## Figures



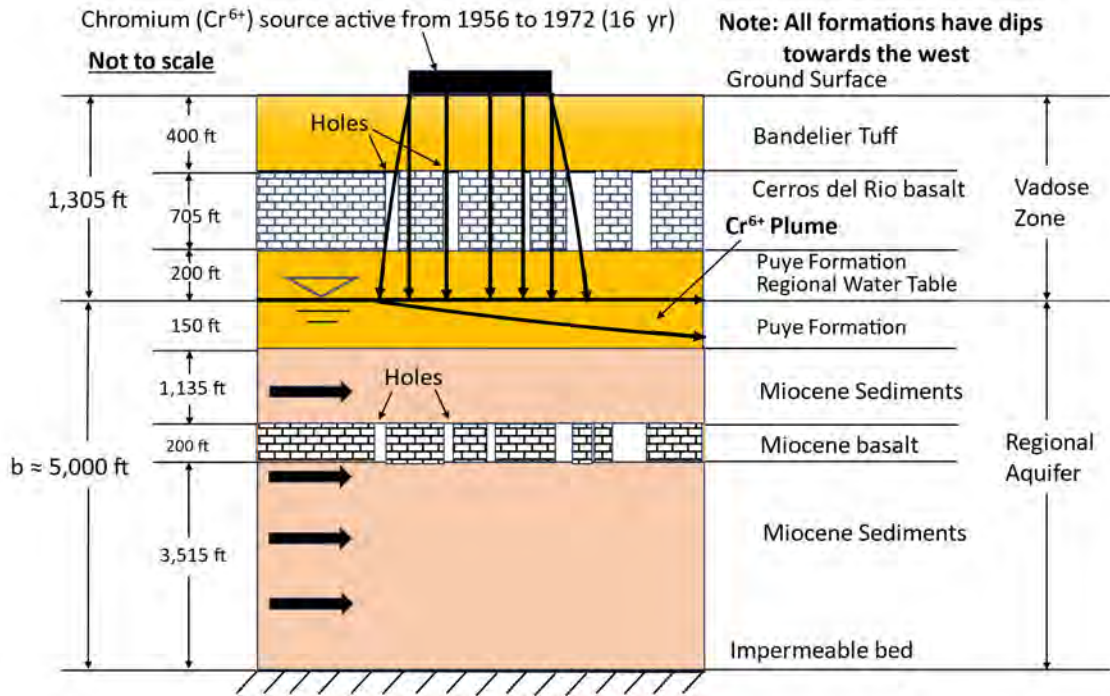


Figure 1. The conceptual model of the LANL site.

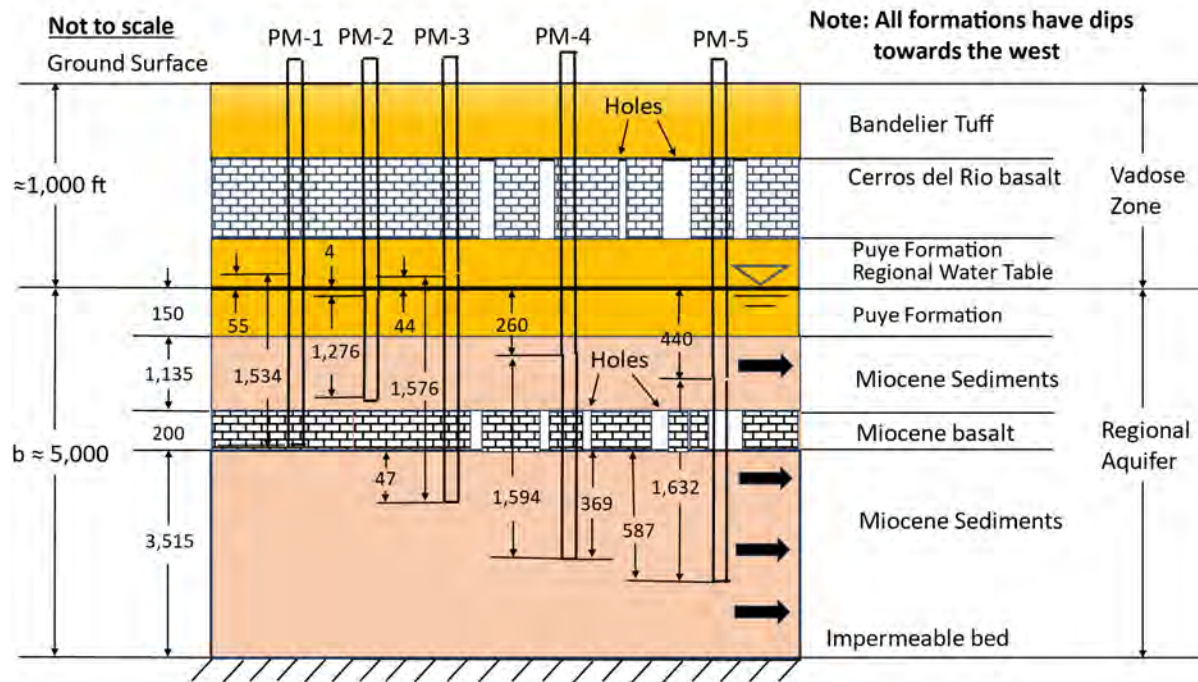


Figure 2. PM well diagrams in the conceptual model of the LANL site.

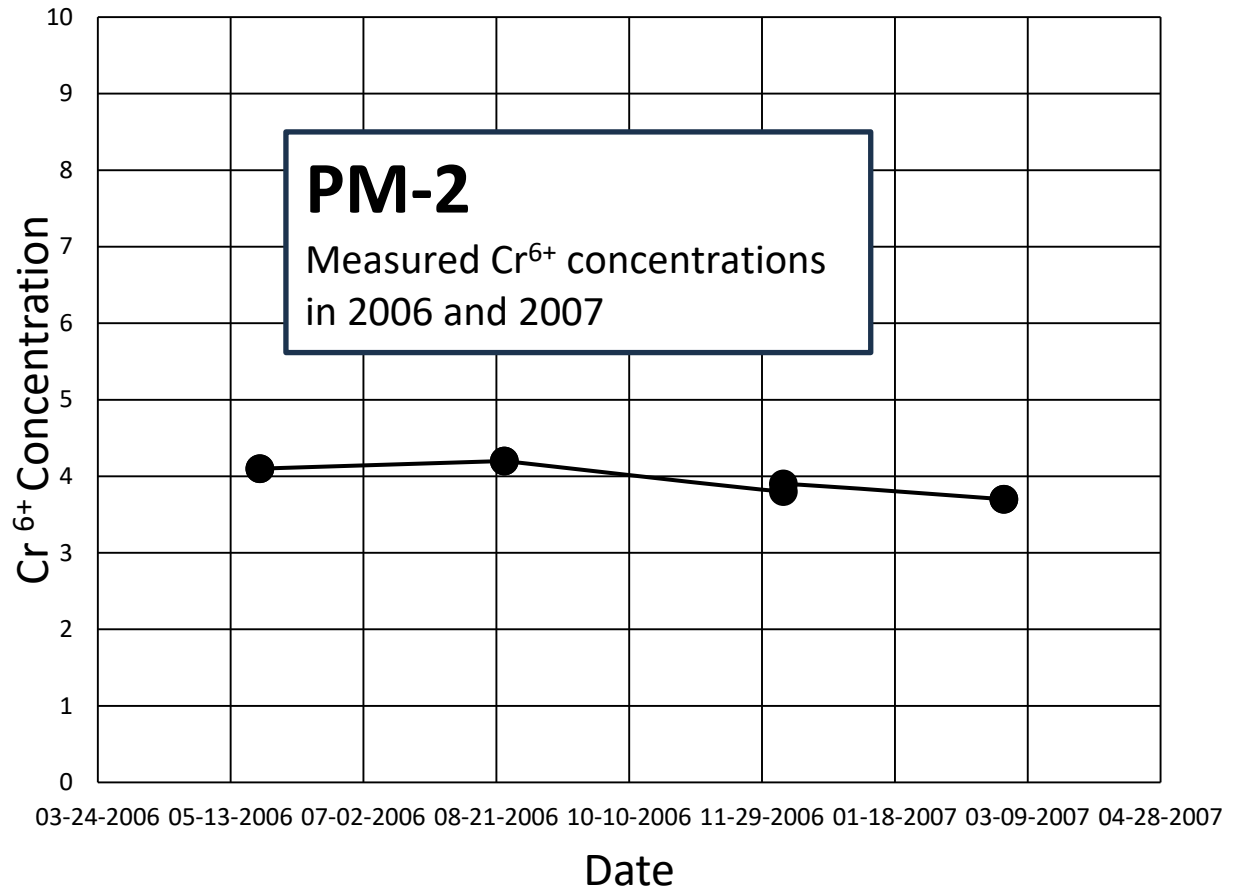


Figure 3. Measured  $Cr^{6+}$  concentrations at PM-2 in 2006 and 2007.

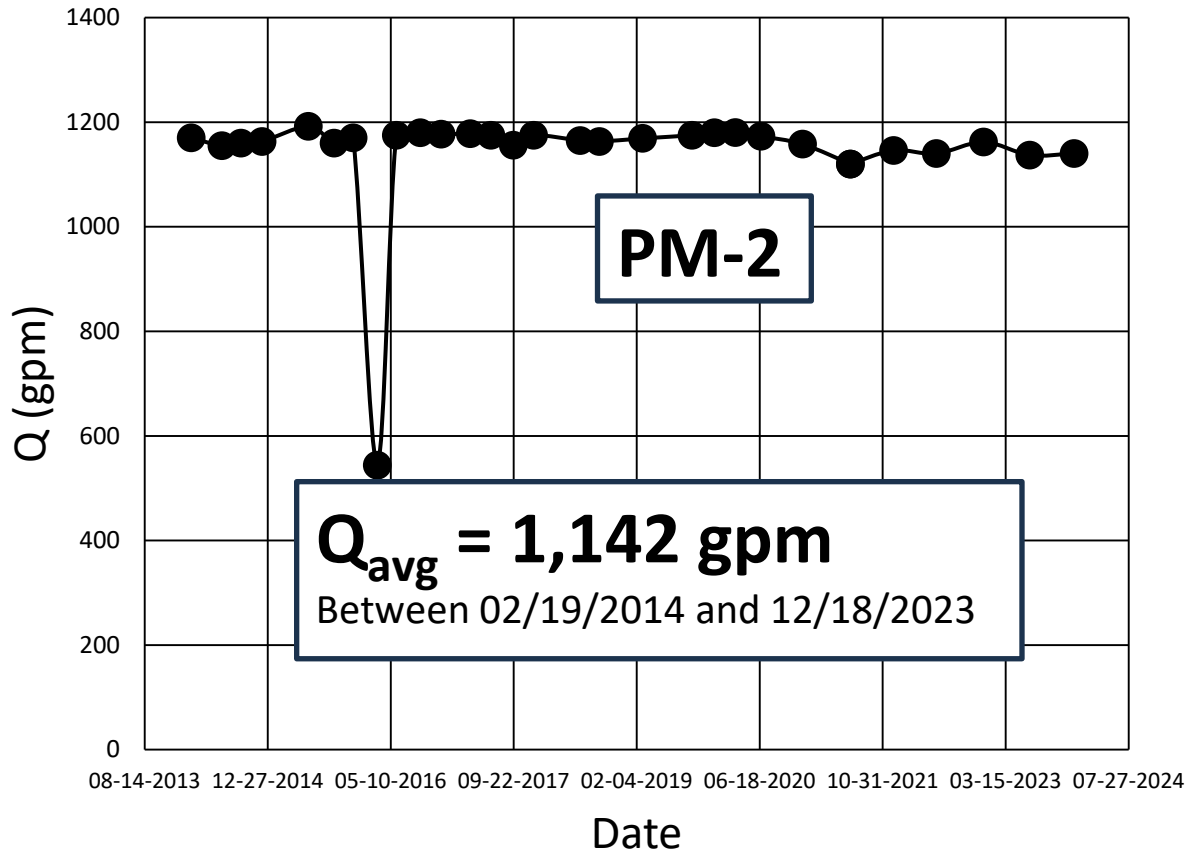


Figure 4. Measured flow rates at PM-2 between 02/19/2014 and 12/18/2023.

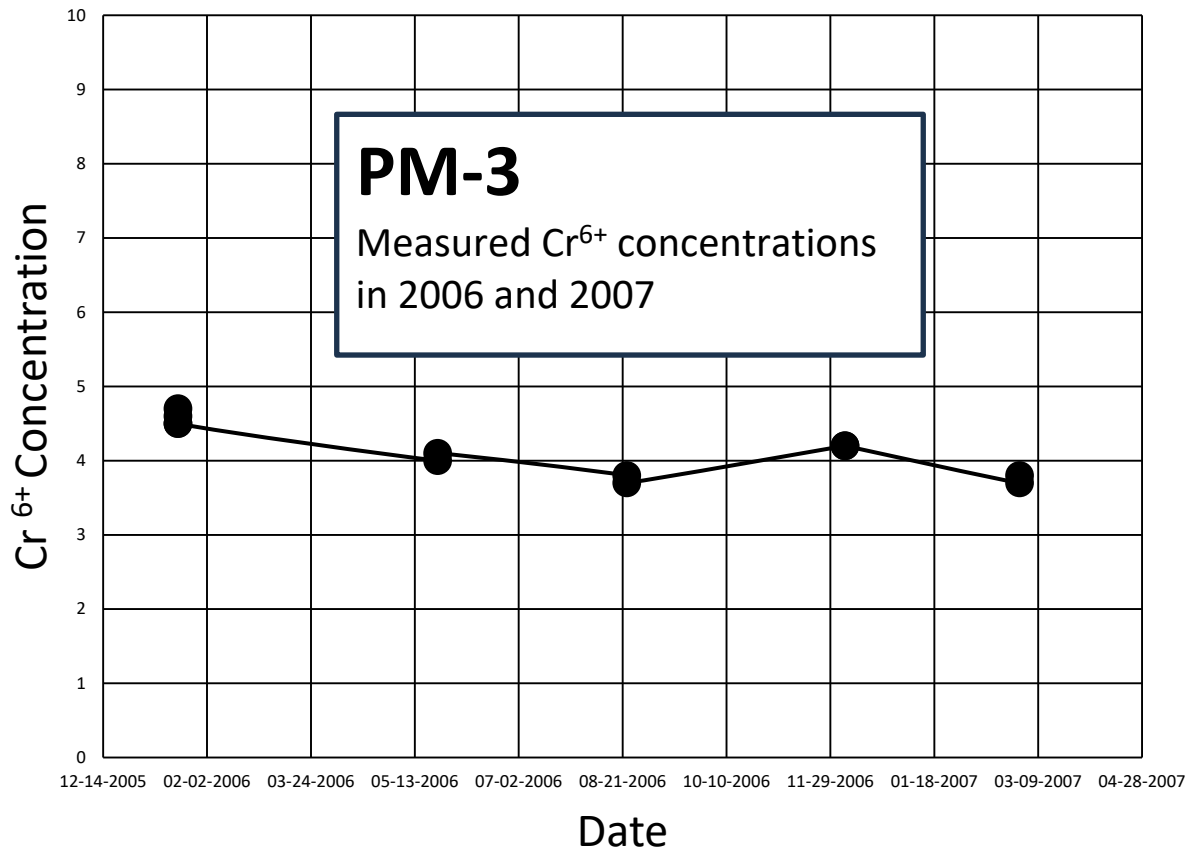


Figure 5. Measured  $Cr^{6+}$  concentrations at PM-3 in 2006 and 2007.

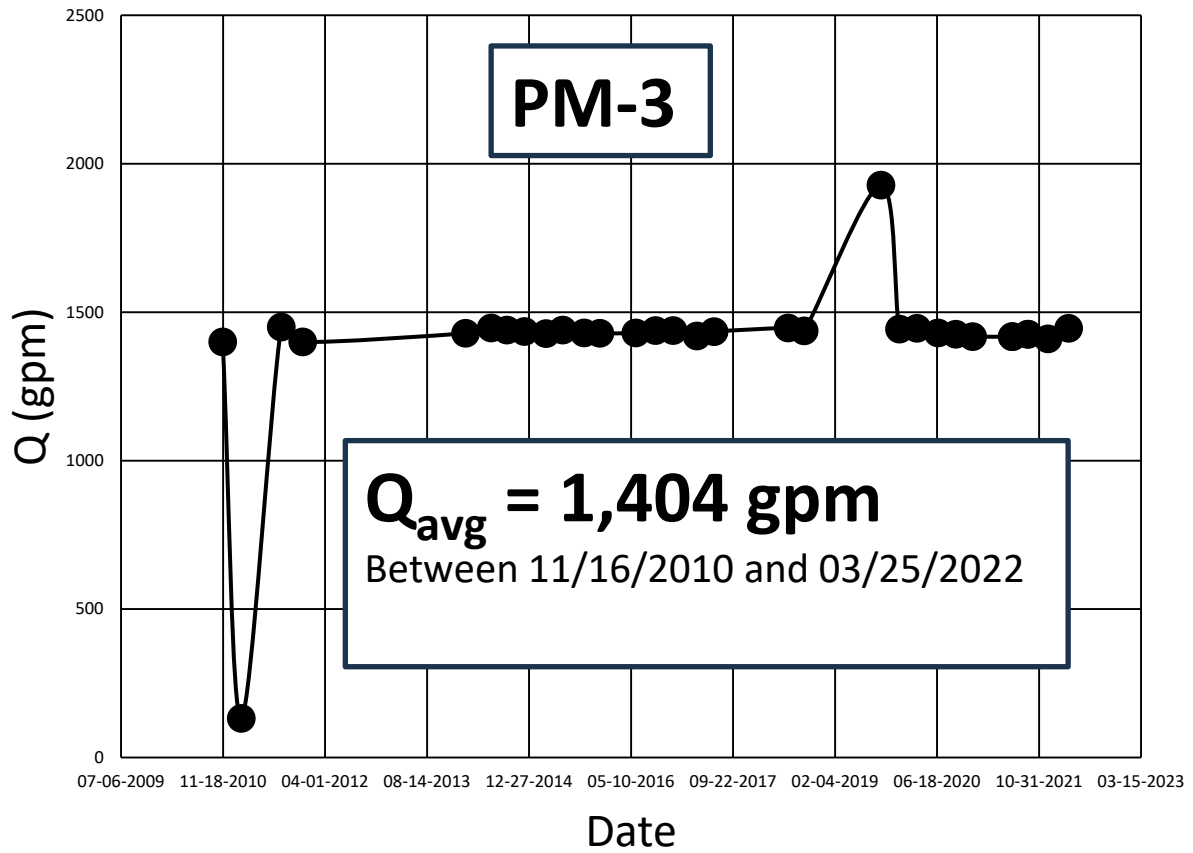


Figure 6. Measured flow rates at PM-3 between 11/16/2010 and 03/25/2022.

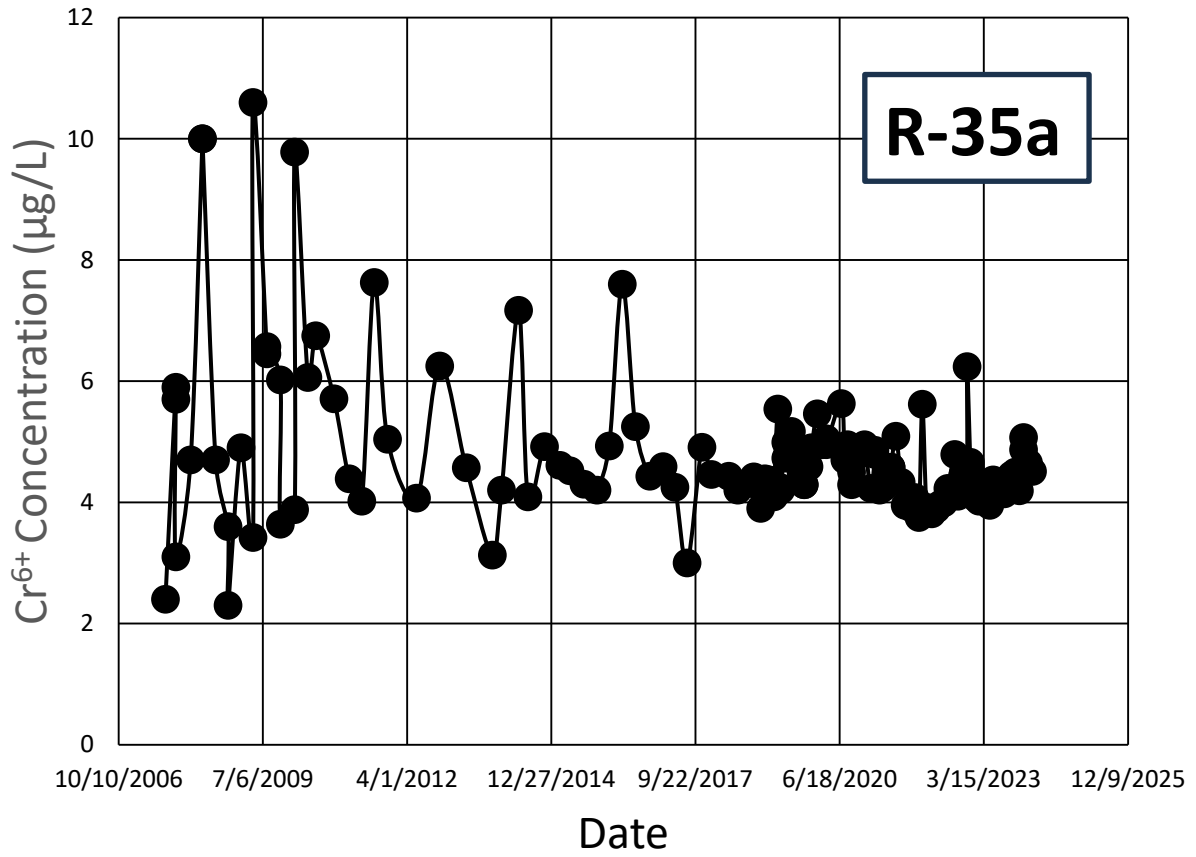


Figure 7. Measured  $Cr^{6+}$  concentrations at R-35a between 8/30/2007 to 2/16/2024.

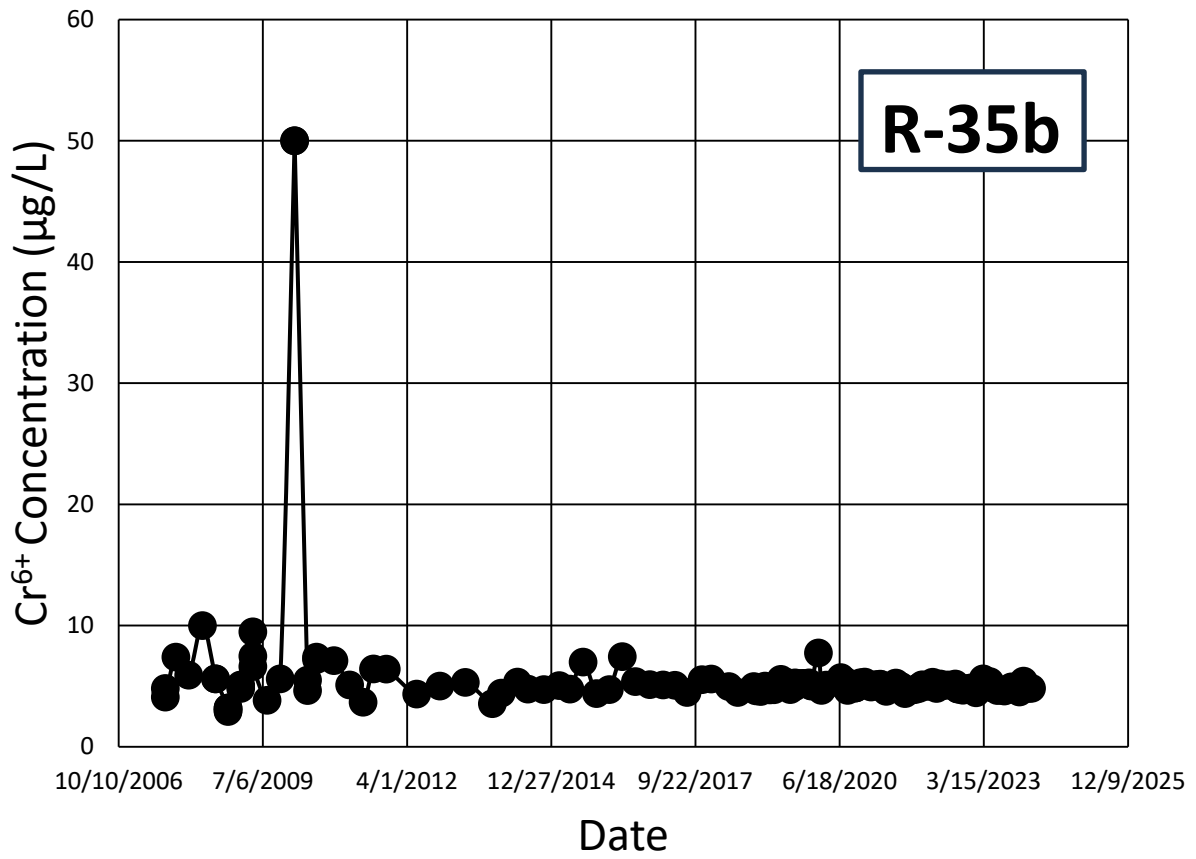


Figure 8. Measured  $Cr^{6+}$  concentrations at R-35b between 8/29/2007 to 2/9/2024.



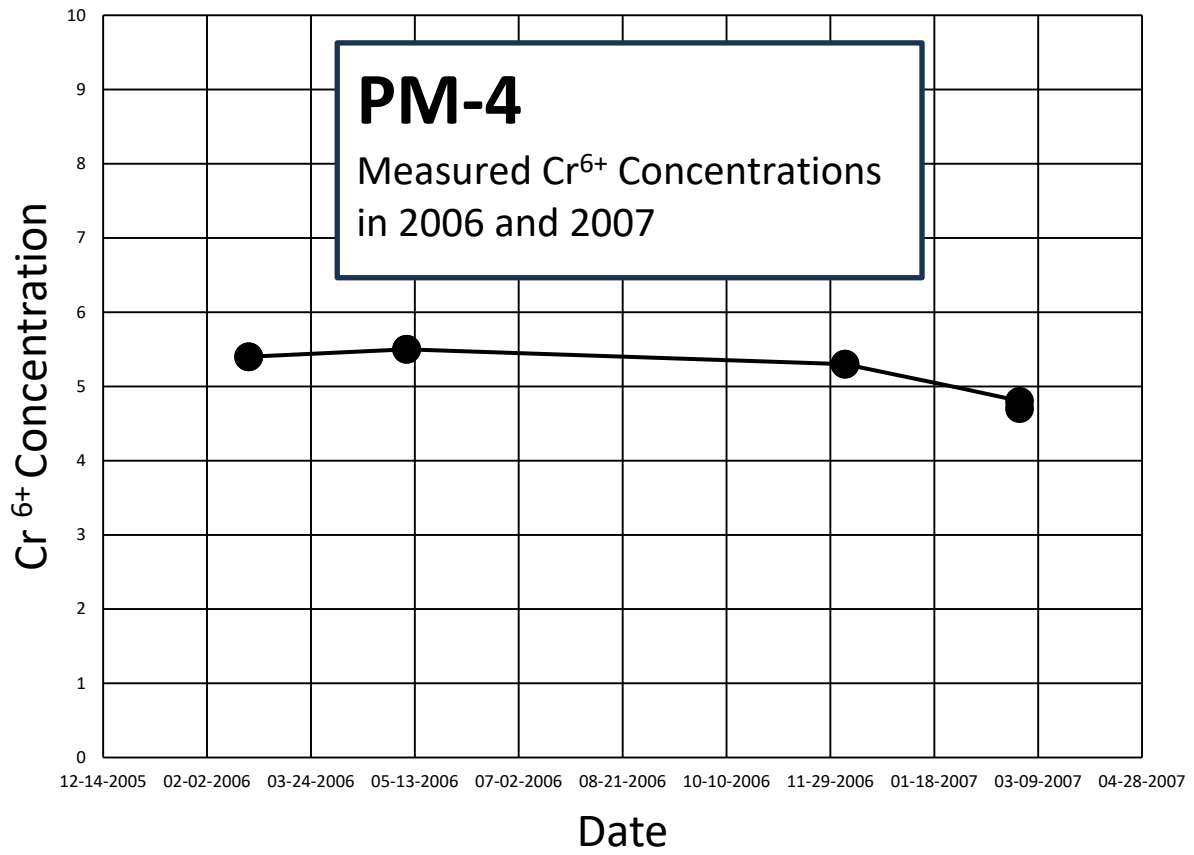


Figure 9. Measured  $Cr^{6+}$  concentrations at PM-4 in 2006 and 2007.

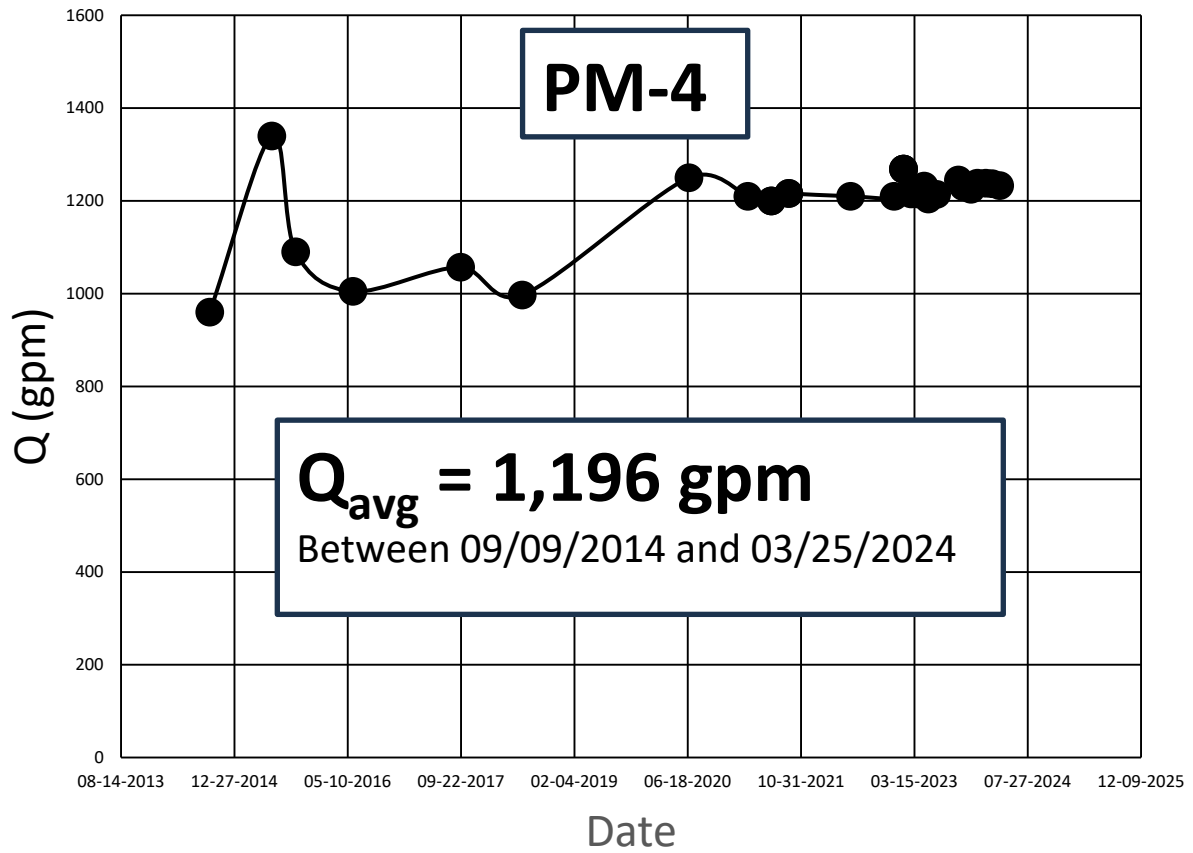


Figure 10. Measured flow rates at PM-4 between 09/09/2014 and 03/25/2024.

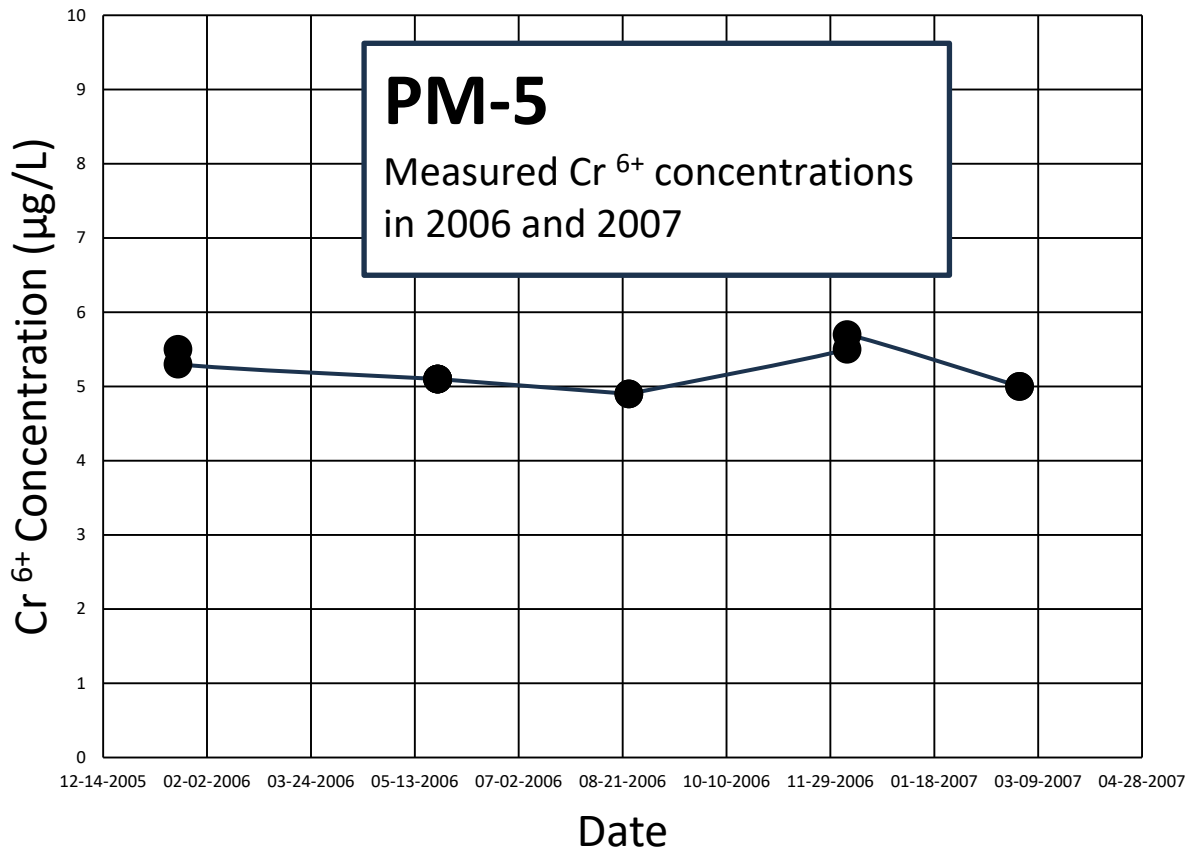


Figure 11. Measured  $Cr^{6+}$  concentrations at PM-5 in 2006 and 2007.

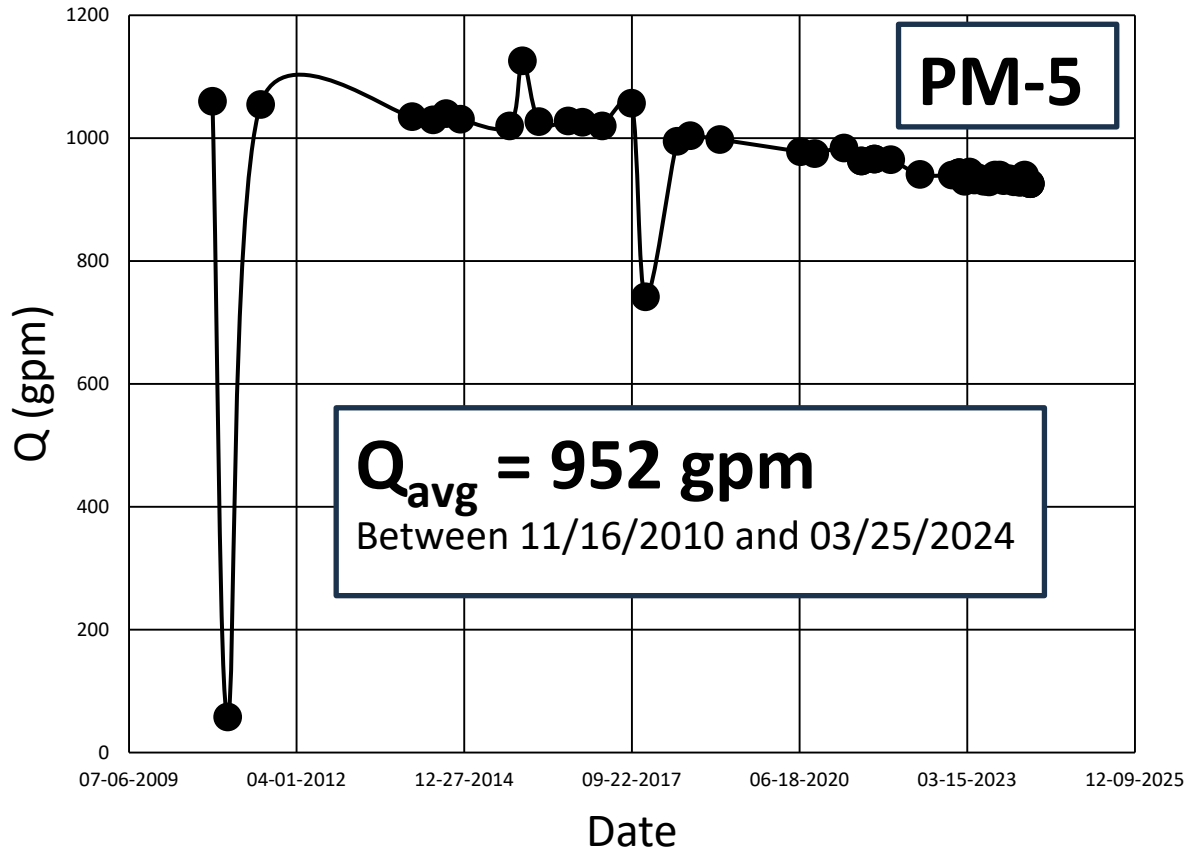


Figure 12. Measured flow rates at PM-5 between 11/16/2010 and 03/25/2024.

**APPENDIX A**  
**PM Wells Geometry Data**

LA-14397-PR  
Progress Report  
Approved for public release;  
distribution is unlimited.

Groundwater Level Status Report for 2008  
Los Alamos National Laboratory

ANL PROJECTS \ EMLA - DOE \  
LA-14397-2008-GROUNDWATER LEVEL REPORT  
EMLA-DOE \ WATER SUPPLY WELL  
DIAGRAMS - PM-1, PM-2, PM-3, PM-4, PM-5.pdf

regional aquifer that can be characterized as an alluvial fan draped up against the Sierra de los Valles located west of well R-26, but the alluvial fan is also constrained by the Rio Grande on the east. Historical information for the regional aquifer below Pajarito Plateau was previously described (Cushman 1965; Griggs 1964; Theis and Conover 1962).

Figure 3 is an enlargement of the area surrounding well PM-2, where numerous observation wells are located. Figure 3 also shows an idealized radius of influence, or maximum extent of measured drawdown, that was observed in the 25-day aquifer test at PM-2. This radius is idealized because one must assume homogeneous and isotropic aquifer properties that generate concentric circles of equal drawdown in response to pumping at a constant rate. Several idealized contours would also decrease in value as the radial distance from the pumping well increases. In reality, we rarely see this idealized aquifer response. Instead, drawdown contours in response to pumping are typically shaped like concentric but distorted ellipses because the subsurface is not homogeneous and isotropic. These irregular shapes are revealed only when a sufficient number

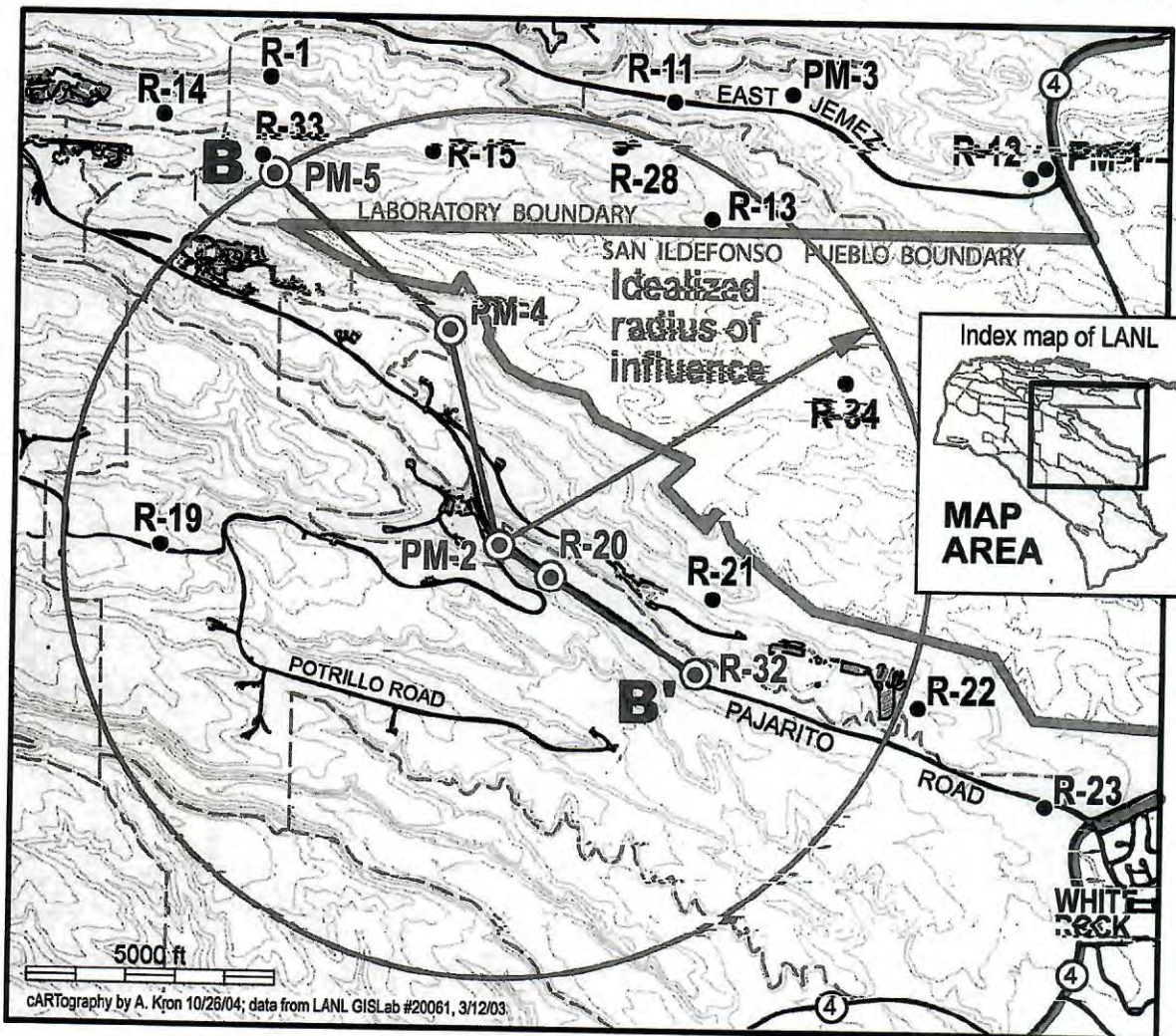


**Figure 3.** Location of wells surrounding the PM-2 aquifer test. Note the location of geologic cross-section B-B'.





**6.11 PM-3**

Location: PM-3 is located in Sandia Canyon about 1 mile west of PM-1 and about 330 ft northeast of monitoring well R-35a.

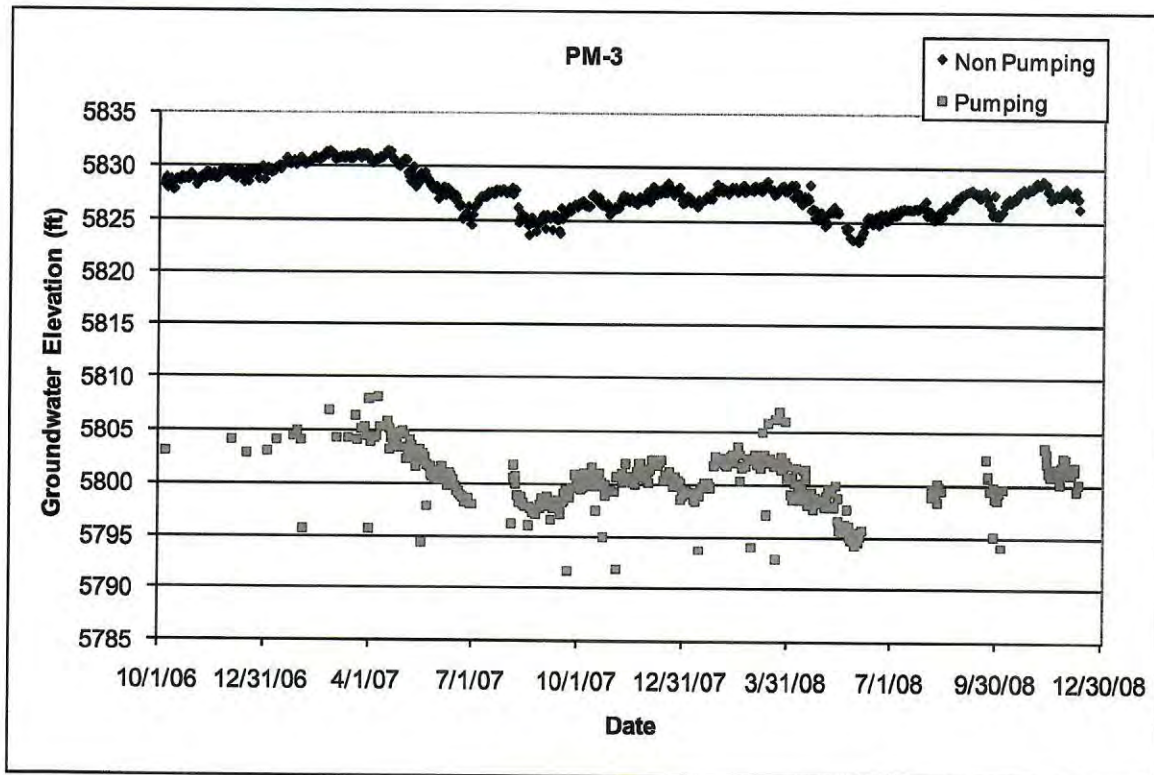
Completion Type: Single completion in Santa Fe Group.

Period of Record: Well completed as a supply well in November 1966; transducer installed October 2006; data through 2008.

Remarks: Drawdown is about 27 ft. PM-3 responds to pumping at O-4.

PM-3 Construction Information														
Screen	Screen Top Depth (ft)	Screen Bottom Depth (ft)	Screen Top Elev (ft)	Screen Bottom Elev (ft)	Screen Length (ft)	Pump Intake Depth (ft)	Pump Intake Elev (ft)	Depth to Top of Sump (ft)	Top of Sump Elev (ft)	Depth to Sump Bottom (ft)	Sump Length (ft)	Sump Volume (L)	Hydro Zone Code	Geo Unit Code
1	956	2532	5654	4078	1576	830	5780	2532	4078	2552	20	605.4	RT	Tsf

Note: Ground Elevation: 6610 ft; all measurements are from this elevation



**6.12 PM-4**

Location: PM-4 is located on Mesita del Buey about midway between supply wells PM-2 and PM-5.

The nearest monitoring well is R-15 in Mortandad Canyon, about 0.67 miles to the north.

Completion Type: Single completion in the Puye Formation and Santa Fe Group.

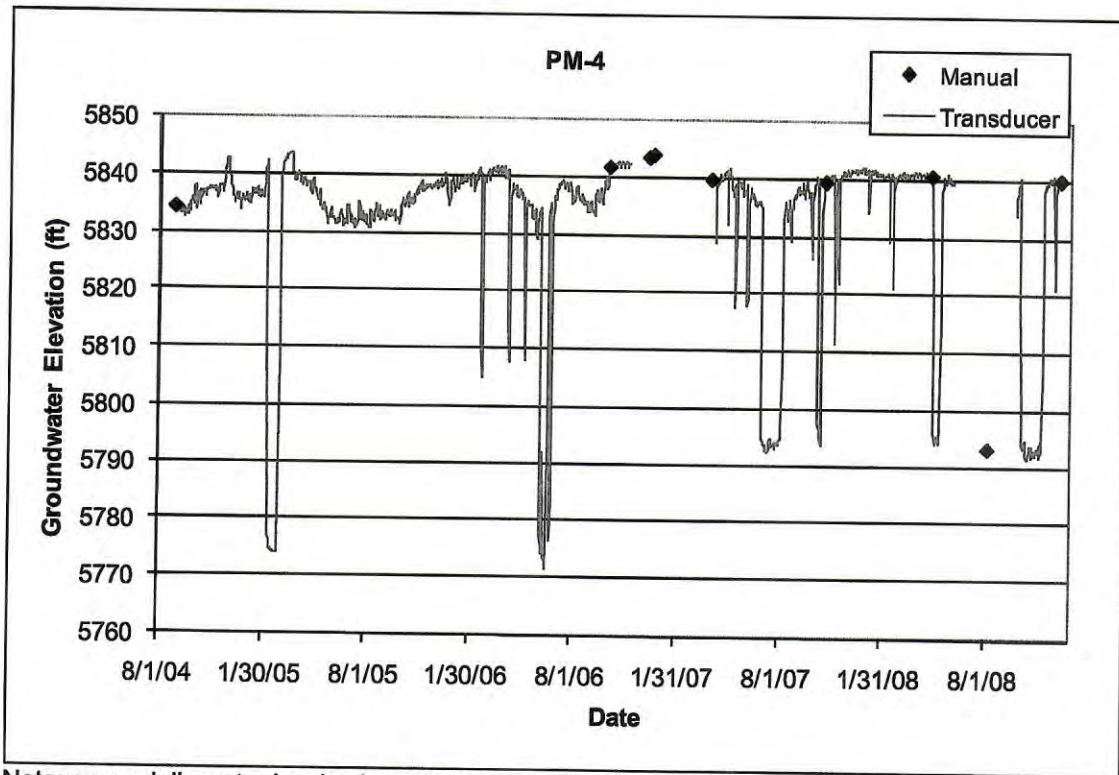
Period of Record: Well completed as a supply well in August 1981; transducer installed August 2004.

The transducer failed in November 2006 and was replaced in April 2007, failed again June 2008, replaced September 2008; intermittent data through 2008.

Remarks: Well is powered by a natural gas motor and when used is operated continuously.  
 Drawdown in 2008 was about 48 ft. PM-4 responds to pumping at PM-2.

PM-4 Construction Information														
Screen	Screen Top Depth (ft)	Screen Bottom Depth (ft)	Screen Top Elev (ft)	Screen Bottom Elev (ft)	Screen Length (ft)	Pump Intake Depth (ft)	Pump Intake Elev (ft)	Depth to Top of Sump (ft)	Top of Sump Elev (ft)	Depth to Sump Bottom (ft)	Sump Length (ft)	Sump Volume (L)	Hydro Zone Code	Geo Unit Code
1	1260	2854	5660	4066	1594	1210	5710	2854	4066	2874	20	790.8	RT	Tp

Note: Ground Elevation: 6920 ft; all measurements are from this elevation



Note: mean daily water level values shown

**6.13 PM-5**

Location: PM-5 is located on a mesa south of Ten Site and Mortandad canyons. The nearest monitoring well is R-33 in Ten Site Canyon about 1500 ft to the northeast.

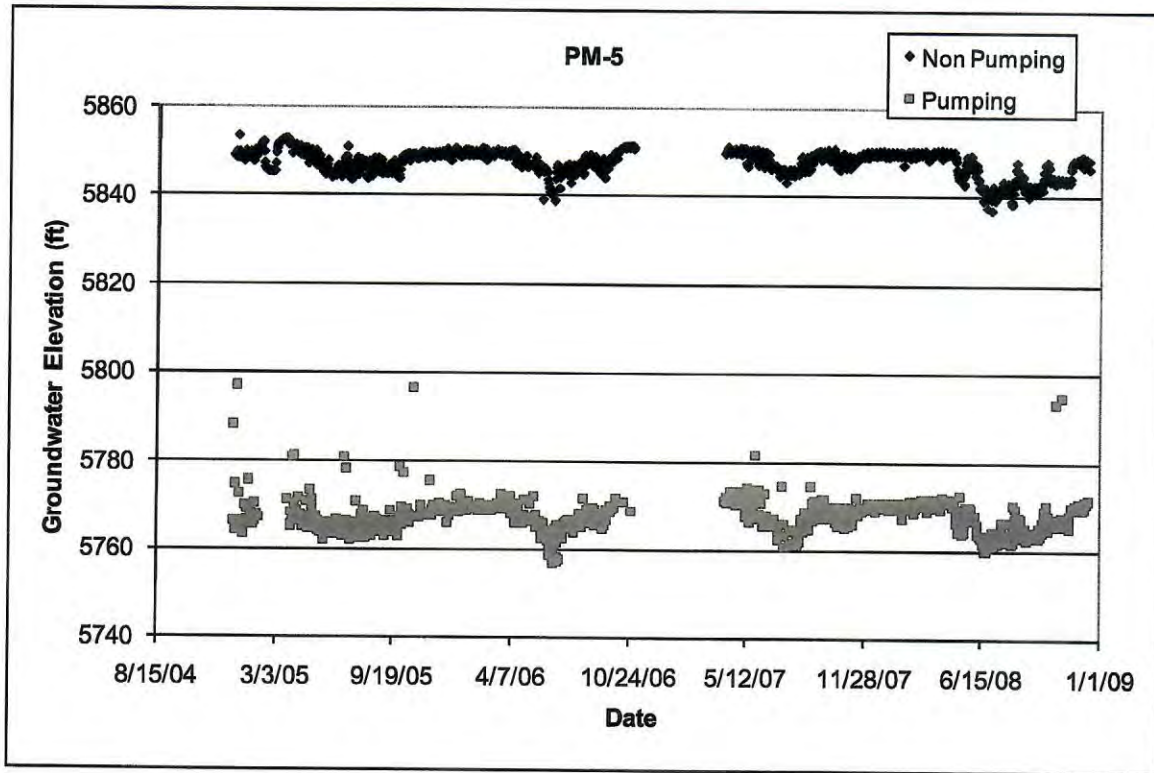
Completion Type: Single completion in the Puye Formation and Santa Fe Group.

Period of Record: Well completed as a supply well in September 1982; transducer installed December 2004. The transducer failed in October 2006 and was replaced in April 2007; data through 2008.

Remarks: PM-5 responds to pumping PM-4. Drawdown is about 80 ft.

PM-5 Construction Information														
Screen	Screen Top Depth (ft)	Screen Bottom Depth (ft)	Screen Top Elev (ft)	Screen Bottom Elev (ft)	Screen Length (ft)	Pump Intake Depth (ft)	Pump Intake Elev (ft)	Depth to Top of Sump (ft)	Top of Sump Elev (ft)	Depth to Sump Bottom (ft)	Sump Length (ft)	Sump Volume (L)	Hydro Zone Code	Geo Unit Code
1	1440	3072	5655	4023	1632		7095	3072	3072	3092	20	790.8	RT	Tp

Note: Ground Elevation: 7095 ft; all measurements are from this elevation



**3.36 R-35a**

Location: R-35a is located in Sandia Canyon about 340 ft southwest of supply well PM-3.

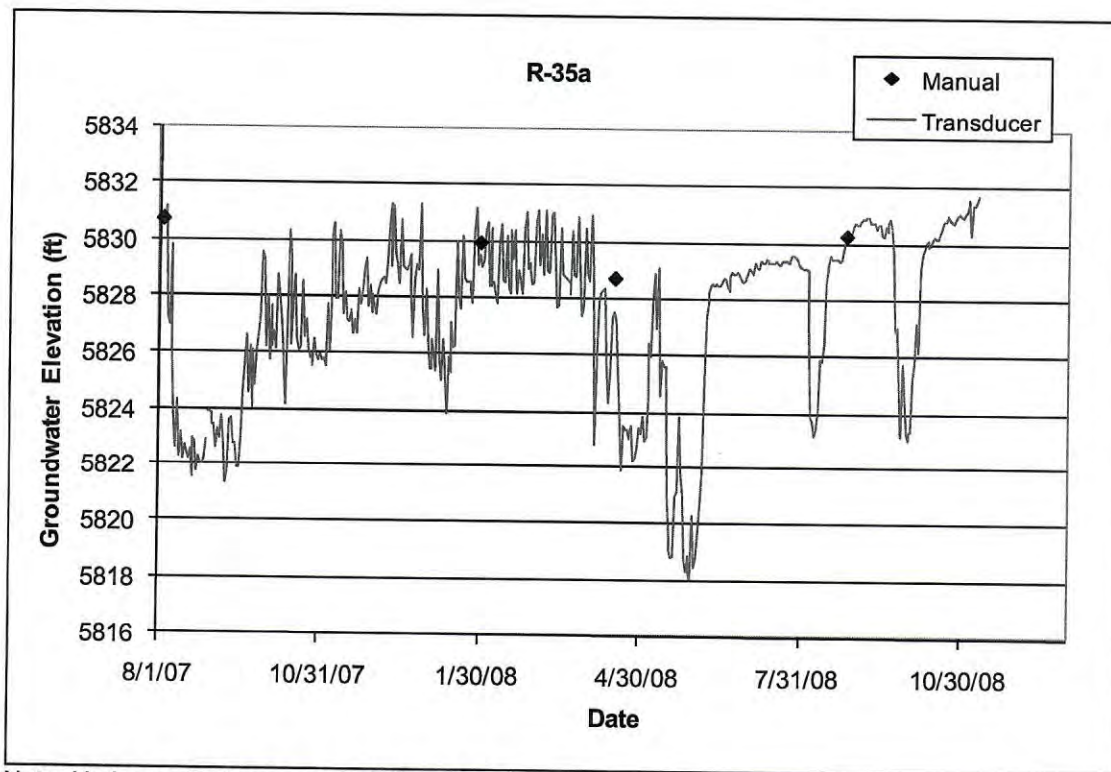
Completion Type: Single completion in the regional aquifer. The top of the screen is about 220 ft below the water table at the same elevation as the top of the PM-3 screen.

Period of Record: Well completed June 2007, transducer installed August 3, 2007; water level data through 2008.

Remarks: R-35a installed at a depth of 1082.2 ft, about 290 ft into the regional aquifer. R-35a responds primarily to pumping supply well PM-3, about 3 to 4 ft daily, but also shows a response to pumping supply well O-4. When the well was completed, the static water level at R-35a was about 7 ft lower than nearby monitoring well R-35b.

R-35a Construction Information														
Screen	Screen Top Depth (ft)	Screen Bottom Depth (ft)	Screen Top Elev (ft)	Screen Bottom Elev (ft)	Screen Length (ft)	Pump Intake Depth (ft)	Pump Intake Elev (ft)	Depth to Top of Sump (ft)	Top of Sump Elev (ft)	Depth to Sump Bottom (ft)	Sump Length (ft)	Sump Volume (L)	Hydro Zone Code	Geo Unit Code
1	1013.1	1062.2	5610.0	5560.9	49.1	998.3	5624.8	1062.2	5560.9	1086.2	24.0	75.1	RD	Tsfu

Note: Brass Cap Ground Elevation: 6623.06 ft; all measurements are from this elevation



Note: Hydrograph shows mean daily values

**3.37 R-35b**

Location: R-35b is located in Sandia Canyon about 90 ft west of R-35a.

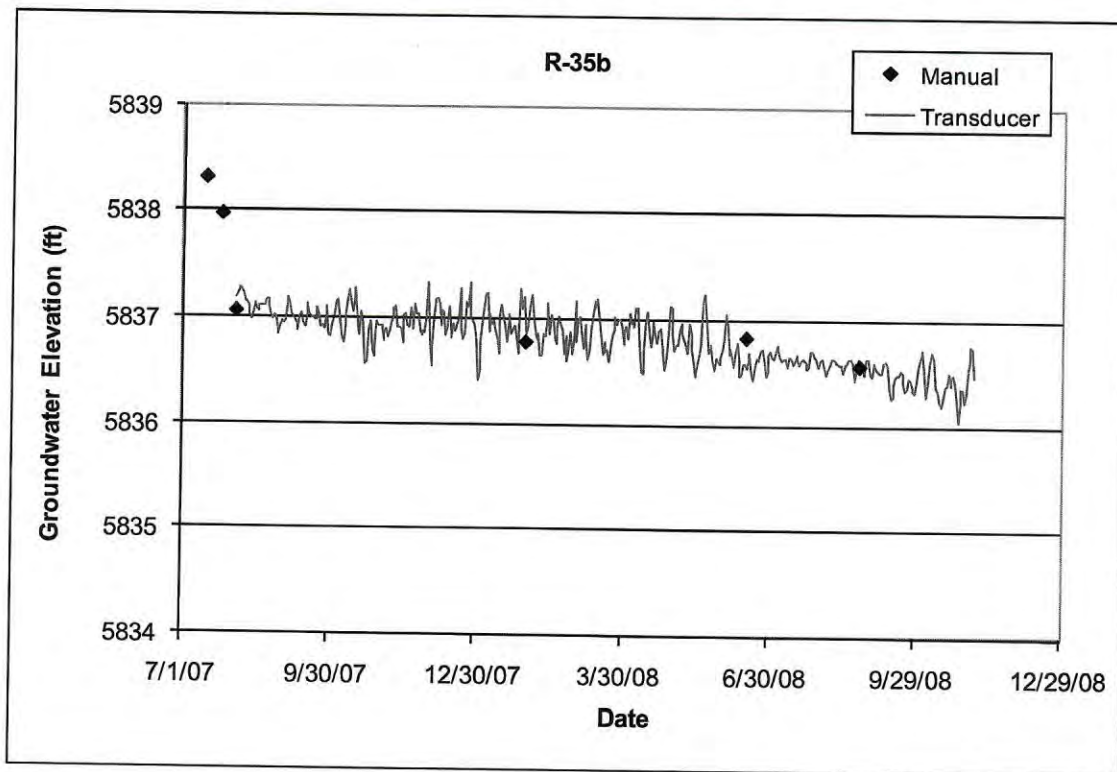
Completion Type: Single completion at the top of the regional aquifer. The top of the screen was about 37 ft below the water table when the well was installed.

Period of Record: Well completed July 2007, transducer installed August 3, 2007; water level data through 2007.

Remarks: R-35b installed near the top of the regional aquifer at a depth of 872.2 ft, about 80 ft into the regional aquifer. The well is 100% barometrically efficient; the aquifer does not respond to atmospheric pressure fluctuations. R-35b does not indicate a response to pumping of nearby well PM-3.

R-35b Construction Information														
Screen	Screen Top Depth (ft)	Screen Bottom Depth (ft)	Screen Top Elev (ft)	Screen Bottom Elev (ft)	Screen Length (ft)	Pump Intake Depth (ft)	Pump Intake Elev (ft)	Depth to Top of Sump (ft)	Top of Sump Elev (ft)	Depth to Sump Bottom (ft)	Sump Length (ft)	Sump Volume (L)	Hydro Zone Code	Geo Unit Code
1	825.4	848.5	5799.8	5776.7	23.1	832.7	5792.5	848.5	5776.7	872.2	23.7	74.1	RT	Tpf

Note: Brass Cap Ground Elevation: 6625.21 ft; all measurements are from this elevation



## **Appendix G**

**Batu (2024f) - Evaluation of the Measured Temporal Chromium (Cr<sup>6+</sup>) Concentrations in the Unconfined Aquifer with Respect to the Transport in the Vadose Zone, Los Alamos, New Mexico**

# **Evaluation of the Measured Temporal Chromium ( $Cr^{6+}$ ) Concentrations in the Unconfined Aquifer with Respect to the Transport in the Vadose Zone, Los Alamos, New Mexico**

---

Vedat Batu, Ph.D., P.E.  
Argonne Associate  
Argonne National Laboratory  
Lemont, Illinois

**August 18, 2024**

This page intentionally left blank.



## Executive Summary

In this report, with the available flow and transport parameters, the measured temporal chromium ( $Cr^{6+}$ ) concentration data in the unconfined aquifer under the vadose zone at the Los Alamos National Laboratory (LANL) site are evaluated using a one-dimensional finite-time analytical solute transport mathematical model with respect to the chromium ( $Cr^{6+}$ ) transport in the vadose zone. Specifically, the measured temporal chromium ( $Cr^{6+}$ ) concentration curves at some selected observation wells are compared with the finite-time theoretical curve with different unsaturated flow parameters based on the available site-specific reports. The conclusions drawn from these analyses are as follows:

1. The measured velocities in the Bandelier Tuff ( $V_{BT} = 4.50 \times 10^{-6} \text{ cm/s} = 0.012756 \text{ ft/d} = 4.656 \text{ ft/yr}$ ) resulted that the  $Cr^{6+}$  mass reaches to the top of the top of the Cerros del Rio basalt after 85.91 yr. This value is unrealistic because the chromium ( $Cr^{6+}$ ) mass has already been reached to the water table which is 1,305 ft below the ground surface. It has been found out that one order of magnitude higher velocity ( $V_{BT} = 4.50 \times 10^{-5} \text{ cm/s}$ ) than the previous value has generated realistic travel time (65 yr) during which the chromium ( $Cr^{6+}$ ) mass reached to the water table.
2. The backward extrapolation of the chromium ( $Cr^{6+}$ ) concentration versus date values indicated that the reaching times to the water table vary between 51 yr and 58 yr at R-42, R-43, and R-62 locations. These values mean that the permeability of the vadose zone changes from location to location.
3. The active time period of the source is less than  $t_0 = 16 \text{ yr}$ .
4. The temporal variation of the chromium ( $Cr^{6+}$ ) concentration at the bottom of the vadose zone through the layered deposits can only be determined with numerical models. However, analytical solute transport models can provide significant insights as presented in the previous items.

# Contents

Executive Summary .....	ES-1
1. Purpose.....	1
2. Vadose Zone Formation Thicknesses and Chromium (Cr <sup>6+</sup> ) Mass Mass Release Information and Data .....	1
3. Vadose Zone Hydraulic Data .....	1
3.1 Travel Time Based on Measured Velocities.....	1
3.2 Travel Time Based On the Unsaturated Hydraulic Conductivity .....	2
4. Method for the Determination the Temporal Chromium (Cr <sup>6+</sup> ) Concentration Variation at the Bottom of the Vadose Zone – Analytical Modeling Approach.....	3
4.1 Conceptual Solute Transport Model in the Vadose Zone.....	3
4.2 Unsaturated Flow Equations .....	3
4.3 One-Dimensional Solute Transport Analytical Solutions for Finite-Time Sources ....	3
4.4 Breakthrough Curves for the Chromium (Cr <sup>6+</sup> ) Concentration at the Bottom of the Vadose Zone .....	3
4.4.1 Usage of Measured Velocities.....	3
4.4.2 Usage of the Estimated Velocity from the Unsaturated Hydraulic Conductivity.....	4
5. Method for the Determination of the Chromium (Cr <sup>6+</sup> ) Concentration Variation at the Bottom of the Vadose Zone by Numerical Modeling Approach .....	5
5.1 Conceptual Site Model .....	5
5.2 Numerical Modeling Approach of Chromium (Cr <sup>6+</sup> ) Migration in the Vadose Zone .....	6
6. Comparison of the Temporal Measured Chromium (Cr <sup>6+</sup> ) Concentrations with the Theoretical Breakthrough Curves at the Bottom of the Vadose Zone.....	6
6.1 Selected Observation Wells for Comparison.....	6
6.1.1 Analysis of the R-42 Cr <sup>6+</sup> Concentration Data .....	6
6.1.2 Analysis of the R-43 S1 Cr <sup>6+</sup> Concentration Data .....	6
6.1.3 Analysis of the R-43 S2 Cr <sup>6+</sup> Concentration Data .....	7
6.1.4 Analysis of the R-62 Cr <sup>6+</sup> Concentration Data .....	7
6.2 Comparisons with the Theoretical Breakthrough Curves at the Bottom of Vadose Zone .....	7
6.2.1 Comparison with of the Measured Cr <sup>6+</sup> Concentrations at R-42.....	7
6.2.2 Comparison with of the Measured Cr <sup>6+</sup> Concentrations at R-43 S1 .....	7
6.2.3 Comparison with of the Measured Cr <sup>6+</sup> Concentrations at R-43 S2 .....	8
6.2.4 Comparison with of the Measured Cr <sup>6+</sup> Concentrations at R-62.....	8
7. Conclusions .....	8
References.....	9

## Figures

- Figure 1. The horizontal layout of conceptual model for chromium ( $Cr^{6+}$ ) release.
- Figure 2. The cross-section of the conceptual model for the vadose zone and aquifer system.
- Figure 3. Hypothetical temporal chromium ( $Cr^{6+}$ ) concentration variation (breakthrough curve) at the bottom of the vadose zone from continuous and finite-time sources at the ground surface.
- Figure 4. Breakthrough curves at the bottom of 1,305 ft thick vadose zone for  $V=4.50 \times 10^{-6}$  cm/s velocity.
- Figure 5. Breakthrough curves at the bottom of 1,305 ft thick vadose zone for  $V=4.50 \times 10^{-5}$  cm/s velocity.
- Figure 6. Breakthrough curves at the bottom of 1,305 ft thick vadose zone for  $V=4.50 \times 10^{-5}$  cm/s velocity with comparison of the first-type solution with the third-type source solution.
- Figure 7. Breakthrough curves at the bottom of 1,305 ft thick vadose zone for  $V=3.38 \times 10^{-5}$  cm/s velocity.
- Figure 8. Breakthrough curves at the bottom of 1,305 ft thick vadose zone for  $V=3.38 \times 10^{-5}$  cm/s velocity with comparison of the first-type solution with the third-type source solution.
- Figure 9a. All data for  $Cr^{6+}$  concentration vs. date at R-42.
- Figure 9b. Data until 2/10/2010 for  $Cr^{6+}$  concentration vs. date at R-42.
- Figure 10a. All data for  $Cr^{6+}$  concentration vs. date at R-43 S1.
- Figure 10b. All data for  $Cr^{6+}$  concentration vs. date at R-43 S1 till April 11, 2022.
- Figure 11a. All data for  $Cr^{6+}$  concentration vs. date at R-43 S2.
- Figure 11b. Data until 11/31/2020 for  $Cr^{6+}$  concentration vs. date at R-43 S2.
- Figure 12a. All data for  $Cr^{6+}$  concentration vs. date at R-62.
- Figure 12b. Data until 1/25/2022 for  $Cr^{6+}$  concentration vs. date at R-62.
- Figure 13. Comparison of the measured  $Cr^{6+}$  concentrations at R-42 well with the calculated breakthrough curve at the bottom of the vadose zone.
- Figure 14. Comparison of the measured  $Cr^{6+}$  concentrations at R-43 S1 well with the calculated breakthrough curve at the bottom of the vadose zone.
- Figure 15. Comparison of the measured  $Cr^{6+}$  concentrations at R-43 S2 well with the calculated breakthrough curve at the bottom of the vadose zone.
- Figure 16. Comparison of the measured  $Cr^{6+}$  concentrations at R-62 well with the calculated breakthrough curve at the bottom of the vadose zone.

## **Appendices**

- Appendix A Vertical Darcy Velocity in an Unsaturated Zone Under Uniform Water Content Conditions
- Appendix B One-Dimensional Advective-Dispersive Analytical Solute Transport Solutions for Finite-Time Source Condition
- Appendix C Estimation of the Longitudinal Dispersivity in the Vadose Zone

# 1. Purpose

In this report, with the available flow and transport parameters, the measured temporal chromium ( $Cr^{6+}$ ) concentration data in the unconfined aquifer under the vadose zone at the Los Alamos National Laboratory (LANL) site are evaluated using a one-dimensional finite-time analytical solute transport mathematical model with respect to the chromium ( $Cr^{6+}$ ) transport in the vadose zone. Specifically, the measured temporal chromium ( $Cr^{6+}$ ) concentration curves at some selected observation wells are compared with the finite-time theoretical curve with different unsaturated flow parameters based on the available site-specific reports. One of the main conclusions is about the release time period of chromium ( $Cr^{6+}$ ) from the ground surface to the water table of the unconfined aquifer. The other feature of this report is to show as to how the solute flux boundary condition at the water table can be handled in a numerical solute transport model in the unconfined aquifer.

## 2. Vadose Zone Formation Thicknesses and Chromium ( $Cr^{6+}$ ) Mass Mass Release Information and Data

The conceptual model is shown in Figures 1 and 2. As shown in Figure 2, the total thickness of the vadose zone above the water table varies between 1,295 ft and 1,315 ft and the water table is in the Puye Formation. The average thickness of the vadose zone is 1,305 ft.

The total 54,000 kg chromium ( $Cr^{6+}$ ) mass was released during the  $t_0 = 16$ -yr time period from 1956 to 1972. However, the temporal release status of this mass in the vadose zone appears to be unknown. It is clear that it will take some time the chromium ( $Cr^{6+}$ ) mass to reach to the water table. Therefore, the chromium ( $Cr^{6+}$ ) concentration at the bottom of the vadose zone will be a time-dependent quantity. After the chromium mass starts to reach to the water table, one should expect that the chromium concentration at the water table will gradually increase. And after reaching to a maximum value, it will decrease as time goes on and eventually it will approach zero. The dynamics of this phenomenon is shown schematically in Figure 3 in which the continuous time ( $t$ ) curve is also shown for comparison purpose.

## 3. Vadose Zone Hydraulic Data

### 3.1 Travel Time Based on Measured Velocities

The report by Rogers and Gallaher (1995) entitled "*The Unsaturated Characteristics of the Bandelier Tuff*" includes some hydraulic data about Bandelier Tuff (see Figure 2) which is just below the ground surface at the LANL site. The thickness of the Bandelier Tuff (BT) varies between 240 ft and 560 ft around the chromium ( $Cr^{6+}$ ) investigation area. Its average thickness is  $b_{BT} = 400$  ft. According to this report (Rogers and Gallaher, 1995, p. 44, Table 8), the observed groundwater velocities at two wells are:

Well MCM-5.9A      Observed Velocity  $> 4.0 \times 10^{-6}$  cm/s

Well LADP-3        Observed Velocity  $> 5.0 \times 10^{-6}$  cm/s

Their average is

$$V_{BT} = 4.50 \times 10^{-6} \frac{cm}{s} = 0.012756 \frac{ft}{d} = 4.656 \frac{ft}{yr}$$

The travel time of the chromium ( $Cr^{6+}$ ) particles to the upper limit of the Cerros del Rio basalt will be

$$t_{BT} = \frac{b_{BT}}{V_{BT}} = \frac{400 \text{ ft}}{4.656 \frac{ft}{yr}} = 85.91 \text{ yr}$$

This value is unrealistic because the chromium ( $Cr^{6+}$ ) mass has already been reached to the water table which is 1,305 ft below the ground surface.

The Bandelier Tuff is underlain by the Cerros del Rio basalt formation which is underlain by the Puye Formation. The average combined thickness of the Cerros del Rio basalt formation and the unsaturated portion of the Fuye Formation is 925 ft. In Section 4.4, the breakthrough curves for chromium ( $Cr^{6+}$ ) concentrations are presented for  $V = 4.50 \times 10^{-6} \text{ cm/s}$  on the assumption that this velocity represents the average velocity along the 1,305 ft average thickness of the vadose zone.

### 3.2 Travel Time Based On the Unsaturated Hydraulic Conductivity

The report of Rogers and Gallaher (1995, p. 43, Table 7) only includes the calculated travel time to well MCM-5.9A as  $5.9 \times 10^{-3} \text{ yr/cm}$  as the arithmetic average of travel time to the depth of 79 ft (2,407.92 cm). Therefore, the travel time will be 14.207 yr.

The average unsaturated hydraulic conductivity at well MCM-5.9A is  $K(\theta) = 1.69 \times 10^{-6} \text{ cm/s} = 0.004791 \text{ ft/d} = 1.748551 \text{ ft/yr}$  (Rogers and Gallaher 1995, p. 41, Table 5) for which the water content  $\theta$  is not given. For example, with an assumed  $\theta = 0.05$  uniform water content value, Eq. (A.5) of Appendix A gives

$$V_{BT} = \frac{q_z}{\theta_{unif}} = \frac{K(\theta_{unif})}{\theta_{unif}} = \frac{1.748551 \frac{ft}{yr}}{0.05} = 34.97102 \frac{ft}{yr} = 0.095811 \frac{ft}{d} = 3.38 \times 10^{-5} \frac{cm}{s}$$

The travel time to the bottom of the Bandelier Tuff will be

$$t_{BT} = \frac{b_{BT}}{V_{BT}} = \frac{380 \text{ ft}}{34.97102 \frac{ft}{yr}} = 10.87 \text{ yr}$$

which is more realistic than the value given above based on the measured  $V_{BT}$  velocity. Also, this value is not significantly different than the calculated travel time given above (14.207 yr).

The Bandelier Tuff is underlain by the Cerros del Rio basalt formation which is underlain by the Puye Formation. The average combined thickness of the Cerros del Rio basalt formation and the unsaturated portion of the Fuye Formation is 925 ft. In Section 4.4, the breakthrough curves for chromium ( $Cr^{6+}$ ) concentrations are presented for  $V = 3.38 \times 10^{-5} \text{ cm/s}$  on the assumption

that this velocity represents the average velocity along the 1,305 *ft* average thickness of the vadose zone.

## **4. Method for the Determination the Temporal Chromium ( $Cr^{6+}$ ) Concentration Variation at the Bottom of the Vadose Zone – Analytical Modeling Approach**

### **4.1 Conceptual Solute Transport Model in the Vadose Zone**

The chromium ( $Cr^{6+}$ ) source is assumed to be located at the ground surface under finite-time conditions. Beneath the chromium ( $Cr^{6+}$ ) source, the water content ( $\theta$ ) in the unsaturated zone is assumed to be uniform and the flow is one-dimensional from the ground surface towards to the water table. Likewise, the transport of chromium ( $Cr^{6+}$ ) solutes is assumed to be one-dimensional as well. Figure 3 presents the expected shape of the concentration versus time curve (or the breakthrough curve) at the bottom of the unsaturated zone (or at the top of the water table) under finite-time conditions. For comparison purpose, the breakthrough curve is also shown under continuous time conditions as well.

### **4.2 Unsaturated Flow Equations**

Appendix A briefly summarizes unsaturated flow equations. The groundwater velocity under uniform water content conditions is given by Eq. (A.5) of Appendix A as  $V = K(\theta)/\theta$ .

### **4.3 One-Dimensional Solute Transport Analytical Solutions for Finite-Time Sources**

The one-dimensional solute transport analytical solutions for both first-type and third-type source conditions are given in Appendix B along with their partial differential equation as well as the initial and boundary conditions. For these solutions, calculations were carried out with Excel.

### **4.4 Breakthrough Curves for the Chromium ( $Cr^{6+}$ ) Concentration at the Bottom of the Vadose Zone**

In this section, the breakthrough curves for the chromium ( $Cr^{6+}$ ) concentration at the bottom of the vadose zone which has average thickness of 1,305 *ft* are presented using different velocities in the unsaturated zone.

#### **4.4.1 Usage of Measured Velocities**

Details about the measured velocities are given in Section 3.1 and the average velocity in the Bandelier Tuff is

$$V_{BT} = 4.50 \times 10^{-6} \text{ cm/s} = 0.012756 \text{ ft/d} = 4.656 \text{ ft/yr}$$

The effective molecular diffusion coefficient  $D^*$  has values between  $1.0 \times 10^{-10} \text{ m}^2/\text{s}$  and  $1.0 \times 10^{-11} \text{ m}^2/\text{s}$ . Their arithmetic average is  $D^* = 5.5 \times 10^{-11} \text{ m}^2/\text{s} = 51.15 \times 10^{-6} \text{ ft}^2/\text{d}$ .

These values are representative of a range of typical nonreactive chemical species in clayey geologic deposits. Values of coarse-grained unconsolidated materials can be somewhat higher than  $1.0 \times 10^{-10} \text{ m}^2/\text{s}$  but less than the coefficients for the chemical species in water (i.e.,  $< 2 \times 10^{-9} \text{ m}^2/\text{d} = 1.728 \times 10^{-4} \text{ m}^2/\text{d} = 1.860 \times 10^{-3} \text{ ft}^2/\text{d}$ ) (e.g., Freeze and Cherry, 1979, p. 393).

According to the Internet, the  $R_d$  values for chromium ( $\text{Cr}^{6+}$ ) varied from 1.1 to 2.4 and are dependent on geochemical conditions. Their average is 1.75. Based on displacement experiments along with the analytical solutions in Appendix B, for chromium ( $\text{Cr}^{6+}$ ) movement through sand, van Genuchten (1980, 1982) found out  $R_d = 1.281$  as the chromium ( $\text{Cr}^{6+}$ ) retardation factor (van Genuchten, 1982, p. 237, Figure 1) which is not significantly off from the average value given above.

Therefore, apart from  $V_{BT}$ , the rest of parameters are as follows:

$$D^* = 2.0 \times 10^{-9} \text{ m}^2/\text{d} = 1.728 \times 10^{-4} \text{ m}^2/\text{d} = 1.860 \times 10^{-3} \text{ ft}^2/\text{d}$$

$$\alpha_L = 6.0 \text{ m} = 19.69 \text{ ft} \text{ (Appendix C)}$$

$$R_d = 1.75$$

$$x = 1,305 \text{ ft}$$

$$C_0 = 2,100 \text{ } \mu\text{g}/\text{L} \text{ (Determined by trial runs)}$$

It is assumed that  $V_{BT} = 4.50 \times 10^{-6} \text{ cm}/\text{s}$  is the average velocity along the 1,305 ft thick vadose zone.

With these values, the breakthrough curves are shown in Figure 4 which shows that the chromium ( $\text{Cr}^{6+}$ ) mass reaches to the water table after 300 yr elapsed time. This means that this velocity cannot be a representative average velocity because the chromium ( $\text{Cr}^{6+}$ ) mass has already been reached to the water table.

Figure 5 corresponds to  $V = 4.50 \times 10^{-5} \text{ cm}/\text{s}$  velocity value, which is one order of magnitude higher than the previous value. The  $C_0 = 2,100 \text{ } \mu\text{g}/\text{L}$  source concentration is specified by trial. The maximum chromium ( $\text{Cr}^{6+}$ ) concentration was measured at well R-42 (1,240  $\mu\text{g}/\text{L}$ ). Figure 5 shows that after 65 yr elapsed time, the concentration is around 800  $\mu\text{g}/\text{L}$  which is comparable with the maximum 1,240  $\mu\text{g}/\text{L}$  concentration at R-42. One should bear in mind that the concentrations in the aquifer potentially may be somewhat less than the bottom values of the vadose zone due to dispersion effects. In Figure 6, the first-type solution results are compared with the third-type solution results which shows that they are close to each other.

#### 4.4.2 Usage of the Estimated Velocity from the Unsaturated Hydraulic Conductivity

In this section, the breakthrough curves for the chromium ( $\text{Cr}^{6+}$ ) concentration at the bottom of the vadose zone which has the average thickness of 1,305 ft are presented using the estimated



velocity from the unsaturated hydraulic conductivity as presented in Section 3.2.1. As mentioned in Section 3.2.1, the average unsaturated hydraulic conductivity at well MCM-5.9A is  $K(\theta) = 1.69 \times 10^{-6} \text{ cm/s}$ . And with an assumed  $\theta = 0.05$  uniform water content value, Eq. (A.5) of Appendix A gives

$$V_{BT} = \frac{q_z}{\theta_{unif}} = \frac{K(\theta_{unif})}{\theta_{unif}} = \frac{1.748551 \frac{ft}{yr}}{0.05} = 34.97102 \frac{ft}{yr} = 0.095811 \frac{ft}{d} = 3.38 \times 10^{-5} \frac{cm}{s}$$

As mentioned in Section 3.2.1, the Bandelier Tuff is underlain by the Cerros del Rio basalt formation which is underlain by the Puye Formation. The average combined thickness of the Cerros del Rio basalt formation and the unsaturated portion of the Fuye Formation is 925 ft. Here, the breakthrough curves for chromium ( $Cr^{6+}$ ) concentrations will be presented for  $V = 3.38 \times 10^{-5} \text{ cm/s}$  on the assumption that this velocity represents the average velocity along the 1,305 ft average thickness of the vadose zone. The rest of parameters are as follows:

$$D^* = 2.0 \times 10^{-9} \text{ m}^2/\text{d} = 1.728 \times 10^{-4} \text{ m}^2/\text{d} = 1.860 \times 10^{-3} \text{ ft}^2/\text{d}$$

$$\alpha_L = 6.0 \text{ m} = 19.69 \text{ ft} \text{ (Appendix C)}$$

$$R_d = 1.75$$

$$x = 1,305 \text{ ft}$$

The breakthrough curve is presented in Figure 7. The maximum chromium ( $Cr^{6+}$ ) concentration was measured at well R-42 (1,240  $\mu\text{g/L}$ ). Figure 7 shows that after 65 yr elapsed time, the concentration is around 980  $\mu\text{g/L}$  which is comparable with the maximum 1,240  $\mu\text{g/L}$  concentration at R-42. One should bear in mind that the concentrations in the aquifer are somewhat less than the bottom values of the vadose zone due to dispersion effects. In Figure 8, the first-type solution results are compared with the third-type solution results and they are close to each other.

## 5. Method for the Determination of the Chromium ( $Cr^{6+}$ ) Concentration Variation at the Bottom of the Vadose Zone by Numerical Modeling Approach

The vadose zone (VZ) is composed of several formations. With the characteristics of these formations, the temporal variation at the bottom of VZ can be determined by numerical models. These are discussed in the sections below.

### 5.1 Conceptual Site Model

As shown in Figure 2, the vadose zone (VZ) has an average thickness of 1,305 ft and is composed of the Bandelier Tuff, Gerros del Rio Basalt, and Puye Formation. As can be seen from Figure 2, the Gerros del Rio Basalt is thickest one (705 ft) and is located between the Bandelier Tuff and Puye Formation having 400 ft and 200 ft thicknesses, respectively. Since the

chromium ( $Cr^{6+}$ ) source at the ground surface is a finite time source, the temporal variation of the chromium ( $Cr^{6+}$ ) concentration will be like a bell-shaped curve shown in Figure 3.

## 5.2 Numerical Modeling Approach of Chromium ( $Cr^{6+}$ ) Migration in the Vadose Zone

The temporal variation of the chromium ( $Cr^{6+}$ ) concentration at the bottom of the vadose zone through the layered deposits can only be determined with numerical models. One of the well-known software is the POLLUTEv7 program (GAEA Technologies Ltd., 2004, Canada) which is based on Rowe and Booker (1985, 1991) and Rowe et al. (1994). POLLUTEv7 is a computer program that implements a solution to the one-dimensional advection-dispersion equation for a layered deposit of finite or infinite extent. POLLUTEv7 calculates the concentrations of a contaminant at user specified times and depths.

## 6. Comparison of the Temporal Measured Chromium ( $Cr^{6+}$ ) Concentrations with the Theoretical Breakthrough Curves at the Bottom of the Vadose Zone

In this section, the observed breakthrough curves at some observation wells are compared with the theoretical breakthrough curves generated from the first-type finite-source solution whose details are presented in Section 4.3 along with Appendix B.

### 6.1 Selected Observation Wells for Comparison

The selected observation wells for comparison are R-42, R-43 S1, R-43 S2, and R-62 and their temporal concentration variations are discussed below.

#### 6.1.1 Analysis of the R-42 $Cr^{6+}$ Concentration Data

The maximum  $Cr^{6+}$  concentration was measured at R-42 observation well on February 10, 2010 (1,240  $\mu g/L$ ) in the plume area (see Figure 9a). As can be seen from Figure 9a, this maximum concentration is an exception value and the concentration varies between 1,070  $\mu g/L$  (August 8, 2012) and 622  $\mu g/L$  (October 19, 2023), averaging 871  $\mu g/L$ . Figure 9b indicates that after the first quarter of 2012, concentrations started to decline and this trend continued till the last quarter of 2023 after which no measured values exist. One should note that during a 6-yr time period from September 2017 till October 2023 no measured concentration values exist.

Figure 9b presents the temporal concentration variation at R-42 from October 2008 till February 2010 which shows a linear trend. By linear extrapolation, it appears that the  $Cr^{6+}$  mass reached to the water table by around the first quarter of 2005, 55 yr after 1956.

#### 6.1.2 Analysis of the R-43 S1 $Cr^{6+}$ Concentration Data

The maximum  $Cr^{6+}$  concentration was measured at R-43 S1 observation well on November 14, 2019 (223  $\mu g/L$ ) in the plume area (see Figure 10a) and after that decline started till the last measurement on January 17, 2024.

Figure 10b presents the temporal concentration variation at R-43 S1 from May 11, 2008 till November 14, 2022 which shows a linear trend. By linear extrapolation, it appears that the  $Cr^{6+}$  mass reached to the water table by around May 2008 which means that the  $Cr^{6+}$  mass reached to the water table within 58 *yr* after its release starting date in 1956.

### 6.1.3 Analysis of the R-43 S2 $Cr^{6+}$ Concentration Data

The maximum  $Cr^{6+}$  concentration was measured at R-43 S2 observation well on March 11, 2020 ( $49.1 \mu g/L$ ) in the plume area (see Figure 11a) and after that decline started till the last measurement on January 17, 2024.

Figure 11b presents the temporal concentration variation at R-43 S2 from October 10, 2008 till November 3, 2020 which shows a linear trend. By linear extrapolation, it appears that the  $Cr^{6+}$  mass reached to the water table by the first quarter of 2009 which means that the  $Cr^{6+}$  mass reached to the water table within 53 *yr* after its release starting date in 1956 which is comparable with the value in Section 6.1.2.

### 6.1.4 Analysis of the R-62 $Cr^{6+}$ Concentration Data

The maximum  $Cr^{6+}$  concentration was measured at R-62 observation well on January 25, 2022 ( $351 \mu g/L$ ) in the plume area (see Figure 12a) and after that decline continued till the last measurement on February 2, 2024.

Figure 12b presents the temporal concentration variation at R-62 from March 26, 2012 till January 1, 2020 which shows a linear trend. By linear extrapolation, it appears that the  $Cr^{6+}$  mass reached to the water table by around 2007 which means that the  $Cr^{6+}$  mass reached to the water table within 51 *yr* after its release starting date in 1956.

## 6.2 Comparisons with the Theoretical Breakthrough Curves at the Bottom of Vadose Zone

In this section, comparisons for the measured concentrations of  $Cr^{6+}$  at R-42, R-43 S1, R-43 S2, and R-62 are presented with the use of the first-type finite-time source as given in Section B.2.2 of Appendix B.

### 6.2.1 Comparison with of the Measured $Cr^{6+}$ Concentrations at R-42

Using the input data in Section 4.4.2, comparison of the measured concentrations of  $Cr^{6+}$  with the theoretical breakthrough curve at R-42 is shown in Figure 13. By trial runs, the concentration at the ground surface is determined as  $C_0 = 2,300 \mu g/L$ . As can be seen from Figure 13, the shape of the measured concentrations curve has similarities with the theoretical breakthrough curve. But it appears that the active time period of the source is less than  $t_0 = 16 \text{ yr}$ .

### 6.2.2 Comparison with of the Measured $Cr^{6+}$ Concentrations at R-43 S1

Using the input data in Section 4.4.2, comparison of the measured concentrations of  $Cr^{6+}$  with the theoretical breakthrough curve at R-43 S1 is shown in Figure 14. By trial runs, the

concentration at the ground surface is determined as  $C_0 = 420 \mu\text{g}/\text{L}$ . As can be seen from Figure 14, the shape of the measured concentrations curve has similarities with the theoretical breakthrough curve. But it appears that the active time period of the source is less than  $t_0 = 16 \text{ yr}$ .

### 6.2.3 Comparison with of the Measured $\text{Cr}^{6+}$ Concentrations at R-43 S2

Using the input data in Section 4.4.2, comparison of the measured concentrations of  $\text{Cr}^{6+}$  with the theoretical breakthrough curve is shown at R043 S2 in Figure 15. By trial runs, the concentration at the ground surface is determined as  $C_0 = 90 \mu\text{g}/\text{L}$ . As can be seen from Figure 15, the shape of the measured concentrations curve has similarities with the theoretical breakthrough curve. But it appears that the active time period of the source is less than  $t_0 = 16 \text{ yr}$ .

### 6.2.4 Comparison with of the Measured $\text{Cr}^{6+}$ Concentrations at R-62

Using the input data in Section 4.4.2, comparison of the measured concentrations of  $\text{Cr}^{6+}$  with the theoretical breakthrough curve at R-62 is shown in Figure 16. By trial runs, the concentration at the ground surface is determined as  $C_0 = 800 \mu\text{g}/\text{L}$ . As can be seen from Figure 16, the shape of the measured concentrations curve almost match with the left side of theoretical breakthrough curve which increases the possibilities that the active time period of the source is comparable with  $t_0 = 16 \text{ yr}$ .

## 7. Conclusions

The conclusions drawn from these analyses are as follows:

1. The measured velocities in the Bandelier Tuff ( $V_{BT} = 4.50 \times 10^{-6} \text{ cm}/\text{s} = 0.012756 \text{ ft}/\text{d} = 4.656 \text{ ft}/\text{yr}$ ) resulted that the  $\text{Cr}^{6+}$  mass reaches to the top of the Cerros del Rio basalt after 85.91 yr. This value is unrealistic because the chromium ( $\text{Cr}^{6+}$ ) mass has already been reached to the water table which is 1,305 ft below the ground surface. It has been found out that one order of magnitude higher velocity ( $V_{BT} = 4.50 \times 10^{-5} \text{ cm}/\text{s}$ ) than the previous value has generated realistic travel time (65 yr) during which the chromium ( $\text{Cr}^{6+}$ ) mass reached to the water table.
2. The backward extrapolation of the chromium ( $\text{Cr}^{6+}$ ) concentration versus date values indicated that the reaching times to the water table vary between 51 yr and 58 yr at R-42, R-43, and R-62 locations. These values mean that the permeability of the vadose zone changes from location to location.
3. The active time period of the source is less than  $t_0 = 16 \text{ yr}$ .
4. The temporal variation of the chromium ( $\text{Cr}^{6+}$ ) concentration at the bottom of the vadose zone through the layered deposits can only be determined with numerical models. However, analytical solute transport models can provide significant insights as presented in the previous items.

## References

- Freeze, R.A., and J.A. Cherry, *Groundwater*, Prentice-Hall, Inc., Englewood Cliffs, New Jersey, 604 pp., 1979.
- GAEA Technologies Ltd., R.K. Rowe and J.R. Booker, POLLUTEv7, Canada, 2004.
- Gelhar, L.W., C. Welty, and K.R. Rehfeldt, "A Critical Review of Data on Field-Scale Dispersion in Aquifers," *Water Resources Research*, Vol. 28, No.7, pp. 1955-1974, 1992.
- Gershon, N.D., and A. Nir, "Effect of Boundary Conditions of Models on Tracer Distribution in Flow Through Porous Mediums," *Water Resources Research*, Vol. 5, pp. 830-840, 1969.
- Lapidus, L., and N.R. Amundsen, "Mathematics of Adsorption in Beds. VI. The Effects of Longitudinal Diffusion in Ion Exchange and Chromatographic Column," *Journal of Physical Chemistry*, Vol. 56, pp. 984-988, 1952.
- Leij, F.J., J.H. Dane, and M.Th. Van Genuchten, "Mathematical Analysis of One-Dimensional Solute Transport in a Layered Soil Profile," *Soil Science Society of America Journal*, Vol. 55, pp. 944-953, 1991.
- Lindstrom, F.T., R. Haque, V.H. Freed, and L. Boersma, "Theory of Movement of Some Herbicides in Soils: Linear Diffusion and Convection of Chemicals in Soils," *Journal of Environmental Science and Technology*, Vol 1, pp. 561-565, 1967.
- Rowe, R.K., and J.R. Booker, "1-D Pollutant Migration in Soils of Finite Depth", *Journal of Geotechnical Engineering*, ASCE, Vol. 111, GT4, pp. 13-42, 1985.
- Rowe, R.K. and J.R. Booker, "Pollutant Migration Through a Liner Underlain by Fractured Soil". *Journal of Geotechnical Engineering*, ASCE, Vol. 118, No. 7, pp. 1031-1046, 1991.
- Rowe, R.M., R.M. Quigley, and J.R. Booker, "Clayey Barriers for Waste Disposal Facilities", E & F N Spon, England, 1994.
- Ogata, A., and R.B. Banks, "A Solution of the Differential Equation of Longitudinal Dispersion in Porous Media," *U.S. Geological Survey Professional Paper 411-A*, pp. A1-A9, 1961.
- van Genuchten, M.Th., "One-Dimensional Analytical Transport Modeling," In: E.M. Arnold, G.W. Gee, and R.W. Nelson (eds.), *Proceedings of the Symposium on Unsaturated Modeling*, Pacific Northwest Laboratory, NUREG/CP-0030, pp. 231-246, Seattle, Washington, March 22-24, 1982.
- van Genuchten, M.Th., W.J. Alves, "Analytical Solutions of the One-Dimensional Convective-Dispersive Solute Transport Equation," U.S. Department of Agriculture, Agricultural Research Service, *Technical Bulletin Number 1661*, 149 pp., June, 1982.
- Warrick, A.W., *Soil Water Dynamics*, Oxford University Press, New York, 391 pp., 2003.

## Figures

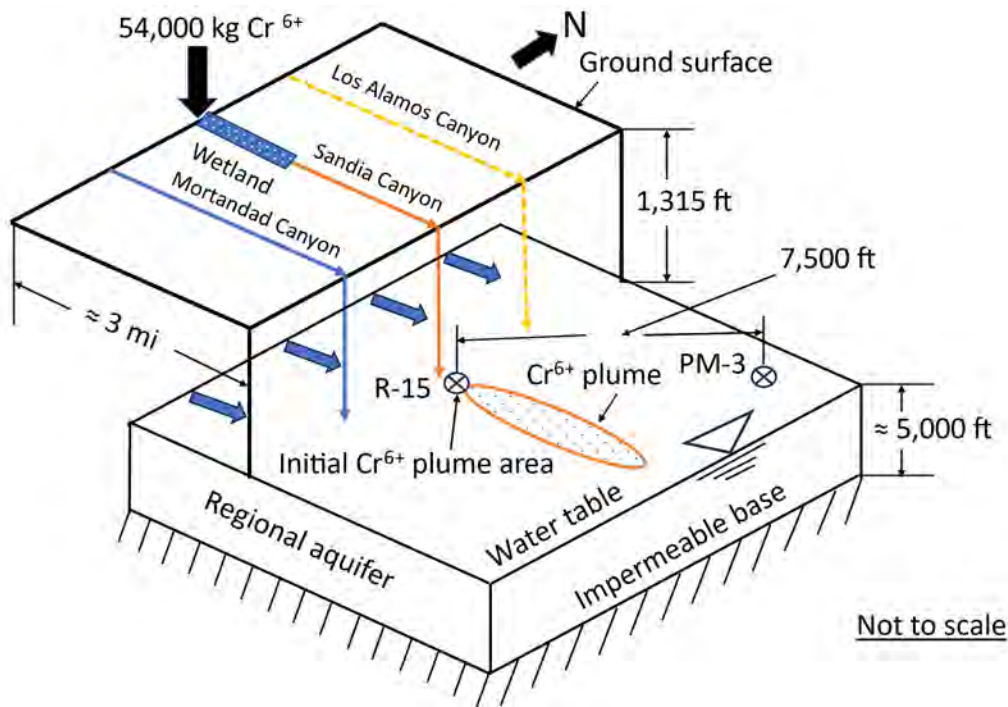


Figure 1. The horizontal layout of conceptual model for chromium ( $Cr^{6+}$ ) release.

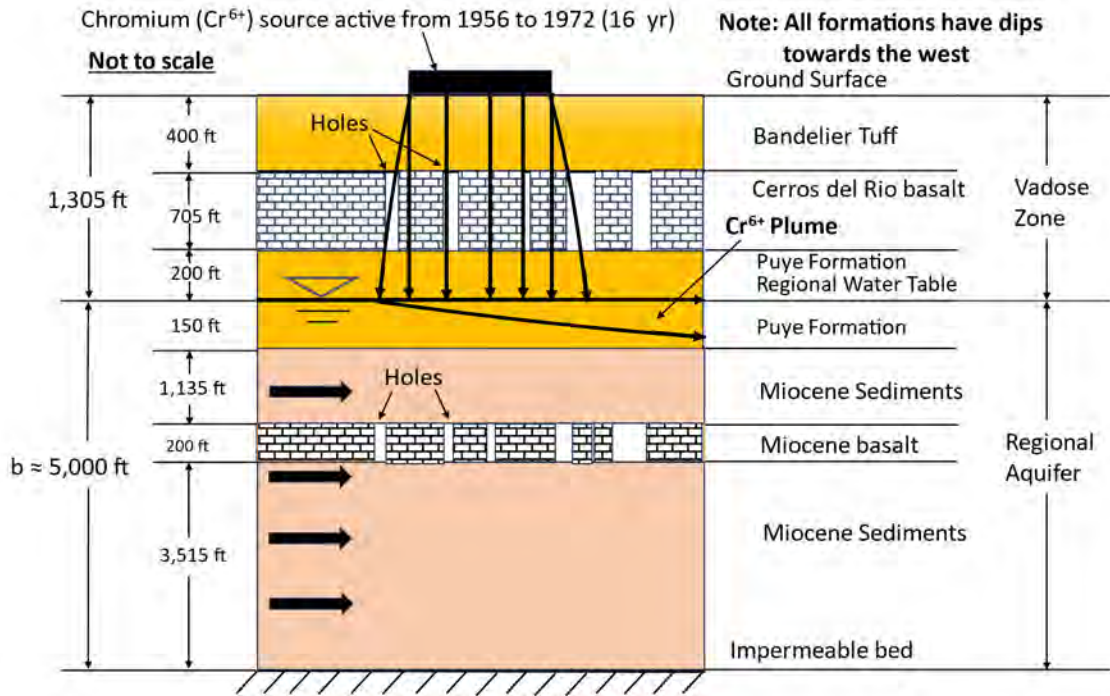


Figure 2. The cross-section of the conceptual model for the vadose zone and aquifer system.



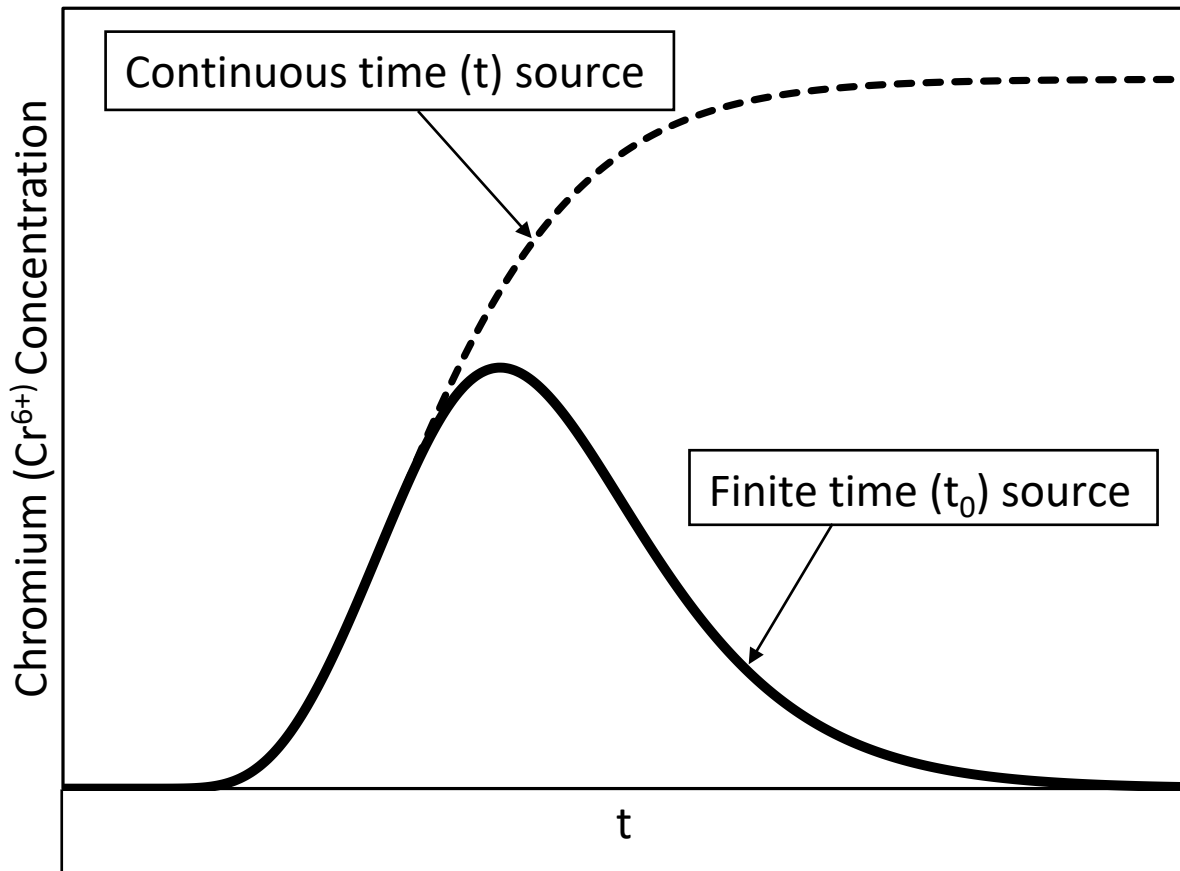


Figure 3. Hypothetical temporal chromium ( $Cr^{6+}$ ) concentration variation (breakthrough curve) at the bottom of the vadose zone from continuous and finite-time sources at the ground surface.

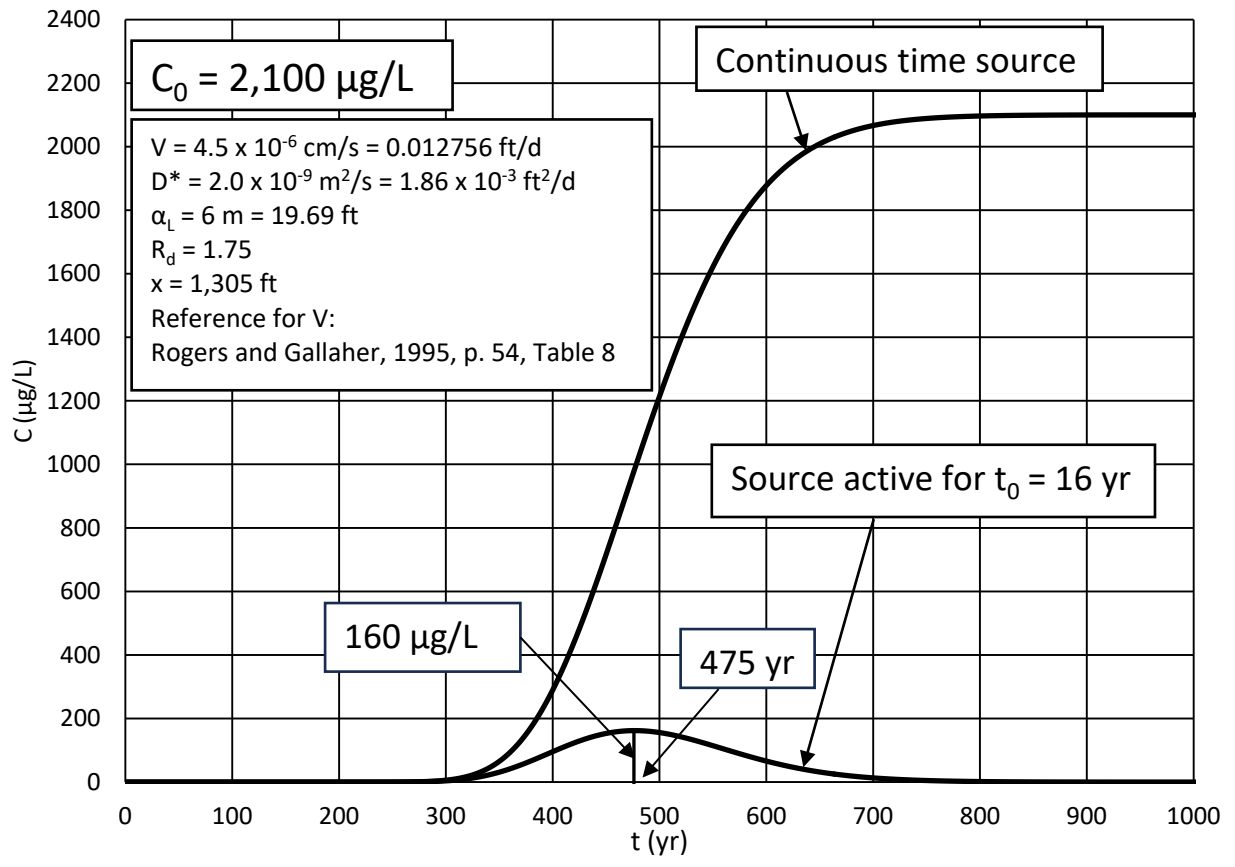


Figure 4. Breakthrough curves at the bottom of 1,305 ft thick vadose zone for  $V = 4.50 \times 10^{-6} \text{ cm/s}$  velocity.

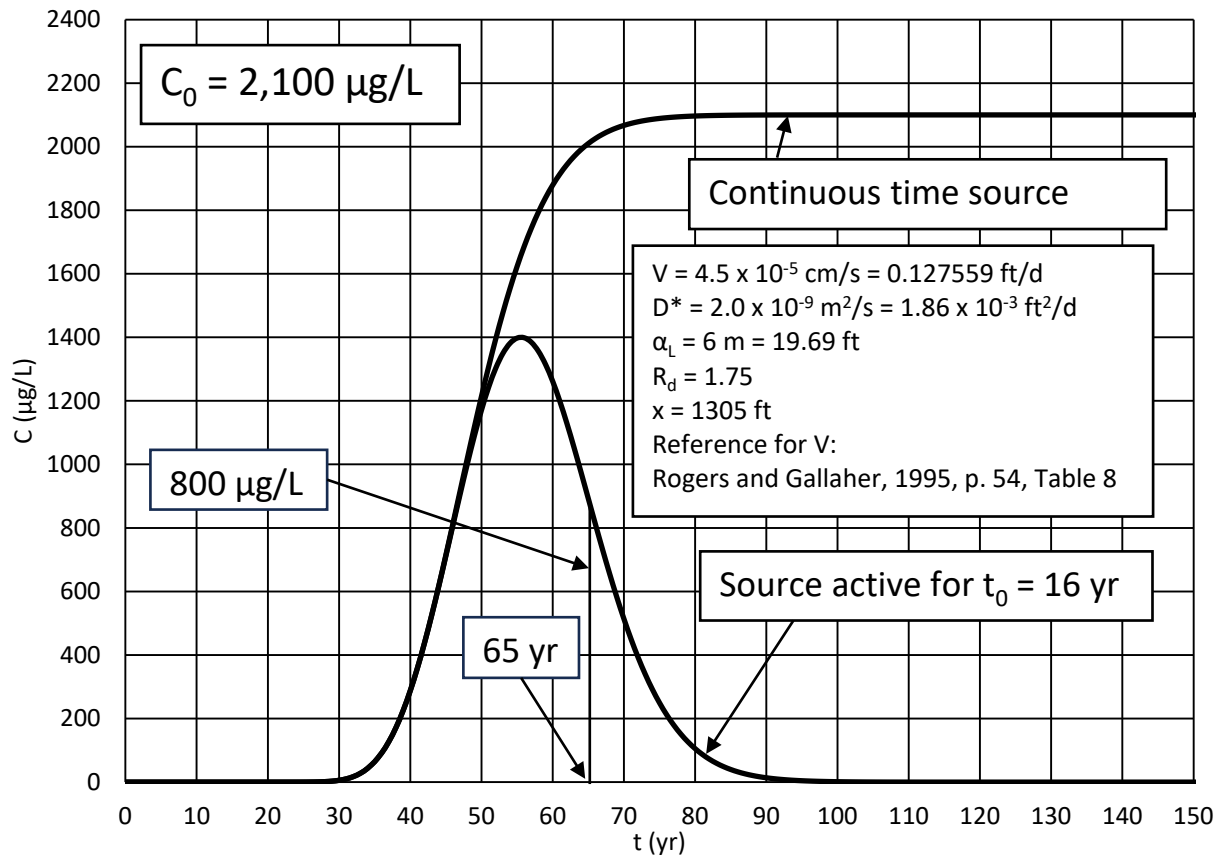


Figure 5. Breakthrough curves at the bottom of 1,305 ft thick vadose zone for  $V = 4.50 \times 10^{-5} \text{ cm/s}$  velocity.

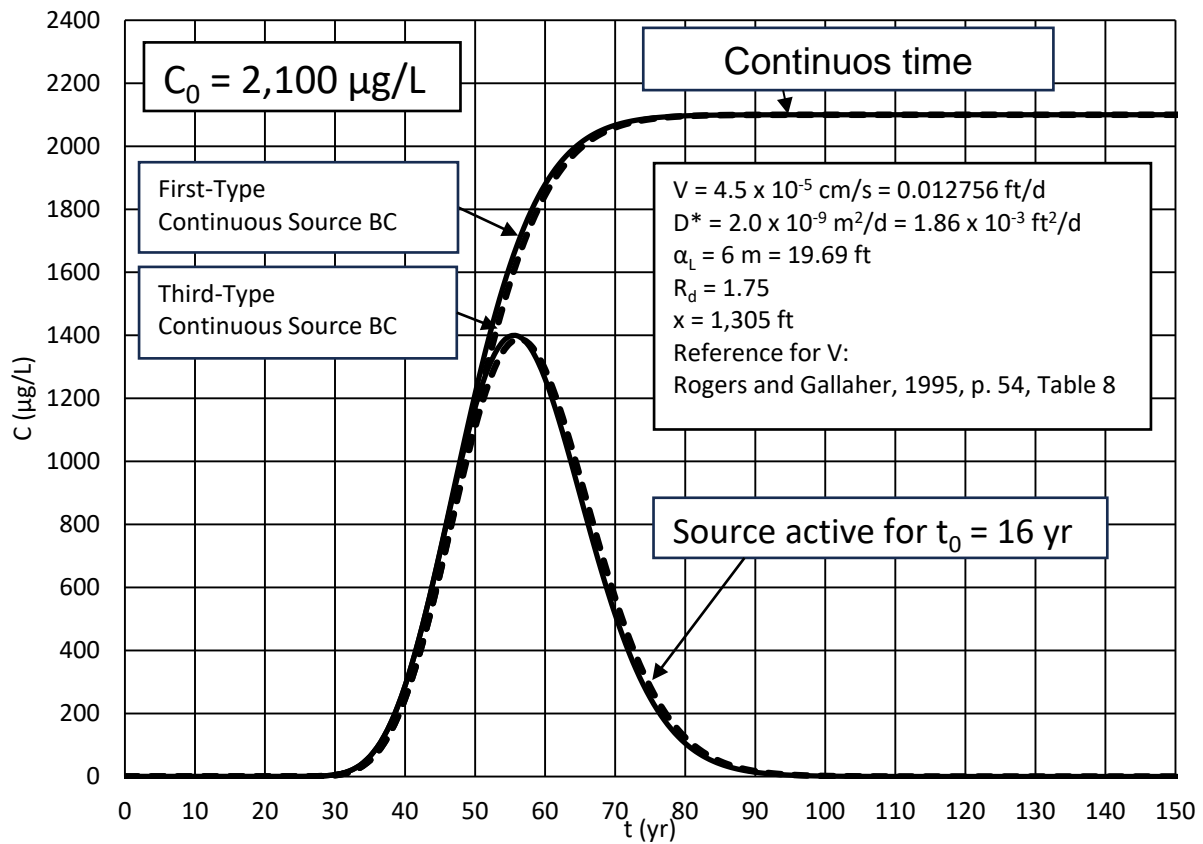


Figure 6. Breakthrough curves at the bottom of 1,305 ft thick vadose zone for  $V = 4.50 \times 10^{-5} \text{ cm/s}$  velocity with comparison of the first-type solution with the third-type source solution.

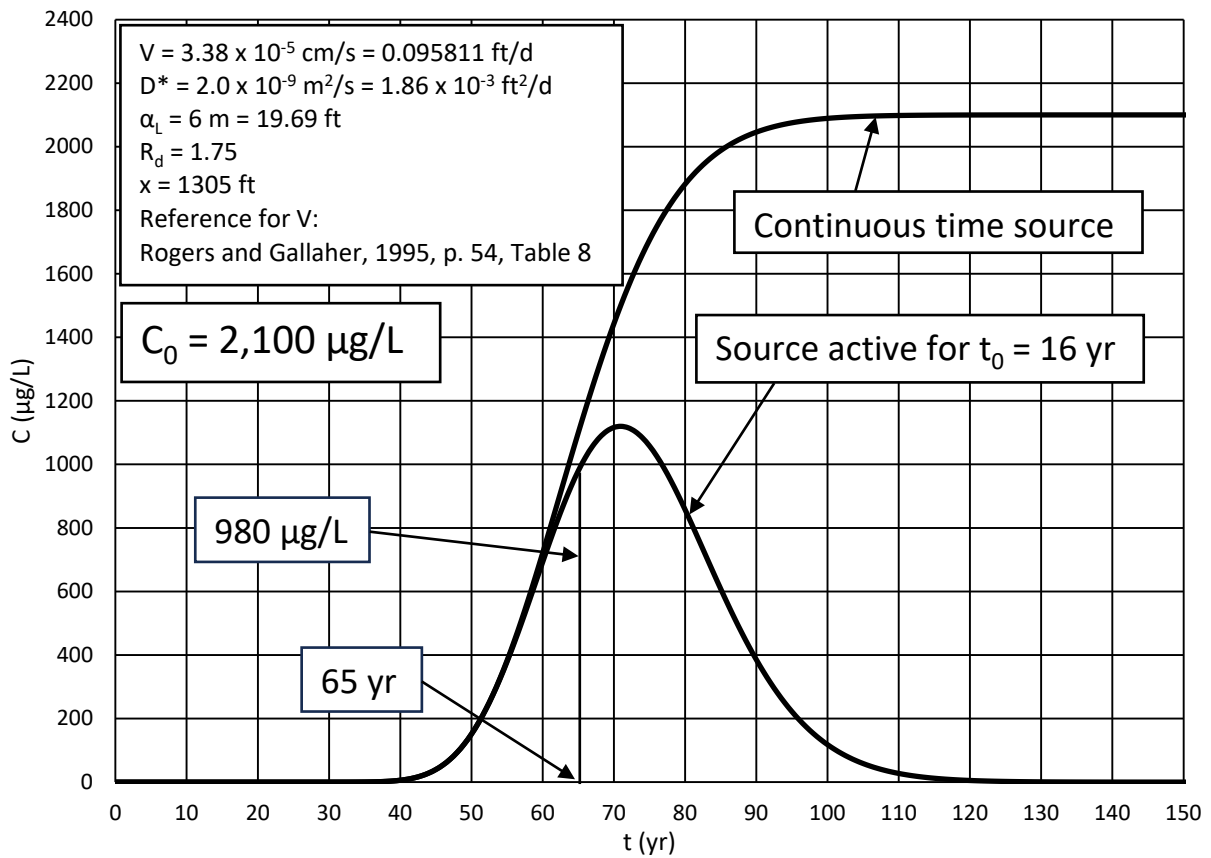


Figure 7. Breakthrough curves at the bottom of 1,305 ft thick vadose zone for  $V = 3.38 \times 10^{-5} \text{ cm/s}$  velocity.

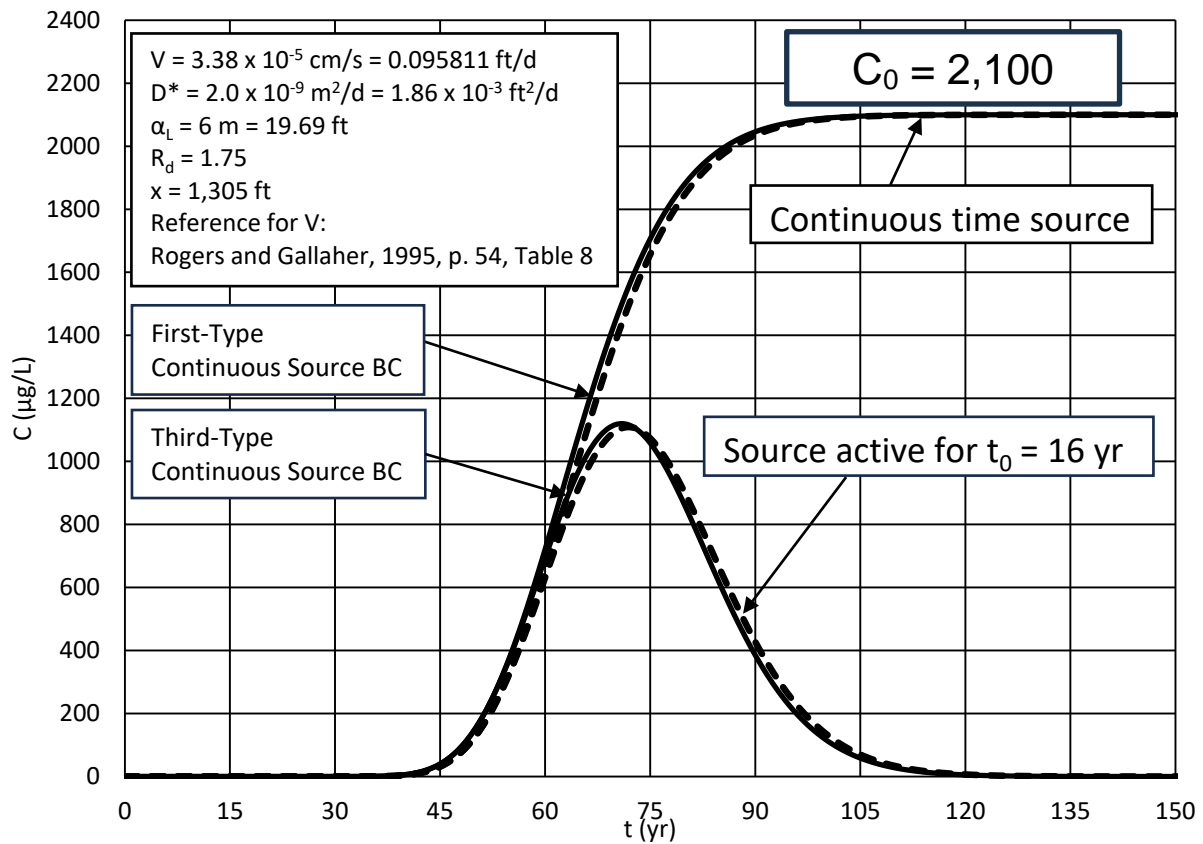


Figure 8. Breakthrough curves at the bottom of 1,305 ft thick vadose zone for  $V = 3.38 \times 10^{-5} \text{ cm/s}$  velocity with comparison of the first-type solution with the third-type source solution.

# R-42

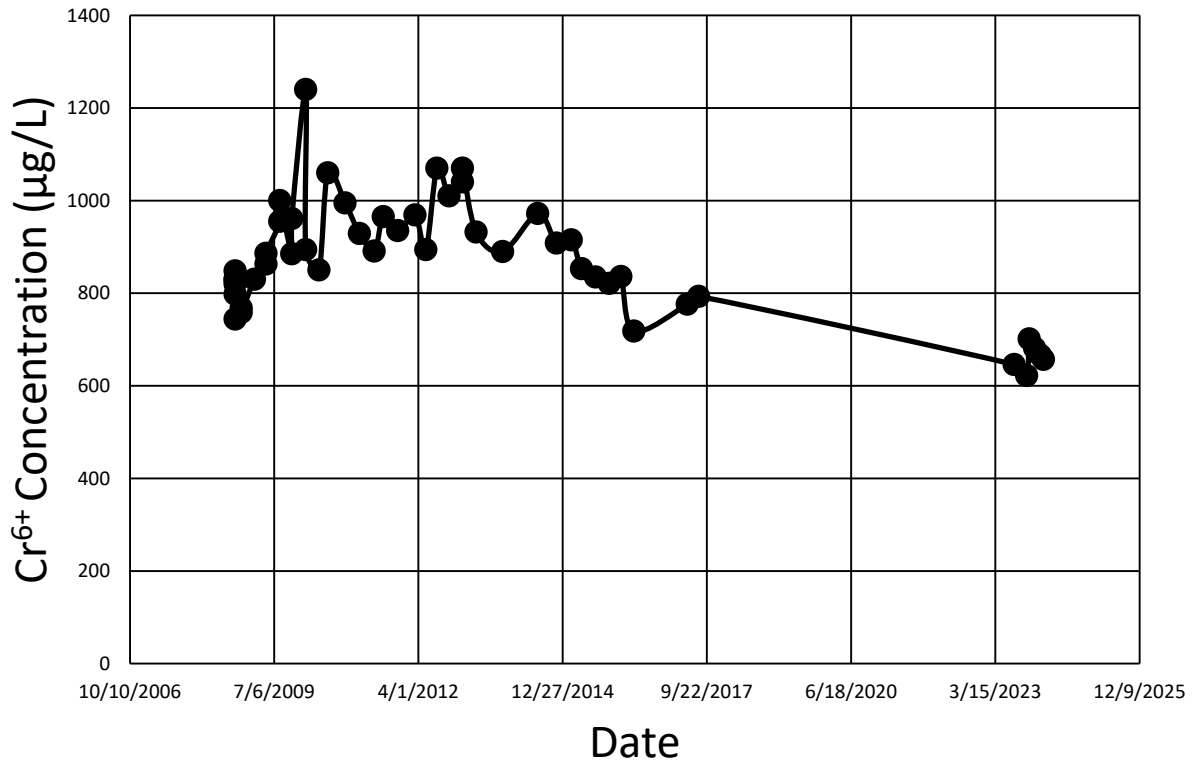


Figure 9a. All data for Cr<sup>6+</sup> concentration vs. date at R-42.

# R-42

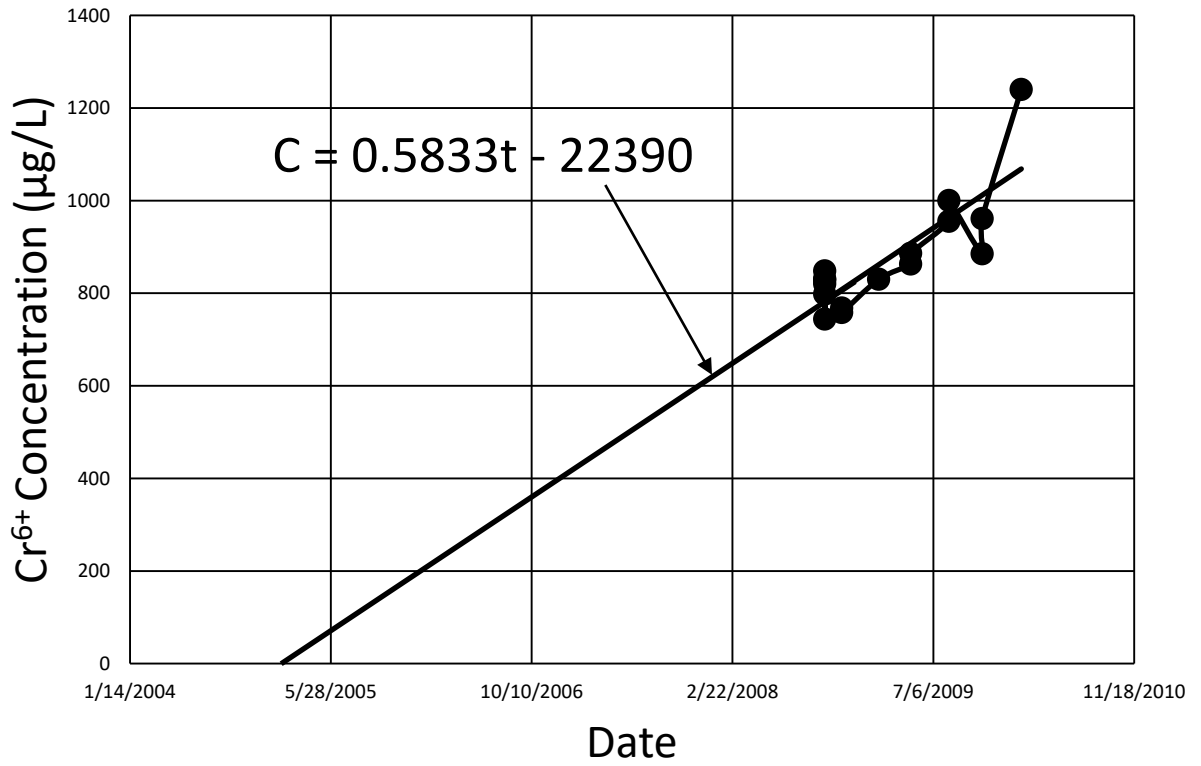


Figure 9b. Data until 2/10/2010 for  $Cr^{6+}$  concentration vs. date at R-42.



# R-43 S1

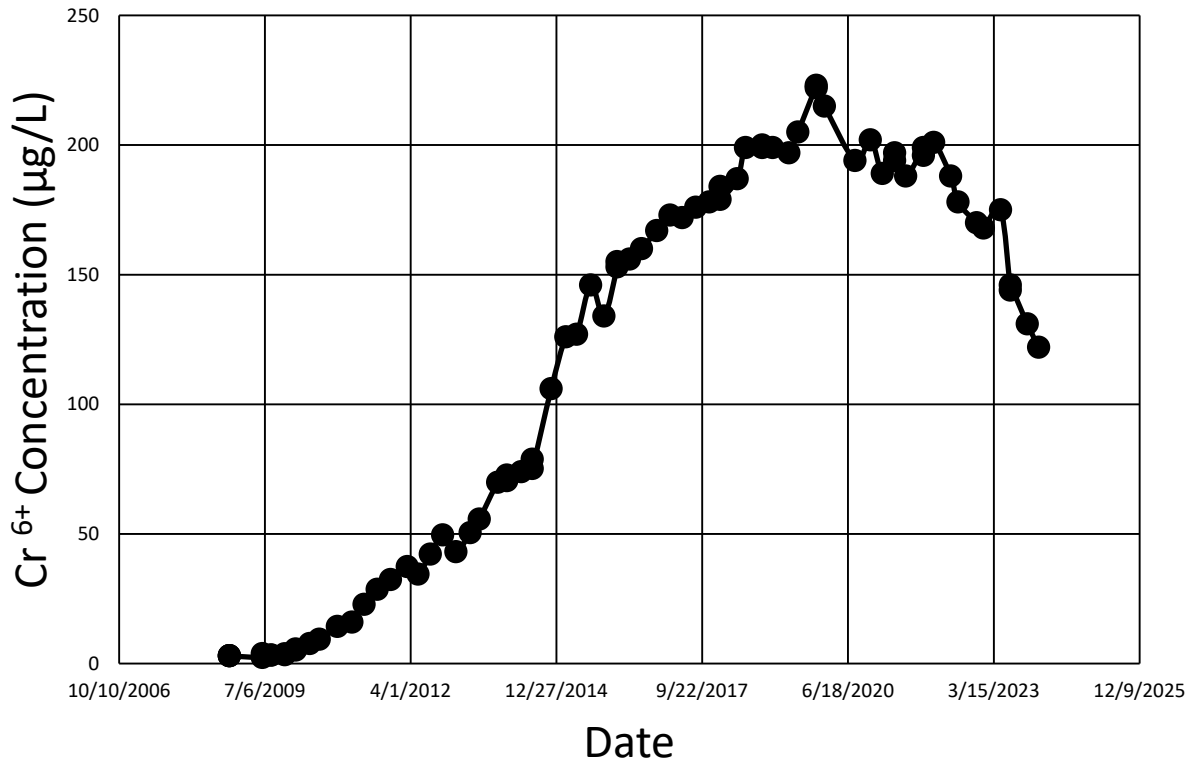


Figure 10a. All data for Cr<sup>6+</sup> concentration vs. date at R-43 S1.

# R-43 S1

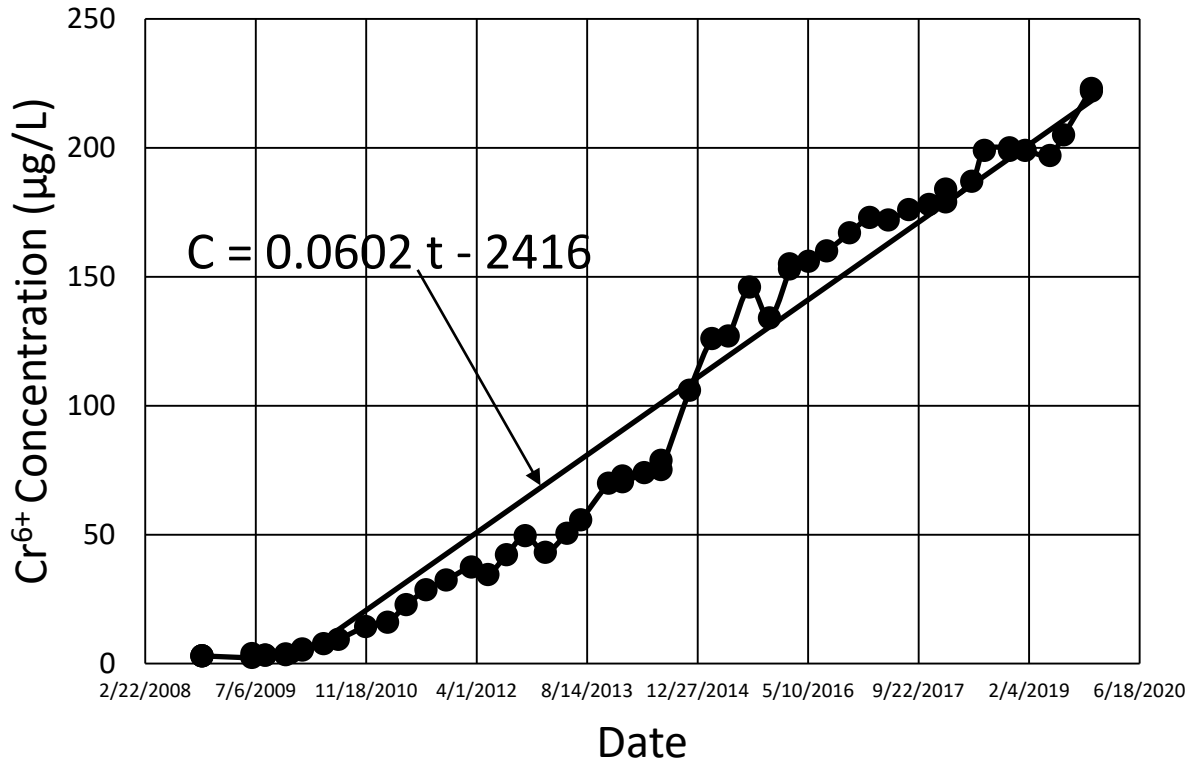


Figure 10b. All data for  $Cr^{6+}$  concentration vs. date at R-43 S1 till April 11, 2022.



## R-43 S2 - Reduced Cr<sup>6+</sup> Concentration Values

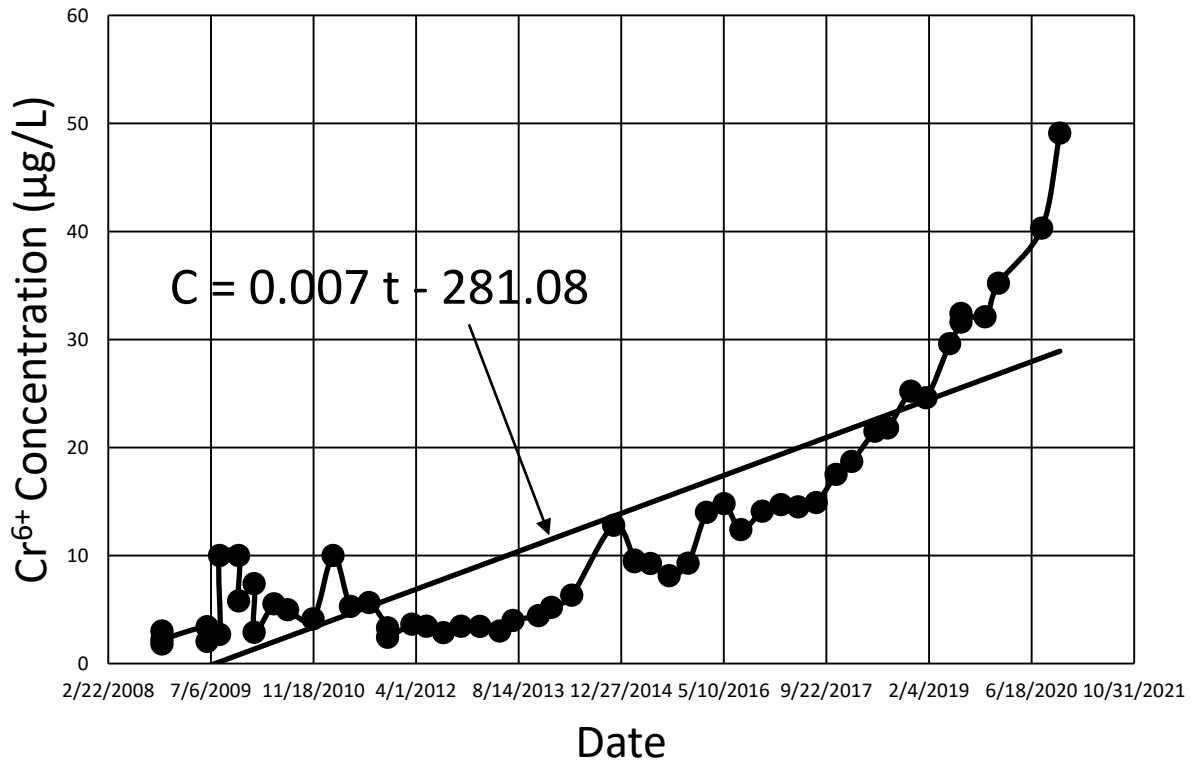


Figure 11b. Data until 11/31/2020 for Cr<sup>6+</sup> concentration vs. date at R-43 S2.

# R-62

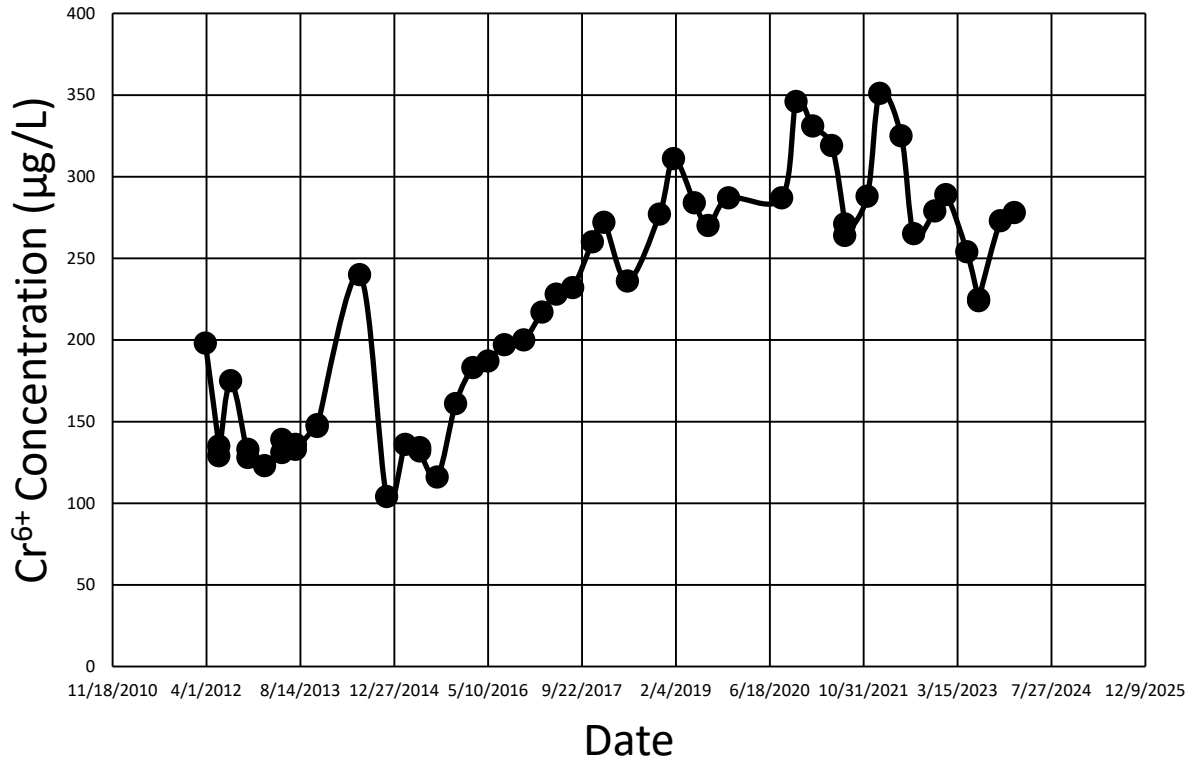


Figure 12a. All data for Cr<sup>6+</sup> concentration vs. date at R-62.

# R-62

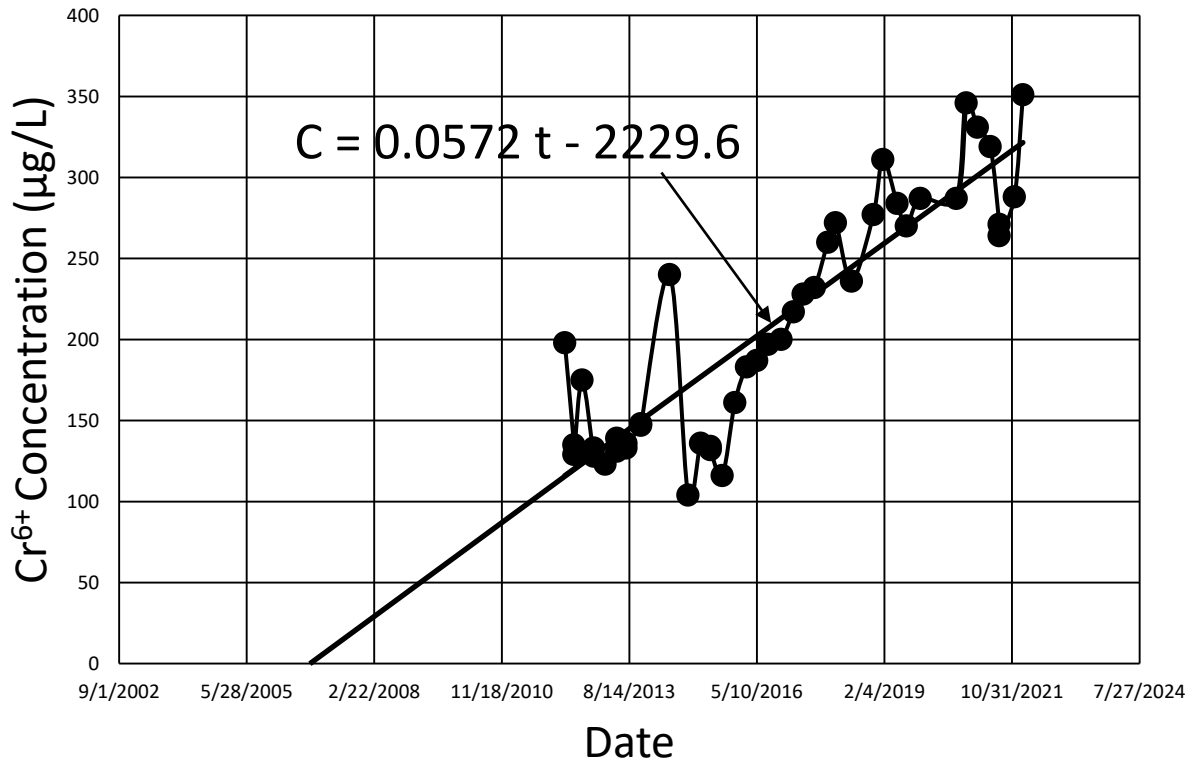


Figure 12b. Data until 1/25/2022 for  $Cr^{6+}$  concentration vs. date at R-62.

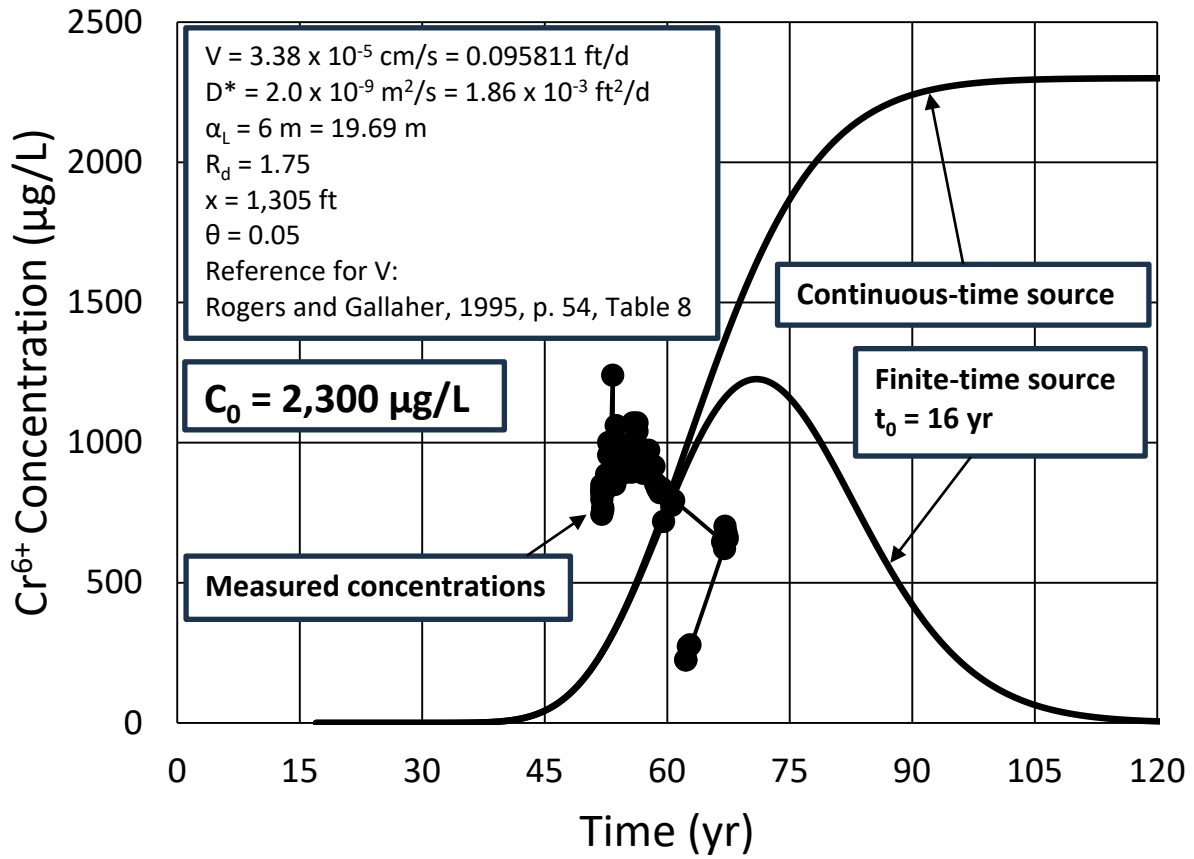


Figure 13. Comparison of the measured  $Cr^{6+}$  concentrations at R-42 well with the calculated breakthrough curve at the bottom of the vadose zone.

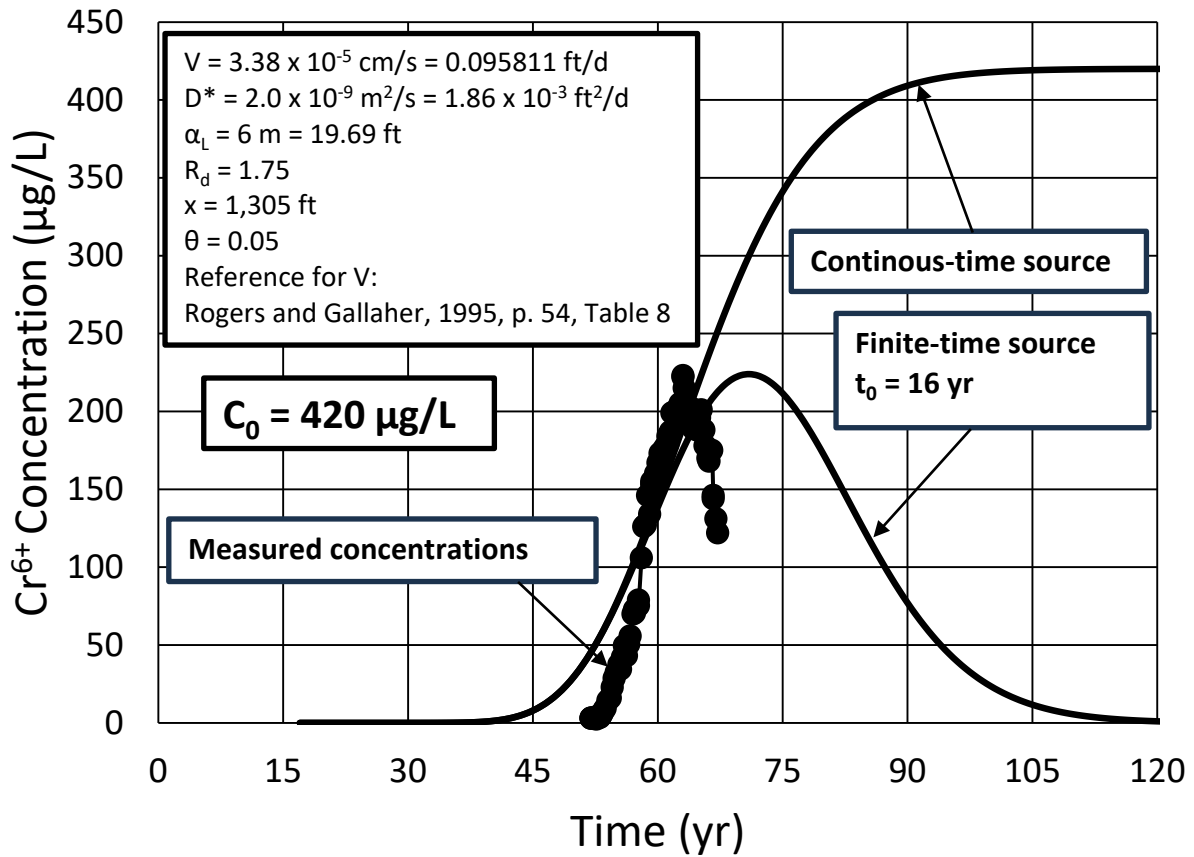


Figure 14. Comparison of the measured  $Cr^{6+}$  concentrations at R-43 S1 well with the calculated breakthrough curve at the bottom of the vadose zone.



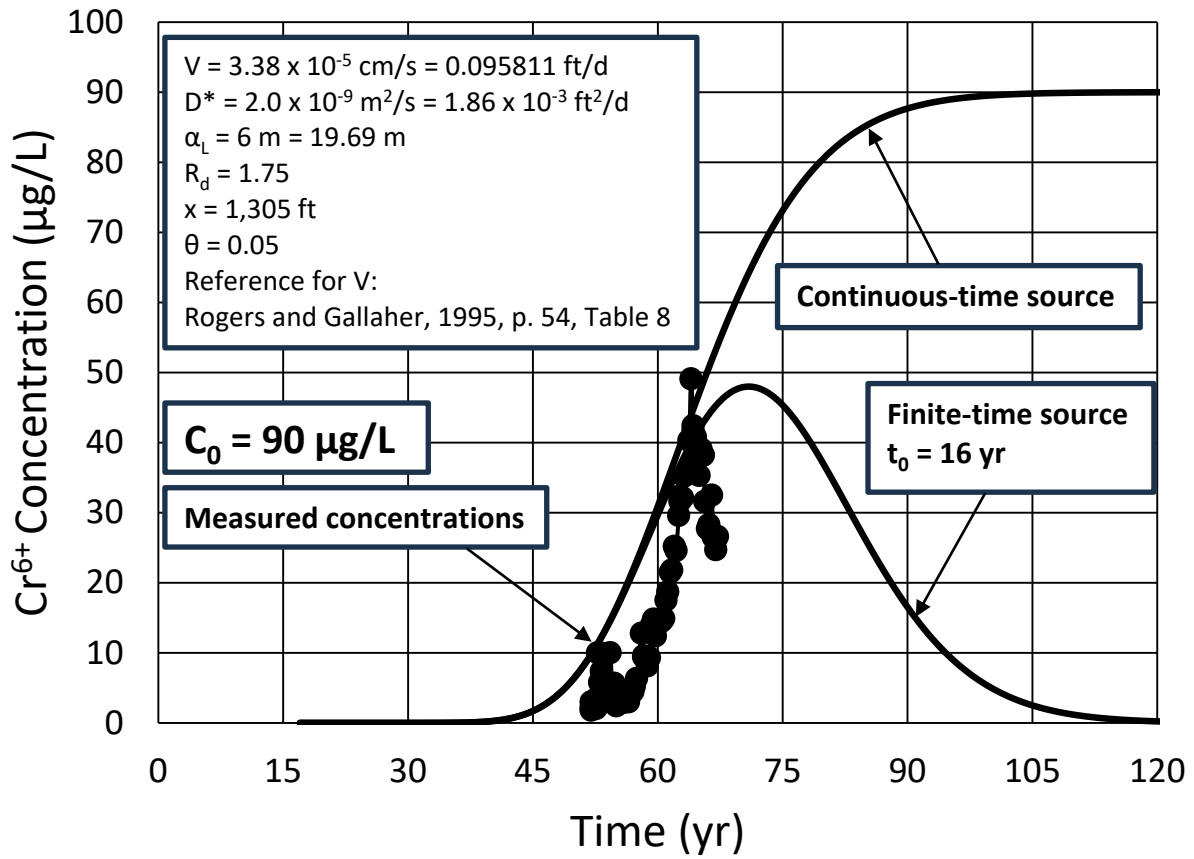


Figure 15. Comparison of the measured  $Cr^{6+}$  concentrations at R-43 S2 well with the calculated breakthrough curve at the bottom of the vadose zone.

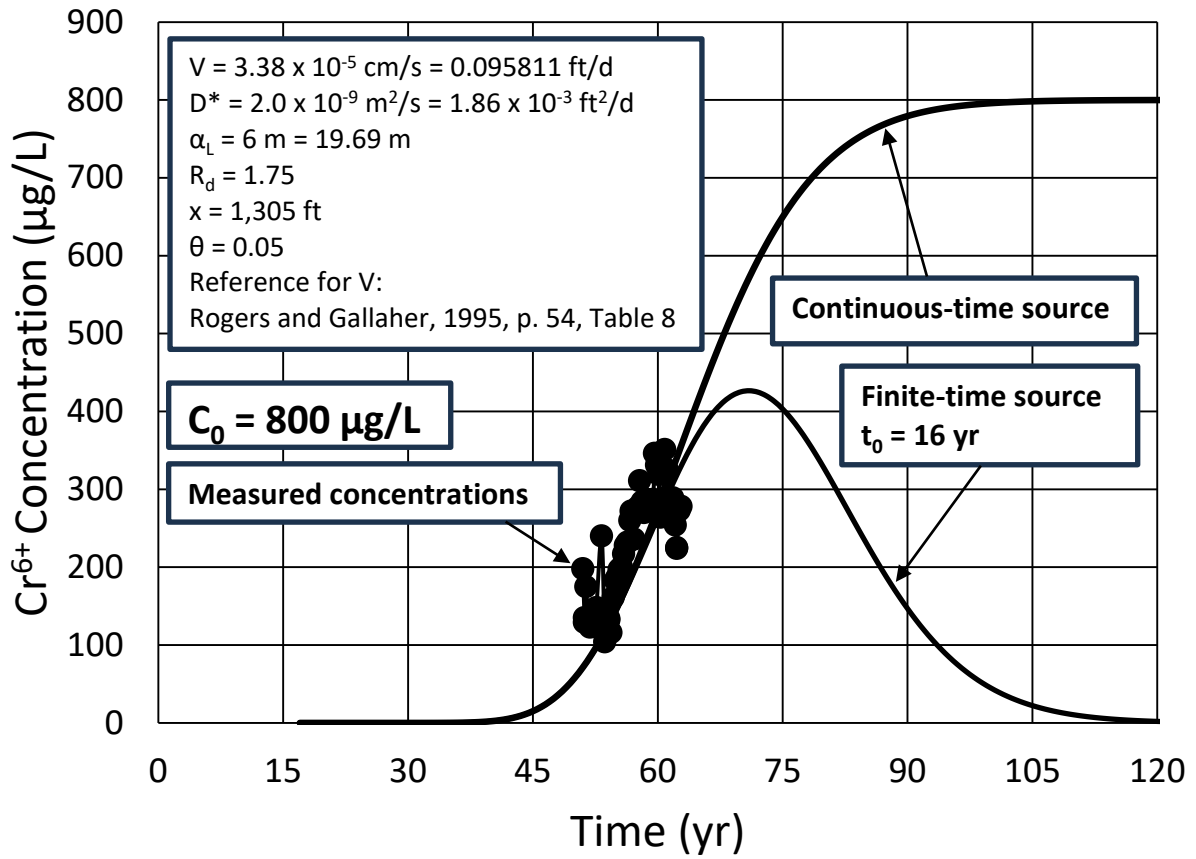


Figure 16. Comparison of the measured  $\text{Cr}^{6+}$  concentrations at R-62 well with the calculated breakthrough curve at the bottom of the vadose zone.

## **Appendices**

## APPENDIX A: VERTICAL DARCY VELOCITY IN AN UNSATURATED ZONE UNDER UNIFORM WATER CONTENT CONDITIONS

The vertical Darcy velocity component for unsaturated formations is given as [e.g., Bear, 1979, page 209, Eq. (6-27); Warrick, 2003, page 63, Eq. (2-24)] as

$$q_z = -K(\theta) \frac{dh(\theta)}{d\theta} \frac{\partial \theta}{\partial z} - K(\theta) \quad (\text{A.1})$$

in which  $K(\theta)$  is the unsaturated hydraulic conductivity,  $h(\theta)$  is matric pressure potential, and  $\theta$  is the water content. Here,  $K$  is a function of  $h$  or  $\theta$ . In Eq. (A.1), the velocity is assumed to be positive in the upward  $z$  coordinate direction. If  $\theta$  is uniform along the thickness of the clayey silt formation, the first term on the right-hand side of Eq. (A.1) becomes zero. Therefore, Eq. (A.1) becomes

$$q_z = -K(\theta) \quad (\text{A.2})$$

If the groundwater velocity is assumed to be positive in the downward direction, Eq. (C.1) becomes

$$q_z = K(\theta) \quad (\text{A.3})$$

in which  $\theta_{unif}$  is the uniform water content in the unsaturated zone. With  $K(\theta_{unif}) \equiv K_v$  and  $\theta_{unif} \equiv \theta$ , Eq. (A.3) becomes

$$q_z = K(\theta_{unif}) \quad (\text{A.4})$$

Then, the linear groundwater velocity is [e.g., Bear, 1979, page 63, Eq. (4-7)],

$$V = \frac{q_z}{\theta_{unif}} = \frac{K(\theta_{unif})}{\theta_{unif}} \quad (\text{A.5})$$

## APPENDIX B: ONE-DIMENSIONAL ADVECTIVE-DISPERSIVE ANALYTICAL SOLUTE TRANSPORT SOLUTIONS FOR FINITE-TIME SOURCE CONDITION

### B.1 GOVERNING SOLUTE TRANSPORT DIFFERENTIAL EQUATION

The governing differential equation for one-dimensional advection and dispersion equation is (e.g., van Genuchten and Alves, 1982, page 9, A1)

$$R_d \frac{\partial C}{\partial t} = D \frac{\partial^2 C}{\partial x^2} - V \frac{\partial C}{\partial x} \quad (\text{B.1})$$

in which  $R_d$  is the retardation factor,  $C$  ( $M/L^3$ ) is the concentration,  $D$  ( $L^2/T$ ) is the dispersion coefficient, and  $t$  is time. The retardation factor equation is

$$R_d = 1 + \frac{\rho_b}{n} K_d \quad (\text{B.2})$$

in which  $\rho_b$  ( $M/L^3$ ) is the bulk density of the porous medium,  $K_d$  ( $L^3/M$ ) is the distribution coefficient, and  $n$  is the total porosity. In Eq. (G.1),  $V$  is the interstitial or pore-water and is given as

$$V = \frac{q}{\theta} \quad (\text{B.3})$$

in which  $q$  ( $L/T$ ) is the volumetric flux and  $\theta$  is the volumetric moisture content. The dispersion coefficient  $D$  is given by

$$D = \alpha_L V + D^* \quad (\text{B.4})$$

in which  $\alpha_L$  ( $L$ ) is the longitudinal dispersivity and  $D^*$  ( $L^2/T$ ) is the effective molecular diffusion coefficient.

### B.2 FIRST-TYPE SOURCE SOLUTION

#### B.2.1 Initial and Boundary Conditions

The initial and boundary conditions are given below (e.g., van Genuchten and Alves, 1982, page 9, A1).

The initial condition is

$$C(x, 0) = C_i \quad (\text{B.5})$$

The boundary conditions at the source are

$$C(0, t) = C_0 \quad 0 < t \leq t_0 \quad (\text{B.6})$$

$$C(0, t) = 0 \quad t > 0 \quad (\text{B.7})$$

The boundary condition at infinity is

$$\frac{\partial C(\infty, t)}{\partial x} = 0 \quad (\text{B.8})$$

### B.2.2 Solution

The analytical solution of the above-defined boundary-value problem is (Lapidus and Amundson, 1952; Ogata and Banks, 1961; as presented in van Genuchten and Alves, 1982, p. 9, A1)

$$C(x, t) = C_i + (C_0 - C_i)A(x, t) \quad 0 < t \leq t_0 \quad (\text{B.9})$$

$$C(x, t) = C_i + (C_0 - C_i)A(x, t) - C_0A(x, t - t_0) \quad t > 0 \quad (\text{B.10})$$

in which

$$A(x, t) = \frac{1}{2} \operatorname{erfc} \left[ \frac{R_d x - Vt}{2(DR_d t)^{\frac{1}{2}}} \right] + \frac{1}{2} \exp\left(\frac{Vx}{D}\right) \operatorname{erfc} \left[ \frac{R_d x + Vt}{2(DR_d t)^{\frac{1}{2}}} \right] \quad (\text{B.11})$$

When the initial concentration is zero ( $C_i = 0$ ), Eqs. (B.9) and (B.10), respectively, become

$$C(x, t) = C_0A(x, t) \quad 0 < t \leq t_0 \quad (\text{B.12})$$

$$C(x, t) = C_0A(x, t) - C_0A(x, t - t_0) \quad t > 0 \quad (\text{B.13})$$

These equations are also given in Leij et al. [1991, page 945, Eqs. (9) and (10)]. In the above equations,  $C_0$  is the source concentration,  $x$  is the distance from the source,  $V$  is the average linear groundwater velocity,  $D$  is the dispersion coefficient,  $t$  is time, and  $t_0$  is the source active time period. The longitudinal dispersion coefficient  $D$  is [e.g., Freeze and Cherry, 1979, page 389, Eq. (9.4)],

$$D = \alpha_L V + D^* \quad (\text{B.14})$$

in which  $\alpha_L$  is the longitudinal dispersivity and  $D^*$  is the effective molecular diffusion coefficient. And  $\operatorname{erfc}$  is the complementary error function and defined as

$$\operatorname{erfc}(u) = 1 - \frac{2}{\pi^{\frac{1}{2}}} \int_u^{\infty} u^{-\xi^2} d\xi \quad (\text{B.15})$$

## B.3 THIRD-TYPE SOURCE SOLUTION

### B.3.1 Initial and Boundary Conditions

The initial and boundary conditions are given below (e.g., van Genuchten and Alves, 1982, page 10, A2).

The initial condition is

$$C(x, 0) = C_i \quad (\text{B.16})$$

The boundary conditions at the source are

$$VC - D \frac{\partial C}{\partial x} = VC_0 \quad 0 < t \leq t_0 \quad (\text{B.17})$$

$$VC - D \frac{\partial C}{\partial x} = 0 \quad t > 0 \quad (\text{B.18})$$

The boundary condition at infinity is

$$\frac{\partial C(\infty, t)}{\partial x} = 0 \quad (\text{B.19})$$

### B.3.2 Solution

The analytical solution of the above-defined boundary-value problem is (Mason and Weaver, 1924; Lindstrom et al., 1967; Gershon and Nir, 1969; as presented in van Genuchten and Alves, 1982, p. 10, A2)

$$C(x, t) = C_i + (C_0 - C_i)A(x, t) \quad 0 < t \leq t_0 \quad (\text{B.20})$$

$$C(x, t) = C_i + (C_0 - C_i)A(x, t) - C_0A(x, t - t_0) \quad t > 0 \quad (\text{B.21})$$

in which

$$A(x, t) = \frac{1}{2} \operatorname{erfc} \left[ \frac{R_d x - Vt}{2(DR_d t)^{\frac{1}{2}}} \right] + \left( \frac{V^2 t}{\pi DR_d} \right)^{\frac{1}{2}} \exp \left[ -\frac{(R_d x - Vt)^2}{4DR_d t} \right] - \frac{1}{2} \left( 1 + \frac{Vx}{D} + \frac{V^2 t}{DR_d} \right) \exp \left( \frac{Vx}{D} \right) \operatorname{erfc} \left[ \frac{R_d x + Vt}{2(DR_d t)^{\frac{1}{2}}} \right] \quad (\text{B.22})$$

When the initial concentration is zero ( $C_i = 0$ ), Eqs. (B.9) and (B.10), respectively, become

$$C(x, t) = C_0 A(x, t) \quad 0 < t \leq t_0 \quad (\text{B.23})$$

$$C(x, t) = C_0 A(x, t) - C_0 A(x, t - t_0) \quad t > 0 \quad (\text{B.24})$$

In the above equations,  $C_0$  is the source concentration,  $x$  is the distance from the source,  $V$  is the average linear groundwater velocity,  $D$  is the dispersion coefficient,  $t$  is time, and  $t_0$  is the source active time period. The longitudinal dispersion coefficient  $D$  is [e.g., Freeze and Cherry, 1979, page 389, Eq. (9.4)],

$$D = \alpha_L V + D^* \quad (\text{B.25})$$

in which  $\alpha_L$  is the longitudinal dispersivity and  $D^*$  is the effective molecular diffusion coefficient. And  $\operatorname{erfc}$  is the complementary error function and defined as

$$\operatorname{erfc}(u) = 1 - \frac{2}{\pi^{1/2}} \int_u^\infty u^{-\xi^2} d\xi \quad (\text{B.26})$$



## APPENDIX C: ESTIMATION OF THE LONGITUDINAL DISPERSIVITY IN THE VADOSE ZONE

The longitudinal dispersivity ( $\alpha_L$ ) has been estimated for  $x = 1,305 \text{ ft} = 397.76 \text{ m}$  scale distance from Gelhar et al. (1992, p. 1968, Figure 2) and is shown in Figure C.1.

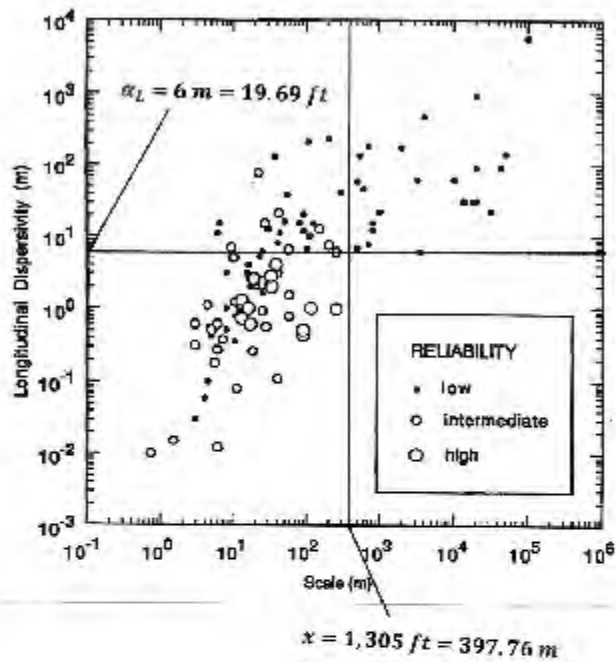


Figure C.1. Estimated longitudinal dispersivity ( $\alpha_L$ ) for  $x = 1,305 \text{ ft} = 397.76 \text{ m}$  scale distance from Gelhar et al. (1992, p. 1968, Figure 2).

## **Appendix H**

**Batu (2024i) - Evaluation of the Flow Parameters and Chromium (Cr<sup>6+</sup>) Concentration Data to Estimate the Plume Extensions in the Longitudinal and Transverse Vertical Directions, Los Alamos, New Mexico**

# **Evaluation of the Flow Parameters and Chromium ( $Cr^{6+}$ ) Concentration Data to Estimate the Plume Extensions in the Longitudinal and Transverse Vertical Directions, Los Alamos, New Mexico**

---

Vedat Batu, Ph.D., P.E.  
Argonne Associate  
Argonne National Laboratory  
Lemont, Illinois

**August 23, 2024**

This page intentionally left blank.

## Executive Summary

In this report, with the available flow and solute transport parameters, the potential longitudinal and transverse vertical dissolved chromium ( $Cr^{6+}$ ) mass plume extensions have been estimated under no extraction and injection well conditions using a two-dimensional analytical solute transport mathematical model. Based on the 2008, 2013, and 2020 hydraulic head values and contours, it has been found out that the streamline formed by R-42, R-28, R-45, and R-13 observation wells is the main flow direction which is oriented towards to the southeast direction. It has been found out that the predicted concentrations at R-45 and R-13 compare well with their measured average values for the  $K_h = 30 \text{ ft/d}$  horizontal hydraulic conductivity value with all potential  $\alpha_L$  longitudinal dispersivity and  $\alpha_{TV}$  transverse vertical dispersivity values. Also the results showed that the estimated site-specific degradation rate of chromium ( $Cr^{6+}$ ) ( $\nu = 0.9 \times 10^{-5} \text{ d}^{-1}$ ) has around 10% to 15% effect on the concentrations. Based on the runs with the analytical model, within 40 *yr* time period, the plume has been migrated longitudinally around 4,000 ft from R-42 observation well. And within 64 *yr* time period, the plume has been migrated longitudinally more than 4,000 ft. Also within 40 *yr* time period, the plume has been migrated from the water table down to 700 ft distance depending on the  $\alpha_H$  and  $\alpha_{TV}$  values. And within 64 *yr* time period, the plume has been migrated from the water table down to 1,300 ft distance depending on the  $\alpha_H$  and  $\alpha_{TV}$  values.

# Contents

Executive Summary .....	ES-1
1. Introduction .....	1
2. Chromium (Cr6 +) Source Area and the Main Flow and Transport Paths in the Unconfined Aquifer .....	1
2.1 The Estimated Chromium (Cr6 +) Source Area .....	1
2.2 The Main Flow and Chromium (Cr6 +) Transport Path Lines and the Average Hydraulic Gradient.....	1
3. Measured Chromium (Cr6 +) Concentrations Along the Main Flow Direction and Distances of the Observation Wells from R-42 .....	2
3.1 Measured Chromium (Cr6 +) Concentrations at R-42 and Their Average Value.....	2
3.2 Measured Chromium (Cr6 +) Concentrations at R-28 and Their Average Value.....	2
3.3 Measured Chromium (Cr6 +) Concentrations at R-45 S1 and R-45 S2 and Their Average Value.....	2
3.4 Measured Chromium (Cr6 +) Concentrations at R-13 and Their Average Value.....	3
3.5 Distances of R-28, R-45, and R-13 from R-42 and Their Average Concentrations ..	3
4. Measured Horizontal Hydraulic Conductivity Values .....	3
4.1 Horizontal Hydraulic Conductivity Values Based on the Previous Studies .....	3
4.1.1 Calculated Horizontal Hydraulic Conductivity (Kh) Values from Figure 13 of Neptune (2023a) Report Based on the Theis Type-Curve (1935) Solution.....	3
4.1.2 Horizontal Hydraulic Conductivity Values from the McLin (2007) Report.....	4
5. Mathematical Modeling Approach.....	4
5.1 Introduction.....	4
5.2 Estimation Approach with a Two-Dimensional Analytical Solution.....	5
6. Flow Parameters.....	5
6.1 Horizontal Hydraulic Conductivity.....	6
6.2 Hydraulic Gradient.....	6
6.3 Effective Porosity.....	6
7. Solute Transport Parameters.....	6
7.1 Dispersivities .....	6
7.2 Molecular Diffusion Coefficient.....	7
7.3 Retardation Factor of Chromium (Cr6+).....	7
7.4 Degradation Rate of Chromium (Cr6+) .....	7
8. Longitudinal and Transverse Vertical Chromium (Cr6 +) Plume Extensions Estimation .....	7
8.1 Longitudinal Chromium (Cr6 +) Concentration Variation Along the Streamline Formed by the Observation Wells R-42, R-28, R-45 S1, R-45 S2, and R-13 .....	8
8.1.1 Cr6 + Concentration Variations for $\alpha L = 50$ m (164.04 ft) After $t = 40$ yr and 64 yr 8	
8.1.2 Cr6 + Concentration Variations for $\alpha L = 100$ m (328.08 ft) After $t = 40$ yr and 64 yr 8	
8.2 Transverse Chromium (Cr6 +) Concentration Variation Perpendicular to the Streamline Formed By the Observation Wells R-42, R-28, R-45 S1, R-45 S2, and R-13.....	9

9. Conclusions .....	10
References.....	11

## Figures

- Figure 1. Head contours for May 1, 2020 and main flow direction.
- Figure 2. Head contours in 2013 and main flow direction.
- Figure 3. Measured Chromium ( $Cr^{6+}$ ) concentrations at R-42 between 10/9/2008 and 7/28/2017 and their average value.
- Figure 4. Measured Chromium ( $Cr^{6+}$ ) concentrations at R-28 between 5/20/2005 and 8/2/2017 and their average value.
- Figure 5. Measured Chromium ( $Cr^{6+}$ ) concentrations at R-45 S1 between 2/28/2009 and 3/23/2022 and their average value.
- Figure 6. Measured Chromium ( $Cr^{6+}$ ) concentrations at R-45 S2 between 3/5/2009 and 3/23/2022 and their average value.
- Figure 7. Measured Chromium ( $Cr^{6+}$ ) concentrations at R-13 between 4/18/2002 and 1/22/2024 and their average value.
- Figure 8. Average  $Cr^{6+}$  concentrations at R-42, R-28, R-45 S1, R-45 S2, and R-13 which are on the same streamline (Or flowline) in the unconfined aquifer beneath the LANL site.
- Figure 9. The geometry of the two-dimensional analytical solute transport model (ST2A) adapted to an unconfined aquifer.
- Figure 10. Longitudinal dispersivity ( $\alpha_L$ ) versus scale (x) with data classified by reliability (Gelhar et al., 1992, p. 1968, Figure 2).
- Figure 11. Ratio of longitudinal to horizontal ( $\alpha_L/\alpha_{TH}$ ) and vertical transverse dispersivities ( $\alpha_L/\alpha_{TV}$ ) versus scale (x) with data classified by reliability (Gelhar et al., 1992, p. 1971, Figure 6).
- Figure 12. Longitudinal  $Cr^{6+}$  concentration variation along the streamline formed by the observation wells R-42, R-28, R-45 S1, R-45 S2, and R-13 for different  $K_h$  values with  $\alpha_L = 50\text{ m}$  (164.04 ft) and  $\alpha_{TV}/\alpha_L = 0.01$  after 40 yr elapsed time.
- Figure 13. Longitudinal  $Cr^{6+}$  concentration variation along the streamline formed by the observation wells R-42, R-28, R-45 S1, R-45 S2, and R-13 for different  $K_h$  values with  $\alpha_L = 50\text{ m}$  (164.04 ft) and  $\alpha_{TV}/\alpha_L = 0.01$  after 64 yr elapsed time.
- Figure 14. Longitudinal  $Cr^{6+}$  concentration variation along the streamline formed by the observation wells R-42, R-28, R-45 S1, R-45 S2, and R-13 for different  $K_h$  values with  $\alpha_L = 100\text{ m}$  (328.08 ft) and  $\alpha_{TV}/\alpha_L = 0.01$  after 40 yr elapsed time.
- Figure 15. Longitudinal  $Cr^{6+}$  concentration variation along the streamline formed by the observation wells R-42, R-28, R-45 S1, R-45 S2, and R-13 for different  $K_h$  values with  $\alpha_L = 100\text{ m}$  (328.08 ft) and  $\alpha_{TV}/\alpha_L = 0.01$  after 64 yr elapsed time.

- Figure 16. Longitudinal  $Cr^{6+}$  concentration variation along the streamline formed by the observation wells R-42, R-28, R-45 S1, R-45 S2, and R-13 for  $K_h = 30 \text{ ft/d}$  with  $\alpha_L = 100 \text{ m}$  (328.08 ft),  $\alpha_{TV}/\alpha_L = 0.01$ , and  $\nu = 0.9 \times 10^{-5} \text{ d}^{-1}$  after 64 yr elapsed time.
- Figure 17. Transverse vertical  $Cr^{6+}$  concentration variation at  $x = 2,500 \text{ ft}$  perpendicular to the streamline formed by the observation wells R-42, R-28, R-45 S1, R-45 S2, and R-13 for  $K_h = 30 \text{ ft/d}$  with  $\alpha_L = 50 \text{ m}$  (164.04 ft) and  $\alpha_{TV}/\alpha_L = 0.01$  and 0.02 after 40 yr elapsed time.
- Figure 18. Transverse vertical  $Cr^{6+}$  concentration variation at  $x = 2,500 \text{ ft}$  perpendicular to the streamline formed by the observation wells R-42, R-28, R-45 S1, R-45 S2, and R-13 for  $K_h = 30 \text{ ft/d}$  with  $\alpha_L = 50 \text{ m}$  (164.04 ft) and  $\alpha_{TV}/\alpha_L = 0.01$  and 0.02 after 64 yr elapsed time.
- Figure 19. Transverse vertical  $Cr^{6+}$  concentration variation at  $x = 2,500 \text{ ft}$  perpendicular to the streamline formed by the observation wells R-42, R-28, R-45 S1, R-45 S2, and R-13 for  $K_h = 30 \text{ ft/d}$  with  $\alpha_L = 100 \text{ m}$  (328.08 ft) and  $\alpha_{TV}/\alpha_L = 0.01$  and 0.02 after 40 yr elapsed time.
- Figure 20. Transverse vertical  $Cr^{6+}$  concentration variation at  $x = 2,500 \text{ ft}$  perpendicular to the streamline formed by the observation wells R-42, R-28, R-45 S1, R-45 S2, and R-13 for  $K_h = 30 \text{ ft/d}$  with  $\alpha_L = 100 \text{ m}$  (328.08 ft) and  $\alpha_{TV}/\alpha_L = 0.01$  and 0.02 after 64 yr elapsed time.
- Figure 21. Transverse vertical  $Cr^{6+}$  concentration variation at  $x = 6,562 \text{ ft}$  (2,000 m) perpendicular to the streamline formed by the observation wells R-42, R-28, R-45 S1, R-45 S2, and R-13 for  $K_h = 30 \text{ ft/d}$  with  $\alpha_L = 200 \text{ m}$  (656.17 ft) and  $\alpha_{TV}/\alpha_L = 0.01$  and 0.02 after 64 yr elapsed time.

## Tables

- Table 1. Construction information of R-42, R-28, R-45, and R-13.
- Table 2. The distances of R-42, R-28, R-45, and R-13 observation wells from R-42 and their average chromium ( $Cr^{6+}$ ) concentrations.



# 1. Introduction

Chromium ( $Cr^{6+}$ ) concentration measurements have started in 2004 and still measurements are going on. As of now, measurements are being made at 47 locations. Of these, 32 of them are observation wells, 5 of them are extraction wells, 5 of them are injection wells, and 5 of them are piezometers.

It appears that the chromium ( $Cr^{6+}$ ) plume till 2009 was only under the effects of some nearby municipal wells (PM-2, PM-3, PM-4, etc.). After that the IM extraction and injection wells were added with intermittent conditions.

Based on the hydraulic head contours analysis, the main flow direction around the chromium ( $Cr^{6+}$ ) plume area as well as the hydraulic gradient in the unconfined aquifer have not changed significantly from 2008 to 2020. But water levels have dropped around 5 to 11 ft.

The purpose of this report is to estimate the potential longitudinal and transverse vertical dissolved chromium ( $Cr^{6+}$ ) mass plume extension under no extraction and injection well conditions using a two-dimensional analytical solute transport mathematical model.

## 2. Chromium ( $Cr^{6+}$ ) Source Area and the Main Flow and Transport Paths in the Unconfined Aquifer

### 2.1 The Estimated Chromium ( $Cr^{6+}$ ) Source Area

Based on the chromium ( $Cr^{6+}$ ) concentration data plots, it appears that the source is likely located inside the polygon formed by R-15, R-62, R-43, R-42, R-50 (Figures 18 and 19), and R-61, which are shown in Figures 1 and 2. The average thickness of the vadose zone around the source area is 1,305 ft.

### 2.2 The Main Flow and Chromium ( $Cr^{6+}$ ) Transport Path Lines and the Average Hydraulic Gradient

In Figure 1, the main flow direction shown by the line CD is based on the head contours corresponding to the May 1, 2020 hydraulic head values. This flow line also represents approximately the main flow direction based on September 6, 2008 hydraulic head data given in the report by Koch and Schmeer (2009) despite the fact that they are 5 to 11 ft higher than the May 1, 2020 head values. Figure 2 shows the hydraulic head contours in 2013 (Los Alamos National Laboratory, 2013, p. 14, Figure 1.0-2). The aforementioned figures clearly indicate that the main flow direction is in the southeast direction. As can be seen from Figure 1, the average hydraulic gradient along the CEDF streamline is  $I = 0.001 \text{ ft/ft}$ . The hydraulic gradient along the same flow direction in Figure 2 is close to this value ( $I = 0.0063 \text{ ft/ft}$ ).

The screen construction information for R-28, R-45, and R-13 are given in Table 1 which shows that the screen intervals are in the shallow part of the unconfined aquifer which is the Puye Formation. The R-42 screen is in the Miocene Formation. Figures 1 and 2 also show that the

R-42, R-28, R-45, and R-13 observation wells are on the main streamline shown by CEDF (Figure 1) and AB (Figure 2).

### **3. Measured Chromium ( $Cr^{6+}$ ) Concentrations Along the Main Flow Direction and Distances of the Observation Wells from R-42**

As can be seen from Figures 1 and 2, the observation wells R-42, R-28, R-45, and R-13 are located on the streamline which represents the main flow direction in the unconfined aquifer beneath Los Alamos National Laboratory. The temporal measured Chromium ( $Cr^{6+}$ ) concentrations at these wells have been analyzed below based on their graphs as presented in a report (Batu, 2024b).

#### **3.1 Measured Chromium ( $Cr^{6+}$ ) Concentrations at R-42 and Their Average Value**

The maximum chromium ( $Cr^{6+}$ ) concentration was measured at R-42 observation well on February 10, 2010 ( $1,240 \mu g/L$ ) in the plume area. This maximum concentration is an exception value and the concentration varies between  $1,070 \mu g/L$  (August 8, 2012) and  $622 \mu g/L$  (October 19, 2023), averaging  $871 \mu g/L$ . After the first quarter of 2012, concentrations started to decline and this trend continued till the last quarter of 2023 after which no measured values exist. One should note that during the 6-yr time period from September 2017 till October 2023 no measured concentration values exist. Potentially, the concentration decline may be attributed to the effects of the extraction and injection wells. Figure 3 presents the concentration values between 10/19/2008 and 7/28/2017 which shows that the  $Cr^{6+}$  concentrations are almost stable around  $900.86 \mu g/L$  average value.

#### **3.2 Measured Chromium ( $Cr^{6+}$ ) Concentrations at R-28 and Their Average Value**

As shown in Figure 1, R-28 observation well is on the CEDF streamline which represents the average flow direction in the aquifer. The chromium ( $Cr^{6+}$ ) concentration variation with time for R-28 (Figure 4) observation well indicates that the concentrations fluctuate around the  $405.50 \mu g/L$  average value from 5/20/2005 to 8/2/2017. The minimum and maximum values are  $310 \mu g/L$  (on 10/26/2006) and  $466 \mu g/L$  (on 8/2/2017), respectively. Therefore, the key characteristic for the R-28 well data is that the chromium ( $Cr^{6+}$ ) concentrations during 12-yr time period remain unchanged. It looks like that the CrEX-3 extraction well which is around 200 ft away from R-28 did not have any significant effect.

#### **3.3 Measured Chromium ( $Cr^{6+}$ ) Concentrations at R-45 S1 and R-45 S2 and Their Average Value**

As shown in Figure 1, the R-45 observation well is very close to the CEDF streamline which represents the average flow direction in the aquifer. As can be seen from Figure 5 (R-45 S1)

and Figure 6 (R-45 S2), although the measured chromium ( $Cr^{6+}$ ) concentration variations have ups and downs, their values are below  $50 \mu g/L$  with the exception of the part after mid 2020 in Figure 6 (R-45 S2). Figure 5 and Figure 6 show the average concentrations between 2/28/2009 and 3/23/2022 at R-45 S1 ( $25.39 \mu g/L$ ) and R-45 S2 ( $29.84 \mu g/L$ ) are close to each other.

### 3.4 Measured Chromium ( $Cr^{6+}$ ) Concentrations at R-13 and Their Average Value

As shown in Figure 1, the R-13 observation well is on the CEDF streamline which represents the average flow direction in the aquifer. As shown in Figure 7, the measured chromium ( $Cr^{6+}$ ) concentrations between 4/18/2022 and 1/22/2024 are stable and their average is  $4.84 \mu g/L$ .

### 3.5 Distances of R-28, R-45, and R-13 from R-42 and Their Average Concentrations

In Figure 1, the distances of R-28, R-45, and R-13 observation wells from R-42 are shown and they are 1,375 ft, 2,625 ft, and 3,940 ft, respectively. Table 2 includes the distances of R-42, R-28, R-45, and R-13 observation wells from R-42 and their average chromium ( $Cr^{6+}$ ) concentrations. Based on the values in Table 2, Figure 8 is generated. As can be seen from Figures 1 and 2, the main flow direction in the unconfined aquifer is predominantly in the southeast direction on which the observation wells R-42, R-28, R-45 S1, R-45 S2, and R-13 are located.

## 4. Measured Horizontal Hydraulic Conductivity Values

### 4.1 Horizontal Hydraulic Conductivity Values Based on the Previous Studies

The measured horizontal hydraulic conductivity ( $K_h$ ) values are included in a draft report (Batu, 2024). From this report, the horizontal hydraulic conductivity ( $K_h$ ) values are given in the following sections.

#### 4.1.1 Calculated Horizontal Hydraulic Conductivity ( $K_h$ ) Values from Figure 13 of Neptune (2023a) Report Based on the Theis Type-Curve (1935) Solution

The horizontal hydraulic conductivity ( $K_h$ ) values are calculated below using different length of screen values of the PM-2 and PM-4. The values are as follows (Batu, 2024a, Section 2.3):

$K_h$  Value from the PM-2 Data for  $b = 850 \text{ ft}$  (Neptune, 2023a, p. 34, Figure 13):

$$K_h = \frac{T}{b} = \frac{3,999 \frac{ft^2}{d}}{850 \text{ ft}} = 4.71 \frac{ft}{d} = 1.66 \times 10^{-3} \frac{cm}{s}$$

$K_h$  Value from the PM-4 Data for  $b = 850 \text{ ft}$  (Neptune, 2023a, p. 34, Figure 13):

$$K_h = \frac{T}{b} = \frac{3,638 \frac{ft^2}{d}}{850 \text{ ft}} = 4.28 \frac{ft}{d} = 1.51 \times 10^{-3} \frac{cm}{s}$$

Their average is

$$K_{h-avg} = 4.49 \frac{ft}{d} = 1.37 \frac{m}{d} = 1.59 \times 10^{-3} \frac{cm}{s}$$

$K_h$  Value the from PM-2 Data for  $b = 1,291 ft$  (Purtymun and Stoker, 988, pp. 13-14, Tables 1 and 2):

$$K_h = \frac{T}{b} = \frac{3,999 \frac{ft^2}{d}}{1,291 ft} = 3.10 \frac{ft}{d} = 1.09 \times 10^{-3} \frac{cm}{s}$$

$K_h$  Value from PM-4 Data for  $b = 1,594 ft$  (Purtymun and Stoker, 988, pp. 13-14, Tables 1 and 2):

$$K_h = \frac{T}{b} = \frac{3,638 \frac{ft^2}{d}}{1,594 ft} = 2.28 \frac{ft}{d} = 8.05 \times 10^{-4} \frac{cm}{s}$$

Their average is

$$K_{h-avg} = 2.69 \frac{ft}{d} = 0.82 \frac{m}{d} = 0.95 \times 10^{-3} \frac{cm}{s}$$

The average of PM-4 values ( $4.49 \frac{ft}{d}$  and  $2.28 \frac{ft}{d}$ ) is

$$K_h = \frac{4.49 \frac{ft}{d} + 2.28 \frac{ft}{d}}{2} = 3.385 \frac{ft}{d} = 1.032 \frac{m}{d}$$

Comparing these values with the median value  $K_h = 12 ft/d$  of Table 1 of Neptune (2023b, p. 12) value, it can be seen that this value is 4 to 6 times higher than the pump test  $K_h$  values given above. In other words, Neptune's value is almost one-half order of magnitude greater.

#### 4.1.2 Horizontal Hydraulic Conductivity Values from the McLin (2007) Report

McLin (2007, p. 488, Table1) presents horizontal hydraulic conductivity ( $K_h$ ) values using the drawdown data at wells G-1A (7.5 ft/d), G-2a (7.9 ft/d), G-3a (6.2 ft/d), G-4a (7.1 ft/d), and G-5a (2.2 ft/d) based on Theis (1935) type-curve analysis. And their arithmetic average is 6.18 ft/d (1.884 m/d) which is around 50% of the median  $K_h = 12 ft/d$  value of Neptune (2023b, p. 12, Table 1). Figure 2 in p. 486 of McLin (2007) paper includes the screen locations of these wells along with aquifer material zones. The Guaje Canyon wells (G-1A, G-2a, etc.) are 5 to 5.7 miles away from PM-2 and PM-4.

## 5. Mathematical Modeling Approach

### 5.1 Introduction

As mentioned in Section 1.0, based on the hydraulic head contours analysis, the main flow direction around the  $Cr^{6+}$  plume area as well as the hydraulic gradient in the unconfined aquifer beneath the LANL site have not changed significantly from 2008 to 2020. As shown in Figures 1

and 2, the main flow direction in the unconfined aquifer is predominantly in the southeast direction on which the observation wells R-42, R-28, R-45 S1, R-45 S2, and R-13 are located.

In this section, the longitudinal and transverse vertical chromium ( $Cr^{6+}$ ) plume extensions will be estimated using a two-dimensional analytical solute transport model.

## 5.2 Estimation Approach with a Two-Dimensional Analytical Solution

The longitudinal and transverse vertical chromium ( $Cr^{6+}$ ) plume extensions have been estimated using a two-dimensional analytical solute transport model called ST2A which is based on the paper (Batu, 1989) entitled “A Generalized Two-Dimensional Analytical Solution for Hydrodynamic Dispersion in Bounded Media With the First-Type Boundary Condition at the Source” published in the journal of *Water Resources Research* in 1989. The same solution is also included in the book (Batu, 2006, pp. 66-93) entitled *Applied Flow and Solute Transport Modeling in Aquifers: Fundamental Principles and Analytical and Numerical Methods*. The model of ST2A has excellent verification status by comparing its results with some numerical codes which are included in Batu (1989) and Batu (2006). Beyond this, it has been proven that some well-known analytical solutions are its special solutions. The ST2A program has more than three decades of usage history in various projects. This model was also accepted by IEPA (Illinois Environmental Protection Agency) in estimating monitoring well spacings according to the IEPA regulations.

The ST2A program has been written in the FORTRAN language in a menu-driven form and it can only be run in XP Windows-based computers. Obviously, it cannot be run in the latest versions computers such as Windows 11.

The geometry of the ST2A model is shown in Batu (1989, p. 1128, Figure 2) and Batu (2006, p. 74, Figure 3-12). Figure 9 shows its adapted form to an unconfined aquifer. As can be seen from Figure 9, the source has a strip form with  $C_M$  source concentration and is infinite along the y-coordinate direction and it can have any location along the  $b$  thickness of the unconfined aquifer. The source width is  $2B$  and its edges distances to the water table and to the impermeable base are  $D_1$  and  $D_2$ , respectively. Since the strip source tends to infinity along the y-coordinate direction the predicted concentrations are conservative. The medium also tends to infinity along the x-coordinate direction. Both the impermeable base as well as the water table are represented as no solute flux boundaries. The flow field in the unconfined aquifer is assumed to be uniform having the pore velocity as  $U = q/n_e$  in which  $q$  is the Darcy velocity and  $n_e$  is the effective porosity.

## 6. Flow Parameters

The flow parameters used in the ST2A model are the horizontal hydraulic conductivity ( $K_h$ ), hydraulic gradient ( $I$ ), and effective porosity ( $n_e$ ).

## 6.1 Horizontal Hydraulic Conductivity

Based on measurements, the average horizontal hydraulic conductivity ( $K_h$ ) values are given in Sections 4.1.1 and 4.1.2. In Section 4.1.1, the value is

$$K_h = 3.385 \frac{ft}{d} = 1.032 \frac{m}{d}$$

In Section 4.1.2, the value is

$$K_h = 6.18 \frac{ft}{d} = 1.884 \frac{m}{d}$$

Both values are used in the ST2A runs.

## 6.2 Hydraulic Gradient

As mentioned in Section 2.2, the average hydraulic gradient along the main flow direction is  $I = 0.001 \text{ ft/ft}$ .

## 6.3 Effective Porosity

The *effective porosity* ( $n_e$ ) is the portion of pore space in a saturated porous material in which water flow occurs. In other words, it is the volume of the interconnected voids of a porous sample. This definition is based on the fact that all the pore space of a porous medium filled with water is not open for water flow. Obviously, the effective porosity  $n_e$  of a porous medium is less than its total porosity  $n$ . The effective porosity in the unconfined aquifer under LANL is estimated at  $n_e = 0.15$ .

# 7. Solute Transport Parameters

## 7.1 Dispersivities

Dispersivity values have been estimated using the diagrams in Gelhar et al. (1992) paper. Assuming that  $x$ ,  $y$ , and  $z$  are principal directions, the dispersivity is simply the ratio of the appropriate component of the dispersion coefficient tensor (e.g., Bear, 1972, pp. 605-615; Bear, 1979, pp. 239-248; Batu, 2006, pp. 17-20) divided by the magnitude of pore velocity (or seepage velocity),  $U$ . To distinguish the field-scale dispersivities from laboratory values, Gelhar et al. (1992) designated the field-scale values by the upper case of letter  $A$  (Gelhar and Axness, 1983) used

$$D_{11} = A_L U \quad (1)$$

$$D_{22} = A_T U \quad (2)$$

$$D_{33} = A_V U \quad (3)$$

in which  $D_{11}$  is the longitudinal dispersion coefficient,  $D_{22}$  is the transverse horizontal dispersion coefficient, and  $D_{33}$  is the transverse vertical dispersion coefficient. And  $A_L$  is the field-scale longitudinal macrodispersivity,  $A_T$  is the field-scale transverse horizontal macrodispersivity, and  $A_V$  is the field-scale transverse vertical macrodispersivity. With

$$A_L \equiv \alpha_L \quad A_T \equiv \alpha_{TH} \quad A_V \equiv \alpha_{TV} \quad (4)$$

Therefore, in Cartesian coordinates, Eqs. (1), (2), and (3) become

$$D_{xx} = \alpha_L U \quad (5)$$

$$D_{yy} = \alpha_{TH} U \quad (6)$$

$$D_{zz} = \alpha_{TV} U \quad (7)$$

Further details can be found in Gelhar and Axness (1983) and Gelhar et al. (1992).

Values of dispersivities have been estimated from the diagrams in Figures 10 and 11 of Gelhar et al. (1992).

## 7.2 Molecular Diffusion Coefficient

Molecular diffusion coefficient values of coarse-grained unconsolidated materials can be somewhat higher than  $1.0 \times 10^{-10} \text{ m}^2/\text{s}$  but less than the coefficients for the chemical species in water, i.e.,  $2.0 \times 10^{-9} \text{ m}^2/\text{s}$  ( $1.86 \times 10^{-3} \text{ ft}^2/\text{d}$ ) (Freeze and Cherry, 1979, p. 303). Therefore,  $D^* = 1.86 \times 10^{-3} \text{ ft}^2/\text{d}$  will be used in the ST2A runs.

## 7.3 Retardation Factor of Chromium ( $\text{Cr}^{6+}$ )

According to the literature, the retardation factor ( $R_d$ ) of varied from 1.1 to 2.4 and is dependent on chemical conditions. Therefore, in the ST2A runs  $R_d = 1.75$  is used the average of these values.

## 7.4 Degradation Rate of Chromium ( $\text{Cr}^{6+}$ )

Based on the measured dissolved  $\text{Cr}^{6+}$  concentrations, its degradation rate is estimated at  $\nu = 0.9 \times 10^{-5} \text{ d}^{-1}$  (Batu, August 16, 2024c) using the method in Batu (2010).

## 8. Longitudinal and Transverse Vertical Chromium ( $\text{Cr}^{6+}$ ) Plume Extensions Estimation

Using the mathematical modeling approach along with flow and solute transport parameters, computer runs with ST2A were conducted in the longitudinal as well as transverse directions at some fixed times. Here, the results of these runs will be presented.

In Figure 9, the following values are used:  $D_1 = 0$ ,  $D_2 = 4,990 \text{ ft}$ , and  $2B = 10 \text{ ft}$ . Here,  $D_1 = 0$  means that the sources is adjacent to the water table. And  $D_1 + 2B + D_2 = 0 + 10 \text{ ft} + 4,990 \text{ ft} = 5,000 \text{ ft} = b$  is the thickness of the unconfined aquifer. The source has  $2B = 10 \text{ ft}$  height and has a strip shape that tends to infinity in both  $-y$  and  $+y$  coordinate directions which is conservative because it predicts maximum concentrations in the solute transport domain.

## **8.1 Longitudinal Chromium ( $Cr^{6+}$ ) Concentration Variation Along the Streamline Formed by the Observation Wells R-42, R-28, R-45 S1, R-45 S2, and R-13**

### **8.1.1 $Cr^{6+}$ Concentration Variations for $\alpha_L = 50 \text{ m}$ (164.04 ft) After $t = 40 \text{ yr}$ and $64 \text{ yr}$**

In Figure 12, the longitudinal  $Cr^{6+}$  concentration variation is presented after 40 yr elapsed time for three different horizontal hydraulic conductivity ( $K_h$ ) values 3.385 ft/d, 6.18 ft/d, and 30 ft/d. The origin of the first two values is described in Section 6.1. The third value, 30 ft/d, is also included as a higher value than the previous ones to demonstrate the effects of  $K_h$ . Figure 12 also shows the measured average  $Cr^{6+}$  concentrations. As can be seen from Figure 12, R-42 is represented as the source, the predicted concentration at R-28 is significantly off than the predicted ones, but the average concentrations at R-45 S1, R-45 S2, and R-13 are close to the predicted concentrations especially to the ones corresponding to  $K_h = 30 \text{ ft/d}$ .

Likewise, Figure 13 shows the longitudinal  $Cr^{6+}$  concentration variation is presented after 64 yr elapsed time for three different horizontal hydraulic conductivity ( $K_h$ ) values 3.385 ft/d, 6.18 ft/d, and 30 ft/d. The origin of the first two values is described in Section 6.1. The third value, 30 ft/d, is also included as a higher value than the previous ones to demonstrate the effects of  $K_h$ . Figure 13 also shows the measured average chromium ( $Cr^{6+}$ ) concentrations. As can be seen from Figure 13, R-42 is represented as the source, the predicted concentration at R-28 is significantly off than the predicted ones, but the average concentrations at R-45 S1, R-45 S2, and R-13 are close to the predicted concentrations especially to the ones corresponding to  $K_h = 30 \text{ ft/d}$ .

### **8.1.2 $Cr^{6+}$ Concentration Variations for $\alpha_L = 100 \text{ m}$ (328.08 ft) After $t = 40 \text{ yr}$ and $64 \text{ yr}$**

In Figure 14, the longitudinal chromium ( $Cr^{6+}$ ) concentration variation is presented after 40 yr elapsed time for three different horizontal hydraulic conductivity ( $K_h$ ) values 3.385 ft/d, 6.18 ft/d, and 30 ft/d. The origin of the first two values is described in Section 6.1. The third value, 30 ft/d, is also included as a higher value than the previous ones to demonstrate the effects of  $K_h$ . Figure 14 also shows the measured average chromium ( $Cr^{6+}$ ) concentrations. As can be seen from Figure 14, R-42 is represented as the source, the predicted concentration at R-28 is significantly off than the predicted ones, but the average concentrations at R-45 S1, R-45 S2, and R-13 are close to the predicted concentrations especially to the ones corresponding to  $K_h = 30 \text{ ft/d}$ . Comparison with Figure 12, indicates that the  $\alpha_L = 100 \text{ m}$  (328.08 ft) value makes slight difference with Figure 12 corresponding to  $\alpha_L = 50 \text{ m}$  (164.04 ft).



In Figure 15, the longitudinal chromium ( $Cr^{6+}$ ) concentration variation is presented after 64 yr elapsed time for three different horizontal hydraulic conductivity ( $K_h$ ) values 3.385 ft/d, 6.18 ft/d, and 30 ft/d. The origin of the first two values is described in Section 6.1. The third value, 30 ft/d, is also included as a higher value than the previous ones to demonstrate the effects of  $K_h$ . Figure 14 also shows the measured average  $Cr^{6+}$  concentrations. As can be seen from Figure 15, R-42 is represented as the source, the predicted concentration at R-28 is significantly off than the predicted ones, but the average concentrations at R-45 S1, R-45 S2, and R-13 are close to the predicted concentrations especially to the ones corresponding to  $K_h = 30$  ft/d. Comparison with Figure 13, indicates that the  $\alpha_L = 100$  m (328.08 ft) value makes slight difference with Figure 13 corresponding to  $\alpha_L = 50$  m (164.04 ft).

Figure 16 compares the chromium ( $Cr^{6+}$ ) concentration profiles for  $\alpha_L = 100$  m (328.08 ft) with  $K_h = 30$  ft/d for  $\nu = 0$  and  $= 0.9 \times 10^{-5} d^{-1}$ . As can be seen from Figure 16, the difference is around 10% to 15%.

## 8.2 Transverse Chromium ( $Cr^{6+}$ ) Concentration Variation Perpendicular to the Streamline Formed By the Observation Wells R-42, R-28, R-45 S1, R-45 S2, and R-13

In Figure 17, the transverse vertical  $Cr^{6+}$  concentration variation with the  $z$  coordinate is presented after 40 yr elapsed time for  $K_h = 30$  ft/d at  $x = 2,500$  ft for  $\alpha_L = 50$  m (164.04 ft) and  $\alpha_{TV}/\alpha_L = 0.01$  and 0.02 after 40 yr elapsed time. Figure 17 shows that the plume extent in the vertical direction increases as the vertical transverse dispersivity  $\alpha_{TV}$  increases. Also, it shows that as  $\alpha_{TV}$  increases, the concentration in the vertical direction decreases due to dilution effects.

In Figure 18, the transverse vertical chromium ( $Cr^{6+}$ ) concentration variation is presented with the  $z$  coordinate after 64 yr elapsed time for  $K_h = 30$  ft/d at  $x = 2,500$  ft for  $\alpha_L = 50$  m (164.04 ft) and  $\alpha_{TV}/\alpha_L = 0.01$  and 0.02 after 64 yr elapsed time. Likewise, Figure 18 has the same characteristics as Figure 17 with the exception that the plume advances more in the vertical direction because the elapsed time is greater.

In Figure 19, the transverse vertical  $Cr^{6+}$  concentration variation is presented with the  $z$  coordinate for  $K_h = 30$  ft/d at  $x = 2,500$  ft for  $\alpha_L = 100$  m (328.08 ft) and  $\alpha_{TV}/\alpha_L = 0.01$  and 0.02 after 40 yr elapsed time which has similar characteristics with the previous ones.

In Figure 20, the transverse vertical  $Cr^{6+}$  concentration variation is presented with the  $z$  coordinate for  $K_h = 30$  ft/d at  $x = 2,500$  ft for  $\alpha_L = 100$  m (328.08 ft) and  $\alpha_{TV}/\alpha_L = 0.01$  and 0.02 after 64 yr elapsed time which has similar characteristics with the previous ones.

In Figure 21, the transverse vertical  $Cr^{6+}$  concentration variation is presented with the  $z$  coordinate for  $K_h = 30$  ft/d at  $x = 6,562$  ft (2,000 m) for  $\alpha_L = 200$  m (656.17 ft) and  $\alpha_{TV}/\alpha_L = 0.01$  and 0.02 after 40 yr elapsed time has similar characteristics with the previous ones.

## 9. Conclusions

The conclusions drawn from this study can be summarized as follows:

1. The main flow direction in the unconfined aquifer is predominantly in the southeast direction on which the observation wells R-42, R-28, R-45 S1, R-45 S2, and R-13 are located (Figures 1 and 2).
2. The maximum chromium ( $Cr^{6+}$ ) concentration was measured at R-42 observation well on February 10, 2010 ( $1,240 \mu g/L$ ) in the plume area. The concentration values between 10/19/2008 and 7/28/2017 show that the chromium ( $Cr^{6+}$ ) concentrations are almost stable around  $900.86 \mu g/L$  average value (Figure 3).
3. The chromium ( $Cr^{6+}$ ) concentration variation with time for R-28 observation well indicates that the concentrations fluctuate around the  $405.50 \mu g/L$  average value from 5/20/2005 to 8/2/2017 (Figure 4).
4. Although the measured chromium ( $Cr^{6+}$ ) concentration variations at R-45 S1 and R-45 S2 have ups and downs, their values are below  $50 \mu g/L$  (Figures 5 and 6) with the exception of the part after mid 2020 in Figure 6 (R-45 S2). Figure 5 and Figure 6 show the average concentrations between 2/28/2009 and 3/23/2022 at R-45 S1 ( $25.39 \mu g/L$ ) and R-45 S2 ( $29.84 \mu g/L$ ) are close to each other.
5. The measured chromium ( $Cr^{6+}$ ) concentrations at R-13 between 4/18/2022 and 1/22/2024 are stable and their average is  $4.84 \mu g/L$  (Figure 7).
6. The average concentrations at R-42, R-28, R-45 S1, R-45 S2, and R-13 show a regular and continuous decline with distance along the main flow direction shown in Figures 1 and 2 (Table 2 and Figure 8).
7. The predicted concentrations at R-45 and R-13 compare well with their measured average values for the  $K_h = 30 ft/d$  horizontal hydraulic conductivity value with all potential  $\alpha_L$  longitudinal dispersivity and  $\alpha_{TV}$  transverse vertical dispersivity values (Figures 12, 13, 14, and 15).
8. The estimated site-specific degradation rate of chromium ( $= 0.9 \times 10^{-5} d^{-1}$ ) has around 10% to 15% effect on the concentrations (Figure 16).
9. Within 40 yr time period, the plume has been migrated longitudinally around 4,000 ft from R-42 (Figures 12 and 14). And within 64 yr time period, the plume has been migrated longitudinally more than 4,000 ft (Figures 13 and 15).
10. Within 40 yr time period, the plume has been migrated from the water table down to 700 ft distance depending on the  $\alpha_H$  and  $\alpha_{TV}$  values (Figures 17, 19, and 21).
11. Within 64 yr time period, the plume has been migrated from the water table down to 1,300 ft distance depending on the  $\alpha_H$  and  $\alpha_{TV}$  values (Figures 17, 19, and 21).

## References

- Batu, V., "Hydraulic Conductivity Data Evaluation of the Neptune's Model for the LANL Site, Los Alamos, New Mexico, April 3, 2024a.
- Batu, V., "Plots of Chromium ( $Cr^{6+}$ ) Concentrations Vs. Date Between 2004 and 2024 and Their, Interpretations, Los Alamos, New Mexico," August 17, 2024b.
- Batu, V., "The Conceptual Model for the Water-Bearing Formations Beneath the LANL Site and Determination Methods of the Breakthrough Curves at the Bottom of the Vadose Zone and Degradation Rates of Chromium ( $Cr^{6+}$ ), Los Alamos, New Mexico, August 16, 2024c.
- Batu, V., "Estimation of Degradation Rates by Satisfying Mass Balance at the Inlet," *Ground Water*, Vol. 48, pp. 560-568, July-August, 2010.
- Batu, V., *Applied Flow and Solute Transport Modeling in Aquifers: Fundamental Principles and Analytical and Numerical Models*, CRC Press, Taylor & Francis Group., Boca Raton, Florida, 667 pp., 2006.
- Batu, V., "A Generalized Two-Dimensional Analytical Solution for Hydrodynamic Dispersion in Bounded Media With the First-Type Boundary Condition at the Source," *Water Resources Research*, Vol. 25, No. 6, pp. 1125-1132, 1989.
- Bear, J., *Hydraulics of Groundwater*, McGraw-Hill Book Company, New York, 569 pp., 1979.
- Bear, J., *Dynamics of Fluids in Porous Media*, (Published first in 1972 by American Elsevier Publishing Company, Inc.), Dover Publications, Inc., 764 pp., New York, 1988.
- Freeze, R.A., and J.A. Cherry, *Groundwater*, Prentice-Hall, Inc., Englewood Cliffs, New Jersey, pp. 604, 1979.
- Gelhar, L. W., and C. L. Axness, "Three-Dimensional Stochastic Analysis of Macrodispersion in Aquifers," *Water Resources Research*, Vol. 19, No. 1, pp. 161-180, 1983.
- Gelhar, L.W., C. Welty, and K.R. Rehfeldt, "A Critical Review of Data on Field-Scale Dispersion in Aquifers," *Water Resources Research*, Vol. 28, No.7, pp. 1955-1974, 1992.
- Koch, R.J., and S. Schmeer, "Groundwater Level Status Report for 2008, Los Alamos National Laboratory," LA-14397-PR, Progress Report, 260 pp., March, 2009.
- Los Alamos National Laboratory, "Interim Measures Work Plan for the Evaluation of Chromium Mass Removal," ERID-241096, LA-UR-13-22534, EP2013-0073, 20 pp., April, 2013.
- McLin, S.G., "Hydrogeologic Characterization of Groundwater System Using Sequential Aquifer Tests and Flowmeter Logs," *New Mexico Geological Society Guidebook*, 58<sup>th</sup> Field Conference, Jemez Mountains II, pp. 485-491, 2007.
- Neptune and Company, Inc., "*Hydraulic Analysis of the Pajarito Plateau*", EMID-702780, prepared by Neptune and Company, Inc. for the U.S. Department of Energy Environmental

Management Los Alamos Field Office, Neptune and Company Inc., Los Alamos NM, 64 pp., June 16, 2023a.

Neptune and Company, Inc., "*Chromium Model: Calibrated with Uncertainty through 2022*", prepared by Neptune and Company, Inc. for the U.S. Department of Energy Environmental Management Los Alamos Field Office, Neptune and Company Inc., Los Alamos NM, 69 pp., June 16, 2023b.

Purtymun, W.D., and A.K. Stoker, "Water Supply at Los Alamos: Current Status of Wells and Future Supply Wells," Los Alamos National Laboratory, LA-11332-MS, 16 pp., August, 1988.

## Figures



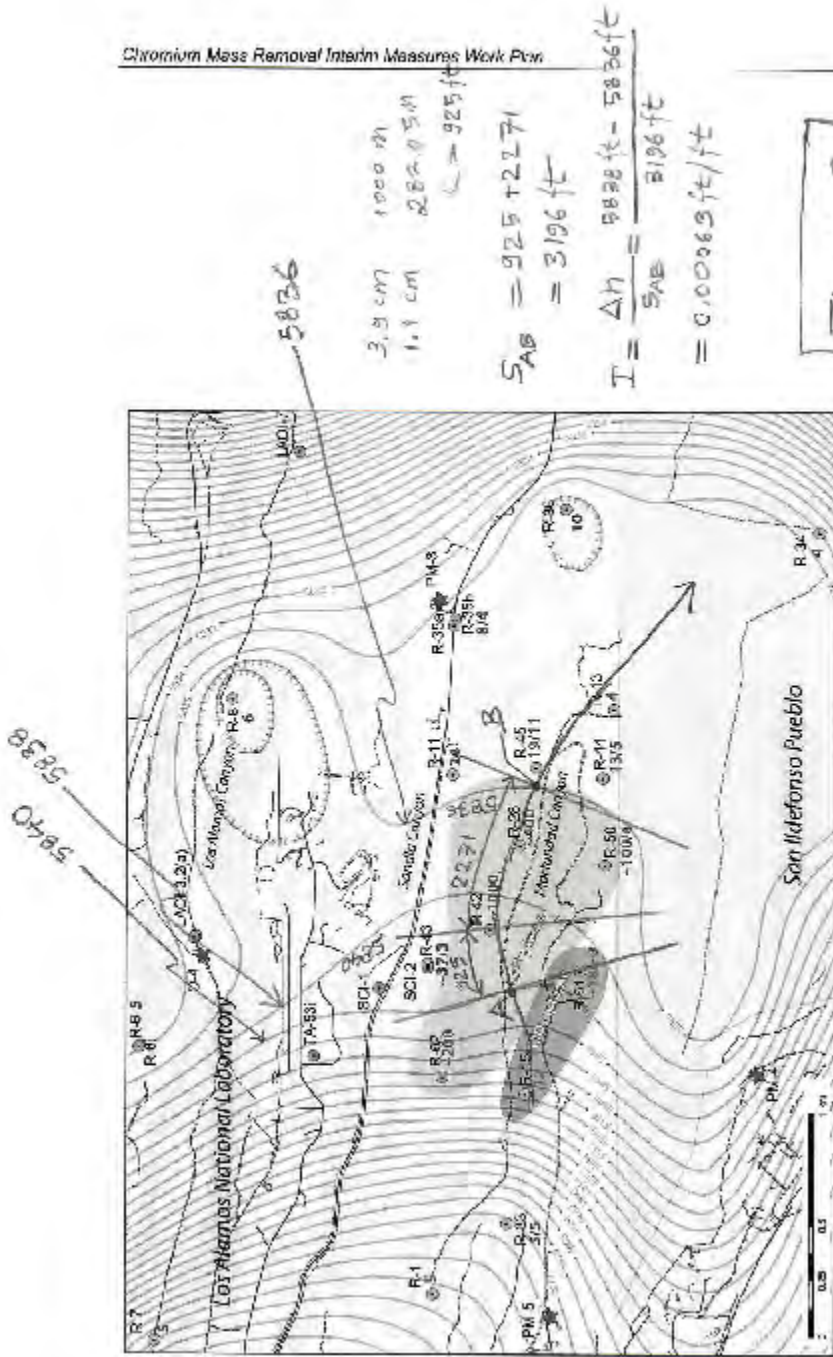


Figure 2

Figure 1.0-2 Plan view of the Cr(VI) plume (>50 ppb contour shown in pink) in the regional aquifer with nearby regional monitoring wells (green circles), perched-intermediate monitoring wells (blue circles), and water-supply wells (red stars). Contour lines (2-ft intervals) represent the regional water table elevations. The approximate area of perchlorate contamination greater than approximately 2 ppb in the regional aquifer is shown in grey. Numbers beneath the well names refer to the approximate chromium concentrations for upper and lower screens.

Ref: "Interim Measure Work Plan for the Evaluation of Chromium Mass Removal," Los Alamos National Laboratory, ERID-241096, 20 pp., Figure 1.0-2, April 2013.

Figure 2. Head contours in 2013 and main flow direction.

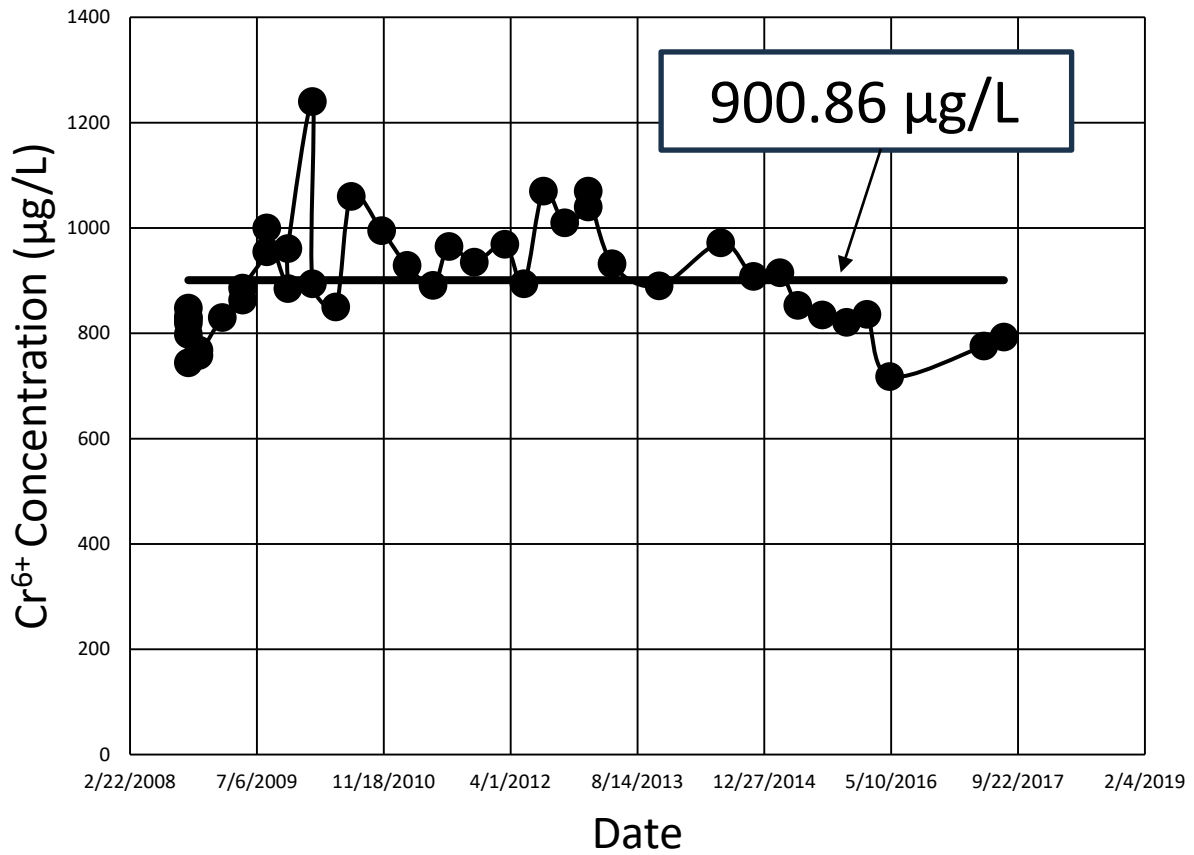


Figure 3. Measured Chromium ( $Cr^{6+}$ ) concentrations at R-42 between 10/9/2008 and 7/28/2017 and their average value.



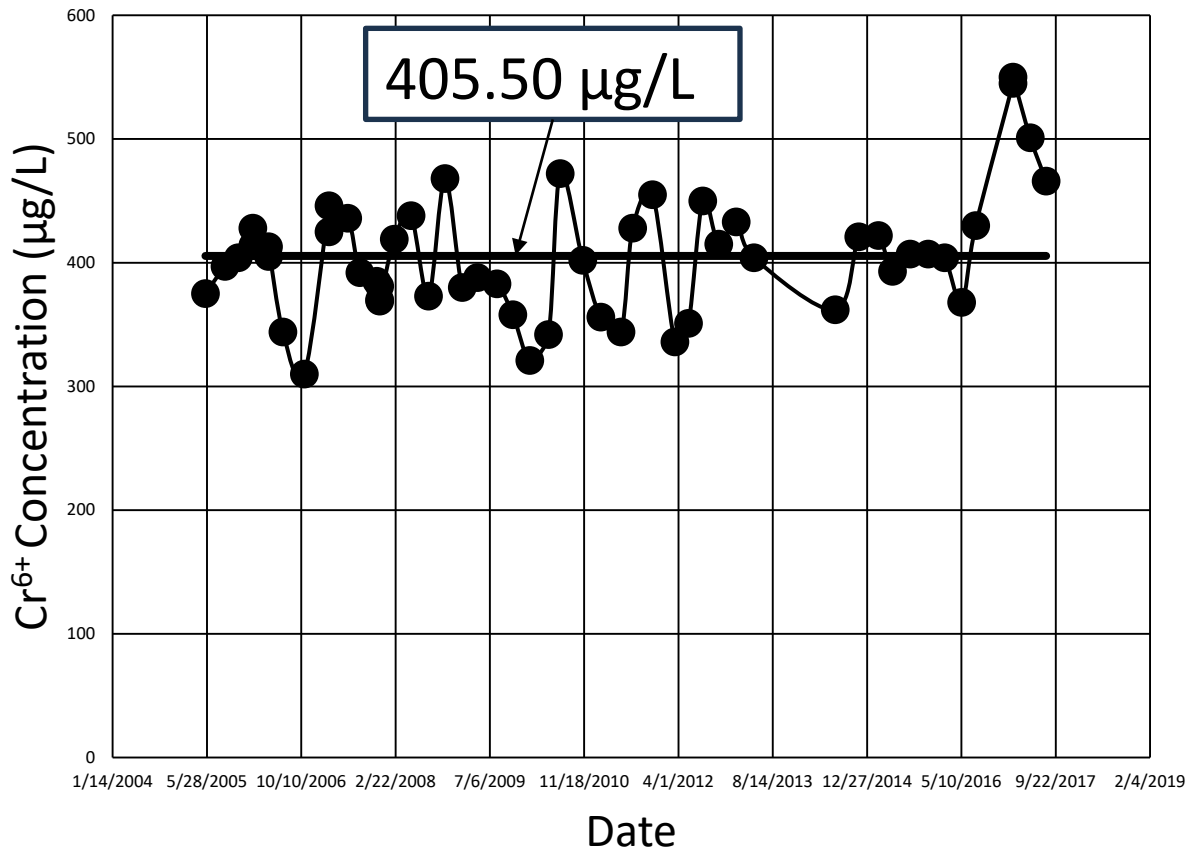


Figure 4. Measured Chromium ( $Cr^{6+}$ ) concentrations at R-28 between 5/20/2005 and 8/2/2017 and their average value.

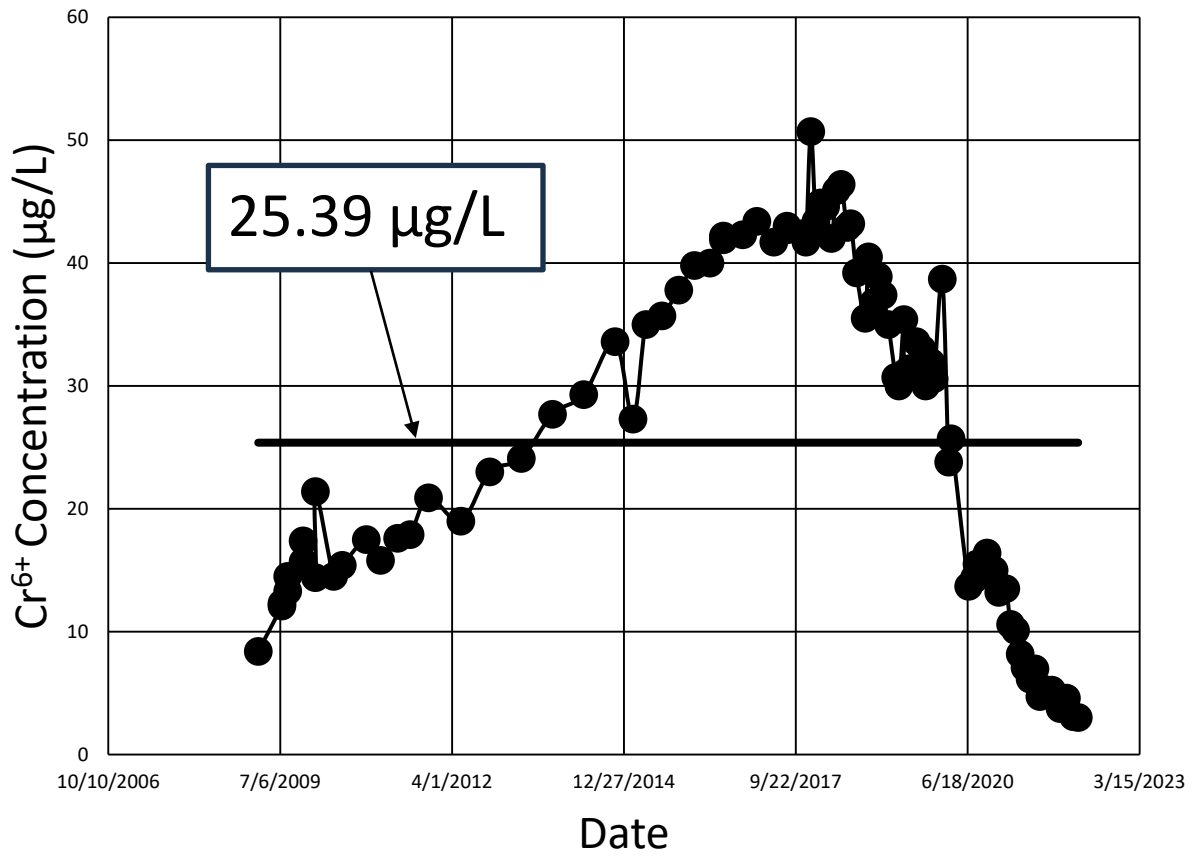


Figure 5. Measured Chromium ( $Cr^{6+}$ ) concentrations at R-45 S1 between 2/28/2009 and 3/23/2022 and their average value.

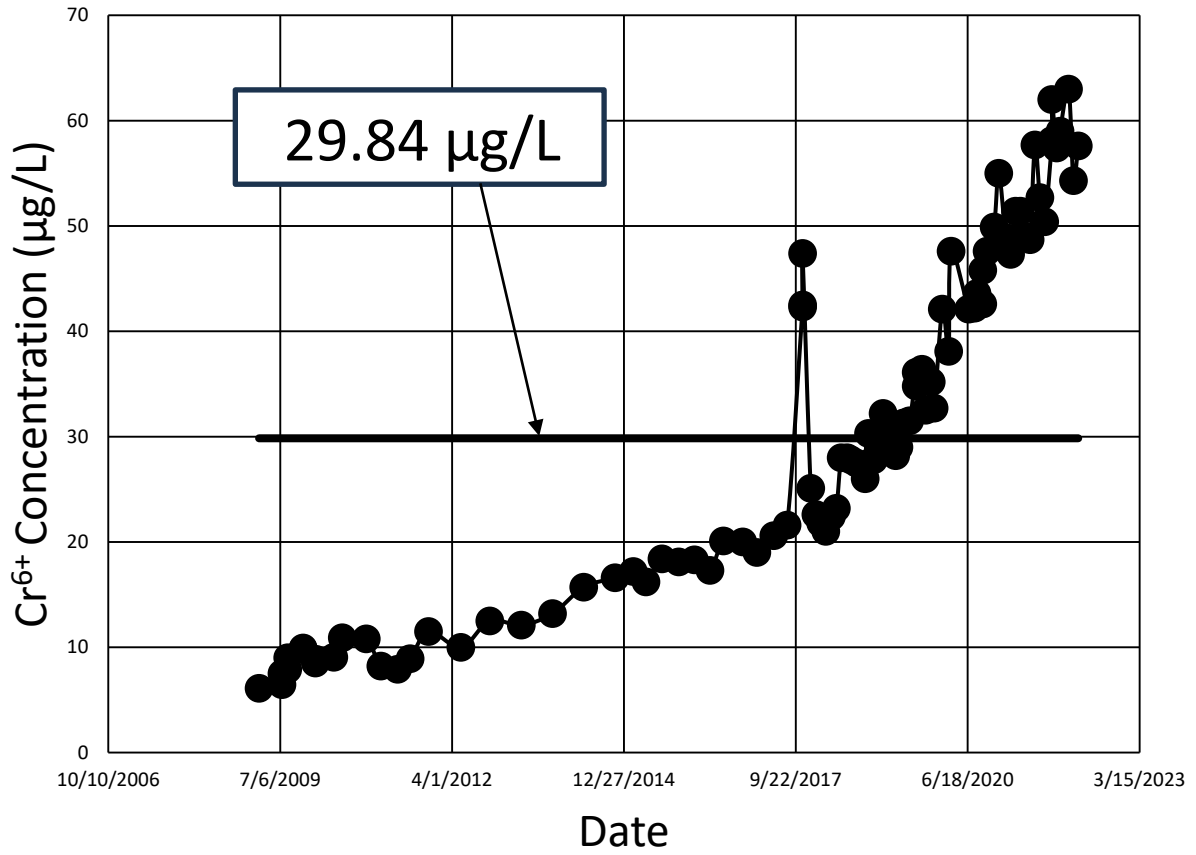


Figure 6. Measured Chromium ( $Cr^{6+}$ ) concentrations at R-45 S2 between 3/5/2009 and 3/23/2022 and their average value.

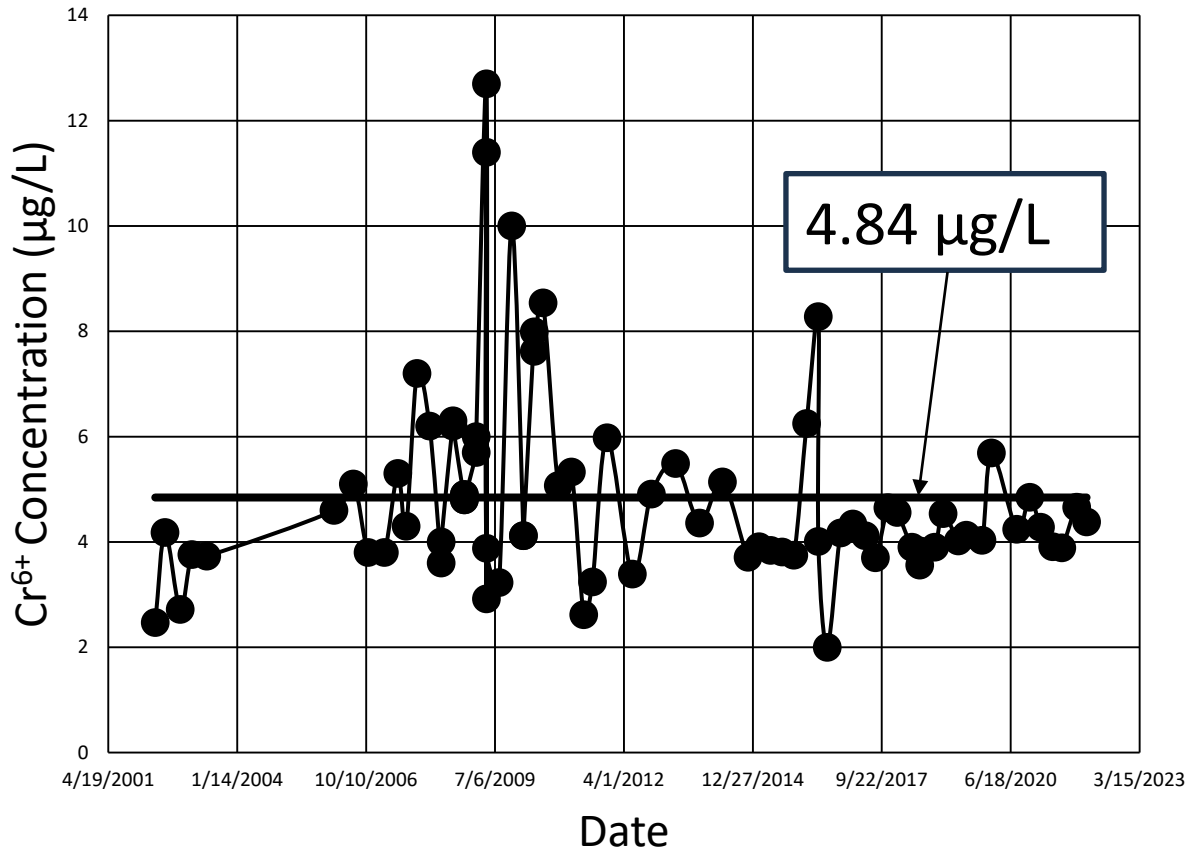


Figure 7. Measured Chromium ( $Cr^{6+}$ ) concentrations at R-13 between 4/18/2002 and 1/22/2024 and their average value.

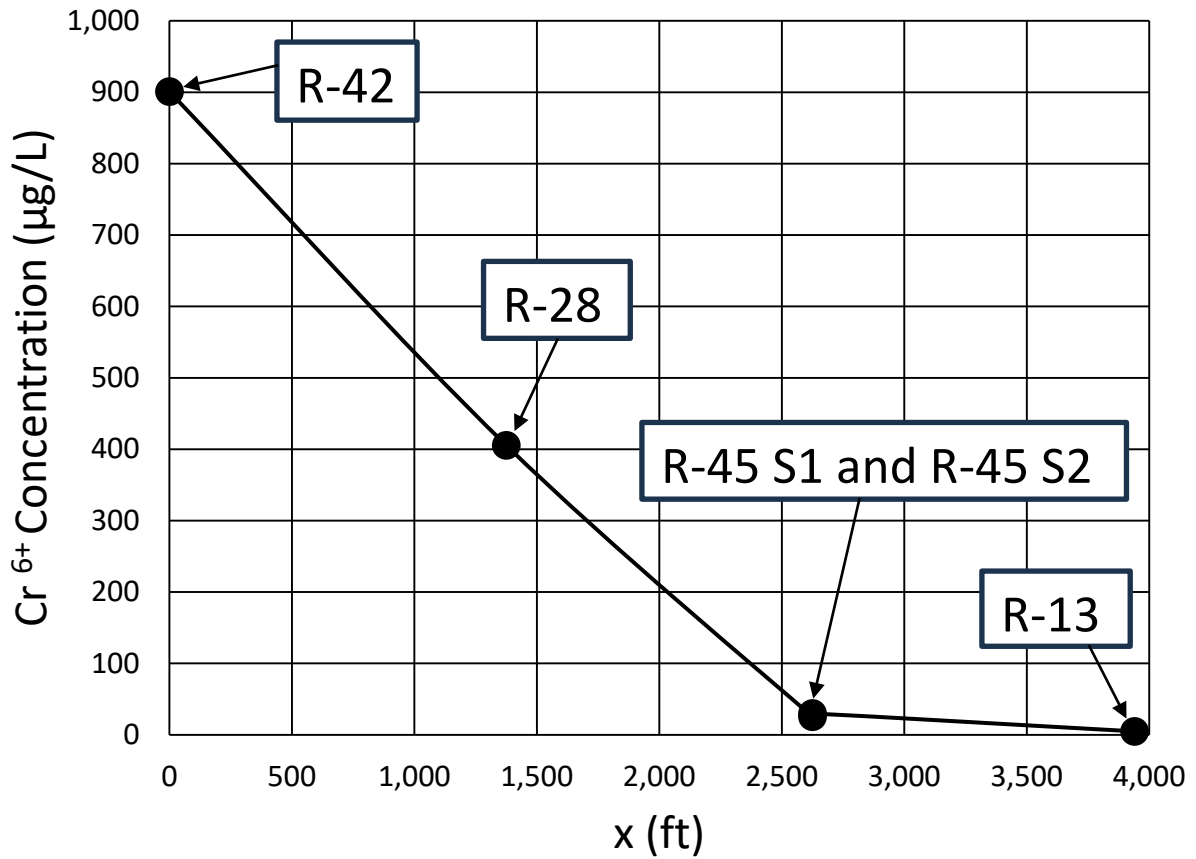


Figure 8. Average  $Cr^{6+}$  concentrations at R-42, R-28, R-45 S1, R-45 S2, and R-13 which are on the same streamline (Or flowline) in the unconfined aquifer beneath the LANL site.

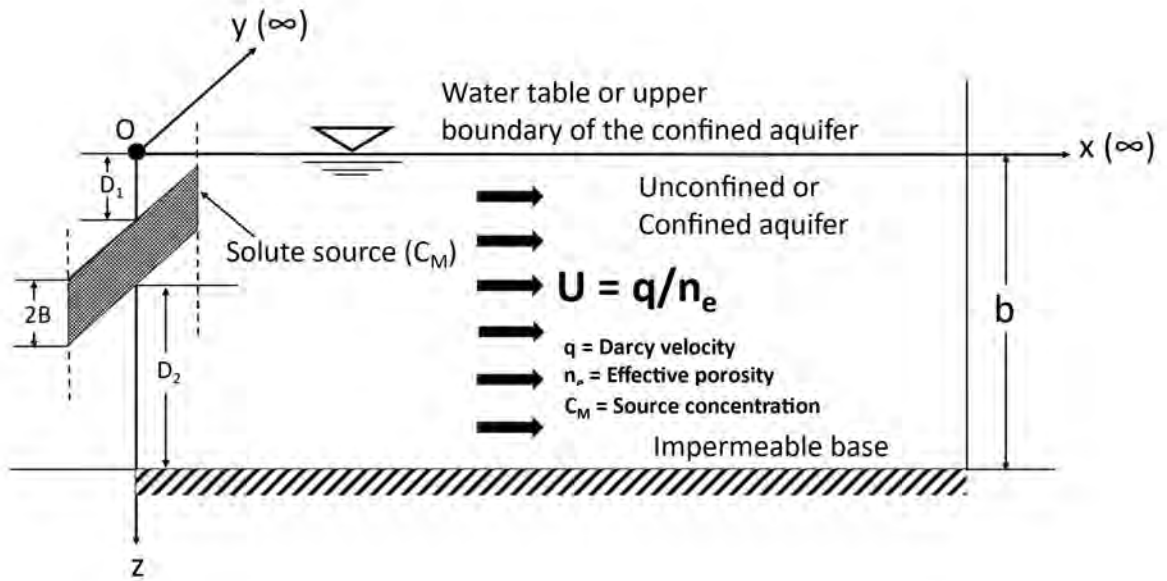


Figure 9. The geometry of the two-dimensional analytical solute transport model (ST2A) adapted to an unconfined aquifer.

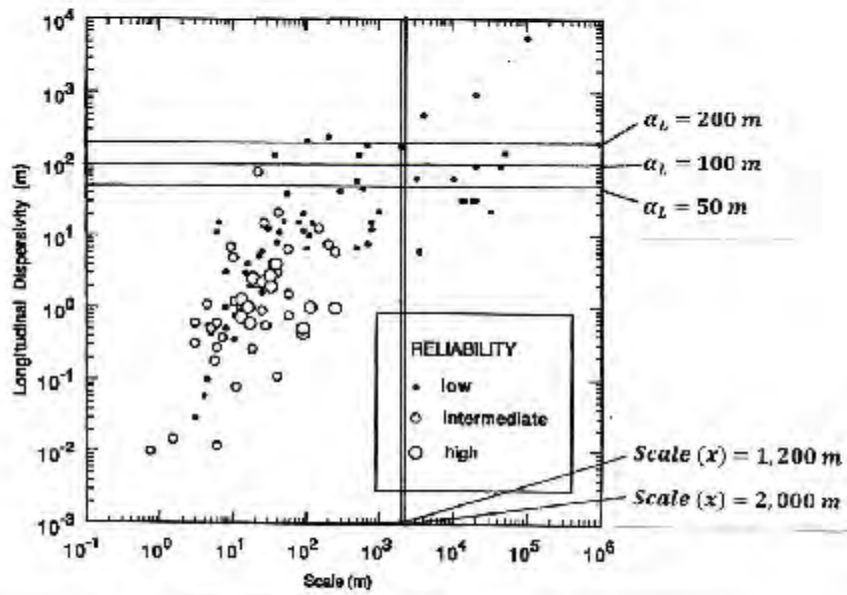


Figure 10. Longitudinal dispersivity ( $\alpha_L$ ) versus scale ( $x$ ) with data classified by reliability (Gelhar et al., 1992, p. 1968, Figure 2).

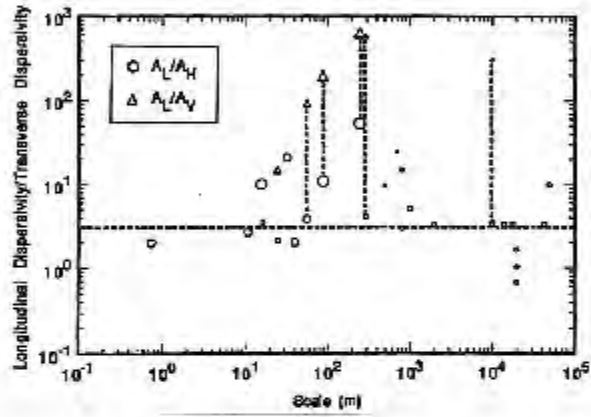


Figure 11 Ratio of longitudinal to horizontal ( $\alpha_L/\alpha_{TH}$ ) and vertical transverse dispersivities ( $\alpha_L/\alpha_{TV}$ ) versus scale ( $x$ ) with data classified by reliability (Gelhar et al., 1992, p. 1971, Figure 6).



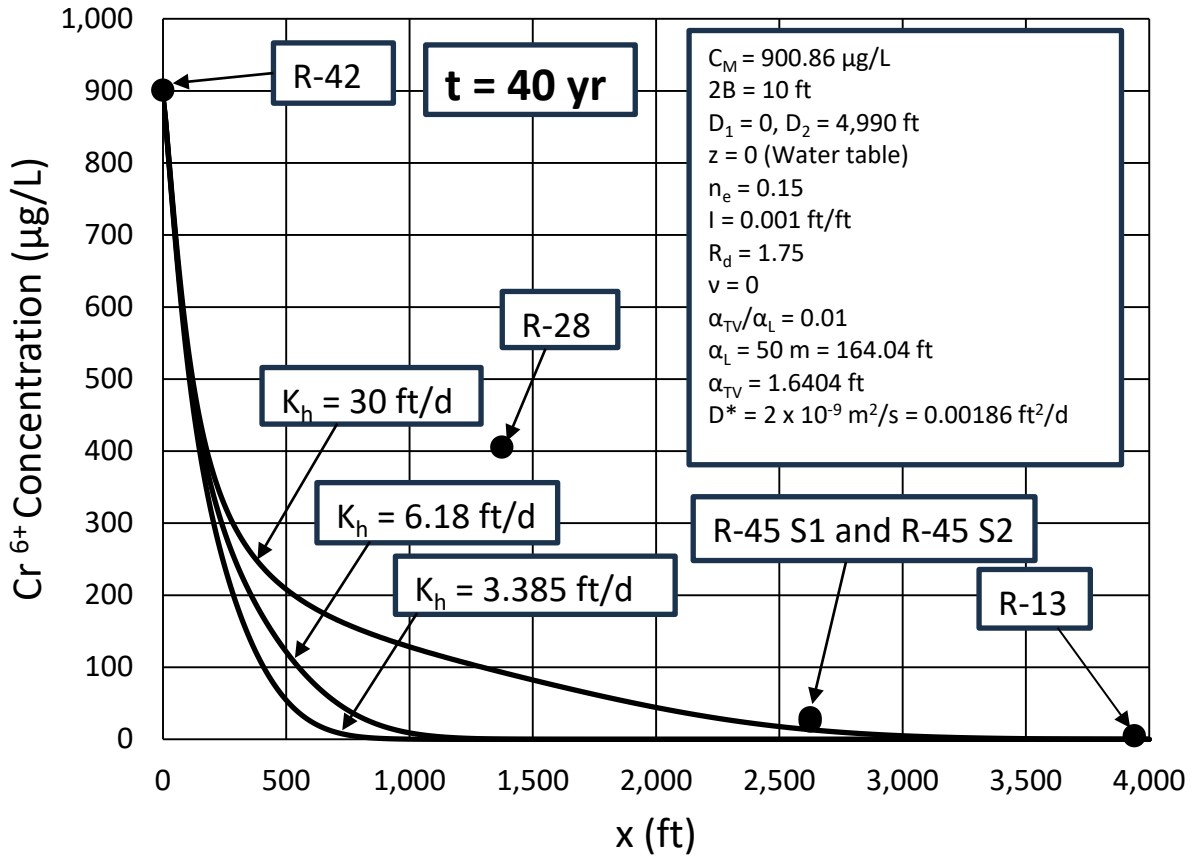


Figure 12. Longitudinal  $Cr^{6+}$  concentration variation along the streamline formed by the observation wells R-42, R-28, R-45 S1, R-45 S2, and R-13 for different  $K_h$  values with  $\alpha_L = 50\text{ m}$  (164.04 ft) and  $\alpha_{TV}/\alpha_L = 0.01$  after 40 yr elapsed time.

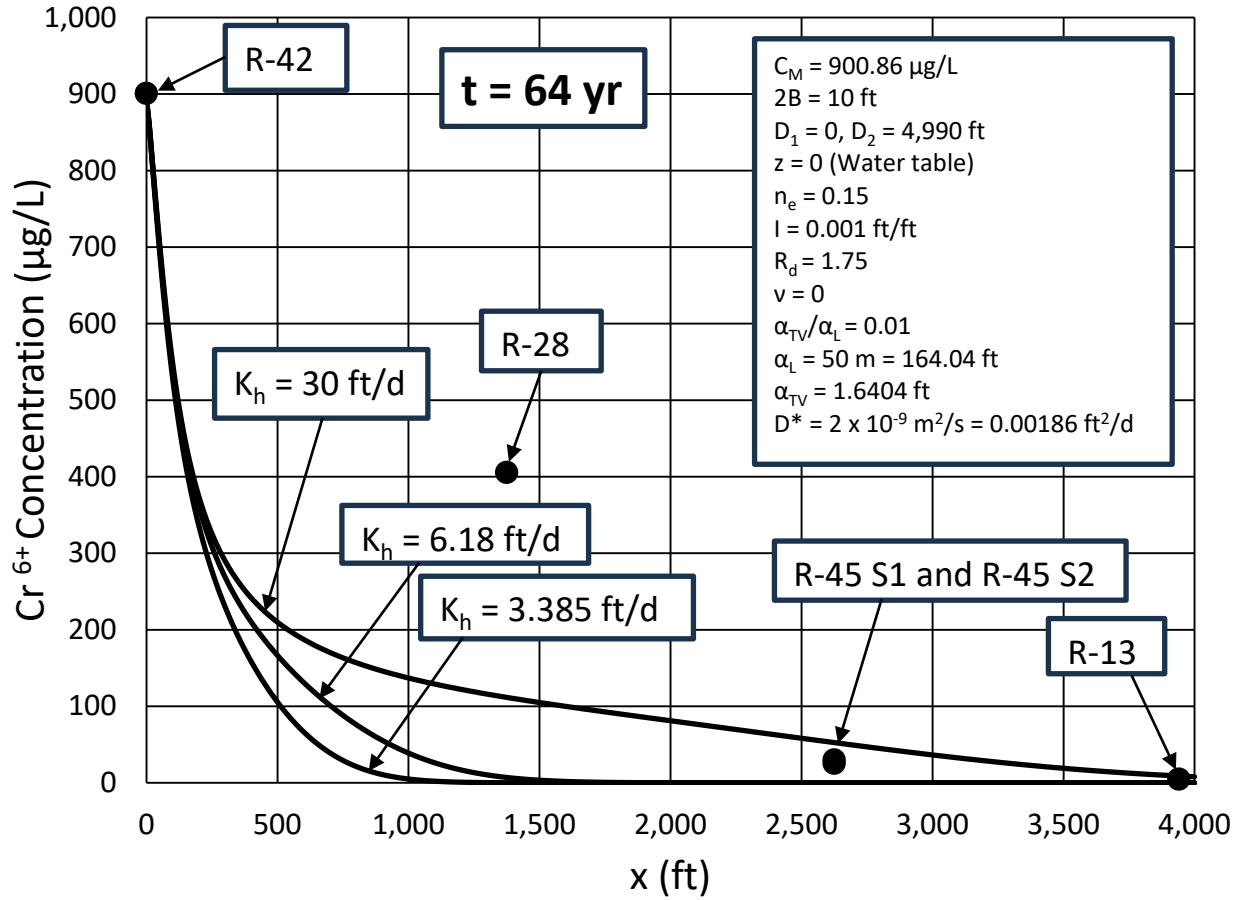


Figure 13. Longitudinal  $Cr^{6+}$  concentration variation along the streamline formed by the observation wells R-42, R-28, R-45 S1, R-45 S2, and R-13 for different  $K_h$  values with  $\alpha_L = 50 \text{ m}$  (164.04 ft) and  $\alpha_{TV}/\alpha_L = 0.01$  after 64 yr elapsed time.

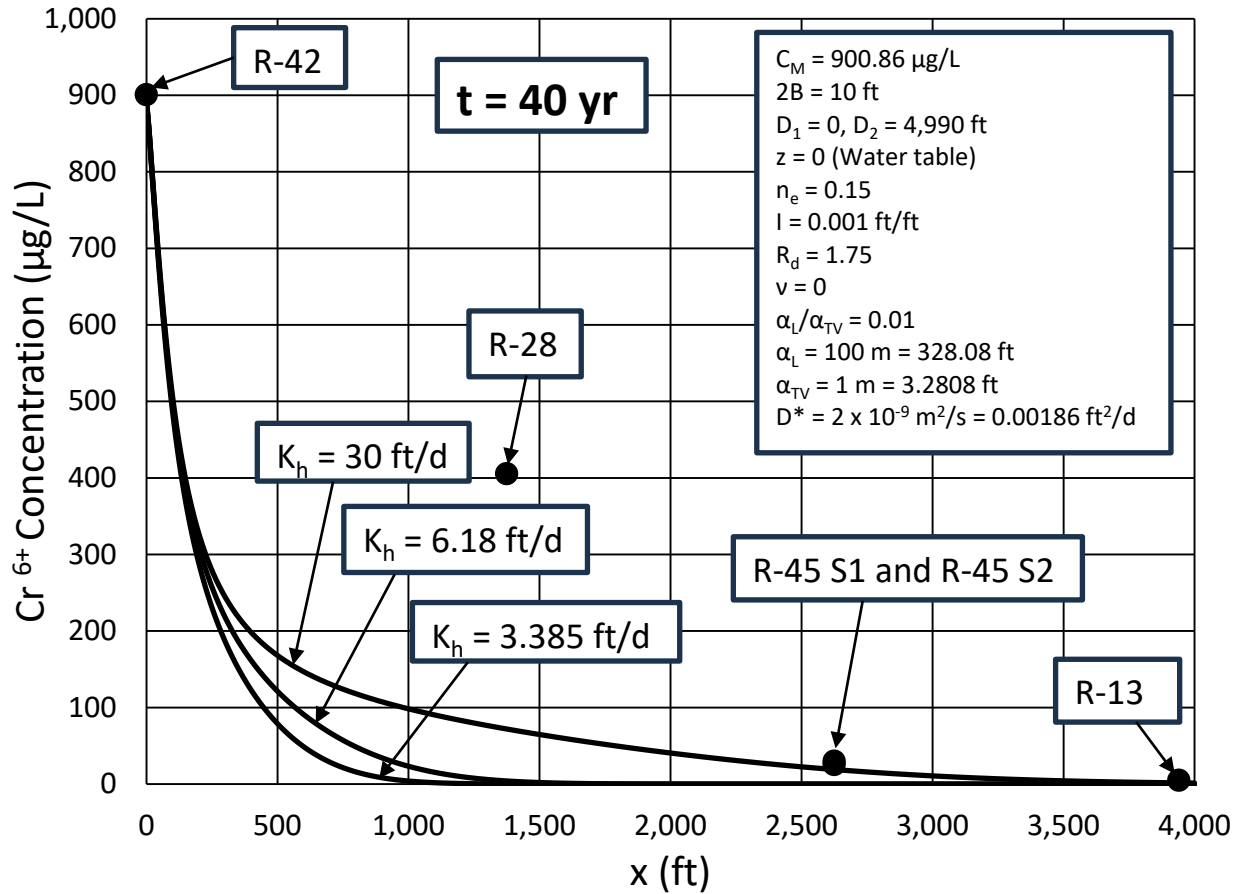


Figure 14. Longitudinal  $Cr^{6+}$  concentration variation along the streamline formed by the observation wells R-42, R-28, R-45 S1, R-45 S2, and R-13 for different  $K_h$  values with  $\alpha_L = 100 \text{ m}$  (328.08 ft) and  $\alpha_{TV}/\alpha_L = 0.01$  after 40 yr elapsed time.

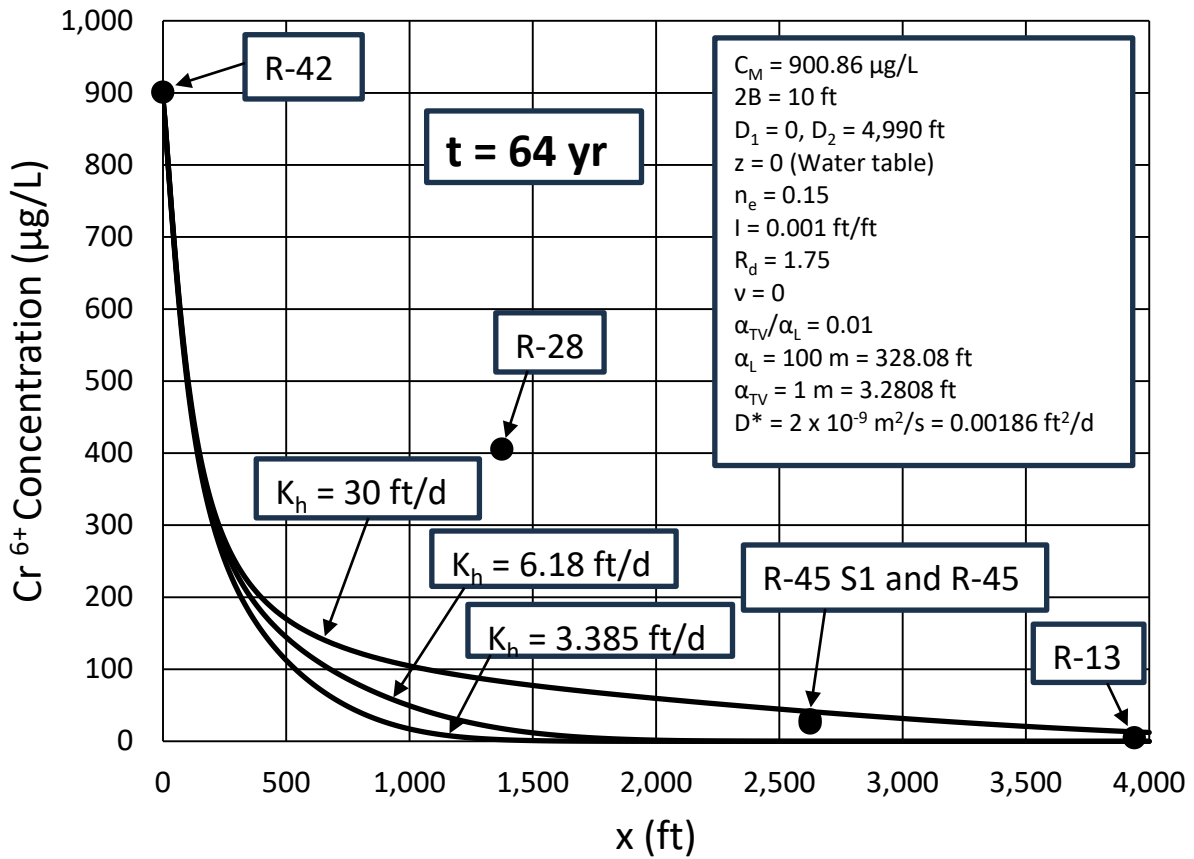


Figure 15. Longitudinal  $Cr^{6+}$  concentration variation along the streamline formed by the observation wells R-42, R-28, R-45 S1, R-45 S2, and R-13 for different  $K_h$  values with  $\alpha_L = 100 \text{ m}$  (328.08  $ft$ ) and  $\alpha_{TV}/\alpha_L = 0.01$  after 64  $yr$  elapsed time.

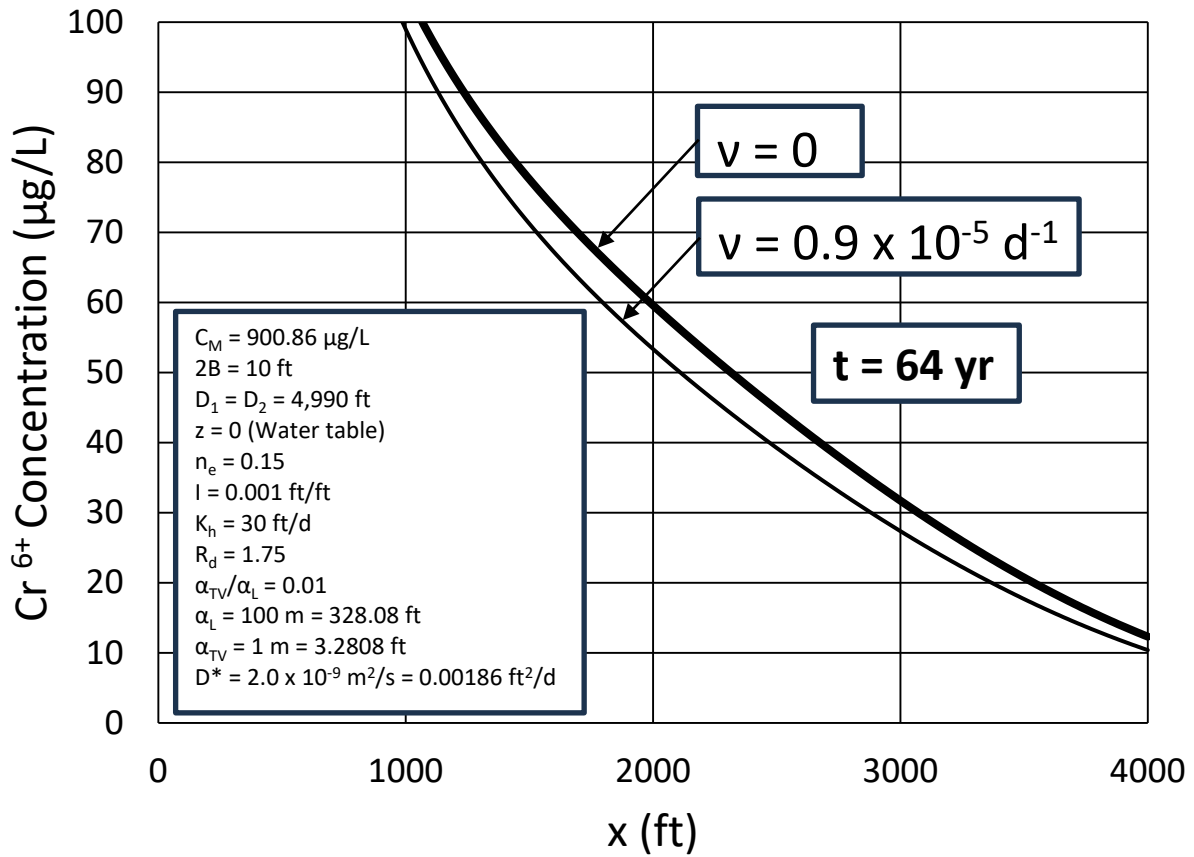


Figure 16. Longitudinal  $Cr^{6+}$  concentration variation along the streamline formed by the observation wells R-42, R-28, R-45 S1, R-45 S2, and R-13 for  $K_h = 30 \text{ ft/d}$  with  $\alpha_L = 100 \text{ m}$  (328.08 ft),  $\alpha_{TV}/\alpha_L = 0.01$ , and  $v = 0.9 \times 10^{-5} \text{ d}^{-1}$  after 64 yr elapsed time.

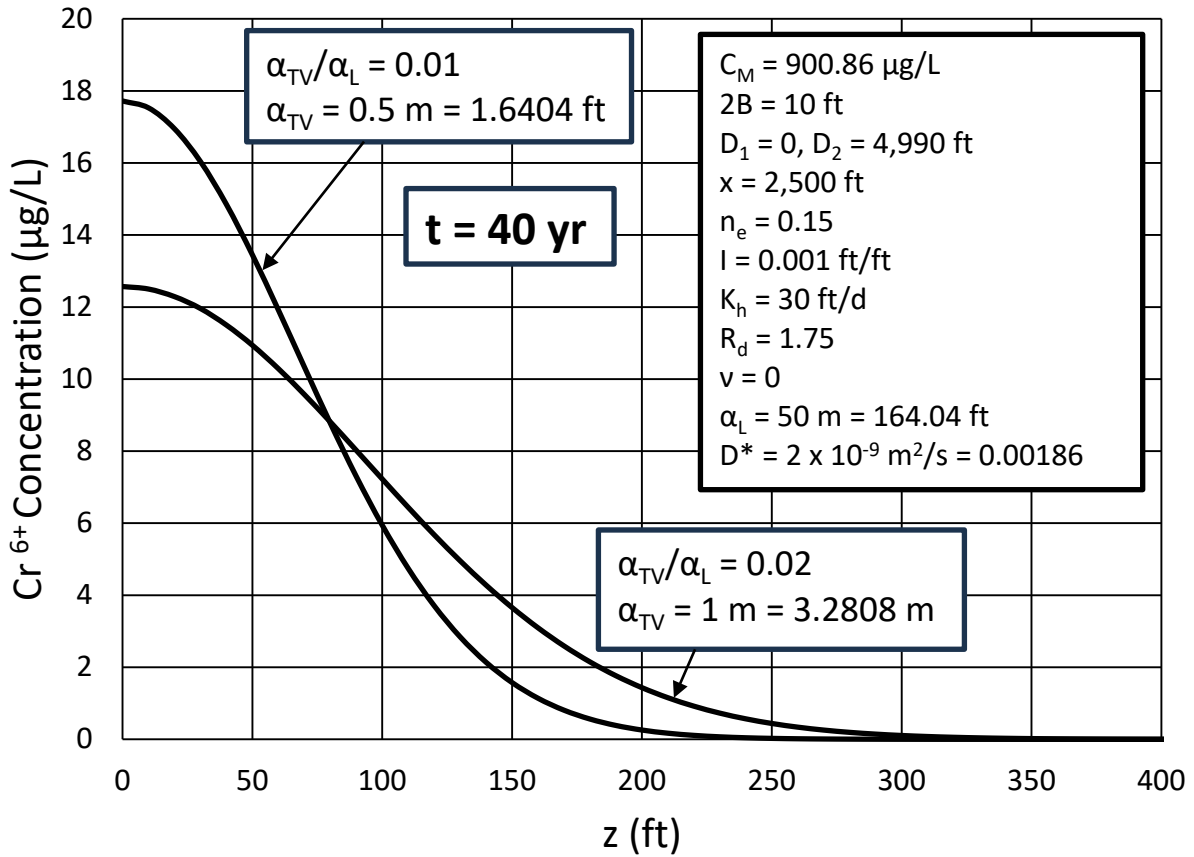


Figure 17. Transverse vertical  $Cr^{6+}$  concentration variation at  $x = 2,500 \text{ ft}$  perpendicular to the streamline formed by the observation wells R-42, R-28, R-45 S1, R-45 S2, and R-13 for  $K_h = 30 \text{ ft/d}$  with  $\alpha_L = 50 \text{ m}$  ( $164.04 \text{ ft}$ ) and  $\alpha_{TV}/\alpha_L = 0.01$  and  $0.02$  after  $40 \text{ yr}$  elapsed time.

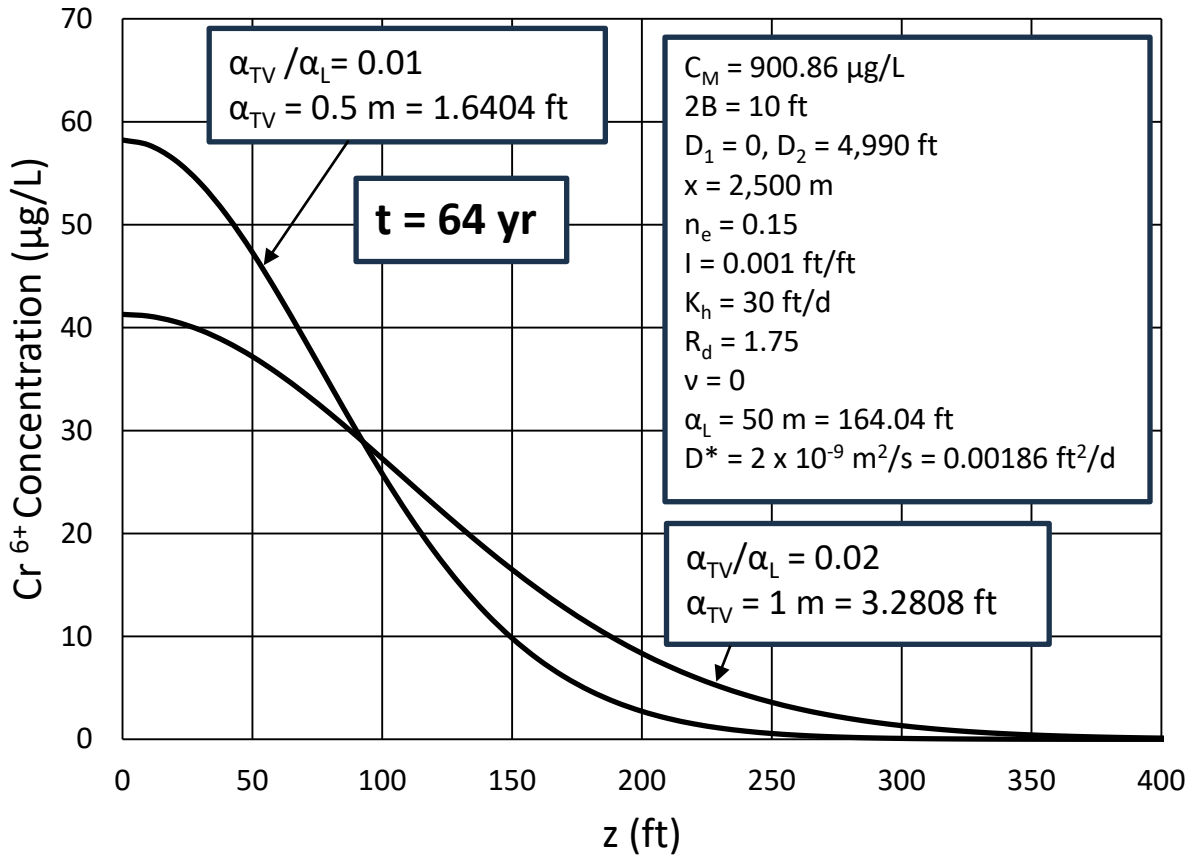


Figure 18. Transverse vertical  $Cr^{6+}$  concentration variation at  $x = 2,500 \text{ ft}$  perpendicular to the streamline formed by the observation wells R-42, R-28, R-45 S1, R-45 S2, and R-13 for  $K_h = 30 \text{ ft/d}$  with  $\alpha_L = 50 \text{ m}$  ( $164.04 \text{ ft}$ ) and  $\alpha_{TV}/\alpha_L = 0.01$  and  $0.02$  after  $64 \text{ yr}$  elapsed time.

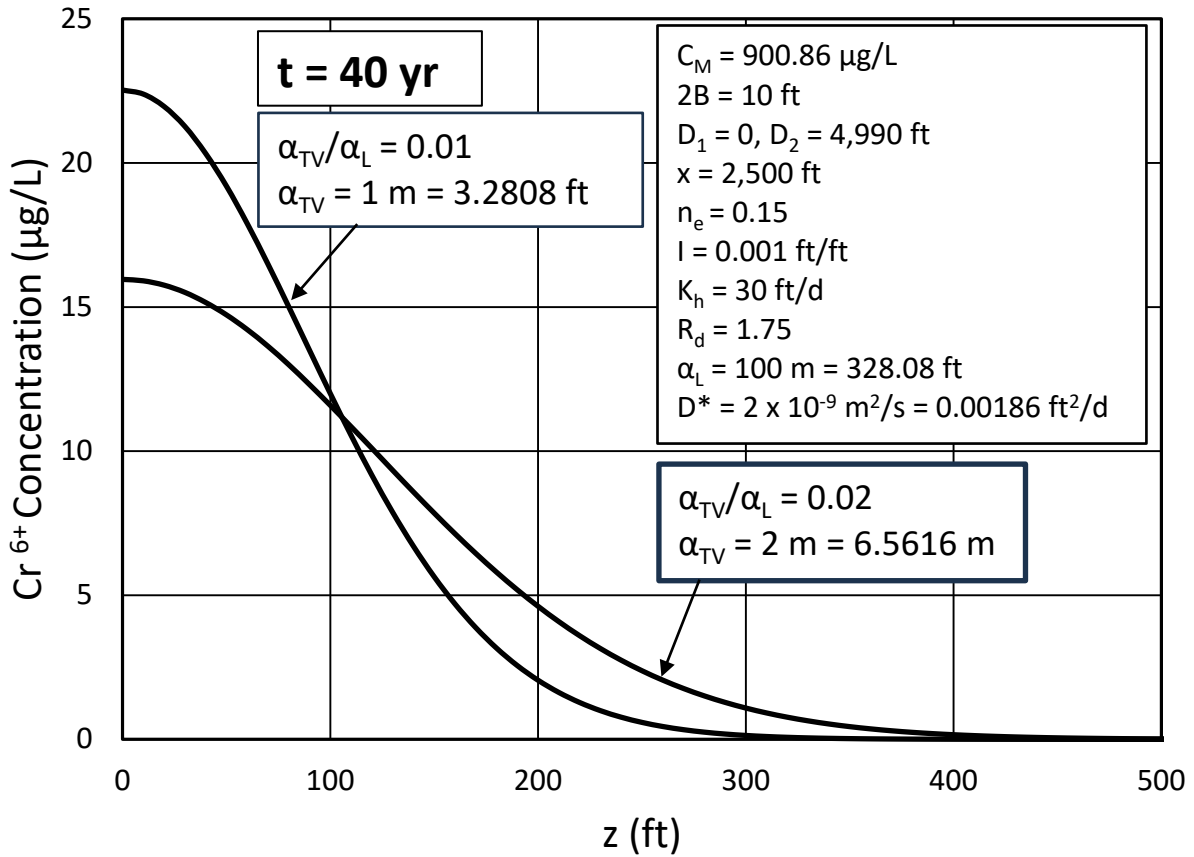


Figure 19. Transverse vertical  $Cr^{6+}$  concentration variation at  $x = 2,500 \text{ ft}$  perpendicular to the streamline formed by the observation wells R-42, R-28, R-45 S1, R-45 S2, and R-13 for  $K_h = 30 \text{ ft/d}$  with  $\alpha_L = 100 \text{ m}$  (328.08 ft) and  $\alpha_{TV}/\alpha_L = 0.01$  and  $0.02$  after 40 yr elapsed time.



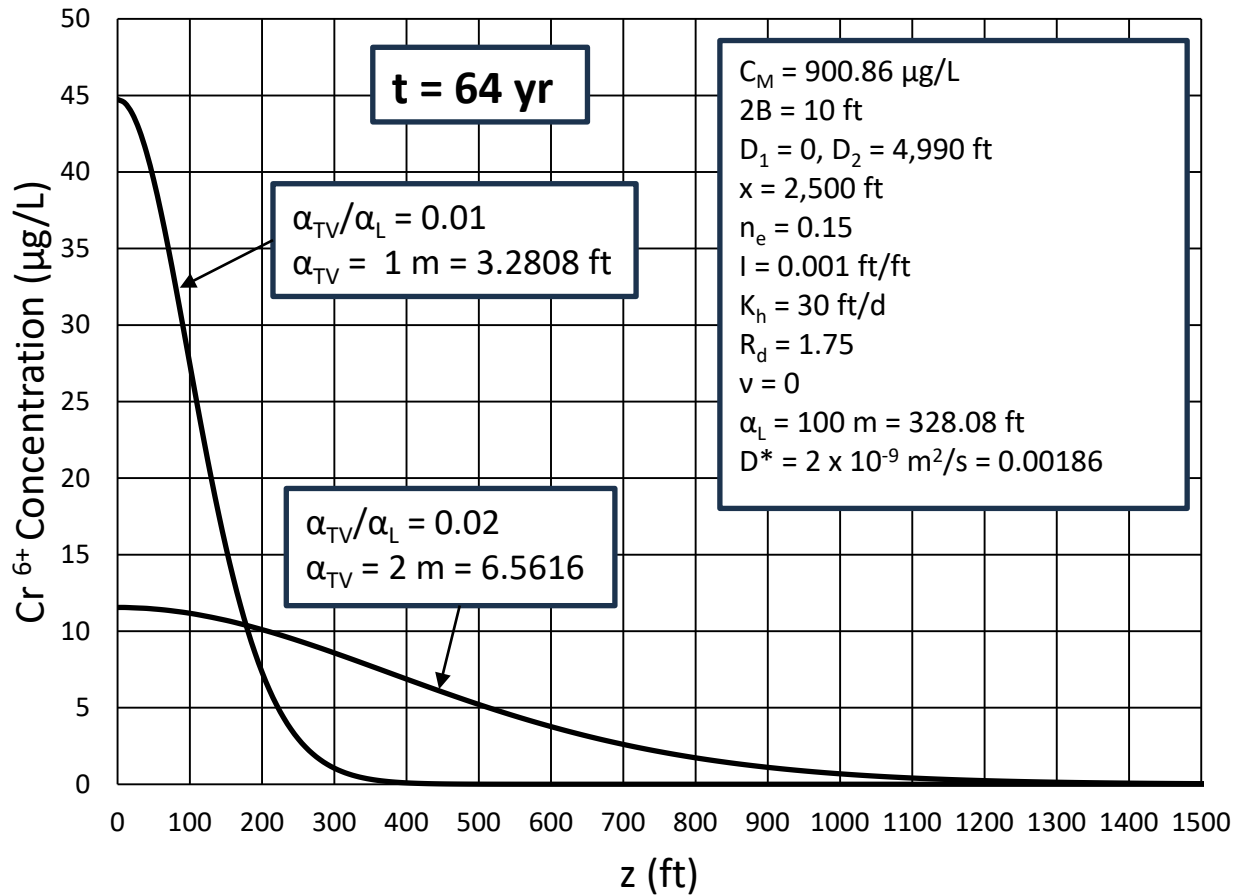


Figure 20. Transverse vertical  $Cr^{6+}$  concentration variation at  $x = 2,500 \text{ ft}$  perpendicular to the streamline formed by the observation wells R-42, R-28, R-45 S1, R-45 S2, and R-13 for  $K_h = 30 \text{ ft/d}$  with  $\alpha_L = 100 \text{ m}$  (328.08 ft) and  $\alpha_{TV}/\alpha_L = 0.01$  and 0.02 after 64 yr elapsed time.

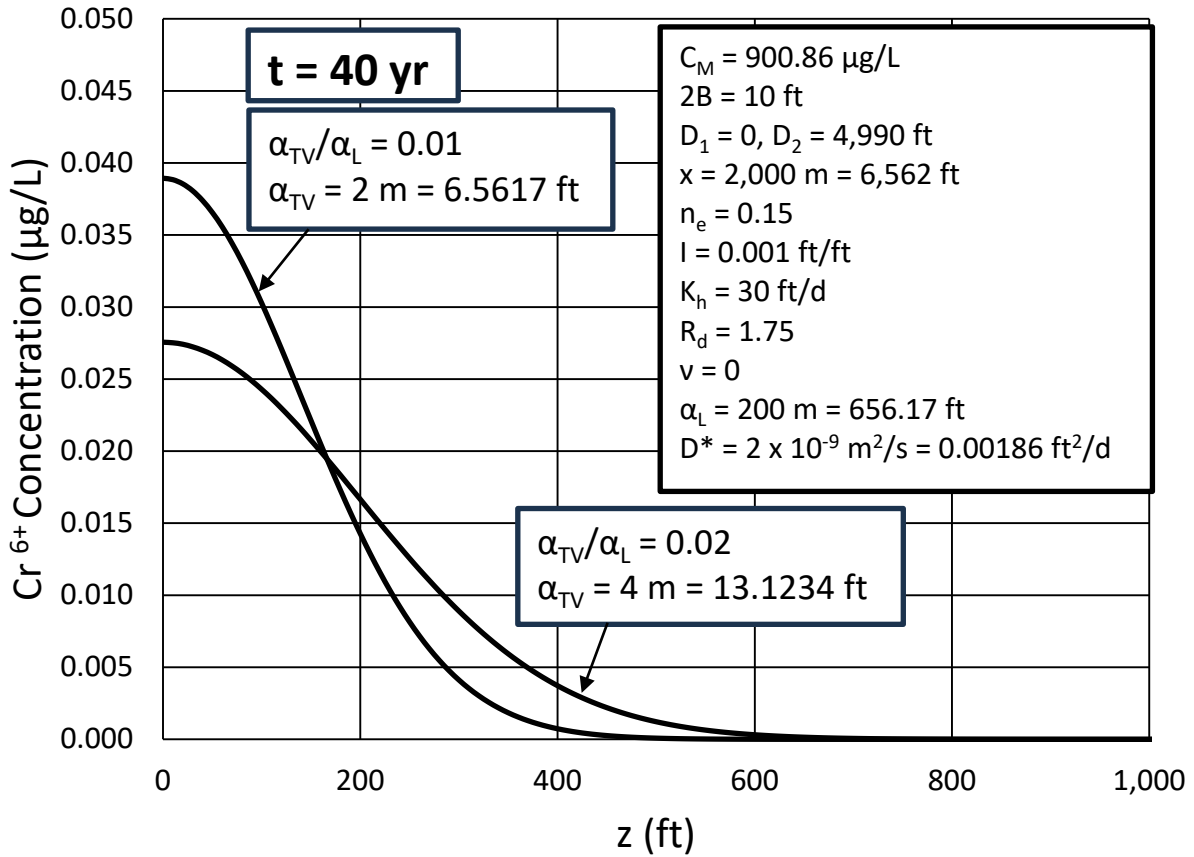


Figure 21. Transverse vertical  $Cr^{6+}$  concentration variation at  $x = 6,562 \text{ ft}$  ( $2,000 \text{ m}$ ) perpendicular to the streamline formed by the observation wells R-42, R-28, R-45 S1, R-45 S2, and R-13 for  $K_h = 30 \text{ ft/d}$  with  $\alpha_L = 200 \text{ m}$  ( $656.17 \text{ ft}$ ) and  $\alpha_{TV}/\alpha_L = 0.01$  and  $0.02$  after  $64 \text{ yr}$  elapsed time.

## Tables

Table 1. Construction information of R-42, R-28, R-45, and R-13.

<b>Well ID</b>	<b>Screen Top Depth (ft)</b>	<b>Screen Bottom Depth (ft)</b>	<b>Screen Top Elevation (ft)</b>	<b>Screen Bottom Elevation (ft)</b>	<b>Screen Length (ft)</b>
R-42	931.8	952.9	5,827.2	5,806.1	21.1
R-28	934.3	958.1	5,794.3	5,770.5	23.8
R-45 S1	880.0	890.0	5,824.0	5,814.0	10.0
R-45 S2	974.9	994.9	5,729.1	5,709.1	20.0
R-13	958.3	1,018.7	5,714.8	5,654.4	60.4

Source: Koch, R.J., and S. Schmeer, "Groundwater Level Status Report for 2008, Los Alamos National Laboratory," LA-14397-PR, Progress Report, 260 pp., March, 2009.

Table 2. The distances of R-42, R-28, R-45, and R-13 observation wells from R-42 and their average chromium ( $Cr^{6+}$ ) concentrations.

<b>Well ID</b>	<b>Distance from R-42 (ft)</b>	<b>Chromium (<math>Cr^{6+}</math>) Average Concentration (<math>\mu\text{g/L}</math>)</b>	<b>Distance from x (ft)</b>
R-42	0	900.86	0
R-28	1,375	405.50	185
R-45 S1	2,625	25.39	0
R-45 S2	2,625	29.84	0
OR-13	3,940	4.84	0

## **Appendix I**

**Batu (2024h) - Determination of the Zone of Influence of the  
PM-4 Water Supply Well and Evaluation of the Effects of  
All Water Supply Wells to the Chromium (Cr<sup>6+</sup>) Plume Area,  
Los Alamos, New Mexico**

# **Determination of the Zone of Influence of the PM-4 Water Supply Well and Evaluation of the Effects of All Water Supply Wells to the Chromium ( $Cr^{6+}$ ) Plume Area, Los Alamos, New Mexico**

---

Vedat Batu, Ph.D., P.E.  
Argonne Associate  
Argonne National Laboratory  
Lemont, Illinois

**August 23, 2024**

This page intentionally left blank.



## Executive Summary

The purpose of this report is to determine the zone of influence of the PM-4 water supply well with a partially-penetrating three-dimensional analytical well hydraulics solution for unconfined aquifers. Specifically, the drawdown variation at the location of R-28, which is located in the chromium ( $Cr^{6+}$ ) plume area, is determined. PM-4 is the second closest water supply well to the main chromium ( $Cr^{6+}$ ) plume around R-28 after PM-3 water supply well. The conclusions drawn from this analysis can be summarized as follows:

1. As can be seen from Figure 3, after 30 d (1 month) of elapsed time the drawdown at R-28 is around 0.1 ft. After 300 d of elapsed time the drawdown at R-28 will be 0.88 ft. And after 1,000 d, the drawdown will be 3.19 ft. The key point is that with the significantly high extraction rate at PM-4 (1,400 *gpm*), the zone of influence of PM-4 will be noticeably at R-28 even after 1 month of elapsed time. And these results are consistent with the points given in Section 5.1 which are based on the actual drawdown measurements when water was extracted from PM-2.
2. The chromium ( $Cr^{6+}$ ) plume is inside of polygon formed large water supply wells such as PM-2, PM-3, PM-4, and PM-5 having recorded extraction rates up to 1,500 *gpm*. Based on the available reports, potentially these wells may extract water simultaneously from the aquifer under intermittent conditions. Therefore, in order to take under the control of the chromium ( $Cr^{6+}$ ) plume, inward gradients need to be generated with CrEx-1, CrEx-2, CrEx-3, and CrEx-4 with comparable water extraction rates. But the screen intervals of these wells are in the Puye Formation and close to the water table which is a drawback as compared with the long and deep screen intervals of the aforementioned water supply wells.
3. Based on Eq. (1), the radius of influence of PM-4 is shown in Figure 4. Figure 4 shows that as the drawdown  $s_w$  at PM-4 increases, the radius of influence  $R$  will be increased. For example, for  $s_w = 250 \text{ ft}$ ,  $R = 2,000 \text{ ft}$ . With the combined effects of the other water supply wells, the radius of influence  $R$  will be much greater.

## Contents

Executive Summary .....	ES-1
1. Purpose.....	1
2. Well Geometry of PM-4 Water Supply Well and its Extraction Rate Range .....	1
3. Hydrogeologic Parameters .....	1
4. The Analytical Solution Used for the Zone of Influence of PM-4.....	2
5. Drawdown Versus Time Curve at the Location of R-28 Well and Zone of Influence of PM-4 .....	2
5.1 Radius of Influence of PM-2 .....	2
5.2 Drawdown Versus Time at R-28 while PM-4 Pumping .....	3
5.3 Radius of Influence of PM-4 .....	3
6. Conclusions .....	4
References.....	4

## Figures

Figure 1. The well geometry of PM-4.

Figure 2. Schematic picture of Neuman's partially-penetrating well hydraulics geometry in an unconfined aquifer (Adapted from Neuman, 1975, p. 304, Figure 1).

Figure 3. Drawdown versus time at R-48 location for  $K_h = 2.05 \text{ ft/d}$  and  $K_v/K_h = 0.020$ .

Figure 4. Radius of influence (R) vs. drawdown ( $s_w$ ) at PM-4 water supply well.

## 1. Purpose

The purpose of this report is to determine the zone of influence of the PM-4 water supply well with a partially-penetrating three-dimensional analytical well hydraulics solution for unconfined aquifers. Specifically, the drawdown variation at the location of R-28, which is located in the chromium ( $Cr^{6+}$ ) plume area, will be determined. PM-4 is the second closest water supply well to the main chromium ( $Cr^{6+}$ ) plume around R-28 after PM-3 water supply well.

## 2. Well Geometry of PM-4 Water Supply Well and its Extraction Rate Range

The well geometry of PM-4 is shown in Figure 1 based on the data in McLin (2005, p. 10, Figure 6). Its screen interval is

$$L = 1,594 \text{ ft}$$

and the other quantities in Figure 1 are

$$d = 184.7 \text{ ft}$$

$$l = d + L = 1,778.7 \text{ ft.}$$

The extraction rate of PM-4 varies between 800 *gpm* and 1,400 *gpm* (Boyle et al., 2024, p. 5) and  $Q = 1,400 \text{ gpm}$  is used in this analysis. This rate is comparable with the PM-2 aquifer test value (1,249 *gpm*) for the 25 –  $d$  aquifer test having  $L = 1,276 \text{ ft}$  screen interval whose upper end is at 135 *ft* depth from the water table.

## 3. Hydrogeologic Parameters

The following parameters were determined from the PM-2 aquifer test analysis (Batu, August 10, 2024):

$$K_r = K_h = 2.05 \frac{\text{ft}}{\text{d}} \dots \text{Horizontal hydraulic conductivity}$$

$$\frac{K_z}{K_r} = \frac{K_v}{K_h} = 0.020 \dots \text{Anisotropy ratio}$$

$$K_z = K_v = (0.020)K_h = (0.020) \left( 2.05 \frac{\text{ft}}{\text{d}} \right) = 0.041 \frac{\text{ft}}{\text{d}}$$

$$S = 0.00284$$

And the specific yield ( $S_y$ ) is estimated at

$$S_y = 0.15$$

## 4. The Analytical Solution Used for the Zone of Influence of PM-4

The analytical solution developed by Neuman for partially-penetrating wells in unconfined aquifers [Neuman, 1974, p. 304, Eqs. (17) and (20); Neuman, 1975, p. 330, Eq. (1)] have been used in determining the zone of influence of PM-4. The geometry of this analytical solution is shown in Figure 2.

Neuman (1974) has developed a FORTRAN computer program called DELAY2 to calculate the drawdown in the aforementioned equations. Since DELAY2 was generated for mainframe computers in the 1970s, later on Batu (1998, p. 514) has generated its personal computers (PC) version and was called DELAY2PC by keeping the original parts and algorithm of the program the same. Later on, the program was renamed as SPN (Shlomo P. Neuman) just for convenience and all runs in this report were generated by running this version of the original DELAY2 program. In running the program, the Type B (for late drawdown data) version of the solution is used.

## 5. Drawdown Versus Time Curve at the Location of R-28 Well and Zone of Influence of PM-4

Since R-28 well is around the center of the chromium ( $Cr^{6+}$ ) plume, the drawdown versus time curve is generated at this location. The distance between PM-4 pumped well and R-28 well is approximately 5,000 ft (McLin, 2005, p. 6, Figure 3).

Before presenting, the results of the analysis regarding the zone of influence of PM-4, it will be instructive to look at the statements regarding the radius of influence of PM-2 from the report of McLin (2005, July) based on measurements.

### 5.1 Radius of Influence of PM-2

Regarding the radius of influence of PM-2 under extraction conditions, McLin (2005, pp. 6-7) states:

*“Figure 3 is an enlargement of the area surrounding well PM-2, where numerous observation wells are located. Figure 3 also shows an idealized radius of influence, or maximum extent of measured drawdown, that was observed in the 25-day aquifer test at PM-2. This radius is idealized because one must assume homogeneous and isotropic aquifer properties that generate concentric circles of equal drawdown in response to pumping at a constant rate. Several idealized concentric circles would actually represent these lines of equal drawdown at some time  $t$ . These contours would also decrease in value as the radial distance from the pumping well increases. In reality, we rarely see this idealized aquifer response. Instead, drawdown contours in response to pumping are typically shaped like concentric but distorted ellipses because the subsurface is not homogeneous and isotropic. These irregular shapes are revealed only when a sufficient number of observation wells are available to record spatial and temporal changes in drawdown. For the PM-2 aquifer test, drawdown was observed in wells*

*PM-2, R-20, R-32, PM-4, and PM-5 (see Figure 3). However, no drawdown was observed in R-22, PM-1, or PM-3 because these deep wells are located too far from well PM-2 to be affected. In addition, no drawdown was observed in R-21, R-23, R-12, R-13, R-15, or R-14 because these wells are either too shallow and do not penetrate into the water-bearing units that yield water to PM-2, or these wells are located too far from PM-2 to be affected. This observation of drawdown in some wells and no drawdown in other wells immediately tells us that the saturated regional aquifer materials surrounding PM-2 are vertically anisotropic with respect to hydraulic transmitting characteristics. More is written about this behavior further on. Finally, no drawdown was recorded at R-19 because the recording transducer system for this well was not deployed during the PM-2 test period. On the basis of the hydraulic transmitting properties obtained from this test (as presented below) and the geologic cross-section shown in Figure 2, we would expect to see recordable drawdown in well R-19 during the 25-day pumping interval.”*

## **5.2 Drawdown Versus Time at R-28 while PM-4 Pumping**

The values  $K_r = K_h = 2.05 \frac{ft}{d}$  and  $\frac{K_z}{K_r} = \frac{K_v}{K_h} = 0.020$  were determined from the PM-2 aquifer test analysis (Batu, June 10, 2024). Based on these values, the drawdown variation with time at the R-28 location is shown in Figure 3. As can be seen from Figure 3, after 30 d (1 month) of elapsed time the drawdown at R-28 is around 0.1 ft. After 300 d of elapsed time the drawdown at R-28 will be 0.88 ft. And after 1,000 d, the drawdown will be 3.19 ft. The key point is that with the significantly high extraction rate at PM-4 (1,400 *gpm*), the zone of influence of PM-4 will be noticeably at R-28 even after 1 month of elapsed time. And these results are consistent with the points given in Section 5.1 which are based on the actual drawdown measurements.

## **5.3 Radius of Influence of PM-4**

The radius of influence  $R$  is the distance from the well where drawdown is zero. Since the 1880s, many attempts have been made to relate it to well, aquifer, and flow parameters in both steady and unsteady flow conditions in confined and unconfined aquifers. Some semi-empirical formulas are given in Bear (1979, p. 306). Of these formulas, the one developed by Sichardt is given in Bear [1979, p. 306, Eq. (8-11) as presented in Chertousov (1962)] is widely being used [e.g., De Filippi et al., 2020; Batu, 2024, p. 1088, Eq. (29-249)]:

$$R = 3000 s_w K_h^{\frac{1}{2}} \quad (1)$$

in which  $R$  and  $s_w$  are in meters (m), and  $K_h$  in meters per second (m/s).

Based on Eq. (1), the radius of influence of PM-4 is shown in Figure 4. Figure 4 shows that as the drawdown  $s_w$  at PM-4 increases, the radius of influence  $R$  will be increased. For example, for  $s_w = 250 ft$ ,  $R = 2,000 ft$ .

## 6. Conclusions

As mentioned in Section 5.1, the  $R$  radius of influence is idealized because one must assume homogeneous and isotropic aquifer properties that generate concentric circles of equal drawdown in response to pumping at a constant rate. In other words, the horizontal hydraulic conductivity ( $K_h$ ) and vertical hydraulic conductivity ( $K_v$ ) are spatially constant. Most importantly, the effects of partial penetration of PM-2 is taken into account. Based on these points, the conclusions drawn from this analysis can be summarized as follows:

1. As can be seen from Figure 3, after 30 d (1 month) of elapsed time the drawdown at R-28 is around 0.1 ft. After 300 d of elapsed time the drawdown at R-28 will be 0.88 ft. And after 1,000 d, the drawdown will be 3.19 ft. The key point is that with the significantly high extraction rate at PM-4 (1,400 *gpm*), the zone of influence of PM-4 will be noticeably at R-28 even after 1 month of elapsed time. And these results are consistent with the points given in Section 5.1 which are based on the actual drawdown measurements when water was extracted from PM-2.
2. The chromium ( $Cr^{6+}$ ) plume is inside of the polygon formed by PM-2, PM-3, PM-4, and PM-5 having recorded extraction rates up to 1,500 *gpm*. Based on the available reports, potentially these wells may extract water simultaneously from the aquifer under intermittent conditions. Therefore, in order to take under the control of the chromium ( $Cr^{6+}$ ) plume, inward gradients need to be generated with CrEx-1, CrEx-2, CrEx-3, and CrEx-4 with comparable water extraction rates. But the screen intervals of these wells are in the Puye Formation and close to the water table which is a drawback as compared with the long and deep screen intervals of the water supply wells.
3. Based on Eq. (1), the radius of influence of PM-4 is shown in Figure 4. Figure 4 shows that as the drawdown  $s_w$  at PM-4 increases, the radius of influence  $R$  will be increased. For example, for  $s_w = 250 \text{ ft}$ ,  $R = 2,000 \text{ ft}$ . With the combined effects of the other water supply wells, the radius of influence  $R$  will be much greater.

## References

- Batu, V., *Fluid Mechanics and Hydraulics: Illustrative Worked Examples of Surface and Subsurface Flows*, Taylor & Francis CRC Press, 1,240 pp., Boca Raton, Florida, 2024.
- Batu, 1998., *Aquifer Hydraulics: A Comprehensive Guide to Hydrogeologic Data Analysis*, John Wiley & Sons, Inc., 727 pp., New York, 1998.
- Batu, V., "Horizontal ( $K_h$ ) and Vertical Hydraulic Conductivity ( $K_v$ ) Values Determined from the Aquifer Tests of the CrIN, CrEX, PM-2, and PM-4 Wells at the LANL Site," August 10, 2024.
- Bear, J., *Hydraulics of Groundwater*, McGraw-Hill Inc., 569 pp., New York, 1979.
- Boyle, D., L. Foster, L. Gains-Germain, A. Rice, and D. Birdsell, "LANL Chromium Plume: Using Water Level Data to Characterize Hydraulic Gradients in the Presence of a Pump-And-Treat System. – 24608," *WM2024 Conference*, March 10-14, Pheonix, Arizona, 18 pp., 2024.

Chertousov, M.D., *Hydraulics* (in Russian), Gosenergouzdat, 630 pp., Moscow, Russia, 1962.

De Filippi, F.M., S. Iacurto, F. Ferranti, and G. Sappa, "Hydraulic Conductivity Estimation Using Low-Flow Purging Data Elaboration in Contaminated Sites," *Water*, Vol. 12, pp. 898-914, 2020.

McLin, S.G., "Analysis of the PM-2 Aquifer Test Using Multiple Observation Wells, LA-14225-MS, Los Alamos National Laboratory," Los Alamos, New Mexico, July, 2005.

Neuman, S.P., "Effect of Partial Penetration on Flow in Unconfined Aquifers Considering Delayed Gravity Response," *Water Resources Research*, Vol. 10, No.2, pp. 303-312, April, 1974.

Neuman, S.P., "Analysis of Pumping Test Data From Anisotropic Unconfined Aquifers Considering Delayed Gravity Response," *Water Resources Research*, Vol. 11, No. 2, pp. 329-342, April, 1975.

## Figures



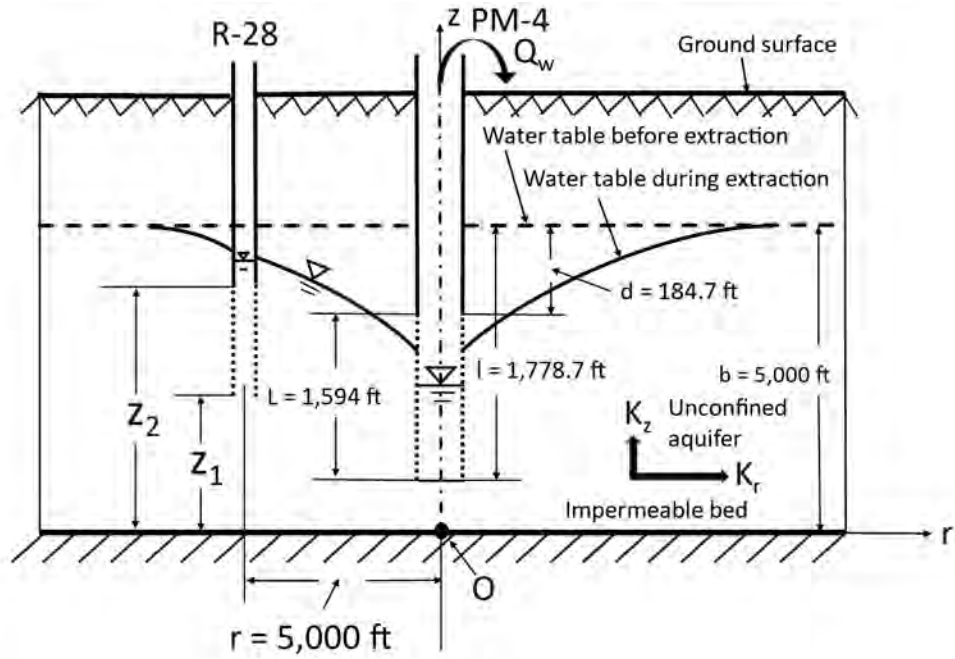


Figure 1. The well geometry of PM-4.

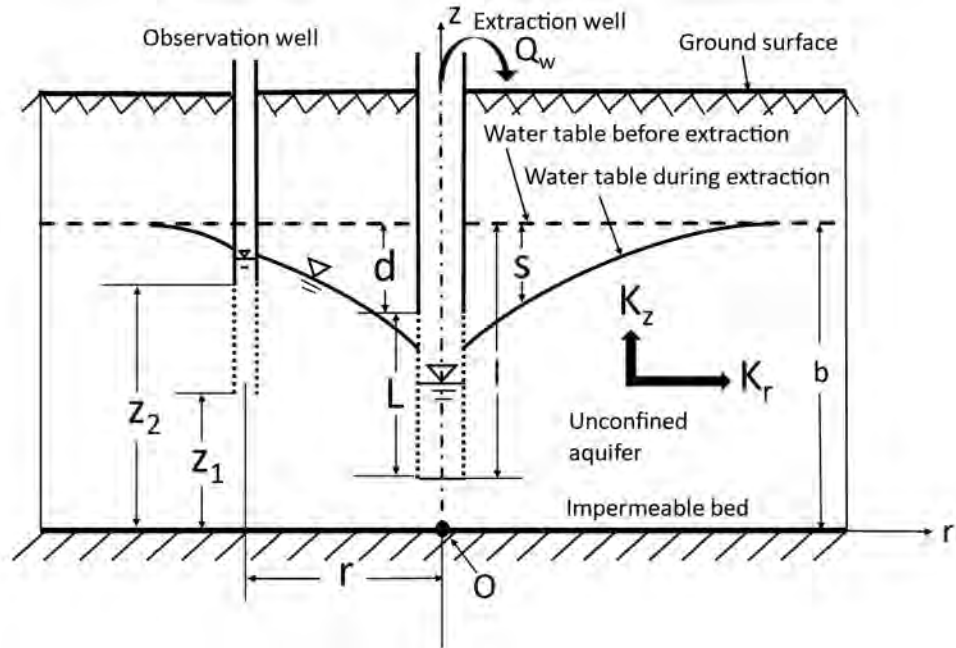


Figure 2. Schematic picture of Neuman's partially-penetrating well hydraulics geometry in an unconfined aquifer (Adapted from Neuman, 1975, p. 304, Figure 1).

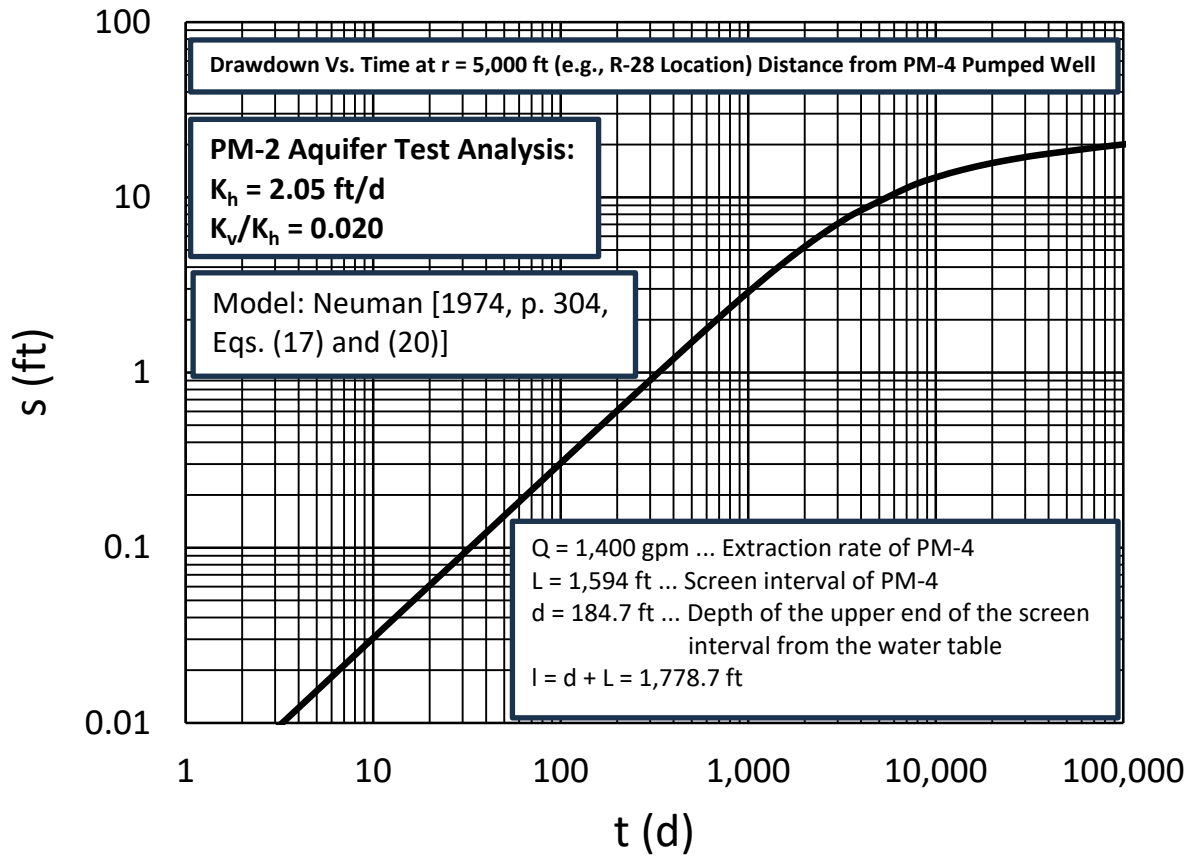


Figure 3. Drawdown versus time at R-28 location for  $K_h = 2.05$  ft/d and  $K_v/K_h = 0.020$ .

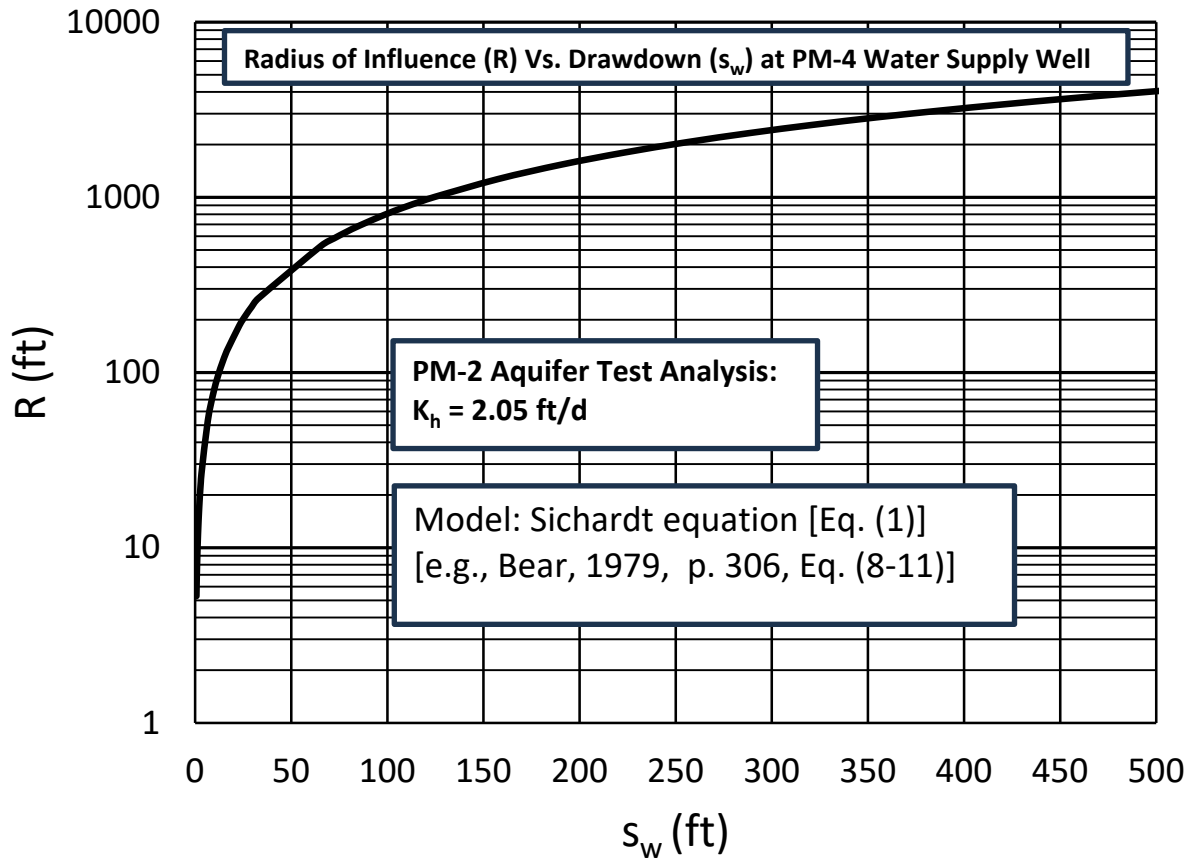


Figure 4. Radius of influence (R) vs. drawdown ( $s_w$ ) at PM-4 water supply well.

## **Appendix J**

**Batu (2024e) - Plots of Chromium ( $\text{Cr}^{6+}$ ) Concentrations vs.  
Date Between 2004 and 2024 and Their Interpretations,  
Los Alamos, New Mexico**

# **Plots of Chromium ( $Cr^{6+}$ ) Concentrations vs. Date Between 2004 and 2024 and Their Interpretations, Los Alamos, New Mexico**

---

Vedat Batu, Ph.D., P.E.  
Argonne Associate  
Argonne National Laboratory  
Lemont, Illinois

**August 17, 2024**

This page intentionally left blank.

## Executive Summary

Chromium ( $Cr^{6+}$ ) concentration measurements have started in 2004 and still measurements are going on. As of now, measurements are being made at 47 locations. Of these, 32 of them are observation wells, 5 of them are extraction wells, 5 of them are injection wells, and 5 of them are piezometers. In this report, the plots of the chromium ( $Cr^{6+}$ ) concentrations vs. date curves have been analyzed in order to better understand the migration dynamics of the chromium ( $Cr^{6+}$ ) mass from the vadose zone to the predominantly unconfined aquifer.

In Section 1, the purpose of the report is described.

In Section 2, the chromium ( $Cr^{6+}$ ) source area and the main flow and transport paths in the unconfined aquifer are presented.

In Section 2.1, the estimated chromium ( $Cr^{6+}$ ) source area is described. Based on the  $Cr^{6+}$  concentration data plots, it has been reached to the conclusion that it appears that the source is likely located inside the polygon formed by R-15, R-62, R-43, R-42, R-50, and R-61.

In Section 2.2, the main flow directions are described based on the September 6, 2008 and May 1, 2020 measured hydraulic head contours.

In the subsections of Section 2.2, the chromium ( $Cr^{6+}$ ) concentrations vs. date plots for a number of wells have been analyzed and some key conclusions have been reached.



## Contents

Executive Summary .....	ES-1
1. Purpose.....	1
2. Chromium (Cr <sup>6+</sup> ) Source Area and the Main Flow and Transport Paths in the Unconfined Aquifer .....	1
2.1 The Estimated Chromium (Cr <sup>6+</sup> ) Source Area .....	1
2.2 The Main Flow and Chromium (Cr <sup>6+</sup> ) Transport Path Lines .....	1
2.2.1 Analysis of the R-42 Cr <sup>6+</sup> + Concentration Data .....	2
2.2.2 Analysis of the R-28 Data Along with the R-11 and R-61 Cr <sup>6+</sup> + Data .....	3
2.2.3 Analysis of the R-45 Data Along with R-35a, R-35b, R-44, R-50, and R-70 Cr <sup>6+</sup> + Data.....	3
2.2.4 Analysis of the R-13 Data Along with SIMR-2 Chromium (Cr <sup>6+</sup> ) Data .....	4
2.2.5 Overall Conclusions for the Transport of Chromium (Cr <sup>6+</sup> ) in the Unconfined Aquifer.....	4
References.....	5

## Figures

- Figure 1. Cr<sup>6+</sup> concentration vs. date at R-1.
- Figure 2. Cr<sup>6+</sup> concentration vs. date at R-11.
- Figure 3. Cr<sup>6+</sup> concentration vs. date at R-13.
- Figure 4. Cr<sup>6+</sup> concentration vs. date at R-15.
- Figure 5. Cr<sup>6+</sup> concentration vs. date at R-28.
- Figure 6. Cr<sup>6+</sup> concentration vs. date at R-33 S1.
- Figure 7. Cr<sup>6+</sup> concentration vs. date at R-33 S2.
- Figure 8. Cr<sup>6+</sup> concentration vs. date at R-35a.
- Figure 9. Cr<sup>6+</sup> concentration vs. date at R-35b.
- Figure 10. Cr<sup>6+</sup> concentration vs. date at R-36.
- Figure 11a. All data for Cr<sup>6+</sup> concentration vs. date at R-42.
- Figure 11b. Data til 2/10/2010 for Cr<sup>6+</sup> concentration vs. date at R-42.
- Figure 12a. Full data for Cr<sup>6+</sup> concentration vs. date at R-43 S1.
- Figure 12b. Full data for Cr<sup>6+</sup> concentration vs. date at R-43 S1 till April 11, 2022.
- Figure 13a. Full data for Cr<sup>6+</sup> concentration vs. date at R-43 S2.
- Figure 13b. Data till 11/31/2020 for Cr<sup>6+</sup> concentration vs. date at R-43 S2.
- Figure 14. Cr<sup>6+</sup> concentration vs. date at R-44 S1.
- Figure 15. Cr<sup>6+</sup> concentration vs. date at R-44 S2.

Figure 16.  $Cr^{6+}$  concentration vs. date at R-45 S1.  
Figure 17.  $Cr^{6+}$  concentration vs. date at R-45 S2.  
Figure 18.  $Cr^{6+}$  concentration vs. date at R-50 S1.  
Figure 19.  $Cr^{6+}$  concentration vs. date at R-50 S2.  
Figure 20.  $Cr^{6+}$  concentration vs. date at R-61 S1.  
Figure 21a. Full data for  $Cr^{6+}$  concentration vs. date at R-62.  
Figure 21b. Data till 1/25/2022 for  $Cr^{6+}$  concentration vs. date at R-62.  
Figure 22.  $Cr^{6+}$  concentration vs. date at R-70 S1.  
Figure 23.  $Cr^{6+}$  concentration vs. date at R-70 S2.  
Figure 24.  $Cr^{6+}$  concentration vs. date at R-71 S1.  
Figure 25.  $Cr^{6+}$  concentration vs. date at R-71 S2.  
Figure 26.  $Cr^{6+}$  concentration vs. date at R-72 S1.  
Figure 27.  $Cr^{6+}$  concentration vs. date at R-72 S2.  
Figure 28.  $Cr^{6+}$  concentration vs. date at SCI-1.  
Figure 29.  $Cr^{6+}$  concentration vs. date at SCI-2.  
Figure 30.  $Cr^{6+}$  concentration vs. date at SIMR-2.  
Figure 31.  $Cr^{6+}$  concentration vs. date at MCOI-5.  
Figure 32.  $Cr^{6+}$  concentration vs. date at MCOI-6.  
Figure 33.  $Cr^{6+}$  concentration vs. date at CrEX-1.  
Figure 34.  $Cr^{6+}$  concentration vs. date at CrEX-2.  
Figure 35.  $Cr^{6+}$  concentration vs. date at CrEX-3.  
Figure 36.  $Cr^{6+}$  concentration vs. date at CrEX-4.  
Figure 37.  $Cr^{6+}$  concentration vs. date at CrEX-5.  
Figure 38.  $Cr^{6+}$  concentration vs. date at CrIN-1.  
Figure 39.  $Cr^{6+}$  concentration vs. date at CrIN-2.  
Figure 40.  $Cr^{6+}$  concentration vs. date at CrIN-3.  
Figure 41.  $Cr^{6+}$  concentration vs. date at CrIN-4.  
Figure 42.  $Cr^{6+}$  concentration vs. date at CrIN-5.  
Figure 43.  $Cr^{6+}$  concentration vs. date at CrPZ-1.  
Figure 44.  $Cr^{6+}$  concentration vs. date at CrPZ-2a.  
Figure 45.  $Cr^{6+}$  concentration vs. date at CrPZ-3.  
Figure 46.  $Cr^{6+}$  concentration vs. date at CrPZ-4.  
Figure 47.  $Cr^{6+}$  concentration vs. date at CrPZ-5.

Figure 48. Head contours in 2008 and 2020 along with the average  $Cr^{6+}$  concentration data.

Figure 49. Head contours in 2013.

# 1. Purpose

Chromium ( $Cr^{6+}$ ) concentration measurements have started in 2004 and still measurements are going on. As of now, measurements are being made at 47 locations. Of these, 32 of them are observation wells, 5 of them are extraction wells, 5 of them are injection wells, and 5 of them are piezometers. The purpose of this report is to analyze the plots of the chromium ( $Cr^{6+}$ ) concentrations vs. date curves to understand better the migration dynamics of the chromium ( $Cr^{6+}$ ) mass from the vadose zone to the predominantly unconfined aquifer.

## 2. Chromium ( $Cr^{6+}$ ) Source Area and the Main Flow and Transport Paths in the Unconfined Aquifer

### 2.1 The Estimated Chromium ( $Cr^{6+}$ ) Source Area

Based on the  $Cr^{6+}$  concentration data plots, it appears that the source is likely located inside the polygon formed by R-15, R-62, R-43, R-42, R-50, and R-61. The average thickness of the vadose zone around the source area is 1,305 ft.

According to the report entitled “Groundwater Level Status Report for 2008: Los Alamos National Laboratory” by Koch and Schmeer (2009), the screen interval data for some of the aforementioned wells are as follows:

Well ID	Screen Top Depth	Screen Bottom Depth	Screen Length	Page No.
R-15	958.6 ft	1,020.3 ft	61.7 ft	26
R-43 S1	903.9	924.6	20.7	60
R-43 S2	969.1	979.1	10.0	60
R-42	931.8	952.9	21.1	59

These values indicate that the measured chromium ( $Cr^{6+}$ ) concentrations belong to the Puye Formation which is the shallow part of the aquifer.

### 2.2 The Main Flow and Chromium ( $Cr^{6+}$ ) Transport Path Lines

In Figure 48, the main flow direction shown by the line CEDF based on the head contours corresponding to the May 1, 2020 data are shown. This flow line also represents approximately the main flow direction based on September 6, 2008 hydraulic head data given in the report by Koch and Schmeer (2009) despite the fact that they are 5 to 11 ft higher than the May 1, 2020 head values. Figure 49 shows the hydraulic head contours in 2013 (Los Alamos National Laboratory, 2013, p. 14, Figure 1.0-2). The aforementioned figures clearly indicate that the main flow direction is in the southeast direction. As can be seen from the chromium ( $Cr^{6+}$ ) concentration values in Figure 48, the R-42, R-28, R-45, and R-13, which are located on the flowline (or streamline), decrease as the distance increases from R-42.

### 2.2.1 Analysis of the R-42 $Cr^{6+}$ Concentration Data

The maximum chromium ( $Cr^{6+}$ ) concentration was measured at R-42 observation well on February 10, 2010 (1,240  $\mu g/L$ ) in the plume area (see Figure 11a). As can be seen from Figure 11a, this maximum concentration is an exception value and the concentration varies between 1,070  $\mu g/L$  (August 8, 2012) and 622  $\mu g/L$  (October 19, 2023), averaging 871  $\mu g/L$ . Figure 11a indicates that after the first quarter of 2012, concentrations started to decline and this trend continued till the last quarter of 2023 after which no measured values exist. One should note that during the 6-yr time period from September 2017 till October 2023 no measured concentration values exist. Potentially, the concentration decline may be attributed to the effects of the extraction and injection wells.

Figure 11b presents the temporal concentration variation at R-42 from October 2008 till February 2010 which shows a linear trend. By linear extrapolation, it appears that the chromium ( $Cr^{6+}$ ) mass reached to the water table by around the first quarter of 2005.

Being in decline mode of the temporal concentrations of R-42 does not mean that all  $Cr^{6+}$  mass reached to the water table. The evidence of this situation is the temporal concentration variations at R-15 (Figure 4), R-62 (Figure 21a), and R-70 S2 (Figure 23) observation wells.

Figure 4 for R-15 shows that although the concentrations are well below from 50  $\mu g/L$ , they are in the increase mode and based on linear extrapolation the chromium ( $Cr^{6+}$ ) mass reached to the water table in the first quarter of 1980 which may be attributed that the vadose zone in the area of R-15 is less permeable than the surrounding areas.

Figure 21a for R-62 shows that the concentrations are significantly above from 50  $\mu g/L$  (Up to 351  $\mu g/L$  on January 25, 2022) and they are generally in the increase mode. And based on linear extrapolation (Figure 21b) the chromium ( $Cr^{6+}$ ) mass reached to the water table sometime in 2007 which may be attributed that the vadose zone in the area of R-62 is less permeable than the surrounding areas.

Figure 23 for R-70 S2 shows that, like R-62, the concentrations are significantly above from 50  $\mu g/L$  (Up to 272  $\mu g/L$  on August 4, 2020). Figure 23 also shows that the chromium ( $Cr^{6+}$ ) concentrations decline continuously till mid 2023 and afterwards start to increase till February 20, 2024 (257  $\mu g/L$ ) to almost the initial value on August 4, 2020 (272  $\mu g/L$ ).

Based on the foregoing analyses, the following conclusions can be drawn:

1. Based on the temporal chromium ( $Cr^{6+}$ ) concentration variations at R-15, R-42, R-62, and R-70, the likely area of the source location in the aquifer is the inside area of the polygon formed by R-15, R-62, R-43, R-42, R-50, and R-61.
2. The permeability of the vadose zone changes from location to location in the source area.
3. The chromium ( $Cr^{6+}$ ) mass front had reached to the water table as early as in 1980 in the west side of the plume (R-15). But in the northwest side of the plume (R-62), the chromium ( $Cr^{6+}$ ) mass front had reached to the water table sometime in 2007.

4. The chromium ( $Cr^{6+}$ ) mass front had reached to the water table in the first quarter of 2005 in the middle part of the plume (R-42).

### 2.2.2 Analysis of the R-28 Data Along with the R-11 and R-61 $Cr^{6+}$ Data

As shown in Figure 48, R-28 (Figure 5) observation well is on the CEDF streamline which represents the average flow direction in the aquifer. And R-11 (Figure 2) and R-61 (Figure 20 for R-61 S1) are the closest observation wells nearby R-28. Here are some key points for the aforementioned figures:

1. The chromium ( $Cr^{6+}$ ) concentration variation with time for R-28 (Figure 5) observation well indicates that the concentrations fluctuate around the  $405.50 \mu g/L$  average value from May 20, 2005 to August 2, 2017. The minimum and maximum values are  $310 \mu g/L$  (on October 26, 2006) and  $466 \mu g/L$  (on August 2, 2017). Therefore, the key characteristic for the R-28 well data is that the chromium ( $Cr^{6+}$ ) concentrations during the 12-yr time period remain unchanged. It looks like that the CrEX-3 extraction well which is around 200 ft away from R-28 did not have any significant effect.
2. One of the closest observation wells R-11 (Figures 2) to R-28 data show that the chromium ( $Cr^{6+}$ ) concentration measurements were made between May 17, 2005 ( $17.2 \mu g/L$ ) and February 7, 2024 ( $9.29 \mu g/L$ ) with the maximum concentration on February 13, 2007 ( $34.9 \mu g/L$ ). As can be seen from Figure 2, they are all below  $50 \mu g/L$ .
3. The other closest observation well to R-28 is R-61 S1 and its chromium ( $Cr^{6+}$ ) concentration with time variation (Figure 20) indicates that there were no measurements before May 20, 2011 ( $16 \mu g/L$ ) and afterwards the concentration started to increase till February 2, 2024 ( $77 \mu g/L$ ). It looks like the nearby extraction well CrEX-2, which is around 100 ft away from R-61, had no effect.
4. Based on the aforementioned points, the chromium ( $Cr^{6+}$ ) mass is around R-28 and there is almost constant mass flux from the vadose zone.

### 2.2.3 Analysis of the R-45 Data Along with R-35a, R-35b, R-44, R-50, and R-70 $Cr^{6+}$ Data

As shown in Figure 48, the R-45 (Figure 16) observation well is very close to the CEDF streamline which represents the average flow direction in the aquifer. And R-35a (Figure 8), R-35b (Figure 9), R-44 (Figure 14 for R-44 S1 and Figure 15 for R-44 S2), R-50 (Figure 18 for R-50 S1 and Figure 19 for R-50 S2), and R-70 (Figure 22 for R-70 S1 and Figure 23 for R-70 S2) are the closest observation wells nearby R-45. Here are some key points for the aforementioned figures:

1. As can be seen from Figure 16 (R-45 S1) and Figure 17 (R-45 S2), although the temporal chromium ( $Cr^{6+}$ ) concentration variations have ups and downs, their values are below  $50 \mu g/L$  with the exception of the part after mid 2020 in Figure 17 (R-45 S2).
2. Figure 8 (R-35a) and Figure 9 (R-35b) show that the measured chromium ( $Cr^{6+}$ ) concentrations are way below from  $50 \mu g/L$ .

3. According to Figure 22 (R-70 S1), the chromium  $Cr^{6+}$  concentrations between August 4, 2020 and February 20, 2024 are around  $15 \mu g/L$  with the exception of one value ( $137 \mu g/L$ ) on September 21, 2023. But Figure 23 for R-70 S2 indicates that there were no measurements before August 4, 2020 ( $272 \mu g/L$ ) and after that it declines and by the first quarter of 2024 it reaches almost to the previous value ( $257 \mu g/L$ ). Perhaps during the decline period the nearby CrEX-5 extraction well was active.
4. Figure 14 (R-44 S1) and Figure 15 (R-44 S2) show that the measured chromium ( $Cr^{6+}$ ) concentrations are below  $50 \mu g/L$ .
5. The only well in the group of wells is R-50 S1 (Figure 18) having chromium ( $Cr^{6+}$ ) concentrations above  $50 \mu g/L$  ( $150 \mu g/L$  on October 26, 2017). And after fourth quarter, the concentrations started to decline due to perhaps nearby extraction and injection wells.

#### 2.2.4 Analysis of the R-13 Data Along with SIMR-2 Chromium ( $Cr^{6+}$ ) Data

As shown in Figure 48, the R-13 (Figure 3) observation well is on the CEDF streamline which represents the average flow direction in the aquifer. The observation well SIMR-2 (Figure 30) is approximately on the same 5,835 ft msl equipotential line like R-13 and the distance between them is around 1,560 ft. Here are the key points:

1. The chromium ( $Cr^{6+}$ ) concentration data for R-13 (Figure 3) are between April 18, 2002 and January 22, 2024 averaging approximately  $5.0 \mu g/L$ .
2. As can be seen from Figure 3 for R-13, the temporal concentration variation does not have significant ups and downs during the 22-yr time period.
3. The chromium ( $Cr^{6+}$ ) concentration data for SIMR-2 (Figure 30) are between September 11, 2015 and February 8, 2024 averaging approximately  $5.0 \mu g/L$  like R-13.
4. As can be seen from Figure 30 for SIMR-2, the temporal concentration variation does not have significant ups and downs during the 9-yr time period like R-13.

#### 2.2.5 Overall Conclusions for the Transport of Chromium ( $Cr^{6+}$ ) in the Unconfined Aquifer

The overall conclusions drawn from this analysis can be summarized as follows:

1. In Figure 48, the main flow direction shown by the line CEDF based on the head contours corresponding to the May 1, 2020 data are shown. Figure 49 shows the hydraulic head contours in 2013 in which the main flow direction is shown by the AB flowline (or streamline) which matches with the flow line CEDF in Figure 48. The flow line in Figure 48 also matches with the flow direction based on September 6, 2008 hydraulic head data given in the report by Koch and Schmeer (2009) despite the fact that they are 5 to 11 ft lower than the May 1, 2020 head values.
2. As can be seen from the average chromium ( $Cr^{6+}$ ) concentration values in Figure 48, the R-42 ( $980.86 \mu g/L$ ), R-28 ( $405.50 \mu g/L$ ), R-45 ( $29.84 \mu g/L$ ), R-45 S1 ( $25.39 \mu g/L$ ), R-45 S2 ( $29.84 \mu g/L$ ), and R-13 (R-45 S1 ( $4.84 \mu g/L$ )), which are located on the flowline (or

streamline), decrease as the distance increases from R-42. Based on the detailed analysis, it is not likely that the extraction and injection wells are the reason of this decline.

## **References**

Koch, R.J., and S. Schmeer, "Groundwater Level Status Report for 2008, Los Alamos National Laboratory," LA-14397-PR, Progress Report, 260 pp., March, 2009.

Los Alamos National Laboratory, "Interim Measures Work Plan for the Evaluation of Chromium Mass Removal," ERID-241096, LA-UR-13-22534, EP2013-0073, 20 pp., April, 2013.



## Figures

# R-1

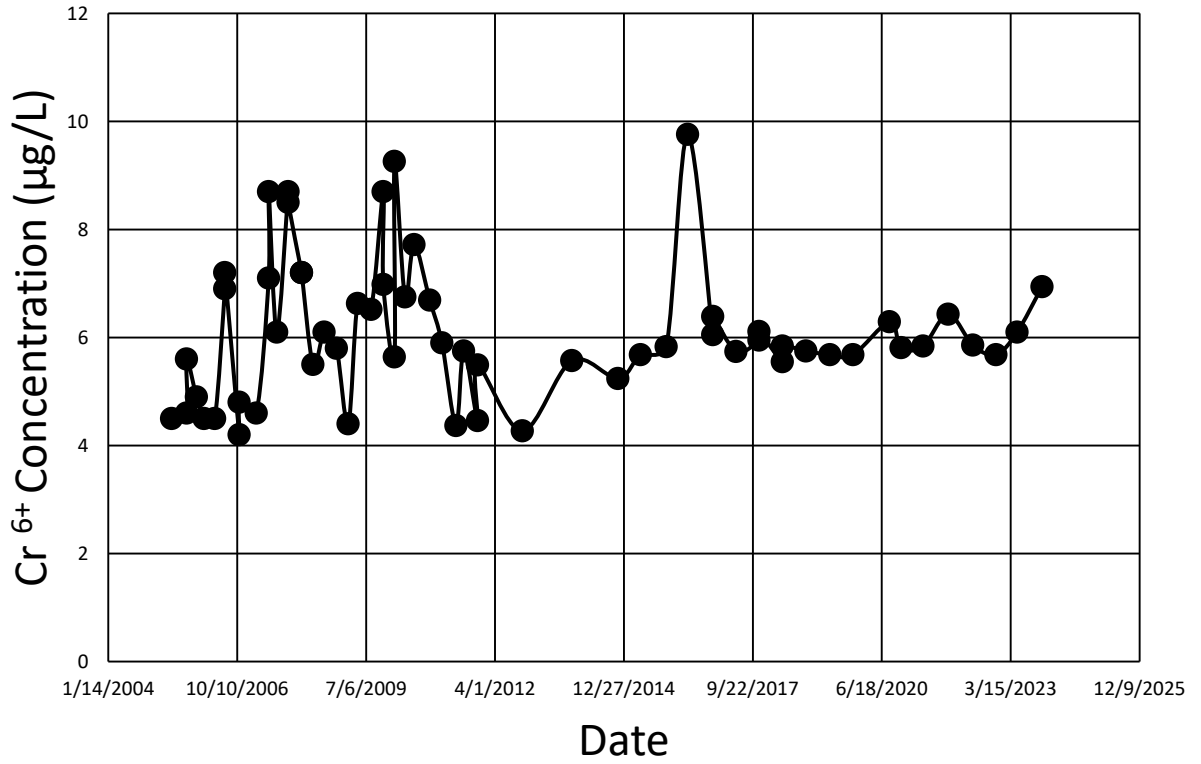


Figure 1. Cr<sup>6+</sup> concentration vs. date at R-1.

# R-11

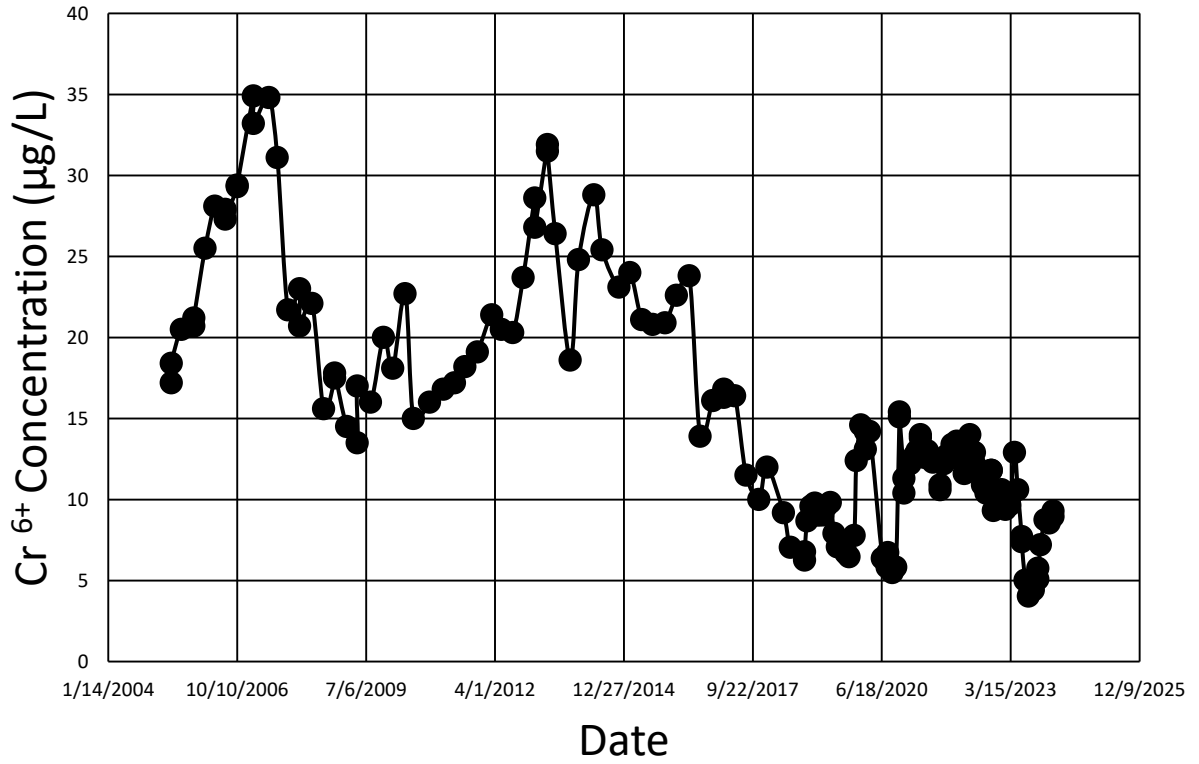


Figure 2. Cr<sup>6+</sup> concentration vs. date at R-11.

# R-13

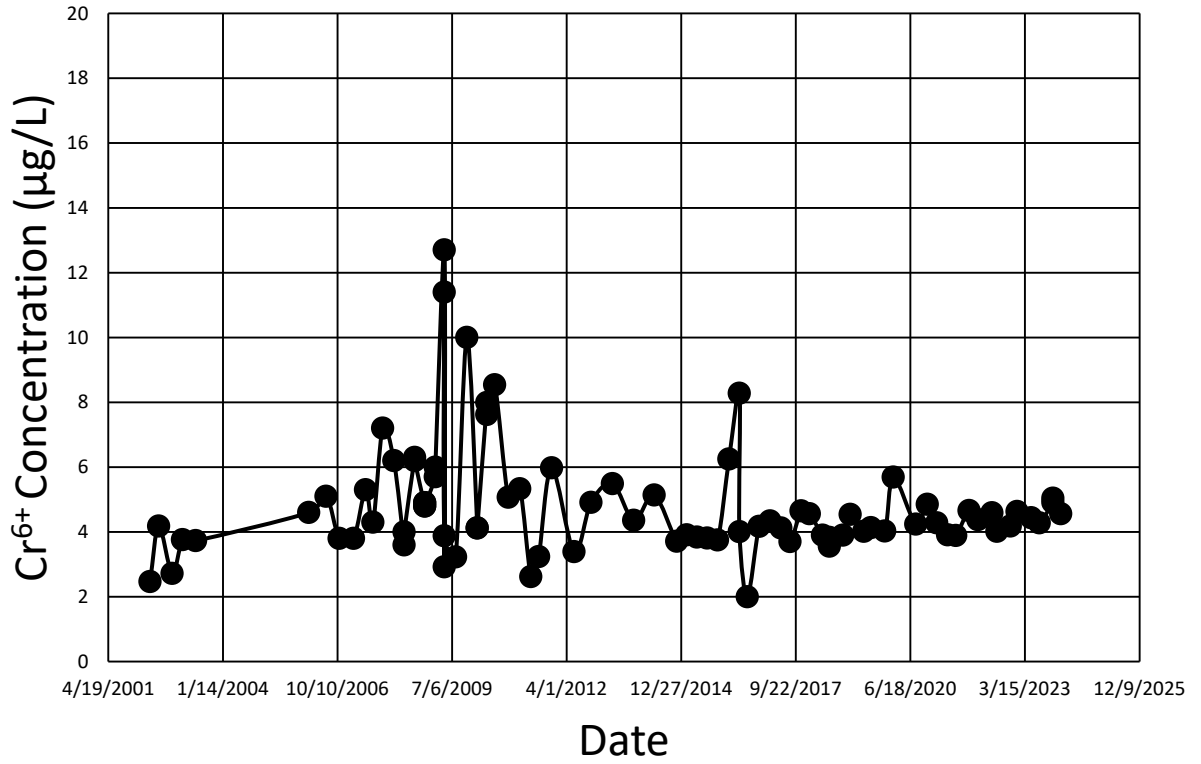


Figure 3. Cr<sup>6+</sup> concentration vs. date at R-13.

# R-15

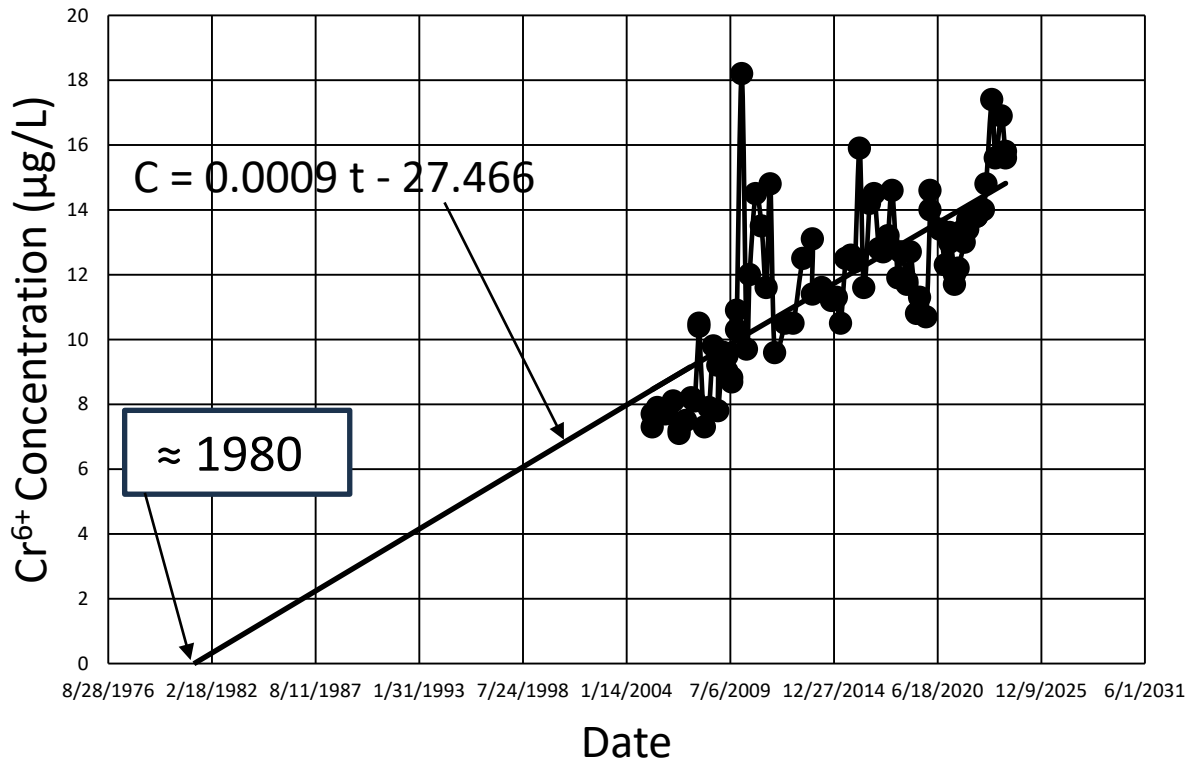


Figure 4.  $Cr^{6+}$  concentration vs. date at R-15.

# R-28

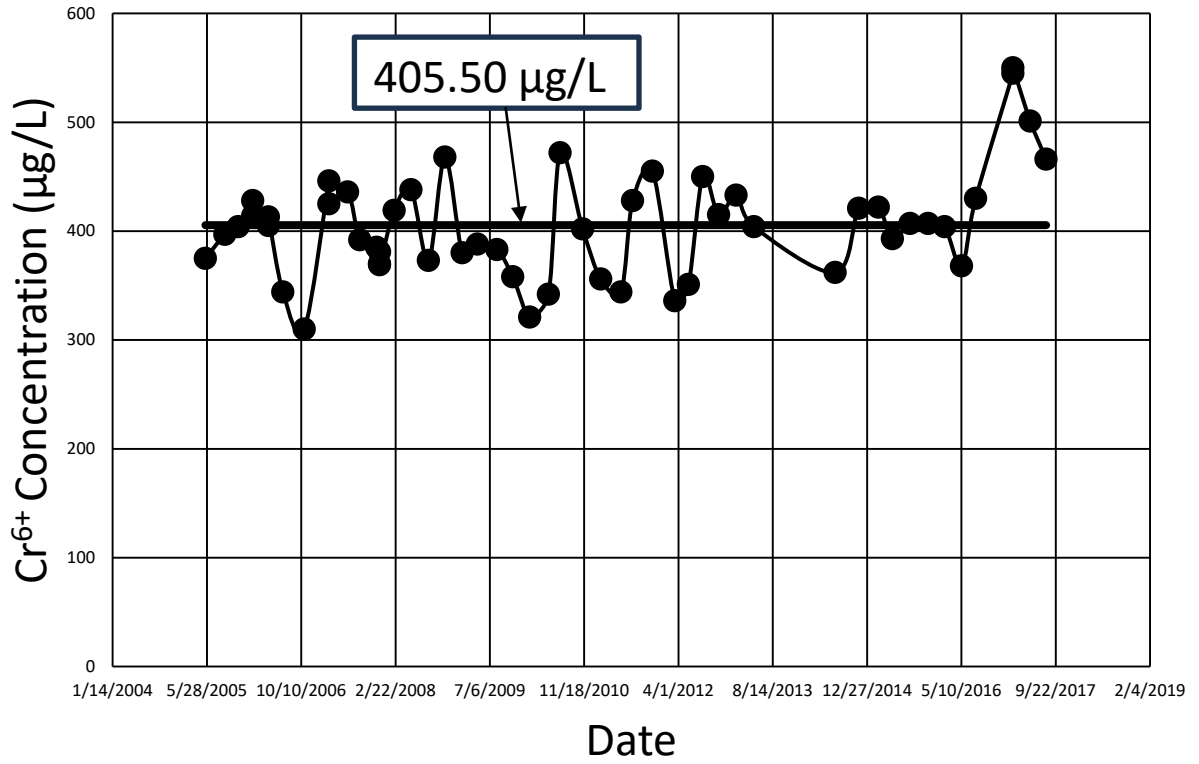


Figure 5. Cr<sup>6+</sup> concentration vs. date at R-28.

# R-33 S1

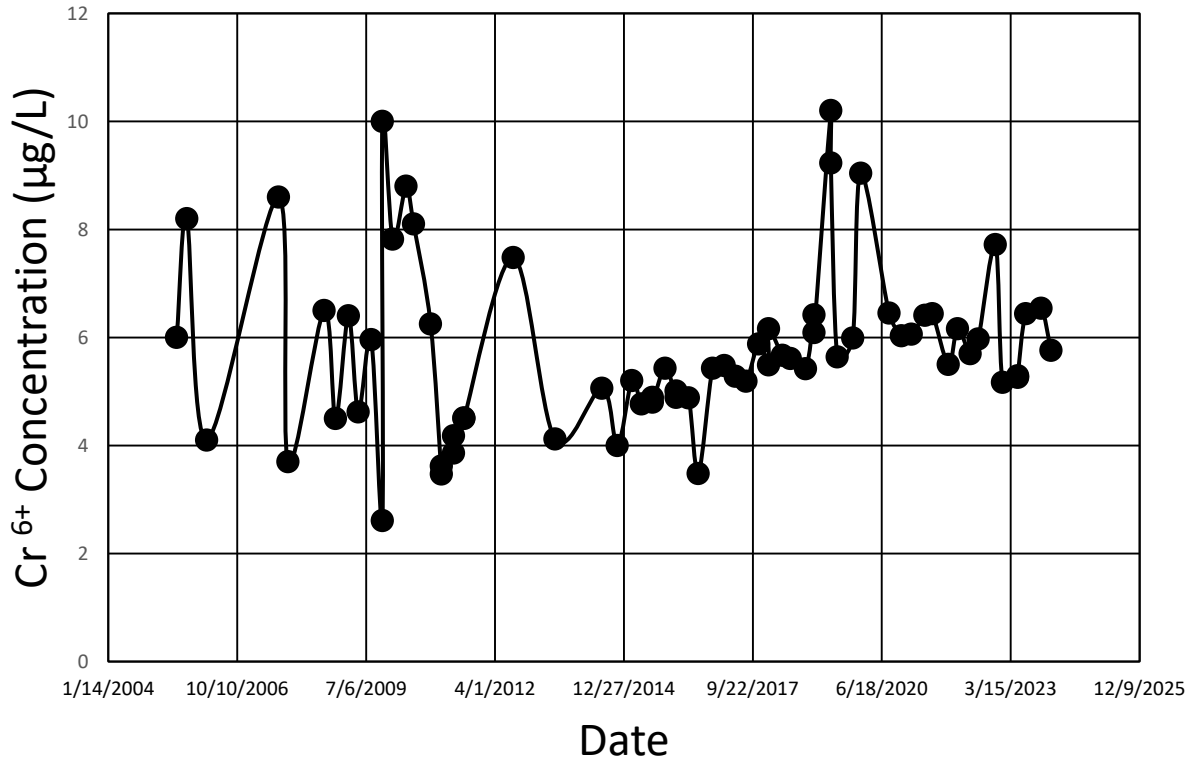


Figure 6. Cr<sup>6+</sup> concentration vs. date at R-33 S1.

# R-33 S2

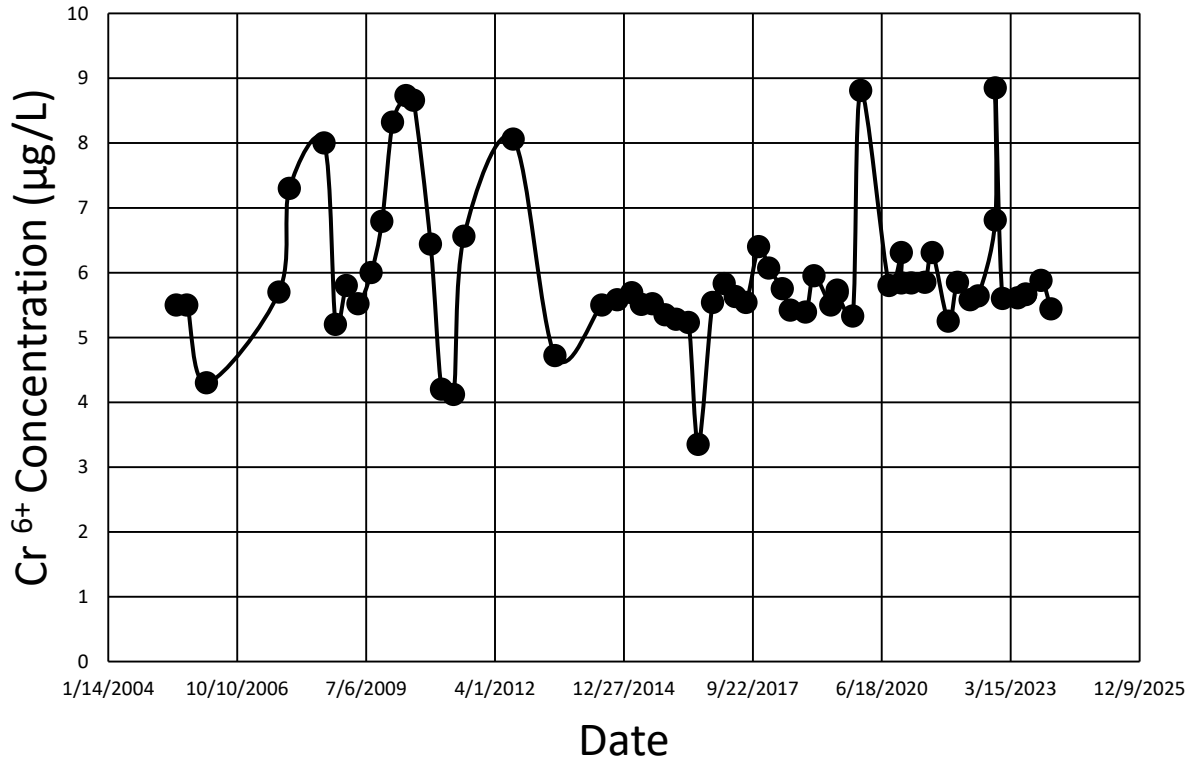


Figure 7. Cr<sup>6+</sup> concentration vs. date at R-33 S2.



# R-35a

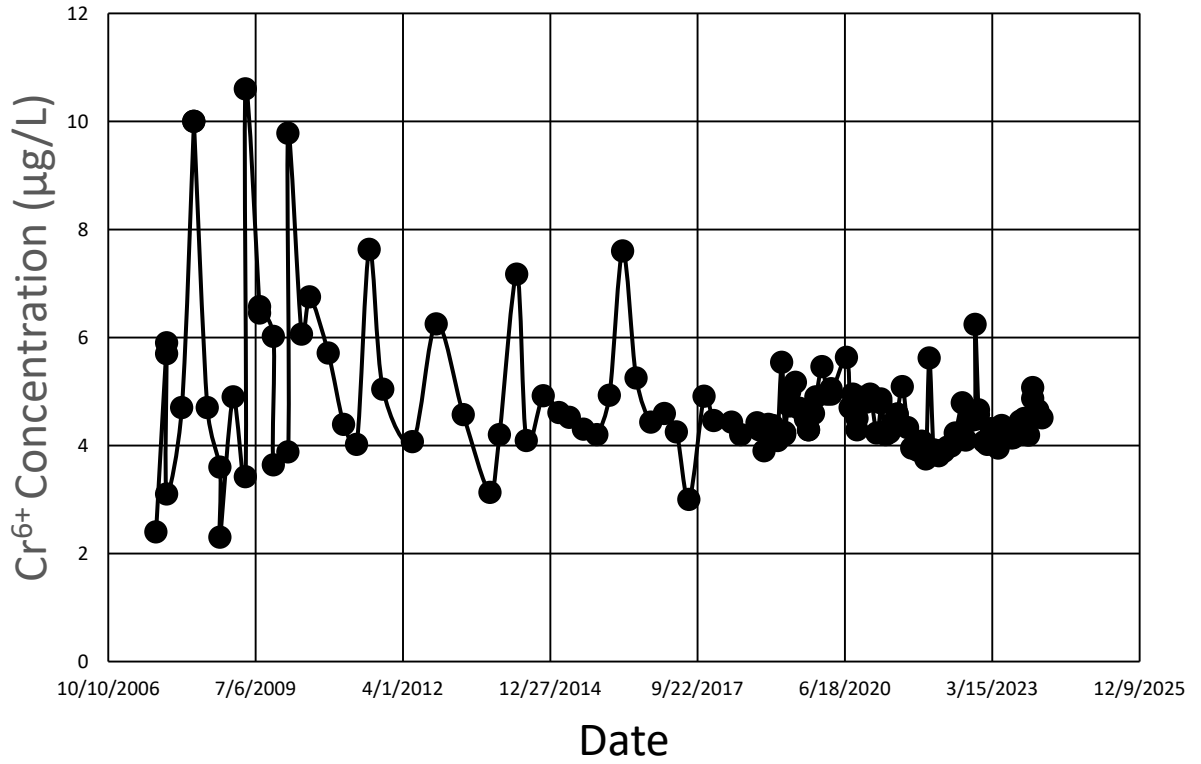


Figure 8. Cr<sup>6+</sup> concentration vs. date at R-35a.

# R-35b

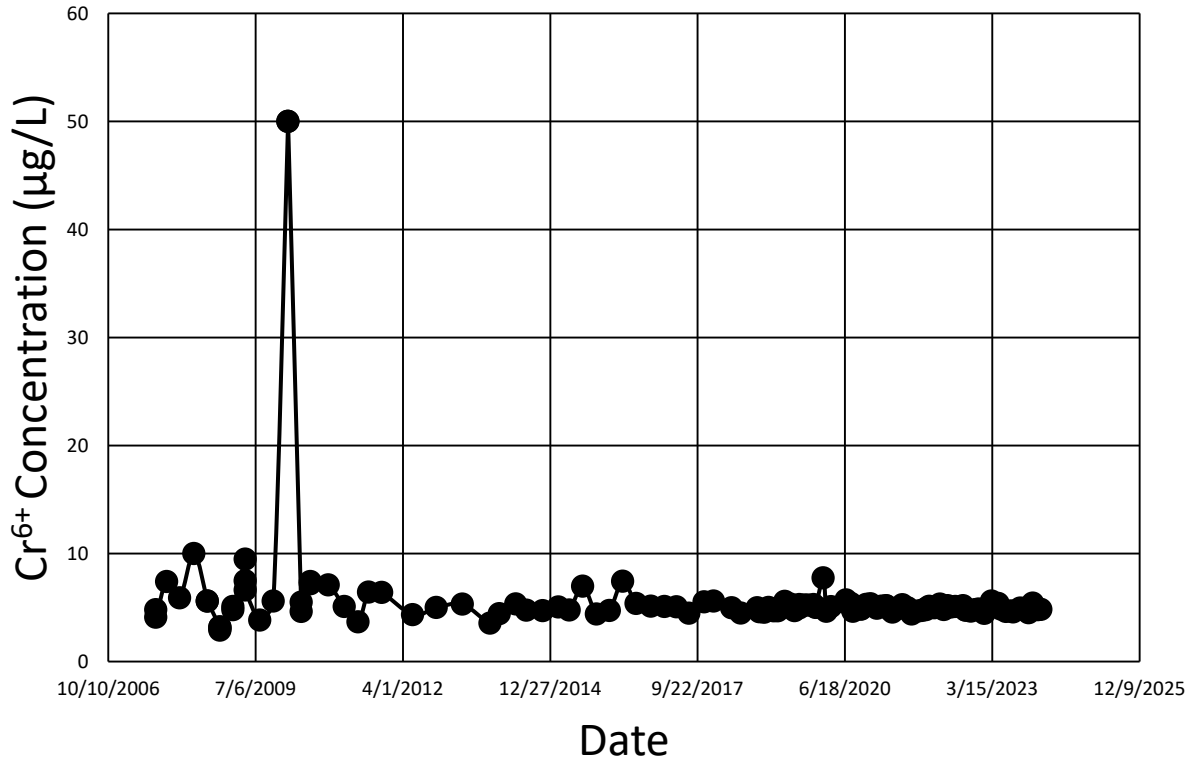


Figure 9. Cr<sup>6+</sup> concentration vs. date at R-35b.

# R-36

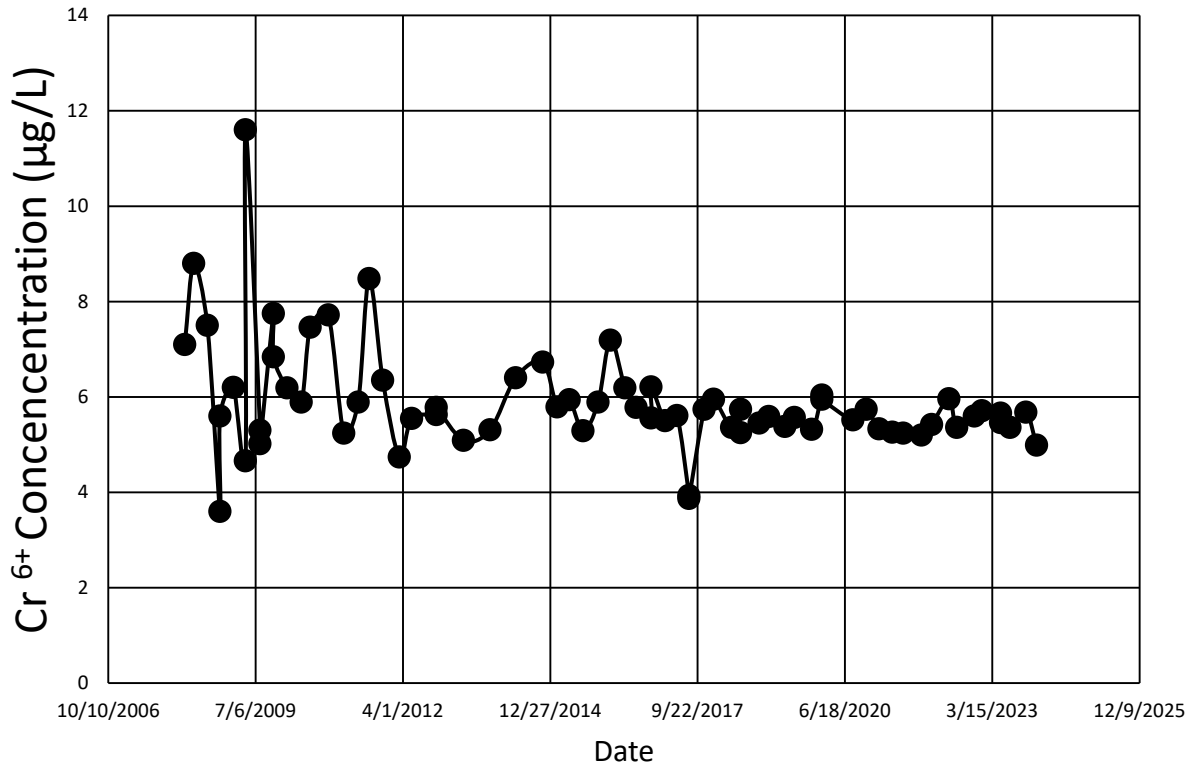


Figure 10. Cr<sup>6+</sup> concentration vs. date at R-36.

# R-42

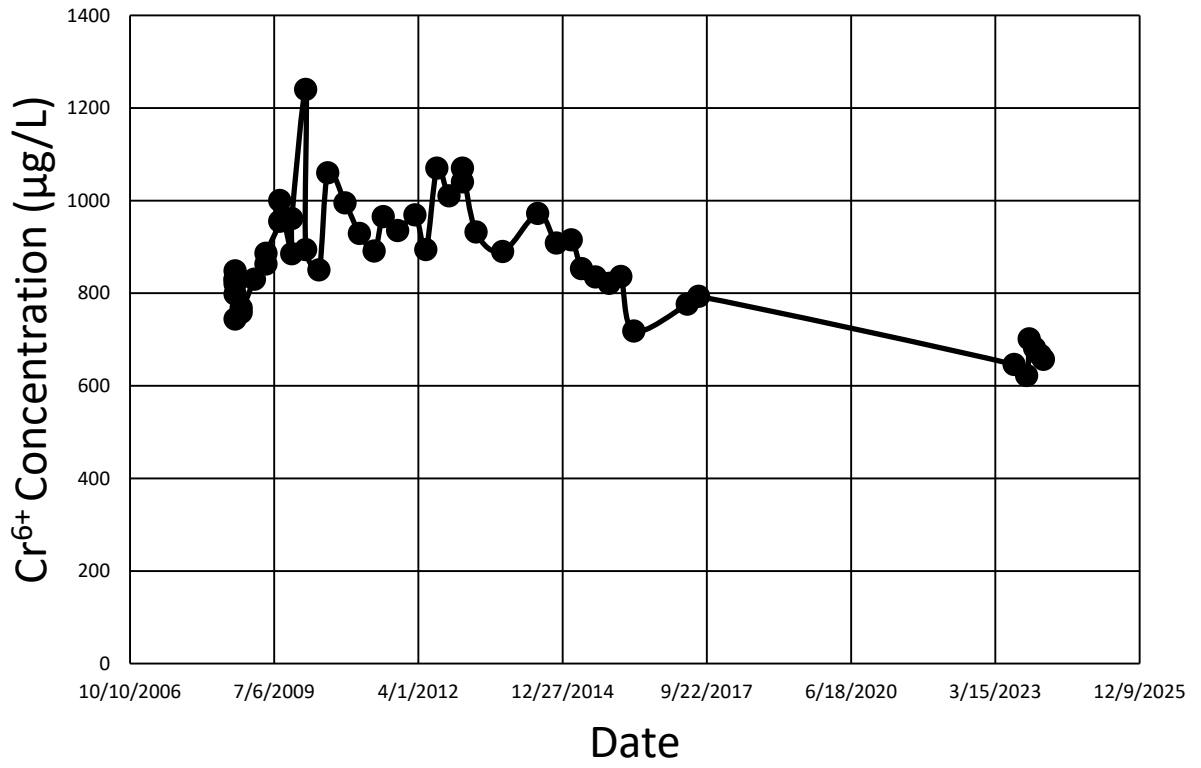


Figure 11a. All data for Cr<sup>6+</sup> concentration vs. date at R-42.

# R-42

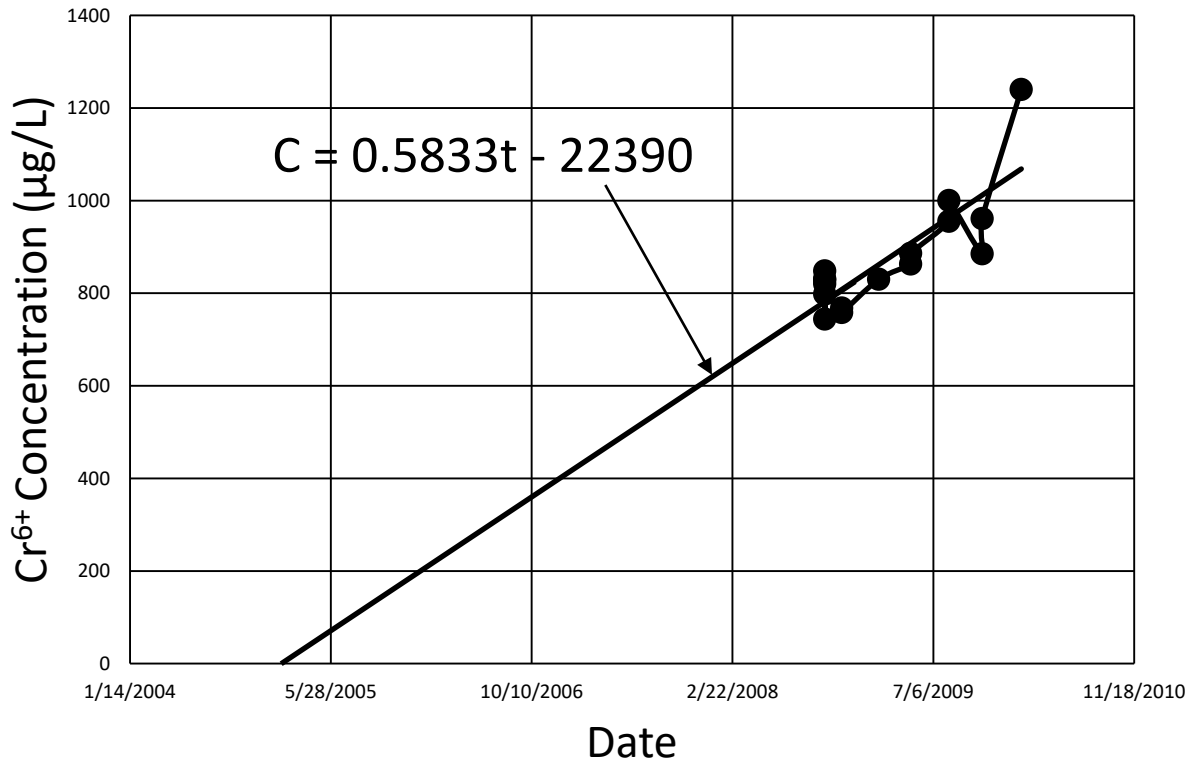


Figure 11b. Data till 2/10/2010 for  $Cr^{6+}$  concentration vs. date at R-42.

# R-43 S1

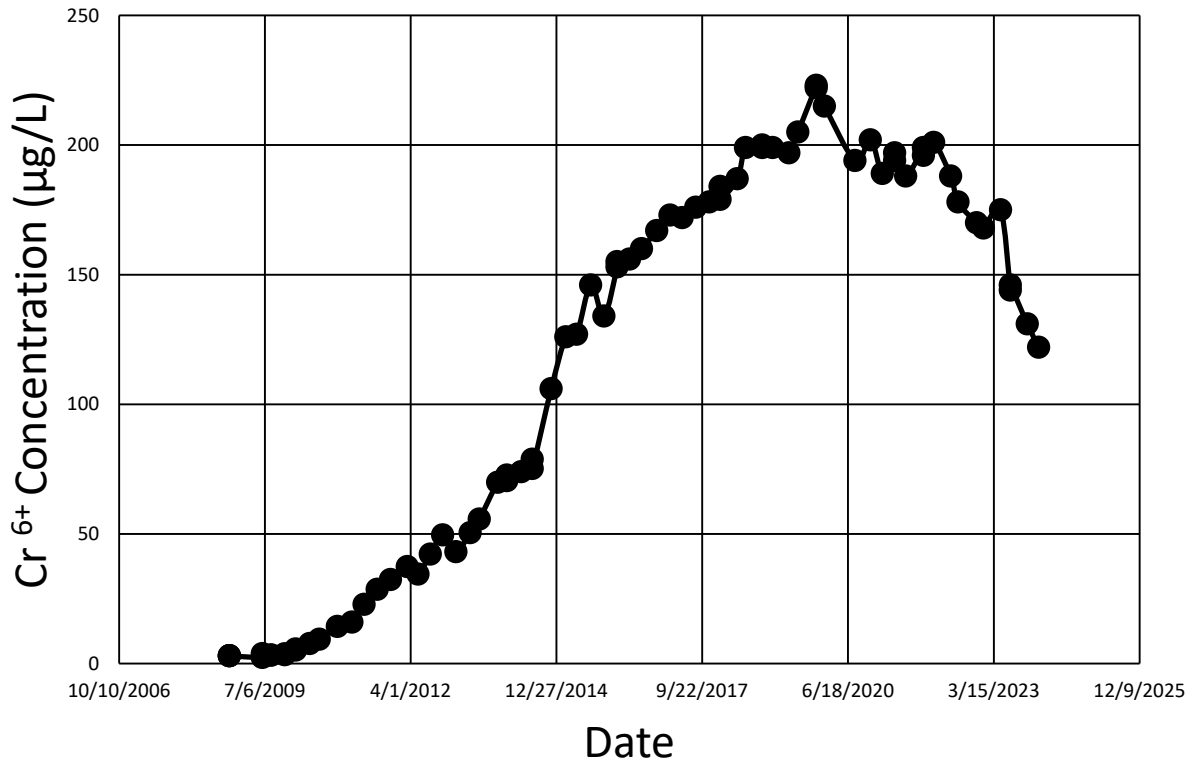


Figure 12a. Full data for  $Cr^{6+}$  concentration vs. date at R-43 S1.

# R-43 S1

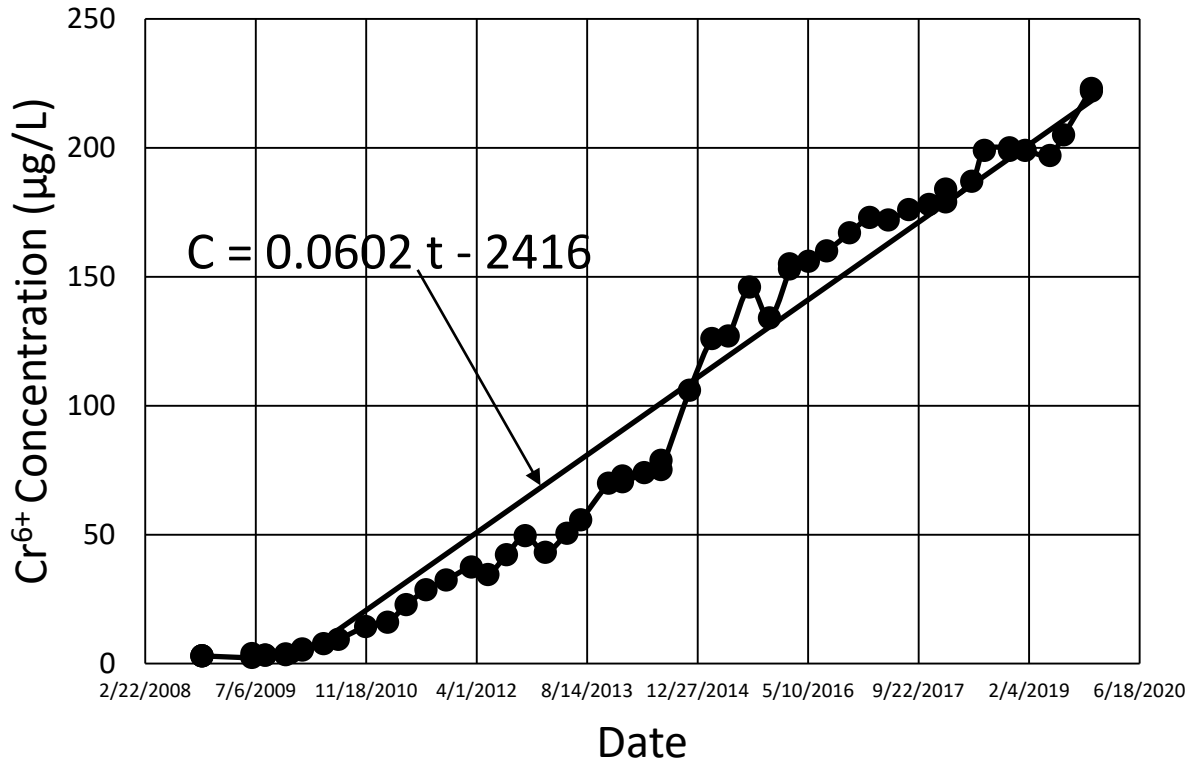


Figure 12b. Full data for  $Cr^{6+}$  concentration vs. date at R-43 S1 till April 11, 2022.

# R-43 S2

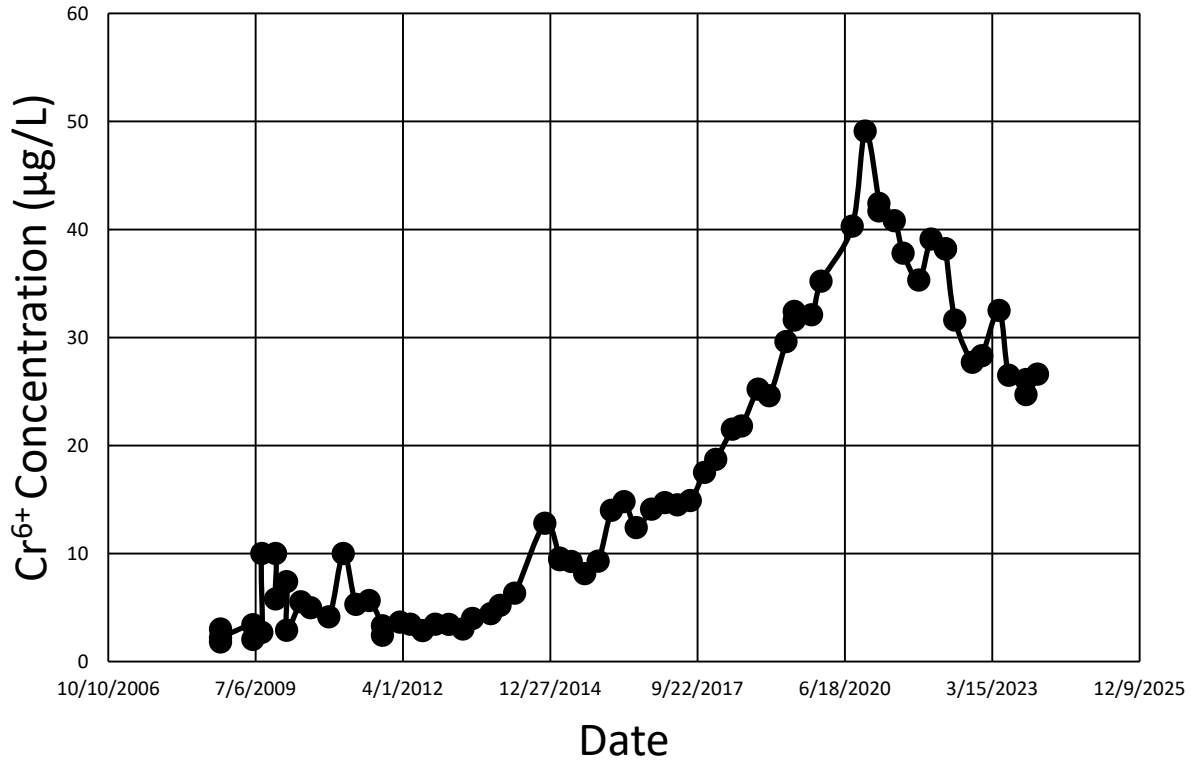


Figure 13a. Full data for  $Cr^{6+}$  concentration vs. date at R-43 S2.



## R-43 S2 - Reduced Cr<sup>6+</sup> Concentration Values

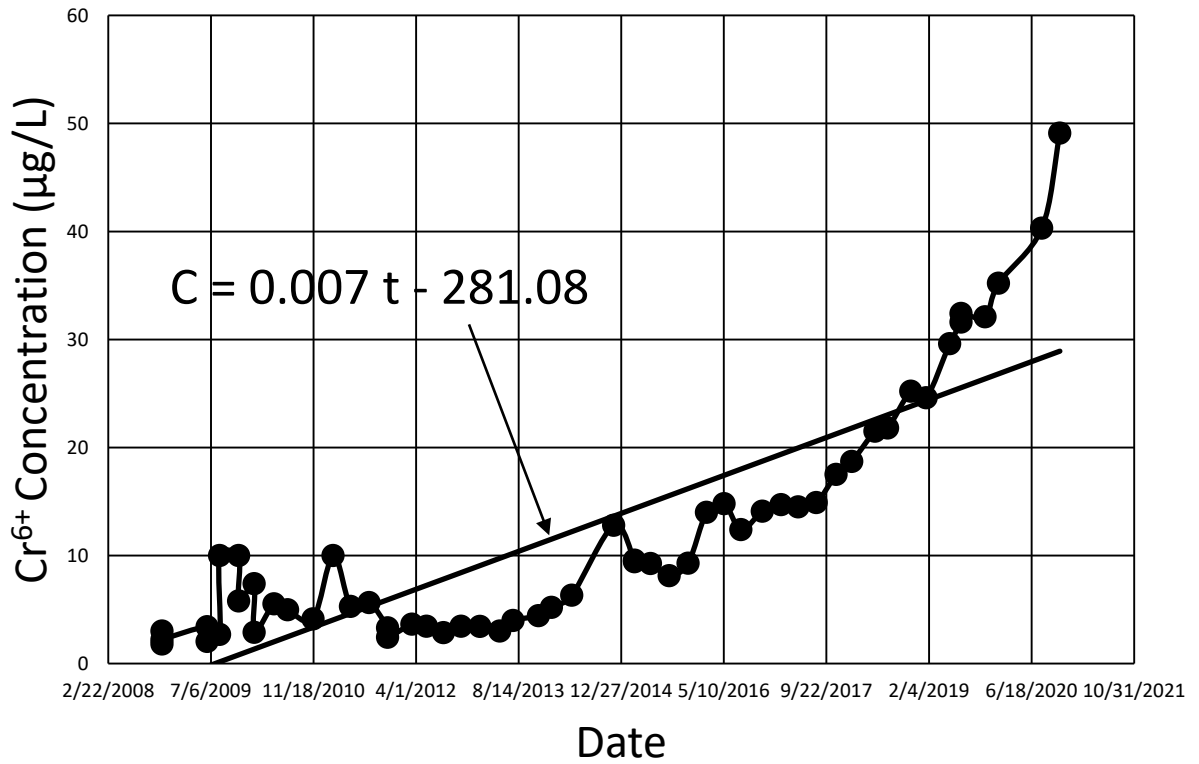
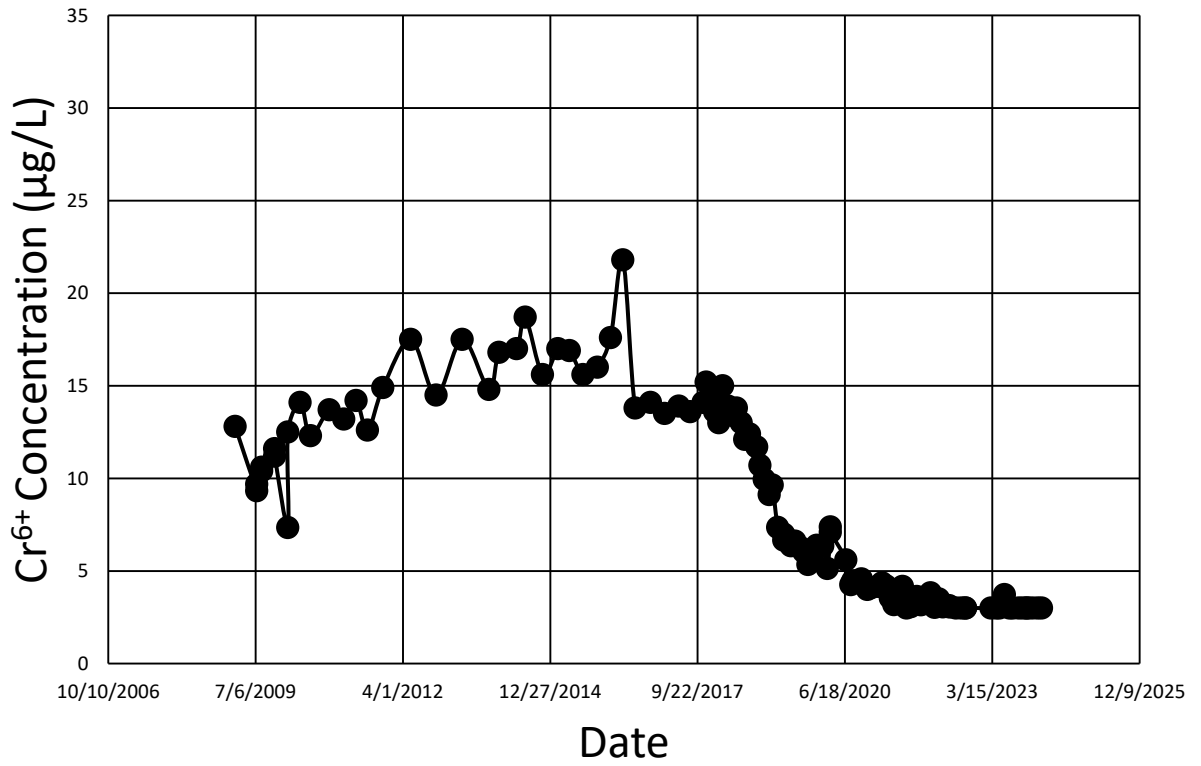


Figure 13b. Data till 11/31/2020 for Cr<sup>6+</sup> concentration vs. date at R-43 S2.

# R-44 S1





# R-45 S1

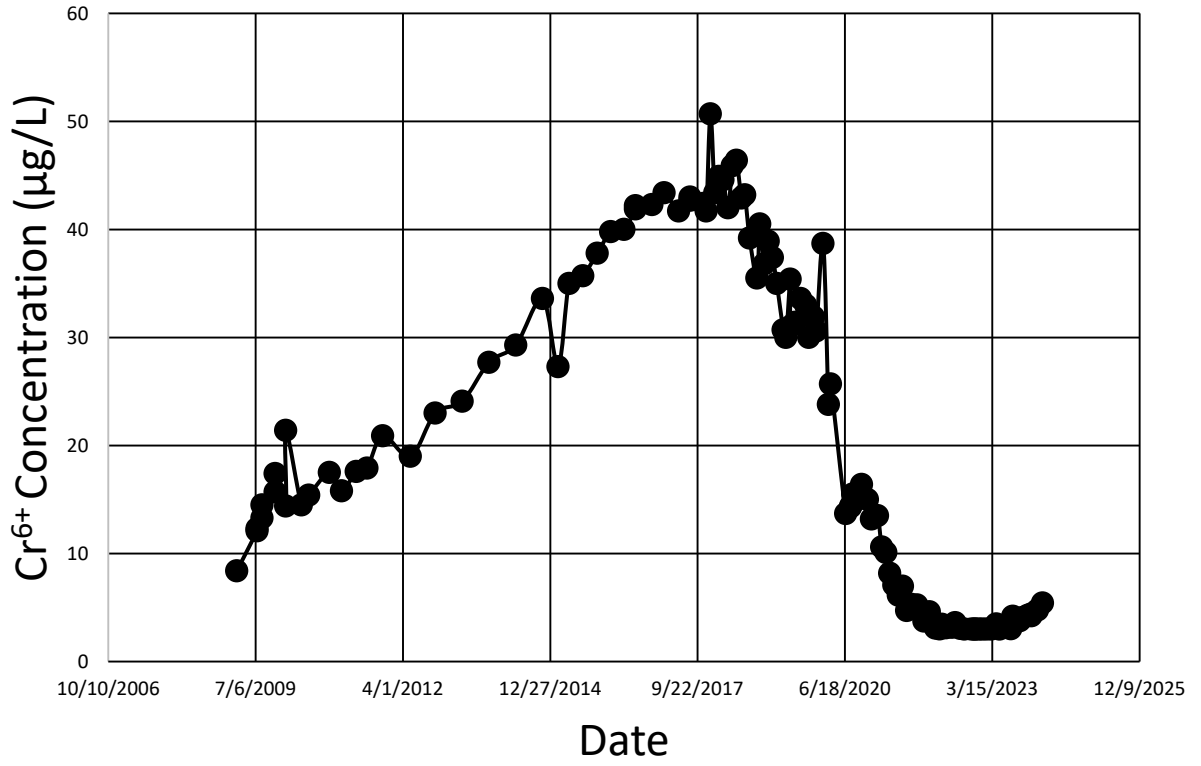


Figure 16. Cr<sup>6+</sup> concentration vs. date at R-45 S1.

# R-45 S2

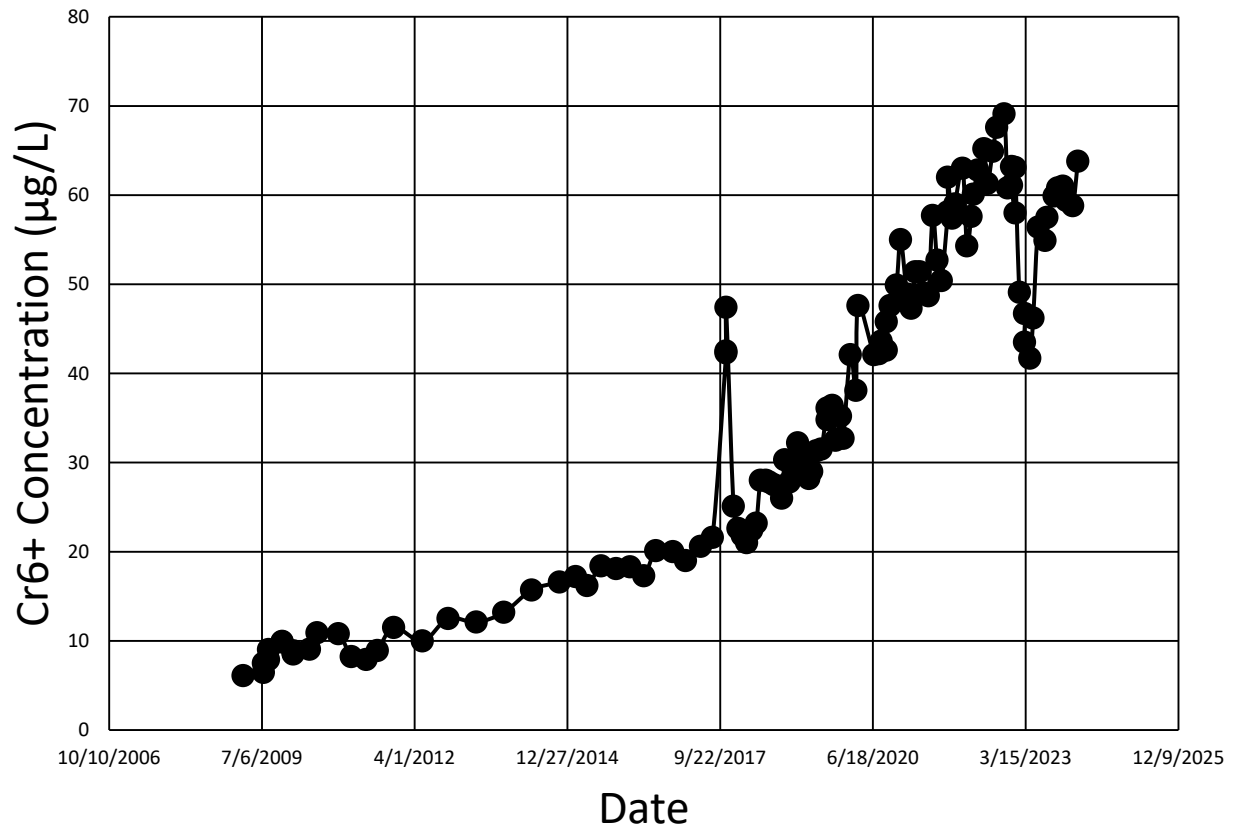


Figure 17.  $Cr^{6+}$  concentration vs. date at R-45 S2.

# R-50 S1

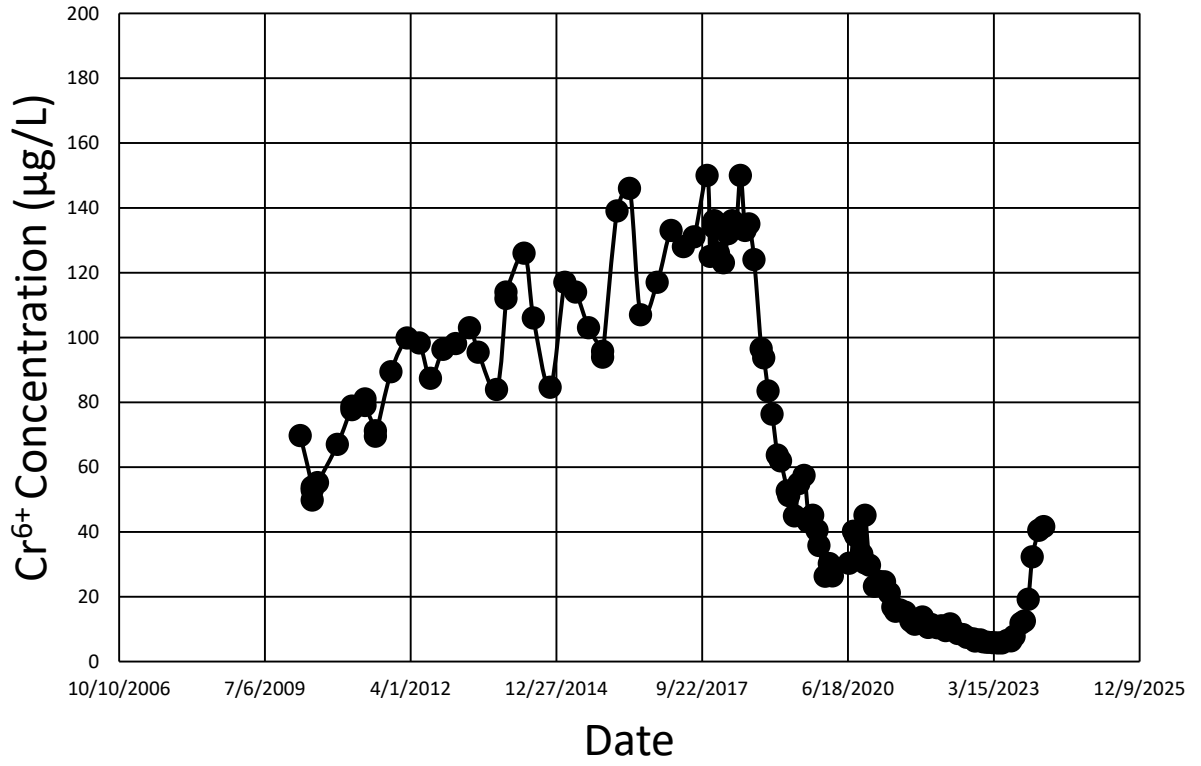
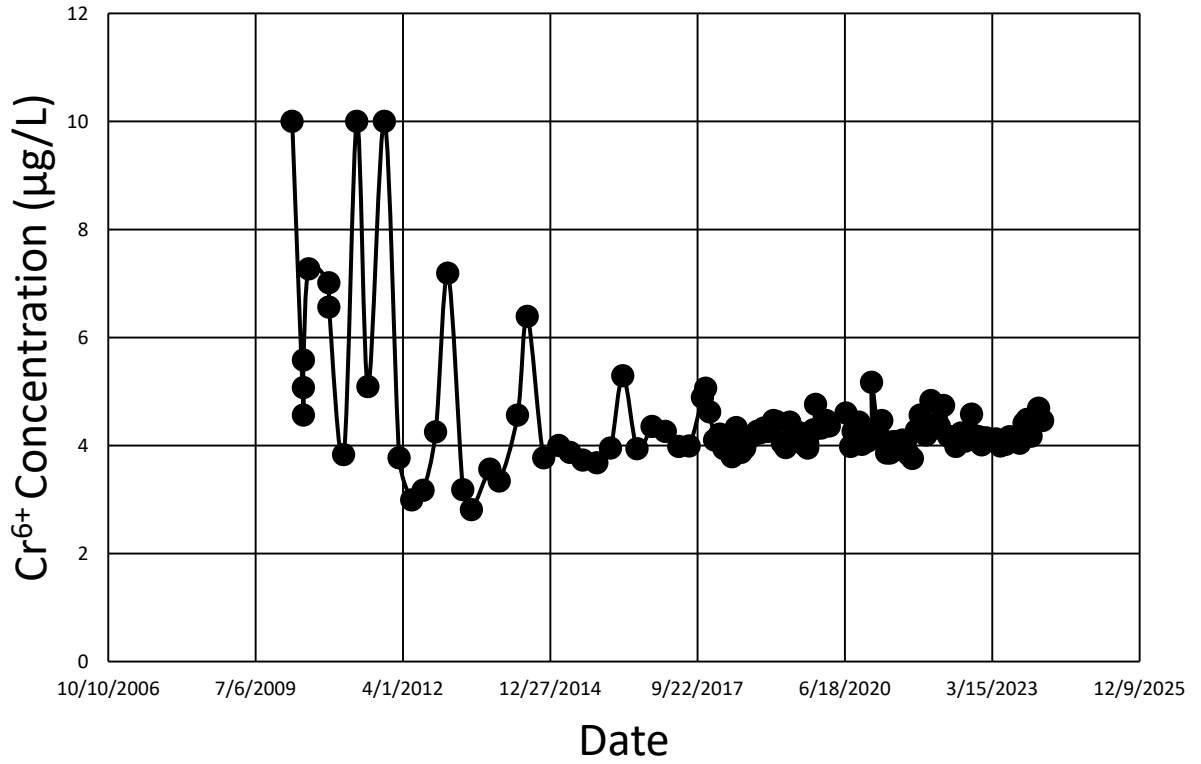


Figure 18. Cr<sup>6+</sup> concentration vs. date at R-50 S1.

# R-50 S2



# R-61 S1

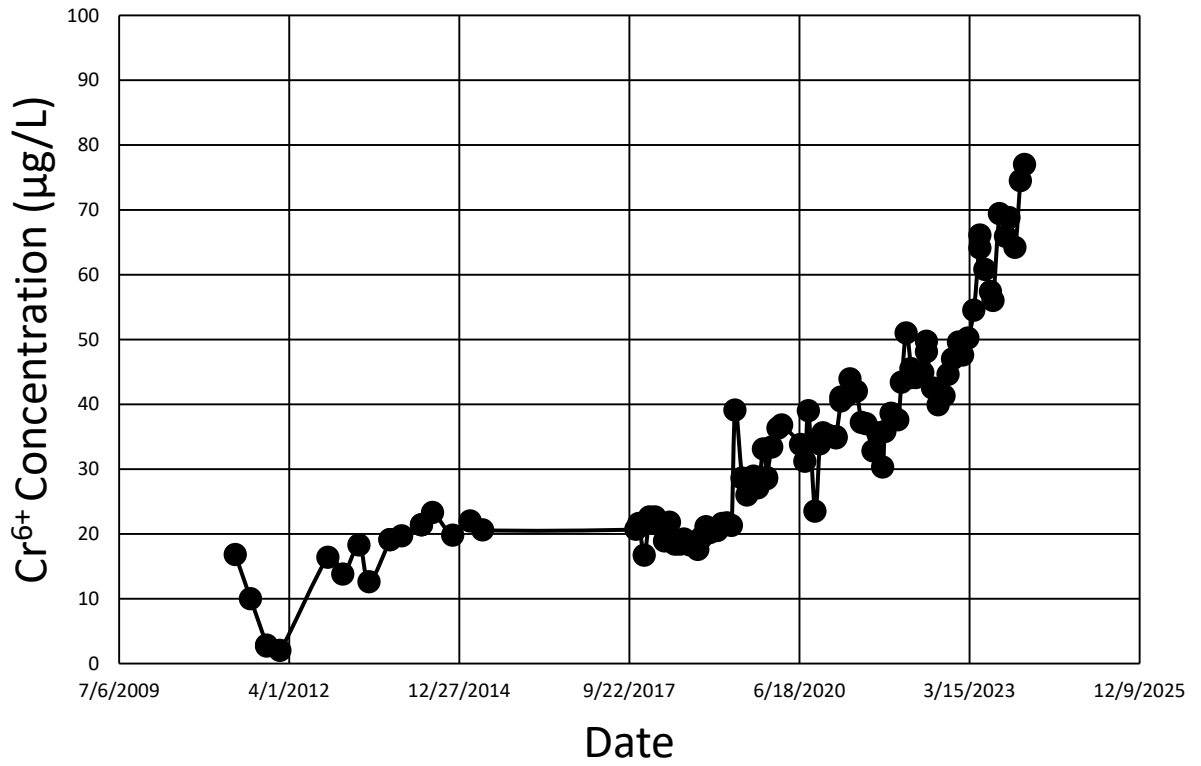


Figure 20. Cr<sup>6+</sup> concentration vs. date at R-61 S1.



# R-62

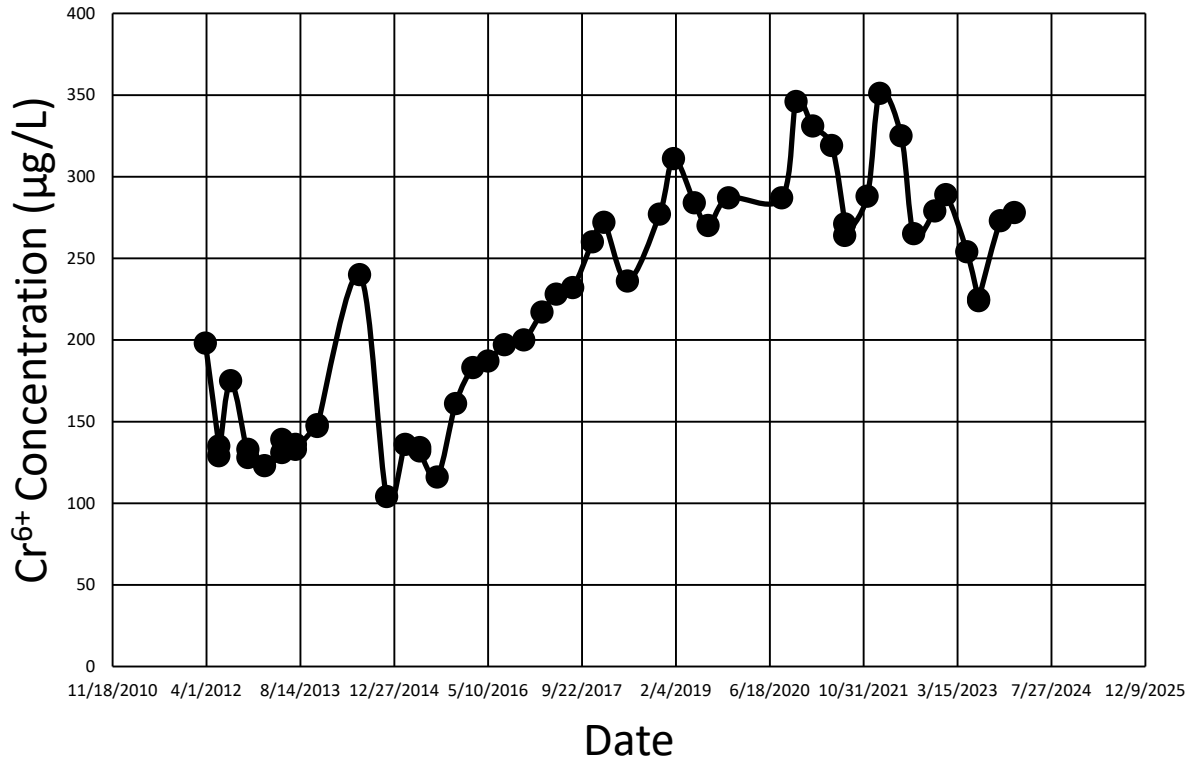


Figure 21a. Full data for  $Cr^{6+}$  concentration vs. date at R-62.

# R-62

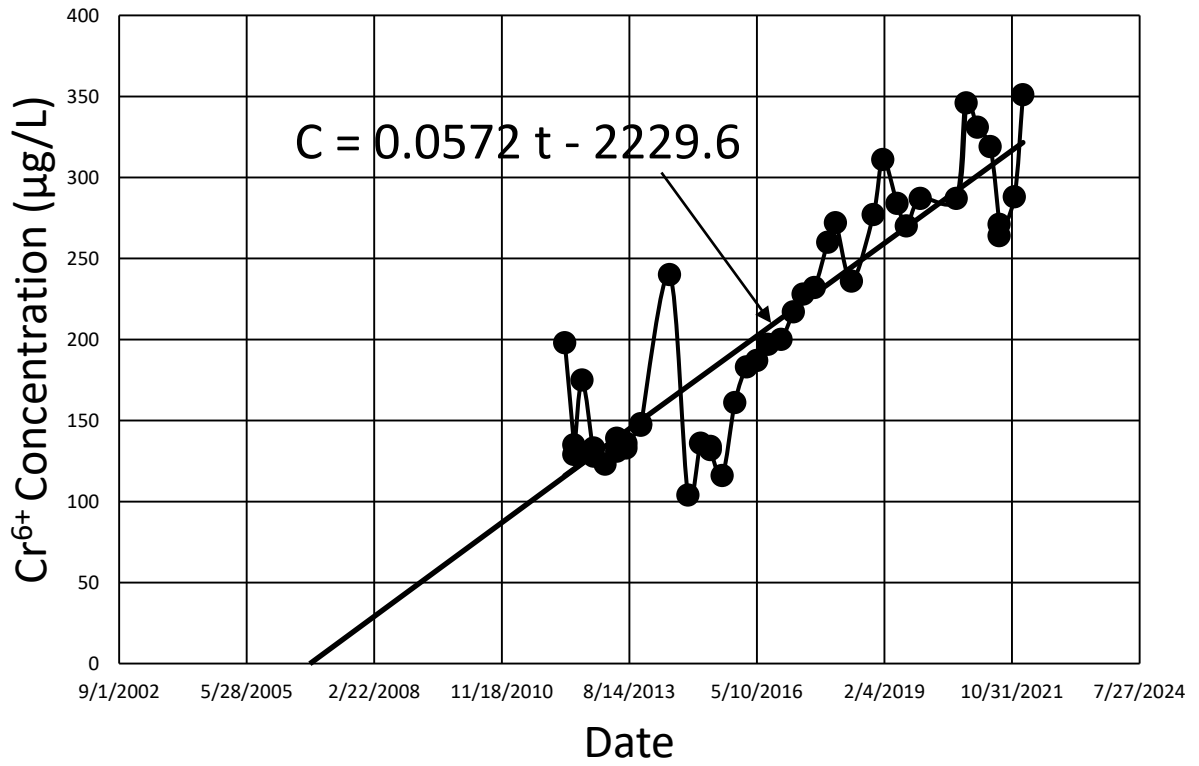


Figure 21b. Data till 1/25/2022 for Cr<sup>6+</sup> concentration vs. date at R-62.

# R-70 S1

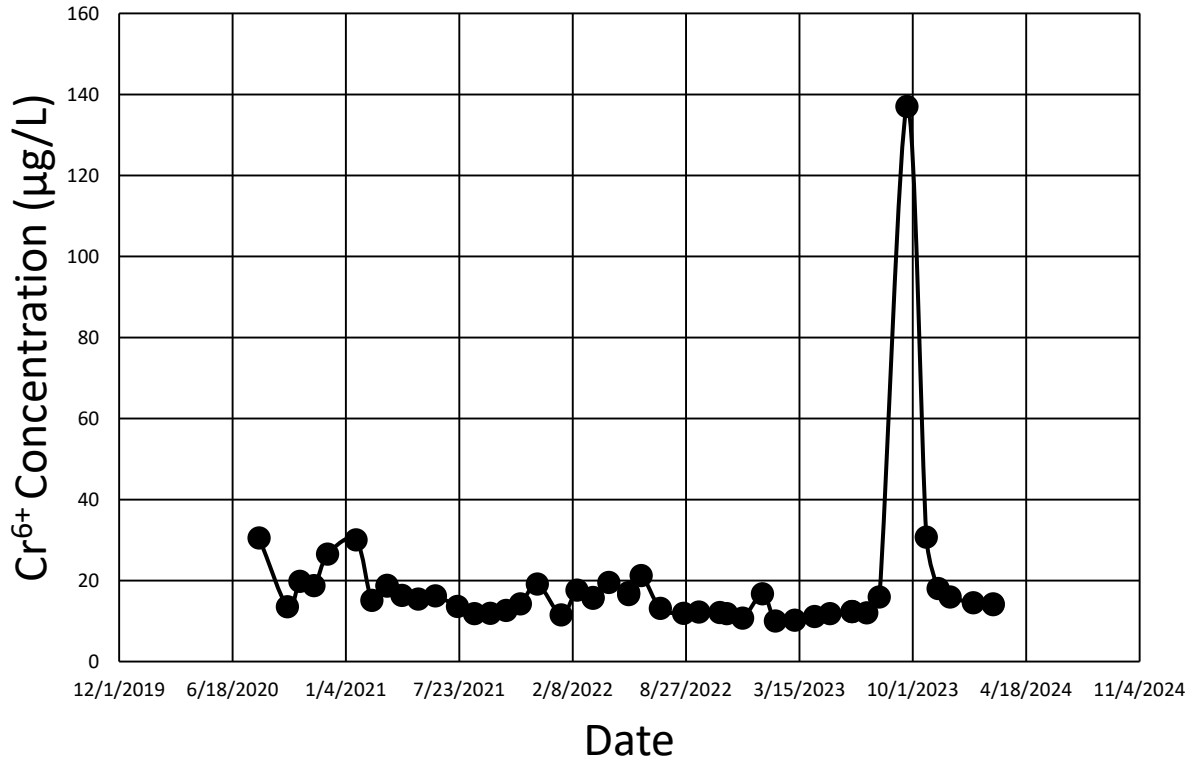


Figure 22.  $Cr^{6+}$  concentration vs. date at R-70 S1.

# R-70 S2

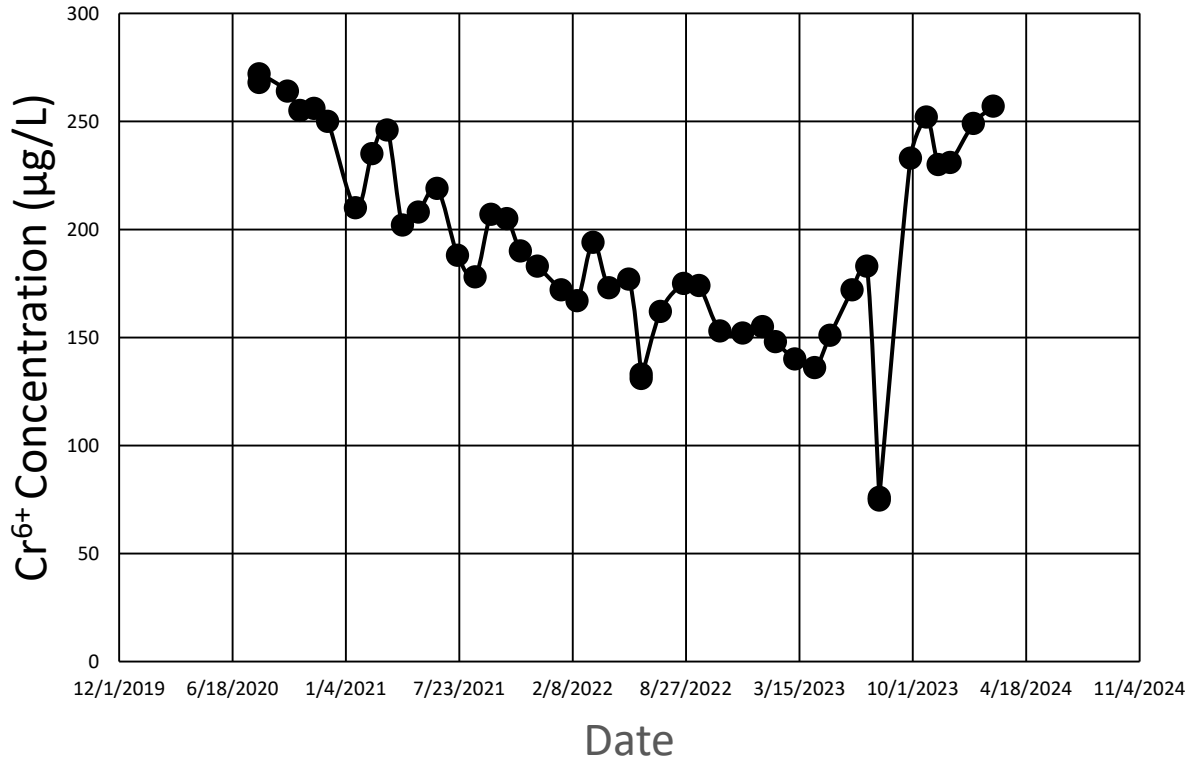


Figure 23. Cr<sup>6+</sup> concentration vs. date at R-70 S2.

# R-71 S1

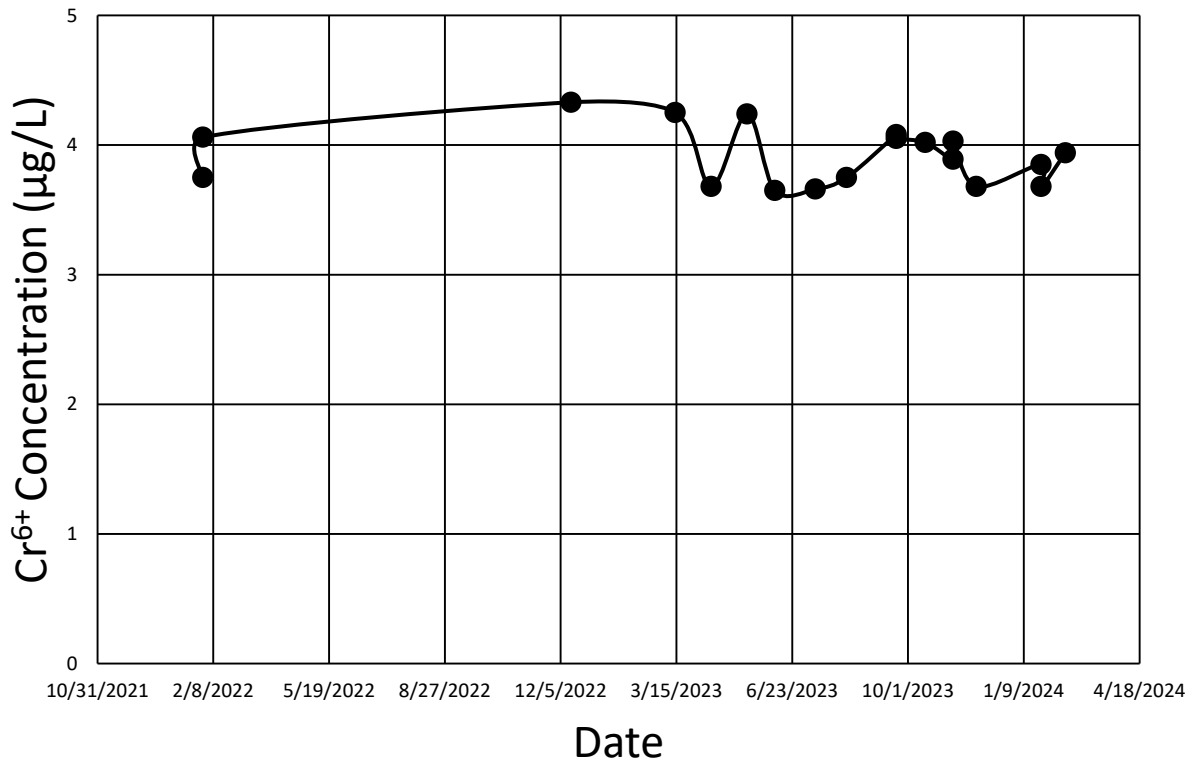


Figure 24. Cr<sup>6+</sup> concentration vs. date at R-71 S1.

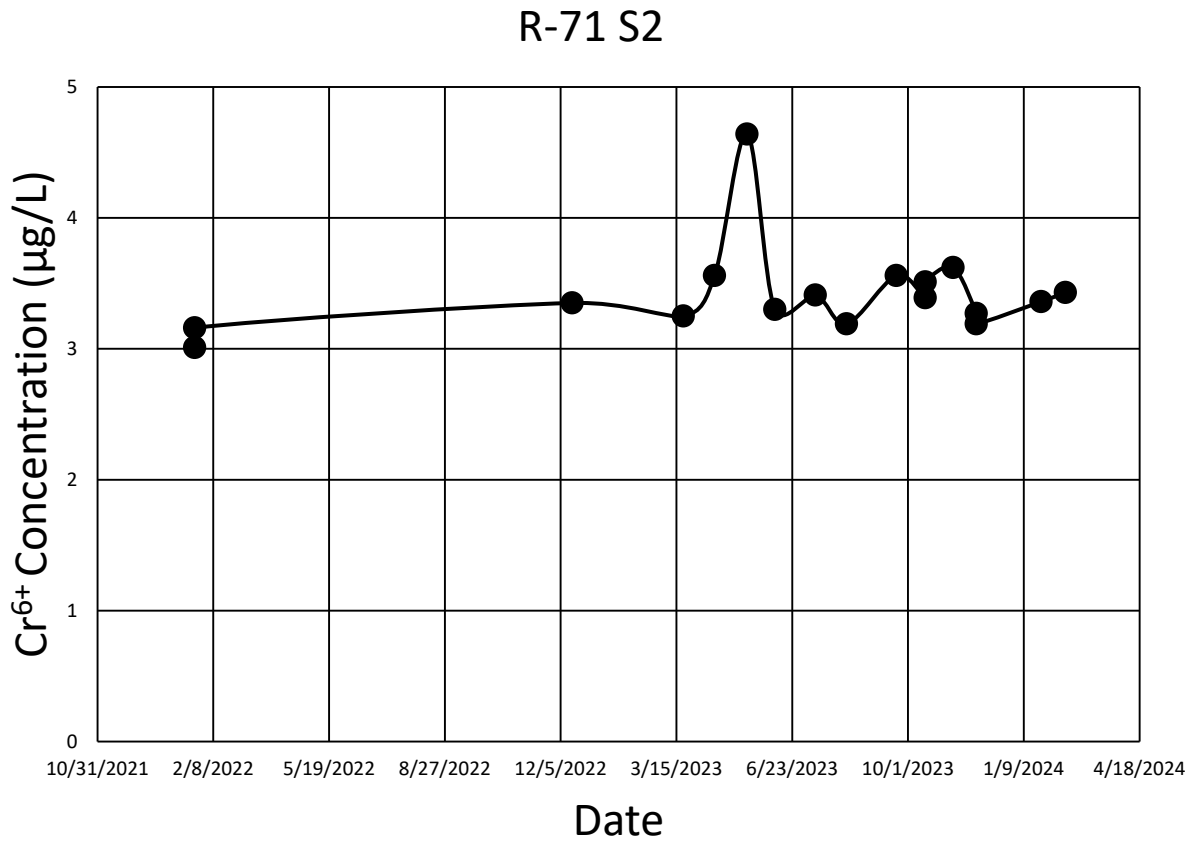


Figure 25.  $Cr^{6+}$  concentration vs. date at R-71 S2.

# R-72 S1

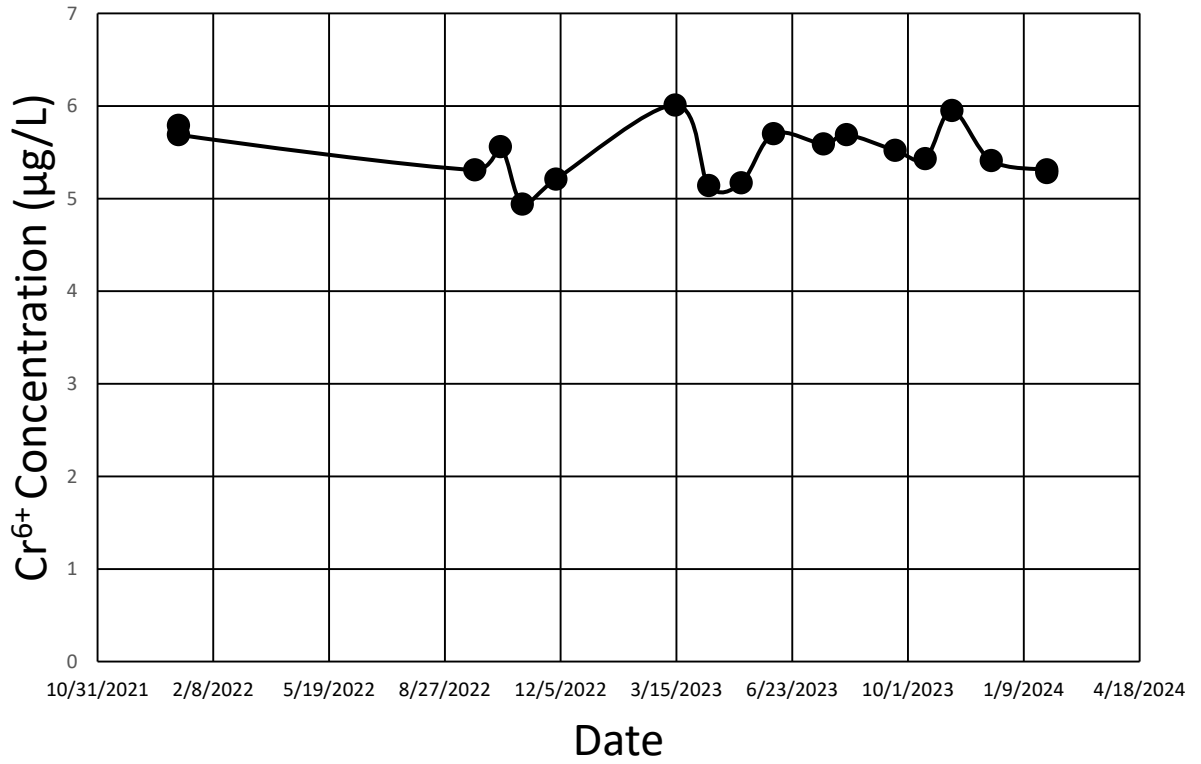


Figure 26. *Cr*<sup>6+</sup> concentration vs. date at R-72 S1.

# R-72 S2

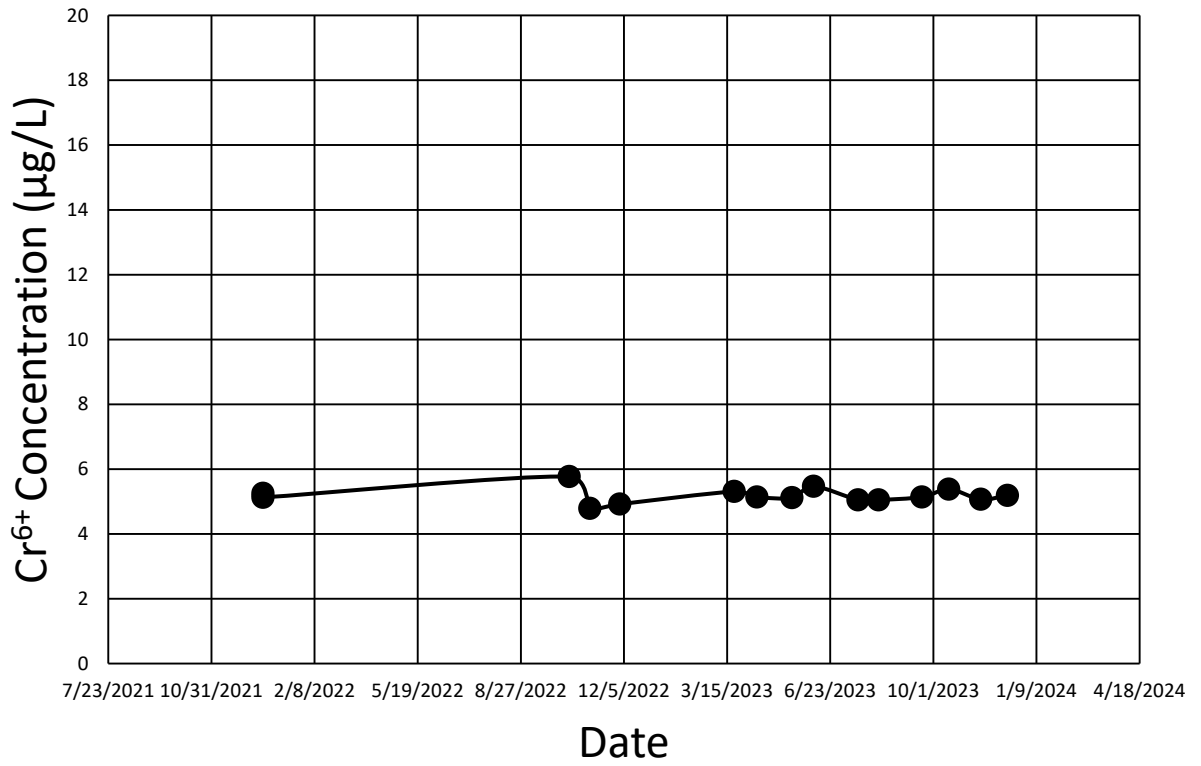


Figure 27.  $Cr^{6+}$  concentration vs. date at R-72 S2.



# SCI-1

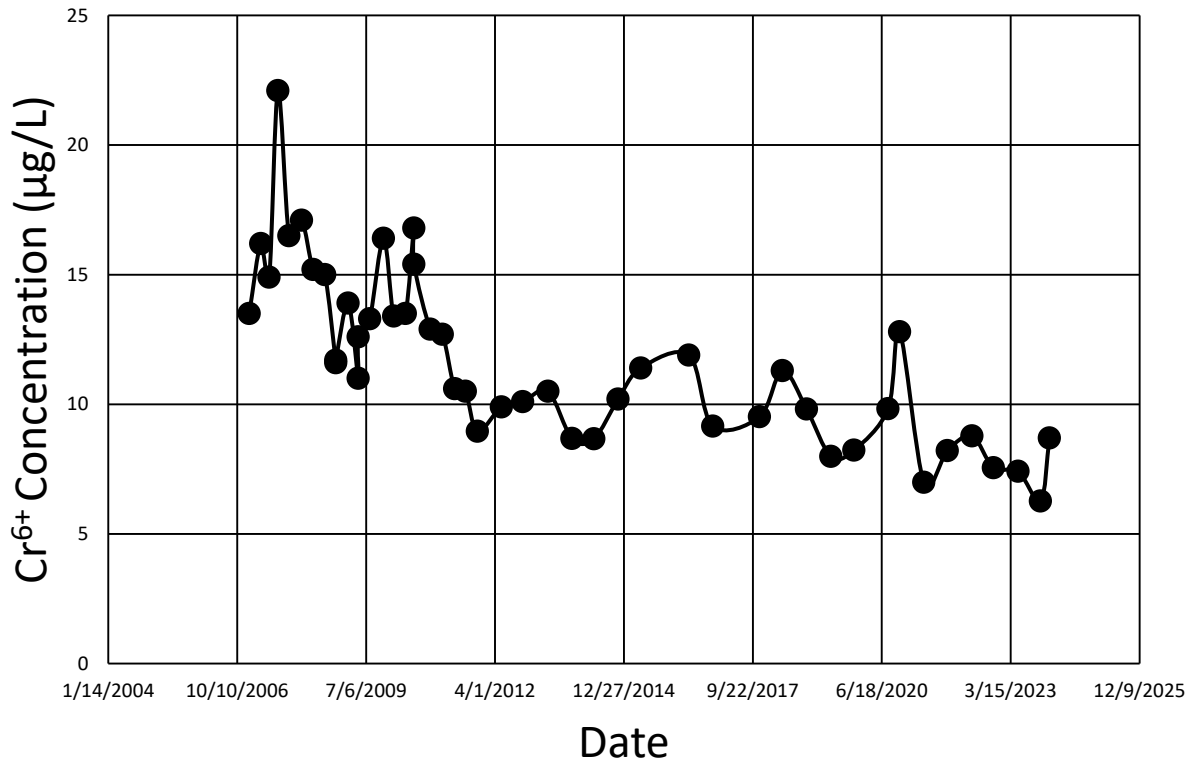


Figure 28. Cr<sup>6+</sup> concentration vs. date at SCI-1.

# SCI-2

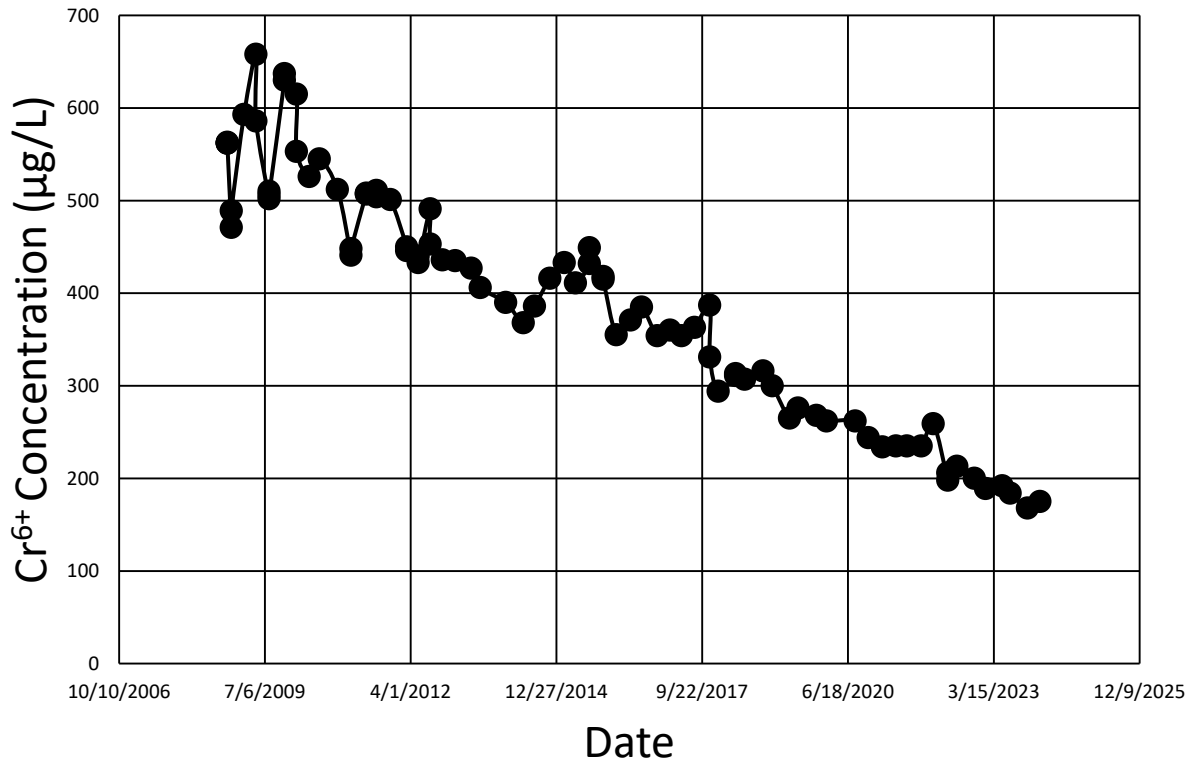


Figure 29. Cr<sup>6+</sup> concentration vs. date at SCI-2.

# SIMR-2

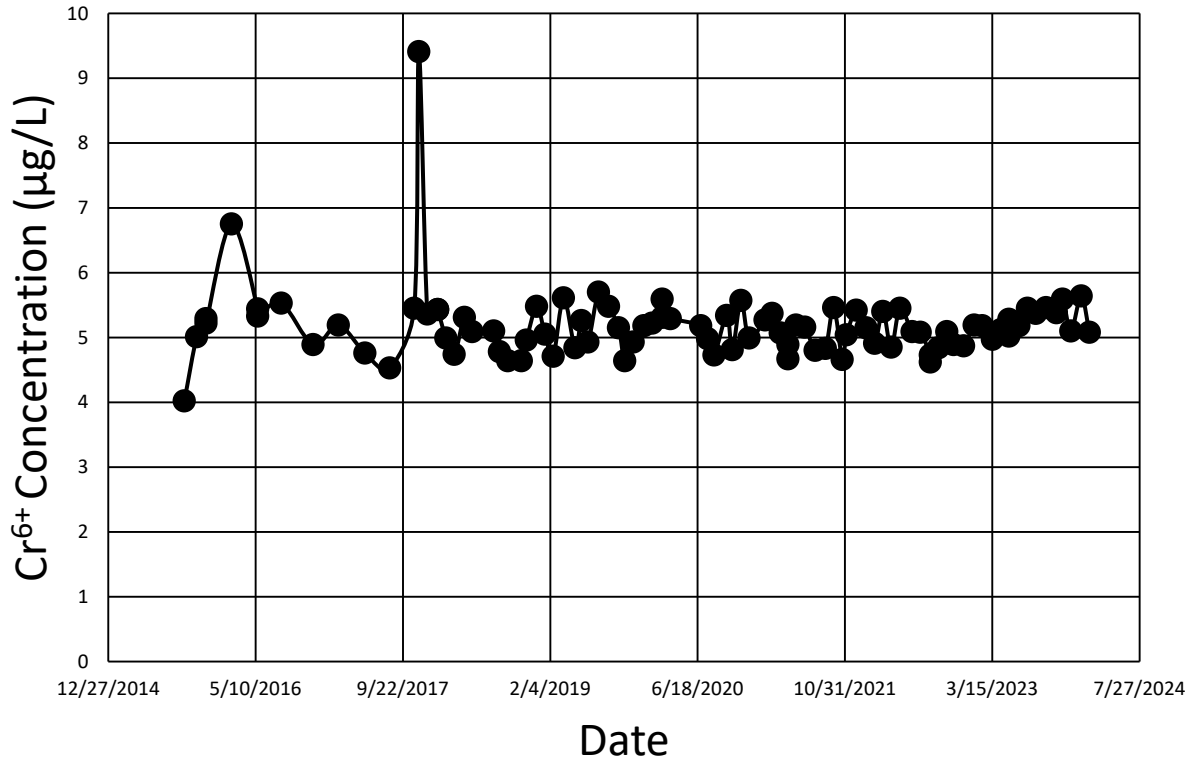


Figure 30. Cr<sup>6+</sup> concentration vs. date at SIMR-2.

# MCOI-5

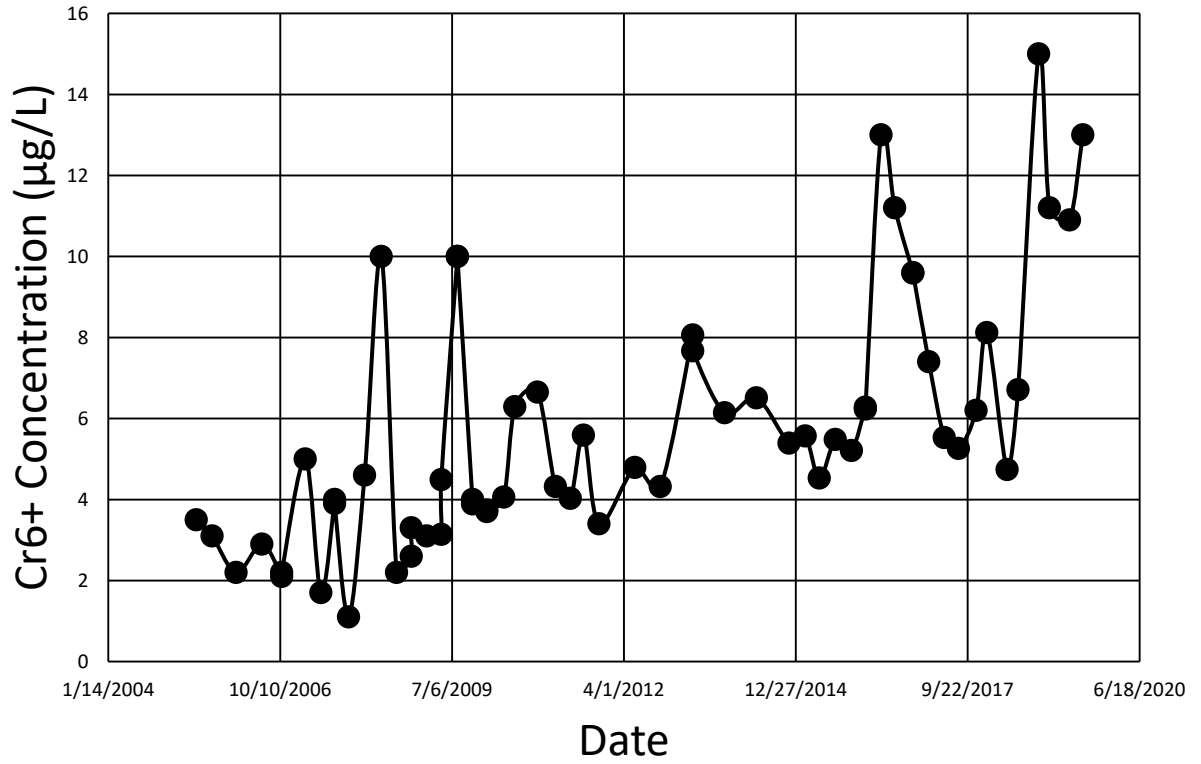


Figure 31. Cr<sup>6+</sup> concentration vs. date at MCOI-5.

# MCOI-6

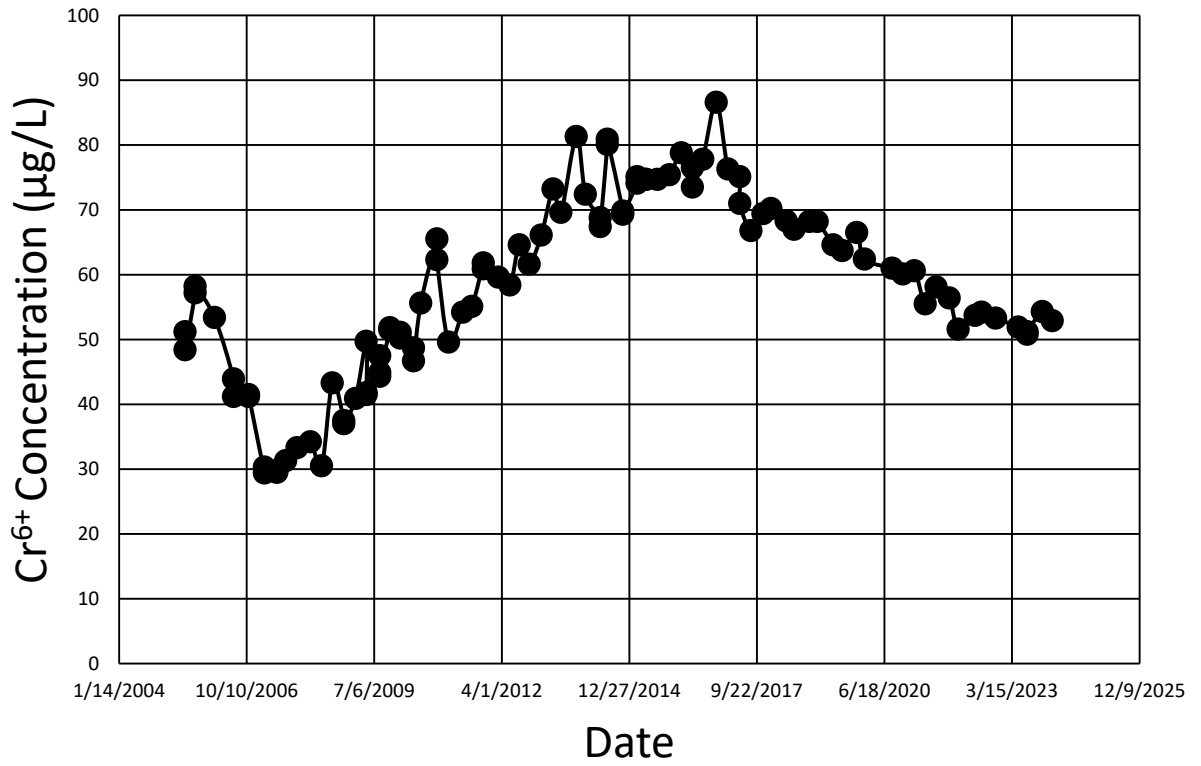


Figure 32. Cr<sup>6+</sup> concentration vs. date at MCOI-6.

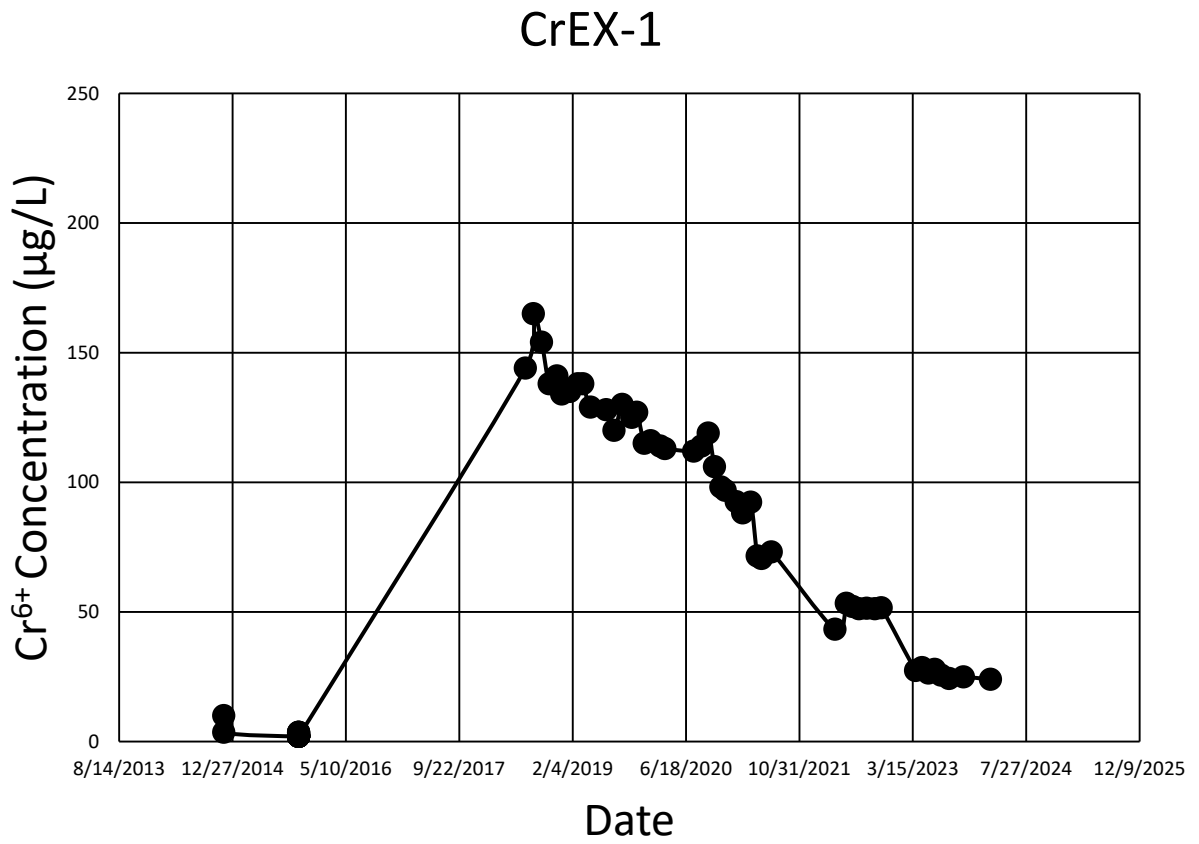


Figure 33.  $Cr^{6+}$  concentration vs. date at CrEX-1.

# CrEX-2

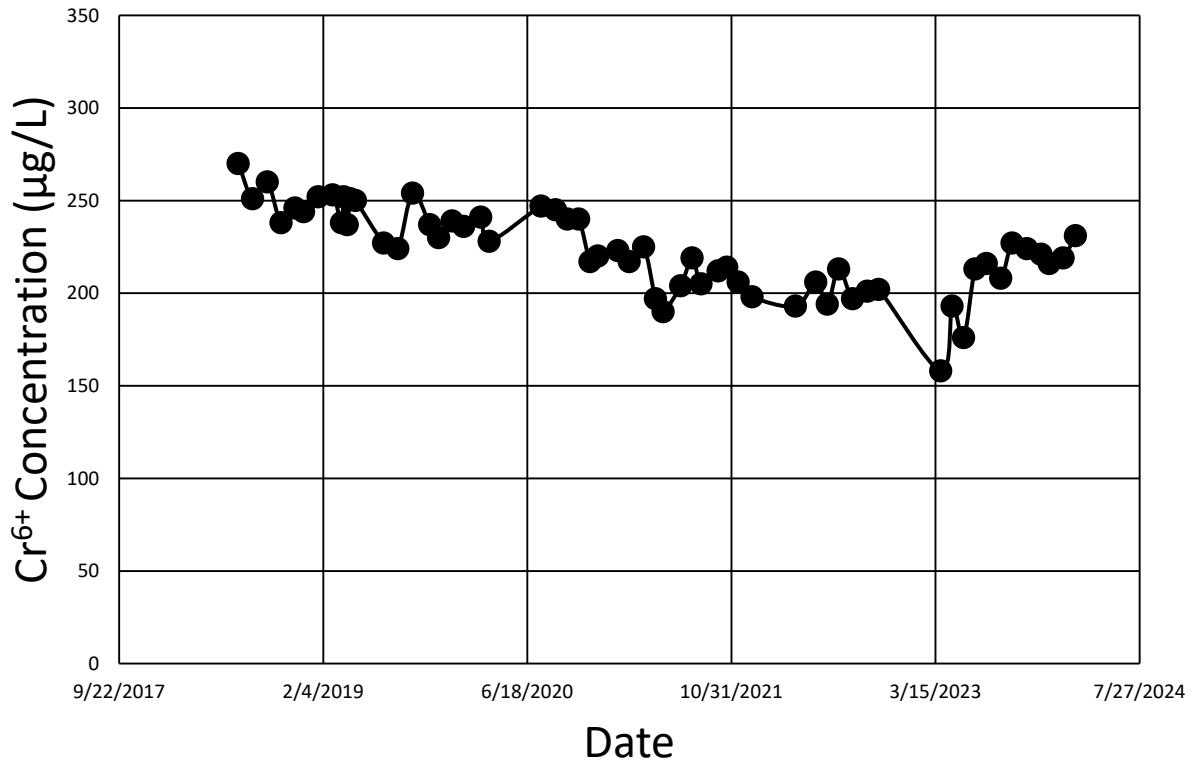


Figure 34. Cr<sup>6+</sup> concentration vs. date at CrEX-2.

### CrEX-3

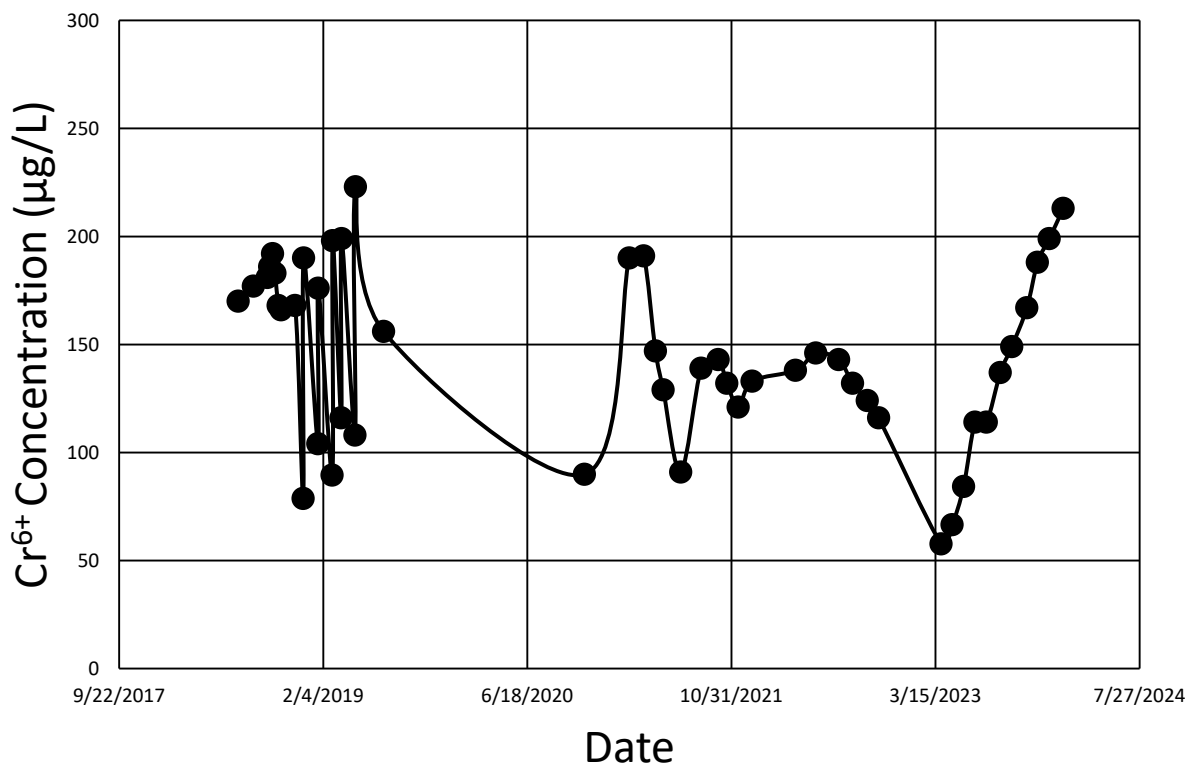


Figure 35.  $Cr^{6+}$  concentration vs. date at CrEX-3.



# CrEX-4

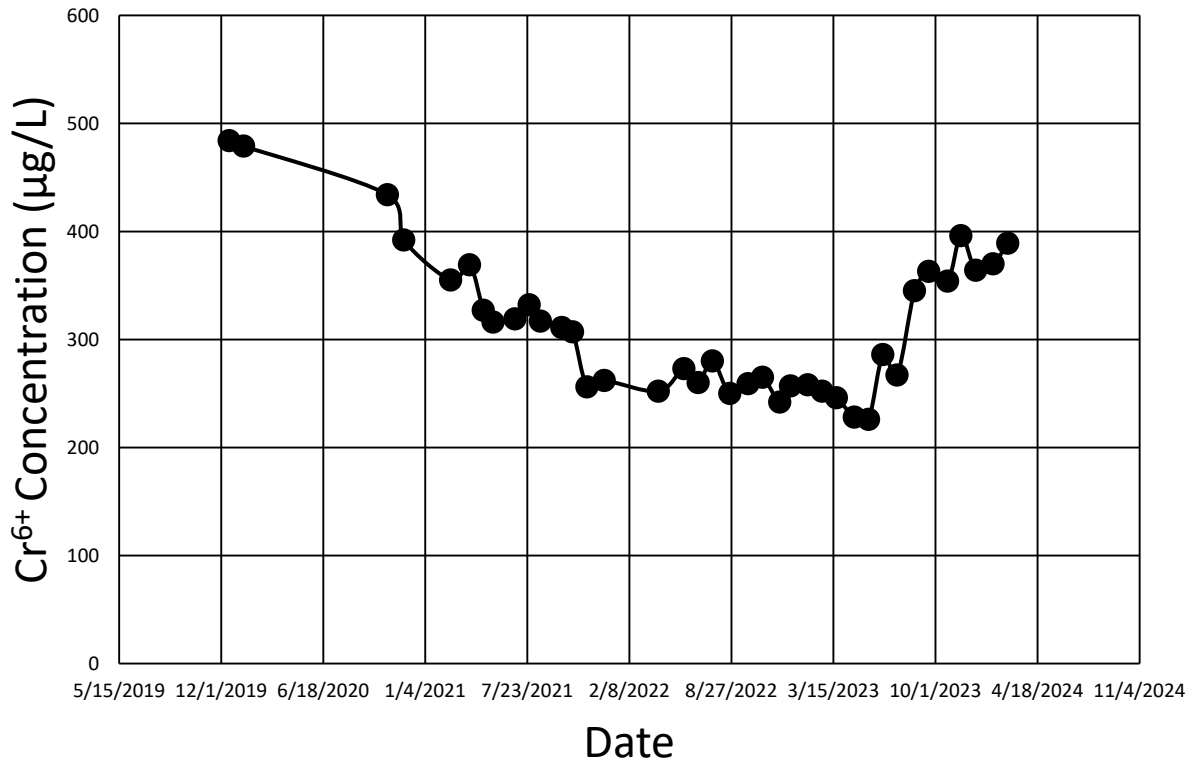


Figure 36.  $Cr^{6+}$  concentration vs. date at CrEX-4.

# CrEX-5

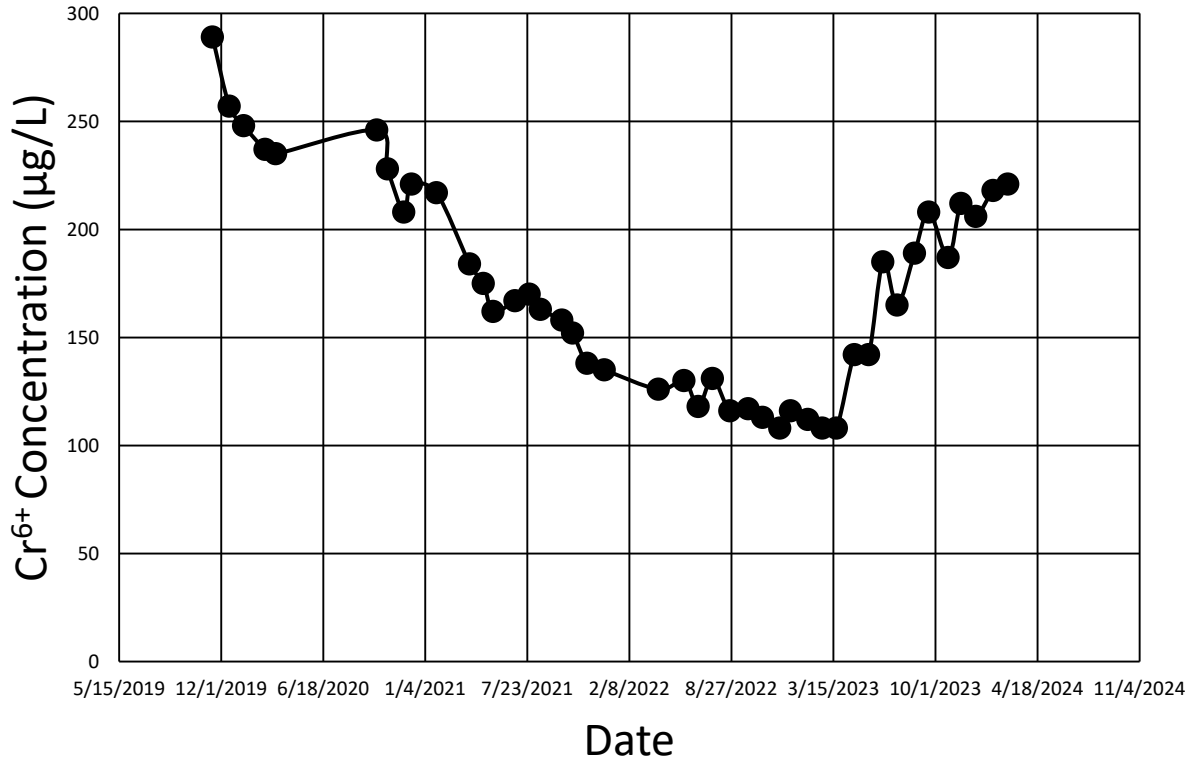


Figure 37. Cr<sup>6+</sup> concentration vs. date at CrEX-5.



# CrIN-2

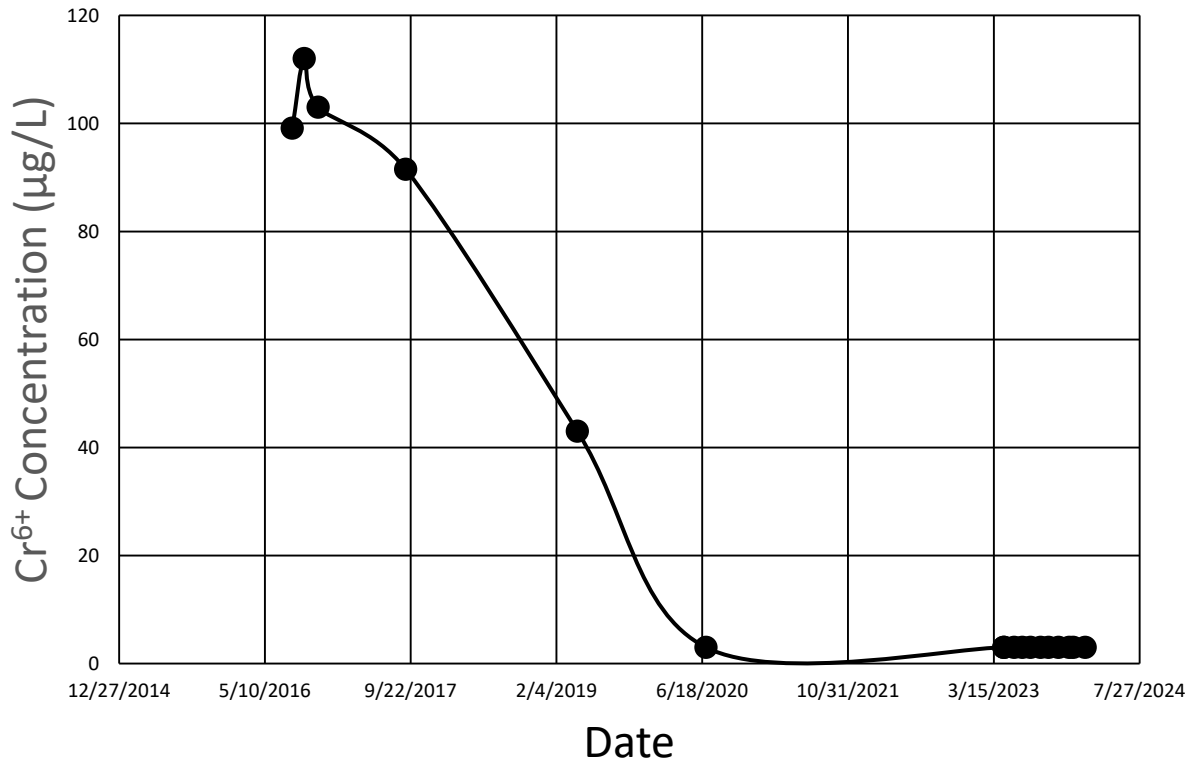


Figure 39.  $Cr^{6+}$  concentration vs. date at CrIN-2.

# CrIN-3

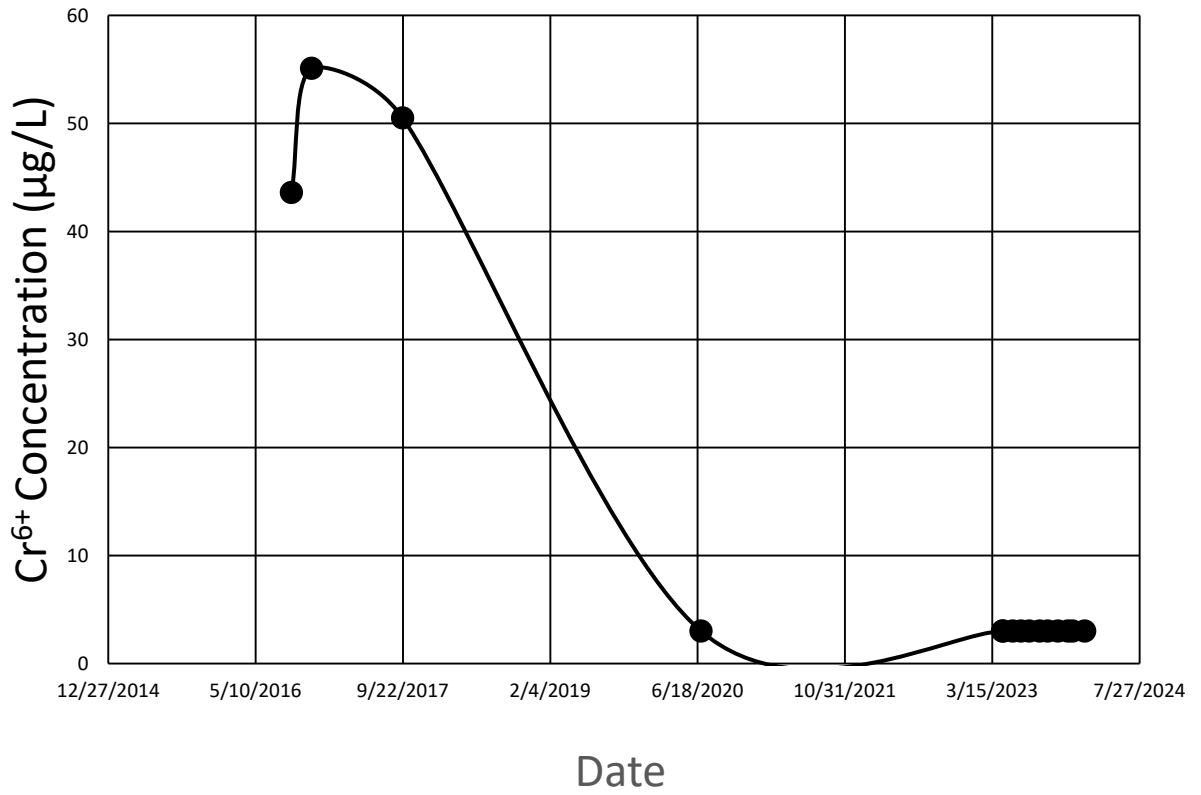


Figure 40.  $Cr^{6+}$  concentration vs. date at CrIN-3.

# CrIN-4

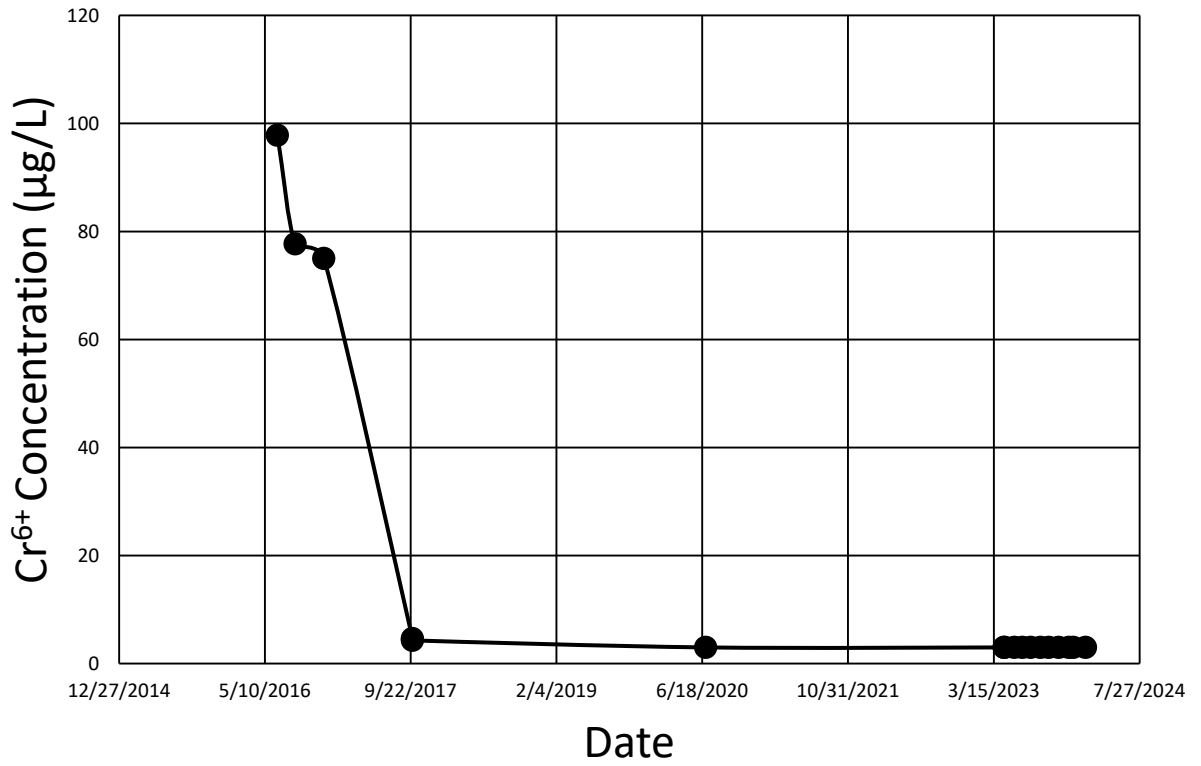


Figure 41.  $Cr^{6+}$  concentration vs. date at CrIN-4.

# CrIN-5

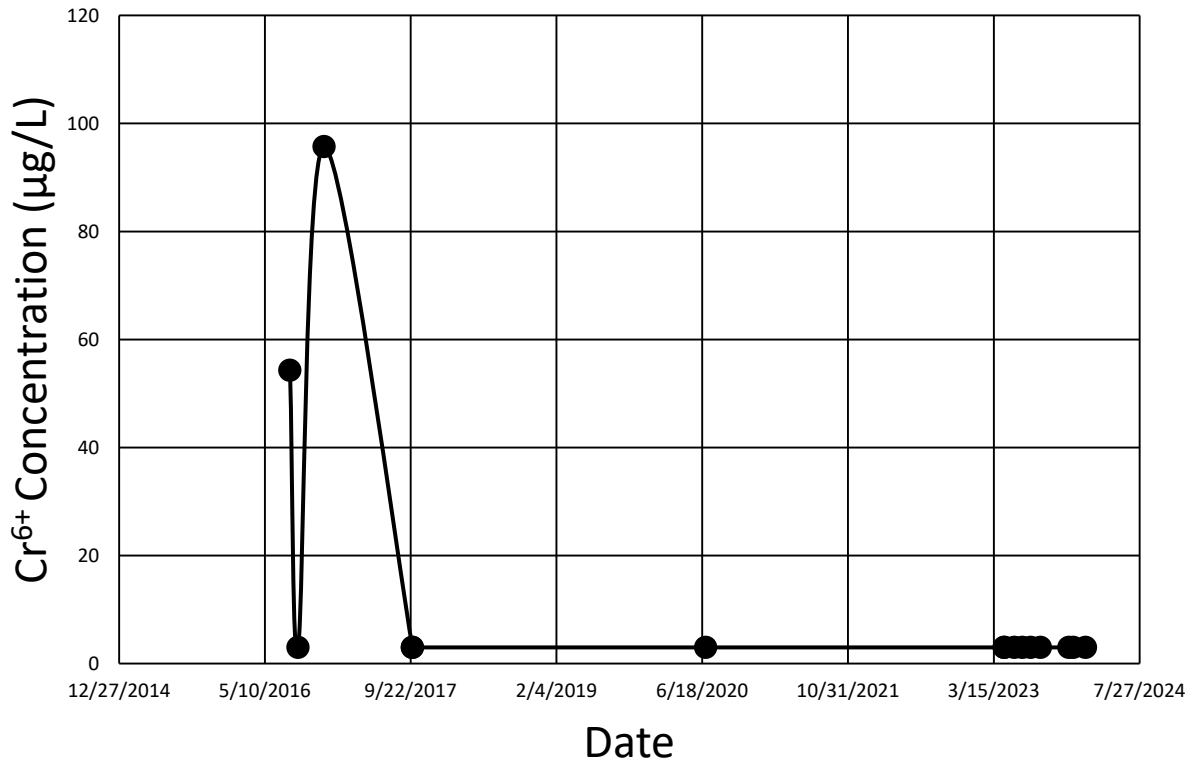


Figure 42.  $Cr^{6+}$  concentration vs. date at CrIN-5.

# CrPZ-1

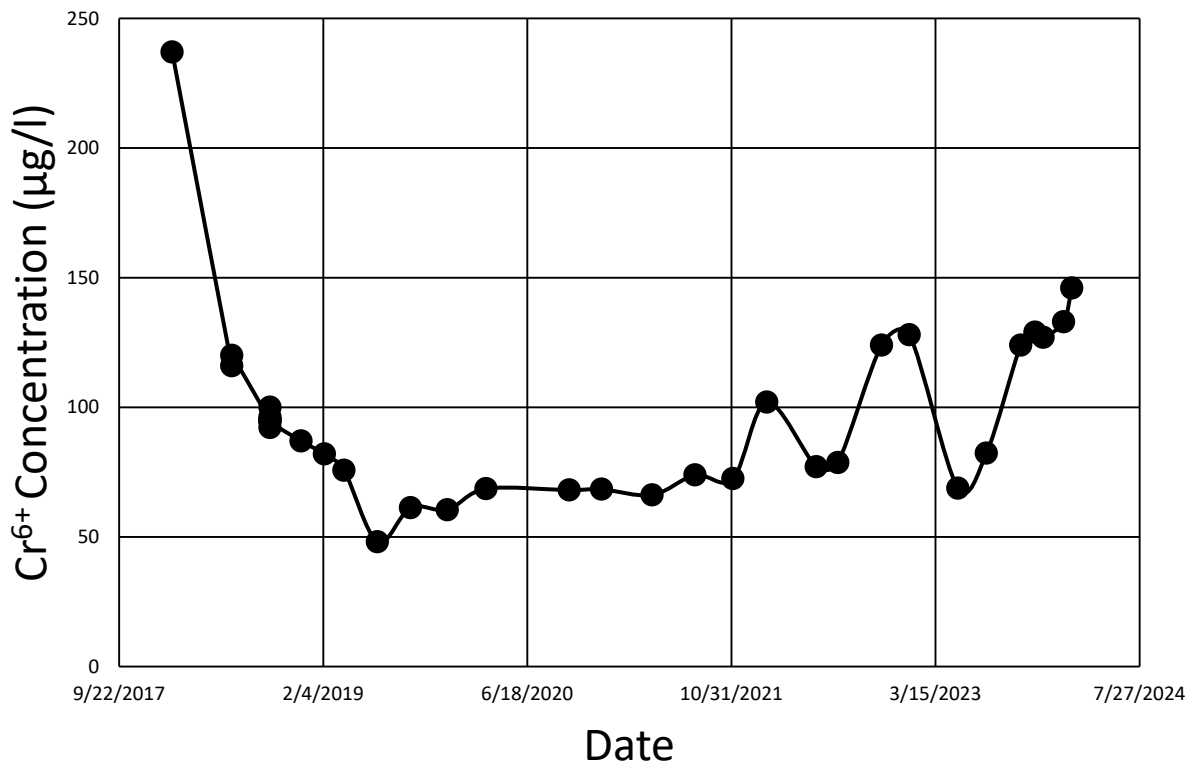


Figure 43. Cr<sup>6+</sup> concentration vs. date at CrPZ-1.



# CrPZ-2a

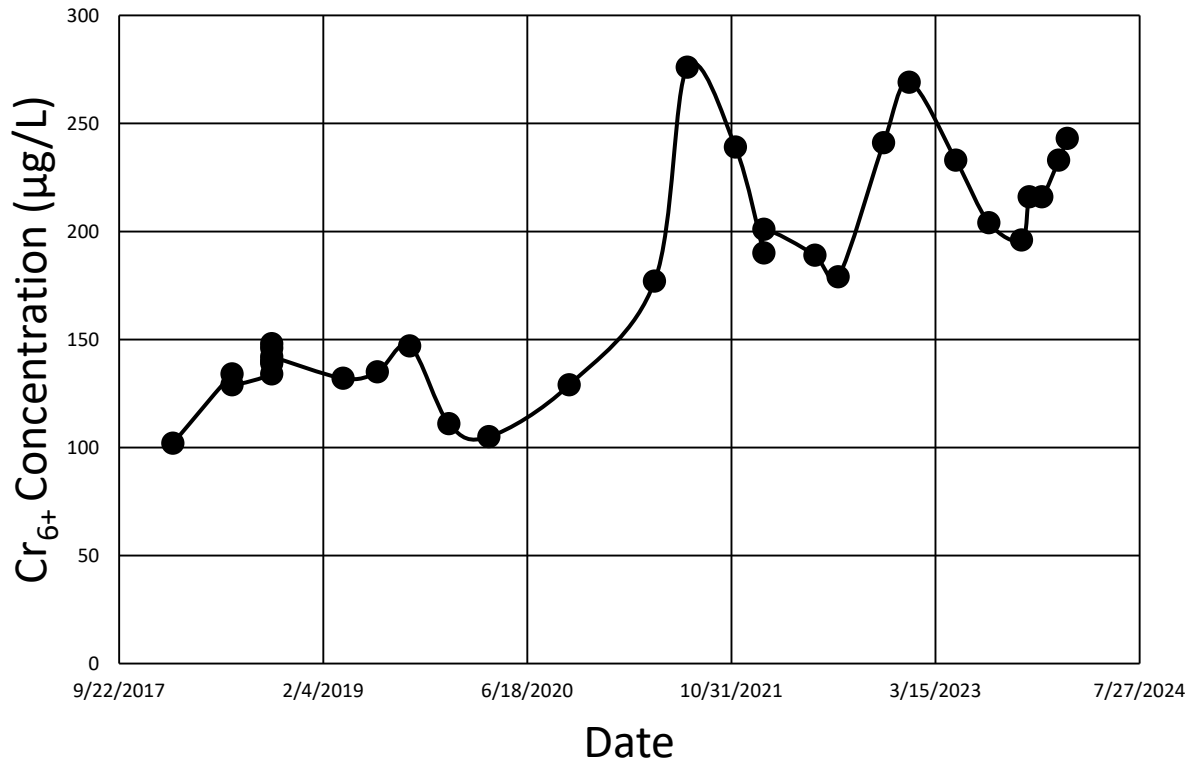


Figure 44. Cr<sup>6+</sup> concentration vs. date at CrPZ-2a.

### CrPZ-3

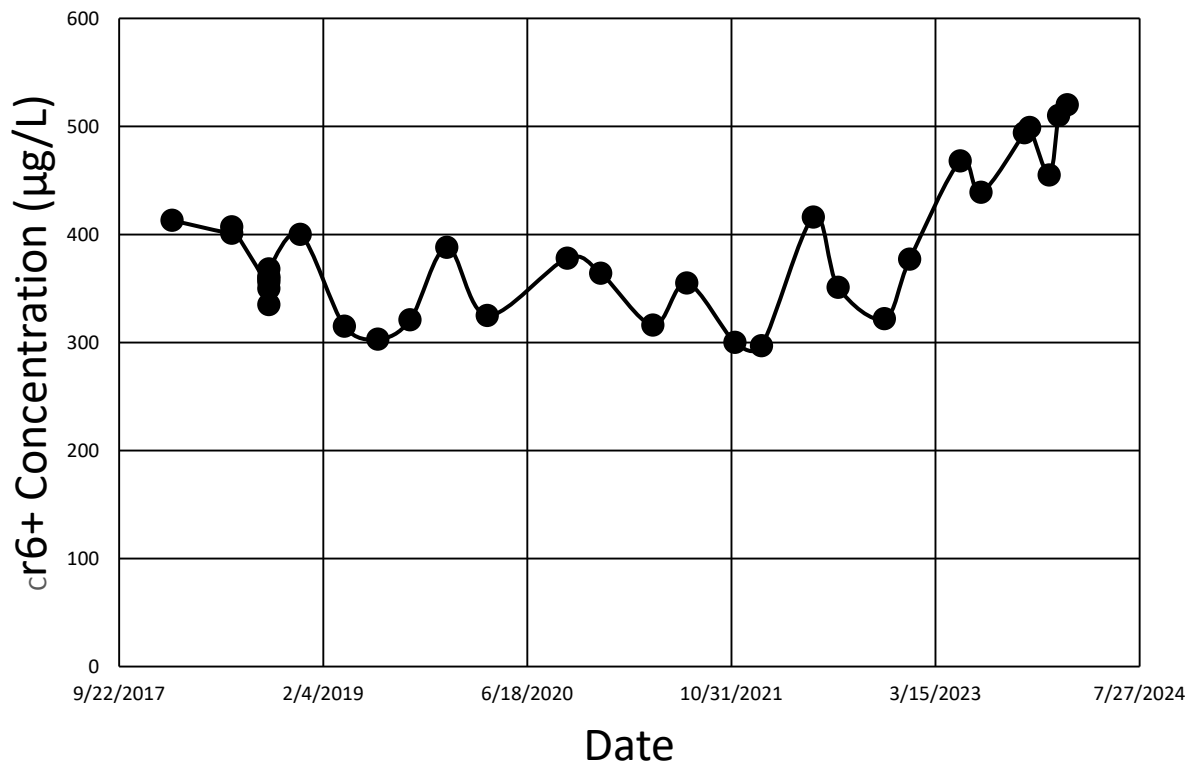


Figure 45. Cr<sup>6+</sup> concentration vs. date at CrPZ-3.

# CrPZ-4

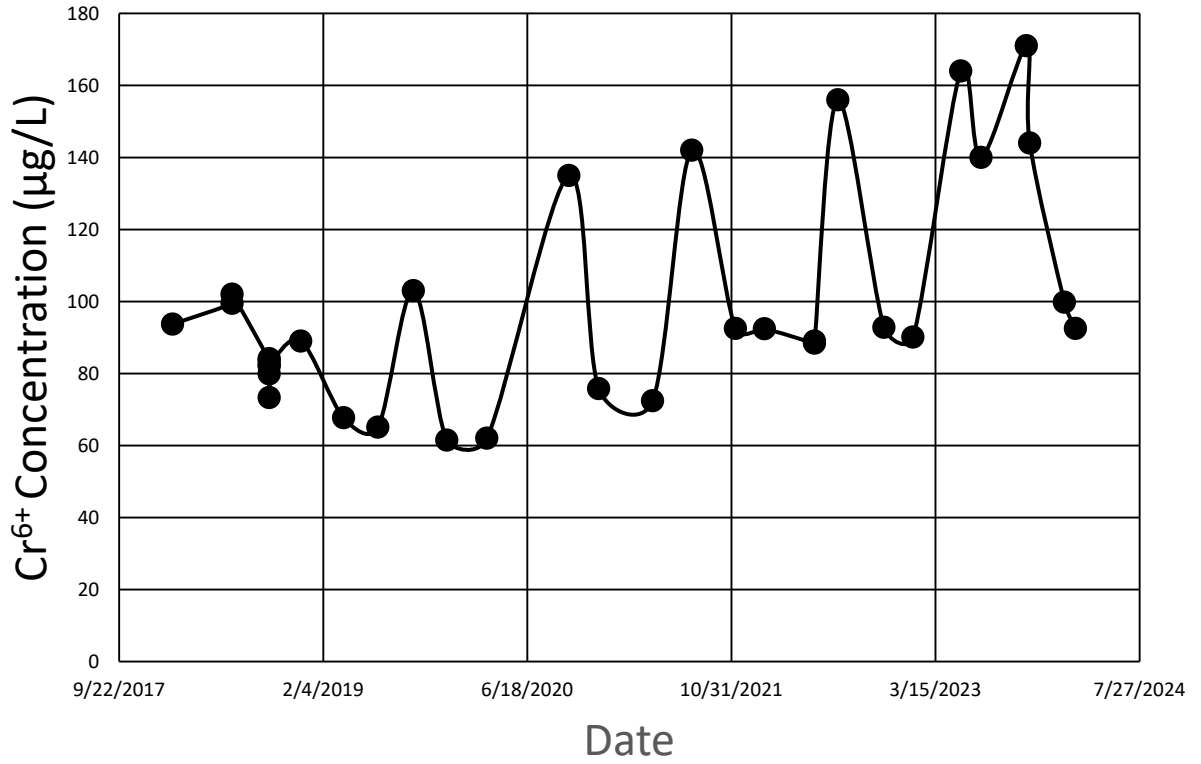


Figure 46. Cr<sup>6+</sup> concentration vs. date at CrPZ-4.

# CrPZ-5

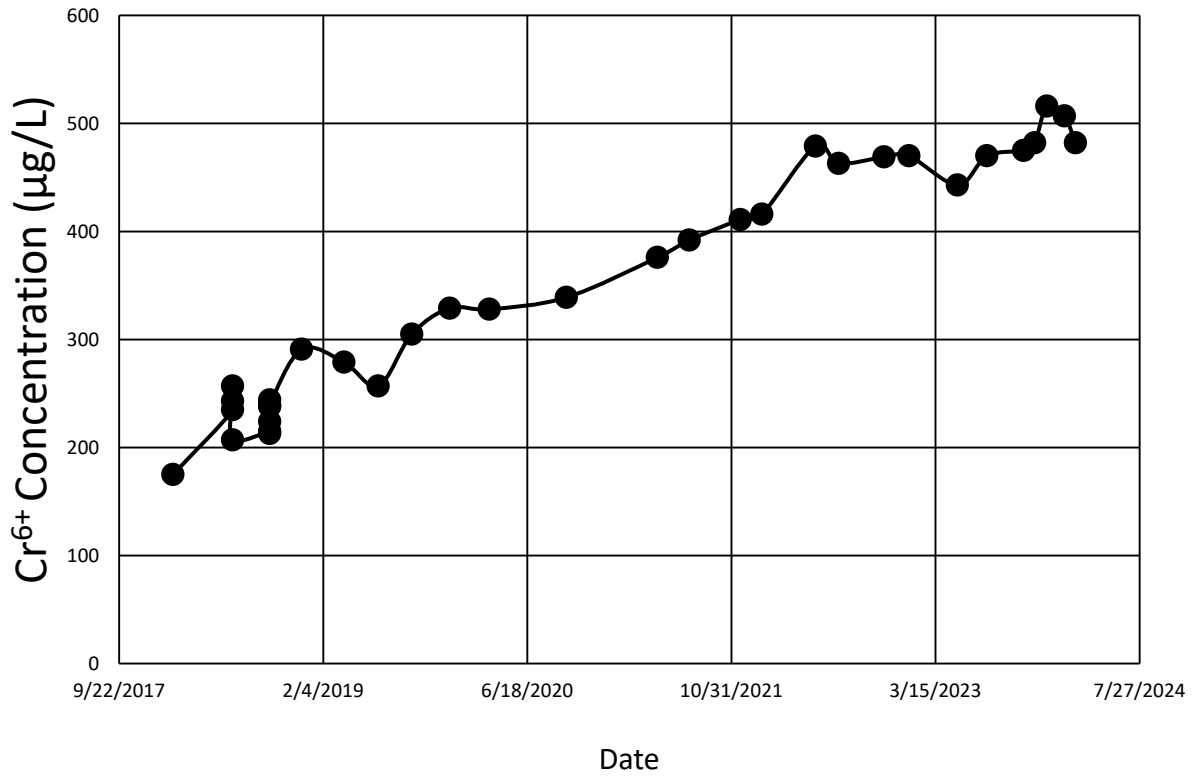


Figure 47. Cr<sup>6+</sup> concentration vs. date at CrPZ-5.

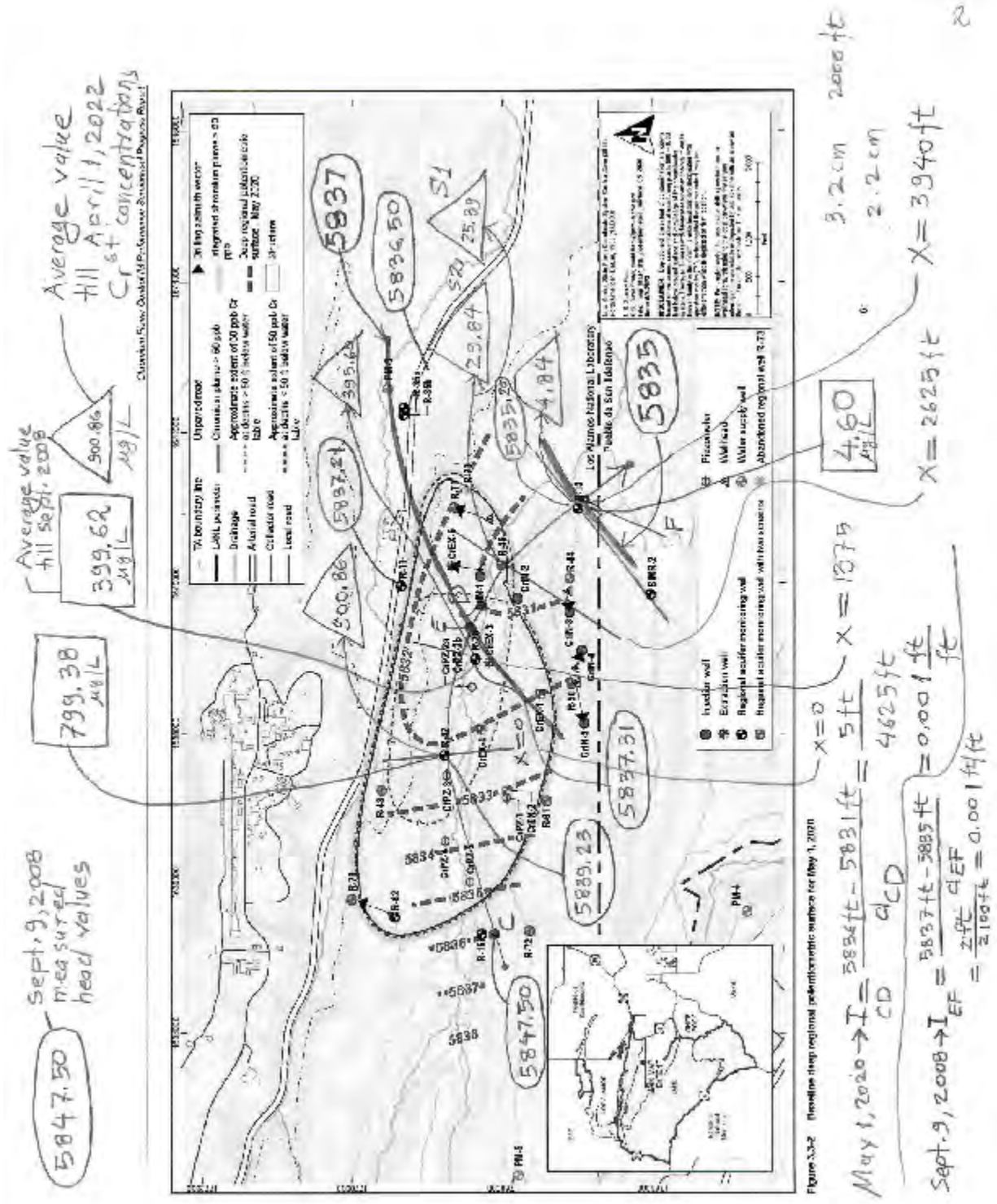


Figure 48. Head contours in 2008 and 2020 along with the average  $Cr^{6+}$  concentration data.

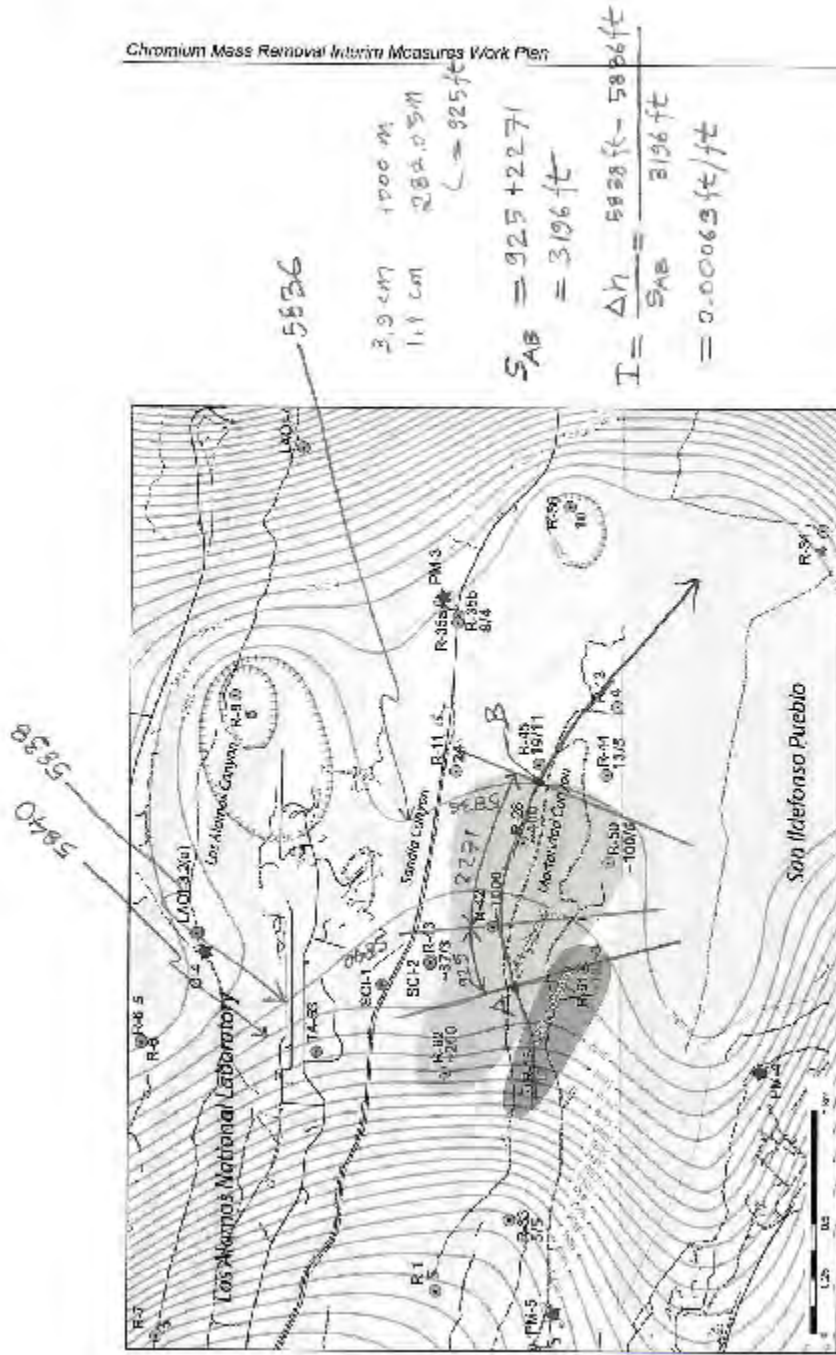


Figure 49.

Figure 1.0-2 Plan view of the Cr(VI) plume >50 ppb contour shown in pink in the regional aquifer with nearby regional monitoring wells (green circles), perched-intermediate monitoring wells (blue circles), and water supply wells (red stars). Contour lines (2-ft intervals) represent the regional water table elevations. The approximate area of perchlorate contamination greater than approximately 2 ppb in the regional aquifer is shown in grey. Numbers beneath the well names refer to the approximate chromium concentrations. Two numbers represent concentrations for upper and lower screens.

Ref: "Interim Measure Work Plan for the Evaluation of Chromium Mass Removal," Los Alamos National Laboratory, ERID-241096, 20pp, Figure 1.0-2, April 2013.

Figure 49. Head contours in 2013.

## **Appendix K**

### **Vertical Gradients and Their Impact on Cr Concentrations (*Wainwright, Newell, Stephens*)**

# Appendix K: Vertical Gradients and Their Impact on Chromium Concentrations

Haruko Wainwright, Charles Newell, Dan Stephens

## Introduction

This appendix addresses one of the charge questions: “To what extent are the increasing chromium concentration trends in R-45 S2 and R-61 the result of an adverse impact of current injection locations? Will the current IM be protective of the environment until a remedial alternative is selected and implemented?” In particular, R45-S2 is the problematic well that led to the notice of violation by NMED. It is also one of the major reasons that eventually led to shutdown of the interim measure (IM).

The initial five-year evaluation of the IM (McFarlane, 2023) has investigated this issue, particularly in Section 4.1 and 5.3. The authors mention the influence of injection on the vertical migration as well as the migration of the higher concentration region between wells. However, the main conceptual model (Figure 1a; Figure 4.1.2 in the white paper)—the migrating contaminants eventually captured in the extraction well—may not be correct, as the injection/extraction well locations are closer to the shallow screen zones, and the vertical gradient at R-45 is downward (Boyle et al., 2024), not toward the extraction wells (Figure 1b).

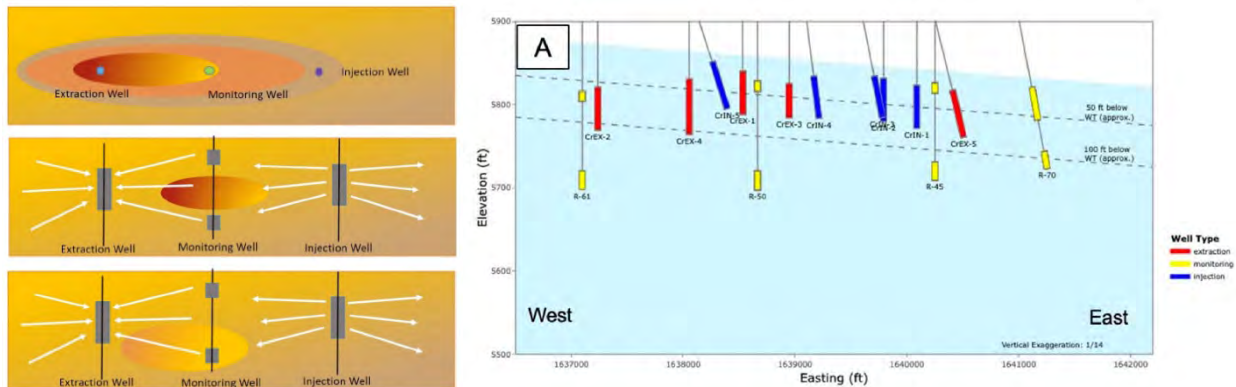


**Figure 1. (a) Depiction of a high concentration zone between the wells under the influence of injection moving toward an extraction well (Figure 4.1.2 in the white paper), and (b) Well screen locations (Figure 4.2.1 in the white paper)**

The vertical gradient has been investigated to test whether PM-4 pumping has a significant impact in the plume region, and to determine whether PM-4 should be included in the modeling efforts (Boyle et al., 2024). The data analysis has shown that IM has an overwhelming impact on the vertical gradient in the region compared to the PM-4 pumping, and that the vertical gradient is downward at most of the wells. Although McFarlane (2023) briefly discusses “the moderate concentration increases observed at R-45 screen 2 since late 2019 are likely due to injection water influencing the vertical migration of higher chromium concentrations that was already present between the screens into the R-45 screen 2 interval.” However, the impact of



this vertical gradient on the plume migration has not been extensively investigated in a quantitative manner.

Vertical downward gradient exists in the unconfined aquifer when there is a significant recharge in the aquifer. Given that chromium comes from the vadose zone, the vertical gradient is the major mechanism to drive contaminant plume downward in groundwater. At the LANL site, the plume has been observed beyond 50 feet below the water table. In fact, R-45 S2 is beyond 100 feet below the water table. The gradient is likely to be larger within or near the hydraulic window, as well as where groundwater is influenced by the IM. Although the vertical hydraulic conductivity is smaller than the horizontal one, the water injection and extraction are likely to impact the vertical gradient.

In this report, we investigate the impact of vertical gradient on the chromium concentrations at R-45 S2 and R-61 S1/S2 as well as at other locations before and during the IM. Although extensive model-based investigation has been done, multiple concerns have been raised for models. Our analysis is observation-based, aiming to provide independent perspectives. We evaluate the time-series of the vertical gradient at the dual screen wells as well as the concentration time-series and their increases  $C(t)/dt$  before and during IM. In addition, using the estimated vertical hydraulic conductivity values, we estimate the plume migration speed and their changes depending on IM. At the end, we provide several recommendations on (a) specific model activities to evaluate the impact of IM on chromium concentrations at R-45 S2 (particularly whether the plume gets eventually captured by the extraction wells), and (b) IM configurations.

## Method

We first processed the groundwater table data at the dual screen wells by (1) removing outliers, (2) taking the difference of the groundwater table between the two screen zones, (3) dividing each difference by the distance of the middle points of the screens, and (4) taking the daily averages. Rather than taking the distribution in each time segment as Boyle et al. (2024) did, we evaluate the time series over time.

In parallel, we processed the chromium concentration time-series,  $C(t)$ , by (1) removing outliers and (2) taking the daily averages. In addition, we computed their changes  $dC(t)/dt$  and fractional changes  $(dC/dt)/C$  based on the smoothed time-series by Friedman's super smoother method (Friedman, 1998).

NMED used  $dC/dt$  (based on the linear regression) to argue that the IM accelerated the concentration increase at R-45 and R-61. However, concentration breakthrough is often approximated by an exponential curve, which means that the increase appears accelerated as  $C(t)$  increases. When  $C(t)$  is exponential, the fractional increase rate  $(dC/dt)/C$  is constant and representative of the increase rate.

## Results

### Vertical Gradient

The vertical gradient and its change are variable across the site (Figure 2).

#### R-43 Vertical Gradient

R-43 has the largest downward gradient in the ambient condition. The seasonal variability is observed, which is likely to be the influence of municipal well pumping. The IM impact is limited, most likely because R-43 is in the northwestern region far away from the IM operations.

#### R-50 Vertical Gradient

R-50—located in the southern area—has the downward vertical gradient, which is increased from the average of -0.0022 in the ambient condition to up to -0.01 during the IM operation. The R-70 time-series starts in 2020 so that there is no data before IM. During the IM, the vertical gradient is downward. After the shutdown in 2023, the vertical gradient is upward up to 0.005, suggesting that the gradient is upward in the ambient condition.

#### R-45 Vertical Gradient and S2 Concentration

The vertical gradient at R-45 (Figures 3 and 4, Table 1) shows that the vertical gradient is slightly negative in the ambient condition ( $-0.0003$  on average) before 2016, although there are some variations. The vertical gradient increases to  $\sim -0.0021$  on average after 2018 when the southern IM operation started, and then to  $\sim -0.007$  after 2019 during the full IM. When the IM is shut down in 2023, the downward vertical gradient is reduced to  $-0.0013$ , which is still higher than the ambient condition. This increased gradient after the shutdown could be the residual of IM, since McFarlane (2023) states that it takes up a year for the hydraulic condition to fully establish after pumping/injection operations change. Alternatively, it could be the impact of increased pumping at PM-4 to compensate for PM-3, which was shut down.

The chromium concentration increase ( $dC/dt$ ) is approximately four times higher during the partial IM (on average) than the ambient condition, and five times higher during the full IM periods. However, it does not respond to the vertical gradient immediately. The fractional increase rate ( $(dC/dt)/C$ ) is approximately two times higher during the partial IM and full IM periods. After the IM shutdown, the fractional increase rate is back to the same value as the ambient condition.

#### R-61 Vertical Gradient and S2 Concentration

The vertical gradient at R-61 shows (Figures 5 and 6, Table 2) that the vertical gradient is slightly upward in the ambient condition before IM ( $0.0016$  on average). The vertical gradient switches to downward after 2018 when the southern IM operation started, and then to  $-0.0018$  during the full IM. When the IM is shut down, the vertical gradient is back to upward; similar to the ambient condition.

The rate of chromium concentration increase ( $dC/dt$ ) is approximately 8 to 10 times higher during the IM compared to the ambient condition. However, after 2021, the concentration slightly decreases during the IM operations. The fractional increase rate ( $(dC/dt)/C$ ) is 4 to 10 times higher during the IM periods, although it decreases in 2021. After the IM shutdown, the fractional increase rate is approximately 10 times higher than the pre-IM ambient condition.

## Discussion

*“To what extent are the increasing chromium concentration trends in R-45 S2 and R-61 the result of an adverse impact of current injection locations?”*

Our analysis suggests that IM increased the downward vertical gradient, and consequently the downward velocity component of the plume migration. The impact is not local around particular wells but across the site, given that the accelerated increase of concentrations is observed in R-45 S2 during the IM period (note that in this document, the partial IM period is from May 2018 to June 2019 before CrIN-1 and CrIN-2 start; Table 1), and also that the difference is small between the full and partial IM operations (the influence of the nearby CrIN-1 injection is not significant). In fact, Boyle et al. (2024) has shown that the downward gradient is increased during the IM across the plume area, including CrPZ-2 near the extraction wells. Even after IM shut down, the concentration continues to increase, possibly because the Cr mass exists in a deeper portion of the aquifer and continues to migrate horizontally.

The exception is R-70 at which the upward gradient is observed. Although the IM still pushed the vertical gradient down at R-70, it is still upward during IM. A significant decrease in the chromium concentration is observed in R-70 S2, which suggests that the extraction is working to pull the plume from the deeper portion towards the extraction wells.

At R-61, the downward gradient is likely the cause of chromium concentration increases in the shallow well, by pulling the plume downward from the vadose zone source. Because the horizontal gradient is toward the northwest (the main source zone), there should be a separate source (the southwestern hydraulic window in MacFarlane, 2023). For R-61, IM would be important to push the plume toward the extraction wells and away from PM-4.

*“Will the current IM be protective of the environment until a remedial alternative is selected and implemented?”*

Although IM is considered to have caused the accelerated migration, it is still protective of the environment. Downward vertical gradients exist even in the ambient condition. The downward gradient at R-43—close to the main source zone—is higher than the one caused by IM at R-45. The downward migration would have happened even without IM, but to a lesser extent. Because IM is removing the significant chromium mass in the upper part of the aquifer, it is considered protective. However, the chromium mass that has escaped capture near R-45 and R-70 necessitates that the current IM system be expanded. In addition, as mentioned above, there is likely to be another source in the southwestern region, impacting R-61. IM would be important to move the plume towards the extraction wells in the north, and to protect PM-4.

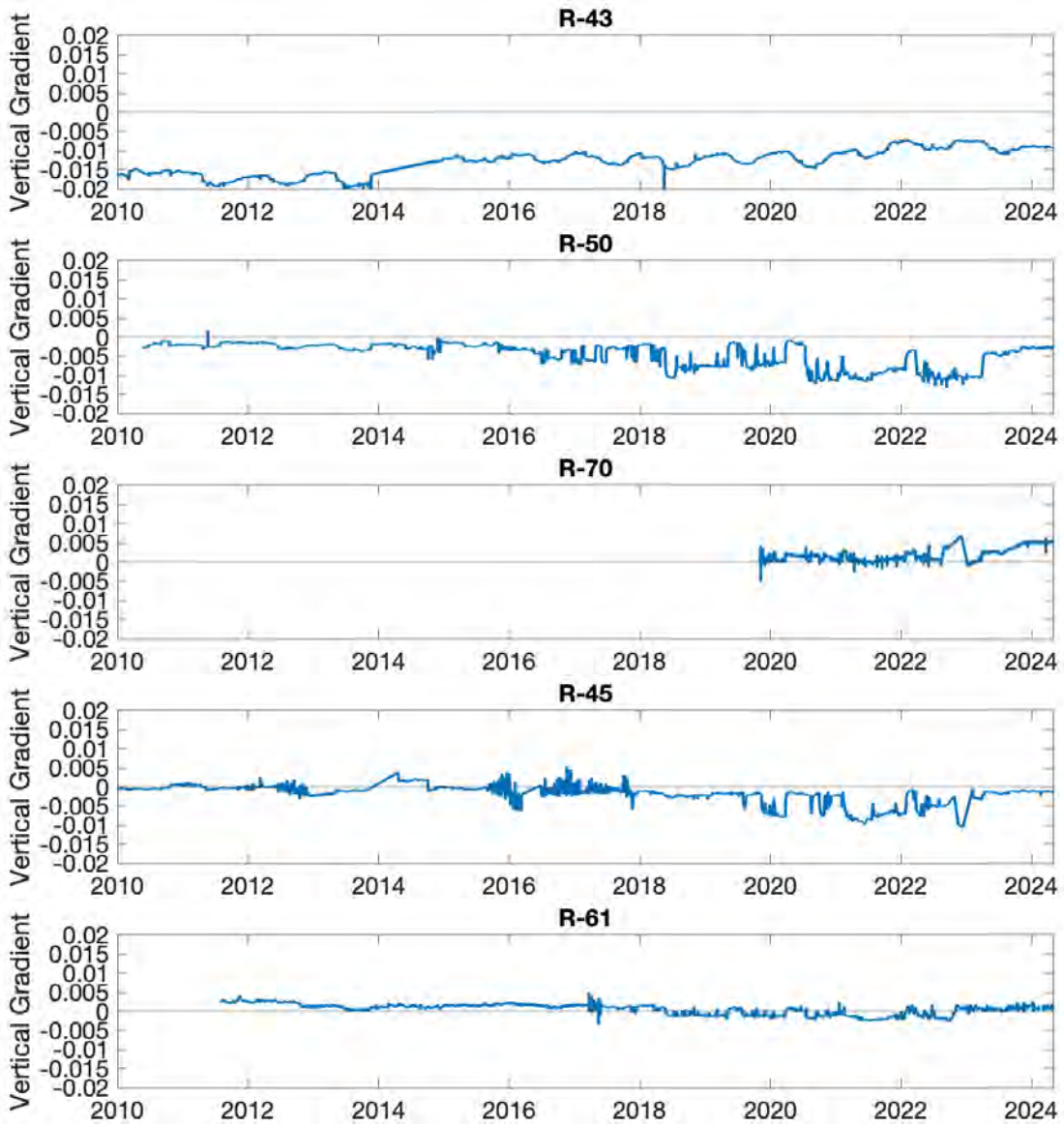


Figure 2. Vertical gradient at the dual screen wells as a function of time.

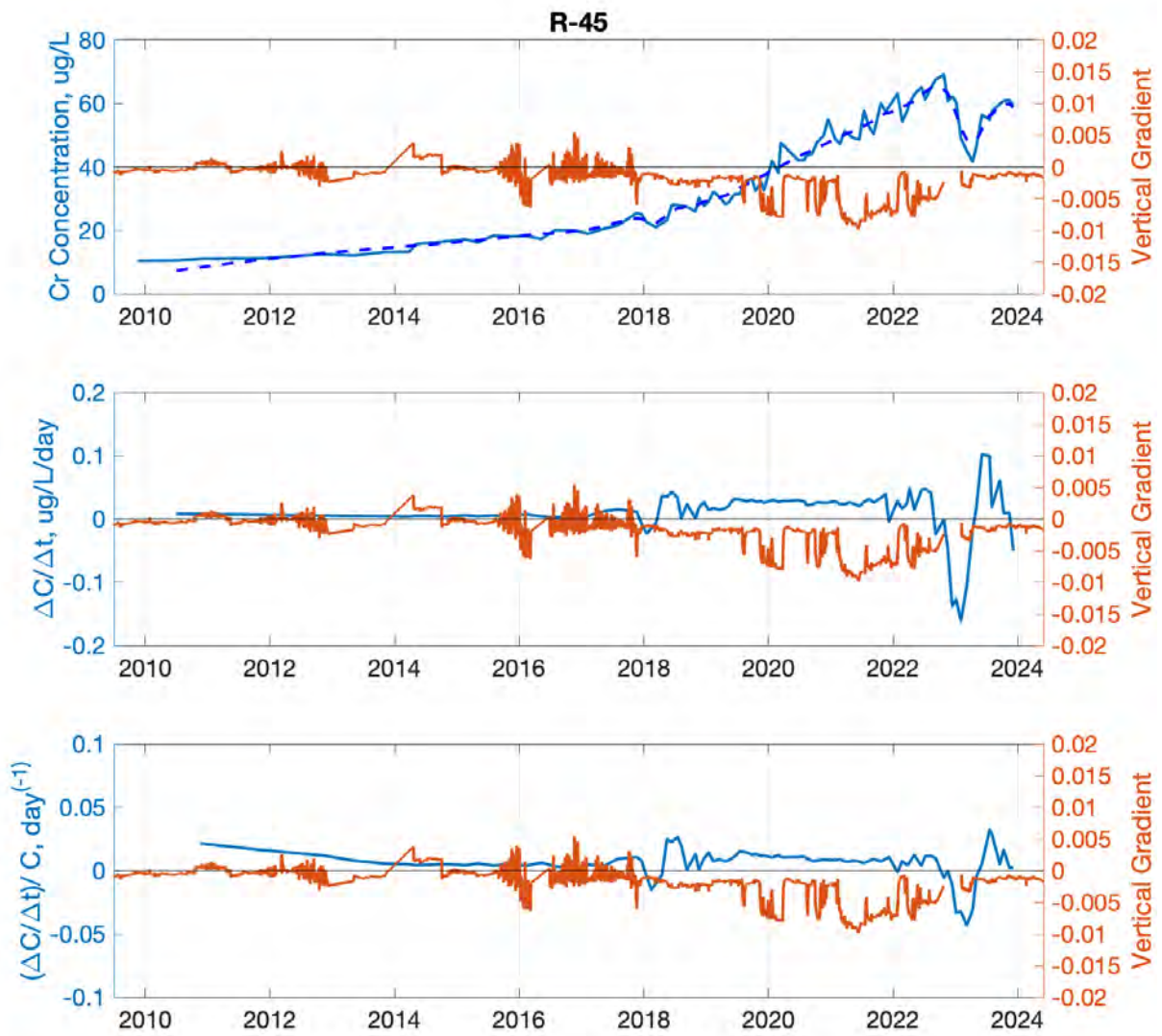
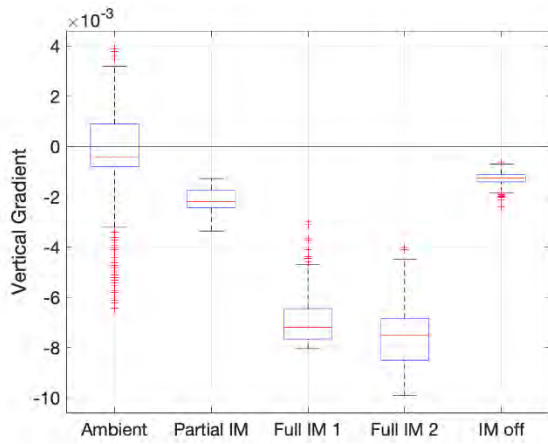
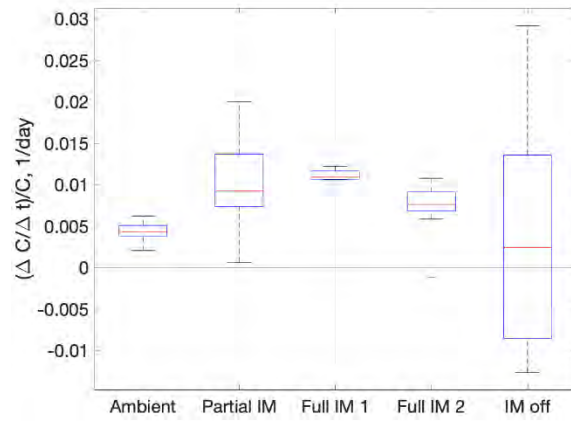


Figure 3. (top) Chromium concentration time series at R-45 S2, (middle) its increase rate, (bottom) its fractional increase rate compared to the vertical gradient.



(a)



(b)

**Figure 4. Boxplots for (a) vertical gradient in the different time period at R-45, and (b) fractional increase of Cr concentration at R-45 S2.**

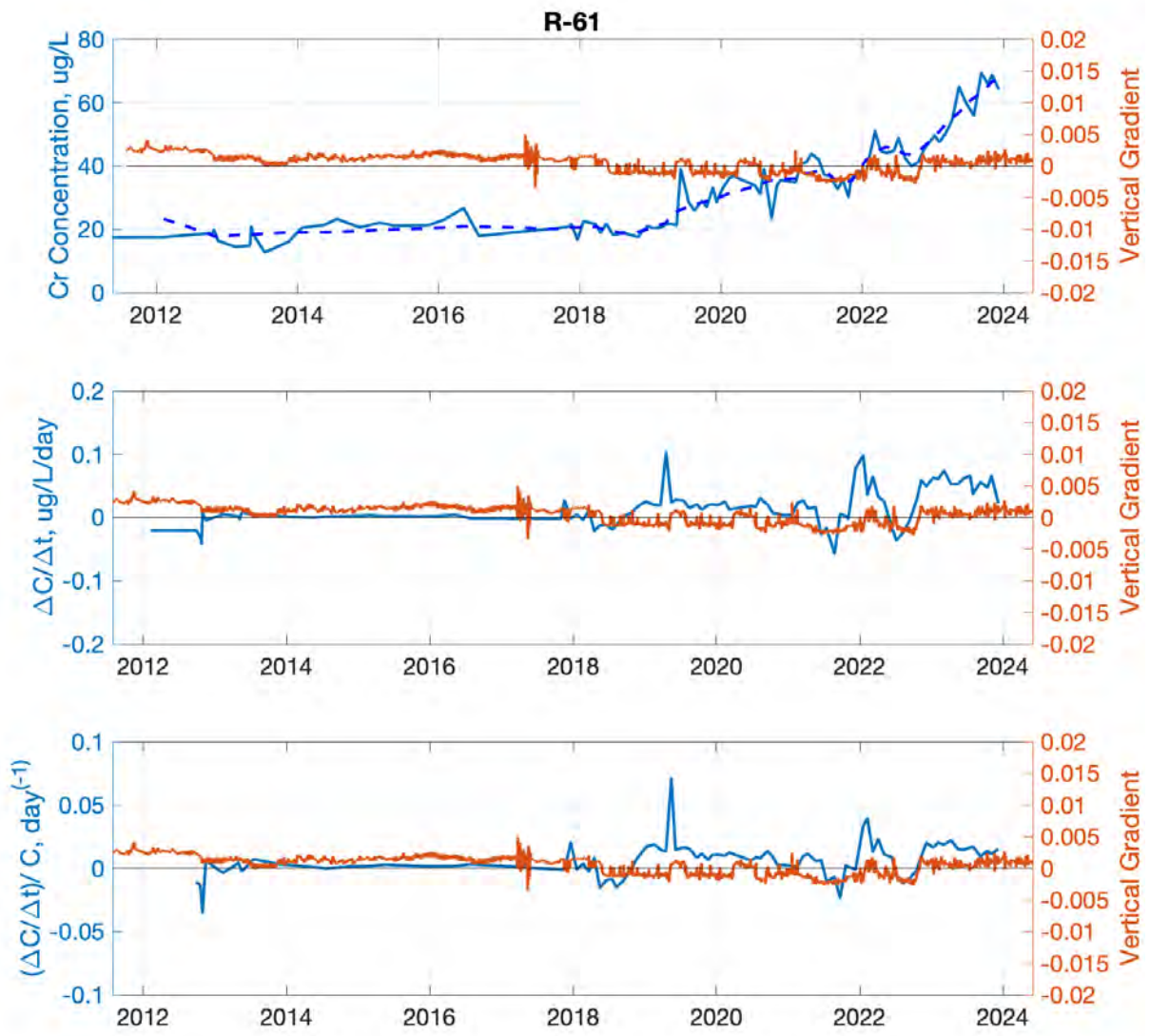
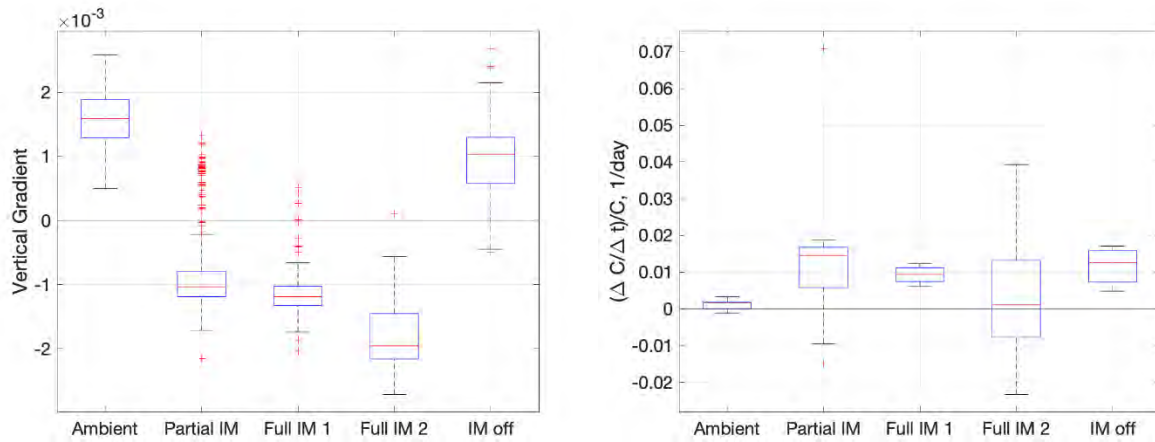


Figure 5. (top) Chromium concentration time series at R-61 S1, (middle) its increase rate, (bottom) its fractional increase rate compared to the vertical gradient.



**Figure 6. Boxplots for (a) vertical gradient in the different time period at R-61, and (b) fractional increase of chromium concentration at R-61 S1.**

**Table 1. Average vertical gradient, concentration increase rates, and fractional increase rates at R-45 S2 during the selected period (between the averaging start and end dates). The full IM period is divided to before and after the COVID-associated shutdown.**

	Ambient	Partial IM	Full IM 1	Full IM 2	IM off
Av. start date	1-Jan-14	30-May-18	29-Nov-19	04-Apr-21	13-May-23
Av. end date	9-Oct-16	13-Jun-19	20-Mar-20	11-Jan-22	13-May-24
Av. vertical gradient	-0.0003	-0.0021	-0.0068	-0.0076	-0.0013
Av. dC/dt, $\mu\text{g/L/day}$	0.0049	0.0184	0.0287	0.0251	0.0248
Av. (dC/dt)/C, 1/day	0.0044	0.0097	0.0112	0.0071	0.0044

**Table 2. Average vertical gradient, concentration increase rates, and fractional increase rates at R-61 S1 during the selected period (between the averaging start and end dates).**

	Ambient	Partial IM	Full IM 1	Full IM 2	IM off
Av. start date	1-Jan-14	30-May-18	29-Nov-19	04-Apr-21	13-May-23
Av. end date	9-Oct-16	13-Jun-19	20-Mar-20	11-Jan-22	13-May-24
Av. vertical gradient	0.0016	-0.0008	-0.0011	-0.0018	0.001
Av. dC/dt, $\mu\text{g/L/day}$	0.0015	0.0202	0.0188	0.0108	0.0509
Av. (dC/dt)/C, 1/day	0.0012	0.0137	0.0093	0.0046	0.0117



## References

- McFarlane (2023), Initial Five-Year Evaluation of the Interim Measures for Chromium Plume Control with an Assessment of Potential Modifications to Operations, Report No. EM2023-0067.
- Boyle et al. (2024), LANL Chromium Plume: Using Water Level Data to Characterize Hydraulic Gradients in the Presence of a Pump-And-Treat System, Proceedings of WM2024 Conference, March 10 – 14, 2024, Phoenix, Arizona, USA 24608.

## **Appendix L**

### **Devlin (2024) - Derivation of Equation 1**

## DERIVATION OF Eq. (1) IN THE IRT REPORT

From Darcy's law, the flux  $q_h$  in the horizontal  $x$  coordinate direction is

$$q_h = -K_h \frac{\Delta H_h}{\Delta x} \quad (1)$$

in which  $K_h$  is the horizontal hydraulic conductivity,  $\Delta H_h$  is the hydraulic head difference along the  $\Delta x$  horizontal distance.

Likewise, the flux  $q_v$  in the vertical  $y$  coordinate direction is

$$q_v = -K_v \frac{\Delta H_v}{\Delta y} \quad (2)$$

in which  $K_v$  is the vertical hydraulic conductivity,  $\Delta H_v$  is the hydraulic head difference along the  $\Delta y$  vertical distance.

Dividing both sides of Eq. (2) to the respective sides of Eq. (1),

$$\frac{q_v}{q_h} = \frac{-K_v \frac{\Delta H_v}{\Delta y}}{-K_h \frac{\Delta H_h}{\Delta x}} = \xi \frac{\frac{\Delta H_v}{\Delta y}}{\frac{\Delta H_h}{\Delta x}} \quad (3)$$

in which

$$\xi = \frac{K_v}{K_h} \quad (4)$$

Eq. (3) can also be expressed as

$$\frac{q_v}{q_h} = \xi \frac{i_v}{i_h} \quad (5)$$

in which

$$i_v = \frac{\Delta H_v}{\Delta y} \quad (6)$$

$$i_h = \frac{\Delta H_h}{\Delta x} \quad (7)$$

Eq. (5) is exactly the same as Eq. (1) in the IRT report.

**Appendix M**  
**Mass Flux Evaluation (*Newell*)**

## APPENDIX M: MASS DISCHARGE ANALYSIS

### *Abstract*

- A risk-based approach is the accepted way to manage groundwater cleanups across the country, including in New Mexico.
- Mass discharge calculations are used to determine the overall strength of groundwater contaminant plume, and the resulting mass discharge can be used to estimate the potential risk of the plume to nearby groundwater users.
- The estimated mass discharge of the highest concentration area of the chromium plume is between 3 and 75 kilograms per year, with a best estimate of 15 kilograms per year (about 33 pounds of chromium per year) being transported by groundwater to the east.
- The Independent Review Team (IRT) was interested in understanding how a plume of this strength might affect nearby water supply wells. Therefore a *hypothetical scenario* was evaluated where the chromium plume was assumed to impact the nearest downgradient water supply well (Los Alamos County well PM-3), even though this scenario cannot happen from a practical perspective for several reasons.
- For an almost impossible, worst case scenario where the Interim Measure or Final Correct Measure are never operated, the analysis indicates a potential increase in chromium concentration in the water supply well between 4 and 85 µg/L **with a mid-range value of 17 µg/L** chromium. In other words, exceedance of the chromium drinking water standard is possible but very unlikely for this scenario.
- For almost impossible, almost worst case scenario where a partial restart of the Interim Measure occurs and is never expanded and the Final Correct Measure is not constructed the analysis indicates a potential increase in chromium concentration in the water supply well of between 1 and 28 µg/L **with a mid-range value of 6 µg/L** chromium. Exceedance of the chromium drinking water standard is very unlikely to occur for this scenario.
- The risk conclusion provides supporting evidence to the IRT that the IM (or some version of an IM) can be put in operation immediately even if some questions about hydrogeology and chromium plume migration are not completely resolved at restart time.

### *Overview of Risk-Based Approach to Managing Groundwater Plume*

Most groundwater cleanup projects use a risk-based approach to manage the contamination in a way to protect human health and the environment based on current and reasonably expected future exposures, rather than aiming to remove all contaminants from the subsurface. This approach recognizes that complete removal of "every last molecule" of contamination is often technically impracticable or prohibitively expensive. Instead, the goal is to reduce contaminant concentrations to levels that do not pose unacceptable risks to human health or the environment.

The U.S. Environmental Protection Agency (EPA) acknowledges this approach in both its Superfund and RCRA programs. For Superfund sites, U.S. EPA (2024a) states that groundwater response actions should "address all exposure pathways that pose an actual or potential risk to human health and the environment," with the goal of returning usable groundwater to beneficial uses "wherever feasible and within a reasonable timeframe." When full restoration is not feasible, the focus shifts to preventing further plume migration and exposure. Similarly, USEPA's RCRA guidance recommends developing groundwater cleanup levels based on "existing cleanup standards" when available, or on site-specific risk assessments that consider "all actual and potential exposures to the contaminant(s)" (USEPA, 2024b). Many states, including New Mexico, have adopted similar risk-based approaches for groundwater cleanup projects, recognizing that this method allows for more efficient and effective management of contaminated sites while still protecting public health and the environment.

Understanding that risk-based approaches are a fundamental part of the groundwater cleanups is important, so several tools have been developed by the groundwater cleanup community to better understand the overall and general risks of groundwater plumes. One such tool is called "mass flux / mass discharge."

#### *Overview of Mass Flux and Mass Discharge in Groundwater Plumes*

*Mass flux* and *mass discharge* calculations are important tools for understanding groundwater contaminant plumes and assessing their potential impacts. While these terms are sometimes used interchangeably, they have distinct meanings that are important to differentiate as described in a key 2010 Interstate Technology and Regulatory Council (ITRC, 2010) guidance document:

- **Mass flux** refers to the mass of contaminant flowing through a unit area of the subsurface per unit time. It is typically expressed in units of mass per area per time, such as grams per square meter per day (**g/m<sup>2</sup>/day**). Mass flux provides information about contaminant movement at specific locations within a plume.
- **Mass discharge** on the other hand represents the total mass of contaminant moving past a vertical plane or imaginary "curtain" perpendicular to groundwater flow per unit time. It is expressed simply as mass per time, such as kilograms per year (**kg/year**). Mass discharge integrates mass flux over an entire plume cross-section to quantify the overall contaminant loading in groundwater.

#### What is the ITRC?

*"Established in 1995, the Interstate Technology & Regulatory Council (ITRC) is a state-led, national coalition of personnel from the environmental regulatory agencies of all 50 states and the District of Columbia, three federal agencies, tribes, and public and industry stakeholders. The organization is devoted to reducing barriers to, and speeding interstate deployment of, better, more cost-effective, innovative environmental techniques." (ITRC)*

The IRT performed a mass discharge calculation to better understand the chromium plume. Mass discharge combines three key elements that relate to the overall risk posed by a groundwater plume:

1. The size of the contaminant plume; specifically the cross sectional area of the plume perpendicular to groundwater flow. A larger plume area will produce a higher mass discharge.
2. The groundwater *flow rate*; specifically the groundwater “Darcy velocity.” Faster groundwater movement increases mass discharge.
3. The *concentration* of the contaminants dissolved and moving in flowing groundwater. Higher concentrations result in greater mass discharge.

By integrating these three factors, mass discharge better reveals the overall plume strength and potential impacts compared to using contaminant concentration data alone. Newell et al. (2011) the usefulness of mass discharge this way: *‘Mass discharge is an important single metric for characterizing a site because it represents an integration of both hydraulic properties and contaminant distribution.’* The ITRC (2010) stressed:

*“Mass discharge and flux estimates quantify source or plume strength at a given time and location. Consideration of the strength of a source or solute plume (i.e., the contaminant mass moving in the groundwater per unit of time) improves evaluation of natural attenuation and assessment of risks posed by contamination to downgradient receptors, such as supply wells or surface water bodies.”*

Overall, the higher the mass discharge, the greater the potential impacts to downgradient receptors like drinking water wells or streams that receive groundwater discharge if the plume reaches these receptors. This is because a high mass discharge plume is conveying more contaminant mass over time. The IRT wanted to know the mass discharge of the chromium plume to assess the hypothetical risk it posed to nearby groundwater users, in particular local water supply wells, if these wells are impacted the chromium plume.

#### *How Groundwater Plumes Can Impact Pumping Wells*

Any groundwater pumping well can effectively “capture” a contaminant plume if it is pumping at a sufficiently high rate. This process, related to the process of “hydraulic containment”, works by altering the local groundwater flow field around the well (Gorelick et al., 1993; U.S. EPA, 2008).

When a well pumps water from an aquifer, it creates a cone of depression in the water table or potentiometric surface around the well. This cone of depression causes groundwater to flow towards the well from all directions, but mostly upgradient. The area from which water is drawn to the well is called the “capture zone” (Figure 1).

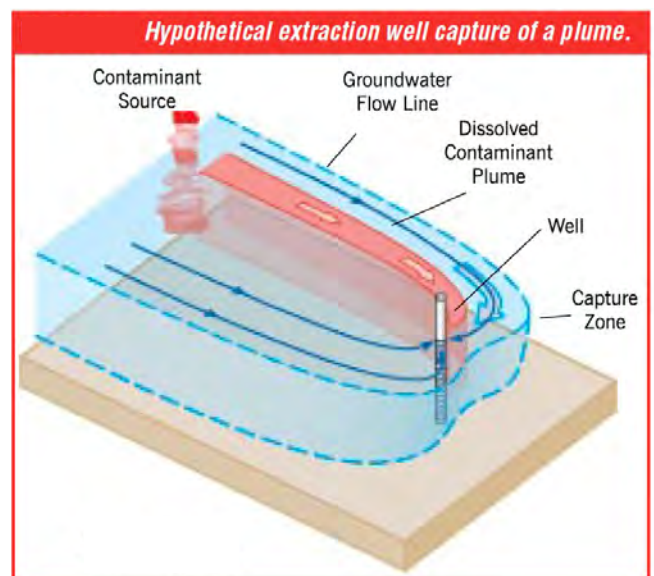


*Figure 1. Hypothetical capture of a groundwater plume by a groundwater extraction well (Nichols and Roth, 2004).*

If the pumping rate is high enough, the capture zone can extend to encompass the entire width and depth of a contaminant plume. In this case, all contaminated groundwater within the plume will eventually be drawn into the well, effectively containing the plume and preventing its further migration downgradient.

The size and shape of the capture zone depend on several factors:

1. Pumping rate: Higher pumping rates create larger capture zones.
2. Aquifer properties: Hydraulic conductivity and thickness of the aquifer influence the extent of the capture zone.
3. Natural groundwater gradient: The capture zone will extend further upgradient in areas with lower natural gradients.
4. Duration of pumping: The capture zone expands over time as pumping continues.

#### *Estimating the Mass Discharge of the Uncontrolled Chromium Plume*

When a groundwater extraction well captures a plume, the resulting contaminant concentration in the extracted water can be estimated by dividing the plume's mass discharge by the well's average pumping rate (Einarson and MacKay, 2001) (Equation 1):

$$\text{Concentration (mass per volume)} = \text{Mass Discharge (mass per time)} \div \text{Pumping Rate (volume per time)}$$

For some combinations of mass discharge and pumping rate, a dilution effect can result in contaminant concentrations below drinking water standards, where unimpacted groundwater mixes with impacted groundwater in the well. **While regulatory agencies and remediation engineers do not typically rely on this dilution alone to achieve compliance** (Einarson and MacKay, 2001<sup>1</sup>), the IRT understanding the potential risk associated with a particular strength groundwater plume provides a useful context on the magnitude of the contamination problem. By combining information on plume size, flow rates, and concentrations, mass discharge offers valuable insights for site characterization, risk assessment, and remediation planning that concentration data alone cannot provide.

The chromium plume mass discharge of the plume was estimated using the following information (Figure 2):

1. A contour map of the chromium plume developed by one member of the IRT, Dr. Daniel Stephens. This plume provide the width of the chromium plume near its highest concentration point (near monitoring well R-42) and the concentrations of the chromium plume along a vertical cross section perpendicular to groundwater flow;

---

<sup>1</sup> Einarson and Mackay (2001) state “We do not advocate reliance on in-well blending to maintain water supply standards but recognize that it must be considered in assessing potential impacts. The process does occur, and understanding it is fundamental to determining the risks posed by contaminant plumes drawn into water supply wells.”



2. Groundwater flow modeling performed by another member of the IRT, Dr. Rick Devlin. This provided the groundwater flow rates (Darcy velocity) through the transect.
3. An estimated plume thickness of 50 feet for the largest area zone of the plume based on site information.

The mass discharge of the plume was then calculated using the Isocontour Method (ITRC, 2010). The vertical transect was divided into 10 separate imaginary flow-through vertical “curtains”, each with its own width, average chromium concentration, groundwater Darcy velocity, and each assumed to be a 50 feet thick layer below the water table. The mass discharge of each plume segment was calculated by multiply the width, thickness, chromium concentration, and groundwater Darcy velocity. Then all of 10 of the plume segments were summed together to yield a mass discharge of about 12 kilograms per year (26 pounds per yr) of chromium flowing the east in groundwater. There is uncertainty in each step of the mass discharge calculation, so a range of mass discharge values is provided.

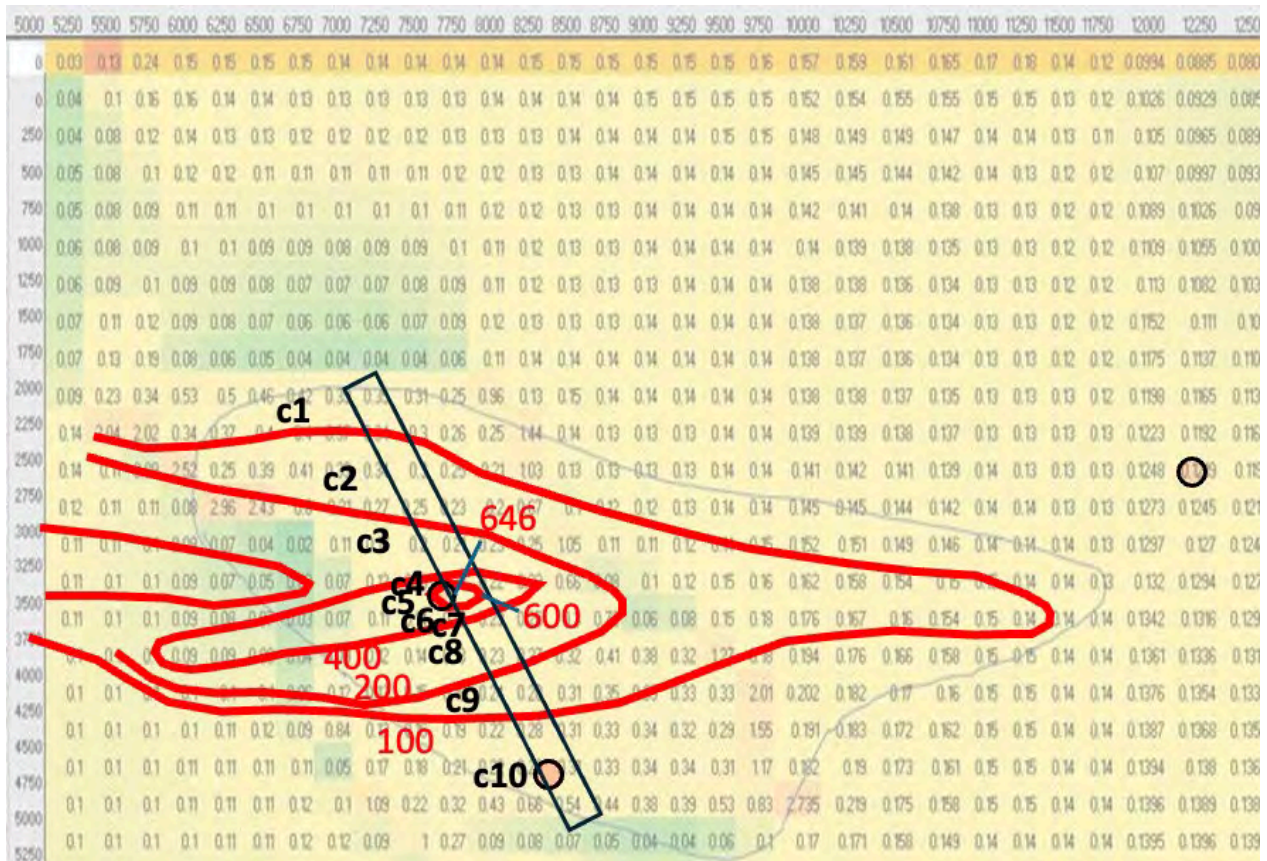


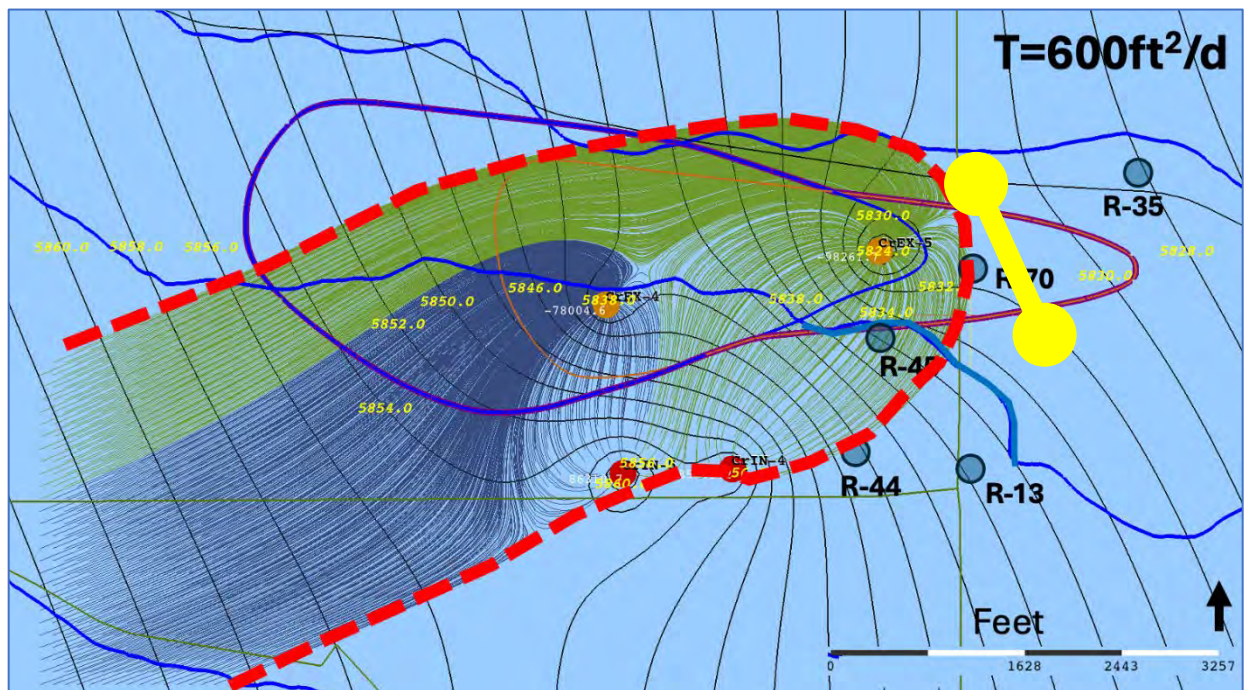
Figure 2. Groundwater seepage velocity map (Devlin) (ft/day), chromium plume contours (Stephens), and the vertical plume transect. c1, c2, c3 etc. are vertical mass flux polygons with individual chromium concentrations based on contours and monitoring well data. Effective porosity used for calculation: 0.15 (Devlin). Red values are chromium concentrations in ug/L. Scale is in feet.

Because some portion of the chromium plume is more than 50 feet below the water table, an additional 25% of the calculated mass discharge of the 12 kilograms was added to the mass discharge estimate. Note that the transect in Figure 2 where this 25% assumption was applied was far upgradient of the R-70 area that shows deeper chromium. Overall this resulted in an overall estimated chromium mass discharge of about **15 kilograms per year (~33 pounds per year), with a possible range of 3 to 75 kilograms per year ( $\pm$  x5) after accounting for uncertainty (based on engineering judgement).**

This value was similar to previous mass discharge estimates from a conference proceedings paper by Vesselinov et al. (2013) who estimated 3-18 kilograms per year “contaminant flux to the regional aquifer” (note their use of an older term “contaminant flux” rather than “mass discharge”).

#### *Estimating the Mass Discharge of the Chromium Plume Under Influence of Interim Measure Restart*

One potential approach to an Interim Measure is to start with a “4s/5s” Scenario where only CrEX 4 and 5 and CrIN 4 and 5 are operated a temporary starting point for an Interim Measure restart. The pumping rates are approximately 60-70 gpm for each well. This is the same configuration that the IM was last operated from late Oct. 2022 to the end of March 2023 where chromium concentrations in the R-45-S2 well declined rapidly.



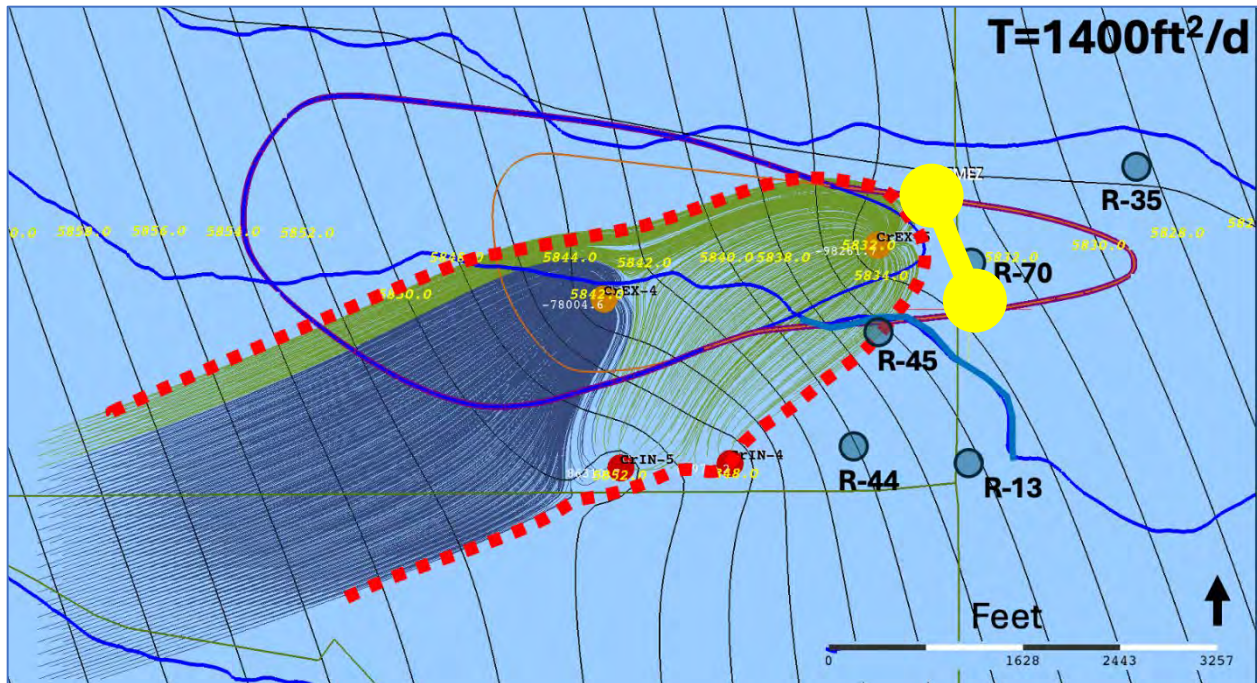


Figure 3. Capture zones for two different regional aquifer transmissivities using the Theis Grid Method (Tonkin) for the “4s/5s” Scenario (pumping CrEx-4,5; injecting CrIN-4,5 at about 60-70 gpm each). Top: Regional aquifer transmissivity assumed to be 600 ft<sup>2</sup>/day. Bottom: Regional aquifer transmissivity assumed to be 1400 ft<sup>2</sup>/day. Red dashed lines indicate approximate capture zone for this scenario. Blue/red line is approximate extent of chromium plume. Yellow line: vertical transect used to estimate mass discharge of uncaptured portion of the chromium plume.

Three different hydrologic analyses of a potential Interim Measure restart based on the 4s/5s Scenario provided three different possible capture zones (red dashed lines) that extend into the eastern portion of the chromium plume (Figure 3 shows two different aquifer characteristics applied to a Theis method analysis: less permeable (Panel A) and more permeable (Panel B) by Dr. Matt Tonkin of the IRT. Figure 4 assumes middle-range aquifer characteristics calibrated to observed water levels to yield a capture zone by Dr. Rick Devlin of the IRT.

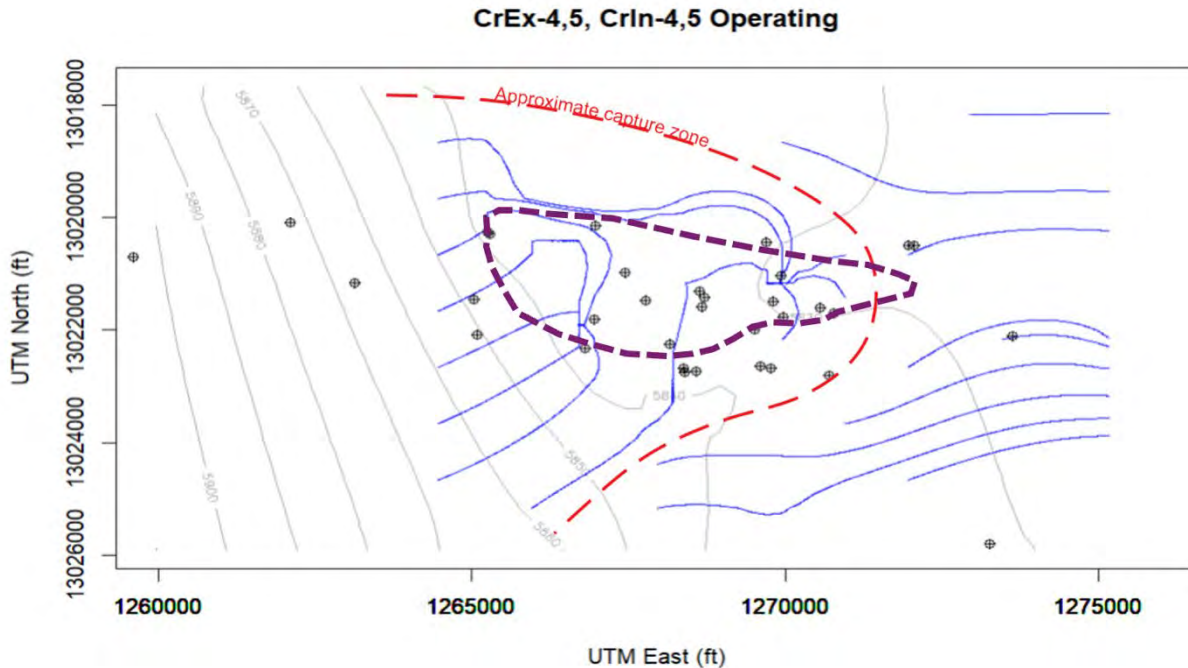


Figure 4. Capture zones using a simple 1-layer model of the regional aquifer for the “4s/5s” Scenario (Devlin). Red dashed lines indicate approximate capture zone indicated by this model. Purple dashed line is approximate location of the chromium plume shown in Fig. 5. This model suggest it is possible the 4s/5s Scenario could capture almost all of the chromium plume, but with significant uncertainty.

#### Summary of All Mass Discharge Estimates Including Uncertainty Ranges

The resulting estimated mass discharges with a range of  $\pm X5$  range include are shown in Table 1.

Table 1. Mass Discharge Estimates for the Chromium Plume (kilograms per year).  
(1 kilogram = 2.2 pounds)

Scenario	Low-Range Mass Discharge (kg/yr)	Mid-Range Mass Discharge (kg/yr)	High-Range Mass Discharge (kg/yr)
No Interim Measure	3.0	15	75
IM 4s/5s Restart (Fig. 3)*	1.0	~5.0	25

\* Figure 4 indicates almost complete capture, but due to uncertainties about the concentrations mass discharge was not estimated. IM: Interim Measure.

Note that all of the scenarios in Table 1 are almost impossible to occur because: (1) PM-3 is no longer being used for water supply and (2) the chromium plume will be either controlled by the recommended initial “4s/5s Scenario” (if figure 4 is correct) or by an expanded Interim Measure or the operation of the Final Corrective Measure.

*Hypothetically What Would Happen if a Nearby Water Supply Well Was Impacted by the Chromium Plume?*

The IRT's mass discharge analysis was then used to help answer the following question: *If the chromium plume continued to advance to the east without any remediation or control for many years, and if the chromium plume was completely impacted by a downgradient water supply, how much would the chromium concentrations increase in the pumped water from this well?*

Note the nearest downgradient water supply wells is Los Alamos County's PM-3 well, located about 800 feet to the east-north-east of the northern edge of the chromium plume (Figure 5). A geologic cross section with PM-3 shows the depth and screened interval (where water enters the well) of this well (Figure 6).

Note this hypothetical scenario of chromium plume impact by water supply well PM-3 is almost certainly *not to occur* for many reasons, from most important to lesser importance:

- An Interim Measure will almost certainly be in place well before the high concentration portion of the chromium plume reaches PM-3;
- Los Alamos County has shut down pumping at water supply well PM-3, so it is no able to draw in any water from the plume.
- All of the high-concentration of the chromium plume may not be draw into PM-3 because:
  - ◇ The PM-3 groundwater supply well screen which allows water to enter the well is or is almost entirely below the high concentration portions of the chromium plume (Figure 6) and therefore some portion of the chromium plume could flow above the PM-3 screened interval without flowing into the well.
  - ◇ Some portion of the chromium plume may flow to the south and therefore not enter PM-3.
  - ◇ When PM-3 was operated in the 2009-2012 timeframe, the average pumping rate was only about 466 gallons per minute (gpm) (data from Figure G-2.1-2 in the LANL 2012 report, a flowrate which might not be enough to draw in all of the chromium plume even all of the plume is flowing towards the east.

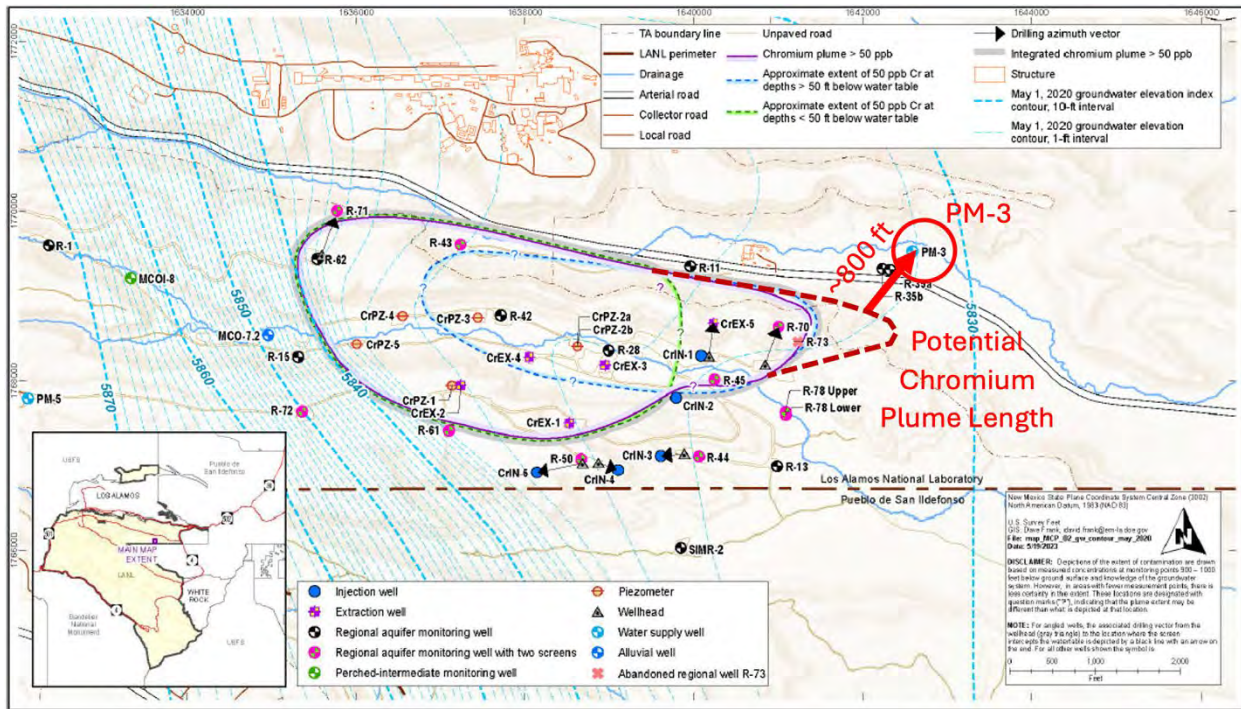


Figure 5. Location of Los Alamos County’s PM-3 water supply well relative to the chromium plume. Base map from NMED presentation “Chromium Plume Cleanup” (Herman and Martinez, 2024) with annotations included expanded plume boundary.

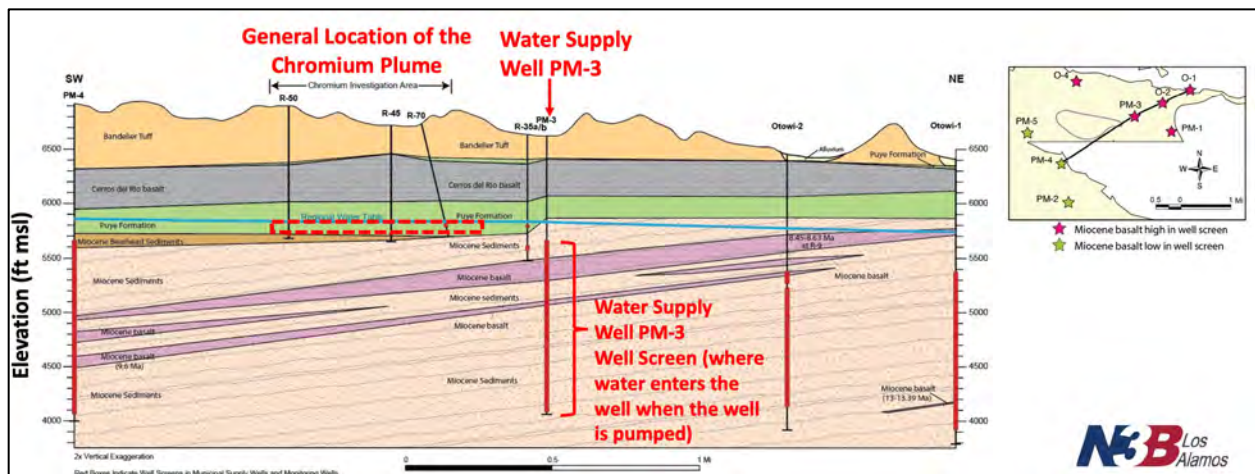


Figure 6. SW to NE Cross Section Showing Dip of Miocene Basalts. Original figure from “Miocene Basalts” presentation by D. Broxton (2023) with annotations. Location of chromium plume is conceptual and not to scale.

Despite the extremely unlikely nature of this scenario (PM-3 capturing the chromium plume), the IRT was interested in understanding the general magnitude of risk that the chromium plume posed to nearby pumping wells. Would an uncontrolled chromium plume that impacts a water supply well increase the chromium concentrations in the pumped water to several hundred  $\mu\text{g/L}$  (parts per billion), thereby exceeding the New Mexico drinking water standard for chromium of

50 µg/L? Or would the increase in chromium concentration be so low that these drinking water standards would not be exceeded?

To answer this question, Equation 1 above was used with the estimated chromium plume mass discharge of 15 kilograms per year for a hypothetical “No Interim Measure” scenario and an average PM-3 flowrate of about 466 gallons per year. Dividing the mass discharge by this flowrate and making the appropriate scientific unit conversions resulted in an estimated increase in the chromium concentration of this hypothetical PM-3 plume impact scenario by only 17 µg/L. Assuming a background chromium concentration of about 5 ug/L results in a chromium concentration of **about 23 µg/L after plume impact**, which is still under half of the New Mexico drinking water standard for chromium of 50 µg/L.

This single value indicates that with the best estimates of site conditions described above, **even if all of the chromium plume impacted PM-3 it may not result in chromium concentrations exceeding the drinking water standard is Los Alamos County water supply PM-3**. This result aligns with a 2018 Long-Range Water Supply Plan for Los Alamos County prepared by Daniel B. Stephens & Associates, Inc., which provided this analysis:

*“The screened interval in monitoring well R-28 is from 934 to 958 feet deep, extending only 69 feet from the top of the regional aquifer, while PM-3 is screened at much greater depths (from 956 to 2532 feet) thereby producing water from a much larger section of the aquifer. If the chromium plume were to reach PM-3 yet be confined to a shallow segment near the top of the aquifer, the concentration is likely to be highly diluted as a result of pumping from an interval of more than 1500 feet. Nevertheless, the presence of hexavalent chromium near the well represents a risk that should be carefully monitored”* (Daniel B. Stephens & Associates, 2018).

While the mass discharge calculation described above with the most likely, middle range values suggested a chromium concentration increase of **only 17 µg/L** assuming a worst-case condition where all of the chromium plume was drawn into the PM-3 (Table 2). However, as described above, there is considerable uncertainty in several areas of the calculation where the actual mass discharge might range from 3 to 75 kilograms per year. In the low-mass discharge case (3 kilograms per year) the chromium concentrations is calculated to be about **4 µg/L**. In the high-mass discharge case (75 kilograms per year) the chromium concentration increase would be about **85 µg/L**, thereby exceeding the New Mexico drinking water standards (Table 2) .

An analysis of the hypothetical impact on PM-3 if the current 4s/5s Scenario was in operation but no further remediation or change in the 4s/5s pumping rates were made in the future (i.e., no Adaptive Site Management). This analysis used the transects shown based on Figures 3a and 3b. The results was about 5 kg/yr mass discharge. This results in a resulting hypothetical increase in chromium concentrations in PM-3 between 1 and 28 µg/L, with a mid-range value of **6 µg/L**. Note these theoretical elevated concentrations would not be permanent because of this part of the plume is cut off from the source by the 4s/5s pumping scenario. However, it is likely that continued chromium plume remediation efforts would prevent this chromium from ever reaching PM-3.

Table 2. Theoretical increase in chromium concentrations in hypothetical impact to PM-3 water supply well for an Interim Measure “4s/5s Scenario”. These are hypothetical scenarios do not account for water supply well PM-3 no longer being in use and likely future full control of the plume.

Scenario	Low-Range Increase in Conc. (ug/L)	Mid-Range Increase in Conc. (ug/L)	High-Range Increase in Conc. (ug/L)
No Interim Measure	4	17	85
IM 4s/5s Restart (Fig. 3, 4)	1.1	5.6	28

IM: Interim Measure

## Conclusions

A risk-based approach is almost always used to remediate groundwater plumes, where the goal is to remove risks to potential receptors and not remove every last molecule of groundwater contamination. A mass discharge analysis, where the plume size, groundwater flowrate, and plume concentrations are integrated together, is an useful way groundwater experts gauge the general risk posed by a particular groundwater plume.

A mass discharge analysis was performed and indicated that using the most likely site data, about 15 kilograms per year (33 pounds a year) flows eastward in groundwater under natural groundwater flow conditions. Because of uncertainties in performing groundwater calculations, the chromium mass discharge could range between 3 and 75 kilograms per year. When a partial restart of the Interim measure was considered, this possible mass discharge range dropped to 5 kilograms per year. (Note 1 kilogram equals about 2.2. pounds).

The IRT wanted to know what the theoretical impact of the chromium plume to local users of groundwater. Therefore a *hypothetical scenario*, one that will not happen for multiple reasons, was evaluated where the chromium plume impacted by the nearest downgradient water supply well. In this analysis, 100% of the high concentration part of chromium plume was assumed to flow into a water supply well sometime in the future. The analysis then assumed that there was a partial Interim Measure restart (the “4s/5s” Scenario where only CrEx-4,5 and CrIN-4,5 are operated) and then only the portion of the plume that was not controlled by the Interim Measure impacted the water supply well. To compare these mass discharge scenarios to the State of New Mexico drinking water standard of 50 µg/L, add about 5 µg/L to account for background chromium concentrations.

Overall this mass discharge analysis provided this information about the general risk associated with the chromium plume:

1. For an almost impossible, worst case scenario where the Interim Measure or Final Correct Measure are never operated, the chromium concentration in the water supply well could increase between 4 and 85 µg/L **with a mid-range value of 17 µg/L**. In other words,



exceedance of the chromium drinking water standard is possible but very unlikely under this scenario.

2. For almost impossible, almost worst case scenario where a partial restart of the Interim Measure occurs and is never expanded and the Final Correct Measure is never constructed, the chromium concentration in the water supply well could increase between 1 and 28 µg/L **with a mid-range value of 6 µg/L**. In other words, exceedance of the chromium drinking water standard is extremely unlikely to occur under this scenario.

Overall these results gives the IRT more confidence that an extremely adverse outcome will not occur upon an immediate restart of the IM (or some version of the IM) even if some questions about the aquifer and plume are not fully resolved at restart time.

### *References*

- Broxton, D. (2023). Miocene Basalts as Potential Confining Beds. N3B Los Alamos/EM-LA.
- Einarson, M. D. & MacKay, D.M. (2001). Predicting impacts of groundwater contamination. *Environmental Science and Technology*, 35(3), 66A-73A. <https://doi.org/10.1021/es0122647>
- Gorelick, S.M., Freeze, R.A., Donohue, D., & Keely, J.F. (1993). *Groundwater Contamination Optimal Capture and Containment*. Lewis Publishers.
- Herman, J. and C. Martinez. (2024). Los Alamos National Laboratory Chromium Plume Cleanup. March 21, 2024. New Mexico Environmental Department.
- Interstate Technology & Regulatory Council (ITRC). 2010. Use and Measurement of Mass Flux and Mass Discharge. MASSFLUX-1. Washington, D.C.: Interstate Technology & Regulatory Council, Integrated DNAPL Site Strategy Team.
- Interstate Technology & Regulatory Council ITRC. (2017). Remediation Management of Complex Sites. In Interstate Technology and Regulatory Council: Vol. RMCS-1 (Issue October 2017, p. 2017). <https://rmcs-1.itrcweb.org>
- LANL. (2012). Phase II Investigation Report for Sandia Canyon. Sept 2012. LA-UR-12-24593. EP2012-0195.
- Newell, C.J., S.K. Farhat, D.T. Adamson, and B.B. Looney. 2011. Contaminant Plume Classification System Based on Mass Discharge. *Ground Water*, 49(6): 914-919.
- Nichols, E. and T. Roth. (2004). Using Mass Flux To Improve Cleanup Decisions. LUSTLine Bulletin 46, March 2004.
- U.S. EPA. (2008). A Systematic Approach for Evaluation of Capture Zones at Pump and Treat Systems. U.S. Environmental Protection Agency. [https://cfpub.epa.gov/si/si\\_public\\_record\\_report.cfm?Lab=NRMRL&dirEntryId=187788](https://cfpub.epa.gov/si/si_public_record_report.cfm?Lab=NRMRL&dirEntryId=187788)
- U.S. EPA. (2024a). How Superfund Addresses Groundwater Contamination. <https://www.epa.gov/superfund/how-superfund-addresses-groundwater->

[contamination#:~:text=Groundwater%20is%20extracted%20and%20conveyed,used%20to%20contain%20contaminant%20plumes.](#)

U.S. EPA. (2024b). Guidance for Cleaning Up Groundwater, Soil and Air at Corrective Action Facilities. <https://www.epa.gov/hw/guidance-cleaning-groundwater-soil-and-air-corrective-action-facilities>

Vesselinov et al. (2013). Data and Model-Driven Decision Support for Environmental Management of a Chromium Plume at Los Alamos National Laboratory. WM2013 Conference, February 24 – 28, 2013, Phoenix, Arizona USA.

## **Appendix N**

**Batu (2024d) - The Conceptual Model for the Water-Bearing Formations Beneath the LANL Site and Determination Methods of the Breakthrough Curves at the Bottom of the Vadose Zone and Degradation Rates of Chromium ( $\text{Cr}^{6+}$ ), Los Alamos, New Mexico**

# **The Conceptual Model for the Water-Bearing Formations Beneath the LANL Site and Determination Methods of the Breakthrough Curves at the Bottom of the Vadose Zone and Degradation Rates of Chromium ( $Cr^{6+}$ ), Los Alamos, New Mexico**

---

Vedat Batu, Ph.D., P.E.  
Argonne Associate  
Argonne National Laboratory  
Lemont, Illinois

**August 16, 2024**

This page intentionally left blank.

## Executive Summary

In this report, the site history and conceptual model for the water-bearing formations beneath the Los Alamos National Laboratory as well as the rationales behind that are presented. Based on the available reports and papers, the temporal release of chromium ( $Cr^{6+}$ ), the formations in the vadose zone, and the formations in the aquifer are briefly described. Also, the methods for the determination of the breakthrough curves with analytical as well as numerical solute transport solutions at the bottom of the vadose zone are presented. Using the chromium ( $Cr^{6+}$ ) concentration data, degradation rates of chromium ( $Cr^{6+}$ ) under different conditions have been estimated.

In Section 1, the purpose of the report is described.

In Section 2, after presenting the site history, the conceptual model is presented.

In Section 3, methods for the determination of the breakthrough curves at the bottom of the vadose zone are presented.

In Section 4, the methods for the determination of potential vertical chromium ( $Cr^{6+}$ ) plume extension are described.

In Section 5.0, estimated degradation rates of chromium ( $Cr^{6+}$ ) are presented. Based on the values of the degradation rate ( $\nu$ ) presented in Sections 5.4.1, 5.4.2, 5.4.3, and 5.4.4, it has been concluded that the estimated average degradation rate of chromium ( $Cr^{6+}$ ) is  $\nu_{avg} = 0.000009 d^{-1}$ .

# Contents

Executive Summary .....	ES-1
1. Purpose.....	1
2. Site History and Conceptual Model.....	1
2.1 Released Mass of Chromium .....	1
2.2 Formations in the Vadose Zone .....	2
2.3 Formations in the Aquifer .....	3
3. Methods for the Determination of the Breakthrough Curves at the Bottom of the Vadose Zone.....	3
3.1 Analytical Solute Transport Modeling Approach .....	3
3.1.1 Unsaturated Flow Equations .....	4
3.1.2 One-Dimensional Solute Transport Analytical Solutions for Finite-Time Sources .....	4
3.2 One-Dimensional Solute Transport Numerical Solutions for Finite-Time Sources....	4
4. Method for the Determination of the Vertical Extent of the Chromium ( $Cr^{6+}$ ) Plume .....	4
5. Estimation of the Degradation Rate of Chromium ( $Cr^{6+}$ ) .....	5
5.1 Estimation Methods for the Degradation Rate of Solutes .....	5
5.1.1 First-Type Source Solution-Based Degradation Rate Estimation Methods.....	5
5.1.2 Third-Type Source Solution-Based Degradation Rate Estimation Method .....	5
5.1.3 Comparative Evaluation of the First-Type and Third-Type Source Solutions...	5
5.2 Natural Attenuation of Chromium ( $Cr^{6+}$ ) .....	6
5.3 Analysis of Chromium ( $Cr^{6+}$ ) Concentration Data at the LANL Site .....	6
5.4 Estimation of Degradation Rates of Chromium .....	7
5.4.1 Degradation Rate for the Maximum Chromium ( $Cr^{6+}$ ) Concentrations.....	7
5.4.2 Degradation Rate for the Minimum Chromium ( $Cr^{6+}$ ) Concentrations.....	7
5.4.3 Degradation Rate Along the Main Flow Direction Along R-42, R-28, R-45, and R-13 Using the Chromium ( $Cr^{6+}$ ) Concentration Till 2022.....	8
5.4.4 Degradation Rate Along the Main Flow Direction Along R-42, R-28, and R-13 Using the Chromium ( $Cr^{6+}$ ) Concentration Till 2009.....	9
5.4.5 Results of the Estimated Degradation Rates .....	10
References.....	10

## Figures

- Figure 1. Cross-section of geology below the chromium ( $Cr^{6+}$ ) plume [References: Neptune (2003a, p. 28, Figure 11) and Neptune and Company, Inc. (2003b, p. 5, Figure 4).
- Figure 2. Hypothetical temporal chromium ( $Cr^{6+}$ ) concentration variation (breakthrough curve) at the bottom of the vadose zone from continuous and finite-time sources at the ground surface.
- Figure 3. The vertical cross-section of the conceptual site model beneath LANL.

- Figure 4. The horizontal layout of the conceptual site model beneath LANL.
- Figure 5. Determination of degradation rate ( $v$ ) from the maximum chromium ( $Cr^{6+}$ ) concentration data between April 2022 and March 2023 ( $K_h=4.493$  ft/d= $1.3695$  m/d).
- Figure 6. Determination of degradation rate ( $v$ ) from the minimum chromium ( $Cr^{6+}$ ) concentration data between April 2022 and March 2023 ( $K_h=4.493$  ft/d= $1.3695$  m/d).
- Figure 7. Chromium ( $Cr^{6+}$ ) versus time between 10/9/2008 and 7/28/2017 at R-42 well.
- Figure 8. Chromium ( $Cr^{6+}$ ) versus time between 5/20/2005 and 8/2/2017 at R-28 well.
- Figure 9. Chromium ( $Cr^{6+}$ ) versus time between 2/28/2009 and 3/23/2022 at R-45 S1 well.
- Figure 10. Chromium ( $Cr^{6+}$ ) versus time between 3/5/2009 and 3/23/2022 at R-45 S2 well.
- Figure 11. Chromium ( $Cr^{6+}$ ) versus time between 4/18/2002 and 1/28/2022 at R-13 well.
- Figure 12. Determination of degradation rate ( $v$ ) from Table 1 chromium ( $Cr^{6+}$ ) concentration data ( $K_h=3.385$  ft/d= $1.032$  m/d,  $n_e=0.15$ ).
- Figure 13. Determination of degradation rate ( $v$ ) from Table 1 chromium ( $Cr^{6+}$ ) concentration data ( $K_h=3.385$  ft/d= $1.032$  m/d,  $n_e=0.20$ ).
- Figure 14. Determination of degradation rate ( $v$ ) from Table 1 chromium ( $Cr^{6+}$ ) concentration data ( $K_h=6.18$  ft/d= $1.884$  m/d,  $n_e=0.15$ ).
- Figure 15. Determination of degradation rate ( $v$ ) from Table 1 chromium ( $Cr^{6+}$ ) concentration data ( $K_h=6.18$  ft/d= $1.884$  m/d,  $n_e=0.20$ ).
- Figure 16. Determination of degradation rate ( $v$ ) from Table 1 chromium ( $Cr^{6+}$ ) concentration data ( $K_h=3.385$  ft/d= $1.032$  m/d,  $n_e=0.15$ ).
- Figure 17. Determination of degradation rate ( $v$ ) from Table 1 chromium ( $Cr^{6+}$ ) concentration data ( $K_h=3.385$  ft/d= $1.032$  m/d,  $n_e=0.20$ ).
- Figure 18. Chromium ( $Cr^{6+}$ ) versus time between 10/9/2008 and 11/20/2008 at R-42 well.
- Figure 19. Chromium ( $Cr^{6+}$ ) versus time between 5/10/2005 and 11/10/2008 at R-28 well.
- Figure 20. Chromium ( $Cr^{6+}$ ) versus time between 4/18/2002 and 11/10/2008 at R-13 well.



- Figure 21. Determination of degradation rate ( $v$ ) from Table 2 chromium ( $Cr^{6+}$ ) concentration data ( $K_h=3.385$  ft/d= $1.032$  m/d,  $n_e=0.15$ ).
- Figure 22. Determination of degradation rate ( $v$ ) from Table 2 chromium ( $Cr^{6+}$ ) concentration data ( $K_h=3.385$  ft/d= $1.032$  m/d,  $n_e=0.20$ ).
- Figure 23. Determination of degradation rate ( $v$ ) from Table 2 chromium ( $Cr^{6+}$ ) concentration data ( $K_h=6.18$  ft/d= $1.884$  m/d,  $n_e=0.15$ ).
- Figure 24. Determination of degradation rate ( $v$ ) from Table 2 chromium ( $Cr^{6+}$ ) concentration data ( $K_h=6.18$  ft/d= $1.884$  m/d,  $n_e=0.20$ ).

## Tables

- Table 1. Chromium ( $Cr^{6+}$ ) concentration versus distance along the main flow direction formed by the wells R-42, R-28, R-45, and R-13 till August 2022.
- Table 2. Chromium ( $Cr^{6+}$ ) concentration versus distance along the main flow direction formed by the wells R-42, R-28, and R-13 till September 2008.

## Appendices

- Appendix A. Vertical Darcy Velocity in the Unsaturated Zone Under Uniform Water Content Conditions
- Appendix B. One-Dimensional Advective-Dispersive Analytical Solute Transport Solutions for Finite-Time Sources

# 1. Purpose

In this report, the site history and conceptual model for the water-bearing formations beneath the Los Alamos National Laboratory as well as the rationales behind that are presented. Based on the available reports and papers, the temporal release of chromium ( $Cr^{6+}$ ), formations in the vadose zone as well as in the aquifer are briefly described.

Then, methods for the determination of the breakthrough curves with analytical solute transport solutions at the bottom of the vadose zone are presented. Under one-dimensional uniform flow assumption in the vadose zone, the breakthrough can be determined with analytical solute transport solutions. For this purpose, the related unsaturated flow equations are presented (e.g., Warrick, 2003). Then, the well-known one-dimensional solute transport solutions under the first-type (constant concentration or Dirichlet) and third-type (flux-type or Cauchy) source conditions are presented in Appendix B (van Genuchten and Alves, 1982).

If there are difficulties in making uniform flow assumption in the vadose zone, numerical models may be needed. One of the well-known softwares is the POLLUTEv7 program (GAEA Technologies Ltd., 2004) which is based on Rowe and Booker (1985, 1991) and Rowe et al. (1994). POLLUTEv7 is a computer program that implements a solution to the one-dimensional dispersion-advection equation for a layered deposit of finite or infinite extent. POLLUTEv7 calculates the concentrations of a contaminant at user specified times and depths.

Using the chromium ( $Cr^{6+}$ ) concentration data, degradation rates of chromium ( $Cr^{6+}$ ) have been estimated. Details of the estimation process are not included in this report.

## 2. Site History and Conceptual Model

### 2.1 Released Mass of Chromium

In the report entitled "Fate and Transport Investigations Update for Chromium Contamination from Sandia Canyon" (LANL, 2008, pp. 2-3), it is stated that the main source of chromium ( $Cr^{6+}$ ) contamination are the cooling towers. Regarding this, the LANL (2008, pp. 2-3) report states:

*"Chromium usage for the TA-03 power plant appears to have averaged 16.3 kg/d (35.9 lb/d) from circa 1956 to 1972, resulting in an estimated total release of 31,000 to 72,000 kg of Cr(VI) as potassium dichromate into the south fork of upper Sandia Canyon, with the lower and upper bounds estimated to be 26,000 to 105,000 kg, respectively (LANL 2007, 098938, Appendix A). Effluent averaging from 7 to 18 mg/L Cr(VI) was discharged to Sandia Canyon at a rate of 380 to 1090 m<sup>3</sup>/d (100,000 to 288,000 gal./d). In addition to potassium dichromate, other cooling water additives were used at the power plant, as summarized in Table 2.0-1 of the Interim Measures Investigation Report for Chromium Contamination in Groundwater (LANL 2006, 094431). Specifically, phosphate was probably used from 1951 to 2001, and sodium molybdate (Na<sub>2</sub>MoO<sub>4</sub>) was used from 1993 to 2001."*

Vesselinov et al. (2013) include somewhat modified and narrated form of the above-given information as:

*“The contaminated effluents were discharged in Sandia Canyon between 1956 and 1972, when treated sanitary wastewater was used for power-plant cooling; the water was treated with potassium dichromate ( $K_2Cr_2O_7$ ), phosphate, zinc, and sulfuric acid. The total  $Cr^{6+}$  mass release into the Sandia Canyon is estimated at 54,000 kg with uncertainty bounds between 31,000 to 72,000 kg. During that period, the water flux released in the canyon was about 500 to 1000 m<sup>3</sup>/d; similar effluent volumes were probably discharged through 1992.”*

The Vesselinov et al. (2013) paper has a total of 15 (fifteen) authors most of which have LANL affiliation.

The vadose zone and aquifer of the site cross-section is shown in Figure 1 which is presented as Figure 11 in Neptune and Company, Inc. (2023a, p. 28) and Figure 4.1-8 in Neptune and Company, Inc. (2023b, p. 5).

In a recent report of U.S. Department of Energy (2022, p. 16), the following statements are included:

*“Site operations at the Los Alamos National Laboratory (LANL) resulted in the release of oxidized chromium, Cr(VI), into Sandia Canyon from cooling tower effluent from 1956 until 1972. The chromium traveled with the surface water approximately 3 miles downstream before migrating below ground surface. Chromium concentrations exceed 50 µg/L in the upper portion of the aquifer (Looney et al., 2012, LANL 2009).”*

## **2.2 Formations in the Vadose Zone**

Based on the aforementioned statements, some key characteristics of the site along with Figure 1 are as follows:

1. The thickness of the vadose zone above the water table varies between 1,295 ft and 1,315 ft and the water table is in the Puye Formation. The average thickness of the vadose zone is 1,305 ft.
2. As can be seen from Figure 1, the thickness of the Puye formation under the water table is between 200 ft and 300 ft around the chromium plume investigation area. The Puye Formation is underlain by the Miocene Sediments whose thickness varies between 1,990 ft and 2,020 ft. The Miocene sediments includes a relatively thin Miocene basalt formation, which is likely fractured, having a total thickness of around 200 ft.
3. As can be seen from Figure 1, the water table and bottom elevations of the unconfined aquifer are 5,585 ft MSL and 3,500 ft MSL, respectively. Therefore, the average aquifer thickness is  $b = 2,085 \text{ ft}$ .
4. As mentioned above, the contaminated effluents were discharged in Sandia Canyon between 1956 and 1972, when treated sanitary wastewater was used for power-plant

cooling; the water was treated with potassium dichromate ( $K_2Cr_2O_7$ ), phosphate, zinc, and sulfuric acid. And the total chromium ( $Cr^{6+}$ ) mass release into the Sandia Canyon is estimated at 54,000 kg with uncertainty bounds between 31,000 to 72,000 kg.

5. The total 54,000 kg chromium ( $Cr^{6+}$ ) mass was released during a 16-yr time period from 1956 to 1972. However, the temporal release status of this mass in the vadose zone appears to be unknown.
6. It will take some time the chromium ( $Cr^{6+}$ ) mass to reach to the water table. Therefore, its mass flux at the water table will be a time-dependent quantity. After the chromium mass front reaches to the water table, one should expect that the chromium concentration at the water table will gradually increase. And after reaching to a maximum value, it will decrease as time goes on and eventually it will approach to zero. This situation is shown schematically in Figure 2.

Using the information and data in Figure 1, the conceptual site model (CSM) is shown in Figure 3. The vadose zone (VZ) has an average thickness of 1,305 ft and is composed of the Bandelier Tuff, Gerros del Rio Basalt, and Puye Formation. As can be seen from Figure 3, the Gerros del Rio basalt is thickest one (705 ft) and is located between the Bandelier Tuff and Puye Formation having 400 ft and 200 ft thicknesses, respectively, and has holes. Since the chromium ( $Cr^{6+}$ ) source at the ground surface is a finite-time source, the temporal variation of the chromium ( $Cr^{6+}$ ) concentration will be like a bell-shaped curve shown in Figure 2 and will be elaborated later on. Figure 4 is the horizontal layout of the conceptual site model (CSM) beneath LANL.

### **2.3 Formations in the Aquifer**

Using Figure 1, the formations in the aquifer are shown in Figure 3 with idealized form. As noted in Figure 3, all formations have dips towards the west. As shown in Figure 3, the Puye Formation extends below the water table approximately 150 ft. And it is underlain by the Miocene Sediments having 1,135 ft thickness. Below this formation, there is the Miocene basalt formation that has approximately a combined 200 ft thickness and has holes. Below this formation, there is again around 1,315 ft thick Miocene Sediments. The formations under the water table in Figure 3 are predominantly under unconfined aquifer conditions and the unconfined aquifer has 5,000 ft thickness. There are two potential questions need to be answered: (a) Is there a bedrock beneath the 5,000 ft unconfined aquifer? and (b) do the Miocene Sediments continue all the way down to the bedrock?

## **3. Methods for the Determination of the Breakthrough Curves at the Bottom of the Vadose Zone**

### **3.1 Analytical Solute Transport Modeling Approach**

The chromium ( $Cr^{6+}$ ) source is assumed to be located at the ground surface under finite-time conditions. Beneath the chromium ( $Cr^{6+}$ ) source, the water content ( $\theta$ ) in the unsaturated zone is assumed to be uniform and the flow is one-dimensional from the ground surface towards to

the water table. Likewise, the transport of chromium ( $Cr^{6+}$ ) solutes is assumed to be one-dimensional as well. Figure 2 presents the expected shape of the concentration versus time curve (or the breakthrough curve) at the bottom of the unsaturated zone (or at the top of the water table) under finite-time conditions. In Figure 2, for comparison purpose, the breakthrough curve is also shown under continuous-time source conditions as well.

### 3.1.1 Unsaturated Flow Equations

Appendix A briefly summarizes the unsaturated flow equations. The groundwater velocity under uniform water content conditions is given by Eq. (A.5) of Appendix A as  $V = K(\theta)/\theta$ .

### 3.1.2 One-Dimensional Solute Transport Analytical Solutions for Finite-Time Sources

The one-dimensional solute transport analytical solutions for both first-type (constant concentration or Dirichlet) and third-type (flux-type or Cauchy) source conditions are given in Appendix B along with their partial differential equation as well as the initial and boundary conditions. For these solutions, calculations can be made with Excel.

## 3.2 One-Dimensional Solute Transport Numerical Solutions for Finite-Time Sources

The vadose zone (VZ) is composed of several formations. With the characteristics of these formations, the temporal variation at the bottom of VZ can be determined by numerical models.

Using the information and data in Figure 1, the cross-section of the conceptual site model (CSM) is shown in Figure 3. The vadose zone (VZ) has an average thickness of 1,305 ft and is composed of the Bandelier Tuff, Gerros del Rio basalt, and Puye Formation. As can be seen from Figure 3, the Gerros del Rio basalt is the thickest one (705 ft) and is located between the Bandelier Tuff and Puye Formation having 400 ft and 200 ft thicknesses, respectively. Since the chromium ( $Cr^{6+}$ ) source at the ground surface is a finite-time source, the temporal variation of the chromium ( $Cr^{6+}$ ) concentration will be like a bell-shaped curve shown in Figure 2.

The temporal variation of the chromium ( $Cr^{6+}$ ) concentration at the bottom of the VZ through layered deposits can only be determined with numerical models. One of the well-known software is the POLLUTEv7 program (GAEA Technologies Ltd., 2004) which is based on Rowe and Booker (1985, 1991) and Rowe et al. (1994). POLLUTEv7 is a computer program that implements a solution to the one-dimensional dispersion-advection equation for a layered deposit of finite or infinite extent. POLLUTEv7 calculates the concentrations of a contaminant at user specified times and depths.

## 4. Method for the Determination of the Vertical Extent of the Chromium ( $Cr^{6+}$ ) Plume

Based on measurements, currently the chromium<sup>6+</sup> plume is migrated several miles away from the source. As shown in Figures 3 and 4, due to vertical dispersion, the chromium<sup>6+</sup> can be extended vertically as the distance increases. Under uniform ground water velocity assumption

in the aquifer, the vertical concentration variations can be determined as function of distance from the source location. These variations can be determined using two-dimensional analytical solutions (e.g., Batu, 1989, 1993) in the x-z coordinate system in which the x coordinate is in the flow direction and the z coordinate is in the downward vertical direction from the water table. The programs were written in the FORTRAN language and they are menu-driven and can only be run in the XP computers.

## **5. Estimation of the Degradation Rate of Chromium ( $Cr^{6+}$ )**

### **5.1 Estimation Methods for the Degradation Rate of Solutes**

#### **5.1.1 First-Type Source Solution-Based Degradation Rate Estimation Methods**

During the past three decades, some methods were developed to estimate the degradation rate constant for various contaminant constituents under laboratory and field conditions (Buscheck and Alcantar, 1995; Chapelle et al., 1995; Zhang and Heathcote, 2003). These methods are all based on the steady-state, one-dimensional solution of the advective-dispersive solute transport differential equation with degradation and sorption effects using the first-type (or Dirichlet-type) source condition. In other words, the source concentration is assumed to be constant in the analytical solution.

The solution used by the aforementioned authors is given in many papers and books [e.g., Bear, 1979, p. 269, Eq. (7-138)]. The same solution is also given by Batu [2006, p. 59, Eq. (3-38)] as a special case of the general two- and three-dimensional analytical solutions. The degradation rate parameter estimation solution used by Buscheck and Alcantar (1995) is also given in Batu [2010, p. 561, Eq. (5)]. Chapelle et al. (1995), and Zhang and Heathcote (2003) also used the same equation.

#### **5.1.2 Third-Type Source Solution-Based Degradation Rate Estimation Method**

During the past four decades, the importance of the third-type source solutions have been emphasized by scientists in soil physics and ground water hydrology (van Genuchten and Parker, 1984; Parker and van Genuchten, 1984; Kreft and Zuber, 1986; van Genuchten and Wierenga, 1986).

Solution details of the one-dimensional steady-state solution are given in Batu (2010, pp. 562-563). And the corresponding solution is also given in [Batu, 2010, p. 562, Eq. (18)].

#### **5.1.3 Comparative Evaluation of the First-Type and Third-Type Source Solutions**

During the past four decades, it has been proven that the first-type (or constant source concentration) solution fails to satisfy the mass balance constraint at the inlet location and the degree of the failure depends on the degradation as well as the flow and solute transport parameters (van Genuchten and Parker, 1984; Parker and van Genuchten, 1984; Batu and van Genuchten, 1990; Batu, 2006).

The third-type source solution [Batu, 2010, p. 562, Eq. (18)], can be used in determining the degradation parameters due to the fact that the third-type source solution exactly satisfies the mass balance constraint at the inlet location, which the first-type source solution fails to do. Drs. Martinus Th. van Genuchten and Jack C. Parker are the pioneers of finding the mass balance violation at the inlet location of the first-type source solutions and exact mass balance satisfaction of the third-type source solutions. In the response of some comments, Vedat Batu, Martinus van Genuchten, and Jack C. Parker (Batu et al., 2012) included the following conclusion: *“In conclusion, we remain behind the statements in Batu (2010) that third-type solutions should be used in transport studies that focus on resident concentrations since they guarantee solute flux continuity across inlet boundaries.”*

## 5.2 Natural Attenuation of Chromium ( $Cr^{6+}$ )

Chromium ( $Cr^{6+}$ ) is a metal used in various industrial processes and ultimately making its way into aquifers. Regarding the **“Perspective on the Natural Attenuation of Chromium ( $Cr^{6+}$ )”**, Palmer and Puls (1994, p. 5) states:

*“If hexavalent chromium can be reduced and immobilized in the subsurface as a result of interaction with naturally existing reductants, then expensive remedial measures may not be required at certain sites. In principle, the natural attenuation of Cr(VI) in the subsurface is feasible. There are several natural reductants that can transform Cr(VI) to Cr(III). If the pH of the contaminant plume is between about 5 and 12, Cr(III) precipitates as Cr(OH)<sub>3</sub>, or as part of a solid solution with Fe(III), thereby keeping Cr(III) concentrations below 1 pmole/L (0.05 mg/L).”*

Whether or not natural attenuation at a particular site is a viable option depends on the characteristics of both the aquifer and the contaminant plume under investigation. Regarding **“Determining the Potential for Natural Attenuation”**, Palmer and Puls (1994, p. 6) states:

*“If “natural attenuation” is to be considered an alternative to expensive remediation efforts, additional characterization is required to demonstrate that the expectations are likely to be met. There is no single test that can tell us if natural attenuation of Cr(VI) will occur at a particular site. Several tests are briefly described which have been utilized to address key factors affecting Cr(VI) transport in the subsurface and describe how the results can be utilized in determining the potential for the natural attenuation of Cr(VI) in the subsurface.”*

## 5.3 Analysis of Chromium ( $Cr^{6+}$ ) Concentration Data at the LANL Site

The chromium ( $Cr^{6+}$ ) concentration data as presented in the report entitled *“Annual Progress Report on Chromium Plume Control Interim Measure Performance, April 2022 through March 2023”* (N3B Los Alamos, June, 2023) have been analyzed to estimate the degradation rate of chromium ( $Cr^{6+}$ ). In the following paragraphs, the results of data analysis are presented.

Inspection of the chromium ( $Cr^{6+}$ ) concentration data from the report of N3B Los Alamos (2023, pp. 25-57) indicate that the concentrations represent approximately steady-state conditions during the period of time of the measurements. The hydraulic head contours especially in the

western side in the aquifer beneath the LANL represent approximately uniform flow conditions (N3B Los Alamos, 2023, pp. 60-67). Under these conditions, using some well-known steady-state one-dimensional analytical solute transport solutions, degradation rates of contaminant constituents can be estimated using field-measured dissolved solute concentrations.

There is a lengthy analysis process in determining the average hydraulic gradient as well as usage of the chromium ( $Cr^{6+}$ ) concentration data which are not presented in this report.

## 5.4 Estimation of Degradation Rates of Chromium

### 5.4.1 Degradation Rate for the Maximum Chromium ( $Cr^{6+}$ ) Concentrations

Figure 5 shows the chromium ( $Cr^{6+}$ ) concentration versus the  $x$ -coordinate calculated from the solution in Batu [2010, p. 562, Eq. (18)] along with the maximum measured concentrations for  $K_{h-avg} = 4.493 \text{ ft/d} = 1.3695 \text{ m/d}$  average horizontal hydraulic conductivity value (Batu, April 3, 20024) [Important Note: This study was done in March 2024 and  $K_{h-avg} = 4.493 \text{ ft/d} = 1.3695 \text{ m/d}$  was taken from Neptune and Company, Inc. (2023a, Figure 13) report and is in the range of the  $K_h$  values of the reanalysis of PM-2 and PM-4 aquifer tests data conducted by ITR]. This is the average value of PM-2 and PM-4 drawdown data with the Theis type-curve matching from Neptune and Company, Inc. (2023a, Figure 13) using 850  $ft$  screen interval. The rest of parameters are shown in the box in Figure 5. The hydraulic gradient  $I = 0.000717 \text{ ft/ft}$  is estimated from the hydraulic head contour maps. The total porosity ( $n$ ) and effective porosity ( $n_e$ ) are assumed to be 0.40 and 0.15, respectively. The retardation factor of chromium ( $R_d = 1.75$ ) is taken from the literature. The bulk density ( $\rho_b = 2.65 \text{ g/cm}^3$ ) and effective molecular diffusion coefficient ( $D^* = 2.0 \times 10^{-9} \text{ m}^2/\text{s} = 1.86 \times 10^{-3} \text{ ft}^2/\text{d}$ ) are taken from the literature as well. The  $K_d$  value ( $0.113208 \text{ cm}^3/\text{g}$ ) is calculated from  $R_d = 1 + K_d\rho_b/n$  equation. The longitudinal dispersivity ( $\alpha_L = 20 \text{ m} = 65.62 \text{ ft}$ ) is estimated from Gelhar et al. (1992, p. 1968, Figure 2).

Based on trial runs with the Excel spreadsheet, it was found that the degradation rate  $\nu = 0.000004 \text{ d}^{-1}$  established the best match with the measured maximum chromium ( $Cr^{6+}$ ) concentration values with  $(Cr)_s = 382.78 \text{ } \mu\text{g/L}$  source concentration.

### 5.4.2 Degradation Rate for the Minimum Chromium ( $Cr^{6+}$ ) Concentrations

Figure 6 shows the chromium ( $Cr^{6+}$ ) concentration versus the  $x$ -coordinate calculated from the solution in Batu [2010, p. 562, Eq. (18)] along with the minimum measured concentrations for  $K_{h-avg} = 4.493 \text{ ft/d} = 1.3695 \text{ m/d}$  average horizontal hydraulic conductivity value [Important Note: This study was done in March 2024 and  $K_{h-avg} = 4.493 \text{ ft/d} = 1.3695 \text{ m/d}$  was taken from Neptune and Company, Inc. (2023a, Figure 13) report and is in the range of the  $K_h$  values of the reanalysis of PM-2 and PM-4 aquifer tests data conducted by ITR]. This is the average value of PM-2 and PM-4 drawdown data with the Theis type-curve matching from Neptune and Company, Inc. (2023a, Figure 13) using 850  $ft$  screen interval. The rest of parameters are shown in the box in Figure 6 and their selection reasons are given in Section 5.4.1.



Based on trial runs with the Excel spreadsheet, it was found that the degradation rate  $\nu = 0.000004 \text{ d}^{-1}$  established the best match with the measured maximum chromium ( $\text{Cr}^{6+}$ ) concentration values with  $(\text{Cr})_S = 160.32 \text{ } \mu\text{g/L}$  source concentration.

#### 5.4.3 Degradation Rate Along the Main Flow Direction Along R-42, R-28, R-45, and R-13 Using the Chromium ( $\text{Cr}^{6+}$ ) Concentration Till 2022

The chromium ( $\text{Cr}^{6+}$ ) concentration versus date data are shown in Figures 7, 8, 9, 10, and 11 for R-42, R-28, R-45 S1, R-45 S2, and R-13, respectively. In these figures, the average chromium ( $\text{Cr}^{6+}$ ) concentrations are also shown. And the average values are listed in Table 1 as function of the  $x$  coordinate for which the origin is R-42 and the  $x$  values are also included in Table 1. The wells R-42, R-45, and R-13 are approximately located on the main flow direction line. The Well R-28 is approximately 185 ft off from this line.

Figure 12 shows the chromium ( $\text{Cr}^{6+}$ ) concentration versus the  $x$ -coordinate calculated from the solution in Batu [2010, p. 562, Eq. (18)] along with the maximum measured concentrations for  $K_{h-avg} = 3.385 \text{ ft/d} = 1.032 \text{ m/d}$  average horizontal hydraulic conductivity (which is the average of  $4.49 \text{ ft/d}$  and  $2.28 \text{ ft/d}$ ) value (Batu, April 3, 20024). The hydraulic gradient  $I = 0.001 \text{ ft/ft}$  is along the main flow direction estimated from the hydraulic head contour maps. The total porosity ( $n$ ) and effective porosity ( $n_e$ ) are assumed to be 0.40 and 0.15, respectively. The retardation factor of chromium ( $R_d = 1.75$ ) is taken from the literature. The bulk density ( $\rho_b = 2.65 \text{ g/cm}^3$ ) and effective molecular diffusion coefficient ( $D^* = 2.0 \times 10^{-9} \text{ m}^2/\text{s} = 1.86 \times 10^{-3} \text{ ft}^2/\text{d}$ ) are taken from the literature as well. The  $K_d$  value ( $0.113208 \text{ cm}^3/\text{g}$ ) is calculated from  $R_d = 1 + K_d \rho_b / n$  equation. The longitudinal dispersivity ( $\alpha_L = 20 \text{ m} = 65.62 \text{ ft}$ ) is estimated from Gelhar et al. (1992, p. 1968, Figure 2). Based on trial runs with the Excel spreadsheet, it was found that the degradation rate  $\nu = 0.000009 \text{ d}^{-1}$  established the best match with the measured maximum chromium ( $\text{Cr}^{6+}$ ) concentration values with  $(\text{Cr})_S = 900.86 \text{ } \mu\text{g/L}$  source concentration at R-42.

Figure 13 shows the chromium ( $\text{Cr}^{6+}$ ) concentration versus the  $x$ -coordinate calculated from the solution in Batu [2010, p. 562, Eq. (18)] along with the maximum measured concentrations with the same data of Figure 12 with the exception that  $n_e = 0.20$ . Comparing Figure 13 with Figure 12, it can be observed that the data points are slightly off from the theoretical curve. Based on trial runs with the Excel spreadsheet, it was found that the degradation rate  $\nu = 0.000009 \text{ d}^{-1}$  established the best match with the measured maximum chromium ( $\text{Cr}^{6+}$ ) concentration values with  $(\text{Cr})_S = 900.86 \text{ } \mu\text{g/L}$  source concentration at R-42.

The data of Figure 14 are exactly the same as Figure 12 with the exception that  $K_{h-avg} = 6.18 \text{ ft/d} = 1.884 \text{ m/d}$  (Batu, April 3, 20024). Based on trial runs with the Excel spreadsheet, it was found that the degradation rate  $\nu = 0.000018 \text{ d}^{-1}$  established the best match with the measured maximum chromium ( $\text{Cr}^{6+}$ ) concentration values with  $(\text{Cr})_S = 900.86 \text{ } \mu\text{g/L}$  source concentration at R-42.

Figure 15 shows the chromium ( $\text{Cr}^{6+}$ ) concentration versus the  $x$ -coordinate calculated from the solution in Batu [2010, p. 562, Eq. (18)] along with the maximum measured concentrations

with the same data of Figure 14 with the exception that  $n_e = 0.20$ . Comparing Figure 15 with Figure 14, it can be observed that the data points are not significantly off from the theoretical curve. Based on trial runs with the Excel spreadsheet, it was found that the degradation rate  $\nu = 0.000014 d^{-1}$  established the best match with the measured maximum chromium ( $Cr^{6+}$ ) concentration values with  $(Cr)_s = 900.86 \mu g/L$  source concentration at R-42.

The data of Figure 16 are exactly the same as the data of Figure 12 with  $\nu = 0.00009 d^{-1}$  which is one order of magnitude higher than the value ( $\nu = 0.000009 d^{-1}$ ) of Figure 12. As can be seen from Figure 16,  $\nu = 0.00009 d^{-1}$  makes significant difference.

The data of Figure 17 are exactly the same as the data of Figure 13 with  $\nu = 0.00009 d^{-1}$  which is one order of magnitude higher than the value ( $\nu = 0.000009 d^{-1}$ ) of Figure 13. As can be seen from Figure 17,  $\nu = 0.00009 d^{-1}$  makes significant difference.

#### 5.4.4 Degradation Rate Along the Main Flow Direction Along R-42, R-28, and R-13 Using the Chromium ( $Cr^{6+}$ ) Concentration Till 2009

The chromium ( $Cr^{6+}$ ) concentration versus date data are shown in Figures 18, 19, and 20 for R-42, R-28, , and R-13, respectively. R-45 S1 and R-45 S2 have measured concentrations after 2009. In these figures, the average chromium ( $Cr^{6+}$ ) concentrations are also shown. And the average values are listed in Table 2 as function of the  $x$  coordinate for which the origin is R-42 and the  $x$  values are also included in Table 1. The wells R-42 and R-13 are approximately located on the main flow direction line. The Well R-28 is approximately 185 ft off from this line.

Figure 21 shows the chromium ( $Cr^{6+}$ ) concentration versus the  $x$ -coordinate calculated from the solution in Batu [2010, p. 562, Eq. (18)] along with the maximum measured concentrations for  $K_{h-avg} = 3.385 ft/d = 1.032 m/d$  average horizontal hydraulic conductivity (which is the average of 4.49 ft/d and 2.28 ft/d) value (Batu, April 3, 20024). The hydraulic gradient  $I = 0.001 ft/ft$  is along the main flow direction estimated from the hydraulic head contour maps. The total porosity ( $n$ ) and effective porosity ( $n_e$ ) are assumed to be 0.40 and 0.15, respectively. The retardation factor of chromium ( $R_d = 1.75$ ) is taken from the literature. The bulk density ( $\rho_b = 2.65 g/cm^3$ ) and effective molecular diffusion coefficient ( $D^* = 2.0 \times 10^{-9} m^2/s = 1.86 \times 10^{-3} ft^2/d$ ) are taken from the literature as well. The  $K_d$  value ( $0.113208 cm^3/g$ ) is calculated from  $R_d = 1 + K_d \rho_b / n$  equation. The longitudinal dispersivity ( $\alpha_L = 20 m = 65.62 ft$ ) is estimated from Gelhar et al. (1992, p. 1968, Figure 2). Based on trial runs with the Excel spreadsheet, it was found that the degradation rate  $\nu = 0.000009 d^{-1}$  established the best match with the measured maximum chromium ( $Cr^{6+}$ ) concentration values with  $(Cr)_s = 799.38 \mu g/L$  source concentration at R-42.

Figure 22 shows the chromium ( $Cr^{6+}$ ) concentration versus the  $x$ -coordinate calculated from the solution in Batu [2010, p. 562, Eq. (18)] along with the maximum measured concentrations with the same data of Figure 21 with the exception that  $n_e = 0.20$ . Comparing Figure 21 with Figure 22, it can be observed that the data points are slightly off from the theoretical curve. Based on trial runs with the Excel spreadsheet, it was found that the degradation rate  $\nu =$

$0.000009 d^{-1}$  established the best match with the measured maximum chromium ( $Cr^{6+}$ ) concentration values with  $(Cr)_S = 799.38 \mu g/L$  source concentration at R-42.

The data of Figure 23 are exactly the same as Figure 21 with the exception that  $K_{h-avg} = 6.18 ft/d = 1.884 m/d$  (Batu, April 3, 20024). Based on trial runs with the Excel spreadsheet, it was found that the degradation rate  $\nu = 0.000018 d^{-1}$  established the best match with the measured maximum chromium ( $Cr^{6+}$ ) concentration values with  $(Cr)_S = 799.38 \mu g/L$  source concentration at R-42.

The data of Figure 24 are exactly the same as Figure 23 with the exception that  $n_e = 0.20$ . Based on trial runs with the Excel spreadsheet, it was found that the degradation rate  $\nu = 0.000014 d^{-1}$  established the best match with the measured maximum chromium ( $Cr^{6+}$ ) concentration values with  $(Cr)_S = 799.38 \mu g/L$  source concentration at R-42.

#### 5.4.5 Results of the Estimated Degradation Rates

Based on the values of the degradation rate ( $\nu$ ) presented in Sections 5.4.1, 5.4.2, 5.4.3, and 5.4.4, it has been concluded that the estimated average degradation rate of chromium ( $Cr^{6+}$ ) is  $\nu_{avg} = 0.000009 d^{-1}$ .

## References

- Batu, V., "Hydraulic Conductivity Data Evaluation of the Neptune's Model for the LANL Site, Los Alamos, New Mexico," April, 3, 20024.
- Batu, V., *Applied Flow and Solute Transport Modeling in Aquifers: Fundamental Principles and Analytical and Numerical Solutions*, CRC Press Taylor & Francis Group, Boca Raton, Florida, 667 pp., 2006.
- Batu, V., "Estimation of Degradation Rates by Satisfying Mass Balance at the Inlet," *Ground Water*, Vol. 48, No. 4, pp. 560-568, 2010.
- Batu, V., "A Generalized Two-Dimensional Analytical Solute Transport Model in Bounded Media for Flux-type Finite Multiple Sources," *Water Resources Research*, Vol. 29, pp. 2881-2892, 1993.
- Batu, V., "A Generalized Two-Dimensional Analytical Solution for Hydrodynamic Dispersion in Bounded Media with the First-type Boundary Condition at the Source," *Water Resources Research*, Vol. 25, pp. 1125-1132, 1989.
- Batu, V., and M.Th. van Genuchten, "First- and Third-Type Boundary Conditions in Two-Dimensional Solute Transport Modeling," *Water Resources Research*, Vol. 26, No.2, pp. 339-350, 1990.
- Batu, V., M. Th. van Genuchten, and J.C. Parker, Reply to the comments of V. Gorokhovski and C.J. Neville, *Ground Water*, Vol. 51, No. 1, pp. 9-13, January-February, 2013.

- Bear, J., *Hydraulics of Groundwater*, McGraw-Hill Book Company, New York, 569 pp., 1979.
- Buscheck, T.E., and C.M. Alcantar, "Regression Methods and Analytical Solution to Demonstrate Intrinsic Bioremediation," in *Intrinsic Bioremediation*, Batelle Press, pp. 109-116, Columbus, Ohio, 1995.
- Chapelle, H.C., P.M. Bradley, D.R. Lovley, and D.A. Vroblesky, "Measuring Rates of Biodegradation in a Contaminated Aquifer Using Field and Laboratory Methods," *Ground Water*, Vol. 34, No.4, pp. 691-698, 1995.
- GAEA Technologies Ltd., R.K. Rowe and J.R. Booker, POLLUTEv7, Canada, 2004.
- Kreft, A., A. Zuber, "On the Physical Meaning of the Dispersion Equation and Its Solution for Different Initial and Boundary Conditions," *Chemical Engineering Science*, Vol. 33, pp. 1471-1480, 1978.
- LANL, "Fate and Transport Investigations Update for Chromium Contamination from Sandia Canyon", LA-UR-08-4702, Los Alamos, New Mexico, 276 pp., July, 2008.
- Neptune and Company, Inc., "*Hydraulic Analysis of the Pajarito Plateau*", EMID-702780, prepared by Neptune and Company, Inc. for the U.S. Department of Energy Environmental Management Los Alamos Field Office, Neptune and Company Inc., Los Alamos NM, 64 pp., June 16, 2023a.
- Neptune and Company, Inc., "*Chromium Model: Calibrated with Uncertainty through 2022*", prepared by Neptune and Company, Inc. for the U.S. Department of Energy Environmental Management Los Alamos Field Office, Neptune and Company Inc., Los Alamos NM, 69 pp., June 16, 2023b.
- N3B Los Alamos, "Annual Progress Report on Chromium Plume Control Interim Measure Performance, April 2022 through March 2023", June, 2023.
- Palmer, C.D., and R.W. Puls, "Natural Attenuation of Hexavalent Chromium in Groundwater and Soils," *EPA Ground Water Issue*, EPA/540/5-94/505, 12 pp., 1994.
- Parker, J.C., and M.Th. van Genuchten, "Flux-Averaged and Volume-Averaged Concentrations in Continuum Approaches to Solute Transport," *Water Resources Research*, Vol. 20, No.7, pp. 866-872, 1984.
- Rowe, R.K., and J.R. Booker, "1-D Pollutant Migration in Soils of Finite Depth", *Journal of Geotechnical Engineering*, ASCE, Vol. 111, GT4, pp. 13-42, 1985.
- Rowe, R.K. and J.R. Booker, "Pollutant Migration Through a Liner Underlain by Fractured Soil". *Journal of Geotechnical Engineering*, ASCE, Vol. 118, No. 7, pp. 1031-1046, 1991.
- Rowe, R.M., R.M. Quigley, and J.R. Booker, "Clayey Barriers for Waste Disposal Facilities", E & F N Spon, England, 1994.

- U.S. Department of Energy, "Independent Review of Groundwater Remediation Strategy of Hexavalent Chromium and RDX Groundwater Plumes at Los Alamos National Laboratory," NNLEMS-2022-00003, Rev. 1, 86 pp., November, 2022.
- van Genuchten, M.Th., W.J. Alves, "Analytical Solutions of the One-Dimensional Convective-Dispersive Solute Transport Equation," U.S. Department of Agriculture, Agricultural Research Service, *Technical Bulletin Number 1661*, 149 pp., June, 1982.
- van Genuchten, M.Th., J.C. Parker, "Boundary Conditions for Displacement Experiments through Short Laboratory Soil Columns," *Soil Science Society of America Journal*, Vol. 48, pp. 703-708, 1984.
- van Genuchten, M.Th., and P.J. Wierenga, "Solute Dispersion Coefficients and Retardation Factors," *Methods of Soil Analysis, Part I. Physical and Mineralogical Methods*, Agronomy Monographs No. 9, Soil Science Society of America, pp., 1025-1054, 1986.
- Vesselinov, V.V., D. Katzmann, D. Broxton, K. Birdsell, S. Reneau, D. Vaniman, P. Longmire, J. Fabryka-Martin, M. Ding, D. Hickmott, E. Jacobs, T. Goering, D. Harp, and P. Mishra, "Data and Model-Driven Decision Support for Environmental Management of a Chromium Plume at Los Alamos National Laboratory – 13264", *WM2013 Conference*, February 24-28, Phoenix, Arizona, 18 pp., 2013.
- Warrick, A.W, *Soil Water Dynamics*, Oxford University Press, New York, 391 pp., 2003.
- Zhang, Y.-K., and R.C. Heathcote, "An Improved Method for Estimation of Biodegradation Rate with Field Data," *Ground Water Monitoring & Remediation*, Vol. 23, No. 3, pp. 112-116, 2003.

## Figures

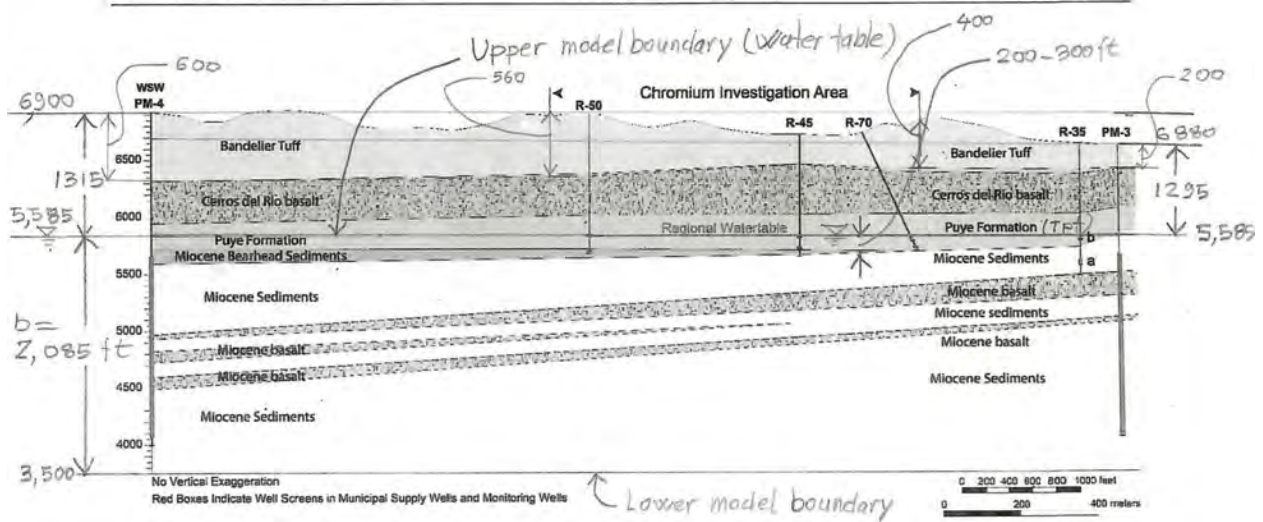


Figure 11. Cross-section of geology below the Cr plume. Supply wells are shown in red, and shallow Cr plume monitoring wells are shown in black (figure modified from (N3B 2021)).

Figure 1. Cross-section of geology below the chromium ( $Cr^{6+}$ ) plume [References: Neptune (2003a, p. 28, Figure 11) and Neptune and Company, Inc. (2003b, p. 5, Figure 4).

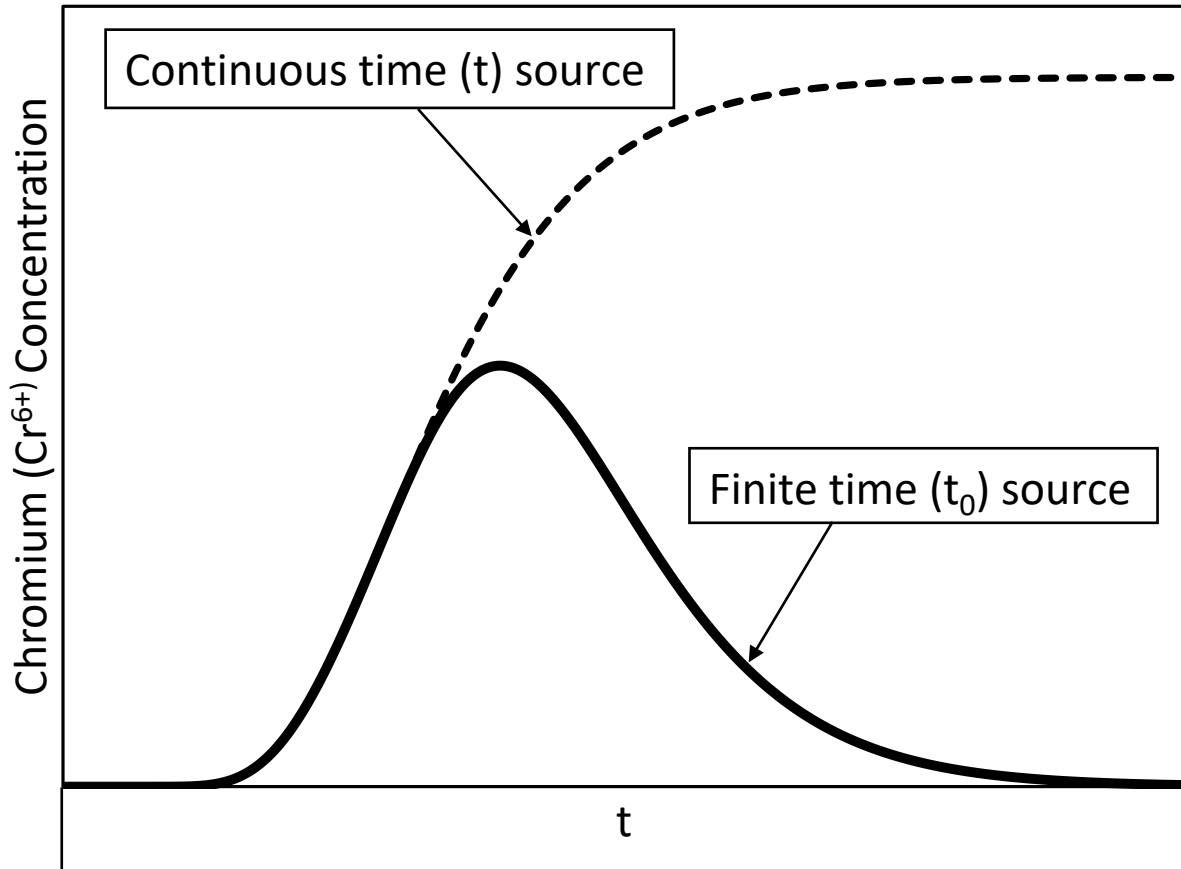


Figure 2. Hypothetical temporal chromium ( $Cr^{6+}$ ) concentration variation (breakthrough curve) at the bottom of the vadose zone from continuous and finite-time sources at the ground surface.



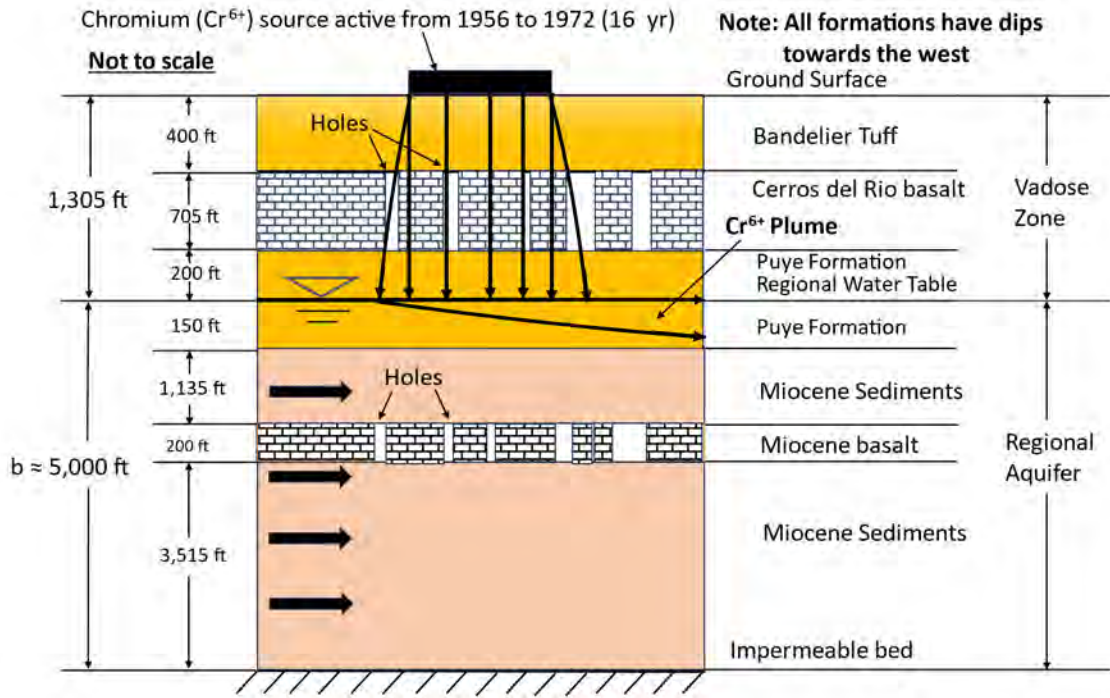


Figure 3. The vertical cross-section of the conceptual site model beneath LANL.

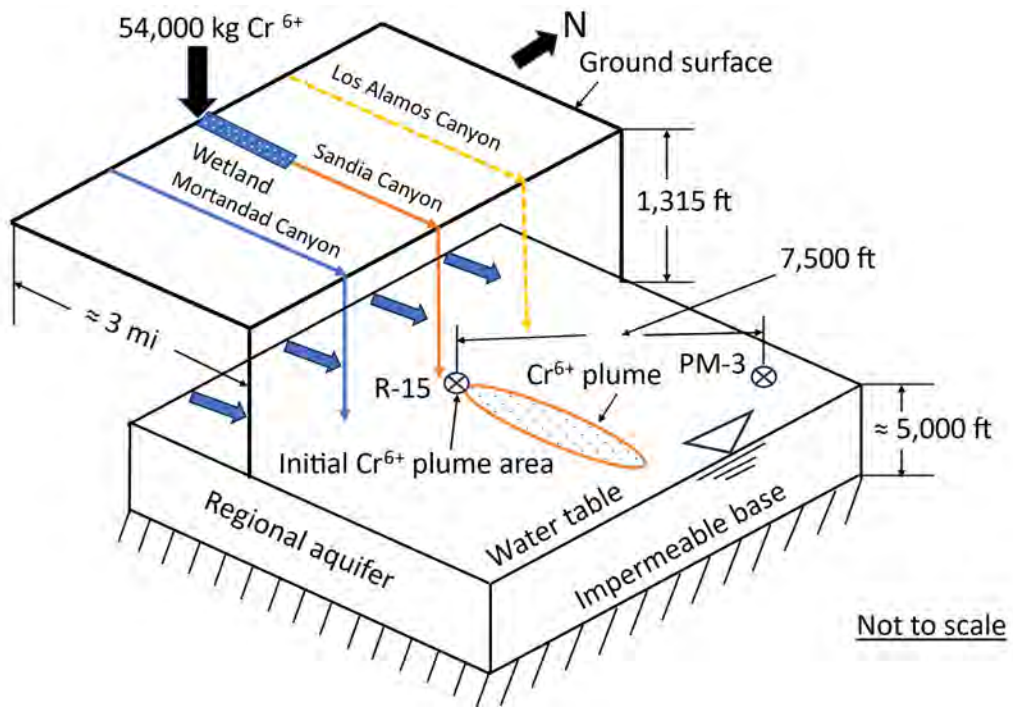


Figure 4. The horizontal layout of the conceptual site model beneath LANL.

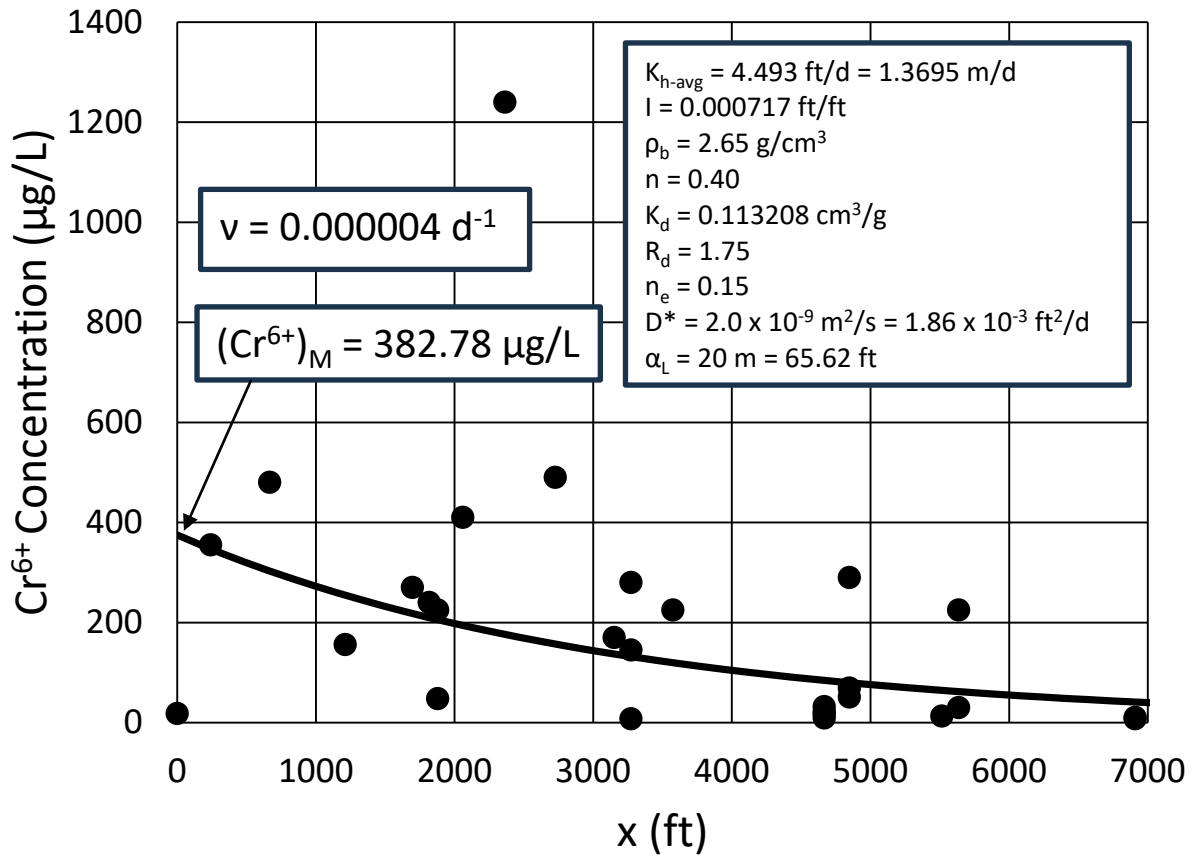


Figure 5. Determination of degradation rate ( $v$ ) from the maximum chromium ( $\text{Cr}^{6+}$ ) concentration data between April 2022 and March 2023 ( $K_h = 4.493 \text{ ft/d} = 1.3695 \text{ m/d}$ ).

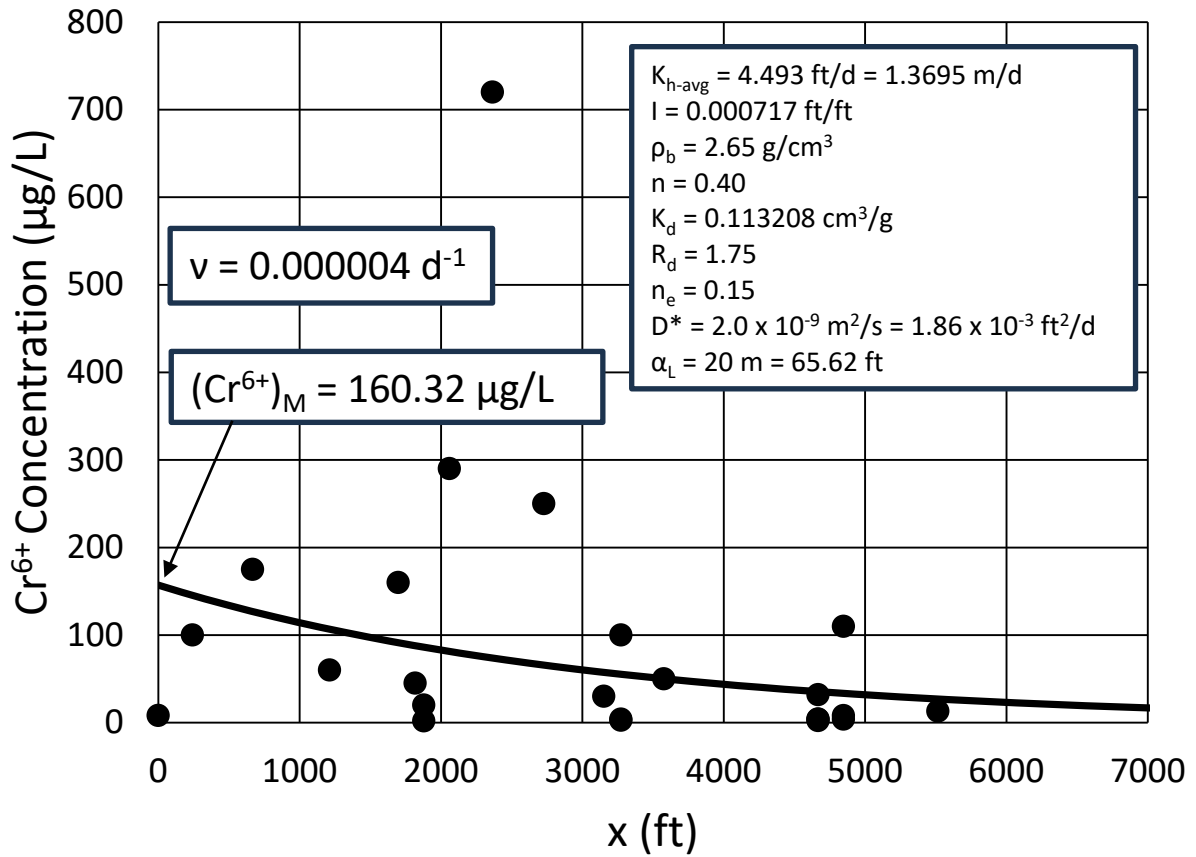


Figure 6. Determination of degradation rate ( $v$ ) from the minimum chromium ( $Cr^{6+}$ ) concentration data between April 2022 and March 2023 ( $K_h = 4.493 \text{ ft/d} = 1.3695 \text{ m/d}$ ).

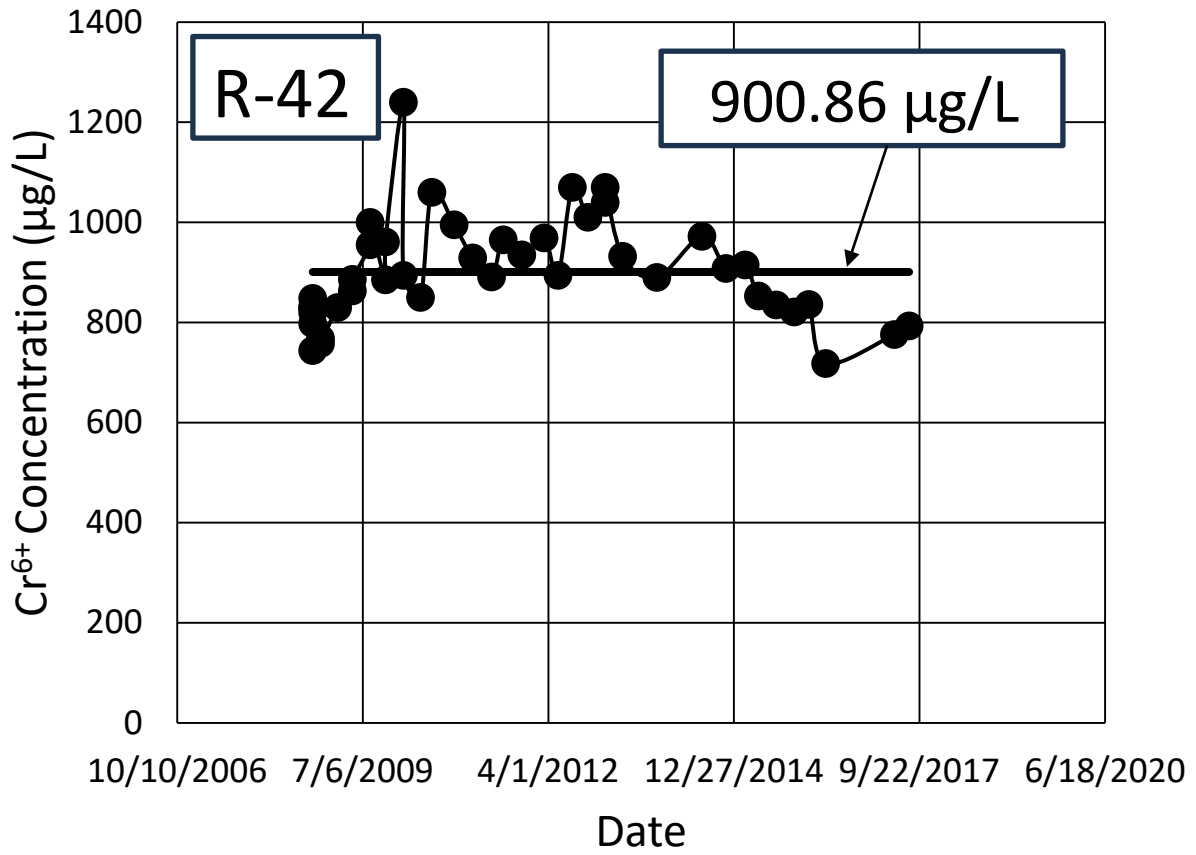


Figure 7. Chromium (Cr<sup>6+</sup>) versus time between 10/9/2008 and 7/28/2017 at R-42 well.

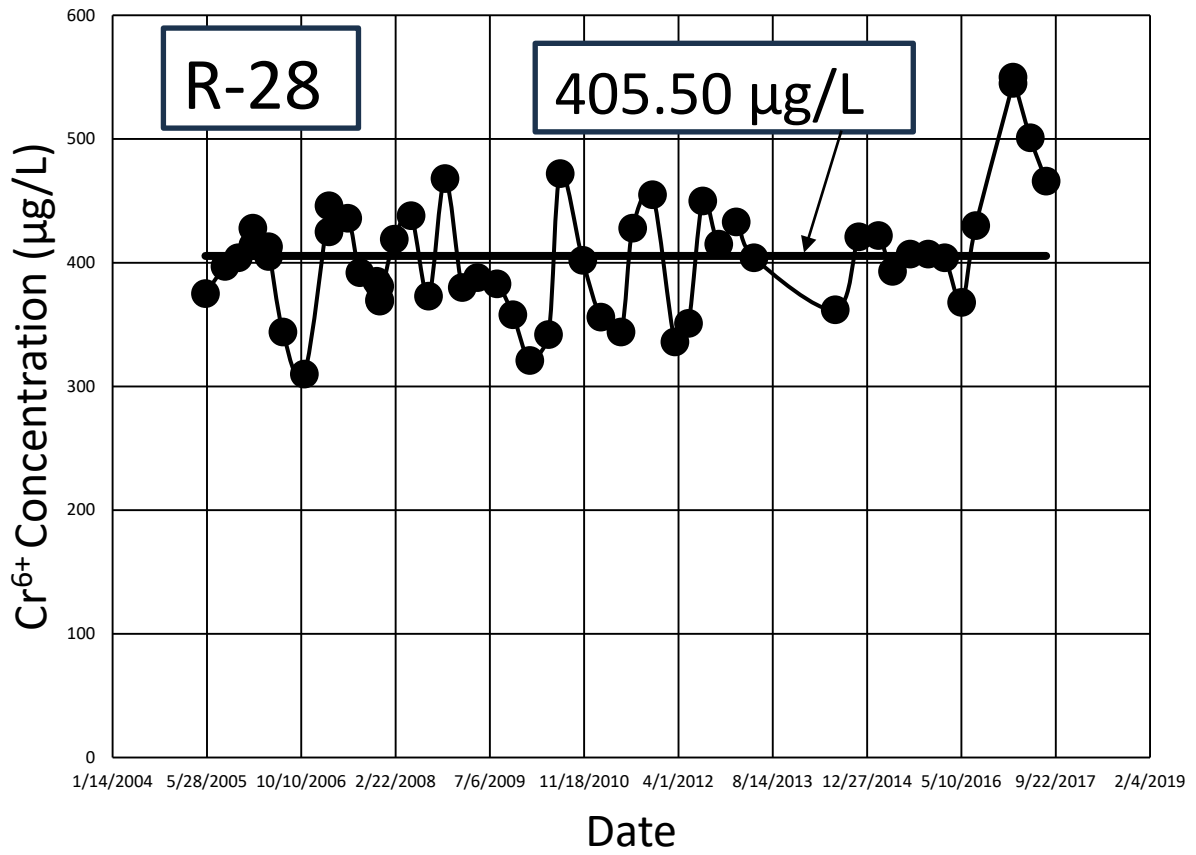
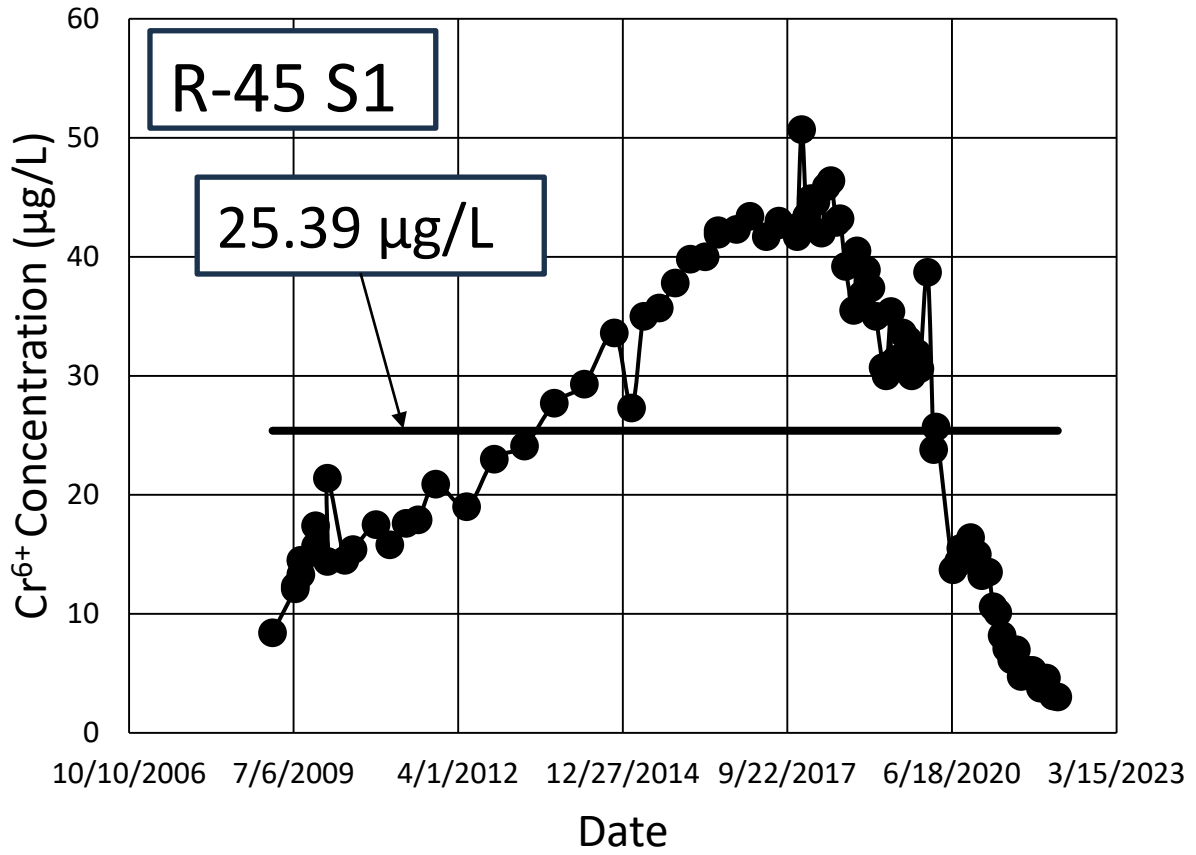


Figure 8. Chromium ( $Cr^{6+}$ ) versus time between 5/20/2005 and 8/2/2017 at R-28 well.



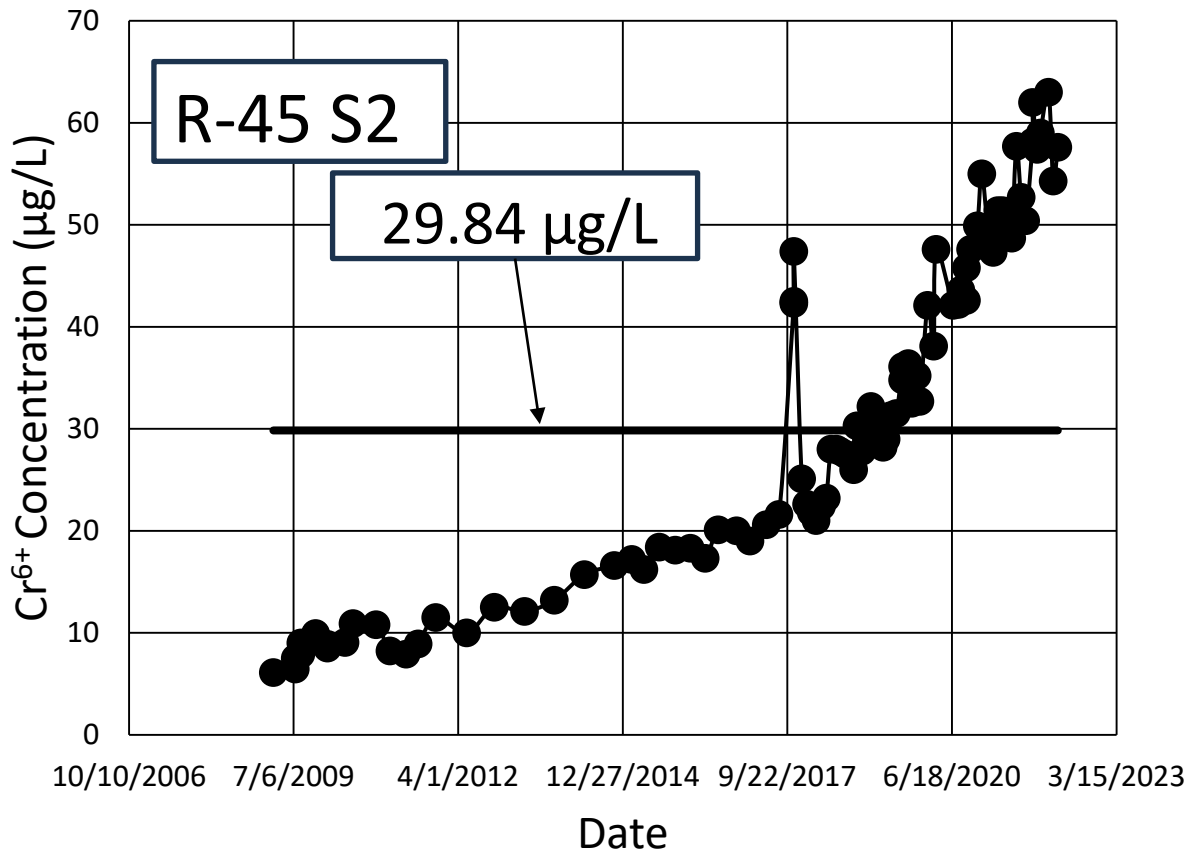


Figure 10. Chromium ( $Cr^{6+}$ ) versus time between 3/5/2009 and 3/23/2022 at R-45 S2 well.



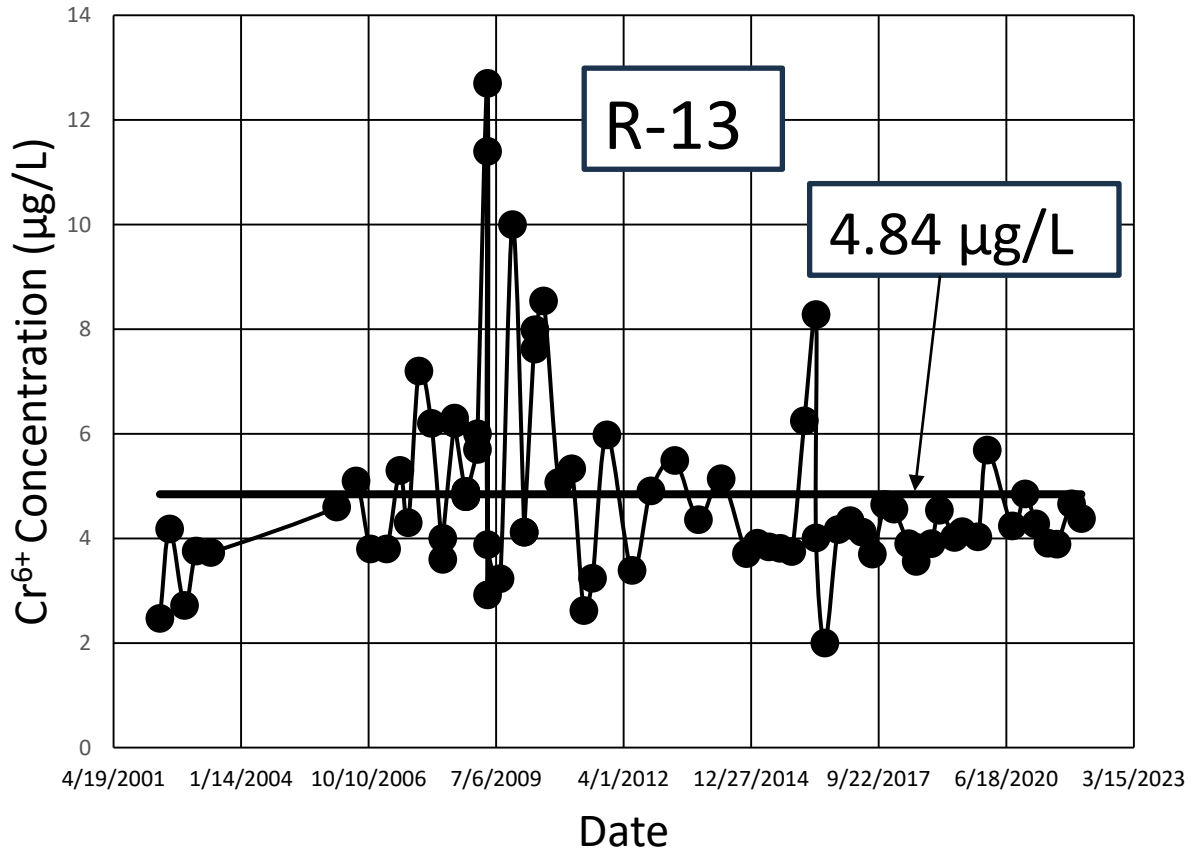


Figure 11. Chromium ( $Cr^{6+}$ ) versus time between 4/18/2002 and 1/28/2022 at R-13 well.

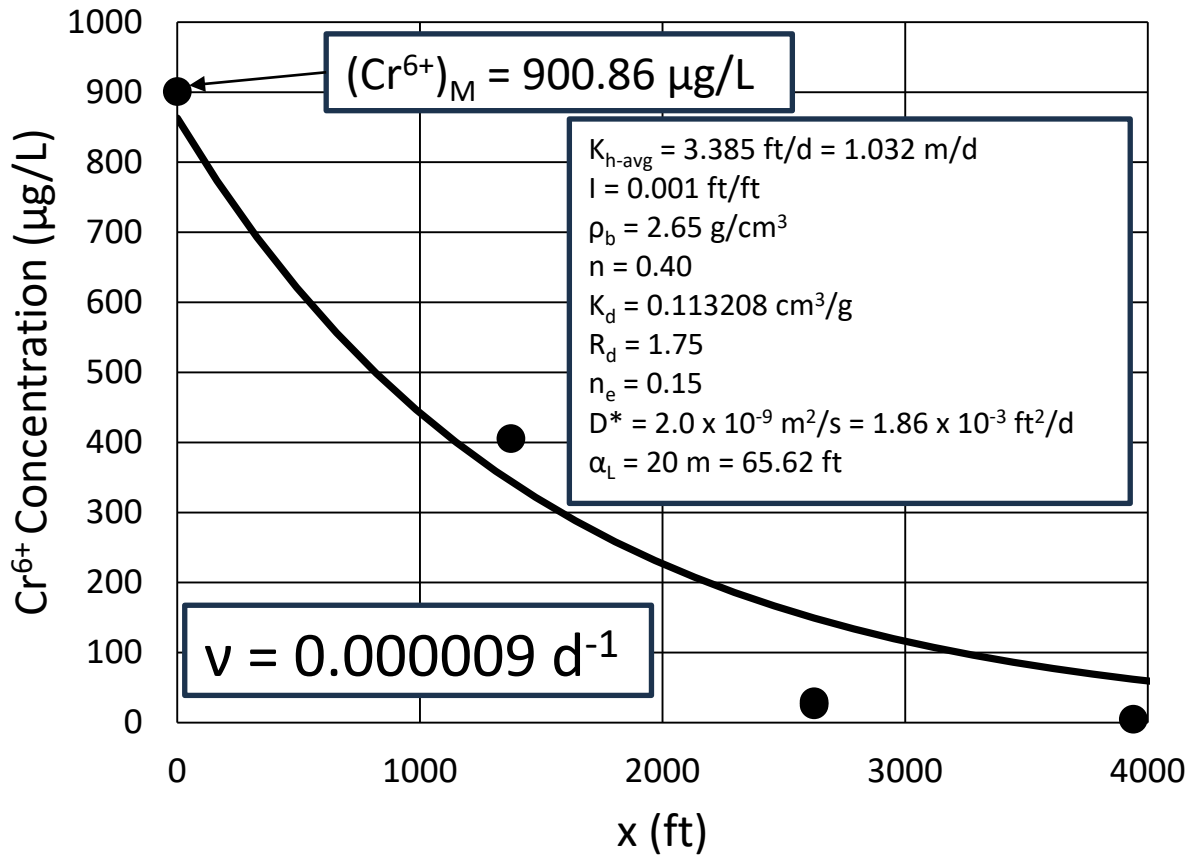


Figure 12. Determination of degradation rate ( $v$ ) from Table 1 chromium ( $Cr^{6+}$ ) concentration data ( $K_h = 3.385 \text{ ft/d} = 1.032 \text{ m/d}$ ,  $n_e = 0.15$ ).

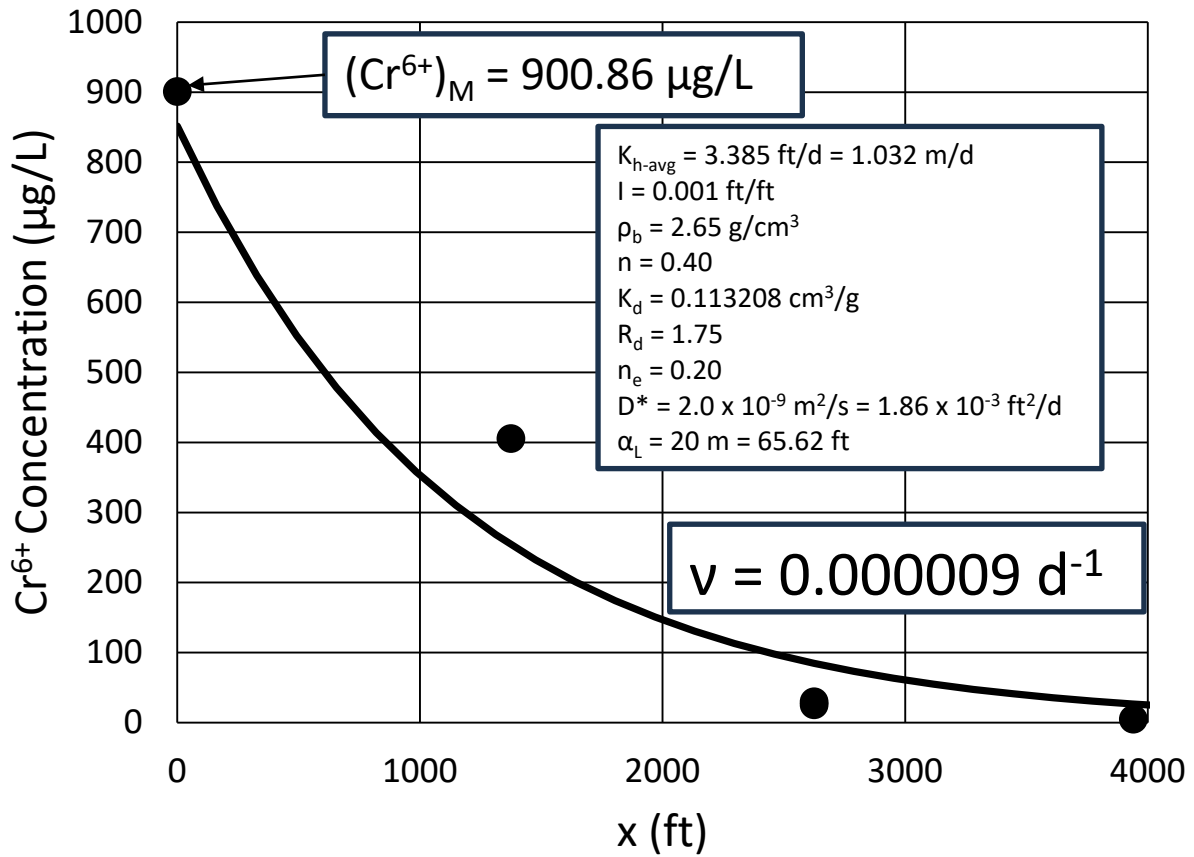


Figure 13. Determination of degradation rate ( $v$ ) from Table 1 chromium ( $Cr^{6+}$ ) concentration data ( $K_h = 3.385 \text{ ft/d} = 1.032 \text{ m/d}$ ,  $n_e = 0.20$ ).

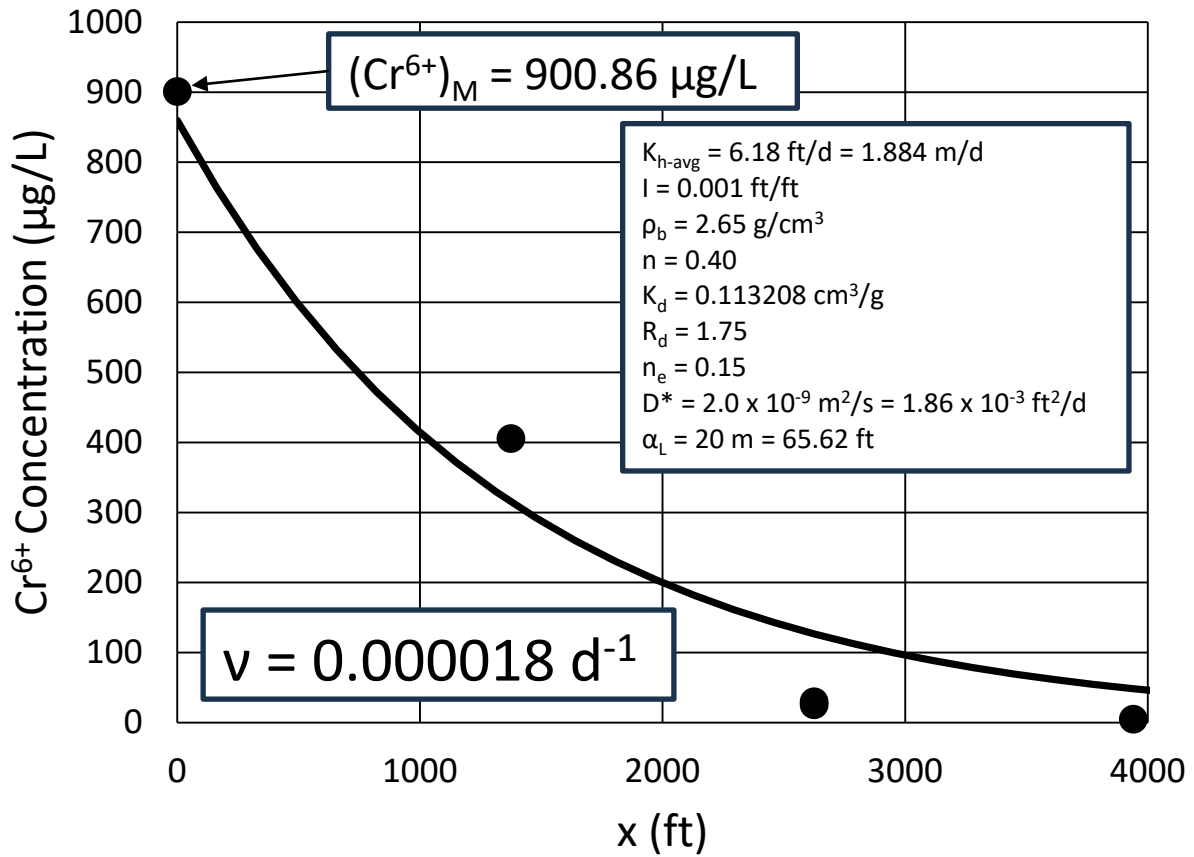


Figure 14. Determination of degradation rate ( $v$ ) from Table 1 chromium ( $Cr^{6+}$ ) concentration data ( $K_h = 6.18 \text{ ft/d} = 1.884 \text{ m/d}$ ,  $n_e = 0.15$ ).

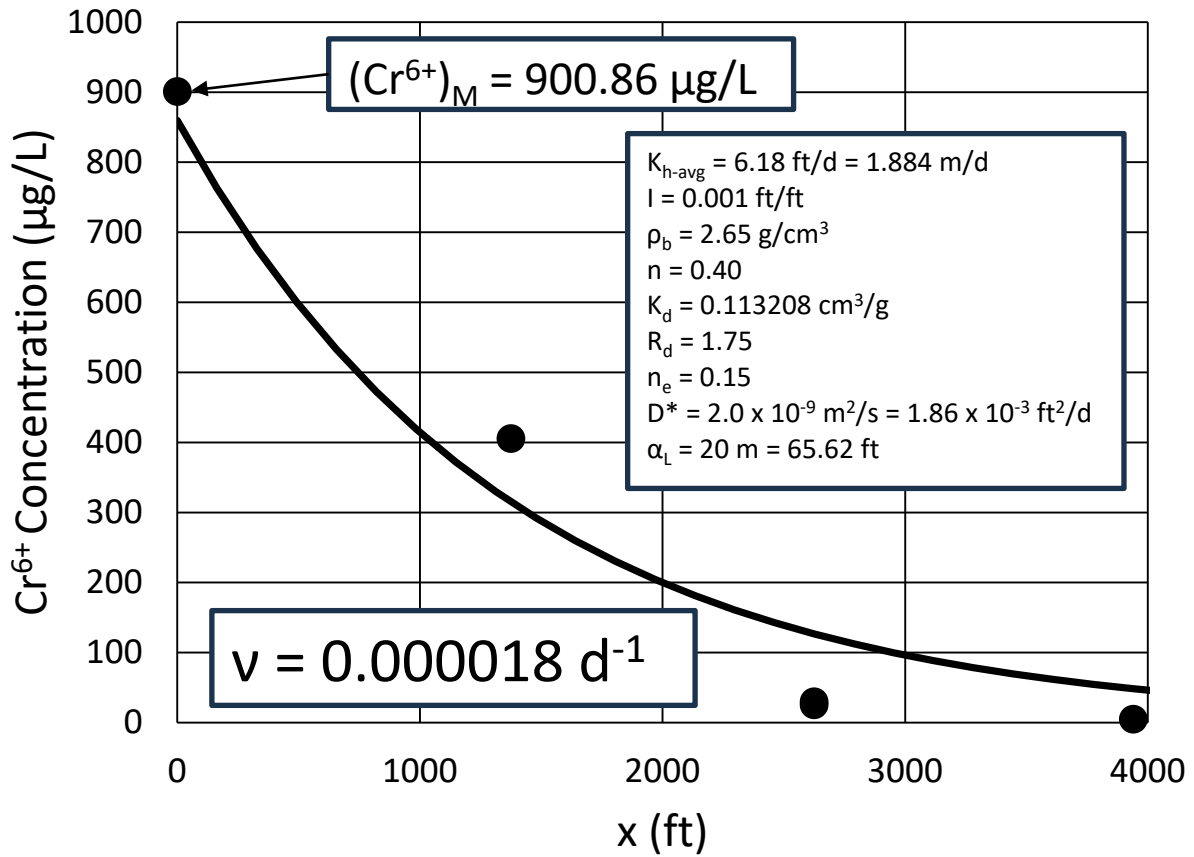


Figure 15. Determination of degradation rate ( $v$ ) from Table 1 chromium ( $Cr^{6+}$ ) concentration data ( $K_h = 6.18 \text{ ft/d} = 1.884 \text{ m/d}$ ,  $n_e = 0.20$ ).

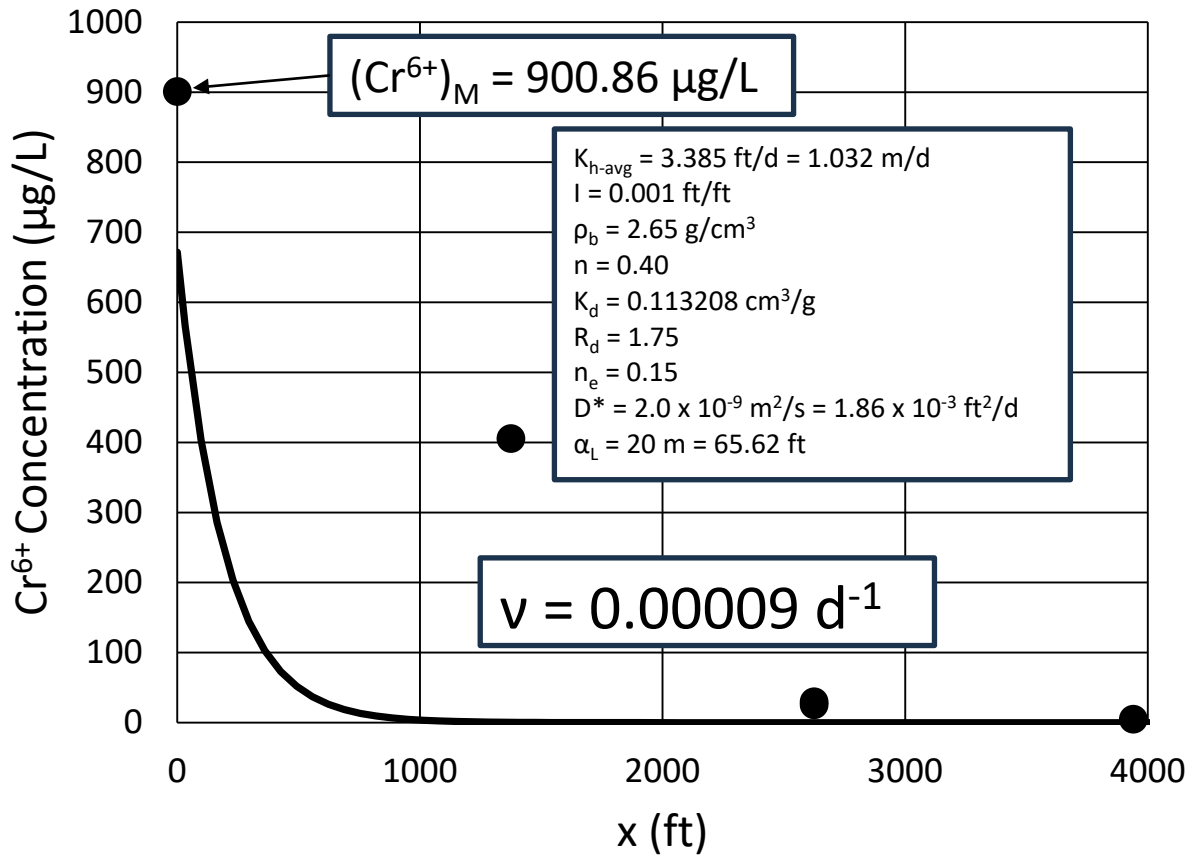


Figure 16. Determination of degradation rate ( $v$ ) from Table 1 chromium ( $Cr^{6+}$ ) concentration data ( $K_h = 3.385 \text{ ft/d} = 1.032 \text{ m/d}$ ,  $n_e = 0.15$ ).

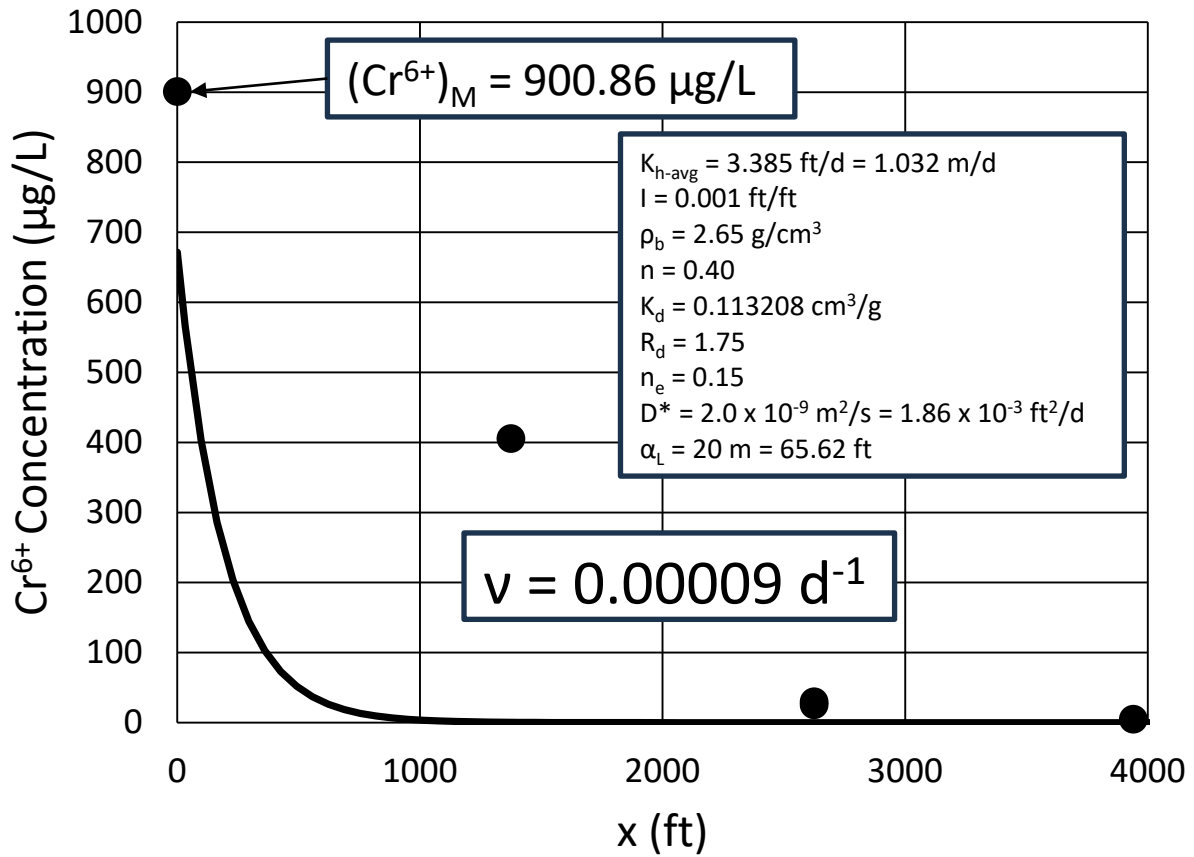


Figure 17. Determination of degradation rate ( $v$ ) from Table 1 chromium ( $Cr^{6+}$ ) concentration data ( $K_h = 3.385 \text{ ft/d} = 1.032 \text{ m/d}$ ,  $n_e = 0.20$ ).

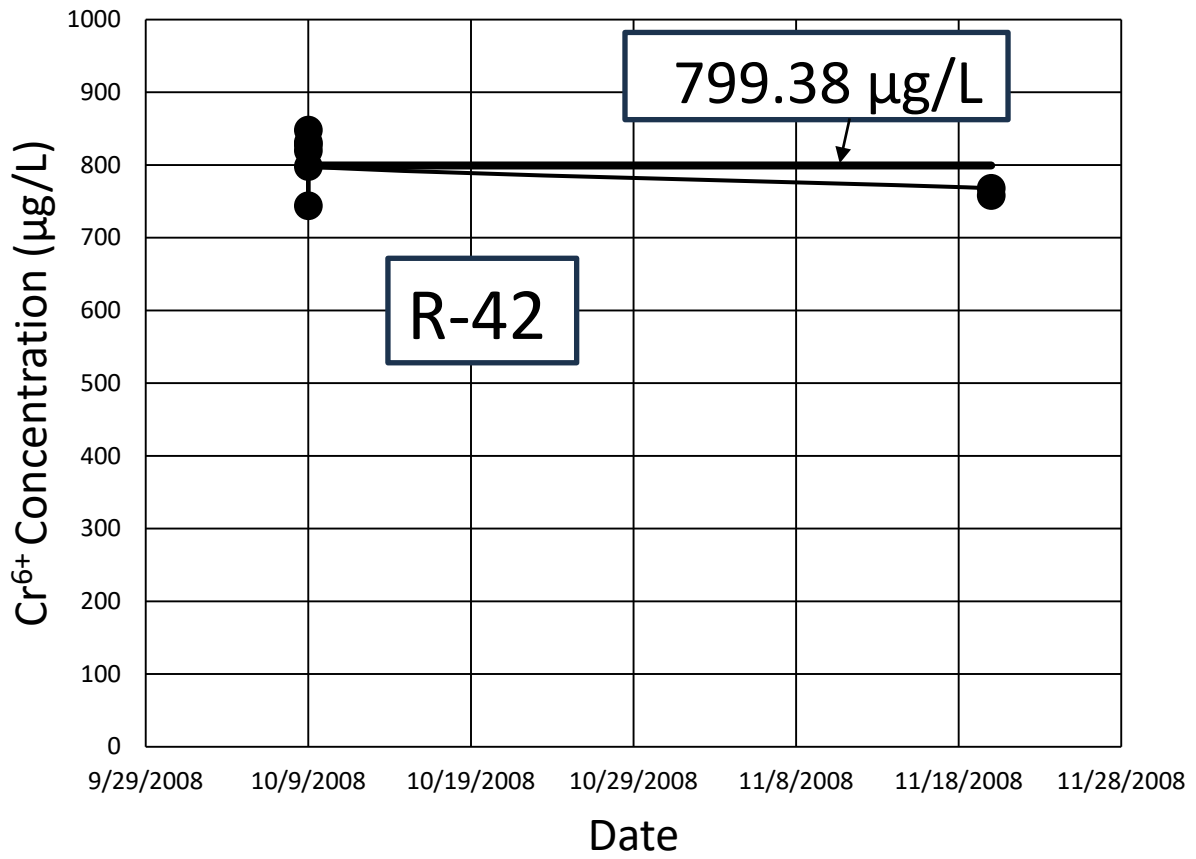


Figure 18. Chromium ( $Cr^{6+}$ ) versus time between 10/9/2008 and 11/20/2008 at R-42 well.



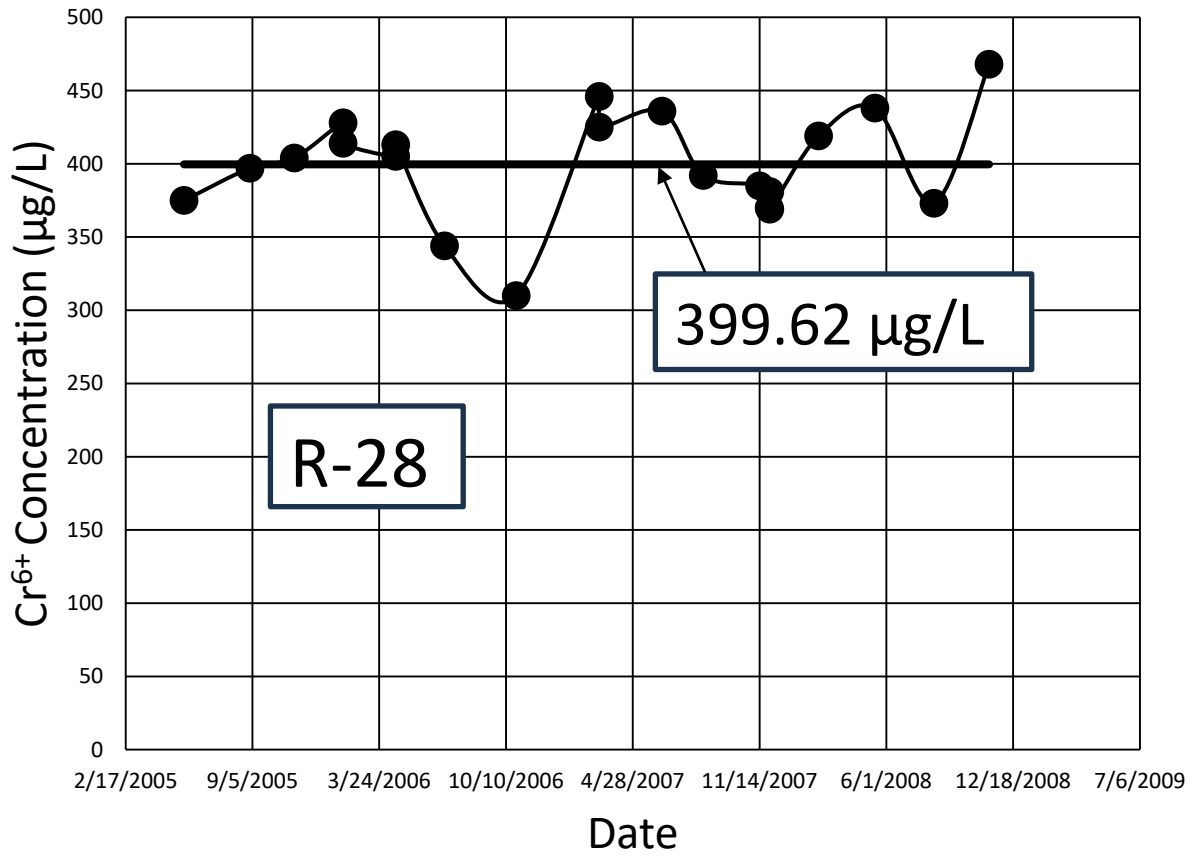


Figure 19. Chromium ( $Cr^{6+}$ ) versus time between 5/10/2005 and 11/10/2008 at R-28 well.

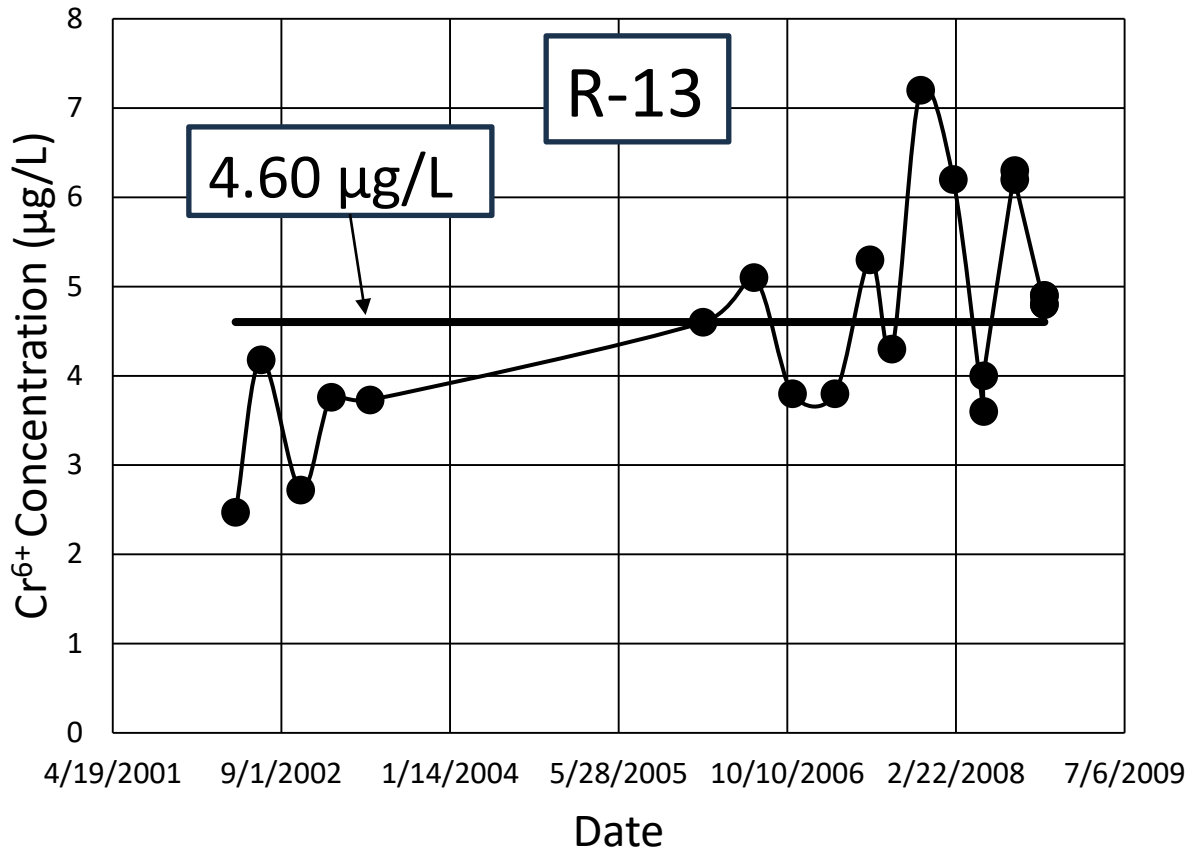


Figure 20. Chromium ( $Cr^{6+}$ ) versus time between 4/18/2002 and 11/10/2008 at R-13 well.

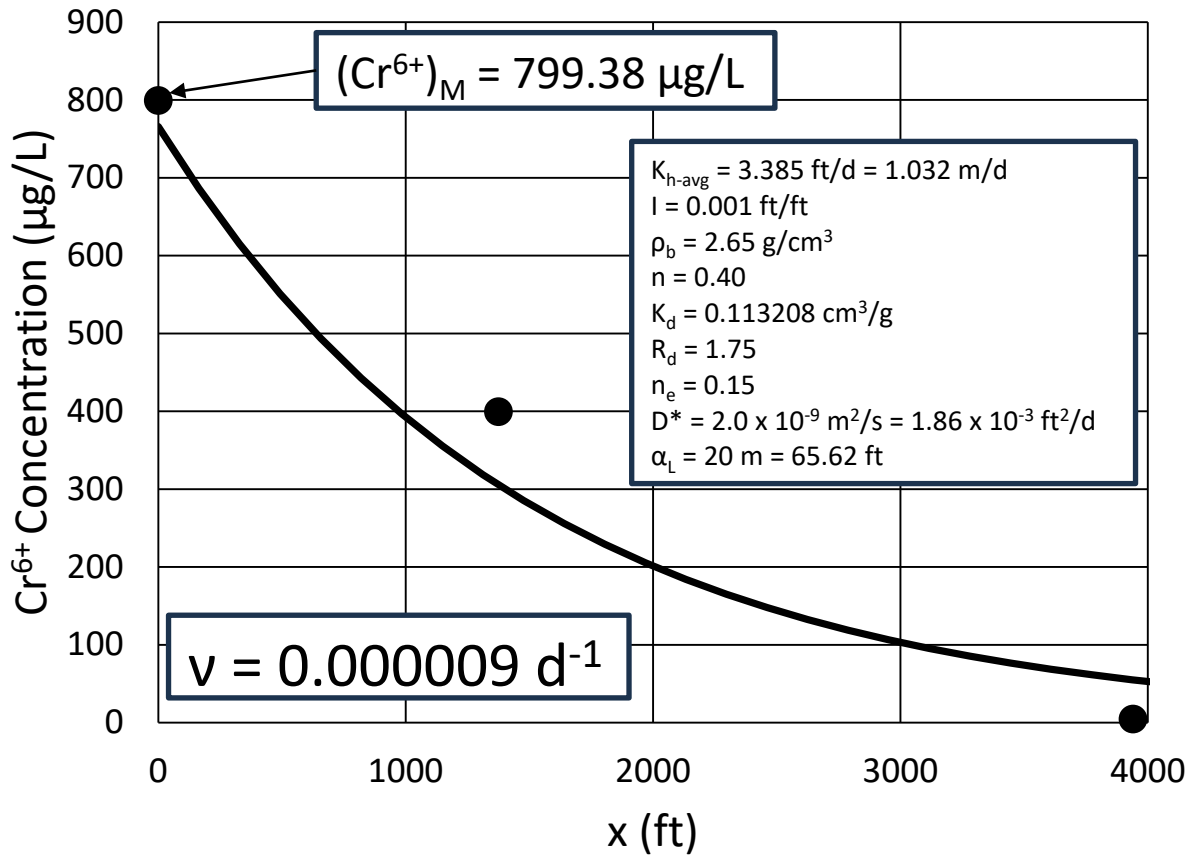


Figure 21. Determination of degradation rate ( $v$ ) from Table 2 chromium ( $Cr^{6+}$ ) concentration data ( $K_h = 3.385 \text{ ft/d} = 1.032 \text{ m/d}$ ,  $n_e = 0.15$ ).

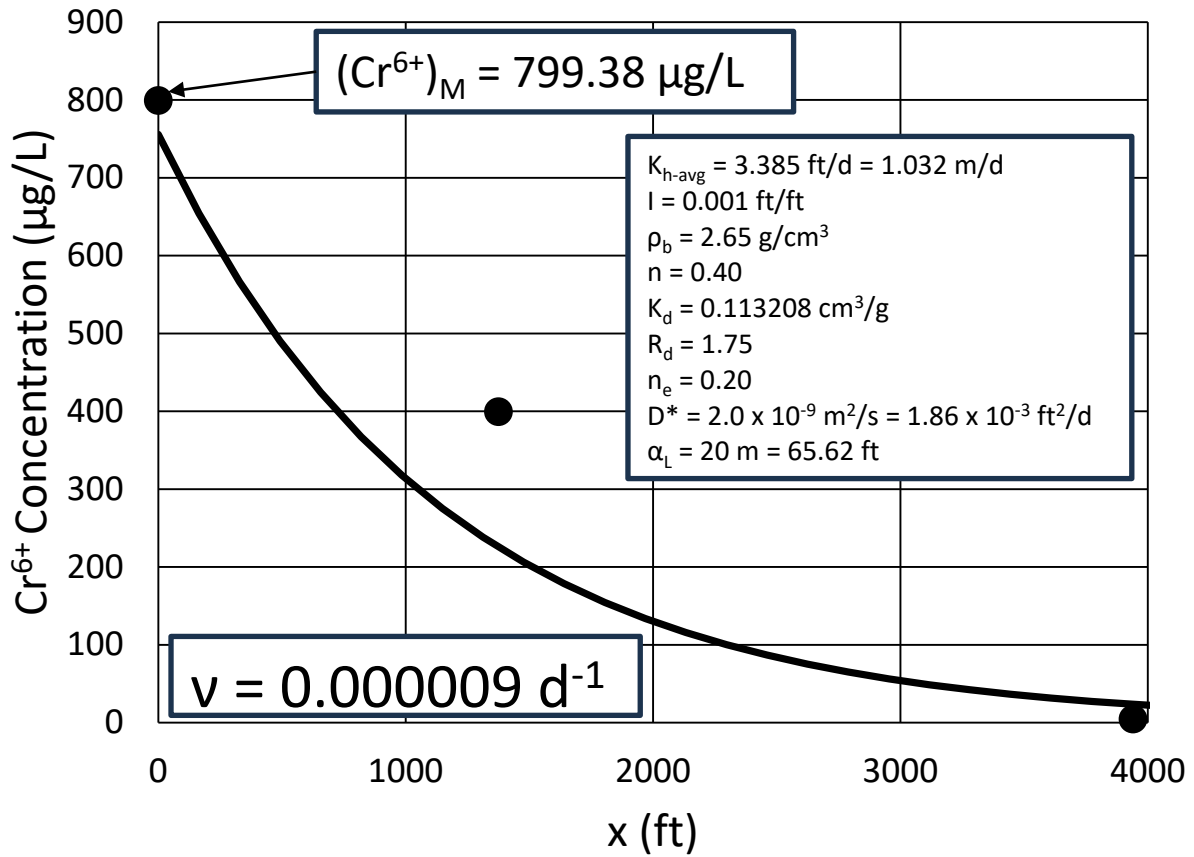


Figure 22. Determination of degradation rate ( $v$ ) from Table 2 chromium ( $Cr^{6+}$ ) concentration data ( $K_h = 3.385 \text{ ft/d} = 1.032 \text{ m/d}$ ,  $n_e = 0.20$ ).

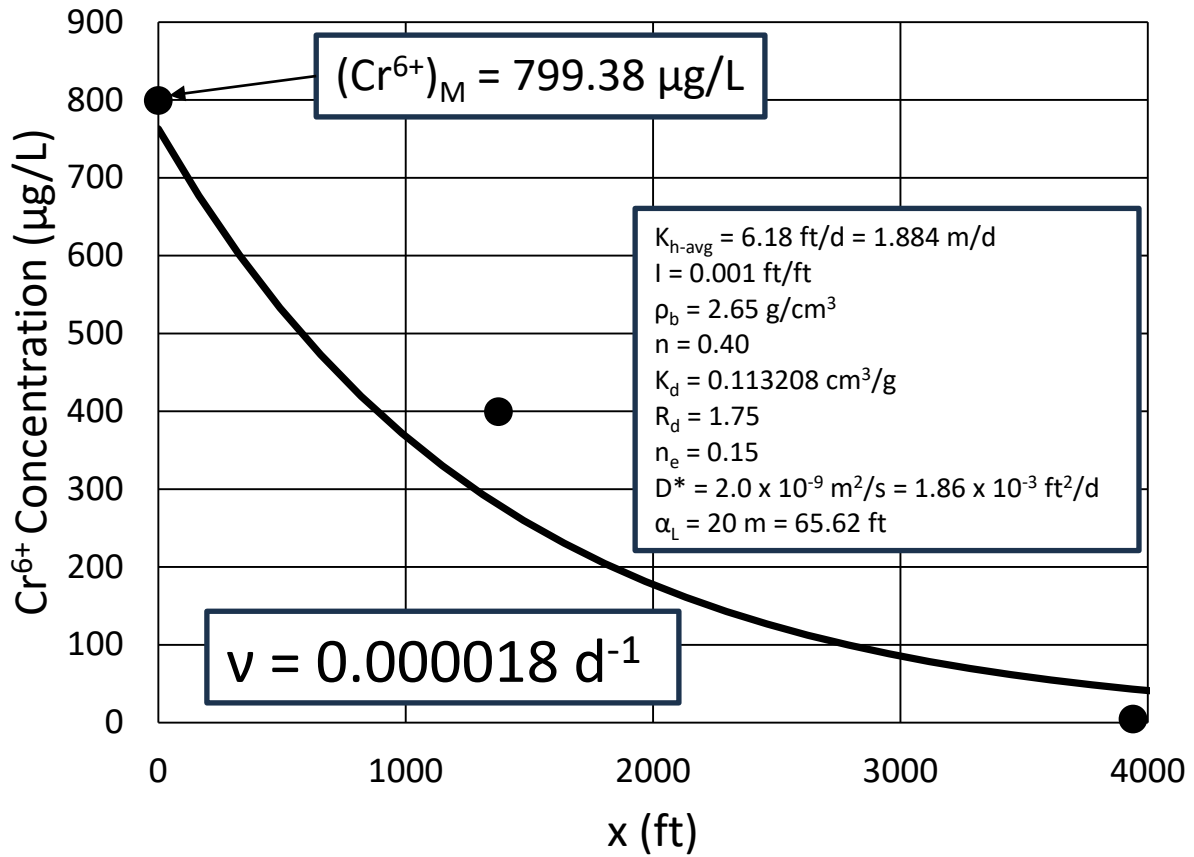


Figure 23. Determination of degradation rate ( $v$ ) from Table 2 chromium ( $Cr^{6+}$ ) concentration data ( $K_h = 6.18 \text{ ft/d} = 1.884 \text{ m/d}$ ,  $n_e = 0.15$ ).

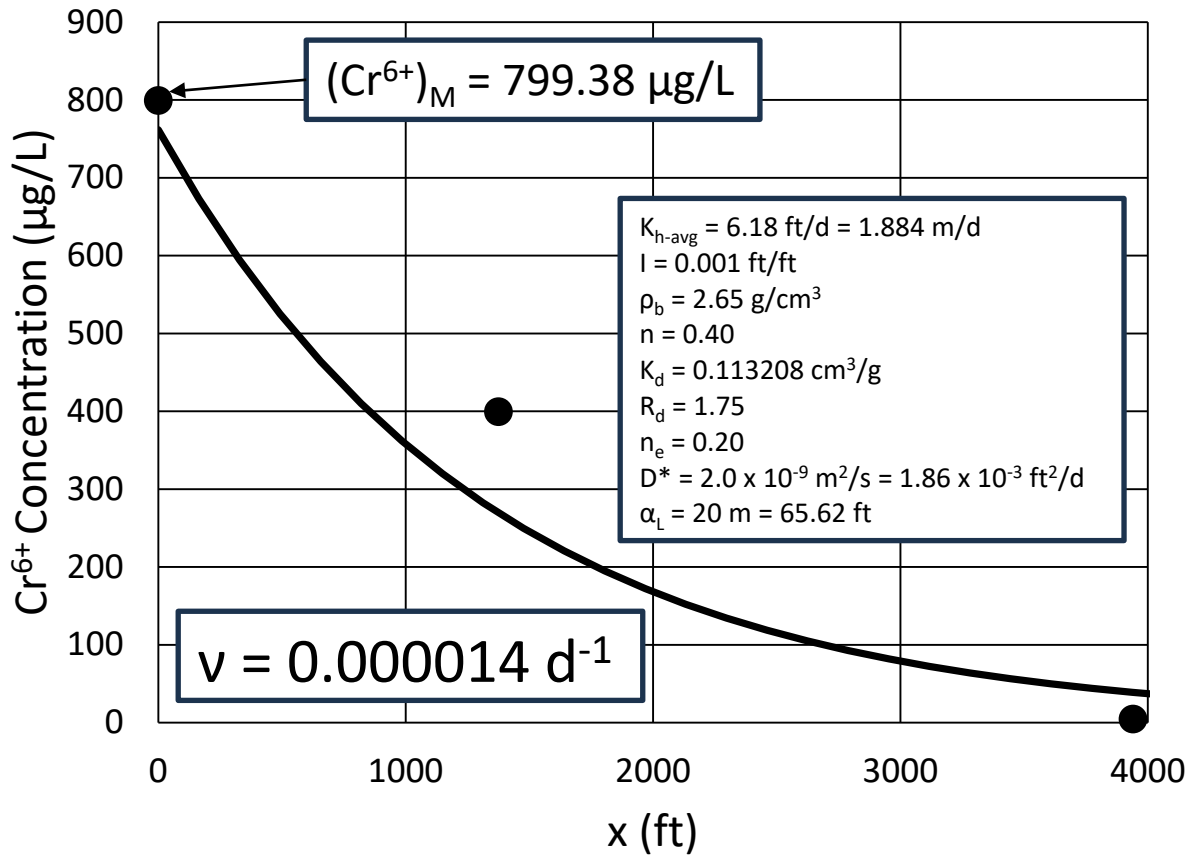


Figure 24. Determination of degradation rate ( $v$ ) from Table 2 chromium ( $Cr^{6+}$ ) concentration data ( $K_h = 6.18 \text{ ft/d} = 1.884 \text{ m/d}$ ,  $n_e = 0.20$ ).

## Tables

Table 1. Chromium ( $Cr^{6+}$ ) concentration versus distance along the main flow direction formed by the wells R-42, R-28, R-45, and R-13 till August 2022.

Well ID	x ft	$Cr^{6+}$ Concentration ( $\mu\text{g/L}$ )	Distance from x (ft)
R-42	0	900.86	0
R-28	1375	405.50	185
R-45 S1	2625	25.39	0
R-45 S2	2625	29.84	0
R-13	3940	4.84	0



Table 2. Chromium ( $Cr^{6+}$ ) concentration versus distance along the main flow direction formed by the wells R-42, R-28, and R-13 till September 2008.

Well ID	x ft	$Cr^{6+}$ Concentration ( $\mu\text{g/L}$ )	Distance from x (ft)
R-42	0	799.38	0
R-28	1375	399.62	185
R-13	3940	4.60	0

## **Appendices**

## APPENDIX A: VERTICAL DARCY VELOCITY IN THE UNSATURATED ZONE UNDER UNIFORM WATER CONTENT CONDITIONS

### A.1 VERTICAL DARCY VELOCITY FOR UNSATURATED FLOWS

The vertical Darcy velocity component for unsaturated formations is given as [e.g., Bear, 1979, page 209, Eq. (6-27); Warrick, 2003, page 63, Eq. (2-24)] as

$$q_z = -K(\theta) \frac{dh(\theta)}{d\theta} \frac{\partial \theta}{\partial z} - K(\theta) \quad (\text{A.1})$$

in which  $K(\theta)$  is the unsaturated hydraulic conductivity,  $h(\theta)$  is matric pressure potential, and  $\theta$  is the water content. Here,  $K$  is a function of  $h$  or  $\theta$ . In Eq. (A.1), the velocity is assumed to be positive in the upward  $z$  coordinate direction. If  $\theta$  is uniform along the thickness of the clayey silt formation, the first term on the right-hand side of Eq. (A.1) becomes zero. Therefore, Eq. (A.1) becomes

$$q_z = -K(\theta) \quad (\text{A.2})$$

### A.2 VERTICAL DARCY VELOCITY FOR UNIFORM WATER CONTENT

If the groundwater velocity is assumed to be positive in the downward direction, Eq. (A.1) becomes

$$q_z = K(\theta) \quad (\text{A.3})$$

in which  $\theta_{unif}$  is the uniform water content in the unsaturated zone. With  $K(\theta_{unif}) \equiv K_v$  and  $\theta_{unif} \equiv \theta$ , Eq. (F.3) becomes

$$q_z = K(\theta_{unif}) \quad (\text{A.4})$$

Then, the linear groundwater velocity is [e.g., Bear, 1979, page 63, Eq. (4-7)],

$$V = \frac{q_z}{\theta_{unif}} = \frac{K(\theta_{unif})}{\theta_{unif}} \quad (\text{A.5})$$

## APPENDIX B: ONE-DIMENSIONAL ADVECTIVE-DISPERSIVE ANALYTICAL SOLUTE TRANSPORT SOLUTIONS FOR FINITE-TIME SOURCE CONDITION

### B.1 GOVERNING SOLUTE TRANSPORT DIFFERENTIAL EQUATION

The governing differential equation for one-dimensional advection and dispersion equation is (e.g., van Genuchten and Alves, 1982, page 9, A1)

$$R_d \frac{\partial C}{\partial t} = D \frac{\partial^2 C}{\partial x^2} - V \frac{\partial C}{\partial x} \quad (\text{B.1})$$

in which  $R_d$  is the retardation factor,  $C$  ( $M/L^3$ ) is the concentration,  $D$  ( $L^2/T$ ) is the dispersion coefficient, and  $t$  is time. The retardation factor equation is

$$R_d = 1 + \frac{\rho_b}{n} K_d \quad (\text{B.2})$$

in which  $\rho_b$  ( $M/L^3$ ) is the bulk density of the porous medium,  $K_d$  ( $L^3/M$ ) is the distribution coefficient, and  $n$  is the total porosity. In Eq. (B.1),  $V$  is the interstitial or pore-water and is given as

$$V = \frac{q}{\theta} \quad (\text{B.3})$$

in which  $q$  ( $L/T$ ) is the volumetric flux and  $\theta$  is the volumetric moisture content. The dispersion coefficient  $D$  is given by

$$D = \alpha_L V + D^* \quad (\text{B.4})$$

in which  $\alpha_L$  ( $L$ ) is the longitudinal dispersivity and  $D^*$  ( $L^2/T$ ) is the effective molecular diffusion coefficient.

### B.2 FIRST-TYPE SOURCE SOLUTION

#### B.2.1 Initial and Boundary Conditions

The initial and boundary conditions are given below (e.g., van Genuchten and Alves, 1982, page 9, A1).

The initial condition is

$$C(x, 0) = C_i \quad (\text{B.5})$$

The boundary conditions at the source are

$$C(0, t) = C_0 \quad 0 < t \leq t_0 \quad (\text{B.6})$$

$$C(0, t) = 0 \quad t > 0 \quad (\text{B.7})$$

The boundary condition at infinity is

$$\frac{\partial C(\infty, t)}{\partial x} = 0 \quad (\text{B.8})$$

### B.2.2 Solution

The analytical solution of the above-defined boundary-value problem is (Lapidus and Amundson, 1952; Ogata and Banks, 1961; as presented in van Genuchten and Alves, 1982, p. 9, A1)

$$C(x, t) = C_i + (C_0 - C_i)A(x, t) \quad 0 < t \leq t_0 \quad (\text{B.9})$$

$$C(x, t) = C_i + (C_0 - C_i)A(x, t) - C_0A(x, t - t_0) \quad t > 0 \quad (\text{B.10})$$

in which

$$A(x, t) = \frac{1}{2} \operatorname{erfc} \left[ \frac{R_d x - Vt}{2(DR_d t)^{\frac{1}{2}}} \right] + \frac{1}{2} \exp\left(\frac{Vx}{D}\right) \operatorname{erfc} \left[ \frac{R_d x + Vt}{2(DR_d t)^{\frac{1}{2}}} \right] \quad (\text{B.11})$$

When the initial concentration is zero ( $C_i = 0$ ), Eqs. (B.9) and (B.10), respectively, become

$$C(x, t) = C_0A(x, t) \quad 0 < t \leq t_0 \quad (\text{B.12})$$

$$C(x, t) = C_0A(x, t) - C_0A(x, t - t_0) \quad t > 0 \quad (\text{B.13})$$

These equations are also given in Leij et al. [1991, page 945, Eqs. (9) and (10)]. In the above equations,  $C_0$  is the source concentration,  $x$  is the distance from the source,  $V$  is the average linear groundwater velocity,  $D$  is the dispersion coefficient,  $t$  is time, and  $t_0$  is the source active time period. The longitudinal dispersion coefficient  $D$  is [e.g., Freeze and Cherry, 1979, page 389, Eq. (9.4)],

$$D = \alpha_L V + D^* \quad (\text{B.14})$$

in which  $\alpha_L$  is the longitudinal dispersivity and  $D^*$  is the effective molecular diffusion coefficient. And  $\operatorname{erfc}$  is the complementary error function and defined as

$$\operatorname{erfc}(u) = 1 - \frac{2}{\pi^{\frac{1}{2}}} \int_u^{\infty} u^{-\xi^2} d\xi \quad (\text{B.15})$$

## B.3 THIRD-TYPE SOURCE SOLUTION

### B.3.1 Initial and Boundary Conditions

The initial and boundary conditions are given below (e.g., van Genuchten and Alves, 1982, page 10, A2).

The initial condition is

$$C(x, 0) = C_i \quad (\text{B.16})$$

The boundary conditions at the source are

$$VC - D \frac{\partial C}{\partial x} = VC_0 \quad 0 < t \leq t_0 \quad (\text{B.17})$$

$$VC - D \frac{\partial C}{\partial x} = 0 \quad t > 0 \quad (\text{B.18})$$

The boundary condition at infinity is

$$\frac{\partial C(\infty, t)}{\partial x} = 0 \quad (\text{B.19})$$

### B.3.2 Solution

The analytical solution of the above-defined boundary-value problem is (Mason and Weaver, 1924; Lindstrom et al., 1967; Gershon and Nir, 1969; as presented in van Genuchten and Alves, 1982, p. 10, A2)

$$C(x, t) = C_i + (C_0 - C_i)A(x, t) \quad 0 < t \leq t_0 \quad (\text{B.20})$$

$$C(x, t) = C_i + (C_0 - C_i)A(x, t) - C_0A(x, t - t_0) \quad t > 0 \quad (\text{B.21})$$

in which

$$A(x, t) = \frac{1}{2} \operatorname{erfc} \left[ \frac{R_d x - Vt}{2(DR_d t)^{\frac{1}{2}}} \right] + \left( \frac{V^2 t}{\pi D R_d} \right)^{\frac{1}{2}} \exp \left[ -\frac{(R_d x - Vt)^2}{4DR_d t} \right] - \frac{1}{2} \left( 1 + \frac{Vx}{D} + \frac{V^2 t}{DR_d} \right) \exp \left( \frac{Vx}{D} \right) \operatorname{erfc} \left[ \frac{R_d x + Vt}{2(DR_d t)^{\frac{1}{2}}} \right] \quad (\text{B.22})$$

When the initial concentration is zero ( $C_i = 0$ ), Eqs. (B.9) and (B.10), respectively, become

$$C(x, t) = C_0 A(x, t) \quad 0 < t \leq t_0 \quad (\text{B.23})$$

$$C(x, t) = C_0 A(x, t) - C_0 A(x, t - t_0) \quad t > 0 \quad (\text{B.24})$$

In the above equations,  $C_0$  is the source concentration,  $x$  is the distance from the source,  $V$  is the average linear groundwater velocity,  $D$  is the dispersion coefficient,  $t$  is time, and  $t_0$  is the source active time period. The longitudinal dispersion coefficient  $D$  is [e.g., Freeze and Cherry, 1979, page 389, Eq. (9.4)],

$$D = \alpha_L V + D^* \quad (\text{B.25})$$

in which  $\alpha_L$  is the longitudinal dispersivity and  $D^*$  is the effective molecular diffusion coefficient. And  $\operatorname{erfc}$  is the complementary error function and defined as

$$\operatorname{erfc}(u) = 1 - \frac{2}{\pi^{\frac{1}{2}}} \int_u^{\infty} u^{-\xi^2} d\xi \quad (\text{B.26})$$

## **Appendix O**

**Compilation of Materials Regarding Well Construction and  
NMOSE Concerns and Correspondence  
(*Stephens/Looney/other*)**



STATE OF NEW MEXICO  
Office of the State Engineer  
Hydrology Bureau



COMMUNICATION MEMORANDUM

**DATE:** June 27, 2024

**TO:** Ines Triay, PhD, Interim Dean of College of Engineering and Computing,  
Director of the Applied Research Center; Florida International University

**THROUGH:** Ramona Martinez; Water Rights Division VI, District Manager  
Katie Zemlick, PhD; Hydrology Bureau Chief

**FROM:** Christopher E. Angel, PG; Senior Hydrologist, Hydrology Bureau *Cc2'*  
Lorraine Garcia, Water Rights Division VI, Deputy District Manager  
Christopher Thornburg, Water Rights Division VI, Upper Pecos Manager

**SUBJECT:** Independent Review Team - LANL Chromium Plume - Questions for the Office  
of the State Engineer (OSE)

**KEYWORD:** Dual Screened Well, Independent Technical Review (ITR) team, ITR, LANL,  
Chromium Plume, Contamination Migration, Bentonite, R-25, R-70, R-73, R-76,  
Wells, Plugging, Construction

---

## INTRODUCTION

On April 24, 2024, the Independent Technical Review (ITR) team posed twenty-two updated questions to the OSE to aid the ITR team in their review of the chromium plume at LANL. The purpose of this memorandum is to answer these questions and to illustrate how a history of communication issues has further complicated addressing the risks posed by drilling activities in the area of the chromium plume. In no way do any statements or answers to the questions constitute a final decision on the construction of any well. Each well is evaluated independently when an application is submitted to the New Mexico Office of the State Engineer (OSE).

The chromium plume at LANL is located proximal to sensitive receptors (e.g. several municipal wells and the Rio Grande) it presents serious health and safety concerns for the public. Improperly constructed wells, particularly those screened in contaminated and uncontaminated aquifers, may provide additional pathways for the plume to migrate. With these receptors being located so close to the plume, the OSE cannot approve drilling and completion methods that pose a risk to previously uncontaminated portions of the aquifer and/or different hydrogeologic units. The OSE has jurisdiction over well construction (New Mexico Administrative Code (NMAC) 19.27.4) and will make the final decision as to the proper construction of a well.

There have been numerous issues with communication between LANL representatives and OSE staff which present additional challenges beyond the specifics of the application. For example, the NMED Hazardous Waste Bureau provided a Department of Energy/N3B (DOE/N3B) presentation



dated May 2, 2024 (Drilling Work Plans (DWP) Discussion Topics) that states "Cement is not required below the bentonite", which is inaccurate. Cement is the OSE approved sealant in the chromium plume or where the chromium plume may occur. According NMAC (2017) 19.27.4.30.C(1), "The well shall be plugged with an office of the state engineer approved sealant for use in the plugging of non-artesian wells." If contamination is present or suspected to be present, NMAC 19.27.4.30.C(2) states "Specialty plugging materials and plugging methods may be required." The OSE has the jurisdiction to determine the appropriateness of annular sealants and plugging materials to insure proper construction that is protective of the resource.

## REVIEW OF ITR QUESTIONS

### Dual Screened Wells

- 1) *Is there anything specific in the monitoring data which suggests to the OSE that the existing dual completion wells are conduits for vertical contaminant migration or otherwise ineffective?*
  - a. Part of the migration pathways issue will be answered via a separate memorandum; OSE will share with the ITR team once complete.
  - b. During the plugging of the R-25 well the casing parted and became wedged into the casing. The plugging of this well started approximately 10 months after the plugging permit was granted. OSE required a downdip regional groundwater monitor well near the R-25 well. At this time, LANL has not inquired or attempted to permit a new well at this location. Therefore, OSE cannot fully determine if there has been vertical migration. However, if this well had not been screened in the contaminated perched aquifer and uncontaminated aquifer, then the potential for contaminating the uncontaminated aquifer by this completion would have been minimized and the need for another monitor well would not be necessary and the risk to the regional aquifer would have been minimized.
  - c. Multiple issues occurred during the failed drilling attempt of R-73. Due to these drilling issues, the Chamita formation was left open for a significant amount of time before plugging activities were initiated. The OSE is still awaiting a replacement well to investigate the potential chromium migration due to this failed drilling attempt with multiple screened intervals.
    1. If the well had been constructed with an artesian casing with cement sealing the contamination in the Puye Formation (upper hydrogeologic unit), the risk of contamination migration would have been significantly reduced.
  - d. R-76 was drilled and has remained open since temporary wells were removed. As the total depth of this well is near the base of the confining hydrogeologic unit, migration may have occurred. Migration has not been determined at this time as wells will need to be completed in the Puye and Chamita. It should also be noted, every time a well fails during the drilling and/or completion process the OSE will not be able to determine if contaminant migration is from the packer, from a nearby poorly completed well, failed drilling attempt, or has migrated into the deeper horizon by natural pathways.
    1. The stop work was initiated when an N3B representative contacted OSE Hydrology Bureau representative (Christopher Angel) on his personal

cellphone on Wednesday, November 22, 2023 at 1705. This was just after the official start of Thanksgiving holiday. Mr. Angel was informed that the drilling contractor had used a larger diameter drill casing and wanted to know about completing the well in a larger borehole. Mr. Angel informed N3B was informed that centralization is to the borehole and not to the casing. As the centralization is to the borehole wall, increasing the borehole size will decentralize the casing. According to the NMAC (2017) casings are to be centralized in the annular sealant; decentralizing the casing and placing an annular seal may lead to poor annular seals that leak.

- 2) *Has NMED reported to OSE that the LANL two-screen wells are not suitable for their intended purpose?*
  - a. NMED has not; however, it is important to note that NMED and OSE possess distinct regulatory authorities. NMED is responsible for monitoring the subject contamination, while OSE has jurisdiction over well construction and the protection of New Mexico's surface and groundwater resources.
- 3) *Has the OSE found any evidence that the process of constructing or operating the dual screen monitor wells has impacted fresh groundwater?*
  - a. The OSE has only been made aware of one well (R-70) being screened in both contaminated and uncontaminated hydrogeologic units. In this well, the uncontaminated hydrogeologic unit overlies the contaminated hydrogeologic unit. However, the upper screen (S1) is 41 feet long and has 52 feet of filter pack overlying the screen. The lower screen (S2) is 19 feet long and has 7.6 feet of filter pack above the screen top. These highly variable screen lengths and filter packs do not allow for an effective evaluation of the groundwater contamination. This is especially true given there is unexpected deep contamination and overlying uncontaminated groundwater.
  - b. Information will be submitted in a separate memorandum that provides evidence that current well construction methods are allowing chromium migration into previously uncontaminated hydrogeologic units/aquifers. Preventing "the flow of contaminated or low quality water" into other hydrogeologic units and/or aquifers is required by NMAC 19.27.4.30.A.
    1. Migration of contamination is one of the reasons the OSE has re-evaluated completion techniques. This information was not presented to the OSE by LANL or their representatives.
    11. Continued evaluations of LANLs wells by OSE personnel is time-consuming and does not allow OSE staff to perform other assigned duties. Therefore, time is allotted to this project when there is an active pending application.
  - c. The OSE is waiting for the replacement wells identified in Question 1 above. Therefore, **it** cannot be determined if the drilling/constructing process has impacted groundwater.
- 4) *Has the OSE found any evidence that the packers inside the casing have led to impacts to fresh groundwater?*
  - a. Only one well (R-70) appears to have a packer separating uncontaminated and contaminated hydrogeologic units and was discussed above. Other wells are completed either in the contaminated or uncontaminated hydrogeologic units.

- b. As was discussed in question 1) above, the risk in drilling wells with screens in both contaminated hydrogeologic unit(s) and the uncontaminated hydrogeologic unit(s) poses significant risk during the entire life span of the well (drilling to plugging).
  - c. LANL has not provided information on all nine dual screened monitor wells to OSE. In addition, the OSE has not been informed of how packer testing is performed or the results of any packer testing. The lack of effective technical communication has been a significant barrier to working with LANL and their representatives.
  - d. NMAC 19.27.4.7.J is the definition of a repair. In this definition, a repair includes the installation of a packer. Packers are considered a material change to the well. As such, NMAC 19.27.4.29.Q requires a description of how the wells will prevent the migration of poor-quality or contaminated water.
  - e. The OSE is providing the ITR team with some initial recommendations for LANL to provide information on the packers currently in use in the Chromium Plume. This includes the methods used to install individual packers, monitoring procedures used by LANL to determine the effectiveness of each packer and any modifications that have been made to the packer over time.
    - i. Each well should be identified by the official OSE well and POD number.
    - ii. Each packer's make and model should be identified along with the materials used for installation and maintenance.
    - iii. Procedures used to install the packers currently in use in the Chromium Plume.
    - iv. Set depth of the packer.
    - v. Procedures used for testing and monitoring the packers.
    - vi. After this is received, the OSE can determine the reporting requirements necessary for evaluating the effectiveness of the packers.
- 5) *Is the OSE open to granting a variance on the concept of using multi-screen monitor wells to determine the vertical depth of contamination, based on the OSE's prior approval of this design, the record of successful performance of prior dual screen wells at LANL, the long time to drill separate wells, and the urgency of filling data gaps identified by NMED to implement a successful remedy?*
- a. OSE is not currently open to grant variances for dual-screened wells that span two separate hydrogeological units; this has already been stated to LANL representatives on several occasions. It should be noted that within the last three years, OSE has granted a permit for one such well, which subsequently failed (R- 73). Many prior permits for dual-screened wells were issued in the past and/or prior to OSE assuming jurisdiction over monitoring wells. Additionally, OSE is not prepared to assert the success of previously installed dual-screened wells, given the limited data and resources available to us at this time.
  - b. The OSE has been hindered by the lack of communication with the DOE and their representatives. An example of this lack of communication occurred during the LANL sponsored geology field trip, OSE technical staff (Christopher Angel) was having a technical discussion with a N3B and Neptune employees at the first stop. At the end of the first stop, these two individuals were taken aside by an N3B

employee and at subsequent stops, the Neptune and N3B employees would not discuss any additional technical topics with Mr. Angel.

- 6) *If yes' to #5, what conditions would need to be imposed by the OSE and why?*
- a. OSE is open to dual screened wells in the same hydrogeologic unit and with similar water qualities. Conditions of approval will be determined by the OSE on a case-by-case basis as geology, hydrology, chemical constituents, construction materials and methods vary.
  - b. The items in 4) d. will need to be addressed along with all construction methods.

### **Annular Sealant**

J) *If properly emplaced, are there any inherent problems with using bentonite below the water table as a sealant to prevent fluid migration outside well casings in the dual screen well design? How can these be overcome?*

- a. The term "properly emplaced" is a misleading term. Properly emplaced would indicate that geologic, hydrogeologic, geochemical, climatic, and human-induced conditions have been accounted for during the installation and during the life of the well (ASTM D5092/D5092M- 16).
  - b. Bentonite has a very low shear and compressive strength, ranging from ~1 psi to ~2 psi. Depending on the amount of induced drawdown during development, aquifer testing, and pressure differentials between different hydrogeologic units during the life of the well, it is possible to breakdown and/or channel the annular seal creating a leak and migration pathways between hydrogeologic units.
  - c. There is sufficient evidence that swelling potential of bentonite is hindered by the introduction of different analytes in the groundwater (Aller et al, 1991). Other research has also shown that the free swell in the presence of chromium is reduced with time and concentration (Ajitha et al, 2018).
  - d. Bentonite is not an appropriate material for use as an annular seal between contaminated and uncontaminated groundwater. There is significant potential for the annular seal to fail and contaminate fresh (uncontaminated) water.
  - e. The OSE allows for cement, sand-cement and bentonite-cement as an annular seal at contaminated sites.
  - f. The OSE is currently approving a layer of bentonite above and below the filter pack to aid in preventing cement migration. However, bentonite must have a cementitious material below the lower bentonite layer and above the upper bentonite layer. Designs will vary on a well-by-well basis due to the varying factors of each well site and construction design.
- 2) *Please discuss OSE's views on the pros/cons vs using cement for this chromium contaminated site.*
- a. Bentonite has no shear and/or compressive strength allowing for possible migration pathways should the applied forces exceed the strength of the bentonite.
  - b. Bentonite may not adequately swell in the presence of some chemicals. There is evidence that Chromium VI impacts the swell potential of bentonite and can be accumulative (Ajitha et al, 2018). This will degrade the annular seal quality.
  - c. Bentonite under injection/production induces pressures that can break down and/or channel the annular seal.

- d. Bentonite in an angled borehole will not have the strength to keep casing from flexing. Adding a pump, tubing and packer will only increase the likelihood of these issues. Other problems may also occur without cement in the annular space.
- e. Cement gives the casing additional mechanical integrity especially when wellbore remedial activities are required.
- f. Cement can more effectively invade into borehole damage preventing and/or minimizing contaminate migration through borehole damage.
- g. Issues with bentonite in the Chromium Plume will be discussed in a separate memorandum; the OSE will share with the ITR team once complete.

### **Documentation**

- 1) *Have there been discrepancies between work plans and site inspections by the OSE or OSE representative?*
  - a. Yes.
    1. On the R-76 well, there have been occasions when the work plan did not match what occurred in the field. For example, the drill casing size is larger than what was planned in the work plan. This drill casing issue was brought to the attention of Mr. Christopher Angel with the OSE Hydrology Bureau after hours on November 22, 2023, during the start of the 2023 Thanksgiving Holiday. The larger drill casing would likely create a decentralized casing in the contaminated interval. Many discussions on this topic have occurred and even a memorandum was written about the methods and equations used in describing casing centralization (Angel, 2022). Variance requests were submitted to the OSE to resume drilling and completion activities. The initial variance requests had errors that did not allow the OSE to grant the variance. The final variance request submitted to the OSE had errors. As these errors were not in critical areas the OSE was able to approve the variance request and issue Conditions of Approval. The OSE provided clarification in a meeting with N3B, T2S and LANL.
    11. During the plugging of the R-25 well, the cement delivered to the site was not the same cement that LANL had designated on the plugging plan. As the cement type is required on the plugging plan and approved as part of the approval process any changes to cement design require approval. The approved cement in the plugging plan is generally considered High Sulfate Resistant (HSR) cement. The API Class C cement delivered to LANL can be designated as Low Sulfate Resistance (LSR), Moderate Sulfate Resistance (MSR) or High Sulfate Resistance (HSR). As the material was not the material approved in the plugging plan LANL had to demonstrate to the OSE representative in the field (Christopher Angel) that either the groundwater did not contain sulfates more than 500 mg/l allowing for a LSR cement to be used and/or the cement delivered to the site contained a HSR cement. The project manager submitted to the OSE evidence that the groundwater did not require sulfate resistant cement and the API Class C cement delivered to the site was acceptable.

- m. There were significant differences to overcome on the R-73 well, especially with centralization. The OSE does not accept centralization to the inside diameter of the casing when the casing is going to be removed. After many attempts to have LANL and/or their representatives explain how their centralization design would comply with the NMAC 19.27.4.30.A, the Hydrology Bureau recommended that the application be denied (Angel, 2022).
- 2) *Are there specific problems with the information provided by DOE on the construction of the dual screen wells, for example based on the well completion reports and as-built diagrams provided to the OSE? Please explain what needs to be done to address OSE's concerns on the reporting.*
- a. There have been no specific issues noted in the well completion reports submitted to OSE. However, an incident occurred at the R-73 well where difficulties encountered during well construction were not immediately reported to OSE by LANL. Instead, NMED notified OSE of the potential issues, prompting OSE to contact LANL directly for clarification. Furthermore, the well driller contracted for the R-73 well informed OSE staff that they were instructed to channel all communications through LANL representatives, rather than directly approaching OSE. This practice is a violation of the administrative code in New Mexico, where OSE has regulatory oversight over well drillers.

#### **Dry Wells/Vadose Zone Wells**

- 1) *If dry/vadose zone wells were proposed as an alternative or complement to land disposal of treated water, what would be the major concerns of the OSE and what are the main obstacles which would need to be overcome in order for OSE to approve of such a well design?*
- a. OSE has not reviewed any plan detailing this proposed approach and is not in a position to approve generalized hypothetical scenarios outside of a formal permit application, due to limited resources.

#### **Additional Questions**

- 1) *What is OSE's current thinking about either retaining or replacing the current dual-screened monitoring wells at the LANL chromium plume site?*
- a. Currently, OSE does not have a definitive stance regarding the replacement of existing dual-screened wells on LANL property. However, the OSE reserves the right to request that these wells be replaced or abandoned in the future should there be evidence of contamination migration or a threat to uncontaminated underground hydrogeologic units/aquifers.
- 2) *Is OSE aware of any other state or groundwater regulatory agency that prohibits the use of bentonite for monitoring well construction?*
- a. The use of the term "prohibit" is confusing as the OSE has not prohibited the use of bentonite. In fact, the OSE just approved the construction of the R-76 utilizing bentonite both below and above the filter pack. Therefore, the term "prohibit" does not allow for an adequate response to this question. However, the EPA has provided guidance on annular seals and several states limit the use of bentonite as an annular seal in the vadose zone and when poor-quality or contaminated water is present (Aller et al, 1991).

1. An incomplete list of states that regulate the use of bentonite in the construction of wells include: Texas, Colorado, Ohio, California, Oregon, Louisiana, Nebraska, Kentucky, Georgia, Florida, North Carolina, Maryland, Delaware, New Jersey, Massachusetts, Washington DC.
- 3) *What were the key factors that caused OSE to implement the changes in monitoring well requirements (e.g., no dual-screen wells. no bentonite) at this time?*
  - a. Bentonite has never been formally approved by OSE as a sealant for contaminated areas. Recent advancements in research, data, and expertise have prompted OSE to reexamine well construction practices in contaminated sites. Consequently, new conditions and requirements may be implemented to ensure the utmost protection of our aquifers.
- 4) *The panel has been presented with some data that suggest there is a permeability increase with depth in each of the Puye, Puye Pumiceous sub unit, and Miocene sediment layers. Even modest stratification in the hydrostratigraphic profile can affect vertical flow paths in important ways over the scale of the chromium plume. Future monitoring should maximize the vertical profile information that can be gathered, both in hydraulic heads and water quality, to assist with remedial design. Given the cost of well installation at the site, and risk introduced by insufficient data, multi-screen wells should be fully excluded as an option only **if** there is clear evidence they expand the plume. What is the maximum screen length the OSE currently considers acceptable?*
  - a. The OSE limits the screen length when there is a potential for the screen to access multiple hydrogeologic units and/or aquifers and/or to prevent the migration of contaminated, lower quality water into uncontaminated hydrogeologic units.
  - b. If the screen does not violate one of the above-mentioned conditions then NMED and their monitoring requirements will be the limiting factor.
- 5) ***If** there is ambiguous evidence of problems associated with multi-screened wells, can we learn from the wells that worked and those that did not how to optimize the multi-screen well construction, so future wells maintain integrity? Is there a chance to ramp up the use of multi-screened wells while it is verified that the newest constructions are reliable, as future drilling proceeds?*
  - a. OSE does not support the use of dual-screened wells in contaminated areas due to the heightened risk they pose. The OSE's position is that such wells significantly increase the potential for contaminating an uncontaminated hydrogeologic unit/aquifer. In addition, the aquifer in question serves as critical water source for one of the state's largest municipalities. Consequently, the OSE is not willing to entertain the risks associated with these wells in contaminated areas.
  - b. In the presence of ambiguity, the OSE takes a conservative approach to the conservation and protection of groundwater resources and its citizenry.
- 6) ***If** OSE decides that multi-screened wells, of the types currently in the ground, are unacceptable, can they recommend any alternative ways to obtain time and space multi-depth profiles the panel can consider?*
  - a. OSE does not offer consultations on well drilling construction. LANL representatives should utilize their contractors and experts to draft and propose alternative solutions for well design, which can then be submitted for OSE review.
- 7) *Future installations of dual screened wells seem to be impeded primarily due to fears about annular seal integrity. Chemical concerns affecting water sample representativeness arise*

*over the pH changes caused by cement seals, and the potential failure of bentonite seals in the presence of contaminants and large pressure differentials is problematic. In addition, bentonite could dry out in the vadose zone, and therefore be unable to create or maintain a seal. The OSE is worried that bentonite seals are not protective. Is there any evidence from the LANL site that shows bentonite is not protective? Regardless, if bentonite is deemed inadequate, does the OSE consider cement reliably protective?*

- a. This will be covered in a separate memorandum; OSE will share with the ITR team once complete.
- 8) *The isolation of hydrogeologic units is important, but the need for data from deep portions of the aquifer is necessary to understand the plume distribution, assess risk, and to inform remediation system designs. Is the objection to dual screen wells the same for single screen wells? Are both subject to the same seals limitations or are dual screen wells subject to additional concerns? If the outer annular seals are the main problems, and cement is acceptable as a sealing material, in principle could dual screen wells be installed with cement seals?*
- a. This is a multifaceted question with multiple areas of increased risk during the drilling, completion, and plugging process.
    1. While the well is being drilled there is a migration pathway through the drilling fluids, drill pipe and/or casing.
      1. Migration can occur through the drilling fluids when the contaminated interval is not sealed prior to entering deeper potentially uncontaminated hydrogeologic unit.
      2. The proposed drilling methods utilize drill casing, which will leave an annular space until the casing is removed and the well is constructed. This annular space can be a contaminant migration pathway until the casing is removed and plugs and/or annular seals have been properly installed.
    11. Issues that have occurred during the drilling of R-73 and R-76 created significant migration pathways have been left open for a significant amount of time.
      - I. The OSE has stated that when penetrating lower porosity and permeability hydrogeologic units, contaminated intervals must be sealed prior to entering the deeper hydrogeologic units.
        - a. These deeper hydrogeologic units have several sensitive receptors (Municipal Supply wells, migration pathways and discharge to the RioGrande).
        - b. Protecting these potentially uncontaminated waters and the citizenry of New Mexico are an utmost importance to the OSE.
      - iii. There is a potential for wellbore stability issues while removing the drill casing and construction of the monitor well. If the stability of the wellbore is compromised, then the annular sealant may not effectively seal the annular space allowing fluids to migrate from one hydrogeologic unit to another. Some of this was seen in the R-73 well with heaving sands and differential sticking of the casing.



- iv. During the construction of a dual screened monitoring well both screens will be left open to flow and contaminant migration until the packer is properly set.
  - v. After the packer is appropriately set in an interval capable of withstanding inflation pressures, then the risk is mitigated to some extent.
    - 1. However, if there are significant changes in pressure from wellbore development/purging, the pressure differentials may cause some migration pathways.
    - 2. If groundwater remediation activities such as injection and/or production create significant differences in pressures, packers may not adequately seal between screen intervals.
    - 3. Other operational issues may include tubing hangers failing, couplers leaking and/or corroding, and check valves failing.
  - vi. If the packer needs to be replaced or repaired the dual screen method will leave the different screens open to the migration of contaminated and uncontaminated between hydrogeologic units. If the casing is damaged through mechanical or chemical degradation, the packer may not seal the contaminated zone from the uncontaminated zone.
  - b. As described above in question 1) b. of the **Dual Screens** section, plugging activities can create significant problems and potential contaminant migration pathways.
  - c. The OSE has not been provided information in a timely, unaltered (without layers of LANL interpretations) manner. Therefore, the OSE would need to have personnel available to witness all aspects of the drilling, completion and testing of packers where these materials were used. At this time, the OSE cannot dedicate the number of professional hours required for this level of oversight.
  - d. LANL and their representatives have not allowed for an open and free exchange of information. Most communication is filtered through multiple levels of management and multiple layers of interpretations prior to anything being released.
    - 1. The OSE has attempted to have informal discussions on hydrology, and well construction. This has not been received well and/or has been used against the OSE. This is not conducive to securing a working relationship and /or protecting the groundwater from contamination migration.
  - e. The OSE has attempted to discuss the issues with bentonite. However, LANL and their representatives have only discussed pH and modifications to water chemistry.
    - 1. The OSE does not necessarily regulate how the annular seal chemistry will react in the groundwater sampling. OSE regulates the materials in the construction of the well to prevent further migration of contaminants, inter-aquifer exchange, and floodwater from entering the borehole/well.
  - f. Properly constructed single screened wells lower the risk of contamination migrations.
- 9) *In order to provide the mechanical strength of cement but prevent the cement chemistry from altering the water chemistry of samples, would the OSE be willing to install wells (single, dual, or other) that layer the bentonite and cement? The concept would be to surround a screened interval with one or more layers of bentonite and separate these*

*isolated zones with cement seals. The cement would provide mechanical strength while the bentonite would keep cement affected water from entering the water in the screens*

- a. The layered system is generally acceptable. However, the thickness of the bentonite in the R-76 is longer than OSEs desired lengths. The OSE prefers five feet or less of bentonite. Bentonite will not generally be accepted as a seal across hydrogeologic units and/or aquifers and/or from contaminated water to uncontaminated water. The use of bentonite in the vadose zone will also be limited as the material desiccates in unsaturated conditions.

*10) The panel understands that a layered system like that mentioned above is currently being installed. Do we have a timeline for data from the new well(s) to help us assess the performance of a layered seal system?*

- a. LANL is responsible for providing data and answering OSE questions. The OSE cannot provide a timeline as it is LANL's responsibility to provide the information for OSE's review.

*11) We heard that a Westbay multilevel well system was installed and abandoned at the RDX site. Could we hear the details that led to the conclusion the system failed?*

- a. This failure was documented and plugging required by NMED. NMED will need to answer questions on the system failure prior to plugging.
- b. From OSEs perspective, the system failed during plugging and abandonment operations.

1. It appears that while the Westbay System was being recovered the PVC components failed to maintain integrity.
- ii. Attempts were made to drill out the remaining portions of the system.
- iii. During these drilling operations the casing was damaged and left a large section of the wellbore open with no casing and/or annular seal.
- iv. A packer was set below one of the contaminated perched zones.
  - I. Based on the information provided it cannot be determined if the packer prevented contaminant migration.
- v. The packer was removed to perform plugging operations.
- vi. It cannot be determined from the information provided if the annular seal stopped contaminant migration in the annular space after the casing was parted.
- vii. Significant risk is left at this location due to the construction of a monitor well with screens in both the contaminated and uncontaminated hydrogeologic units.
- viii. Due to the risk imposed on the uncontaminated hydrogeologic unit (regional aquifer), the OSE required a down flow gradient (down dip) monitor well be constructed in regional aquifer.
- ix. NMED in a letter to LANL dated October 24, 2023, noted that LANL is supposed to establish a monitoring well in the regional aquifer.
  - I. Based on conversations with the NMED Hazardous Waste Bureau, there has been no progress on monitoring the regional aquifer down dip of the R-25 well.

## **CONCLUSION**

The OSE has provided answers to the 22 questions requested by the ITR team. Some of these questions may need to be supplemented either by NMED and/or LANL and their representatives. For clarification, it is the applicant's responsibility to provide evidence supporting assertions about claims made in reports, applications and/or during variance requests. The OSE has provided some evidence to support how the wells have failed and do not comply with NMAC (2017). A separate memorandum will address bentonite as an annular seal and/or plugging material, which the OSE will share with the ITR team once complete.

## REFERENCES

- Ajitha, A.R., S. Chandrakaran, and Y. Evangeline. "Effect of Chromium on the Engineering Properties of Amended Clay Liner." *International Journal of Engineering and Advanced Technology* 7 (February 2018): 114-18.
- Aller, L., T. W. Bennett, G. Hackett, R. J. Petty, J. H. Lehr, H. Sedoris, D. M. Nielsen, and J. E. Denne. *Handbook of Suggested Practices for the Design and Installation of Groundwater Monitoring Wells*. EPA160014-891034. Las Vegas, Nevada 89193-3478: Environmental Monitoring Systems Laboratory Office of Research and Development U.S. Environmental Protection Agency, 1991.
- D18 Committee. "Practice for Design and Installation of Groundwater Monitoring Wells." ASTM International. Accessed May 7, 2024. [https://doi.org/10.1520/D5092\\_D5092M-16](https://doi.org/10.1520/D5092_D5092M-16).
- N38 Los Alamos. "Drilling Work Plans (DWPs) Discussion Topics." Los Alamos, New Mexico, May 2, 2024.
- NMAC. "New Mexico Annotated Code Title 19 -Natural Resources and Wildlife; Chapter 27 - Underground Water; Part 4: Well Driller Licensing; Construction, Repair and Plugging of Wells." In *New Mexico Register*, Issue 11. Vol. Volume XXVII. New Mexico, 2017.
- Rick Shean. Letter to Arturo Duran. "Review 2022 Annual Progress Report for the Corrective Measures Evaluation for Royal Demolition Explosive in Deep Groundwater (November 2022) Los Alamos National Laboratory; EPA ID #NM0890010515; HWB-LANL-22-10I," October 24, 2023.

# **IRT's Response to the June 27, 2024 OSE Communication Memorandum**

The IRT requested clarifications from the New Mexico Office of the State Engineer (OSE) on their position that (1) the agency would not approve of dual-screen monitoring wells, (2) the agency would not approve of a monitor well with an annulus sealed with bentonite, and (3) the agency would not approve of drilling a monitor well through a contaminated zone into a fresh water zone. The questions posed and the OSE responses are provided in OSE's Communication Memorandum. The independent review team (IRT) response to the OSE Communication Memorandum is presented below.

## **Dual-Screen Wells**

- The question has to do with dual-screen monitoring wells, and the context is with respect to the chromium investigation area. OSE's review speaks of R-25, R73, and R76, none of which are dual-screen monitoring wells.
- NMED has been reviewing groundwater monitoring data and has not informed the IRT of any concerns that the existing or proposed monitoring wells are not adequately designed to protect groundwater and obtain representative sample of groundwater chemistry.
- OSE presents no evidence here, but refers to a separate memorandum on the subject.

Instead, in their report here, OSE cites to its concerns at R-70, where the upper zone is uncontaminated and the lower zone is contaminated. Their main comment is about the length of the well screens because it would "not allow for an effective evaluation of groundwater contamination." NMED has not informed the IRT of any concern about screen length or the effective evaluation of contamination here.

The dual-completion monitoring well R-70 appears to be a good example of an effective monitoring well. The OSE is concerned that drilling across different hydrogeologic units contaminates fresh water. At R-70, the vertical hydraulic gradient is upward. The contaminated zone is below the fresh water zone. When the well reached total depth, the contamination should have migrated up the well bore and into the freshwater zone, but OSE found that the upper screen was uncontaminated. If there was migration in the well bore during the time the hole was open, there is no evidence that this happened to an extent that compromised the interpretation of the data collected from these two well screen intervals.

- The question asked for evidence that packers placed inside the casing have led to impacts of fresh groundwater. OSE indicated it was only aware of one well, R-70, that has a packer separating contaminated and uncontaminated zones. OSE cites to no evidence that this well is a problem, however. In fact, OSE clearly notes that in R-70 there are two separate zones, at different depths, with different water levels and different chemistry, with the upper zone uncontaminated. If the packer were not effective, there would be upward flow from the lower contaminated zone through the casing, up to the upper well screen, and flow of contaminated water out into the shallower part of the formation.

OSE claims “LANL has not provided information on all nine dual screened monitor wells to OSE.” Later in their memorandum, in response to Documentation question 2, OSE finds “there have been no specific issues noted in the well completion reports submitted to OSE.” This last response suggests that in fact OSE has received the well completion reports. The IRT agrees with OSE that relevant information on monitor well design, including packer operations, should be made available to the OSE.

At our initial meeting in March 2024, Catherine Goetz briefed the IRT on the detailed methodology followed for monitor well construction, including using Baski packers inside the casing. She explained how the Baski system allows one to determine whether there is a loss of packer pressure and potential for water bypassing the packers as well as the use of a monitoring system that alarms and alerts to the control room for immediate response and restoration of the packer system integrity. The IRT recommends that DOE-EM-LA and OSE to meet to review the packer and screen isolation and contingency response protocols and that these be formally included in the well construction planning and documentation.

- OSE’s position appears to be intractable—that a dual-screen monitoring well cannot span two separate hydrogeologic units. The IRT finds that the upper part of the aquifer at in the chrome remediation area appears to be essentially one aquifer. David Broxton has presented to the IRT that while there are geological nomenclature distinctions, such as the proportion of pumice, the system behaves as a single hydrogeologic unit. Geologists use subtle differences in grain size and shape, mineralogy, or color to log core or drill cuttings to develop geological maps and cross-sections to better understand the geological process of the past which deposited the aquifer materials (e.g., the fanglomerates of the Puye formation and the fluvial deposits of the Santa Fe Group). Both of these geologic units are considered water-bearing and productive.

However, these subtle geologic distinctions within a formation do not always translate into distinct hydrogeologic units. The IRT has observed that the LANL chromium plume has migrated within and across these units, as though they were a single system. As another example, deep (2,000 feet +) regional high-capacity production wells of the Pajarito well field have been shown to induce a hydrologic response in the monitoring wells in the shallow groundwater in the chromium remediation area. To the extent that there may be some zones within a geologic formation that are relatively more permeable than others within the aquifer in the chromium plume area, these do not seem to be sufficiently distinct or laterally extensive to require separate monitoring wells, one in each different material. And contrary to OSE statements elsewhere in their memorandum, the IRT has not found evidence of a confining bed or artesian condition within the chromium-impacted area.

Although OSE has maintained a position that it has evidence that dual-screened bentonite-sealed wells have impacted fresh water, OSE also in this section of the memorandum said that “OSE is not prepared to assert the success of previously installed dual-screened wells, given the limited data and resources available to us at this time.” The OSE disclosure that it has not been able to review the performance of the dual-screened wells seems inconsistent with its firm position on not approving dual-screened monitoring wells, the timeliest method to obtain much needed data on the depth of contamination. The OSE’s Well Construction

Memorandum and the IRTs review of that are presented in subsequent sections of this appendix.

- OSE is open to dual-screened wells within the same hydrogeologic unit. DOE-EM-LA represents the shallow portion of the aquifer system in the chromium remediation area as a single hydrogeologic unit (a heterogeneous aquifer comprising various interbedded and interconnected geologic materials emplaced by various deposition processes and characterized as fanglomerates and similar geologic descriptors). OSE further would want to consider the hydrology and chemical characteristics as evidence for separate hydrogeologic units. The IRT suggests that OSE technical staff meet with Dr. Broxton to discuss details of the site geology and with Dr. Patrick Longmire for a discussion about the chemistry of groundwater. If OSE can find that the chromium plume essentially lies within a single hydrogeologic unit, dual-screen wells should be approved by OSE. This sort of information exchange could be critical to resuming site characterization efforts.

## **Annular Sealant**

- There is no compelling evidence seen by the IRT that the existing dual-screen monitoring wells constructed with bentonite have impacted fresh groundwater. Nonetheless, the topic of annular sealants is critically important and the IRT concurs with OSE that the sealants should be selected to assure sealing performance, minimize logistical issues that might impact emplacement, and minimize any adverse collateral impacts. Based on balancing these factors, the IRT urges consideration of the following strategy: monitoring well construction using coated bentonite granules (tablets) below the water table and cement above the water table to seal the annulus outside the casing. The IRT recommended strategy urges analysis of the cement for the presence of chromium and consideration of uncoated bentonite granules in the vadose zone as an alternative sealing material. The IRT recommendation is a compromise bridging the LANL and the previously stated OSE positions. Additional detail on the balancing criteria and basis for the IRT recommendation are provided in the main body of the IRT report.

In developing their argument that bentonite should not be used for sealing the casing annulus, OSE cites to a publication by Ajitha et al. (2018) finding that “free swell in the presence of chromium is reduced with time and concentration.” Further, OSE relies on that report to conclude that “there is evidence that Chromium VI impacts the swell potential of bentonite and can be accumulative. This will degrade the annular seal quality.” The IRT infers that the OSE is concerned that the chromium will react with bentonite to cause it to shrink and/or otherwise increase the permeability of the bentonite seal to cause it to leak significantly.

In this paper by Ajitha et al. (2018), the type of bentonite used was a calcium montmorillonite (bentonite). In the U.S., bentonite pellets for well seals are usually a sodium montmorillonite. Sodium montmorillonite has much better swelling characteristics. It is not possible to directly extrapolate the experimental findings in this research to the type of bentonite used in the LANL monitor wells.

Further, the paper actually concludes that there was only a “marginal increase in permeability of the liner due to chromium...” During the experiment by Ajitha et al. (2018), the hydraulic conductivity (coefficient of permeability) increased from about 5 to about  $7 \times 10^{-8}$  centimeters per second (cm/s). There was little difference in results after 1 month or 2 months. For comparison, a landfill clay liner is considered protective if its permeability is no more than  $1 \times 10^{-7}$  cm/s.

During the experiment by Ajitha et al. (2018) with the calcium montmorillonite, there was a 22 percent decline in plasticity index over 60 days. Because sodium montmorillonite clay would swell more than the calcium montmorillonite and have a greater plasticity index, the results here cannot be extrapolated to the LANL wells.

Because the experiment did not use the type of clay used in constructing the monitor wells, the Ajitha et al. (2018) article cited by the OSE should not be relied upon for evaluating the integrity of bentonite in the presence of chromium.

- The OSE raises a legitimate concern about the strength of bentonite. During well development, elevated water pressures may occur in the well screen interval that have the potential to compromise the integrity of the bentonite seal between the dual screens. This may occur most likely after the well is drilled, during the well development process to remove residual drilling fluids from the well. It is not clear to the IRT whether tests or calculations have been conducted to ensure that bentonite seals are not likely to fail during well development or during injection/extraction.

It is reassuring, however, that in the completed dual-screen well, there is over 1,000 feet of material, about 3 inches thick in the annular ring, including bentonite, along with some sand and a surface cement, to resist displacement of the bentonite seal in the interval between the two well screens in the regional aquifer during well development or operations.

## **Other Observations**

From the OSE comments, it is clear that the OSE perceives that the communication between LANL and OSE could be improved. The IRT recommends that efforts by both DOE-EM-LA and OSE be made to improve communications, share information, learn, and build mutual appreciation for the unique challenges and sense of urgency presented by the chromium contamination remediation.





STATE OF NEW MEXICO  
OFFICE OF THE STATE ENGINEER  
Hydrology Bureau



WELL CONSTRUCTION MEMORANDUM

**DATE:** May 21, 2024

**TO:** Lorraine Garcia, Deputy District Manager, Water Rights Division, District VI

**THROUGH:** Katie Zemlick, Ph.D., Hydrology Bureau Chief *KZ*  
Chris Angel, P.G., Water Resources Professional IV, Hydrology Bureau *CA*

**FROM:** Christopher Krambis, P.G., Water Resources Professional IV, Hydrology Bureau *CK*

**SUBJECT:** Bentonite well sealant failures in unsaturated and pressurized environments

**KEYWORD:** Well Construction, Sealant Guidelines, Bentonite, District VI, Los Alamos County, Northern Rio Grande Ground Water Basin, Espanola Basin Aquifer System Sole Source Aquifer, LANL, Chromium Plume

**ID:** WLC\_2024\_004

---

**EXECUTIVE SUMMARY**

The New Mexico Office of the State Engineer (NMOSE) has recently received submittals of Form WR-07 *Application for Permit to Drill a Well with No Water Right* from the Department of Energy (DOE) Environmental Management – Los Alamos Field Office (EM-LA) for the purpose of installing monitoring wells in the Los Alamos National Laboratory (LANL) legacy waste groundwater chromium plume (Figure 1). The legacy waste resulted from LANL’s effluent discharge to canyons, which impacted a portion of the Espanola Basin Aquifer System Sole Source Aquifer. The legacy waste requires remediation under a consent order with the New Mexico Environment Department (NMED) Hazardous Waste Bureau (HWB). The contamination present condition requires an Artesian Plan of Operation (APOO) to demonstrate that the proposed well construction will prevent the intermingling of groundwater within a hydrogeologic unit and between two or more hydrogeologic units. NMOSE is legally obligated to protect groundwater rights and quality from improper drilling techniques and well construction designs.

The EM-LA proposed well design involves placement of two wire-wrapped screens vertically separated on the same production casing with bentonite placed in the annulus between the screens to create a seal for discrete depth monitoring (the dual screen design). At LANL, this design is often used when drilling through a contamination zone to place the top screen in a position to monitor the contamination and the bottom screen in a position to evaluate for the vertical extent of

contamination and may involve drilling through separate hydrogeologic units. It has also been used to monitor separate perched aquifers in one installation. A packer separates the two screens inside the production casing.

When hydrated, bentonite is a gelatinous material that, while it has little compressive and shear strength, produces some pressure that forms a seal along the formation and casing walls. However, it does not form a chemical bond with the casing wall and does not “invade” several feet into the formation to form a sufficient hydrologic seal between the screens like cement. Its minimal strength does not withstand pressurization.

The New Mexico Administrative Code (NMAC) requires a permanent surface or artesian casing be installed by pressure or tremie grouting an NMOSE approved annular sealant at depth to provide an adequate seal before drilling through a contaminated zone and/or into an artesian (confined) zone where potable groundwater occurs. The strength of such a seal must achieve 500 pounds per square inch (psi) within 48 hours. NMOSE reviews the APOO to evaluate whether the surface, artesian and production casing material, size, weight, and seals meet NMAC. NMOSE concluded that EM-LA’s proposed design does not meet the NMAC. Despite this, EM-LA later stated in writing to NMED “*in the future EM-LA will continue to pursue a technical basis to advance dual screen well designs...*”.

Several case studies involving increasing chromium trends along the water table in the regional aquifer were analyzed and are presented herein. LANL has postulated that these increasing trends are due to natural breaks (hydraulic windows) in the lower confining unit of the overlying contaminated perched intermediate aquifer. Two other case studies are also presented and are specific to perched groundwater monitoring where desiccation and/or strength failures of the bentonite annular seal are apparent. The Hydrology Bureau shows that improper well construction is the more plausible explanation for the documented increasing chromium trends in the regional aquifer and tracer arrivals from one perched zone to underlying perched groundwater zones. This memorandum (Memorandum) provides empirical evidence to demonstrate that LANL’s universal use of and belief that bentonite materials provide a proper annular well sealant is misguided.

## INTRODUCTION

NMOSE published the Sealant Guidelines for Well Construction and Plugging (OSE, 2020). These Guidelines allow for the use of bentonite as an annular well seal under appropriate conditions, specifically in uncontaminated, unconfined, and non-flowing artesian conditions. The RG-00485-POD14 application process illustrates NMOSE's experience dealing with the applicant regarding the improper use of bentonite products as annular seals at LANL. The following outlines the chronological evolution of the RG-00485-POD14 monitoring well application.

- 1) On August 2, 2022, EM-LA, and their subcontractor N3B-Los Alamos (N3B), submitted an application for a permit to drill vertically through two distinct geologic formations in the east portion of the chromium plume to install monitoring well RG-00485-POD14 (R-76) using the dual screen design (Thomson and Bishop, 2022).
- 2) On November 15, 2022, NMOSE denied the application due to the proposed dual screen design being located where contamination is present and separate hydrogeologic units will be penetrated (Garcia, 2022).
- 3) On December 14, 2022, at their request EM-LA and N3B met with NMOSE in the Concha Ortiz y Pino Building in Santa Fe to discuss their drilling practices and to continue to advocate for the dual screen design and the use of bentonite sealants. Following the meeting, NMOSE conveyed to EM-LA and N3B that their argument for the design to assure protection of groundwater was unconvincing.
- 4) On March 8, 2023, EM-LA submitted Revision 1 of the application (Thomson and Bishop, 2023a), which maintained the dual screen design and the use of bentonite seals despite NMOSE's position on the design where contamination is present.
- 5) On March 15, 2023, Mike A. Hamman, P.E., the State Engineer of New Mexico responded to Revision 1 by explaining NMOSE's legal obligation to protect groundwater where proposed well designs will penetrate separate hydrogeologic units where contamination is present or suspected (Hamman, 2023).
- 6) On May 31, 2023, EM-LA submitted a drilling work plan (DWP) to the HWB for a single screen design (Duran, 2023) due to NMOSE's March 15, 2023, letter. In their cover letter to this submittal, EM-LA stated "*in the future EM-LA will continue to pursue a technical basis to advance dual screen well designs, while also protecting groundwater.*"
- 7) On June 8, 2023, the HWB approved the revised DWP with modifications that require the well be installed as a single screen design, that the Chamita Formation not be penetrated by the borehole, and that a separate monitoring well be installed in the Chamita Formation at this location (Shean, 2023).
- 8) On June 29, 2023, EM-LA submitted Revision 2 of the application to NMOSE (Thomson and Bishop, 2023b) with a single screen design that included the revised DWP. Revision 2 is the third submittal to NMOSE to obtain a permit to drill monitoring well RG-00485-POD14.
- 9) On August 14, 2023, the Hydrology Bureau completed review of Revision 2 and recommended special conditions that require Portland cement be used to plug the bottom 40 feet of the exploratory borehole and to seal the annulus of the well (Krambis, 2023).

- 10) On August 15, 2023, EM-LA met with NMOSE to discuss Revision 2. EM-LA agreed to use cement in lieu of bentonite as a sealant in the installation of RG-00485-POD14.
- 11) On September 18, 2023, NMOSE sent EM-LA the permit to drill RG-00485-POD14 (R-76) that included 19 Special Conditions of Approval (Garcia, 2023a).
- 12) On September 22, 2023, EM-LA began drilling the RG-00485-POD14 (R-76) borehole.
- 13) On November 2, 2023, NMOSE notified EM-LA via email that they were in violation of one of the Special Conditions of Approval. This violation was quickly rectified by EM-LA.
- 14) On November 22, 2023, N3B contacted NMOSE after hours to discuss borehole dimensions differing from the drilling work plan. NMOSE determined that the centralization of the casing in the borehole may be compromised and halted the drilling until the proper variances could be obtained.
- 15) On November 24, 2023, N3B contacted NMOSE requesting a variance from the permit.
- 16) On November 28, 2023, NMOSE suspended the permit (Garcia, 2023b) due to EM-LA's failure to follow their own drilling protocol approved and included in the permit by NMOSE.

To date, drilling of RG-485-POD14 (R-76) has been suspended. The lower 40 feet of the borehole has not been sealed per Permit Special Condition No. 19. The potential for downward migration of contaminated groundwater has been left unabated.

Ultimately, it is NMOSE that has the sole legal authority to determine appropriate well construction in the State of New Mexico. EM-LA's intent to continue to advocate for the dual screen design and bentonite sealants where contamination is present and their refusal to regard NMOSE's determination of confined conditions warrant a detailed technical understanding. The purpose of this Memorandum and a pending memorandum on artesian conditions at LANL is to provide NMOSE with a sound technical basis to make a final determination on these matters regarding current and future permit application submittals.

## HYDROGEOLOGY

Regionally, groundwater beneath the Pajarito Plateau is part of the Espanola Basin Aquifer System (EBAS) – a sole source aquifer that is the source of potable groundwater to Los Alamos County including LANL. The EBAS is comprised of deep basin fill sedimentary deposits mostly from the adjacent Sangre de Cristo Mountains to the east and the Jemez Mountains to the west and occurs within a major rift basin within the Rio Grande Rift. LANL and Los Alamos County occupy a portion of the Pajarito Plateau, which overlies a small portion of the EBAS west of the Rio Grande. Beneath the Pajarito Plateau, the basin fill deposits are comprised of a thick sequence of sedimentary deposits that include the Tesuque Formation, the Chamita Formation, and the Puye Formation. Volcanics including two major basalt layers occur within and above the Chamita and Puye Formations. Overlying volcanics above the Puye Formation include tuffs. These overlying volcanics are largely unsaturated.

The upper Cerros del Rio Basalt is a prevalent layer within the top of the Puye Formation at the chromium plume. Saturation within and on top of the Cerros del Rio Basalt and within the top of the Puye Formation forms the Perched Intermediate Aquifer (PIA). Chromium contamination persists in the PIA. The PIA remains poorly characterized but can occur as separate hydrogeologic units on top of and within the Cerros del Rio Basalt, possibly under water table and artesian conditions. At the west portion of the chromium plume the direction of groundwater flow within the PIA appears southwesterly with the dip of the basalt. Boreholes drilled through the lower confining unit of the PIA at the base of the Cerros del Rio Basalt have leaked contamination down through the desiccated and/or strength failures of the bentonite seals.

The top of the EBAS beneath the Pajarito Plateau is referred to as the Regional Aquifer (RA). Groundwater flow in the RA is easterly and appears to follow the trends of the major canyons that dissect and drain the Pajarito Plateau. County municipal supply wells draw groundwater from the top 2,000 feet of the RA. Since the late 1940's, the decline in the groundwater levels due to groundwater mining from these supply wells and possibly climatic changes have caused a steady linear decline in the groundwater levels (potentiometric surface). At PM-3 – one of the County production wells located east of the chromium plume – the potentiometric surface of the Chamita Formation has declined about 50 feet since its installation in 1966, whereas the water table in the overlying Puye Formation declined about 25 feet over the same time.

Groundwater at LANL is contaminated in the shallow unconfined portion of the RA. The deeper confined portion of the RA has been explored by only a few wells that indicate the deeper portions of the RA may be uncontaminated. However, there has been no exploration in the confined portion of the RA within LANL's chromium plume to verify the vertical extent. The existence of a shallow unconfined and a deep confined hydrogeologic unit beneath the Pajarito Plateau is well established by multiple publications and will be the subject of a follow up NMOSE memorandum.

## EVALUATION OF WELL CONSTRUCTION

A series of case studies are presented in this section to provide NMOSE with empirical evidence that bentonite materials do not make adequate well sealants under many conditions encountered at LANL.

### **Case Study I: RDX Plume Monitoring Well Nest CdV-9-1(i)**

An example of a failed bentonite seal is evident in monitoring well CdV-9-1(i) installed at the southwest portion of LANL (Figure 1). CdV-9-1(i) was constructed as a well nest that penetrates a 1,200-foot-thick unsaturated zone (vadose zone) where a series of alternating unsaturated and perched saturated hydrogeologic units occur within the RDX plume (Appendix A and B). RDX, also known as Royal Demolition explosive, cyclonite, hexogen and T4, has the chemical name 1,3,5-trinitro-1,3,5-triazine and is a synthetic explosive that when found in the environment is considered an emerging contaminant (USEPA, 2011). RDX has been detected in the alluvial, shallow perched, deep perched, and regional aquifers (LANL, 2011b). Initial RDX concentrations at CdV-9-1(i) were detected at about 250 micrograms per liter ( $\mu\text{g/L}$ ) during January 2015 but stabilized at about 25  $\mu\text{g/L}$  by July 2015 where they have remained to date. These detections exceed the tap water screening levels established by NMED (NMED, 2021) and the U.S. Environmental Protection Agency (USEPA, 2017) of 9.66  $\mu\text{g/L}$  and 0.7  $\mu\text{g/L}$ , respectively.

CdV-9-1(i) was completed in January 2015 to monitor a portion of the RDX plume at various depths within the upper perched zone (UPZ) of the deep perched groundwater system (LANL, 2015). The UPZ occurs in the Otowi Member tuffs and Puye Formation and ranges in thickness from 150 to 250 feet (LANL, 2011b). The lower perched zone (LPZ) occurs deeper within the Puye Formation and has a thickness between 30 and 80 feet (LANL, 2011b). Both the UPZ and the LPZ contain the deep perched groundwater in layered saturated hydrogeologic units that are vertically separated from one another by intervening confining units that create multiple intervening unsaturated zones (Appendix A). The UPZ and LPZ constitute the PIA at the RDX plume but include different hydrogeologic units compared to the chromium plume. These layered hydrogeologic units overlie the RA. The LPZ and the RA were not penetrated by the CdV-9-1(i) borehole (LANL, 2015).

### **CdV-9-1(i) Well Nest Construction**

Appendix B shows the configuration of well nest CdV-9-1(i), which consists of a shallow piezometer (PZ-1) that monitors the top of the UPZ, a second piezometer (PZ-2) that monitors a deeper portion of the UPZ, Screen 1 and Screen 2 that monitor separate saturated portions of the vadose zone that appears between the UPZ and the LPZ (LANL, 2017b). Screen 2 was set 31.3 feet below Screen 1 within a deeper perched zone separated from Screen 1 by a 10-foot-thick unsaturated zone (LANL, 2015), but was abandoned in 2015 when a temporary packer became lodged within the well (LANL, 2015). No information relevant to this study appears to have been collected from Screen 2 since the abandonment.

Each screen in CdV-9-1(i) is set within the same borehole and are separated from one another by 3/8-inch bentonite chips as is the bottom 133.2 feet of the borehole, which terminated at a depth of 1,220 feet below land surface (fbls) within the Puye Formation above the RA (LANL, 2015).

The 10-foot-long screens of PZ-1 and PZ-2 are vertically spaced about 180 feet apart and are set between 662.9 and 672.4a fbls and 852.9 and 862.4 fbls, respectively (Appendix B). PZ-1 is screened with the Otowi Member of Bandelier Tuff whereas PZ-2 is screened within the upper portion of the Puye Formation (LANL, 2015). The Cerro del Rio Basalt is not present at this location. PZ-2 is 75 feet above the 55-foot-long Screen 1 that extends from 937.4 fbls to 992.4 fbls as shown in the diagram in Appendix B. PZ-2 and Screen 1 both are screened within the Puye Formation but have a head difference of about 281 feet (LANL, 2011b), with PZ-2 having the higher head (Appendix A). The head difference indicates the portions of the UPZ monitored by PZ-2 and Screen 1 are separate perched hydrogeologic units within the Puye Formation with a downward vertical hydraulic gradient of 2.2 as determined using the EPA low to high vertical gradient calculator (USEPA, 2021). The horizontal gradient of the UPZ, as determined from Figure 3.1-3 (N3B, 2019) is about 0.18. The relatively steep vertical gradient indicates predominantly unsaturated conditions between screens and not predominantly saturated flow between screens (LANL, 2011b). These observations show that the UPZ is a series of stacked, individual hydrogeologic units that are hydraulically separated from one another by low permeability lower confining units, and influence among them is due to channeling within the borehole seal.

### **CdV-9-1(i) Hydrographs**

The data to create Figures 2 through 7 were downloaded from Intellus on September 20, 2023. Figure 2 shows the groundwater levels from each CdV-9-1(i) installation plotted over time (hydrographs). The near identical hydrographs for PZ-1 and PZ-2 suggest that these two installations monitor the same hydrogeologic unit – namely the UPZ – despite being installed in different formations (Otowi Member and Puye Formation). LANL assessed the vertical connection between these two formations and concluded that a vertical preferential pathway is present between them but considered this to be unique because pumping from the upper Puye (e.g., PZ-2) caused little or no response in the overlying Otowi Member and that the Otowi/Puye contact to be an important hydrostratigraphically because it causes a high lateral to vertical anisotropic condition (LANL, 2017c). Considering that the response between PZ-1 and PZ-2 is unique, channeling within the bentonite seal at CdV-9-1(i) appears to be the reason for the near identical hydrographs. In contrast, the Screen 1 hydrograph (Figures 2 and 3) clearly shows it is placed within a separate hydrogeologic unit than the portion of the UPZ that the piezometers monitor despite PZ-2 being screened in the Puye Formation like Screen 1.

### **CdV-9-1(i) Screen 1 Pumping Test**

Figure 3 shows the CdV-9-1(i) hydrographs during the July 2016 Screen 1 pumping test. Pumping tests consist of a background phase, a pumping phase, and a recovery phase. The pumping test was preceded by a month-long snowmelt recharge event during May 2016 that deflected the hydrograph upward by 12 feet (LANL, 2017c). While LANL attributed this to natural recharge, LANL also noted that previous studies on natural recharge to the PIA from snowmelt were much smaller in magnitude and that the May 2016 rise was unusual for a natural recharge event (LANL, 2017c). The pumping phase of this test was conducted from June 7 to July 12, 2016, at 1.88 gallons per minute (gpm) and includes a five-day hiatus from June 9 to June 14, 2016 (LANL, 2017c). The pumping phase was followed by a period of recovery from July 12 to July 25, 2016 (LANL, 2017c). Figure 3 shows the CDV-9-1(i) well nest hydrograph during the 1.88 gpm pumping test

conducted within Screen 1 resulted in a 40-foot drawdown in that well. However, the groundwater in the upper UPZ monitored by PZ-2 (also screened in the Puye Formation) showed no response. This indicates the Puye is a highly stratified formation that prevents the vertical movement of groundwater, similar to the Otowi/Puye contact. Intra-Puye Formation confining units are also observed between CdV-9-1(i) Screen 1 and 2, at monitoring well R-25 S4 (LANL, 2002), and in regional aquifer monitoring wells R-42 (LANL, 2009a) and R-62 (LANL, 2012a) in the chromium plume. This indicates that stacked confining conditions are a widespread hydrogeological characteristic of the Puye Formation.

The five-day hiatus is apparent early in the hydrograph (Figure 3) as a brief period of recovery that followed the initial drawdown. Variable pumping rates are apparent at the end of the hydrograph as slight inflections in the drawdown that were due to mechanical reasons (LANL, 2017c). Downward leakage through the borehole between PZ-2 and Screen 1 is not apparent in the hydrograph. The water levels measured in nearby observation wells during the CdV-9-1(i) S1 pumping test, shown and discussed in Figures D7 through D12 do not show obvious influence from the pumping at Screen 1 (LANL, 2017c). Considering the 40-foot drawdown curve in Screen 1, these observations indicate that the cone of depression had not moved to those locations hundreds of feet away in over a month of pumping and indicates that the UPZ either has a low transmissivity or does not extend laterally in those directions.

The May 2016 month-long snowmelt recharge was preceded by the November 2015 tracer injection test, which created a 30-foot pulse that lasted about 25 days. A 30-foot-high slug of water added above the well screen would result in an additional 13.5 psi pressurization above the natural static water level height of about 25 feet above the screen. The total pressure of about 23 psi exceeds the shear strength of bentonite provided by Ogden and Ruff (1993). These pulses are shown in the CdV-9-1(i) S1 hydrograph (Figures 2 and 4) and are much smaller in magnitude and duration compared to the two subsequent and much larger pulses discussed below, which are of unknown origin.

#### *Anomalous Pulses in CdV-9-1(i) Screen 1 Hydrograph*

The hydrograph shown in Figure 2 and Figure 4 shows two large pulses or spikes in the groundwater level monitored by Screen 1. The first spike appears to have occurred from late March to May 2017, and the second between mid-March and mid-May 2019. Both occurred after the 2016 CdV-9-1(i) Screen 1 pumping test. CdV-9-1(i) Screen 1 groundwater levels during these two periods rose by 79 and 116 feet, respectively. The groundwater levels in the upper UPZ monitored by the piezometers rose about 12 feet during the first spike and 23 feet during the second spike (Figure 4).

LANL attributed the 2017 spike to natural seasonal recharge to the UPZ from subvertical fracture pathways in the canyon bottom (LANL, 2017c, 2018b; N3B, 2019). However, this is purely speculative because it is highly unlikely that natural recharge would increase the groundwater level in the deeper Screen 1 more than the groundwater levels in the shallower CdV-9-1(i) piezometers and other nearby UPZ monitoring wells. Additionally, LANL considered the much smaller May 2016 snowmelt rise that preceded the July 2016 pumping test to be unusually large for natural recharge observed in the past at LANL. Furthermore, the Puye Formation is not a fractured



formation, but is predominantly unconsolidated. It is unlikely that a discrete fracture pathway that propagates from the surface and through the differentially competent geologic units to Screen 1 exists.

Groundwater levels in nearby UPZ wells CdV-16-1(i), R-25b, CdV-16-4ip S1 and CdV-16-2i(r) located 500 feet and 810 feet south and 835 feet and 1690 feet southeast, respectively (Figure 1) do not show the spikes (Figure 5) exhibited in CdV-9-1(i) Screen 1 (Figures 2 and 4). However, the CdV-16-1(i) hydrograph (Figure 5) shows a 3.5-foot and an 8.6-foot rise, respectively, about two months after the first and second spikes. Additionally, a delayed and muted two-foot spike in CdV-16-4ip S1 occurred on May 21, 2019, after the second spike. No response to the first spike is evident in CdV-16-4ip S1. The R-25b hydrograph may exhibit a slight rise following the second spike, but it is not as well-defined as the other two UPZ wells. Each of these wells are screened within the upper portion of the UPZ in the same stratigraphic horizon as PZ-2.

Conceptually, these delayed and muted responses in the adjacent UPZ wells are more likely attributed to water loss from the CdV-9-1(i) borehole flowing laterally outward into the upper UPZ as a cone of impression developed, and not from natural recharge. Recharge would have affected these water levels far more equally in space and time than what is shown in Figure 5. Also, a much smaller previous spike exhibited in the CdV-9-1(i) Screen 1 hydrograph during May 2016 immediately prior to the pumping test (Figure 5) was attributed to a spring snowmelt recharge event (LANL, 2017c). This smaller spike affected the water level in Screen 1 by about 12 feet (small by comparison to the latter spikes), which at the time LANL considered to be unusually high in magnitude and not observed at other wells completed in the perched intermediate aquifer (LANL, 2017c). The 2016 spike is about seven to 10 times less than the 2017 and 2019 spikes, respectively.

The pattern of water level spikes in the hydrographs of nearby UPZ monitoring wells shown in Figure 5 indicates that the further away a UPZ monitoring well is from the CdV-9-1(i) borehole, the less the response is in magnitude and the greater the lag time becomes with the furthest well exhibiting no response. This indicates the source emanated from the CdV-9-1(i) borehole and not from natural recharge. The source created a cone of impression centered around CdV-9-1(i) screen 1 that was detectable in nearby wells that are known not to have responded to the 2016 CdV-9-1(i) Screen 1 pumping test. Additionally, local precipitation events prior to these spikes are similar in duration and magnitude to later precipitation events when corresponding spikes are absent (Figure 5). This indicates that local precipitation was not the cause of the two spikes. In addition, earlier studies concluded that the deep PIA groundwater monitoring wells CdV-16-2(i)r do not respond to snowmelt runoff like the shallower CdV-16-1(i) and R-25b have (LANL, 2011b). Considering that Screen 1 is situated deeper in the UPZ than CdV-16-2(i)r, it is highly unlikely that the spikes recorded at CdV-9-1(i) are due to natural recharge events originating from the canyon floors.

### **CdV-9-1(i) Borehole Integrity**

If the bentonite seals within the CdV-9-1(i) borehole were competent, the pressurization of Screen 1 during these spikes would have propagated laterally into the Puye Formation adjacent to Screen 1 and not upward to PZ-1 and PZ-2. In order to obtain the water level changes seen in PZ-2 and PZ-1 with a competent annular seal, it would be necessary to breakdown the overlying formation

including the perching confining layers within the Puye Formation and at the Otowi/Puye contact, which are demonstrated to have high vertical anisotropy that prevent vertical groundwater movement, and the intervening unsaturated zone between Screen 1 and PZ-2 would have had to become saturated. The groundwater should move laterally away from the well and into the formation due to the higher permeability indicated by the Screen 1 dilution tracer test (LANL, 2017b, 2018b). However, lateral movement of the water from the spikes were not detected in R-25 S3, which monitored the same portion of the UPZ. This suggests that most of the water from the two spikes went into the upper UPZ nearest the two piezometers.

A more plausible explanation for the two groundwater level spikes is that two separate injection operations took place within Screen 1. These hypothesized injections are hereafter referred to as apparent injection operations (AIO). The AIOs pressurized the CdV-9-1(i) borehole, which compromised the bentonite seal between Screen 1 and the piezometers and pushed water up through the compromised seal and into the upper UPZ. The AIOs raised the water level within the borehole, not within the Puye Formation, to a level that connected the three CdV-9-1(i) screens. This affected the water levels in PZ-1 and PZ-2 immediately. Later, the pressurization expanded laterally outward within the upper UPZ creating a large cone of impression that affected groundwater levels at CdV-16-1(i), and perhaps CdV-16-4ip S1 and R-25b (Figure 5). These distant wells were demonstrated by the 2016 pumping test to not be hydraulically connected to CdV-9-1(i) Screen 1.

The breakdown of bentonite is easily achieved because it has very little compressive strength. The compressive strength of a compacted bentonite ranges from 9.4 psi to 14.5 psi (Muhmed, Mohamed and Khan, 2022) and about 2.19 psi for bentonite seals emplaced down boreholes (Ogden and Ruff, 1991, 1993). The compacted values are likely overstated for an uncompacted bentonite in the annular space of the borehole. An estimate of the added pressure exerted on the bentonite by these large spikes in water level can be calculated by multiplying the change in water level (ft) by the weight of water (0.43 psi/ft). Therefore, a 79-foot increase in water equates to approximately 34 psi and a 116-foot increase equates to approximately a 50-psi increase. These increases can channel the bentonite compromising the annular seal. As this is a pressure dependent calculation, it can also be used to determine the pressures acting on a bentonite seal during pumping where drawdown occurs. According to Ogden and Ruff (1993), the shear strength can be related to the well ratio and ranges between 2.19 psi and 1.40 psi depending on the well ratio. In this article they conclude that the difference in head per length of annulus seal, equal to the aquitard thickness should be less than or equal to 30 without a safety factor. As these wells are in a contaminated aquifer (that will likely impact the swelling capacity of the bentonite) with municipal water wells immediately adjacent to the plume a large safety factor should be applied.

Considering that the vertical separation between the top of Screen 1 and the bottom of PZ-2 is about 75 feet, that there is a highly competent confining unit between the two that perches groundwater to a point that it creates an intervening unsaturated zone, and that the water level rises measured in PZ-2 and CdV-16-1(i) coincide with the spikes in Screen 1, it is evident that flow from Screen 1 must have travelled up the borehole and pressurized the upper UPZ to a lateral distance of at least 500 feet. Pressurizing of the upper UPZ by the Screen 1 spikes is also evident by the responses at CdV-16-1(i) and CdV-16-4ip S1, which are screened at about the same

stratigraphic interval as PZ-2. Confirmation of preexisting CdV-9-1(i) borehole integrity issues is provided by the following analysis of a series of tracer tests conducted by LANL.

### **CdV-9-1(i) Tracer Tests**

A tracer test conducted in 2015 within CdV-9-1(i) had an unexpected result. Each CdV-9-1(i) piezometer (PZ-1 and PZ-2) was injected with a different tracer during November 2015, both of which were detected in underlying CdV-9-1(i) Screen 1 after a three-to-four-month period. 25 kilograms (Kg) of 1,3,6-NTS tracer was poured into PZ-1 and 25 Kg of 1,3,5-NTS tracer was poured into PZ-2 (LANL, 2017b). The subsequent detection of these tracers in Screen 1 demonstrates vertical flow path connections that represent natural flow paths or short-circuiting along the well bore or in the adjacent formation (LANL, 2017b, 2018b). Detected concentrations of both tracers in Screen 1 increased during the July 2016 pumping test conducted on Screen 1, were continually detected following breakthrough in mid-2017 and were continually detected afterward (LANL, 2017b).

LANL (2017a) concluded that *“However, this transport time does not represent rates under natural hydraulic gradients because the tracer deployments in piezometers 1 and 2 increased heads substantially during addition of the tracers, and the pump test at screen 1 appeared to have increased gradients that would also promote faster transport. At this time, it is also unclear whether the connections between the piezometers and screen 1 represent natural flow paths or if the detections of tracers in the piezometer are related to short-circuiting along the well bore or in the adjacent formation. Additional data and evaluations are required to evaluate this issue.”* It is unknown whether additional evaluations were conducted. However, the Hydrology Bureau finds the natural flow path scenario proposed by LANL to be the least plausible because:

- The intervening confining unit and vadose zone between PZ-2 and Screen 1 would prevent a natural vertical pathway within the Puye Formation just as it does with groundwater,
- The highly stratified nature of the Puye Formation would create a vertical anisotropy that would impede vertical migration of the tracers within saturated zones,
- The relatively high horizontal hydraulic conductivity of 10.2 feet per day (LANL, 2017a) of the saturated zone monitored by Screen 1 would provide a strong lateral preferential pathway that would cause the tracers to migrate away from Screen 1 over this prolonged period as indicated by the Screen 1 tracer test (LANL, 2017b),
- The July 2016 Screen 1 pumping test (LANL, 2017c) did not influence the water levels in PZ-2, proving that the two zones are not naturally hydrogeologically connected, and
- The gradients between Screen 1 and the two piezometers induced by the 2015 tracer injection tests and the 2016 pumping test are not relevant in the case of the natural pathway due to the natural confining conditions but promotes the idea of an intra-borehole connection.

The hydrographs demonstrate that there is no natural flow path between PZ-2 and Screen 1. While the PZ-2 hydrograph shows no response during the 2016 Screen 1 pumping test, tracer did leak from PZ-2 down to Screen 1 during this test. The only rational conclusion is that the tracers entered

Screen 1 from within the borehole and not through the formation. This must have occurred as intermittent pulses along the casing, through the desiccated bentonite seal and/or exceeding the shear strength of the bentonite and/or by the short-circuiting of the bentonite seal as hypothesized by LANL (LANL, 2017a).

It is believed that the piezometer tracers had not initially moved beyond the vicinity of the screens following the tracer injection (LANL, 2017b). While LANL credits the 2016 Screen 1 pumping test as the cause for the piezometer tracers to be detected in Screen 1, the breakthrough occurred during the 2017 spike, about two years after the pumping test (Figure 4). The 2017 AIO forced water up through the leaking annular seal likely mobilized the tracers around the piezometer screens as the cone of impression continued to pressurize the upper UPZ. When the 2017 AIO ceased, depressurization followed. The resulting reverse gradient pushed the tracer-laden water back down the borehole to Screen 1 creating the breakthrough observed in Figure 4. Following the 2017 AIO induced tracer breakthrough, the mass decreased significantly until the second spike occurred.

During the second (2019) spike, the tracer detections in Screen 1 temporarily decreased due to the dilution from the Screen 1 2017 AIO water invading that zone. Following the second AIO, detections of both tracers have been gradually increasing in Screen 1 to date. This indicates that most of the piezometer tracer mass were removed during the first spike or that the larger second spike forced the tracers further out into the UPZ so that more time was required for the tracers to flow back to the wellbore and down to Screen 1 under the natural downward vertical hydraulic gradient. The latter explanation better accounts for the more subdued and long-term breakthrough following the second spike in 2019. The tracers injected into Screen 1 were never recovered during the 2016 pumping test, indicating that they migrated away from the well and into the Puye Formation (LANL, 2017b). This suggests that the lower UPZ is much more permeable than the upper portion of the UPZ monitored by PZ-1 and PZ-2.

The Hydrology Bureau believes that the portion of the bentonite annular seal that spans across the thin intervening vadose zone between the stacked perched aquifers desiccated over time, which compromised the seal even before the subsequent testing was conducted. Later, the 2015 tracer test and the 2016 pumping test conducted at CdV-9-1(i) further compromised the bentonite seal. Furthermore, the 2017 and 2019 AIO spikes appear to have caused significant damage to the seal. These four factors provide conclusive evidence that bentonite does not provide an adequate annular seal when installed across an unsaturated, partially saturated, and/or intermittently saturated vadose zone – especially when placed under pressurization and depressurization such as injection and extraction operations. Other well nests and clusters installed at LANL also demonstrate that contaminants have migrated in a similar fashion as the CdV-9-1(i) tracers when bentonite seals were installed across an intervening vadose zone.

### **Case Study II: Monitoring Well R-25**

Monitoring well R-25 was completed to a depth of 1,942 fbls on May 25, 1999, as a multi-screened well with three screens in the UPZ, one in the LPZ, and five in the RA. Each screen consisted of a 10-foot long 10-slot stainless steel wire wrap section welded onto a single 5-inch inside diameter (ID) Schedule 40 304-stainless steel production casing (LANL, 2002). The nine screened intervals

were isolated from one another with a 50:50 mix of 20/40-gradation sand and granular bentonite in the annular space and a packer system within the wellbore (LANL, 2002). From 1,942 to 1,026 fbls, the seals were installed using a mix of bentonite, water, and a retardant, the latter to keep the bentonite from expanding in the tremie line within the saturated zone (LANL, 2002). From 1,026 to 610 fbls, above the top of the upper saturated zone, the transport fluid was municipal water, and “[a]bove the saturated zone, the bentonite was introduced dry” (LANL, 2002).

The well was used for monitoring groundwater quality and levels at various depths (Figure 7) from November 2000 to December 2016. The main groundwater contaminant was RDX. The UPZ was encountered between 711 to 1,132 fbls where Screens 1 through 3 were placed within the lower part of the Otowi Member and upper part of the Puye Formation (LANL, 2002). Alternating wet and dry zones were encountered from 1,132 to 1,286 fbls within the LPZ of the Puye Formation where Screen 4 was placed. The RA was encountered at a depth of 1,286 ft in the Puye Formation where Screens 5 through 9 were placed (LANL, 2002). A downward vertical hydraulic gradient is present among all screened zones with Screen 1 having the highest head and Screen 9 the lowest.

R-25 was declared an unsuitable monitoring well by the HWB in 2012 due to improper construction and downward leakage of contaminated groundwater (Kieling, 2012). R-25 was properly plugged and abandoned on February 5, 2023 (N3B, 2023). Despite R-25 being plagued with construction issues, the 16 years of monitoring exhibit patterns of downward movement of RDX mass within the UPZ to the LPZ.

Figure 6 shows the RDX concentration in Screen 1 gradually decrease from an initial concentration of 65 µg/L to 21 µg/L over the 16-year monitoring period. The trendline shows a consistent negative slope of  $-0.0062$ . Simultaneously, the RDX concentrations in Screen 2 and 4 (Screen 3 was not monitored for water quality testing due to damage) increased from background to about 20 µg/L. The trendlines for these two datasets exhibit a consistent positive slope of 0.0034 and 0.0023, which are about half that of Screen 1 and nearly sum to the slope of Screen 1. It should be noted that the RDX concentrations detected in each of these three screens are about the same at the end of the monitoring period. This indicates a transfer of the RDX mass from the top portion of the UPZ down to Screens 2 and 4 to a point when the concentrations equilibrated. It should also be noted that Screen 4 was within an isolated zone of alternating unsaturated conditions so that there should have been no natural hydraulic communication between it and the overlying perched hydrogeologic units. The introduction of RDX into Screen 4 must have been through the annulus or the damaged zone along the borehole.

The HWB identified that water levels also show downward leakage from Screen 1 and 2 to Screen 4 and that the “*excessively long filter-packs may have been set across perching horizons, providing a conduit for downward leakage*” (Kieling, 2012). The Hydrology Bureau notes that the filter pack for Screen 1 extended about four feet below the bottom of the screen and that the filter pack/sand seal below Screen 4 extended about seven feet below that screen. The filter pack and sand seal below Screen 2 is about 12 feet, which can possibly breach a thin perching horizon if located immediately below the screen. However, thin alternating saturated and unsaturated horizons only existed between 1,132 and 1,286 fbls where Screen 4 was placed (LANL, 2002) so that the filter pack extents cited by HWB should not have been the issue. Furthermore, the 39-foot-thick cement seal between Screen 3 and Screen 4 (LANL, 2002) should have prevented downward migration of

contaminants between those two points assuming it was not compromised during construction. Instead, the Hydrology Bureau proposes the following scenario as the likely cause of the downward leakage.

The lengths of the bentonite seals between Screen 1 and 2 is 103 feet, between Screens 2 and 3 is 135 feet and between Screens 3 and 4 is 111 feet including the cement seal (LANL, 2002). It is more plausible that the bentonite seals were damaged during well construction as stated by the HWB (Kieling, 2012) and may have been further compromised by subsequent desiccation where the seals cross unsaturated zones, such as those between the interval of 1,132 and 1,286 fbls (Screen 4). While the fully saturated conditions between Screens 1 and 2, and 2 and 3 may have prevented desiccation, the bentonite seals were half coarse sand and installed via gravity, not pressure. This likely created channeling. Coupled with the vertical downward gradient exhibited by all the screens, these factors appear to have created a downward leaky condition within the annulus between screens. The R-25 issue documents how poor well design and construction in a setting where multiple hydrogeologic units are penetrated, and where groundwater in the overlying hydrogeologic unit occurs at a higher head and is contaminated can cause inter-aquifer exchange to a degree that underlying hydrogeologic units become contaminated over time. This downward leakage pattern is observed at other well nests at LANL.

### **Case Study III: Chromium Plume Monitoring Wells R-43 and SCI-2**

At dual screen regional aquifer monitoring well R-43, sampling conducted since 2008 of nearby PIA monitoring well SCI-2 (Figure 1) established that the groundwater to be contaminated with total chromium due to exceedances of the 50 µg/L New Mexico groundwater standard established by 20.6.2.3103 NMAC. The borehole each well was installed within penetrated the lower confining layer of the PIA and was advanced deep into the RA across an intervening vadose zone. The boreholes for SCI-2 and R-43 are about 75 feet apart and penetrate to a depth of 890 and 1,006 fbls, respectively (LANL, 2009b) with SCI-2 located west and upgradient (in the RA) of the R-43 borehole. No casing or cement seal was installed prior to drilling the SCI-2 borehole through the lower confining unit at the base of the Cerro del Rio Basalt, which comprises the contaminated PIA.

#### **Perched Intermediate Aquifer Monitoring Well SCI-2**

PIA monitoring well SCI-2 was completed on August 31, 2008, with a two-inch ID polyvinyl chloride casing (LANL, 2009b). The bottom 310 feet of the SCI-2 borehole was plugged with a mix of bentonite pellets and chips from a depth interval of 890 up to 580 fbgl (LANL, 2009b). This spans the 260-foot-thick vadose zone within the Puye Formation between the overlying contaminated PIA and the then uncontaminated underlying RA. The annulus above the SCI-2 well screen interval (568 and 548 fbgl) was filled with ¼-inch bentonite pellets to 418 fbgl, 3/8-inch bentonite chips to 400 fbgl, and a high solids bentonite grout to 46 fbgl (LANL, 2009b).

The perched water table was encountered at a depth of 514 fbls following well construction (LANL, 2009b). The water table depth and the depth of the bottom of the SCI-2 well screen indicate that the PIA was at least 54 feet thick upon well completion. However, the actual thickness is evident when considering the depth to the base of the Cerros del Rio Basalt encountered at about

630 fbgl (LANL, 2009b) to be 115 feet thick then, which is close to the estimate of 100 feet by LANL (LANL, 2012b). LANL (2012b) estimated the thickness to decrease to 20 to 40 feet at PIA monitoring wells MCOI-5 and MCOI-6 in Mortandad Canyon to the south (Figure 1).

### Dual Screen Regional Aquifer Monitoring Well R-43

RA monitoring well R-43 was completed on October 17, 2008, with two screened intervals welded to a five-inch ID stainless steel casing (LANL, 2009b). During drilling, the open-hole interval between 408.3 fbgl and 640 fbgl was cemented on August 23, 2008, to seal off the PIA groundwater (LANL, 2009b). This was confirmed by subsequent video logging (LANL, 2009b). This cemented interval corresponds to the Cerros del Rio Basalt that contains the contaminated PIA groundwater at this location. Following cementation, the drilling of the R-43 borehole resumed to a total depth of 1,006 fbgl. The bottom screen (Screen 2) spans a depth interval of 979.1 to 969.1 fbgl and the top screen (Screen 1) spans a depth interval of 924.6 to 903.9 fbgl (LANL, 2009b). Thirty-four feet of the 44-foot-long annulus between the two screens was filled with bentonite chips to create a hydraulic seal between the two screens (LANL, 2009b). The annulus above Screen 1 was filled with bentonite chips from 897.6 to 868.8 fbgl, high solids bentonite grout from 868.8 to 629.8 fbgl, bentonite chips to 400.1 fbgl and cement-bentonite slurry to land surface (LANL, 2009b). RA groundwater was encountered at a depth of 892.9 fbgl following well completion.

### Evidence of Inter-aquifer Exchange

Figure 7 illustrates the evidence that the chromium-contaminated groundwater in the PIA at SCI-2 has migrated down to the unconfined portion of the RA at R-43. Figure 7 was prepared using data downloaded from Intellus on October 24, 2023. The total dissolved chromium behaves like a tracer between these two aquifers because the high dissolved oxygen concentration present in groundwater at LANL prevents the reduction of the chromium VI to chromium III – making the total dissolved chromium relatively chemically unreactive in the environment. Consequently, the apparent depletion of the total dissolved chromium concentration in the PIA at SCI-2 is not due to chemical alteration, but to physical migration.

### First Decline

Figure 7 shows that about two years following the completion of monitoring well SCI-2, the high chromium concentration, which initially fluctuated between about 470 and 658  $\mu\text{g/L}$ , began to decrease linearly (decline) with a slope of -0.095 in May 2010. While the trendline shown in Figure 7 exhibits a low coefficient of determination ( $R^2$ ) due to the large variations in laboratory detected chromium concentrations; it does indicate a rate of loss of total dissolved chromium from the PIA was about 34  $\mu\text{g/L}$  per year. The PIA water level was stable during the first decline with an elevation of about 6,208 feet above mean seal level (famsl). The first decline lasted until October 2013.

Two pumping tests conducted on SCI-2 from October 24 to November 23, 2013 (LANL, 2014) and August to September 2014. These pumping tests appear to have disrupted the first decline (Figure 7). During the first test, SCI-2 was pumped at 0.7 gallons per minute (gpm) for 30 days and resulted in 13 feet of drawdown in that well. A transmissivity of 1,600 gallons per day per foot

(gpd/ft) was determined from the first test (LANL, 2014), which is about 214 square feet per day (ft<sup>2</sup>/d). Considering the PIA at SCI-2 was 115 feet thick at the time of the test, the hydraulic conductivity is about 1 foot per day (ft/d) or 3.5E-04 cm/s. These tests appear to have impacted the bentonite seal as shown by the second decline.

### Second Decline

Following these two pumping tests, the water level in the PIA at SCI-2 also began to decline until August 2016. By this time, the chromium concentration had resumed a downward trend from August 2015 to February 2019. This second decline had a slightly greater rate and slope (-0.1) than the first decline. During the second decline, the chromium concentration decreased at a rate of 36 µg/L per year. Although the PIA water table was stable at an elevation of about 6,198 famsl during the second decline, the head loss of about 10 feet since the first decline appears to coincide with the first pumping test. The 10-foot head loss indicates a significant loss of fluid from the PIA occurred. The second decline continued until 2020. At this time, a two-year hiatus or period of stable water levels and chromium concentrations followed the second decline until about January 2022. While the cause of the end of the second decline and the start of the two-year hiatus is not known, it may be attributed to the depletion of chromium mass in the PIA equilibrating with the rising concentration in the RA.

### Third Decline

Starting in 2022, a third decline in the chromium concentration and water level measured in SCI-2 followed the two-year hiatus. During the third decline, the chromium concentration decreased at a rate of 34 µg/L per year with a slope of -0.094, which is the same as the rate of the first decline. The PIA water level dropped another five feet since the second decline. Although the third decline is ongoing, the chromium concentration at SCI-2 is now below 200 µg/L for the first time since monitoring began in 2008, which is nearly the same as the concentration now measured in R-43 Screen 1.

Overall, from May 2010 to date, the chromium plume concentration and water level in SCI-2 decreased from about 658 µg/L to below 200 µg/L and 15 feet, respectively. There was no remediation of the PIA during this time and the PIA hydraulics have been described as limited in aerial extent and lacking influence on other portions of the PIA (LANL, 2014) so that the contaminant transport was likely to be low. This is supported by the low transmissivity and hydraulic conductivity of the PIA at SCI-2. Dilution of the chromium from local recharge and permitted effluent discharge to Sandia Canyon are unlikely causes of the decrease in chromium concentration considering temperature and water level responses indicate isolation from the surface (LANL, 2012b, 2014). Additionally, the long-term drought (or climatic changes) discounts natural dilution from surface recharge as a cause of the concentration decrease over this period.

Another reason for the chromium concentration and head losses should be considered. The issue of where the fluid and chromium mass migrated to is apparent after a review of the chromium concentrations in R-43 Screen 1 that monitors the top of the RA.



### Effects on the Regional Aquifer

The head difference between the PIA and RA indicates a downward vertical gradient of 0.9455 exists based on the low to high value as calculated by the U.S. EPA Vertical Gradient Calculator (USEPA, 2021). Other values were calculated to range from 1.017 to 1.182 downward. This indicates that there is a strong potential for downward migration of fluids from the PIA to the RA if the lower confining unit of the PIA becomes compromised.

Following initial sampling of R-43 in November 2008, the chromium concentrations in R-43 Screen 1 and Screen 2 were below background concentrations over six quarterly sample events (Figure 7). This indicates that the RA was initially uncontaminated. However, the overlying PIA as monitored by SCI-2 was highly contaminated at this time. By May 2010, about a year and a half after completion of R-43, the total chromium concentration began to steadily exceed background in R-43 Screen 1. On May 15, 2013, the total chromium first exceeded the regulatory limits of 50 µg/L, and on November 14, 2019, the total chromium concentrations peaked from below background to 223 µg/L. Subsequent sampling showed a steady decrease in the total chromium concentrations in both SCI-2 and R-43 following the two-year hiatus when the chromium concentrations in the two aquifers equilibrated.

Following the initial Screen 1 chromium concentration increase in May 2010, two subsequent Screen 1 increasing trends appear to correspond to two SCI-2 declines (Figure 7). During the first SCI-2 decline, total chromium concentrations in Screen 1 steadily increased at a rate of 15 µg/L per year – slightly less than half of the rate of loss from SCI-2 over the same period. During the second SCI-2 decline, chromium concentrations in Screen 1 steadily increased at a rate of 21 µg/L per year – slightly more than half the rate of loss from SCI-2. The slope of the second decline is greater than the first. The pattern of increasing chromium concentration in Screen 1 mirrors the pattern of chromium concentration decreases in SCI-2. Following the second decline, the hiatus marked by a static period of about two years occurs in both wells. The hiatus is followed by a third decline in the chromium concentration in SCI-2 and the first decline in Screen 1.

This indicates a correlating trend with a slightly greater rate of loss in SCI-2 than gain in Screen 1. It is obvious the two are related and that the chromium plume in the RA at R-43 is a result of leakage from the SCI-2 borehole. It is not suspected that the perched groundwater encountered at R-43 has leaked down that borehole because the open-hole interval between 408.3 fbls and 640 fbls was cemented on August 23, 2008, during drilling to seal the PIA (LANL, 2009b).

After a lag of six years relative to the first two SCI-2 declines, the total chromium concentrations in R-43 Screen 2 began to increase from about 14 µg/L in early 2016 up to 50 µg/L on November 3, 2020. The lower concentrations and lag time are to be expected considering Screen 2 monitors a deeper portion of the RA than Screen 1. After about 11 and 12 years, the chromium concentrations detected in R-43 S1 and R-43 S2, respectively, began to decrease with the third SCI-2 decline. This is due to the depletion of the chromium concentration in the PIA through the SCI-2 borehole entering the RA and the vadose zone between the two.

To explain the increasing trend in the regional aquifer, LANL hypothesized the existence of an “hydraulic window” – a location where downward groundwater flow from the contaminated PIA

enters the RA (LANL, 2018a). The locations of the LANL-hypothesized hydraulic windows are provided in Figure 8. Although modeled, actual geological evidence supporting the hydraulic window concept has not been demonstrated. It is postulated here that hydraulic windows exist, but not as a natural phenomenon. It is far more likely that it is the result of an improper well/borehole seal at SCI-2 that connects the contaminated PIA to a previously uncontaminated RA. This condition violates 19.27.4.30(4) NMAC.

#### **Case Study IV: Monitoring Wells R-15, MCOI-5 and MCOI-6**

In contrast to the SCI-2/R-43, RA monitoring well R-15 and nearby PIA monitoring well MCOI-6, both located about 2,800 feet southwest of R-43/SCI-2 (Figure 1) exhibited a different relationship between the PIA and RA over the same period. MCOI-6 exhibited total chromium exceedances since it was completed on January 13, 2005 (Figure 9), but at lower concentrations than those detected at SCI-2 (Figure 7). However, the adjacent R-15 RA monitoring well has not had exceedances of this contaminant. Additionally, the trend of chromium concentration in MCOI-6 exhibits a seven-year increase between 2007 and 2014 followed by a decreasing trend beginning in 2017 (Figure 9). The termination of 051 effluent release into Mortandad Canyon in mid-2017 (Figure 9) does not appear to be related to this trend. No inverse response is noted between R-15 and MCOI-6 (Figure 9) as it is with R-43 and SCI-2 (Figure 7).

When compared to the relationship exhibited at the R-43/SCI-2 well cluster, the lack of a similar response in the R-15/MCOI-6 well cluster appears to be due to the drilling and well construction. The MCOI-6 wellbore did not penetrate through the lower confining unit of the PIA (the base of the Cerros del Rio Basalt) as in the case of the SCI-2 borehole. The MCOI-6 borehole terminated at a depth of 720 fbls (Kleinfelder, 2006), about 26 feet above the base of the Cerros del Rio Basalt and was screened between 686 and 709 fbls (Kleinfelder, 2006). Groundwater was noted to enter from the bottom of the borehole during geophysical logging, and initially had a static depth to water at about 664 fbls and a very slow recovery time following development (Kleinfelder, 2006). The R-15 borehole was sealed with 119 feet of a cement-bentonite slurry (LANL, 2001) like at R-43 to prevent the downward seepage of contaminated PIA groundwater from entering the RA.

MCOI-5 was drilled nearby to a shallower depth of 717 fbls (Kleinfelder, 2006), about 30 feet above the base of the Cerros del Rio Basalt. MCOI-5 is screened from 689 and 699 fbls and had an initial static water level of about 686 fbls (Kleinfelder, 2006), indicating the screen intercepted the water table. MCOI-5 is currently dry. Although, the hydrographs of MCOI-5 and MCOI-6 exhibit the same trend (Figure 9), the head difference indicates an upward gradient is present in the Cerros del Rio Basalt PIA and the chromium concentrations show contamination is present only at depth in this aquifer. This suggests that the PIA within the Cerros del Rio Basalt at this location exists as an unconfined water table aquifer (MCOI-5) and a separate artesian aquifer (MCOI-6). However, the PIA has not been adequately characterized at LANL to determine if this is observed elsewhere.

The MCOI-5 and MCOI-6 hydrographs (Figure 9) also exhibit a similar overall trend with SCI-2 (Figure 7) – suggesting the two locations may be hydrogeologically connected. SCI-2 is hydraulically upgradient of MCOI-6 based on the consistent 50-foot head difference between them. Conceivably, some of the chromium mass from SCI-2 can migrate to MCOI-6. An apparent horizontal hydraulic gradient of about 0.02 and the chromium mass and trend differences between

these two points indicate high resistance to flow due to a low hydraulic conductivity in the basal part of the Cerros del Rio Basalt. This is corroborated by the observed slow recovery rate following development of MCOI-6 (Kleinfelder, 2006). These observations indicate a slow transport time between the two points is likely. It appears that the loss of chromium at SCI-2 is best explained by borehole leakage as previously discussed. Additionally, it should be noted that the drilling and well construction at the MCOI-5/MCOI-6/R-15 well cluster appears to meet code regarding inter-aquifer exchange and that LANL did not hypothesize evidence of a hydraulic window at the R-15/MCOI-6 location (Figure 8).

### **Case Study V: Chromium Plume Monitoring Wells R-61, R-62, and CRPZ-5**

Other locations in the RA where long-term steady increasing trends in chromium concentration are occurring include R-61, R-62, and CrPZ-5 (Figure 1).

#### **Regional Aquifer Monitoring Well R-62**

Monitoring well R-62 was completed as a single screen RA monitoring well on October 3, 2011, about 2,000 feet west-southwest of SCI-2. Bentonite chips and 10/20 sand were used to plug the open borehole below the well from a depth interval of 1,239 to 1,182 fbls and the annulus above the screen from 1,128.9 to 916.5 fbls (LANL, 2012a). The rest of the annulus was filled with Barotherm Gold bentonite grout to 50 fbls followed by cement to land surface (LANL, 2012a). During the drilling, three perched groundwater zones were encountered at R-62, but unlike R-15 and R-43 no PIA monitoring well was installed (LANL, 2012a) despite the proposal by the HWB to install SCI-4 there (LANL, 2011a).

Although SCI-4 was not installed, groundwater samples GW62-11-25564 through GW62-11-25566 were collected on August 9, 2011, from the first encountered perched groundwater zone at 628 fbls within the Puye Formation above the Cerros del Rio Basalt (LANL, 2012a) and yielded detectable total chromium concentrations between 1.8173  $\mu\text{g/L}$  to 2.3202  $\mu\text{g/L}$  (Intellus October 27, 2023, download). This is a similar zone detected at SCI-1 to the northeast and MCOI-4 to the southwest (Figure 1). Bentonite chips (not cement) were installed from 688 to 672 fbls to seal off the top perched zone before drilling resumed (LANL, 2012a). Two deeper perched groundwater zones were later detected during the drilling operation at 843 and 853 fbls within the Cerros del Rio Basalt and at 881 to 893 fbls in the underlying Puye Formation (LANL, 2012a). One sample, GW62-11-25567 was collected on August 26, 2011, from one of these two deeper zones. The perched groundwater samples were noted to be turbid and unfiltered (Intellus download on October 27, 2023) and collected directly from the R-62 drilling discharge line (LANL, 2012a). While these samples had chromium detections below background, they were heavily diluted by drilling fluids and may have had similar concentrations detected at SCI-2 and MCOI-6 at this time. The significance of the GW62-11-25564 through GW62-11-25567 samples is that they document the presence of chromium in the perched intermediate groundwater at R-62. However, unlike R-43 and R-15, the R-62 annulus across the perched groundwater zones was not sealed with cement to prevent the downward movement of contaminated groundwater to the RA through the annulus.

The area around R-62 is the location of another hypothesized hydraulic window (Figure 8) to explain the rising chromium concentration detected in the RA at R-62. The improper well construction of R-62 is the most likely cause of the high chromium concentrations in that well and

the increasing concentrations detected during the annual extended purge sampling events (Figure 10). Figure 10 compares outlier chromium concentrations at R-61, R-62 and CrPZ-5 that have steadily increased over time.

These three RA monitoring wells are in line with each other roughly along an apparent hydraulic gradient. R-62 is the upgradient location and CrPZ-5 is located between R-62 and R-61, with R-61 being much further downgradient than CrPZ-5. It is plausible that chromium contamination from the PIA migrated down the R-62 annulus to the RA and migrated along this pathway. This is evident in the similar concentrations between R-62 and CrPZ-5 in magnitude and the similar timing and increasing trend between CrPZ-5 and R-61. While the concentration trends are similar for the two downgradient wells, the concentration detected in R-62 has begun to decrease as the chromium mass in the PIA becomes depleted. Also, the annual extended purges conducted on R-62 are evident on Figure 10 as repetitious early year spikes in chromium concentration. The longer R-62 is purged, the greater the chromium concentration becomes. The only upgradient well to R-62 is a mile to the west and shows background chromium concentrations. With no documented upgradient source of chromium in the RA, the most likely source is the PIA at R-62.

#### Regional Aquifer Monitoring Wells R-61 and CrPZ-5

At RA monitoring wells R-61 and CrPZ-5 more recent increasing trend in chromium concentration are evident (Figure 10). To explain these long-term increases, LANL has informally postulated that a separate source (i.e. a new “hydraulic window”) is present there. It should be noted that like R-62, a cement plug was not used in R-61 or CrPZ-5 to prevent the downward migration of groundwater from the PIA to the RA as was done in R-15 and R-43. However, during the drilling of these two wells, no perched water was encountered. While it is possible that perched water was missed during the drilling, another explanation is considered here.

Figure 10 shows that the chromium concentrations in CrPZ-5 and R-61 began to suddenly increase in mid-2018 and mid-2019, respectively. While the CrPZ-5 increase coincides with the startup of the interim measures (IM) operation, which may have mobilized chromium from other parts of the plume, the positions of the IM extraction wells preclude this as a source to CrPZ-5. The most viable scenario to explain these two increasing trends is that a large mass of chromium was released to the RA upgradient (west) of both wells and continues to migrate from west to east reaching CrPZ-5 first then R-61.

An apparent source may be the herein postulated releases of chromium contaminated groundwater from the PIA to the RA at SCI-2 and R-62. However, the natural hydraulic gradient and the IM operation would preclude the PIA at SCI-2 as a source. The PIA at R-62 provides the best explanation for the progressive chromium concentration increases documented at CrPZ-5 first and R-61 second. This pathway would not be affected by the IM to the point of the source being intercepted, although it could pull the bulk of the pathway toward CrPZ-5 while skirting R-61. Assuming this scenario to be valid, it shows the impact that a continually leaking seal emplaced across an intervening vadose between an overlying contaminated aquifer and an underlying non-contaminated aquifer can have on water quality in another aquifer. Such a situation violates 19.27.4.30 NMAC.

## **Dual Screen Wells and Bentonite**

Bentonite chips emplaced between the two screens in a dual screen monitoring well can provide an adequate seal are noted at regional aquifer monitoring well nest R-33 and R-69. These two inter-screen seals have remained fully submerged since emplacement, and the boreholes do not penetrate a contaminated perched intermediate aquifer. The large divergence and different patterns in the hydrographs from R-33 and R-69 are evidence that the screens monitor different hydrogeologic units. These patterns and divergences in head appear like those from well clusters R-10/R-10a, R-16/R-16r, and R-35a/R-35b, which unlike the two R-33 and R-69 well nests are not installed within the same borehole – eliminating the potential for intra-borehole leakage. With the continual declining water table at LANL and lack of information regarding the longevity of bentonite seals, it is prudent to avoid them at LANL, especially considering bentonite is not permitted for use in wells where contamination is present (OSE, 2020). Without a proper seal between the two screens in the nested dual screen well design, the hydrographs may present with a similar pattern and head, such as those exhibited by the typical chromium plume dual screen monitoring well. Without a proven way to test the bentonite seal in a dual screen or other nested well design, it is difficult to assess the adequacy of the seal between the screens. In contrast, cement seals are routinely pressure tested and cement bond logs provide additional ways to test cement seals. These tests are typical conditions issued by NMOSE for approval of drilling applications. Additionally, cement seals can be repaired in the case of channeling by casing perforation and cementation through the casing to plug the channel in the seal. There are no proven test and repair methods for bentonite seals.

## CONCLUSION

The Hydrology Bureau's concern for the continued approval of bentonite products as materials to emplace well seals across vadose zones, or where pressures exceeding the compressive and shear strength of bentonite are to be exceeded (e.g., artesian conditions, extraction and injection operations and excessive static water columns) include:

- Hydration of bentonite is unlikely to be sustained in the vadose zone and where there is a declining water table as the unsaturated condition desiccates the seal.
- Bentonite has little shear or compressional strength to withstand pressurized conditions.
- Bentonite does not provide invasion of the formation like cement.
- There is no industry standard method to test a bentonite seal like there is with a cement seal, such as pressure testing and bond logs.
- There is no proven way to repair a bentonite seal like there is with a cement seal.

While use of bentonite as a well seal may be feasible in an uncontaminated, unconfined, fully saturated condition where the water table is not in decline, it should not be considered as an appropriate well seal material in the vadose zone or where a declining water table is present, for environmental wells where contamination is present, or in any artesian or pressurized condition due to the lack of strength and ability to remain hydrated.

## REFERENCES

- Duran, A. (2023) ‘Drilling Work Plan for Groundwater Regional Aquifer Monitoring Well R-76 (Replacement of Groundwater Regional Aquifer Monitoring Well R-28), Revision 2’. Department of Energy, Environmental Management, Los Alamos Field Office.
- Garcia, L. (2022) ‘Well R-76 Monitoring Permit Application, OSE File No. RG-00485-POD14’.
- Garcia, L. (2023a) ‘Approval of RG-485-POD14 (R-76)’. New Mexico Office of the State Engineer.
- Garcia, L. (2023b) ‘Temporary Suspension of Permit RG-485-POD 14 (R-76)’. New Mexico Office of the State Engineer.
- Hamman, M.A. (2023) ‘Well R-76 Monitoring Permit Application, Revision 1, OSE File No. RG-00485-POD14’.
- Kieling, J.E. (2012) ‘Approval with Modifications, Technical Area 16 Well Network Evaluation and Recommendations, Los Alamos National Laboratory, EPA ID#NM0890010515, HWB-LANL-12-022’.
- Kleinfelder (2006) *Final I Wells Completion Report, 2004-05 Mortandad Canyon Drilling Program*. Well Construction Project No. 49436. Los Alamos, New Mexico: Los Alamos National Laboratory, p. 320.
- Krambis, C. (2023) ‘Application for Permit to Drill a Well with No Water Right, RG-00485-POD14 Contamination Present Rio Grande Underground Water Basin, Los Alamos County, New Mexico’.
- LANL (2001) *Characterization Well R-15 Completion Report*. Well Construction LA-13749-MS. Los Alamos, New Mexico: Los Alamos National Laboratory, p. 119.
- LANL (2002) *Characterization Well R-25 Completion Report*. Well Construction LA-13909-MS, ER2001-0697. Los Alamos, New Mexico: Los Alamos National Laboratory, p. 77.
- LANL (2009a) *Completion Report for Regional Aquifer Well R-42*. Well Construction LA-UR-09-0217, EP2009-0003. Los Alamos, New Mexico: Los Alamos National Laboratory, p. 14.
- LANL (2009b) *Completion Report for Wells R-43 and SCI-2*. Well Construction LA-UR-09-1337, EP2009-0141. Los Alamos, New Mexico: Los Alamos National Laboratory, p. 176.
- LANL (2011a) *Completion Report for Regional Aquifer Well R-61*. LA-UR-11-5091, EP2011-0274. Los Alamos, New Mexico: Los Alamos National Laboratory, p. 122.
- LANL (2011b) *Investigation Report for Water Canyon/Cañon de Valle*. Investigation Report LA-UR-11-5478. Los Alamos, New Mexico: Los Alamos National Laboratory, p. 572.

LANL (2012a) *Completion Report for Regional Aquifer Well R-62*. Well Construction LA-UR-12-0605, EP2012-0037. Los Alamos, New Mexico: Los Alamos National Laboratory, p. 30.

LANL (2012b) *Phase II Investigation Report for Sandia Canyon*. Investigation Report LA-UR-12-24593, EP2012-0195. Los Alamos, New Mexico: Los Alamos National Laboratory.

LANL (2014) *Summary Report for the 2013 Chromium Groundwater Aquifer Tests at R-42, R-28, and SCI-2*. Summary Report LA-UR-14-21642, EP2014-0066. Los Alamos, New Mexico: Los Alamos National Laboratory, p. 122.

LANL (2015) *Completion Report for Intermediate Aquifer Well CdV-9-1(i)*. Well Construction LA-UR-15-23954. EP2015-0094. Los Alamos, New Mexico: Los Alamos National Laboratory, p. 28.

LANL (2017a) *Annual Progress Report for Corrective Measures Implementation and Deep Groundwater Investigations for Consolidated Unit 16-021(c)-99*. Annual Progress LA-UR-17-30538, EP2017-0152. Los Alamos, New Mexico: Los Alamos National Laboratory, p. 14.

LANL (2017b) *Status Report for the Tracer Tests at Consolidated Unit 16-021(c)-99, Technical Area 16*. Status Report LA-UR-17-20782, EP2017-0009. Los Alamos, New Mexico: Los Alamos National Laboratory, p. 11.

LANL (2017c) *Summary Report for Intermediate Groundwater System Characterization Activities at Consolidated Unit 16-021(c)-99*. Summary Report LA-UR-17-22550, EP2017-0008. Los Alamos, New Mexico: Los Alamos National Laboratory, p. 56.

LANL (2018a) *Compendium of Technical Reports Conducted Under the Work Plan for Chromium Plume Center Characterization: Attachment 9 - Groundwater Modeling Status Report*. Compendium LA-UR-18-21450. Los Alamos, New Mexico: Los Alamos National Laboratory, p. 630.

LANL (2018b) *Compendium of Technical Reports Related to the Deep Groundwater Investigation for the RDX Project at Los Alamos National Laboratory*. LA-UR-18-21326, EP2018-0006. Los Alamos, New Mexico: Los Alamos National Laboratory, p. 52.

Muhmed, A., Mohamed, M. and Khan, A. (2022) ‘The Impact of Moisture and Clay Content on the Unconfined Compressive Strength of Lime Treated Highly Reactive Clays’, *Geotech Geol Eng*, 40, pp. 5869–5893. Available at: <https://doi.org/10.1007/s10706-022-02255-x>.

N3B (2019) *Investigation Report for Royal Demolition Explosive in Deep Groundwater*. Investigation Report EM2019-0235. Los Alamos, New Mexico: Newport News Nuclear BWXT-Los Alamos, LLC, p. 191.

N3B (2023) *Plugging and Abandonment Report for Well R-25*. Well Construction EM2023-0262. Los Alamos, New Mexico: Newport News Nuclear BWXT-Los Alamos, LLC, p. 218.

NMED (2021) ‘Risk Assessment Guidance for Site Investigations and Remediation,’ Volume I Soil Screening Guidance for Human Health Risk Assessments’. Available at: chrome-



extension://efaidnbmnnnibpcajpcgiclfndmkaj/https://www.env.nm.gov/hazardous-waste/wp-content/uploads/sites/10/2021/12/NMED\_SSG-VOL\_I\_Dec\_2\_2021.pdf.

Ogden, F.L. and Ruff, J.F. (1991) 'Setting Time Effects on Bentonite Water-Well Annulus Seals', *Journal of Irrigation and Drainage Engineering*, 117(No. 4), pp. 534–545.

Ogden, F.L. and Ruff, J.F. (1993) 'Strength of Bentonite Water-Well Annulus Seals In Confined Aquifers', *Journal of Irrigation and Drainage Engineering*, 119(No. 2), pp. 242–250.

OSE (2020) *Guidelines and Handbooks, OSE Sealant Table, Well Drillers Forms*. Available at: <https://www.ose.nm.gov/Statewide/wdForms.php>.

Shean, R. (2023) 'Approval with Modifications Drilling Work Plan for Groundwater Regional Aquifer Monitoring Well R-76 (Replacement of Groundwater Regional Aquifer Monitoring Well R-28), Revision 2, Los Alamos National Laboratory EPA ID#Nm0890010515 HWB-LANL-22-019'.

Thomson, T. and Bishop, L. (2022) 'Submittal of Regional Aquifer Well R-76 WR-07 Permit Application and WD-09 Artesian Well Plan of Operations'.

Thomson, T. and Bishop, L. (2023a) 'Submittal of Regional Aquifer Well R-76 WR-07 Permit Application and WD-09 Artesian Well Plan of Operations, Revision 1'. N3B-Los Alamos/U.S. Department of Energy Environmental Management Los Alamos Field Office.

Thomson, T. and Bishop, L. (2023b) 'Submittal of Regional Aquifer Well R-76 WR-07 Permit Application and WD-09 Artesian Well Plan of Operations, Revision 2 (OSE File No. RG-00485-POD14)'. N3B-Los Alamos/U.S. Department of Energy Environmental Management Los Alamos Field Office.

USEPA (2011) 'Emerging Contaminants – Hexahydro-1,3,5-trinitro-1,3,5-triazine (RDX) Fact Sheet EPA 505-F-10-009'. United States Environmental Protection Agency Office of Solid Waste and Emergency Response (5106P). Available at: [chrome-extension://efaidnbmnnnibpcajpcgiclfndmkaj/https://cluin.org/download/techdrct/emerging\\_contaminant\\_rdx.pdf](chrome-extension://efaidnbmnnnibpcajpcgiclfndmkaj/https://cluin.org/download/techdrct/emerging_contaminant_rdx.pdf).

USEPA (2017) 'Technical Fact Sheet – Hexahydro-1,3,5-trinitro- 1,3,5-triazine (RDX) TECHNICAL FACT SHEET EPA 505-F-17-008'. United States Environmental Protection Agency Office of Land and Emergency Management (5106P).

USEPA (2021) *Vertical Gradient Calculator, EPA On-line Tools for Site Assessment Calculation*. Available at: <https://www3.epa.gov/ceampubl/learn2model/part-two/onsite/vgradient.html>.

## FIGURES

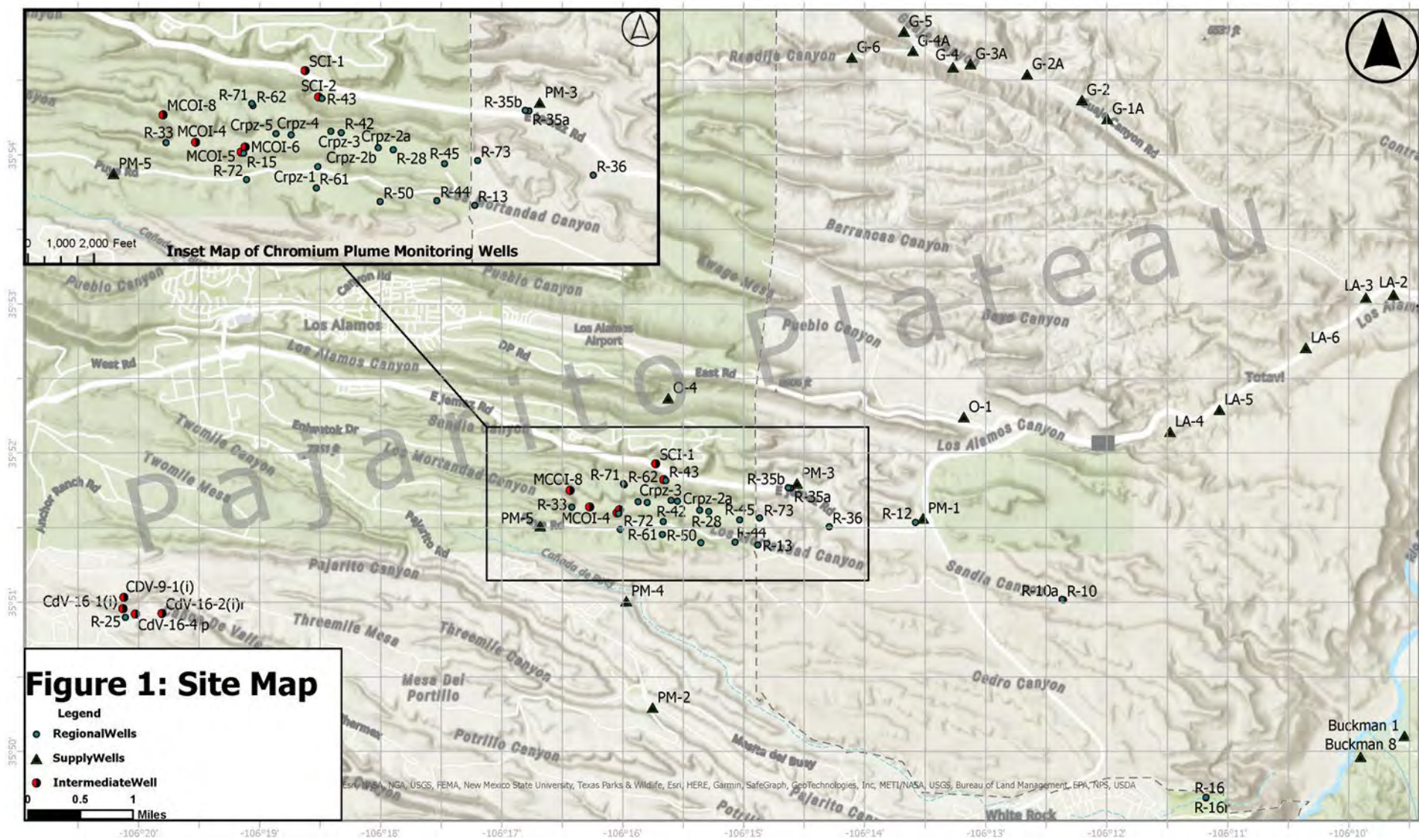


Figure 1) Locations of production wells and LANL monitoring wells on the Pajarito Plateau.

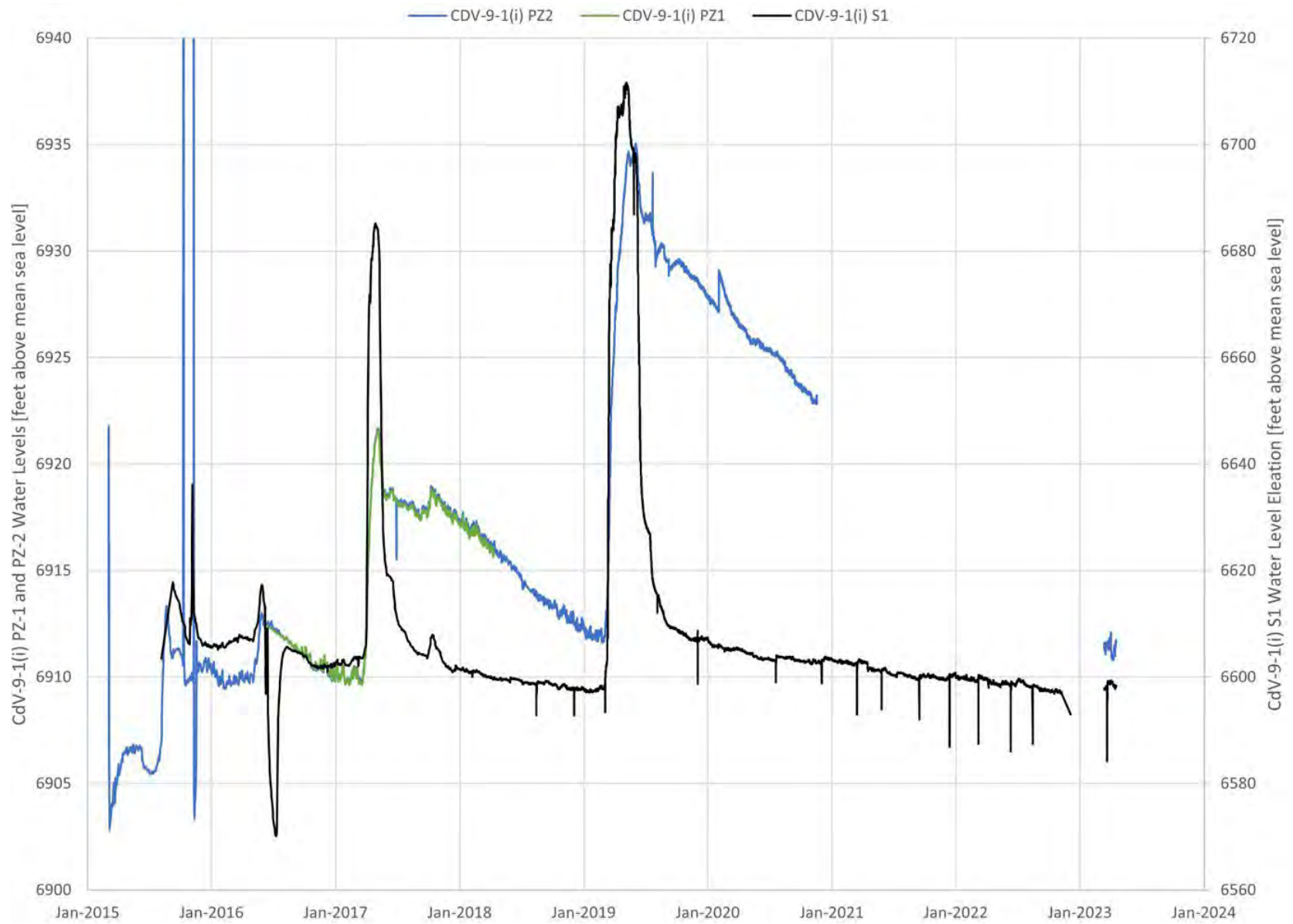


Figure 2) CdV-9-1(i) well nest hydrographs.

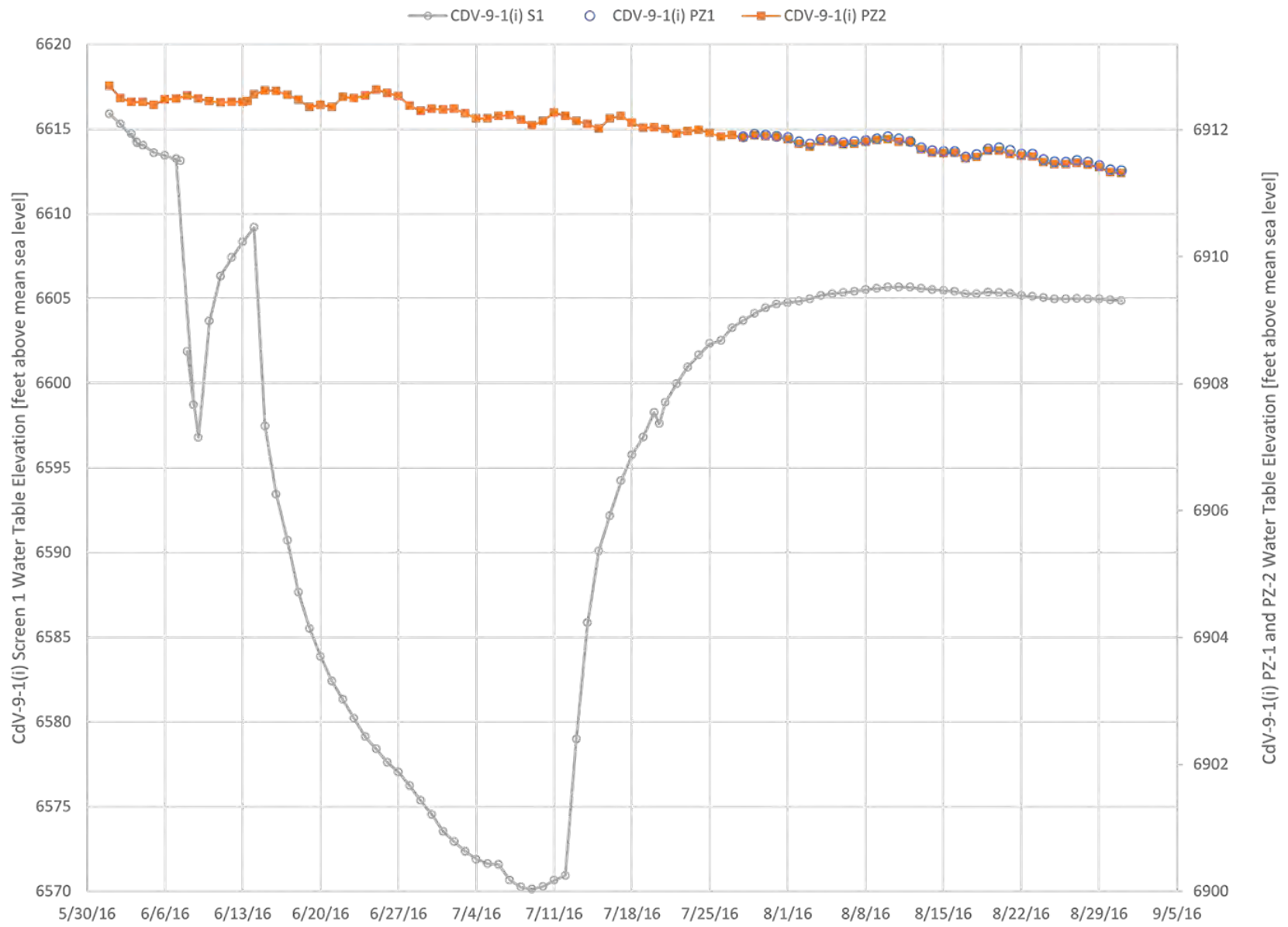


Figure 3) CdV-9-1(i) well nest hydrographs during the July 2016 Screen 1 pumping test.

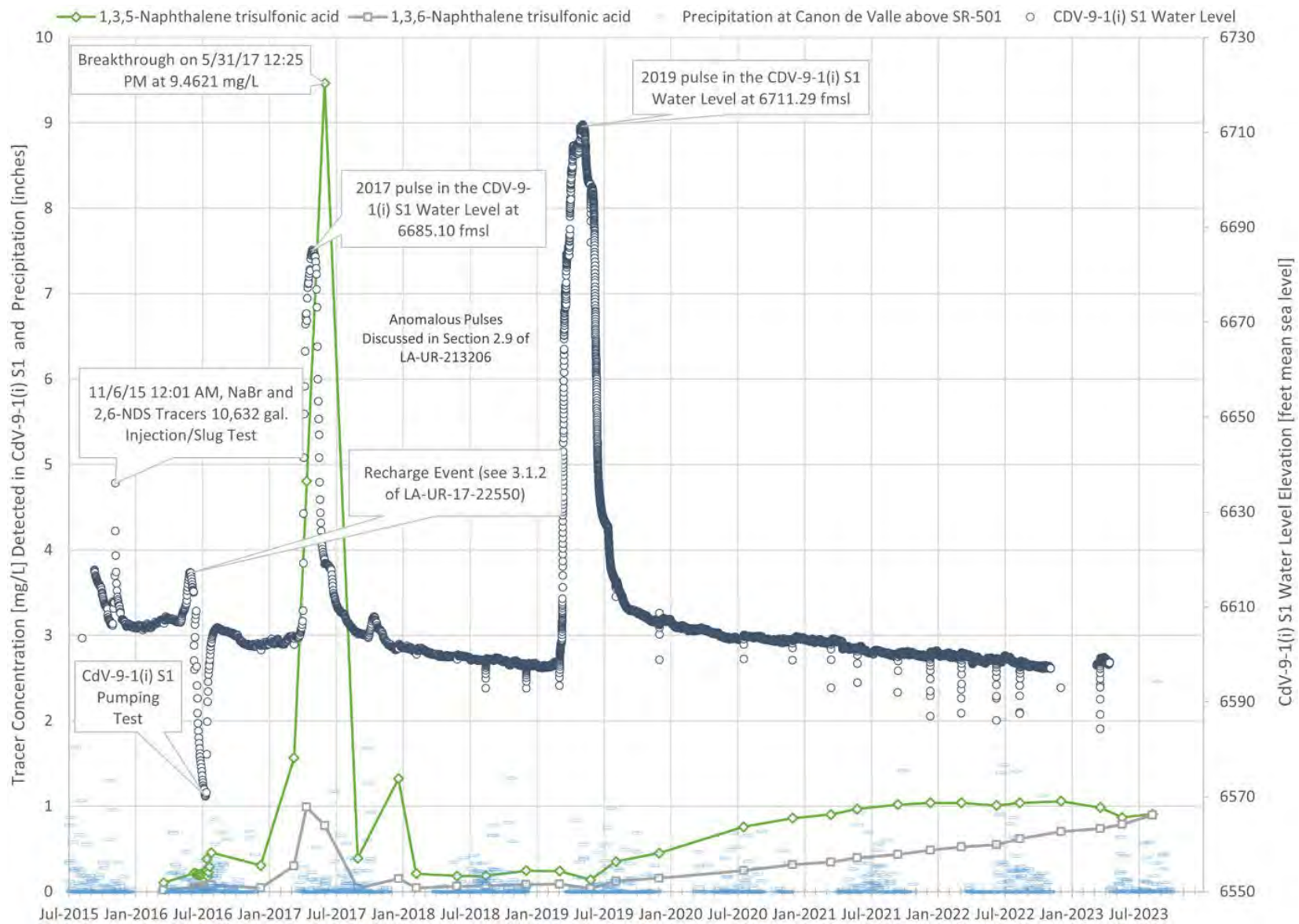


Figure 4) CdV-9-1(i) Screen 1 hydrograph and CdV-9-1(i) PZ-1 and PZ-2 tracer detections.

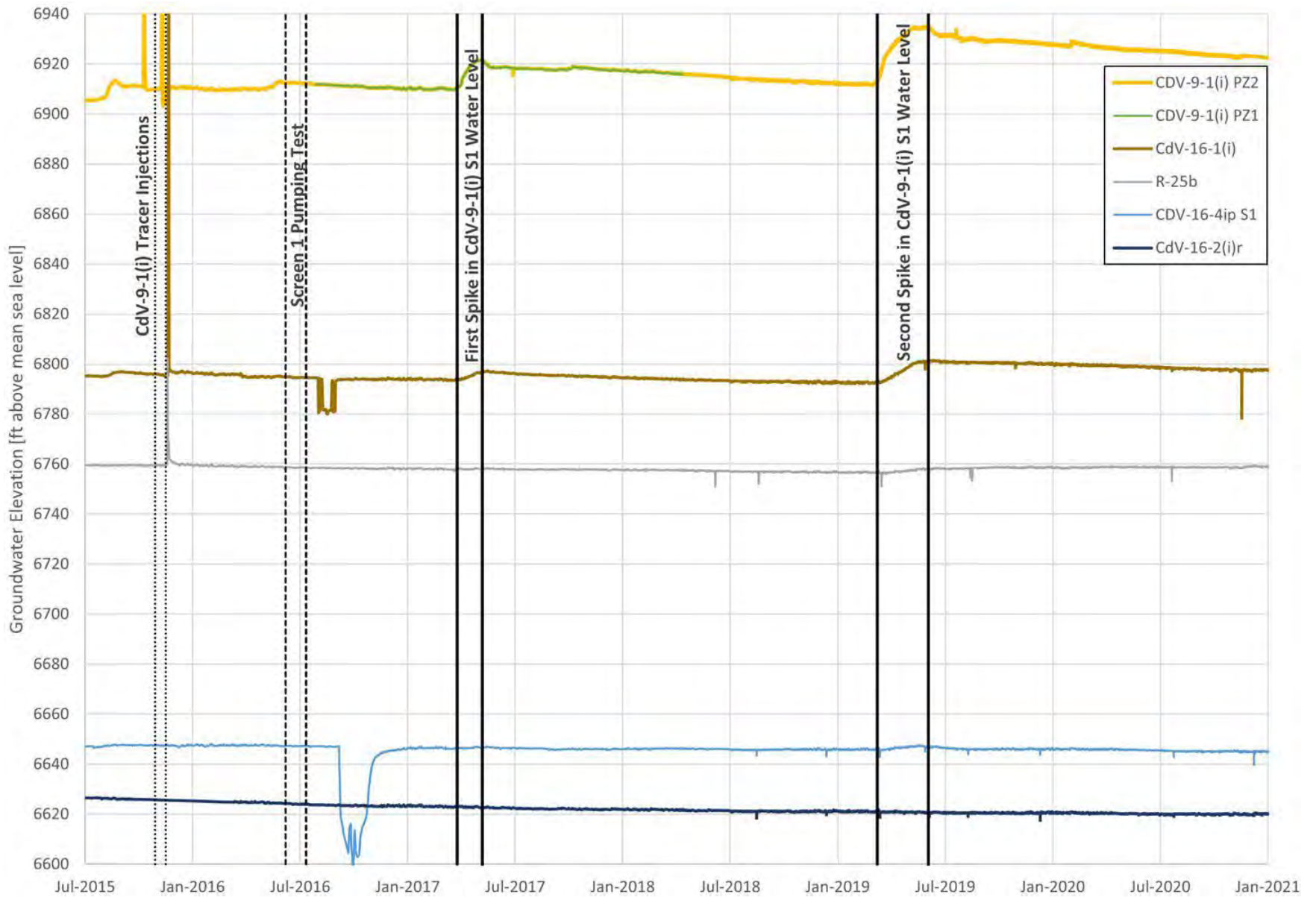


Figure 5) Hydrographs of Upper Perched Zone Monitoring Wells near CdV-9-1(i).

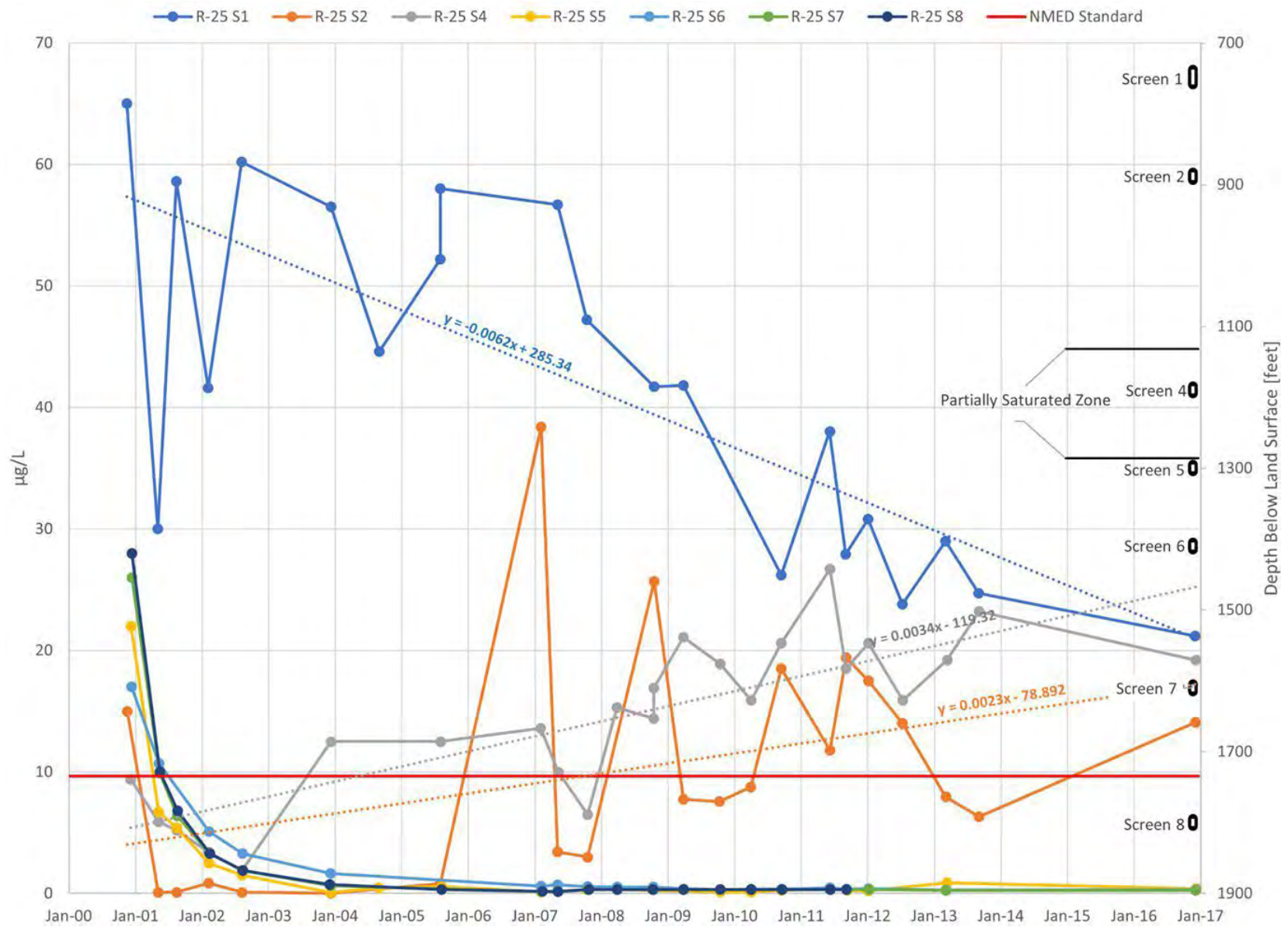


Figure 6) Monitoring Well R-25 RDX concentration trends among screened intervals.



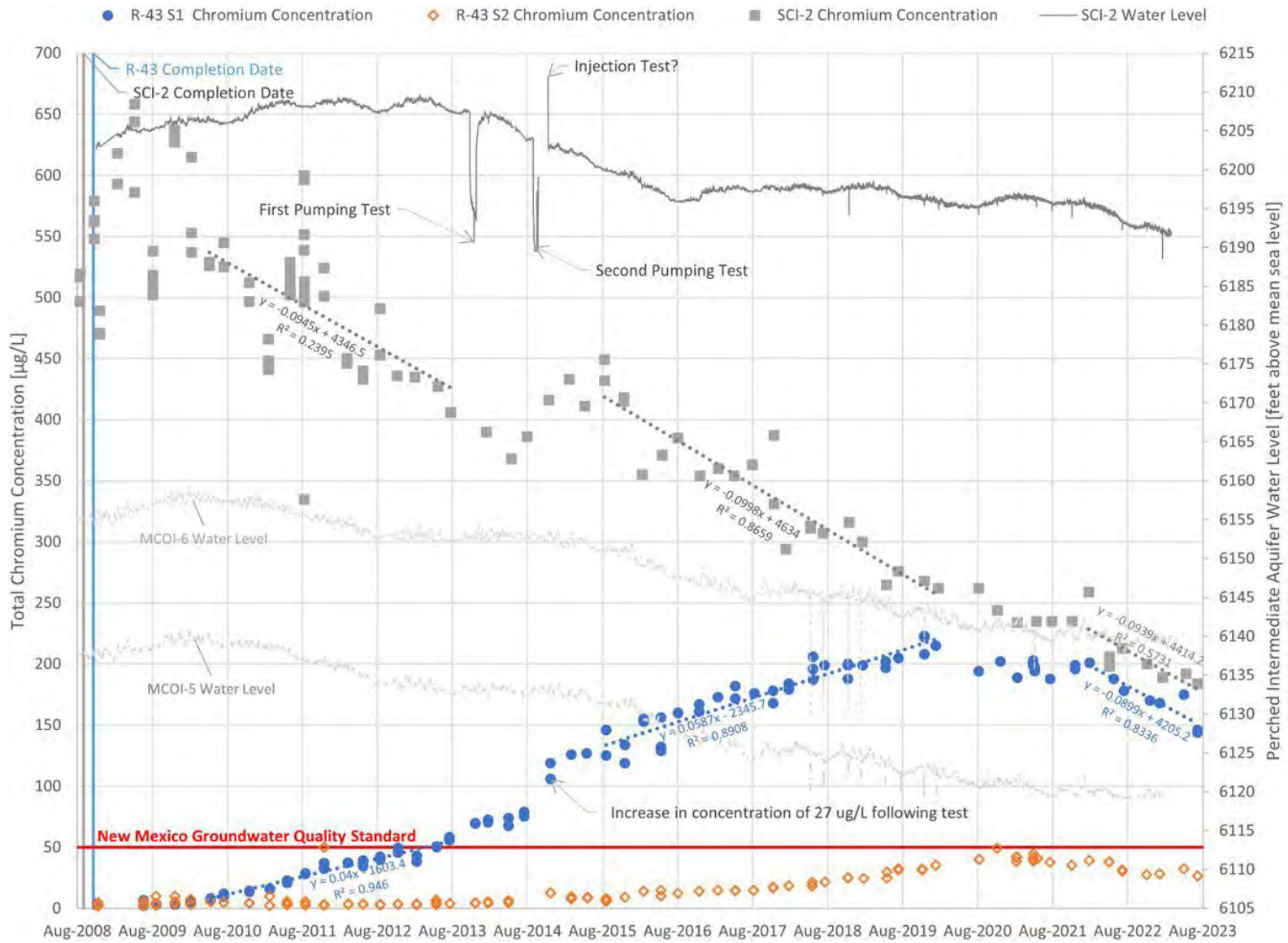


Figure 7) Total dissolved chromium concentration trends between hydrogeologic units at Regional Aquifer Monitoring Well R-43 and Intermediate Aquifer Monitoring Well SCI-2.

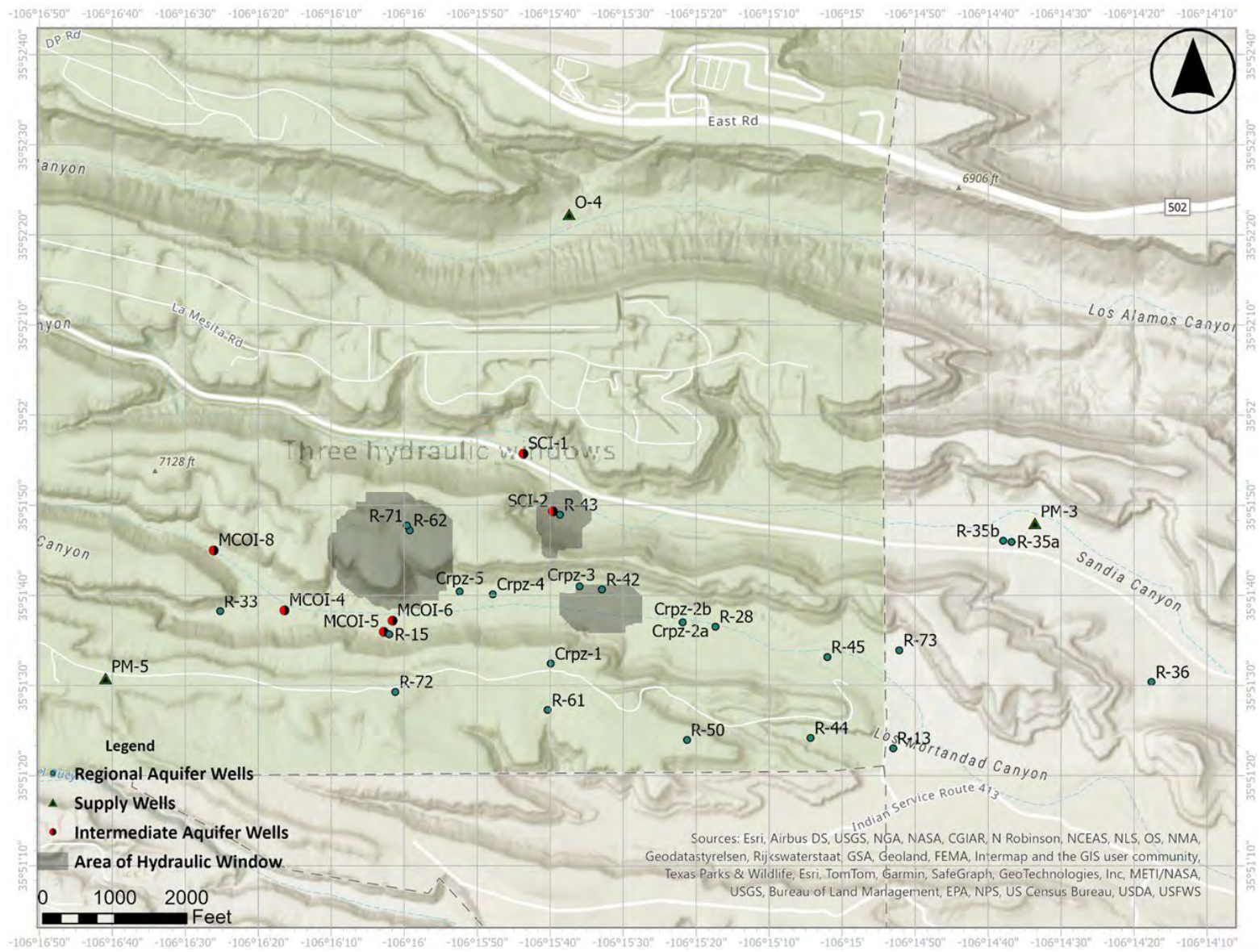


Figure 8) Hydraulic windows in the chromium plume.

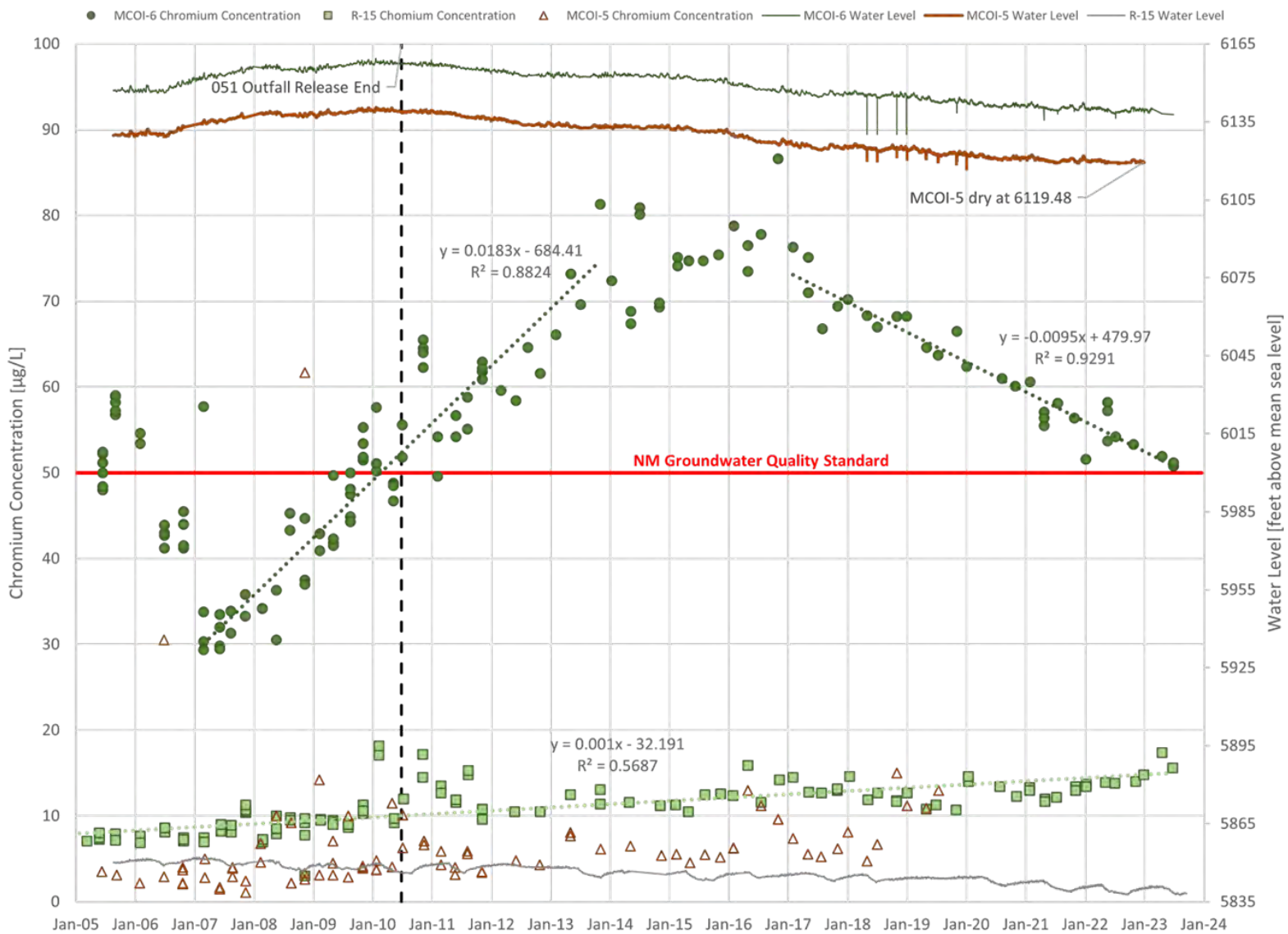


Figure 9) Total dissolved chromium concentration trends between Regional Aquifer Monitoring Well R-15 and Intermediate Aquifer Monitoring Wells MCOI-6 and MCOI-5.

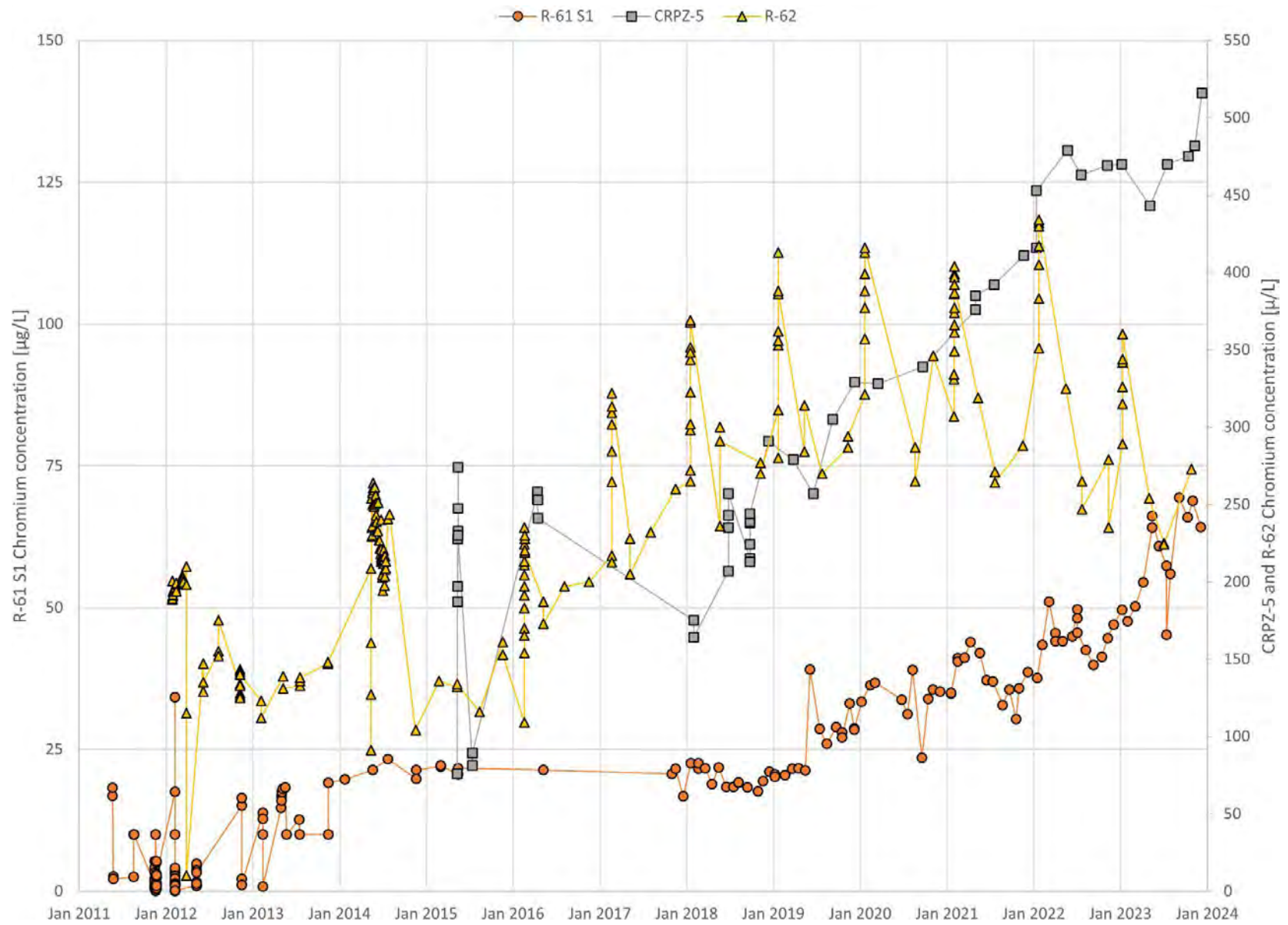
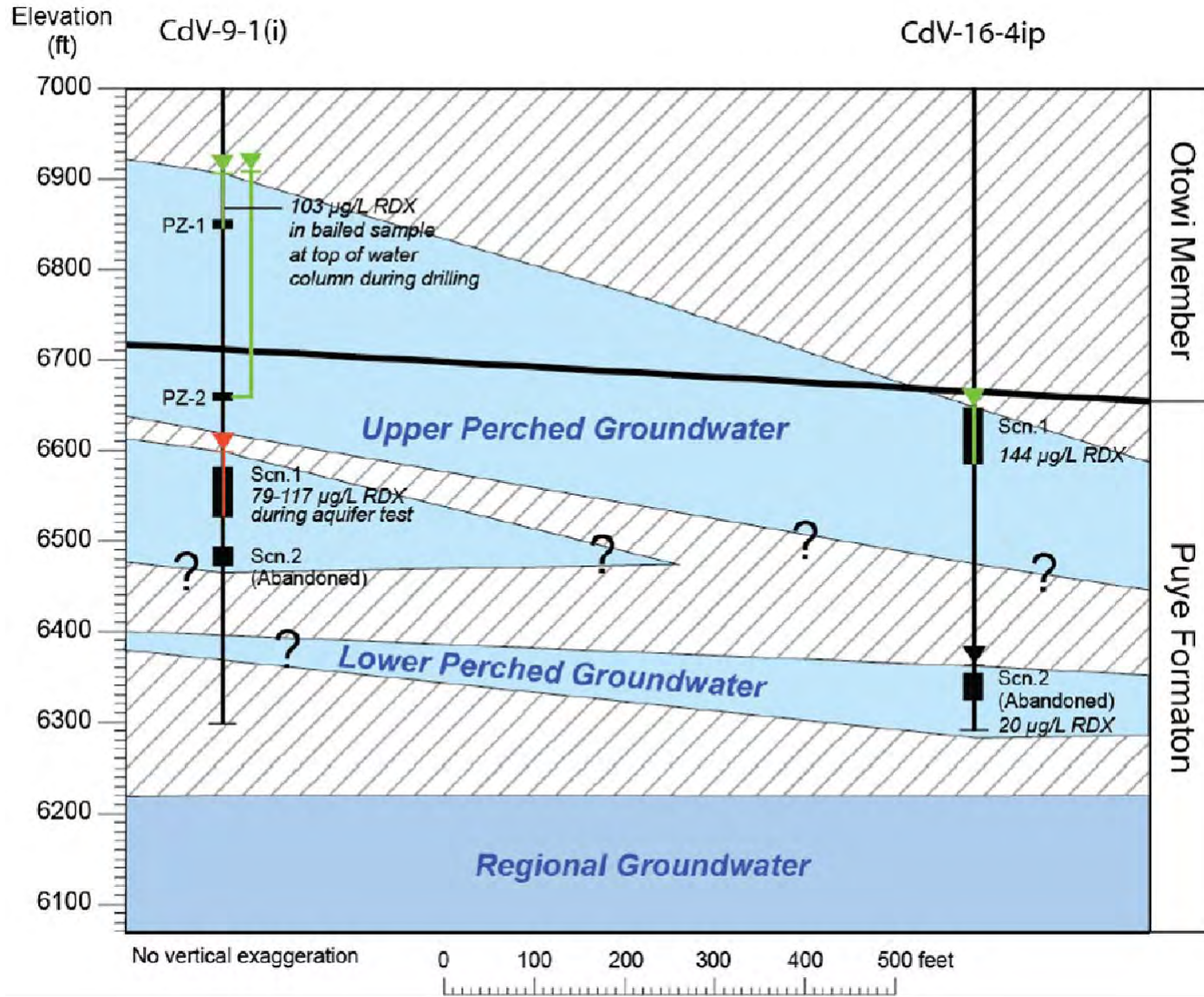


Figure 10) Total Chromium Concentrations among Regional Monitoring Wells R-62, R-61, and CrPZ-5.

## APPENDICES

Appendix A

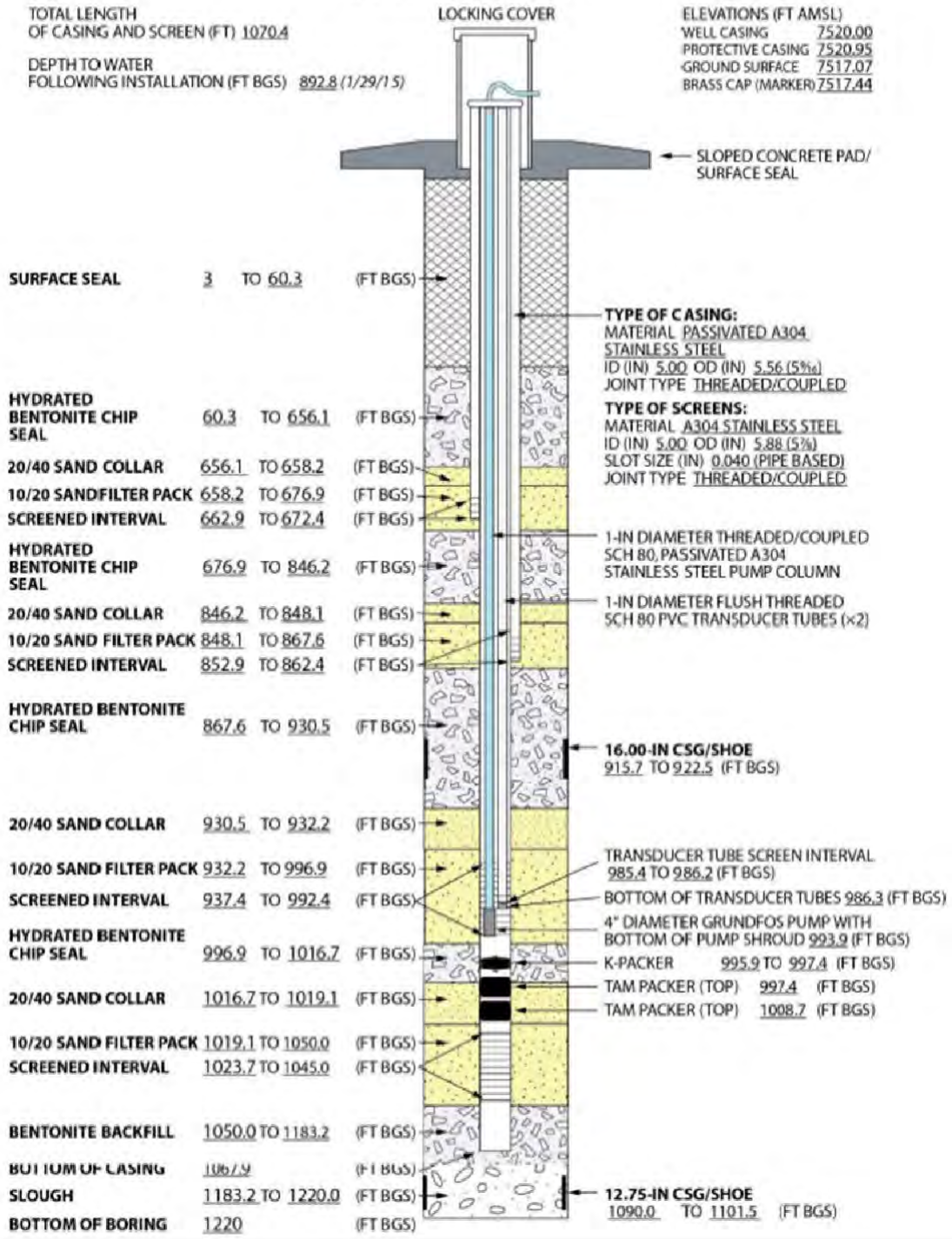


Conceptual model of the aquifer systems at LANL's Technical Area 16 RDX plume (LANL, 2017a).

## Appendix B

### MONITORING WELL CdV-9-1(i) AS-BUILT WELL DIAGRAM

Technical Area 9 (TA-9)  
Los Alamos National Laboratory  
Los Alamos, New Mexico



From: (LANL, 2015).

# IRT Review of May 21, 2024 OSE Well Construction Memorandum

The following comments are based on the headings and pagination in the Well Construction Memorandum.

## Executive Summary

Page 2, par. 2. There is no evidence that the upper portion of the regional aquifer where the chromium contamination occurs is under artesian (confined) conditions.

Page 2, par. 3. OSE is correct that that the chromium occurs “along the water table in the regional aquifer.” An aquifer under water table (unconfined) conditions is not the same as an artesian (confined) aquifer.

Page 2, par. 3. There is no evidence of a “lower confining unit,” or any “confining unit,” anywhere in the vadose zone. The vadose zone lies between the land surface and the water table; it may include saturated zones, such as perched aquifers. A confining unit is a term used to describe a relatively low-permeability layer/unit/stratum that caps a more permeable underlying water-bearing unit that is under some hydraulic pressure. When a borehole or well penetrates through the confining unit, the water level rises in the borehole/well above the top of the water-bearing unit/aquifer. We have seen no evidence that this phenomenon occurs in the upper regional aquifer where the chromium contamination occurs. In fact, throughout much of the area, there is a small downward hydraulic gradient, as determined by monitoring wells screened at various depths below the water table.

The term “confining unit” is not applicable to the vadose zone in the chromium remediation area. The vadose zone contains perched water-bearing zones within it. The perched zones are created when infiltrating water in an unsaturated state percolates downward and reaches a relatively low-permeability zone/layer/stratum that resists the downward passage of the water, causing the water to “perch,” or to saturate the sediments on top of the “perching layer.” The upper surface of the perched zone is under atmospheric pressure. That is, it is a water table, called a “perched water table.” The perched zone is a saturated lens or layer that also has a bottom where the pressure is atmospheric. The perched water-bearing zone is under unconfined conditions, not artesian conditions; thus, it is not appropriate to characterize the perching layers as a “confining unit,” as it is not under pressure from an overlying cap created by a low-permeability layer.

## Introduction

Page 3, items (1) and (5). Regarding R-76, OSE refers to drilling through “two distinct geologic formations” in item (1) and penetrating “separate hydrogeologic units” in item (5). Based on the available data presented to us, the hydrogeologic system comprising the upper regional aquifer has various geologic materials that differ based on mineralogy, grain size, grain shape, and color, from drill cuttings and core samples, for example. These have been identified as primarily the Puye Formation, along with its subunits, the Miocene pumiceous unit and the Chamita



Formation. The Chamita is recognized as a formation within the Santa Fe Group, a productive regional aquifer. From the available information on water levels and inorganic chemistry, including the migration habit of the chromium plume, for purposes of characterizing contaminant transport and designing a remedy, the aquifer containing the chromium appears to behave as a single hydrogeologic unit. There are no confining beds separating the productive water-bearing formations in the chromium remediation area, including the Puye and Chamita.

Page 4, last paragraph. The IRT has seen no evidence of “confined conditions” or “artesian conditions” in the upper part of the regional aquifer and chromium remediation area.

## **Hydrogeology**

Page 5, par. 2. Artesian conditions are not known to exist in the vadose zone, including in the perched zones. The perched intermediate aquifer (PIA) consists of one or more saturated zones that lie above the regional aquifer. The occurrence of these perched zones depends on sources of recharge as well as the permeability, slope, and lateral continuity of the Cerro del Rio Basalt layers. Water infiltrating downward through the tuff and Puye sediments is slowed by the lower permeable basalt. Information available indicates that the water collecting on top of the basalt flows along the slope of the basalt perching layer, likely to a location where the perching horizon drains through vertical open fractures or to where the basalt layer is truncated. Here, the water continues downward migration. If that water encounters another low-permeability basalt layer, perching can again develop. Thus, the water generally migrates vertically downward in the vadose zone tuffs and sediments, then laterally along the basalts. Where the infiltrating water migrates vertically downward, the sediments are not fully saturated. On top of the basalt layers, the perched water is saturated and flows more horizontally, except where the basalt might be fractured. There would be a water table within the saturated sediments of the upper Puye Formation that are just above the basalt, a perched water table. The basalts are perching layers holding up discontinuous, local unconfined water-bearing zones, contrary to the description by OSE.

OSE states that “[B]oreholes drilled through the lower confining unit of the PIA at the base of the Cerros del Rio Basalt have leaked contamination down through the desiccated and/or strength failures of the bentonite seals.” Perched aquifers are indicative of locations where there is potentially significant flow and likely recharge to the regional aquifer. Because the vadose zone has surface water infiltrating downward from the canyon bottoms, the vadose zone sediments contain moisture, a generalized downward flux of water, patchy areas of perched water, and a generalized (patchy) source of water to the regional water table aquifer after transiting the 1,000+ feet of vadose zone. The fact that there is a downward hydraulic head gradient within the upper regional aquifer is consistent with the conceptual model that there is a source of recharge beneath the plateau, including Sandia and Mortandad Canyons. The perched groundwater and the unsaturated but moist sediments in the Puye Formation, make it unlikely that complete desiccation of the bentonite occurred. OSE has provided no evidence of desiccated conditions. The IRT concurs that shrinkage of annular sealing materials in low moisture vadose conditions occurs (including cements and bentonite). The two materials that appear to provide the mode competent sealing capabilities for these conditions are cement (not

bentonite amended) and uncoated bentonite granules (tablets). Thus, these materials are highlights in the IRT recommendations. Additional detail on the IRT assessment of various annular sealants is provided in the main body of the IRT report.

Page 5, par. 3. OSE states that at PM-3, the water table in the Puye has declined about 25 feet since 1966 and the potentiometric surface of the underlying Chamita formation has declined 50 feet over the same time period. It is not clear where the OSE has obtained this information. According to the U.S. Geological Survey (Purtymun, 1966), PM-3 was constructed with gravel in the annulus below 552 feet below ground surface (bgs). The water table was noted at 740 feet bgs upon completion. The geologic report of the well indicates that both the Puye conglomerate and the underlying Tesuque sandstone are saturated. There are no plugs in the well separating different zones. There does not appear to be any way to measure fluid pressure in the PM-3 well at multiple depths. (Note: The Santa Fe group includes both the Tesuque and the Chamita formations; both are fluvial sedimentary formations that fill the basin.)

Page 5, par. 4. OSE is correct that “[G]roundwater at LANL is contaminated in the shallow unconfined portion of the RA” (regional aquifer).

OSE indicates there is also a confined portion of the RA within LANL’s chromium plume and that its existence is well established. The IRT is not aware of confined conditions within the chromium plume. There are Miocene basalt layers deep below the chromium plume, within the Santa Fe Group, perhaps below the Chamita Formation. These basalts very well could create confined aquifer conditions below them. There are no monitoring wells to establish pressure below the basalts which lie about a few hundred or more feet below the water table in the chromium remediation area. There is no evidence at this time that there has been migration below the basalt. In fact, where the Miocene basalts are closest to the surface, on the east side of the chromium plume, near R-70, there is upward groundwater flow. Thus, the chromium plume appears to be forced upward and above the basalt. The OSE indicates that they will present information to establish the presence of confining conditions, but this has not yet been provided to us.

## **Evaluation of Well Construction**

OSE presents empirical evidence that bentonite seals leak, including at CdV-9-1(i), R25, and in the R-43/SCI-2. The issues essentially center on migration between the well casing and the formation across perching zones within the vadose zone. Throughout the OSE discussion, reference is made to “confining units” as creating perched zones. This is not correct use of hydrogeologic terminology.

### **Case Study I: CdV-9-1(1)**

This well is located about 4 to 5 miles west of the chromium remediation area. This is an intermediate zone well with three well screens apparently within three different perched zones. OSE is correct that the behavior of this well is peculiar. Something is wrong with this well. In particular, the hydraulic heads in the upper two perched zone well screens are essentially identical, even though they are separated by about 169 feet of bentonite. OSE notes that

DOE-EM-LA concluded that it is “unclear whether the connections between the piezometers and screen 1 represent natural flow paths or if the detections of tracers in the piezometer are related to short-circuiting along the well bore or in the adjacent formation. Additional data and evaluations are required to evaluate this issue.” The IRT agrees. It is beyond the time available to the IRT to determine the exact cause of the problems, which, in addition to bentonite failure, could include casing or packer leaks.

### **Case Study II: Monitoring Well R-25**

This well is located about 4 miles west-southwest of the chromium remediation area. This well was impacted by explosives. The well consists of nine screen intervals in one well, each separated by bentonite of some mix in the annulus and a packer system inside the casing; this most likely is a Westbay type monitor well. Four screens were in the perched zones and five were in the regional aquifer. The contamination in the perched zone is alleged by OSE to have migrated into the regional aquifer via the well. NMED found that excessively long sand filter packs were the problem, while OSE concluded that the bentonite desiccated or that the bentonite had been improperly emplaced to allow channeling. Apparently DOE-EM-LA found that the samples from R-25 were of poor quality, so R-25 was plugged and abandoned in 2023. The IRT does not have the time or resources to independently review all the relevant data about the construction of this well. There are no monitoring wells of similar construction in the chromium remediation area.

### **Case Study III: Chromium Plume Monitoring Wells R-43 and SCI-2**

These are two wells in the chromium remediation area 75 feet apart. SCI-2 is an intermediate perched zone well drilled to 890 feet bgs. The lower part of the hole was filled with bentonite to 580 feet bgs, a 20-foot well screen and sand filter pack was set, and the overlying interval was filled with more bentonite. R-43 has two screens in the regional aquifer separated by bentonite, and the casing annulus in the perched zone is cemented. OSE believes that R-43 and the regional aquifer were contaminated by migration downward from SCI-2. This is based on chromium time-series, which for a large part of the record showed that concentrations in the perched zone decreased while concentrations in the regional aquifer increased.

The IRT is not convinced by the OSE argument. It is clear there was chromium discharged to Sandia Canyon for many years. This water would have infiltrated the alluvium and fractured tuff beneath it and continued migrating downward through the permeable Puye Formation. The less permeable Cerro del Rio basalts caused perched conditions; the perched conditions would have occurred from the impeded infiltration beneath Sandia Canyon, not SCI-2 or any other well. No areally extensive impermeable strata have been identified at LANL that would prevent downward migration from the vadose zone perched aquifers to the regional aquifer.

The IRT understands OSE's interpretation. However, it also seems plausible that, of course after some time lag, the decline in concentration in the perched zone noted in OSE Figure 7 has occurred as the source in Sandia Canyon was stopped. In fact, the water level in SCI-2 begins to decline after about 2012, about the same time concentrations there decline. The chromium increase in the regional aquifer may be explained by downward percolation through the Puye,

beyond the construction materials of SCI-2, to the regional aquifer. There is only a poor understanding at this time of the pathways through the vadose zone, but it is clear that chromium migration to the regional aquifer would be expected without a pathway via a desiccated bentonite seal in the annulus of a 2-inch-diameter PVC casing such as SCI-2. OSE presented no quantitative analysis of whether a crack or other flaw in SCI-2 along several hundred feet of the bentonite filled borehole annulus, from 580 feet bgs to the water table, was the most likely cause of impact at R-43.

#### **Case Study IV: Monitoring Wells R-15, MCOI-5 and MCOI-6**

The IRT disagrees with parts of the OSE interpretation here. These three wells are located just west of the chromium remediation area. R-15 is completed only in the regional aquifer, and it has bentonite amended cement to seal off the perched zones, in accordance with OSE requirements. Chromium at R-15 did not exceed standards. MCOI-5 and -6 are perched zone wells in Mortandad Canyon where there was discharge of contaminated water from the 051 Outfall until 2017. MCOI-5 is closest to R-15 and chromium did not exceed standards. MCOI-6 is a few hundred feet northeast of MCOI-5/R-15 and has chromium concentrations above standards.

OSE concluded that there is confined groundwater in the perched zone, that there is upward flow between MCOI-6 (deeper) to MCOI-5 (shallower), that the perched zone wells are not recharged by discharge from Mortandad Canyon, that contamination at MCOI-6 may have come from SCI-2, and that LANL does not include a source of contamination near MCOI-6. We offer the following comments.

An upward gradient within a perched zone Cerro del Rio basalt is highly unlikely. The top of the well screen at MCOI-5 extends to an elevation of 6,130 feet above mean sea level (feet msl), and after construction the water level was at about 6,130 feet msl in 2005/2006. The top of the well screen at MCOI-6 extends to 6,125 feet msl and after construction the water level was at about 6,147 feet msl in 2005/2006. MCOI-6 is closest to the main channel of Mortandad Canyon, and the water level elevation in MCOI-6 is higher/shallower than at MCOI-5. This suggests that infiltration from Mortandad Canyon outfall 051 infiltrated near MCOI-6, that there was a hydraulic head gradient from MCOI-6 toward MCOI-5, and that the contaminants in the outfall and MCOI-6 apparently had not yet reached to MCOI-5 200 feet away.

The complex lava flow geology, spatial variability in hydraulic conductivity, connectiveness, and distance between MCOI-5 and MCOI-6 is large enough to expect significant differences in water levels. Yet both monitor wells show similar hydrographs, which indicates some hydraulic connection within a low-permeability water-bearing perched basalt aquifer. If MCOI-6 were truly confined and tapping a separate artesian aquifer, its hydrograph response would be much different, due to a confining cap above it that would impede/prevent recharge from reaching the lower perched zone, as well as from the difference in storage coefficients.

The OSE text states that discharge to Mortandad Canyon at NPDES Outfall 051 stopped in 2017, but their Figure 9 notations indicate discharge stopped in 2010; the latter is correct. When discharge stopped in 2010, the chromium continued to increase, but more slowly until about

2016 when concentrations declined. About this time, water levels in MCOI-5 and -6 both began to decline. The time lag of a few to several years between the halt of discharge and a response in the perched zone is reasonable. This is a good indication that recharge from the shallow alluvial aquifer reached the perched zone. MCOI-5 dried up in 2023.

The perched zone contamination in Mortandad Canyon, including at MCOI-6, contained significant tritium (up to 13,100 picocuries per liter [pCi/L]) and perchlorate ( up to 218 micrograms per liter [µg/L]), along with chromium. The perched zone at SCI-2 has minor tritium (from Los Alamos Canyon), but no perchlorate. Although the perched zone at MCOI-6 may be at a lower elevation than the perched zone at SCI-2 (about ½ mile to northeast), it is more likely that the Sandia Canyon chromium (only) discharge emptied into the regional aquifer closer to R-43 and probably at other locations between Sandia and Mortandad Canyons. Although chromium was greater in SCI-2 than MCOI-6, the latter does not have the fingerprints of SCI-2.

In the briefing and reports provided to the IRT on FEHM, N3B does in fact have a “hydraulic window” in the regional aquifer near MCOI-6. The center of this source extends from near R-15 to southeast of R-61 and toward R-50. It appears that the OSE source of information is out of date. The upper Mortandad Canyon contamination fingerprints can be found in the southern part of the IM area, for example near R-61-S1.

#### **Case Study V: Chromium Plume Monitoring Wells R-61, R-62, and CrPZ-5**

##### ***Regional Aquifer Monitoring Well R-62***

R-62 is about 2,000 feet west of SCI-2. It is in the regional aquifer and has no screens in perched zones. Bentonite seals most of the annular spaces. OSE notes that this well has increasing concentrations of chromium. Although no chromium above background was found in the perched zones, OSE concluded that the increasing concentrations must be due to downward migration of chromium through the bentonite-filled annulus.

OSE should consider the possibility that there is a source of chromium upgradient of R-62, and that the source at the regional water table is either increasing in strength or that a plume is advancing. For example, chromium detected in CrPZ-6 west-northwest of R-62 deserves further investigation and consideration as evidence of the source upgradient of R-62. N3B includes a “hydraulic window” near R-62, but it could be located farther to the west or west-northwest of R-62. This source would likely have followed a similar path from Sandia Canyon infiltration step-wise through the perched zones down to the regional aquifer, upgradient from R-62. The increasing concentration over time may simply be the result of the slow migration rate vertically and horizontally through the vadose zone.

OSE concludes that “continually leaking seal” at R-62 is the source of contamination at downgradient wells CrPZ-5 and R-61 because these two wells have increasing concentrations over time, as at R-62. The OSE has not analyzed the amount of chromium that could be leaking or the nature and trajectory of a postulated plume emanating from from a crack or channel in the bentonite seal.

CrPZ-5 is over 1,000 feet directly *southeast* of R-62. Most water level elevation maps show the direction of groundwater flow from R-62 is more to the *east or east-southeast*, not directly southeast toward CrPZ-5. And R-61 has fingerprints of tritium and perchlorate, not found at R-62. Further, the concentrations at R-61 do not significantly increase and exceed standards until the IM system is turned on and the hydraulic gradient at R-61 is to the *northeast*, which would be about 90 degrees from the direction of R-62.

## **Appendix P**

### **Evaluation of Borehole Leakage (*Tonkin*)**

## **Appendix P: Evaluation of Borehole Leakage**

### **1. Introduction**

This appendix presents calculations of the approximate rates of vertical flow within a cased boring that is open at two different vertical intervals within an aquifer.

#### **1.1 Background**

At the Los Alamos National Laboratory (LANL) chromium investigation area, the characterization of subsurface conditions has historically included installation of dual-screen well completions. Using this well design, a single boring is completed with two open-screened intervals separated by blank casing. Within the casing, a Baski packer system is inflated to prevent flow occurring in the casing that could cross-connect the two open screened intervals, which might otherwise cause potentially contaminated water to flow from one vertical interval within the unconfined aquifer to another vertical interval within the unconfined aquifer. Figure 1 depicts this type of dual-screen well completion as it has been typically implemented at the chromium investigation area.

This potential mode of cross-contamination can be a very real concern under conditions with large diameter well completions, in settings where there are strong vertical gradients, and very high contaminant concentrations. Under such conditions, flow of contamination within unpumped boreholes that possess multiple screens can lead to substantial mass flux between the screens. However, in settings where such conditions are less evident—in particular, where concentrations are not highly elevated, and vertical gradients are relatively small—and where there is good evidence that the packer system in use is typically reliable, the concern regarding cross-contamination is outweighed by the cost-benefit of obtaining data (water levels and concentrations) from multiple screens within a single boring. The concern has been expressed by the NMED and the New Mexico Office of the State Engineer (OSE) that the subsurface conditions and historical dual-screen well completions at the chromium investigation area are such that should a Baski packer fail, it would lead to hydraulic connection of the upper and lower screened intervals and unacceptable cross-contamination.

It is important to note that as detailed in Section 3 of the main report, based on geology and the spatial distribution of hydraulic conductivity, the IRT sees no evidence of a confining layer or aquitard within the upper portion of the regional aquifer where chromium is present. Therefore, dual-screened wells completed within this portion of the regional aquifer are effectively completed within a single unconfined aquifer and do not lie above and below materials that exhibit aquitard properties that would serve to prevent vertical migration within the aquifer. It is also noted that the wellheads of the dual-screened completion wells are fitted with telemetry systems that report continually on the status of the packer installed within the wells in the event of a failure of the packer inflation and seal.



## 1.2 Purpose

The calculations presented here are intended to estimate the range of likely flow rates between two vertically-separated screen intervals, over defined time periods, under conditions and assumptions representative of the LANL chromium plume investigation area.

## 2. Calculations

The data, methods, inputs, results and conclusions of the calculations are presented in this section.

### 2.1 Methods

Sokol (1963) present an analytical expressions that describe how both the single water level measured in a non-pumping well that is perforated at more than one vertical interval, and any flow that occurs within the cased portion of the well under unpumped conditions, are determined by each open-screened interval in proportion to the transmissibility and the head potential of each interval. The expressions presented by Sokol (1963) were implemented within Microsoft Excel™ for the purpose of the calculations presented in this Appendix.

### 2.2 Data and Calculation Inputs

The following data were used as the basis for the inputs to the calculations of potential flow within dual-screen wells in the event of a packer failure. The values listed below were considered broadly representative of conditions encountered within the chromium investigation area and were used to complete a series of calculations across a reasonable range.

- Vertical separation of upper and lower well screens: 75 ft
- Screen length: 30 ft (includes sand pack)
- Radius of cased well: 0.33 ft (diameter 8 inches)
- Well effective radius of influence: 1000 ft
- Vertical hydraulic gradient: 0.004, 0.012 ft/ft
- Horizontal hydraulic conductivity: 10, 25, 75 ft/d

Given the heterogeneous conditions encountered in the unconfined aquifer throughout the chromium investigation area, a range of values was used for the horizontal hydraulic conductivity and the vertical hydraulic gradient, the basis for which is summarized below:

Vertical gradients: although it is anticipated that there may be a small regional downward gradient given that this is interpreted as an area of low but non-zero recharge, work completed by the IRT suggests that absent the pumping of the IM system and regional water supply wells, vertical gradients are small-valued and depending on the location may be upward or downward. Work completed by the IRT suggests that downward vertical gradients increase under the

influence of both IM pumping and pumping of the regional (PM-series) supply wells, and that under these conditions the vertical gradients may be on the order of 0.012 (downward) feet-per-foot.

Horizontal hydraulic conductivity: work was completed by the IRT to summarize previous aquifer testing results, interpret values for the hydraulic conductivity used in FEHM modeling, and re-interpret available groundwater response data as summarized in Section 3 of the main report. That work suggests that the hydraulic conductivity of the Puye Formation is variable due to the heterogeneous nature of the sediments, ranging depending on the analyst and method of analysis from low (on the order 1 ft/d) to high (on the order several 100 ft/d). However, work completed by Batu using analyses of larger-scale aquifer response data from the CrEx and CrIN wells suggests narrower ranges of 12 ft/d and 172 ft/d (CrEx wells) and 13 ft/d to 75 ft/d (CrIN wells). Overall, the Miocene age sediments beneath the Puye formation (e.g. Chamita Formation of the Santa Fe Group) appear to be sedimentologically similar to those within the Puye Formation, down to an elevation of 5740 f-asl. The hydrogeologic properties of sediments down to an elevation of about 4000 ft msl may be inferred from the re-analysis of PM-2 pumping test analyses reported by Batu for which a  $K_h$  of between 0.8 and 19.9 ft/d was obtained depending on the observation well used for the analysis. These results suggest that the permeability of the deeper sediments are slightly less than those in the Puye Formation and upper Miocene sediments.

This evaluation does not consider the trivial cases where either (a) there is no meaningful vertical head difference between the two screened intervals, or (b) there is no meaningful concentration difference between the two screened intervals. Under the first condition, there would be no flow between the screened intervals despite a failure with the packer; and under the second condition despite the fact there could be flow between the screens (if there is a meaningful head difference) and transfer of some chromium mass, there would be no change in the chromium concentration at the elevation within the aquifer of the receiving screen interval.

### **2.3 Results and Conclusions**

The table below lists the calculation results: the column headers are hydraulic conductivity (ft/d), the row headings are the calculated vertical head difference between the two screened intervals, and the table entries are the calculated flow in gallons per day (gpd) assuming that the situation was not rectified within one day (i.e., 1,440 minutes). In summary, across the range of conditions that might be reasonably encountered by dual-screen wells completed within the chromium investigation area, and setting aside the trivial conditions discussed above, flows within the cased boring between screened intervals might range between about 0.2 and 4 gpm—that is, between about 256 and 5768 gpd assuming that the situation was not rectified within one day.

These estimated rates can be assumed to be “upper-bound” values for the presumed conditions for the following reasons:

1. The Sokol (1963) solution assumes steady-state conditions.

2. The Sokol (1963) solution assumes that there is no additional resistance to flows either into or out of the screened intervals - i.e., that there are no linear or non-linear “skin” effects resulting from the filter pack, drilling fluids, formation disturbance, or other factors.
3. The Sokol (1963) solution assumes that flow within the annulus itself is uninhibited – i.e., that it can occur through the entire cross-sectional area of the cased boring – in this instance, assumed to be of radius 4 inches (diameter 8 inches) as listed on well completion logs. In reality, however, (a) the Baske packer system occupies a substantial proportion of this cross-sectional area thereby reducing the area for flow, and (b) the presence of the Baske system may lead to non-laminar flow, again reducing the flow rate within the remaining area for flow in the annulus.

Consequently, the actual flow rates experienced in the field are likely to be substantially smaller than the rates listed in the table below.

	Conductivity		
H <sub>Diff</sub>	10	25	75
0.30	256	641	1923
0.90	769	1923	5768

## References

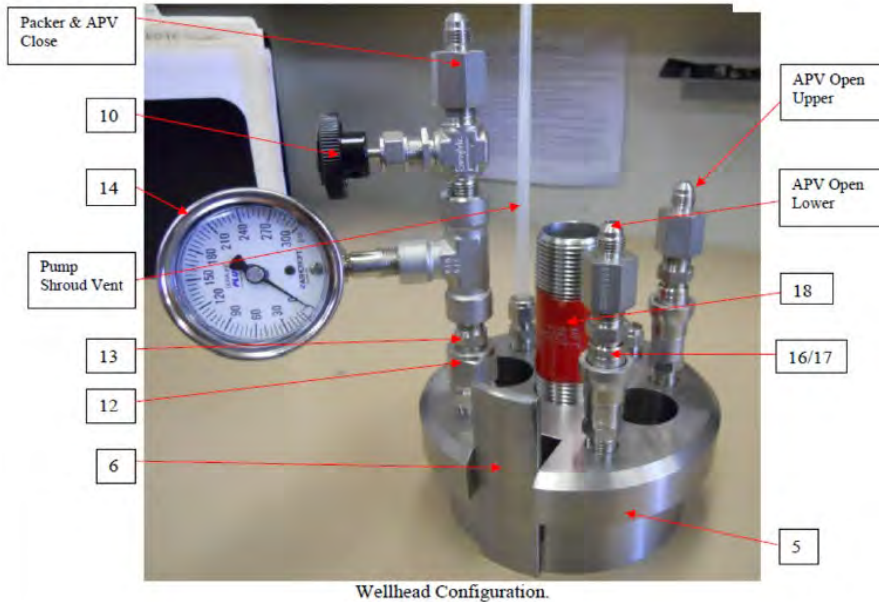
Sokol, D., 1963. Position and Fluctuation of Water Level in Wells Perforated in More than One Aquifer. *Journal of Geophysical Research*, Vol. 68 No. 4, February.



- Baski system for screen separation
  - Telemetry for QA/QC

Baski, Inc.

Viton Covered Packer



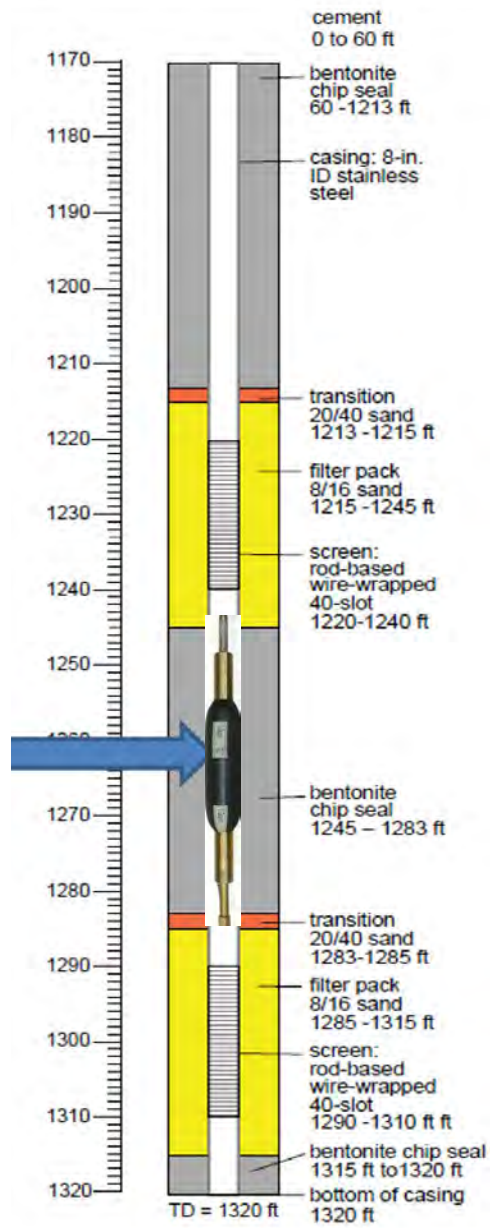


**Figure 1: Typical dual-screen well completion as implemented at the chromium investigation area.**